THE UNIVERSITY *of* EDINBURGH

Late Quaternary sedimentation off the Queensland continental margin (northeast Australia) in response to sea level fluctuations

Ian T. Alexander

Thesis submitted for a degree of
Doctor of Philosophy

University of Edinburgh

January 1996

ACKNOWLEDGEMENTS

First and foremost to Dick Kroon for his endless enthusiasm, encouragement and patience. To Graham Shimmield for acting as second supervisor and giving valuable support. To Erica Kroon and Kate Darling for trying to keep Dick organized, and preventing him drowning under the paperwork. To Peder Aspen and Roy Gill for providing a wealth of information and humouring my constant visits.

Special thanks to all the secretaries, both past and present, especially Nicky McEwan, Helena Jack and Heather Hooker, without whom the department would rapidly come to a standstill.

I would also like to thank Tony Fallick and Terry Donnelly of the Scottish Universities Research reactor Centre at East Kilbride for their assistance and endless patience with the "PRISM", Ann Mennim for help in choosing foraminifers, and Mike Saunders and Tim Brand for their guidance in matters chemical. To Godfrey Fitton, Geoff. Angell and Dodie James for help in all things emitting X-rays, to Janet Cuthill and Yvonne Cooper for being there in a crisis, to Jim Smith and Bob Pringle for providing a window into real life, and to Liz Pickett, Nicki Alison, Helen Trivias and Clare Bradshaw for endless cups of tea and gossip. Also, thanks to Alistair Matthewson, Jerry Lloyd, Gavin McNeill, Steve Mowbray, Christian Robinson and Alan Collins for help and encouragement along the way.

Thanks to Peter Davies (formerly at BMR/AGSO, Canberra) for his hospitality while visiting the antipodes, and to Alex Isern, Dave Feary, Chris Pigram, Charlie Barton and Frank Peerdeman for useful discussion. To Richard Young, Alistair Lomax and Derek Parsons, (formerly at Geol. Dept., Hull University) for nurturing my interest in geology and providing the encouragement to leave (even if it did take the best part of a decade)- cheers !!

And finally to Marianne

ABSTRACT

Drilling during ODP Leg 133 offshore Cairns, northeast Queensland, provided a unique opportunity to document carbonate production and facies development on a mixed carbonate-siliciclastic margin. Recent studies have shown that variations in the sedimentology of Late Quaternary and Pliocene periplatform sediments (Schlager and James, 1978), deposited on continental slopes and in deep basins surrounding shallow carbonate platforms, are linked to changes in sea-level (Droxler *et al.*, 1993; Schlager *et al.*, 1994). However, considerable debate has arisen to the timing of the production and export of shallow water carbonate material, with respect to sea level change. Two main hypotheses have been proposed to explain the response of shallow water carbonate platforms to variation in Late Quaternary sea level: 1) 'highstand shedding' and 2) 'lowstand shedding'. Proponents of highstand shedding argue that depositional systems shed most of its carbonate sediments onto the platform slopes during highstands of sea level. Conversely, during lowstands of sea level bank top production and export of carbonate material is restricted, and platform slopes are largely starved of bank derived carbonate (Schlager, 1992; Schlager *et al.*, 1994). Supporters of lowstand shedding maintain that significant carbonate production and export of shallow water carbonate material occurs during lowstands (and highstands) of sea level (Bosellini, 1989; Goldhammer and Harris, 1989; Grammer and Ginsburg, 1992).

In order to investigate the response of mixed carbonate-siliciclastic systems to variations in Late Quaternary sea level and climate change, core material was collected from Ocean Drilling Program (ODP) Leg 133, Sites 819 and 823 (northeast Australian margin). These two sites form part of an eastward extending transect of drill localities, offshore Cairns, Queensland, from the outer-shelf/upper-slope of the Great Barrier Reef (Sites 821/820/819), into the Queensland Trough (Site 823) and ultimately onto the flanks of the Queensland Plateau (Sites 824 and 811/825). Pelagic to hemipelagic sediments collected from these two sites were examined for the downcore distribution of grain size, magnetic susceptibility, carbonate content, variations in carbonate mineralogy (XRD), and major and minor element (XRF) geochemistry.

Using high resolution foraminiferal stable oxygen isotopes, coupled with biostratigraphic and magnetostratigraphic datums, well defined age models for Hole 819A and Hole 823A have been constructed, although it was not an easy task as hiatuses occur in these records. Age models for the sequences recovered from Hole 819A and Hole 823A have been further refined using correlation with existing isotopic stratigraphies in the Pacific Ocean (ODP Hole 677, Raymo *et al.*, 1989), and comparison with high resolution sedimentologic records from other ODP Leg 133 marine sequences.

Analysis of the mineralogical, sedimentological and geochemical records from Holes 819A and 823A indicate that, over the last 1.1 million years, highstands of sea level (and during the early regression) are characterized by increased shallow water carbonate production, and deposition on the upper slope. This pattern of carbonate deposition is consistent with the highstand carbonate shedding scenario outlined by Schlager *et al.* (1992), and Schlager *et al.* (1994). Lowstands of sea level (and particularly the early transgression) are characterized by increased deposition of non-carbonate (mainly terrigenous) material and/or were not diluted by shallow water carbonate platform material. During the lowstands of sea level the shallow water carbonate factories were switched off. Therefore, the sediments deposited during lowstands of sea level tend to record the greater influence of pelagic driven carbonate.

Although the above mentioned scenario of highstand shedding applies to the entire record of 1.1 million years, mineralogical and geochemical data indicate that shallow burial diagenesis, and dissolution of solution sensitive carbonate, occurred in the lower part of the records. The diagenesis and dissolution, however, have played only a minor role in determining the composition of the Queensland margin sediments.

Variations in the terrigenous input (Cr/Al and Ti/Al ratios) in Queensland margin sediments indicate that interglacial periods were generally wetter than corresponding glacials or lowstands of sea level, during the Late Quaternary.

TABLE OF CONTENTS

APPENDICES

LIST OF FIGURES, TABLES AND PLATES

LIST OF FIGURES

Chapter 3

LIST OF TABLES

Chapter 1

Chapter 3

Chapter 4

Chapter 5

Chapter 6

PHOTOGRAPHIC PLATES

Chapter 1. Introduction

1.1 Main objectives of this study

The goal of this thesis is fourfold: 1) to examine the composition of sediments that have accumulated on the outer-shelf and upper-slope of the Great Barrier Reef and in the Queensland Trough, offshore Cairns, northeast Australian margin, throughout the Late Quaternary; 2) to establish a relationship between the production and shedding of carbonate sediment and sea-level on the continental margin throughout the Late Quaternary; 3) to test the current ideas on carbonate platform production and preservation on a mixed carbonate-siliciclastic platform margin and 4) to ultimately relate the sedimentary history to the development of the shelf margin associated with the buildup of the Great Barrier Reef (GBR). This is however a future objective as the GBR was not yet drilled during the production of this thesis.

1.2 Rationale and background

Coral reef and carbonate platforms are extremely sensitive indicators of environmental change. Environmental parameters such as temperature, light, nutrients, sedimentation, salinity, pressure and water depth, conspire with the processes of erosion to determine how much sediment is produced by a carbonate platform or build-up. Of these parameters, possibly temperature and water depth (which to a greater or lesser extent controls light, pressure and temperature) are the two most important controlling factors determining carbonate production. Modern reefs are constructed mainly of Scleractinian frame-builders (hermatypic corals) and crustose coralline algae (Tucker and Wright, 1990). Hermatypic corals typically live in water depths less than 100 m deep and mainly under 20 m (although this largely depends on the depth at which symbiotic zooxanthellae can photosynthesize- Wells, 1957). Temperatures are in the range between 16-36°C, with an optimum of 23 to 27°C (Tucker and Wright, 1990). Carbonate platforms generally build-up so close to sea level that even small rises and falls will alternately flood and expose the platform top and so drastically effect the carbonate production (Reijmer, 1991). Much of the shallow water carbonate material produced on carbonate bank tops is shed down the platform flanks, due to the lack of accommodation space. This shallow water carbonate material mixes with pelagic/planktonic carbonate to produce the so-called "periplatform deposits" of Schlager and James (1978). These complex and often enigmatic sediments may provide a more continuous record of variations in sea level and climate change, than shallow water neritic deposits, particularly during lowstands of sea level when bank top deposition is often interrupted by karst and erosion (Reijmer, 1991).

Two main hypotheses have been proposed to explain the response of shallow water carbonate bank tops and platforms to variations in Late Quaternary sea level, namely: 'highstand shedding' and 'lowstand shedding' (Schlager, 1992; Schlager *et al.*, 1994). The term 'highstand shedding' means that a depositional system sheds most of its sediment onto the platform slopes during highstands of sea level. Conversely, during lowstands of sea level carbonate production on shallow water shelves and platforms is restricted, and adjacent slopes and basins are largely starved of bank top derived carbonate (Schlager, 1992). This pattern of carbonate sedimentation contrasts with siliciclastic depositional systems which shed most sediment onto the upper-slope during lowstands of sea level, when the shelf becomes subaerially exposed, and rivers become incised, by-passing the shelf (Vail *et al.*, 1977). Some of this material is transported downslope by turbidity currents and deposited in submarine fans (Wilson, 1991). Highstand shedding of carbonate banks and platforms has been documented in the Bahamas (Kier and Pilkey, 1971; Lynts *et al.*, 1973; Droxler *et al.*, 1983; Boardman and Neumann, 1984; Droxler and Schlager, 1985; Mullins *et al.*, 1986; Reijmer *et al.*, 1988; Wilber *et al.*, 1990), the Caribbean (Glaser and Droxler, 1991, 1993), the Indian Ocean (Droxler *et al.*, 1990), and the southwest Pacific (Davies *et al.*, 1989; Davies *et al.*, 1991; Haddad *et al.*, 1993). Reports of highstand shedding are not confined solely to the Cenozoic. In the ancient record, highstand shedding has been documented for Triassic calciturbidites in the Northern Alps (Reijmer and Everaars, 1991; Reijmer, 1991; Reijmer *et al.*, 1992). Similarly, a strong case for highstand carbonate production in Middle Permian strata of the Permian basin (West Texas and New Mexico) has been made by Meissner (1972).

In general, sedimentation rates are high during highstands of sea level and low during glacial lowstands. Furthermore, turbidites are generally more frequent and thicker during highstand intervals, than glacial lowstands, and often forming "highstand bundles" (Droxler and Schlager, 1985). This pattern is opposite to that of the siliciclastic environments where turbidites are more abundant during glacial lowstands (Damuth, 1977). According to Schlager *et al.* (1994) highstand shedding is generally caused by two common attributes of carbonate platforms: their relatively flat tops and their tendency to lithify prior to burial. Sediment production of a platform increases with its size, and the production area of an emergent platform/reef system is normally several orders of magnitude smaller than the production area of a flooded platform (Schlager, 1992; Schlager *et al.*, 1994). In the marine environment, carbonate sediments tend to lithify and form hardgrounds in areas of slow sedimentation and high

current activity (Milliman, 1974). Thus, extensive sea floor lithification will protect highstand deposits when sea level starts to fall and wave base is lowered. Once exposed, shallow water carbonate sediments lithify even faster (particularly in contact with fresh water), as metastable aragonite and high magnesian calcite, reprecipitate as stable low magnesian calcite.

The general concept of highstand shedding of carbonate depositional systems has not gone unchallenged. Several authors have suggested that significant carbonate shedding and platform progradation occurs during both highstands and lowstands (Bosellini, 1989; Goldhammer and Harris, 1989; Grammer and Ginsburg, 1992). A case for lowstand shedding of carbonate depositional systems has been made by Thiede (1981) and Thiede *et al.* (1981) from the analysis of Tertiary turbidite aprons around carbonate atolls in the central Pacific. However, Schlager *et al.* (1994) noted that in many cases a compositional difference (skeletal vs. non-skeletal grains) exists between highstand and lowstand carbonate deposits (in addition to geometric differences). As a consequence much of the evidence presented for lowstand shedding can be reconciled in terms of highstands of sea level (Schlager *et al.*, 1994). Fundamental to many of the arguments for lowstand shedding is the notion that carbonate platforms are not completely shut off during lowstands of sea level. Carbonate sediments may continue to be produced along a narrow zone, parallel to the platform edge, from fringing reefs, eroding sea cliffs and marginal foreslopes. However, Schlager *et al.* (1994) argue that during the Quaternary there is generally insufficient evidence to suggest that lowstand production reaches anywhere near the volume of carbonate produced during highstands of sea level. More recently, Droxler *et al.* (1993) has proposed a new 'lowstand shedding' hypothesis, in which carbonate platform production is tied to the position of the carbonate bank tops relative to the photic zone. According to Schlager *et al.* (1994) the only detailed documentation of lowstand shedding refers to temperate carbonates (see Driscoll *et al.*, 1991).

The northeast Australian carbonate platforms have not been studied in any great detail and provides an unique opportunity to study the effects of variations in late Quaternary sea level and climate change on a mixed carbonate-siliciclastic margin, and, importantly, provides a modern analogue for many ancient sequences (Davies et al., 1987; 1988).

"the question whether carbonate systems show the same response to changes in sea level as siliciclastic systems is one of the major controversies in the recent environment" -Reijmer (1991).

1.3 General Background: Ocean Drilling Program Leg 133

The primary scientific objectives of Ocean Drilling Program (ODP) Leg 133 [4th. August- 11th. October, 1990] drilling offshore Cairns, northeast Australia margin, were: 1). to define the sedimentary response of the passive Queensland continental margin to global sea-level change in the Late Cenozoic, and in particular the Quaternary and, 2) to define the influences of variations in palaeochemistry, palaeoclimate and palaeoceanography on the initiation, growth, and demise of carbonate platforms and build-ups, particularly the Great Barrier Reef complex. In addition, secondary objectives included investigations aimed at defining: 1) the slope-to-basin stratigraphic and facies variations on both sides of the Queensland margin rift basins and, 2) the diagenetic history and processes operating on pure carbonate and mixed carbonate- siliciclastic margins.

In order to carry out the above scientific aims, a series of 16 high resolution drill cores were taken along two transects, across the northeast Australian margin: one orientated east-west, from the outer shelf off the Queensland continental margin (Sites 819 through 822) into the Queensland Trough (Site 823) and ultimately onto the western flanks of the Queensland Plateau (Sites 824 and 811/825), and the second transect orientated north-south across the Townsville Trough (Sites 816/826 and 815 on the northwest margin of the Marion Plateau) to the southern margin of the Queensland Plateau (Sites 817/818) (see Figure 1.1). The work carried out onboard the scientific research vessel the *JOIDES Resolution*, during ODP Leg 133, coupled with extensive post-cruise shore based research, form the basis of a comprehensive data set, the results of which are largely presented in the ODP Leg 133 Initial Reports (Davies *et al.*, 1991) and Scientific Results (McKenzie *et al.*, 1993).

1.4. Study Sites

This study is concerned primarily with the sedimentary sequences recovered from the Queensland margin drilling transect, in particular Hole 819A and Site 823 (Holes 823A and 823B). However, extensive use will be made of both shipboard and post-cruise core data from neighbouring ODP Leg 133 drill sites (see Table 1.1), and from marine sequences outside the study area.

Drilling Site 819 (NE-3[1]) occurs in 565.2 m of water in Grafton Passage, a navigatable channel through the outer Great Barrier Reef (GBR), on the continental slope east of

[1]Original ODP site code

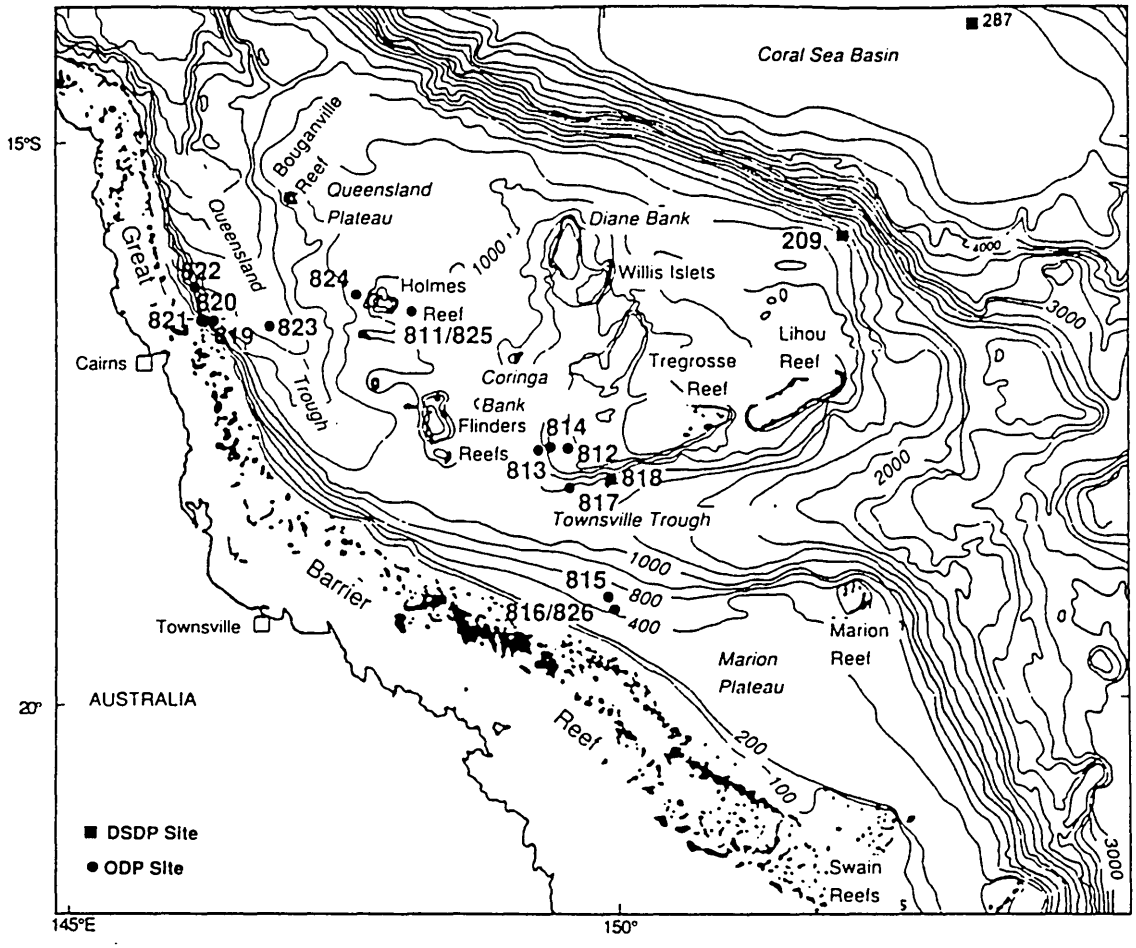

Figure 1.1. Map of ODP Leg 133 drill sites and prior DSDP drill sites, northeast Australian margin (after, Shipboard Scientific Party, 1991). Bathymetry in meters

Cairns, northeast Queensland (see Figure 2.14). The location of Hole 819A represents the distal and deeper water end of an outer-shelf upper-slope transect, on the GBR shelf. Site 819, together with Sites 821, 822 and 820, were drilled in a general location where the GBR changes from a dominantly narrow, rimmed carbonate platform in the north to a narrow, partially rimmed, ramp-shaped continental margin in the south (Davies *et al.*, 1991). Study Site 823 (NE-5) is located in the central-western Queensland Trough, towards the deepest part of the basin, in 1637.9 m water, between the GBR shelf and the Queensland Plateau (see Figures 1.1 and 1.2).

Table 1.1. Ocean Drilling Program Leg 133 Site locations and summary statistics

Site	Latitude (south)	Longitude (East)	Water depth (m)	Penetration (m) total	APC	Bottom age (Ma)	Notes
821	16° 38.793′	146° 17.366′	212	400.0	165.9	< 1.48	46 km from shore
820	16 °38.220′	146° 18.224′	278	400.0	160.2	< 1.48	1.9 km NE of Site 821
819	16 °37.439′	146° 19.486′	565	400.0	123.0	< 1.48	2.7 km NE of Site 820
822	16° 25.379′	146° 12.904′	955	433.9	95.9	> 2.60	25 km NW of Site 819
823	16° 36.981′	146° 36.045′	1638	1011.0	120.5	10.80	29 km E of Site 819
817	18° 09.496′	149° 45.494′	1016	700.0	214.7	> 10.40	30 km SW of Site 818
818	18° 03.767′	150° 02.533′	745	303.0	303.0	< 3.70	30 km SW of Tregrosse Reef

Note: APC = advanced hydraulic piston corer

The marginal Queensland Plateau, and its associated carbonate bioherms, is about 140 and 170 km distance from Site 823 and Site 819, respectively. Site 823 (Queensland Trough) is approximately 60 km to the southeast-east of the GBR shelf edge. The nearest, present-day, source of shallow water carbonate, to the study sites, is Euston Reef (on the outer-shelf of the GBR), located about 14 km to the southwest of Site 819. Other neighbouring reefs on the Queensland margin shelf include the atoll-type Arlington Reef Complex (~16 km^2 in area), and the smaller Flynn, Fin and Milln reefs (see Figure 1.3). In the following chapter a brief introduction to the geological history of Australia, and the region offshore northeast Queensland is presented. In addition, a summary of the main physiographic, climatic and oceanographic elements of the Great Barrier Reef Province (including the marginal troughs and plateaus) is given, in order to introduce the complex environmental setting of the northeast Australian margin.

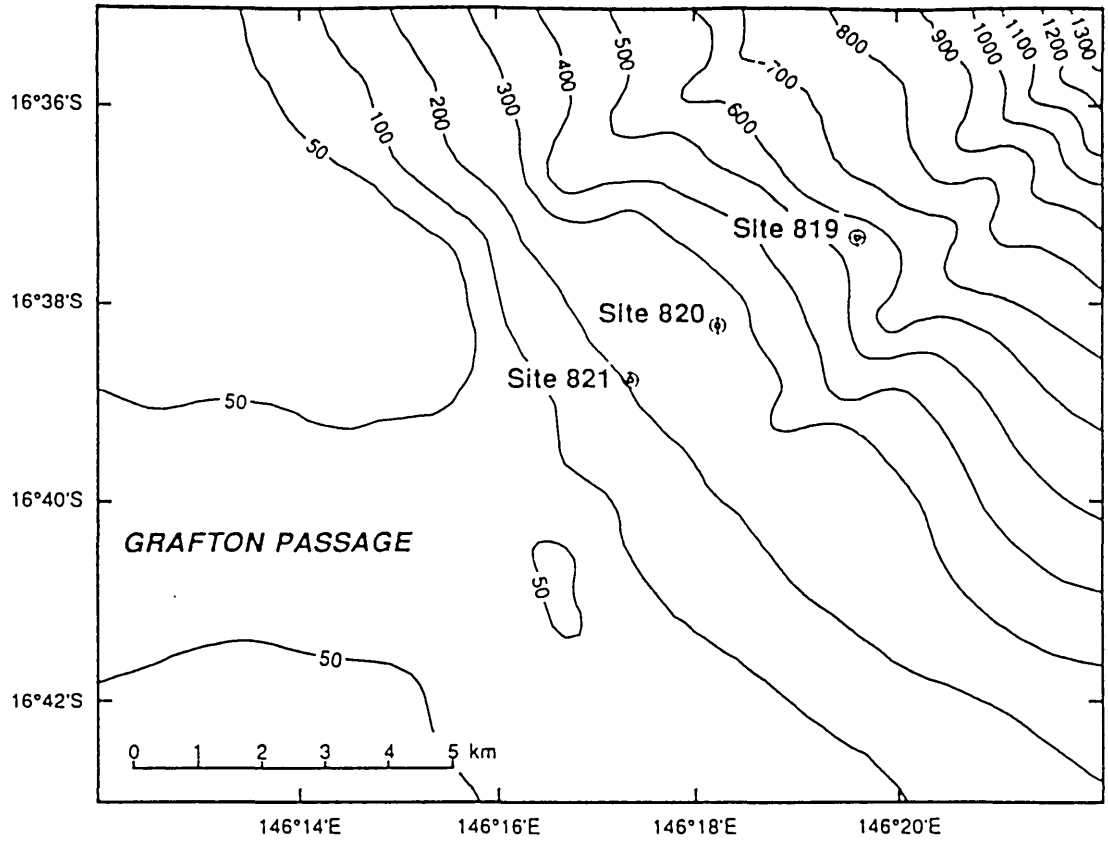

Figure 1.2. Location of Site 819 with bathymetry in meters. Site 819 is approximately 13 km from the outer edge of the Great Barrier Reef (GBR) and 53 km from the Queensland shoreline. Locations of Sites 821 and 820 are also shown. Site 822 is off the map approximately 25 km to the north (after, Barton et al., 1993).

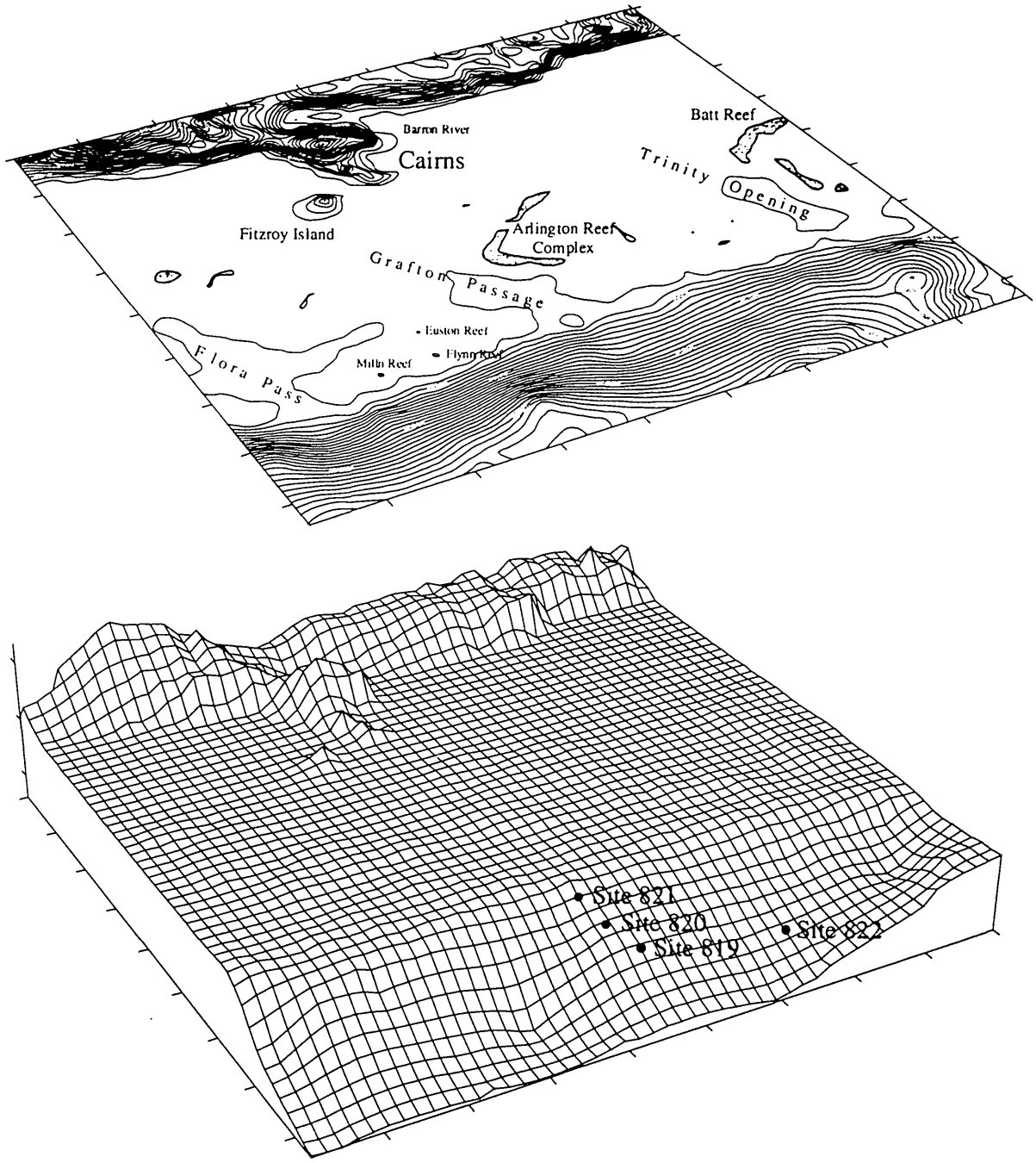

Vertical
exaggeration x 6

Figure 1.3. 2-D (upper plot) and 3-D (lower plot) topographic/bathymetric diagrams of the northeast Queensland continental margin. Sites 821 to 819 are located on the outer-shelf/upper-slope of the Great Barrier Reef. Site 822 is located approximately 26 km to the NW of Site 819. The distance from shore to shelf edge is about 60 km.

Chapter 2 Physiographic and Oceanographic Setting

2.1 Introduction

Examination of the geological and hydrological character of the northeast Australian margin leads to a clearer understanding of the Great Barrier Reef Province, especially with respect to its evolution, its areal distribution, its regional facies differentiation, the nature of the sedimentation and the effect which the province is having and has had on the character of the Queensland continental shelf (Maxwell, 1968). In this chapter, a brief review is given of the tectonic evolution of Australia and the Queensland continental margin, and the modern-day physiographic, oceanographic and climatic setting of the Great Barrier Reef Province, and the Tasman Sea and Coral Sea.

2.2 Tectonic Framework and Evolution

The tectonic evolution of the Southwest Pacific region, and Australia, is very complex, and not yet fully understood (Kennett, 1982). Several possible configurations of continental fragments and plate boundaries in the South Pacific at successive times in the past have been proposed to explain the evolution of the Australian continent (Rutland, 1976; Veevers and McElhinny, 1976; Coleman, 1980; Yan and Kroenke, 1993). Although the various tectonic models differ with regard to spatial and temporal details, they broadly follow the same pattern of plate migration and evolution. A simple overview of the tectonic evolution of Australia is presented below.

2.2.1 Tectonic History of Australia

It is widely believed that during the Proterozoic most of Australia was part of a supercontinent called Gondwanaland that remained virtually intact between 1800 and 450 Ma (Veevers and McElhinny, 1976; Lindsay *et al.*, 1987). Geological studies suggest that the first clearly recorded separation of lithospheric plates occurred during the late Precambrian (Veevers and McElhinny, 1976). These events are interpreted as marking the inception of the eastern (Pacific) and northwestern (Tethys) margins of Australia (Veevers and McElhinny, 1976). Thereafter, the active Pacific margin drifted eastward by the accretion of island-arc material (in the Tasmanides), and the passive Tethyan margin, after its complete development in the early Palaeozoic, remained virtually static until the Mesozoic (Veevers and McElhinny, 1976).

During the Mesozoic the Gondwanaland supercontinent began to break up with the formation of the Indian Ocean, Tasman and Coral Seas, and finally the Southern Ocean (Falvey and Mutter, 1981). These ocean basins formed at normal spreading ridges (divergent plate boundaries). The initial fragmentation of the supercontinent occurred

between western Gondwanaland (Africa and South America) and eastern Gondwanaland (Madagascar, Antarctica, India, and Australia) during the late Jurassic (140-160 Ma). Further continental breakup led to the separation of Greater India from Antarctica/Australia, during the Early Cretaceous (125 Ma ago); the separation of the Campbell Plateau, Chatham Rise, and New Zealand from West Antarctica (Kennett, 1982), and the separation of the New Zealand Plateau and Lord Howe Rise in the late Cretaceous (80 Ma) (Hayes and Ringis,1973); and the separation of Antarctica from Australia, at the end of the Palaeocene (53 Ma ago) (Veevers and McElhinny, 1976; Coleman, 1980).

From about 53 to 32 Ma (Late Palaeocene to Early Oligocene), Greater India, Antarctica, and Australia each lay on separate lithospheric plates. When spreading between India and Australia stopped (at about 32 Ma), these two plates became one. The resultant plate (Indo-Australian Plate) continued to separate by spreading from the Antarctic Plate, creating an ocean between the two continents, and migrated northward at a rate of about 8 cm/yr (Weissel and Hayes, 1972; Cande and Mutter, 1982). Continued plate divergence enabled the South Tasman Rise (which linked Australia with Antarctica) to clear Antarctica, by a sufficient margin to enable the development of the Circum-Antarctic Current during the mid-Tertiary (35-20 Ma) (Coleman, 1980). Northward migration of the Australian craton led to its collision with several island arc complexes, oceanic plateaus and microcontinents (Silver and Smith, 1983), and ultimately to the formation of the New Guinea Orogen (Pigram *et al.*, 1989). The middle Oligocene docking of the Australian continental margin with the complex New Guinea subduction system resulted in the emplacement of a thrust mass and formation of a foreland basin that extended from the Coral Sea to the Indian Ocean (Pigram and Davies, 1987; Pigram *et al.*, 1989). Throughout the Neogene, orogenesis involving large-scale strike-slip and vertical faulting, continued in Papua New Guinea. With the beginning of the Quaternary at about 2 Ma the picture of land and sea was substantially as it is today for Australia and New Zealand (although New Guinea and Tasmania were land extensions of Australia proper) (Coleman, 1980).

About 6 ka ago the coastline attained its modern configuration as the sea rose to its present level in response to the melting of the glaciers of the last ice age. At present Australia is moving toward Papua New Guinea at a rate of several centimetres per year (Struckmeyer, 1990). Associated with the collision are seismic activity, volcanoes, and continuous uplift in the order of millimetres to centimetres per year. Figure 2.1 illustrates the present day position of the Australian continent with respect to the major lithospheric plates and their mean spreading directions.

2.2.2 Outline of the Geological Structure of Queensland

The complex geology of northeast Queensland is the result of convergent interaction between the continental lithosphere of the eastern Indo-Australian Plate with both oceanic lithosphere, and terranes of various affinities. The main tectonic framework of eastern Queensland evolved during the Palaeozoic and consists essentially of the various units of the Tasman Fold Belt (TFB), or Tasmanides (Scheibner, 1978; 1987; Coney *et al.*, 1990; Powell *et al.*, 1990). The TFB stretches over 4000 km from Tasmania in the south to Cape York in northern Queensland, and is at its maximum 1500 km wide (see Figure 2.2). The TFB can be considered as made up of a number of tectonostratigraphic terranes, each with a distinctive history (Powell *et al.*, 1990). However, considerable controversy exists to the exact paleogeographic and paleotectonic setting between the identified terranes and the Australian craton, and between many of the terranes themselves (Scheibner, 1985).

The Queensland Portion of the TFB, or Orogenic System, comprise the Thomson Orogen in the northwest, the Hodgkinson-Broken River Orogen in the northeast and the New England Orogen in the centre and south (Day *et al.*, 1978) (Fig. 2.2). The TFB, is mostly made up of fairly deep-marine Palaeozoic sedimentary and volcanic rocks, and Palaeozoic to lower Mesozoic volcanic and plutonic material. Much of this material is buried beneath mostly flat-lying upper Palaeozoic to Mesozoic-Cenozoic cover, such as the Murray and Great Australian Basins (Coney *et al.*, 1990). The western border of the TFB consists of Precambrian metamorphic rocks that, at least in the north, are separated from the Palaeozoic sediments by a major fault (the Palmerville Fault) (see Figure 2.2).

Offshore, the marginal plateaus and rift troughs of northeast Australia formed during a rifting event which may have commenced in the Early Cretaceous but was certainly in progress in the late Cretaceous (Taylor and Falvey, 1977; Mutter and Karner, 1980; Symonds *et al.*, 1984). The rifting preceded continental breakup and seafloor spreading in the Coral Sea basin during the Palaeocene and Early Eocene (Weissel and Watts, 1979) or latest Cretaceous (Symonds *et al.*, 1983). The Queensland Plateau appears to have formed part of the TFB until the Mesozoic, when it began to subside after grabens coinciding with the Townsville and Queensland Troughs formed along its southern and western margins (Falvey, 1974). Opening of the Coral Sea to the northeast of the plateau during the Palaeocene may have pre-dated formation of the grabens (Falvey and Taylor, 1974). Mutter and Karner (1980) have suggested that the geometry of the Townsville and Queensland Troughs and Osprey Embayment may

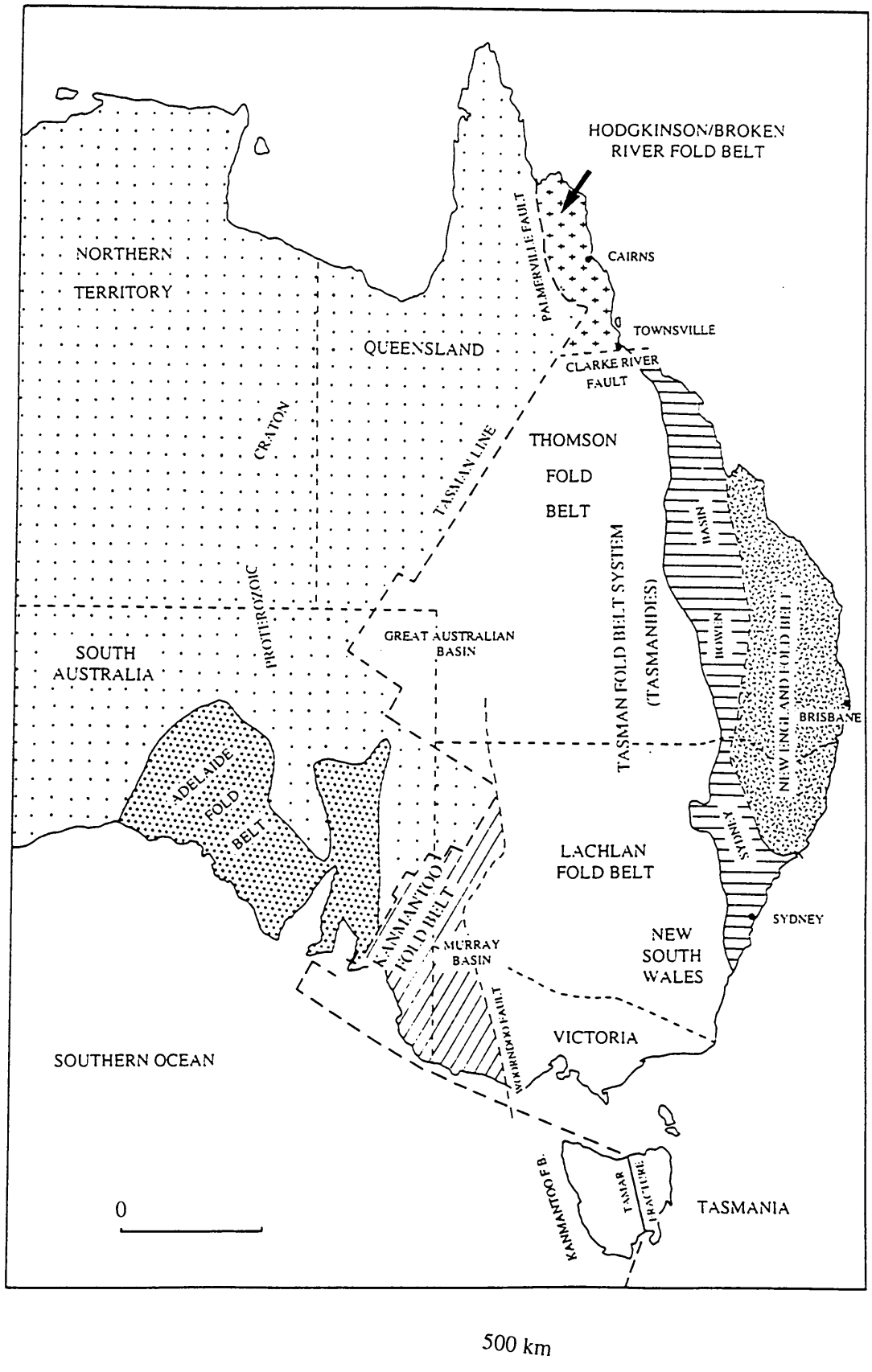

Figure 2.2. Selected tectonic elements of the Tasman Fold Belt (after Scheibner, 1987).

have resulted from the failed arms of a 'three branch rift system' (after Burke and Dewey, 1973). More recently, Scott (1993) has suggested that the Queensland Trough is a product of oblique rifting and possibly pre-dates either the Coral Sea or Tasman Sea taphrogenesis. According to Symonds *et al.* (1983), the Queensland and Townsville Troughs are the most important structural elements associated with the development of the Great Barrier Reef Province. Figure 2.3 illustrates the regional setting and location of the main sedimentary basins offshore northeast Australia.

2.2.3 Carbonate Platform development off the northeast Australian margin

Cenozoic carbonate platform development off the passive northeast Australian margin has been summarized by Davies and Symonds (1988) and Davies *et al.* (1989, 1991). These studies suggest that reef growth has developed primarily in response to five inter-related factors which have acted on the continental margin since the Cretaceous. These factors are: continental rifting, subsidence, plate motion (with climatic and oceanographic consequences), variations in sea-level, and plate collision. Davies *et al.* (1989) further differentiated between short-term (eustatic sea-level, paleoclimatic and paleoceanographic variations) controlling factors, and longer-term (plate motion and subsidence) controls on platform growth and development.

The northward movement of the Indo-Australian plate, throughout the Cenozoic, is thought to have controlled the distribution of carbonate related facies within the Great Barrier Reef sequence, particularly as plate motion was essentially normal to developing climatic zones (Davies *et al.*, 1989). As a consequence of plate drift, the temperate conditions that applied to northeast Australia during the early Tertiary were progressively replaced by tropical conditions, resulting in the development of a southward thining and younger tropical carbonate wedge overlying temperate and subtropical facies (Davies *et al.*, 1987; 1989; 1991) (see Figure 2.4). Superimposed upon latitudinal plate migration, throughout the Cenozoic, have been the effects of global paleoclimatic and paleoceanographic change, producing periods of enhanced and restricted carbonate platform development (see Figure 2.5). Davies *et al.* (1989) suggest that during periods of rising and high sea-levels carbonate production was switched on, whereas falling and low sea-levels restricted carbonate production, caused increased terrigenous input along the shelf and, in many cases resulted in subaerial exposure and karstification (see Figure 2.6).

Davies and his co-workers (1989) suggest that reefs grew first in the north, probably along the margins of a developing foreland basin (New Guinea Orogen), and this early reef growth was closely followed by reef growth on the Marion and Queensland

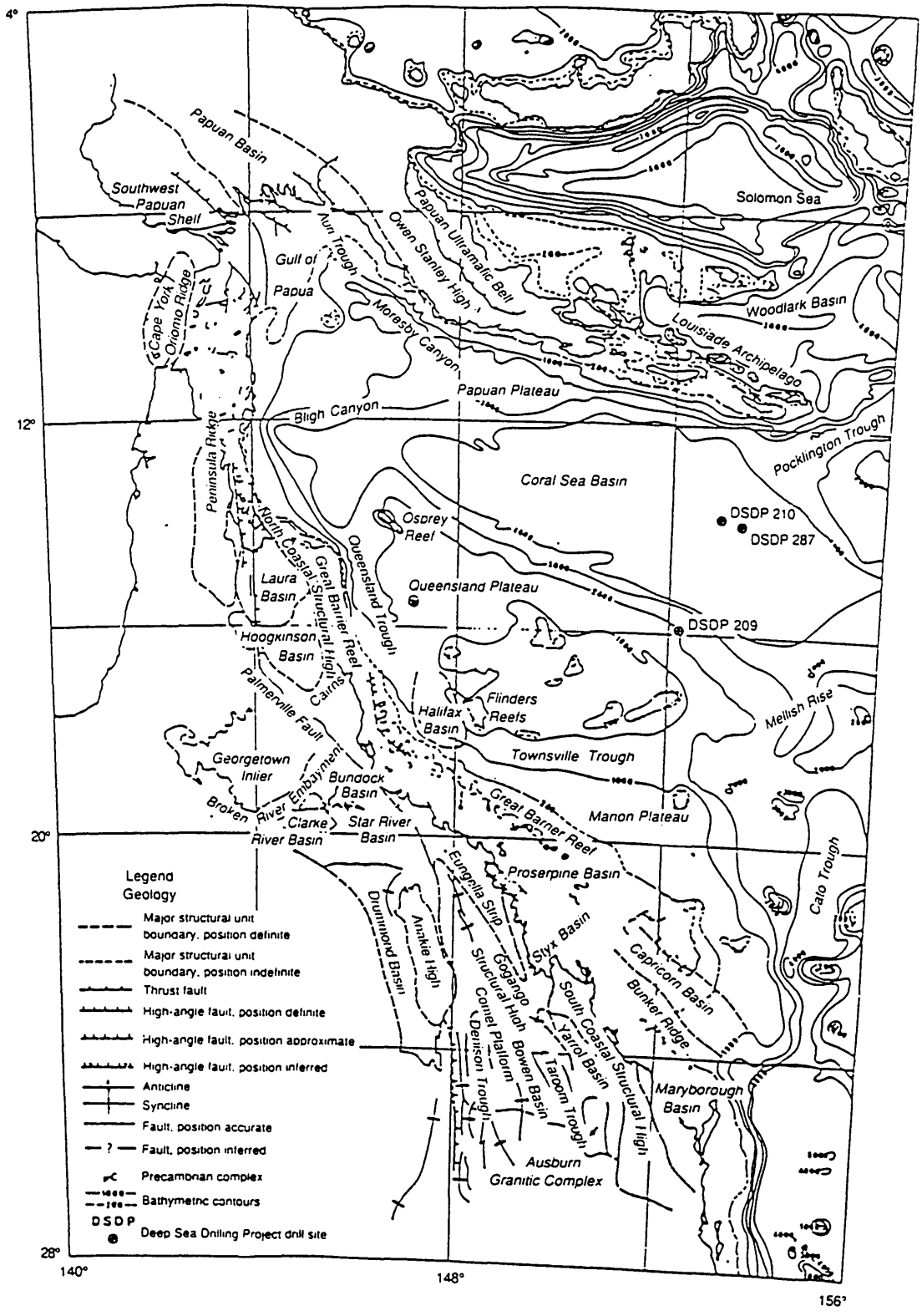

Figure 2.3 Regional setting and location of the main sedimentary basins offshore northeastern Australia. Bathymetry in meters (after Davies et al., 1991).

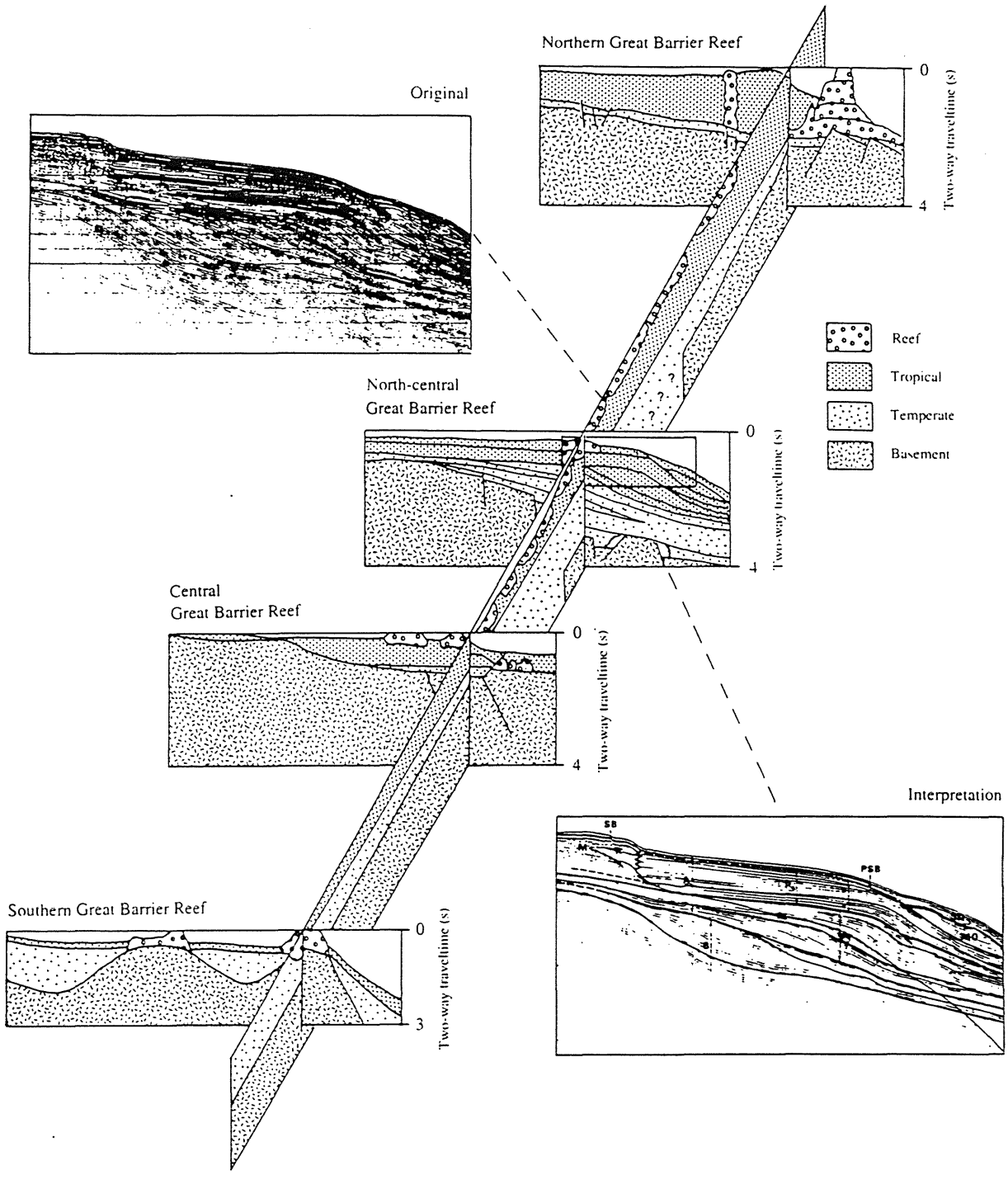

Figure 2.4 Schematic north-to-south section illustrating variations in thickness of temperate and tropical facies of the Great Barrier Reef shelf and slope (after Davies et al., 1991). The northward-thickening tropical wedge implies that reef growth began earlier in the north than in the south (from Davies et al., 1987).

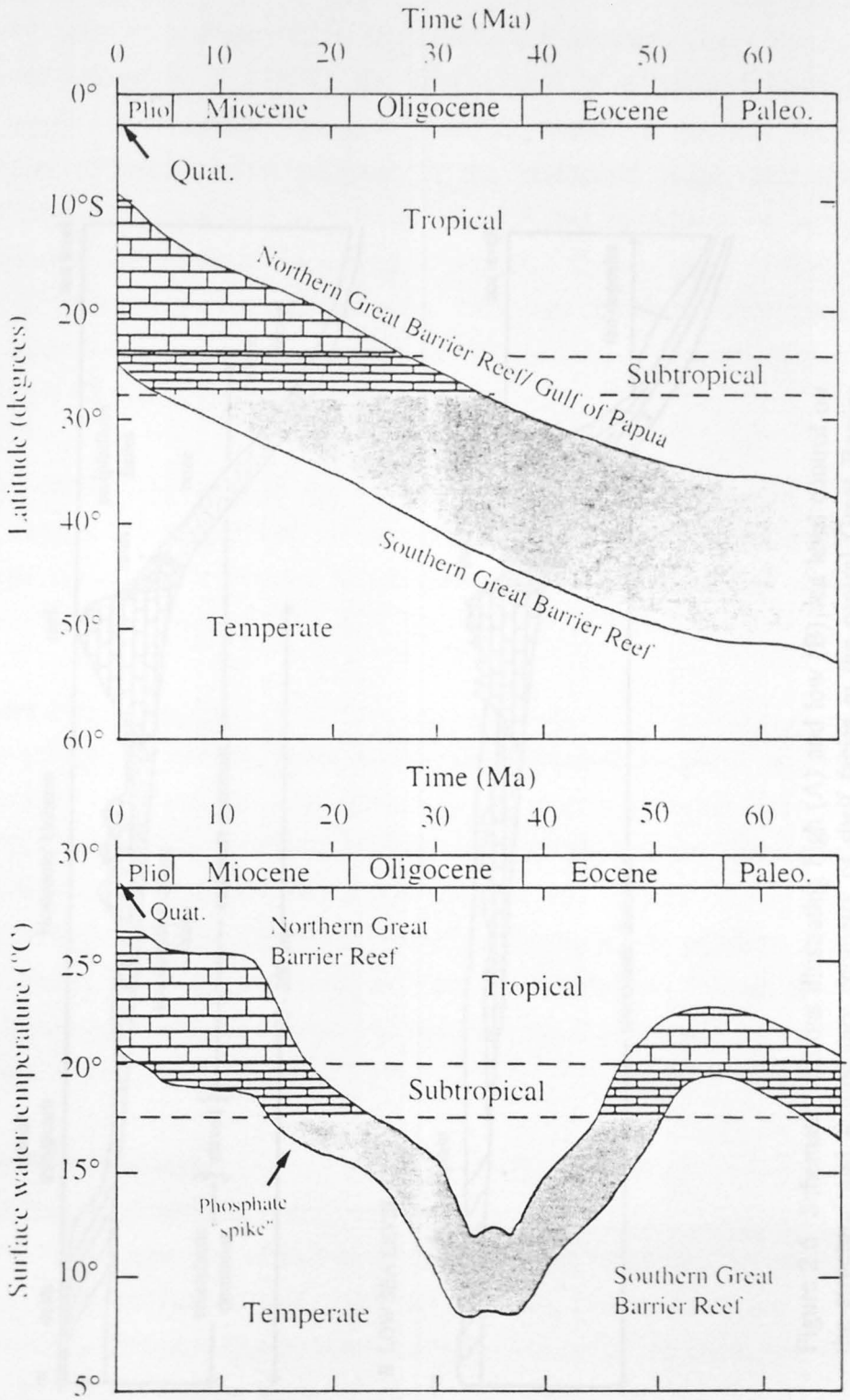

Figure 2.5 **A**. Projected latitudinal movement of the northeastern Australia region throughout the Cenozoic (after Davies et al., 1991). The northern boundary corresponds to Anchor Cay 1 (presently at 9° 30′S) and the southern boundary to Heron Island (presently 24°S) (see Figure 2.7). **B**. Surface-water envelope for the northeastern Australia region throughout the Cenozoic, showing periods when temperatures were suitable for reef growth. The Miocene "phosphate spike", which inhibited reef growth, is also shown (Riggs, 1984).

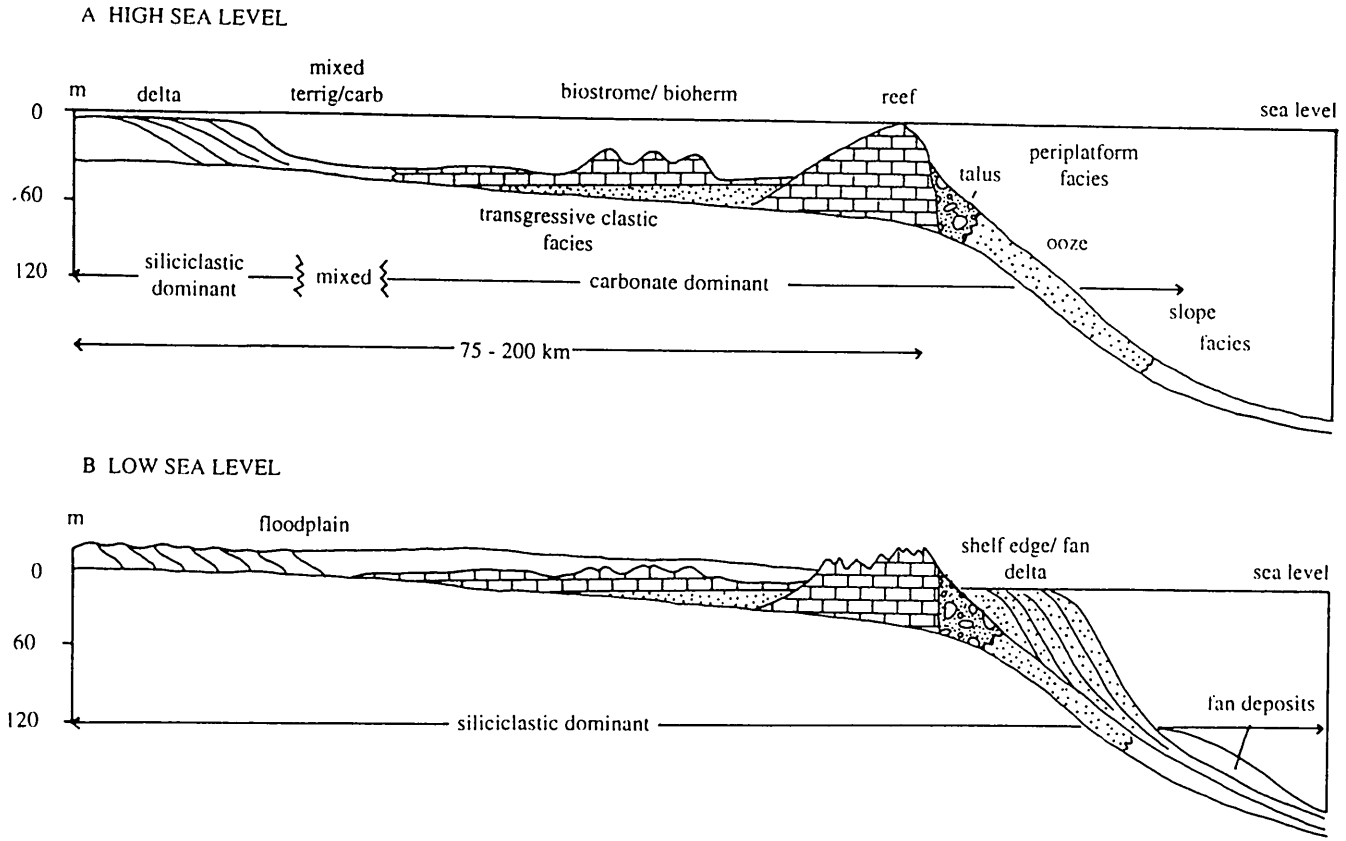

Figure 2.6 Schematic sections illustrating high (A) and low (B) sea level control on the structural and sedimentary geometry of shelf facies in the central Great Barrier Reef Province (after Davies et al., 1989). Note the predominance of carbonate facies in the highstand sea level scenario.

Plateaus, and later by reef growth on the central and southern Great Barrier Reef. According to Pigram *et al.* (1989), the development of a foreland basin on the northeast margin of Australia, during the Tertiary, caused a dramatic increase in shallow water carbonate facies adjacent to the peripheral bulge, but ultimately terminated carbonate deposition as a result of uplift and inundation by terrigenous clastic sediments derived from the emergent orogen. Davies *et al.* (1989) further suggest that prior to continental collision, carbonate platform development off northeast Australia was largely controlled by the location of shallow water areas, associated with rift bounded structural highs.

For a more detailed account of the Cenozoic evolution of the passive northeast Australian continental margin and the primary factors effecting carbonate platform development, the reader is referred to the concise work of Davies and co-workers (1989).

2.3 Offshore Physiography

The region offshore of the northeast Australian continental margin is an extremely complex product of rifting, sea-floor spreading, and margin accretion (Davies *et al.*, 1987; 1989). The passive continental margin comprises the Eastern, Queensland, and Marion plateaus; the Pandora and Bligh troughs; the Osprey Embayment; the Queensland Trough, and the Townsville and Cato Troughs. In addition, a zone of narrow rift basins, which extend southeast from the Queensland Trough toward the Capricorn Basin, separates the Marion Plateau from the Queensland continental shelf (see Figures 2.7 and 2.8).

2.3.1 Carbonate Platforms

The modern day physiographic setting on the northeast Australian continental margin is dominated by the presence of extensive shallow water carbonate bioherms, which border deep rift basins (Davies *et al.*, 1989; Harris *et al.*, 1990). There are three main carbonate build-ups offshore Queeensland, northeast Australia: the Great Barrier Reef, the Queensland Plateau and the Marion Plateau.

The Great Barrier Reef is an extensive assembly of coral reefs and lagoons, extending from about 9.1°S, just south of Papua New Guinea, to about 24°S, off the east coast of Queensland, Australia (Figure 2.7) (Pickard *et al.*, 1977). The Reef as a whole extends roughly in a northwest-southeast direction, with an outer reef length of about 2300 km; within which lie over 2500 reefs (Bennett, 1971) varying in size from small isolated pinnacles to massive reefs up to 25 km long and 125 km^2 in area (Hopley,

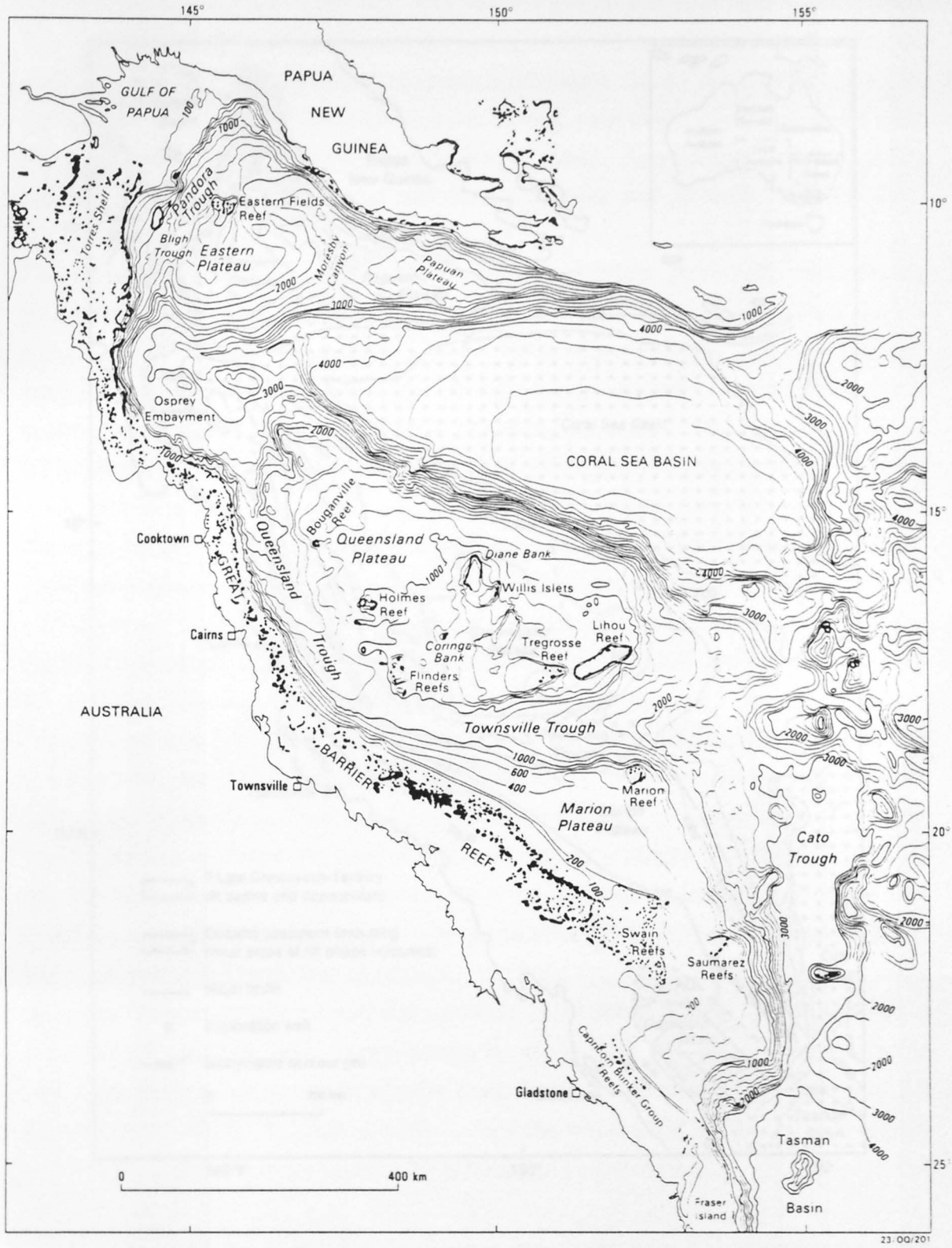

Figure 2.7 Locality map showing the principle bathymetric features of the northeastern Australia continental margin (courtesy of AGSO- formerly BMR). Areas of modern reef growth are shaded. Bathymetry in meters.

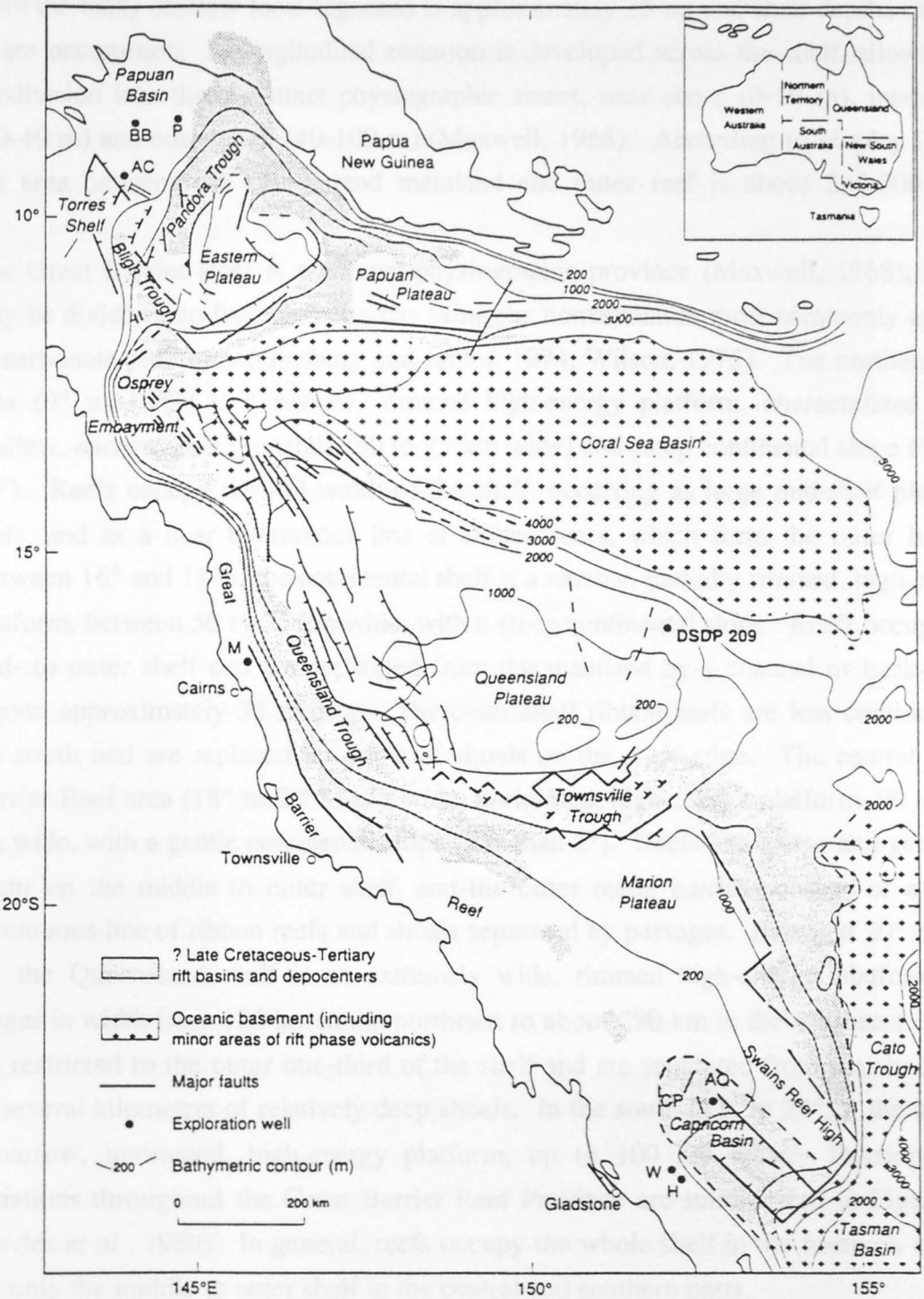

Figure 2.8 Map showing the major structural features offshore northeastern Australia margin. The location of exploration wells (BB Borabi 1; P = Pasca A1 and C1; AC = Anchor Cay; M = Michaelmas Cay; AQ = Aquarius 1; CP = Capricorn 1A; W = Wreck Reef; H = Heron Island) and DSDP Site 209 also are shown. (after Davies et al., 1991).

1982). The width from shore to outer reef varies from 23 km at 14°S to 260 km at 22.5°S and averages about 100 km. The mean depth of the main lagoon (as distinct from the many shallow local lagoons) is approximately 35 m, and shelf depths over 60 m are uncommon. A longitudinal zonation is developed across the shelf, allowing its subdivision into three distinct physiographic zones: near shore (0-10 m), inner shelf (10-40 m) and outer shelf (40-100 m) (Maxwell, 1968). According to Hopley (1982) the area between the Queensland mainland and outer reef is about 230,000 km^2.

The Great Barrier Reef is a diverse physiographic province (Maxwell, 1968), which may be divided into five distinct areas using the nomenclature most commonly applied to carbonate platforms (Ginsburg and James, 1974; Wilson, 1975). The northernmost area (9° to 16°S) is a narrow, rimmed high-energy platform, characterized by a shallow, narrow shelf (generally 50 to 75 km wide) and steep continental slope (10° to 60°). Reefs occupy the full width of the shelf, occurring as large mid-shelf platform reefs, and as a near continuous line of ribbon reefs, which form the outer barrier. Between 16° and 18°S, the continental shelf is a narrow, partially rimmed, high-energy platform, between 50 to 75 km wide, with a steep continental slope. Reefs occupy the mid- to outer shelf and are separated from the mainland by a channel or back-reefal lagoon approximately 35 m deep. The outer-shelf ribbon reefs are less continous to the south and are replaced by a line of shoals on the shelf edge. The central Great Barrier Reef area (18° to 20°S) is a wide, unrimmed, high-energy platform, 90 to 125 km wide, with a gentle continental slope (less than 2°). Reefs are sparse and generally occur on the middle to outer shelf, and the outer reefal barrier consists of a semi-continuous line of ribbon reefs and shoals separated by passages. Between 20° and 22 °S, the Queensland shelf is an extremely wide, rimmed high-energy platform that ranges in width from 125 km in the northeast to about 290 km in the southeast. Reefs are restricted to the outer one-third of the shelf and are separated from the shelf edge by several kilometers of relatively deep shoals. In the south (23° to 24°S), the shelf is a narrow, unrimmed, high-energy platform, up to 100 km wide. Physiographic variations throughout the Great Barrier Reef Province are summarized in Figure 2.9 (Davies *et al.*, 1989). In general, reefs occupy the whole shelf in the northern region, but only the middle to outer shelf in the central and southern parts.

Despite its name the Great Barrier Reef is not continuous and certainly does not present an impermeable barrier to the passage of water. In the more continuous stretches of reef, water from the Western Coral Sea may enter not only through the gaps between the coral reefs (e.g., Grafton Passage, Trinity Opening, Flora Pass), but also over the reefs as swell breaks on them (Pickard *et al.*, 1977).

The Queensland Plateau is the largest marginal plateau on the Australian continental margin (Orme, 1977) (see Figures 2.7 and 2.8). It has an area within the 1000 m isobath of approximately 181,000 km^2, and about 373,000 km^2 overall (Mutter, 1977). It is one of the largest features of its type and is approximately the same size as the Bahamas Platform. The plateau is bounded to the northeast by the Coral Sea Basin, and to the west and south by the Queensland and Townsville Troughs, respectively. The plateau is roughly triangular in shape, with its western margin striking north-northwest, its northeastern margin which faces the Coral Sea Basin striking northwest, and its southern margin striking east-west. The Queensland Plateau consists of subsided continental crust with basement rocks of Palaeozoic age which are tectonically part of the Tasman Geosyncline (Ewing *et al.*, 1970; Falvey, 1974). The Queensland Plateau surface is dissected by many canyons and valleys (particularly in the northern part of the plateau), which lead into the adjacent troughs, and the Coral Sea Basin (Winterer, 1970).

The plateau is punctuated by a number of atoll-like, isolated carbonate platforms which rise to the sea surface (Mullins, 1983). The largest modern day reef complexes are the Tregrosse and Lihou reefs (>50 km^2), lying along the southern margin of the plateau. Other major areas of modern reef growth are the Coringa, Willis and Diana complexes in the centre of the plateau, and the large isolated pinnacles of Flinders, Holmes, Bougainville, and Osprey reefs, which lie along the western margin of the plateau. Away from the reef areas the plateau surface is generally very smooth and flat, and has a very gentle northwest tilt.

The Marion Plateau, with an area of about 77,000 km^2, lies directly east of the central Great Barrier Reef and is fringed along its northern margin by the Townsville Trough and along its eastern margin by the Cato Trough (Figures 2.7 and 2.8). In addition, a series of north-south orientated, narrow discontinuous half-grabens separates the plateau from the continental margin to the west. The present plateau surface forms a deeper-water extension of the Australian continental shelf and has water depths ranging from 100 m along the western (landward) border to 500 m along the eastern (seaward) margin (Davies *et al.*, 1989). A large part of the Marion Plateau is underlain by several shallow-water carbonate platform complexes of different ages: the oldest (probably Early Miocene) occurs in the north: and the youngest (Late Miocene-Pleistocene) in the south (Davies and Symonds, 1988). At the present time, reef growth is restricted to Marion Reef on the northeastern corner and Saumarez Reef at the southeast extremity of the plateau (Davies *et al.*, 1989). Prior to ODP Leg 133,

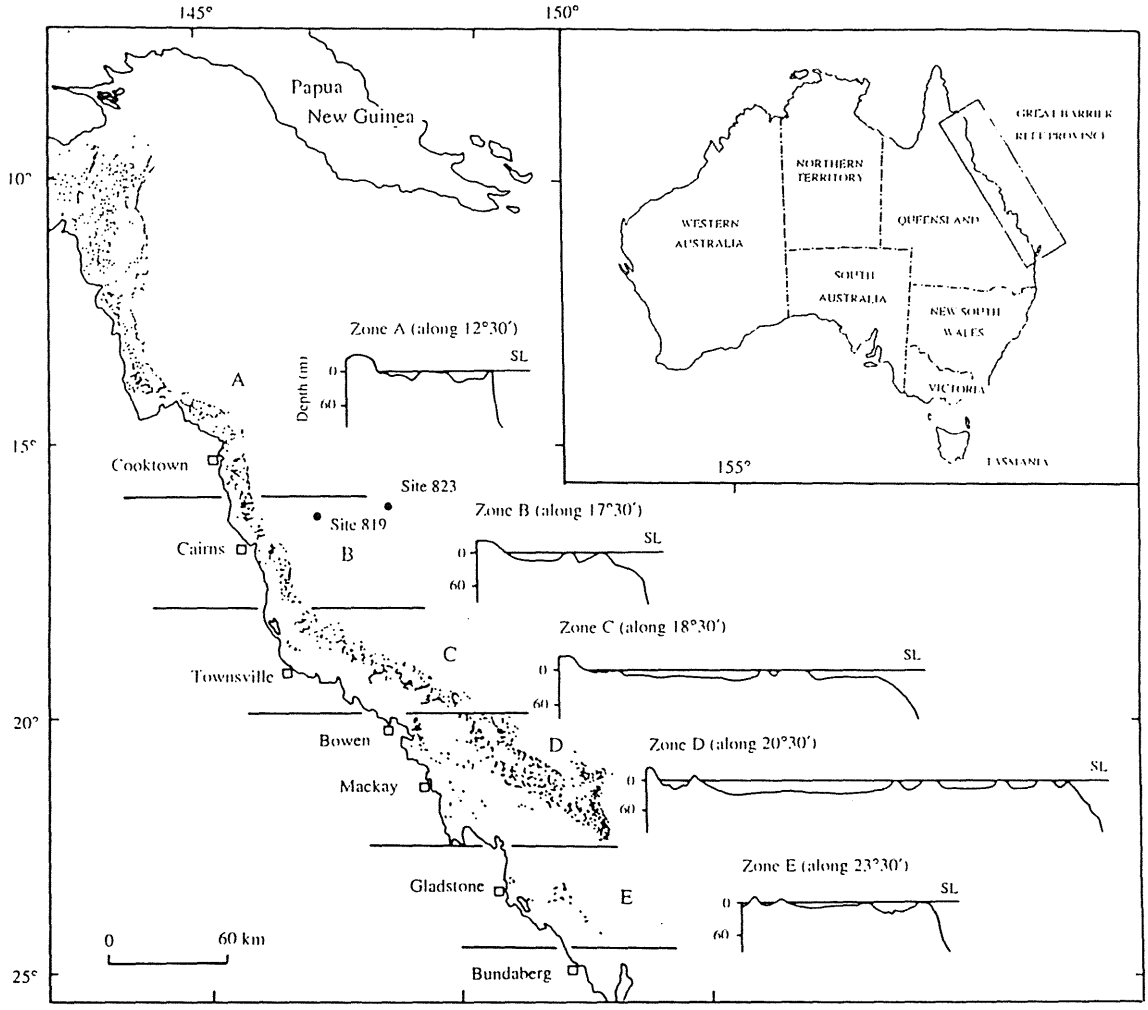

Figure 2.9 Physiographic variations throughout the Great Barrier Reef Province (after Davies *et al.*, 1991). A. Narrow, rimmed platform; B. Narrow, partially rimmed platform; C. Wide, unrimmed platform; D. Extremely wide, rimmed platform; E. Narrow, unrimmed platform. Nomenclature after Ginsburg and James (1974) and Wilson (1975). Note the position of Sites 819 and 823 in Zone A/B reefs.

little detailed subsurface structure and facies distribution information existed for the Marion Plateau.

2.3.2 Queensland and Townsville Troughs

The Queensland Trough is a roughly north-south trending feature separating the Queensland continental margin, to the west, from the Queensland Plateau, to the east (see Figures 2.7 and 2.8). The strike of the trough is that of the dominant structural grain of the Tasman Fold Belt in northern Queensland (Hill and Denmead, 1960; Falvey, 1972). The trough has a gradient of about 1:300 and ranges in depth from 1100m in the south to abyssal depths in the north (Gartner, 1970). The western margin is much steeper than its eastern margin, with gradients up to 1:3 (at 15°S). The steepness of this slope implies a tectonic origin for the western margin (Mutter, 1977). A schematic cross section across the Queensland Trough illustrating its general structural style and that of its margins is shown in Figure 2.10a (ODP Leg 133 Shipboard Scientific Party, 1991).

The Townsville Trough is an east-west striking topographic feature that separates the Queensland Plateau from the Marion Plateau. The trough is roughly perpendicular to the main structural trends of Queensland (Mutter, 1977), which suggests either an erosional origin or a reflection of a tectonic trend not apparent on mainland Australia (Gartner, 1970). The trough is characterized by a broad, flat floor, gently sloping wall, and a gradient of 1:300. The trough has a symmetric, U-shaped profile that is maintained over most of its length. At its eastern end, at about 154°E, a bifurcation sends one branch south into the Cato Trough and the other winds sinuously north into the Coral Sea Basin. Mutter (1977) speculated that sediment derived from the Queensland Plateau or from mainland Queensland might have reached the adjacent deep ocean floor via the Townsville Trough and its offshoots. A composite section across the Townsville Trough from the Queensland Plateau in the north to the Marion Plateau in the south is illustrated in Figure 2.10b (ODP Leg 133 Shipboard Scientific Party, 1991).

2.4 Oceanographic Setting

A bewildering multitude of water masses, water types, water mass components and mixing circuits have been proposed to explain the physical oceanography of the waters of the GBR region, and the adjacent Coral and Tasman Seas (Wyrtki 1960, 1962; Maxwell, 1968; Rochford, 1969; Sculley-Power, 1973a; Pickard *et al.*, 1977; Tomczak and Hao, 1989). However, many of these studies are largely based on non-synoptic and individually sparse data sets, which in many cases have been collected over several

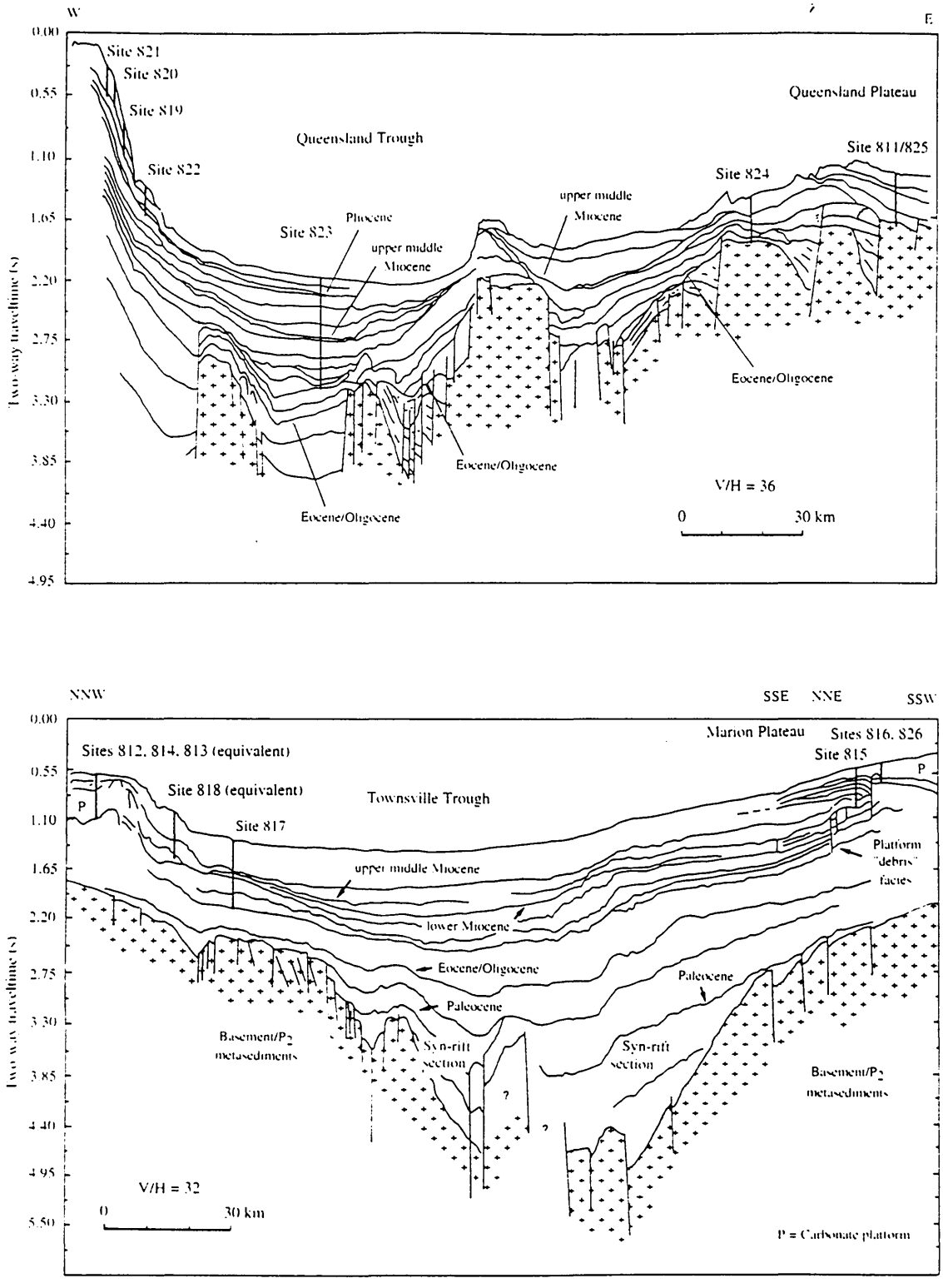

Figure 2.10 **A.** Schematic section tying east-west seismic profiles across the Queensland Trough from the GBR slope to the western flanks of the Queensland Plateau (after, Davies et al., 1991). **B.** Composite section across the Townsville Trough from the Queensland to Marion plateaus, based on seismic profiles.

years. Thus, there exists considerable scope for refinement, particularly with respect to understanding the large scale movements of water masses and the influence of Coral Sea waters on the Great Barrier Reef ecosystem.

2.4.1 Water Masses

Several attempts have been made to summarize the water masses occurring in the South-Pacific Ocean (Wrytki, 1960, 1962; Maxwell, 1968; Pickard *et al.*, 1977). According to Wrytki (1962) five major water masses can be recognized in the Western Coral Sea (WCS) namely: Surface Water; Subtropical Lower Water (SLW); Antarctic Intermediate Water (AAIW); Deep Water and Bottom Water. The essential characteristics of these different water masses are summarized below:

(1) WCS surface water is characterized by a high temperature (>24°C) and salinities between 34.0 ‰ and 35.6 ‰. It can be further subdivided into several components of different origin (Rochford, 1957, 1959). In the northwest, surface water is augmented by Arafura and Gulf Water which enters through the Torres Strait, and mixes along the Queensland shelf and the western part of the Coral Sea (see Figure 2.11). Arafura Water is characterized by mean salinity and temperature values of 34.2 ‰ and 29.0°C, respectively (Pickard, 1977).

(2) The Subtropical Lower Water (SLW), is derived from the Subtropical Surface Water of the South Pacific Ocean. SLW is characterized by a salinity maximum, and can be separated into northern and southern components based on dissolved oxygen (3-4 ml/l and >4.4 ml/l, respectively). SLW has salinities between 35.5 ‰ and 36.0 ‰, combined with temperatures between 18° and 25°C, in the WCS. The SLW core layer is found between the surface and 250 m depth.

(3) The Antarctic Intermediate Water (AAIW), characterized by a salinity minimum found at the 1000 m level in the whole region. In the WCS, the AAIW has a salinity between 34.37 ‰ and 34.53 ‰, a temperature between 4.2° and 6.0°C, and a density (σ) near 27.2 g/cm^3. AAIW is further characterized by relatively high O_2 concentrations of about 4.2 ml/l (Pickard *et al.*, 1977). AAIW is found at depths between 650 to 1100 m.

(4) The Deep Water, characterized by a weak salinity maximum of the order of 34.74 ‰, a temperature at or near 1.7°C and a relatively high oxygen content. The maximum is found only in the East Australian Basin, but the Deep Water fills the Coral Sea Basin and the Solomon Basin. Deep Water is situated between 2500 m and 3000

m water depth. In general, deep-water represents a mixed water type, which is formed by the bottom water (AABW) and intermediate water (AAIW and North Atlantic Deep Water - Deitrich *et al.*, 1980).

(5) The Bottom Water, characterized by the minimum of potential temperature and by salinities slightly lower than those exhibited by the Deep Water. Its origin is in the Antarctic and is found in the deepest layers of the East Australian Basin. Bottom Water is found below the Deep Water.

Alternatively, Maxwell (1968) recognises four major water masses, Equatorial, Central Water Mass, Coral Sea and Gulf-Arafura (see Figure 2.11), in the WCS, all with different temperature-salinity characteristics (Rochford, 1959). The salient characteristics of these water masses (except for the Gulf-Arafura surface water mass) are listed below:

(1) The Equatorial Water Mass (EWM), is the main surface water mass that is swept into the province under the influence of the Trade Wind Drift. It forms a band between 10°S and 10°N latitude and extends to depths of 1000 m (average salinity 35.3 ‰, temperature 27°C).

(2) The central Water Mass (CWM) of the South Pacific, extends to depths of 900 m (in the west) and is variable in character (mean salinity 35.7 ‰, temperature16-26°C.

(3) The Coral Sea Water Mass (CSWM) with an average salinity of 35.0 ‰ and a temperature of 21.3°C. This water mass is developed in the northwestern region adjacent to the EWM.

Typical vertical profiles of temperature (T), salinity (S), density (σ) and dissolved oxygen (O_2) for the Western Coral Sea (15.0°S, 149.5°E, 1200 m water column) are illustrated in Figure 2.12 (data from Sculley-Power and France, 1969). An important point to note is that, in the above scenario, the present-day position of ODP Leg 133 Site 819 (and location of one of the main study cores), in 565.2 m water depth, is just below the main thermocline, the zone of rapid physiochemical change. In terms of watermasses, Site 819 located on the upper-slope of the GBR is situated between the cores of SCW (water depth 50-250 m) and AAIW (water depth 650-1150 m). The present day position of ODP Leg 133 Site 823 (axis of the Queensland Trough), drilled in 1638.4 m water depth, lies below the core of the AAIW.

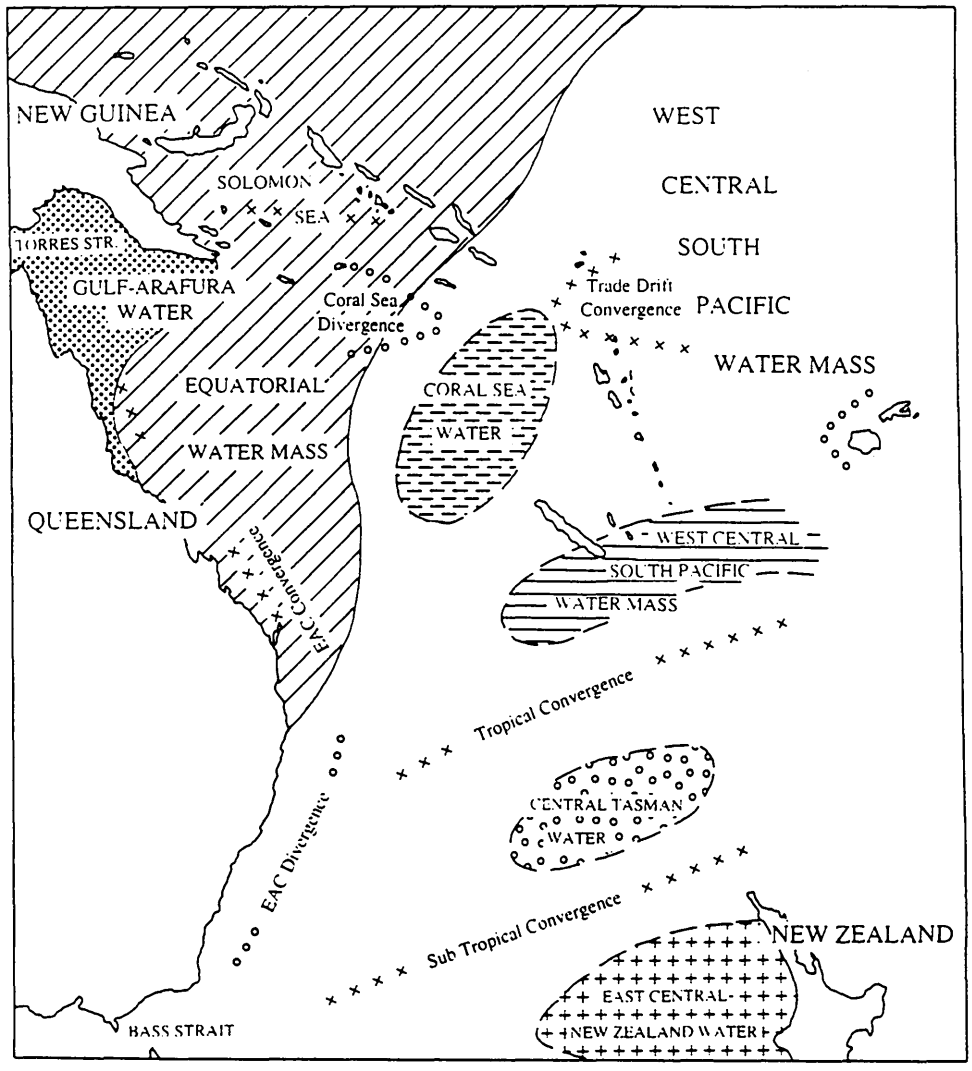

Figure 2.11 The main water masses of the South-West Pacific, and the zones of convergence and divergence (after Maxwell, 1968). Note the southern extension of Equatorial Water and Gulf Arafura Water.

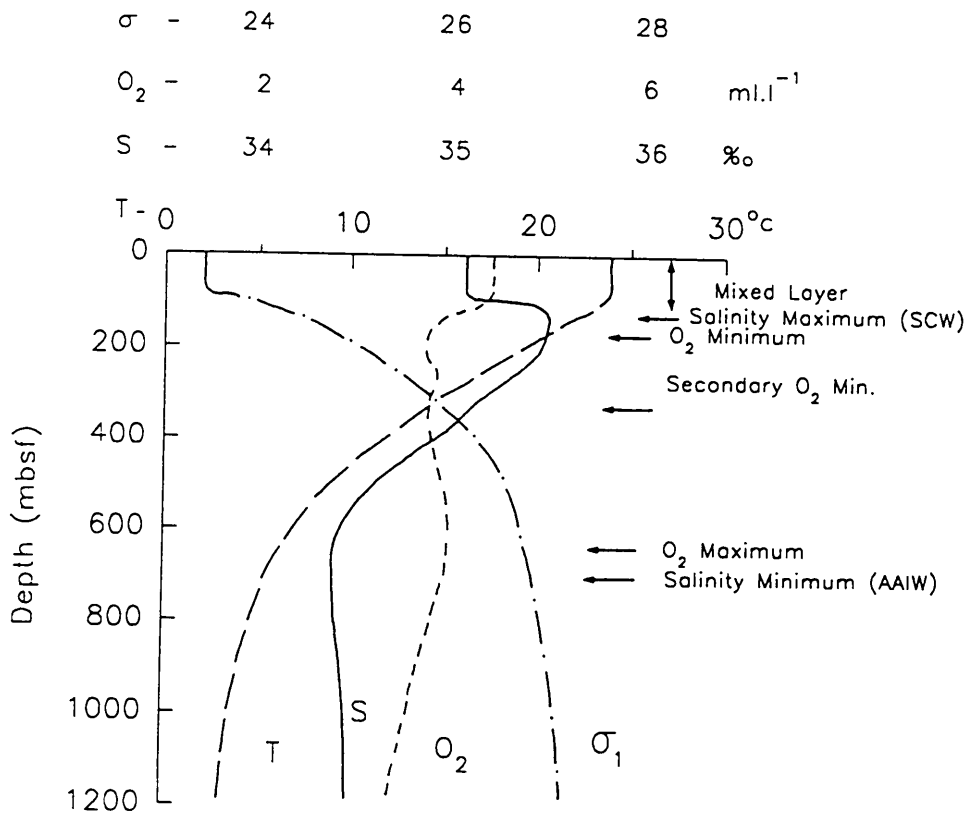

Figure 2.12 Typical vertical profiles of temperature (T), salinity (s), density (σ) in 1200 m of water in the western Coral Sea (redrawn after Pickard et al., 1977). Note the changes in the structure of the thermocline/ mixed layer in a water depth of between 200 and 550 m.

2.4.2 Circulation

Both surface and subsurface water circulation patterns in the Western Coral Sea are very complex, and are not fully understood (Andrews and Clegg, 1989). For example, whereas seasonal changes can be clearly identified in the surface water circulation patterns, the affect of seasonality on deep water circulation remains ambiguous. The essential hydrologic character of the Coral Sea and Tasman Sea is provided by Wyrtki (1960; 1962) and Scully-Power (1973a; 1973b). Figures 2.11 and 2.13 illustrate the surface and subsurface circulation patterns in the South-West Pacific Ocean and Western Coral Sea, respectively.

The surface circulation of the oceans is closely related to that of the atmosphere and the currents in general follow the direction of the wind, but slightly turning to the left (Rotschi and Lemasson, 1967). Surface water circulation patterns in the Western Coral Sea are largely dominated by the westward flowing South Equatorial Current (SEC), see Figure 2.13. The SEC normally flows with considerable velocity (>20 cm/s), but fluctuates widely with seasonal changes in the wind pattern (Maxwell, 1968). Upon entering the Western Coral Sea, the SEC either diverges or is turned southward depending on the austral season (Pickard *et al.*, 1977). Parts of the northern branch flow into the Solomon Sea and the Gulf of Papua, while a drift continues westward to the Northern Queensland Shelf. The southern component, of the SEC, sweeps over the Queensland shelf between 20°S and 25°S latitude, and becomes the East Australian Current (western boundary current) at about 20°S (Orme, 1977). During the monsoon season (December to February), the bifurcation point moves north to at least 14°S (Church, 1987). The East Australian Current (EAC) reaches maximum velocities of about 175 cm/s in the upper 100 m, and decreases to 10-20 cm/s at 1200 m water depth (Hamon, 1970). Further south, in the region of the Subtropical Divergence (near latitude 30°S), the EAC turns to the east, passing to the north of the barrier formed by New Zealand (Kennett, 1982). Church and Boland (1983) demonstrated that between 18-20°S the continental margin was subject to an northward-flowing undercurrent (the Great Barrier Reef Undercurrent). Maxwell (1968) speculated that the undercurrent was possibly forced by strong southerly winds, particularly during the austral winter. The northward limits of the Great Barrier Reef Undercurrent remain speculative, as does its relationship to the New Guinea Coastal Undercurrent (Lindström *et al.*, 1987). Donguy and Henin (1975) noted the existence of an eastward surface flow between 15° and 20°S, at 170°, 163° and 158°E, this has been called the South Tropical Counter Current (STCC). Jarrige (1968) suggested that the STCC originated in the western part of the Coral Sea rather than north of New Guinea like the South Equatorial Counter Current (SECC). The mean transport of the

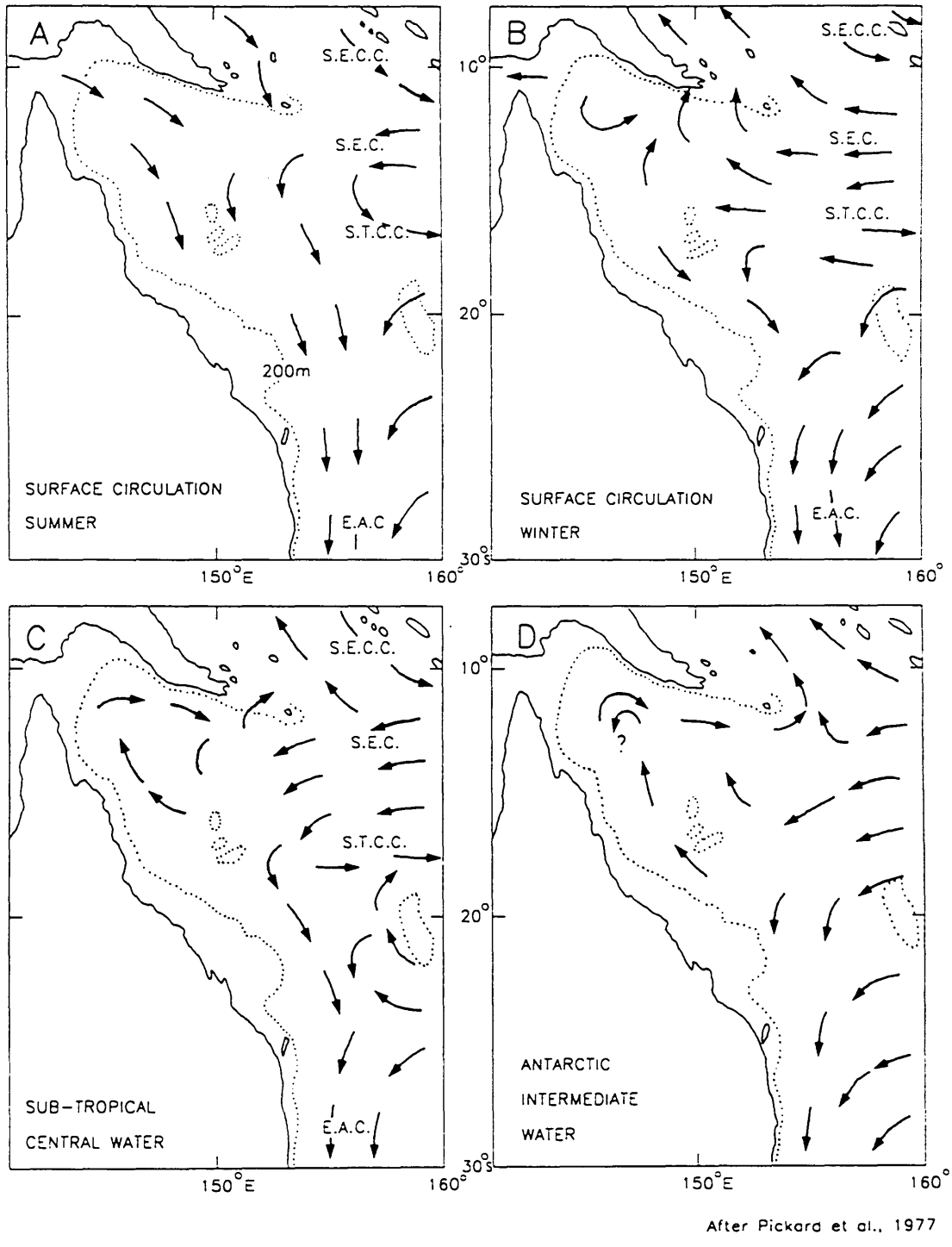

Figure 2.13 Surface and subsurface circulation patterns in austral summer and winter in the western Coral Sea (modified after Pickard et al., 1977). The South Equatorial Counter Current (SECC), the South Equatorial Current (SEC), the South Tropical Counter Current (STCC), and the East Australian Current (EAC) are illustrated in blocks A through to D.

STCC (as deduced from the velocity in the upper (0-100 m) layer is about 2 x 10^6 m^3/s (Donguy and Henin, 1975).

Antarctic Intermediate Water (AAIW), dominates the subsurface ocean circulation patterns in the Western Coral Sea (Wyrtki, 1961, 1962; Pickard *et al.*, 1977). AAIW forms within the Antarctic Polar Frontal Zone(APFZ), in the vicinity of the Antarctic Polar Front (APF) (Glasby, 1990). Its core lies near the sea surface north of the APFZ and deepens northward to more than 1000 m in mid-latitudes (Piola and Georgi, 1982). AAIW participates in the general eastward circulation associated with the Antarctic Circumpolar Current (ACC). From its source region, AAIW flows northward into the South Atlantic, the Indian, and the South Pacific oceans (Dietrich *et al.*, 1980). AAIW enters the Tasman Sea from the south (between Tasmania and New Zealand) and the east (between New Zealand and Fiji). The eastern branch originates from a strong northward flow of AAIW around Chatham Ridge east of New Zealand. AAIW watermass flows into the Townsville Trough from the southeast at a depth of 650 to 1100 m (AAIW core depth 700-1000 m) (Wyrtki, 1962).

The present day bottom and deep water circulation patterns are, as might be expected, strongly influenced by the distribution of passages between the various deep-sea basins (Edwards, 1975). Antarctic Bottom Water (AABW) is formed predominantly along the slope of the Antarctic Continent in the Weddell Sea (Dietrich *et al.*, 1980). After formation AABW circulates eastwards around the Antarctic continent, perhaps a number of times, before branching off and spreading northward into the deeper parts of the ocean basins.

In the East Australian Basin (the Thomson Basin), Deep Water spreads north at the 3000 m level. Part of this water overflows two sills of about 2850 m into the Coral Sea Basin forming its bottom water. Once in the Coral Sea Basin, the bottom water ascends slowly, becoming slightly heated and diluted by mixing with the water above it, and flows northward into the Solomon Basin (Wyrtki, 1960) (see Figure 2.14).

Pickard *et al.* (1977) suggest that due to the build up and sinking of water masses associated with the SEC along the Australian continental margin today, there is at present little significant upwelling. Present-day evidence of upwelling, however, along the margin of the Great Barrier Reef has been documented by Andrews and Gentien (1982), Andrews (1983) and Wolanski and Bennett (1983). Several mechanisms have been proposed to account for upwelling along the Queensland continental margin. Brandon (1973) considered the possibility of upwelling induced by the shearing of

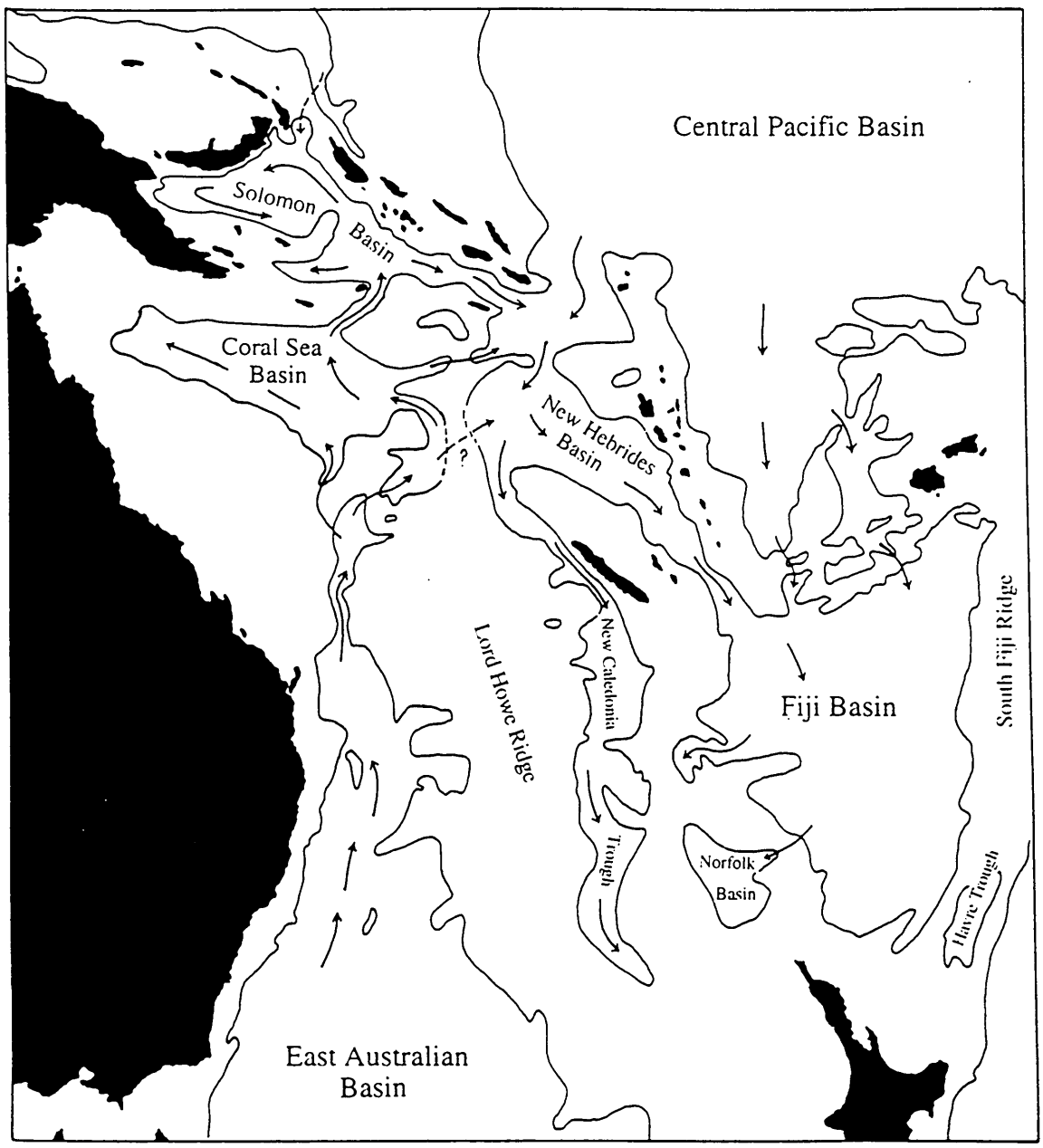

Figure 2.14 Map of the deep sea basins of the western South Pacific Ocean showing circulation patterns of bottom waters. The shape of the basins is indicated by the 3000 m line (after Wyrtki, 1960).

contrary currents, within and outside the Great Barrier Reef. Further, Brandon (1973) suggested that a southerly current adjacent to the outer Barrier, would be deflected away from the reefs by the coriolis effect, resulting in upwelling adjacent to the reefs. The probability of contact with living reefs he considered to be fairly good.

Currents within the Great Barrier Reef Province are a combination of wind and tide generated movements. Except in restricted channels the wind component dominates, generating currents to the north or northwest over most of the reef, with speeds of between 0.25 and 0.6 m/s (Hopley, 1982). The northward longshore drift developed over much of the GBR has significant implications for fluviatile discharge and the movement of terrigenous sediments across the shelf (Belperio and Searle, 1988; Flood and Orme, 1988). In comparison to other major reef provinces, tides across the GBR region are unusually high and range from 2.3 m (near its southern margin) to 10.4 m (between latitudes 21° and 22°S - Broad Sound). The mean tidal range throughout the rest of the province is about 2.9 m (Maxwell, 1968). The semi-diurnal tidal exchange involves up to 15 % of the total volume of water, approximately 30,000 km^3, contained within the Great Barrier Reef (Hopley, 1982). Water circulation is further complicated by small islands and reefs throughout the Great Barrier Reef province.

2.5 Climate and Weather

The Great Barrier Reef province lies almost entirely within the tropics, extending from latitude 24°07'S to latitude 9°15'S, a latitudinal spread of 14°52'. It forms a meridional belt between the Australian continental mass and the vast oceanic region of the South Pacific. As a consequence it is influenced by both regions, and incorporates several distinct climatic zones (Hopley, 1982). Antipodean seasons are the antithesis of those experienced in Europe and America.

2.5.1 Temperature

Temperature variations along the Queensland coastal belt is gradual and is controlled almost entirely by latitude. Seasonal variation in temperature in the tropical zone is extremely small. Air temperatures decrease over the ocean from north to south and in general are higher over the oceans than those over the coastal areas (Maxwell, 1968). Temperature values in the Western Coral Sea range from over 28°C in the north to 24° C in the south during the austral summer, and about 26°C in the north to 18°C in the south in the austral winter (Pickard *et al.*, 1977).

Although not as important in open waters, evaporation, as a result of the thermal regime, has important influences on salinity of the sea surface. Zones of restricted

circulation within lagoonal reefs salinities may show significant increases due to evaporation, but these are areally unimportant (Maxwell and Swinchatt, 1970). Average monthly evaporation totals range from 200 cm in the south to in excess of 250 cm in the northern reefal areas (Hopley, 1982).

2.5.2 Rainfall

The relief along the coast of Queensland exerts a strong influence on the incidence of rainfall. Isohyets, both seasonal and annual, largely parallel the coastline (see Figure 2.15), indicating the general importance of moisture from the east (Hopley, 1982). There are two dominant rain influences: the northern summer one which is dependent on the trades, monsoons and tropical cyclones, and the southern winter influence dependent on the troughs and fronts that develop over the continent in the south (Maxwell, 1968). The rainfall pattern in Queensland is characterised by its great variability from year to year. The variability is due largely to the generation of tropical cyclones and depressions which, although short lived, lead to extremely heavy rainfall. Such fall in reef areas have resulted in abruptly lowered surface salinities (particularly in shallow water lagoonal areas) that have proved fatal for reef organisms (Hedley, 1925).

Rainfall is not the sole cause of reduced salinity to the Great Barrier Reef lagoon. River discharge, introduced at specific points along the coastal areas (e.g., the Burdekin, Barron and Fitzroy rivers), is also an important albeit local factor. The actual effect of continental runoff on the salinity of the lagoonal waters will be a function of the rate of discharge in relation to the width and depth of the lagoon at the point of discharge (Maxwell, 1968). Wolanski and Jones (1981) found no evidence of freshwater runoff directly reaching the Great Barrier Reef, but suggested that small buoyant patches, detached from the river plumes, found further offshore might reach the Great Barrier Reef. Wrytki (1960) estimated the average annual river discharge of the Burdekin, Barron and Fitzroy rivers to be in the order of 15.9 km^3. Estimates of the coastal stream discharge average 3.6 km^3, so that the total land drainage of eastern Queensland contributes approximately 19.5 km^3 of water annually to the GBR Province. Wrytki (1960) concluded that the contribution of land water to the GBR Province is volumetrically insignificant, when compared to the estimated 900,000 km^3 of water moved annually by the EAC.

2.5.3 Winds

The main wind systems affecting the GBR province and the Coral Sea are the southeast trade winds for most of the year and the northwest monsoon winds during

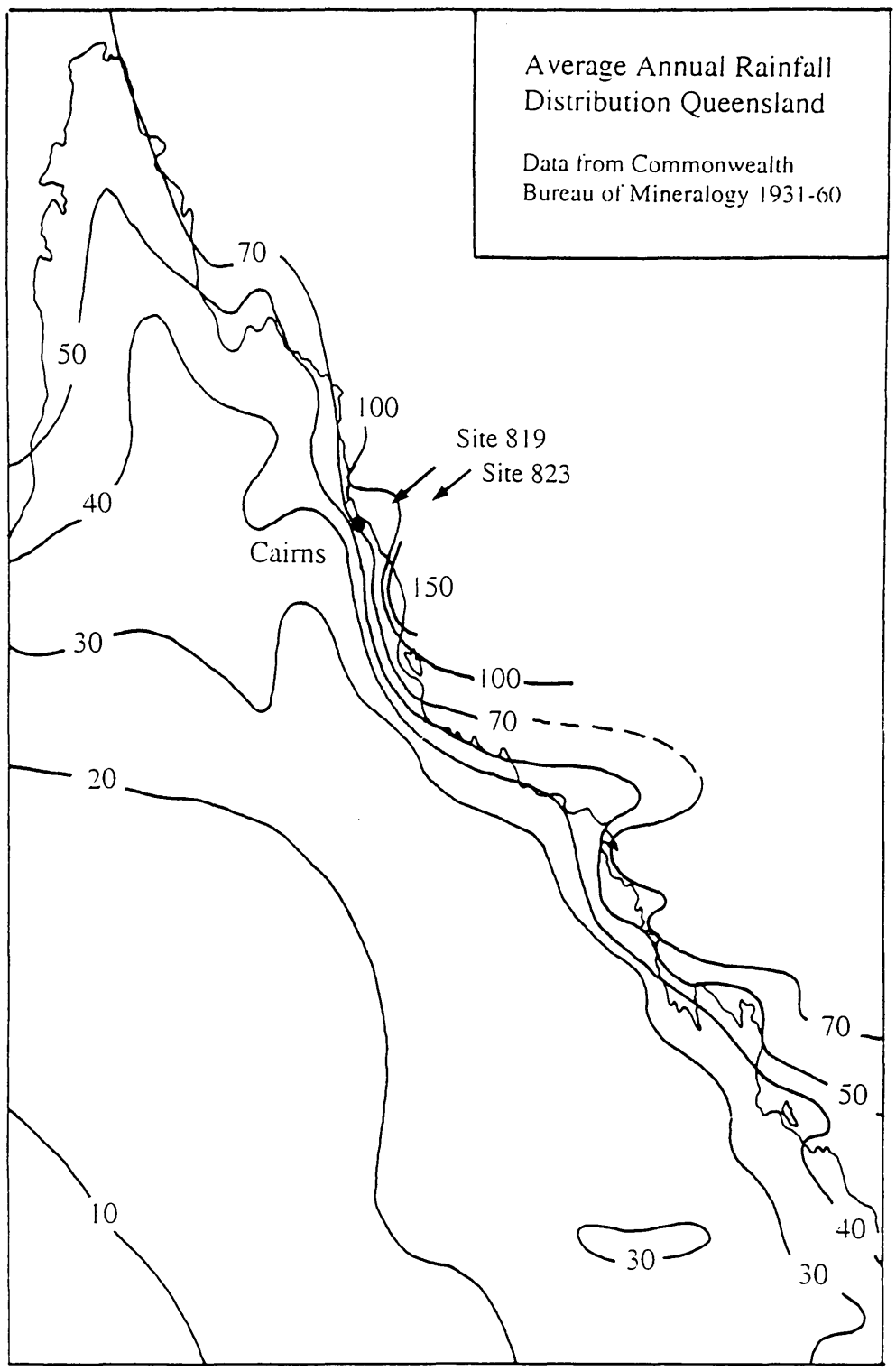

Figure 2.15 Annual average rainfall distribution in inches for Queensland (redrawn after Maxwell, 1968). Note the striking parallelism of the rainfall isohyets with the coast of northeast Australia.

the austral summer (Pickard *et al.*, 1977). The southeast trade winds consist essentially of warm stable, moist, air and the weather in the oceanic region is fair and clear. The monsoon wind is initially extremely cold and as it moves into the tropical regions, it encounters warm maritime air and a cold front develops with all its complications. In general, winter wind speeds (over the reef) tend to be higher than in summer, with wind speeds of 31-40 km/hr (Hopley, 1982). Away from the coast wind speeds in excess of 41 km/hr become less common toward the northern end of the reef.

On average two to three tropical cyclones per year affect the Queensland coast (Pickard *et al.*, 1977). These are extremely important events for reef morphology, for wind speeds may exceed 150 km/hr, passing through important process thresholds not normally experienced (Hopley, 1982). Although very unpredictable, tropical cyclones tend to originate in the Intertropical Convergence Zone between 8° and 18°S, in the Coral Sea, and either, move in a southerly direction, reaching the Tasman Sea as rain depressions, or cross the Queensland coast from an easterly to northeastlerly direction. A number of cyclones also develop in the Gulf of Carpentaria and either move southward as rain depressions or across Cape York, regenerating in the Coral Sea. Circulation in these southern hemisphere storms is clockwise, with maximum velocity wind coming from a southeasterly or northeasterly direction (i.e., coinciding with the predominant wind direction). The main oceanographic effects of cyclones are to cause a reduction in salinity, from the associated rainfall, and an increase in the mixed layer depth, presumably due to strong winds. In addition to heavy rainfall, very rough seas associated with cyclonic winds may cause considerable physical damage to carbonate platforms (Boss and Neumann, 1993; Scoffin, 1993). Important rises in sea-level (rarely greater than 3 m), as storm surges, may also accompany cyclones, although the influence of these is largely governed by storm intensity and off-shore morphology (Hopley, 1974). Cyclones tend to be most common during the austral summer/autumn (Pickard, 1977). The southern Great Barrier Reef is the most prone to cyclonic activity, both in terms of frequency and intensity.

Chapter 3 Chronostratigraphy using oxygen-isotope stratigraphy, bio- magnetostratigraphy and magnetic susceptibility

3.1 Introduction

In order to make meaningful interpretations of the Australian continental margin carbonate platform evolution, sedimentation, and paleoceanography, it is first necessary to produce an accurate chronostratigraphic framework, for the piston cores examined in this study. One of the most successful methods for producing accurate age models in high resolution deep-sea records involves the use of stable oxygen isotope stratigraphy. In this study the principles of oxygen isotope stratigraphy and bio- magnetostratigraphy were used to produce age models for the sedimentary successions recovered from Hole 819A and Site 823 (Holes 823A and 823B). A brief account of the fundamentals of stable oxygen isotope geochemistry is given below.

Oxygen can exist in several isotopic forms, but only two, ^{16}O and ^{18}O (about 99.8 % and 0.2 %, respectively, of the natural levels of the common oxygen isotopes), are of importance in oxygen isotope analysis. Ratios of oxygen isotopes are measured not in absolute terms but as relative deviations from the mean ratios present in a standard. The deviations are given in parts per thousand (δ ‰).

Equation 1.

$$\delta^{18}O \text{ sample } ‰ = 1000 \times (^{18}O/^{16}O \text{ sample} - ^{18}O/^{16}O \text{ standard})/(^{18}O/^{16}O \text{ standard}).$$

(Shackleton and Opdyke, 1973).

The δ ‰ value is thus a standardised indication of the ratio of $^{18}O/^{16}O$ present in the sample. For example a $\delta^{18}O$ value of 2.5 ‰ indicates the sample measured has 2.5 parts per thousand more ^{18}O atoms than the standard to which it is compared. For carbonate materials, the ratio of $^{18}O/^{16}O$ are measured with reference to the ratio present in the PDB standard (defined from the rostrum of a Cretaceous belemnite *Belemnitella americana*, B-1, from the Pee Dee Formation of South Carolina, by Epstein *et al.*, 1953). The ^{18}O content of the standard, PDB-1, is +0.20 per thousand, relative to standard mean ocean water (SMOW standard, distributed by the International Atomic Energy Agency, Vienna). This means that analysis can show whether a sample represents water colder or warmer than the standard as fractionation is dependent on temperature, provided that the isotopic difference is not a function of isotopic composition.

Oxygen isotope ratios on a global scale are principally affected by natural fractionation

processes in the hydrological cycle (Aharon and Chappell, 1983). During evaporation of sea water, from low latitude oceans, the lighter oxygen isotope (^{16}O) is preferentially removed, so that water vapour becomes relatively enriched in ^{16}O. Fractionation is particularly marked at higher latitudes and altitudes (Dansgaard, 1964) where cold air masses are increasingly less able to support the heavier ^{18}O isotope. Thus, moisture-bearing winds moving into higher latitudes become increasingly depleted in ^{18}O. Subsequent precipitation at high latitudes, causes the polar ice sheets to become enriched in the lighter oxygen isotope (^{16}O). During periods of expanded ice masses (glacial periods) large quantities of ^{16}O are trapped in the ice sheets leaving the oceans relatively enriched in ^{18}O, and thus more isotopically positive. Conversely, melting of the ice masses, during interglacial periods, liberates large quantities of ^{16}O back into the oceans. The magnitude of the glacio-eustatic/ice-volume effect from glacial-interglacial changes has been estimated to be about 1.2 ‰ (Shackleton and Opdyke, 1973). Fluctuations in the relative abundance of ^{18}O in seawater are recorded in the calcareous tests of those marine organisms which precipitate $CaCO_3$ in approximate isotopic equilibrium with the surrounding ocean waters (Urey, 1947; McCrea, 1950; Emiliani, 1954). Urey *et al.* (1951) coined the term 'vital effect' as a label for precipitation of carbonate by marine organisms out of equilibrium with ambient ocean waters. An extensive review of isotopic disequilibria in calcareous marine organisms (the 'vital effect') can be found in Wefer and Berger (1991). Detailed accounts of the theory and methods of stable isotope chronostratigraphy and geochemistry is given by Berger (1979); Hoefs (1987); and Williams *et al.* (1988).

The foundations of modern stable isotope palaeontology were laid down by Harold Urey, and his colleagues, who studied the thermodynamic properties of oxygen isotopes and their use as potential geothermometers (Urey, 1947; McCrea, 1950; Epstein *et al.*, 1951, 1953). However, it was Cesare Emiliani who first applied the isotopic paleotemperature technique to fossil foraminifera. In a series of classic papers, Emiliani came to recognise that the stable isotopic signal, in the tests of foraminifera, are due to two main features: growth temperature and isotopic composition of seawater (Emiliani 1955a, 1966, 1972). The problem of disentangling the two potential effects on the $\delta^{18}O$ record, can be partly resolved by analysing both benthic and planktonic foraminifera (Hoefs, 1987). Although there has been considerable controversy over the extent of the "temperature effect" as opposed to the "ice-volume effect", it is now generally accepted that the dominant signal (about two-thirds) is due to changes in seawater composition (Dansgaard and Tauber, 1969; Shackleton and Opdyke, 1973; Kennett 1982). Given the relatively short mixing time of the oceans (~10^3 years- Craig and Gordon, 1965), the potential exists for

synchronous $\delta^{18}O$ records throughout the global oceans. Thus, oxygen isotope signals can provide stratigraphic markers enabling correlation between cores which may be thousands of kilometres apart (Hoefs, 1987).

Since the pioneering work of Emiliani, numerous cores from the Atlantic, Caribbean and equatorial Pacific have been analysed. These have been accurately dated, and correlated to produce a well established oxygen isotope curve for the Pleistocene (Emiliani, 1972; Shackleton and Opdyke, 1973; Emiliani and Shackleton, 1974; Emiliani, 1978). Imbrie *et al.* (1984) took the isotope records from five high resolution cores from low latitudes, combined or statistically 'stacked' them, to produce a standard global isotope record known as the SPECMAP record. Scaled in standard deviation units (σ) this curve provides an approximate measure of global ice volume. This stacked record was accurately dated, using radiometric techniques, in association with biostratigraphic and magnetostatigraphic methods, and is often used as a reference curve when constructing age models for poorly dated cores. In this study the oxygen isotope records from Holes 819A and 823A were correlated primarily with the equatorial Pacific ODP Hole 677A (Shackleton and Hall, 1989; Raymo *et al.*, 1990). The reasons for comparing Holes 819A and 823A with ODP Hole 677A, are that (1) all sites lie in the tropical zone of the equatorial Pacific, (2) all sites contain oxygen isotope information that primarily reflects changes in ice volume (Shackleton and Opdyke, 1973), and (3) Hole 677A contains a complete and relatively detailed stratigraphy for the Pleistocene.

Specific magnetic susceptibility is a measure of the ease with which a sample can be magnetized, that is, the extent to which it is attracted to or repelled by a magnetic field (Tarling, 1983). It is primarily dependent on the concentration of magnetic minerals present in a sediment sample, such as magnetite and maghemite (γ-Fe_2O_3), although it is related to other parameters, such as magnetic mineral grain-size and shape (Thompson, 1979; Hounslow, 1990). Magnetic susceptibility is easily determined (measurements are both rapid and non-destructive) which has led in its widespread use, with other mineral/rock parameters, as an environmental indicator and as a means of characterizing sediment sources (Thompson *et al.*, 1975; Thompson and Oldfield, 1986). It has also been used in the detailed stratigraphic analysis and correlation of lacustrine sediments (Sandgren *et al.*, 1990; Snowball and Thompson, 1990), marine sequences (Bloemendal, 1989; Hounslow, 1990; Robinson, 1990), and terrestrial deposits (Beget *et al.*, 1990; Maher and Thompson, 1991). Magnetic susceptibility has also been used for ultra-high-resolution lithostratigraphic correlation between

subsidiary holes drilled at ODP sites (Ruddiman *et al.*, 1987; Prell *et al.*, 1989; Robinson, 1990).

In the present study, correlation between magnetic susceptibility and foraminferal oxygen isotope stratigraphies, and inter-hole correlation using magnetic susceptibility, has been used to refine the age models, for Holes 819A and 823A, during periods of low resolution in the oxygen isotope stratigraphies. Also, the magnetic susceptibility profiles of Hole 823A has been correlated to Hole 820 (Barton *et al.*, 1993a), to show that the stable oxygen isotope stratigraphy of this hole interpreted by Peerdeman *et al.* (1993), has been influenced by diagenesis, which renders the interpretation of assignment of stable oxygen isotope stages very difficult. Note that in this chapter magnetic susceptibility is introduced in the context of a correlative tool, a more detailed account of the sedimentological and paleoenvironmental significance of downcore magnetic susceptibility variations will be discussed in Chapters 4 and 7.

3.2 Oxygen Isotope Analysis

Sampling densities throughout Holes 819A and 823A were typically one sample every 20 and 25 cm, respectively. Splits of each sample were oven-dried at 60°C, weighed, and washed over a mesh N°100 (British Standard Sieves, Wire Mesh Series B.S.410: 1969) (63 μm aperture) stainless steel sieve. During the washing procedure the fine (<63 μm) fraction was retained and later oven-dried at 60°C. The coarse sediment fraction (>63 μm) was dry-sieved through mesh N°45 (355 μm) and mesh N°60 (250 μm) stainless steel sieves. Tests of the foraminiferal species *Globigerinoides ruber* (planktic) [d'Orbigny, 1839] and epifaunal *Cibicidoides spp.* (benthic) (see Plate 1) were hand-picked under a binocular microscope from the 250 μm to 355 μm sediment fraction. Care was taken in selecting only complete and undamaged foraminiferal tests. After selection, tests were soaked in methyl alcohol (analytical reagent) for several minutes and later cleaned in an ultrasonic bath to remove adherent contaminants. Following ultrasonic cleaning, excess methyl alcohol was drawn off with tissue paper and any residual alcohol allowed to evaporate. Foraminiferal sample weights were typically less than 0.1 mg and composed of between five to eight planktic specimens and between two to four benthic specimens.

Following cleaning, foraminiferal tests were reacted in orthophosphoric acid (specific gravity 1.9) at 90°C, and the resulting CO_2 gas analysed using a VG Isogas Precision Isotope Ratio Mass Spectrometer (PRISM) (under the supervision of A.E. Fallick and T. Donnelly), located at the Scottish Universities Research and Reactor Centre (SURRC), East Kilbride, Scotland. A brief account of the standard working

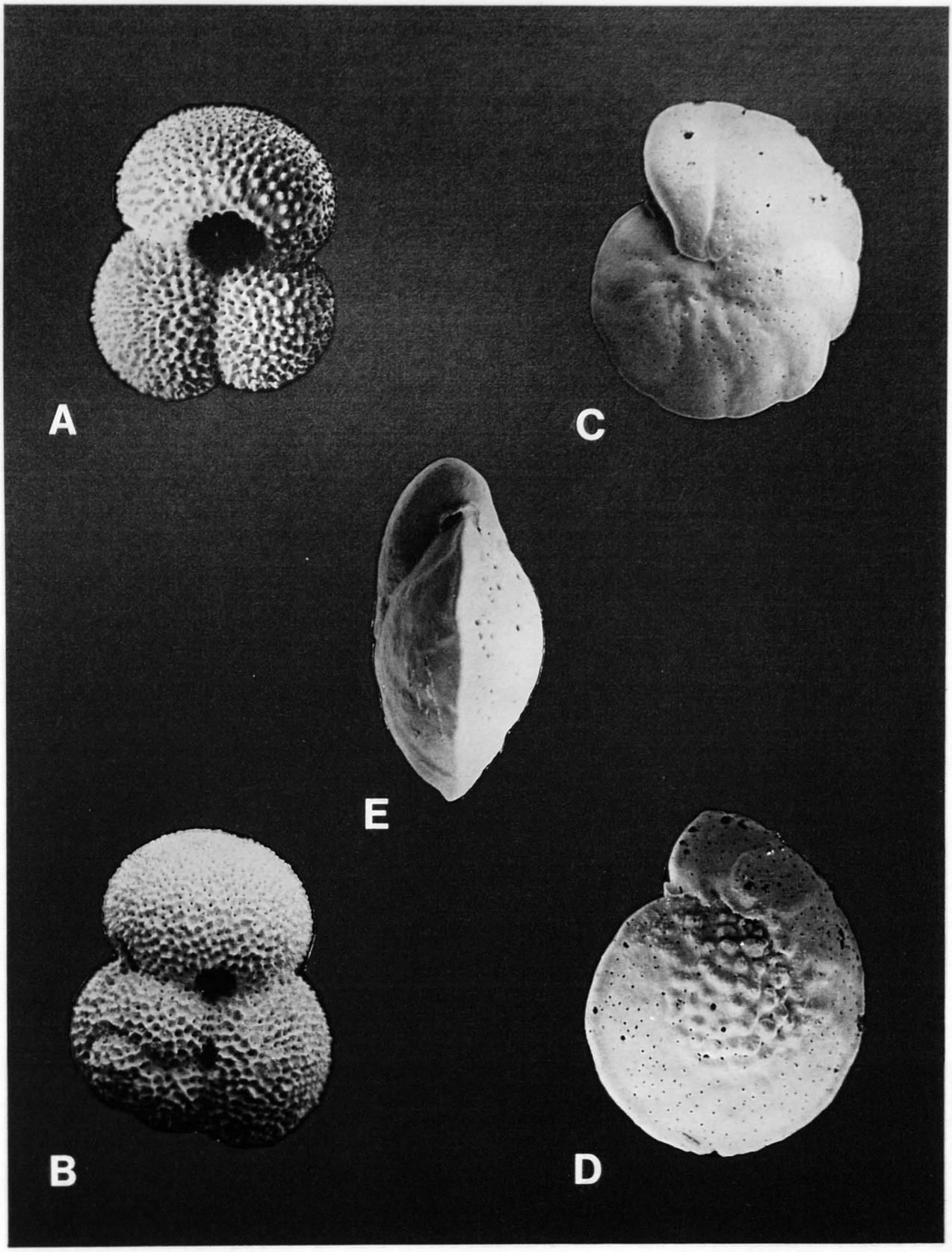

Plate 1. SEM microphotographs of foraminifers from Leg 133 samples used for oxygen isotope analysis. (A). An example of a well preserved *Globigerinoides ruber* (d'Orbigny, 1839), umbilical view x 110. (B) *G.ruber* spiral view, x 110. (C) Typical *Cibicidoides sp.* showing spiral view x 95. (D) *Cibicidoides sp.* showing umbilical view x 120. (E) Axial view of *Cibicidoides sp.*, x 75.

conditions of the PRISM is given in Appendix A. Planktic and benthic foraminiferal samples were analysed using an internal laboratory standard (marble reference SM1), and values thus obtained were converted to a PDB standard (Craig, 1957). Precision for oxygen isotope analysis was 0.085 ‰ (standard deviation for 100 analyses of an 'in-house' standard carbonate (SM1) conducted over several months) using SM1 sample weights of between 0.05 mg to 0.1 mg. Duplicate $\delta^{18}O$ measurements of separate aliquots of *G. ruber* and *Cibicidoides spp.* from Hole 819A and Hole 823A are given in Appendix A, Table A.2. Standard deviations for duplicate foraminiferal samples gave typical ranges from 0.015 to 0.275 for the planktic oxygen isotope ratios and 0.093 to 0.250 for the benthic $\delta^{18}O$ ratios (see below).

3.3 Description of the $\delta^{18}O$ records from Holes 819A and 823A

The $\delta^{18}O$ values of the foraminiferal species *Globigerinoides ruber* (planktic) and *Cibicidoides spp.* (benthic) for Holes 819A and 823A are listed in Appendix A, Tables A.3. and A.4., respectively. These data are presented in Figures 3.1 and 3.2, plotted against depth (mbsf- metres below sea floor). Core breaks are indicated by horizontal dotted lines, and are included to aid the identification of potential sample recovery hiatuses (J.W. Farrell, pers. comm., 1994). Hereafter, for the sake of brevity, both the planktic and benthic foraminiferal oxygen isotope records will be referred to as the planktic and benthic $\delta^{18}O$ record, respectively.

3.3.1 Hole 819A (upper-reef slope of the GBR)

Although lacking the classic "sawtooth" shape or profile familiar to many deep-sea $\delta^{18}O$ records (Shackleton and Opdyke, 1973; Emiliani, 1978), the high resolution isotopic records from Hole 819A display a reasonably well-defined cyclical pattern, characterized by episodes of isotopic maxima and minima (see Figure 3.1). This periodicity is particularly evident in the planktic $\delta^{18}O$ record, from Hole 819A.

The planktic $\delta^{18}O$ signal ranges from -2.68 ‰ at the top of the core to about +0.93‰ at about 40 mbsf. The planktic $\delta^{18}O$ record is characterized by two intervals, marked by a distinct change in the variability of the isotopic signal. Below about 45 mbsf, the isotope signal is dominated by broad cyclic variations in $\delta^{18}O$. Values throughout this part of the core range from about 0 ‰ to -1.75 ‰. The upper 45 m of the sequence from Hole 819A is characterized by high amplitude isotopic variations, coupled with a trend of enrichment in mean ^{18}O values with depth (or conversely a pattern of isotopic depletion with decreasing depth). The difference in mean planktic $\delta^{18}O$ values between the top of the core and 45 mbsf is approximately 2 ‰ (i.e., mean ^{18}O values

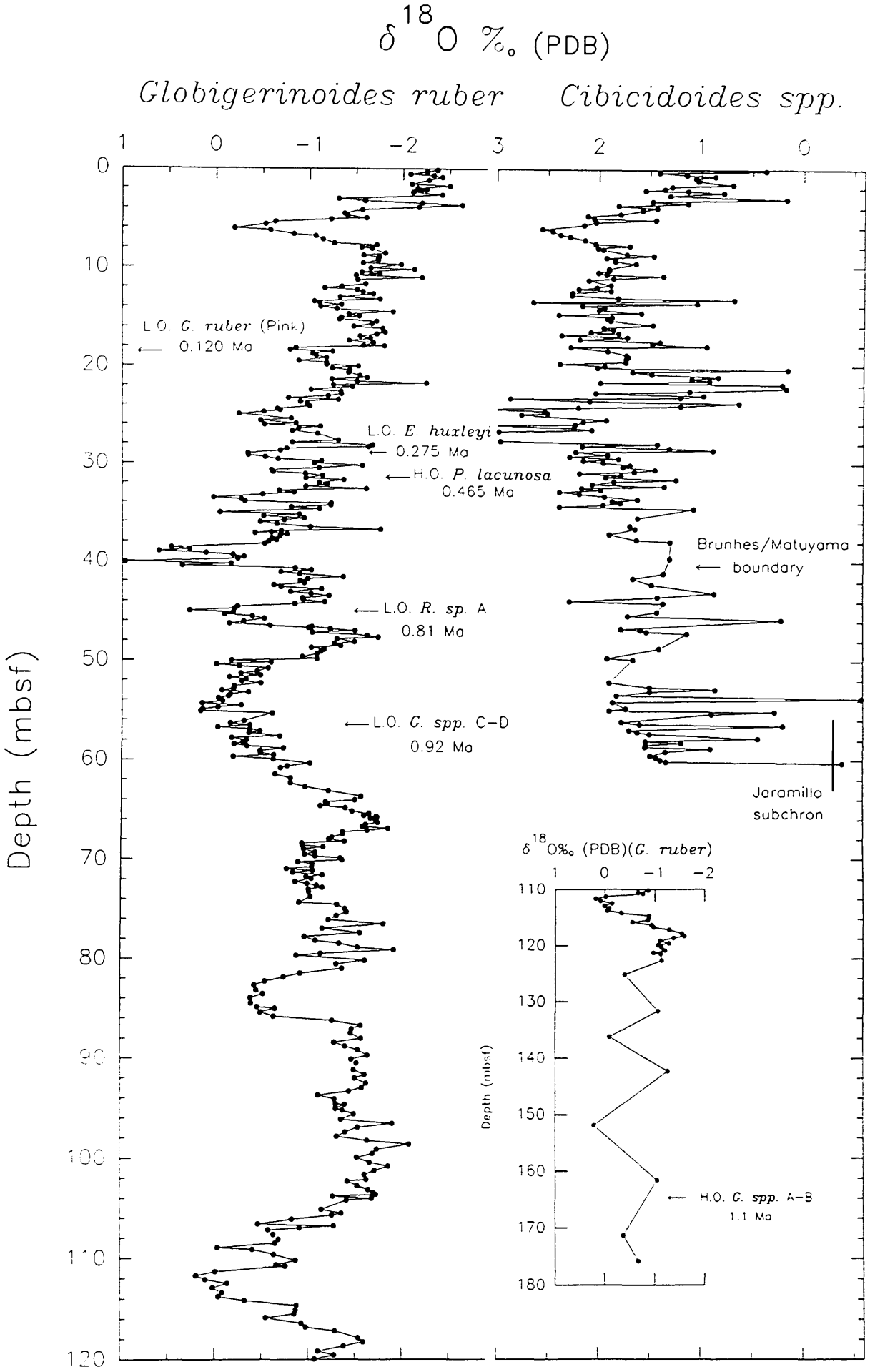

Figure 3.1. Planktic and benthic foraminiferal oxygen isotope records for Hole 819A. Magnetostratigraphic and biostratigraphic datums from Barton et al. (1993) and Wei and Gartner (1993), respectively. Horizontal dotted lines indicate positions of core–breaks.

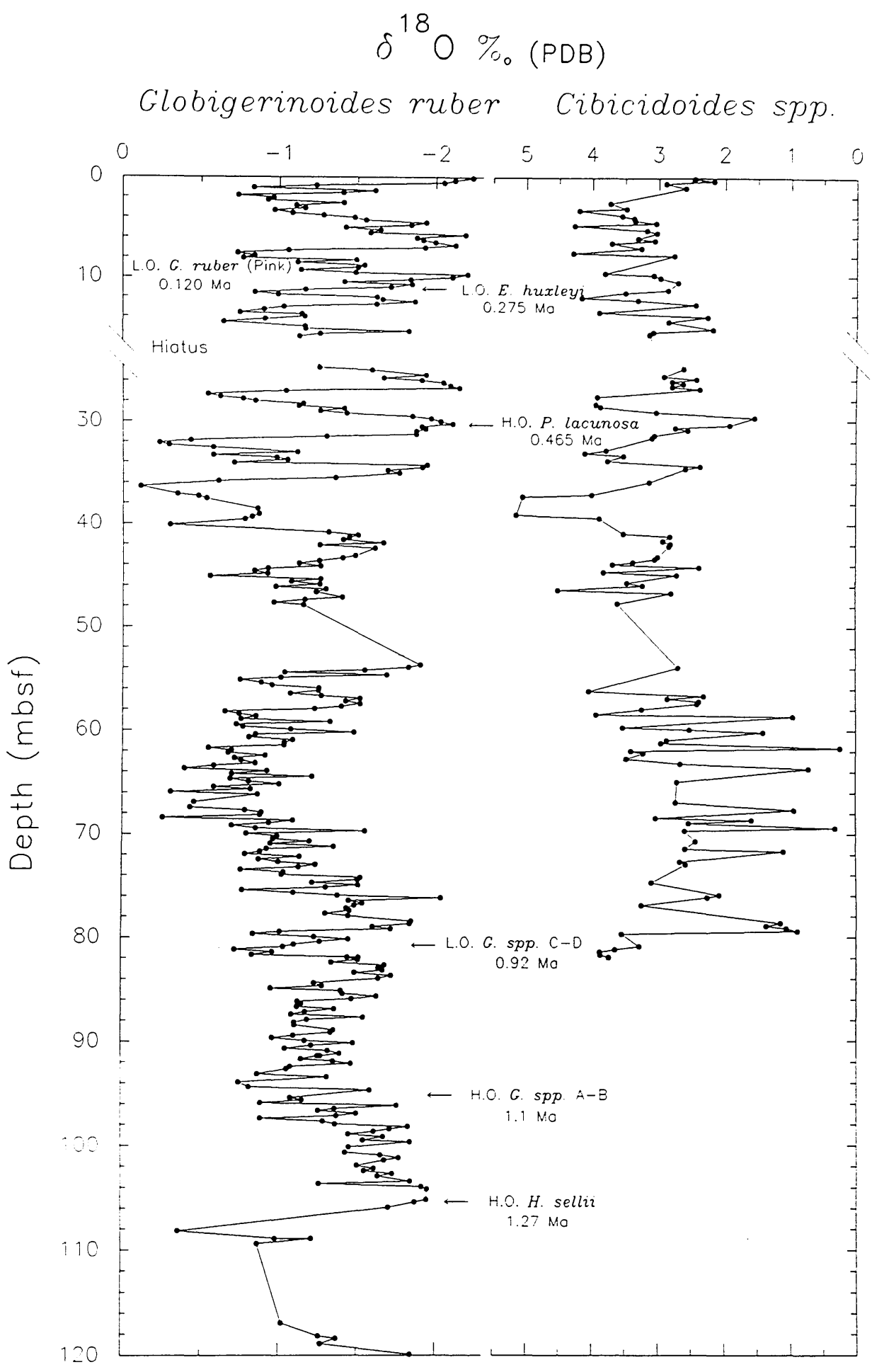

Figure 3.2. Planktic and benthic foraminiferal oxygen isotope records for Hole 823A. Magnetostratigraphic and biostratigraphic datums from Barton et al. (1993) and Wei and Gartner (1993), respectively. Horizontal dotted lines indicate positions of core–breaks. Note the presence of a sampling hiatus (slump) between 16.5 and 24.5 mbsf.

at the top of the core are about 2 ‰ lighter than those at 45 mbsf). This trend is not so clear in the benthic $\delta^{18}O$ record (see Figure 3.1).

In general, the benthic $\delta^{18}O$ record is characterised by high amplitude variations in isotopic values, particularly below 20 mbsf. This gives the record an anomalous or 'spikey' appearance (see discussion). Benthic oxygen isotope values typically range from about +3.24 ‰ to +1.0 ‰, although occasional samples gave values as isotopically light as -2.28 ‰. On average benthic $\delta^{18}O$ values are between 2.5 ‰ to 3.5 ‰ heavier (or enriched in ^{18}O) than planktic isotopic values. In the lower part of the sequence, mean benthic $\delta^{18}O$ values decrease steadily from about +2.5 ‰ at about 25 mbsf, to approximately +1.5 ‰ toward the bottom of the record (60 mbsf).

The [1]oxygen isotope difference between benthic and planktic foraminifera ($\Delta\delta^{18}O_{B\text{-}P}$) is shown in Figure 3.3. Comparison of the $\Delta\delta^{18}O_{B\text{-}P}$ record in the upper and lower parts of the sequence at Hole 819A indicates that below about 50 mbsf the mean isotopic difference is about 1.75 ‰. This compares with a mean value of approximately 3.0 ‰ in the upper part (<30 mbsf) of the sequence, at Hole 819A.

3.3.2 Hole 823A (Queensland Trough)

Unlike Hole 819A, the planktic $\delta^{18}O$ record from Hole 823A displays a well-developed 'sawtooth' profile, characterized by gradually increasing $\delta^{18}O$ values toward a maximum, followed by an abrupt and rapid decline in $\delta^{18}O$ values, with decreasing depth (see Figure 3.2). This pattern is particularly evident in the upper 45 m of the $\delta^{18}O$ record from Hole 823A. Superimposed upon the cyclicity is a trend of mean isotopic depletion (although not as pronounced as in the Hole 819A record) with decreasing depth. Below about 50 mbsf, the planktic $\delta^{18}O$ record is distinguished by low amplitude cyclical variations in isotopic value. In general, planktic $\delta^{18}O$ values in Hole 823A range from about -0.11 ‰ to -2.23 ‰, and are slightly lower (i.e., more depleted with respect to ^{18}O) than Hole 819A planktic values (0 ‰ to -1.75 ‰).

The comparatively low resolution benthic oxygen isotope curve for Hole 823A is very messy and, as such, very difficult to summarize. Tentative analysis of this record suggest a gradual decrease in $\delta^{18}O$ values from the Holocene down to about 30 mbsf. Below about 30 mbsf $\delta^{18}O$ values increase to a maximum at about 38 mbsf then gradually decline toward the bottom of the record (~70 mbsf). Benthic $\delta^{18}O$ values

---

[1]The $\delta^{18}O$ response of benthic and planktic foraminifera, and the oxygen isotope difference between benthic and planktic froraminifera ($\Delta\delta^{18}O_{B\text{-}P}$), can be used as a speculative tool to estimate palaeobathymetry in terms of both absolute and relative water depth (Williams *et al.*, 1988).

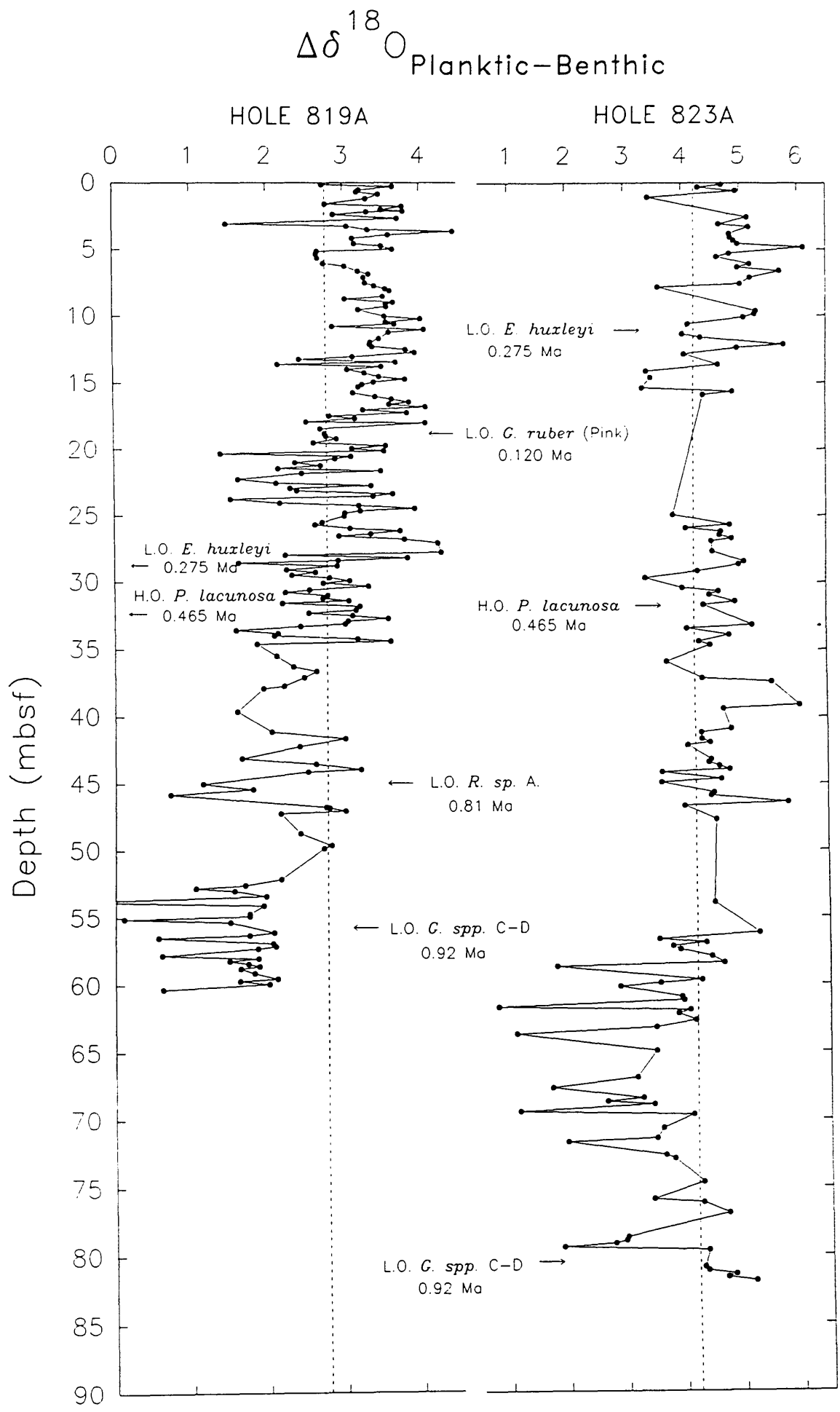

Figure 3.3. The oxygen isotope difference between planktic and benthic foraminifera from Holes 819A and 823A. The vertical dashed line, in each plot, represents the mean of each data set. Note the difference in the $\Delta\delta 180_{P-B}$ values in the upper and lower parts of each record. Dashed lines indicate downcore mean.

typically range between +2.5 ‰ and +4.0 ‰, although occasional (possibly reworked) samples gave anomalous values of between +0.37 ‰ and +0.5 ‰.

The oxygen isotope difference between Hole 823A benthic and planktic foraminifera ($\Delta\delta^{18}O_{B-P}$), plotted against depth, are illustrated in Figure 3.3. In general, $\Delta\delta^{18}O_{B-P}$ values are significantly higher in Hole 823A, than in the record from Hole 819A. Tentative analysis of the Hole 823A $\Delta\delta^{18}O_{B-P}$ record suggest that, compared to the lower part of the record (i.e., between about 57 to 80 mbsf), mean values are slightly higher in the upper part the record. Mean $\Delta\delta^{18}O_{B-P}$ values in the upper part of the Hole 823A record are about 4.2 ‰.

3.4 Measurement of Magnetic Susceptibility

Magnetic susceptibility measurements were taken on 10 cm^3 sample core plugs using a Bartington Instruments susceptibility meter, which is based on a modification of the principle used by metal detectors (Lancaster, 1966). Instrument calibration was achieved using a paramagnetic salt ($FeSO_4.7H_2O$) standard. Noise levels were typically below 0.1 $10^{-6}m^3kg^{-1}$. Mass specific susceptibility measurements were obtained for Hole 819A and Hole 823A samples by dividing the total magnetic susceptibility value by the sample weight and are expressed in mass specific units of 10^{-6} m^3 kg^{-1} (see Appendix A, Table A.5 and A.6).

3.4.1 Description of the magnetic susceptibility records

Figures 3.4 and 3.5 summarize the variations in mineral magnetic susceptibility and planktic oxygen isotope ratio with depth in Hole 819A and Hole 823A sediments, respectively. Note that magnetic susceptibility values are plotted using a logarithmic scale in order to suppress the dominance of high values and to enhance variations at low values. Plotting on a logarithmic scale enables better correlation between susceptibility and the oxygen isotope records, and between the magnetic susceptibility signatures from adjacent ODP Leg 133 drill holes (Barton *et al.*, 1993).

3.4.1.1 Hole 819A

Magnetic susceptibilities in Hole 819A are generally low throughout most of the sequence, with the majority of samples having susceptibilities of greater than 0.008 $10^{-6}m^3kg^{-1}$ (see Figure 3.4). Superimposed upon this low value background signal are three prominent peaks: Peak 1 (4.2-6.1 mbsf), Peak 2 (24.52-24.87 mbsf), and Peak 3 (21.3-21.7 mbsf). Peaks 1 and 2 have susceptibilities greater than 0.021 $10^{-6}m^3kg^{-1}$, and Peak 3 is slightly smaller, reaching 0.008 $10^{-6}m^3kg^{-1}$. Several smaller broader peaks occur in the sequence in Hole 819A (for example, at 10-15 mbsf and 65-78

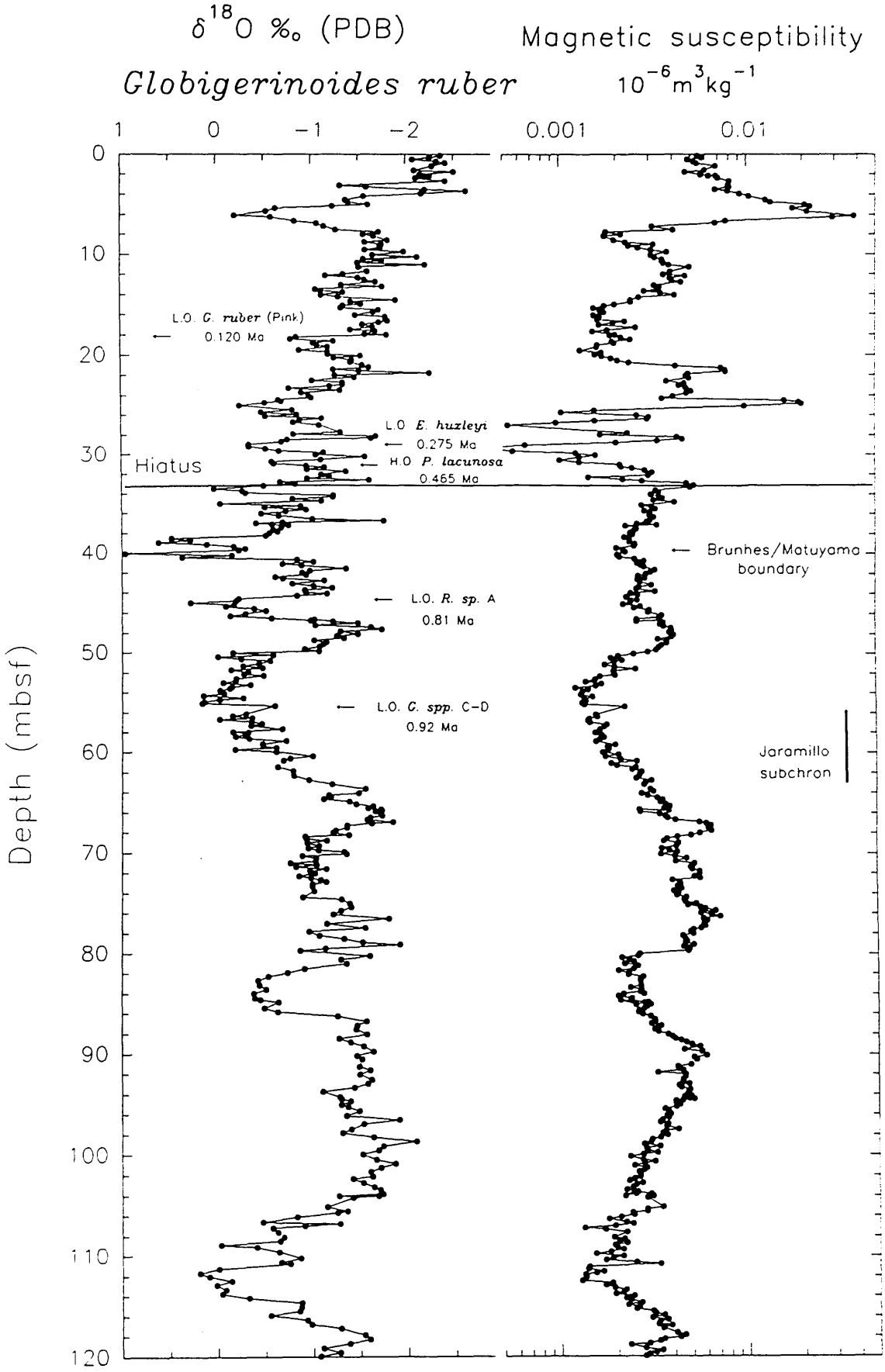

Figure 3.4. Magnetic susceptibility and planktic $\delta^{18}O$ values, plotted aginst depth, for Hole 819A sediments. Note that magnetic susceptibility values have been plotted on a logarithmic scale.

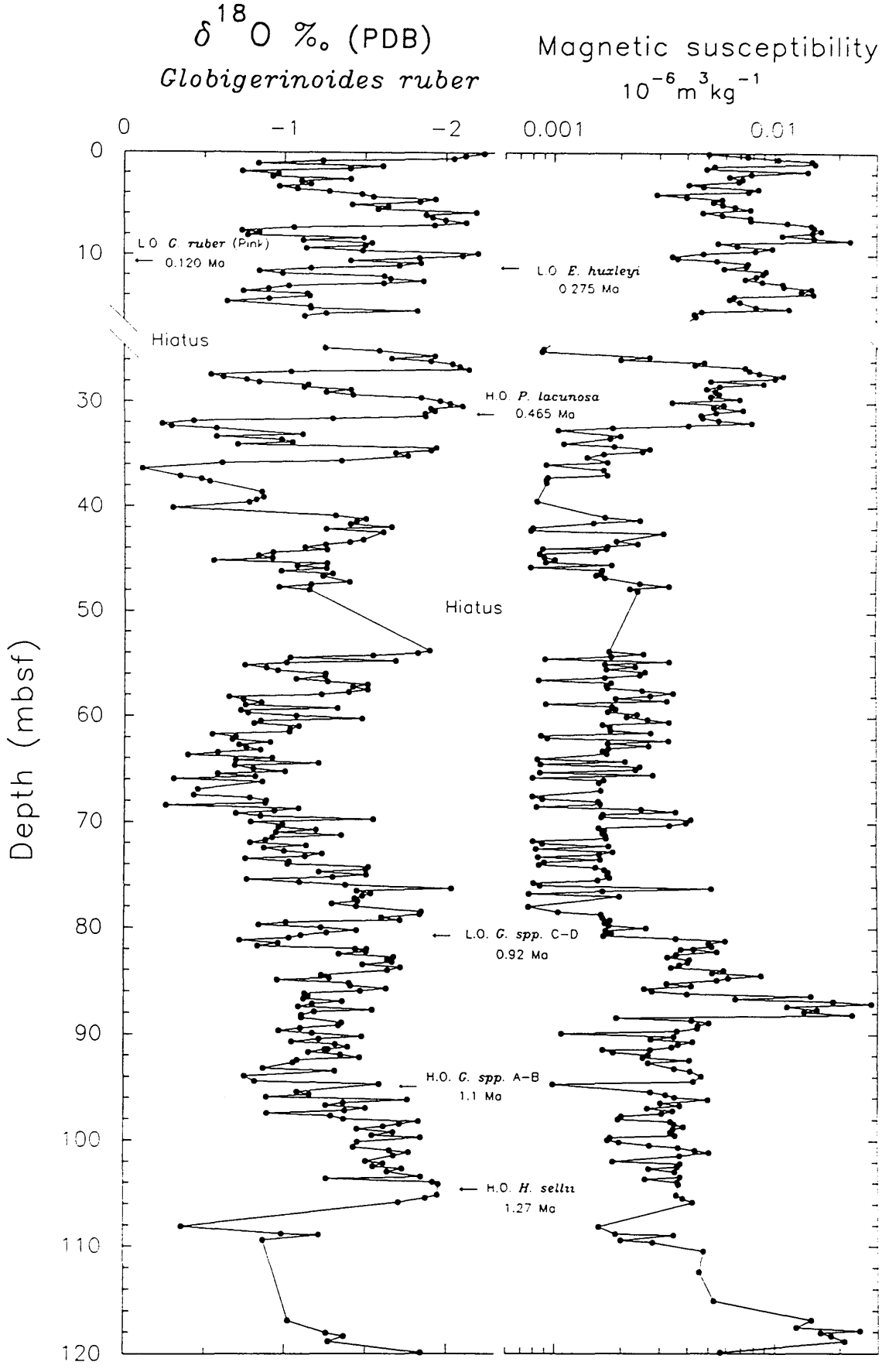

Figure 3.5 Magnetic susceptibility and planktic $\delta^{18}O$ values, plotted aginst depth, for Hole 823A sediments. Note that the magnetic susceptibility has been plotted on a logarithmic scale. Note the presence of a sampling hiatus (slump) between 16.5 and 24.5 mbsf.

Table 3.1 Oxygen isotope, biostratigraphic and magnetostratigraphic control for depth to age conversion.

Age (Ma)	Datum Levels	Depth (mbsf)	
Biostratigraphy		**Hole 819A**	**Hole 823A**
0.0125	Stage 1/ 2 boundary	4.0	-
0.024	Stage 2/ 3 boundary	6.7	-
0.059	Stage 3/ 4 boundary	18.2	-
0.071	Stage 4/ 5 boundary	19.7	3.975
~ 0.125	H.O. *Globigerinoides ruber* (pink) [1]	18.5	10.55
0.128	Stage 5/ 6 boundary	22.31	7.27
0.186	Stage 6/ 7 boundary	27.1	9.275
(0.204-0.220)	Hiatus 819A	(28.6/ 28.8)	-
0.245	Stage 7/ 8 boundary	-	13.025
0.275	L.O. *Emiliania huxleyi* [2]	29.4	12.2
(0.300-0.306)	Hiatus 823A	-	(16.15/ 24.9)
(0.310-0.530)	Hiatus 819A	(32.3/ 32.7)	-
0.339	Stage 9/ 10 boundary	-	27.15
0.362	Stage 10/ 11 boundary	-	28.025
0.423	Stage 11/ 12 boundary	-	31.65
(0.444-0.454)	Hiatus 823A	-	(32.65/ 33.15)
0.465	H.O. *Pseudoemiliania lacunosa* [2]	32.4	32.0
0.478	Stage 12/ 13 boundary	-	34.275
(0.512-0.530)	Hiatus 823A	-	(35.65/ 35.90)
0.565	Stage 14/ 15 boundary	33.9	-
(0.600-0.660) ?	Hiatus 823A	-	(47.9/ 53.65)
0.620	Stage 15/ 16 boundary	38.45	-
(0.659-0.721)	Hiatus 819A	(40.5/ 40.7)	-
0.790	Stage 21/ 22 boundary	44.45	-
0.810	L.O. *Reticulofenestra spp.* A [3]	45.0 ?	-
0.838	Stage 24/ 25 boundary	46.65	-
0.870	Stage 25/ 26 boundary	50.1	-
0.920	Stage 27/ 28 boundary	67.22	-
0.920	L.O. small *Gephyrocapsa spp.* C-D [2]	56.1	80.2
0.930	Stage 28/ 29 boundary	74.72	-
0.956	Stage 29/ 30 boundary	81.65	-
0.975	Stage 30/ 31 boundary	85.6	-
0.994	Stage 31/ 32 boundary	93.5	-
1.020	Stage 32/ 33 boundary	95.92	-
1.033	Stage 33/ 34 boundary	105.9	-
1.100	H.O. small *Gephyrocapsa spp.* A-B [2]	166.9	95.5
1.270	H.O. *Helicosphaera sellii* [2]	189.2	105.7
Magnetostratigraphy			
0.73	Brunhes-Matuyama Chron Boundary	40.8	-
0.91	Top of Jaramillo subchron	54.0 ?	-
0.97	Bottom of Jaramillo subchron	65.5 ?	-

Note: Ages for isotopic stages 1 through 17 are from SPECMAP (Imbrie et al., 1984); stages 18 through 29 are from Ruddiman et al. (1989); and stages 30 through to 36 are taken from Raymo et al. (1990). Foraminiferal and nannofossil biostratigraphy taken from [1] Thompson et al. (1979) and [2] Wei and Gartner, (1993), respectively. The L.O. of *Reticulofenestra spp.* A is taken from [3] Barton *et al.*, (1993). Magnetostratigraphic datums after Barton et al. (1993). ? denotes uncertainty. L.O. = Lowest occurrence, H.O. = Highest occurrence. Dashes indicate that the specified boundary is not identified

mbsf). In general, magnetic susceptibility values correlate positively with the planktic oxygen isotope record in the lower part (45-120 mbsf) of the sequence at Hole 819A. In the upper 45m of the record from Hole 819A the relationship between magnetic susceptibility and planktic $\delta^{18}O$ values is more complex, than the lower section, and the nature of the relationship between these two parameters will be discussed fully in Chapter 4.

3.4.1.2 Hole 823A

Downcore fluctuations in magnetic susceptibility and planktic $\delta^{18}O$ values in Hole 823A are illustrated in Figure 3.5. In general, Hole 823A susceptibility values are comparable in magnitude to those displayed by Hole 819A sediments. Susceptibility values typically range between 0.001 to 0.005 $10^{-6}m^3kg^{-1}$, with occasional maxima exceeding 0.010 $10^{-6}m^3kg^{-1}$, in Hole 823A. In total six major peaks, or clusters of related peaks, with susceptibility values greater than 0.010 $10^{-6}m^3kg^{-1}$ can be recognised in the sequence from Hole 823A. Four of these peaks are located in the upper 35 m of the sequence at Hole 823A (i.e., between 0.60-1.10 mbsf, 6.65-8.64 mbsf, 12.90-13.90 mbsf and 26.90-27.40 mbsf). The remaining significant susceptibility peaks occur in the lower part of the succession and are located between 86.39-88.4 mbsf and 116-118.9 mbsf. In common with the record from Hole 819A, the association between planktic $\delta^{18}O$ values and magnetic susceptibility in Hole 823A is very complex. However, unlike the Hole 819A record, the lower part of the sequence in Hole 823A lacks any clear relationship between magnetic susceptibility and $\delta^{18}O$ value. The significance of the departure from covariance, between susceptibility and $\delta^{18}O$, in the lower part of the record in Hole 823A, will be discussed in Chapter 4.

3.5 Depth Age Relationships

Age models for the sequences recovered from Holes 819A and 823A, are illustrated in Figures 3.6 and 3.7, respectively. The equatorial Pacific (Panama Basin) ODP Hole 677A benthic $\delta^{18}O$ record (Shackleton and Hall, 1989; Raymo *et al.*, 1990) and the SPECMAP stack (Imbrie *et al.*, 1984) are presented for reference. In addition, Figure 3.8 illustrates the oxygen isotope event taxonomy of Prell *et al.* (1986), and provides a useful means of peak description and numerical coding.

Oxygen isotope stage assignment has followed the numbering scheme first outlined by Emiliani (1955a), and later extended by Shackleton and Opdyke (1973), and Ruddiman *et al.* (1989). Even-numbered stages represent glacial intervals (enriched ^{18}O values), and odd-numbered stages represent interglacial periods (depleted ^{18}O values). The

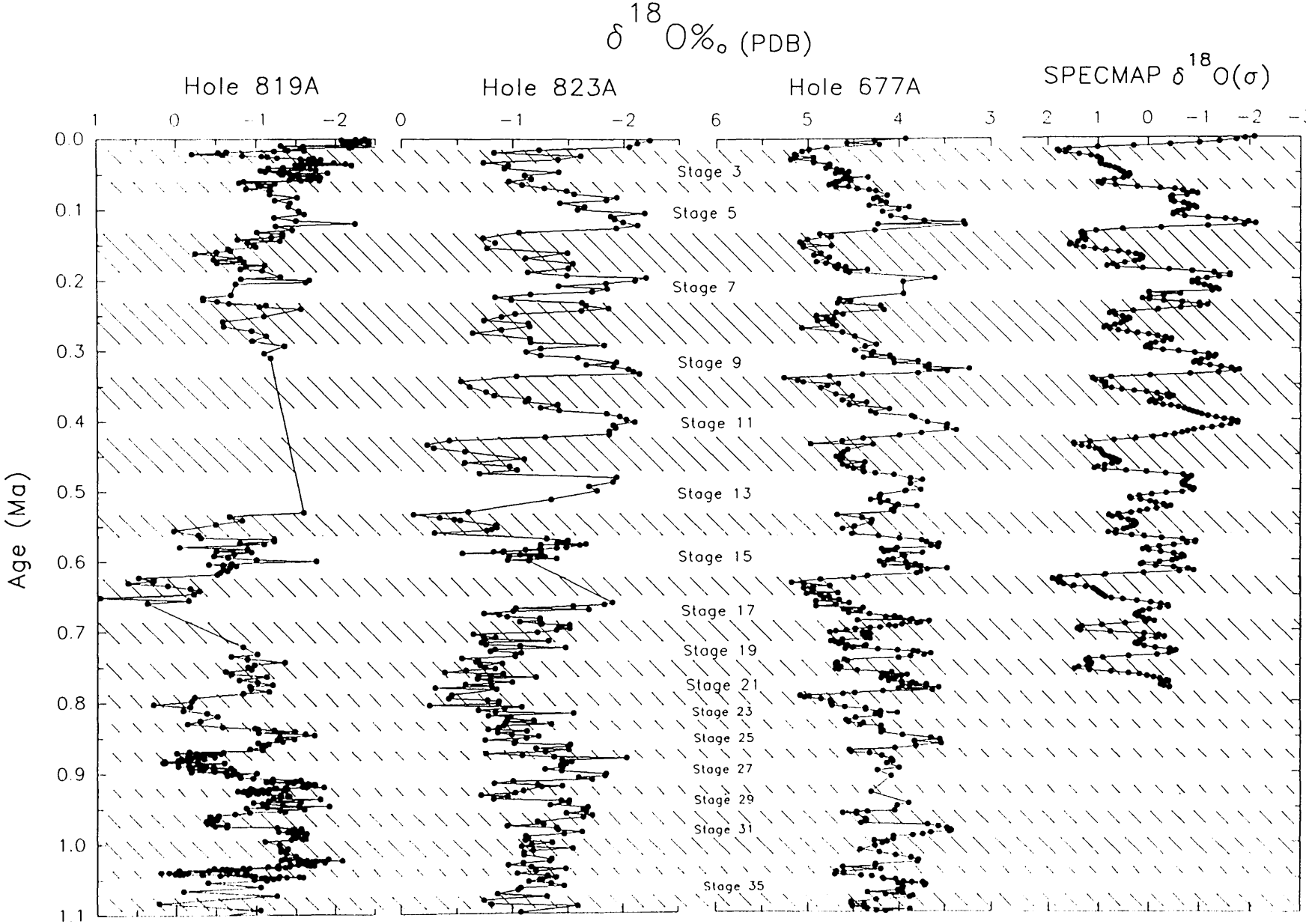

Figure 3.6. Comparison of the planktic foraminiferal oxygen isotope stratigraphies proposed for Holes 819A and 823A (this study), with the benthic foraminiferal $\delta^{18}O$ record at Hole 677A (Raymo et al., 1989) and the stacked record of Imbrie et al., 1984 (SPECMAP).

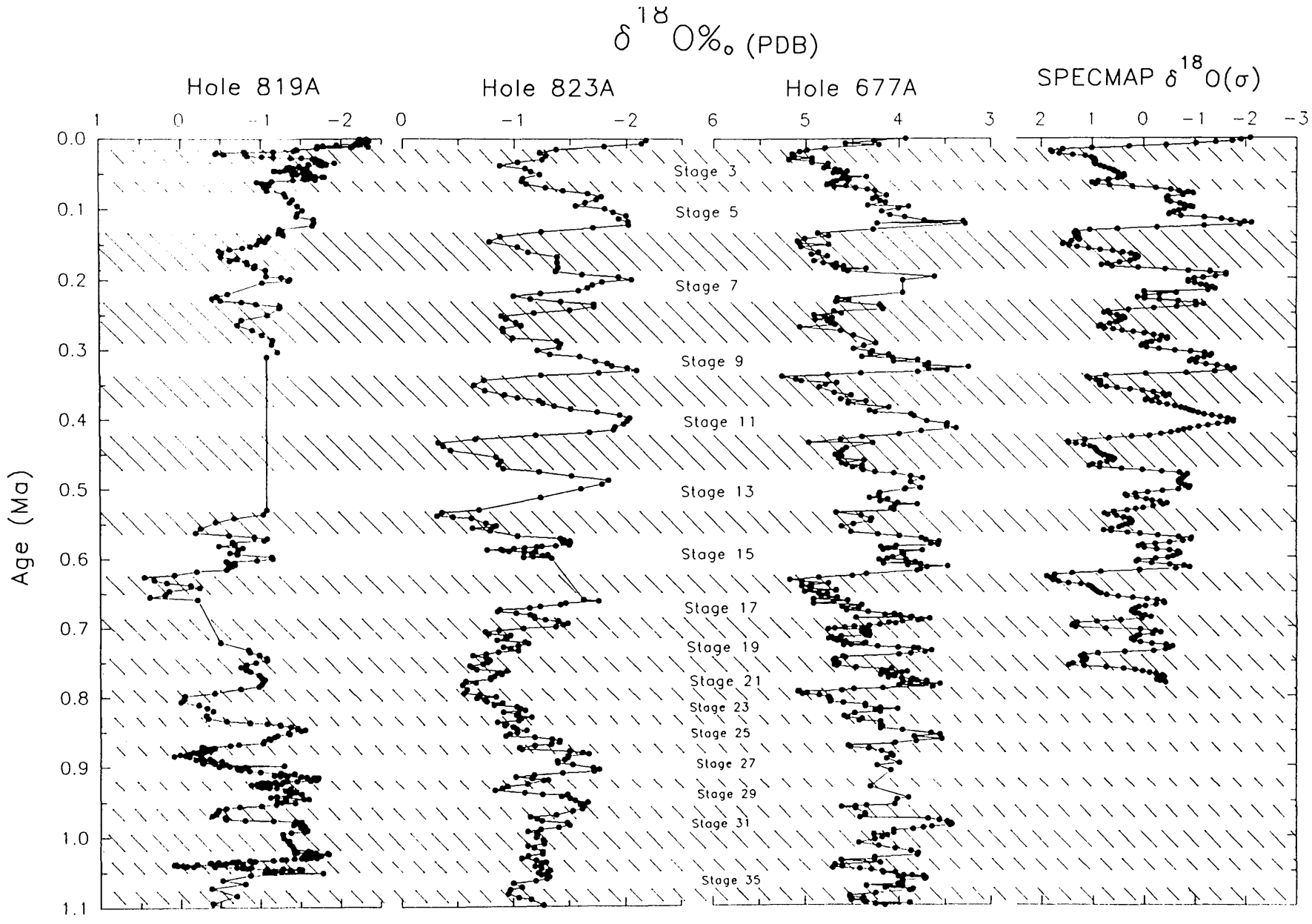

Figure 3.7. Comparison of the planktic foraminiferal oxygen isotope stratigraphies proposed for Holes 819A and 823A (this study), with the benthic foraminiferal $\delta^{18}O$ record at Hole 677A (Raymo et al., 1989) and the stacked record of Imbrie et al., 1984 (SPECMAP). The data for Holes 819A and 823A has been smoothed using a 3 point average.

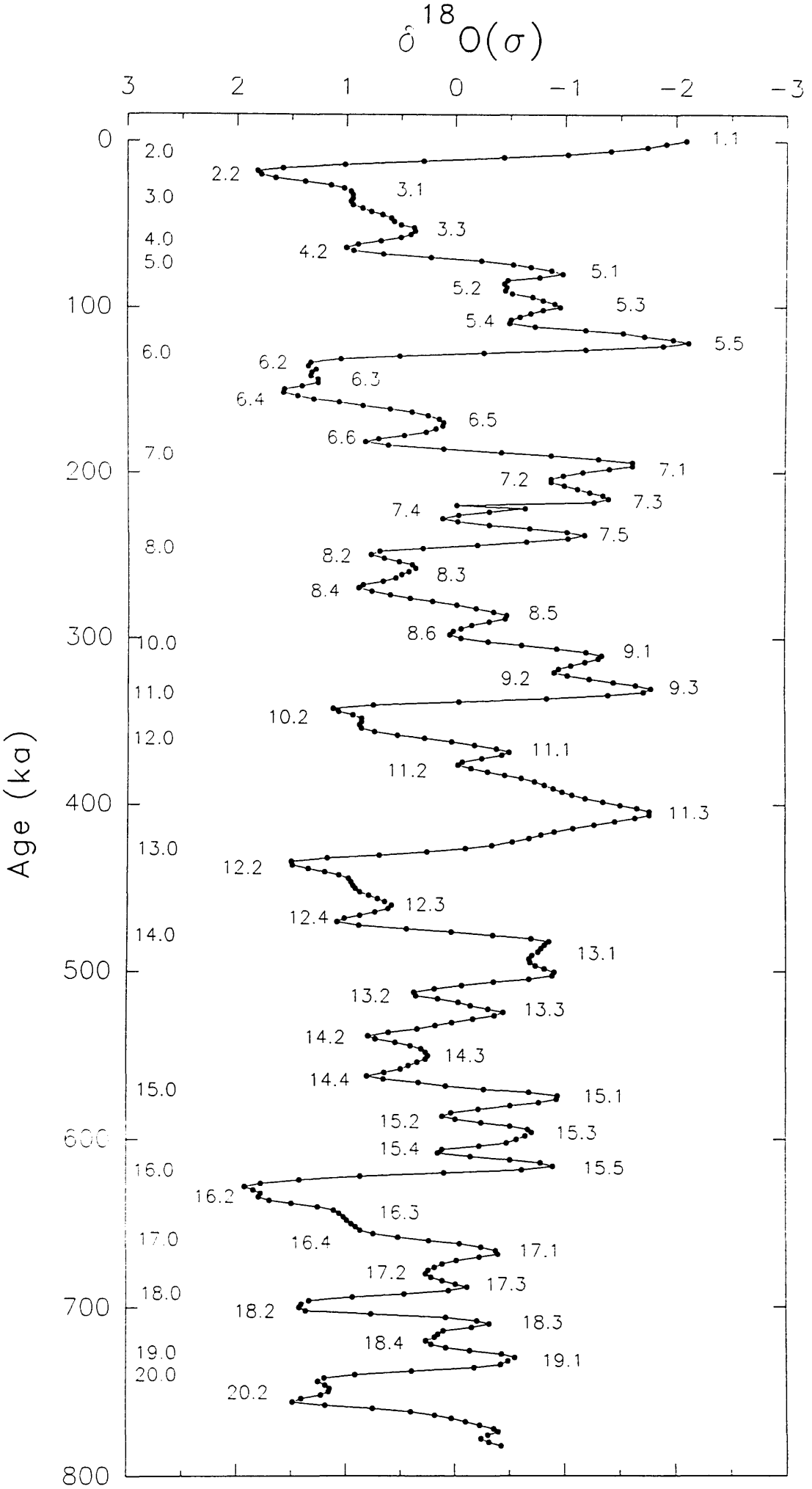

Figure 3.8. Oxygen isotope taxonomy (Prell et al., 1986) applied to the stacked isotopic records of Imbrie et al. (1984). Note that all events do not occur in SPECMAP.

depths (mbsf) and ages (ka) of the control points used for the age models in Holes 819A and 823A are given in Table 3.1. Ages of oxygen isotope stages (and stage boundaries) were taken from Imbrie *et al.* (1984); Ruddiman *et al.* (1989) and extrapolated from the stacked record of Raymo *et al.* (1990).

3.5.1 Hole 819A

An attempt was made to correlate the foraminiferal oxygen isotope stratigraphy of Hole 819A with the equatorial Pacific ODP Hole 677A $\delta^{18}O$ record (Shackleton and Hall, 1989; Raymo *et al.*, 1990) and the stacked record of Imbrie *et al.* (1984). However, isotopic stage recognition and assignment has in sections proven extremely difficult given the atypical profile of the foraminiferal $\delta^{18}O$ records, recovered from Hole 819A (i.e., the shape of the Hole 819A records is significantly different from the SPECMAP and Hole 677A curves). Therefore, the presented isotopic stage assignment is tentative and represents a refinement of the isotopic stratigraphy presented earlier by Alexander *et al.* (1993).

Both biostratigraphic datums and magnetostratigraphic data have been used to validate the foraminiferal oxygen isotope stratigraphy presented here. Mainly calcareous nannofossil data (Shipboard Scientific Party, 1991; Wei and Gartner, 1993) were used to constrain isotopic stage assignment. The lowest occurrence (L.O.) of *Emiliani huxleyi* was located at 29.4 mbsf and indicates the approximate position of late stage 8 (Thierstein *et al.*, 1977). The highest occurrence (H.O.) of *Pseudoemiliania lacunosa* was located at 32.4 mbsf in Hole 819A. This datum normally coincides with the middle of oxygen isotope stage 12 (Berggren *et al.*, 1980; Thierstein *et al.*, 1977). The L.O. of *Reticulofenestra sp.* A, was identified by Barton *et al.* (1993) at 45 mbsf, and has been used to fix the approximate position of the stage 22/23 boundary (Wei, 1993). The L.O. of *Gephyrocapsa spp.* C-D, at 56.1 mbsf, and the H.O. of *Gephyrocapsa spp.* A-B, at 166.9 mbsf , were used to place the approximate positions of stages 27/28 and stage 37 (Wei, 1993), respectively. The foraminiferal datum event, the H.O. of the pink-pigmented planktic foraminifera *Globigerinoides ruber* , was used to fix the position of the 6/5e oxygen isotope boundary (Thompson *et al.*, 1979) at about 18 mbsf.

The Brunhes/Matuyama (B/M) Chron boundary has been identified at about 41 mbsf (Barton *et al.*, 1993). Two alternatives have been suggested for the age of the B/M Chron boundary, either; 0.73 Ma (Mankinen and Dalrymple, 1979) or 0.79 Ma (Shackleton *et al.*, 1990; Berger *et al.*, 1994). In an attempt to remain consistent with other ODP Leg 133 workers (i.e., Barton *et al.*, 1993) the author has adopted the

dating scheme of Mankinen and Dalrymple (1979). The location of the B/M Chron boundary (0.73 Ma), and the Jaramillo subchron (0.91-0.97 Ma) are taken as defining the approximate positions of oxygen isotope stage 19, and stages 27 through to 31 (Ruddiman *et al.*, 1989), respectively. Two depth intervals have been proposed for the position of the Jaramillo subchron, in Hole 819A; namely the intervals between 115 and 120 mbsf and 54 to 60 mbsf (Barton *et al.*, 1993). The author has decided to adopt the later interpretation because this interval (54 to 60 mbsf) encompasses the biostratigraphic marker L.O. of *Gephyrocapsa spp.* C-D, at 56.1 mbsf (Wei and Gartner, 1993).

According to the biostratigraphy the Late Quaternary sequence from Hole 819A appears to be incomplete. A major hiatus is present at 32.5 mbsf as indicated by the condensed nature of the nannofossil stratigraphy, i.e., the H.O. of *P. lacunosa* (0.465 Ma) is almost at the same depth as the location of the L.O. of *E. huxleyi* (0.275 Ma) (Shipboard Scientific Party, 1991). Also, both the upper part and lower portion of the foraminiferal isotopic records are punctuated with minor hiatuses and unconformities.

In the upper part of the planktic and benthic $\delta^{18}O$ records, in Hole 819A, isotopic stages 1 through to 4 are clearly distinguishable (although the exact position of stage 4 is doubtful- see chapter 4), and correlate well with the equatorial Pacific Hole 677A isotopic record (Figures 3.1 and 3.6). However, below glacial stage 4, isotopic stage recognition and assignment becomes more difficult. For example, oxygen isotope stage 5 (substages 5a to 5e) in the planktic $\delta^{18}O$ record are very indistinct, and only when an averaged (3 point running mean) benthic $\delta^{18}O$ data curve is utilized (Figure 3.9), can a reasonable correlation be achieved with the Hole 677A isotopic record. The averaged benthic $\delta^{18}O$ record (and the magnetic susceptibility data of Barton *et al.*, 1993) suggest that the stage 4/5 boundary can be located at about 18 mbsf (see Figure 3.9). However, this implies that the recorded datum level of H.O. of the pink-pigmented planktic foraminifera *Globigerinoides ruber* (Thompson *et al.*, 1979), at about 18 mbsf, is unreliable and possibly indicates either reworking (Hutson, 1980), or sample contamination. Further problems with isotope stage assignment occur between the stage 6/7 boundary (27.1 mbsf) and the major hiatus at 32.5 mbsf. Several possible interpretations exist for this part of the $\delta^{18}O$ record, either: (1) a minor hiatus at about 28.7 mbsf has removed isotopic event 7.3, and the nannofossil datum L.O. of *Emiliani huxleyi* (at 29.4 mbsf) is reworked, or (2) the position of the L.O. of *Emiliani huxleyi* datum is correct and isotopic events 7.3 through to 8.3 are absent. Both interpretations are equally valid. However, comparison with the records from Hole 677A suggests that the former scenario (reworked *Emiliani huxleyi* datum) is more

likely than the second interpretation (see Figure 3.9). Clearly there is no easy solution to the problem of isotopic stage assignment above 32.5 mbsf.

Below 32.5 mbsf, the oxygen isotope stratigraphy in Hole 819A is thought to be more complete. Reasonably good correlation can be achieved between the planktic $\delta^{18}O$ record and the Hole 677A stratigraphy (see Figures 3.6 and 3.7). However, the benthic $\delta^{18}O$ record during this interval is very disappointing. A drastic reduction in the number of benthic foraminifera (particularly *Cibicidoides spp.*) in the lower part of the sequence has resulted in a poorly defined and unreliable $\delta^{18}O$ record. Interpretation of the benthic record is also hampered by the large amplitudinal fluctuations in isotopic value, thought to reflect the contemporaneous redeposition of isotopically depleted *Cibicidoides spp.* specimens from higher up the continental slope/shelf. Redeposition of benthic specimens would also account for the large variations in isotopic value mentioned in section 3.3.2. In the present interpretation of the isotopic records from Hole 819A, stages 17 and 18 are absent, and are believed to have been removed during stage 16, a time of recognised global sea-level lowstand (Shackleton and Opdyke, 1973). Alternatively, it could be argued that, in point of fact, isotopic stages 14 to 16 are absent and that stages 17 through to 35 (as far as can be determined) are present. However, this interpretation would present two problems; (1) explaining why stage 18 is so isotopically enriched in ^{18}O with respect to other glacial values, and (2) why the sedimentation rate (SR) over doubled during this interval, from about 6 cm/ka (stages 19-25) to about 14 cm/ka (stages 17-19)? Perhaps the effects of preferential dissolution of ^{16}O rich foraminifera, resulting in heavier $\delta^{18}O$ values (Wu *et al.*, 1990) might explain the unusual stage 18 values?, although we still have to explain the increase in SRs. In conclusion, if we assume a linear sedimentation rate and the integrity of the Hole 677A and SPECMAP isotopic profiles, then our arguments point in favour of the former interpretation, with the presence of a clear stage 16 (see Figures 3.6 and 3.7).

3.5.2 Hole 823A

In common with Hole 819A, the $\delta^{18}O$ record of Hole 823A was primarily correlated with the equatorial Pacific record of Hole 677A (Figures 3.6 and 3.7). Biostratigraphic and magnetostratigraphic age control, for the sequence recovered from Hole 823A, was taken from Wei and Gartner (1993) and Barton *et al.* (1993), respectively, and are summarised in Table 3.1.

The following biostratigraphical datums were used to constrain the $\delta^{18}O$ stratigraphy in Hole 823A: the L.O. of *Emiliani huxleyi* and the H.O. of *Pseudoemiliania*

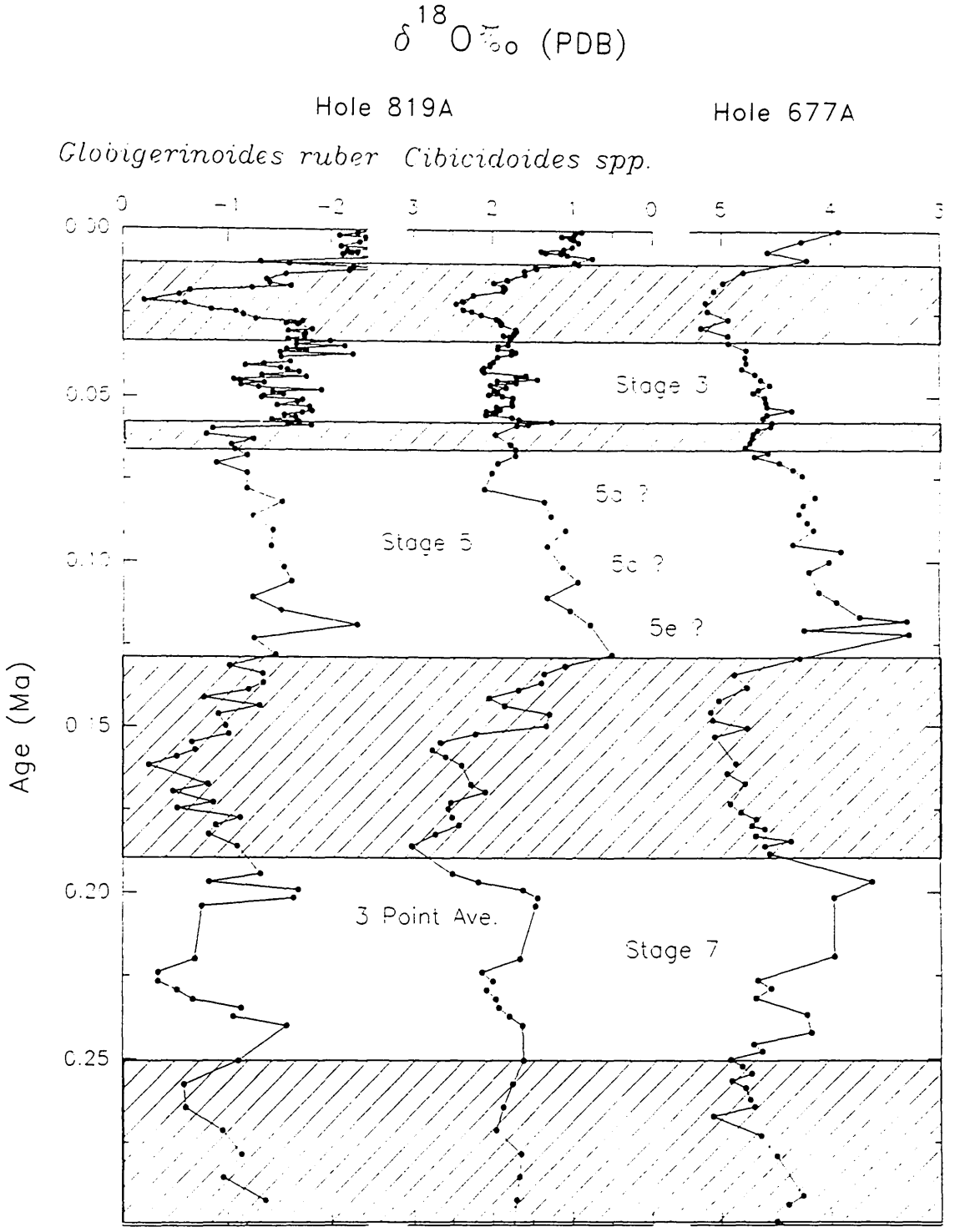

Figure 3.9. Comparison between the planktic foraminiferal oxygen isotope record at Hole 819A and the benthic foraminiferal records from Holes 677A and 819A. A 3 point running average has been used to smooth the benthic $\delta^{18}O$ data presented for Hole 819A. Note the absence of a clear stage 5 (substages a–e) in the planktic record from Hole 819A.

lacunosa were located at 12.2 mbsf and 32.0 mbsf, respectively; the L.O. of *Gephyrocapsa spp.* C-D was identified at 80.2 mbsf, and the H.O. of *Gephyrocapsa . spp.* A-B was located at 95.5 mbsf. The H.O. of *Helicosphaera sellii* was located at 105.7 mbsf, and is used to define the approximate position of the stage 44/45 boundary (Ruddiman *et al.*, 1989). The H.O. of the planktic foraminifera *Globigerinoides ruber* (pink variety) was located at 10.55 mbsf (Watts *et al.*, 1993).

Relative to Hole 819A, oxygen isotope stage recognition and assignment in the upper 50 m of the sequence recovered from Hole 823A, was appreciably clearer. Stable oxygen isotope stages 1 through to mid stage 15 (substage 15.3), at about 48 mbsf, were clearly identifiable in the planktic $\delta^{18}O$ record recovered from Hole 823A (see Figures 3.6 and 3.7). Thus, excellent correlation was achieved with the isotopic record from Hole 677A and the SPECMAP stack. Several minor hiatuses of correlative significance are thought to be present in the upper part of the record at Hole 823A. These small breaks are thought to have removed isotopic event 13.3 and possibly part of isotopic event 12.3 (0.445 Ma and 0.51 Ma, respectively) (see Figure 3.8). Surprisingly, the large sampling hiatus between 16.15 mbsf and 24.90 mbsf, identified by the Shipboard Scientific Party (1991) as a possible slump, was found to have little effect on the integrity of the isotopic record (see Figures 3.2 and 3.6). Examination of the planktic $\delta^{18}O$ record suggests that stages 8 and 9 are complete in detail (i.e., substages 8.2 through to 9.3 can be clearly identified). This suggests that the upper slump possibly occurred prior to isotopic events 8.5, and served to artificially thickened the stratigraphic sequence, without significant reworking or loss of any part of the record.

The effects of a second sampling hiatus (and slump- Shipboard Scientific Party, 1991), between 47.9 mbsf and 53.65 mbsf, on the integrity of oxygen isotope record have been more difficult to assess. The lack of any reliable magnetostratigraphic control (in particular the absence of a definitive B/M Chron boundary- Barton *et al.*, 1993) has severely hampered the age determination of the sequence between the H.O. of *Pseudoemiliani lacunosa* and the L.O. of *Gephyrocapsa spp.* C-D (0.465 to 0.92 Ma, respectively) in Hole 823A. In the final age model, the lower limit of the sampling hiatus (and slump) has been placed tentatively at 0.66 Ma. This position implies that oxygen isotope substage 15.4 (Prell *et al.*, 1986) through to glacial stage 16 are missing. However, given the uncertainty associated with the age of the lower boundary, the exact size of the hiatus is open to speculation. Analysis of the sedimentation rates (SRs) in the lower part of the sequence, provide little help in determining the extent of the hiatus. Sedimentation rates between 1.27 to 1.1 Ma and

1.1 to 0.92 Ma, are approximately 6 cm/ka and 8.5 cm/ka, respectively, (based on the nannofossil stratigraphy provided by Wei and Gartner, 1993). Applying these sediment accumulation rates upcore from the L.O. *Gephyrocapsa spp.* C-D at 80.2 mbsf (0.92 Ma), ages of about 0.478 Ma and 0.608 Ma, respectively, are obtained for the lower boundary of the sampling hiatus located at 53.65 mbsf. An age of 0.478 Ma, for the lower limit of the hiatus, conflicts with the present position of isotopic stage 13 to mid stage 15, and would imply a greatly increased SR between the lower boundary and the biostratigraphic datum the H.O. of *Pseudoemiliania lacunosa*, at 32.0 mbsf. The second alternative, an age of 0.608 Ma for the lower boundary of the hiatus, would suggest that only a small part of the isotopic record is absent, and that stage 16 was abnormally depleted with respect to ^{18}O? In the authors opinion neither of the two alternatives is particularly appealing (or likely). As mentioned earlier, in the final age model the lower boundary of the hiatus has been placed at 0.66 Ma, and SRs between this tie-point and the 0.92 Ma datum are only slightly higher (10.21 cm/ka) than rates lower down the sequence. This slightly elevated figure may, in part, be a function of the large slump occurring between 60 and 80 mbsf, in Hole 823A (Watts *et al.*, 1993).

Below 53.65 mbsf isotopic stage recognition and assignment has proved extremely difficult. The high incidence of gravity-flow deposits, coupled with the presence of numerous minor hiatuses, and the absence of reliable magnetostratigraphic datums (Barton *et al.*, 1993) have made correlation with Holes 819A and 677A (and SPECMAP) very difficult. Furthermore, because several of the biohorizons occur within gravity deposits, their ages may be inaccurate (Watts *et al.*, 1993). Attempts using visual correlation techniques (pattern matching) between the isotopic records from Holes 823A and 819A, and the equatorial Pacific Hole 677A, have largely proved disappointing. For while a reasonable match can be achieved between the $\delta^{18}O$ records, in the lower part of Holes 819A and 823A (see Figures 3.10 and 3.11), the results are at serious odds with the biostratigraphy outlined by Wei and Gartner (1993). Thus, these alternative age models, although superficially convincing, must be rejected. Therefore, in the lower part of the sequence in Hole 823A a speculative isotopic interpretation is presented based on depth/age relationships calculated assuming constant sedimentation rates between fixed biostratigraphic datums (see Table 3.1). In Chapter 7 (Concluding remarks and considerations), however, an improved age model for the lower part of the record will be presented based on strontium/calcium ratios. From the geochemistry of Hole 823A periplatform sediments it appears that the stable isotope stratigraphy is seriously affected by diagenesis.

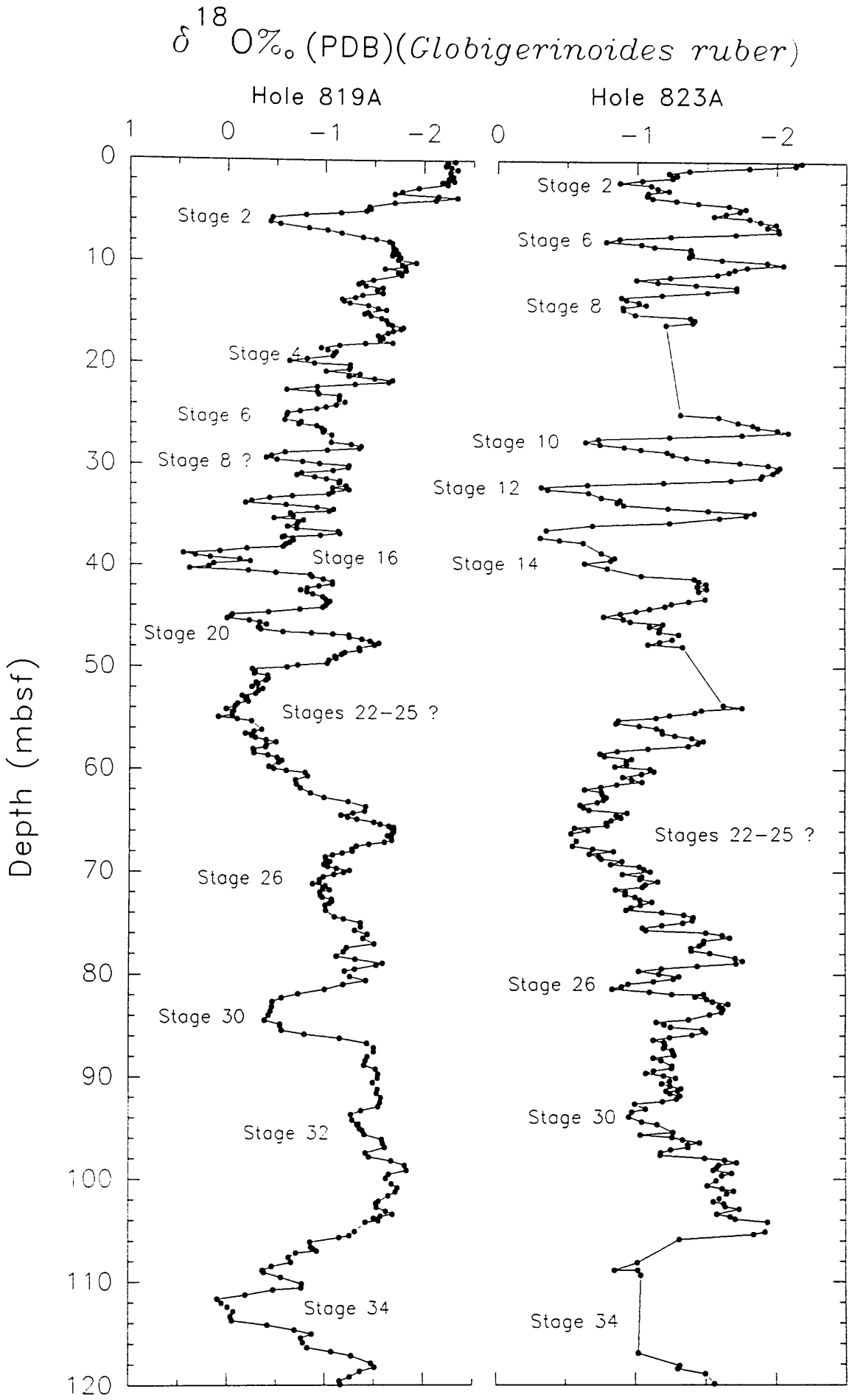

Figure 3.10. Alternative interpretations of the isotopic records from Holes 819A and 823A, based on a tentative visual correlation with the equatorial Pacific Hole 677A isotopic record (Raymo et al., 1989). A 3 point running average has been applied to both data sets.

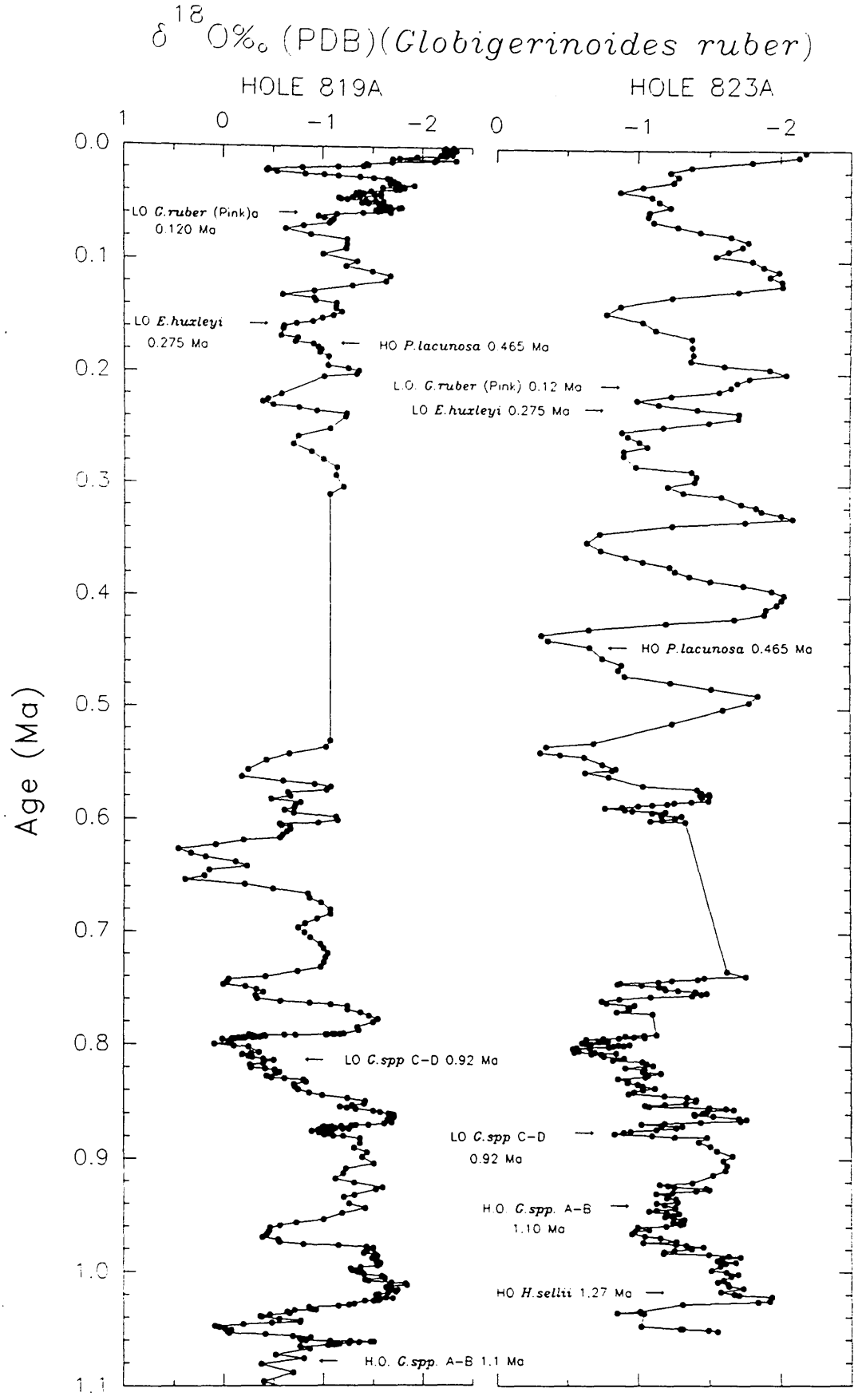

Figure 3.11. Alternative age models, based on visual correlation with the isotopic record of Raymo et al. (1989), for Holes 819A and 823A. Note that the biostratigraphic datums are largely at odds with the proposed stable isotope stage assignments (see Figure 3.9) The isotopic data for both holes have been smoothed using a 3 point running average.

3.6 Correlation of the isotopic chronologies from Holes 819A and 823A with adjacent ODP Leg 133 drill sites (northeast Australian margin)

As mentioned previously in Chapter 1 (Introduction), the principal study sites (819 and 823) form part of an eastward extending transect of drill localities from the outer-shelf/upper-slope of the GBR (Sites 819A through 822), to the Queensland Trough (Site 823) and onto the Queensland Plateau (Sites 811/825 and 824) (see Figures 1 1. and 1.2). The question arises as to how representative are the stable isotopic records from Holes 819A and 823A? And how do these records compare to those from adjacent ODP Leg 133 drill sites? Three ODP Leg 133 drill sites are of particular interest; Sites 822, 821 and 820.

Unfortunately, due to the effects of early diagenesis, particularly in the lower carbonate-poor half couplets of Unit I (Shipboard Scientific Party, 1991), it has not been possible to produce a reliable Late Pleistocene $\delta^{18}O$ stratigraphy for the sequence recovered from Hole 821A (Kenji Konishi, pers. comm., 1993). The only isotopic record available for Hole 821A is that provided by Kroon *et al.* (1993) covering the last 17 m of the sequence (i.e., stage 1 through to late stage 3). While at Site 822 a foraminiferal oxygen isotope record has yet to be produced, and the influence of variations in Late Pleistocene sea level and climate change at this site remains speculative.

Thus, the high resolution isotopic records of Peerdeman *et al.* (1993) for Site 820 (Holes 820A and 820B) provide the only other complete Late Pleistocene $\delta^{18}O$ record on the outer-shelf/upper-slope of the GBR, available for comparison with the authors records. Given the close proximity of Site 820 with Holes 819A (2.7 km apart) and 823A (approximately 31 km apart) might we not expect their isotopic signals to be alike? However, although superficially similar in many respects, significant discrepancies occur between the presented isotopic stratigraphies for Site 820 (Peerdeman *et al.*, 1993), and Holes 819A and 823A (this study). These differences and their implications for the age models presented for Holes 819A and 823A are discussed below.

The calculated differences in the $\delta^{18}O$ values between Holes 819A and 823A, with Site 820, at equivalent oxygen isotope stages are listed in Table 3.2. Broadly speaking, absolute planktic $\delta^{18}O$ values are similar in each drill hole. The $\Delta\delta^{18}O$ value between Site 820 and Hole 819A range from between 0.15 ‰ to 1.06 ‰, while the difference between the records from Site 820 and Hole 823A range between 0.09 ‰ to

Table 3.2. Approximate difference in the planktonic foraminifera $\delta^{18}O$ values between Hole 820A (Peerdeman *et al.*, 1993) and Holes 819A and 823A at equivalent oxygen isotope stages.

Stage	$\delta^{18}O‰$ Hole 820A	$\delta^{18}O‰$ 819A	$\delta^{18}O‰$ 823A	$\Delta\delta^{18}O‰$ 820A-819A	$\Delta\delta^{18}O‰$ 820A-823A
1	-2.60	-2.60	-2.25	0.00	0.35
2	-0.97	-0.53	-0.74	0.44	0.23
(3)	-1.98	-1.70	-1.40	0.28	0.58
(4)	-1.45	-1.20	-0.93	0.25	0.52
5	-2.66	-2.25	-2.19	0.41	0.50
6	-1.13	-0.24	-0.77	0.89	0.36
(7)	-2.11	-1.60	-2.20	0.51	-0.09
(7.5)	-2.09	-	-1.86	-	0.23
8.5	-2.20	-1.36	-1.80	0.84	0.40
8.6	-0.82	-	-1.12	-	-0.30
(8.4)	-0.82	-0.58	-0.64	0.24	0.18
(8.5)	-1.83	-1.36	-1.80	0.47	0.03
(8.6)	-1.24	-	-1.12	-	0.12
9	-1.74	-	-2.14	-	-0.40
10	-0.25	-	-0.54	-	-0.29
11	-1.49	-	-2.11	-	-0.62
12	-0.41	-	-0.23	-	0.18
13	-1.60	-	-1.94	-	-0.34
14	-0.21	+0.03	-0.35	0.24	-0.14
15.1	-1.85	-1.22	-1.61	0.63	0.24
15.3	-1.61	-1.76	-0.55	-0.15	-1.06
15.5	-1.47	-0.41	-	1.06	-
16	+0.09	+0.97	-	-0.88	-
17	-1.45	-	-	-	-
18	-0.28	-	-	-	-
19	-1.71	-1.00	-0.79	0.71	0.92

Oxygen isotope values for various stages in Hole 820A taken from Peerdeman *et al.* (1993). The stages indicated by brackets denote isotopic events as proposed by the first age model (Graphic correlation concepts- Prell *et al.*, 1984), for Hole 820A.

1.06 ‰. Significantly, the planktic records from Site 820 and Hole 819A (and to a lesser extent Hole 823A) display a comparable trend of mean isotopic depletion with decreasing depth, from about stage 16 through to the Holocene.

Peerdeman *et al.* (1993) presented two possible interpretations of the planktic $\delta^{18}O$ data, from Site 820. The first age model was based on a comparison of the oxygen isotope data from Holes 820A and 820B with records obtained from the western equatorial Pacific deep sea Core V28 -238 (Shackleton and Opdyke, 1973) and from ODP Hole 677A (Shackleton and Hall, 1989), and used the graphic correlation concepts outlined by Prell *et al.* (1986). This age model suggests that the oxygen isotope stratigraphy at Site 820 is complete, from stage 1 through to stage 19 at about 150 mbsf. The second age model proposed by Peerdeman and co-workers adhered more closely to the nannofossil biostratigraphy established by Wei and Gartner (1993), and suggested that oxygen isotope stages 4 and 7 are absent, and stages 8 and 5 are greatly expanded, in the record from Site 820. Below approximately 73 mbsf (~ stage 8/9 boundary) both age models presented for Site 820 are the same. In their final synthesis Peerdeman *et al.* (1993) expressed a preference for the second age model (based on the biostratigraphy proposed by Wei and Gartner, 1993), and suggested that the L.O. of *Emiliania huxleyi* datum at 35.8 mbsf was either; diachronous, or possibly reworked in Hole 820A? Support for the idea of a regional diachroneity of the *E. huxleyi* datum might be gained from both Holes 819A and 823A, where the nannofossil occurs later than the established 0.275 Ma datum. However, this supposition will require further work, in the western Coral Sea and the GBR province, to substantiate.

A comparison of the different age models proposed by Peerdeman *et al.* (1993) for Site 820, with the oxygen isotope stratigraphies from Holes 819A and 823A (this study) are presented in Figures 3.12 and 3.13. In each diagram planktic $\delta^{18}O$ values are plotted against depth. Correlation between these high resolution records has proved very difficult, especially given the atypical nature or shape of the isotopic curves from Site 820 and Hole 819A. An examination of these records suggest that the first age model proposed by Peerdeman *et al.* (1993) is in most agreement with the chronology presented for Hole 819A (and Hole 823A), particularly between stage 1 and stage 8. However, below stage 8, problems arise with the isotopic interpretation of the records from Site 820. For example, why is there no evidence for a hiatus in the record from Hole 820A, when oxygen isotope stages 10 to 14 are missing in Hole 819A, and a distance of only 2.7 km separates these two holes? Similarly, the second age model presented by Peerdeman and co-workers (despite being more consistent

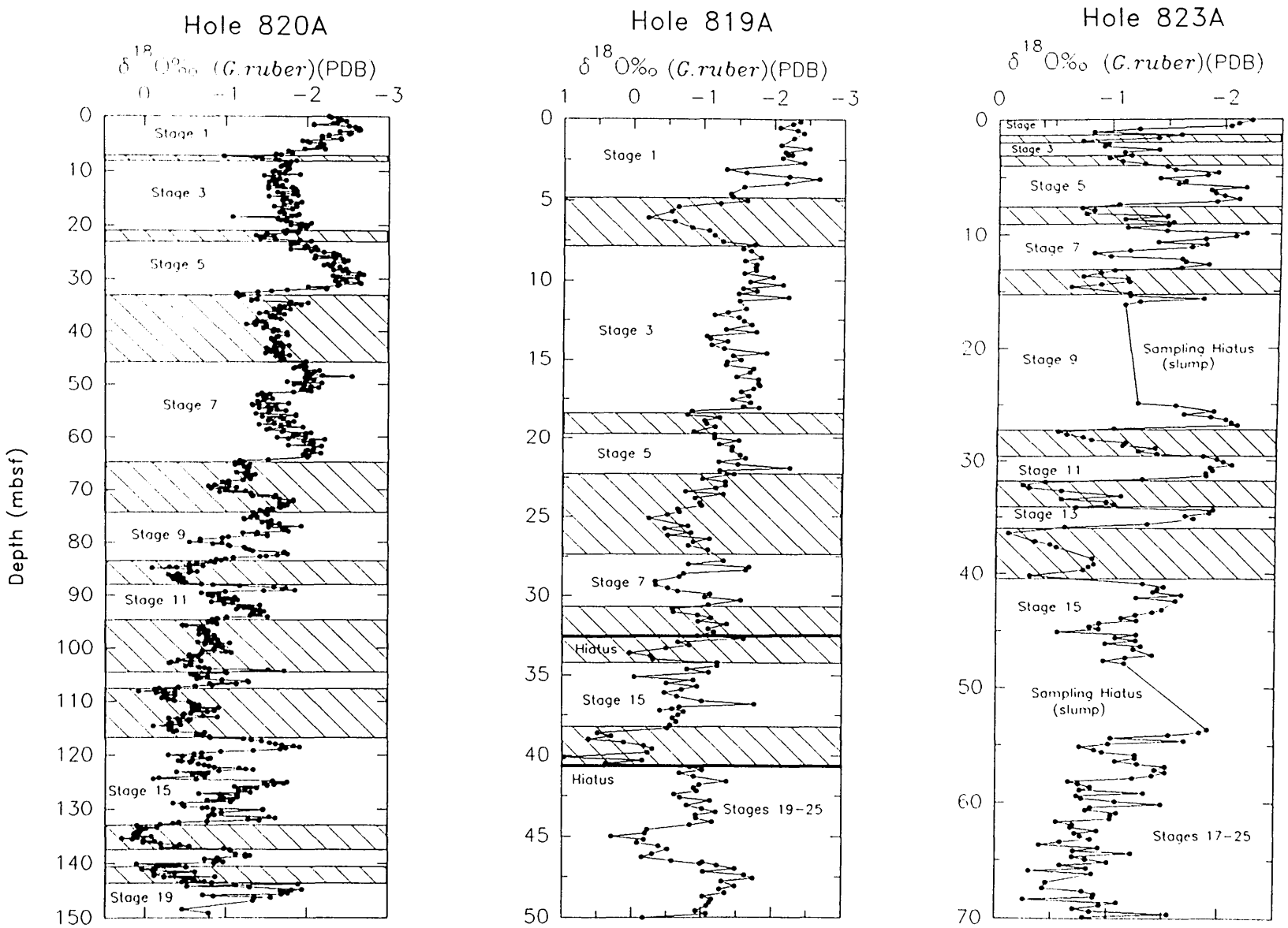

Figure 3.12. Oxygen isotope stratigraphy from Holes 819A and 823A in comparison to the isotope chronostratigraphy from Hole 820A (Peerdeman et al., 1993). Age model for Hole 820A is based on the graphic correlation concepts outlined by Prell et al., 1986. Solid line indicates position of a major stratigraphic hiatus.

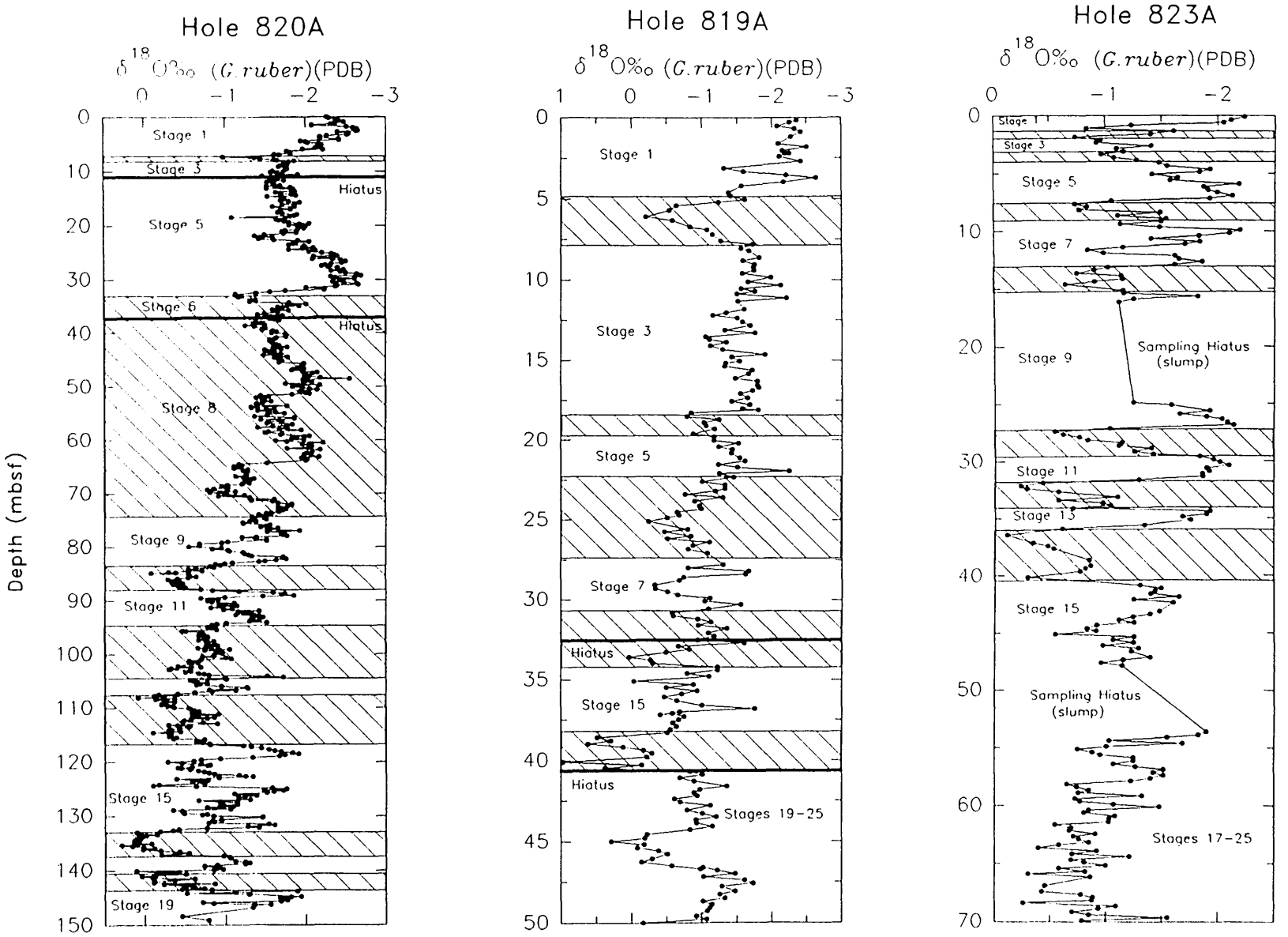

Figure 3.13 Oxygen isotope stratigraphy from Holes 819A and 823A in comparison to the isotope chronostratigraphy from Hole 820A (Peerdeman et al., 1993). Age model for Hole 820A is based primarily on the calcareous nannofossil stratigraphy of Wei and Gartner, (1993). Solid line indicates position of a major stratigraphic hiatus.

with the nannofossil biostratigraphy presented by Wei and Gartner, 1993) shows serious discrepancies with the isotopic chronologies presented for Hole 819A and Hole 823A, particularly with respect to the position and size of glacial stage 8.

In an attempt to resolve some of the inconsistencies associated with the age models presented for Site 820, and the chronologies proposed for Holes 819A and 823A, the high resolution magnetic susceptibility data from these cores have been plotted in Figures 3.14 through to 3.16. In these plots the main magnetic susceptibility peaks are numbered according to the scheme outlined by Barton *et al.* (1993). Note that not all correlation numbers or magnetic susceptibility peaks are present in the records from Holes 820A, 819A and 823A. Analysis of these plots suggest that, with the possible exception of the exact location of the stage 5/6 boundary, there is good agreement between the magnetic susceptibility and isotopic records from Hole 819A and 823A, over the last two main glacial/interglacial cycles (see Figure 3.14). However, below glacial stage 6 the absence of any obvious or prominent magnetic susceptibility peaks in the records from Hole 819A, makes correlation with the sequence from Hole 823A very difficult. Tentative comparison of the records from Hole 820A with the well defined stable oxygen isotope and magnetic susceptibility records from 823A suggest that, in the former record: (1) stages 1 to 5 are present; (2) part of stage 6 is absent [note: the position of the stage 5/6 boundary has been placed by Barton *et al.* (1993) centred over magnetic susceptibility tie-point 8.0]; (3) stage 7 should lie between 33 and 45 mbsf; (4) the stage 7/8 and 8/9 isotopic boundaries should be placed at approximately 45 mbsf and 50 mbsf, respectively; (5) possibly stage 10 is absent, and (6) stage 12 is located between 65 to 70 mbsf. Alternatively, interglacial stage 7 may be absent from the record in Hole 820A, and the magnetic susceptibility tie-point 10 could be 12.0 (see Figure 3.16). This would imply that the isotopic depletion events between 47 to 52 mbsf and 60 to 65 mbsf were interglacial stages 9 and 11, respectively. Below 70 mbsf the magnetic susceptibility record from Site 820 lacks obvious peaks or tie-points, and as a result the Hole 820A record becomes increasingly more difficult to correlate with the records from Holes 819A and 823A. Thus, according to the high resolution magnetic susceptibility records both of Peerdeman's isotopic models are possibly incorrect, and many hiatuses occur in this record, just as in the record from Hole 819A.

Clearly there is no easy solution to oxygen isotope stage assignment in Holes 820A and 820B. Alternative interpretations using the oxygen isotope and magnetic susceptibility records from Holes 819A and 823A, suggest that the isotopic record at Site 820 has been subjected to factors other than temperature and seawater

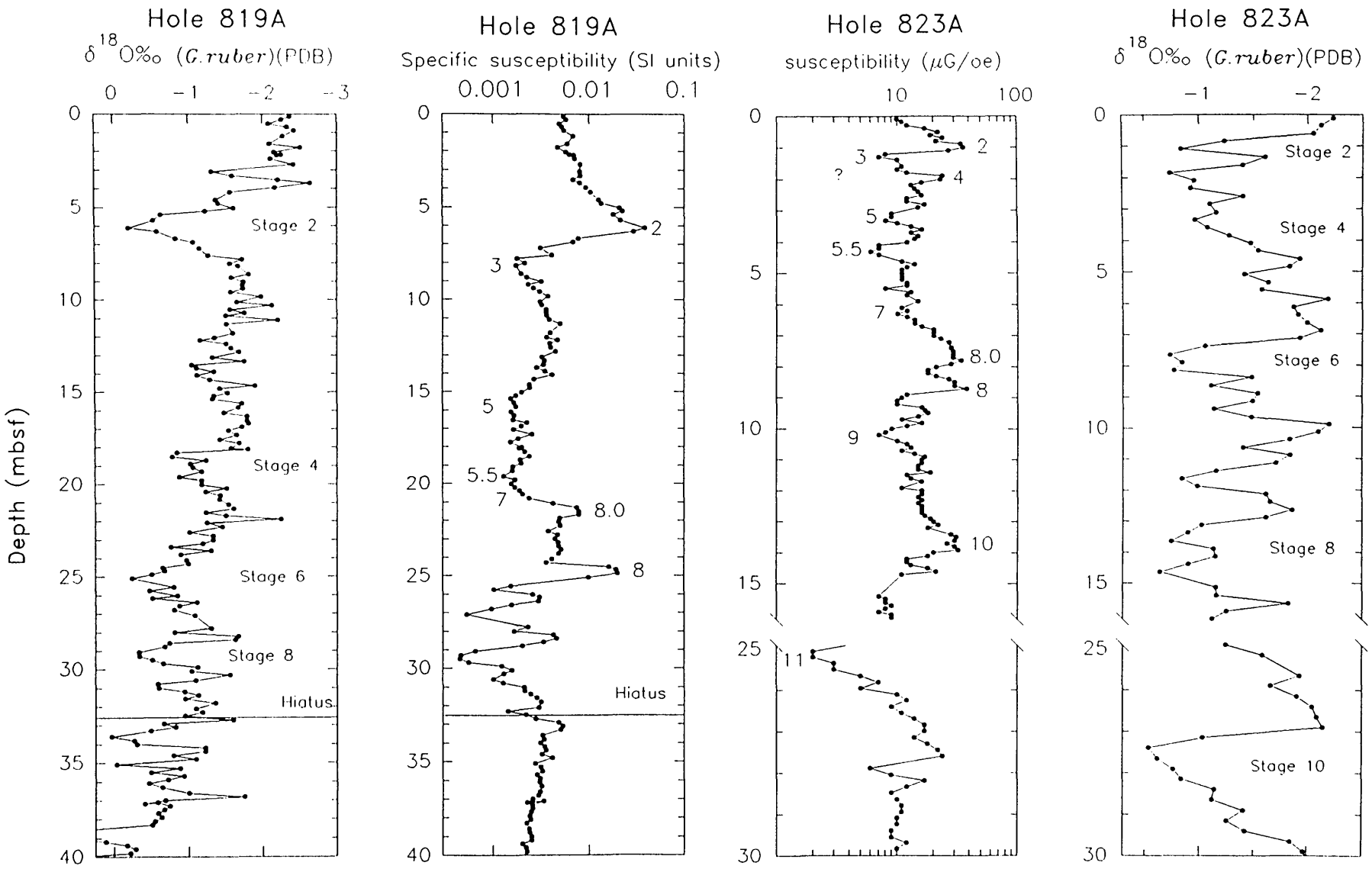

Figure 3.14. Comparison of the magnetic susceptibility and $\delta^{18}O$ records for the upper part of Holes 819A and 823A. Tie-point numbers of matching features are marked on the figure (after Barton et al., 1993). The interval 16–25 mbsf, in Hole 823A, indicates the position of a slump (and Shipboard sampling hiatus).

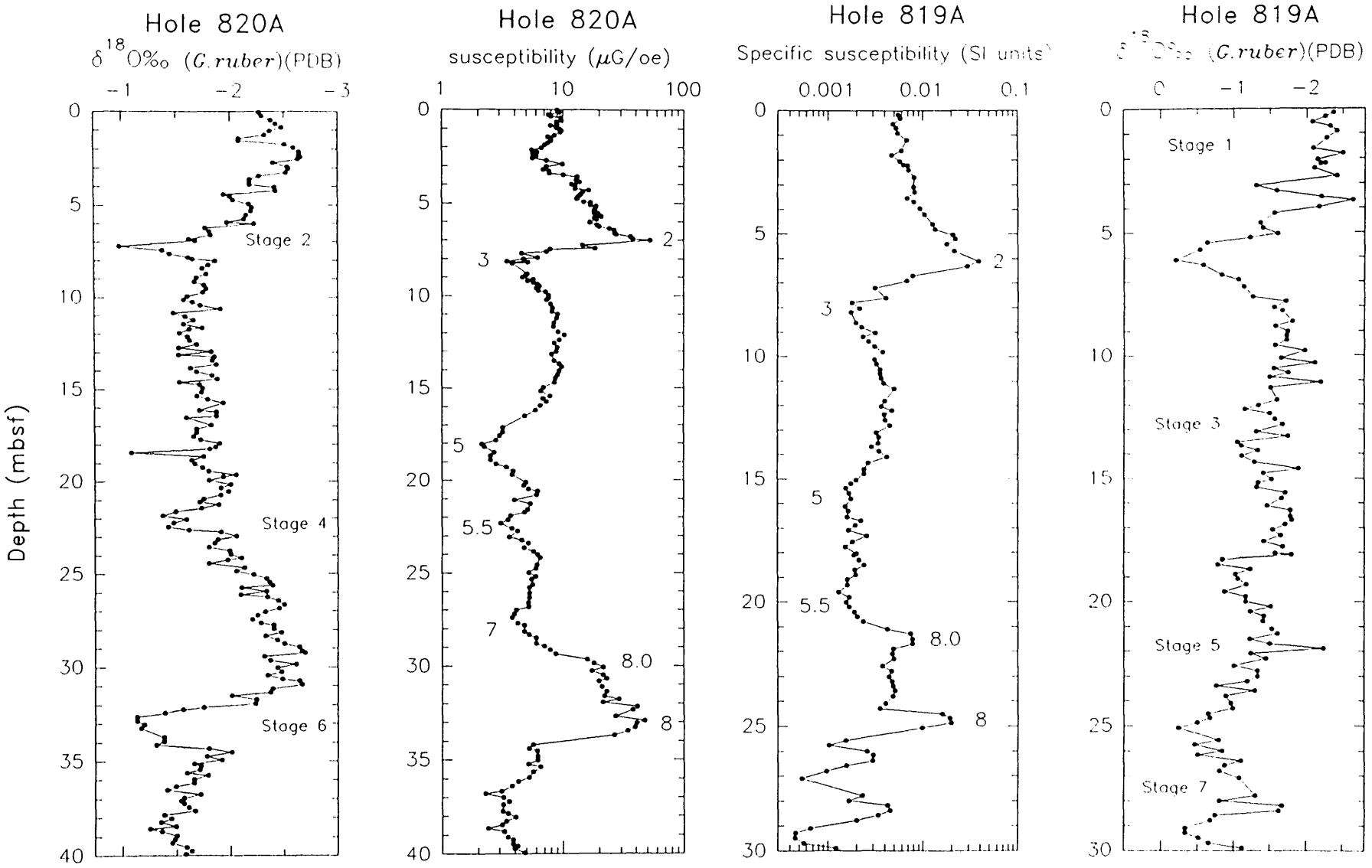

Figure 3.15. Comparison of the magnetic susceptibility and $\delta^{18}O$ records for the upper parts of Holes 820A and 819A. Tie-point numbers of matching features are marked on the figure (after Barton et al., 1993).

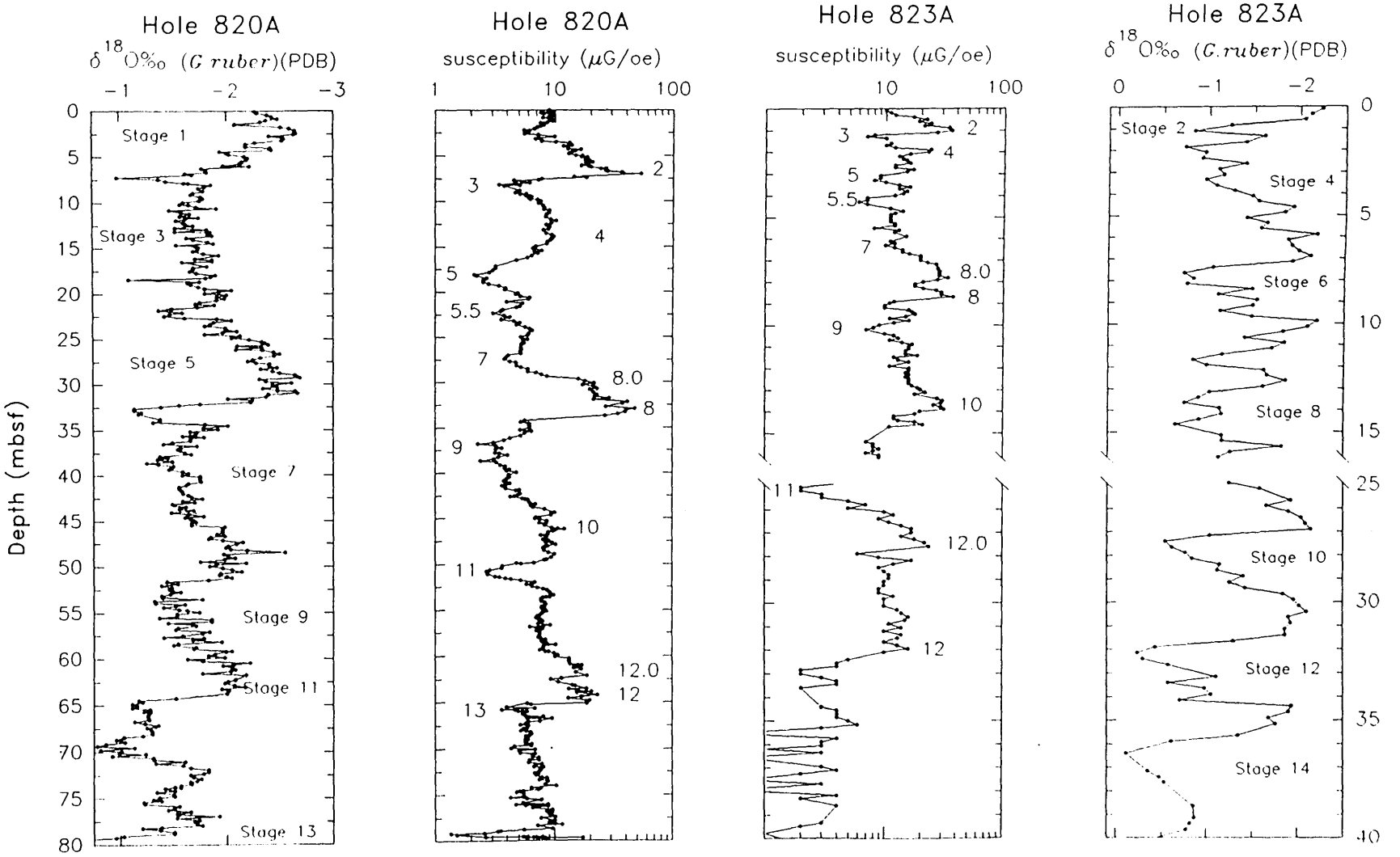

Figure 3.16. Comparison of the magnetic susceptibility and $\delta^{18}O$ records for the upper parts of Holes 820A and 823A. Tie-point numbers of matching features are marked on the figure (after Barton et al., 1993). The interval 16–25 mbsf in Hole 823A indicates the position of a major slump (and sampling hiatus).

composition. Diagenesis may have played a major role in changing the isotopic signal of the shallow sites and erroneous age models are the result if only the oxygen isotope variations are taken into account. Possibly the Hole 823A isotope stratigraphy is the more reliable one. The deep sea (Queensland Trough) hole was probably less affected by shallow burial diagenesis.

3.7 Time-Series Analysis

In an attempt to check the validity of the age models proposed for Holes 819A and 823A, time series analysis techniques were applied to the planktic $\delta^{18}O$ records from each core, and the results compared to spectra obtained from the benthic $\delta^{18}O$ record from ODP Hole 677A (Shackleton and Hall, 1989; Raymo *et al.*, 1990). Unfortunately, the poor and often incomplete nature of the benthic $\delta^{18}O$ records from Holes 819A and 823A precluded detailed analysis using time-series techniques.

Power spectral and cross (power) spectral analysis are two common quantitative statistical methods of correlation in the frequency domain (Patience and Kroon, 1991). Each method plots the amount of spectral power (concentration of variance) present against a harmonic number (1/time window). Power spectral techniques estimate the spectral density function, or spectrum, of a given time series (Chatfield, 1989), whereas, cross spectral methods quantify the degree of similarity between two records in the frequency domain. Both spectral techniques are commonly employed in palaeoclimatic studies to evaluate the relationships between potential climatic proxies and orbital/astronomical forcing (Hays *et al.*, 1976; Imbrie *et al.*, 1984). Spectral methods also provide a powerful tool for the refinement of time series, in particular isotopic age models. For example, peaks of spectral power should be sharp and well defined if stage boundaries are correctly positioned, for a given age model. However, caution should be exercised to avoid excessive refinement, or tuning, in order to force a time series to yield preconceived periodicities. A comprehensive review of spectral analysis techniques is provided by Pestiaux and Berger (1984).

Cross (power) spectral analysis (hereafter referred to as cross-spectral analysis) results are generally discussed in terms of the variance-, coherency-, and phase -spectra between two time series/data sets. In this study, the variance-, coherency-, and phase -spectra were calculated according to the standard Blackman-Tukey Fourier spectral method described by Jenkins and Watts (1968). Spectral and cross spectral analysis was performed using the Arand software package developed by Philip Howell (Department of Geological Sciences, Brown University, Providence, Rhode Island).

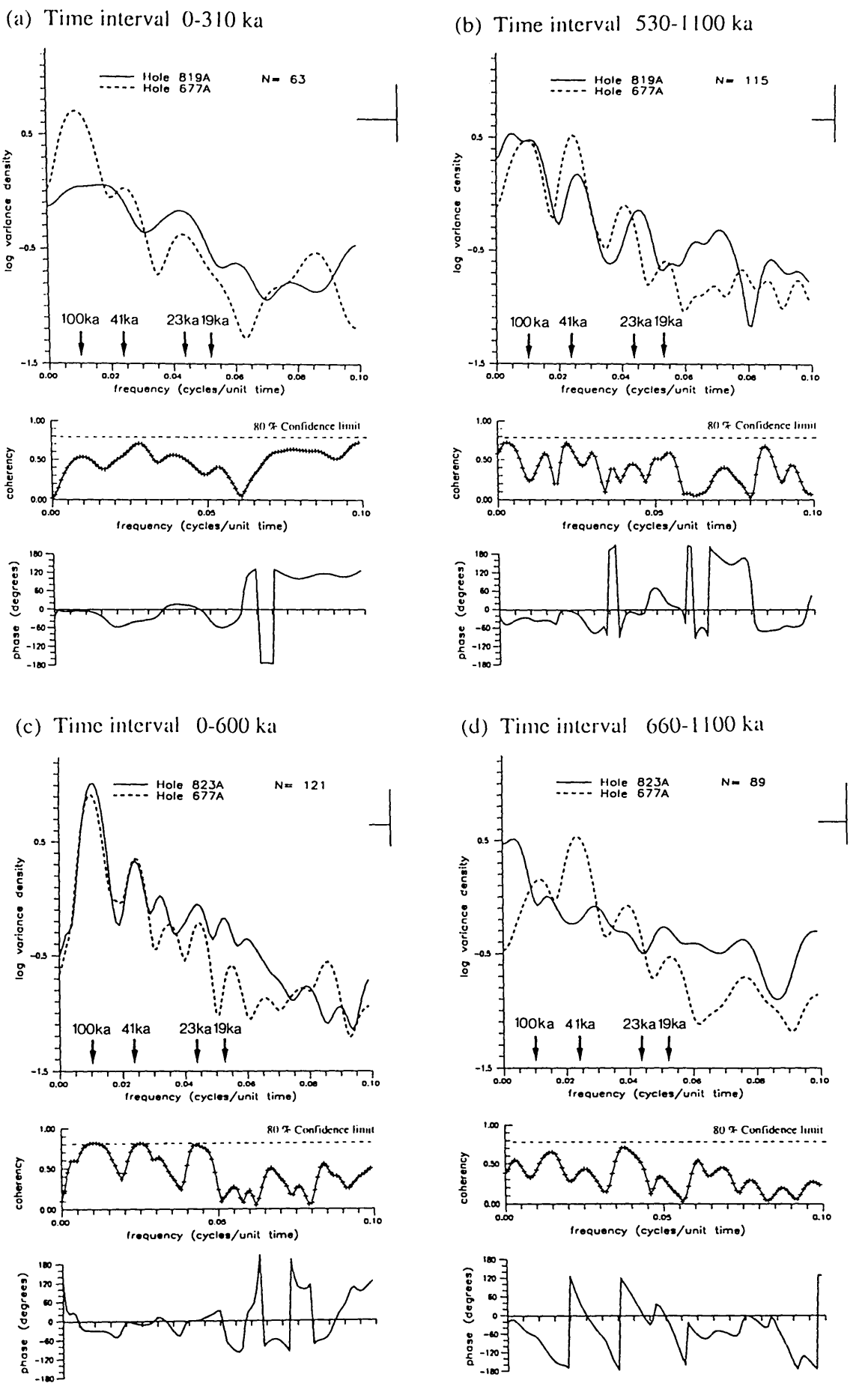

Figure 3.17. Spectral and cross-spectral analyses of the upper and lower parts of the stable oxygen isotope records from Holes 819A and 823A (this study), and Hole 677A (Raymo et al., 1986). Note the presence of well-defined Milankovitch (orbital) periodicities in the upper and lower section of the isotope records from Holes 823A and 819A, respectively.

Variance spectra are used to identify the dominant periods of variation in a time series as indicated by major spectral peaks. Coherency (k) is a measure of the linear correlation between two time series over a given frequency band when the phase difference is set to zero. A coherency of one is indicative of perfect correlation whereas a coherency of zero indicates no correlation. On the coherency spectra an 80 % confidence limit is displayed, above which statistical significance exists between the two time series under investigation. Phase (ϕ) spectra describe the relative timing of variations in two time series. Although phase estimates are generated for the same range of frequencies as the coherency spectra, the phase estimates are only significant where coherency is significant. On the phase spectra illustrated, negative phase values indicate that the first named parameter lags (or follows variations in) the second.

Each periodogram indicates the proportion of the total observed variance accounted for by the individual frequency components. The amount of variance per frequency band (log variance density) is plotted against frequency (cycles/unit time). The 80 % confidence interval (C.I.) is represented on the plot by a vertical bar. The shorter horizontal bar defines the bandwidth (B.W.) of the filter used in the smoothing of the spectra in the frequency domain, and is inversely related to the number of lags (M) used to calculate the autocorrelation/autocovariance function. For every time series the number of lags selected was about one third the number of interpolated values (N), i.e., M = N/3. The highest frequency which can be resolved is the Nyquist frequency (f_n) =1/2 Δt (where t = time interval between data points). In the high resolution isotopic spectra presented below (f_n) = 0.10. The absolute amplitudes of the various time series in this study (see following chapters) vary by orders of magnitude making comparison on the same variance density scale difficult. In order to overcome this problem time series were standardised by subtracting the mean of the distribution from each observation and dividing by the standard deviation of the distribution (Davis, 1986). This allows direct comparison of relative variance density without affecting the shape of the spectra. In general (unless otherwise stipulated) time series were linearly detrended, a prewhitening constant of zero selected, and a fixed time interval of 5.0 ka used during spectral/cross-spectral analysis.

Log variance spectral density and cross-spectral analysis of the planktic $\delta^{18}O$ records, in Holes 819A and 823A, with the equatorial Pacific benthic isotopic record in Hole 677A (Shackleton and Hall, 1989; Raymo, 1990) are illustrated in Figure 3.17.

3.7.1 Hole 819A (outer-shelf/upper-slope of the GBR)

Due to the presence of a major stratigraphic hiatus in Hole 819A, at 32.5 mbsf, spectral and cross-spectral analyses were carried out on the upper (0-310 ka) and lower (530-1100 ka) sections (Figures 3.17a and 3.17b, respectively) of the stable isotope records from Hole 819A and Hole 677A.

Analysis of the $\delta^{18}O$ records, from Holes 677A and 819A, shows a preponderance of variation associated with the astronomical or "Milankovitch" frequencies (Imbrie *et al.*, 1984), cycles with periods of about 19 ka and 22 ka (components of precession), 41 ka (obliquity/tilt), and 100 ka (eccentricity). In addition to variance at the primary orbital periods, the stable isotopic records from Holes 819A and 677A contain variance at heterodyne frequencies of the primary orbital periods (for example at ~29 ka, in Hole 819A) resulting from ill-defined primary peaks (Clemens *et al.*, 1991).

Unlike the stable oxygen isotope record from Hole 819A, the $\delta^{18}O$ variance spectrum for Hole 677A, between 0-310 ka, is dominated by well defined spectral peaks at the 100 ka and 23 ka, frequency bands. The spectrum for Hole 819A is poorly defined with respect to concentrations in variance. However, strong coherencies are recorded over the 41 ka band, and moderate to strong coherencies are documented over the 100 ka, 23 ka and 19 ka orbital frequencies, for the isotopic records from Holes 819A and 677A. Phase is only significant at the 41 ka obliquity band, where the two isotopic records differ by about +20° (see Figure 3.17).

The 530 to1100 ka periodogram (Figure 3.17b.) shows well defined peaks in variance at the 100 ka, 41 ka and 23 ka bands, in both $\delta^{18}O$ records. Relative to the upper time-slice, the amplitude of the concentration of variance, has increased and decreased for the obliquity and eccentricity bands, respectively. Further, the 19 ka cycle is only clearly distinguishable in the isotopic record from Hole 677A. Significant coherencies occur at the 400 ka and 41 ka frequencies, and moderately strong and moderate coherencies at the 19 ka and 23 ka bands, respectively. The lack of strong coherency over the eccentricity band is probably associated with poorly aligned spectral peaks (Clemens *et al.*, 1991). Phase is significant at the 400 ka and 41 ka frequencies, where the isotopic records, differ by about -20° and +20°, respectively.

3.7.2 Hole 823A (Queensland Trough)

In a similar manner to that described for Hole 819A (section 3.7.1), time series analyses were carried out on the upper and lower sections (corresponding to 0-600 ka

and 660-1100 ka, respectively) of the isotopic records from Holes 677A and 823A (see Figure 3.17). Note that because of the presence of significant sampling hiatuses (depositional slumps) within the sequence from Hole 823A the time-slices used for this piston core are different from those used in Hole 819A (see section 3.7.1).

The spectra for the upper part of the isotopic records at Holes 823A and 677A are dominated by well developed peaks in variance at the 100 ka and 41 ka, primary orbital frequencies (Figure 3.17a). Relative to the isotopic spectra for Holes 819A and 677A, the amplitude of the 100 ka peak in variance is significantly larger, for Holes 823A and 677A. Significant peaks in coherency, between the isotopic records at Holes 823 and 677A, occur at the 100 ka, 41 ka and 23 ka orbital frequencies, and these records differ in phase by about -10°, +20° and +30°, respectively. Although represented by a well-defined peak in variance, in Hole 677A, the 19 ka precessional frequency has weak coherency.

The periodogram for lower part of the isotopic record (660-1100 ka), in Hole 823A, is very difficult to interpret. The isotopic record for Hole 677A, across the same time-interval shows well-defined concentrations of variance at the primary orbital frequencies. However, apart from the 400 ka cycle, the spectrum for Hole 823A is very incoherent and lacks any readily identifiable peaks in variance. Furthermore, coherency is below the 80 % C.I for the two isotopic records, during the early to mid Pleistocene.

3.7.3 Summary of Time-Series Analyses

Although not as pronounced as the ODP Hole 677A $\delta^{18}O$ data, comparison of the variance spectra for Holes 819A and 823A show a distinct change in the frequency of isotopic variation, between the lower and upper parts of the $\delta^{18}O$ records. These results are consistent with the findings of other workers (Shackleton and Opdyke, 1976; Pisias and Moore, 1981; Prell, 1982) which suggest changes in the frequency of isotopic variation, from high frequency and low amplitude Milankovitch cycles (41 ka) during the early late Pleistocene, prior to 0.9 Ma, to low frequency and high amplitude cycles (100 ka) during the late Pleistocene, after 0.73 Ma.

3.8 Conclusions

In order to reconstruct the sedimentologic and paleoceanographic history on the northeast Australian continental margin, reliable age control is of the utmost importance. The isotopic records from Holes 819A and 823A (this study), and from Hole 820A (Peerdeman *et al.*, 1993), are not easy to interpret. The uppermost part of

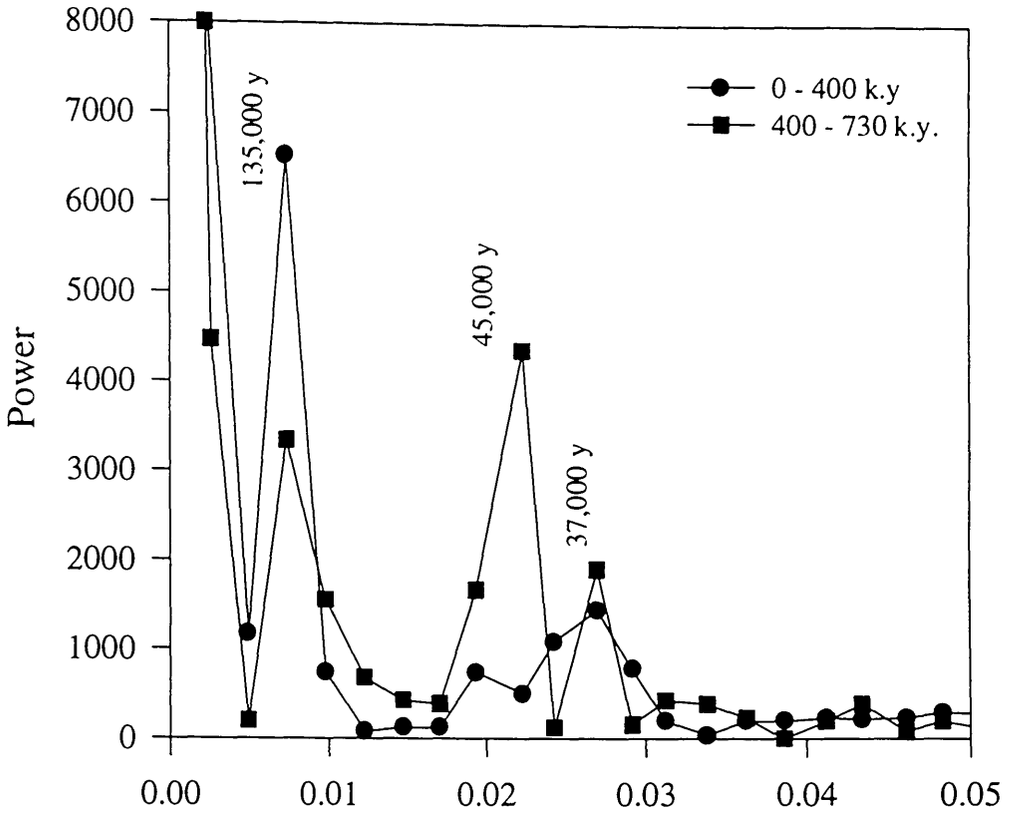

Figure 3.18 Time-frequency analysis of the oxygen-isotope signal of Holes 820A and 820B for the intervals 0-400 and 400-730 k.y. for the second age model proposed by Peerdeman *et al.* (1991) (see Figures 3.12 and 3.13).

Hole 823A (Queensland Trough) is probably the best record available for interpreting the stable oxygen isotope record. It has well defined biostratigraphic and magnetostratigraphic control, and demonstrates the dominance of the 100 ka Milankovitch cycle, and the presence of the 41 ka and 23 ka orbital frequencies, over the last 600 ka. Extrapolating this well defined stable isotope stratigraphy to the outer-shelf/upper-slope Hole 819A and Site 820 records appears at first sight impossible. However, we can successfully correlate the Queensland Trough record to the outer-shelf/upper slope of the GBR holes by using the high-resolution magnetic susceptibility stratigraphy. This shows that the stable isotope record in Site 820 must have been influenced by factors other than seawater composition and/or water temperature, and that many hiatuses are present in this record. Possibly the Site 820 record has been extensively bioturbated in a manner outlined by Hutson (1980) or been affected by shallow-water diagenesis? The fact that the Site 820 record spectrum did not show the usual orbital frequencies over the last 600 ka (Peerdeman *et al.*, 1993), further suggests that the stable isotope record has been influenced by post-depositional factors. Thus, we conclude that the mid to late Pleistocene isotopic record in Hole 823A is coherent and provides good age control which can be tentatively extrapolated to the outer-shelf/upper slope of the GBR by using variations in magnetic susceptibility.

The interpretation of the lower part of Hole 823A, however, gives many problems due to an abundance of gravity-flow deposits, the lack of magnetostratigraphic control, and possibly unreliable biostratigraphic datum levels. The only reasonable approach, taking into account the sediment accumulation rate, is to take the available datum level control points and extrapolate between them. In chapter 6 (Geochemistry of Queensland Trough Hole 823A sediments) another method will be presented for refining the age model of the lower part of Hole 823A. The lower part of Hole 819A, however, shows a better defined oxygen isotope stratigraphy, and in addition has reasonably good magnetostratigraphic and biostratigraphic control. The frequency spectrum, for the lower part of the $\delta^{18}O$ record at Hole 819A shows, in addition to the 100 ka and 23 ka orbital cycles, a strong 41 ka periodicity. The lower part of the sequence recovered from Hole 819A thus provides good age control from 600 to 1100 ka (mid- to late Pleistocene), although it is not clear whether shallow burial diagenesis has also affected this part of the record and thus care must be taken when interpreting these records.

Chapter 4 Sedimentological response to fluctuations in late Pleistocene sea level and climate change, northeast Australian margin.

4.1 Introduction

Models for both siliciclastic and carbonate continental margin sedimentation have been developed for a wide range of physiographic, oceanographic and climatic settings (Wilson, 1975; Reading, 1978; Reid, 1985; Reineck and Singh, 1980). However, relatively few detailed studies have dealt with the complex carbonate-siliciclastic transitional environment associated with many continental margins. Previous studies, largely based along the west Florida continental margin and in the Bahamas, have concentrated on the response of mixed carbonate-siliciclastic systems having carbonate ramp slopes (Gardulski *et al.*, 1986; Roof *et al.*, 1991) and carbonate rimmed platforms (Kier and Pilkey, 1971; Boardman and Neumann, 1984; Droxler *et al.*, 1983; Boardman *et al.*, 1986), to fluctuations in Late Quaternary sea level and climate change. These studies have demonstrated that carbonate mineral cycles in Quaternary periplatform slope sediments in the Bahamas and on the Florida ramp slope are driven by different mechanisms: carbonate mineral dissolution (Droxler *et al.*, 1983) or autocyclicity controlled by alternate flooding and exposure of the bank top carbonate 'factory' (Boardman, *et al.*, 1986), and productivity and dilution by terrigenous material (Gardulski *et al.*, 1986), respectively. These two fundamental carbonate depositional systems highlight the effect of variations in the physiography, oceanographic setting, sediment source and proximity to terrigenous input on carbonate facies development.

As noted by Peerdeman and Davies (1993), the continental margin offshore Cairns, northeast Queensland, is characterized by a transition from a dominantly rimmed carbonate platform in the north to a ramp-shaped continental margin in the south, and as such provides a scenario unlike anything previously described for the Bahamas and the Florida regions. The north-central Great Barrier Reef Province offers a unique opportunity to study the effects of variations in late Quaternary sea level and climate change on a mixed carbonate-siliciclastic margin, and, importantly, provides a modern analogue for many ancient sequences (Davies *et al.*, 1987; 1988).

The aim of this chapter is threefold: 1) to examine the present-day facies distribution and composition in the north-central Great Barrier Reef Province, 2) to evaluate the sedimentological response of the Queensland margin to oscillations in late Pleistocene sea level (as inferred from the foraminiferal oxygen isotope records), and 3) to determine the effects of sea level and climate change on carbonate production and accumulation on the upper-slope and in the Queensland Trough.

4.1.1 Modern Sediment Distribution

In order to understand the nature and composition of periplatform[1] sediments recovered from Queensland continental margin Sites 819 and 823, it is first necessary to consider the distribution patterns of the major components which contribute to the present-day sediment mass on the northeast Australian continental margin, in particular the region offshore Cairns, northeast Queensland.

Extensive studies of facies development and distribution patterns have been carried out for the inner shelf and coastal regions of the north-central GBR (Maxwell, 1968; Belperio 1983a, 1983b). However, detailed information on Holocene sedimentary processes on the middle- and outer-shelf (>20 m water depth) is sparse, and is largely deduced from surficial sediment distribution patterns (Orme and Flood, 1977; Marshall and Davies, 1978; Davies *et al.*, 1983; Orme, 1985;), sedimentary bedform analysis (Scoffin and Tudhope, 1985; Harris and Davies, 1989), and continuous high-resolution seismic reflection profiles (Searle, 1983; Orme and Salma, 1988). Many more studies on the GBR shelf have concentrated on the carbonate reef complexes, dealing with various aspects of skeletal carbonate production, sediment transport and growth rates (Swinchatt, 1968; Jell and Flood, 1978; Marshall and Davies, 1978; Davies *et al.*, 1983). However, according to Belperio and Searle (1988) these studies have generally failed to appreciate the significance of terrigenous sedimentation in the context of Quaternary shelf evolution.

Early studies by Maxwell (1968), suggested that the GBR shelf sediments could be classified into three broad facies, based on the proportion of carbonate and siliciclastic components, namely: 1) terrigenous facies identified by less than 60 % acid-soluble content, 2) carbonate facies distinguished by greater than 80 % acid-soluble content, and 3) mixed (or transitional) facies characterized by 60 to 80 % acid-soluble content. Subsequently, Maxwell and Swinchatt (1970) and Maxwell (1973) provided a more comprehensive account of the sediment facies distribution patterns on the GBR shelf. Consequently it was thought that the shelf-floor sediments showed a semi-meridonal zonation of lithofacies with a near-shore and inner shelf dominated by terrigenous sediments, a zone of carbonate sediments on the outer shelf, and a mixed or transitional zone on the mid-shelf (see Figure 4.1). More recently, Flood and Orme (1988) have suggested that the carbonate-terrigenous end-member mixing model of Maxwell (1968) represent an oversimplified picture of an across the shelf carbonate

[1]Broad realm of transitional sediments between the shallow, bank-top carbonate deposits and the pelagic oozes of the deep ocean basins- Schlager and James (1978).

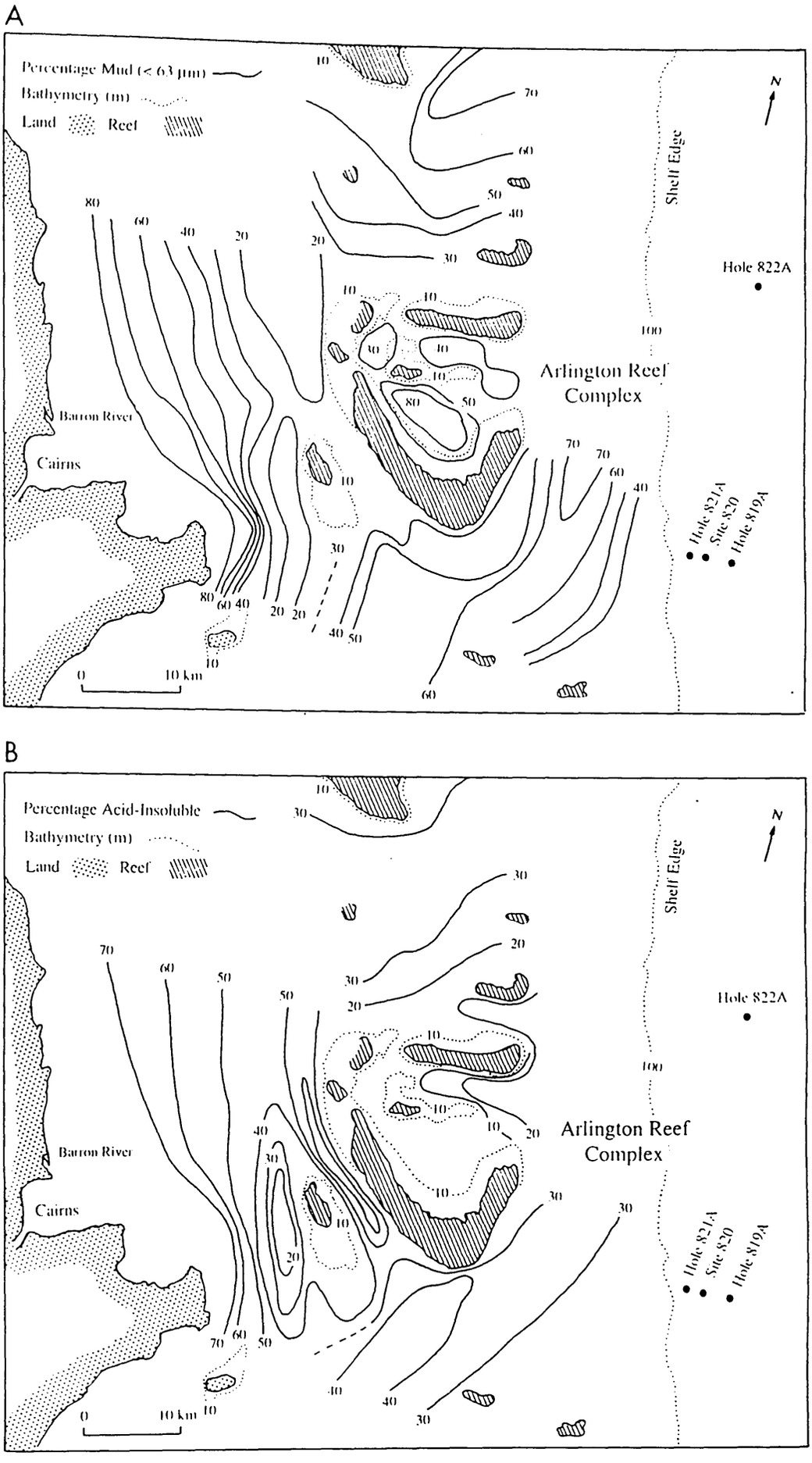

Figure 4.1 A). Present day distribution of fine-grained sediment (< 63μm) in the region of Arlington Reef Complex, Queensland shelf, northeast Australian margin. B). Variation of acid insoluble material in shelf sediments in the vicinity of Arlington Reef Complex, offshore Cairns, Queensland (after, Maxwell and Swinchatt, 1970).

C

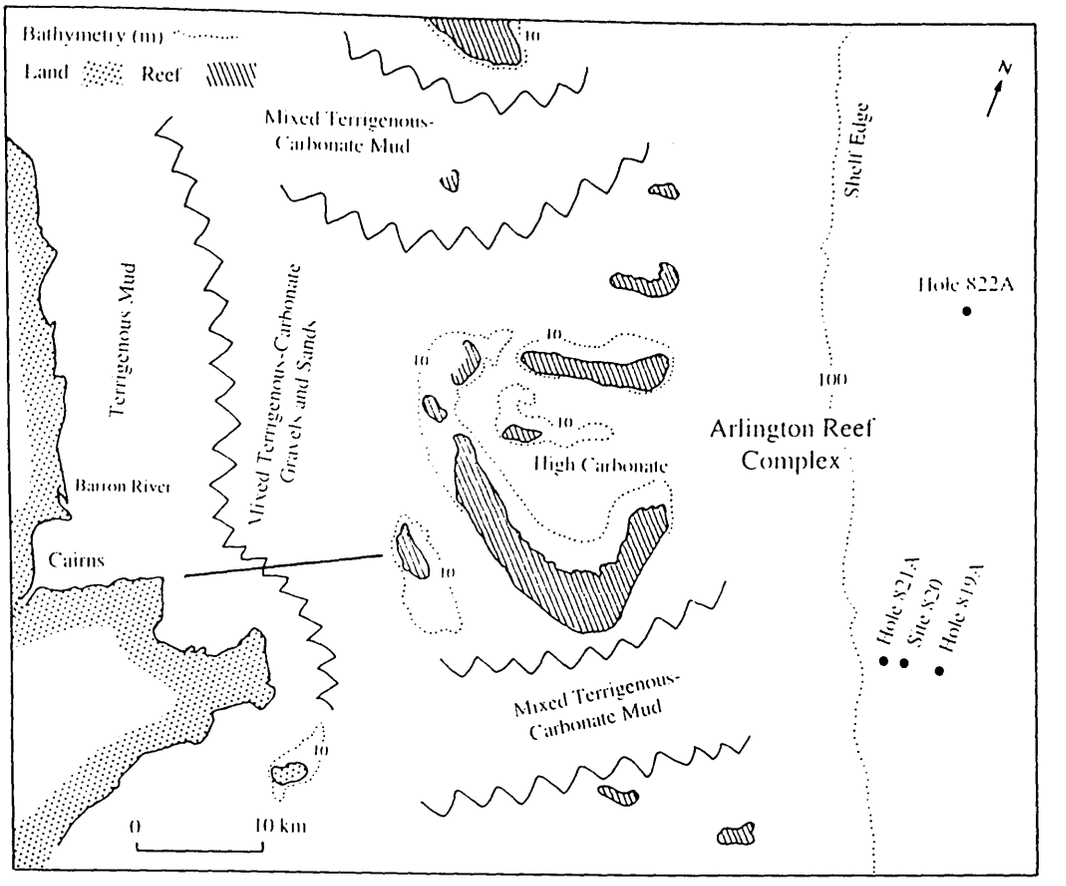

D

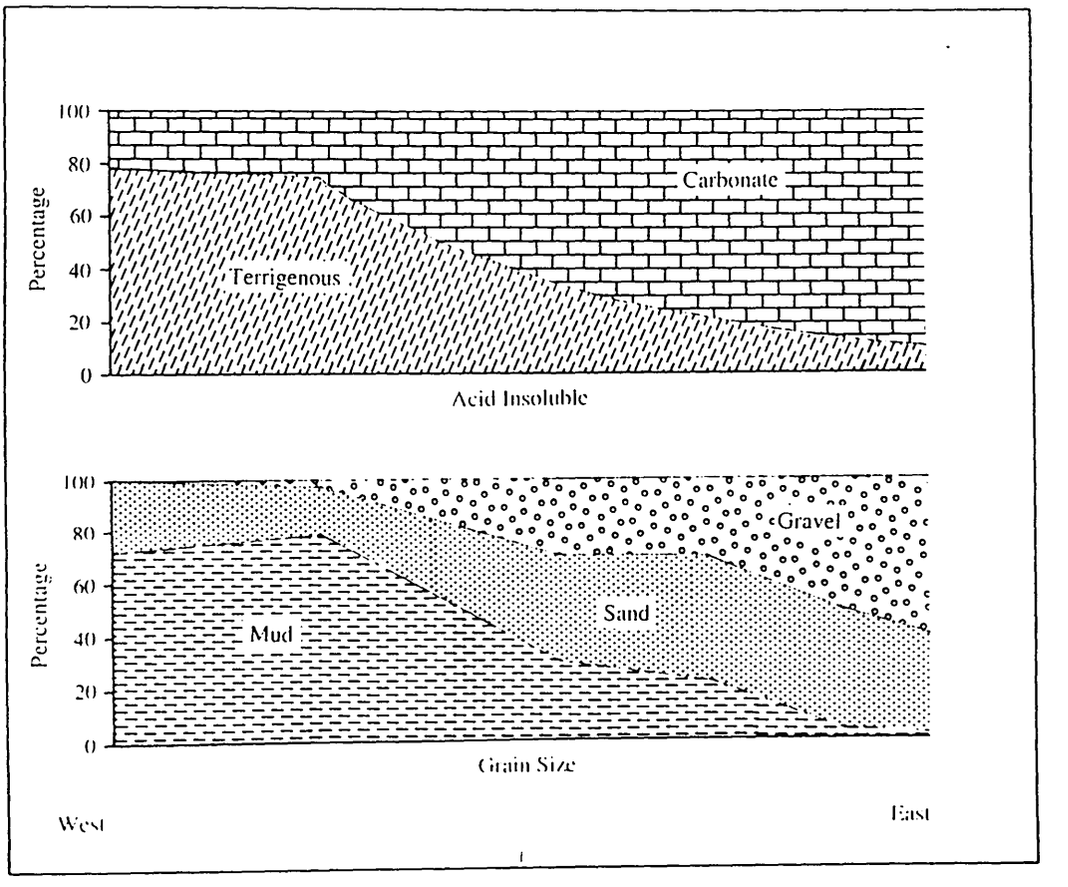

Figure 4.1. C). Distribution of lithofacies on the Queensland continental shelf offshore Cairns, northeast Australia. The mixed terrigenous-carbonate gravels and sands belong mainly to the impure carbonate facies. D). Variation of acid-insoluble and grainsize of shelf sediments along one traverse (solid line in Figure 4.1c) (after, Maxwell and Swinchatt, 1970).

source. These authors point out that the decrease in siliciclastic components across the shelf is not gradual, as previously held, and that modern transport of sediment beyond the inner shelf is limited because of the dominance of along-the-shelf sediment transport in the near shore and inner-shelf regions. Despite these new findings the early work of Maxwell (1968) and Maxwell and Swinchatt (1970) still provides a useful introduction to sediment distribution patterns across the Queensland continental shelf.

In the north-central GBR region, the terrigenous facies is restricted to the inner-shelf, adjacent to the mainland (Maxwell and Swinchatt, 1970) (see Figure 4.1). According to these authors, detrital quartz sand is the main constituent and appears to be derived from the granitic and sandstone hinterlands drained by the eastern rivers (for example, the Barron and Daintree rivers), from the large dune systems of the present coastal region, as well as from the ancient dune systems of the continental shelf and older fluviatile deposits. Indeed, Belperio (1983b) suggests that significant amounts of relic terrigenous sediment is incorporated into modern, actively accumulating shelf floor sediments, particularly where the Holocene sedimentary cover is thin and patchy. In general, the carbonate facies occurs on the outer-shelf in the vicinity of reefs, and consists largely of reef derived bioclastic carbonate sand and gravel, as well as *in situ* skeletal material of benthic foraminifera, bryozoans, molluscs, Codiacean green algae (e.g., *Halimeda, Penicillus*) and calcareous red algae (Marshall and Davies, 1978). Echinoderm, crustacean and clay mineral fractions are generally subordinate sediment components of the carbonate facies (Maxwell, 1968). Ooids and cemented aggregate grains of the type found in the Florida-Bahamas area are generally absent in GBR shelf sediments, and cemented faecal pellets are rare (Maxwell and Swinchatt, 1970). The major contributors to the inter-reefal carbonate sediments are benthic foraminifers (Tudhope and Scoffin, 1988), and on the outer-shelf (between 60-100 m water depth) *Halimeda spp.* debris. Recent figures published by Scoffin and Tudhope (1985) suggest that modern corals contribute less than 2 % of the total carbonate sediment to inter-reefal shelf areas. The mixed facies represents a transition between the terrigenous (siliciclastic) facies and the carbonate facies. Figure 4.1 (a-d) illustrate schematically the modern carbonate-terrigenous and mud-sand distribution patterns for the north-central GBR, and in particular the Arlington Reef Complex.

According to Maxwell (1968) the mud of the Queensland shelf is predominantly terrigenous in origin and very little fine carbonate material is contributed by the reefs. In this respect, the province differs from others such as Florida (Ginsburg *et al.*, 1963), Bahamas (Purdy, 1963; Stieglitz, 1972), Bermuda (Neumann, 1963) and the Persian

Gulf (Kendal and Skipwith, 1969) where the mud fraction is largely composed of carbonate.

4.2 General characteristics of Hole 819A (upper-slope of the GBR) and Site 823 (Queensland Trough) sediments

This section provides a synopsis of the main sedimentological observations made onboard the *JOIDES Resolution* by the Shipboard Scientific Party (1991), during the Ocean Drilling Program Leg 133, northeast Australian margin.

4.2.1 Hole 819A (upper-reef slope of the GBR)

Marine sediments were recovered from Site 819 using an advanced hydraulic piston corer (APC) between 0-123 meters below seafloor (mbsf), and by the use of an extended piston core barrel (XCB) between 123-400 mbsf (Davies *et al.*, 1991). Above 123 mbsf, a total of 133.5 m of sediment was recovered (gas expansion of cored sediment gave values of 108.6 % recovery). Below 123 mbsf, 277 m of sediment was cored, with a 205.5 m (74.3 %) recovery.

Site 819 yielded an expanded late Pleistocene section (spanning <1.48 Ma) of rhythmically bedded, hemipelagic, carbonate and siliciclastic sand and muds (see Plate 2). Five major sedimentary units were identified by the Shipboard Scientific Party (1991), of which only the upper three fall within the scope of this study. Figure 4.2 illustrates the major lithologic units identified in the periplatform sequence recovered from Hole 819A (upper-slope of the Queensland shelf). Unit I, representing Cores 133-819A-1H through to -4H-3 (0-32.5 mbsf), were found to consist of rhythmically bedded sediment couplets about 9.6 m long; the upper half-couplet consisting of light greenish-gray clayey nannofossil ooze with assorted shallow water bioclasts and the lower half-couplet made up of dark greenish gray clayey nannofossil ooze with numerous silt intercalations. A typical upward coarsening sedimentary couplet is illustrated in Figure 4.3 (Shipboard Scientific Party, 1991). Unit II, Cores 133-819A-4H-3 through to -11H-2 (32.5-97.0 mbsf), is composed of five rhythmic sedimentary couplets, each approximately 13 m thick. The lower half-couplets, in Unit II, were characterised by the presence of abundant intercalations of silt; these grade upward into the dolomitized clayey nannofossil ooze of the upper half-couplet. A stratigraphic hiatus separates sedimentary Unit I from Unit II, and was visually characterised by steeply inclined bedding and a rapid change in calcium carbonate content (Shipboard Scientific Party, 1991). Unit III, Cores 133-819A-11H-2 through to -13H-2 (97.0-179.7 mbsf), consists of predominantly rhythmically interbedded bioclastic and micritic oozes. Carbonate contents are similar to those found in Unit II sediments, but

A

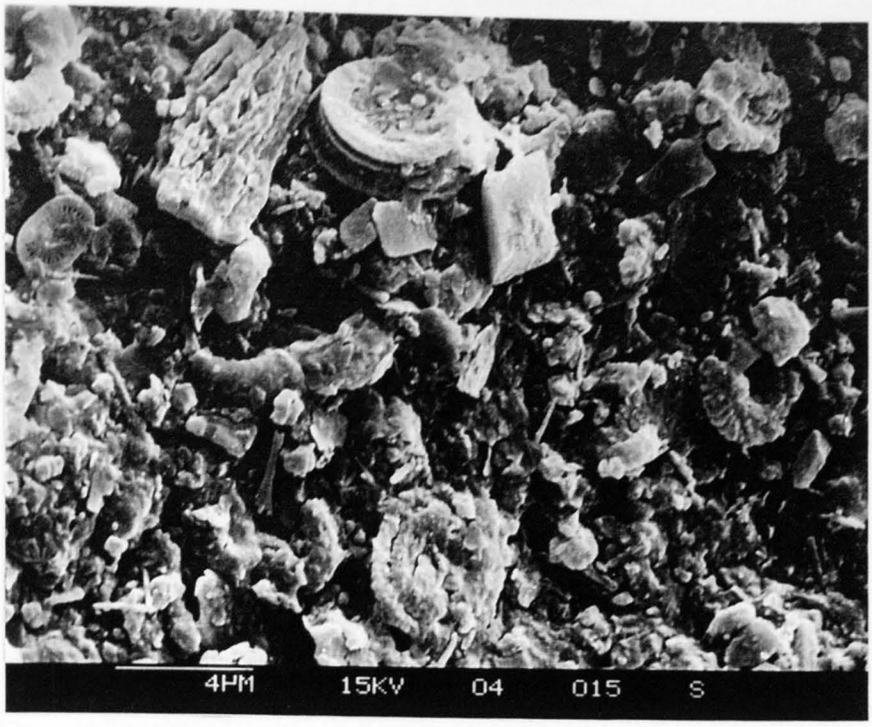

X 4500

B

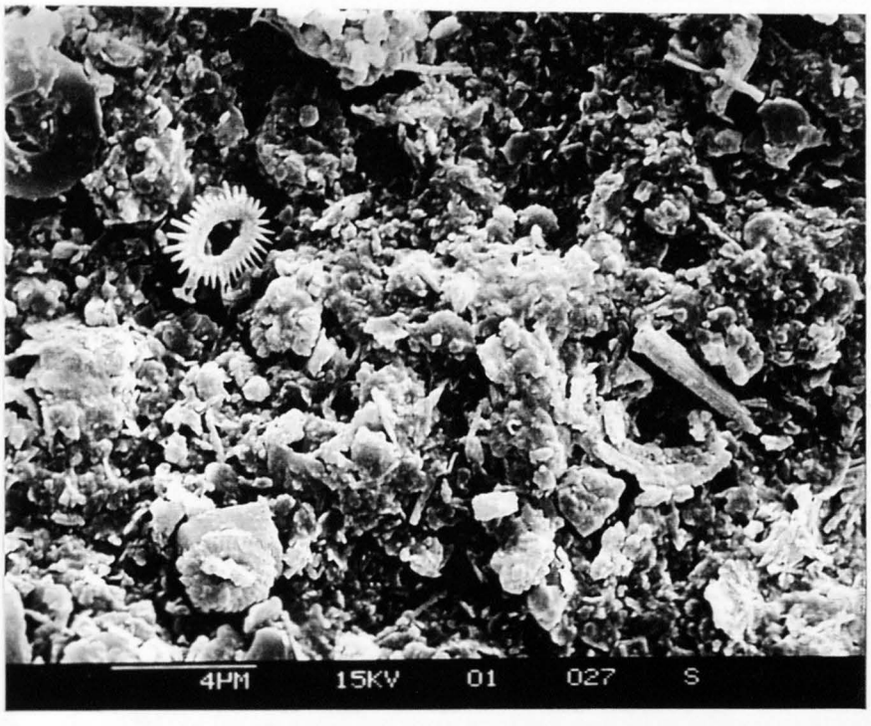

X 4750

Plate 2. Scanning Electron Microscope (SEM) photomicrographs of typical Hole 819A (GBR margin) periplatform muds (<63 μm size fraction). (A) Sample 133-819A-01H01-54/56 (0.54 mbsf) corresponding to an isotopically inferred sea level highstand. (B) Sea level lowstand sample 133-819A-01H05-30/32 (6.30 mbsf).

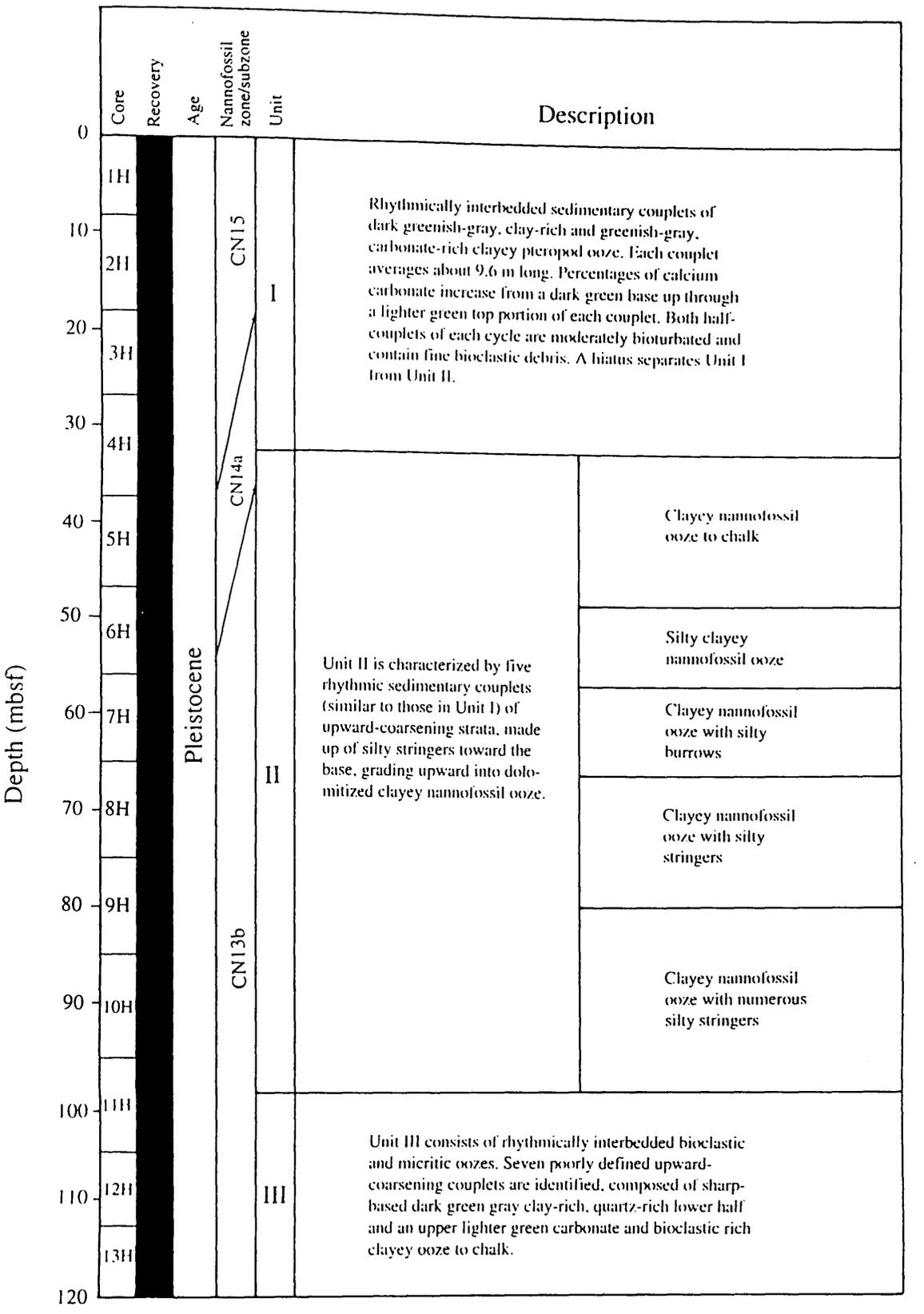

Figure 4.2 Summary chart showing the main lithological units identified in Hole 819A (Shipboard Scientific Party, 1991). Note excellent recovery throughout cored intervals.

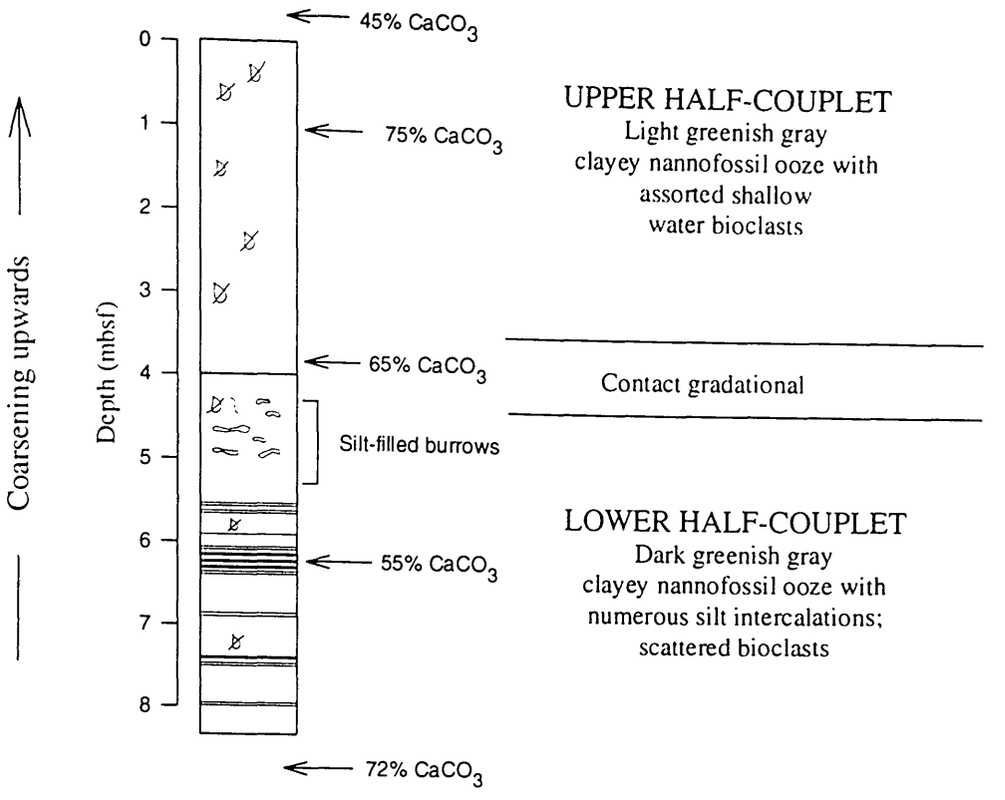

Figure 4.3 Schematic illustration of a typical upward-coarsening sedimentary couplet (cycle E-1 at about 140 mbsf) at Hole 819A (Shipboard Scientific Party, 1991).

Key to graphic logs

Pelagic Sediments

Foraminiferal Ooze

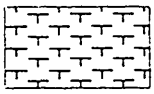

Nannofossil Ooze

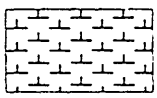

Calcareous Ooze

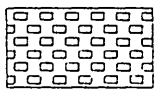

Non-pelagic Carbonate Sediments

Unlithified Rudstone

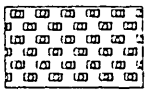

Unlithified Floatstone

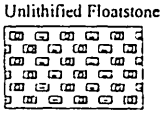

Unlithified Packstone

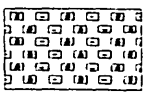

Siliciclastic Sediments

Silty clay/ clayey silt

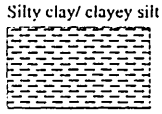

Shells (complete)

Shell fragments

Symbols for drilling disturbance & sedimentary structure

Slump blocks or slump folds

Load casts

Gradational contact

Sharp contact

Graded bedding (normal)

Graded bedding (reversed)

Lithoclast

Isolated pebbles cobbles/ dropstones

Convoluted and contorted bedding

Cross-bedding

Cross-laminae (including climbing ripples)

Concretions/ nodules

Bioturbation, minor (<30% surface area)

Bioturbation, moderate (30-60% surface area)

Bioturbation, strong (>60% surface area)

Interval over which primary sedimentary structures occur

F Fining-upward sequence

C Coarsening-upward sequence

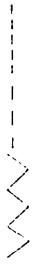

Slightly disturbed

Moderately disturbed

Highly disturbed

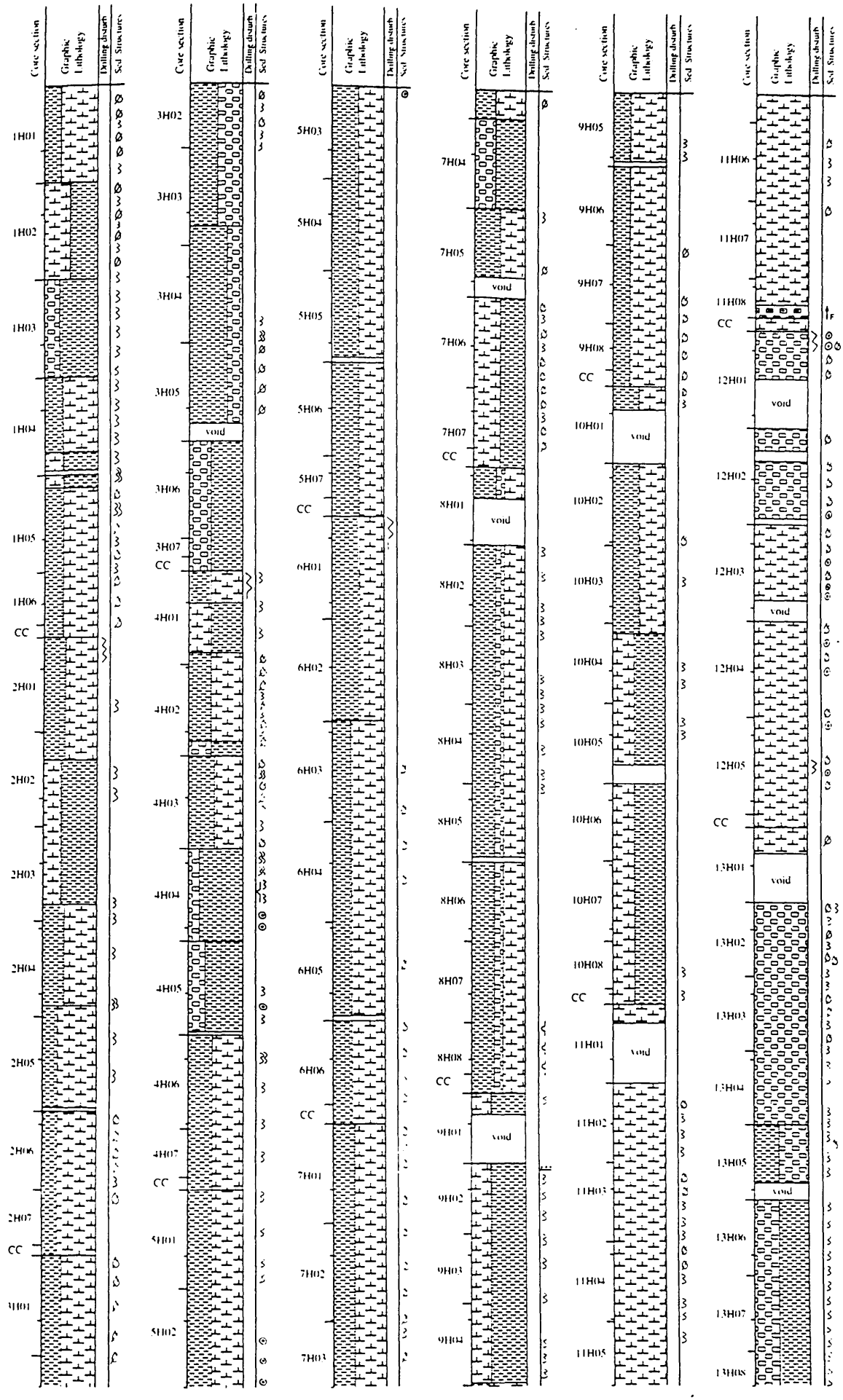

Figure 4.4. General graphic log of the succession in Hole 819A (Shipboard Scientific Party, 1991). Each column represents 20 m of cored sediment. Note that cored intervals (usually 9.5 m in length) have been adjusted for gas expansion. See opposite page for key to symbols.

generally decrease upward in response to increasing proportion of siliciclastic mud. Bioclastic silt-sized grains tend to increase toward the base of the unit, where calcium carbonate contents reach their acme for the site. Seven poorly defined upward-coarsening rhythmic couplets are identified in Unit III, composed of an often sharp-based, dark green grey clay-rich, quartz rich lower half and an upper lighter green carbonate and bioclastic-rich clayey ooze to chalk. Major slumping has disturbed the base of the Unit III. An unrecovered interval between Units III and IV occurs from 179.7-198.1 mbsf. A graphic lithological profile of Hole 819A periplatform sediments is presented in Figure 4.4 (see also Davies *et al.*, 1991).

The general depositional setting for all five sedimentary units has been interpreted as being that of an upper-slope environment, perhaps tapping fluviodeltaic terrigenous sources (Shipboard Scientific Party, 1991). According to the Shipboard Scientific Party (1991), benthic foraminiferal assemblages indicate an upper bathyal paleodepth (200-600 m) for Hole 819A during the Late Quaternary. Tentative interpretation of the sedimentary couplets suggest that the basal clay-rich half-couplets of each sedimentary cycle may relate to periods of sea level lowstand (glacial periods) and enhanced terrigenous influx, while coarser upper portions are related to periods of sea level highstand with enhanced neritic carbonate production and detrital shedding onto the upper-slope (Shipboard Scientific Party, 1991) (see Figure 2.6).

4.2.2 Site 823 (axis of the Queensland Trough)

APC/XCB and rotary core barrel (RCB) drilling recovered an uppermost middle Miocene to Pleistocene, 1011 m thick, sequence of hemipelagic to pelagic sediments, from Site 823 (see Plate 3). Sediment core recovery was excellent with approximately 92 % retrieval. Site 823 sediments are interbedded with numerous gravity flow deposits that are interpreted as turbidites, debris flows and slumps (Watts, 1993). More than 1860 sediment gravity-flow deposits, occur throughout more than 1000 m of sediment cored at Site 823. The majority of these have been interpreted as representing contemporaneous redeposition of periplatform sediments (Shipboard Scientific Party, 1991; Watts *et al.*, 1993). According to the Shipboard Scientific Party (1991) benthic foraminiferal faunal assemblages indicate that the depositional environment remained at lower bathyal paleodepths (1000-2000 m) during the late Pleistocene.

Seven major sedimentary units were recovered from Site 823 (Queensland Trough), of which only the upper two fall within the scope of this study. Figure 4.5 illustrates these major lithologic units and their subdivisions (Shipboard Scientific Party, 1991).

A

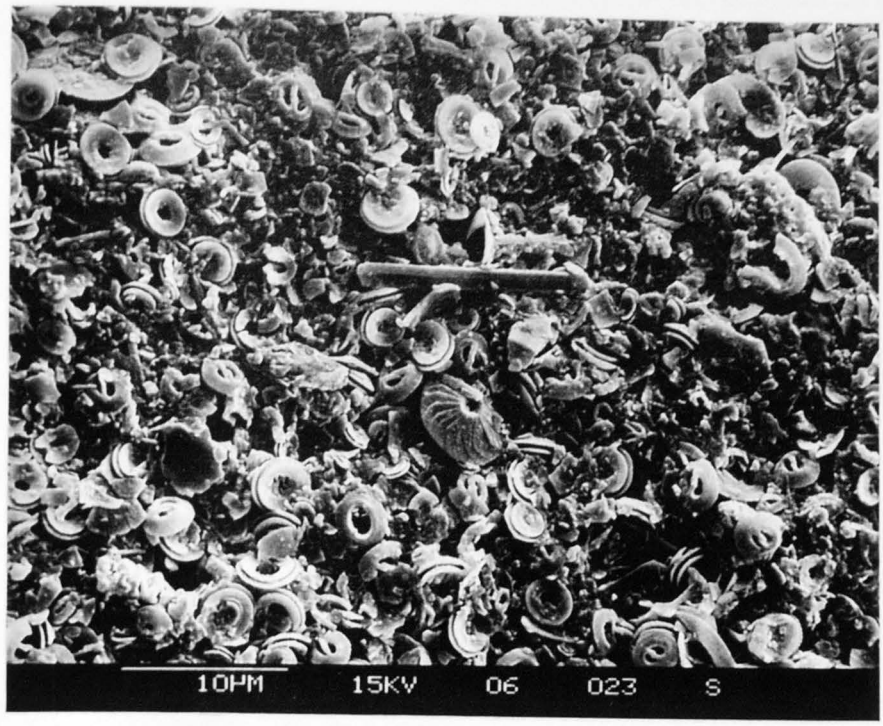

X 2100

B

X 5250

Plate 3. Scanning Electron Microscope (SEM) photomicrographs of typical Hole 823A (Queensland Trough) periplatform muds (<63 μm size fraction). (A) Sample 133-823A-01H02-110/112 (2.60 mbsf) corresponding to an isotopically inferred sea level highstand. (B) Sea level lowstand sample 133-823-04H02-10/12A (26.40 mbsf).

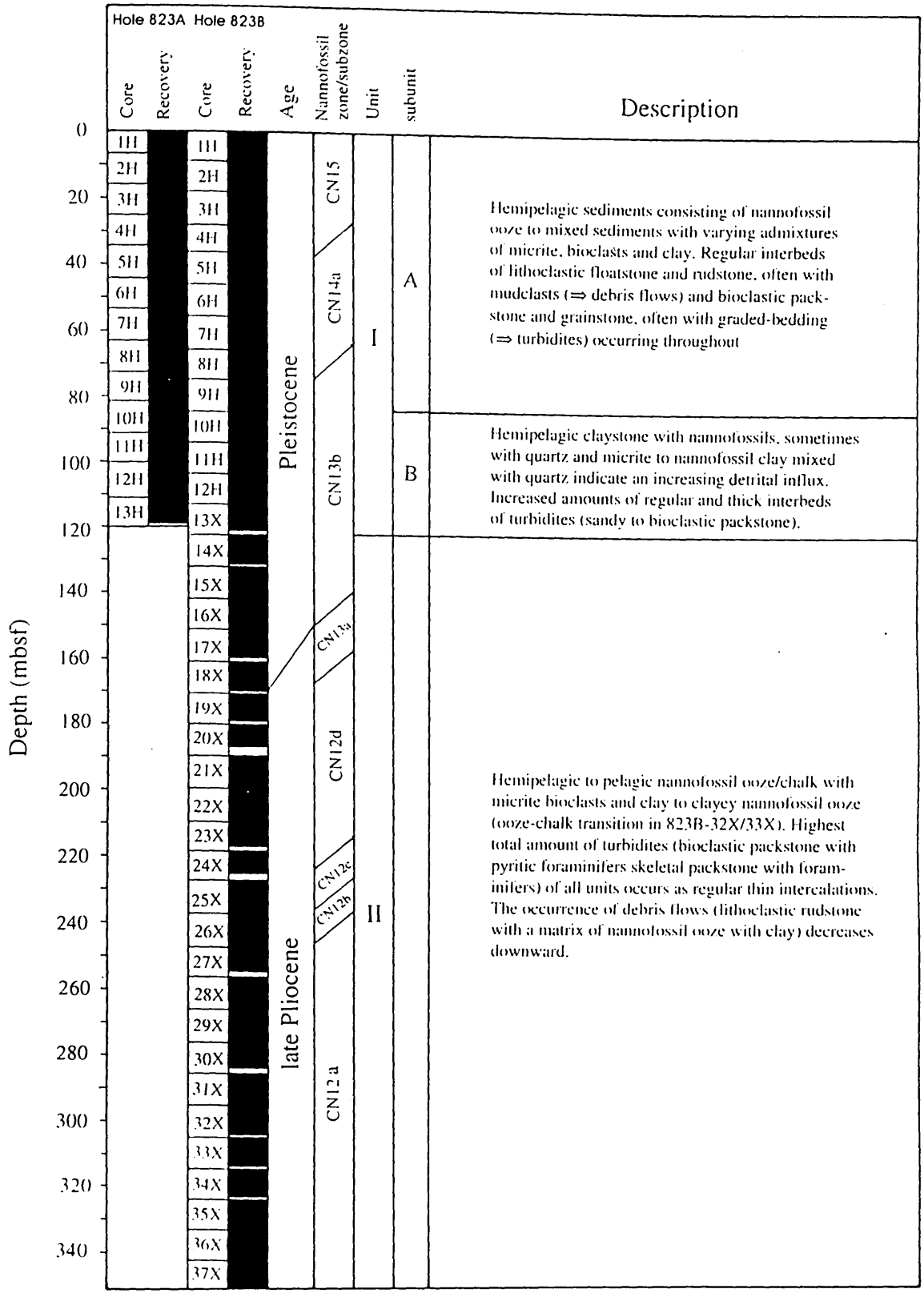

Figure 4.5 Summary chart showing the main lithological units identified at Site 823 (Shipboard Scientific Party, 1991). Note excellent recovery throughout cored intervals.

Key to graphic logs

Pelagic Sediments

Foraminiferal Ooze

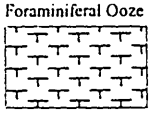

Nannofossil Ooze

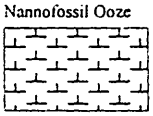

Calcareous Ooze

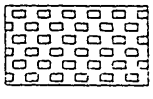

Non-pelagic Carbonate Sediments

Unlithified Rudstone

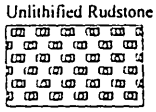

Unlithified Floatstone

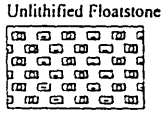

Unlithified Packstone

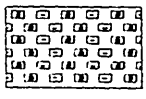

Siliciclastic Sediments

Silty clay/ clayey silt

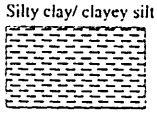

 Shells (complete)

 Shell fragments

Symbols for drilling disturbance & sedimentary structure

 Slump blocks or slump folds

 Load casts

 Gradational contact

 Sharp contact

 Graded bedding (normal)

 Graded bedding (reversed)

 Lithoclast

 Isolated pebbles cobbles/ dropstones

 Convoluted and contorted bedding

 Cross-bedding

 Cross-laminae (including climbing ripples)

 Concretions/ nodules

 Bioturbation, minor (<30% surface area)

 Bioturbation, moderate (30-60% surface area)

 Bioturbation, strong (>60% surface area)

 Interval over which primary sedimentary structures occur

 F Fining-upward sequence

 C Coarsening-upward sequence

 Slightly disturbed

 Moderately disturbed

 Highly disturbed

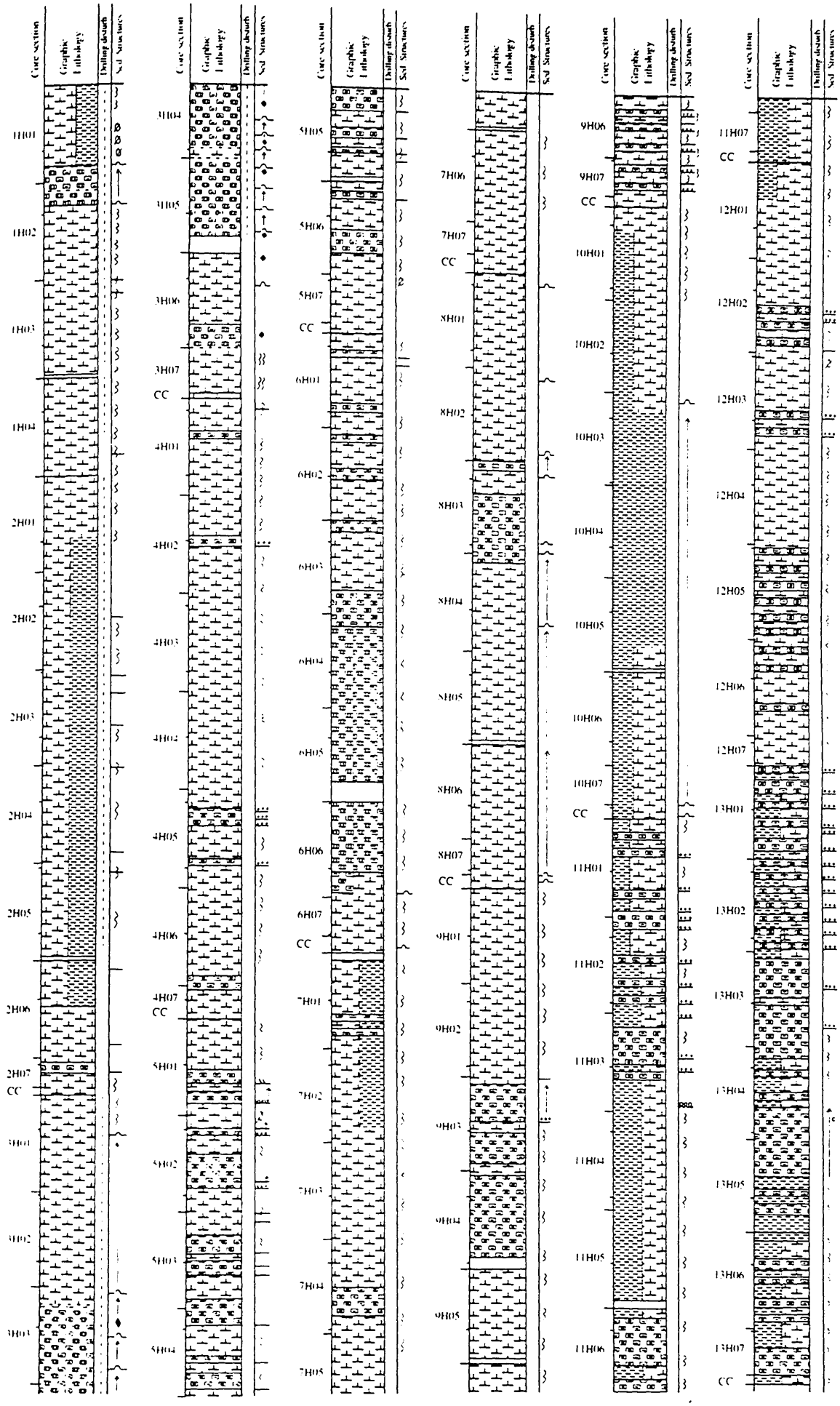

Figure 4.6. Graphic lithological log of the sedimentary succession in Hole 823A. Each column represents 20 m of cored sediment. Note that cored intervals (usually 9.5 m in length) have been adjusted for gas expansion. See opposite page for key to symbols.

In addition a graphic sedimentary log of the periplatform sequence recovered from Hole 823A is presented in Figure 4.6.

Unit I, Cores 133-823A-1H through to 13H (0-119.8 mbsf) were found to consist of pelagic to hemipelagic sediments interbedded with redeposition layers that have been interpreted as turbidites and debris flows (Shipboard Scientific Party, 1991; Watts *et al.*, 1993). Unit I has been divided into two lithological subunits based on differences in clay contents and abundance of gravity flows. Subunit IA: depth 0-85.4 mbsf, consists of light greenish gray nannofossil micritic ooze with clay, foraminifers and bioclasts; clayey nannofossil mixed sediments with micrite, foraminifers and bioclasts; nannofossil ooze with micrite and clay; and clayey nannofossil ooze. These sediments are interbedded with lithoclastic floatstone and rudstone (Dunham, 1962; Embry and Klovan, 1971), often containing mud clasts, that are interpreted as debris flows, and bioclastic packstone and grainstone, often showing normal grading, that are interpreted as turbidites (Shipboard Scientific Party, 1991). Subunit IB: depth 85.4-120.7 mbsf, consists of dark greenish gray claystone with nannofossils and, occasional, quartz and micrite; dark gray nannofossil clayey to clayey nannofossil mixed sediments; clayey nannofossil ooze; and nannofossil clay mixed sediments with quartz. Interbedded layers of gray sandy packstone with foraminifers, quartz and nannofossils and bioclastic packstone with quartz, micrite and nannofossils are interpreted as turbidites.

Unit II, Cores 133-823B-14X through to 37X (120.7-352.75 mbsf) consists of gray to greenish gray hemipelagic to pelagic nannofossil ooze with clay and bioclasts interbedded with gray to dark gray lithoclastic rudstone, and gray to greenish gray bioclastic and skeletal packstone (Shipboard Scientific Party, 1991). Debris-flow and slump deposits are abundant in the upper part of the unit. Turbidites are particularly abundant in this unit and show significant variation in composition, grain-size and bed thickness (Watts *et al.*, 1993). At about 305 mbsf, there is a distinct transition in lithology, from predominately ooze to chalk. In general, the thickness of debris-flow deposits and slumped intervals decreases with depth.

4.3 Sediment Accumulation Rates

Sedimentation rates or sediment accumulation rates (SARs) are critically dependent on the accuracy of the age-model proposed for any marine sequence. Any slight error in the identification or positioning of a isotopic stage boundary could result in a large change in the sedimentation rate, both, above and below the control horizons (McNeill, 1993). In addition, SARs can be greatly affected by a number of other important factors, for example: inaccurate biostratigraphic zonation; the presence of stratigraphic

hiatuses; sediment winnowing and redeposition, and the selective dissolution of metastable carbonate (and silicate) components (Brummer and Eijden, 1992). Unfortunately, variations in these parameters, whether collectively or individually, will make the calculation of accurate fluxes extremely difficult and subject to significant errors. Thus, given the occurrence of numerous minor (and occasional major) stratigraphic hiatuses in the marine sequences from Holes 819A and 823A, and the uncertainties associated with the age models presented for these piston cores (see previous chapter), mass accumulation rates[2] (MARs) or sediment fluxes will not be used in this study.

Figures 4.7 and 4.8 illustrate the depth-age relationships for periplatform sediments recovered from Holes 819A and 823A. The calculated SARs between oxygen isotope stage boundaries (and datums) used in the depth/age conversion of these cores are listed in Table 4.1 (see previous chapter, Table 3.1). The SARs for each oxygen isotope stage were calculated by simply taking the depth (mbsf) for a particular stage and dividing by the corresponding time interval (this assumes a constant rate of sediment accumulation for each isotopic stage). For example, interglacial stage 5 located between 397.5-1055 cm in Hole 823A (corresponding to the interval 71-125 ka) represents 657.5 cm of sediment accumulation over a 54 ka time period, or a SAR of about 12.18 cm/ka. Several notable gaps occur in the depth-age records from Holes 819A and 823A, related to the presence of gravity flow deposits (Shipboard Scientific Party, 1991). These have made the calculation of accurate SARs in these piston cores very difficult.

In general, the depth-age plot for Hole 819A periplatform sediments is characterized by several intervals, punctuated by abrupt changes in the downcore SAR. The first interval extends from about 50 to 170 mbsf (0.86-1.11 Ma) and is distinguished by an extremely high SAR of about 48 cm/ka (see Figure 4.7). The interval between 20 to 50 mbsf (corresponding to the period between 63-86 ka) identifies a second trend with a significantly lower SAR of about 5.2 cm/ka (taking into account the major stratigraphic hiatus at 32.5 mbsf- Shipboard Scientific Party, 1991). The third trend extends from the seafloor to about 20 mbsf (0-63 ka) and has a mean SAR approaching that of the first interval (i.e., about 32 cm/ka). In contrast the Hole 823A record is characterized by a near linear SAR throughout much of the core (see Figures 4.7 and 4.8). The majority of Hole 823A biostratigraphic datums (ignoring the major slump between 16.5-24.5 mbsf) form a near straight line from the Holocene to the mid-

[2]Mass accumulation rate (MAR) is the weight of sediment (or component) accumulating in a specific area over time (generally measured in g/cm^2/kyr).

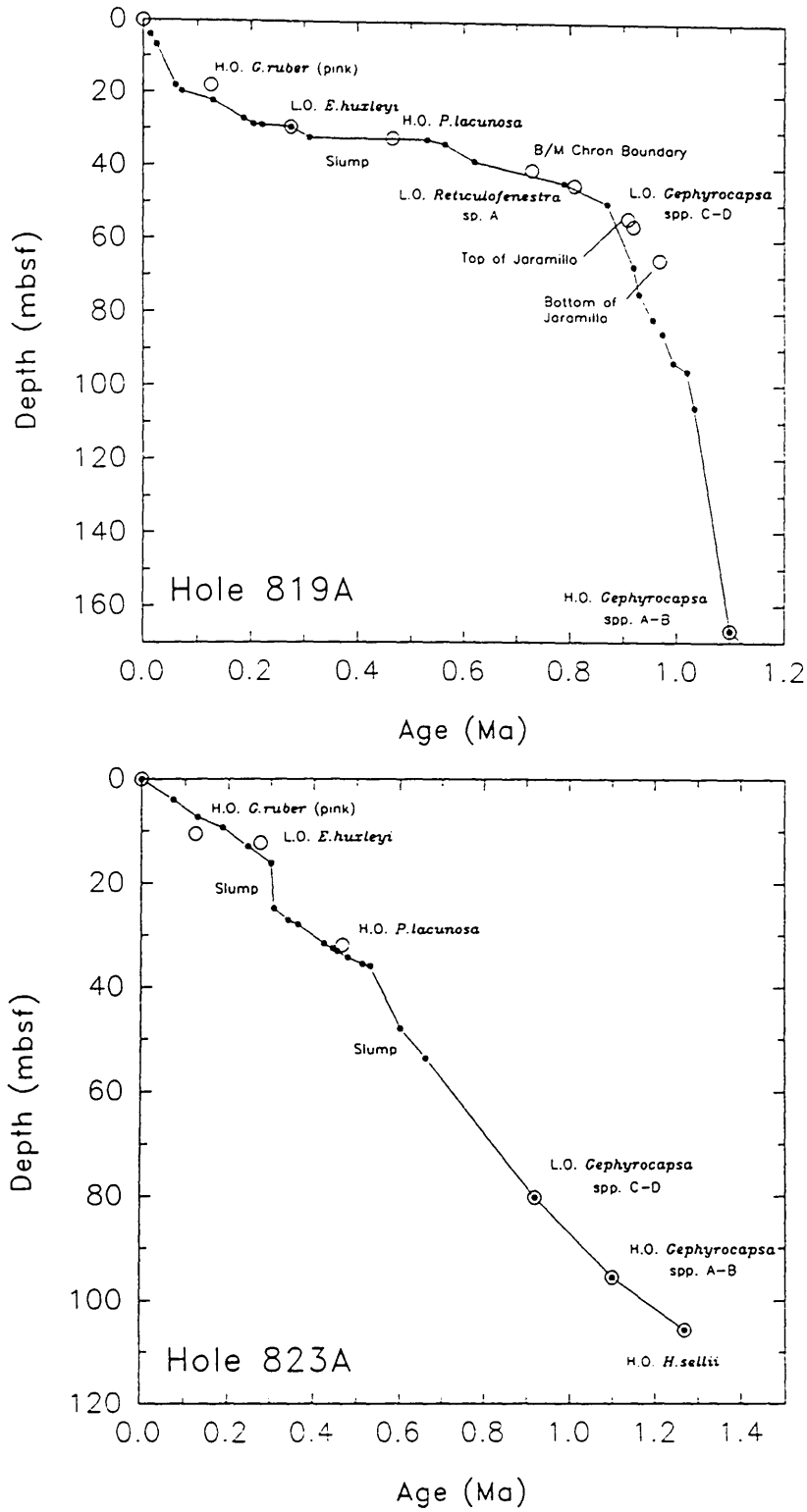

Figure 4.7. Age/depth plots for Holes 819A and 823A based on age models discussed in Section 3.3 (see main text). Biohorizon and magnetostratigraphic datums are shown for reference (open) symbols. In these plots, the nearer horizontal, or shallower, the line connecting datum points the slower the sedimentation rate (or conversely the steeper the line the faster the rate).

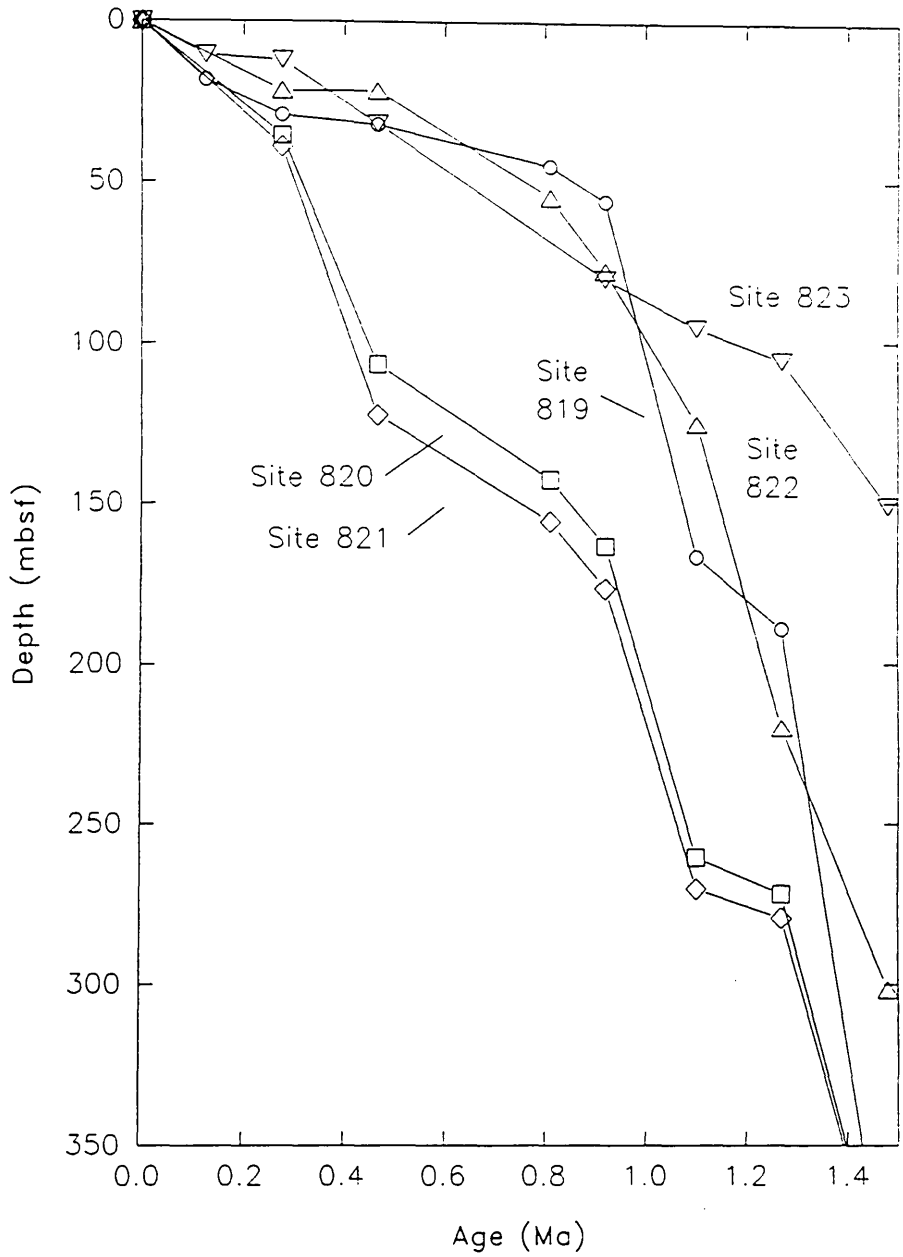

Figure 4.8. Age–depth plots for Queensland margin transect drill localities (Sites 819, 820, 821), Site 822 (26 km north–northwest of Grafton Passage) and Site 823 (Queensland Trough), based on biostratigraphic datums provided by Shipboard Scientific Party (1991) and Wei and Gartner (1993).

Pleistocene. Typical SARs in Hole 823A range from about 5 to 10 cm/ka, with the highest sedimentation rates occurring during the mid to late Pleistocene (i.e., between about 35 to 95 mbsf).

The exact nature of the relationship between sea level (as inferred from the stable oxygen isotope record) and SARs on the northeast Queensland margin is very complicated. Interpretation of the upper part of the Hole 819A record (taking into account the presence of a possible hiatus at, or near, the stage 5/6 boundary- see section 3.5) suggests that interglacial periods are characterized by high SARs (or, conversely glacial intervals are distinguished by low sedimentation rates). However, below about 32 mbsf the precise relationship between SAR and the planktic $\delta^{18}O$ record is difficult to discern, although there is some suggestion that interglacial periods are slightly more expanded than corresponding glacial intervals (see Figure 3.1). Similarly, in the record from Hole 823A, glacial periods tend to be more condensed, while interglacial periods are expanded (see Table 4.1).

Disregarding the major stratigraphic hiatus in Hole 819A, the SAR follows a near identical pattern to that observed in adjacent ODP Leg 133 Sites 820 and 821: a relatively high rate of between 28 to 42 cm/ka during the mid to late Pleistocene (1.10 to 0.93 Ma); followed by a slightly lower of rate of about 6 to 12 cm/ka from 0.93 to 0.465 Ma; and lastly a more modest rate of approximately 35 to 49 cm/ka between 0.465 to 0.275 Ma; and again a slightly lower rate of 10.3 to 11.3 during the latest Pleistocene (0.275 to 0 Ma) (based on the nannofossil datums provided by Wei and Gartner, 1993- see Figure 4.8). These general trends are more difficult to discern at Site 822 (located approximately 26 km to the north of the Queensland margin transect sites), and appear to be absent in Hole 823 (Queensland Trough).

The general similarity of the depth/age profiles, between ODP Leg 133 Sites 819, 820 and 821, reflect the close proximity of the sites to each other, whereas, sedimentation rates in Hole 823A reflect the more distal setting of this core, less under the influence of shallow water sedimentary processes occurring on the Queensland continental shelf. In Hole 823A, SARs are relatively high compared to many pelagic to hemipelagic depositional settings but are comparable to those associated with many highly productive reef and periplatform environments (Tucker and Wright, 1990). The high sedimentation rates in Hole 823A are probably due to the high incidence of gravity flow deposits at this site (Shipboard Scientific Party, 1991; Watts *et al.*, 1993).

Table 4.1. Sediment accumulation rates (SARs) for periplatform sequences recovered from Holes 819A and 823A based on the age models discussed in chapter 3 and the nannofossil biostratigraphy provided by Wei and Gartner (1993).

	Hole 819A (cm/ka)	Hole 823A (cm/ka)		Hole 819A (cm/ka)	Hole 823A (cm/ka)
Stage 1	32.0	6.8 ?	Stage 12	-	4.8
Stage 2	23.5	-	Stage 13	-	3.1 ?
Stage 3	32.9 (18.0)	-	Stage 14	-	10.5 ?
Stage 4	12.5 (25.0)	6.0	Stage 15	8.3	-
Stage 5	4.6 (11.1)	5.8	Stage 16	-	-
Stage 6	8.3	3.5	Stage 17	-	-
Stage 7	-	6.4	Stage 18	-	-
Stage 8	-	5.4 ?	Stage 19	-	-
Stage 9	-	6.3 ?	Stage 20	-	-
Stage 10	-	3.8	Stage 21	-	-
Stage 11	-	5.9	Stage 22	-	-

Numbers in brackets refer to SARs based on revised stage assignments discussed in section 4.6. ? denotes uncertainty, dashes indicate the absence of sufficient data to calculate SAR..

Nannofossil datum (Wei and Gartner, 1993)	Hole 819A cm/ka	Hole 823A cm/ka
Core top - L.O. *E.huxleyi* (0-0.275 Ma)	10.7	4.4
L.O. *E.huxleyi* - L.O. *P.lacunosa* (0.275-0.465 Ma)	1.6	10.4
L.O. *P.lacunosa* - L.O. small *G.spp.* C-D (0.465-0.92)	5.2	10.6
L.O. small *G.spp.* C-D - L.O. small *G.spp.* A-B (0.92-1.10 Ma)	61.6	8.5
L.O. small *G.spp.* A-B - H.O. *H.sellii* (1.1-1.27 Ma)	13.2	6.0
H.O. *H.sellii* - H.O. *C.macintyrei* (1.27-1.48 Ma)	-	21.5

4.4 Variations in Particle Size Distribution in response to changes in late Pleistocene Sea level

Particle size is a fundamental property of sedimentary materials that may tell us much about their origins and history (McCave and Syvitski, 1991). Detailed studies on sediment grain-size characteristics and distribution patterns can also provide information on the depositional processes and flow conditions (Middleton, 1976), and combined with studies of sediment composition and mineralogy, can be most useful in facies description and palaeoenvironmental analysis. In this section, particle size analysis measurements for the sedimentary sequences recovered from Holes 819A and 823A are described and correlated with adjacent ODP Leg 133 drill sites in order to obtain a better understanding of the influence of variations in late Pleistocene sea level (as inferred from the stable oxygen isotope record) and climate change, on the mixed carbonate-siliciclastic grainsize distribution.

4.4.1 Methods

Two analytical methods were employed in order to determine particle size variations in Hole 819A and Hole 823A pelagic to hemipelagic sediments.

Method 1

Discrete sediment samples (taken from shipboard piston cores) were oven-dried at 60° C for 24 hours, weighed, and a 0.5 g subsamples taken from each. Samples were then wet sieved over a mesh N^{o}·250 (63 μm aperture) stainless steel sieve. Both sediment fractions, fine (<63 μm) and coarse (>63 μm) (hereafter referred to as the mud and sand fractions, respectively) were retained, oven-dried at 60°C, and later weighed to five decimal places. Mud fraction and sand fraction dry weights were then expressed as percentages of the original dry sample weight.

Method 2

Hole 819A subsamples (0.5g) were analysed for particle size variations using a Coulter LS-100 particle size analyser (hereafter referred to as the LS-100). This precision instrument uses the principle of Fraunhofer diffraction of laser light in which light falling on suspended sediment particles is deflected (diffracted) by an amount that depends on, amongst other things, the size of the particle (McCave and Jarvis, 1973, 1986; Agrawal *et al.*, 1991). The LS-100 resolves grain sizes into 72 separate particle size classes ranging from 0.4 to 900 μm with an exact logarithmic progression (Loizeau *et al.*, 1994). LS-100 particle size analyses provide data on the abundance of silt (3.91-63 μm), clay (<3.91 μm), very fine sand (63-125 μm), fine sand (125-250 μm) and medium sand (250-500 μm) (Tucker, 1981). In addition, the LS-100 provides

data to determine the abundance of coarse silt (>31 μm) for distinguishing between mudstones and wackestones (Dunham, 1962).

Sediment subsamples were allowed to soak overnight in mains water, to facilitate sediment deflocculation. After a visual check for good dispersion, the samples were wet-sieved through a mesh N°·32 (500 μm) stainless steel sieve, and the suspension retained. Sample volume was made up to approximately 150 ml, using degassed mains supply water (Loizeau *et al.*, 1994). During the sieving procedure, occasional scattered shell fragments and grains greater than the upper running limit of the Coulter LS-100 particle size analyser (i.e., approximately 900 μm) were found in some of the sediment samples (this material was removed prior to sample analysis, accurately weighed and later included in the calculation of downcore mean particle size). Samples were further disaggregated with ultrasound for about 3 minutes before being analysed by the LS-100. No chemical deflocculents or surfactants (i.e., Calgon® or Sodium carbonate) were used in the preparation of the samples prior to analysis (see Matthews, 1991). The software used to run the LS-100 analyser unit and to compute grain size distributions is Coulter® LS100/130, version 1.44. A detailed appraisal of the accuracy, precision, and resolution of particle size measurements made by the Coulter LS-100 particle size analyser, in relation to other sizing techniques, is provided by Loizeau *et al.* (1994), and further discussion is beyond the scope of this study.

Unfortunately because of the limited size of Hole 823A shipboard subsamples (approximately 10 g dry weight) and the priority given to extracting reliable stable isotope signatures (both planktonic and benthic records) for the sequence at Site 823, particle size analyses using the LS-100 were only carried out on Hole 819A periplatform sediments. These results are presented below.

4.4.2 Description of the particle size variations in Queensland margin periplatform sediments

4.4.2.1 Hole 819A (upper-slope of the GBR)

Downcore variations in the proportion of mud (as determined using the wet sieving method- see above) and mean particle size (μm) (using the Coulter Counter), plotted against the planktic $\delta^{18}O$ record for the sequence recovered from Hole 819A, are illustrated in Figures 4.9 and 4.10, respectively. Particle size distribution data are presented in Appendix B, Table B.1. Typical mud content values for Hole 819A sediments range between 80 to 90 %, with occasional minima at or slightly below 70 % (by weight). The amplitude of fluctuations in mud content (and mean particle size) within the sequence at Hole 819A is significantly higher above 32.5 mbsf (position of a

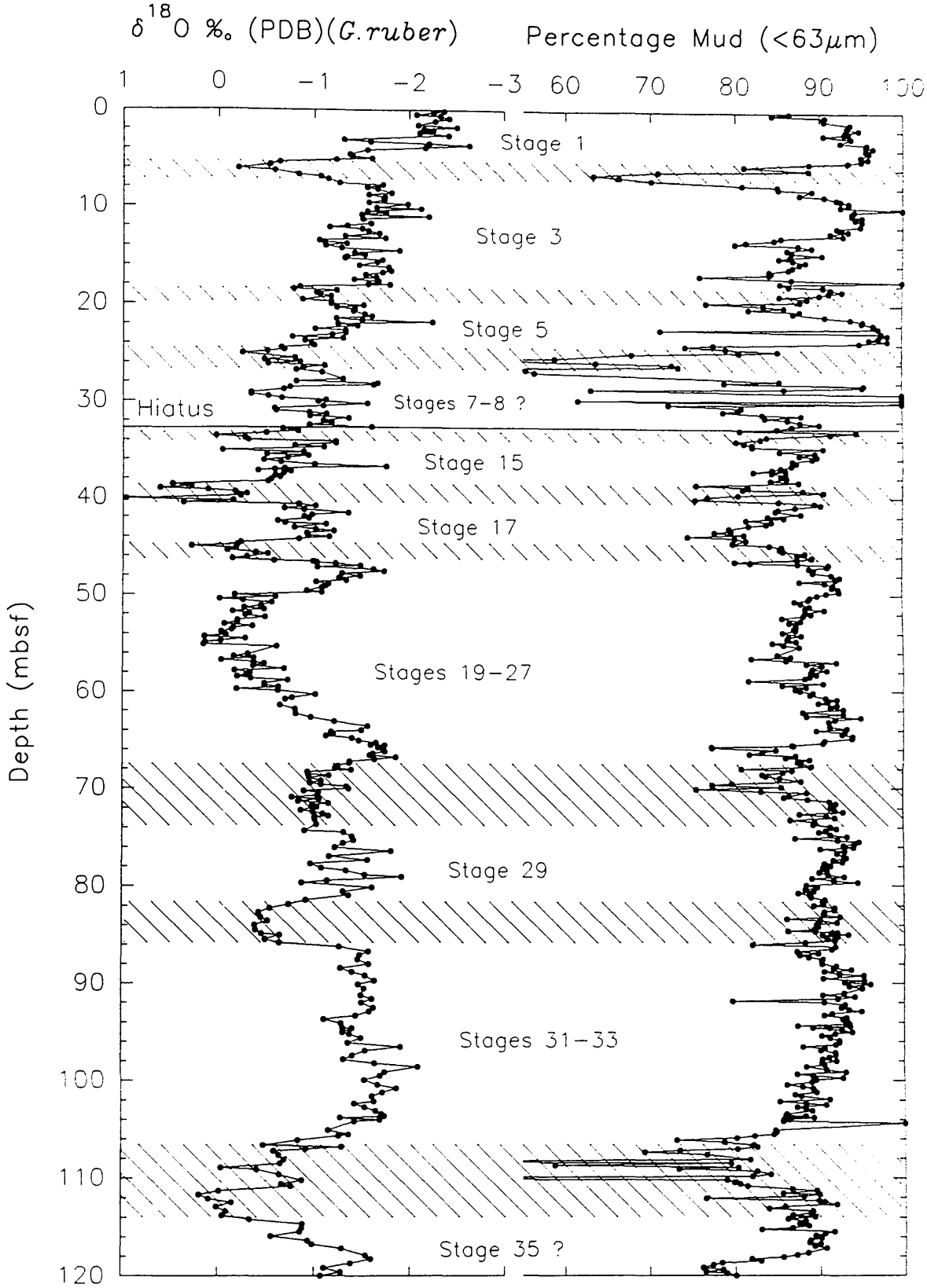

Figure 4.9. Comparison between percentage mud content and planktic $\delta^{18}O$ values, in Hole 819A. Note the presence of a major stratigraphic hiatus at 32.5 mbsf (Shipboard Scientific Party, 1991).

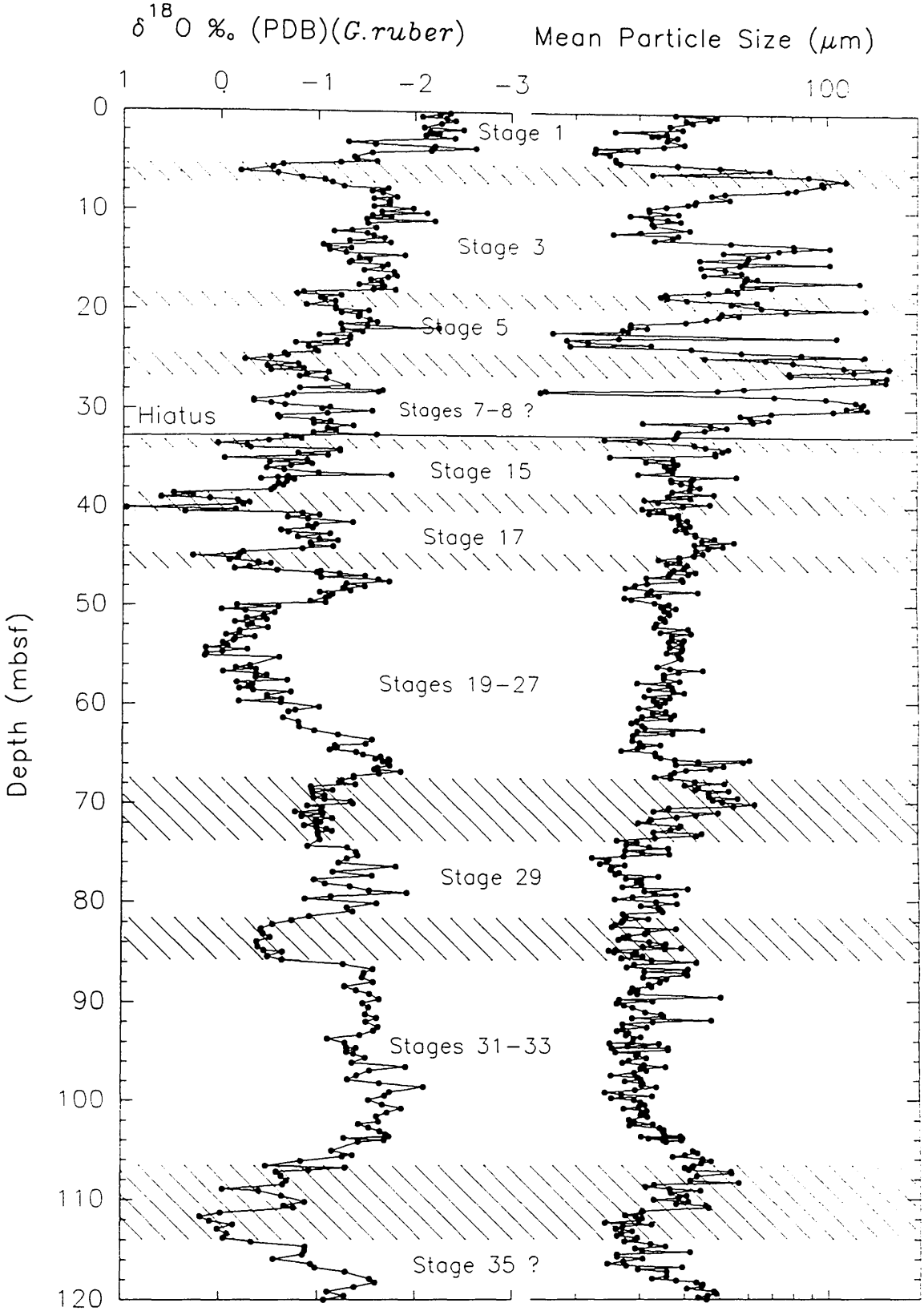

Figure 4.10. Mean particle size (μm) and planktic $\delta^{18}O$ values in Hole 819A, plotted against depth (mbsf). The particle size data has been produced using a Coulter LS−100 particle size analyser. Note that the particle size data has been plotted on a logarithmic scale.

major stratigraphic hiatus- Shipboard Scientific Party, 1990), than below 32.5 mbsf. Tentative interpretation of the mud content curve suggests a gradual decrease in mean value from the core top down to about 40 mbsf (~ Stage 16). Below 40 mbsf, mean mud values increase to a maximum of about 90 % at 95 mbsf, then decline to approximately 80 % at 120 mbsf. As expected, the mean particle size curve is the antithesis of that for percentage mud (i.e., when the mud content is high the mean particle size is low). Mean particle size varies from about 16 μm to 63 μm and between 16 μm to 150 μm, for sediments below and above 32.5 mbsf, respectively.

The relationship between percentage mud content and planktic $\delta^{18}O$ value is very complicated (see Figure 4.9). Below 32.5 mbsf, a clear association between these two parameters is difficult to establish. However, above 32.5 mbsf, tentative interpretation of the grain-size and isotopic records suggest that glacial periods are characterized by low percentages of mud (or conversely high sand content), and interglacial periods are characterized by high mud content. Although broadly similar, both the grain size and planktic $\delta^{18}O$ records are significantly out of phase in places; for example, during glacial Stages 2 the peak in percentage sand content clearly occurs prior to the glacial maxima (see Figure 4.11). Similar offsets in peak position can also be seen in the mean particle size record (see Figure 4.10). For example, the broad peaks centred on 68 mbsf and 106 mbsf (stages 28 and 34, respectively), clearly occur slightly later than the corresponding isotopic enrichment events.

Figure 4.12 illustrates a smoothed (3 point average) version of the LS-100 grain size distribution data, plotted alongside the planktic $\delta^{18}O$ record, for Hole 819A sediments. The original (unsmoothed) data is presented in Appendix B, Table B.2. Note that because of the scarcity of particles greater than 500 μm (i.e., <2 %) coarse sand results are not included in Figure 4.12. In general, the LS-100 analyses confirm the dominance of mud in Hole 819A samples, as indicated by the sieving method outlined above. In addition, LS-100 data suggest that clay-sized particles (<3.91 μm) are subordinate, in total abundance, to silt grains (3.91-63 μm) throughout the full length of the Hole 819A record. Further, the LS-100 particle size distribution results suggest that the majority of Hole 819A sediments can be classified as wackestone/ packstones (i.e., >10 % grains between >0.03 to <2 mm), using the terminology of Dunham (1962) (see Figure 4.12).

In general, Hole 819A sediments contain about 70-72 % silt, 10-12 % clay, 10-14 % very fine sand and between 2-3 % fine sand. Only in the upper 35 m of the core is medium sand present in significant quantities. Coarse sand (>500 μm) is generally

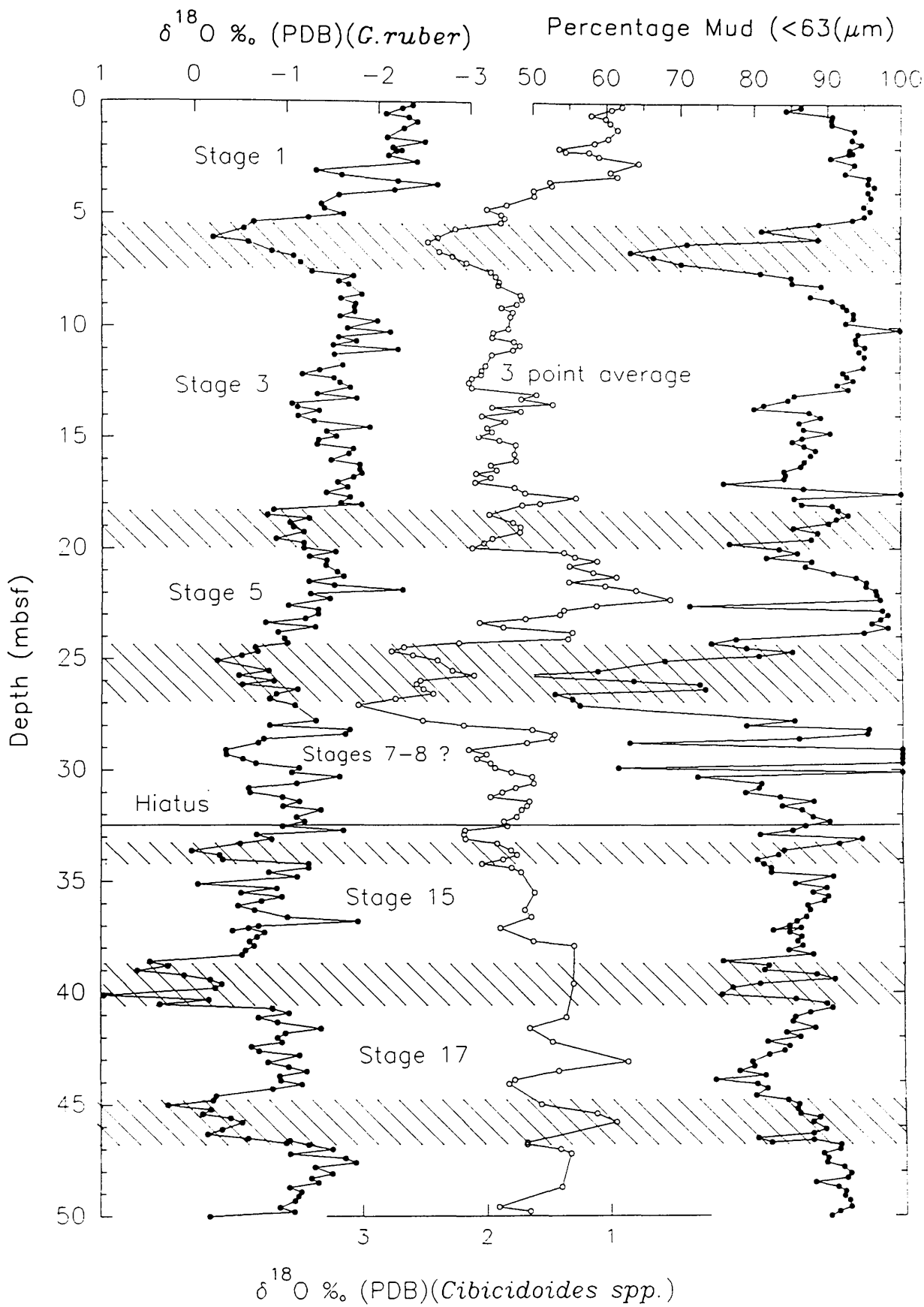

Figure 4.11. Diagram illustrating the relationship between percentage mud content and the foraminiferal oxygen isotope records in the upper 50 m of the sequence from Hole 819A. Note that the benthic. isotopic record has been smoothed using a 3 point average.

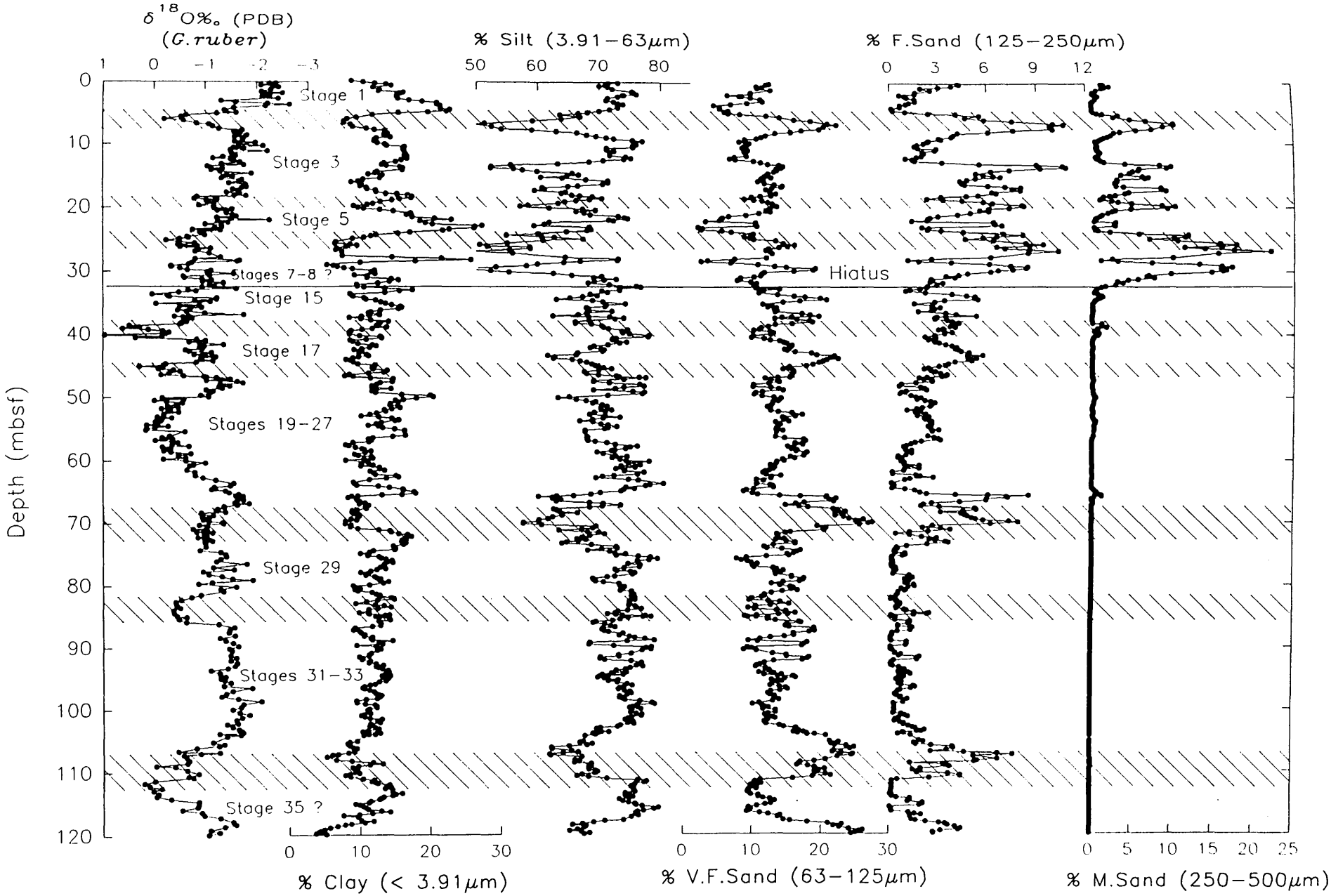

Figure 4.12. Grain-size distribution characteristics of Hole 819A bulk sediments, as generated using the Coulter LS-100 particle size analyzer.

absent or rare in Hole 819A sediments. In common with the mean particle size and mud content records, the LS-100 particle size distribution data display greater amplitudinal variation in value in the upper 32.5 m of the core, than in the lower part of the record. Similarly, the very fine-, fine- and medium sand size fractions all display significant shifts in peak position, relative to planktic $\delta^{18}O$ values, comparable to those seen in the mud content (sieving method) record.

4.4.2.2 Hole 823A (Queensland Trough)

The downcore variation in percent mud content and the planktic $\delta^{18}O$ record for Hole 823A sediments, are illustrated in Figure 4.13. Mud content data are tabulated in Appendix B, Table B.3. In general, the downcore percentage mud content for Hole 823A sediments is characterised by large fluctuations in amplitude, particularly in the lower part of the record (i.e., below about 50 mbsf). Mud content values in Hole 823A hemipelagic sediments are slightly higher than those found at Site 819, and typically range between about 85 % to 95 %, with occasional mud content values less than 75 %. There is little evidence to suggest any significant long-term trend or change in mean downcore mud content value at Site 823.

The relationship between percent mud content and the planktic $\delta^{18}O$ record, at Site 823, is very complex, particularly given the small scale fluctuations in mean mud content seen in the upper part of the sequence (see Figure 4.13). Tentative interpretation of these records suggest, however, that interglacial or isotopically light periods are characterised by high percentage mud content and, conversely, glacials or isotopically heavy intervals are dominated by low percentage mud content. Notable exceptions to this general association occur, for example, during stable oxygen isotope stages 10 and 11 (see Figure 4.14). In the lower part of the sequence in Hole 823A (i.e., below about 50 mbsf) no clear relationship seems to exist between the percentage mud content and isotopic value.

4.4.3 Particle size distribution variations from the outer continental shelf, upper slope, to the Queensland Trough Basin (Sites 821 through to 823) and onto the Queensland Plateau (Sites 817/ 818)

Having extracted particle size distribution data for both Hole 819A and Hole 823A the question now arises as to how representative are these records to those from adjacent Leg 133 drill sites, and how do these grain-size distribution records compare to those from sites located on the relatively isolated Queensland Plateau? In order to answer these, and other questions, the grain size records from these holes are compared and correlated with other particle size records collected during Leg 133.

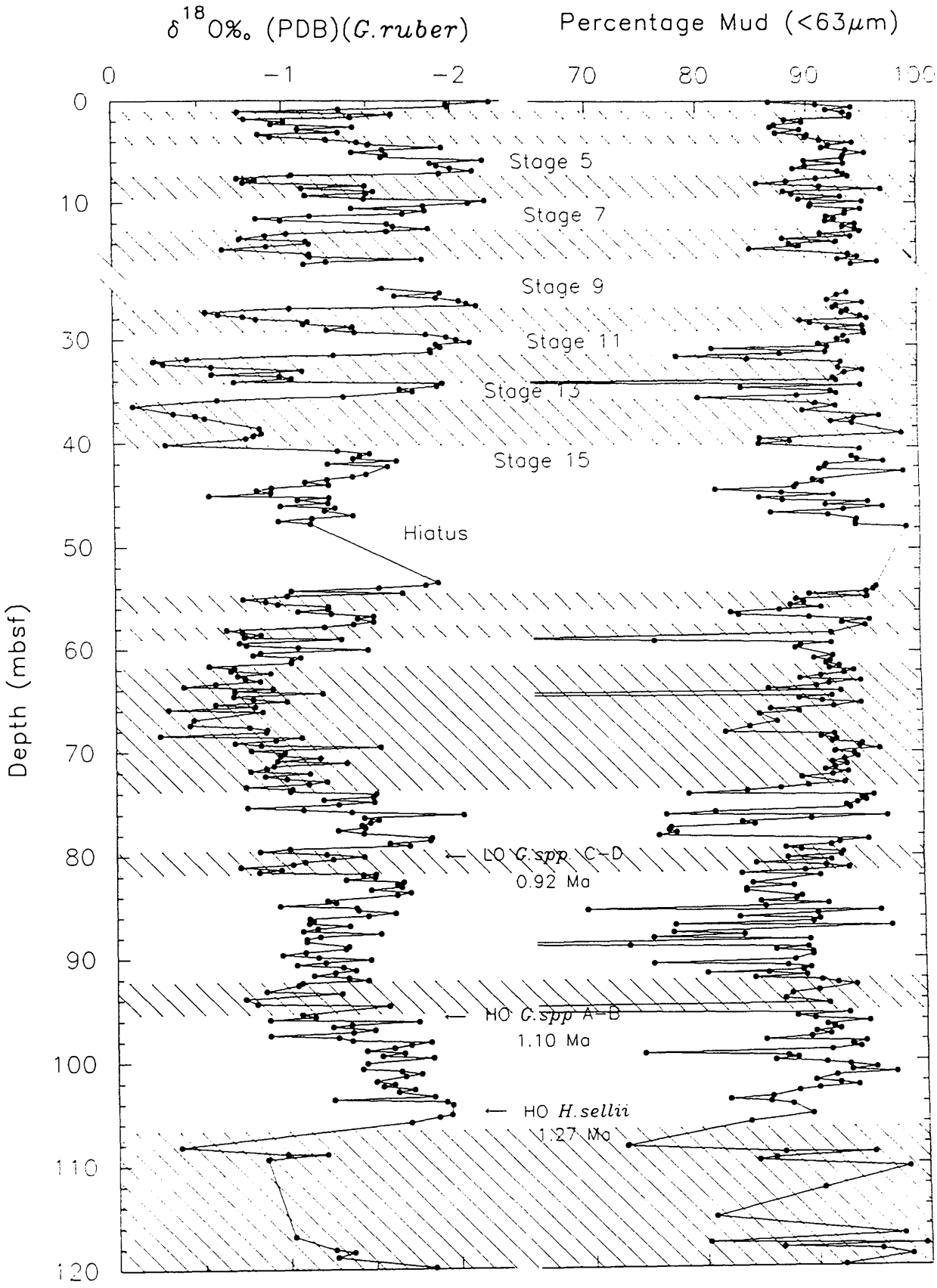

Figure 4.13. Comparison between the percentage mud content and planktic oxygen isotope values in Hole 823A. Note the presence of major sampling hiatus (slump) between 16.5–24.9 mbsf.

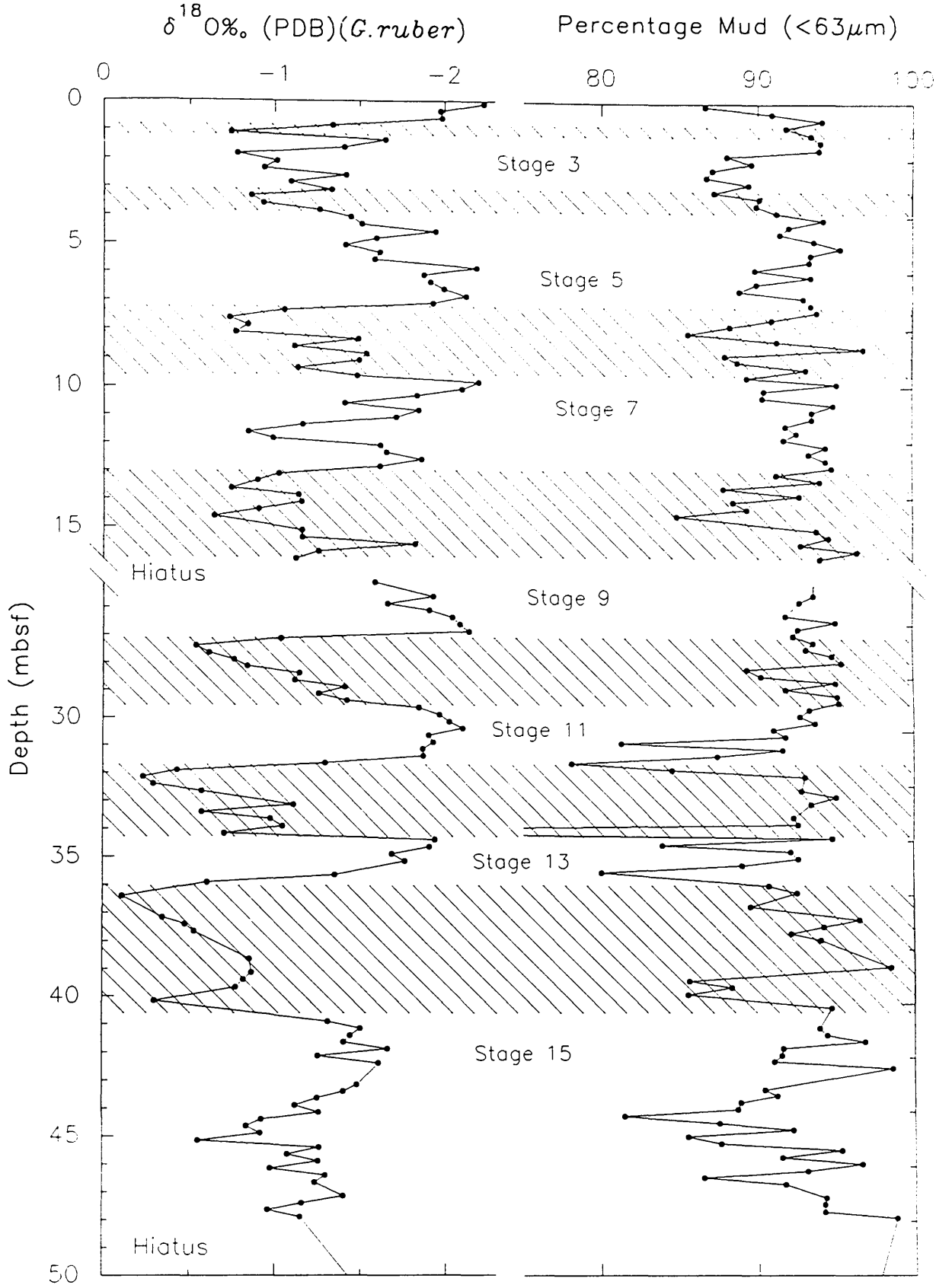

Figure 4.14. Comparison between the percentage mud content and planktic oxygen isotope values for the upper part of the sequence from Hole 823A. Note the presence of a major hiatus between 16.5 and 24.9 mbsf.

The percentage of fine fraction, or mud (<63 μm) content, in Queensland margin transect Holes 821A through to 823A, are illustrated in Figures 4.15 and 4.16. Unfortunately high resolution percentage mud content data is only available for the upper 23 m of the sequence from Hole 821A. Thus, any correlation with this site is severely restricted unless the downcore variation in "fine grains" (<150 μm) (Konishi and Ikehara, pers comm., 1991) is used as a substitute or proxy for the limited percentage mud content data, in Hole 821A. In Figure 4.14 this alternative grain-size distribution data has been plotted alongside the limited Hole 821A mud content values, in order to aid correlation with neighbouring ODP Leg 133 drill sites.

Comparison of the various Queensland margin transect mud content records (Sites 821 through to 823) suggests an outer-shelf to basin gradient of decreasing sand content (or conversely increasing mud content) with distance from the Queensland mainland. In general, mud content values at Hole 821A (present water depth 212 m) range from about 35 to 85 %, with a mean value of about 80 % (Davies and Peerdeman, pers. comm., 1992). By comparison, the more distal Site 823 (1637.8 m water depth) hemipelagic sediments contain between about 80 to 94 % mud, with an average value of about 90 %. In addition, the percentage mud records from Hole 821A through to Hole 819A display a significant proximal to distal decrease in the difference in average mud content between glacial and interglacial periods. For example, the difference in mean mud content between interglacial stage 1 and glacial stage 2 is approximately 55 %, 45 % and 25 % for Hole 821A, Hole 820A and Hole 819A sediments, respectively (see Figure 4.16).

In general, excellent correlation can be achieved between the short-term (Late Pleistocene-Recent) mud content records from Sites 820 and 819. For example, the prominent peaks in sand content associated with glacial stages 2 and 6 can be traced between each of the sites with comparative ease (see Figure 4.16). However, correlation of these records with the Hole 821A and Hole 823A sequences has proved more difficult. In Hole 823A the condensed nature of the record, coupled with low amplitudinal fluctuations in mud content value, particularly in the upper 30 m of the sequence, have made correlation highly speculative. Similarly, correlation with the mud content record from Hole 821A, is fraught with difficulties, especially given the absence of a reliable oxygen isotope record below late stage 3 (Kroon *et al.*, 1993), and doubts concerning the integrity of the stratigraphic record between about 20 to 40 mbsf (i.e., the condensed nature of the record between late stage 3 and the recorded nannofossil datum F.O. *E. huxleyi* (0.275 Ma) at 35.8 mbsf (Wei and Gartner, 1993)

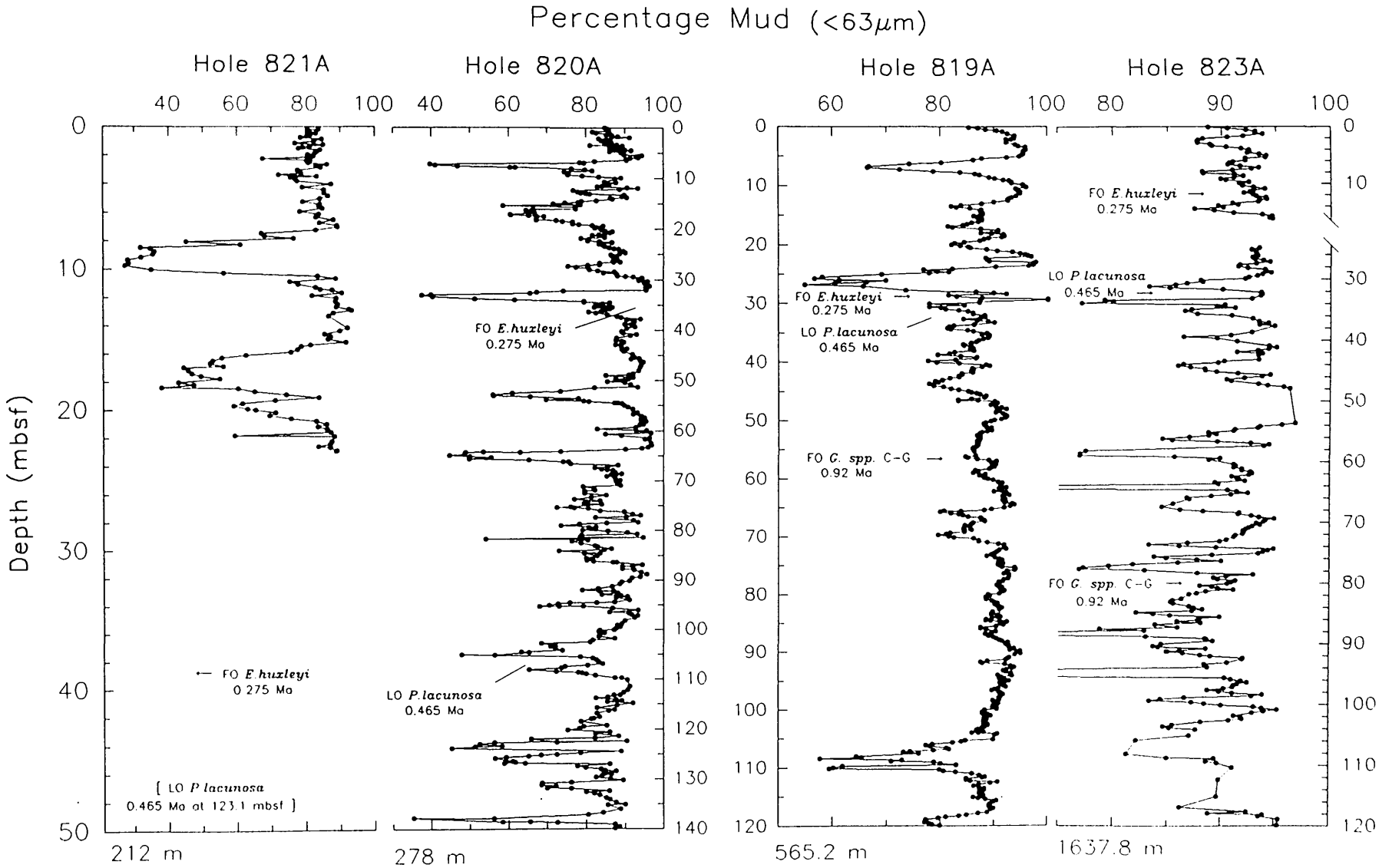

Figure 4.15. Downcore variations in percentage mud (<63μm) content in Queensland margin transect sediments (Holes 821A to 823A). Present day water depths are given at the bottom of each plot.

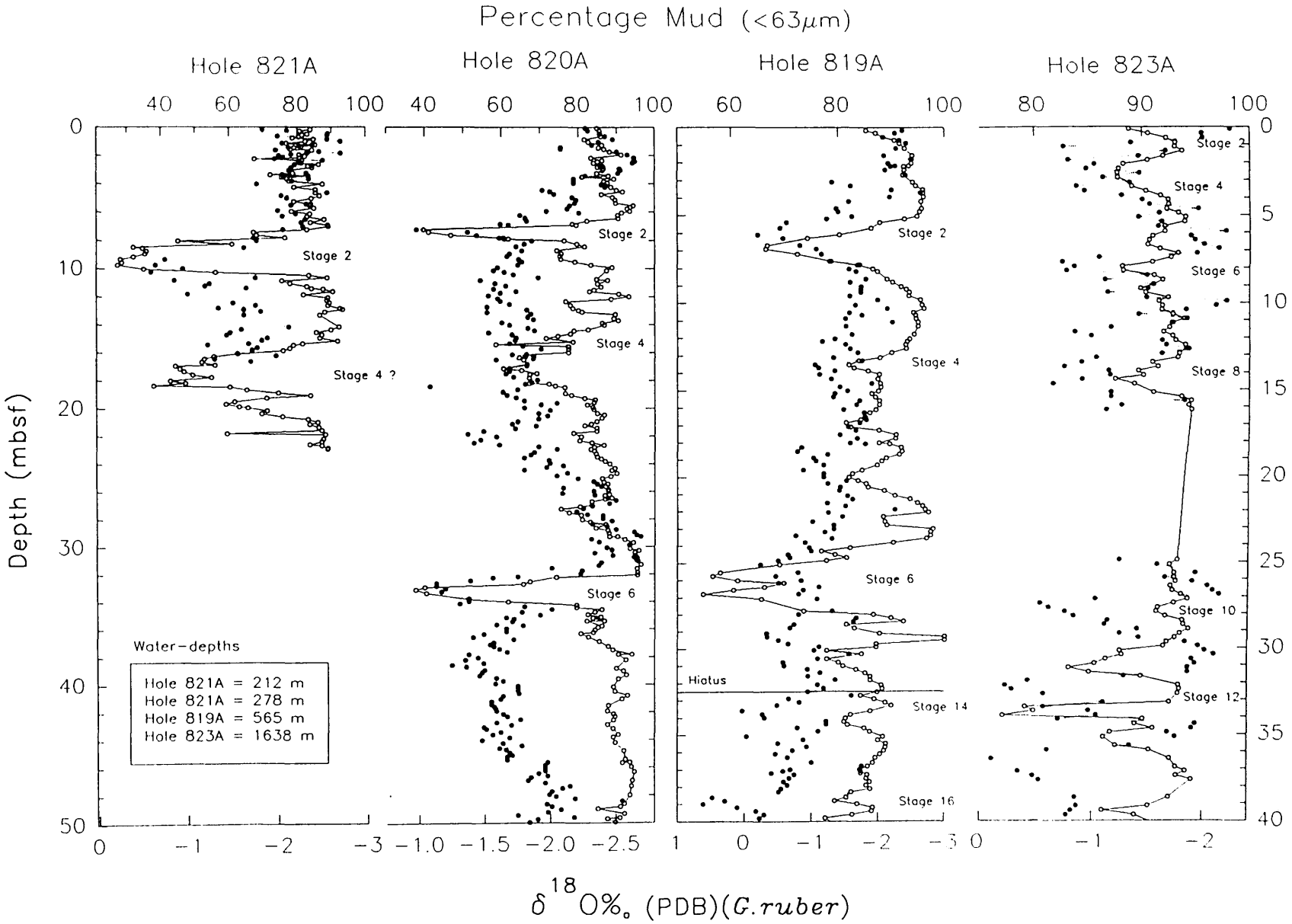

Figure 4.16. Comparison between the percentage mud content in Queensland margin transect cores. The planktic oxygen isotope record for each record is given for reference (dotted line/closed symbols).

would suggest the presence of a major stratigraphic hiatus?). Problems with inter-hole correlation also occur in the lower parts (i.e., below about glacial stage 6) of the mud content records from Sites 821 through to 823. These are largely due to inconsistencies between the age models proposed for Site 820 (Peerdeman *et al.*, 1993), and Holes 819A and 823A (this study). Problems are further accentuated by the lack of any obvious correlative mud peaks or datums across this interval.

In general, total mud content values in Holes 821A through to 823A are similar to those reported by Haddad *et al.*, (1993) for drill sites located on the southern margin of the Queensland Plateau (i.e., Holes 817A and 818B located in 1015 and 745 m water, respectively) (see Figures 1.1 and 4.17). Mean percentage mud content values in Hole 817A and Hole 818B sediments typically range between about 85 to 94 % and 68 to 88 %, respectively. In common with the Queensland margin transect sites (Sites 821 through to 823), the mud content records from Holes 817A and 818B display a trend of increasing mean value with increasing water depth (and distance from the nearest modern source of shallow-water carbonate on the Queensland Plateau- the Tregrosse Reef complex- see Haddad *et al.*, 1993), and a proximal to distal gradient, away from the reef, in the difference in mean mud content between glacial and interglacial periods (although this latter point is a little tenuous in the Hole 817A record). Although broadly similar, the Queensland Plateau mud content records differ from those seen in Holes 821A through to 819A in one important detail, unlike the aforementioned holes there is no significant offset in peak position between the Hole 817A and 818B mud content and isotopic records (i.e., peaks in sand abundance (or conversely minima of mud content) are concomitant with isotopically inferred glacial maxima).

4.4.4 Summary of the principal results

1) Queensland margin transect sites (Holes 821A through to 823A) show an outer-shelf/upper-slope to basin gradient of increasing mud content, with distance from the Queensland coast. In addition, Sites 821 to 819 display a general trend of decreasing difference in mean mud content between glacial and interglacial periods, with distance from the mainland.

2) The relationship between particle size and isotopically inferred sea level is more clearly developed in the upper parts, than the lower portions of the various grain-size records examined. In general, lowstands of sea level (glacials) are characterized by low mud content (or conversely high sand content), whereas highstand periods (interglacials) are dominated by high mud content.

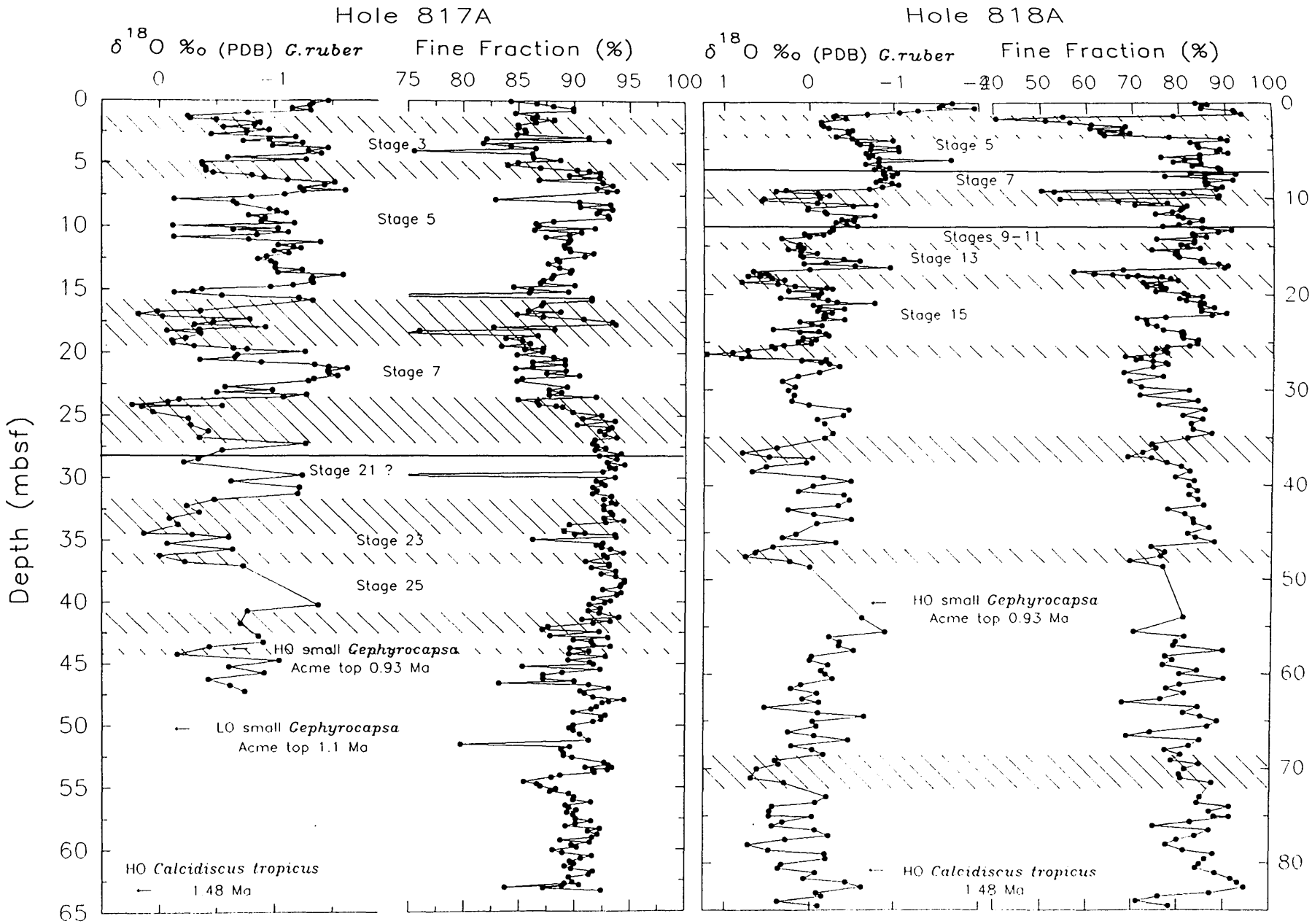

Figure 4.17. Comparison of the percentage fine fraction (<63μm) with the planktic oxygen isotope record from Queensland Plateau Holes 817A and 818B (after, Haddad et al.,1993). Solid horizontal lines indicate the position of major stratigraphic hiatuses.

3) The particle size record in Hole 819A (and to a certain extent Hole 823A) show a significant offset in the position of the main peaks in sand content (or conversely minima of mud content) relative to isotopically inferred glacial maxima, particularly over the last two main glacial/interglacial cycles. A similar trend is not observed in the records from Hole 820A, or in sediments recovered from the marginal Queensland Plateau (Sites 817/818).

4.5 Calcium carbonate cyclicity and variations in late Pleistocene sea level and climate change

Calcium carbonate accumulation and preservation patterns have varied between and within ocean basins throughout geological time (Peterson and Prell, 1985a). In the equatorial Pacific, Arrhenius (1952) was the first to observe that deep-sea cores contained lower percentages of carbonate in sediments deposited during inferred periods of warm climate than those deposited during inferred periods of cold climate. These were subsequently the subject of numerous studies on correlation and cause (Hays *et al.*, 1969; Berger, 1973; Arrhenius, 1988; Farrell and Prell, 1989; Wu *et al.*, 1991). However, considerable debate has arisen regarding the mechanisms behind these depositional cycles. Studies have suggested that carbonate cycles may be driven by fluctuations in pelagic productivity (i.e., by variation in the rates of sediment flux and by changes in the ratio of calcareous to siliceous material- Arrhenius, 1988), or by fluctuation of carbonate dissolution intensity (Berger, 1973; Broecker and Broecker, 1974; Farrell and Prell, 1989; Wu *et al.*, 1990; Le and Shackleton, 1992), or a combination of these two effects. Dilution by non-carbonate material (so-called '*dilution cyclicity*'- Seibold and Berger, 1993), such as terrigenous or lithogenic input, aeolian dust and volcanic debris, may also provide a forcing mechanism behind late Pleistocene carbonate cycles (see Rea 1990; and references therein). In addition, variations in shallow water carbonate production and export may provide a mechanism behind late Pleistocene carbonate (and in particular aragonite) cycles (Schlager, 1982; Droxler *et al.*, 1988; Davies *et al.*, 1989, 1991).

In this section, high-resolution carbonate content records for Hole 819A and Hole 823A periplatform sediments, and adjacent ODP Leg 133 drill sequences (both on the GBR shelf and on the southern flanks of the Queensland Plateau), are examined in order to determine the effect of Late Quaternary oscillations in sea level and climate change on patterns and processes of carbonate production and preservation.

4.5.1 Method

Percentages of carbonate content were determined using a modified version of the acid-base titration method, first described by Grimaldi *et al.* (1966). In brief, the analytical technique involved taking approximately 0.5 g of oven-dried (110°C) sediment and digesting it overnight in 25 ml 0.5 N Hydrochloric acid (HCL), then back titrating the excess acid with 0.35 N Sodium hydroxide (NaOH) using Bromophenol blue (0.1 % w/v aqueous solution) as indicator. Analytical reagent (AR) grade calcium carbonate (~100 % $CaCO_3$) was used in the standardization procedure. A worked example of the method employed in calculating the percentage carbonate content of an unknown sample from the wet chemical results is given in Appendix B. To demonstrate the precision of the acid-base titration technique (expressed as the standard deviation of 12 replicate analyses) results are presented in Table 4.2 for a single arbitrarily chosen sample (133-819A-6HCC at 56 mbsf). The accuracy of 12 replicate analyses of standard $CaCO_3$ (AR), used in the final calculation of percentage carbonate content, are also listed below:

Table 4.2

Sample 133-819A-6HCC			Standard $CaCO_3$ (AR)		
Weight (g)	NaOH (mls)	Carbonate (%)	Weight (g)	NaOH (mls)	Carbonate (%)
0.59019	16.22	59.58	0.57499	3.54	97.58
0.52149	18.53	60.13	0.48268	8.48	99.34
0.49406	19.51	60.19	0.56696	4.02	97.56
0.47879	20.06	60.21	0.54850	4.63	99.01
0.53165	18.20	60.00	0.53019	5.95	98.32
0.60448	15.68	59.65	0.57142	3.70	97.72
0.54749	17.71	59.74	0.58542	2.81	97.90
0.60812	15.40	60.06	0.44212	10.76	99.94
0.47789	20.03	60.43	0.62818	0.50	97.30
0.56942	16.94	59.68	0.58000	3.14	97.87
0.50725	19.10	59.96	0.61000	1.40	97.77
0.59754	16.10	59.19	0.51757	6.71	98.29
Standard deviation		0.34			0.81
Mean		59.90			98.21

In this study, acid-base titration, carbonate content evaluation measurements were carried on the coarse (>63 μm) and bulk sample size fractions, and on the mud size fraction, for Hole 819A and Hole 823A periplatform sediment samples, respectively. These sample sizes were chosen in order to enable a direct comparison with adjacent Leg 133 carbonate records (in the case of Hole 819A bulk samples), and because of

the high mud content of Hole 823A samples (and associated difficulty in obtaining sufficient coarse fraction for accurate carbonate content analysis).

4.5.2 Description of Carbonate Content Results

4.5.2.1 Hole 819A (upper-slope of the GBR)

The downcore variation in percent carbonate content, plotted with the planktic $\delta^{18}O$ record, for sediments collected from Hole 819A, are illustrated in Figures 4.18 and 4.19. These data are tabulated in Appendix B, Table B.4. Both the coarse fraction (sediments > 63 μm) and bulk sample curves are characterized by cyclic variations in percent carbonate, punctuated by abrupt changes in carbonate content. In general, carbonate content values range from about 55 % to 90 % and between 20 % to 85 % for the coarse and bulk Hole 819A samples, respectively. Carbonate content values, at Site 819, are typically higher (by as much as 45 %) in the coarse fraction than those reported for depth equivalent bulk samples (see Figure 4.18).

The percentages of carbonate content within both size fractions in Hole 819A display less variation below 32.5 mbsf (position of a major stratigraphic hiatus- Shipboard Scientific Party, 1991) than above this level (see Figure 4.18). Below 32.5 mbsf, glacial lowstands are characterized by high carbonate content, and interglacial highstands of sea level are distinguished by low carbonate content. Above 32.5 mbsf the relationship between planktic $\delta^{18}O$ values and carbonate content in Hole 819A periplatform sediments is more complex. For example, whereas, high percentage of carbonate content occur during late interglacial stage 1 and late stage 3, low carbonate content values characterize mid stage 3 and early/mid stage 5 (see Figure 4.18). Although the curve for the coarse fraction is broadly similar to the bulk sample carbonate curve, it does display significant differences, particularly in the position of minima and maxima of value (for example, at 5 mbsf and between 10 to 15 mbsf).

4.5.2.2 Hole 823A (Queensland Trough)

Downcore variations in the abundance of carbonate in Hole 823A periplatform muds (<63 μm sediment size fraction), plotted alongside the planktic $\delta^{18}O$ record, are illustrated in Figures 4.20 and 4.21. Carbonate content data are listed in Appendix B, Table B.5. Carbonate content values in Hole 823A muds typically range between about 40 % to 80 %, by weight. In general, mean carbonate values increase with depth to a maxima of about 90 % at 45 mbsf. Below 45 mbsf the mean proportion of carbonate decreases steadily with increasing depth to a minima of about 40 % (~100 mbsf). Despite the difference in size fractions analysed, carbonate content values in Hole 823A mud samples are similar to those displayed by Hole 819A sediments.

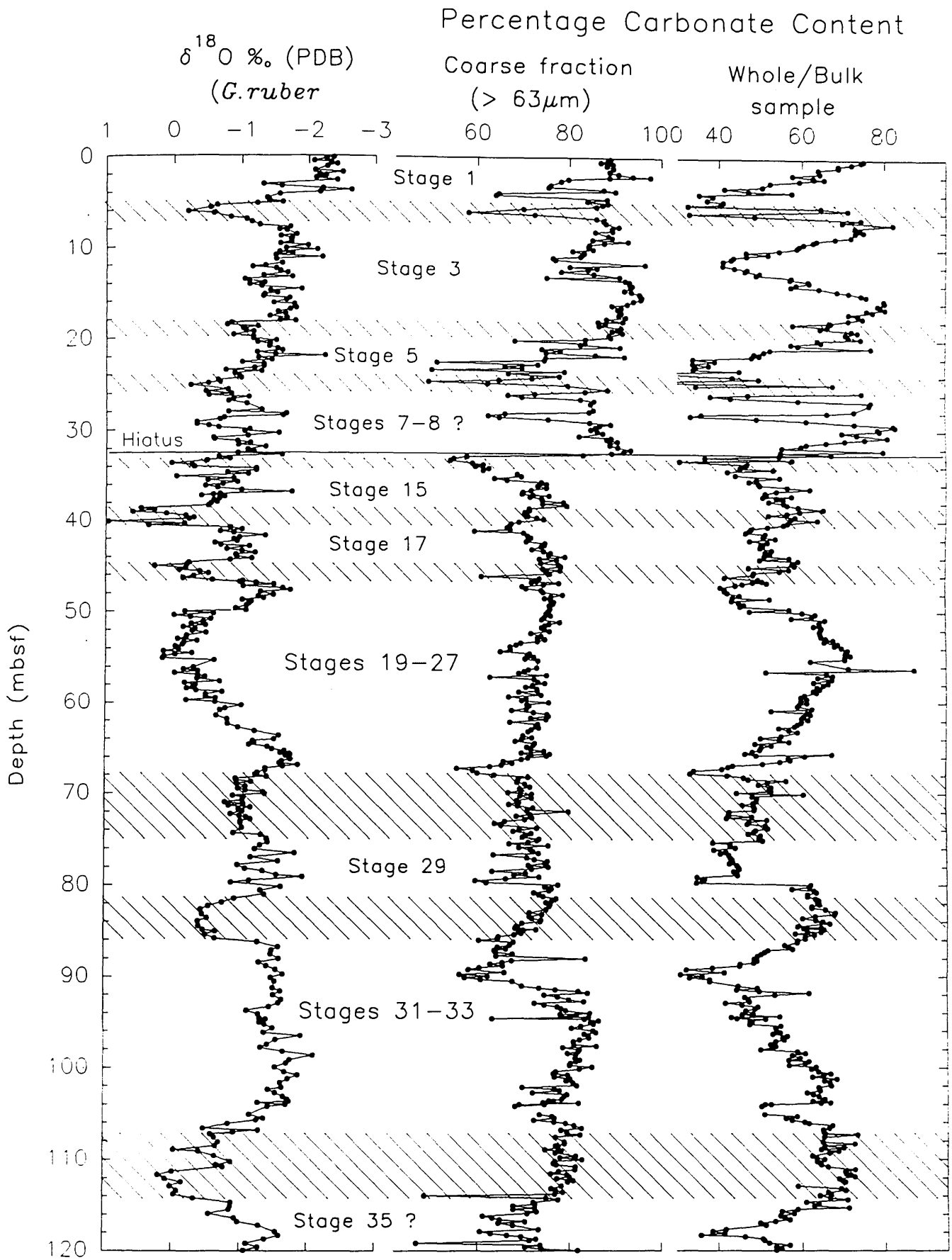

Figure 4.18. Downcore variations in carbonate content of the coarse (> 63μm) and bulk sediment fractions in Hole 819A, plotted alongside the planktic oxygen isotope record.

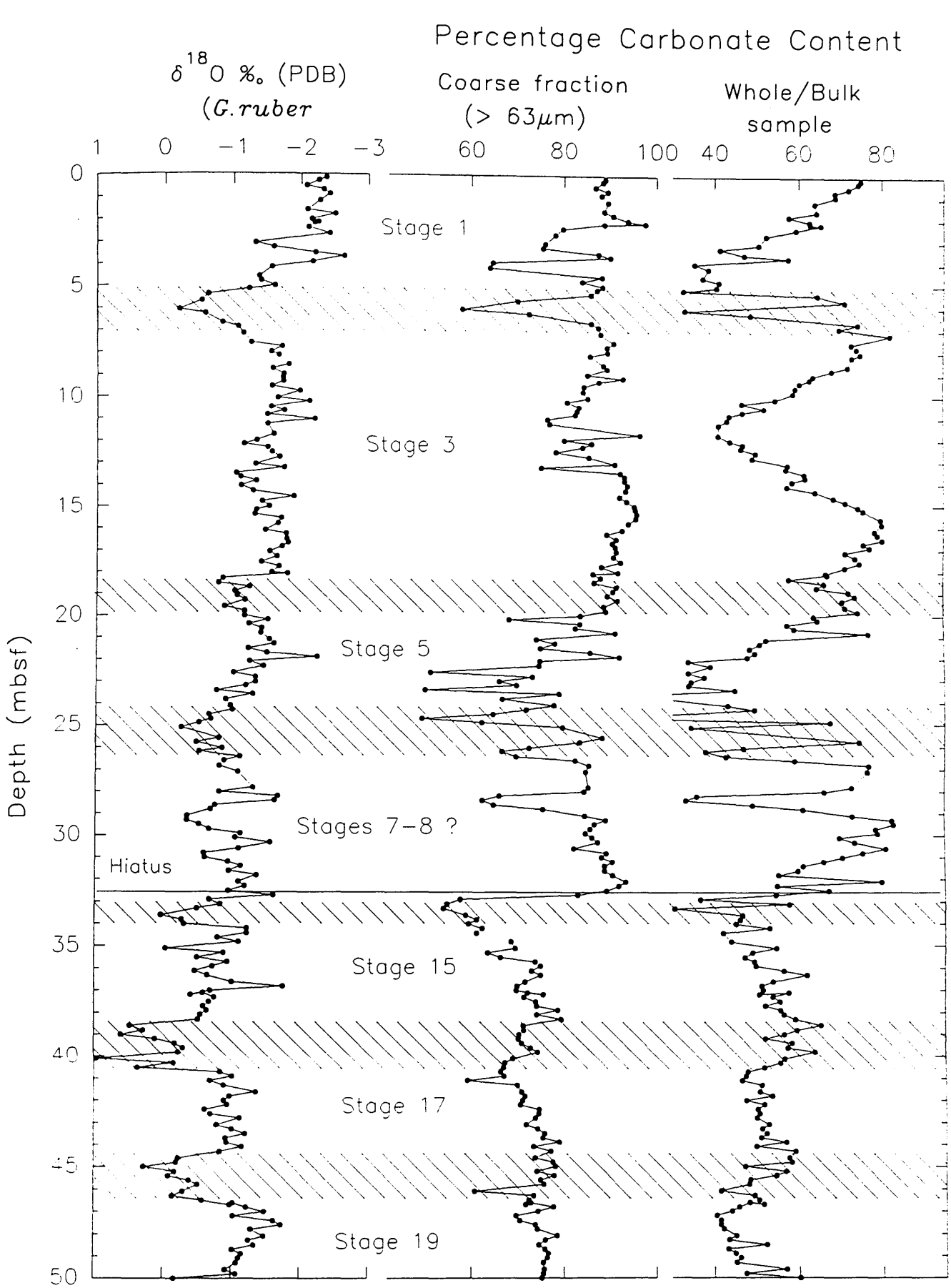

Figure 4.19. Downcore variations in percentage carbonate content of coarse and bulk sediment samples, plotted with the planktic oxygen isotope record, for the upper 50 m of the sequence from Hole 819A.

However, relative to the Hole 819A coarse fraction and bulk samples, Hole 823A muds display greater amplitudinal fluctuations in mean carbonate content throughout the sequence recovered.

The relationship between planktic $\delta^{18}O$ values and the abundance of carbonate in Hole 823A muds is illustrated in Figures 4.20 and 4.21, plotted against depth. In the lower part of the sequence a clear antithetical relationship exists between eustatic sea level (as inferred from the oxygen isotope record) and the carbonate content of the muds i.e., during sea level lowstands the carbonate content of the muds is high. This association is particularly well developed between 55 and 85 mbsf, where these two parameters are clearly inversely related. However, in the upper part of the sequence from Hole 823A the inverse relationship seen in the lower part of the record no longer holds true, and the mud size fraction is dominated by high carbonate content during highstands of sea level. For example, interglacial stages 5, 7 and 9 are all characterized by mud containing a high proportion of carbonate material. Between about 32 to 55 mbsf the association between percentage carbonate content and planktic $\delta^{18}O$ values is unclear, and remains speculative.

4.5.3 Correlation of high-resolution Late Pleistocene carbonate stratigraphies, northeast Australian margin

In this section, the high resolution carbonate stratigraphies from Holes 819A and 823A are compared to neighbouring Leg 133 Queensland margin sites (primarily Holes 820A and 820B), and with carbonate records from drill sites located on the Queensland Plateau (Holes 817A and 818A), in order to answer the following questions: are the records seen in Hole 819A and Hole 823 representative of the general patterns of carbonate deposition occurring on the GBR outer-shelf/upper-slope, and how do these records differ from patterns of carbonate production and buildups on the relatively isolated Queensland Plateau ?

As mentioned previously, a reliable high-resolution late Pleistocene stable isotope stratigraphy, below late stage 3 (Kroon *et al.*, 1993) is unavailable for the sequence at Hole 821A. Thus, any attempt to correlate the carbonate content record from Hole 821A (Konishi and Ikehara, pers. comm., 1992) with other Leg 133 carbonate stratigraphies remains highly speculative. However, despite the lack of reliable age control, the carbonate record at Hole 821A does still provide some useful clues to the general relationship between sea level and carbonate deposition on the outer shelf of the GBR. Figure 4.22 illustrates the downcore carbonate content record, in Hole 821A, plotted alongside the limited isotopic record provided by Kroon *et al.*, 1993.

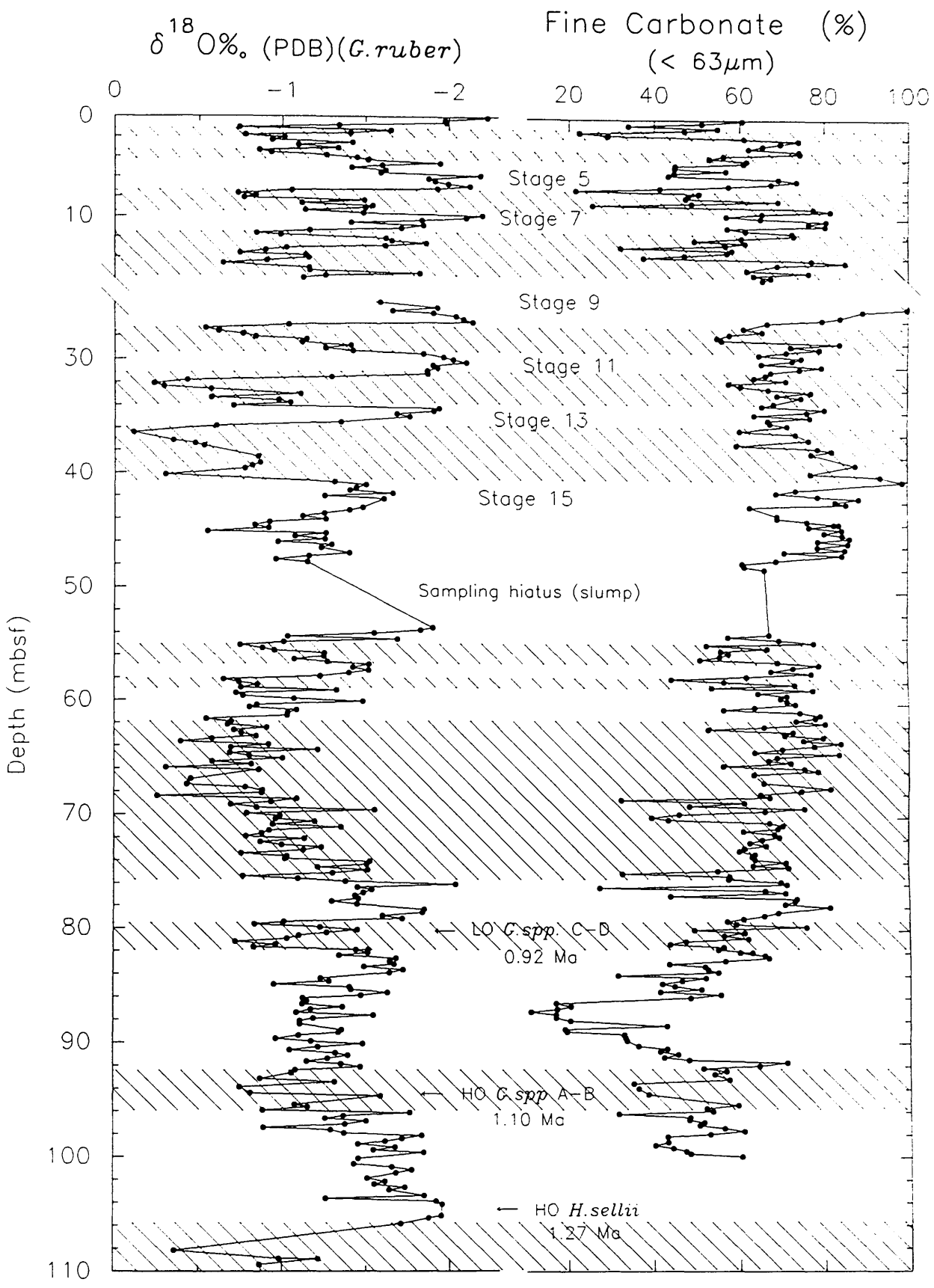

Figure 4.20. Comparison between percentage carbonate in the fine (<63μm) fraction and planktic oxygen isotope values in Hole 823A periplatform sediments. Note the presence of a major sampling hiatus between 16.5–24.9 mbsf.

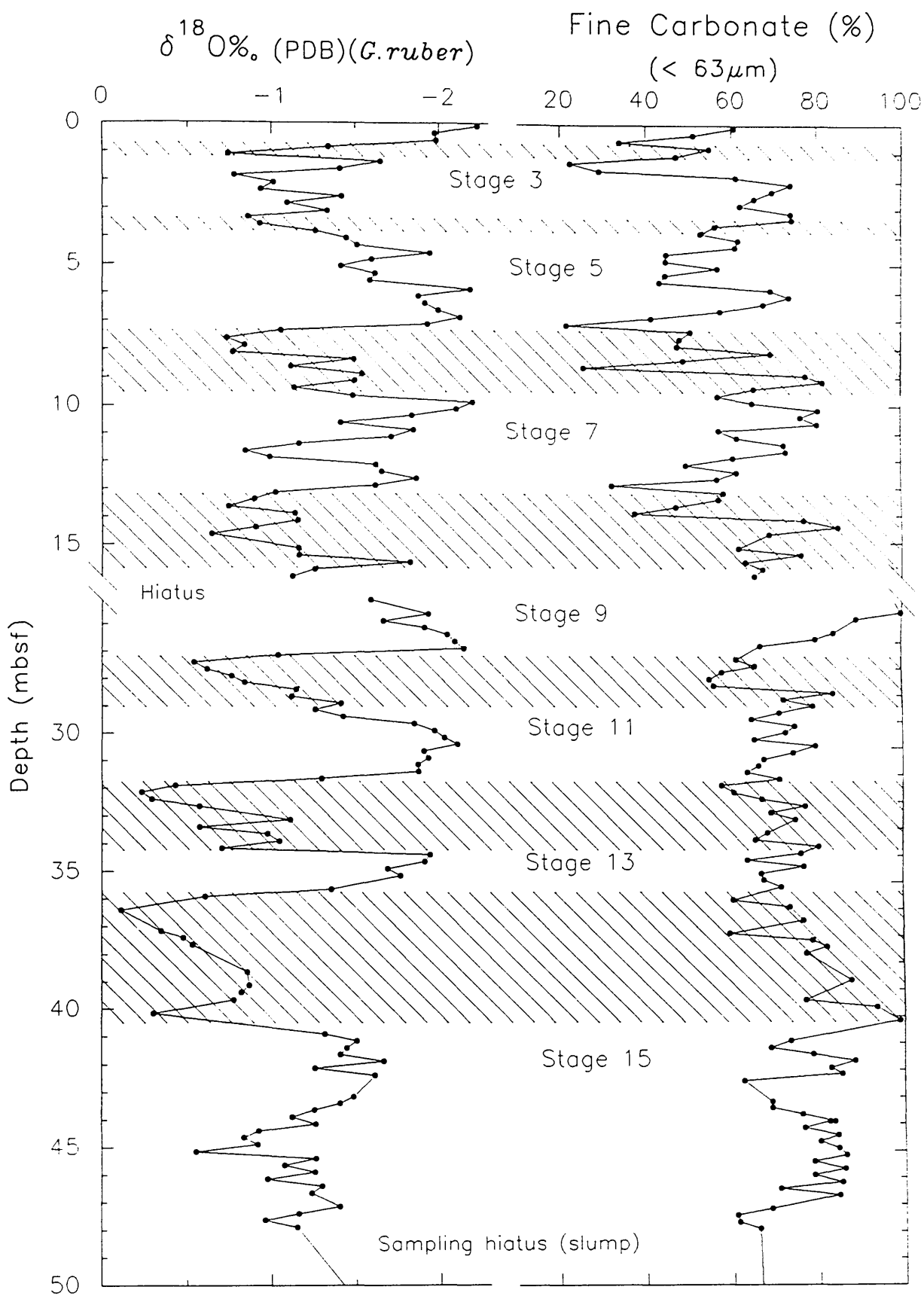

Figure 4.21. Comparison between the percentage carbonate in the fine (<63μm) fraction and the planktic oxygen isotope record, in the upper 50 m of the sequence recovered from Hole 823A. Note the presence of a major sampling hiatus (slump) between 16.5–24.9 mbsf.

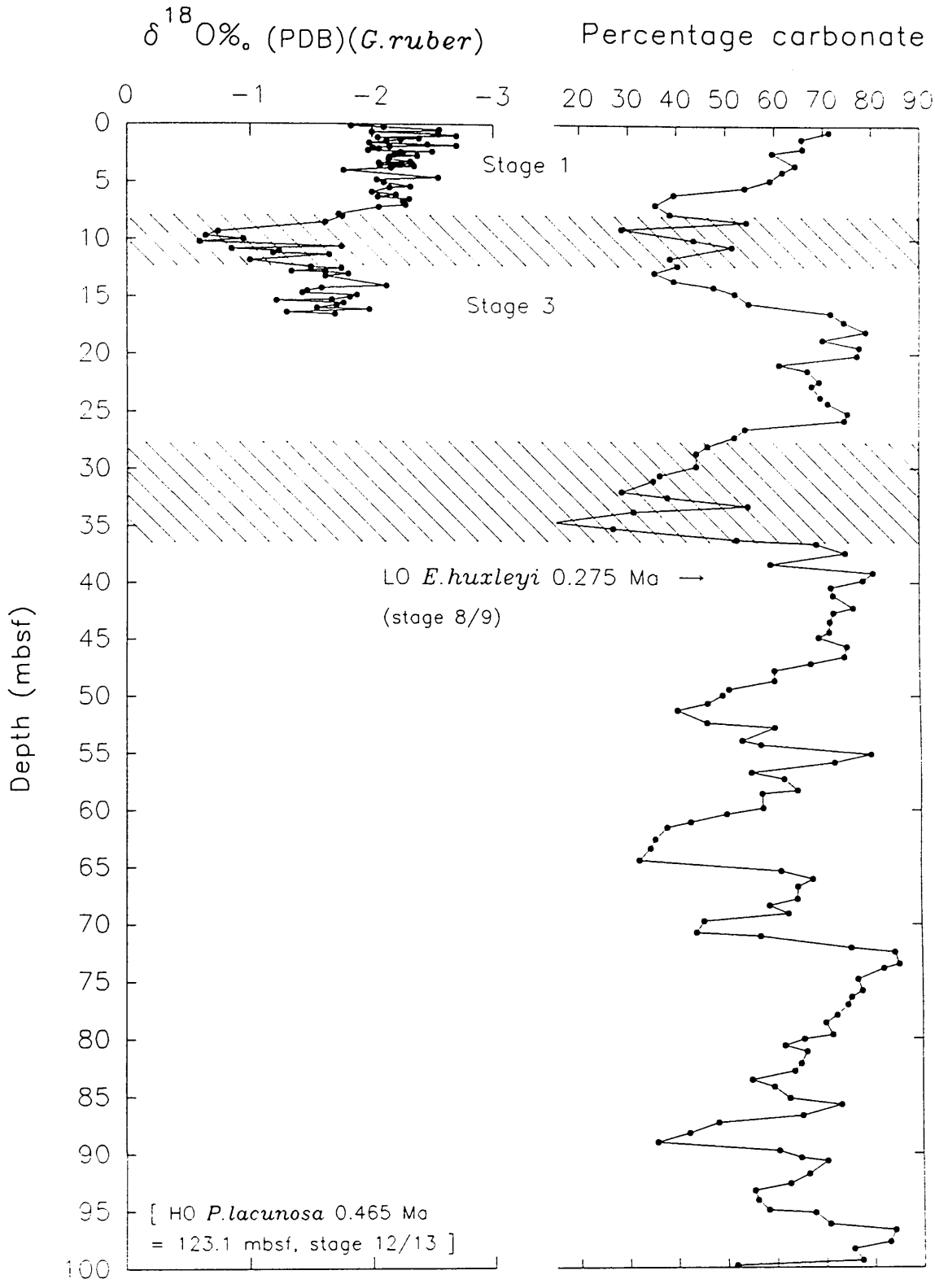

Figure 4.22. Comparison between the limited planktic oxygen isotope curve provided by Kroon et al (1993) and the carbonate content record for Hole 821A periplatform sediments (Konishi and Ikehara, 1992). The condensed nature of the stratigraphy suggests either: a) a hiatus occurs between late stage 3 and the L.O. *E.huxleyi* datum, or b) the nannofossil datum has been misplaced.

The carbonate content record in Hole 821A is characterized by a well developed cyclicity, similar to the records from Hole 819A (see Figure 4.18). In general, carbonate content values, in Hole 821A, range from about 45 to 80 %, and comparable to values obtained for Hole 819A and Hole 823A sediments. Interpretation of the Hole 821A record, suggest that (at least over the last 20 ka) carbonate production has followed variations in the isotopic record (i.e., carbonate production is high during interglacial or isotopically light periods). However, beyond late stage 3 the relationship between sea level and carbonate content becomes speculative and remains open to interpretation (see discussion).

Figure 4.23 illustrates the downcore variation in carbonate content for sediments collected at Site 820, plotted with the planktic $\delta^{18}O$ record (Peerdeman *et al.*, 1993). This figure represents a composite of carbonate data provided by Shipboard Scientific Party (1991), Feary and Jarrard (1993), and Peerdeman *et al.* (1993). All these data sets agree within a few percent and so provide a high-resolution carbonate content record for Site 820 (Holes 820A and 820B). Carbonate content values at Site 820 range from about 40 to 80 %, with a mean of about 60 %, and are similar to values reported for Site 820 (Konishi and Ikehara, pers. comm., 1992), and Sites 819 and 823 (this study). In general, the sequence at Site 820 is characterized by low-frequency/ high amplitude and high frequency/low amplitude fluctuations in carbonate content, in the upper and lower parts of the record, respectively. The transition from high to low amplitude variations in carbonate content occurs at about 95 mbsf, or slightly earlier, and is equivalent to about mid-stage 12 (~ 0.465 Ma) using either version of the age models proposed for Site 820 by Peerdeman *et al.* (1993). This position differs significantly from the proposed change in dominant frequency and amplitude by Peerdeman *et al.* (1993), seen in the stable oxygen isotope record at Site 820, at about 80 mbsf (~ 400 ka).

In common with Holes 819A and 823A, the relationship between carbonate content and planktic $\delta^{18}O$ value at Site 820 is not straightforward (see Figure 4.23). Throughout the majority of the sequence at Site 820, carbonate content and planktic $\delta^{18}O$ value exhibit a clear antithetical relationship, inasmuch as carbonate content is high during lowstands of sea level. The coefficient of correlation ([3]Pearson's *r*) between these two parameters is r = 0.61 (number of observations *N* = 189), for the upper 95 m of the sequence. This depth corresponds to a significant change in the frequency and amplitude of the carbonate record. Below 95 mbsf the relationship

[3]The calculated value of Pearson's r can vary between +1.0 (perfect positive correlation) through zero (no relationship) to -1.0 (perfect negative correlation).

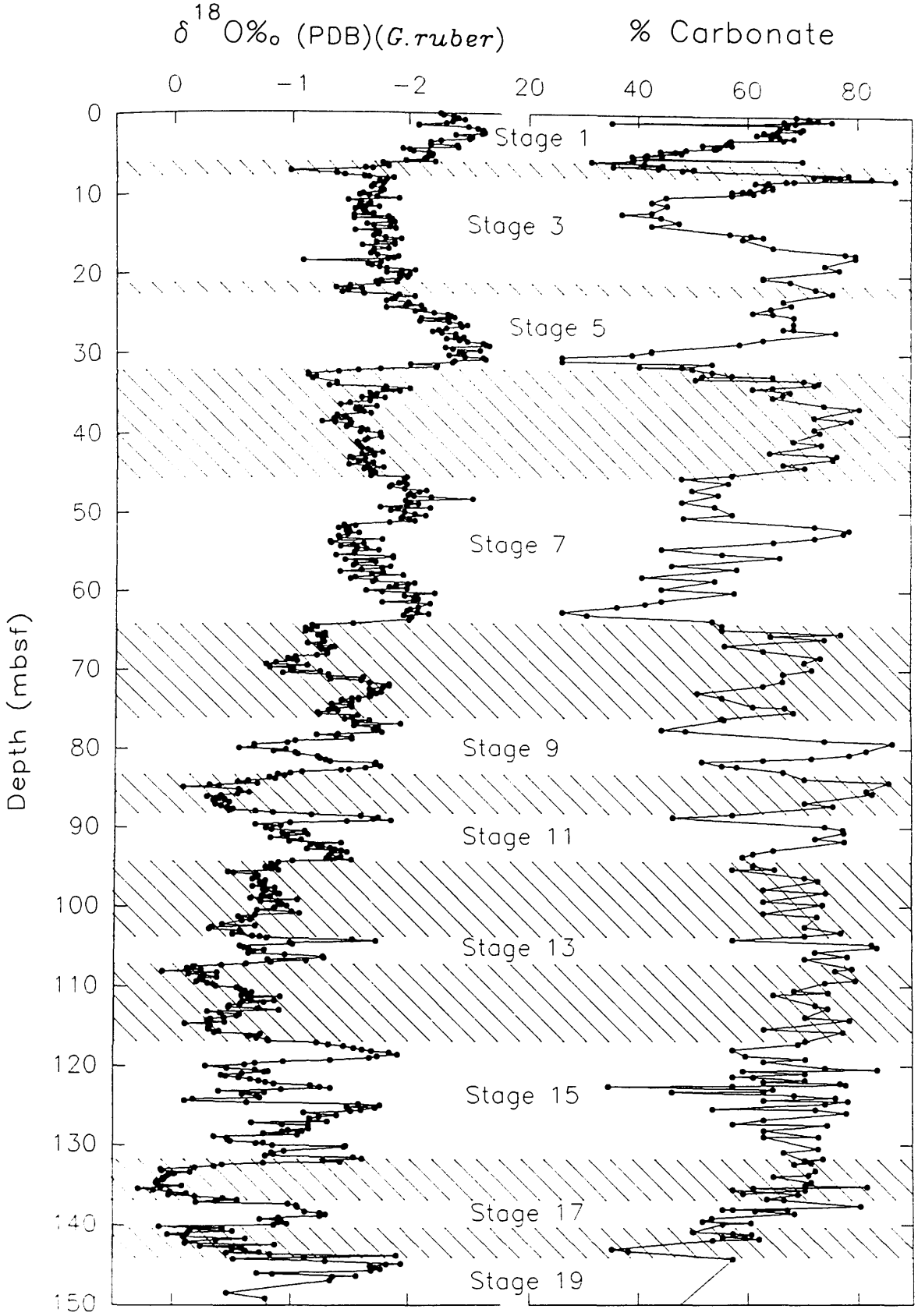

Figure 4.23. Composite carbonate content record at Site 820 (see main text) plotted alongside the planktic $\delta^{18}O$ record (Peerdeman et al.,1993) Isotopic stage assignments follow Age Model 1 (Peerdeman et al.,1993) and are based on the the graphic correlation concepts outlined by Prell et al. (1986). Note the change in amplitude in the carbonate record at about 95 mbsf.

between carbonate content and isotopic value becomes unclear. This is demonstrated in the comparatively low correlation coefficient of $r = 0.18$ ($N = 113$). A notable exception to the general positive relationship between carbonate content and planktic $\delta^{18}O$ values occurs between the core top and 6.5 mbsf (i.e., throughout the duration of the Holocene). This indicates a noteworthy change in dominant depositional style, from lowstand to highstand carbonate sedimentation, since the last glacial maximum.

In a similar manner to that described for the records in Hole 819A and Hole 823A, significant offsets in the position of carbonate content and isotopic minima and maxima occur in the sequence recovered from Hole 820A, particularly over the last two main glacial/interglacial cycles. These peaks shifts are largely responsible for the, somewhat lower than expected, correlation coefficient value ($r = 0.61$) obtained for the upper part of the sequence in Hole 820A. A detailed description of these peak shifts, in particular over the last two main glacial perturbations, is provided by Peerdeman *et al.* (1993), and their sedimentologic significance will be discussed later.

Carbonate content records for Queensland Plateau Site 817 and Site 818 sediments, plotted against depth, are illustrated in Figures 4.24 and 4.25. Also shown in these figures are the planktic oxygen isotope records from these sites. These data are provided by Haddad *et al.* (1993) and Shipboard Scientific Party (1993). In general the total carbonate content within Hole 817A and Hole 818B sediments is higher than values found on the outer-shelf/upper-slope of the GBR (Sites 821 to 819), and in the Queensland Trough basin (Site 823). Carbonate content values typically range from about 93 to 96 % and 95 to 98 % for Hole 817A and Hole 818B sediments, respectively (see Figure 4.24). Interpretation of the Hole 817A and Hole 818B carbonate content and isotopic records, suggests that, unlike the Queensland margin transect sites (Sites 821 through to 823), carbonate content is high during highstands or isotopically depleted periods. For example, during interglacial stages 11, 13 and 15 in Hole 818B, and between 2 to 5 mbsf and during stage 5 in the records from Hole 817A carbonate content is high. This relationship is better developed in the Hole 818B record than the sequence recovered from Hole 817A. Further, unlike the records from Sites 821 through to 823, the carbonate records from Holes 817A and 818B do not show any significant lead/lag relationships with the isotopic records (although this is slightly difficult to substantiate across some interval, given the non-standard profile of the planktic oxygen isotope records).

Despite the relative isolated position of the marginal Queensland Plateau, and Sites 817 and 818, a significant proportion of the sediments analysed at these two drill sites is

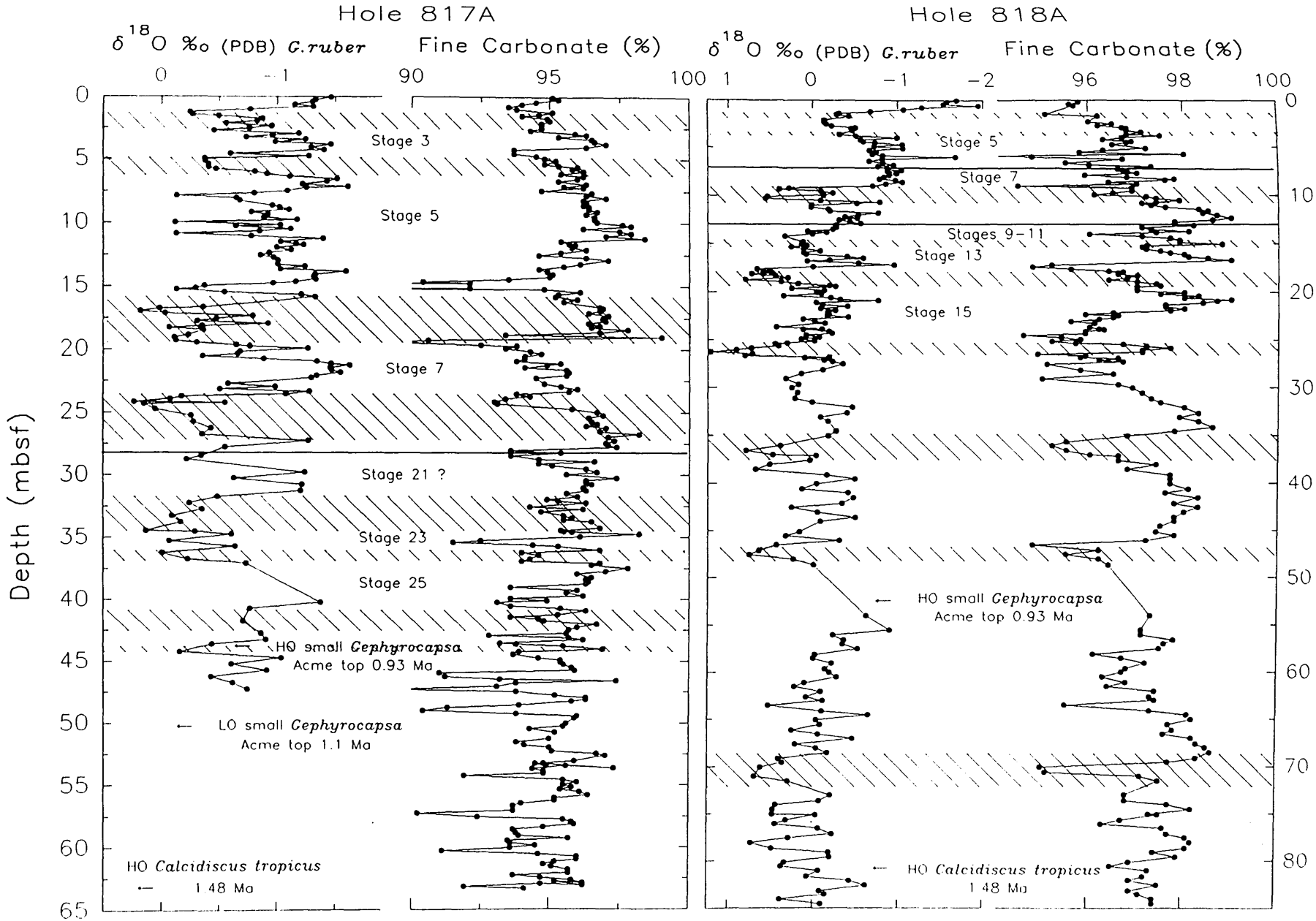

Figure 4.24. Comparison of the percentage of carbonate in the fine fraction (<63μm) with the planktic oxygen isotope record from Queensland Plateau Holes 817A and 818B (after, Haddad et al., 1993). Solid horizontal line indicate the position of major stratigraphic hiatus.

composed of non-carbonate material (i.e., between about 1 to 5 %, with occasional maxima exceeding 10 %- see Figure 4.25). The question therefore remains as to what are the origins of this non-carbonate material? Has this material come from the GBR shelf, as suggested by Davies *et al.* (1991)? or is it driven by fluctuations in the productivity of siliceous organisms ? Possibly this material has been introduced into the area by some other mechanism such as, increased fluvial discharge associated with the Fly River, New Guinea, or as ocean circulation driven volcanic pumice rafts as suggested by Beiersdorf (1989)?

4.5.4 Summary of main points

1) Carbonate content in sediments collected from Sites 821 through to 823 are similar in magnitude, but are significantly lower than values reported for Sites 817A and 818A located on the marginal Queensland Plateau (Haddad *et al.*, 1993), reflecting the greater influence of terrigenous input on the former sediments.

2) In general, throughout the lower part of the records at Holes 819A and 823A, carbonate content and planktic $\delta^{18}O$ values display a clear antithetical relationship (i.e., carbonate content is high during isotopically heavy periods). In the upper part of the sequences, the association between these two parameters is more complex, and on occasions is the reverse of that seen in the lower sections.

3) In general, the pattern of carbonate sedimentation in Hole 820 is remarkably similar to that seen in Hole 819A and Hole 823A, particularly over the last two main glacial/interglacial cycles. At Site 821 the relationship between carbonate deposition, and sea level and climate change, beyond late stage 3, remains speculative.

4) The switch from predominately lowstand carbonate deposition to a more complex pattern of carbonate sedimentation, in Holes 819A and 823A, is difficult to date accurately, particularly given the uncertainties associated with the age models. Tentative interpretation of the Site 820 carbonate record suggests that, at least at this site, the transition occurred close to mid-stage 12 (~0.465 Ma).

5) Tentative analysis of the records from Holes 817A and 818B suggest that, in general, carbonate content is high during highstands of sea level, i.e., the carbonate content and the planktic oxygen isotope records correlate negatively.

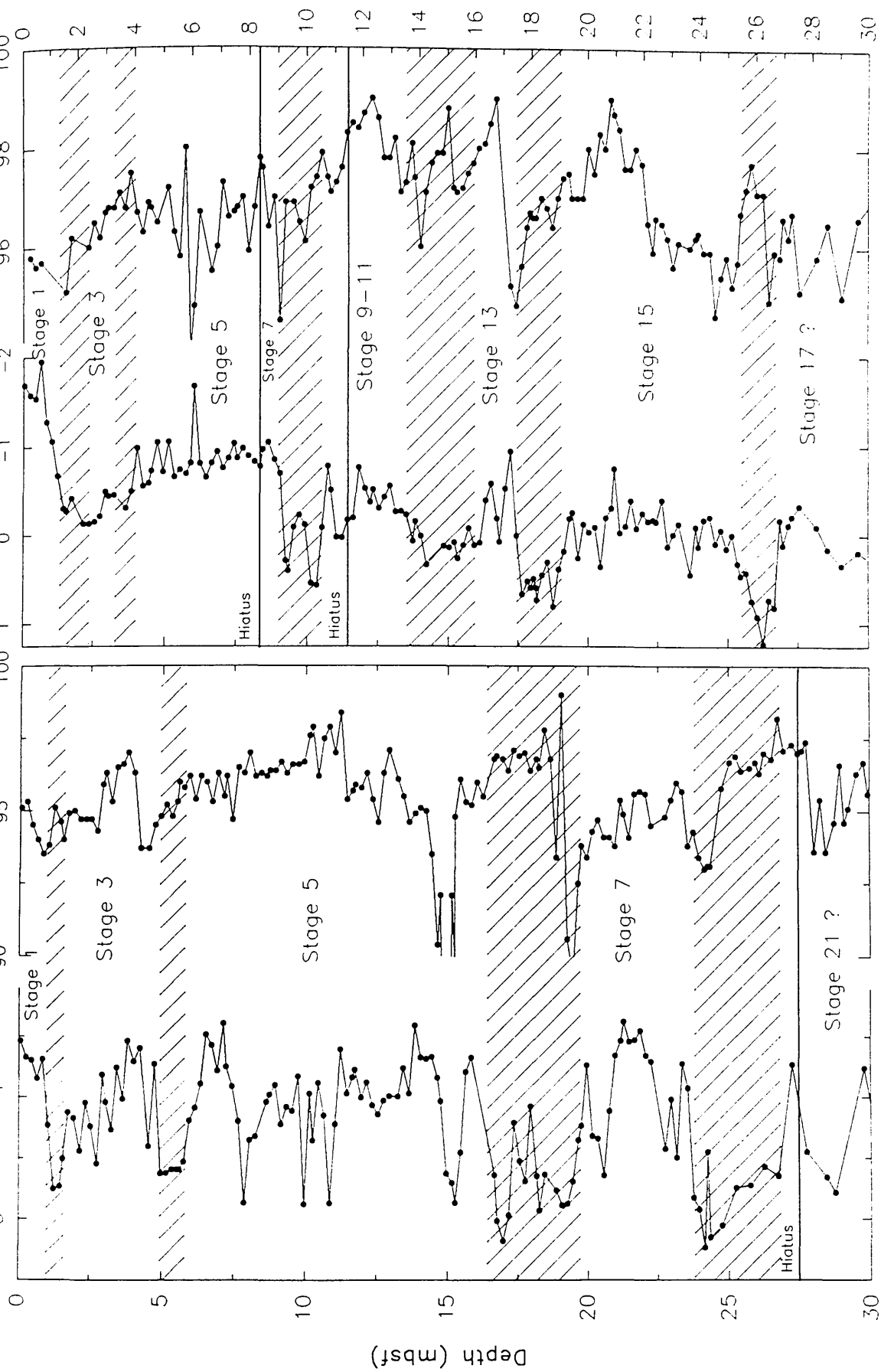

Figure 4.25. Comparison of the percentage of carbonate in the fine fraction (<63μm) with the planktic oxygen isotope record from Queensland Plateau Holes 817A and 818B (after, Haddad et al., 1993).

4.6 Discussion

4.6.1 Carbonate content and carbonate stratigraphy, northeast Australian margin.

Figure 4.26 illustrates the downcore fluctuations in carbonate content in sediments recovered from Sites 821 through to 823, for the last 300 ka. Also shown in this figure are the planktic oxygen isotope records from each site, plotted against depth. Analysis of these high-resolution records suggests that these two parameters are out of phase, such that peaks in non-carbonate material occur slightly later than the isotopically inferred glacial maxima (i.e., during periods of rising sea level/early to late transgression). For example, analysis of the Hole 820A records between 5 to 8 mbsf shows that the prominent peak in non-carbonate material clearly occurs after the stage 2 glacial maximum (see Figure 4.26). Similarly, in Holes 821A through to 823A the percentage carbonate content lags the planktic $\delta^{18}O$ record over the last main glacial/interglacial cycle. Further scrutiny of the records suggest that the lead-lag relationship seen between carbonate content and isotopic value can be traced back as far as stage 6 in the records from Holes 820A and 819A, and possibly glacial stage 8 in Hole 823A. Beyond stage 8, the carbonate content records from Sites 820 to 823 become more difficult to interpret, while, unfortunately in Hole 821A (where the carbonate cyclicity is the best developed?) the absence of a reliable long-term isotopic signature precludes further detailed analysis.

One important implication of the association between carbonate content and isotopic value is that the present age models proposed for the top of Hole 820A (Peerdeman *et al.*, 1993) and Hole 819A (this study) may be incorrect, in terms of the positioning of glacial stage 4 (see Figure 4.26). For example, in the Hole 820A, record if we assume that percentage carbonate content follows the isotopic record (albeit with a slight lag), then the prominent low in carbonate content between 10 and 14 mbsf should indicate the approximate position of stage 4 (i.e., between about 12 to 16 mbsf). According to Peerdeman *et al.* (1993) isotopic stage 4 is either absent in the sequence from Hole 820A or is located between 21.45 and 23.55 mbsf (based on age models constructed using pattern matching techniques and the graphic correlation concepts outlined by Prell *et al.*, (1986), respectively). However, unlike the age models proposed by Peerdeman *et al.* (1993) this new interpretation of the Hole 820A record is consistent with the F.O. *E. huxleyi* acme at 12.1 mbsf proposed by Wei and Gartner, (1993), and in the authors opinion seems more likely.

Using the same rationale, the position of the major peak in non-carbonate content between 10 and 14 mbsf, in Hole 819A, suggests that the correct position for stage 4

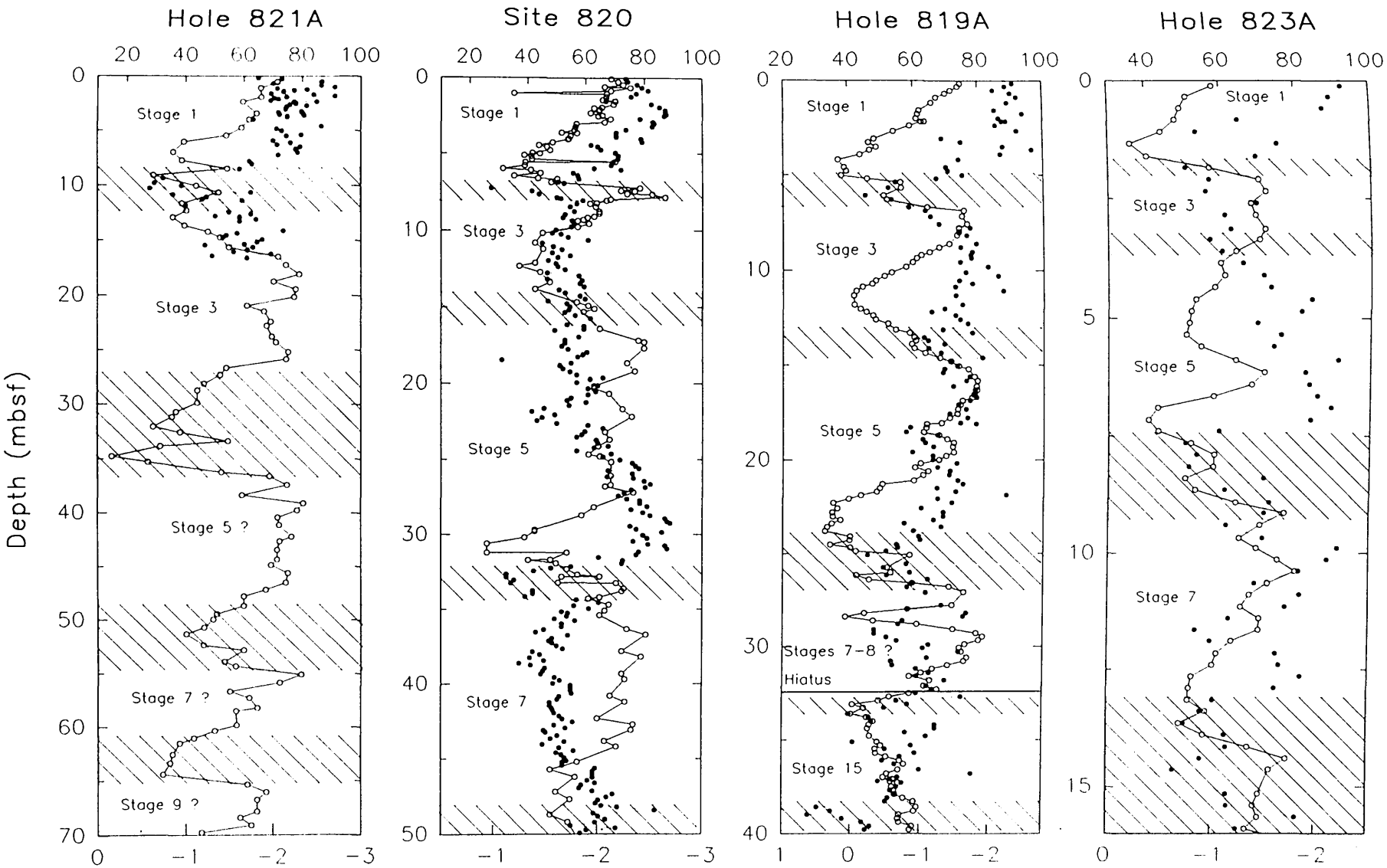

Figure 4.26. Comparison between the planktic $\delta^{18}O$ (dotted line) and percentage carbonate content (solid line) in Queensland margin Holes 821A, 820A, 819A and 823A.

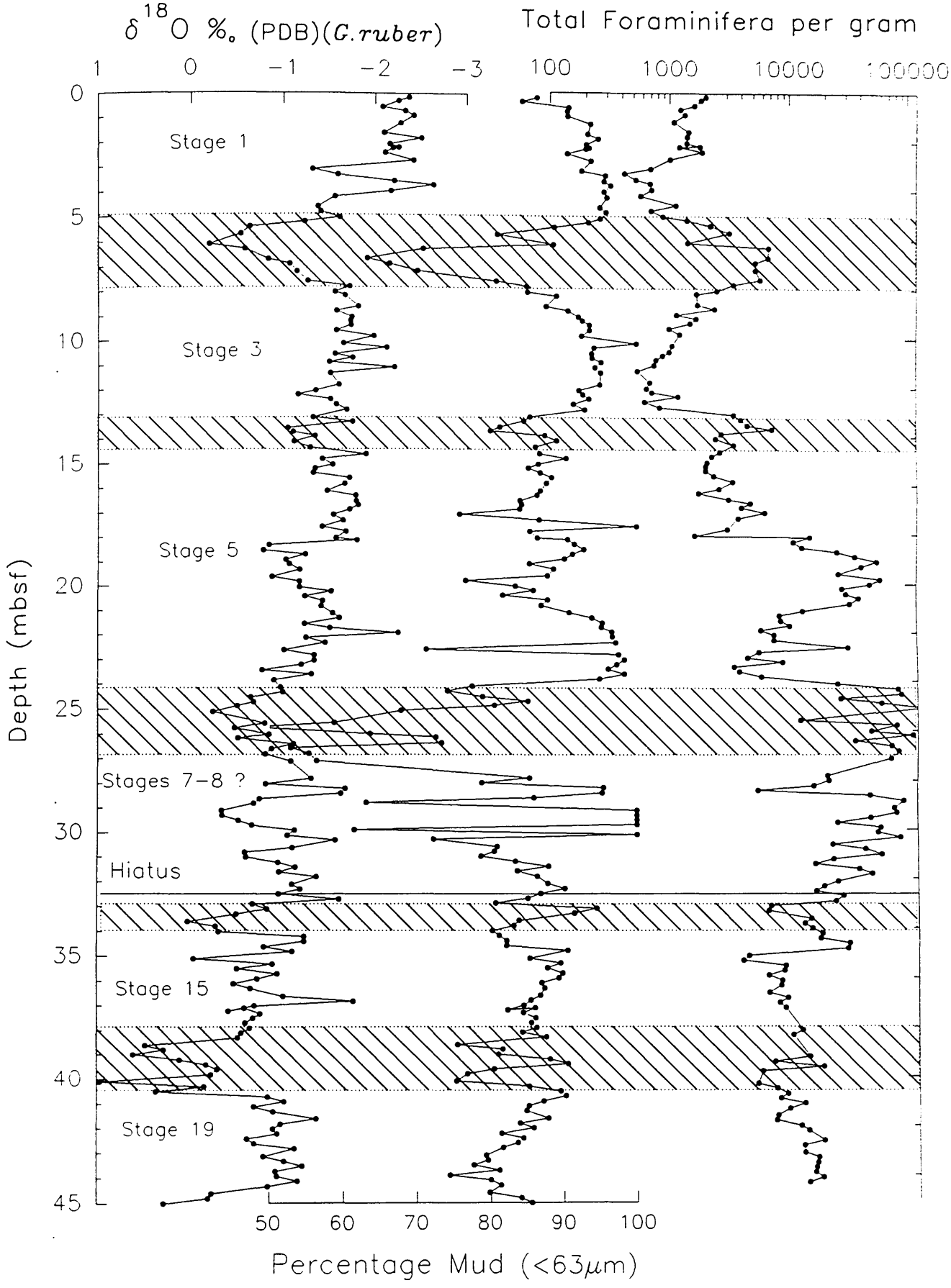

Figure 4.27. Comparison between the percentage mud content, the total number of foraminifers per gram (Kroon et al., 1993) and the planktic oxygen isotope record in Hole 819A.

should be slightly earlier in the sequence[4], i.e., between about 13 to 16 mbsf. This revised interpretation is consistent with an earlier version of the age model proposed for Hole 819A by Alexander *et al.* (1993), which was subsequently revised based on foraminiferal abundances provided by Kroon *et al.* (1993). These data indicate that high foraminifer numbers generally occur during glacial periods, thus the prominent peak in abundances between 18 to 21 mbsf (see Figure 4.27) was interpreted as representing glacial stage 4. Alternatively, the present position of stage 4 in the isotope stratigraphy for Hole 819A (and in the first age model proposed by Peerdeman *et al.* (1993) for Hole 820A) may be correct? However, this would present the problem of explaining why the carbonate content in Hole 819A (and Hole 820A) sediments should fall so dramatically during the last interstadial (mid-stage 3)?, possibly this event is related to a similar phenomenon seen in deep-sea cores collected off Namibia, southwest Africa, where low carbonate content within the marine sediments has been explained in terms of enhanced organic matter decomposition and increased carbonate dissolution (Summerhayes *et al.*, 1995).

4.6.2 Sedimentological response of the northeast Australian margin to fluctuations in late Pleistocene sea level and climate change

Previous studies on the effects of late Pleistocene sea level change on patterns and processes of sedimentation on the northeast Australian margin, suggest that during periods of relative high sea level (interglacial periods), deposition on the Queensland shelf with the GBR is dominated by either; the progradation of prodeltaic sediments on the inner shelf, primarily concentrated on wave-dominated deltas, or as aggradation of sediments on the mid- to outer shelf as a result of reef growth and inter-reef sedimentation (Harris *et al.*, 1990; Davies *et al.*, 1991). According to these authors, high sea level sedimentation is characterized by reefal and inter-reefal carbonate deposition with restricted siliciclastic deposition largely concentrated on the inner shelf. Continental slope sedimentation reflect the reduced or restricted fluvial input to the shelf edge, and sediments are distinguished by higher carbonate and lower terrigenous mud content. In contrast, during periods of relative low sea level (to minus 120 m sea level fall- Harris *et al.*, 1990) continental margin sedimentation is characterized by the aggradation of fluvial sediments, on the mid- to outer shelf, and the progradation of shelf edge deltas (composed mainly of terrigenous sand and sandy muds) beneath the outer shelf and upper-slope (see Chapter 2, Figure 2.26). During low sea level conditions fluvial inputs were effectively point sources onto the Queensland shelf (e.g., the Burdekin River) with terrigenous material ultimately

[4] see Appendix C, Table C.6 for corrections to the age model proposed for Hole 819A.

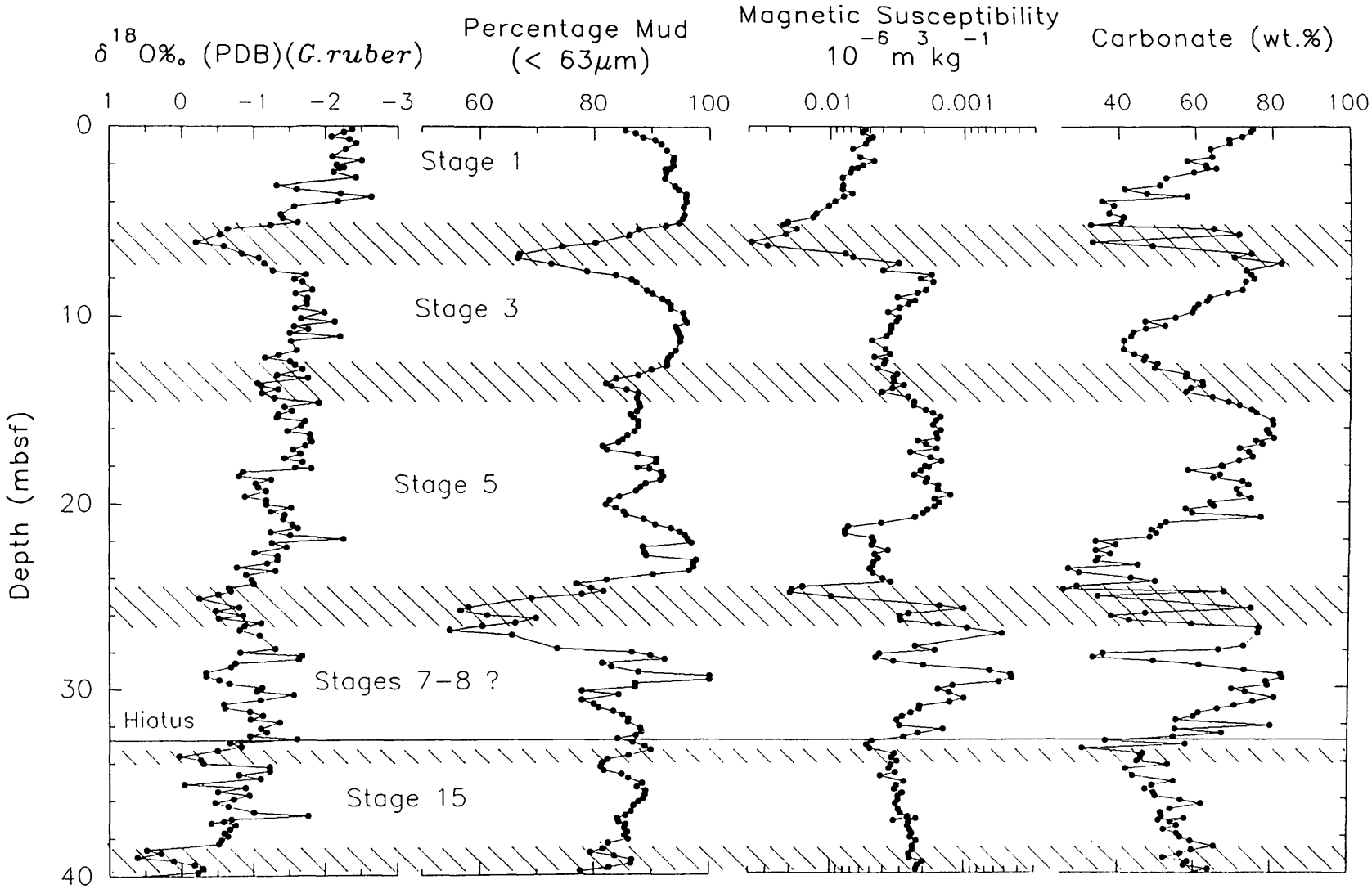

Figure 4.28 Oxygen isotope signal compared to abundance of mud, magnetic susceptibility and carbonate content for sediments recovered from Hole 819A. The numbers on the left diagram represent successive oxygen isotope stages. Note that stage 4 has been positioned slightly below the main peak in non carbonate material (see text for discussion).

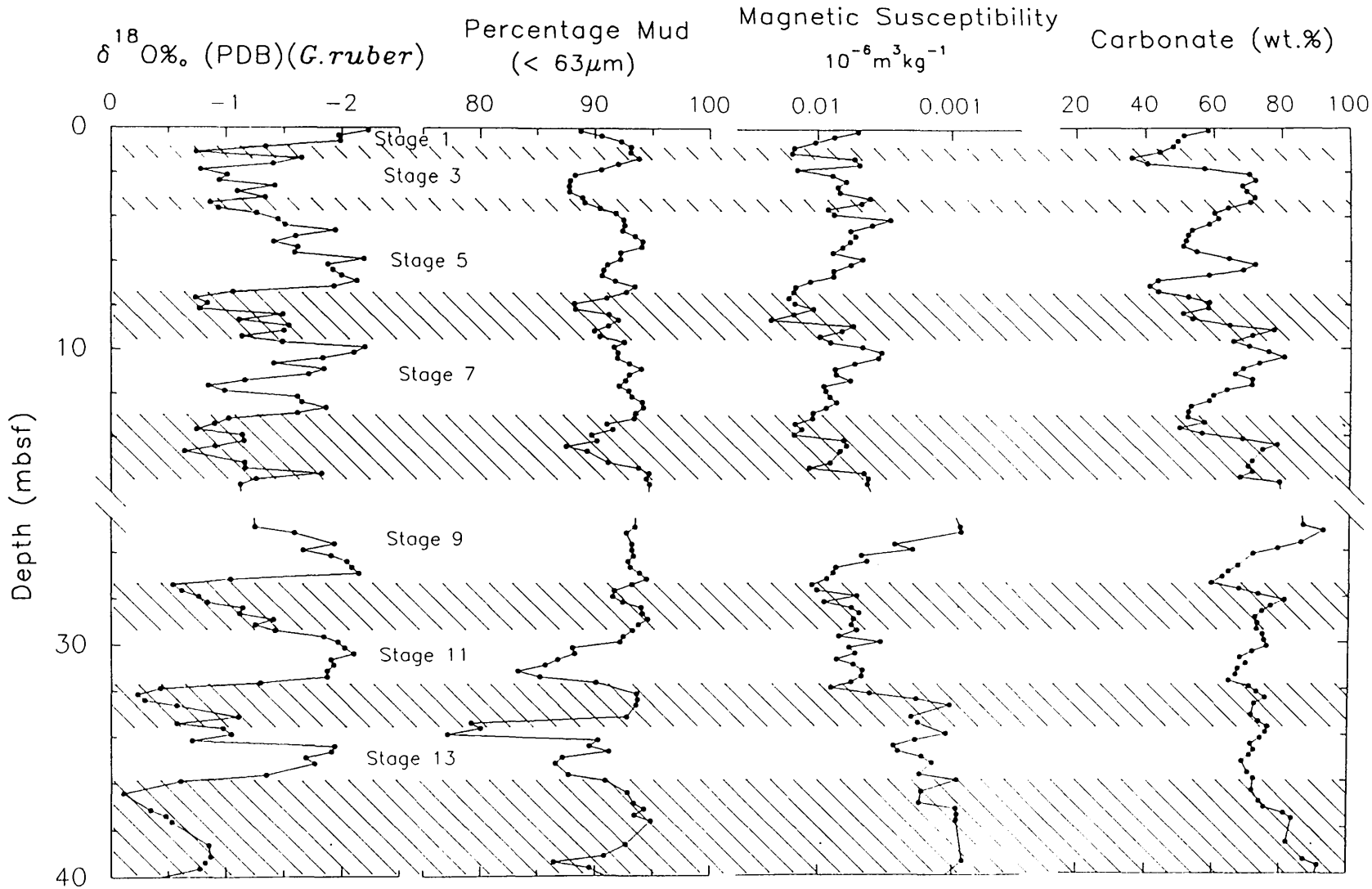

Figure 4.29 Oxygen isotope signal compared to abundance of mud, magnetic susceptibility and carbonate content for sediments recovered from Hole 823A. The numbers on the left diagram represent successive oxygen-isotope stages. Note the presence of a haitus between 16.5–24.9 mbsf.

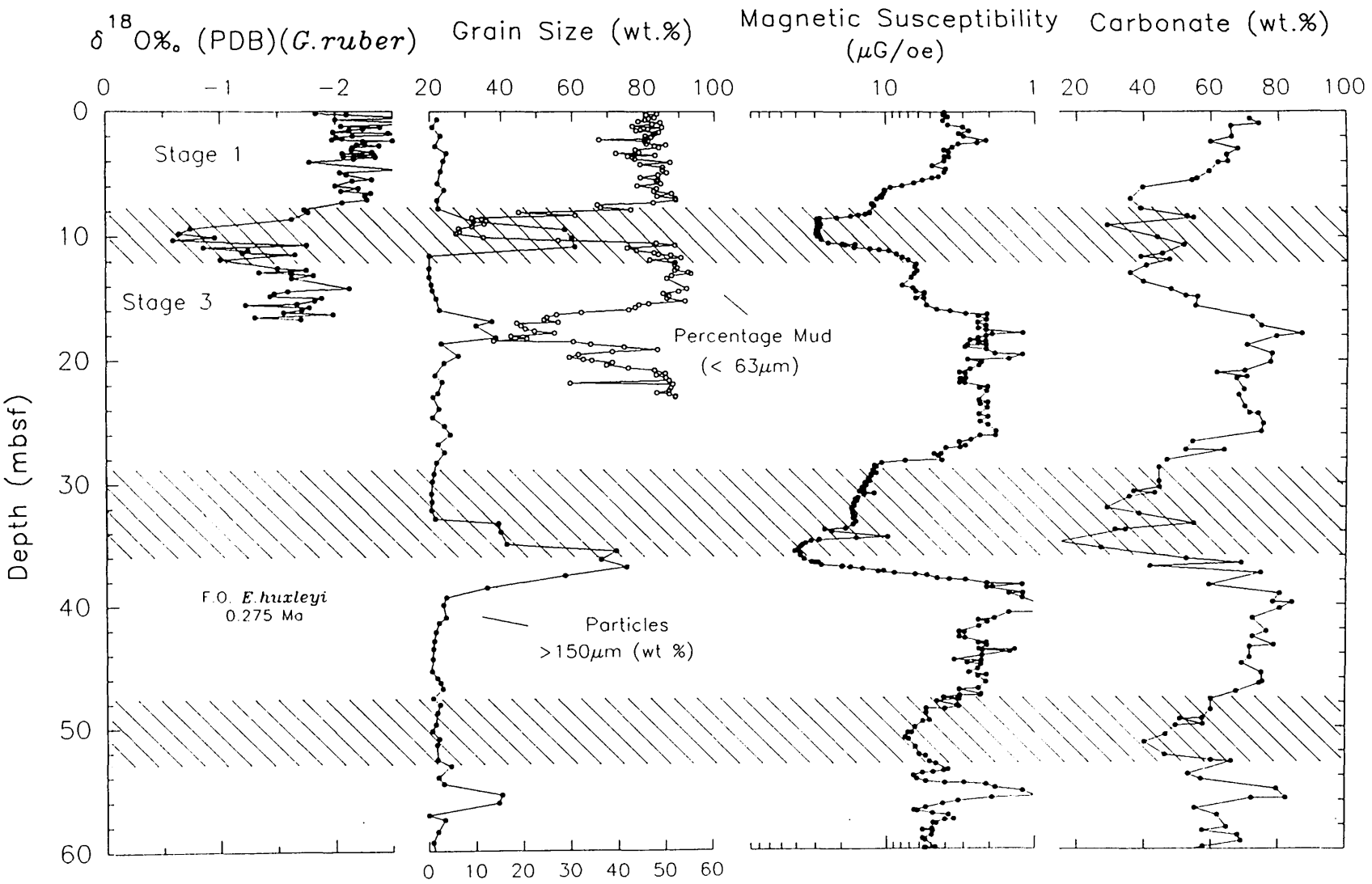

Figure 4.30. Grain-size, carbonate content, magnetic susceptibility and planktic $\delta^{18}O$ values, plotted against depth (mbsf), for Hole 820A periplatform sediments. Note the absence of an isotopic record below 18 mbsf.

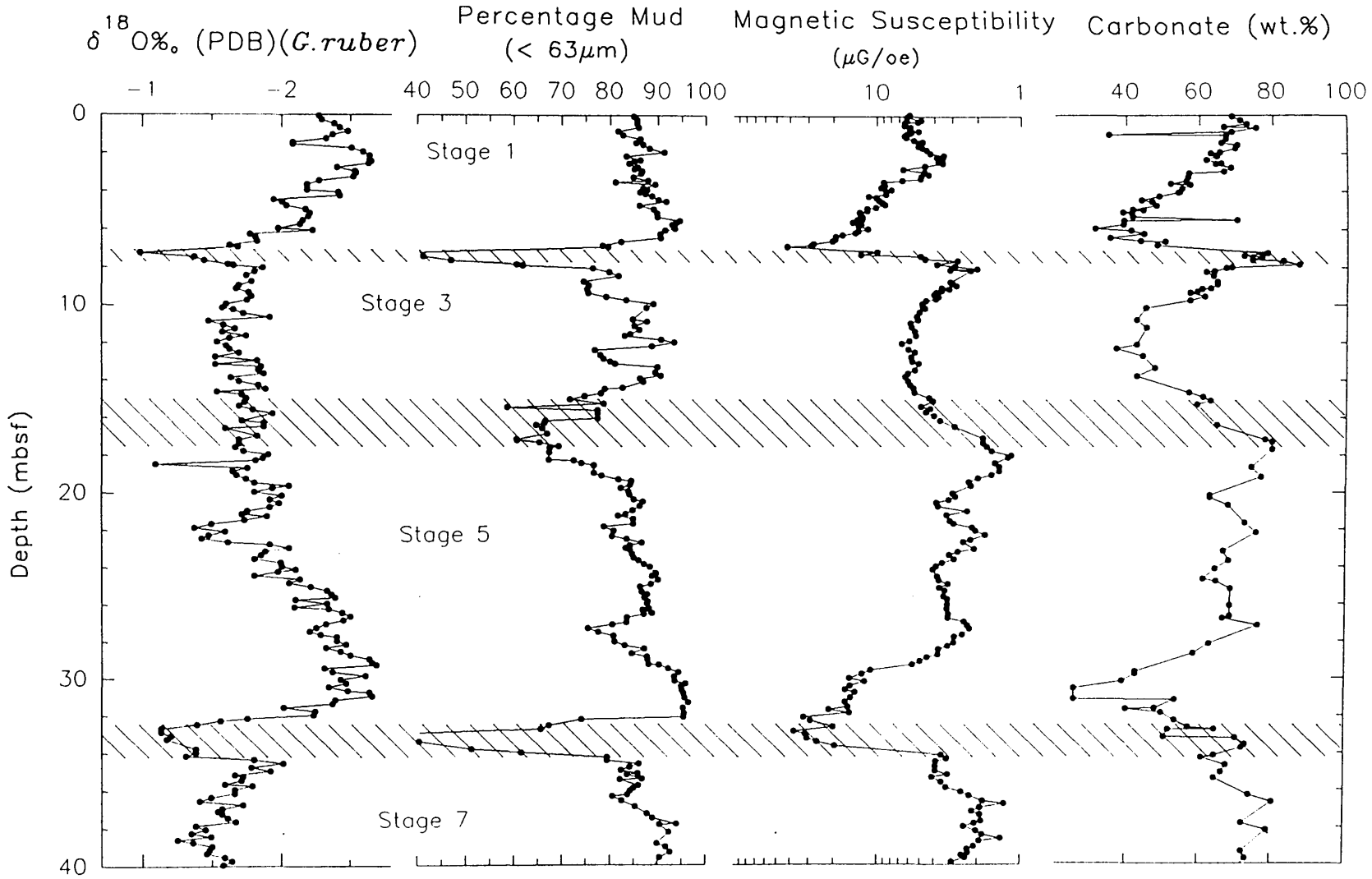

Figure 4.31 Oxygen isotope signal compared to abundance of mud, magnetic susceptibility and carbonate content for sediments recovered from Site 820. The numbers on the left diagram represent successive oxygen-isotope stages. Note that the position of stage 4 has been placed slightly earlier than the main main peak in non-carbonate material centered at 11 mbsf (see text for discussion).

reaching the upper-slope, through gaps and breaks in the carbonate reefs (Harris *et al.*, 1990).

In general, previous studies of the effects of variations in late Pleistocene sea level and climate change on patterns of carbonate buildup and deposition on the northeast Australian margin, suggest that during highstands of sea level carbonate production increases. In contrast, during periods of relative low sea level carbonate production is restricted, largely because of the emergence of previous high sea level stand carbonate buildups (Harris *et al.*, 1990; Davies *et al.*, 1991). The results of these studies, are consistent with the general principle of "highstand shedding" of carbonate platforms, previously described for the Bahamas banks (Droxler *et al.*, 1983; Mullins, 1983; Reijmer *et al.*, 1988), the carbonate platforms of the Caribbean (Glaser and Droxler, 1991, 1993), and the Indian Ocean (Droxler *et al.*, 1990).

For comparison, the grain-size distribution, carbonate content, magnetic susceptibility and oxygen isotope records, for the sequences recovered from Hole 819A and Hole 823A, are presented in Figures 4.28 and 4.29, respectively. Careful examination of these high resolution records suggest that the pattern of sedimentation on the upper-slope of the GBR, and in the Queensland Trough, during the Late Pleistocene is more complex than that previously suggested for the northeast Australian margin. Detailed analysis of the various sedimentologic records from these two cores (and from Holes 821A and Site 820- see Figures 4.30 and 4.31, respectively) reveal significant offsets in the position of minima and maxima in value, both with respect to sea level, and to each other. These peak shifts are particularly well developed in the high-resolution upper-slope Hole 819A records.

In order to characterize the response of the upper-slope (Hole 819A) and Queensland Trough (Hole 823A) sequences to fluctuations in late Pleistocene sea level and climate change, in particular over the last main glacial/interglacial cycle, the various sedimentologic and isotopic records have been interpreted in terms of a sea level cycle comprising: a regression, a lowstand, an early transgression, a late transgression and a highstand and/or stillstand. Using this rationale, the sedimentologic and isotopic records from Hole 819A (and to a lesser extent 823A) can be accurately correlated and compared with adjacent Leg 133 sequences, in particular the high-resolution records from Site 820 (Shipboard Scientific Party, 1991; Feary and Jarrard, 1993; Peerdeman *et al.*, 1993) (see Figure 4.31). Furthermore, correlation of the upper part of the sequence, recovered from Hole 819A, with the records from Site 820 (including the topmost 10 m, which has been accurately dated using accelerated mass-spectrometry

(AMS) radiocarbon techniques- Peerdeman *et al.*, 1993), has enabled bulk sedimentation rates for the various phases of the last glacial/interglacial cycle in Hole 819A to be calculated (see Figure 4.32). Unfortunately, a similar exercise with the sequence recovered in Hole 823A has not been possible, because of the comparatively low resolution (and low sedimentation rates) associated with this core.

In general, petrological examination of selected Hole 819A periplatform sediments, coupled with an analysis of the grain-size distribution, carbonate content, magnetic susceptibility and foraminiferal isotopic records from this core (see Figure 4.29), corresponding to the last main glacial/interglacial cycle, suggest that:

- The regression is characterized by a coarse grained bioclastic packstone showing: the highest and lowest abundances of sand and mud sized particles, respectively; the highest carbonate content in both bulk and coarse fraction samples; moderately high magnetic susceptibility values, and comparatively high sedimentation rates. The sand fraction (>63 μm) comprises abundant planktic foraminifera and thecosomatous pteropods and heteropods. Other bioclasts include: benthic foraminifera, molluscs, bryozoan fragments, gastropods, occasional coral fragments, bivalves, rhodoliths, echinoderm debris, ostracods and a variety of assorted skeletal (?) carbonated particles (see Plate 4, Figure A). The very fine sand (63-125 μm) fraction (i.e., the dominant sediment particle size fraction greater than 63 μm) is distinguished by abundant foraminifers (both planktic and benthic), Octocorallian (Gorgonian) sclerites, Ascidian (tunicate) spicules, and many carbonate grains of unknown origin (see Plate 4, Figure B).

- The pattern of lowstand (and/or stillstand) sedimentation is distinguished by medium grained bioclastic wackestone/packstone displaying: the highest magnetic susceptibility values; the lowest carbonate content values in both bulk and coarse sediment size fractions; moderately high percentage mud content in bulk samples, and very low sedimentation rates (cf. condensed section). Sand size bioclasts are similar to those deposited during the regression, with pteropod and benthic foraminiferal (particularly agglutinated species) debris being the most dominant constituent (Plate 5, Figure A). The very fine sand size sediment fraction is characterized by abundant angular to sub-angular quartz grains and, in general, a paucity of carbonate particles and fragments (Plate 5, Figure B).

- The early-transgression, is dominated by fine to medium grained bioclastic wackestone/packstone characterized by: the highest abundance of mud; medium to

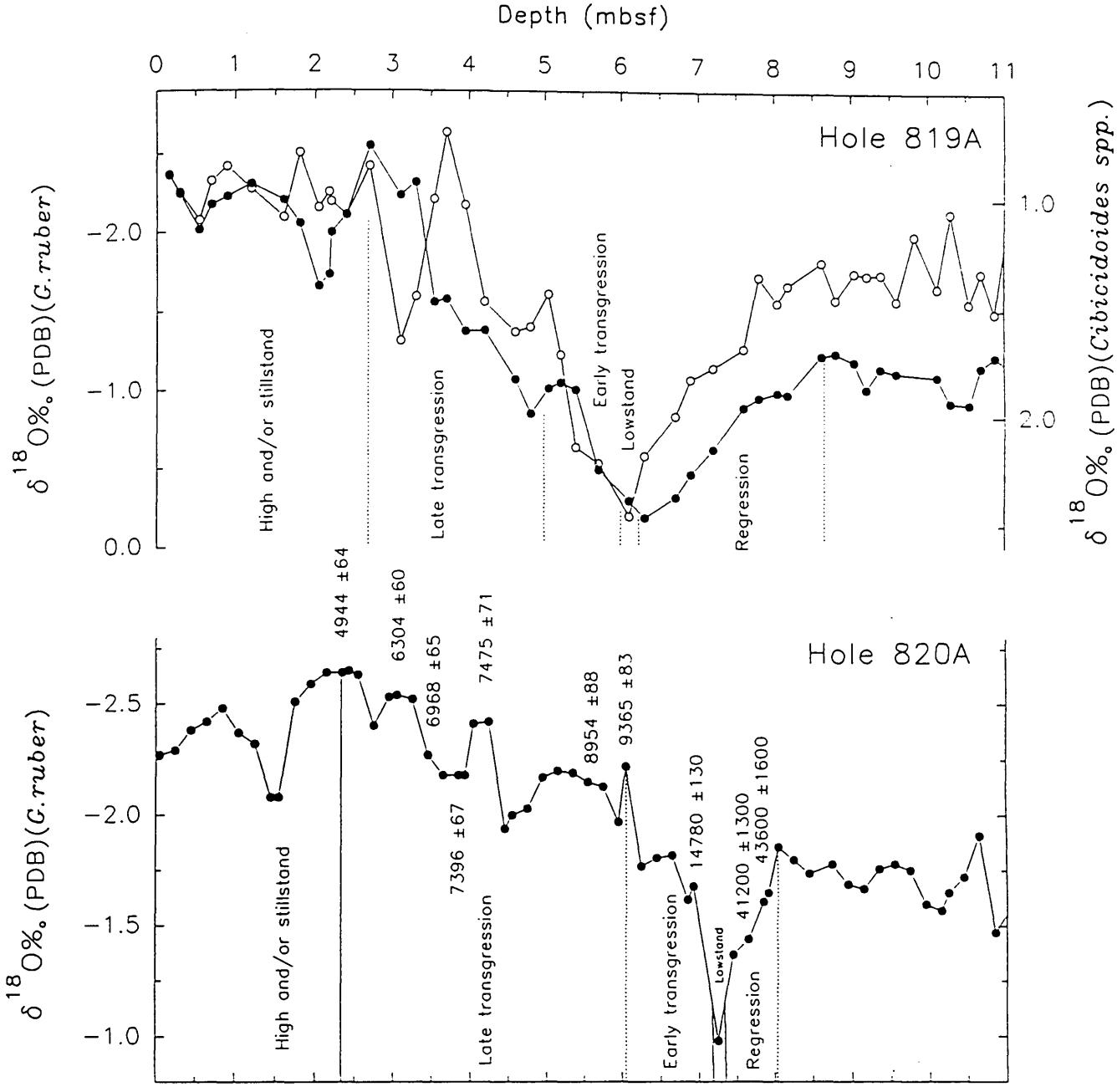

Figure 4.32. Comparison of the isotopic records from Hole 819A and Hole 820A (Peerdeman et al.,1993) over the last main glacial/interglacial cycle. The numbers on the lower plot refer to AMS carbon dates. In the upper diagram solid symbols refer to the benthic isotopic record.

high magnetic susceptibility values, and low carbonate content in both the bulk and coarse fractions. Sedimentation rates of around 22 cm/ka. Sand size bioclasts are similar to those deposited during the lowstand, however pteropods fragments appear to be more abundant, and a significant proportion of the planktic foraminifera are pyritized (Plate 6, Figure A). Although not as abundant as in the lowstand, the very fine sand fraction (63-125 μm) contains significant amounts of quartz (see Plate 6, Figure B).

- The late-transgression, comprising organic rich fine grained bioclastic wackestone is characterized by: the highest and lowest proportions of mud and sand size particles, respectively; low to medium and generally high carbonate content in the bulk and coarse sediment fractions, respectively; medium to high magnetic susceptibility values, and moderately high sedimentation rates (~53 cm/ka). Again bioclasts include planktonic foraminifers, as well as pteropods, but also include abundant plant remains (Plate 7, Figure A). Pyrite is particularly abundant within the sand size fraction, often occurring as framboids (Scholle, 1978) or as overgrowths. Analysis of the very-fine sand fraction reveals a general paucity of quartz grains, and an abundance of pteropod fragments and assorted carbonate debris (Plate 7, Figure B).

- The Holocene highstand (stillstand) is dominated by fine to medium grained bioclastic wackestone/packestone characterized by: high percentage mud content; moderately low magnetic susceptibility values, and high carbonate content values. Sedimentation rates are similar to those seen during the late transgression (~55 cm/ka). Sand size bioclasts are similar to those seen during the regression, with abundant planktonic foraminifera, pteropods, and agglutinated benthic foraminifera (Plate 8, Figure A). The very fine sand fraction (63-125 μm) is distinguished by low quartz content, and an abundance of: planktic foraminifers; tunicate spicules; octocorallian sclerites; and a variety of unidentifiable carbonate grains (Plate 8, Figure B).

Further, examination of the sedimentological and isotopic records from Hole 819A suggest that the pattern of mixed carbonate-siliciclastic deposition seen during the last main glacial/interglacial cycle is similar to that occurring during glacial stage 6. The only significant difference in these records, is that during stage 6 the foraminiferal abundances (both planktic and benthic species) are considerably higher (by several orders of magnitude) than those recorded for stage 2 sediments (Kroon *et al.*, 1993) (see Figure 4.27). This implies that the particle size characteristics of stage 6 sediments are being forced by foraminiferal abundances. In stage 2, the low foraminifer numbers, and high carbonate content, indicate that particle size (i.e.,

A

X 20

B

X 160

Plate 4. Photographs showing representative sand fraction (> 63 μm) (A) and very fine sand fraction (63-125 μm) sediments (B) for the sea level regression associated with the last main glacial/ interglacial cycle in Hole 819A.

A

B

x 20

x 160

Plate 5. Photographs showing representative sand fraction (> 63 μm) (A) and very fine sand fraction (63-125 μm) sediments (B) for the sea level lowstand (stillstand), associated with the last main glacial/ interglacial cycle in Hole 819A. Note the abundance of angular to subangular quartz grains.

A

X 20

B

X 82·5

Plate 6. Photographs showing representative sand fraction (> 63 μm) (A) and very fine sand fraction (63-125 μm) sediments (B) for the early transgression, associated with the last main glacial/ interglacial sea level cycle in Hole 819A.

A

X 20

B

X 160

Plate 7. Photographs showing representative sand fraction (> 63 μm) (A) and very fine sand fraction (63-125 μm) sediments (B) for the sea level late transgression, associated with the last main glacial/ interglacial cycle in Hole 819A. Note the organic contribution in these sediments.

A

x 20

B

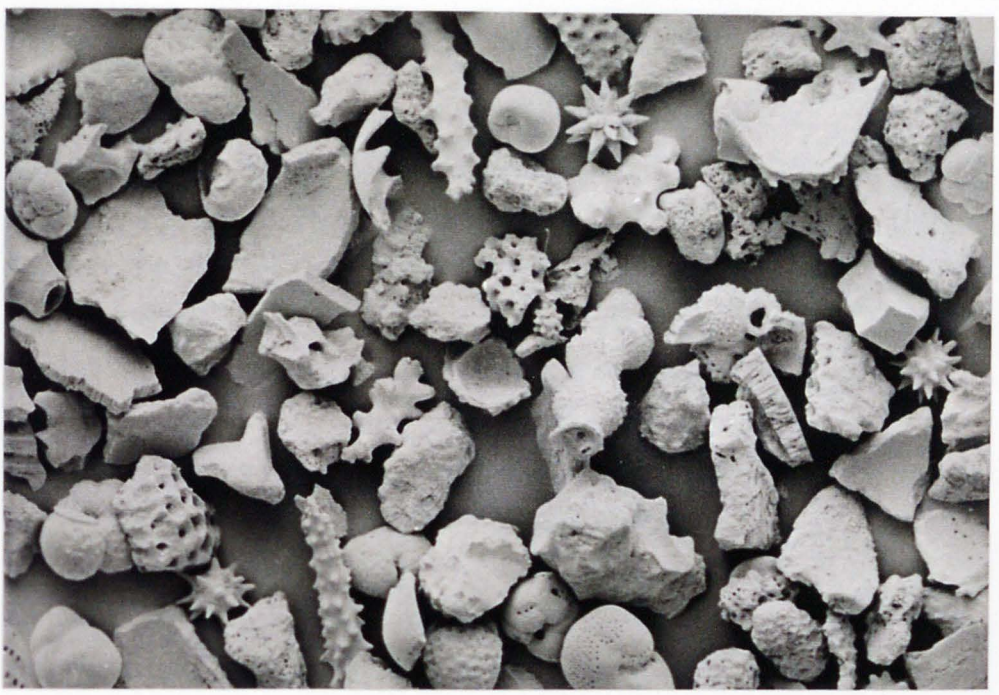

x 160

Plate 8. Photographs showing representative sand fraction (> 63 μm) (A) and very fine sand fraction (63-125 μm) sediments (B) for the Holocene highstand (stillstand) of sea level, in Hole 819A periplatform sediments.

percentage sand content) is being forced by an alternative source of carbonate (i.e., molluscan or pteropod aragonite). The relationship between grain size, carbonate content, magnetic susceptibility and isotopically inferred sea level, in the interval between lowstand stages 2 and 6 is more speculative, particularly given the uncertainty over the location of stage 4. As mentioned earlier, it now seems highly likely that the present position of stage 4 is incorrect. If the position of stage 4 is indeed moved to a new position between 13 to 16 mbsf, in accordance with the arguments discussed above, then analysis of the various records suggests that the downcore succession of peak positions (excluding the isotopic signal) is similar to the succession as seen in stage 2 and stage 6 (i.e., the peak in non-carbonate content lags the magnetic susceptibility, which in turn lags the peak in percentage sand content) (see Figure 4.28).

Having extracted a detailed record of the sedimentological response of upper-slope Site 819 to variations in sea level and climate change, the question arises as to how do these records compare to those from Hole 820A (280.8 m water depth) located 2.7 km further up the continental slope ? and how do these outer-shelf/upper slope of the GBR records compare to the more distal and deeper water Queensland Trough Hole 823A sediments ?

The high resolution sedimentologic and isotopic records from Hole 820A and Hole 819A show significant differences in the position of minima and maxima in value, with respect to the last main glacial/interglacial cycle. To emphasize these differences, the upper 11 m of the records from Holes 820A and 819A are presented in Figure 4.33 and 4.34, respectively. In addition, these data are summarized schematically in Figure 4.35. The main points, to be drawn from these figures are that:

(1) The highest magnetic susceptibility values occur during the sea level lowstand and early transgression in Hole 819A and Hole 820A, respectively.

(2) The highest percentage sand (or conversely the lowest mud) content occurs during the regression and lowstand in Hole 819A and Hole 820A, respectively.

(3) Both Hole 819A and Hole 820A records show the highest carbonate (or lowest acid-insoluble material) content during the sea level regression and highstand.

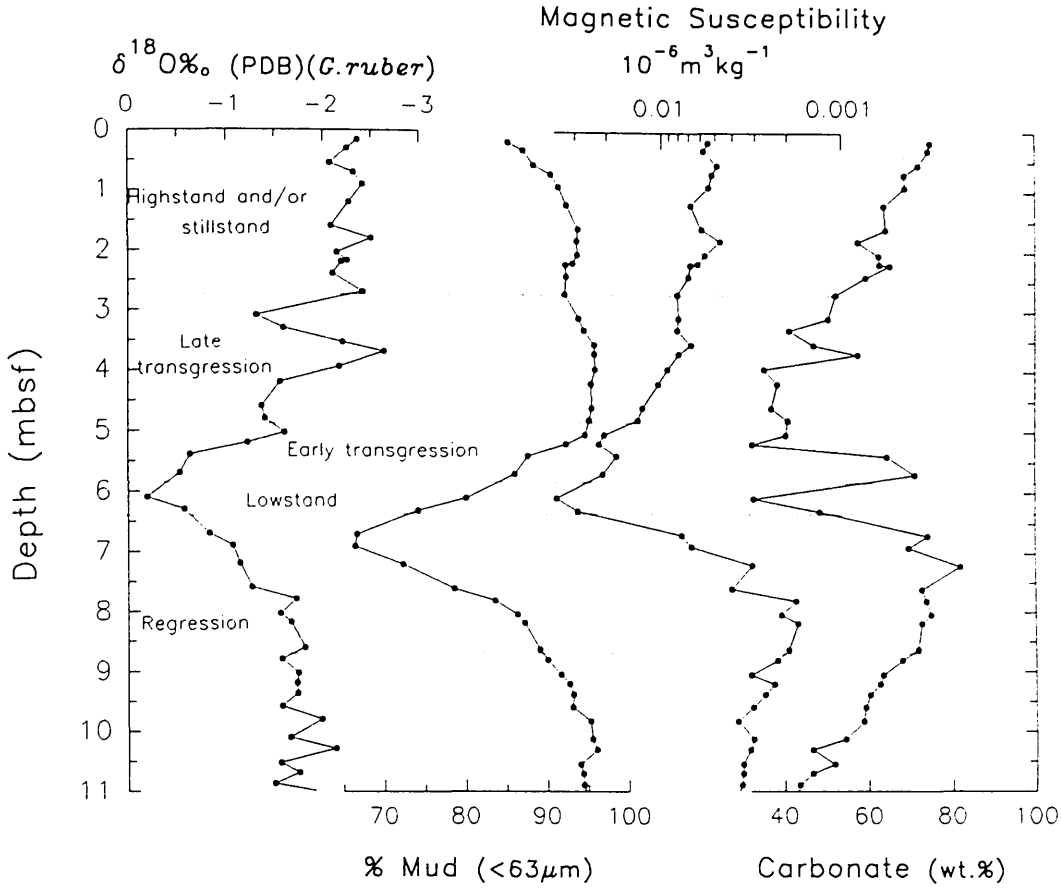

Figure 4.33. Hole 819A

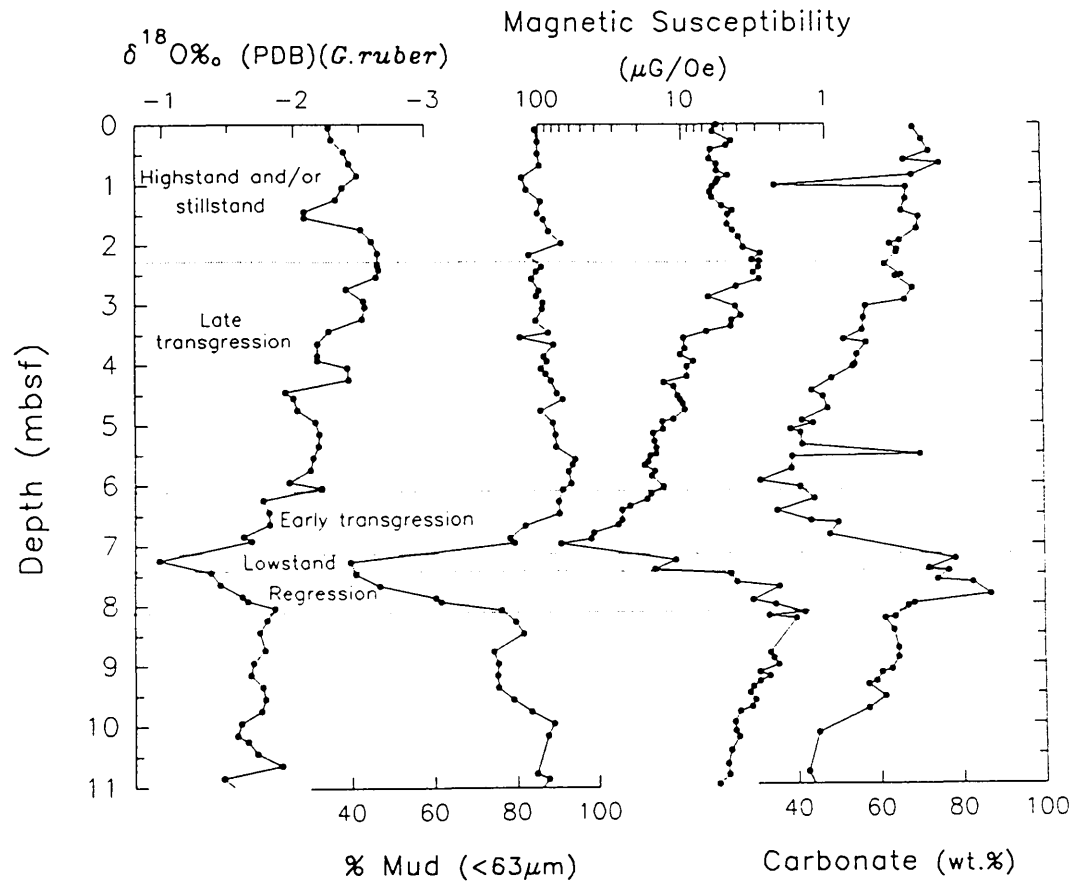

Figure 4.34. Hole 820A

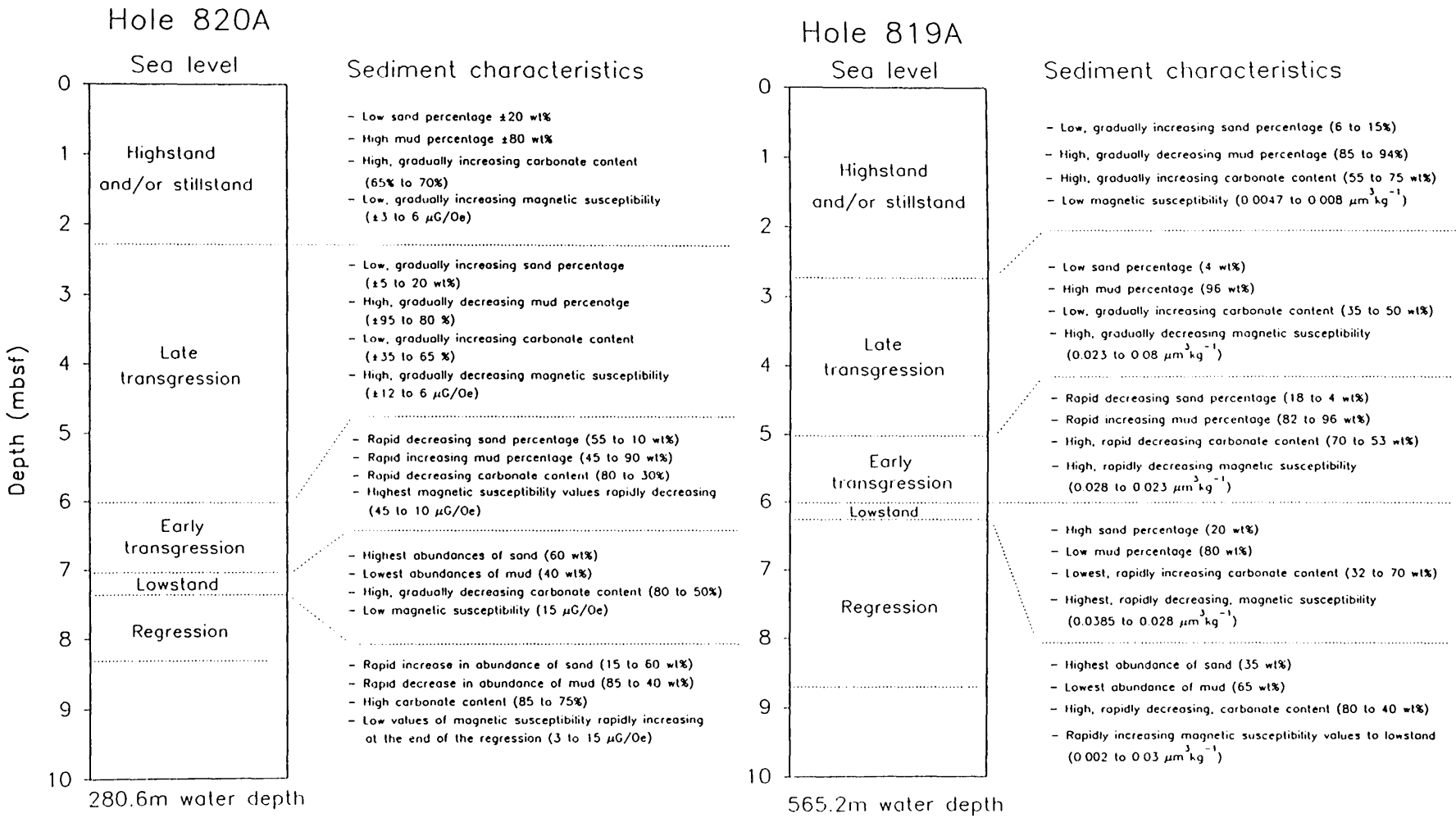

Figure 4.35. Comparison of the main sedimentological characteristics in Hole 819A (this study) and Hole 820A (Peerdeman et al., 1993), over the last main glacial/ interglacial cycle.

(4) The lowest mean carbonate content (highest acid-insoluble material) values, in Hole 820A and Hole 819A hemipelagic sediments, occur during the early transgression.

(5) Mean sedimentation rates in Hole 820A are higher during the early- and late transgression, and lower in the highstand, lowstand and regression, than values in Hole 819A.

The difference in the position of the magnetic susceptibility and sand content peaks, with respect to the last glacial/interglacial cycle, in Holes 820A and 819A, can be explained in several different ways. Sediment bypassing, via excavated shelf river channels (Feary *et al.*, 1990, 1993), is one possible explanation for the occurrence of high sand content during the regression and lowstand, in Hole 819A and Hole 820A sediments, respectively (i.e., during the regression sand size particles, rich in bank-derived carbonate (?), bypass Hole 820A and are deposited at Site 819). However, a more likely (and indeed simpler) explanation is that a hiatus has removed part of the lowstand record in Hole 820A (possibly containing the true peaks in magnetic susceptibility and sand content). Thus, the present glacial stage 2 isotopic enrichment peak in Hole 820A may in fact be part of the late regression or the early transgression? A hiatus would also account for the difference between the planktic oxygen isotope values, during stage 2, in these two holes (i.e, $\Delta\delta^{18}O_{819A\text{-}820A}$ = -0.44 ‰). Although, this line of argument should be treated with caution, because of the general lack of agreement, between the isotopic records from Hole 819A and Hole 820A, throughout the mid- to Late Pleistocene (see Chapter 3, Table 3.2). Similarly, the difference in magnetic susceptibility values, during the last main glacial perturbation, between these two cores (i.e, values are about 50 μG/Oe lower in Hole 820A- Barton *et al.*, 1993), suggests a gap in the records from Hole 820A. It seems highly likely that a lowstand erosional hiatus has removed a vital section of the Hole 820A record. In contrast, the sequence from Hole 819A appears to be more complete, particularly over the last main glacial/interglacial cycle. Thus, Hole 819A provides a better record to investigate the sedimentological response of the outer-shelf/upper-slope environment to variations in sea level.

In general, the comparatively low resolution of the Queensland Trough Hole 823A sequence has, to a certain extent, precluded the detailed interpretation/examination of the various sedimentological parameters in terms of sea level cycles. However, analysis of these records, over the last 300 ka, suggests that some of the key elements discussed above, between sea level and sedimentology, are present in the records from

Hole 823A. For example, in a similar manner to the records from Hole 820A and 819A, peaks in non-carbonate content in Hole 823A occur slightly later than glacial maxima. This association is particularly well developed during stage 2 and 6 (see Figure 4.26). However, as mentioned earlier, the relationship between particle size and magnetic susceptibility, and isotopically inferred sea level is more complex. The low amplitude variations in the mud (or conversely sand) content, coupled with the possible effects of incomplete sulphate reduction and dissolution of the primary iron-oxide signal (the process and its rock-magnetic effects are described by Karlin and Levy, 1983) in the upper 32 m of the sequence from Hole 823A (Barton *et al.*, 1993), have made detailed interpretation of these records highly speculative.

A further discussion of the implications of the offsets in sedimentologic peak position, with respect to sea level, on our current understanding of the complex depositional processes occurring on the northeast Australian margin will be provided in the concluding chapter.

4.6.3 Mid- to Late Pleistocene (~ 300 ka to 1.1 Ma) record of mixed carbonate and siliciclastic deposition on the Queensland margin.

Having examined the detailed response of the outer-shelf/upper-slope records to variations in eustatic sea level and climate change, over the last two main glacial/ interglacial cycles, the question now remains as to what is the relationship between the various sedimentologic and geochemical parameters in the lower part of the records from Holes 821A through to 823A? and, is there any difference in the dominant style of sedimentation between the upper and lower parts of the records from Holes 821 through to 823A ?

The lower part of the sedimentologic and isotopic records from Holes 821A through to 823A, spanning the mid- to Late Pleistocene, are illustrated in Figures 4.36 to 4.39, respectively. Correlation of these high resolution records has proved extremely difficult, particularly given the problems associated with the accuracy of the age models proposed for Site 820 (Peerdeman *et al.*, 1993) and Holes 819A and 823A (this study), and the poor isotopic record in Hole 821A. Furthermore, the change in dominant frequency of isotopic variation, between high frequency/low amplitude 40 ka cycles to 100 ka high amplitude/low frequency Milankovitch periodicities (between 400 and 780 ka- Imbrie, 1985; Ruddiman *et al.*, 1986, 1989), has made the detailed analysis of the sedimentologic records exceedingly difficult (and precludes the same degree of interpretation/ resolution achieved in the upper part of the records).

In general, analysis of the sequences from Site 820 and Hole 823A indicates a progressive decoupling of the sedimentologic and isotopic records with increasing depth (i.e., the older the records the more obscure the relationship between sedimentology and eustatic sea level becomes). Only in the upper-slope records from Hole 819A is a there a clear association between sedimentology and isotopically inferred sea level. Comparison of these records indicate that the mid- to Late Pleistocene is characterised by high carbonate content (or conversely low acid-insoluble material), low magnetic susceptibility and a slight decrease in the proportion of mud during periods of relative isotopic enrichment, i.e., during lowstands. This relationship is particularly well developed between 51 to 62 mbsf and 80 to 87 mbsf (see Figure 4.36). The near excellent correlation between the carbonate content and magnetic susceptibility is demonstrated by a high negative correlation coefficient (r = -0.82, where n = 378). Similarly, a correlation coefficient of r = 0.51 (n = 264) demonstrates a reasonable agreement between the percentage carbonate content and the planktic $\delta^{18}O$ values, from Hole 819A. These observations are the opposite of the general style of deposition seen during the last two main glacial perturbations (see Figures 4.28 and 4.33). Thus, the sedimentologic records from Hole 819A suggest a significant change in the style of mixed carbonate-siliciclastic deposition, on the Queensland margin, between the Mid- to Late Pleistocene and the Holocene. Unfortunately, the exact age of the change from lowstand and highstand carbonate deposition remains speculative, because of the presence of a major hiatus at 32.5 mbsf. Tentative interpretation of the records suggest that the change occurs between stage 16 and stage 9 (i.e., between about 630 to 330 ka).

The cause of the switch in the dominant style of carbonate deposition remains speculative. Possibly it is related to a change in the climate and/or palaeoceanography (as suggested by Alexander *et al.*, 1993), which caused the initiated of significant highstand carbonate platform production? Prior to this, conditions on the Queensland continental margin may have been unfavourable for reef growth, and carbonate deposition may have by driven by the productivity of pelagic organisms? Given the present data, however, there is insufficient evidence to suggest that carbonate is solely a function of platform production vs. pelagic productivity. These records could equally be interpreted in terms of variations in dissolution intensity and/or shallow-burial diagenesis.

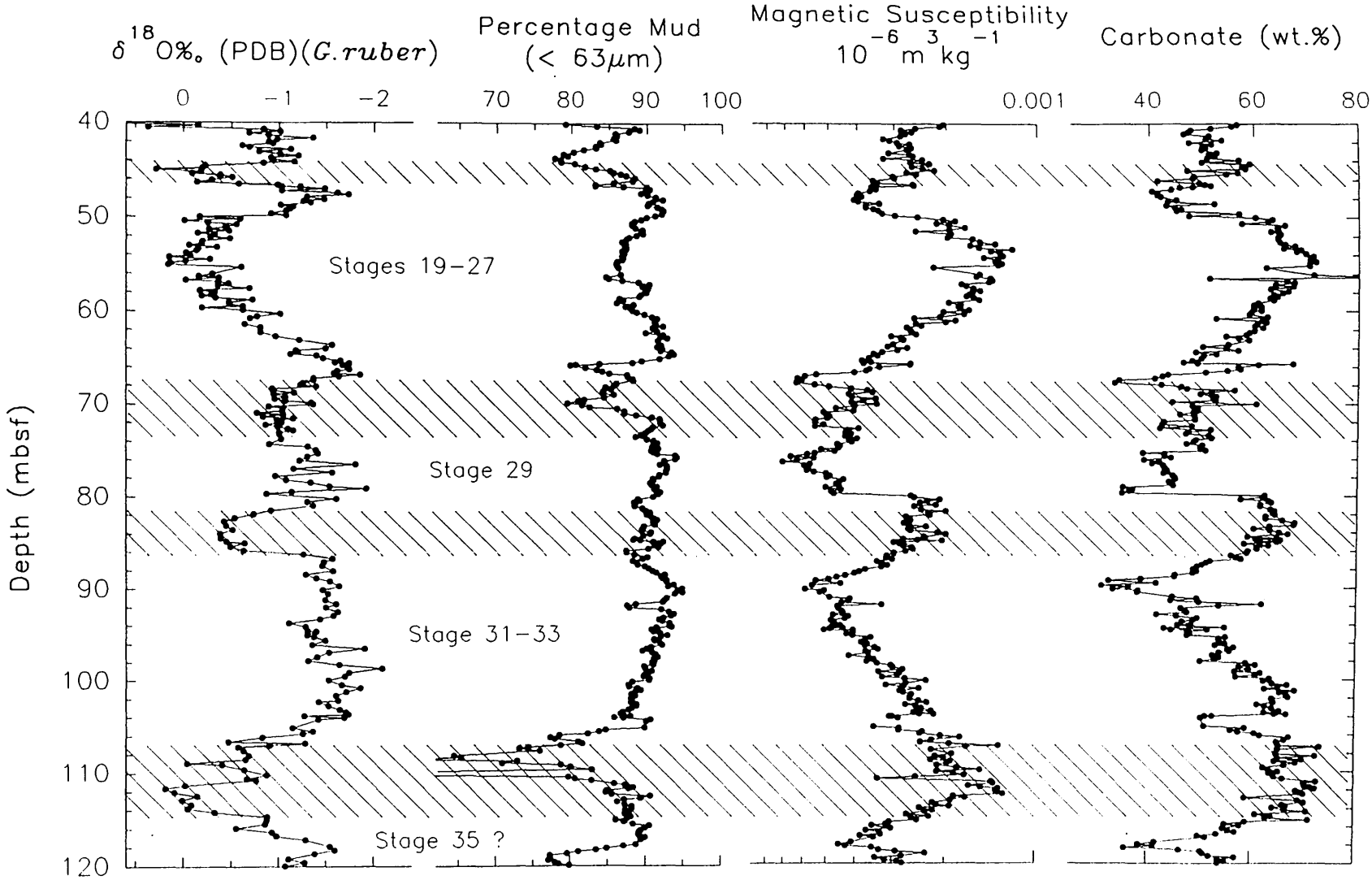

Figure 4.36. Oxygen isotope signal compared to abundance of mud, magnetic susceptibility and carbonate content for sediments recovered from Hole 819A. The numbers on the left diagram represent successive oxygen−isotope stages.

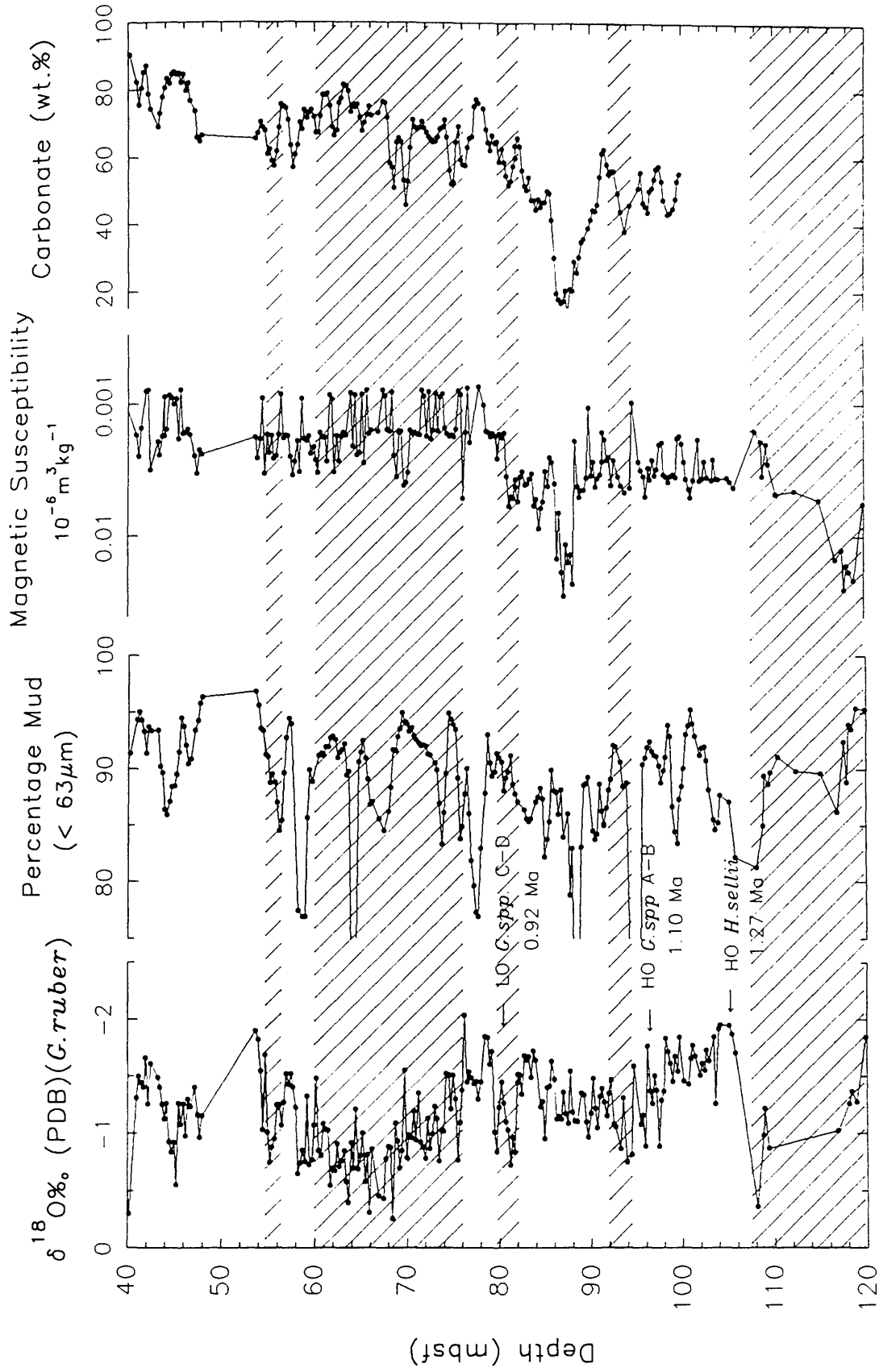

Figure 4.37. Oxygen isotope signal compared to abundance of mud, magnetic susceptibility and carbonate content for sediments recovered from the lower part of Hole 823A.

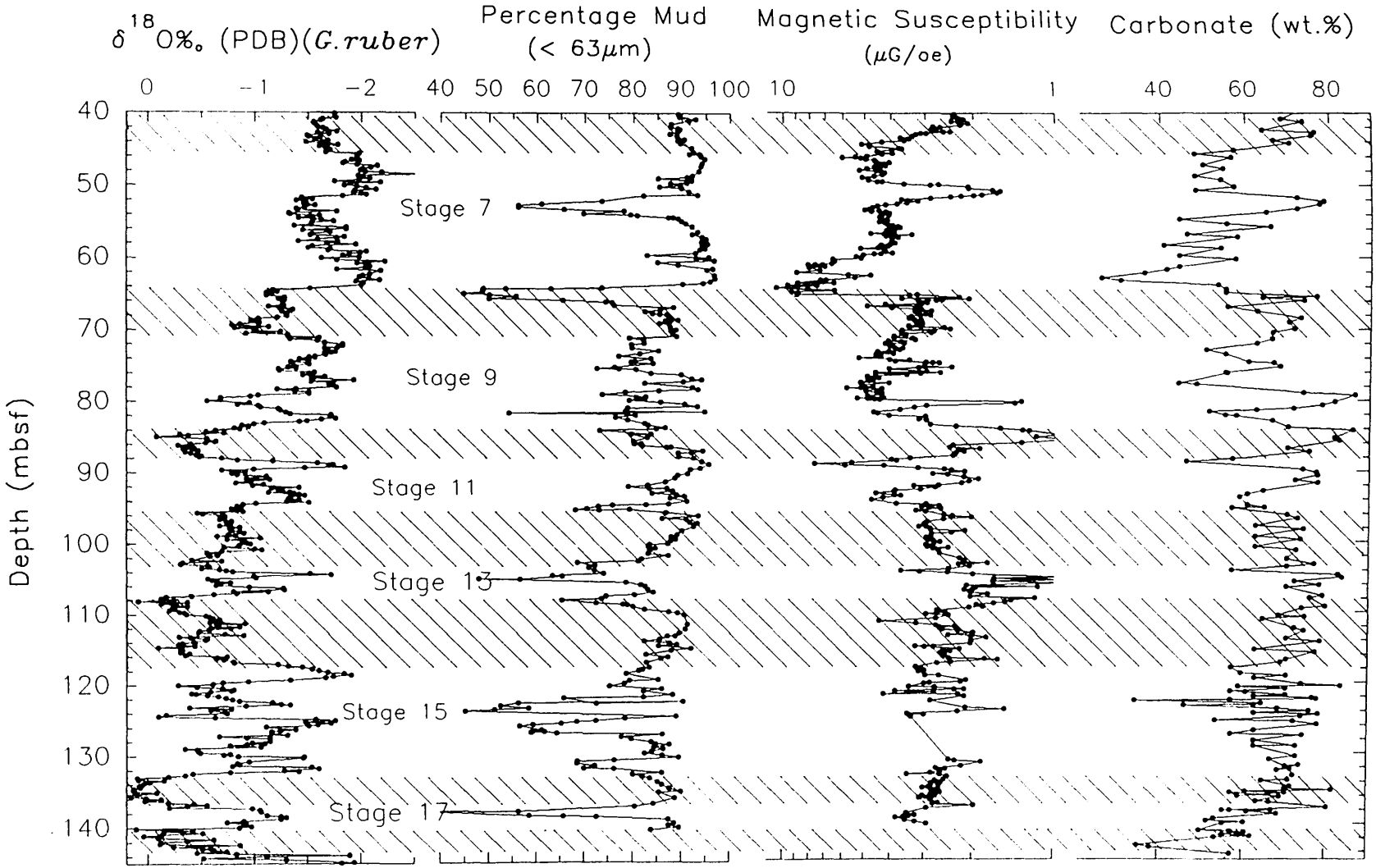

Figure 4.38. Oxygen isotope signal compared to abundance of mud, magnetic susceptibility and carbonate content for sediments recovered from Site 820. The numbers on the left diagram represent successive oxygen–isotope stages (based on Age Model 1, after Peerdeman et al., 1993).

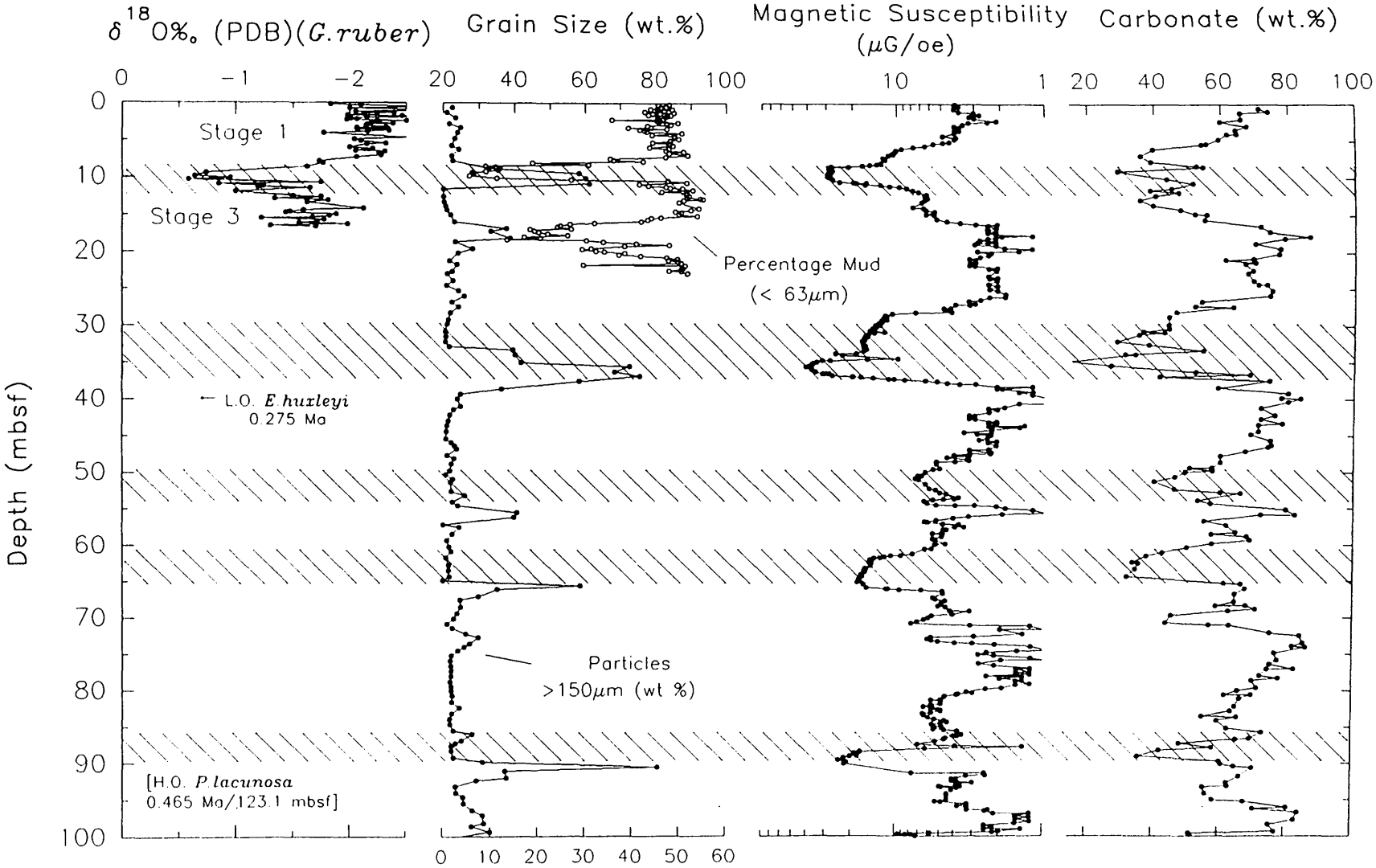

Figure 4.39. Grain-size, carbonate content, magnetic susceptibility and planktic $\delta^{18}O$ values, plotted against depth (mbsf), for Hole 820A periplatform sediments. Note the absence of an isotopic record below 18 mbsf.

4.7 Conclusions

Comparison of the high-resolution records from Sites 821 through to 823 suggests that, during the last 300 ka, the pattern of mixed carbonate-siliciclastic deposition on the outer-shelf/upper slope of the GBR, and in the Queensland Trough, has varied in a systematic or cyclical manner, in response to fluctuations in sea level and climatic change. Detailed analysis of the sedimentological and isotopic records, from these sites, suggest that high carbonate content typically occurs during periods of relative sea level highstand and during the early to mid- regression, and that a significant lag in the abundance of non-carbonate material occurs relative to glacial maxima. These observations are unlike the mixed carbonate-siliciclastic systems in the eastern Gulf of Mexico where regression and lowstand are reported to reflect the influx of terrigenous mud from the continents, during the lowstand, thereby diluting out the pelagic component and reducing the relative sand concentration (Gardulski *et al.*, 1986; Roof *et al.*, 1991).

During the mid- to late Pleistocene the pattern of mixed carbonate-siliciclastic sedimentation on the northeast Australian margin is more complex, than that seen during the last 300 ka. For example, the carbonate content record in Hole 819A (and to a certain extent Hole 823A), clearly demonstrate lowstand carbonate deposition during the mid- to Late Pleistocene. The implications of these observations are that either: the general pattern of carbonate deposition on the Queensland shelf changed from predominately lowstand deposition during the mid- to Late Pleistocene, to highstand deposition over the last 300 ka, or that factors other than carbonate productivity and dilution by terrigenous material are responsible for the carbonate signature seen in the lower part of the record from Hole 819A.

In summary: the carbonate-siliciclastic cycles seen in Hole 819A and Hole 823A (and in Hole 821A and Site 820) periplatform sediments can be interpreted as having formed via a number of fundamentally different processes. These processes are: (1) dilution of the biogenic carbonate fraction of the sediment by terrigenous or lithogenic material (and/or siliceous material); (2) dissolution of the metastable carbonate constituents of the sediment by seawater under saturated with respect to $CaCO_3$ (Ca^{2+} and HCO_3^- ions); and/or (3) productivity variations in calcium carbonate secreting organisms (shallow water platform production versus pelagic productivity).

On mixed carbonate-siliciclastic continental margins, such as that associated with the northeast Australian margin, including the GBR Province, analysis of the total carbonate content of core sediments provides insufficient information to enable all the

possible forcing mechanisms behind carbonate cyclicity to be determined. In order, to further understand the effects of variations in Late Pleistocene sea level and climate change on carbonate production and preservation on the Queensland margin, high resolution X-ray diffraction (XRD) analyses were carried out on Hole 819A and Site 823 periplatform sediments. These results, and their implications for our understanding of the sedimentological and palaeoenvironmental processes acting on the northeast Australian margin, throughout the Late Quaternary, are discussed in the ensuing section (Chapter 5).

Chapter 5 X-Ray Diffraction and Variations in Sediment Mineralogy, northeast Australian margin

5.1 Introduction

The aim of this chapter is to investigate, using X-ray diffractometry, the complex mineralogy of Hole 819A and Site 823 periplatform sediments in order to address the following questions: (1) what are the driving mechanisms behind carbonate production and preservation on the outer-shelf/upper-slope of the GBR, and in the Queensland Trough? (2) what has been the effect, if any, of dissolution and diagenesis on the carbonate mineralogy of Hole 819A and Site 823 periplatform sediments? and, (3) how do patterns of carbonate deposition on the Queensland shelf compare with variations in carbonate production and preservation on the marginal Queensland Plateau?

Most materials are crystalline and hence show some degree of symmetry and regularity, at the atomic level. This order can be made apparent or visible by X-ray powder diffraction or diffractometry. When irradiating crystalline material by monochromatic X-rays, a pattern (or signal) is obtained which is characteristic for the material. The X-ray diffraction (XRD) pattern of a crystal structure contains sufficient information to determine both the dimensions of the unit cell of the crystal lattice and the atomic arrangement within the cell. Qualitative identification of structures can be made by comparison of the interplanar spacing values (d) of the specimen pattern with an index of standard patterns (e.g., McClune, 1987). Standard X-ray diffraction techniques make use of the Bragg equation to obtain a measure of the atomic structure of a substance. The Bragg law (or equation) states that:

Equation 5.1. $$n\lambda = 2d \sin \theta$$

where: Lambda (λ) is the wavelength of the incident radiation (and also the emerging undiffracted X-ray beam), d is the atomic lattice spacing measured in angstroms (Å), theta (θ) is the angle between an incident monochromatic X-ray beam and the chosen atomic plane, and n is an integer (see Figure 5.1).

X-ray (powder) diffraction is commonly used in the study of modern and ancient carbonate sediments, limestones and dolomites. XRD analysis data can yield information on the chemical composition of carbonate minerals. For example, the Mg content of calcite and the Ca or Mg excess in dolomite (Hardy and Tucker, 1988). They can also be used to determine the percentages of the various $CaCO_3$ minerals

(a)

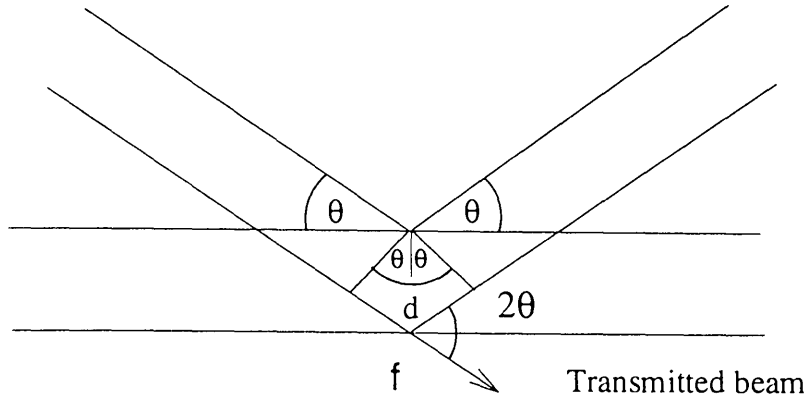

(b)

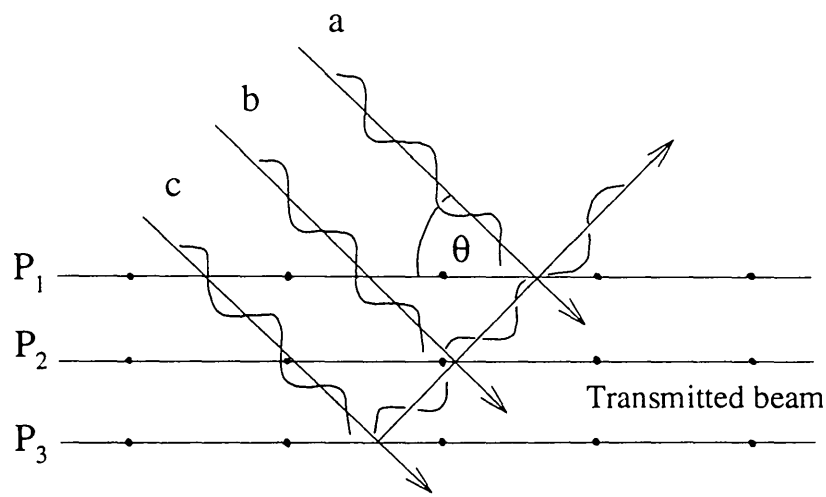

Figure 5.1. Conditions for diffraction of X-rays from a regular crystal lattice: (a) Bragg angle of diffraction (P_1, P_2 and P_3) are successively deeper atomic planes uniformly spaced within the crystal.

(b) path-length difference in condition for diffraction, i.e., when the incidence angle is q and d is the interplanar distance.

present in an unknown mixture or carbonate (although estimates of the amount of dolomite in a dolomitic limestone are less precise- Milliman, 1974). Because of the complexity of the quantitative approach, however, no standard technique of X-ray diffraction analysis has been established (Gavish and Friedman, 1973; Fang and Zevin, 1985). Recent studies of carbonate sediments show two dominant analytical approaches to quantitative X-ray diffraction analysis, both based on peak intensity.

The first approach, and the simplest method of quantification, involves the technique of XRD peak height measurement (Lowenstam, 1954; Turekian and Armstrong, 1960; Friedman, 1964; Gevirtz and Friedman, 1966). Peak height analysis is based on the assumption that a carefully prepared mineral sample will display a constantly reproducible peak height relative to a fixed concentration of internal standard. The second method of quantifying diffraction data is based on measurements of the total peak intensity (Chave, 1962; Neumann, 1965; Milliman and Bornhold, 1973). Intensity is directly related to diffractogram peak area, which can be calculated by planimeter (Neumann, 1965), by tracing the area under each peak on tracing paper, cutting them out and weighing them on an analytical balance (Pilkey, 1964), or in simple mixtures, by geometric analysis (Milliman, 1974). Chave (1962) suggests the accuracy of the peak area method to be about 5 %. In both methods peak intensity is taken above a base line, normally measured just above background level.

Considerable debate has arisen as to which quantitative method of analysis is the more accurate, both methods have their drawbacks and merits. Gavish and Friedman (1973) considered that peak height analysis was more reliable for separating low Mg-calcite (LMC) and high Mg-calcite (HMC)[1]. They also demonstrated that particle size and the degree of structural damage suffered by component minerals in a sample, through excessive grinding, affected the peak areas more than the peak heights. Both authors concluded that, for quantitative analysis of calcite and Mg-calcite in inhomogeneous carbonates, which require different grinding times and have variable amounts of calcite and Mg-calcite, the peak height measurement is the better method of analysis. Milliman and Bornhold (1973), on the other hand, showed that although HMC peak heights and peak shapes varied between different algal genera, the total peak intensity remained relatively constant, and that for aragonite and calcite mixtures, the peak area method was more reliable. In addition, Milliman (1974) noted that, whereas any one type of calcite tends to display a relatively constant peak height, calcites of different

[1]High-magnesian calcite and Low-magnesian calcite have more than 4 mole percent $MgCO_3$ and between 0-4 mole percent $MgCO_3$ in solid solution, respectively (Milliman, 1974).

biogenic origin (for example coralline algae versus oyster calcite) can display markedly different peak heights. Milliman (1974) concluded that in complex mixed carbonates the use of peak heights can result in significant errors, and that peak area analysis (although more lengthy) was more reliable.

In addition to the effects of excessive grinding, different sources of biogenic carbonate and particle size, several other factors can seriously affect X-ray peak intensities; among these are $MgCO_3$ content and the degree of crystallinity of carbonate components (Milliman, 1974). In general, marine biogenic calcites (and all aragonites) have similar peak intensities, largely because the crystallite size is similar (Hardy and Tucker, 1988). However, those calcites with large crystal size, such as reagent grade calcite, some dolomite crystals and echinoid plates (Towe, 1967), show anomalous X-ray diffraction intensities and, according to Hardy and Tucker (1988) should be avoided as standards for calcite analysis. According to Milliman (1974), the substitution of calcium ions by magnesium, iron or manganese cations decreases the lattice spacing in the calcite lattice, and can greatly reduce the peak intensity of various carbonates.

Despite the complex nature of Hole 819A and Site 823 sediments (Shipboard Scientific Party, 1991), given the large number of samples to be analysed and the complexity of the peak area method of quantification, the method of peak heights analysis was used to determine semi-quantitative mineral abundances. A comprehensive review of X-ray diffraction theory and analysis techniques is provided by Klug and Alexander (1974) and Hardy and Tucker (1988), respectively.

5.2 Analytical Procedure

The relative abundance of a variety of minerals present in Hole 819A and Site 823 (Holes 823A and 823B) sediments were quantified by X-ray diffraction. These minerals[2] include aragonite, LMC, HMC, dolomite and quartz. X-ray diffraction was typically performed on approximately 0.5 g of the bulk sediment. Each sample was oven-dried at 60°C, before being hand ground in an agate mortar (with analytical grade acetone) for exactly 4 minutes (Milliman, 1974). Individual samples were then drawn up in a pipette, dispersed on a glass slide (diameter 2 cm), smeared out to produce a sediment slurry of standard thickness and diameter, and dried at room temperature before being subject to X-rays. The rapid evaporation of acetone and drying of the

[2]Other minerals which were detected in Site 819 and 823 periplatform sediments were: chlorite, kaolinite, feldspar (albite), zircon, tourmaline, gypsum, pyrite, epidote, smectite. These in most cases were present at such low concentrations as to preclude accurate quantification.

sediment slurry is advantageous because, according to Archer (1969), slow drying can result in differential settling which enhances the X-ray response of fine components. In addition, the use of acetone during grinding can serve as a crude coolant, reducing the effects of excess heat produced through over-grinding, and the conversion of aragonite to calcite (Goodell and Kunzler, 1965). Each individually prepared sample was then analysed using a Philips PW 1011/1050 automatic powder diffractometer (PW 1808 sample changer) (under the supervision of Geoff. Angell, University of Edinburgh) at 40 kV and 50 mA, through a scan from 5° to 40° 2θ (Cu-kα), at a low scanning speed of 0.040° per second for optimal resolution. X-ray tube parameters were checked periodically for machine drift[3]. Typical X-ray diffractometer system parameters are summarised in Appendix C, Table C.1.

X-ray diffractogram peak intensities (or peak heights) for aragonite, LMC, dolomite, and quartz were measured, corresponding to the degrees 2θ given in Appendix C Table C.2 (after Chao, 1969). During analysis the mineral α-quartz (3.343Å, 26.66° 2 θ) was used as an internal standard, thus enabling subtle shifts in peak position (related to sample preparation and/or machine drift) to be detected and a suitable correction applied. The position of the HMC peak is normally located to the right, or on the shoulder of the LMC peak (i.e., between about 29.84° to 30.0° degrees 2θ). According to Chave (1952) the greater the quantity of magnesium within the calcite lattice the larger the shift in peak position toward that of dolomite (or conversely, the less Mg within the calcite lattice the closer the peak position to that of LMC). In some X-ray diffractograms the peaks of LMC and HMC are clearly separated, whereas in others the LMC peak merges with that of the HMC (see Figure 5.2). In the later case, the asymmetry of the LMC peak was used to estimate the position (and hence peak height) of the HMC peak.

Separate XRD calibration curves were produced for aragonite, LMC, HMC, dolomite and quartz using a modified version of the sample spiking method proposed by Gunatilaka and Till (1971). Calibration involved taking a 'base' or reference bulk sediment sample[4] and adding to it a given quantity of a single mineral, in order to produce a series of dilutions of the original poly-mineralic sample (or conversely

[3]During the course of the experimental work the diffractor X-ray emission tube was replaced. Subsequent sample peak height analyses were corrected to the old X-ray tube parameters.

[4]Sample 133-819A-6CC was chosen as a base or reference sample (in preference to a monomineralic spiking agent such as haematite- Roy Thompson, pers.comm., 1993) because it was thought to have the same diffracting efficiency and characteristics of preferred orientation, uniformity of crystallite size, and adsorption effects as the samples under investigation (particularly if both are prepared in the same manner).

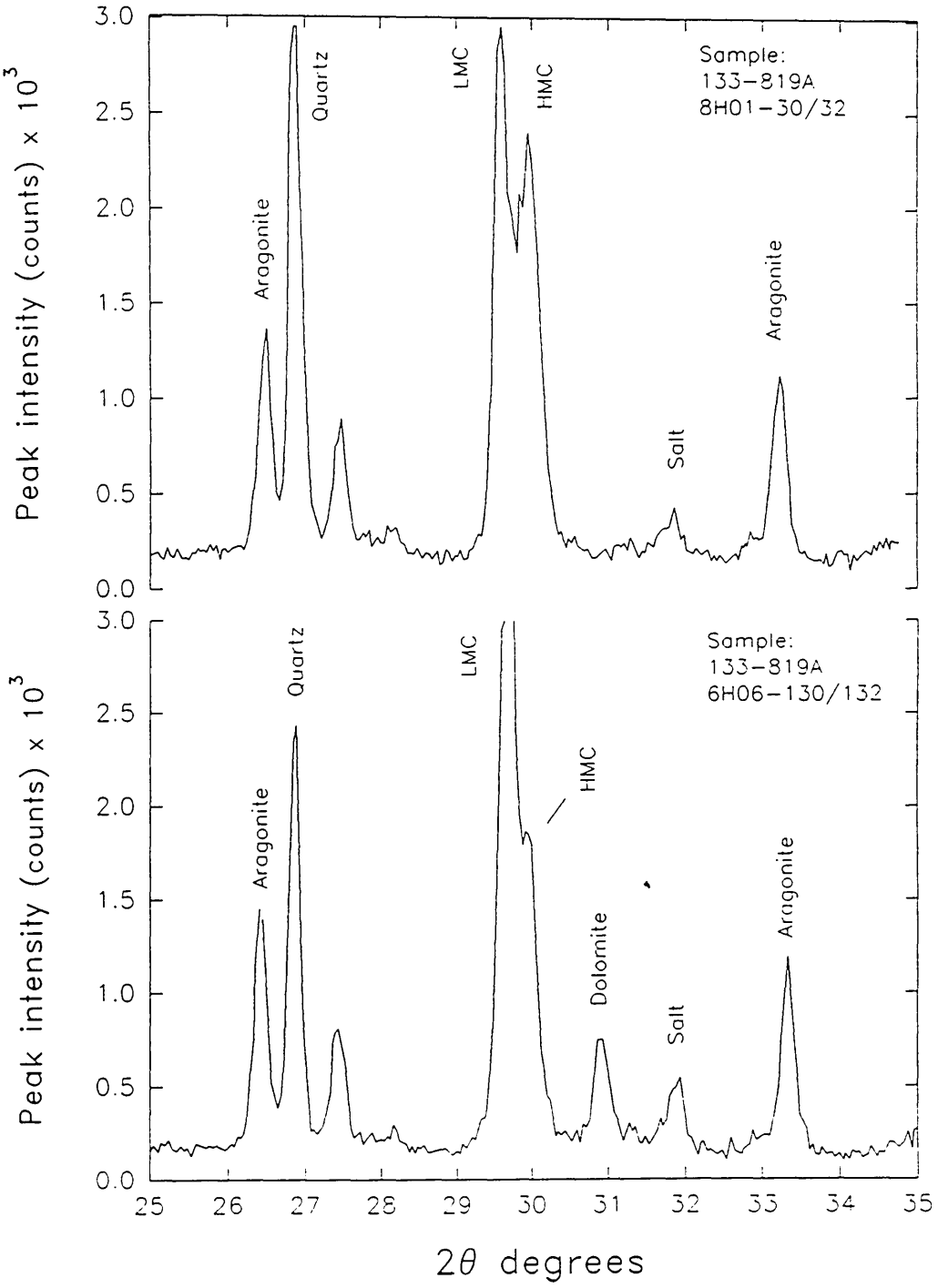

Figure 5.2. Whole sediment XRD diffractograms illustrating the positions of the principle minerals. Note that in the upper plot the low Mg calcite (LMC) and high Mg calcite (HMC) peaks are clearly separated, whereas in the lower chart the HMC peak merges with that of the LMC.

mono-mineralic enrichments). In other words an additional 10 %, 20 %, 30 % etc. (up to 100 % by weight) of a specific mineral was added to the base sample. This procedure was repeated for each mineral analysed, resulting in a set of XRD calibration curves for aragonite, LMC, HMC, dolomite and quartz. Sample mineral abundances (expressed as volume percent) were then calculated by converting peak heights listed by the diffractometer (supplemented by measurements taken directly from XRD diffractogram graphs in the case of HMC, and for any ill-defined or ragged peaks- see Hardy and Tucker, 1988) into semi-quantitative values using the gradient or slope of the relevant calibration graph (see Appendix C, Figures C.1 to C.5).

The standards used to produce the calibration curves in this study were; Recent coral (*Porites lutea*) from Thailand, 'Iceland Spar' calcite from an unknown locality in Scotland, and recent temperate coralline algae (*Phymatolithon calcareum*) from the Sound of Iona (Inner Hebrides, Scotland), for aragonite, LMC and HMC, respectively. The dolomite and quartz standards were both commercially available analytical reagents (AR). Iceland Spar calcite was used as a spiking agent/ calibration standard (instead of a biogenic source of LMC such as: foraminiferal, arthropodan, or brachiopodan calcite) because of its chemical homogeneity, availability (thus avoiding the laborious task of hand picking sufficient biogenic LMC grains needed to spike unknown samples), and ease of preparation (producing a uniformity of crystallite size). A comparison of the diffraction behaviour of Iceland Spar calcite and various biogenic sources of LMC is presented in Table 5.1. The assayed $MgCO_3$ content of the dolomite standard was quoted as 47.25 mole percent. Estimates of the $MgCO_3$ content of the HMC standard, based on 2θ degree values of between 29.84° to 30.0°, using the calibration curves of Goldsmith *et al.* (1961), suggest that the calcite contains between 13 to 18 mole percent $MgCO_3$ (see Figure 5.3). These $MgCO_3$ content values are similar to those cited by Chave (1954) for a variety of different algal genera. Similarly, the range in LMC 2θ degree values between 29.42 and 29.56 (average 29.51 degrees 2θ for 20 replicate analyses), suggests that the Iceland Spar calcite contains less than 3 mole percent $MgCO_3$ (see footnote on previous page).

To check the errors inherent in using multiple calibration/ standardisation curves, the sum of the independently determined carbonate phases, for samples collected at Site 819, were plotted against the total percent carbonate content as determined by the acid-base titration method outlined in the previous chapter (section 4.3) (see Figure 5.4). Comparison of these two high-resolution records suggests that, while individual values differ, on the whole both methods show the same pattern of variation with depth. A similar comparison with sediments from Hole 823A was not made because of

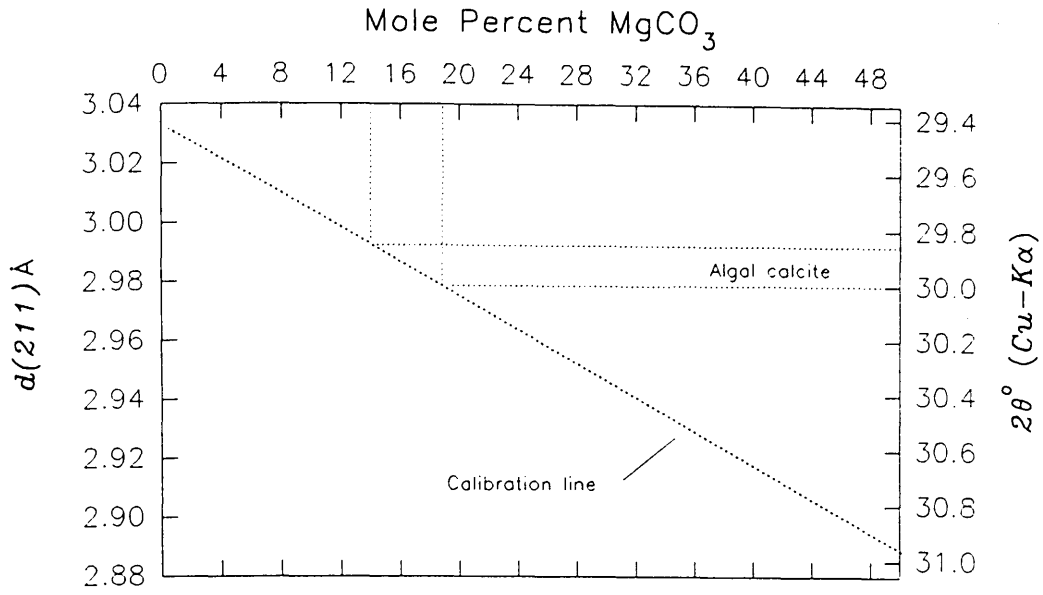

Figure 5.3. Calibration curve relating the mole percent $MgCO_3$ in a calcite (or dolomite) with the position of the d(211) XRD peak (after Goldsmith et al., 1961). Shifts in the position of the HMC peak, between 29.84 and 30.00 2θ degrees, suggest that the coralline algae standard contains on average between 14 to 19 mole percent $MgCO_3$.

Table 5.1. Comparison of XRD peak intensities (peak height) for Iceland Spar calcite and a variety of biogenic low magnesian calcite (LMC) sources, measured at 29.40 2θ degrees (see Appendix C, Table C.2).

LMC Source	Peak Intensity*
Iceland Spar	11363
Benthic foraminifera (*Cibicidoides spp.*)	7414
Planktic foraminifera (*G.ruber*)	7588
L. Cretaceous Nannofossil Chalk (Swanage, Dorset, U.K.)	10076
L. Cretaceous Nannofossil Chalk (Studland, Dorset, U.K.)	11089

Note that Iceland Spar calcite peak intensities quoted in the above table are significantly higher than those recorded whilst producing the calibration curves (see Appendix C). The difference between the two set of figures is a result of the instalation of a new X-ray tube shortly after the construction of the calibration curves (and all of the samples had been analysed). Both foraminiferal samples were from Site 819. *Average of six analyses.

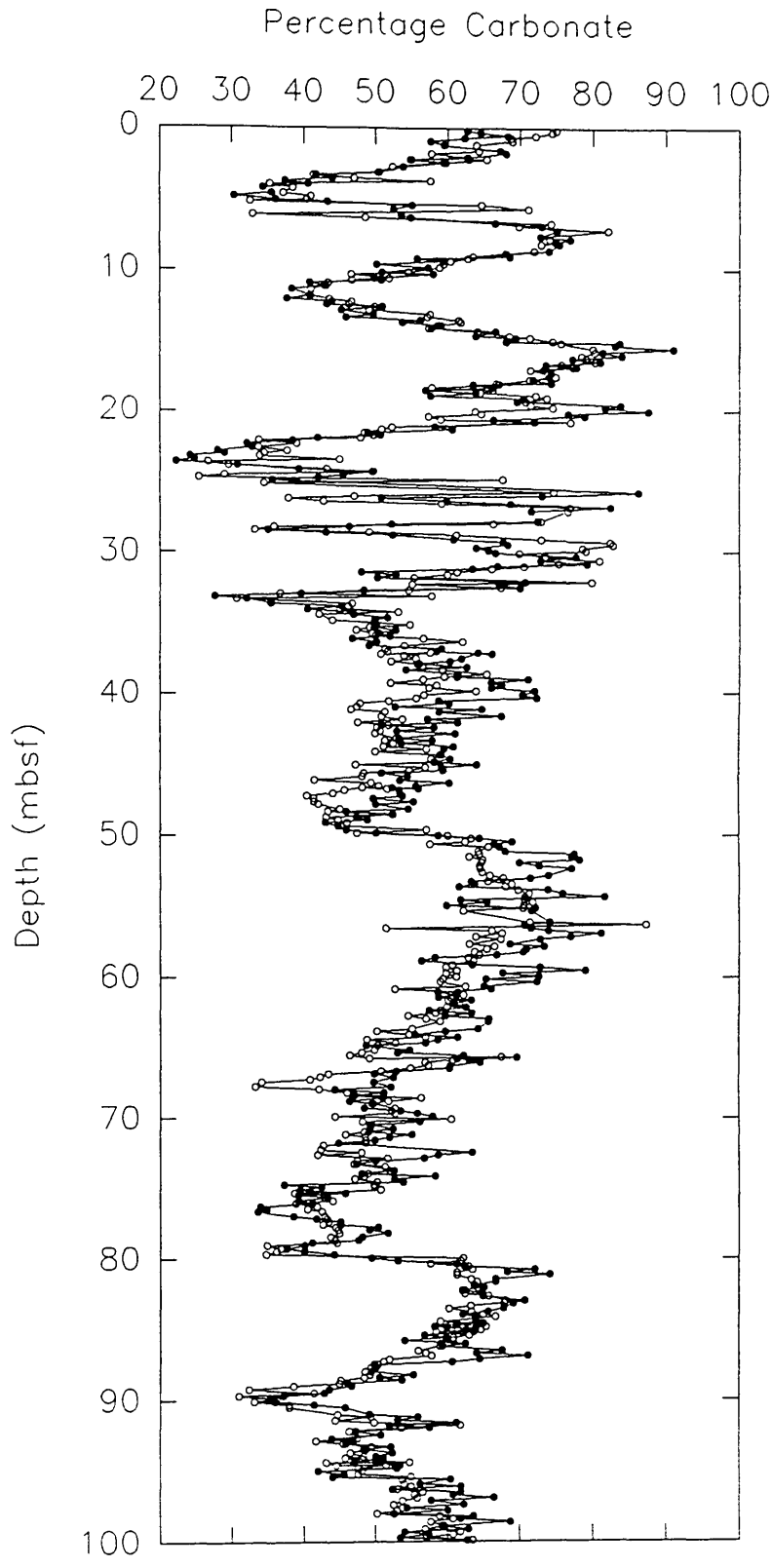

Figure 5.4. Comparison between the XRD (closed circles) and titration (open circles) methods of carbonate content analysis in Hole 819A. Note the good agreement between both records, as exemplified by a correlation coefficient (Pearson's r) of 0.782 (where N=356)

the difference between the size fractions analysed (i.e., XRD and carbonate titration analyses were undertaken on the whole sediment sample and mud size fractions, respectively). However, an alternative check on the accuracy of the titration method, and carbonate content in Hole 823A, is provided in chapter 6, based on X-ray Fluorescence (XRF).

5.3 Description of XRD Results

5.3.1 Hole 819A (outer-shelf/upper-slope of the GBR)

Downcore variations in carbonate mineralogy and quartz content for Hole 819A piston cores, plotted alongside the planktic oxygen isotope record, are illustrated in Figures 5.5 to 5.7. These XRD results are tabulated in Appendix C, Table C.3. In addition, a ternary plot illustrating the variation in main carbonate mineralogy (based on individual values corrected to 100 % carbonate) for Hole 819A hemipelagic sediments is presented in Figure 5.8. Total carbonate content values (sum of the concentration of individual carbonate phases) typically range from 30 % to 80 %, and are similar to those obtained using the acid-base titration method described in the previous chapter (Section 4.3) (see Figure 5.4).

Analyses of the XRD results indicate that aragonite is the most abundant mineral present in Hole 819A sediments (see Figure 5.5). Downcore aragonite content values typically range from about 20 % to 50 %, with a mean of approximately 32 % (by volume). In contrast to the upper section, the lower part of the record at Hole 819A (i.e., below the major stratigraphic hiatus at 32.5 mbsf- Shipboard Scientific Party, 1991), is characterized by expanded cycles and lower amplitudinal fluctuations in percentage aragonite content. In common with the LMC content curve, the aragonite record displays a prominent 'saw-tooth' pattern or profile, characterized by a gradual downcore decrease in aragonite value, followed by a sharp increase in mineral abundance. This relationship is particularly well developed between 40 to 95 mbsf, in both the aragonite and LMC records (and the total carbonate content record- see Figure 5.4). Below about 45 mbsf, aragonite abundance and planktic $\delta^{18}O$ values display a clear antithetical relationship (i.e., aragonite content is high during periods of relative isotopic enrichment) (see Figure 5.5). The correlation coefficient (Pearson's r) for the relationship between aragonite content and planktic $\delta^{18}O$ for this part of the core is 0.38 (n = 250). Above 45 mbsf, however, the association between these two parameters is more complex. For example, the aragonite content low at about 23 mbsf appears to follow the prominent isotopic enrichment event at approximately 25 mbsf (see Figure 5.5). Similarly, the prominent low in aragonite content centred at about 5 mbsf, clearly lags the last main glacial maximum (isotopic stage 2) by several metres.

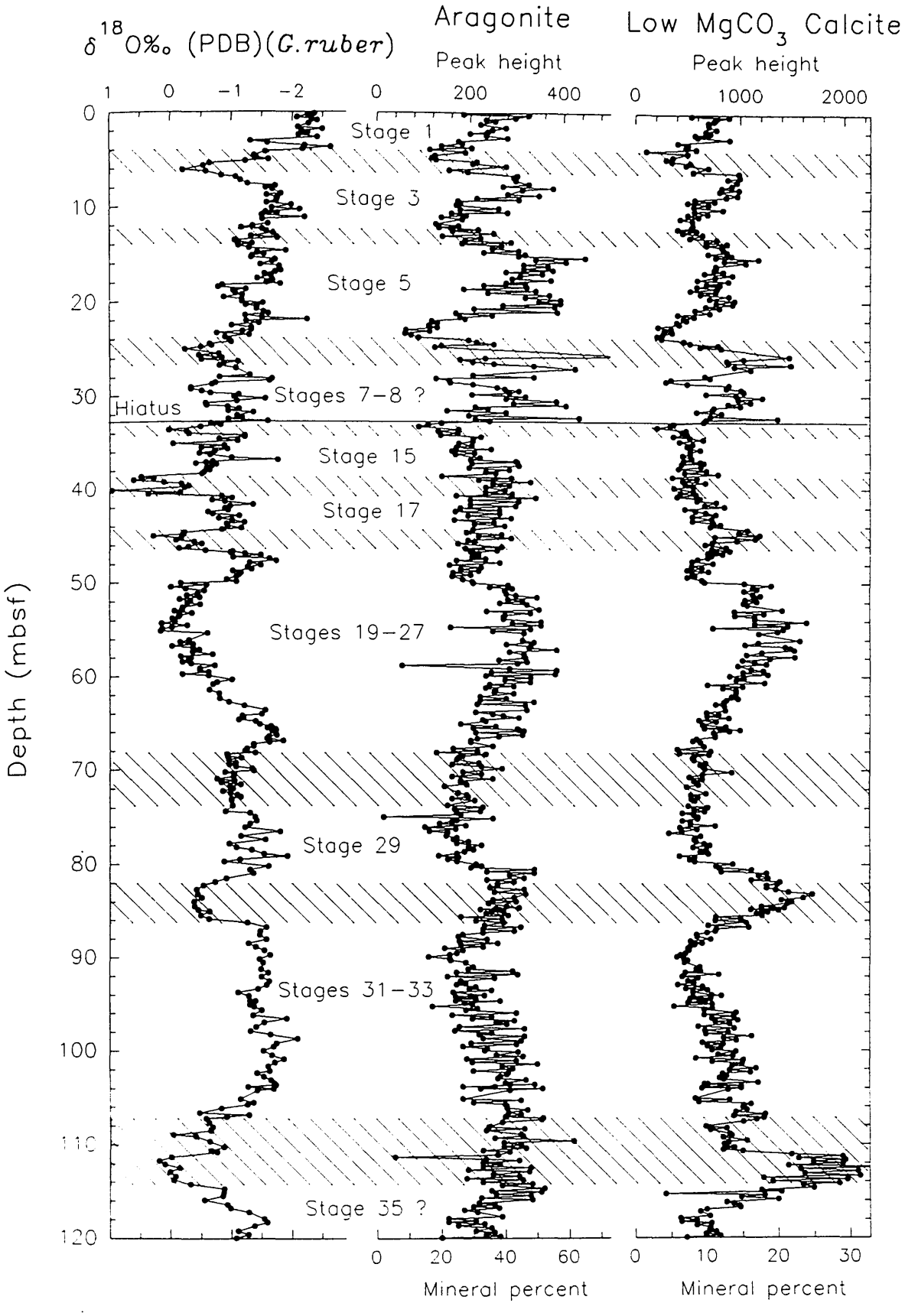

Figure 5.5. Downcore variations in percentage aragonite and low Mg calcite (LMC) in Hole 819A periplatform sediments. Also shown is the planktic oxygen isotope record from this core.

After aragonite, LMC and HMC are the next most abundant carbonate minerals found in Hole 819A piston cores. LMC and HMC content values typically range from about 6 % to 16 % and between 0 % to 15 % (by volume), respectively. In general, LMC values tend to follow the fluctuations in the aragonite content (correlation coefficient r = 0.58, N = 563), although notable exceptions to this relationship occur, particularly at 113 and 45 mbsf, where LMC content is high, but aragonite content is low (see Figure 5.5). HMC content values typically follow those observed for aragonite and LMC, in the upper part of the sequence at Hole 819A, but are antithetical to other carbonate phases in the lower part of the record. Below 32.5 mbsf, HMC values are typically low during periods of oxygen isotope enrichment (or conversely high during episodes of isotopic depletion).

Dolomite is the least abundant carbonate mineral present in Hole 819A sediments, with values rarely exceeding 5 % by volume. Dolomite is almost totally restricted to the lower part of the record in Hole 819 (see Figure 5.6). Below 32.5 mbsf (position of major stratigraphic hiatus/ sedimentary slump), the relationship between dolomite and aragonite, LMC and HMC is unclear. For example, whereas the peaks in dolomite content between 50 to 60 mbsf and centred at 84 mbsf are clearly sympathetic with the aragonite and LMC records, the dolomite peaks at 38 and 117 mbsf correlate negatively with LMC and positively with aragonite (see Figures 5.6 and 5.7). Dolomite abundances are typically high when HMC content values are very low, suggesting a direct relationship between these two minerals. An exception to this general association occurs between 30 and 38 mbsf, where both HMC content and dolomite values are high. Throughout the sequence in Hole 819A, peaks in dolomite content typically occur during periods of isotopic enrichment (i.e., during periods of inferred low sea-level).

In general, percentage quartz content values in Hole 819A sediments ranges between about 2 % to 16 %, although the downcore mean is about 6 % (by volume). Typically, quartz content is low when the carbonate content is high. Interpretation of the lower part of the record in Hole 819A suggests that quartz content is high during periods of relative isotopic depletion (or conversely low during times of isotopic enrichment). This relationship is particularly well developed between 50 to 60 mbsf, and 82 to 86 mbsf (see Figure 5.7) In contrast, throughout the upper part of the record at Hole 819A, the relationship between quartz content and isotopic value is more complex, with peaks in quartz content occurring during both highstands and lowstands of sea level.

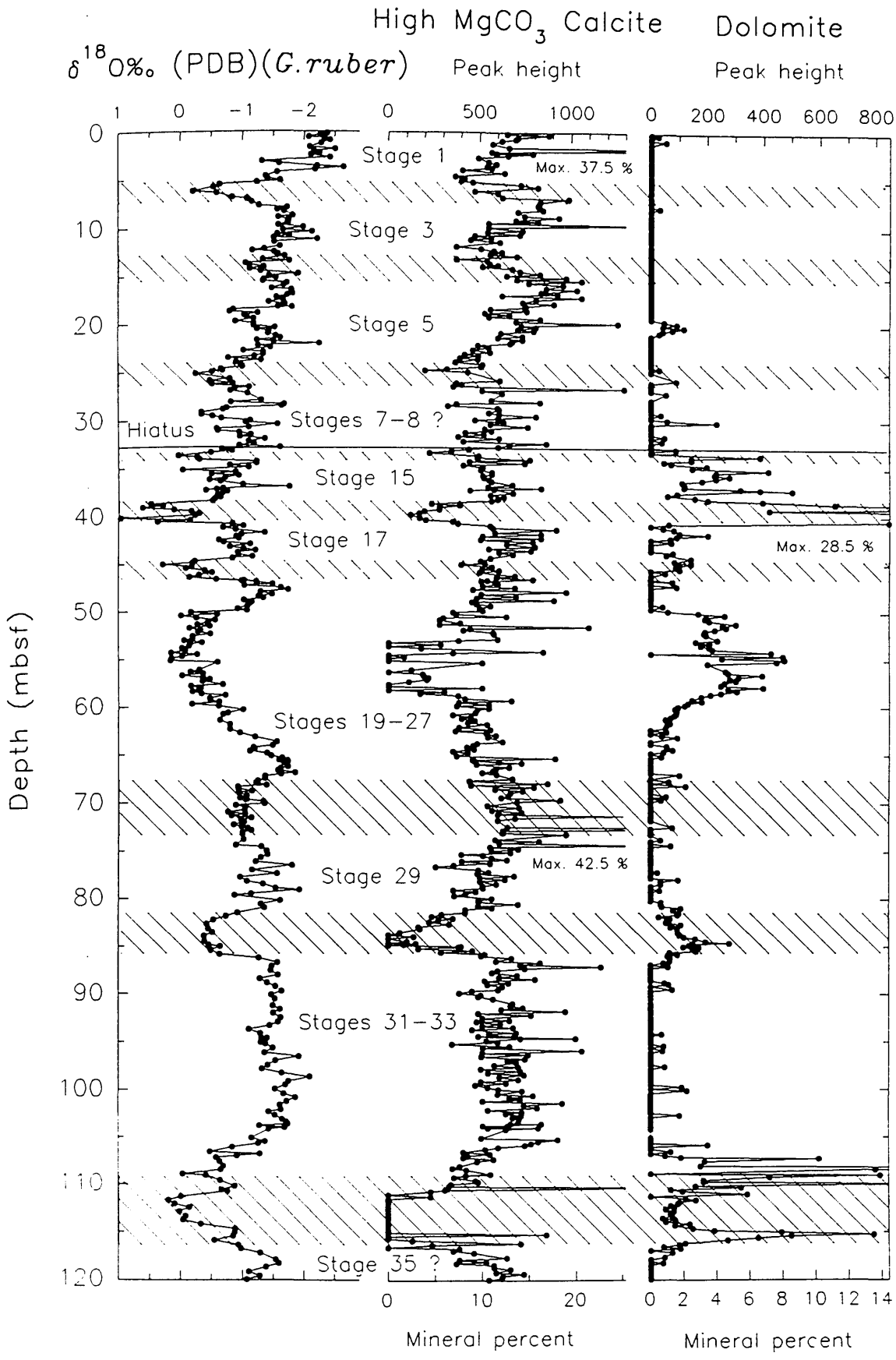

Figure 5.6. Downcore variations in percentage high Mg calcite (HMC) and dolomite in Hole 819A periplatform sediments. Also shown is the planktic oxygen isotope record from this core. Significant peaks off the scale are marked. Note the occurrence of high dolomite during lowstands of sea level.

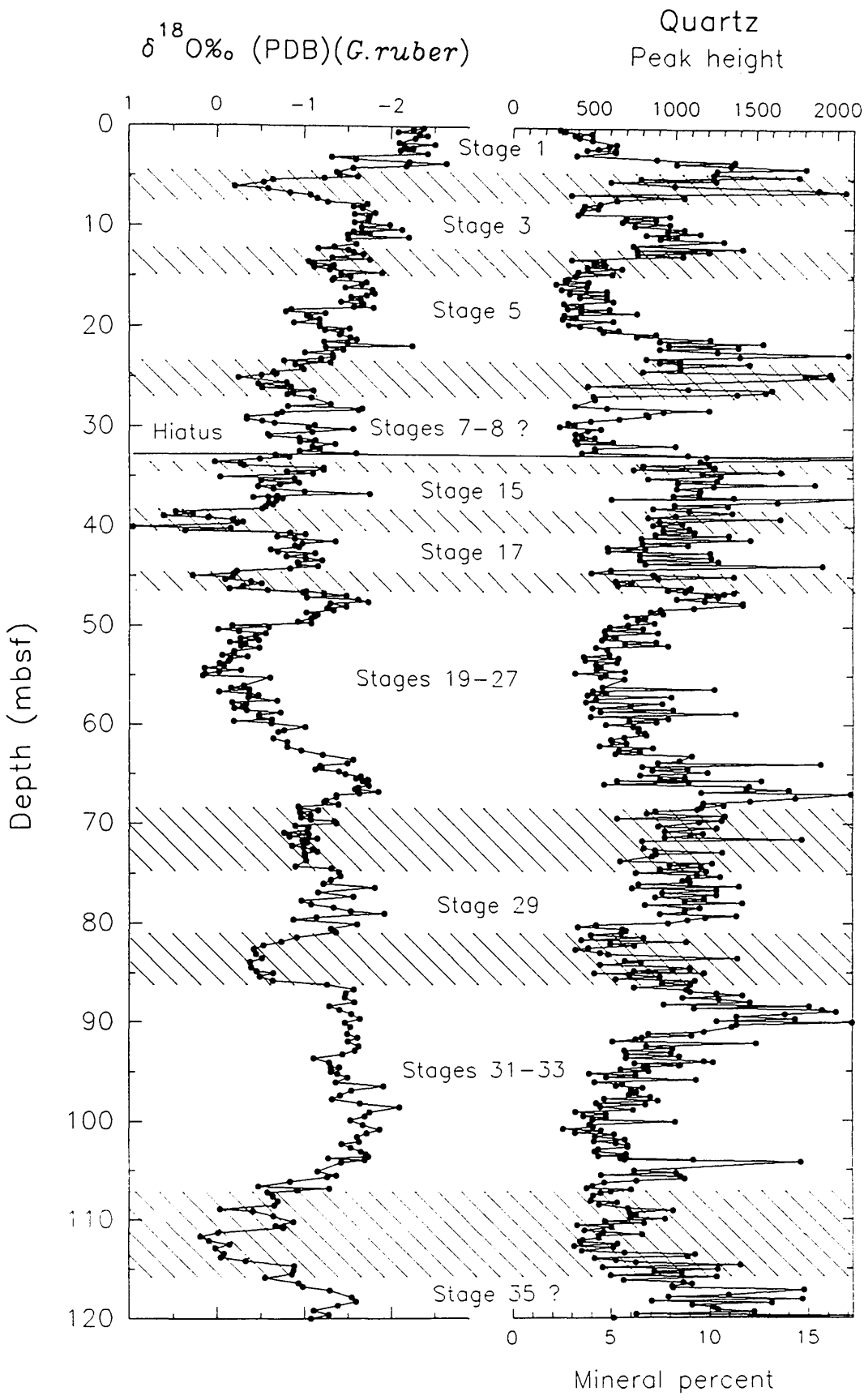

Figure 5.7. Downcore variations in percentage quartz content plotted alongside the planktic oxygen isotope curve from Hole 819A. Note the presence of a major hiatus at 32.5 mbsf.

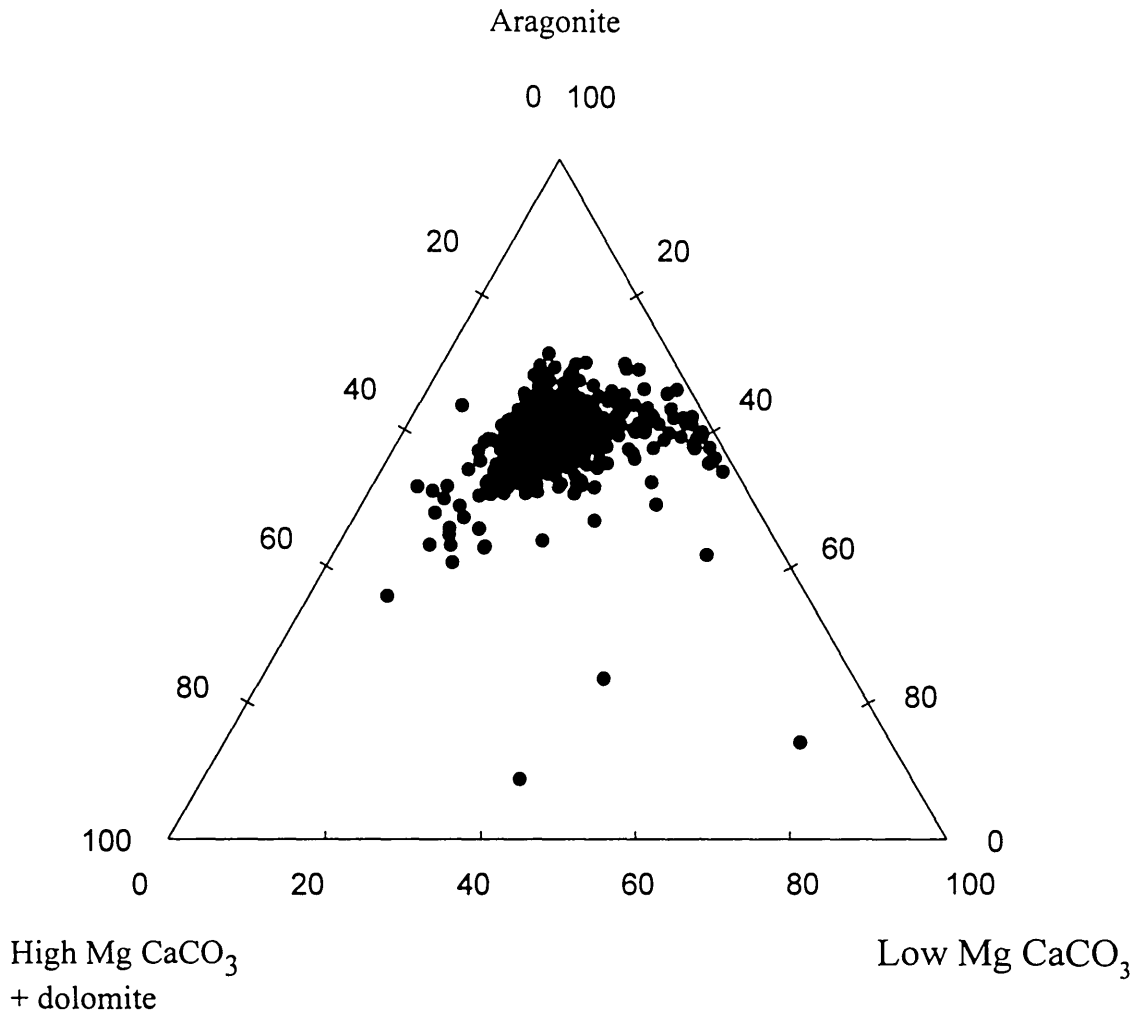

Figure 5.8. Variations in HMC, dolomite and aragonite content in Hole 819A sediments. Values are corrected to 100% carbonate using the sum of the individual carbonate phases. Note that Hole 819A sediments are composed of mainly aragonite with subordinate amounts of HMC, dolomite and LMC.

5.3.2 Queensland Trough Hole 823A (0-120 mbsf)

Figures 5.9 through to 5.11 illustrate the variation in dominant carbonate and terrigenous mineralogy, plotted against depth and alongside the planktic $\delta^{18}O$ record, in Hole 823A. Also, a ternary plot illustrating the variation in dominant carbonate mineralogy (based on LMC, HMC and aragonite content values corrected to 100 % carbonate) for Hole 823A periplatform sediments is presented in Figure 5.12.

The total carbonate content in Hole 823A samples (sum of the concentration of individual carbonate phases, as determined using the XRD technique described above) typically ranges from about 40 to 70 %, although the mean value throughout the core is approximately 50 % (see Figure 5.13). These whole sediment bulk values are similar to the percentage carbonate contents obtained for the mud or fine fraction (<63 μm), using the acid-base titration method described in the previous chapter.

In general, Hole 823A sediments are characterized by a mixture of dominantly aragonite and LMC, with minor amounts of HMC and dolomite (see Figure 5.12). Percentage aragonite content typically range from about 15 to 40 %, although the downcore average is about 20 % (by volume) (see Figure 5.9). The highest aragonite content values occur between about 55 to 80 mbsf (~670 to 920 ka). In the lower part of the sequence from Hole 823A (>50 mbsf), the aragonite content record exhibits a weak antithetical relationship to planktic $\delta^{18}O$ values (correlation coefficient $r = 0.4$, $N = 199$). Throughout the upper part (<50 mbsf) of the sequence from Hole 823A, however, the relationship between these two parameters is more complex. For example, during glacial stage 6 and interglacial stage 13 aragonite content is high, whereas during stages 12 and 14 aragonite values are low (see Figure 5.14).

Sediment mineralogy in the upper part of the sequence recovered from Hole 823A (<50 mbsf) is mainly dominated by LMC, with subordinate amounts of aragonite and HMC and (with the exception of a few horizons) a general absence of dolomite. In contrast, between 55 to 80 mbsf (~670 to 920 ka), Hole 823A sediments are distinguished by high aragonite content, with varying amounts of LMC and HMC, and significant quantities of dolomite. In general, below 80 mbsf sediments have equal proportions of aragonite and LMC, and contain subordinate amounts of HMC, with very little dolomite. Typically, LMC content values are high when aragonite content is low (or conversely low when aragonite content is high). LMC values range from about 20 to 40 % and 10 to 30 % in the upper (<50 mbsf) and lower (>50 mbsf) parts of the core, respectively. Throughout the upper part of the core, the LMC record is

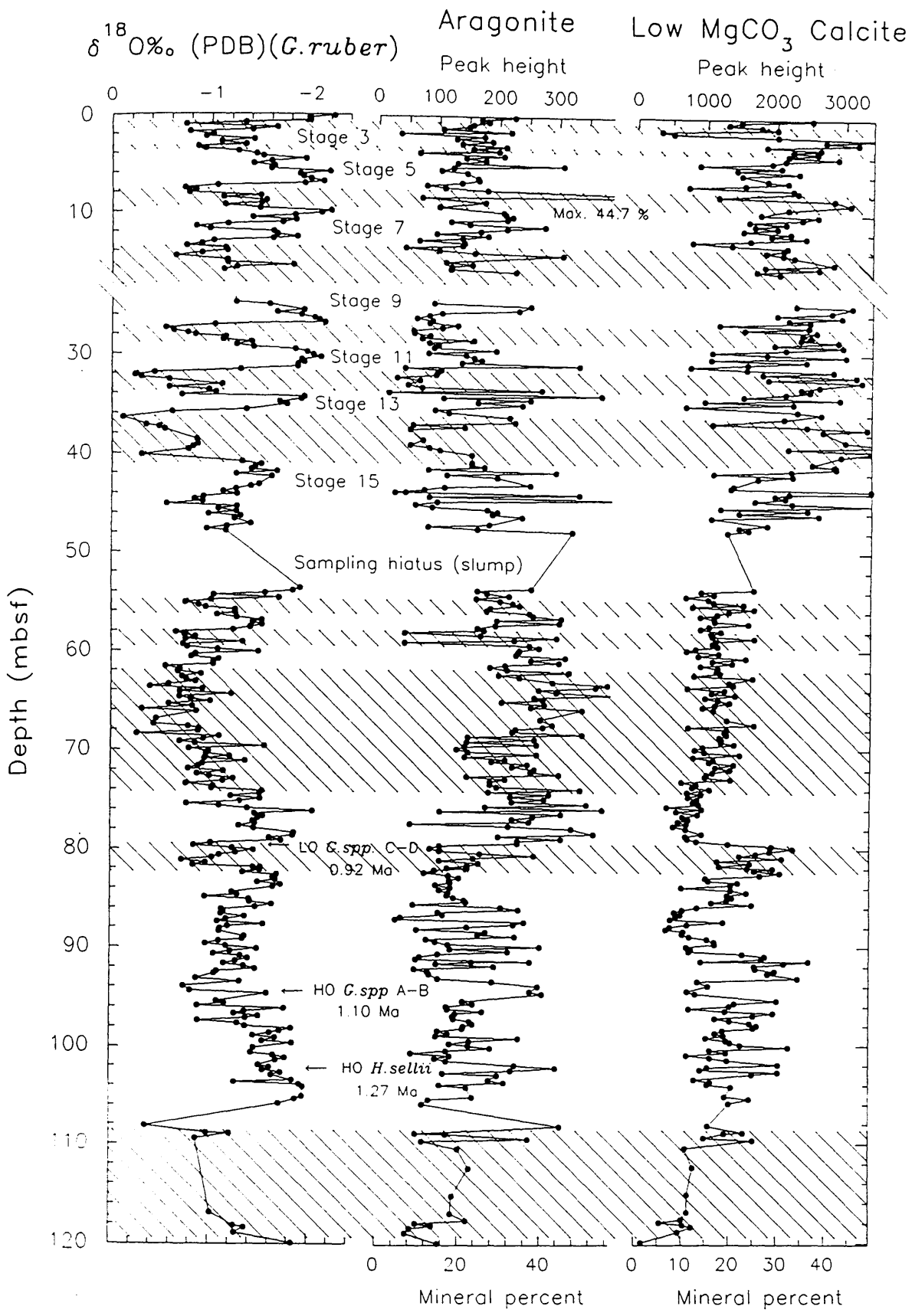

Figure 5.9. Downcore variations in percentage aragonite and low Mg calcite content in Hole 823A periplatform sediments. Also shown is the planktic oxygen isotope record from this core.

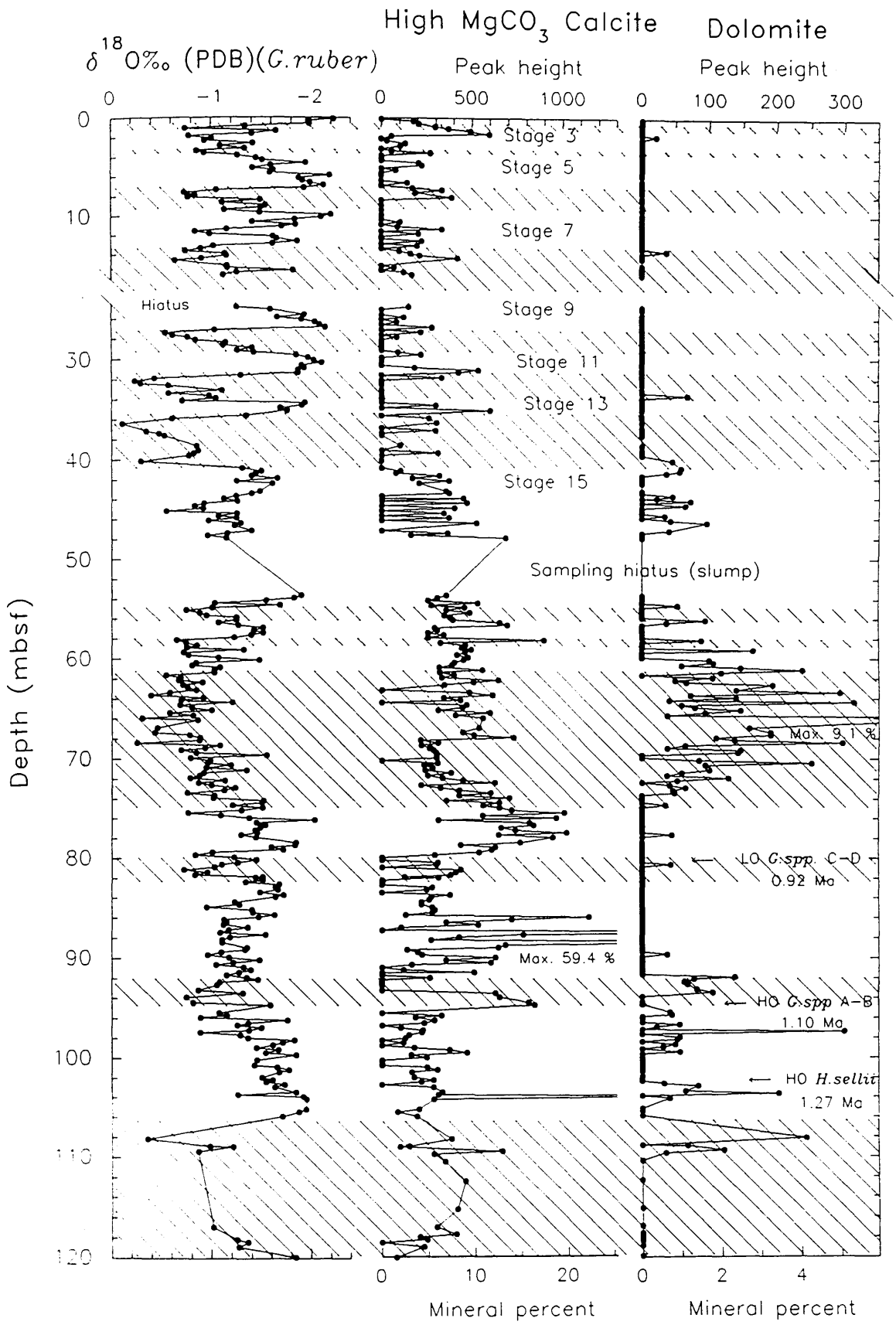

Figure 5.10. Downcore variations in percentage high Mg calcite (HMC) and dolomite in Hole 823A periplatform sediments. Also shown is the planktic oxygen isotope record from this core.

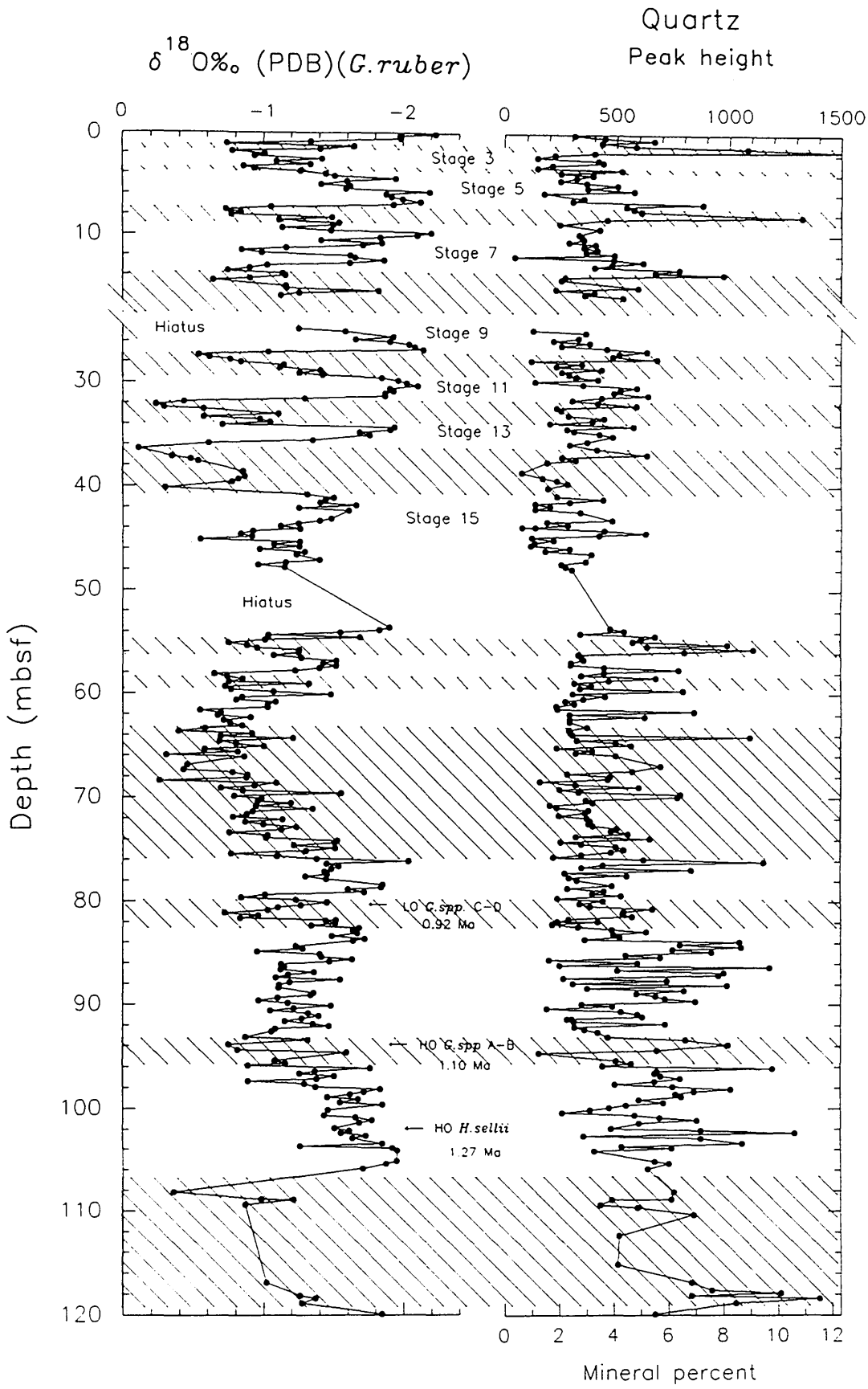

Figure 5.11. Downcore variations in quartz content plotted alongside the planktic oxygen isotope record from Hole 823A.

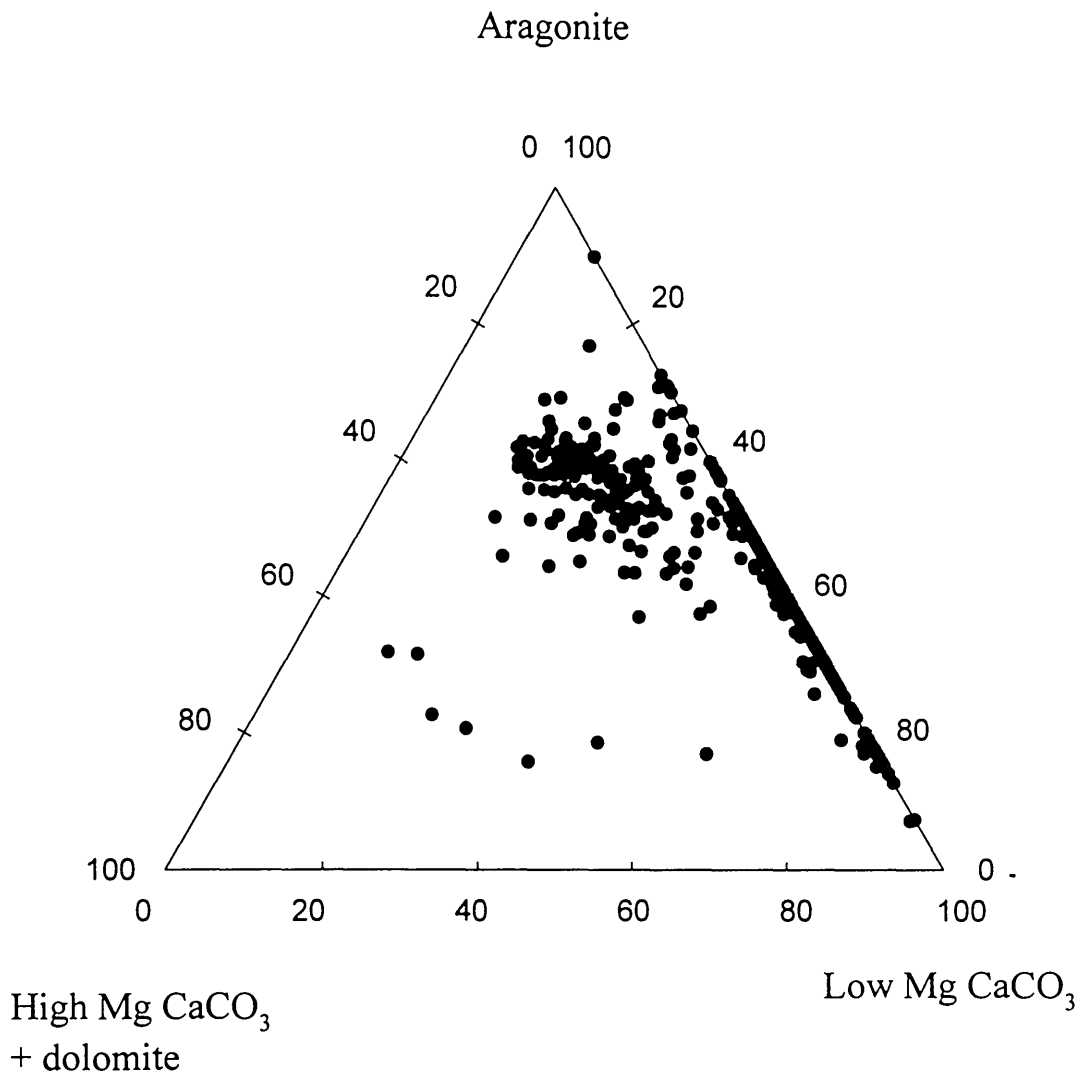

Figure 5.12. Ternary diagram showing the composition of Hole 823A periplatform sediments. Note that Hole 823A sediments are composed of an admixture of aragonite and LMC with subordinate amounts of dolomite and LMC.

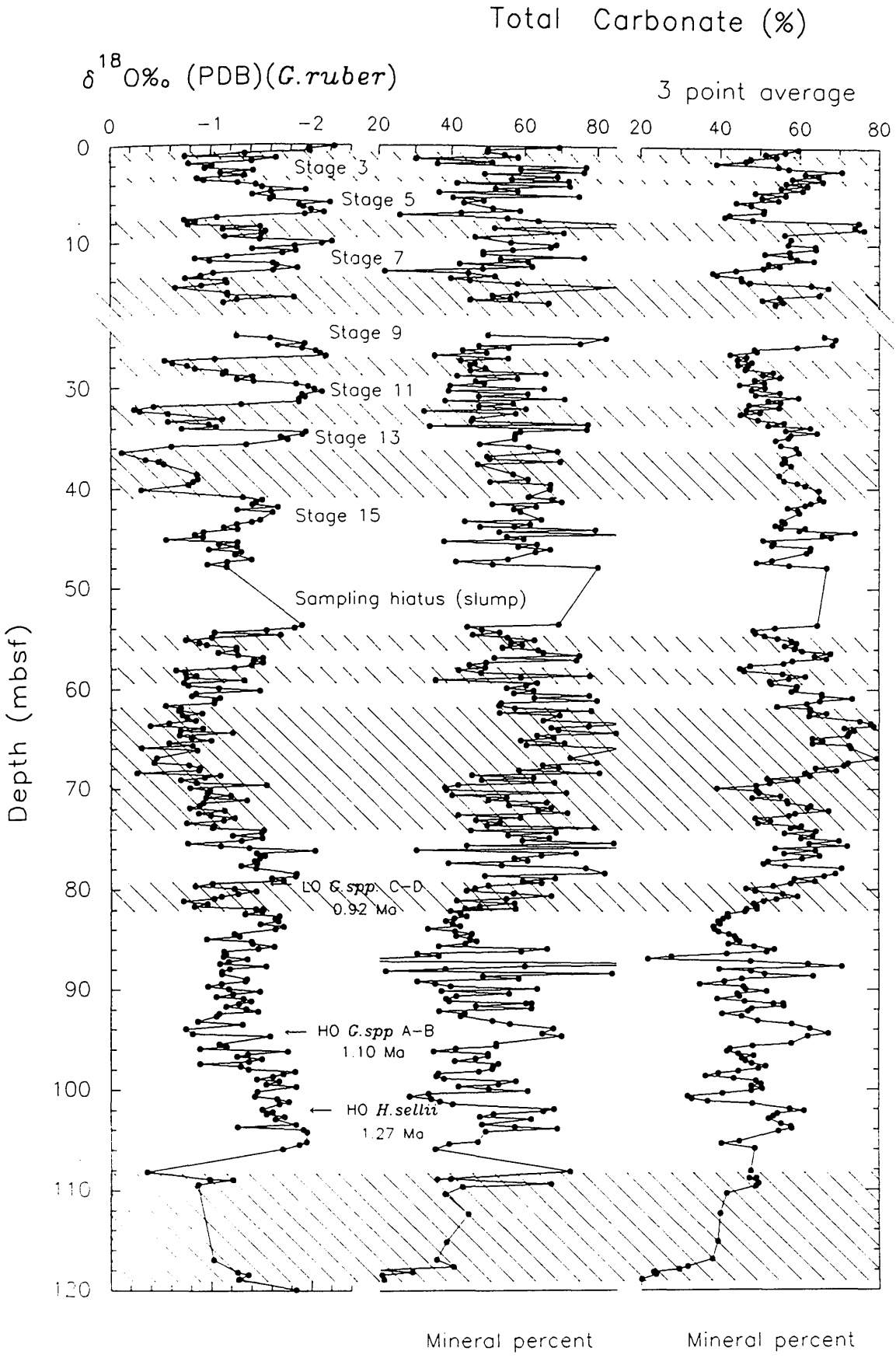

Figure 5.13. Downcore variations in percentage total carbonate (sum of the individual carbonate carbonate minerals measured using the X-ray diffractometer) in Hole 823A. Also shown is the planktic oxygen record from this core.

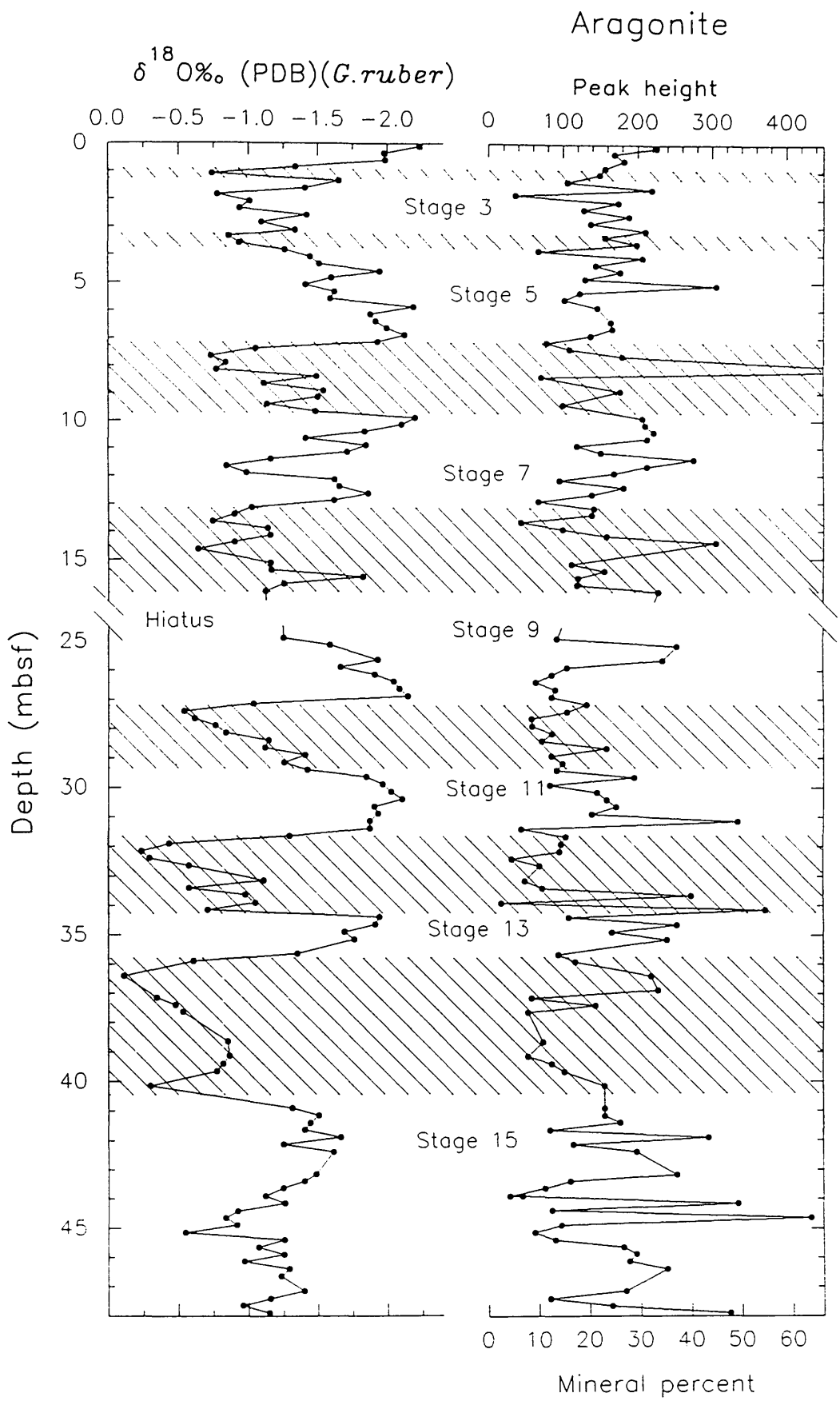

Figure 5.14. Comparison between percentage aragonite content and the planktic oxygen isotope values in the upper 48 m of the sequence from Hole 823A.

characterized by marked fluctuations in value. The transition in dominant carbonate mineralogy, from aragonite to LMC, is relatively sharp and corresponds to the upper surface of a sequence of disturbed sediments interpreted as a slump (Shipboard Scientific Party, 1991), at about 48 mbsf (~590 ka) (see Figure 5.9). The relationship between LMC and planktic $\delta^{18}O$ values is very complicated, particularly in the lower part of the core. Above 50 mbsf, tentative analysis of these records suggest that generally LMC content is high during glacial periods. This relationship can be best seen in a smoothed version of the downcore LMC content data (see Figure 5.15).

In general, the HMC content in Hole 823A sediments is very low (particularly in the upper 48 m of the record), and values rarely exceed 15 % by volume. Tentative interpretation of the HMC content curve suggests a gradual increase in mean value with depth, to a maximum of 15 % at about 80 mbsf. Below 80 mbsf mean HMC values are slightly higher than values for the upper 50 m of the core. HMC values correlate negatively with LMC content, but positively with aragonite values in the lower part of the Hole 823A record. Throughout the sequence in Hole 823A there is a general absence of any clear relationship between HMC content and the planktic $\delta^{18}O$ record (see Figure 5.10).

Dolomite is the least abundant carbonate mineral present in Hole 823A sediments, and only occurs in any significant abundance between about 58 to 72 mbsf (~710 to 840 ka), where concentrations reach a maximum of about 9 % (by volume). This interval marks the position of a series of inclined, folded or overturned beds interpreted as a slump deposit by the Shipboard Scientific Party (1991) (see Figure 4.6) In general, dolomite, where present, correlates positively with the planktic oxygen isotope record (i.e., dolomite is high during inferred periods of low sea level) in Hole 823A (see Figure 5.10).

Quartz is a minor component in Hole 823A periplatform sediments, and values rarely exceed 10 % by volume (see Figure 5.11). Tentative interpretation of the quartz content record suggests a gradual increase in mean value from about 48 mbsf through to the core-top. These concentration maxima tend to be associated with periods of isotopic enrichment/depletion (see Figure 5.16). Below 48 mbsf, mean quartz content values increase to a maximum of about 6 % toward the bottom of the core (~120 mbsf). Throughout this interval the relationship between quartz content and isotopic value remains rather speculative, and no clear association seems exists between these two parameters.

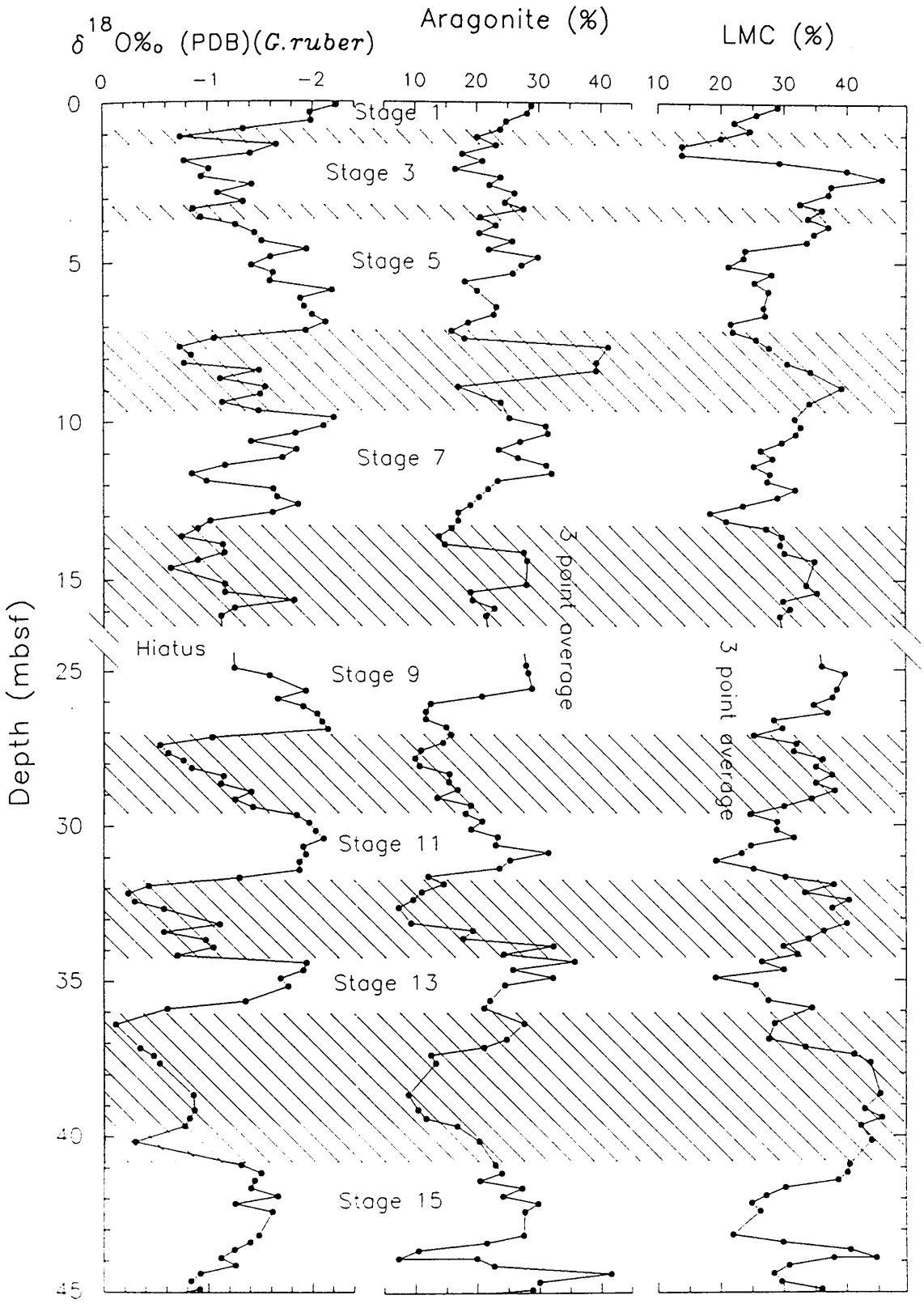

Figure 5.15. Comparison of the upper 45 m of the aragonite and low Mg calcite (LMC) content records from Hole 823A. Also shown is the planktic oxygen isotope record for this core. Note that the carbonate curves have been smoothed using a 3 point average.

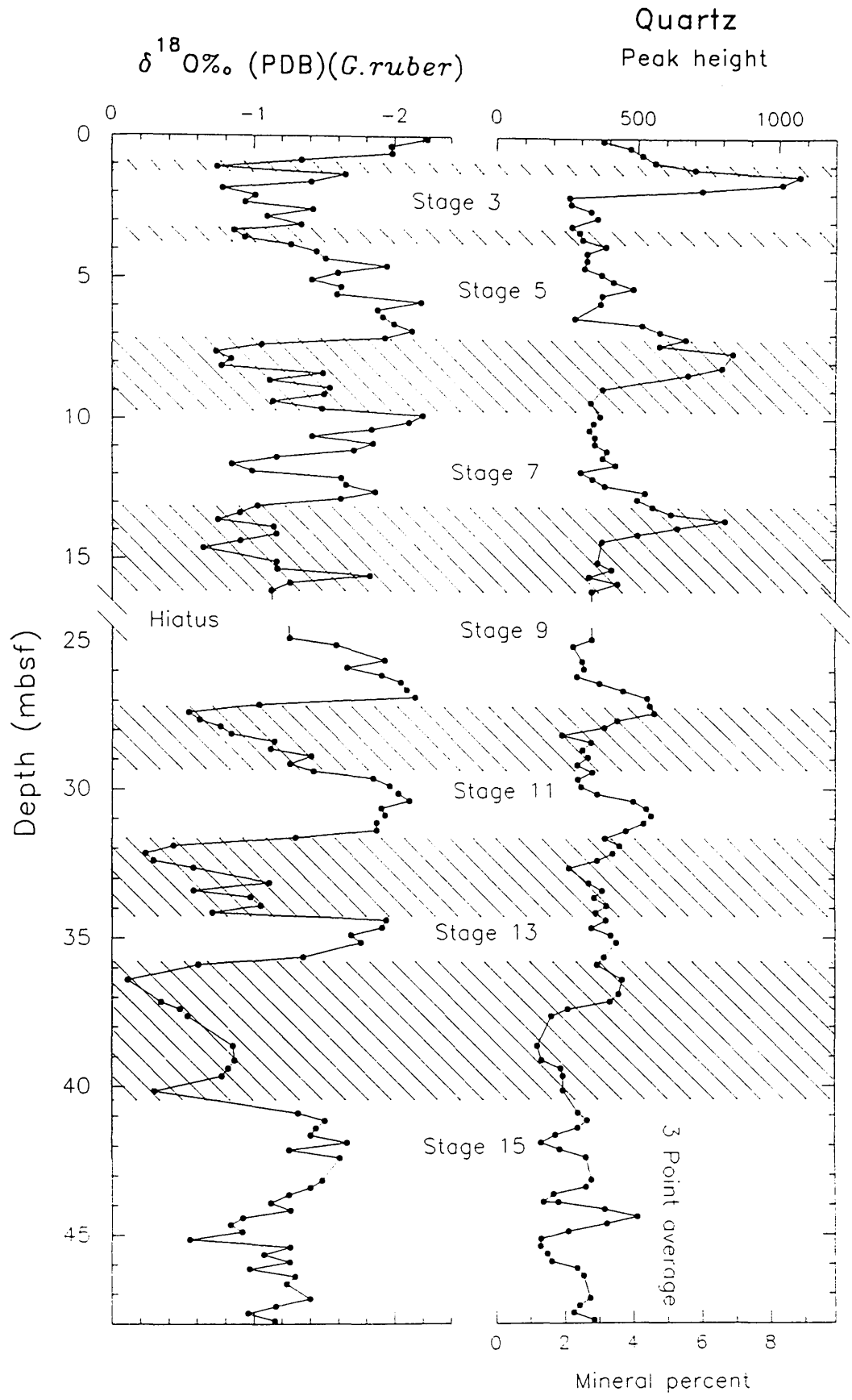

Figure 5.16. Comparison between percentage quartz content and planktic oxygen isotope values in the upper 48 m of the sequence from Hole 823A. Note that the quartz content curve has been smoothed using a 3 point average.

5.3.3 Queensland Trough Hole 823B (120-360 mbsf)

Figures 5.17 and 5.18 illustrate the variation in LMC, HMC, aragonite and quartz content, plotted against depth (mbsf), for Hole 823B sediments. In addition, as with the Hole 819A and Hole 823A records, a ternary diagram (with carbonate corrected to 100 %) showing the variation in carbonate mineralogy is presented in Figure 5.19. Unfortunately, a stable oxygen isotope curve for Hole 823B has yet to be produced. Thus, in the absence of an oxygen isotope stratigraphy, the depth/age conversion for Hole 823B sediments has been made exclusively on the calcareous nannofossil and planktic foraminiferal datums provided by Wei and Gartner (1993), and Kroon (1993), respectively.

Total carbonate content (sum of the individual carbonate phases) in Hole 823B hemipelagic sediments ranges from about 20 to 60 % (or conversely 40 to 80 % non carbonate material), and are significantly lower than values found in either Hole 823A or Hole 819A. Although fluctuating markedly throughout the sequence, the total carbonate abundance record displays a general trend of decreasing value with increasing depth (or increasing abundance of non-carbonate material with depth) (see Figure 5.17). Mean carbonate content values range from about 49 % at the top of the core (1.1 Ma), to approximately 37 %, near the top of sedimentary Unit II at about 360 mbsf (~3.51 Ma) (see previous chapter Figure 4.5).

In general, Hole 823B sediments are characterized by mainly LMC and aragonite, with minor amounts of HMC and quartz[5]. Typically, dolomite is absent or rare (i.e., less than 2 % by volume) in Hole 823B hemipelagic sediments. LMC content values range downcore from about 10 to 45 %. The LMC content record exhibits a general trend of increasing value with depth, from approximately 20 % at the core top (~100 mbsf) to about 37 % at 360 mbsf (see Figure 5.17). In general, LMC values correlate negatively with both the aragonite record and the total carbonate record (i.e., when LMC content is high, both the aragonite and total carbonate content is low). After LMC, aragonite is the next most abundant carbonate mineral present in Hole 823B sediments. Mean aragonite and HMC values decrease steadily from about 35 % and 6 %, respectively, at the top of the core (~100 mbsf), to trace quantities (<1 %) toward the bottom of the record (>300 mbsf).

In general, quartz content values are very low in Hole 823B sediments, and typically

[5]Other minerals which were detected in Hole 823B pelagic to hemipelagic sediments were: chlorite, kaolinite, feldspar (albite), zircon, tourmaline, gypsum, pyrite, epidote, smectite. These in most cases were present at such low concentrations as to preclude accurate quantification.

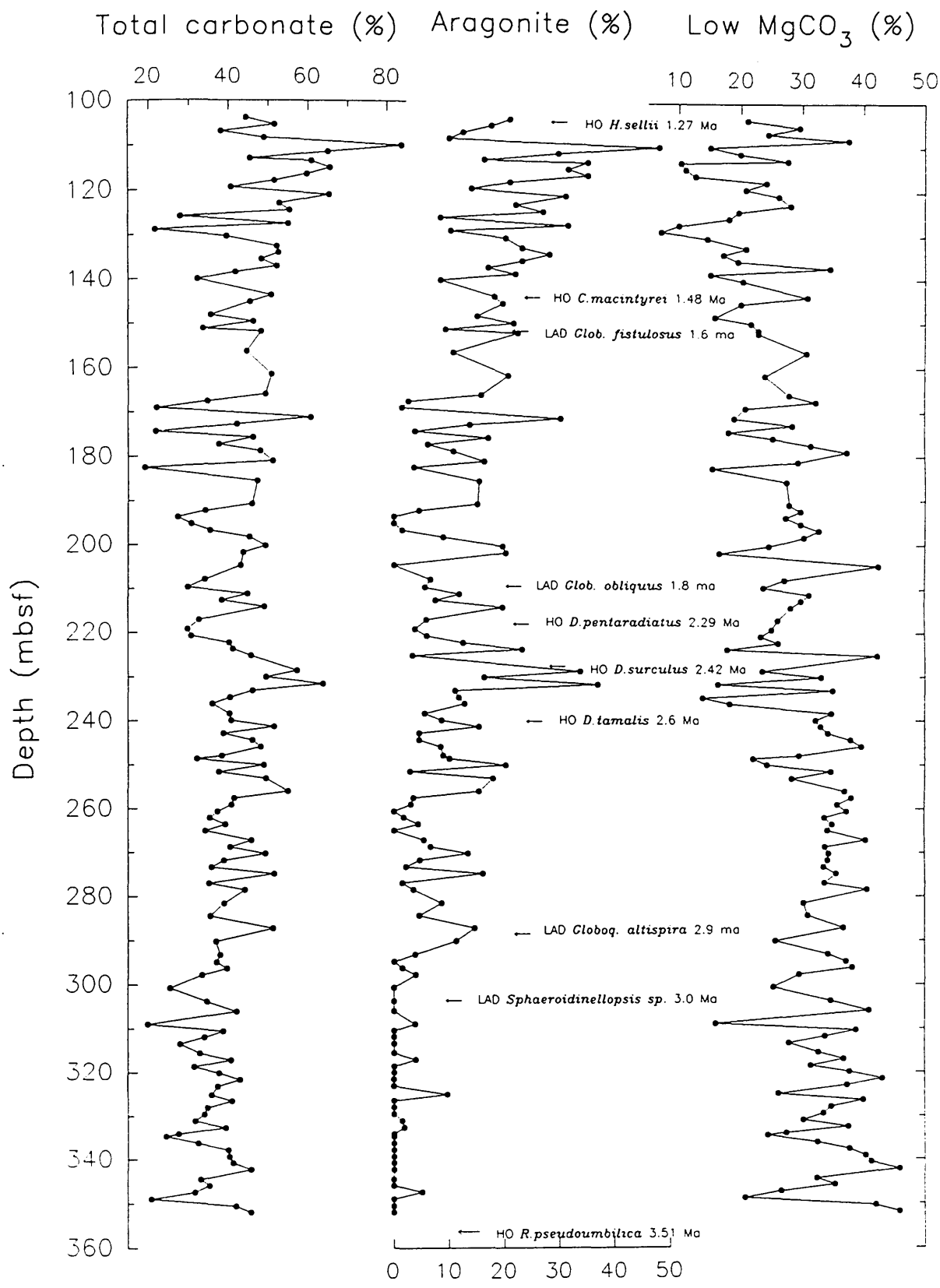

Figure 5.17. Comparison between the total carbonate, aragonite and low Mg calcite (LMC) contents in Hole 823B (Queensland Trough) sediments. Nannofossil and foraminiferal datums provided by Wei and Gartner (1993) and Kroon (1993), respectively (see Table 5.2).

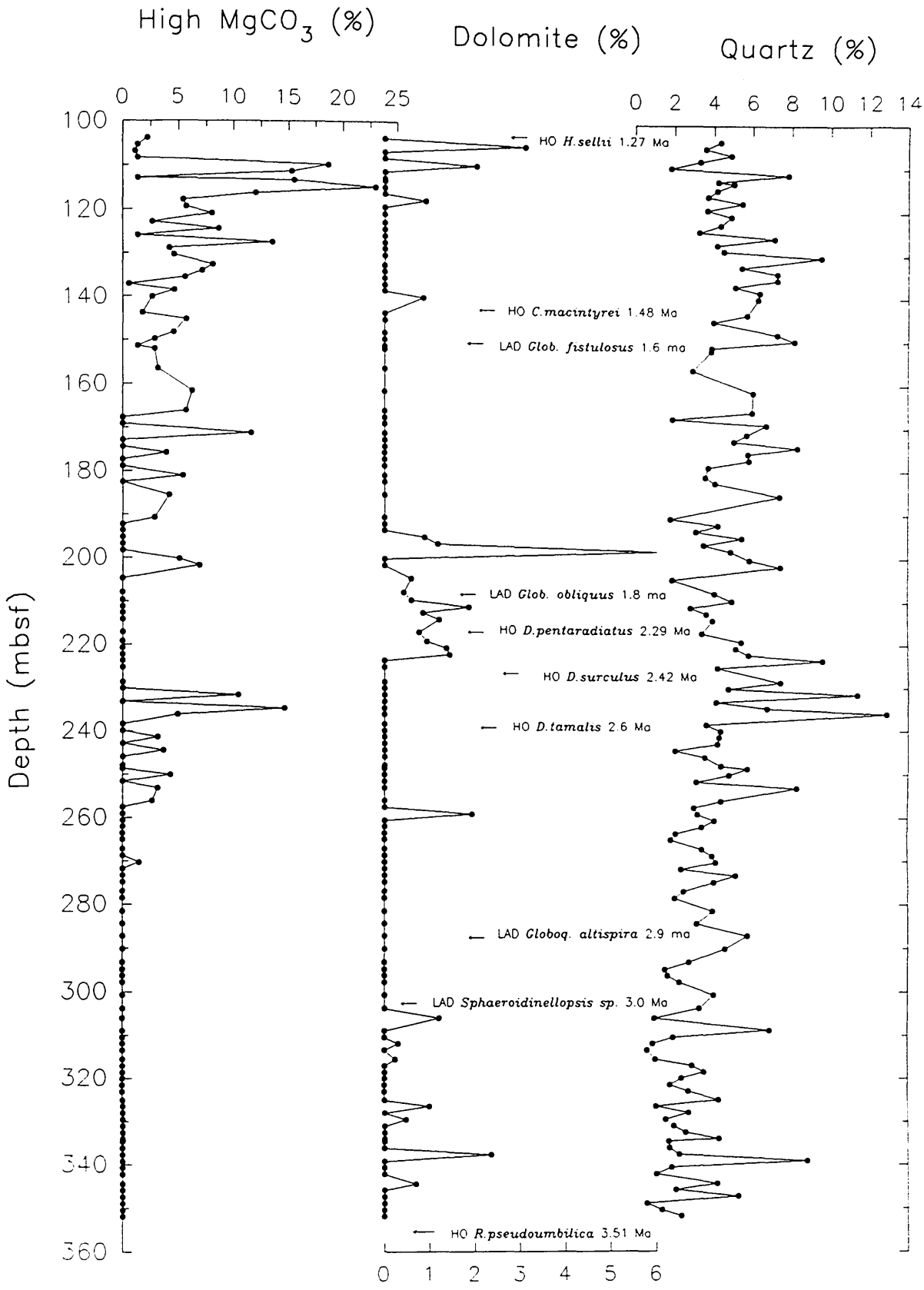

Figure 5.18. Comparison between the high Mg calcite (HMC) dolomite and quartz contents in Hole 823B (Queensland Trough) sediments. Nannofossil and foraminiferal datums provided by Wei and Gartner (1993) and Kroon (1993), respectively (see Table 5.2).

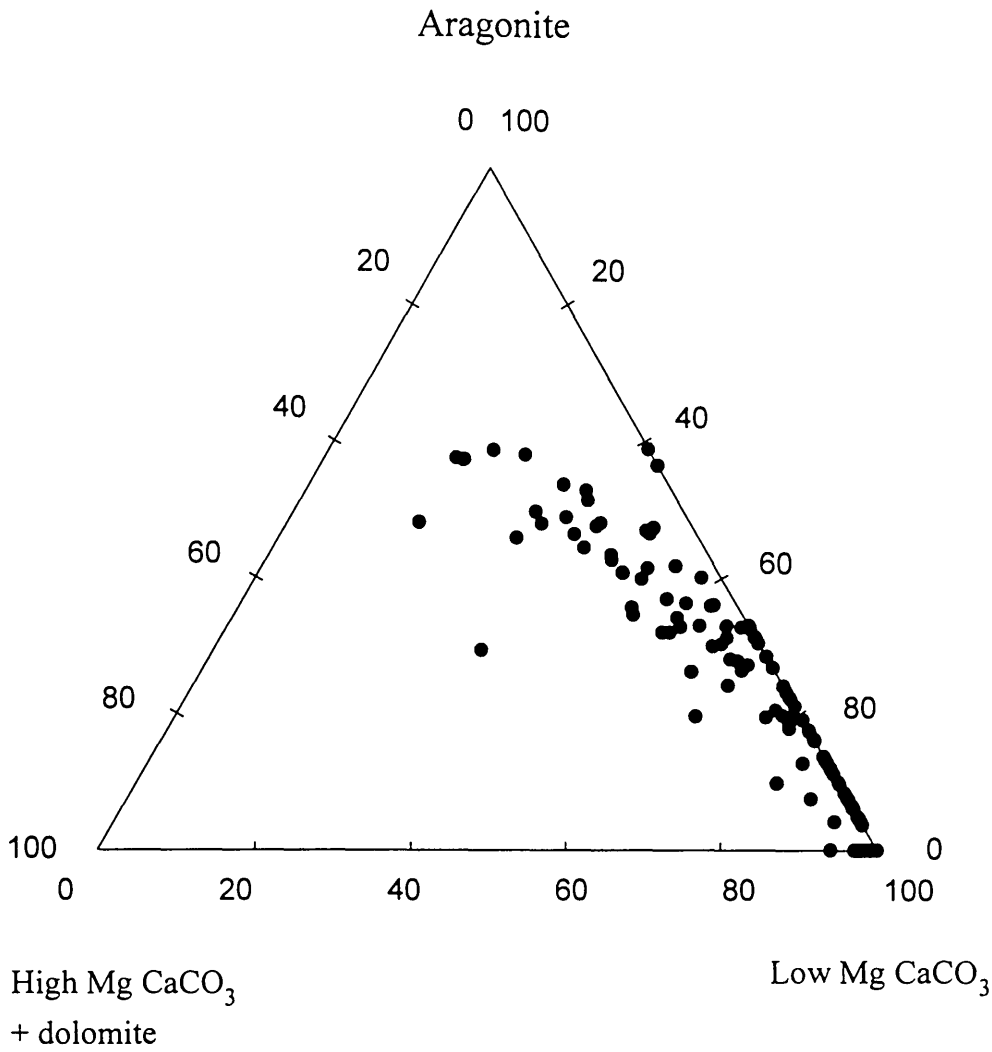

Figure 5.19. Ternary diagram showing the variation in principal carbonate mineralogy in Hole 823B periplatform sediments. Note the general paucity of shallow water carbonate material (i.e., aragonite and HMC) in Hole 823B sediments.

range from about 2 % to 10 % by volume. Mean quartz values decrease gradually with depth, from a maximum of 6 % at the core top, to about 2 % at the base of the section (~360 mbsf) (see Figure 5.18). Variations in quartz content in Hole 823B sediments are apparently independent of fluctuations in carbonate mineralogy, i.e., no clear relationship seems to exist between quartz content and aragonite, LMC, HMC or dolomite.

5.4 Discussion

The cyclic variations in carbonate content and mineralogy, in Hole 819A and Site 823 (Holes 823A and 823B) periplatform sediments, and their relationship to Late Quaternary sea level change may be related to: (a) changes in biological productivity, on the shelf and/or open ocean, (b) dilution by terrigenous sediment, (c) marine diagenesis, (e) current winnowing, and/or (d) carbonate dissolution. In order to fully understand the mechanisms behind the mineralogical variations and carbonate cycles observed in periplatform sediments recovered from Sites 819 and 823, we must attempt to separate these different variables.

5.4.1 Variations in carbonate bank-top production and pelagic productivity as recorded in Hole 819A and Site 823 periplatform sediments

Modern tropical shallow -water carbonate sediments (<200 m water depth) are primarily composed of aragonite and high-magnesian calcite and subordinate amounts of low-magnesian calcite (Friedman, 1965; Land, 1967; Milliman, 1974; Schlager and James, 1978). This mineralogy reflects the composition of the principal skeletal and non-skeletal components dominating the shallow-water setting. Skeletal material may be derived from a variety of invertebrate and algal sources (i.e., bryozoan, echinodermal, benthic foraminifera, barnacle, brachiopod, bivalve, coral and coralline algae). In contrast the mineralogy of deep-water (1000-2000 m) carbonate sediments is largely controlled by the environment and the faunal assemblage, and by the selective dissolution of the more soluble carbonate minerals (Friedman, 1965). In general, deep-water carbonate-rich sediments contain abundant low-magnesian calcite (LMC) with minor amounts of aragonite and high-magnesian calcite (HMC). Deep-water carbonate sediments are typically dominated by planktic foraminifera, calcareous nannofossils (coccoliths) and pelagic molluscs (mainly pteropods and heteropods) (Berger, 1968). Marine sediments accumulating on basin and ocean floors adjacent to shallow-water carbonate banks and platforms (<200 m water depth), termed "periplatform ooze" by Schlager and James (1978), consist predominantly of a mixture of carbonate platform-derived and planktic-derived sediments (Boardman *et al.*, 1986).

Variations in the carbonate mineralogy of periplatform sediments may accurately record fluctuations in sea level, as carbonate platforms and bank-tops are alternately flooded and exposed (Kier and Pilkey, 1971; Droxler *et al.*, 1983; Boardman and Neumann, 1984). The term 'highstand shedding' has been coined to describe the shedding of bank-top derived material rich in aragonite into adjacent basins during highstands of sea level (Schlager *et al.*, 1994). In contrast, during glacial periods or lowstands of sea level, production and export of bank-top aragonite is restricted, and periplatform sediments record the greater influence of planktic or pelagic carbonate production (although, considerable controversy has arisen as to influence of dissolution and dilution on carbonate cycles and the mineralogy of periplatform sediments during glacial periods). Recently Droxler *et al.*, (1993) have questioned the general principle of highstand shedding, and have proposed a 'lowstand shedding' hypothesis, in which carbonate production and export is intimately linked to the position of carbonate bank-tops relative to the photic zone.

In this section, carbonate mineral abundances and their ratios[6] are examined in order to test current ideas on carbonate platform production and shedding (i.e., highstand vs. lowstand shedding), and to assess the influence of pelagic productivity on the carbonate cyclicity seen in Hole 819A and Hole 823A periplatform sediments. Unfortunately the absence of a stable oxygen isotope record has precluded a similar analysis of Hole 823B Pliocene/ Pleistocene periplatform sediments.

5.4.1.1 Hole 819A (outer-shelf/upper-slope of the GBR)

As mentioned earlier, Hole 819A periplatform sediments are composed of predominately aragonite with subordinate amounts of LMC and HMC (see Figures 5.5 to 5.7). Analysis of these records, particularly over the last two main glacial/ interglacial cycles, suggests that highstands of sea level are characterized by high aragonite, LMC, and total carbonate content. In contrast, lowstands of sea level are distinguished by low aragonite and total carbonate content, and high LMC. Similarly, the aragonite/LMC and HMC/LMC records display high ratios during interglacial periods and low values during glacial periods (see Figure 5.20 to 5.22). For example, interglacial stage 5 and glacial stage 2 and 6 are distinguished by high and low ratios, respectively (see Figures 5.21 and 5.22). Using the rational that high aragonite/LMC

[6]Ratios formed between individual carbonate minerals are essentially independent of carbonate concentration in periplatform sediments, and are therefore also free of climatic influences wrought by terrigenous oscillations in the cores. Thus, ratios provide a means of examining more closely variations in shallow-water/carbonate bank-top production and pelagic productivity.

and HMC/LMC ratios indicate a greater influence of platform derived carbonate material over pelagic material, these records suggest that highstand shedding (Droxler and Schlager, 1985; Boardman *et al.*, 1986; Glaser and Droxler, 1991; Grammer and Ginsburg, 1992; Schlager *et al.*, 1994), in which carbonate production and off-bank transport is greatly increased during periods of high sea level, has dominated carbonate deposition during the last two main glacial/interglacial cycles in Hole 819A. Alternatively, in the absence of detailed geochemical data [i.e., Strontium concentrations] it could be argued that the aragonite/LMC ratio is being forced by variations in pelagic pteropod [aragonite] versus coccolith [LMC] productivity, and that the contribution of shelf-derived aragonite during this period was minimal. Thus, high aragonite/LMC values in Hole 819A may represent intervals of high pteropod productivity, while low values may indicate the greater influence of coccoliths.

In contrast to the upper 32.5 m of the sequence in Hole 819A, records from the lower part of the core indicate that total carbonate content is high during isotopically inferred lowstands of sea level (see Figure 4.17). Although percentage aragonite and LMC are typically high during glacial periods, HMC values are very low (see Figures 5.5 and 5.6). Comparison of the aragonite/LMC and HMC/LMC records with the planktic $\delta^{18}O$ record reveal that mineral ratios are generally low during lowstands of sea level (or conversely high during highstands of sea level) (see Figure 5.22). A notable exception to this relationship occurs during glacial stage 16 (~40 mbsf), when aragonite/LMC values are extremely high, but HMC/LMC ratios are very low. The general pattern of carbonate deposition in the lower part of Hole 819A, suggests a greater influence of pelagic driven LMC during glacial periods (as indicated by the low aragonite/LMC and HMC/LMC ratios). Conversely, during interglacial periods aragonite/LMC and HMC/LMC ratios are high suggesting the greater influence of bank-derived material in Hole 819A. Alternatively, it could be argued that low aragonite/LMC and HMC/LMC ratios are the result of the preferential removal of the more dissolution sensitive carbonate minerals (i.e., aragonite and HMC). However, although this is possible, dissolution would not explain the high aragonite/LMC and low HMC/LMC ratios during stage 16, unless the source of HMC contained more than 12 mole % $MgCO_3$ (i.e., calcareous red algae, Chave, 1954), and was more sensitive to dissolution than aragonite (Walter and Morse, 1984). Alternatively, the low HMC/LMC ratios found in glacial stage 16 may, in fact, be a product of shallow burial diagenesis and the precipitation of dolomite (see below).

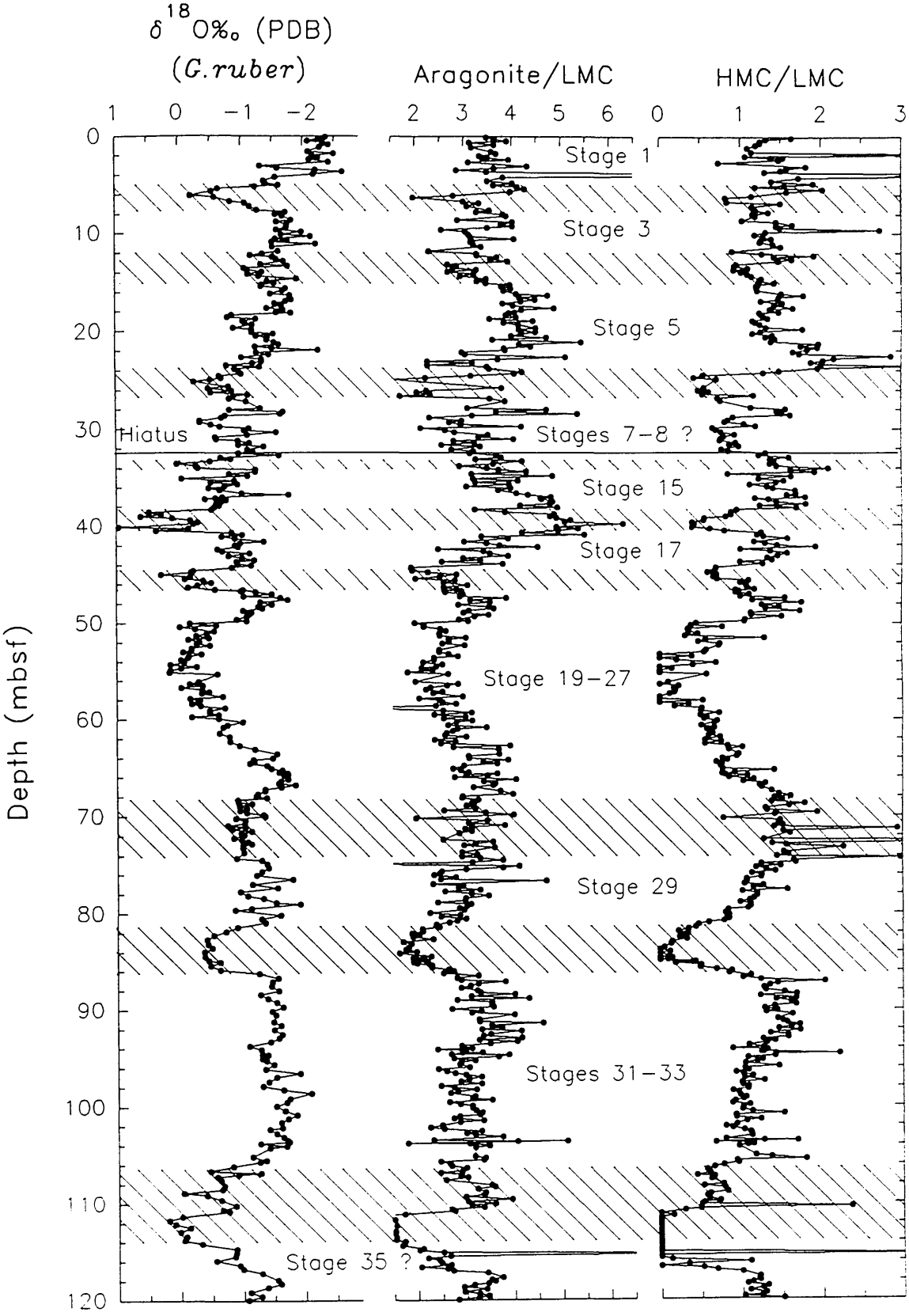

Figure 5.20. Diagram illustrating the downcore variations in the Aragonite /LMC and HMC/LMC ratios in Hole 819A. In addition the planktic stable oxygen isotope record is presented for reference. High carbonate mineral ratios are thought to represent a greater influence of shallow−water derived carbonate material in Hole 819A periplatform sediments.

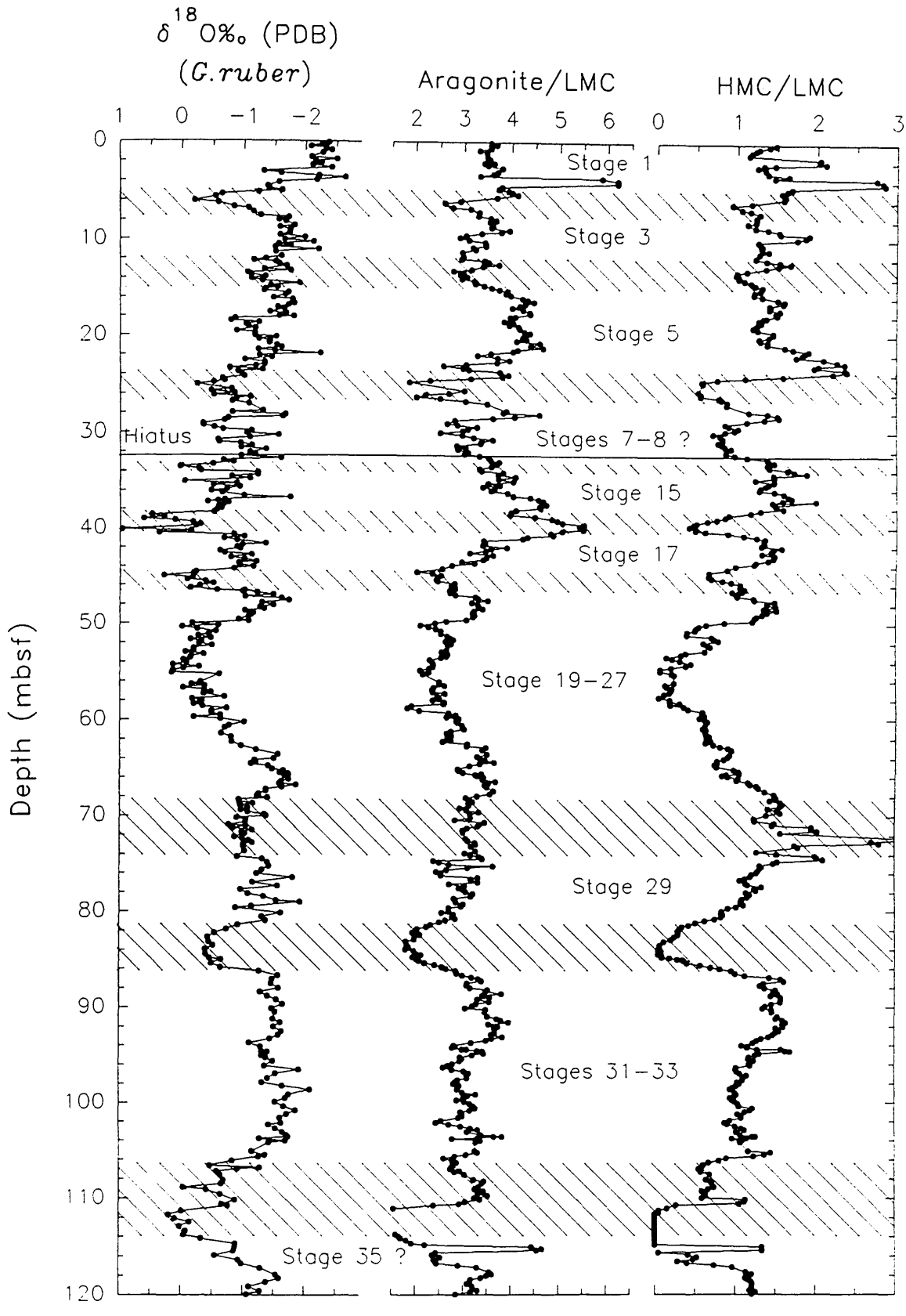

Figure 5.21. Diagram illustrating the downcore variations in the Aragonite /LMC and HMC/LMC ratios in Hole 819A. In addition the planktic stable oxygen isotope record is presented for reference. Note that carbonate ratios have been smoothed using a 3 point average.

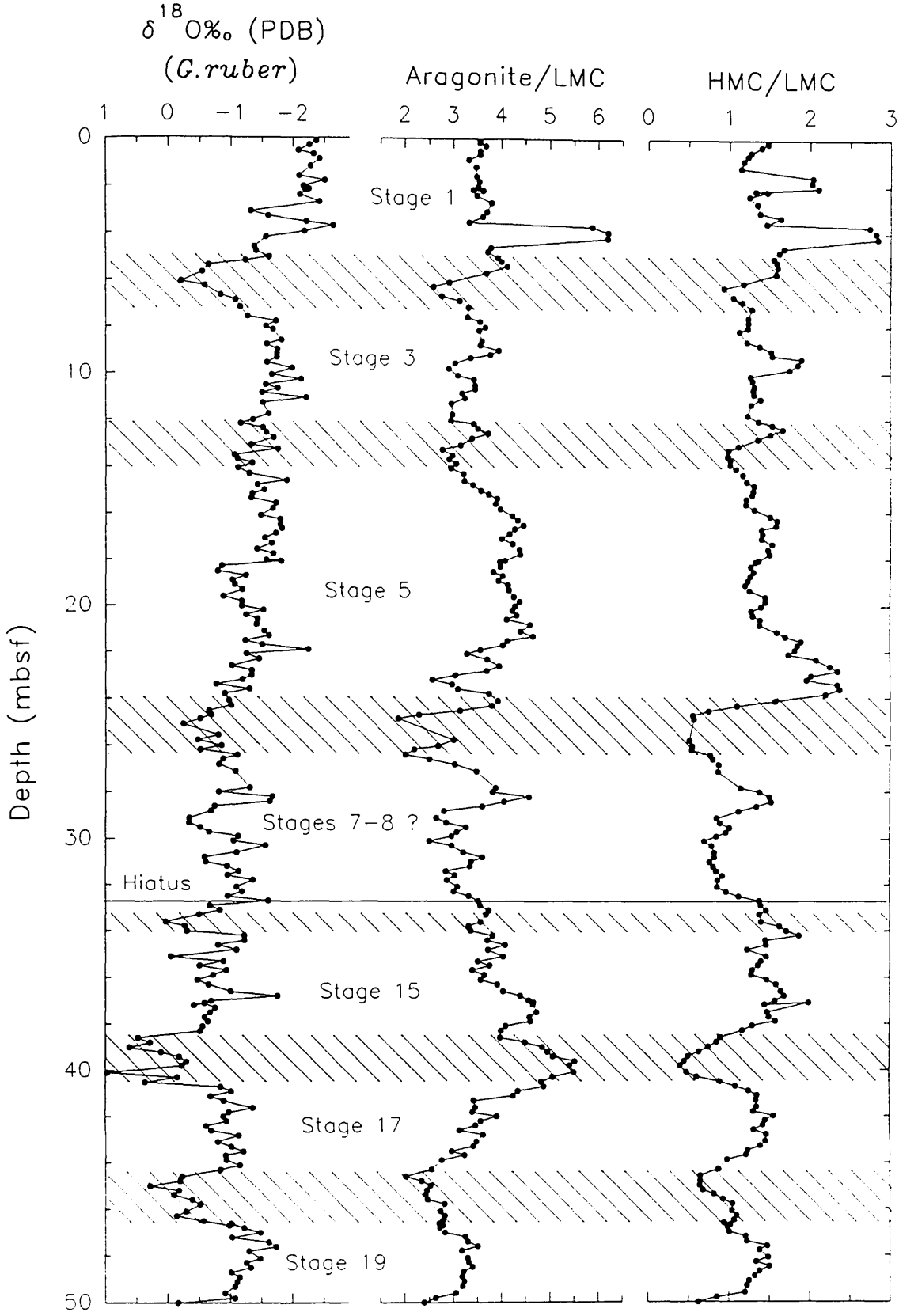

Figure 5.22. Diagram illustrating the downcore variations in the Aragonite /LMC and HMC/LMC ratios in the upper 50 m of the sequence from Hole 819A. In addition the planktic stable oxygen isotope record is presented for reference. Note that carbonate ratios have been smoothed using a 3 point average.

5.4.1.2 Hole 823A (Queensland Trough)

Hole 823A, located toward the deepest part of the Queensland Trough, is the most distal of the Leg 133 Queensland margin transect drill localities (Sites 820 through to 823) (Davies *et al.*, 1991; 1993), and potentially provides a more complete record of bank-top carbonate production and variations in planktic/ pelagic productivity, less under the influence of dilution by terrigenous material.

As mentioned earlier, the carbonate records in Hole 823A can be divided into three distinct intervals, separated by abrupt and distinct changes in mineralogy: 1) an upper section (0-45 mbsf), characterized by high LMC, low aragonite and minor amounts of HMC, 2) a middle section (45-80 mbsf) distinguished by high aragonite and HMC content and low LMC values and, 3) a lower section (80-120 mbsf) with variable amounts of all three minerals (see Figures 5.9 and 5.11). The question now arises as to what is the relationship between sea level change and variations in carbonate mineralogy across, and between, these different intervals? And, is there any evidence to suggest that banktop production and export of shallow water carbonate has significantly changed during the Pleistocene in Hole 823A?

Analysis of the carbonate records from Hole 823A indicates an abrupt and permanent increase in LMC content at about 45 mbsf (~0.58 Ma) (see Figures 5.9 and 5.15). However, because of the presence of a prominent hiatus/slump (between 47.9 and 53.65 mbsf, Shipboard Scientific Party, 1991) corresponding to the interval between 0.6 and 0.66 Ma, the extent of this feature remains somewhat speculative. Nevertheless, the sudden increase in LMC content seems to be related to the general change in the frequency and amplitude of the isotopic record seen in Hole 823A (see Figure 5.23). Previous studies have suggested that a significant change in isotopic character, from high frequency and low amplitude 41 ka Milankovitch cycles during the early Pleistocene, prior to 0.9 Ma, to high amplitude and low frequency 100 ka orbital periodicities during the late Pleistocene, occurred after 0.73 Ma (Shackleton and Opdyke, 1976; Pisias and Moore, 1981; Ruddiman *et al.*, 1989; Raymo *et al.*, 1990). Although, there is a slight discrepancy between the age of the lower boundary of the hiatus between 47.9 and 53.65 mbsf, and the change in the frequency and amplitude of the isotopic records, it seems likely that increased LMC levels, in the upper 50 m of the core, are related to the greater magnitude of sea level change (up to 120 m- Fairbanks *et al.*, 1989; Bard *et al.*, 1990) associated with the 100 ka Milankovitch cycles.

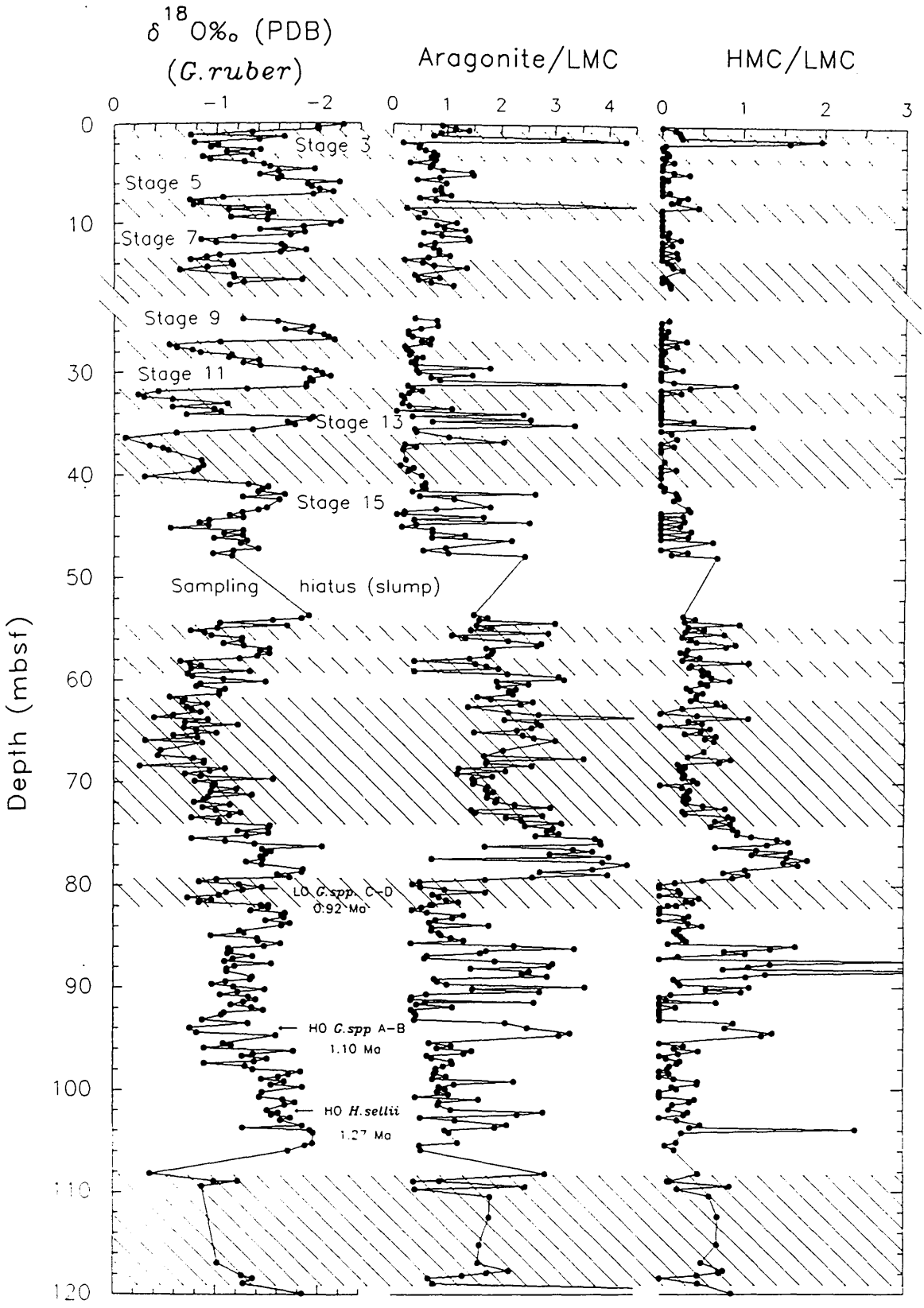

Figure 5.23. Downcore variations in the aragonite/LMC and HMC/LMC ratios in Hole 823A periplatform sediments. Also shown is the planktic oxygen isotope record from this core.

Comparison of the isotopic record with the XRD record from Hole 823A indicates that, a significant correlation exists between LMC, aragonite content and sea level, in the upper 45 m of the core. Analysis of these records suggests that glacial periods are characterized by high LMC and low aragonite content (particularly between 27 to 45 mbsf). This relationship is more clearly developed in the smoothed (3 point average) LMC and aragonite content records (although care must be exercised to avoid over-interpretation of averaged data) (see Figure 5.15). In contrast, during highstands of sea level LMC content is generally low, while aragonite content is comparatively high. Kier and Pilkey (1971) have described a similar pattern of carbonate deposition in periplatform sediments collected from the Tongue of the Ocean (TOTO), Bahamas. These authors attributed increased LMC content to enhanced pelagic productivity (primarily coccoliths) during lowstands of sea level, rather than erosion of subaerially altered carbonate from the adjacent carbonate banktops (Rucker, 1968). Further, intervals of high aragonite content in Bahamian periplatform sediments were interpreted as indicating increased offbank transport of fine-grained lagoonal sediments during highstands of sea level (Kier and Pilkey, 1971). Although, not as well developed in the records of Kier and Pilkey (1971), there is a strong suggestion that Hole 823A sediments have responded to variations in sea level, in a similar manner to Bahamian periplatform sediments (i.e., highstands of sea level are distinguished by greater off-bank transport of carbonate, while glacial periods are characterized by a greater influence of pelagic calcite). However, examination of the aragonite/LMC and HMC/LMC records for Hole 823A are less convincing in terms of documenting off-bank transport of shallow-water carbonate material during highstands of sea level (see Figure 5.24). For example, isotopic stages 11 and 13 (and possible late stage 15), provide the only significant evidence of inferred highstand shedding (i.e., high aragonite/LMC and HMC/LMC ratios). Throughout the remainder of the records there is little evidence to suggest the increased production and export of shallow water carbonate occurred during highstands of sea level. Similarly, during lowstands of sea level there is little evidence to support the notion of the increased influence of pelagic calcite in Hole 823A periplatform sediments. Although several prominent peaks in the carbonate mineral ratios occur during lowstands of sea level, these horizons are thought to represent either; isolated lowstand turbidites, or periods of enhanced pteropod productivity (see Figures 5.9 and 5.23).

As mentioned earlier, the lower part (>45 mbsf) of the sequence from Hole 823A is distinguished by several abrupt and significant changes in carbonate mineralogy (see Figures 5.9 to 5.10). For example, at about 82 mbsf (~0.9 Ma) there is an sudden increase in both aragonite and HMC content in Hole 823A periplatform sediments,

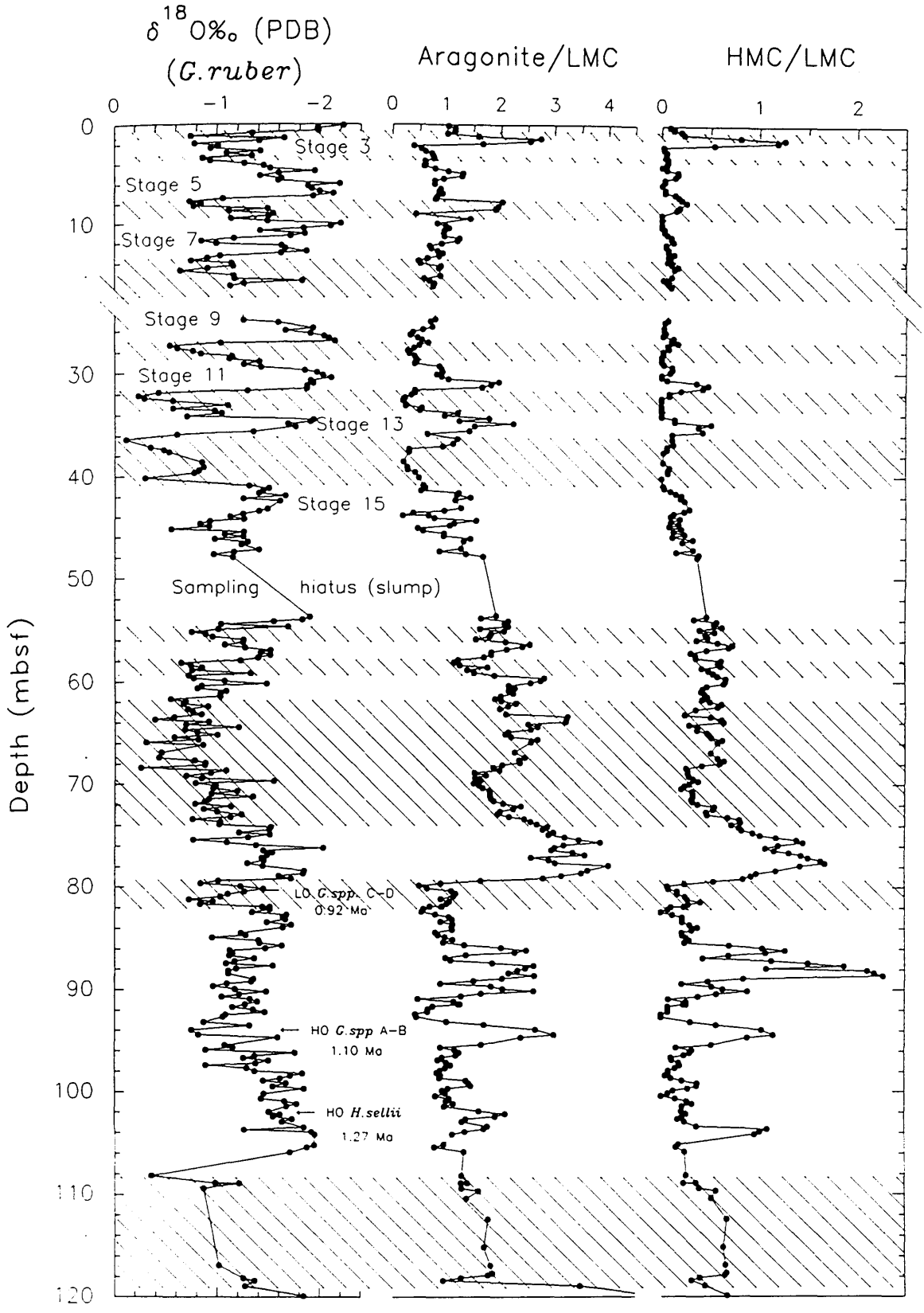

Figure 5.24. Downcore variations in the aragonite/LMC and HMC/LMC ratios in Hole 823A periplatform sediments. Also shown is the planktic oxygen isotope record from this core. Note that the carbonate ratio curves have been smoothed using a 3 point average.

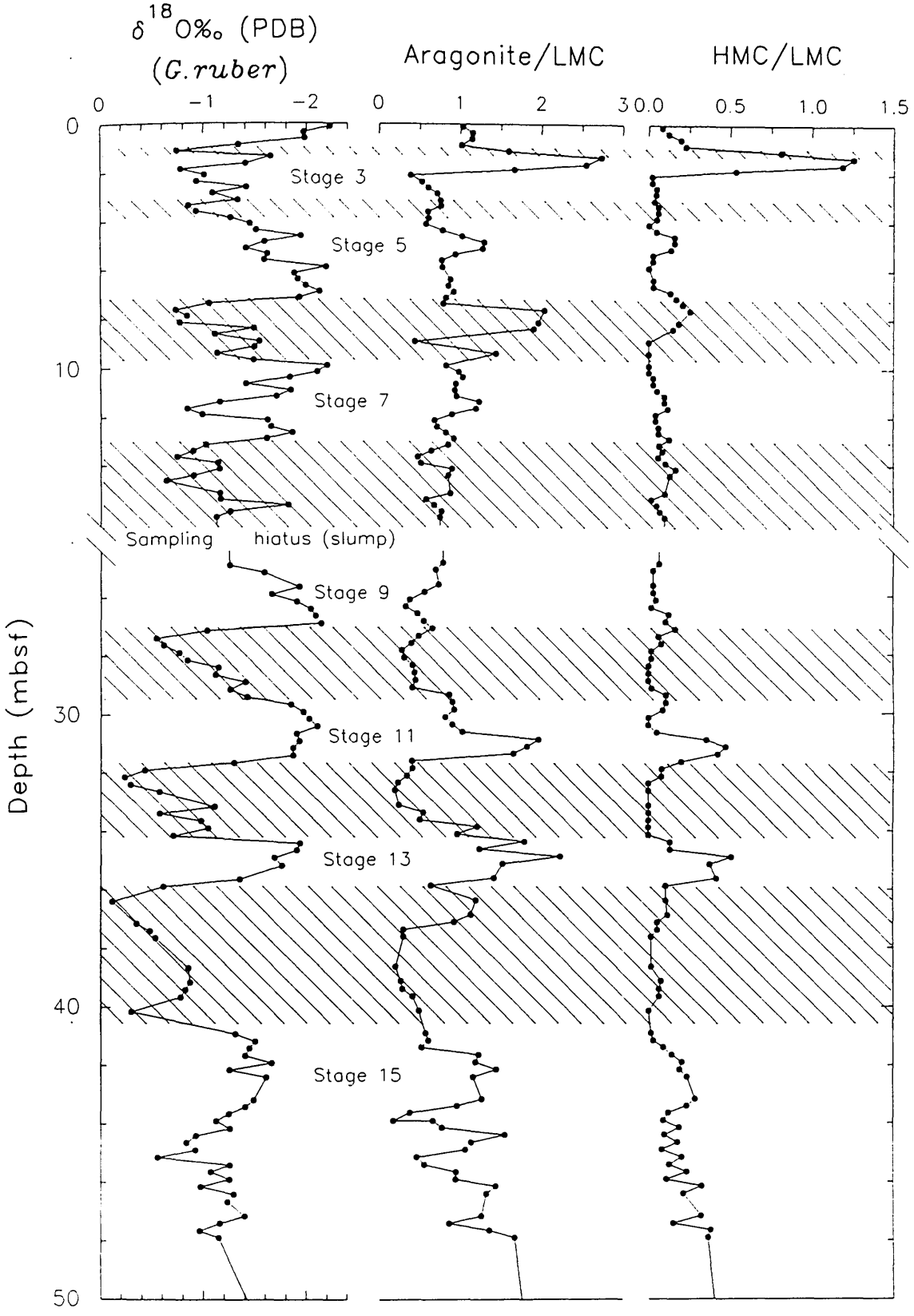

Figure 5.25. Downcore variations in the aragonite/LMC and HMC/LMC ratios in the upper 50 m of Hole 823A. Also shown is the planktic oxygen isotope record from this core. Note that the carbonate ratio curves have been smoothed using a 3 point average.

coupled with a dramatic decrease in average LMC values. This event is also seen in the aragonite/LMC and HMC/LMC records (see Figure 5.24). Using the rationale that high carbonate mineral ratios indicate a greater influence of bank-top derived carbonate, these records suggests a dramatic increase in the amount of bank-derived material at this time. This event coincides with an abrupt shift toward lighter (more depleted) isotopic values, and may be interpreted as a period of significant highstand carbonate shedding (Schlager *et al.*, 1994). However, while the records indicate highstand shedding at about 82 mbsf (~0.9 Ma), at about 66 mbsf (~0.78 Ma) the aragonite/LMC, HMC/LMC and planktic $\delta^{18}O$ records clearly demonstrate lowstand shedding (see Figure 5.23). Alternatively, the decrease in aragonite/LMC and HMC/LMC values seen between 0.9 and 0.58 Ma (82 and 45 mbsf, respectively) may simply represent the progressive removal of dissolution sensitive carbonate material, in response to changes in water chemistry.

Although, useful as a first approximation of platform production, the lack of consistency between the aragonite/LMC and HMC/LMC ratios and the planktic $\delta^{18}O$ record suggests that processes other than banktop flooding and exposure may have played a more important role in determining the composition of Hole 823A periplatform sediments, particularly in the lower part of the core. Factors such as variations in water chemistry (and dissolution intensity), and shallow burial diagenesis, may have exerted a stronger influence on the mineralogy of Hole 823A sediments, than in the shallower, more proximal, Queensland shelf drill sites (Sites 820 to 819). These factors and their effects on the carbonate signature of Hole 823A periplatform sediments are discussed below.

5.4.2 Burial diagenesis and the origin of dolomite in Hole 819A and Hole 823A periplatform sediments, northeast Australian margin

As mentioned earlier, periplatform sediments consist mostly of shallow-water bank-derived aragonite and magnesian calcite, plus pelagic calcite derived principally from foraminifera and coccolithophorids. According to Schlager and James (1978) these complex sediments possess a high diagenetic potential, including dissolution, dolomitization, and lithification (Bathurst, 1975), because of the metastability of aragonite and high magnesian calcite (HMC) in deep, cold seawater (James and Choquette, 1983). Friedman (1965) suggested that the stability or solubility sequence for carbonate minerals, under normal deep-sea conditions was, in order a increasing stability: aragonite < HMC < LMC. However, according to Chave (1962), if HMC contains more than 12 mole % Mg (such as concentrations generally found in calcareous red algae- Milliman, 1974), it is often more dissolution sensitive than

aragonite, and thus may be preferentially removed over aragonite. In this section, the effects of shallow-burial diagenesis (in the absence of high-resolution pore-water geochemical data) on the metastable carbonate records from Holes 819A and 823A are examined.

As noted by Swart *et al.* (1993), geochemical analysis of periplatform sediments recovered from previous ODP Sites (for example during Legs 101 and 115, in the Bahamas and the Maldives, respectively) have shown that many marginal marine sequences are characterized by relatively high interstitial pore-fluid strontium (Sr^{2+}) concentrations. Elevated Sr^{2+} concentrations have been subsequently explained in terms of the release of Sr^{2+} in response to the recrystallization of metastable aragonite and HMC to LMC (Gomberg and Bonatti, 1970; Baker *et al.*, 1982). Thus, Sr^{2+} profiles should provide an indication of the degree of alteration of metastable aragonite and HMC. In order to assess the effect of burial diagenesis on the primary carbonate signal, the ODP Leg 133 shipboard pore water inorganic geochemistry data (Davies *et al.*, 1991) were compared to the aragonite records from Hole 819A and Site 823. However, shipboard pore-water Sr^{2+} measurements were taken approximately every 10 m at both sites, thus care must be exercised to prevent over-interpretation of these low resolution data.

In Hole 819A, pore water strontium [Sr^{2+}] values increase from present day seawater values of 98 μM at the core top, to approximately 273 μM at 54.0 mbsf (~0.88 Ma), below which values decrease slightly before rising to 292 μM at 118.4 mbsf (~1.05 Ma). Comparison of the percentage aragonite content and interstitial pore-water [Sr^{2+}] values in Hole 819A sediments is illustrated in Figure 5.26. Analysis of these records suggests that below about 30 mbsf, variations in percentage aragonite follow pore-water [Sr^{2+}] concentrations. For example, the peaks in aragonite content centred at 55 and 82 mbsf are both associated with slightly elevated pore-water [Sr^{2+}] values (see Figure 5.26). Above 30 mbsf, the aragonite record displays high amplitude fluctuations ranging from about 20 to 60 %, while pore-water [Sr^{2+}] values are typically low. If, as suggested by Baker *et al.* (1982), variations in the aragonite content were simply the result of downcore burial dissolution, then pore-water [Sr^{2+}] values would increase as aragonite decreases. Clearly this is not the case in Hole 819A (even taking into account the poor resolution of the shipboard pore-water [Sr^{2+}] data). The lack of correspondence between aragonite content and pore-water [Sr^{2+}] values indicates that, although there may have been some burial dissolution, and release of strontium [Sr^{2+}] into the interstitial pore-waters, the primary aragonite signal has been largely preserved. A similar, conclusion was reached by Haddad *et al.* (1993),

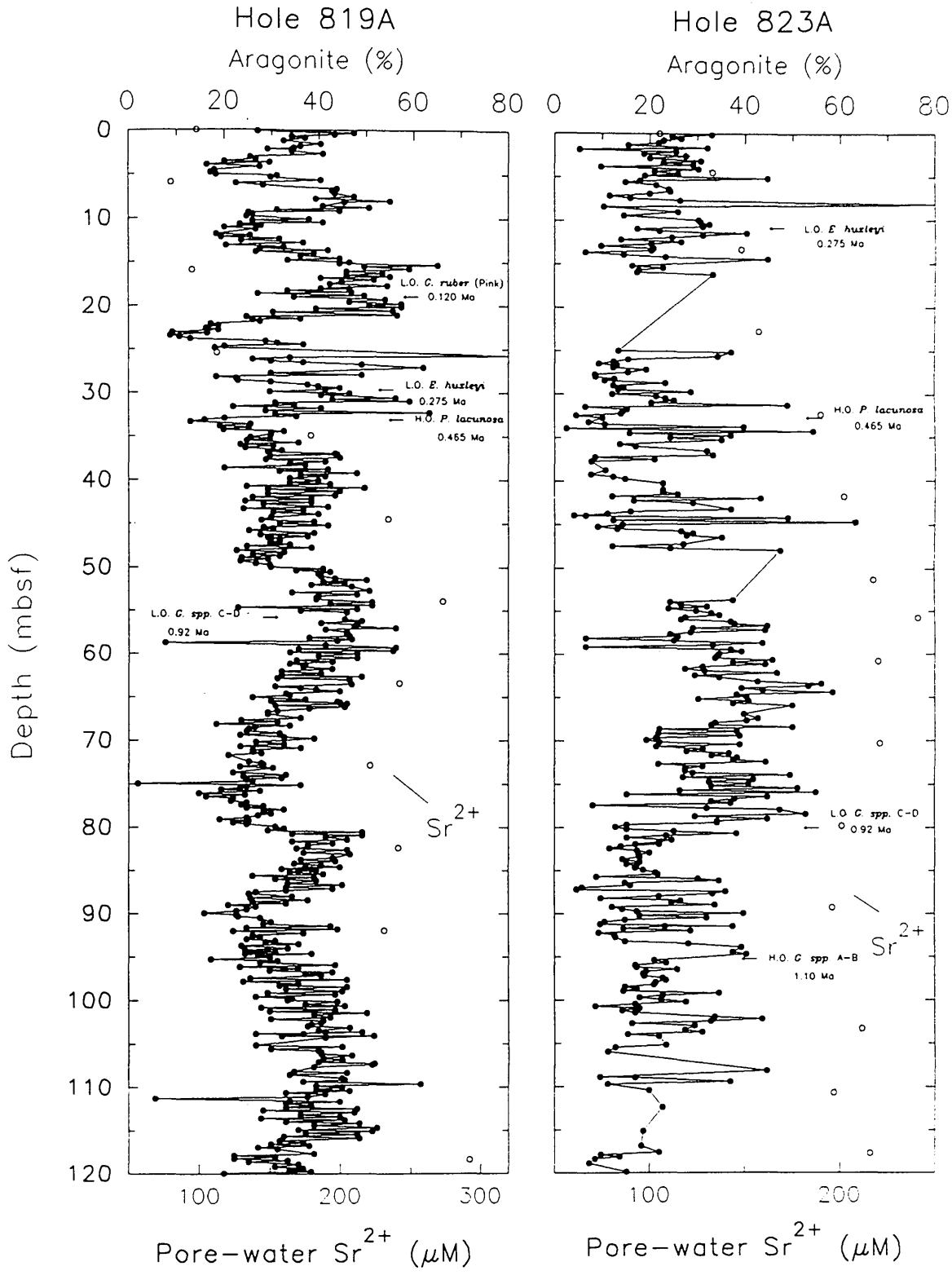

Figure 5.26. Diagram illustrating downcore variations in aragonite content and interstitial pore-water Sr^{2+} concentration data (Shipboard Scientific Party, 1991) in Hole 819A and Hole 823A sediments. Note the dramatic decrease in Sr^{2+} values in the upper part of each core.

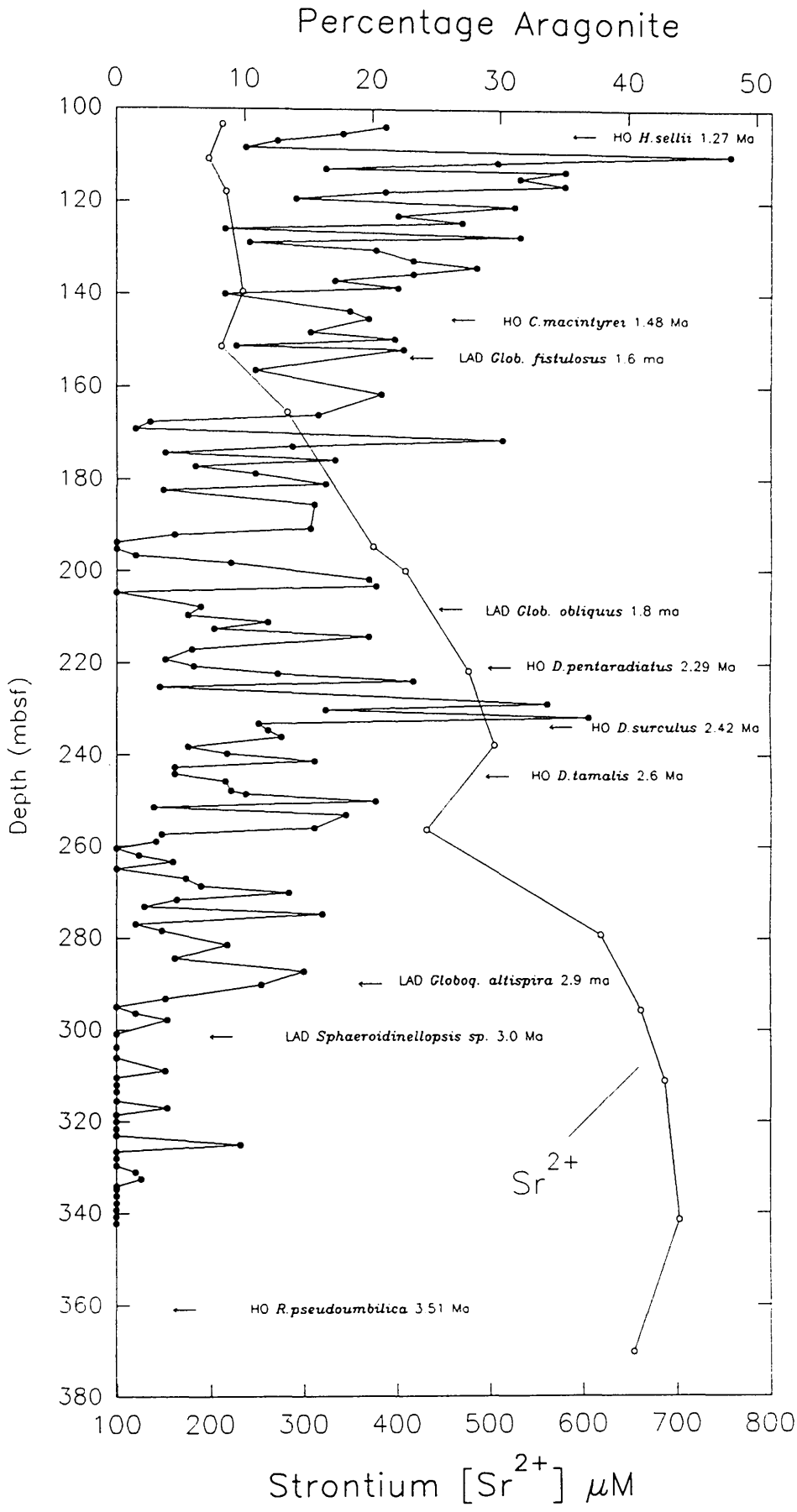

Figure 5.27. Downcore variations in metastable aragonite content and pore-water strontium [Sr^{2+}] concentration (Shipboard Scientific Party, (1991) in Hole 823B (Queensland Trough) sediments. Note the gradual increase in pore-water Sr^{2+} with increasing depth.

working on the metastable carbonate records from Sites 817 and 818, on the flanks of the Queensland Plateau.

Figure 5.26 illustrates the pore-water [Sr^{2+}] concentration and percentage aragonite content in Hole 823A, plotted against depth. In general, pore-water [Sr^{2+}] values in Hole 823A are similar in magnitude to those found in Hole 819A sediments. Pore-water [Sr^{2+}] values, in Hole 823A, gradually increase downcore to a maximum of 241 μM at 55.8 mbsf (~0.68 Ma). Below 55.8 mbsf, pore-water [Sr^{2+}] concentrations decrease slightly to a base level of about 200 μM at 120 mbsf (~1.05 Ma) (see Figure 5.25b). The general downcore increase in pore-water [Sr^{2+}] values, down to about 45 mbsf, and decrease in mean aragonite values is consistent with a diagenetic explanation for the aragonite content in Hole 823A sediments. However, a direct link between these two parameters is difficult to establish given the low resolution of the pore-water [Sr^{2+}] data. At about 45 mbsf, there is an abrupt increase in the mean aragonite content, from about 15 to 25 %, however this is not matched by a corresponding kick in pore-water [Sr^{2+}] values, suggesting that diagenetic alteration is not the primary control on the aragonite record in Hole 823A. Similarly, below 45 mbsf, variations in aragonite content are independent of fluctuations in pore-water [Sr^{2+}]. For example, the abrupt decrease in aragonite content at 80 mbsf (~0.86 Ma) (also seen in the aragonite records from Hole 818A) correlates, rather disappointingly, with a slight decrease in pore-water [Sr^{2+}] content. Thus, as with Hole 819A, fluctuations in aragonite content in Hole 823A sediments are thought to reflect the primary aragonite signal, with possibly some overprint of shallow water burial dissolution.

The long-term (Pliocene-Pleistocene) record of aragonite deposition, plotted against depth and alongside the shipboard pore-water [Sr^{2+}] data, for Hole 823B is illustrated in Figure 5.27. Pore-water [Sr^{2+}] concentrations gradually increase from 200 μM at 100 mbsf (1.02-1.26 Ma) to approximately 700 μM at 340 mbsf (3.2-3.35 Ma). The gradual increase in pore-water values is mirrored by a steady decrease in mean aragonite content values from about 22 % at 100 mbsf to <1 % at approximately 340 mbsf. Despite the low resolution of the geochemical data, the negative relationship between pore-water [Sr^{2+}] content and aragonite content in Hole 823B suggests that shallow burial diagenesis may have been a significant factor in controlling the aragonite signal in Hole 823B. These observations are consistent with the conclusions from the Leg 133 shipboard pore-water [Sr^{2+}] study that suggests that significant dissolution of metastable aragonite and HMC and recrystallization to LMC occurs with increasing core depth (Davies *et al.*, 1993).

Neither of the pore-water geochemistry records, from Hole 819 and Site 823, are particularly convincing in terms of providing positive evidence of dissolution or shallow burial diagenesis. Perhaps, the most persuasive evidence for shallow burial diagenesis and the alteration of metastable aragonite and HMC to LMC can be seen in the HMC 2θ° records. As mentioned earlier in section 5.2, the magnesium ion can substitute for calcium in the calcite lattice, and since the Mg^{2+} ion is smaller than the Ca^{2+} ion, this results in a decrease in the lattice spacing (Goldsmith *et al.*, 1961). Several authors have produced calibration graphs relating the mole % $MgCO_3$ against atomic lattice spacing (d_{104}) in ångstrom units (10^{-10} m) and 2θ° for Cu $K\alpha$ radiation (e.g., Goldsmith *et al.*, 1961) (see Figure 5.3). According to Gomberg and Bonatti (1970), as magnesium is removed from HMC there is a gradual shift in the intervening HMC peak toward lower 2θ° values (see Figure 5.28). Thus, variation in the Mg content of HMC may provide an indication of the degree of alteration and shallow burial diagenesis (Dix and Mullins, 1988) in Hole 819A and Hole 823A periplatform sediments.

The difference between LMC and HMC degrees 2θ ($\Delta 2\theta^{\circ}_{HMC\text{-}LMC}$), and the planktic $\delta^{18}O$ record, for Hole 819A and Hole 823A sediments, plotted against depth (mbsf) are illustrated in Figures 5.29. and 5.30, respectively. The Hole 819A $\Delta 2\theta^{\circ}_{HMC\text{-}LMC}$ record is characterised by an irregular cyclic pattern, punctuated by several prominent minima in value. Minima in $\Delta 2\theta^{\circ}_{HMC\text{-}LMC}$ generally correspond to significant shifts in HMC peak position toward that of LMC (see Figure 5.28). Tentative interpretation of the Hole 819A $\Delta 2\theta^{\circ}_{HMC\text{-}LMC}$ record suggests a significant, albeit gradual, decrease in mean value with increasing depth. Typical, $\Delta 2\theta^{\circ}_{HMC\text{-}LMC}$ values in Hole 819A periplatform sediments range from about 0.1 to 0.45, and according to Goldsmith *et al.* (1961) are equivalent to a difference in $MgCO_3$ content of between about 4 to 15 mole percent (see Figure 5.3). Assuming LMC to have a composition of <4 mole % $MgCO_3$, these figures suggest that HMC in Hole 819A sediments may contain a maximum of about 19 mole % $MgCO_3$. According to Heath and Mullins (1984) calcite containing between 12 to 14 mole % $MgCO_3$ generally indicate a shallow-water/ platform-derived origin of the HMC.

The relationship between the planktic $\delta^{18}O$ record and mean $\Delta 2\theta^{\circ}_{HMC\text{-}LMC}$ values in Hole 819A periplatform sediments is very complex. Above 50 mbsf, no clear relationship seems to exist between these two parameters. However, below about 50 mbsf both curves, although differing in precise details, are broadly similar (i.e., $\Delta 2\theta^{\circ}$

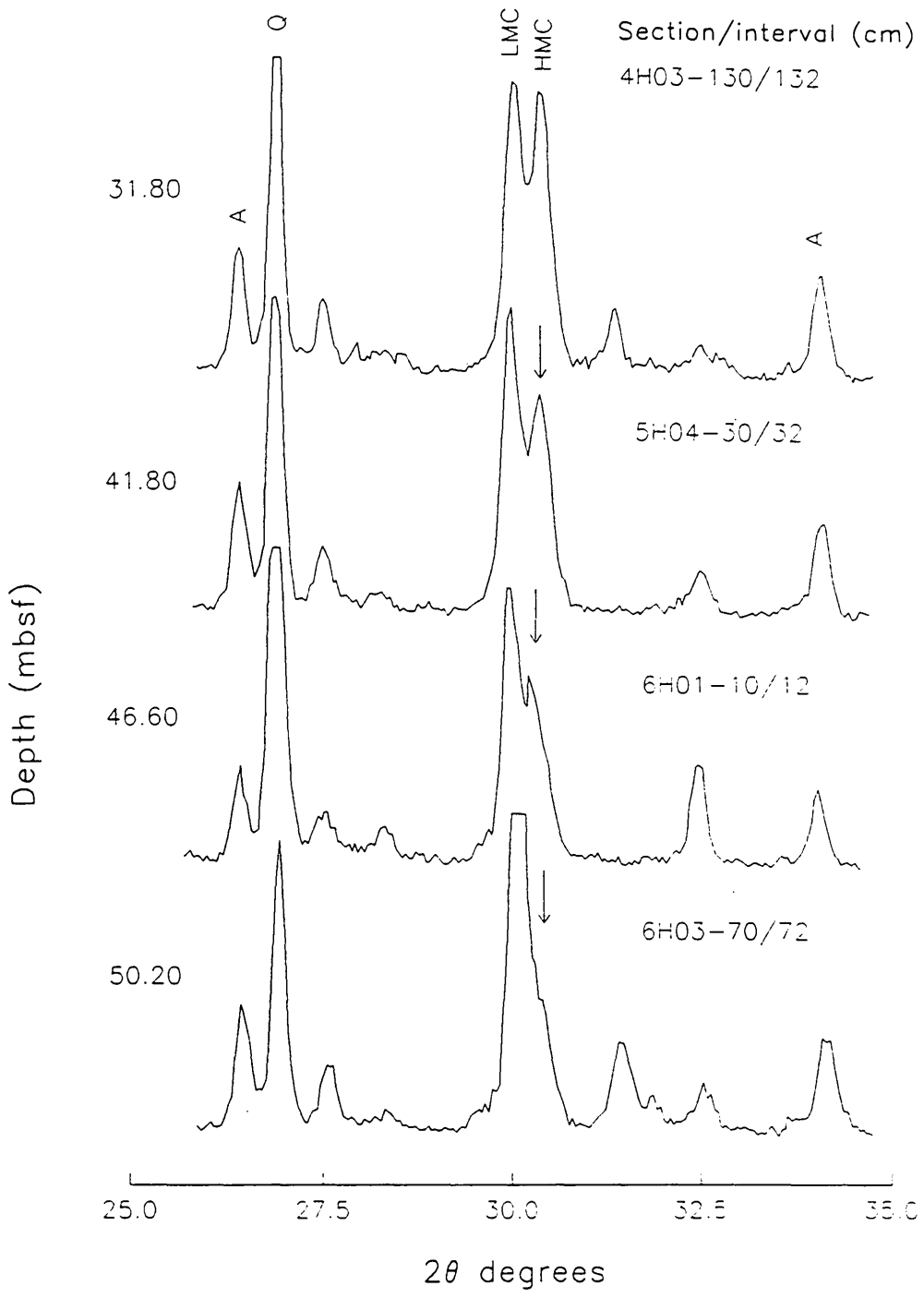

Figure 5.28. Diagram illustating the shift in HMC peak position; relative to LMC, over the interval 31.8–50.2 mbsf, in Hole 819A. The difference in HMC peak position between the upper and lower part of the core correspond to a decrease in $MgCO_3$ content in HMC of approximately 4 Mol. % (see Figure 5.3). Depths are given on left, and core sections and intervals from Hole 819A are indicated. Q = quartz; A = aragonite; LMC = low Mg calcite; HMC = high Mg calcite.

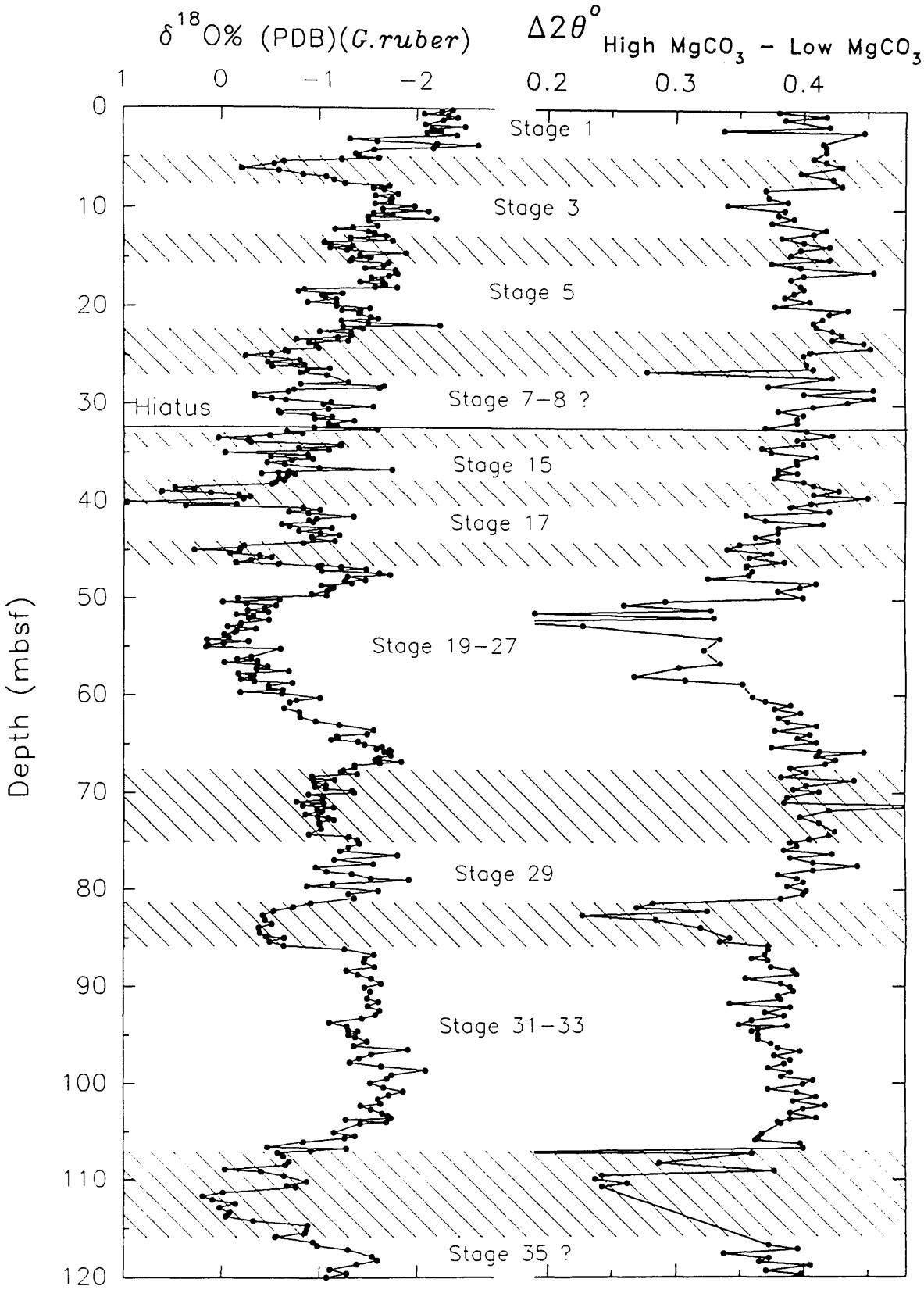

Figure 5.29. The difference between high Mg calcite (HMC) and low Mg calcite (LMC) XRD peak positions ($\Delta 2\theta^{\circ}_{HMC-LMC}$) for Hole 819A sediments.

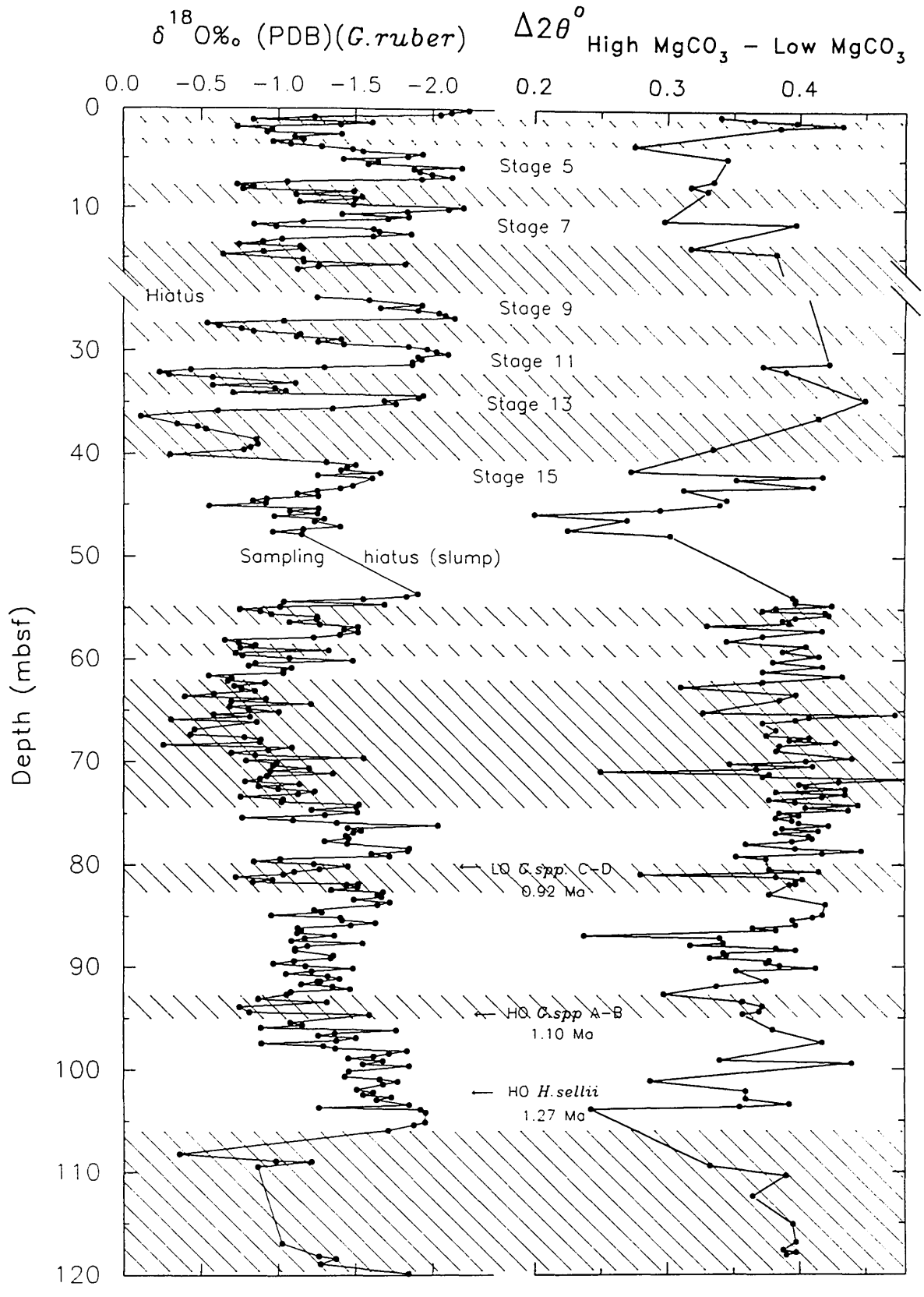

Figure 5.30. The difference between high Mg calcite (HMC) and low Mg calcite (LMC) XRD peak positions ($\Delta 2\theta^{\circ}_{HMC-LMC}$) for Hole 823A sediments. The lack of data in the top 50 m of the XRD record reflects the general absence of HMC across this interval.

$_{HMC\text{-}LMC}$ values are low when oxygen isotope ratios are enriched). A notable exception to this relationship occurs at about 72 mbsf (~0.926 Ma) where the $\Delta 2\theta^{\circ}_{HMC\text{-}LMC}$ and planktic $\delta^{18}O$ records correlate positively.

Relative to Hole 819A, the $\Delta 2\theta^{\circ}_{HMC\text{-}LMC}$ record at Site 823 is poorly defined, largely because of the low abundance of HMC in Hole 823A sediments. In the upper part of the sequence in Hole 823A, HMC content is low and detailed evaluation of the amount of $MgCO_3$ in HMC has not been possible. However, in the lower part of the periplatform sequence in Hole 823A the HMC and LMC records are more complete. Below about 40 mbsf, in Hole 823A, $\Delta 2\theta^{\circ}_{HMC\text{-}LMC}$ values typically range between 0.2 to 0.47. These values suggest a maximum difference in $MgCO_3$ content of about 20 mole % (using the calibration curve of Goldberg *et al.*, 1961). Between about 55 to 120 mbsf, the Hole 823A $\Delta 2\theta^{\circ}_{HMC\text{-}LMC}$ record suggests a progressive decrease in mean value, from about 0.4 to 0.32 (corresponding to a difference in $MgCO_3$ content of approximately 13 to 10 mole %, respectively) (see Figure 5.3). Above, about 55 mbsf the general absence of HMC precludes detailed correlation and interpretation of the $\Delta 2\theta^{\circ}_{HMC\text{-}LMC}$ record. Tentative analysis of the records below 55 mbsf, however, suggests that mean $\Delta 2\theta^{\circ}_{HMC\text{-}LMC}$ values correlate positively with average planktic $\delta^{18}O$ values (i.e., $\Delta 2\theta^{\circ}_{HMC\text{-}LMC}$ values are generally high during periods of isotopic enrichment, or inferred lowstands of sea level).

The downcore variations in $\Delta 2\theta^{\circ}_{HMC\text{-}LMC}$ values, recorded in Hole 819A and Hole 823A periplatform sediments, can be explained in several different ways. Dix and Mullins (1988) suggested that a gradual loss of magnesium from HMC in shallow-water Bahamian periplatform sediments, indicates the neomorphism of HMC to LMC with the subsequent loss of Mg to the ambient pore-waters (the so called *'solution cannibalization'* of Goodell and Garmen, 1969). Thus, the gradual loss of Mg in Queensland margin periplatform sediments could represent the neomorphism of metastable HMC to stable LMC. Alternatively, the reasonably good correlation between the oxygen isotope and $\Delta 2\theta^{\circ}_{HMC\text{-}LMC}$ records, in Hole 819A, suggests a possible link between temperature and the Mg content of HMC. Hardy and Tucker (1988) note that the Mg^{2+} content of biogenic calcite is determined by water temperature, i.e., lower Mg^{2+} occurs in calcareous skeletons precipitated in cooler waters. Thus, variations in $\Delta 2\theta^{\circ}_{HMC\text{-}LMC}$ value may well reflect temperature fluctuations associated with a deterioration of the climate, and not shallow-burial diagenesis as suggested by Dix and Mullins (1988). However, not all glacial periods are associated with low Mg content in HMC. For example, glacial stage 16 (a time of

recognised global sea-level lowstand- Shackleton and Opdyke, 1973) is characterized by high $\Delta 2\theta^{\circ}_{HMC\text{-}LMC}$ values. Similarly, between 60 to 70 mbsf in Hole 823A, isotopic values are enriched with respect to ^{18}O, while $\Delta 2\theta^{\circ}_{HMC\text{-}LMC}$ values remain relatively high. The good correlation between high LMC content and low $\Delta 2\theta^{\circ}_{HMC\text{-}LMC}$ values, particularly below 45 mbsf in Hole 819A, suggests that HMC was neomorphosed to LMC, with the loss or expulsion of Mg from the calcite lattice. Thus, the records suggest that shallow burial diagenesis (in a manner outlined by Dix and Mullins, 1988) has played a significant role in modulating carbonate mineralogy in Hole 819A and Hole 823A periplatform sediments, particularly in the lower part of each record.

Origin and distribution of Dolomite at Site 819 and Site 823

The origin of dolomite rock is still a major problem in carbonate sedimentology (Chilingar *et al.*, 1979). The lack of good modern analogues, coupled with the difficulty of studying its formation in laboratory experiments, have made dolomite a problem mineral. Dolomite is known to form in a variety of depositional and diagenetic settings ranging from hypersaline supratidal sabkhas to organic-rich deep sea sediments, indicating that there is no unique environment of dolomitization (Land, 1980). The controlling factors of dolomite formation or dolomitization and their roles are variable and not always well established. Many different models have been proposed to explain the spatial and temporal distribution of dolomite. These have included: evaporitic-Sabkha (Shinn, 1968; McKenzie *et al.*, 1980; Frisia, 1994), seepage-reflux (Müller and Tietz, 1971; Clark, 1980), meteoric-marine mixing (Hanshaw *et al.*, 1971; Sibley, 1980), shallow-burial (Mountjoy and Amthor, 1994), and seawater models (Kastner, 1984; Land, 1985). In this section, the spatial and temporal distribution of dolomite is briefly examined in Hole 819A and Hole 823A (a more comprehensive account is given by Swart, 1993), in order to determine the origin and significance of dolomite in periplatform sediments deposited on the northeast Australian margin.

According to the Shipboard Scientific Party (1993) significant amounts of dolomite occur in Grafton Passage transect Sites 819, 820 and 821, and in Queensland Trough Site 823. In general, the concentration of dolomite at these sites decreases with increasing distance from the Queensland shelf margin, and thus define a proximal-to-distal/ shelf-basin gradient. For example, in Hole 820 (present-day water depth 212 m) dolomite reaches up to 40 % and is present throughout the section between 40 and 400 m; in Hole 819A (565.2 m water depth) levels are generally <12 % and dolomite is almost totally restricted to the interval below the major hiatus at 32.5 mbsf; in Hole

823A (1637.8 m water depth) dolomite is present only in limited amounts (<5 %) and is largely confined to a prominent interval centred at 65 mbsf (see Figures 5.6 and 5.10).

Several plausible explanations are available to account for the distribution of dolomite in these cores. Given the proximal-to-distal gradient of dolomite content in cores collected from Sites 820 to 823, it is reasonable to suggest that dolomite is detrital in origin. Possibly dolomite formation occurred in restricted shallow water hypersaline lagoons located on the Queensland shelf, in a similar manner to that reported in Holocene sediments from the Caicos Islands, British West Indies (Perkins *et al.*, 1994). During lowstands of sea level this material may have been reworked and directed toward the continental shelf edge/upper slope, and finally into the Queensland Trough. This would explain the shelf-basin gradient of decreasing dolomite content with increasing distance from the Queensland shelf margin. However, temporal variations in dolomite content, in Hole 819A and Hole 823A sediments (and in other Leg 133 sites) provide little evidence of a possible detrital origin or the contemporaneous deposition of this mineral (see Figures 5.6 and 5.10). Thus, an authigenic or diagenitic origin to dolomite in these cores seems most likely.

Extensive dolomitization has been found to occur in many deep-sea cores, many of which are confined to the ocean margins (Kelts and McKenzie, 1982). In a significant number of studies dolomite is thought to have precipitated *in situ* under the oxidation of organic matter by sulphate reducing bacteria (Kelts and McKenzie, 1984; Compton, 1988). According to Berner (1974), bacterial mediated sulphate reduction is a common process of organic matter decomposition in continental margin sediments, both in and below the zone of bioturbation. Seawater sulphate is used as an energy source by sulphate reducing bacteria, which reduce sulphate to H_2S, via the following reaction:

Equation 5.1 $$2CH_2O + SO_4^{2-} \Rightarrow H_2S = 2HCO_3^-$$

This process can only occur in the complete absence of oxygen (i.e., the bacteria are obligate anaerobes) (Berner, 1980). High-concentrations of dissolved methane are often found in organic-rich sediments. Methane often forms micro biologically from the breakdown of organic matter via a sequence of fermentation reactions (Claypool and Kaplan, 1974). Methane builds up in appreciable concentrations, in the marine environment, only at depths where sulphate is exhausted and has been removed by bacterial sulphate reduction. The explanation for this association offered by Berner

(1980) is that in the presence of sulphate any methane produced locally or diffusing up from sediments below is consumed by sulphate reducing bacteria and associate fermentative micro-organisms. Thus, methane concentrations are kept low within the zone of sulphate reduction, whereas they may build up where sulphate concentrations are low or absent (Berner, 1980).

Figure 5.31 illustrates the spatial and temporal distribution of dolomite in Hole 819A and Hole 823A periplatform sediments. Also shown in this figure are the interstitial pore-water sulphate (SO_4^{2-}) and methane (CH_4) data collected onboard the *"Resolution"*, during ODP Leg 133 (Davies *et al.*, 1991). The most striking feature of these curves is that dolomite is almost totally restricted to the interval below the sulphate reduction zone and the zone of methanogenesis in both cores. This suggests that dolomite may be intimately linked to the processes of sulphate reduction and methanogenesis and possibly diagenetic in origin. The process of organic carbon oxidation by sulphate reducing bacteria typically generates an extremely depleted carbon isotopic composition (or an enriched carbon isotopic ratio) in the pore water dissolved carbon (DIC) (Irwin *et al.*, 1977; Kelts and McKenzie, 1982). However, according to Swart (1993) the $\delta^{13}C$ of the interstitial dissolved inorganic carbon (DIC), in the majority of Grafton Passage transect sequences show no conclusive evidence of these diagenetic processes (no samples for DIC were measured from Site 823). Similarly, the carbon and oxygen isotopic signature of dolomites retrieved from Hole 819A reveal no significant evidence of having been formed in either the sulphate reduction zone or the zone of methanogenesis (despite evidence to the contrary from interstitial pore-water data) (see Figure 5.32). Swart (1993) suggested that the lack of any clear isotopic evidence for the diagenetic origin of dolomite in Hole 819A was probably related to the high carbonate content in this core. Recrystallization of calcium carbonate buffers the isotopic composition of the system, masking the addition of isotopically light or heavy CO_2 derived from the processes of sulphate reduction and methanogenesis.

As mentioned earlier, the association of dolomite with the lack or reduced HMC content in both Hole 819A and Hole 823A periplatform sediments suggests that the Mg for dolomitization may have come from the dissolution of HMC (see Figures 5.6 and 5.10). Swart and Guzikowski (1988) have estimated that the dissolution of sediments containing 20 % HMC (containing 20 mole % Mg) might produce sufficient Mg^{2+} to form a sediment containing about 8 % dolomite. Using the same rationale, the reduction in mean HMC values by about 10-12 %, associated with the prominent

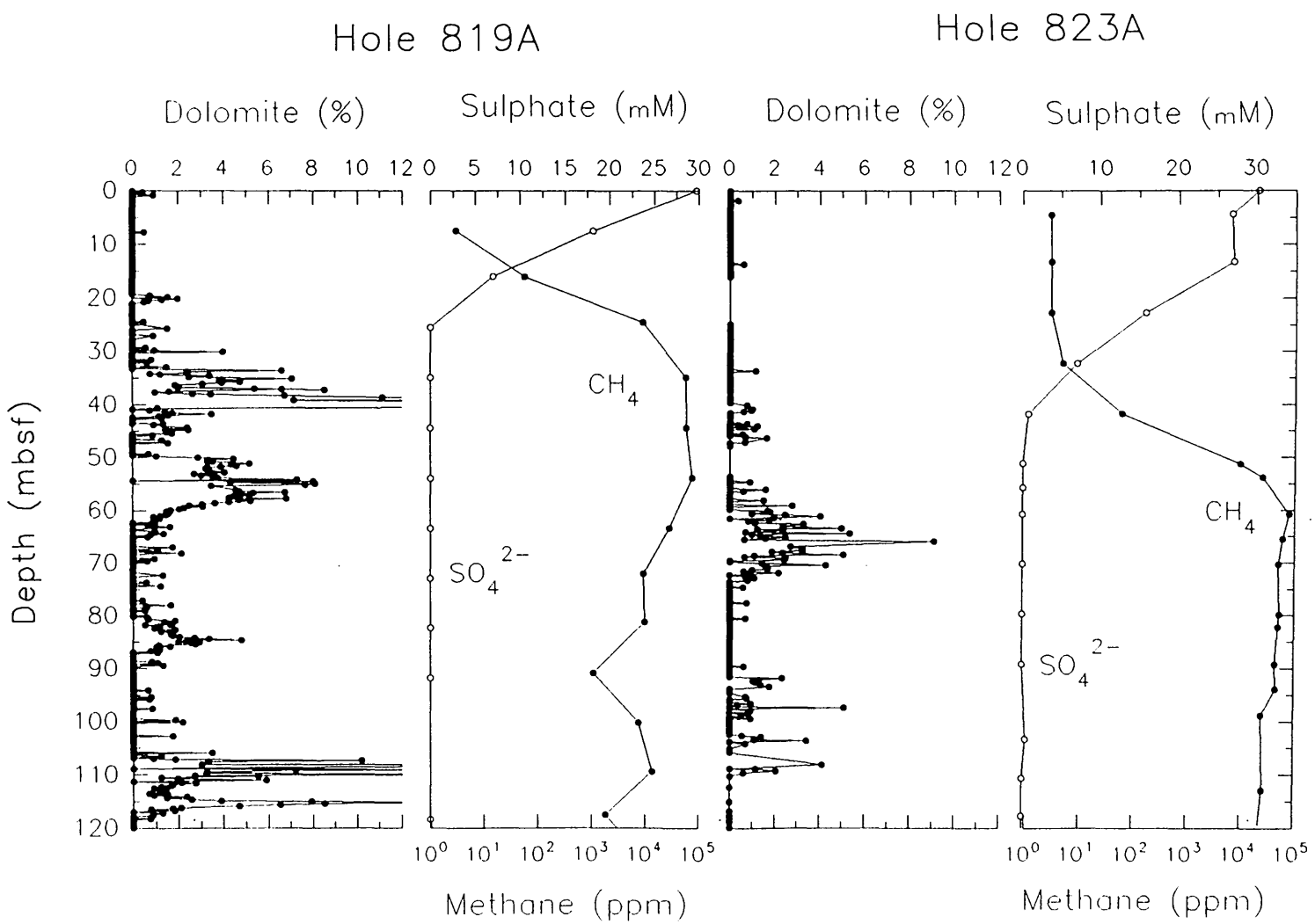

Figure 5.31. Percent dolomite content in Hole 819A and Hole 823A periplatform sediments plotted alongside the pore-water sulphate and methane concentration data (Shipboard Scientific Party, 1991). Note the general absence of dolomite in the upper part of each core.

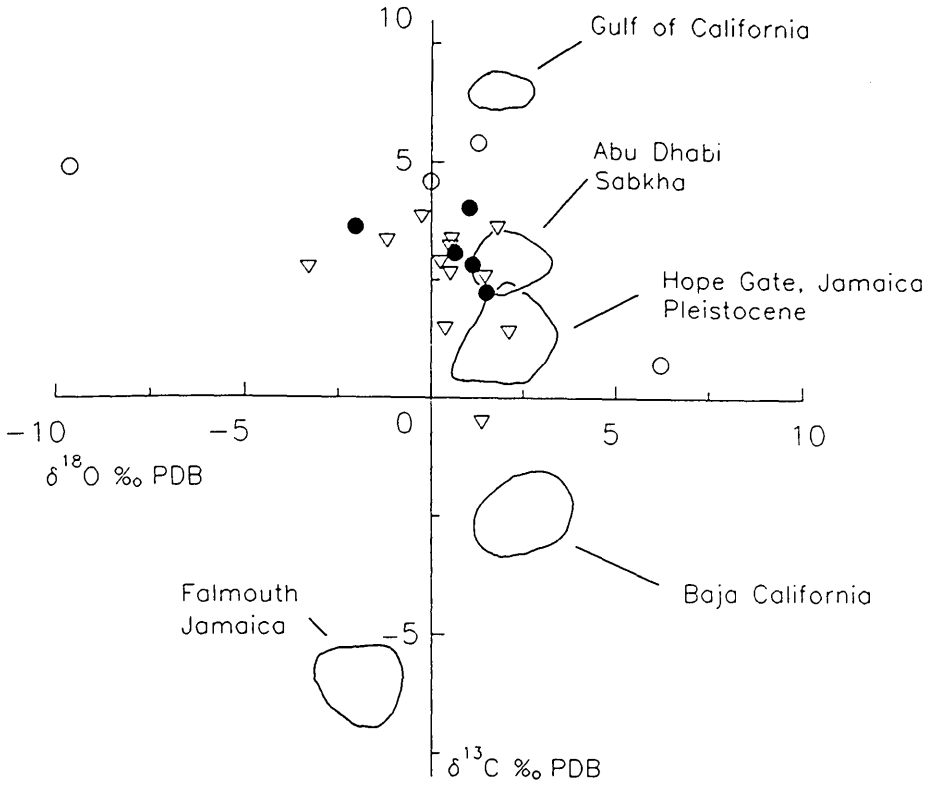

Hole 819A open circles
Hole 820A closed circles
Hole 821A diamonds

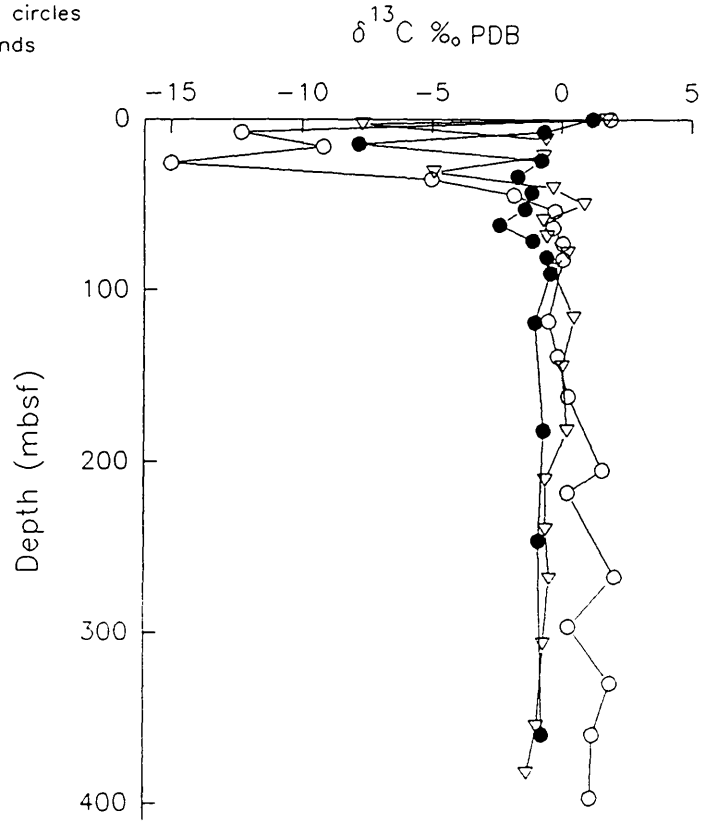

Figure 5.32 The $\delta^{13}C$ and $\delta^{18}O$ of the dolomite (upper plot) and the $\delta^{13}C$ of the pore–water dissolved inorganic carbon (DIC)(lower plot) at Sites 819, 820 and 821 (after Swart, 1993). Also shown for comparison are selected carbon–oxygen isotopic compositions of some recent and Pleistocene dolomites (after Tucker and Wright, 1990).

sufficient Mg^{2+} to allow the formation of about 4-5 % dolomite. These values are close to the average amount of dolomite found in Hole 819A and Hole 823A sediments, and thus support the hypothesis that the dissolution of HMC may have provided the Mg necessary for the formation of dolomite in these sediments. A similar conclusion was reached by Davies *et al.* (1991) who argued that dolomite formation was probably promoted by the dissolution of HMC and the degradation of feldspar (primarily albite) and organic matter. Thus, the shelf-basin gradient of decreasing dolomite content, within Queensland margin transect sites (Holes 820A through to 823A), with increasing distance from the Queensland margin shelf may well reflect the greater influence of shallow water platform derived calcite (HMC) in the more proximal sites.

Preliminary SEM (scanning electron microscopy) examination of Hole 819A and Hole 823A sediments (corresponding to both glacial and interglacial periods) indicate that, where present, dolomite typically occurs as well-developed euhedral rhombs, ranging in size from 2-10 μm, that are fresh in appearance, and are occasionally twinned or showing inter-penetrating rhombs. In general, these characteristics all suggest an *in situ* precipitation of dolomite (Shimmield and Price, 1984; Mullins *et al.*, 1985). Typical dolomite rhombohedra found in Hole 819A and Hole 823A periplatform muds (<63 μm sediment size fraction) are illustrated in Plates 9 and 10.

5.4.3 Carbonate dissolution and preservation on the slope of the GBR and in the Queensland Trough, northeast Australian margin

Late Pleistocene carbonate cycles in the equatorial Pacific were first described by Arrhenius (1952). The carbonate content of the eastern equatorial Pacific sediments oscillate at 10^4 and 10^5 years, generally showing lower values during isotopically inferred interglacial periods and higher content during glacial episodes (Arrhenius, 1952; 1988; Hays *et al.*, 1969; Pisias and Prell, 1985; Pisias and Rea, 1988). Arrhenius (1952) claimed that the $CaCO_3$ cycles were caused by enhanced productivity linked to periods of upwelling driven by variations in the Pleistocene climate. Since the pioneering work of Arrhenius, numerous cores have been collected over the Pacific region (Hays *et al.*, 1969; Berger, 1973; Arrhenius, 1988; Farrell and Prell, 1989; Wu *et al.*, 1991), and these have been the topic of great debate over correlation and cause of $CaCO_3$ cycles. Two main hypothesis have been proposed to explain fluctuations in carbonate content, namely: productivity and dissolution. Proponents of productivity argue that $CaCO_3$ flux from the surface of the ocean (euphotic zone) largely determines the resulting $CaCO_3$ mass accumulation rate (Arrhenius, 1952; Parkin and Shackleton, 1973; Adelseck and Anderson, 1978; Emerson and Bender, 1981; Archer,

A

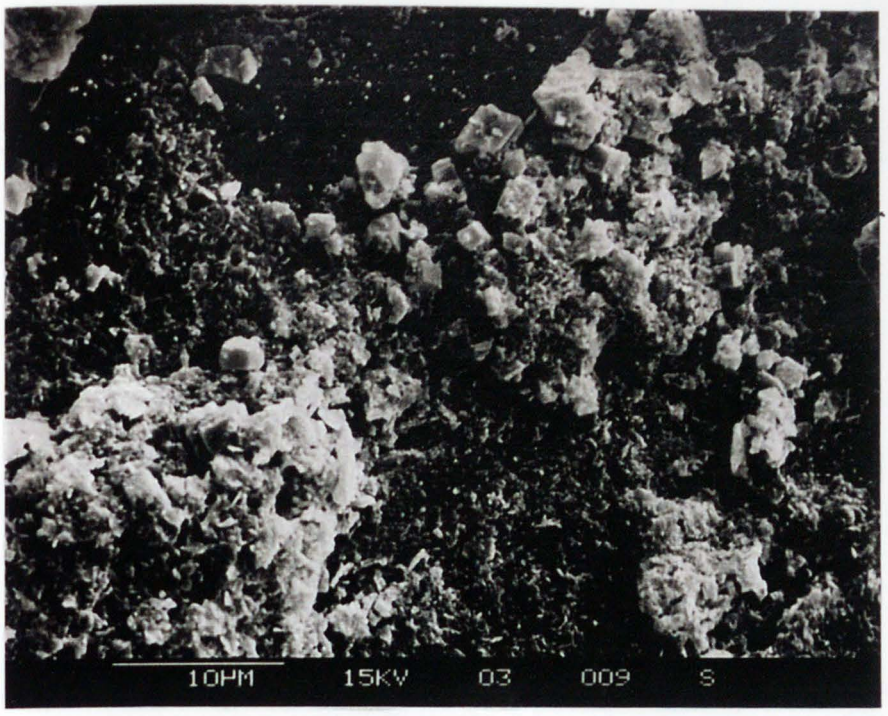

X 1200

B

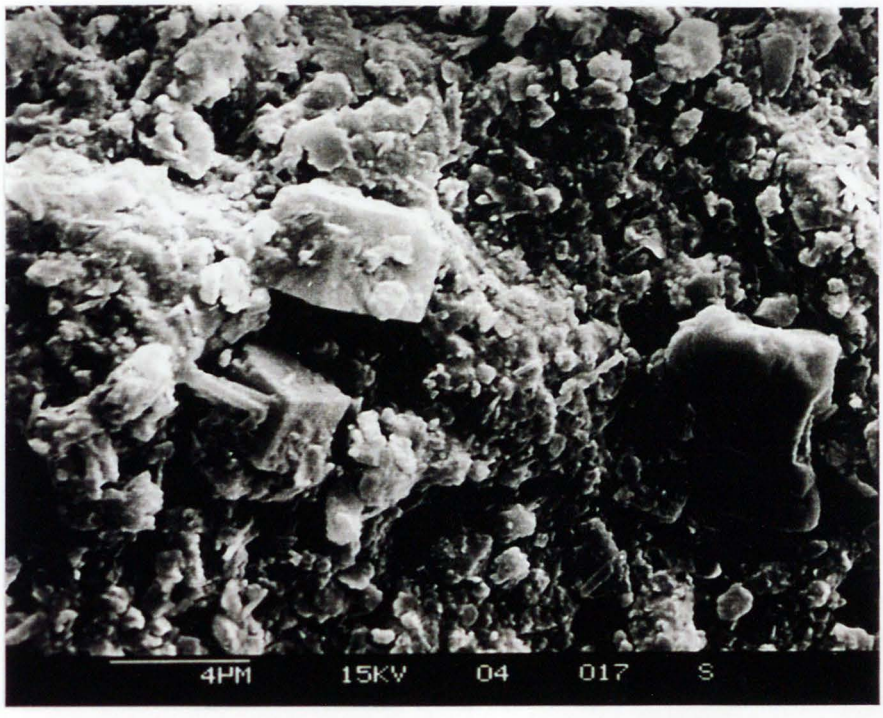

X 4500

Plate 9. SEM photomicrographs showing typical dolomite morphology in Hole 819A periplatform sediments (Samples 133-819A-09H03-90/92 (77.75 mbsf) and 133-819A-10H02-30/32 (85.20 mbsf), Figures (A) and (B), respectively). Note that crystal terminations are sharp and well defined which indicate that no abration or other transport effects have taken place.

A

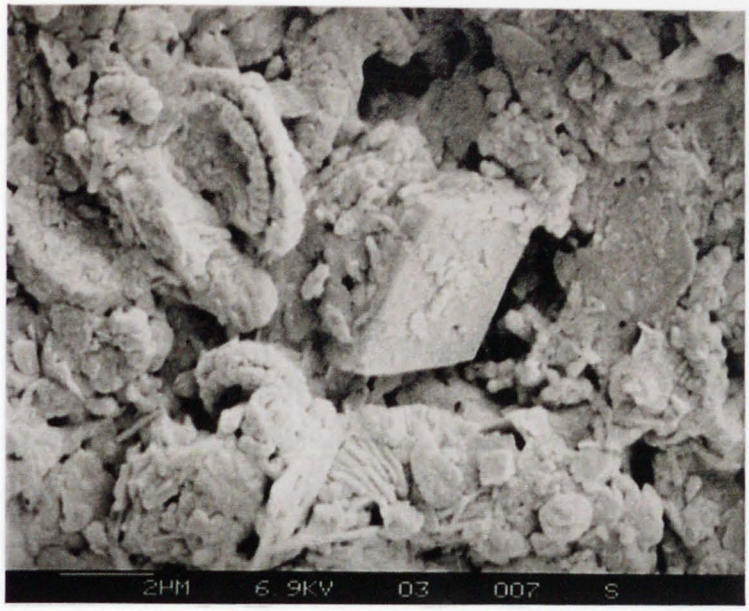

X 6000

B

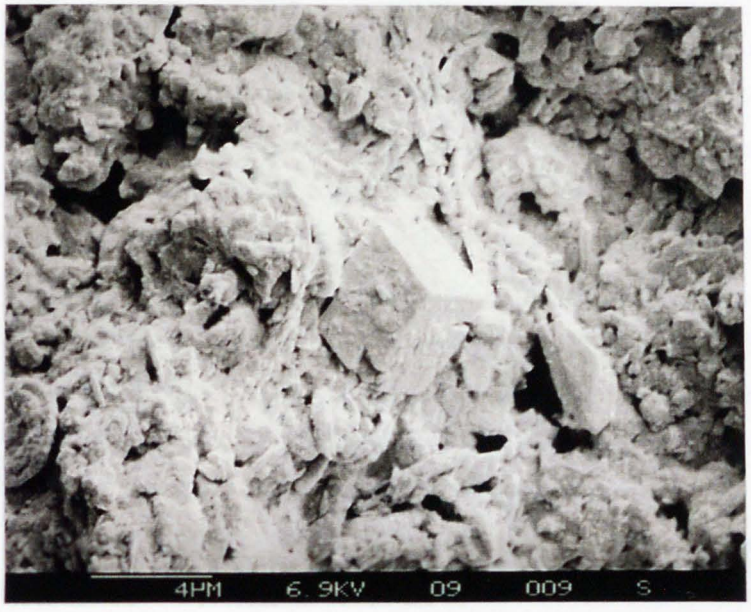

X 3875

Plate 10. SEM photomicrographs showing dolomite morphology in Hole 823A pelagic to hemipelagic sediments (Samples 133-823A-8H02-110/112 (65.4 mbsf) and 133-823A-8H04- 135/137 (68.65 mbsf), Figures (A) and (B), respectively).

1990). Supporters of dissolution suggest that Pleistocene $CaCO_3$ cycles primarily reflect changes in water column chemistry (i.e., the corrosiveness of intermediate and bottom waters) that are most likely related to variations in ocean circulation (Olausson, 1965; Berger, 1975; Farrell and Prell, 1989, 1991). Despite earlier differences of opinion, most authors now agree that although surface productivity (and dilution by non-carbonate input) can locally influence carbonate concentrations (Emerson and Bender, 1981; Arrhenius, 1988; Archer, 1991), dissolution is often the main factor controlling the accumulation of $CaCO_3$ in ocean sediments.

The distribution of $CaCO_3$ in marine sediments is primarily controlled by the effect of hydrostatic pressure on the solubility of carbonate minerals (Hawley and Pykowitcz, 1969). Dissolution of $CaCO_3$ increases with depth as a result of the thermodynamic effects of lower temperature and greater hydrostatic pressure which both serve to increase the solubility of $CaCO_3$. In addition to the bathymetric effect are regional preservation patterns related to water mass chemistry and sediment input (Farrell and Prell, 1991).

In discussing the changes in $CaCO_3$ content in sediments with depth the concepts of the "lysocline" and "carbonate compensation depth" (CCD) have been formed as indicators of $CaCO_3$ preservation status (Bramlette, 1961; Berger, 1968). The lysocline is identified by the break in slope of a particular sedimentological or microfossil dissolution index. For example, the level which separates well-preserved from poorly-preserved assemblages of planktic foraminifera is called the foraminiferal lysocline, pteropods (pteropod lysocline), and coccoliths (coccolith lysocline) (Kennett, 1982). Other sedimentary lysoclines have been defined based on the percentage of $CaCO_3$ content (Berger, 1975), and the mass accumulation rate (MAR) of $CaCO_3$ (Van Andel *et al.*, 1975; Rea and Leinen, 1985). Below the lysocline dissolution occurs at increasing rates, such that there is a progressive decrease in the proportion of biogenic $CaCO_3$ preserved in the sediments (although substantial dissolution can occur in the supra-lysoclinal oxygen minimum zone- Steens *et al*, 1991). In theory, the CCD marks the water depth where the rate of input and dissolution of carbonate are balanced, and there is no net $CaCO_3$ accumulation in the seafloor sediments (Bramlette, 1961). However, in practice, the depth of the CCD is taken where pelagic sediments contain 0 % $CaCO_3$. The CCD should not be confused with the carbonate critical depth (CCrD)[7] at which level sediments contain ≤10 %

[7]Some authors prefer to use the term CCrD to describe the carbonate preservation status of sediments, because seafloor redeposition makes difficult the precise mapping of the CCD based on the 0 % $CaCO_3$ level (Berger *et al.*, 1976; Farrell and Prell, 1989).

$CaCO_3$ (Lisitzin and Peltelin, 1967). The lysocline and CCD are shallower for aragonite than for calcite and unless otherwise stated, the terms usually refer to calcite, because skeletal material is more commonly formed of calcite than aragonite (Milliman, 1974).

The lysocline is not found at a uniform depth, being deepest in the North Atlantic (Biscaye *et al.*, 1976) and shallowest in the North Pacific (Parker and Berger, 1971). Most workers believe the depth of the lysocline is primarily related to the concentration of carbonate ions (CO_3^{2-}) in the intermediate and deep-water masses (Pytkowicz, 1970; Morse, 1974; Broecker and Takahashi, 1978), although the exact relationship is unclear. Broecker and Takahashi (1978) have shown that in deep water the position of the lysocline can be explained to an accuracy of 200 m solely by variations in the concentration of CO_3^{2-} ions. The CO_3^{2-} ion concentration of bottom waters is dependant upon the mix of three main water types: North Atlantic Deep Water (NADW), Antarctic Bottom Water (AABW), and North Pacific Deep Water (NPDW) (Kennett, 1982). The lysocline is deepest where the NADW extends to the bottom and shallowest in the North Pacific, where low CO_3^{2-} (nutrient-rich) deep water overlies the AABW (Broecker and Takahashi, 1978).

Numerous studies have suggested possible secondary mechanisms for controlling carbonate dissolution and the depth of the lysocline. These models include: the rate of rain of calcareous and organic matter in the water column (Berger, 1970); whether the carbonate grains have an organic coating to retard dissolution (Chave and Suess, 1970); the concentrations of kinetic inhibitors such as phosphate ions in deep-water (Morse, 1974); and the turbulence or velocities of bottom waters (Edmond, 1974). According to Kennett (1982) such influences may locally change the depth of the lysocline.

The depth of the CCD is controlled, in part by how undersaturated the water is with respect to CO_3^{2-} ions, but also by the flux or 'rain rate' of $CaCO_3$ rich debris to the sediments. The greater the biogenic $CaCO_3$ flux rate the more likelihood of material being buried before it dissolves. The CCD, and associated aragonite compensation depth (ACD), varies between and within ocean basins. In general, the CCD and ACD are depressed beneath areas of upwelling and high productivity distant from the continental margins, while values tend to shoal toward high latitudes and on the continental slopes where productivity is often higher (Berger, 1978). The reason for the apparent contradiction, between productivity and the depth of the CCD on the continental slopes, is because of enhanced CO_2 development (and associated pH

reduction of the waters) by benthic organisms (including bacteria), in response to high concentrations of organic matter (Berger and Winterer, 1974).

The depth of the lysocline is thought to have fluctuated markedly during the Pleistocene climatic cycles while the CCrD has remained relatively constant (Farrell and Prell, 1991). The reason for the transition zone between the lysocline and the CCD is that pore waters in the uppermost few millimetres of the seafloor sediments become saturated with respect to $CaCO_3$. Dissolution can only take place when they become undersaturated again, through exchange with bottom waters (by diffusion and/or advection). The greater the difference between the saturation concentration of CO_3^{2-} for carbonate and the actual concentration of CO_3^{2-} in the water ($-\Delta CO_3^{2-}$) the longer it takes for saturation to occur and the easier it is for exchange with bottom waters to restore the undersaturation. Thus, significant changes in the thickness of the $CaCO_3$ transition zone, between the lysocline and CCrD, have occurred over time (Van Andel *et al.*, 1975; Farrell and Prell, 1989; Rea *et al.*, 1991). These changes, observed as fluctuations in $CaCO_3$ preservation, are recorded in many deep sea cores (Farrell and Prell, 1989).

According to Beiersdorf (1989) the depth of the Late Quaternary CCD in the western Coral Sea was about 4670 m. The modern position of the aragonite lysocline in the western South Pacific is about 1000 m, as projected from the Geochemical Oceans Sections Study program (GEOSECS) Station 269 (Broecker *et al.*, 1982). It is important to appreciate that the present day positions of Sites 819 and 823, located in 565.2 and 1637.9 m water depth, respectively, straddle the modern position aragonite lysocline. Any variations in water depth, surface productivity and/or ocean circulation, in the past, may have significantly influenced the depth of the lysocline, and hence the pattern of carbonate deposition recorded at these sites.

Dissolution indices

A wide range of microfossil and sedimentological parameters have been used to provide an estimate of the degree of $CaCO_3$ dissolution in deep-sea sediments (Berger, 1968, 1970; Thunell, 1976; Volat *et al.*, 1980; Wu *et al.*, 1990; Howard and Prell, 1994). However, the most useful Late Quaternary deep-sea carbonate preservation records are those provided by Peterson and Prell (1985a, 1985b) and Farrell and Prell (1987, 1989, 1991).

In the eastern equatorial Indian Ocean, Peterson and Prell (1985a) developed a high resolution composite dissolution index (CDI) using principal component analysis of a

suite of dissolution sensitive indices (foraminiferal-based) for sediments collected across the Ninety East Ridge (at latitude 6°S), over a depth range of 2900 to 4600 m (see Figure 5.33). The Peterson and Prell record is displayed as water-depth contours of equal CDI (isopleths) which range from -12 to +4. Positive values indicate better preservation, whereas negative numbers indicate poorer preservation. The CDI = 0 isopleth approximates to the modern calcite saturation horizon of 3800 m based on the critical carbonate ion concept of Broecker and Takahashi (1978) (Peterson and Prell, 1985b). The 700 ka record of Peterson and Prell (1985a) shows that variations in carbonate preservation rate are proportional to and in phase with maximum rates of change in the benthic $\delta^{18}O$ record. This pattern, whereby carbonate preservation is generally best at glacial to interglacial boundaries and is poor during interglacial to glacial transitions, is particularly well developed over the last 250 ka (Peterson and Prell, 1985a). The CDI record of Peterson and Prell also shows a broad interval of relatively high dissolution during the mid- Bruhnes Chron from about 0.25 to 0.6 Ma, superimposed on a general trend of increasing $CaCO_3$ preservation since the Late Pleistocene (700 ka) (see Figure 5.33).

Farrell and Prell (1987, 1989, 1991) used the $CaCO_3$ content of sixteen deep-sea cores from the central equatorial Pacific to construct a continuous 3.9 Ma record of bathymetric variations in carbonate preservation. This records show cyclic deepening and shallowing of carbonate preservation over a water depth range from 4300 to 4800 m. The Farrell and Prell record shows that $CaCO_3$ preservation has been generally increasing since 1.6 Ma with two intervals of poor preservation from 0.87 to 0.9 Ma and from 0.2 to 0.4 Ma (see Figures 5.34 and 5.35). The long-term record of Farrell and Prell is characterized by a first order periodicity of about 100 ka, over the last 0.9 Ma. These orbital eccentricity cycles were give way to lower frequency oscillations between 1.0 to 3.0 Ma[8], with higher frequency cycles returning in the last 900 ka of the record (i.e., between 3.0-3.9 Ma). The preservation record of Farrell and Prell suggests that during the last 800 ka, the $CaCO_3$ lysocline in the central equatorial Pacific deepened by a least 400 m, to about 800 m. In common with the preservation record of Peterson and Prell (1985a), the Farrell and Prell curve shows that carbonate preservation maxima generally coincide with the latter half of glacial and interglacial cycles rather with the mid-point of climate intervals (see Figure 5.35). A similar pattern of carbonate preservation, in which high carbonate content occurs during periods of deglaciation, has been reported by Wu *et al.* (1991) in sediments from

[8]Because of low resolution, a decrease in data intensity, and smoothing introduced by contouring, Farrell and Prell (1991) were unable to clearly distinguish high frequency (≤ 40 ka) fluctuations.

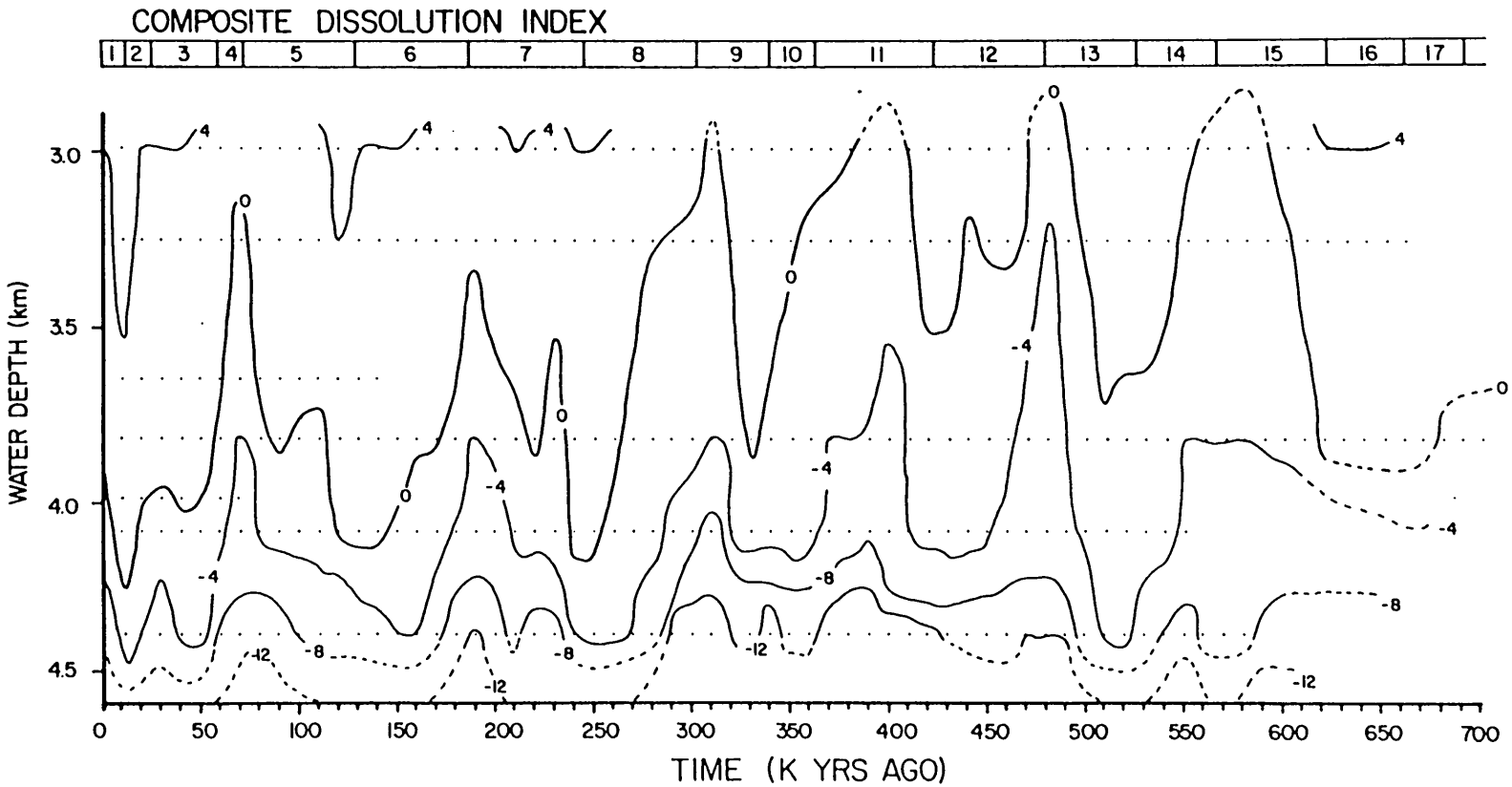

Figure 5.33 Bathymetric variations in relative preservation through time, as expressed by the Composite Dissolution Index (after Peterson and Prell, 1985). The numbered legend across the top shows the standard oxygen isotope stages.

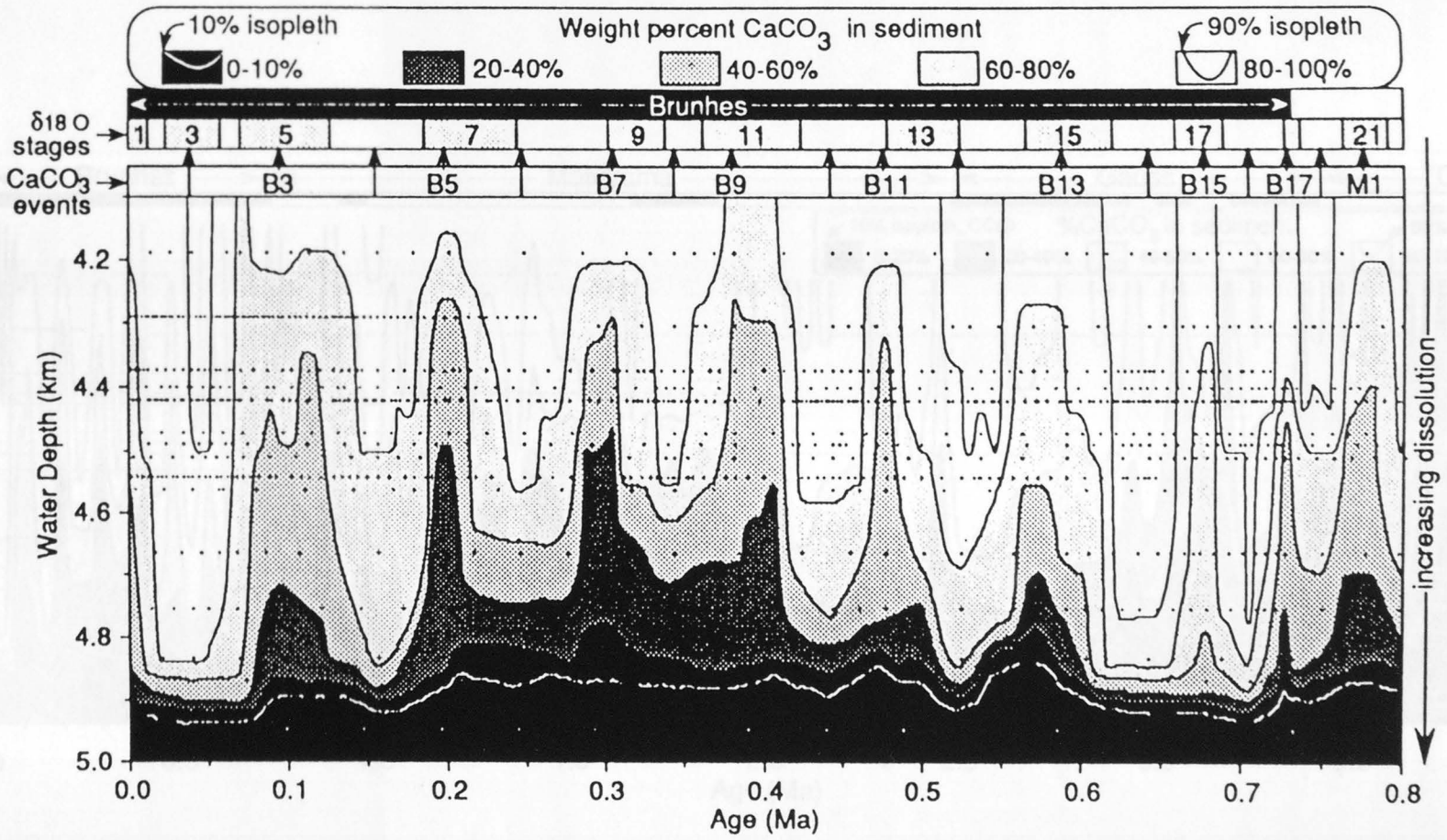

Figure 5.34 Bathymetric variations in $CaCO_3$ preservation through time, as expressed by $CaCO_3$ (after Farrell and Prell, 1989). The four legends above the plot, from top to bottom, are the $\%CaCO_3$ isopleths which delimit water depth intervals of sedimentary $CaCO_3$ content by weight percent, the paleomagnetic time scale of Berggren *et al.* (1985), the SPECMAP oxygen isotope stages from Imbrie et al. (1984), and $CaCO_3$ event scale with midpoints of the preservation maxima and minima marked by arrows. Preservation minima are labelled by event name.

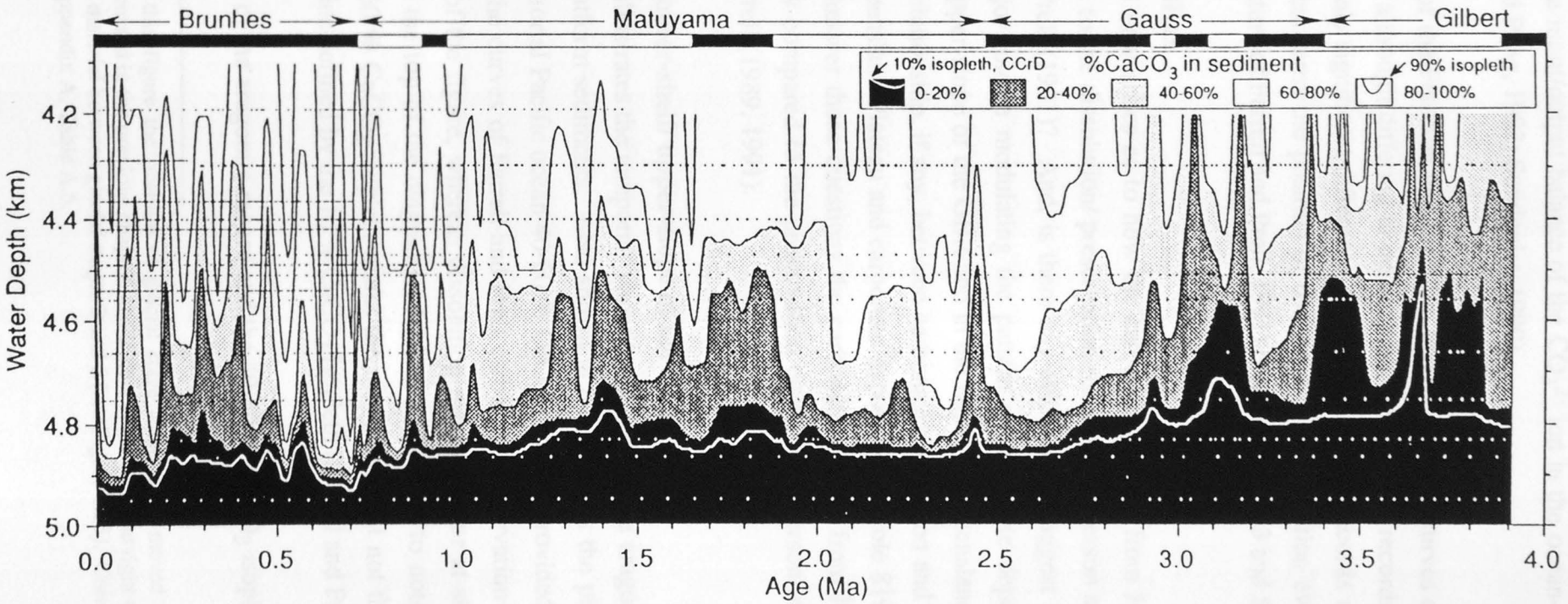

Figure 5.35 Bathymetric variations in $CaCO_3$ preservation through time, as expressed by $CaCO_3$ (after Farrell and Prell, 1989). The legends above the plot are the $\%CaCO_3$ isopleths which delimit water depth intervals of sedimentary $CaCO_3$ content by weight percent and the paleomagnetic time scale of Berggren *et al.* (1985).

Ontong Java Plateau, western equatorial Pacific ocean. This lag, first described by Luz (1973), has been attributed to the response time of the oceans and $CaCO_3$ sediments to changes in the input/output balance of the CO_3^{2-} ion in the ocean-atmosphere system (Broecker and Peng, 1982; Sundquist, 1990).

Comparison of the Peterson and Prell and Farrell and Prell curves over the last 700 ka suggest that, although differing in detail, both preservation records are essentially the same. The only significant difference between these two records occurs over the last 100 ka, and concerns the position of the last major dissolution event (peak B3 using the nomenclature of Farrell and Prell, 1991) (see Figures 5.33 and 5.35).

Study objectives

The question now arises as to how the carbonate records from Hole 819A and Site 823 compare to the dissolution/ preservation records of Peterson and Prell (1985) and Farrell and Prell (1991)? And, is there any evidence to suggest that dissolution has played a major role in modulating the pattern of carbonate deposition seen on the outer-shelf/upper-slope of the GBR and in the adjacent Queensland Trough? Further, what is the relationship, if any, between carbonate production and preservation on the marginal Queensland Plateau and carbonate deposition in Hole 819A and Hole 823A? In order to answer these questions the carbonate records from Hole 819A and Site 823, are now compared to the preservation curves of Peterson and Prell (1985) and Farrell and Prell (1989, 1991).

Hole 819A (outer-shelf/ upper-slope of the GBR)

Figure 5.36 illustrates the temporal[9] variations in metastable aragonite content in Hole 819A periplatform sediments. Also shown in this figure is the planktic $\delta^{18}O$ record, and the equatorial Pacific ocean 40-60 % $CaCO_3$ isopleth provided by Farrell and Prell (1991). In the curves of Farrell and Prell carbonate preservation maxima are toward the bottom of the figure, whereas dissolution maxima occur at shallow water depths (i.e., toward the top of the diagram). An important point to note with these plots is that the 40-60 % $CaCO_3$ isopleth tracks the movement, but not the absolute position, of the lysocline defined by the 10 % $CaCO_3$ isopleth (Farrell and Prell, 1991).

Comparison of the aragonite record and the 40-60 % $CaCO_3$ isopleth record of Farrell

[9]Note that in this figure the position of glacial stage 4 has been moved in accordance with the arguments discussed in the previous chapter, and is now centered to the right of the prominent peak in non-carbonate material between glacial stages 2 and 6 (see Figure 4.25). Corrections to the age model are listed in Appendix A, Table A.6.

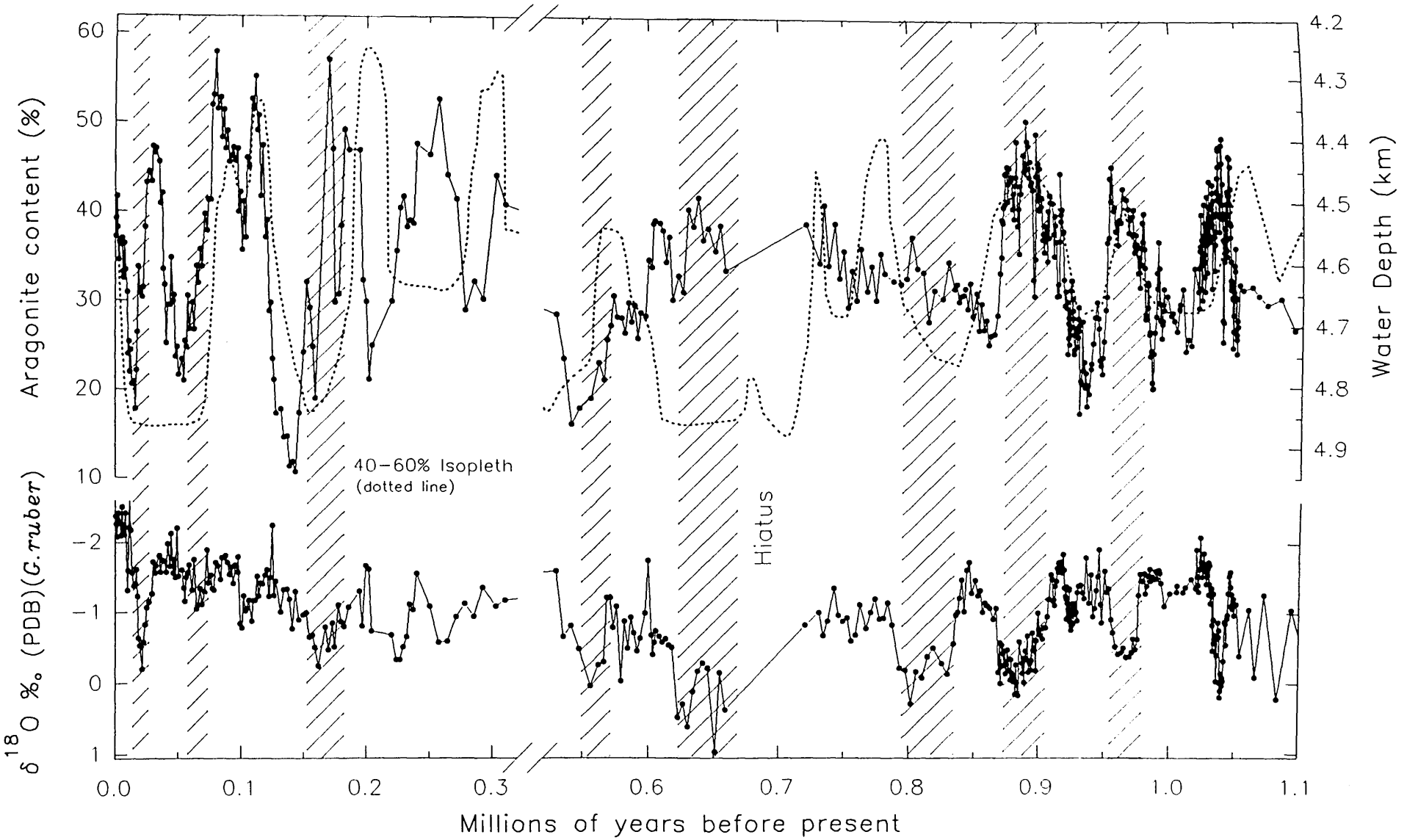

Figure 5.36. Temporal variations in aragonite content in Hole 819A, plotted alongside the carbonate preservation record of Farrell and Prell (1991)(dotted line). Also shown is the planktic oxygen isotope record from Hole 819A. Carbonate preservation increases toward the bottom of the diagram. Note the presence of a major hiatus between 0.31–0.53 Ma.

and Prell suggests that between 1.10 and 0.8 Ma aragonite content follows fluctuations in dissolution intensity (see Figure 5.36). For example, the prominent dissolution peaks of Farrell and Prell centred at 0.9, 0.95 and 1.06 Ma are each associated with high aragonite content (the slight difference in peak position between the aragonite record and the 1.06 Ma dissolution spike is thought to represent either an artifact of the age model and/or digitizing error). This association suggests that either: (1) aragonite input was so high during glacial periods, between 0.7-1.10 Ma in Hole 819A, as to depress the lysocline and ACD (i.e., the pattern of carbonate deposition seen during this interval is a local phenomenon related to high aragonite input), or (2) aragonite deposition occurred in water depth significantly shallower than the lysocline and therefore was largely unaffected by dissolution, during the mid-late Pleistocene (0.7-1.10 Ma), or (3) variations in watermass dissolution intensity may have been significantly out of phase, with the equatorial Pacific and Indian oceans, on the northeast Australian margin, during the mid-late Pleistocene. Paleodepth calculations by the Shipboard Scientific Party (1991) and Kroon *et al.* (1993) suggest that Site 819 was significantly shallower during the mid-late Pleistocene, than at present. Thus, it seems likely that water depth and variations in metastable carbonate input have been the major factors controlling aragonite accumulation between 0.7 and 1.1 Ma, in Hole 819A.

Throughout the majority of the Brunhes Chron (0-730 ka) the association between aragonite content and the preservation record of Farrell and Prell is very complex. Unfortunately, the mid-Brunhes Chron interval (0.3 to 0.6 Ma) is largely absent in the periplatform sequence of Hole 819A due to a major hiatus at 32.5 mbsf (Shipboard Scientific Party, 1991), corresponding to the interval from 0.31 to 0.53 Ma. Thus, possible evidence of this global event is absent from the records in Hole 819A. The mid-Brunhes Chron dissolution interval apparently occurred oceanwide and affected $CaCO_3$ sediments within intermediate waters of the Bahamas (Droxler *et al.*, 1988), the Maldives (Droxler *et al.*, 1990), and the deep and bottom waters of the middle and low latitude oceans (Peterson and Prell, 1985; Farrell and Prell, 1989). According to Jansen *et al.* (1986) this interval correlates to a deterioration in continental climate that may be linked to a perturbation in the Earths 400 ka eccentricity cycle. Between about 0.25 and 0.7 Ma aragonite content and preservation index exhibit a poorly developed antithetical relationship, with significant peaks in aragonite content located at 0.65 and 0.25 Ma (between B13-B15 and B5-B7, respectively- using the nomenclature of Farrell and Prell, 1989; 1991) (see Figures 5.35 and 5.36). However, percentage aragonite content in Hole 819A sediments appear to fluctuate independently of the position of the 40-60 $CaCO_3$ isopleth with respect to water depth. For example, the percent

aragonite content is lower at 0.65 Ma than 0.25 Ma, despite a 200 m deepening of the 40-60 $CaCO_3$ isopleth between 0.25 and 0.65 Ma. This association is the opposite of what might be expected, under normal conditions, particularly had the accumulation of aragonite been solely under the control of dissolution. Thus, the primary factor controlling the distribution of aragonite (and total carbonate) content, in the periplatform sequence of Hole 819A, is thought to be input.

Throughout the last 0.25 Ma of the record from Hole 819A, the relationship between aragonite content and the $CaCO_3$ isopleth curves of Farrell and Prell is somewhat unclear, largely because of the low resolution of the preservation record. Comparison of the aragonite content and 40-60 % $CaCO_3$ isopleth curves, over the last 0.25 Ma, suggests that peaks in aragonite content lag the preservation record (see Figure 5.36). However, comparison of the aragonite record in Hole 819A with the CDI = 0 $CaCO_3$ isopleth of Peterson and Prell (1985) suggest that it is in fact it is former that leads the later (see Figure 5.37). For example, the prominent aragonite content maxima centred at 30 ka and about 80 ka clearly precede inferred dissolution maxima. Thus, it seems likely that the distribution of aragonite in the upper part of the sequence from Hole 819A has been little effected by dissolution, and that input has been the dominant control on aragonite deposition on the outer-shelf/upper-slope of the GBR, as recorded in the periplatform sequence from Hole 819A.

Middle to Late Pleistocene metastable $CaCO_3$ record in Hole 823A (Queensland Trough) periplatform sediments

Having examined the possible effects of dissolution on the comparatively shallow-water carbonate records from Site 819, the question now remains as to what effect, if any, have variations in Pacific deep-water dissolution intensity had on the metastable carbonate signal recorded in the Queensland Trough Hole 823A periplatform sediments? Given the present-day water depth at Site 823 (1638 m), and the position of the modern aragonite lysocline in the western South Pacific (~1000 m, Broecker *et al.*, 1982), we might expect that sediments recovered from Hole 823A contain a clearer record of mid-late Pleistocene variations in Pacific ocean $CaCO_3$ dissolution intensity.

Comparison of the percentage aragonite in Hole 823A periplatform sediments, plotted with the deep-sea equatorial Pacific 40-60 % $CaCO_3$ isopleth of Farrell and Prell (1991), is illustrated in Figures 5.38 and 5.39. Analysis of these records suggest that aragonite content follows variations in the 40-60 % $CaCO_3$ isopleth of Farrell and Prell (1991). For example, the prominent peaks in aragonite content at approximately 0.2,

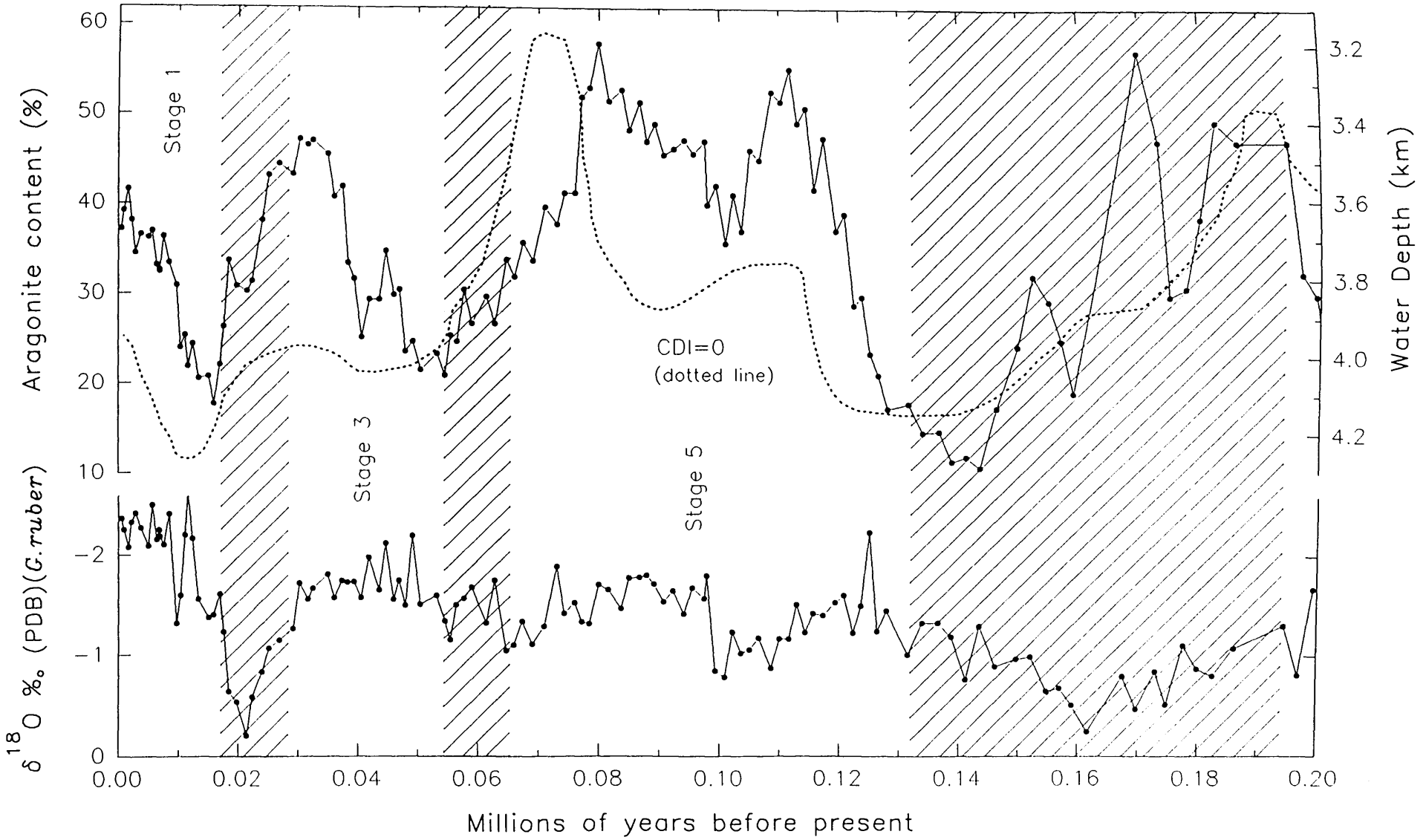

Figure 5.37. Temporal variations in aragonite content in Hole 819A, plotted alongside the Composite Dissolution Index (CDI) record of Peterson and Prell (1985)(dotted line). Also shown is the planktic oxygen isotope record from Hole 819A.

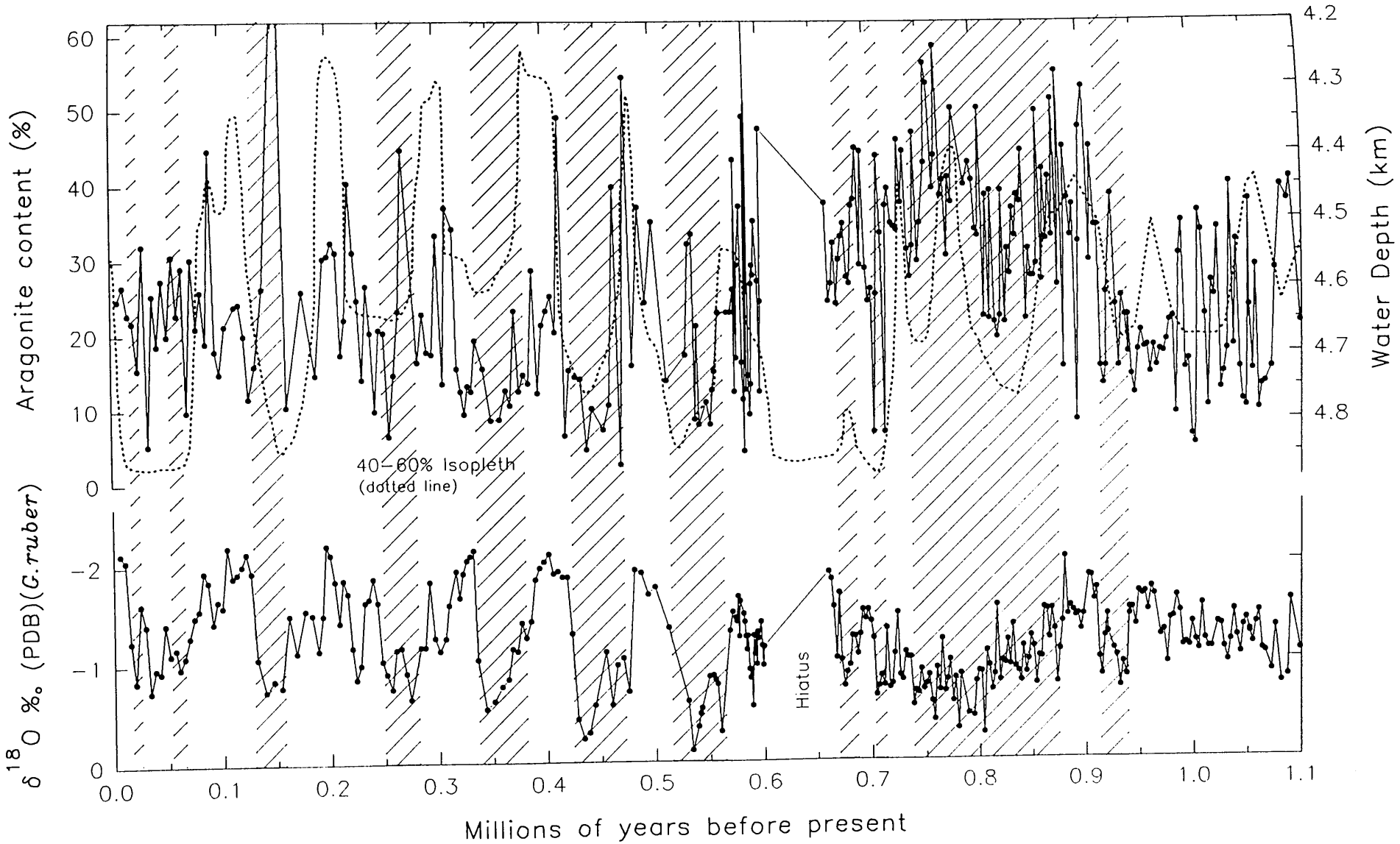

Figure 5.38. Comparison between the aragonite content in Hole 823A and the carbonate preservation record of Farrell and Prell (1991)(dotted line). Also shown is the planktic oxygen isotope record from Hole 823A. Note that carbonate preservation increases toward the bottom of the diagram.

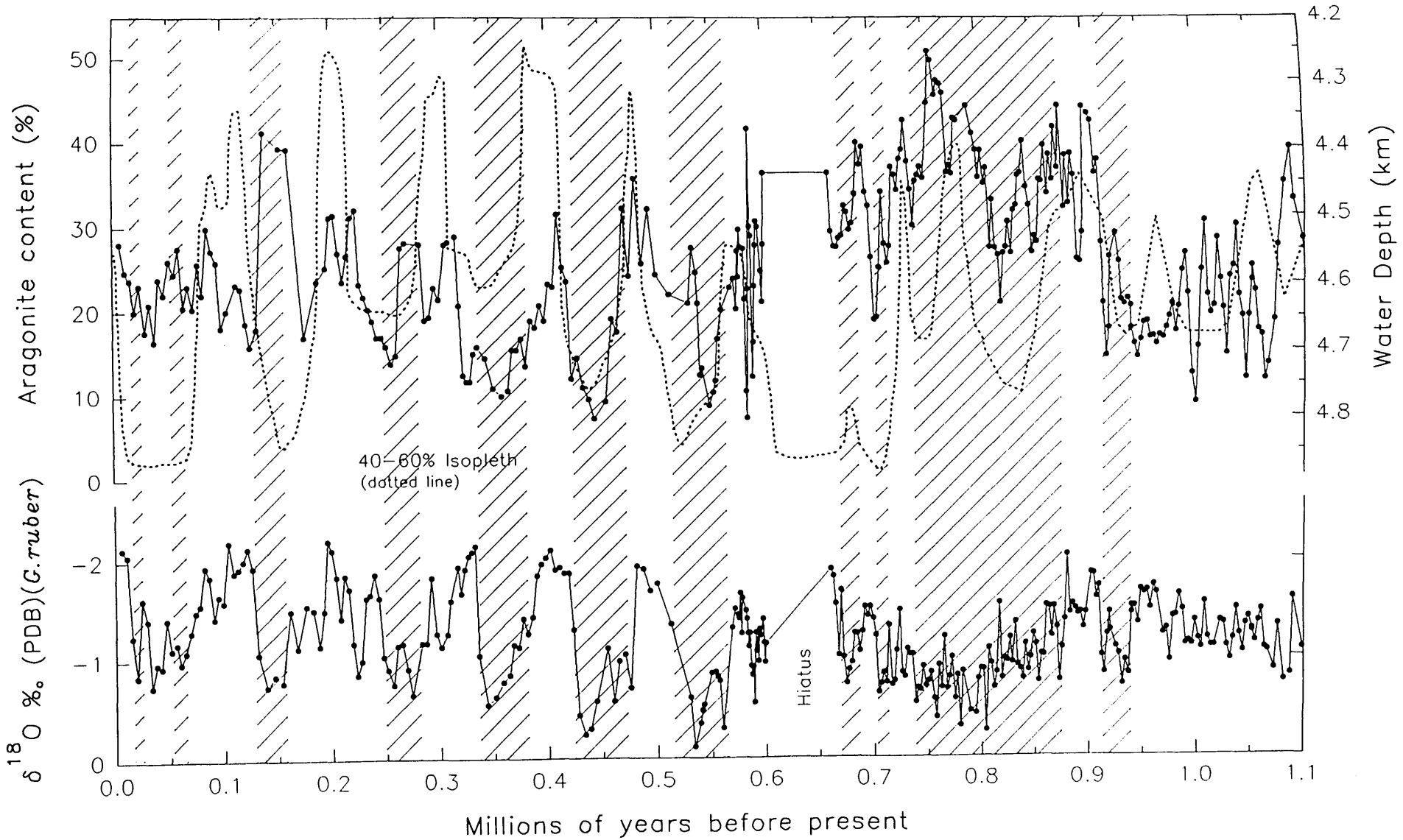

Figure 5.39. Comparison between the aragonite content in Hole 823A and the carbonate preservation record of Farrell and Prell (1991)(dotted line). Also shown is the planktic oxygen isotope record from Hole 823A. Carbonate preservation increases toward the bottom of the diagram. Note that the aragonite record has been smoothed using a 3 point average.

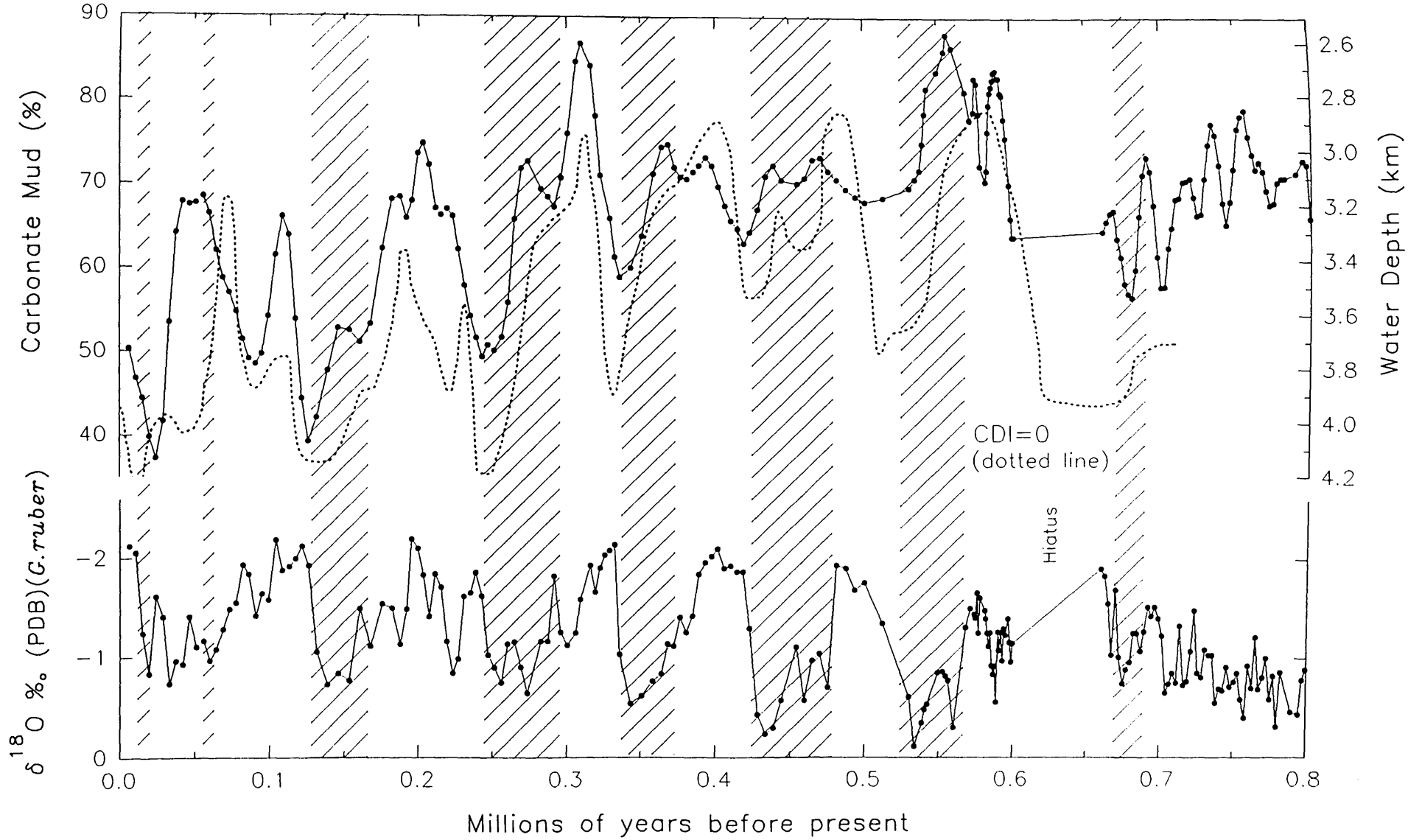

Figure 5.40. Comparison between the carbonate content in Hole 823A muds.and the Composite Dissolution Index (CDI) of Peterson and Prell (1985)(dotted line). Also shown is the planktic oxygen isotope record from Hole 823A. Note that the carbonate record has been smoothed using a 3 point average.

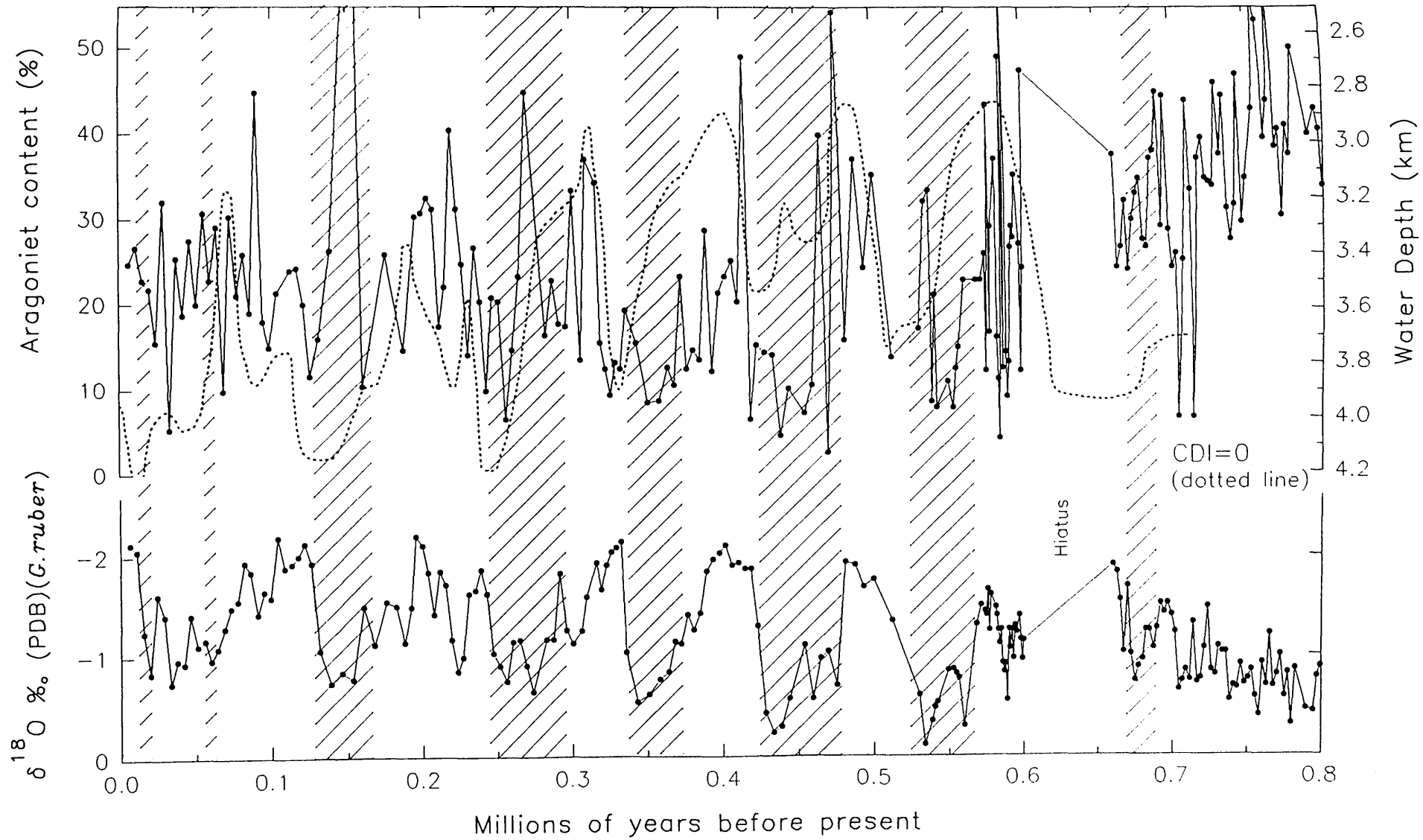

Figure 5.41. Comparison between the Hole 823A aragonite content record and the Composite Dissolution Index (CDI) record of Peterson and Prell (1985)(dotted line). Also shown is the planktic oxygen isotope record from Hole 823A.

0.3, 0.4 and 0.5 Ma in the upper part, and at about 0.75 and 0.9 Ma in the lower section, in Hole 823A, are all centred on or about preservation minima (or conversely dissolution maxima). This positive relationship is particularly well developed in the percent fine carbonate (<63 μm) record (see Figure 5.40). However it must be appreciated that this record contains both dissolution sensitive and dissolution resistant carbonate phases, and therefore must be treated with caution, as an accurate dissolution proxy. Comparison between the aragonite content in Hole 823A periplatform sediments and the CDI = 0 isopleth record of Peterson and Prell (1985b), over the last 700 ka, shows that, in general, peaks in aragonite content are associated with episodes of inferred poor $CaCO_3$ preservation (see Figure 5.41 and 5.42). A notable exception to this relationship occurs at about 0.15 Ma (~8 mbsf), however, this may be related to the high occurrence of turbidites and gravity flow deposits in Hole 823A (Shipboard Scientific Party, 1991; Watts *et al.*, 1993). Superimposed upon the late Pleistocene 100 ka cycles, of high aragonite content during interglacial periods and low aragonite content during glacial intervals, is an abrupt and dramatic increase in mean aragonite value at 0.9 Ma and at 0.82 Ma, in Hole 823A (see Figures 5.38 and 5.39). These records are further characterized by a rapid decline in aragonite values between 0.82 and 0.55 Ma, followed by a gradual increase in mean aragonite content values toward the top of the core (see Figure 5.39).

In general, the pattern of aragonite deposition seen in Hole 823A, is inconsistent with the preservation records of Farrell and Prell (1991) and Peterson and Prell (1985b), particularly since high aragonite (and total carbonate mud) content tend to occur during interglacial periods. However, several aspects of the aragonite record are in agreement with long-term trends inferred from the $CaCO_3$ preservation provided by these authors. For example, since about 0.55 Ma, following a dramatic fall in aragonite content, the records from Hole 823A indicate a gradual increase in mean aragonite value, consistent with a significant deepening of the CDI = 0 $CaCO_3$ isopleth since about 0.5 Ma. Similarly, throughout the mid- Brunhes Chron dissolution interval (Jansen *et al.*, 1986; Farrell and Prell, 1989; Wu *et al.*, 1990), between 0.3 and 0.6 Ma, the aragonite record from Hole 823A displays a broad interval of reduced (albeit slightly rising) aragonite content suggesting a possible link between aragonite content in Hole 823A periplatform sediments and low latitude $CaCO_3$ preservation patterns. Thus, these records indicate that the primary control on carbonate accumulation in the upper part of Hole 823A has been input.

In the lower part of Hole 823A the relationship between aragonite (and carbonate mud) content and the $CaCO_3$ preservation records is less clear than in the upper part

(prior to 0.55 Ma) of the record. Between 1.10 and 0.9 Ma, the 40-60 $CaCO_3$ isopleth record of Farrell and Prell (1991) suggests a general deepening of the calcite lysocline and a shift toward better carbonate preservation in the central equatorial Pacific (see Figure 5.34). However, the aragonite record in Hole 823A shows little evidence of enhanced preservation patterns during this interval. Similarly, the prominent $CaCO_3$ dissolution event centred on 0.9 Ma (correlating to the deep water calcite dissolution event M3 of Hays *et al.*, 1969) suggested by the Farrell and Prell records, is discordant with an abrupt increase in aragonite content seen across this interval in the aragonite records from Hole 823A.

An abrupt increase in aragonite content, at about 0.9 Ma (early/ middle Pleistocene), has also been reported in ODP Leg 133 Holes 818B and 817A, drilled on the flanks of the Queensland Plateau (Haddad *et al.*, 1993). In these piston cores, a sudden and permanent increase in aragonite content occurs between 0.86 and 0.875 Ma (Haddad *et al.*, 1993). The general agreement in the timing of this event, between Queensland Trough and Queensland Plateau records (and the lack of such a feature in the Queensland shelf margin Hole 819A records) suggests that this was a regional phenomenon, possible restricted to intermediate water depths (see Figure 5.43). Several possible explanations have been offered for the abrupt increase in aragonite, in Queensland Plateau cores, at about 0.9 Ma (early/ middle Pleistocene). According to Haddad *et al.* (1993) the dramatic and permanent increase in aragonite at this time, in Holes 818B and 817A, may be related to: (1) an abrupt and permanent increase in the depth of the lysocline; (2) a change in local environmental conditions (e.g., temperature, salinity, nutrients), which promoted a dramatic increase in shallow-water bank-top production and sediment export; or (3) an increase in carbonate bank top production and shedding possible related to a change in amplitude and frequency of sea level changes related to a shift from high frequency and low amplitude 41 ka Milankovitch cycles, prior to 0.9 Ma, to low frequency and high amplitude 100 ka orbital periodicities, after about 0.73 Ma (Shackleton and Opdyke, 1976; Pisias and Moore, 1981; Prell, 1982; Ruddiman *et al.*, 1989; Raymo *et al.*, 1990). In their final analysis, Haddad *et al.* (1993) attributed the abrupt increase in aragonite content, seen in these piston cores, to a possible rebound toward good carbonate preservation between 0.85 and 0.9 Ma, following an oceanwide $CaCO_3$ dissolution increase near 0.9 Ma (early/ middle Pleistocene).

Isern *et al.*, (1993) have proposed, based on $\delta^{18}O$ temperature calculations, that surface-water temperatures increased on the Queensland Plateau, reaching optimum levels for reef growth (20-25°C, Veron, 1986) during the middle Pleistocene (1.2-0.5

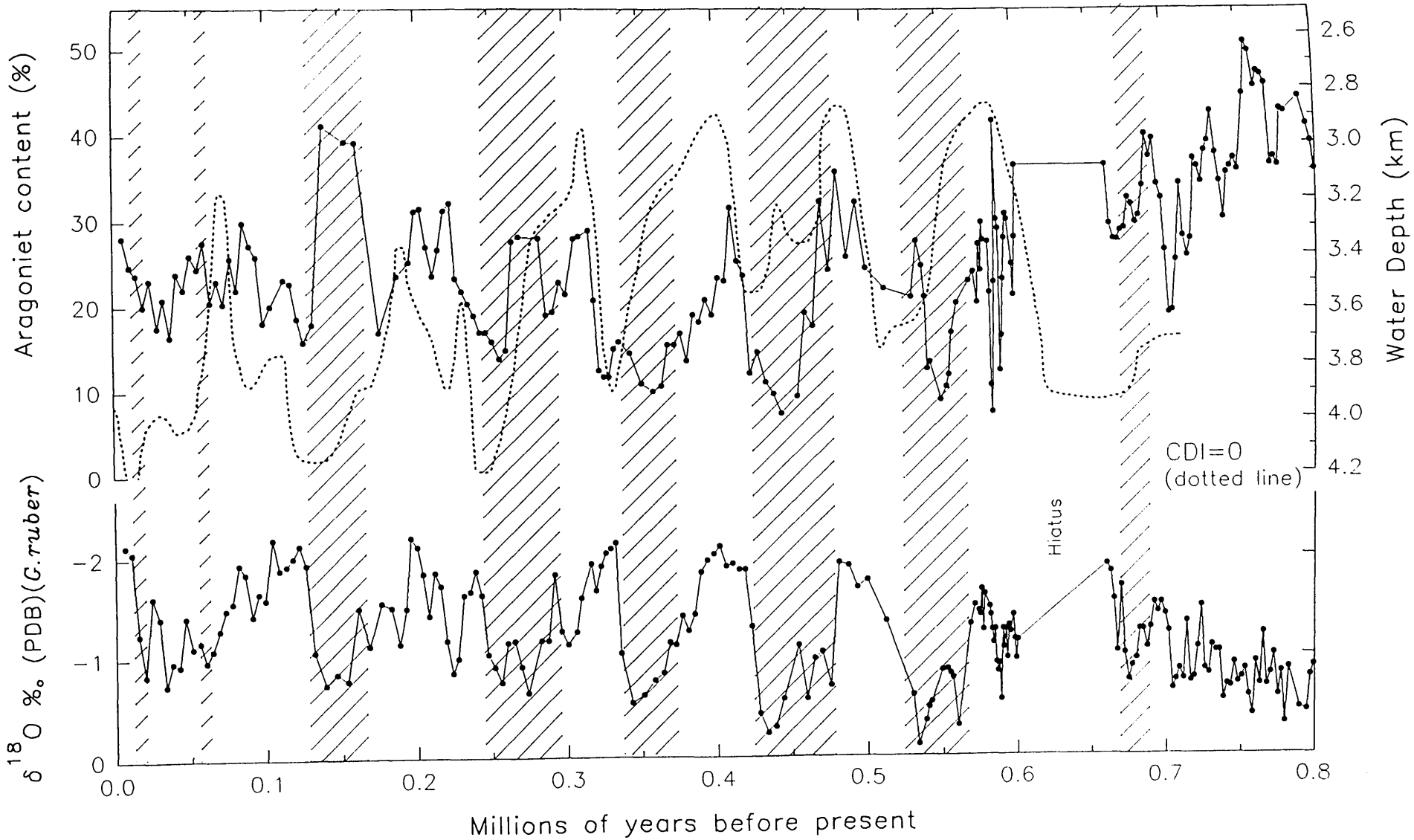

Figure 5.42. Comparison between the Hole 823A aragonite content record and the Composite Dissolution Index (CDI) record of Peterson and Prell (1985)(dotted line). Also shown is the planktic oxygen isotope record from Hole 823A. Note that a 3 point average has been used to smooth the aragonite content record.

Ma). This apparent temperature increase was attributed to a change in the circulation patterns, possibly promoted by sea level variations and subsidence, which allowed warmer surface-waters to flow over the platform. Isern *et al.*, (1993) suggest that the warming trend during the Pleistocene may have been responsible for the initiation of the Great Barrier Reef. It is possible, therefore, that the aragonite peak at 0.9 Ma in the records from Hole 823A (and in Hole 818B) may represent a period of increased bank-top carbonate production and shedding, in response to higher sea water temperatures. Alternatively, it could be argued that an increase in productivity, possibly related to enhanced upwelling, produced the dramatic increase in aragonite content in these cores. However, Hallock and Schlager (1986) have argued that nutrient excess can reduce or kill off reef growth, by stimulating plankton production, which reduces water transparency, and both coral and calcareous algal growth. In addition, enhanced nutrient levels can stimulate the growth of non-calcareous organisms, increasing both competition and bioerosion. Thus, an increase in nutrient levels, during the mid- late Pleistocene is inconsistent with the initiation of reef growth on the northeast Australian shelf. Alternatively, the abrupt increase in aragonite at 0.9 Ma, seen in these cores, may represent an interval of greater productivity and sediment export by calcareous algae (i.e., *Halimeda, Penicillus*), rather than framebuilding corals particularly since these organisms can tolerate much deeper and nutrient-rich waters than corals (Hallock *et al.*, 1988).

In summary, Hole 823A periplatform sediments generally record an 'North Atlantic-type' pattern of carbonate deposition (Peterson and Prell, 1985; Farrell and Prell, 1991), characterized by high carbonate content during interglacial periods and low carbonate during glacials. This pattern is the opposite to many marine sequences recovered from the Pacific (Hays *et al.*, 1969; Berger, 1963; Thompson and Saito, 1977; Pisias *et al.*, 1974; Crowley, 1985; Farrell and Prell, 1989; Berger, 1982). This suggests that carbonate productivity and sediment input have played a more important role in determining the signature of Hole 823A periplatform sediments, than variations in dissolution intensity.

The long-term (Plio- Pleistocene) record of $CaCO_3$ input and preservation in the periplatform sequence of Hole 823B (Queensland Trough)

Having examined in detail the mid-late Pleistocene record of carbonate input and preservation in periplatform sequences recovered from Hole 819A and Hole 823A, the question now arises as to what has been the long-term (Pliocene/ Pleistocene) response of the carbonate systems on the northeast Australian margin to global climate and sea level change.

Temporal variations in aragonite content in Hole 823B periplatform sediments, plotted alongside the 40-60 % $CaCO_3$ preservation isopleth of Farrell and Prell (1991) are illustrated in Figures 5.44 and 5.45. However, the absence of a stable oxygen isotope record for this core has made the conversion of depth to age rather speculative. In addition, the comparatively low resolution in Hole 823B has precluded detailed correlation with high resolution carbonate stratigraphies on the Queensland Plateau (Droxler *et al.*, 1993), the Bahamas (Droxler *et al.*, 1988), and the Maldives (Droxler *et al.*, 1990). Thus, two speculative age models are presented for the Plio-Pleistocene section in Hole 823B (see Appendix A, Tables A.8). The first age model is based exclusively on the foraminiferal datums provided by Kroon (1993) and is illustrated in Figure 5.44. The second age model is founded on a combination of both nannofossil datums (Wei and Gartner, 1993) and foraminiferal dates (Kroon, 1993) (see Figure 5.45). However, in this interpretation, the nannofossil H.O. *Discoaster brouweri* datum (Wei and Gartner, 1993) has been omitted, because it is inconsistent with the H.O. *Globigerinoides fistulosus* and H.O. *Globigerinoides obliquus* foraminiferal datums provided by Kroon (1993). In the following discussion, the later age model is adopted because of the greater time constraints on Hole 823B sediments provided by using both foraminifers and calcareous nannofossils (see Table 5.2).

Comparison of the different age models presented for Hole 823B suggests that, although differing in detail, the general relationship between aragonite content and the preservation record of Farrell and Prell (1991) is essentially the same. In general aragonite content in Hole 823B sediments is high during periods of inferred better $CaCO_3$ preservation (i.e., when the 40-60 % $CaCO_3$ isopleth of Farrell and Prell (1991) is depressed), suggesting that unlike the records from Holes 819A and 823A preservation may have played a more important control on the occurrence of aragonite in this core.

Although, minor amounts of aragonite have been reported in the lower part of the Pliocene/ Pleistocene sequence in Hole 823B (Shipboard Scientific Party, 1991), the first significant appearance of this mineral occurs at 350 mbsf, and corresponds to the interval between 3.2 to 3.4 Ma (see Figure 5.44 and 5.45). This period marks the initiation of a gradual and stepwise deterioration in the global palaeoclimate, from about 3.4- 2.9 Ma, culminating in a series of glacial events at 2.85 (Raymo *et al.*, 1986) and 2.45 Ma (Shackleton *et al.*, 1984). Prior to this period, early Pliocene (5.0-3.6 Ma) sediments in Hole 823B (Queensland Trough) are essentially pelagic in nature and consist mostly of calcareous nannofossil and foraminifer oozes/chalks rich in LMC. These hemipelagic to pelagic sediments were deposited during a prolonged

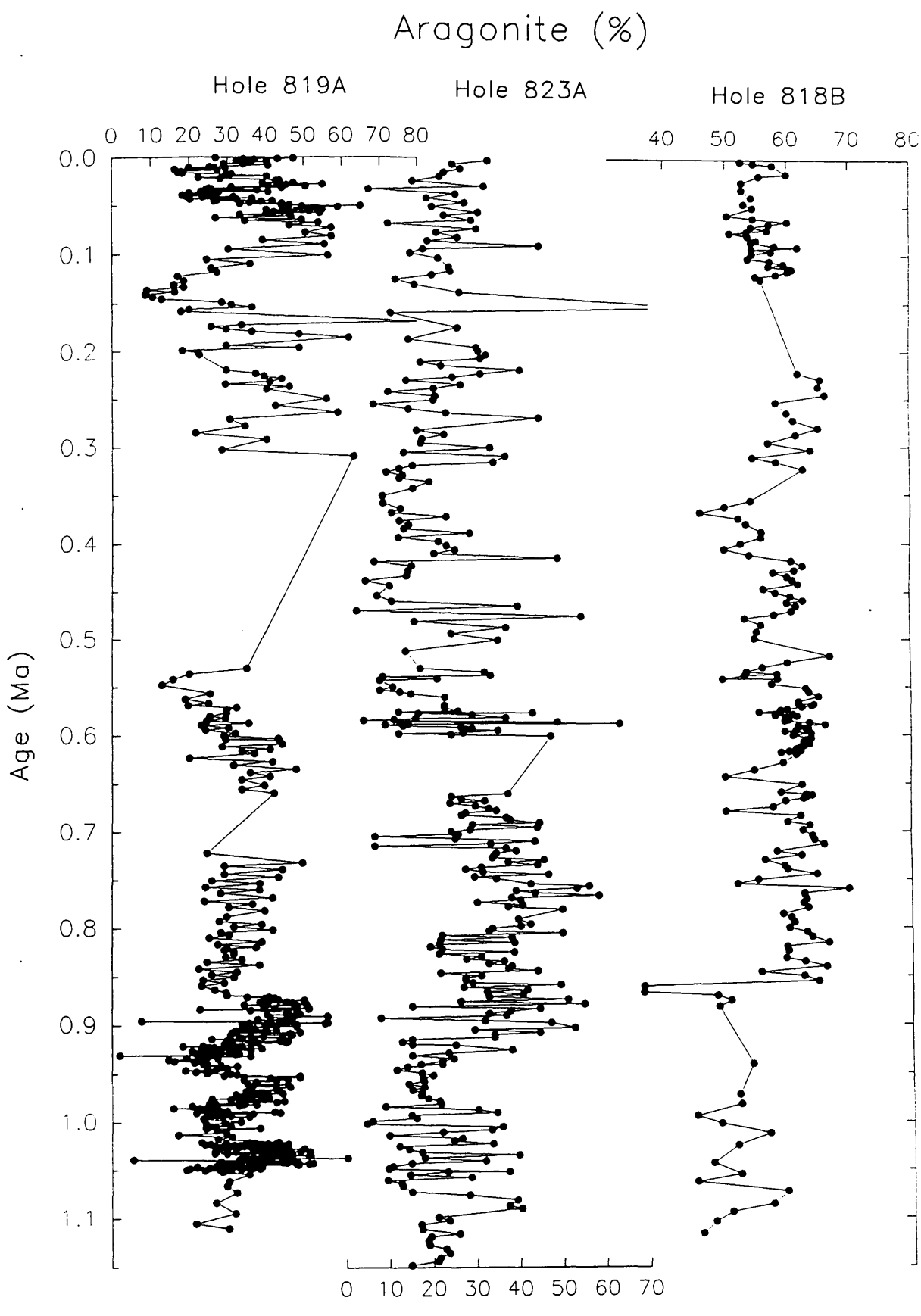

Figure 5.43. Temporal variations in the aragonite content in Hole 819A (GBR margin), Hole 823A (Queensland Trough) and Hole 818B (Queensland Plateau) periplatform sediments. Data for Hole 818B provided by Haddad et al. (1993).

'interglacial' period distinguished by increased warming and elevated sea levels (Keany, 1978; Keigwin, 1979; Hay *et al.*, 1987; Mercer, 1987). Estimates based on stable oxygen isotope values suggest that early Pliocene sea level may have been in the order of 60 to 100 m higher than the present day (Kennett, 1982; Raymo *et al.*, 1986).

Table 5.2. Data for depth intervals of planktic foraminiferal datum levels (Kroon, 1993) and calcareous nannofossil biohorizons (Wei and Gartner, 1993) for Hole 823B (Queensland Trough).

Species	Age (Ma)	Depth (mbsf)	Organism
HO *Helicosphaera sellii*	1.27	105.7	N
HO *Calcidiscus macintyrei*	1.48	150.9	N
HO *Globigerinoides fistulosus*	1.6	151.4-154.9	F
HO *Globigerinoides obliquus*	1.8	199.8-209.1	F
HO *Discoaster brouweri*	1.88	163.0	N
HO *Discoaster pentaradiatus*	2.29	222.3	N
HO *Discoaster surculus*	2.42	236.2	N
HO *Discoaster tamalis*	2.60	244.3	N
HO *Globoquadrina altispira*	2.9	288.7-291.7	F
HO *Sphaeroidinellopsis sp.*	3.0	295.6-299.3	F
HO *Reticulofenestra pseudoumbilicus*	3.51	359.3	N
LO *Discoaster asymmetricus* ac.	3.88	435.5	N
HO *Globigerina nepenthes*	3.9	487.3-491.2	F

Note: LO = lowest occurrence; HO = highest occurrence; F = foraminifera, N = calcareous nannofossil (coccolith)

The onset of aragonite (and traces of dolomite) deposition in Hole 823B coincides with a prominent deepening of the 40-60 % $CaCO_3$ isopleth of Farrell and Prell (1991), centred at about 3.25 Ma (see Figure 5.45). This is close to the timing of the onset of northern hemisphere glaciation at 3.2 Ma, proposed by Shackleton and Opdyke (1977). Recent evidence from benthic foraminiferal $\delta^{18}O$ records, however, suggests that the 3.2 Ma event represents only a brief excursion in ice volume, and that large scale and permanent northern ice sheet growth (advance of Arctic ice sheets) did not occur until about 2.5 Ma (Prell, 1982; Shackleton *et al.*, 1984; Kennett and Hodell, 1986). Farrell and Prell (1991) suggest that during this interval, in the southern latitudes, colder bottom waters were produced which were less corrosive in the Pacific and more corrosive in the Atlantic. Hodell *et al.* (1985) suggested that the 3.2 Ma event may have resulted from a pulse-like increase in the cooling and formation of Antarctic Bottom Water (AABW). Ice sheet growth at about 3.2 Ma was also accompanied by an increase in the intensity of the Antarctic Circumpolar Current (Turnau and Ledbetter, 1989). In the southern latitudes this period was characterized by increased ice volume in Antarctica (Shackleton and Opdyke, 1977), enhanced

continental aridity and supply of aeolian sediments to the oceans (Leinen and Heath, 1981; Rea and Janecek, 1982), and more intense intermediate water circulation in the southwest Pacific (Stein, 1986).

The most dramatic increase in aragonite content in Hole 823B periplatform sediments occurs at 2.9 Ma, and coincides with an abrupt and prolonged deepening in the $CaCO_3$ preservation records of Farrell and Prell (1991) (see Figure 5.45). This interval also corresponds to the first occurrence of bank-derived fine aragonite (and traces of dolomite) in Site 818, on the Queensland Plateau (Droxler *et al.*, 1993). Comparison of the isotopic records from Hole 818B (Queensland Plateau) and Hole 806B (Ontong Java Plateau) (Droxler *et al.*, 1993 and Jansen *et al.*, 1993, respectively), with the aragonite content from Hole 823B, suggest that this event may be related to a distinct decrease in mean planktic $\delta^{18}O$ values (between about 2.95 and 2.85 Ma), interpreted as an interval of enhanced ice volume and cooling trend (Jansen *et al.*, 1993) (see Figures 5.46 and 5.47). Farrell and Prell (1991) suggest that both productivity and deep-water chemistry (in particular the formation of less corrosive Pacific ocean deep waters) may have been responsible for the $CaCO_3$ preservation increase at this time. A second interval of major cooling centred on about 2.35 Ma (close to the Matuyama-Gauss Chron boundary- Berggren *et al.*, 1985), corresponding to the initiation of major northern hemisphere glaciation (Shackleton and Opdyke, 1977) and to a significant extension of the ice cap on Antarctica (Raymo *et al.*, 1986; Jansen *et al.*, 1993), is distinguished by a significant increase in aragonite content in the records from Holes 823B (and in Hole 818B on the Queensland Plateau). This interval coincides with a period of enhanced $CaCO_3$ preservation (event M20 using the nomenclature of Hays *et al.*, 1969), characterized by a significant deepening of the lysocline to 4500 m, in the equatorial Pacific, (Farrell and Prell, 1991).

The dramatic increase in aragonite content in Hole 823B periplatform sediments, between about 2.9 and 2.3 Ma (excluding the M21 dissolution event of Hays *et al.* [1969] centred at 2.45 Ma) are comparable to the inferred changes in $CaCO_3$ preservation in Farrell and Prell's record which indicate a rapid and major deepening of the calcite lysocline during the early late Pliocene (see Figure 5.45). As mentioned previously, this interval corresponds to a stepwise deterioration in the global climate, culminating in the onset of the onset of major northern hemisphere glaciation (Shackleton *et al.*, 1984). Droxler *et al.* (1993) have related the onset of aragonite deposition seen in the periplatform sequence in Hole 818B, at about 2.9 Ma, to the re-entry of parts of the Queensland Plateau carbonate system into the photic zone, related to an well-established interval of eustatic lowering of sea level that occurred between

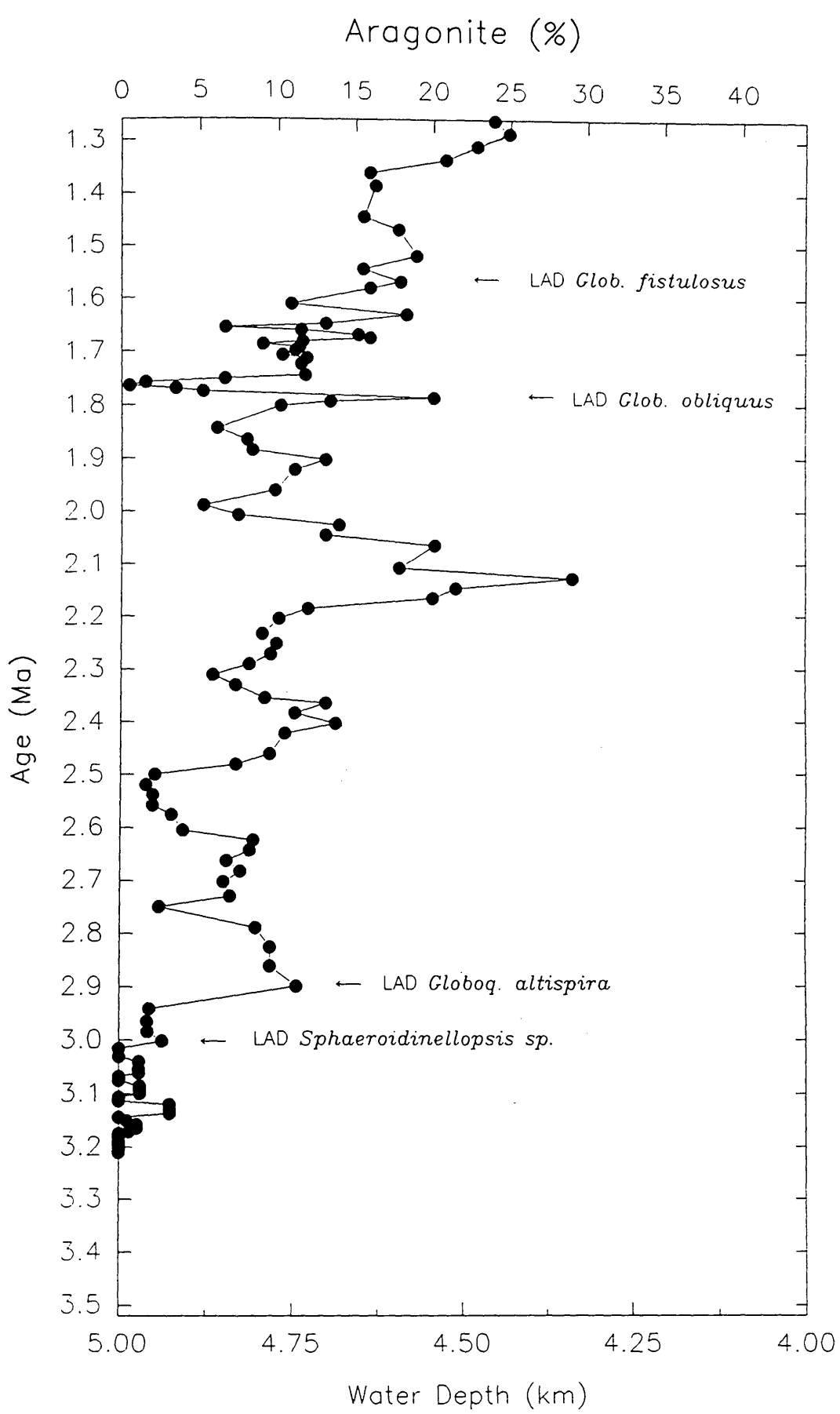

Figure 5.44. Comparison between aragonite content in Hole 823B sediments and the 40–60% carbonate preservation isopleth of Farrell and Prell (1991) (dotted line). Increased carbonate preservation is to the left of the plot. The depth/age conversion has been made using the foraminiferal biostratigraphy provided by Kroon (1993). Note that the major peaks in aragonite content generally coincide with periods of inferred good carbonate preservation.

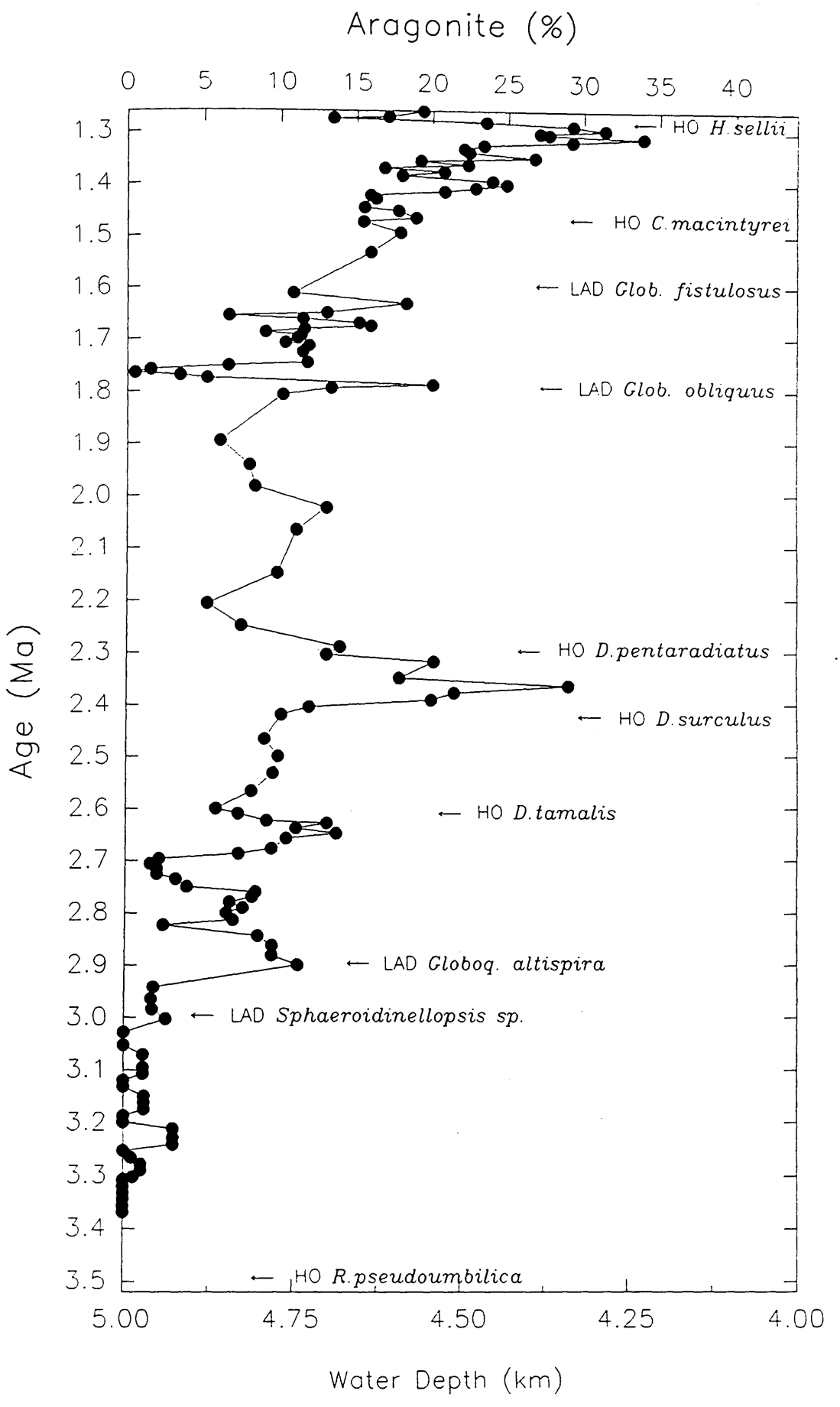

Figure 5.45. Comparison between aragonite content in Hole 823B sediments and the 40–60% carbonate preservation isopleth of Farrell and Prell (1991) (dotted line). Increased carbonate preservation is to the left of the plot. The depth/age conversion have been made using a combination of nannofossil and foraminiferal biostratigraphic datums, provided by Wei and Gartner (1993) and Kroon (1993), respectively. Note that major aragonite peaks mainly occur during periods of inferred good carbonate preservation.

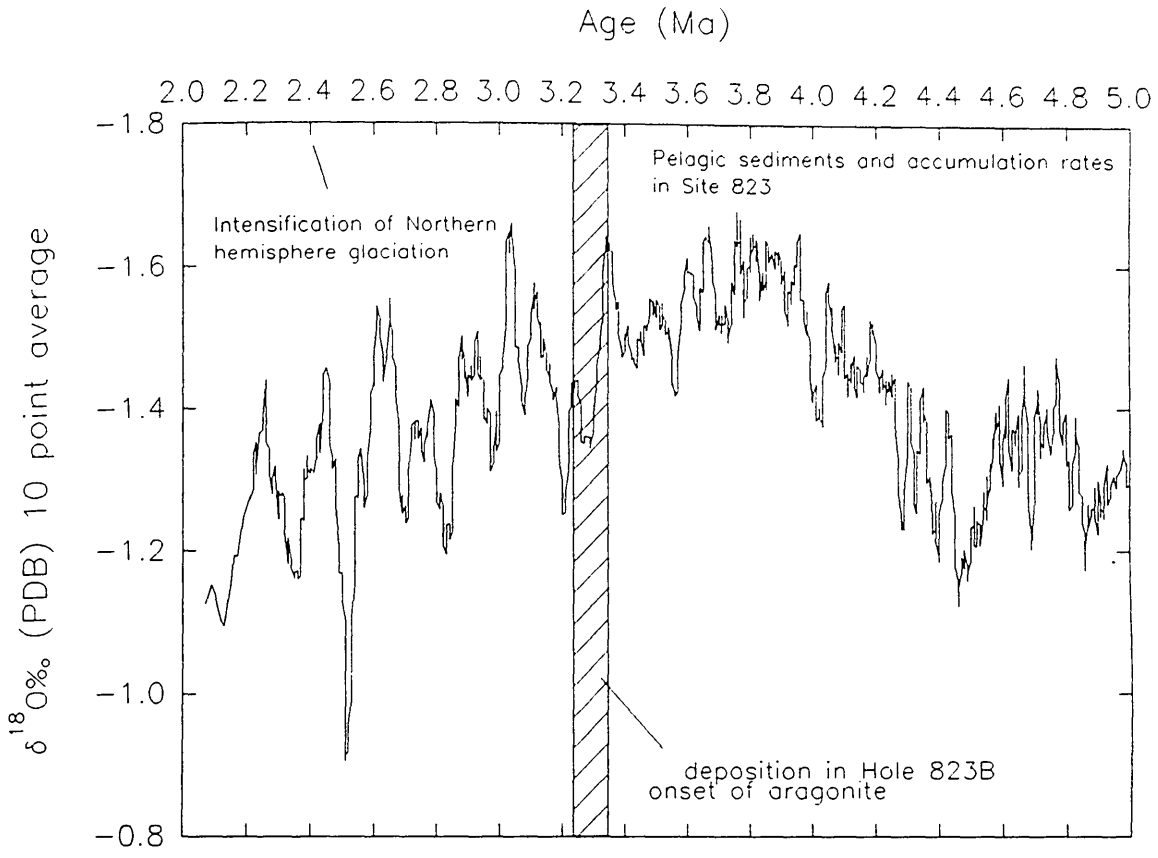

Figure 5.46 Planktonic foraminifer $\delta^{18}O$ record (10 point average) between 5.0 and 2.0 Ma from ODP Leg 130 Site 806 on Ontong Java Plateau (Jansen et al., 1993) used as a proxy for variations in sea level. Note the general lowering in sea level starting at 3.7 Ma. Also note that the onset of significant aragonite in Hole 823B correlates with a major lowering in sea level event at 3.2 Ma.

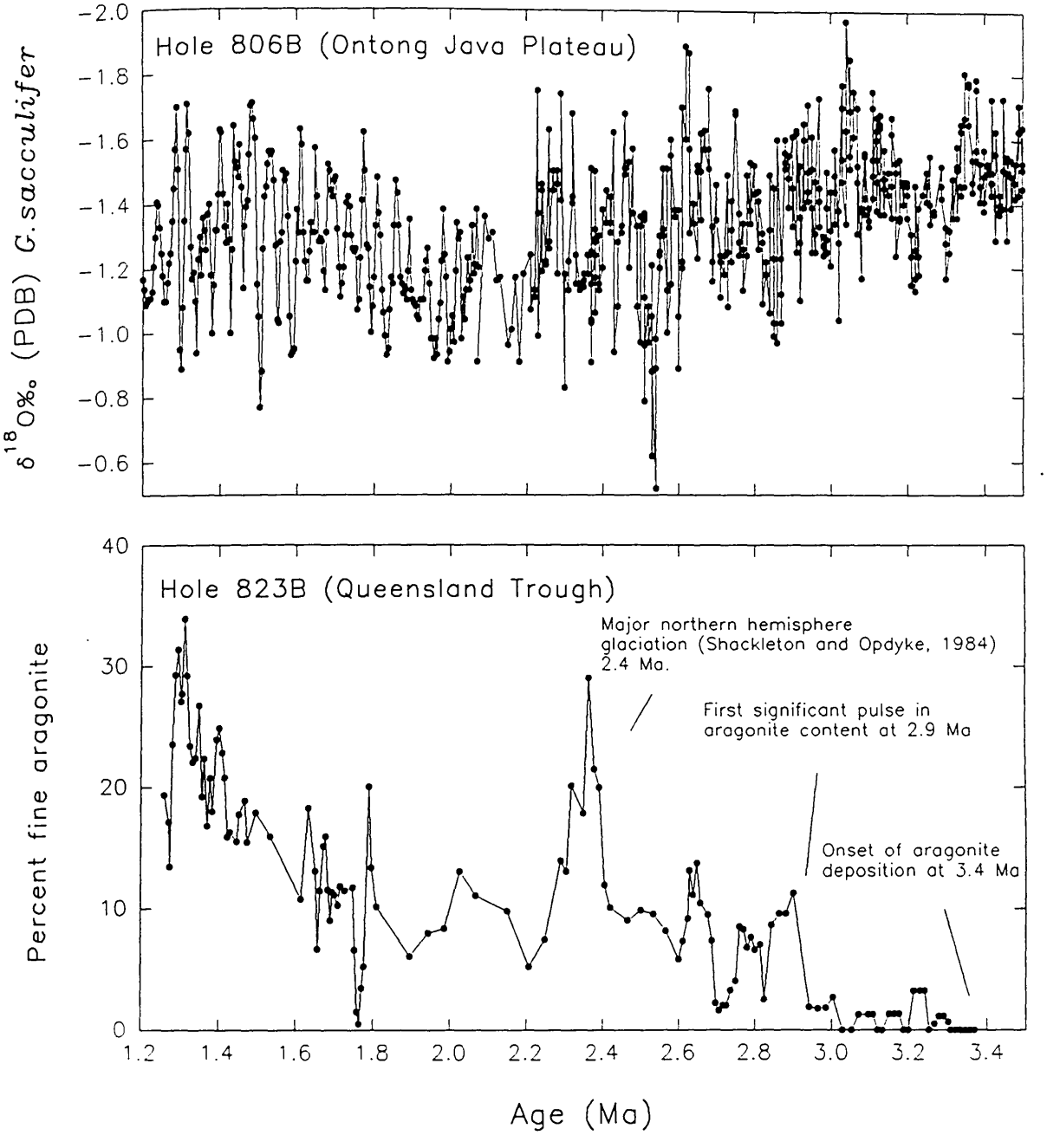

Figure 5.47. Comparison between the aragonite content record in Hole 823B (Queensland Trough) and the planktic oxygen isotope record from Hole 806B (Ontong Java Plateau) (after Berger et al.,1993 and Jansen et al., 1993).

2.9 and 2.45 Ma. High sedimentation rates, in the "deep" sites on the Queensland Plateau (Sites 811/817/818) during this interval would seem to support the idea of a period of increased banktop production and shedding. However, palaeotemperature estimates of Isern *et al.* (1993) suggest that during the late Pliocene (3.1-2.4 Ma) mean sea surface temperatures (SSTs) decreased to below 20° (the minimum temperature required for tropical reef growth- Veron, 1986) and, may have been too cold for reef growth. This would imply that either: the aragonite being deposited during this interval at Site 823 and Site 818 was derived primarily from calcareous algae (i.e., *Halimeda*), or that the palaeotemperature calculations of Isern *et al.* (1993) are incorrect. Prior to this period, Droxler *et al.* (1993) propose that high eustatic sea level, coupled with high subsidence rates during the latest part of the Miocene and early Pliocene (corresponding to the interval between 6 to 3.6 Ma), resulted in the drowning of the Queensland Plateau, with the cessation of bank top carbonate production and export.

The earlier occurrence of aragonite in Hole 823B sediments, between about 3.2-3.4 Ma, in comparison to the records in Hole 818B (Queensland Plateau), suggests that aragonite production occurred first in the north, possible in the region of the present day Holmes Reef (see Figure 2.7). Alternatively, the first appearance of aragonite at about 3.2 Ma in Hole 823B may well reflect the more northward and protected position of this site, in comparison to Hole 818B, with respect to cool surface waters flowing from the south. Support for this hypothesis may be gained from the work of Betzler *et al.* (1995) who suggest that turbiditic intervals, rich in shallow water derived sediments, tend to accumulate on the leeward sides of actively growing reefs and bioherms. While during intervals of reef emergence neritic derived sediments are directed toward the windward side of carbonate buildups. Thus, prior to 2.9 Ma, shallow water derived carbonate material was possibly directed away from Hole 818B (located on the windward side of the Queensland Plateau), and accumulated on the leeward side of the platform, some of this material possibly even reaching the Queensland Trough.

However, the question still remains as to whether the carbonate cycles seen in Hole 823B (and Hole 818B) reflect a pure aragonite input signal related to bank top flooding (i.e., Boardman and Neumann, 1986) or a combination of both aragonite input and preservation (related to climatically modulated variations in intermediate water production and water column chemistry).

5.4 Conclusions:

In general, the pattern of sedimentation seen in the upper part (<32 mbsf) of the sequence from Hole 819A is consistent with an 'Atlantic type' style of carbonate deposition, characterized by high carbonate (and aragonite) content during highstands of sea level (or conversely low carbonate content during glacial lowstands). This suggests that input (and/or productivity) must have been the dominant mechanism behind carbonate cyclicity in Hole 819A. However, the separation of the carbonate signal into platform and pelagic components has proved very difficult. Analysis of aragonite/LMC and HMC/LMC ratios suggests that, at least since glacial stage 6, highstands of sea level have been chararcterized by increased production and off-bank transport of shallow water carbonate material. Variations in water chemistry and/or dissolution intensity are thought to have played only a minor role in modulating the pattern of carbonate deposition in this core. Throughout the lower part of the record (i.e., >32.5 mbsf) dissolution and diagenesis have played a more important role in determining the composition of Hole 819A periplatform sediments, particularly during lowstands of sea level. The good correlation between the occurrence of dolomite and the lack or reduced HMC content in these sediments, coupled with a concomitant increase in LMC content suggest that dolomite formation occurred in response to shallow burial diagenesis and the neomorphism of HMC to LMC. The Mg^{2+} released into the interstitial pore-waters was then probably used in the formation of authigenic dolomite. Superimposed upon this pattern of dissolution and recrystallization is a pattern of high shallow-water carbonate production and export during isotopically inferred periods of sea level highstand.

Analysis of the periplatform sequence in Hole 823A suggest that, during the last 0.6 Ma (i.e., since about glacial stage 16), highstands of sea level are distinguished by increased production and shedding of shallow water/bank top material rich in carbonate. Conversely, during glacial periods or lowstands of sea level marine sediments are characterized by increased pelagic carbonate production. These observations are consistent with the highstand shedding scenario outlined by Schlager (1992) and Schlager *et al.* (1994). In the lower part of the record from Hole 823A the pattern of carbonate deposition is more complex than that seen in the upper part of the sequence. Despite this, the covariance of aragonite (and carbonate mud) content with the $CaCO_3$ preservation records of Farrell and Prell (1991) suggests that fluctuations in Pleistocene dissolution intensity may have played a secondary role in modulating the pattern of carbonate deposition seen in this core. As with the upper part of the record from Hole 823A, it seems likely that carbonate production and input have been the dominant controls on sedimentation, in the lower section of Hole 823A.

Superimposed on this signal has been the effects of early diagenesis, resulting in the neomorphism of HMC and aragonite to LMC, with the concomitant precipitation of dolomite.

In contrast to Hole 823A, the long-term (late Pliocene- Pleistocene) carbonate records from Hole 823B indicate a 'Pacific-type' pattern of carbonate deposition. This suggests that variations in water column chemistry (dissolution intensity) may have played a more important role in modulating the pattern of carbonate deposition seen in this core, than in late Pleistocene Hole 823A (or Hole 819A). However, the precise effects of variations in late Pliocene sea level and/or sea surface temperature (SST) across the Queensland Plateau, on shallow-water carbonate sediment production are at present unclear. Analysis of the Hole 823B records suggests that the first occurrence of significant amounts of shallow water carbonate in Hole 823B may be related to a gradual lowering of global sea level at about 3.2 Ma. This may be related to the re-entry of the shallower parts of the Queensland Plateau into the photic zone, and a switching on of the shallow water carbonate factory (Droxler *et al.*, 1993) as reflected in increased sedimentation rates during this period. Prior to this interval, aragonite accumulation was most likely controlled by water chemistry and variations in dissolution intensity Since 3.2 Ma, aragonite content in Hole 823B has generally followed the carbonate preservation records of Farrell and Prell (1989, 1991), with low aragonite during periods of enhanced dissolution. Significant increases in the proportion of aragonite in Hole 823B between 2.4 and 3.2 Ma can be correlated with recognized changes in global sea level (and ice-volume).

Despite the relatively good agreement between sea level and carbonate mineralogy in the upper part of the cores, in the absence of detailed faunal analysis, the question remains as to the origin of the aragonite in Hole 823A (and Hole 819A) periplatform sediments (i.e., what component of the aragonite record is contributed by pelagic organisms). Primarily, in an attempt to evaluate the contribution of pelagic calcite to the total carbonate (and aragonite) signal, high resolution geochemical (XRF) analysis were conducted on Hole 823A periplatform sediments. These results and their implications for our understanding of the sedimentologic processes acting on the northeast Australian margin during the Late Quaternary form the basis of the following chapter.

Chapter 6 XRF Geochemistry of Queensland Trough- Hole 823A periplatform sediments

6.1 Introduction

The aim of this chapter is to present some of the major and minor elemental results of the geochemical analysis of Hole 823A periplatform muds (<63μm fraction), and to examine the implications of these high-resolution data on our understanding of mixed carbonate-siliciclastic deposition on the northeast Australian margin. In particular, what has been the effect, if any, of late Pleistocene sea level and climate change on the composition of terrigenous sediments deposited on the Queensland margin. Furthermore, what can these complex geochemical data tell use about the timing of carbonate platform evolution relative to highstand or lowstands of sea level.

X-ray fluorescence (XRF) spectroscopy is a standard analytical technique in both hard rock and soft rock petrology, allowing the accurate determination of a wide variety of major and minor elements in an unknown sample (Fairchild *et al.*, 1991). XRF analysis of recent and ancient sedimentary rocks provides an extremely versatile and powerful tool enabling a greater understanding of former environments and climates (particularly when combined with standard sedimentological, petrological and XRD studies). The various geochemical parameters used in this study serve as proxy-palaeoceanographic and palaeoclimatic records of sedimentologic and climatic processes acting on the northeast Australian margin during the late Pleistocene.

In brief, the principle behind this rapid and non-destructive analytical technique is that when a composite sample is bombarded with a beam of sufficiently high energy photons (which include polychromatic X-rays) secondary radiation is emitted with wavelengths and intensities dependent on the elements present. Careful measurement of the intensity of the characteristic radiation for a particular element gives a value reflecting its concentration in the sample (i.e., using the Bragg equation, if a crystal of known *d* spacing is used to diffract the X-rays obtained from the unknown specimen then the measured values of θ will allow values of λ to be calculated- see section 5.1). The normal method of XRF operation is to measure the emission from a series of standards to produce calibration curves, against which the unknown samples can be compared. However, unlike X-ray diffractometry (outlined in chapter 5), XRF spectrometry generates chemical data rather than specifically mineralogical information, i.e., XRF analysis does not provide direct evidence of the identities, natures or properties of the minerals in a complex specimen. However, overall elemental information can be used to derive estimates of the mineral proportions in an

unknown sample (Jones, 1987). A more detailed account of XRF spectrometry and X-ray analytical techniques is provided by Jenkins and de Vries (1970); Johnson and Maxwell (1981), Potts (1987) and Fairchild *et al.* (1991).

Unfortunately, due to time restrictions and the priority given to extracting a reliable isotope signature from Hole 819A sediments, high-resolution XRF analyses were only carried out on Hole 823A (Queensland Trough) periplatform sediments. To date, this core provides the only detailed late Pleistocene geochemical record (to the authors knowledge) from the northeast Australian margin. Thus, comparison and correlation with other ODP Leg 133 marine sequences and a detailed investigation of possible shelf-to-basin geochemical gradients has not been possible. Nonetheless, the XRF geochemical record from Hole 823A does provide a valuable insight into the complex depositional processes, occurring on the northeast Australian margin, during the late Pleistocene.

6.2 Analytical methods

X-ray fluorescence spectrometry (XRF) was performed on Hole 823A periplatform muds (<63μm sediment size fraction) using a Philips PW 1480 sequential X-ray spectrometer, with an automatic PW1510 sample changer (under the supervision of Godfrey Fitton and Dodie James, Grant Institute, University of Edinburgh). Pressed sediment powder discs (~32 mm in diameter) were used for both major and minor element analysis. About 3 grams (±0.1g) of oven-dried sample, was reduced to an average particle size of about 5 μm, using a tungsten carbide Tema® ball-mill. The resulting finely ground/powdered sediment sample was then placed onto a highly polished tungsten carbide disc, and enclosed in a stainless steel inner sleeve (which itself was enclosed in a larger stainless steel cylinder). A perspex plunger was then inserted down the inner sleeve, carefully compacting the sediment under hand pressure. After removal of both the plunger and inner sleeve, boric acid (H_3BO_3) powder was added sufficient to cover the sediment sample disc. Then a large, stainless steel plunger was lowered onto the boric acid powder/sediment sample and, using a hand operated hydraulic press at approximately 7 tons/in^2 (1200 kg/cm^2) for approximately 2 minutes, until the disc was fully compacted. The pressed powder disc or 'briquette' was then stored in a sealed polythene bag and within a desiccator prior to XRF analysis. Storage under vacuum conditions prevented the absorption of excess atmospheric moisture, and errors associated with matrix effects (see Jenkins and de Vries, 1970) and the migration of residual sea salt toward the surface of the XRF sample briquette (Brian Price, pers. comm., 1992).

The International rock and sediment standards used during XRF analysis gave linear calibration lines for all the minor elements (Ba, Sc, V, Ni, Cu, Zn, Sr, Nb, Cr, Zr, Pb, Th, U, Rb, Mo, I, Br, Y, La, Ce and Nd) and major elements (Si, Al, Fe, Mg, Ca, Na, K, Mn, Ti, and P) measured over a wide range in concentration (see Appendix D, Table D.1). Typical analytical conditions for XRF major and minor element analysis are given in Table D.2, with precision for selected elements listed in Table D.3 (see Appendix D). Unfortunately, the limited core Hole 823A subsample size (~10g dry weight) has precluded the preparation of multiple samples from the same horizon, and hence the determination of accurate sample reproducibility. Also, note that because of the absence of detailed sediment sample water content data, major and minor elemental results are presented on a non-salt free basis (i.e., elemental data presented are uncorrected for residual sea salt). These high resolution data are presented in Appendix D, Tables D.4 and D.5.

6.3 Results and Discussion

Although a full suite of major and minor elemental data were obtained for Hole 823A periplatform sediments using XRF analyses, only selected elements (and their ratios) are examined in this section. These have been chosen in order to illustrate some of the more important sedimentary processes occurring on the Queensland continental margin, during the late Pleistocene. These elements include Aluminium (Al), Barium (Ba), Calcium (Ca), Chromium (Cr), Strontium (Sr) and Titanium (Ti). Variations in the downcore abundance of minor elements, in Hole 823A muds, are given in parts per million (ppm). Major element data are presented on an oxide free basis, and are typically expressed in weight percent (wt.%).

6.3.1 The Strontium (Sr) and Calcium (Ca) signals, and variations in shallow-water bank-top production and export

In this section, the downcore distribution of strontium (Sr) and calcium (Ca), and temporal variations in the Sr/Ca ratio, in Queensland Trough Hole 823A periplatform sediments, are examined in order to determine the influence of fluctuations in late Pleistocene sea level, and climate change, on shallow water bank-top production and export. In particular, can we distinguish between variations in carbonate platform production and pelagic/planktic productivity using the concentration of Sr and Ca in Hole 823A sediments?

The distribution of strontium (Sr) in chemical and biological sediments has been extensively studied because of its potential utility as a diagnostic palaeoenvironmental

and diagenetic tracer element (Wedepohl, 1969). Strontium in marine sediments occurs mainly in carbonate, phosphate, barite (Church, 1970) and aluminosilicates (Goldberg and Arrhenius, 1958; Hirst, 1962). Despite there being several possible sources of Sr in marine sediments, by far the most important is that contributed by carbonate (see Table 6.1). This fact is reinforced because an average deep-sea clay holds only around 180 ppm Sr, and the mean value for marine organisms is approximately 862 ppm Sr (Martin and Knauer, 1973). It is because the Sr^{2+} cation has a similar ionic radius, as well as the same ionic charge, to Ca^{2+} (Sr^{2+} = 1.12 Å, Ca^{2+} = 0.99 Å, Ahrens, 1952), that Sr can easily substitute for Ca in most minerals. Sr substitution for Ba in marine barite (Ba SO_4) only occurs to a relatively small degree (0.2-3.4 mol.%, Church, 1979) which allows for a potential contribution of approximately 30-150 ppm strontium to the total Sr concentration in most marine sediments (Patience, 1992).

In shallow water carbonate sediments strontium can be derived from a number of important biogenic sources, these include: molluscs; foraminifera, corals and calcareous algae (Milliman, 1974). In general, calcite and molluscan aragonite contain low concentrations of strontium (<2000 ppm), whereas high concentrations of strontium (>7500 ppm) occur in aragonite from corals, calcareous green algae (e.g., *Halimeda, Penicillus*), inorganically precipitated ooids, and shallow water marine cements (Milliman, 1974). This general type of aragonite is termed high strontium aragonite[1] and is an indicator of sediment derived primarily from a shallow water environment (Boardman *et al.*, 1986). Of the two main carbonate contributors of strontium in deep-sea sediments, coccolithophorids (which are composed of low magnesium calcite) contain on average about 1800 ppm strontium, while pelagic foraminifera (typically LMC and HMC) contain between 1500-1710 ppm strontium (Turekian, 1964). In general, pteropods secrete aragonite with a low content of strontium (about 1500 ppm, Milliman, 1974). However, as noted by Patience (1992) the Sr from the celestite or celestine ($SrSO_4$) in pelagic pteropods tends not to survive burial in sediments of oceanic deposits. Table 6.1 lists the Sr concentration (and Sr/Al ratio) previously found in selected marine organisms and sediments.

[1]High Sr aragonite and low Sr aragonite are not distinguishable from each other by XRD methods (Boardman *et al.*, 1984).

Author	Organism/ Sediment type	Strontium (Sr) (ppm)	Sr/Ca ratio (x 10^{-3})
Emiliani (1955b)	Foraminifera tests	1200	-
Thompson & Chow (1956)	Foraminifera tests	1300	-
	Pacific *Globigerina* ooze	-	3.3
Turekian (1957)	Foraminifera tests	1200	-
Turekian & Wedepohl (1961)	Deep-sea clay	180	-
	Deep-sea carbonate	2000	-
Turekian (1964)	Pure foraminifera ooze	1600	-
	Pure coccolith ooze	1000	2.5-2.6
Milliman (1974)	Green algae (*Halimeda*)	7700-9700	22.6-28.0
	Coralline algae	1200-5600	3.49-19.3
	Coral (Scleractinian)	6900-10000	16.8-28.5
	Bryozoans	1600-8800	4.27-25.6
Khan (1989)	Arabian deep-sea sediment	-	3.0-4.5
Shimmield & Mowbray (1991)	N.W. Arabian Sea sediments	740-1489	3.3-4.5
Patience (1992)	E. Equatorial Pacific sediments	330-1207	3.2-6.4
Rao & Adabi (1992)	Tasman temperate carbonates	2000-4500	-
Alexander & Kroon (in prep.)	N.E. Australian margin sediments	443-3671 (1857)	6.1-15.4 (9.95)

Table 6.1 Total strontium (Sr_{total}) content (ppm) and Sr/Ca weight ratio of selected marine organisms and oceanic sediments. Mean values are given in parentheses.

Figures 6.1 and 6.2 illustrate the downcore fluctuations in total Sr (Sr_{total}) and Ca (Ca_{total}) content in Hole 823A muds (<63 μm), plotted alongside the planktic $\delta^{18}O$ record. Both these high resolution XRF records are characterized by well developed cyclical variations in element concentration, punctuated by an abrupt increase in mean value at about 80 mbsf (corresponding to an age of about 0.865 Ma). In general, the downcore Sr profile broadly mirrors the Ca curve, indicating a strong dependency (coefficient of correlation, r = 0.853, where N = 311) of Sr on Ca (and presumably carbonate). Total Sr and Ca content values in Hole 823A sediments typically range between 1000-3000 ppm and 9.664-26.35 x 10^4 ppm in the upper 80 m of the sequence in Hole 823A, respectively. Below 80 mbsf, mean Sr and Ca values are slightly lower, and generally range between 500-2000 ppm and 5.15-22.87 x 10^4 ppm, respectively. The abrupt increase in total Sr (and total Ca) concentration at about 80 mbsf (0.865 Ma) coincides with a dramatic increase in the abundance of aragonite in Hole 823A periplatform sediments (see Figure 5.44).

As mentioned earlier, a proportion of the total Sr (Sr_{total}) and total Ca (Ca_{total}) content present in marine sediments is associated with the terrigenous/detrital aluminosilicates or clay fraction and this needs to be removed in order to examine any variation in the "biogenic source" of these elements. In order to remove the

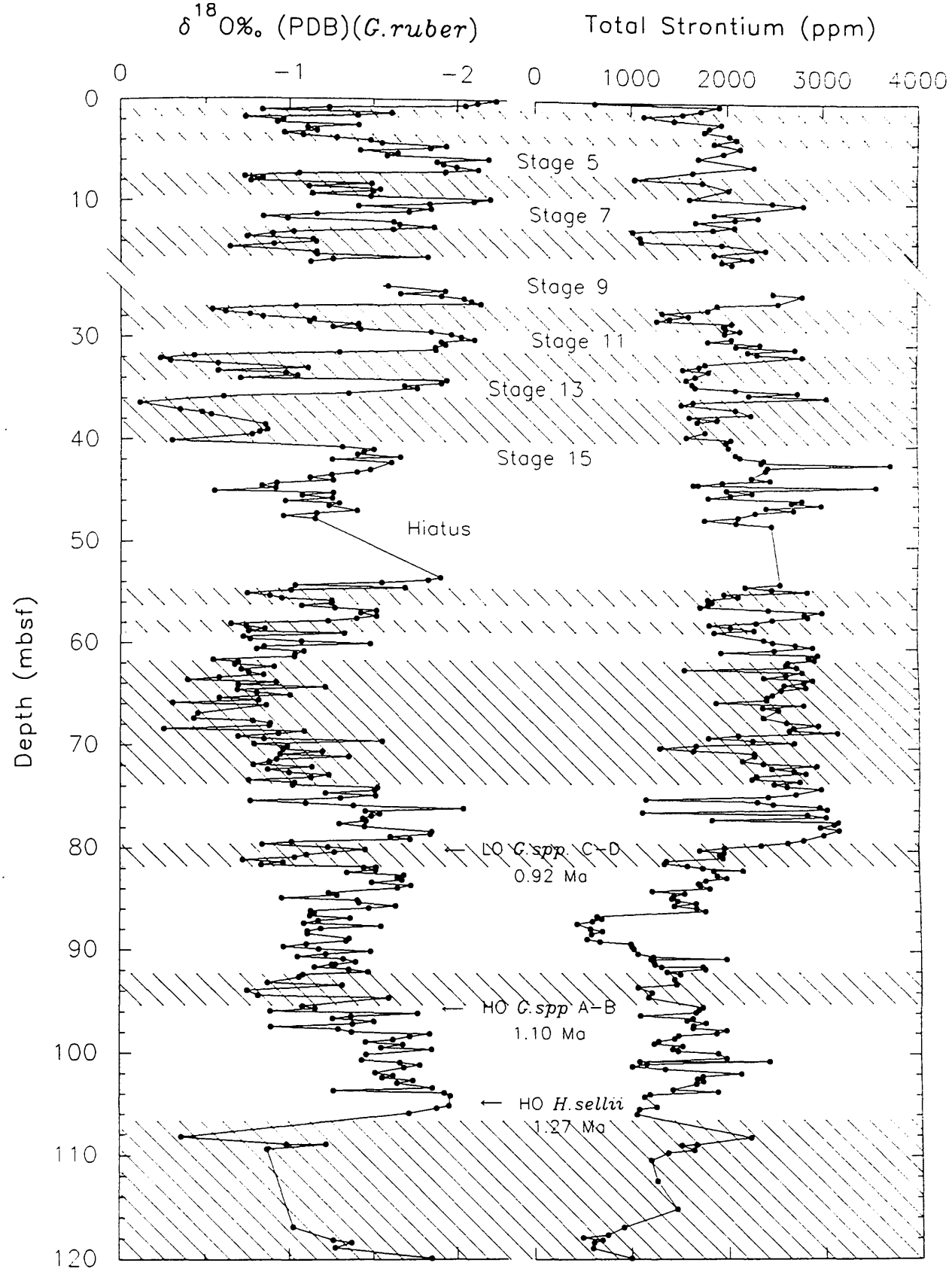

Figure 6.1. Comparison between the total strontium (Sr) content and the planktic oxygen isotope record in Hole 823A periplatform muds.

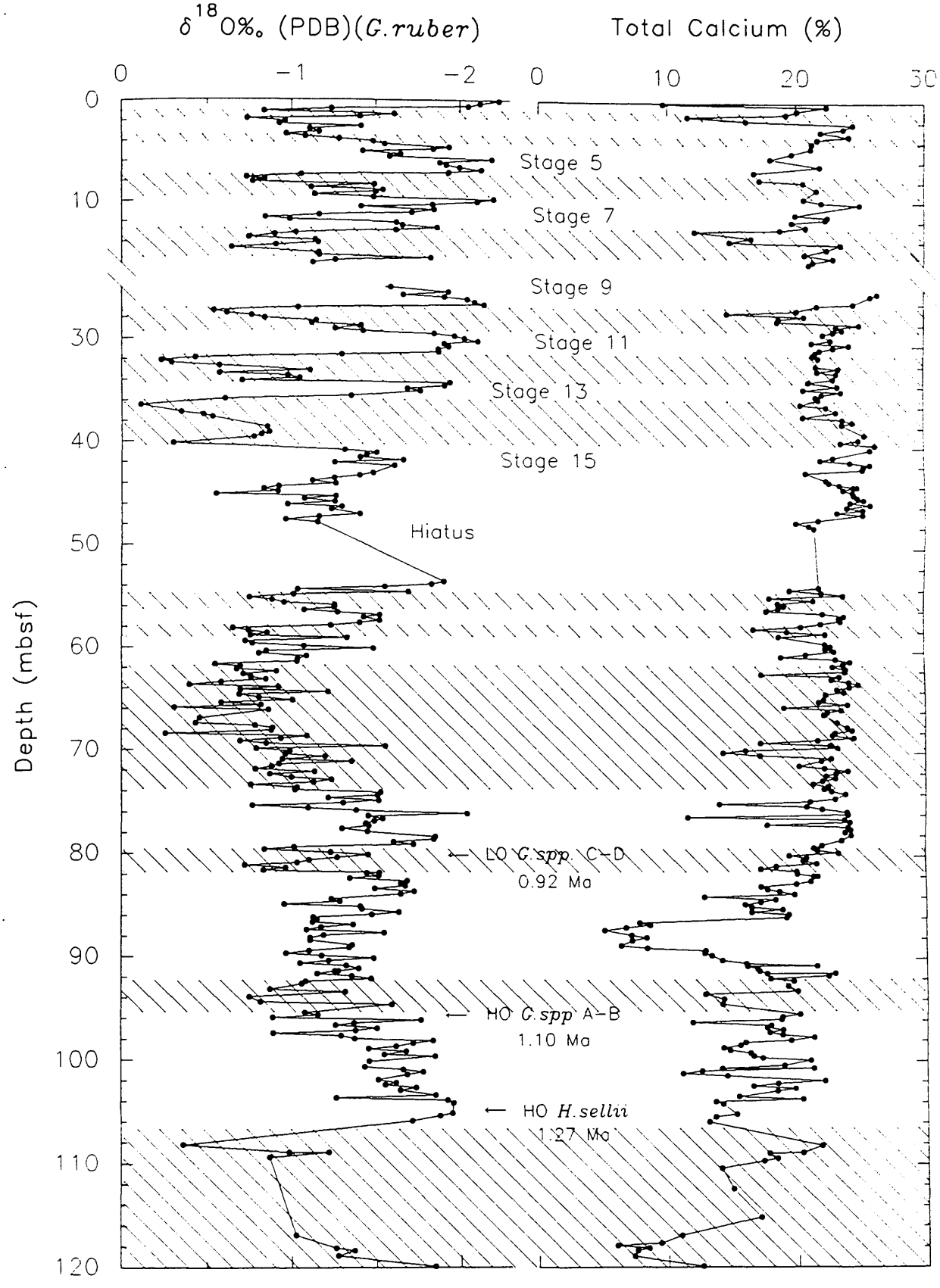

Figure 6.2. Comparison between the total calcium (Ca) content and the planktic oxygen isotope record in Hole 823A periplatform muds.

contribution made by terrigenous aluminosilicates, total element concentrations are corrected for using the following relationship:

Equation 6.1 $$Element_{excess} = Element_{total} - (Al_{total} \times element/Al\ ratio)$$

(Patience, 1992)

where: $Element_{total}$ and Al_{total} are the total elemental concentrations (ppm) measured by XRF analysis. This technique relies on the fact that Al is restricted to clay minerals and that the lithogenic aluminosilicate component (element/Al ratio) is relatively invariant (which is not the case in Hole 823A sediments- see Figure 6.3). Nevertheless, by normalizing elemental contents to Al it is possible to investigate both spatial and temporal changes in the biogenic Sr component in Hole 823A sediments. In this core, the contribution of Sr ($Sr_{terr.}$) from average deep-sea clay has been removed leaving an excess Sr ($Sr_{ex.}$) value by assuming a Sr/Al ratio for aluminosilicates in deep-sea clay of 0.00214 (Turekian and Wedopohl, 1961) (see Figure 6.4). The mean Sr/Al ratio in Hole 823A is 0.0619, with values generally ranging from 0.0048 to 0.2262 (see Figure 6.5). In a similar manner to Sr, a proportion of the Ca concentration present in most marine sediments is associated with the clay fraction or aluminosilicates. The contribution to the Ca_{total} content made by this detrital material is corrected for using a Ca/Al ratio of 0.345 (Turekian and Wedopohl, 1961) (see Figure 6.6). This correction factor compares to an average Ca/Al value in Hole 823A sediments of about 6.25, with values ranging from 0.5552 to 26.33. After correcting for the elemental contribution from terrigenous aluminosilicates, the $Sr_{ex.}$ signal was then ratioed against the $Ca_{ex.}$ record, in order to remove the element of dilution by another element or component, and to examine the downcore variations in Sr content within the carbonate material. These data are illustrated in Figures 6.6 to 6.9.

The Sr_{ex}/Ca_{ex} ratio in Hole 823A periplatform muds varies between approximately 6.1-15.4 x 10^{-3}, with a downcore mean of about 9.95 x 10^{-3}. These values are significantly higher than Sr/Ca ratios for selected deep-sea sediments from around the world (see Table 6.1). Analysis of the Sr_{ex}/Ca_{ex} and planktic $\delta^{18}O$ records in Hole 823A indicate that there is a strong tendency toward high values during interglacial periods (highstands of sea level) and low Sr_{ex}/Ca_{ex} ratios during glacial intervals (lowstands). In general, Sr_{ex}/Ca_{ex} values during highstands of sea level are approximately twice the magnitude of those reached during glacials. The strong covariance displayed between the planktic $\delta^{18}O$ and Sr_{ex}/Ca_{ex} records is particularly well developed in the upper 50 m of the core. For example, interglacial stages 5, 7, 9,

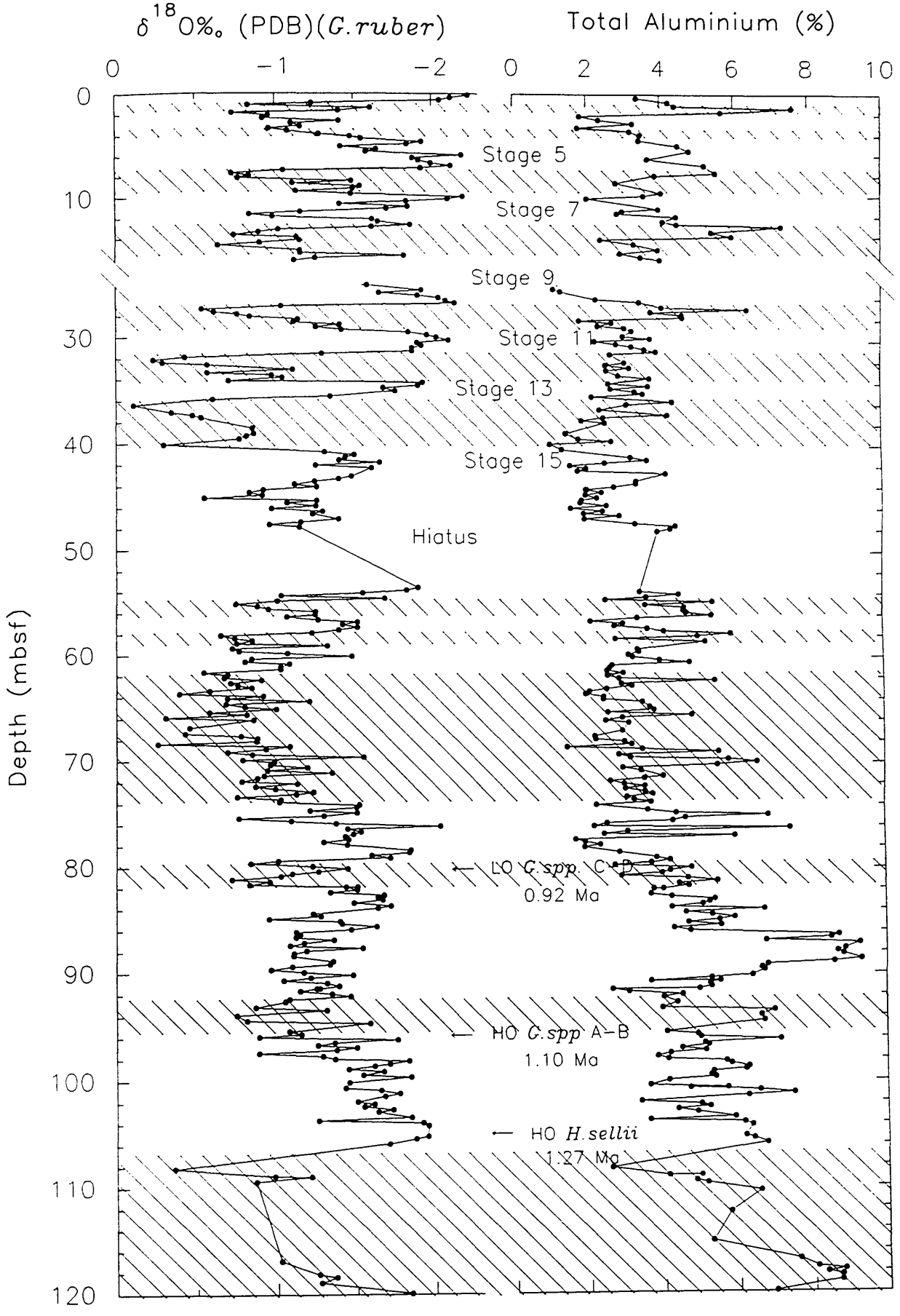

Figure 6.3. Comparison between the total aluminium (%) content and the planktic oxygen isotope record in Hole 823A periplatform muds.

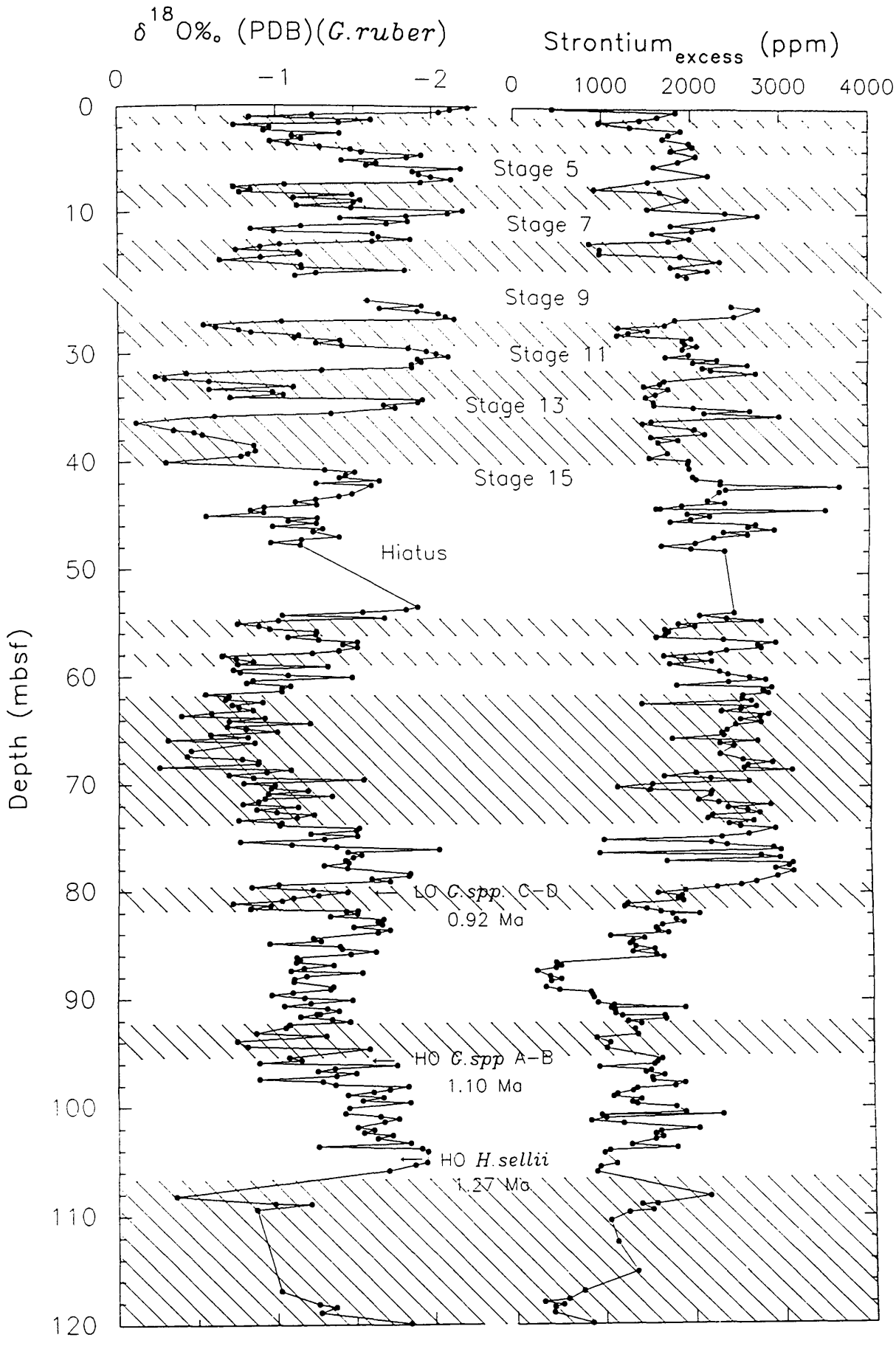

Figure 6.4. Comparison between the excess strontium (Sr) content and the planktic oxygen isotope record in Hole 823A periplatform muds.

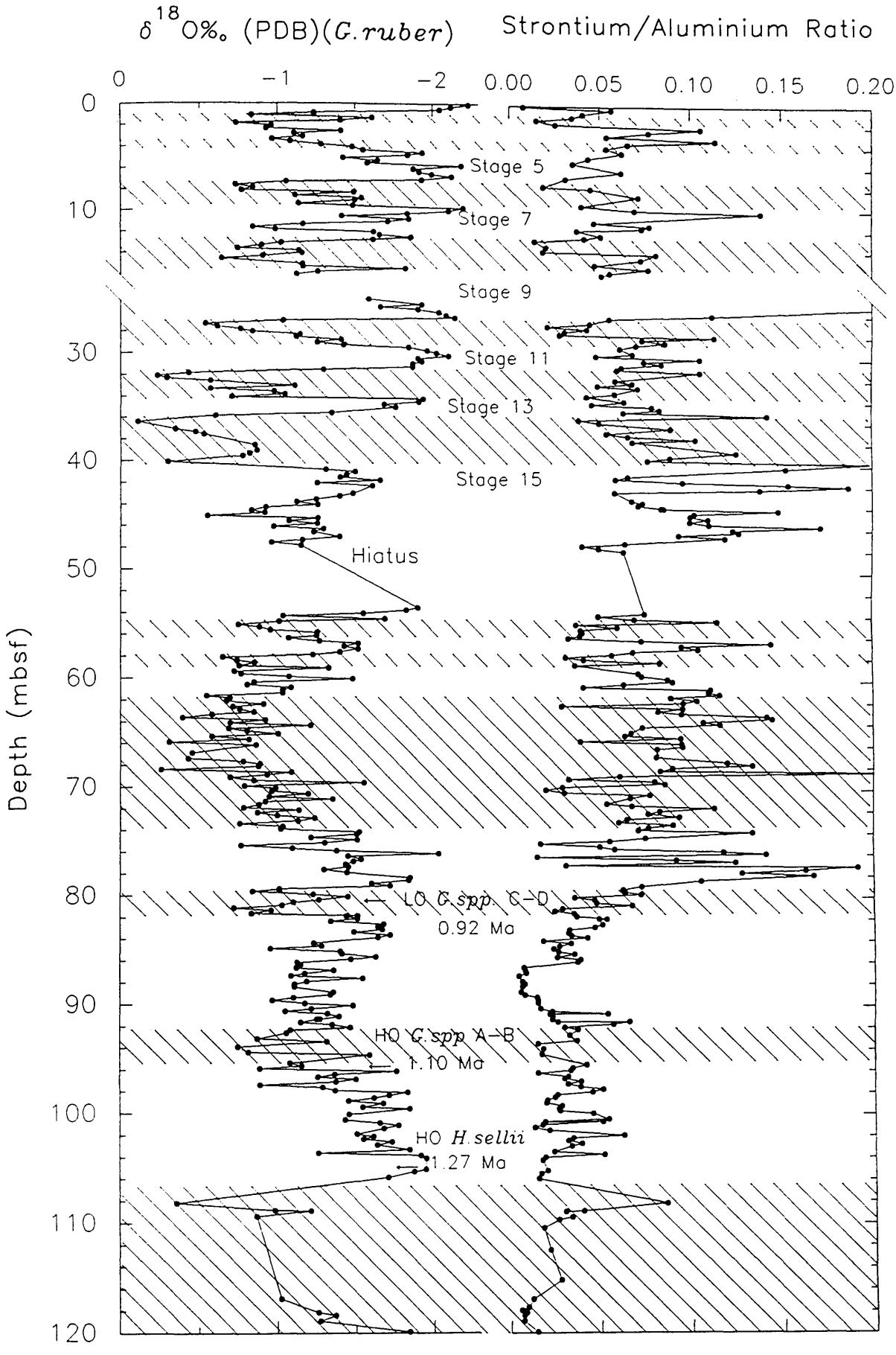

Figure 6.5. Comparison between the Sr/Al ratio and the planktic oxygen isotope record in Hole 823A periplatform muds.

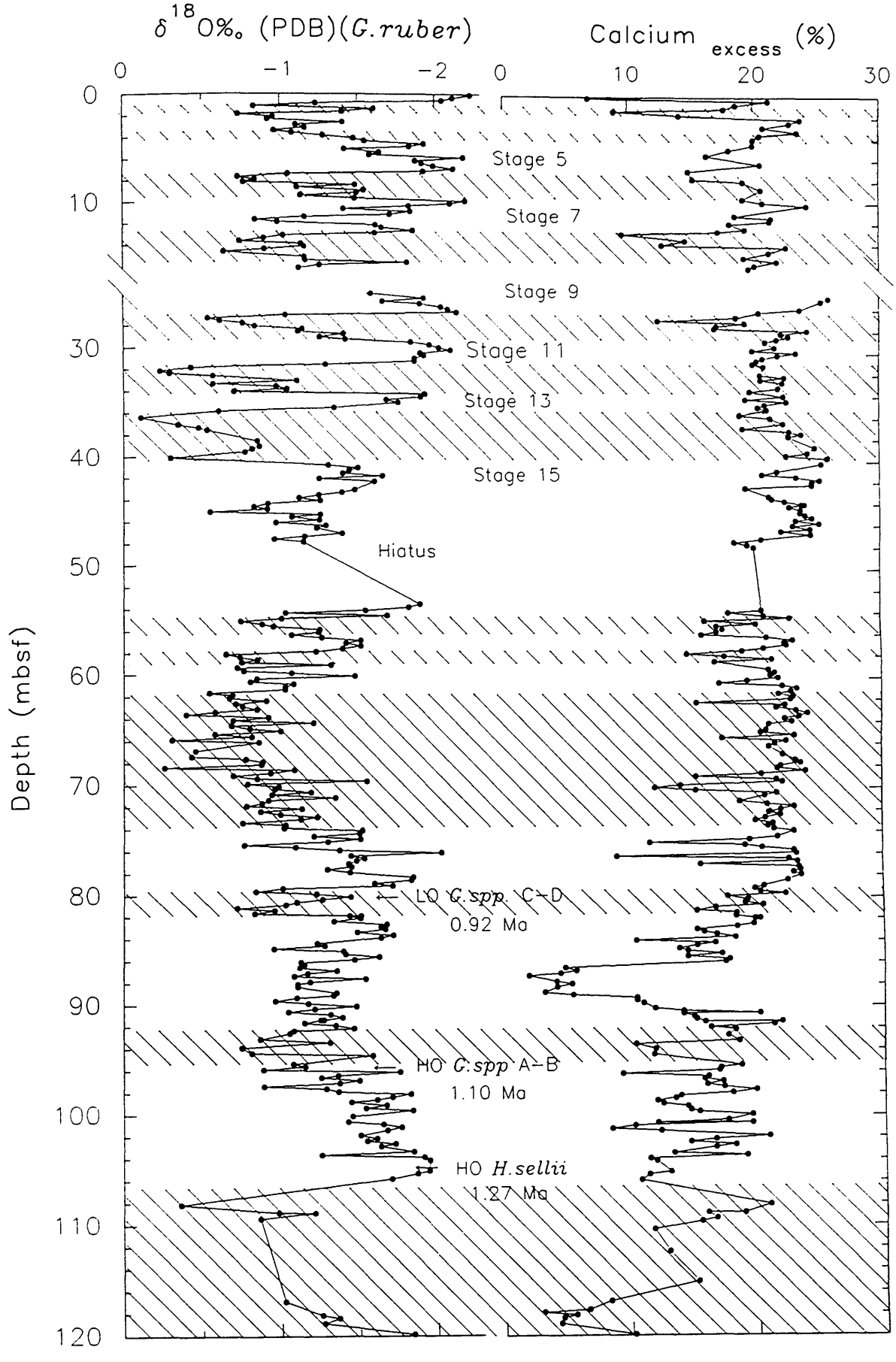

Figure 6.6. Comparison between the excess calcium (Ca) content and the planktic oxygen isotope record in Hole 823A periplatform muds.

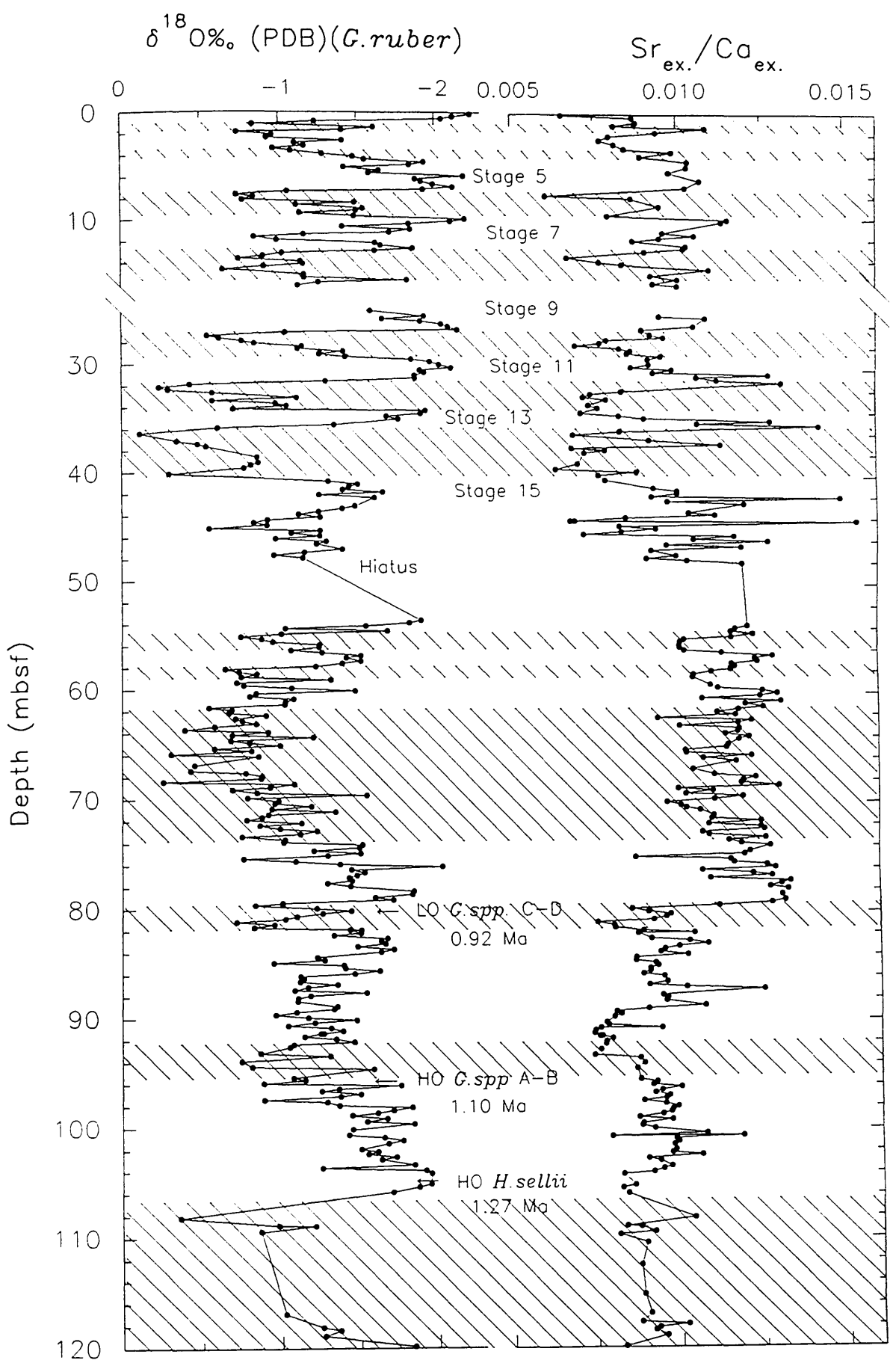

Figure 6.7. Comparison between $Sr_{ex.}/Ca_{ex.}$ values and the planktic oxygen isotope record in Hole 823A periplatform muds.

11, 13 and 15 are all associated with high Sr_{ex}/Ca_{ex} ratios (see Figure 6.7). In the lower part of the core (>50 mbsf), the relationship between Sr_{ex}/Ca_{ex} ratio and isotopically inferred sea level is broadly similar to the upper part of the core, inasmuch as interglacial periods are characterized by high Sr_{ex}/Ca_{ex} values (see Figure 6.8 and 6.9). However, between about 45 to 80 mbsf, the negative relationship between these two parameters is overprinted by an abrupt increase in mean downcore Sr_{ex}/Ca_{ex} values. Significantly, a careful examination of the averaged records between 45 to 80 mbsf indicate a high degree of correlation between individual peaks. For example, minor peaks (or clusters of related peaks) in value centred at 57, 60, 74 and 79 mbsf can be successfully correlated between both records, suggesting that the relationship between these two parameters is maintained during this interval (see Figure 6.8).

Patience (1992) and McNeill (1993) interpreted variations in Sr_{ex}/Ca_{ex} ratios in Eastern Equatorial Pacific and Peruvian continental margin sediments, respectively, in terms of changes in the relative dominance of coccoliths to foraminifera in the oceanic waters. However, in both these studies the contribution of high Sr carbonate (presumably platform derived Sr-rich aragonite) to the overall carbonate signal was considered to be very low. In contrast to these studies, the high Sr/Ca (and Sr_{ex}/Ca_{ex}) values in Hole 823A periplatform sediments, indicate that shallow water platform production and export of Sr rich carbonate (high Sr aragonite), has played a more significant role in determining carbonate deposition, than variations in pelagic productivity (foraminifers and/or coccoliths), in this core. Alternatively, it could be argued that the high Sr_{ex}/Ca_{ex} ratios seen during highstands of sea level represent periods of increased shallow water carbonate preservation, and that during glacial periods enhanced dissolution of the more soluble carbonate phases resulted in the preferential loss of high Sr carbonate (aragonite). However, as mentioned previously (section 5.4.3), the carbonate content records from Hole 823A are in opposition to the classic 'Pacific-type' pattern of intensified dissolution during interglacials and enhanced preservation during glacial (Arrhenius, 1952). Thus, variations in the intensity of carbonate dissolution between glacial/interglacial periods is thought to have played only a minor role in modulating the pattern of carbonate deposition in Hole 823A.

Apart from the good correlation between variations in isotopically inferred sea level and Sr_{ex}/Ca_{ex} ratios, the most striking feature of the Sr_{ex}/Ca_{ex} record in Hole 823A is an dramatic increase in mean values at about 80 mbsf (0.865 Ma). This event may be interpreted in terms of either: a dramatic increase in shallow water banktop production and export (possibly associated with the initiation of the Great Barrier Reef and/or a period of increased shallow water carbonate production on the Queensland Plateau), or

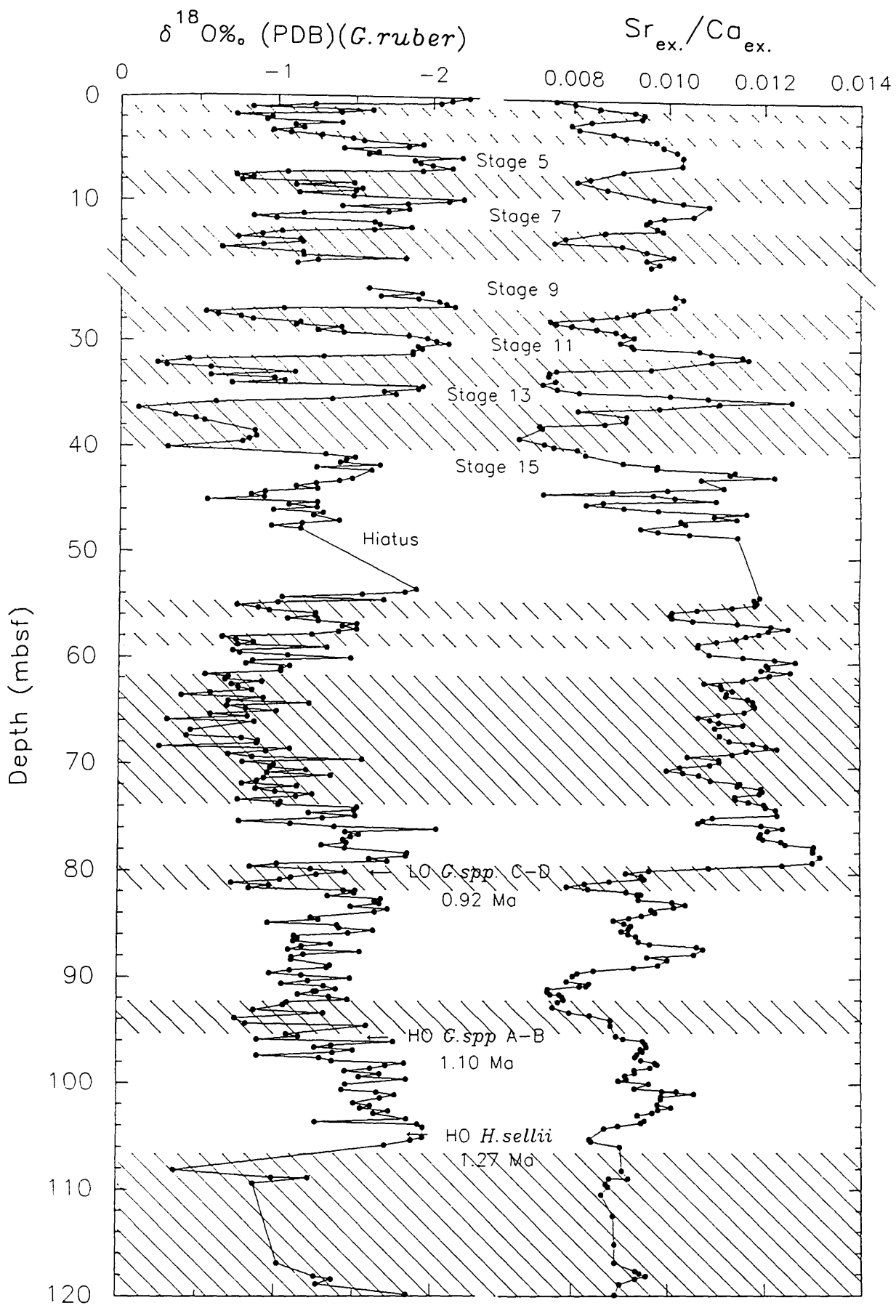

Figure 6.8. Comparison between $Sr_{ex.}/Ca_{ex.}$ values and the planktic oxygen isotope record in Hole 823A periplatform muds. Note that the Sr/Ca curve has been smoothed using a 3 point average.

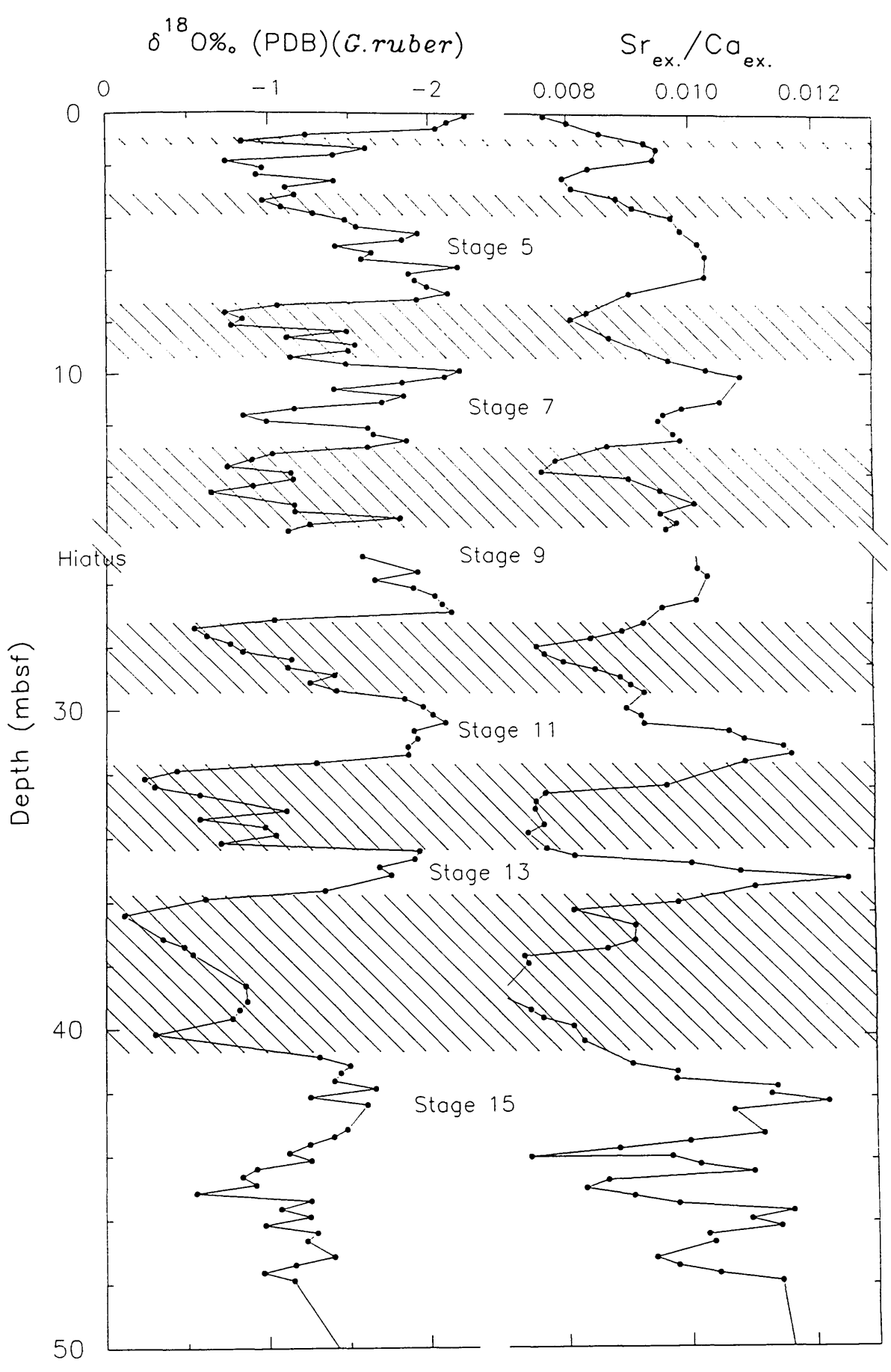

Figure 6.9. Comparison between $Sr_{ex.}/Ca_{ex.}$ values and the planktic oxygen isotope record in the upper 50 m of the sequence from Hole 823A. Note that the Sr/Ca curve has been smoothed using a 3 point average.

marking the onset of a period of enhanced carbonate preservation (see Farrell and Prell, 1989, 1991). Similarly, the sudden decrease in mean Sr_{ex}/Ca_{ex} values at about 45 mbsf (0.59 Ma) may well indicate a reduction in shallow water carbonate material reaching the Queensland Trough, and Hole 823A, or increased dissolution of high Sr carbonate, associated with a significant deepening of the lysocline on the northeast Australian margin.

Thus, the pattern of variation seen in the Sr_{ex}/Ca_{ex} ratio can be interpreted as representing increase production and export of shallow water bank-top carbonate (rich in high Sr aragonite) during highstands of sea level. During glacial lowstands reduced Sr_{ex}/Ca_{ex} ratios may indicate a greater influence of pelagic calcite (mainly coccoliths composed primarily of LMC) low in Sr. This pattern of carbonate deposition is consistent with the 'highstand' shedding scenario outlined by Droxler and Schlager (1985); Mullins *et al.* (1986); Eberli and Ginsburg (1989); Glaser and Droxler (1991), and more recently reviewed by Schlager *et al.* (1994).

6.3.2 Barium as a possible late Pleistocene palaeoproductivity indicator

The search for a reliable chemical proxy for biological productivity preserved in deep-sea sediments has continued for many years (Dymond *et al.*, 1992), and because most proxy indicators previously used (organic carbon, $CaCO_3$, biogenic silica) are indicators of one or more oceanographic processes, the ideal palaeoproductivity indicator has still to be found (Rea *et al.*, 1991). Since Revelle *et al.* (1955) first commented on the association of Ba, opal and biogenic sedimentation, many authors (Chow and Goldberg, 1960; Church, 1970, 1979; Schmitz, 1987; Dehairs *et al.*, 1991; Shimmield and Mowbray, 1991; Dymond *et al.*, 1992; McNeill, 1993), have used Barium (Ba) as a diagnostic tool for palaeoproductivity.

The main barium carrier in deep-sea sediments is barite (Ba SO_4), a marine mineral first reported by Murray and Renard (1898), although locally manganese oxides and phillipsite (Zeolite group mineral) will accumulate significant amounts of Ba (Puchelt, 1969). According to Chan *et al.* (1976) the production of particulate barite from dissolved Ba in the water column seems to be related to the marine biogeochemical cycle. There are two main hypothesis for the formation of barite in the oceans:- (1) Formation in microenvironments (for example, siliceous plankton tests, faecal pellets, marine snow) where the decay of organic matter provides an enrichment of dissolved sulphate (Bishop, 1988).

(2) Active precipitation by marine organisms, such as benthic foraminifera (Lea and Boyle, 1989), corals (Lea *et al.*, 1989) and benthic protozoans such as *Xenophyophoria* and *Loxodes* (Finlay *et al.*, 1983).

However, the use of barium as a proxy for palaeoproductivity is not without its problems. Barium is prone to dissolution under strongly reducing conditions (von Breymann *et al.*, 1990), although not affected to the same degree as biogenic opal (Archer *et al.*, 1993) or calcite (Thunell, 1982; Crowley, 1983) and is thus a more reliable indicator of ocean fertility (Dymond, 1981; Dymond, 1992). As with many elements, a proportion of the total barium (Ba_{total}) concentration present in marine sediments is associated with the terrigenous, detrital aluminosilicates and, therefore, in order to examine any variation in the "biogenic source" of this element, geochemical analyses are usually expressed in two ways (1) Ba/Al ratio:- using Al as a terrigenous normalizing element and, (2) Excess Ba:- Ba in excess of that normally held in marine aluminosilicates.

Equation 6.2 Excess Ba (Ex.Ba) = $Ba_{total} - (Al_{total} \times Ba/Al_{Aluminosilicate})$
(after Dymond *et al.*, 1992)

where: Ba_{total} and Al_{total} are the total elemental concentrations (ppm) measured by XRF, and $Ba/Al_{Aluminosilicate} = 0.003$. According to Dymond *et al.* (1992) a typical Ba/Al value for detrital/terrigenous aluminosilicates is 0.0075 (although this value can be adjusted for specific oceanic provenances- Rösler and Lange, 1972). This technique supposes that the terrigenous aluminosilicate content is relatively invariant, which is not the case with the Queensland Trough sediments (see below).

Figures 6.10 and 6.11 illustrate the downcore variation in Ba_{total} and $Ba_{ex.}$, plotted alongside the planktic oxygen isotope record, respectively, in Hole 823A. In addition the downcore variation in Ba/Al ratios in this core are illustrated in Figure 6.12. Mean $Ba_{ex.}$ content values are generally about 167 ppm in the upper 45 m of the core, and approximately 59 ppm Ba in the lower 75 m of the sequence. Ba/Al values in Hole 823A sediments typically range from about 0.0022 to 0.0228, with a core mean of about 0.00614. These values are significantly lower than the mean normative Ba/Al value (0.02738) for deep-sea shale proposed by Turekian and Wedopohl (1961), or a typical mean normative Ba/Al value of 0.0075 suggested by Dymond *et al.* (1992). The most striking feature of the Ba_{total}, Ba_{ex} and Ba/Al records is the abrupt and permanent increase in mean values at about 45 mbsf, corresponding to an age of approximately 0.59 Ma. Below this depth, the Ba_{ex} and Ba/Al (and to a certain extent

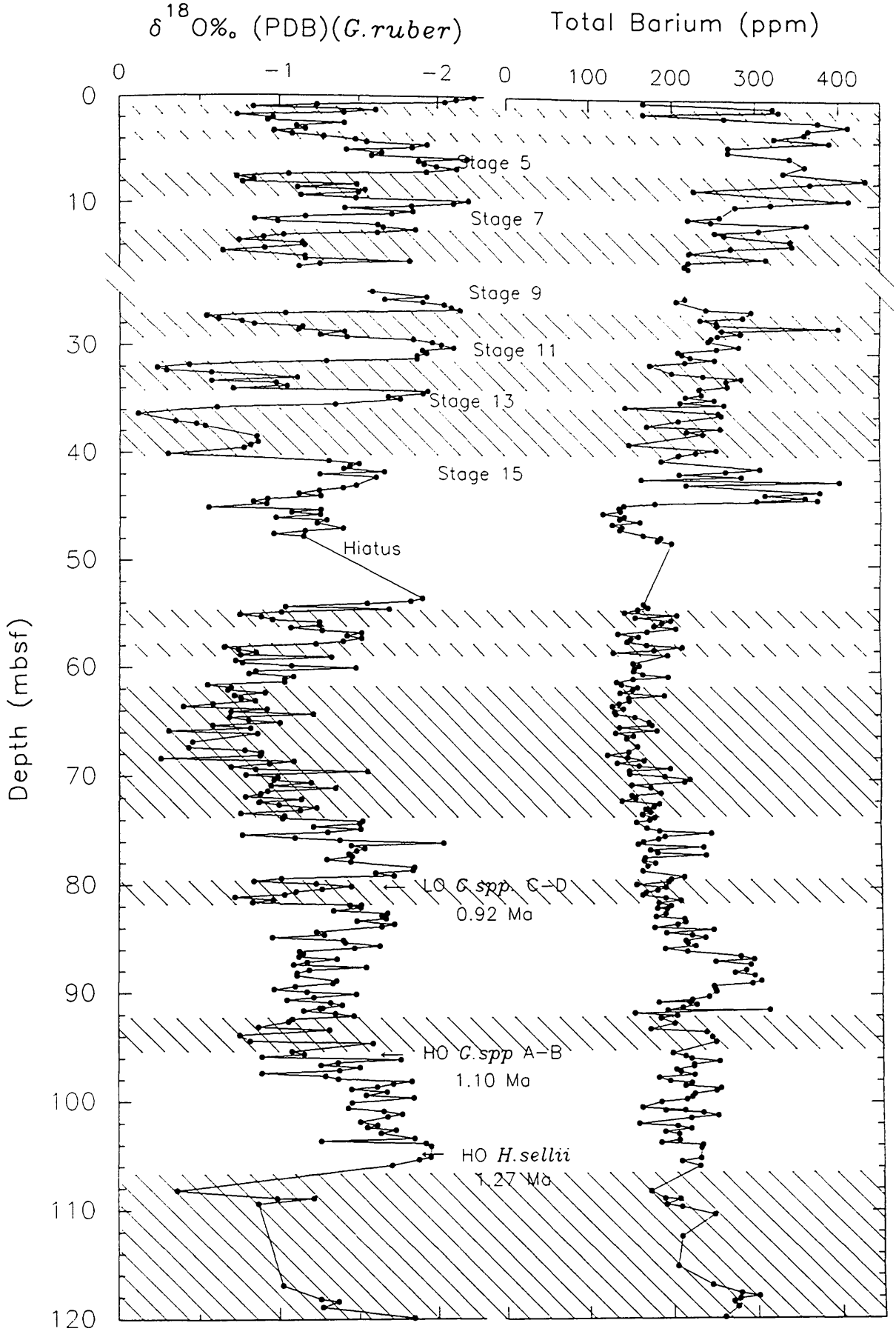

Figure 6.10. Comparison between the total barium (ppm) content and the planktic oxygen isotope record in Hole 823A periplatform muds.

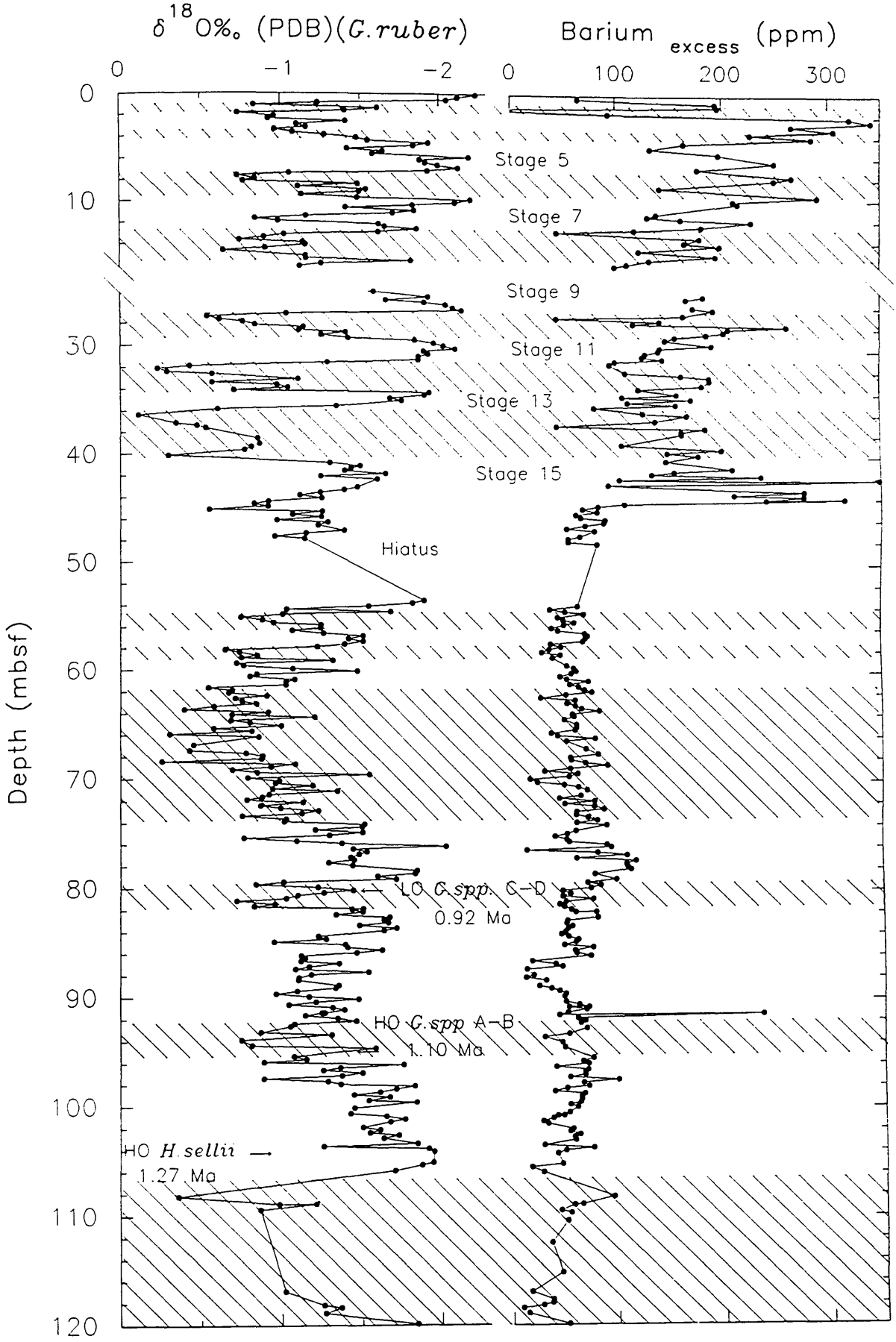

Figure 6.11. Comparison between the excess barium (ppm) content and the planktic oxygen isotope record in Hole 823A periplatform muds.

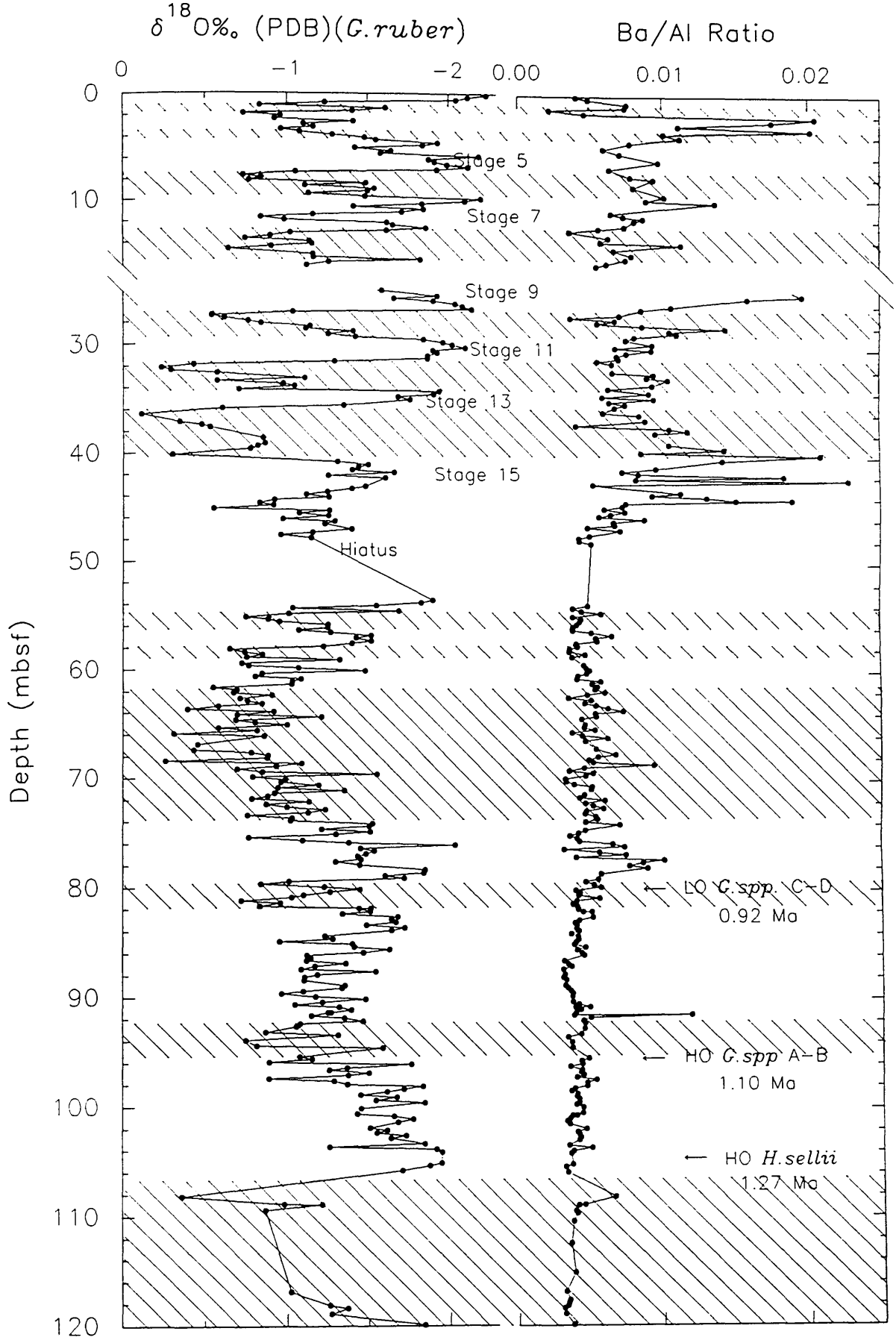

Figure 6.12. Comparison between the Ba/Al ratio and the planktic oxygen isotope record in Hole 823A periplatform muds. Note the presence of a major hiatus between 16.5–24.9 mbsf.

the Ba_{total}) records are characterized by comparatively low values (see Figures 6.11 and 6.12). The abrupt increase in these parameters seems to coincide with a significant change in the dominant amplitude and frequency of the isotopic record (see section 3.8). It is tempting to suggest a direct link between these two phenomenon. However, throughout the majority of the record in this core, Ba content (and the Ba/Al ratio) seem to fluctuate independently of sea level (as inferred from the stable oxygen isotope record) (see Figures 6.10 to 6.12), which suggests that Ba content in Hole 823A is being forced by some other mechanism such as shallow burial diagenesis and/or dissolution.

Comparison of the Ba (and Ba/Al) profiles with the Leg 133 shipboard pore-water geochemistry data indicate that the abrupt increase in values, seen at about 45 mbsf, coincides with the base of the sulphate reduction zone and the top of the zone of methane formation in Hole 823A (see Figure 5.31). Furthermore, a significant reduction in the pore-water dissolved Sr^{2+} content data (Shipboard Scientific party, 1991) occurs at about the same depth (see Figure 5.26b). Thus it seems likely that the main reason for the low $Ba_{ex.}$ concentrations and Ba/Al ratios (and negative $Ba_{ex.}$ values) is that Ba is being lost upon burial in the sediment during diagenetic mobilization (von Breymann *et al.*, 1992). According to Dymond (1981) and Dymond *et al.* (1992) this can only occur in sediment during diagenesis within a suboxic/ anoxic environment, due to pore-water undersaturation with respect to barite at the base of the sulphate reduction zone. The good agreement between the abrupt increase in Ba content and the base of the sulphate reduction zone (and the top of the zone of methanogenesis) at about 45 mbsf (0.59 Ma) support the theory that the Ba (and Ba/Al) signal in Hole 823A is a relic (diagenetic) feature, and not a true indication of late Pleistocene palaeoproductivity on the Queensland margin.

As noted by Dymond *et al.* (1992) the use of barium in nearshore environments is limited not only because of the uncertainties associated with the aluminosilicate contribution (i.e., the element/Al ratio) but also by the diagenetic remobilization of biobarite under sulphate reducing conditions. These authors conclude that:

".....deposits from these areas (nearshore environments) should not be used for palaeoproductivity reconstructions using barium accumulation, because of the remobilization of biogenic barite, in reduced and/or suboxic environments...."

In conclusion, most likely because of diagenesis and the remobilization of Ba, variations in the downcore concentration of this element (and Ba/Al ratios) cannot be

used as an accurate proxy for late Pleistocene ocean fertility, in Hole 823A periplatform sediments.

6.3.3 Variations in the composition of the lithogenic fraction

As mentioned previously, periplatform sediments (Schlager and James, 1978) are composed predominantly of a mixture of shallow water bank-derived carbonate and pelagic/planktonic driven calcite. However, on complex carbonate-siliciclastic margins, such as the northeast Australian margin, incorporating the Great Barrier Reef (GBR), late Quaternary sediments accumulating on the continental slope are invariably mixed with the products of terrestrial/ continental weathering and erosion. Similarly, marine sediments accumulating in deep-sea basins adjacent to continental landmasses often carry a continental-derived terrigenous signal. Variations in the composition of the non-carbonate and/or detrital fraction in marine sediments often provide valuable information concerning provenance or terrigenous source variations, processes of weathering and erosion, and mechanisms of sediment transport/ deposition. In this section, the palaeoenvironmental and palaeoclimatic implications of variations in titanium (Ti) and chromium (Cr) content (and ratios formed with Al) in Hole 823A periplatform sediments are examined.

Titanium (Ti) and chromium (Cr) in marine sediments may have several sources including terrigenous material (Shimmield and Mowbray, 1991), basaltic debris (Goldberg and Arrhenius, 1958; Bostrom *et al.*, 1973), hydrothermal deposits and exhalations (Bonatti *et al.*, 1983; Nath *et al.*, 1989), authigenic/ hydrogenous precipitates (ferromanganese nodules) (Chester, 1965) and biological phases (Bostrum *et al.*, 1974; Martin and Knauer, 1973). Despite this wide variety of possible sources, most Ti and Cr in deep sea sediments occurs in the continentally derived terrigenous materials such as aluminosilicates (typically clays) and heavy minerals (Chester and Aston, 1976). Spears and Kanaris-Sotiriou (1976) and Schmitz (1987) found that Ti and Cr are preferentially concentrated in the coarser sediment fractions, in marine sediments, due to their incorporation in heavy minerals. According to Wedepohl (1960) there is only a limited number of minerals which contain Cr as a major constituent, these include: chromite, magnetite, olivines and garnet. Heavy mineral sources of Ti include anatase (diagenetic TiO_2), rutile and ilmenite (Patience, 1992). Shiraki (1966) has shown that the ratio of mafic to granitic rocks in provenance is most important in controlling the Cr content in terrigenous sediments. Typical Ti and Cr concentrations in recent pelagic to hemipelagic marine sediments are listed in Table 6.2.

Area	Cr (ppm)	Ti (wt.%)	Reference
Pacific	93		Goldberg and Arrhenius (1958)
Atlantic	86	0.46	Wedepohl (1960)
Weddell Sea	104		Angino and Andrews (1968)
East Indian ocean	40		Cronan and Tooms (1969)
northwest Arabian Sea	107	0.45	Shimmield *et al.*, (1990)
Panama Basin	0-120	0.01-0.5	Patience (1992)
Peru continental margin	50-128	0.18-0.61	McNeill (1993)
Northeast Australian margin	7.7-89.0	0.06-0.61	Alexander (this study)
	(40.64)	(0.24)	

Table 6.2 Titanium (Ti) and Chromium (Cr) in pelagic clay sediments. Mean values are given in parentheses.

The downcore variation in Ti and Cr content in Hole 823A muds, plotted alongside the planktic $\delta^{18}O$ record are shown in Figures 6.13 and 6.14. In general, Ti content in Hole 823A sediments ranges between 0.060-0.612 wt.%, with a downcore mean of about 0.244 wt.%. Chromium concentrations in this core typically range between 7.70-89.00 ppm, although the mean for the core is closer to 40 ppm. Comparison of the downcore variations in Ti and Cr content suggests a high degree of coherency between these two records (coefficient of correlation, Pearson's r = 0.975, where N = 311). In general both element curves broadly show the same pattern of variation with depth. For example, the downcore Ti and Cr records are both distinguished by an abrupt decrease in mean elemental value at about 85 mbsf (corresponding to an age of about 0.97 Ma) (see Figure 6.13).

In order to illustrate any variations in the composition of the terrigenous material, it is first necessary to convert the simple elemental concentration (which can be influenced by the dilution effects of another component) into an elemental/Al ratio. Aluminium is chosen as a normalizing agent because of its strong association with the terrigenous/ detrital component (Arrhenius, 1952; Bostrum, 1973; Bischoff *et al.*, 1979), and its use as an indicator of clay detritus of continental terrigenous origin (Shimmield and Mowbray, 1991) (although the alteration of oceanic basalts and/or hydrothermal exhalations (Shankar *et al.*, 1987; Nath *et al.*, 1989) may also contribute to the marine sediment record). The linearity of the relationship between Ti (and Cr) and Al in Hole 823A demonstrate that the majority of Ti (and Cr) is held in the aluminosilicate material in Hole 823A sediments (see Figure 6.15), and therefore the weathering of submarine basalts is unlikely to be a major contributor to the Ti and Cr content of Hole 823A sediments. Figures 6.16 and 6.17 illustrate the downcore variation in Ti/Al and Cr/Al ratios in Hole 823A sediments plotted alongside the planktic $\delta^{18}O$ record.

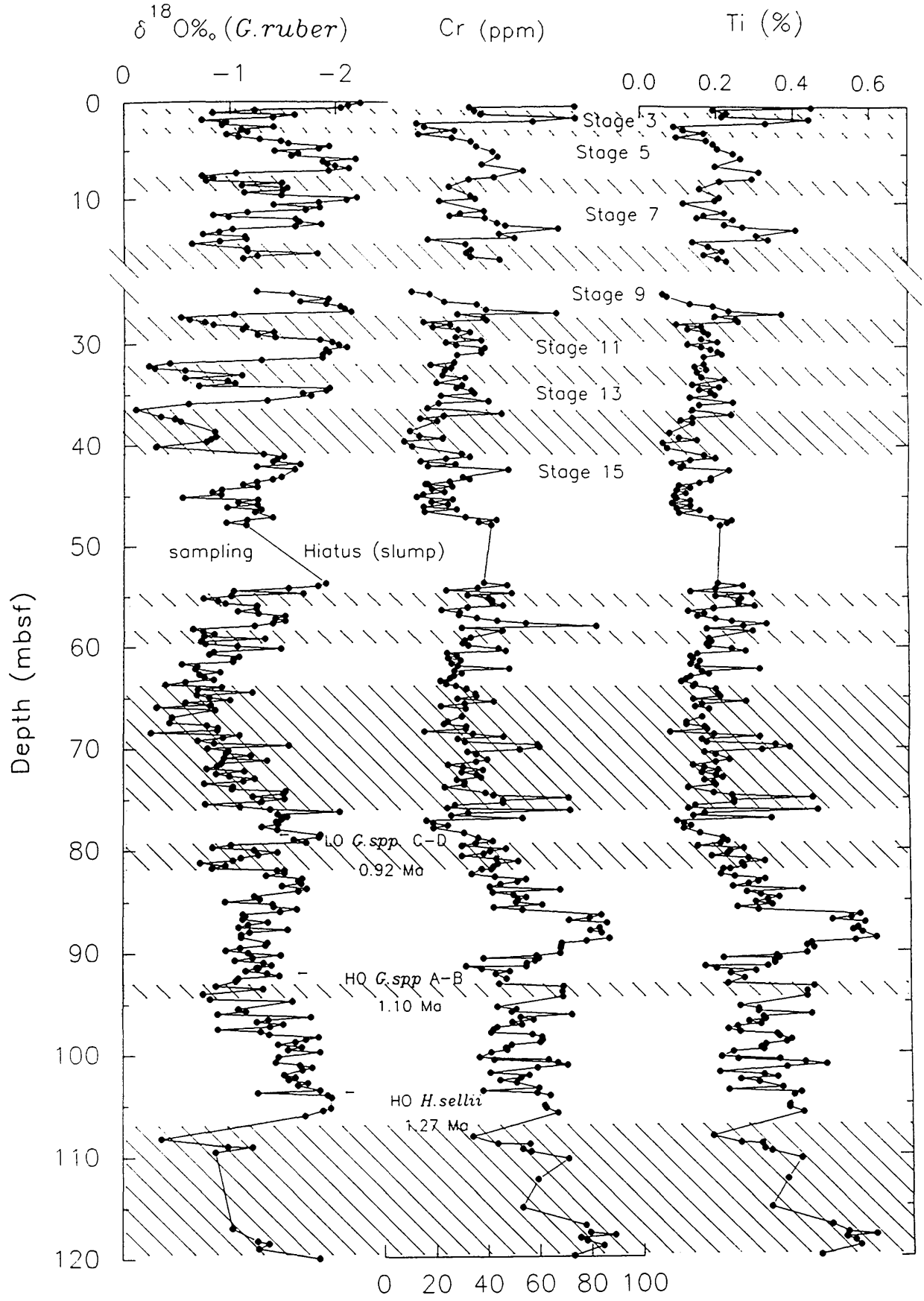

Figure 6.13. Comparison between chromium (Cr) and titanium (Ti) content in Hole 823A periplatform muds and the planktic oxygen isotope record from this core.

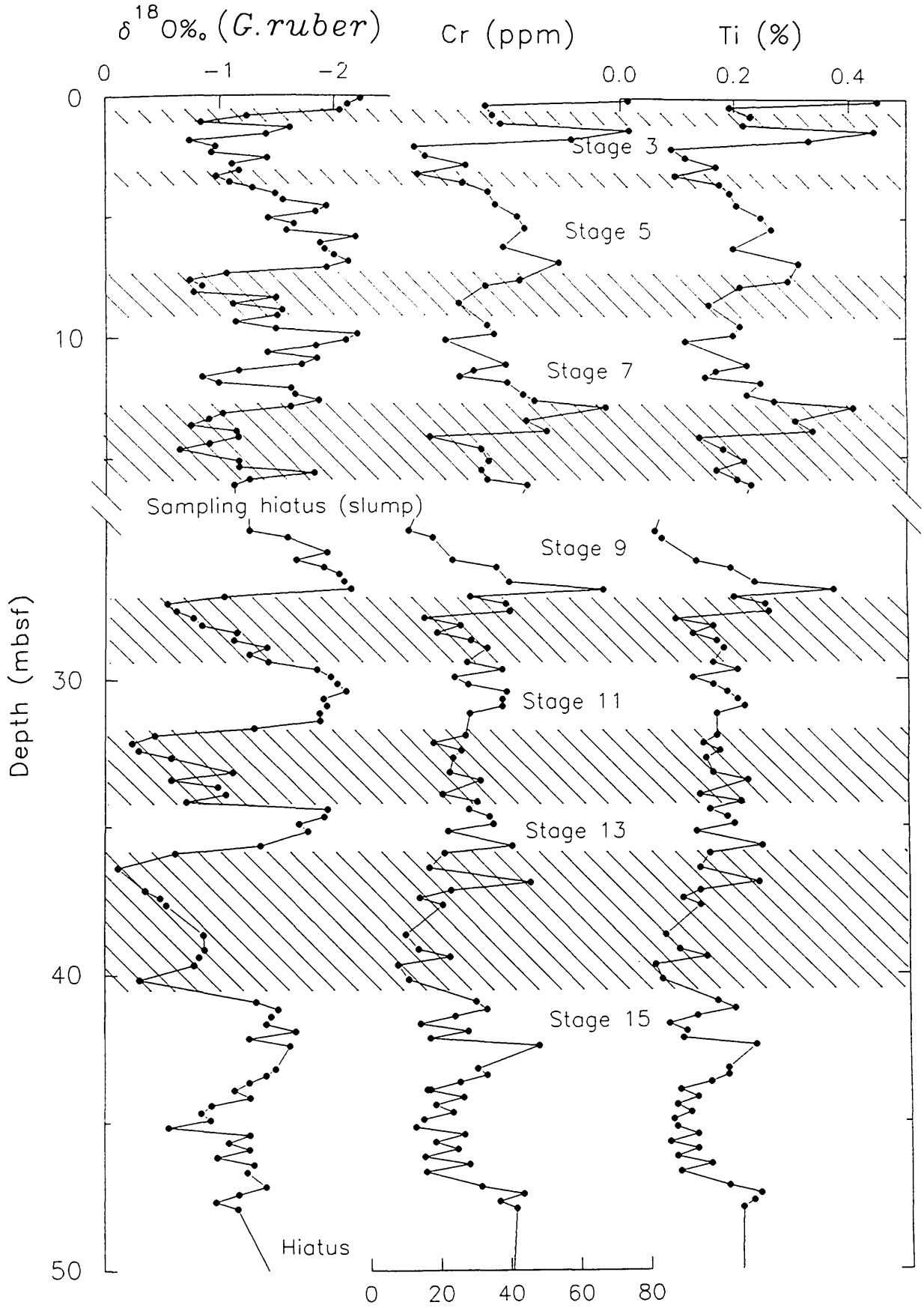

Figure 6.14. Comparison between the chromium (Cr) and titanium (Ti) content in the upper 50 m of the periplatform sequence from Hole 823A Also shown is the planktic oxygen isotope record from this core.

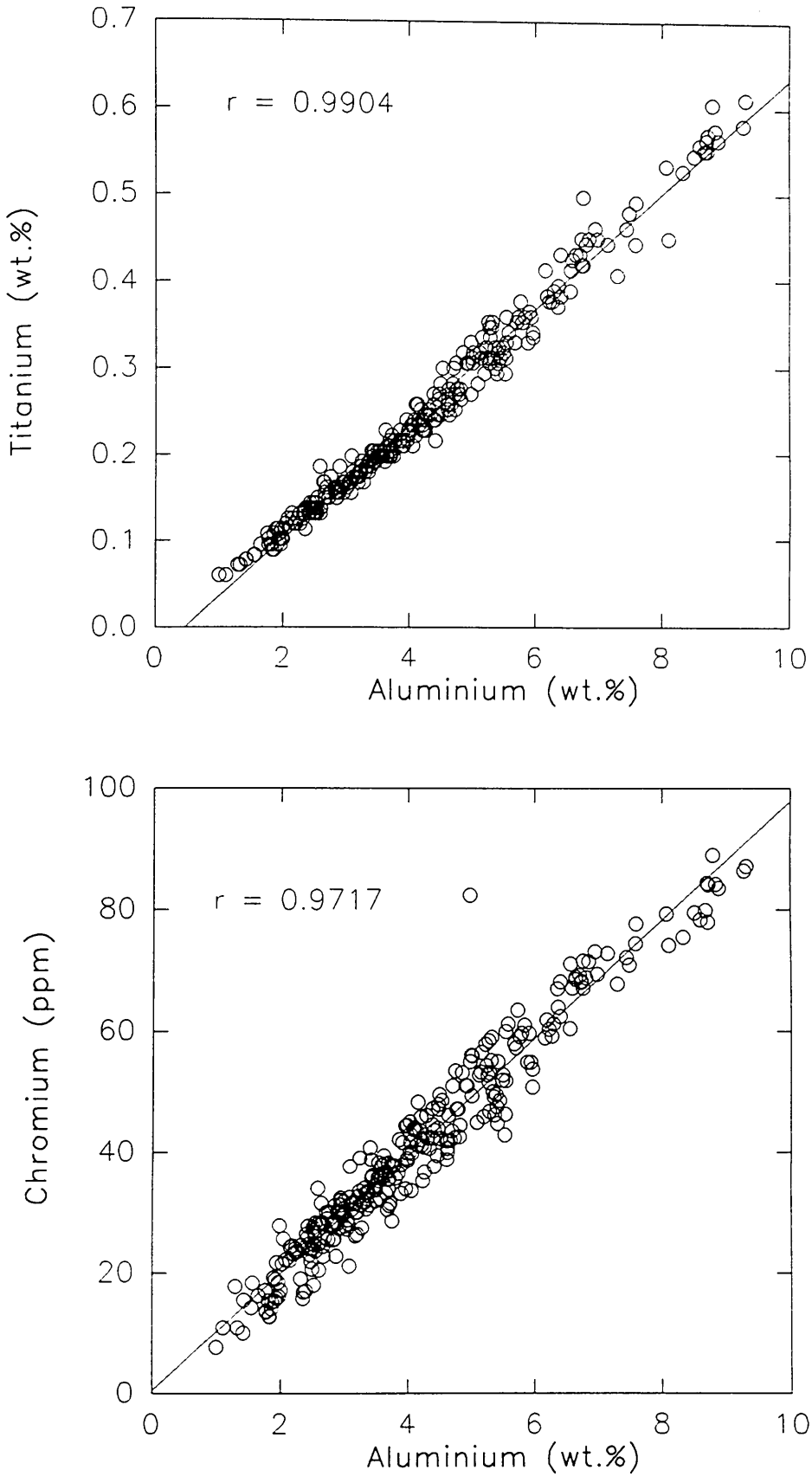

Figure 6.15. Biplots showing the relationship between chromium (Cr) and titanium (Ti), and aluminium (Al) in Hole 823A periplatform muds. The near linear association between these elements indicate that terrigenous alumino-silicate minerals are the primary source of Cr and Ti in this core.

Downcore Ti/Al values range between 0.05 and 0.06, with a mean of about 0.058. These figures are similar to mean values for pelagic sediments from the northwest Arabian Sea sediments (Shimmield *et al.*, 1990), and are close to the average deep-sea clay Ti/Al value provided by Turekian and Wedepohl (1961) (i.e., 0.0548). In contrast, Cr/Al ratios in Hole 823A range between 0.0008 to 0.0012, with a downcore mean of approximately 9.8×10^{-4}, and are significantly lower than values reported for many pelagic sediments (see Table 6.2). Examination of these high resolution data indicate that unlike the Ti/Al ratio, a strong correlation exists between the planktic $\delta^{18}O$ record and variations in the Cr/Al ratio. In general, throughout the length of the core Cr/Al values are high during highstands of sea level (or conversely low during glacial lowstands) (see Figure 6.16). This relationship is particularly well developed in the upper part of the periplatform sequence in Hole 823A (see Figure 6.17).

Boyle (1983) suggested that variations in the Ti/Al ratio in sediments accumulating under the Peru Current could be attributed to changes in the intensity of aeolian transport associated with glacial/ interglacial cycles. Similarly, Shimmield and Mowbray (1991) reported increased Ti/Al ratios (and Cr/Al ratios) in late Pleistocene (last 400 ka) sediments collected from northwest Arabian Sea, related to enhanced wind strength associated with the southwest monsoon. Shiraki (1966) has shown that the ratio of mafic to granitic rocks in provenance is most important in controlling the Cr (and Ti) content in terrigenous sediments. The downcore variations in Cr/Al ratio (and to a certain extent Ti/Al ratio) in late Pleistocene Hole 823A periplatform sediments may represent either changes in: (a) wind strength (possibly associated with the Austral northwest monsoon), (b) variations in source area and/or continental aridity, (c) increased rainfall and/or river discharge, and/or (d) sediment winnowing and bottom transport.

Of these factors, there is little evidence to suggest that wind transport has played a significant role in determining the composition of Hole 823A non-carbonate sediments. As mentioned previously (section 4.6.2), preliminary petrological and SEM analysis of Hole 823A (and Hole 819A) sediments, in particular the non -carbonate fraction, indicate that the majority of quartz grains are angular to sub-angular, lacking a frosted or pitted surface to the grains, all features indicating a likely river-borne or fluviatile origin (see Plate 11). Furthermore, the occurrence of high Cr/Al (and to a certain extent Ti/Al) ratios, during highstands of sea level in Hole 823A sediments, are inconsistent with the hypothesis of increased late Pleistocene southern hemisphere continental aridity and wind strength during glacial periods, as suggested by Rea (1990).

A

X 500

B

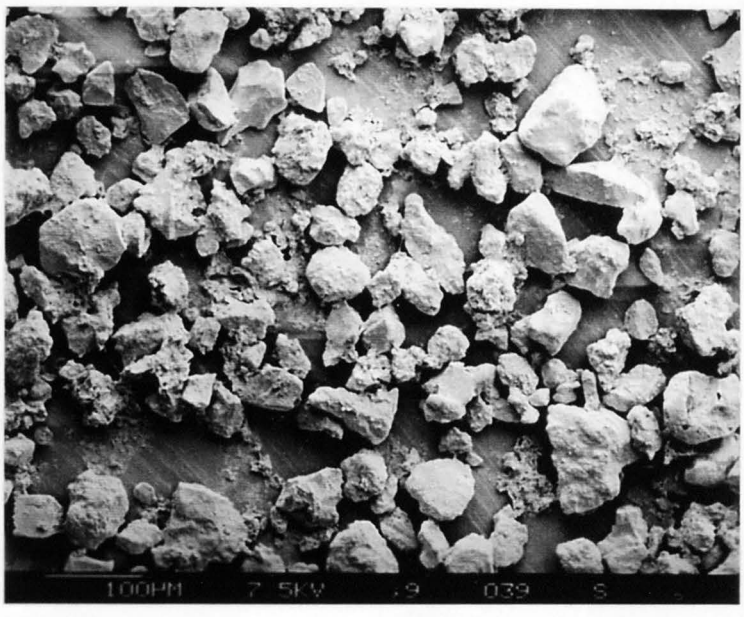

X 125

Plate 11. SEM photomicrographs of representative non-carbonate material within the mud size fraction in Hole 819A periplatform sediments (Sample 133-819A-01H02-70/72). Sediments were dissolved overnight in 15 % acetic acid in order to concentrate the terrigenous fraction. Note the abundance of angular to sub-angular quartz grains (Qtz) indicating a possible fluviale origin.

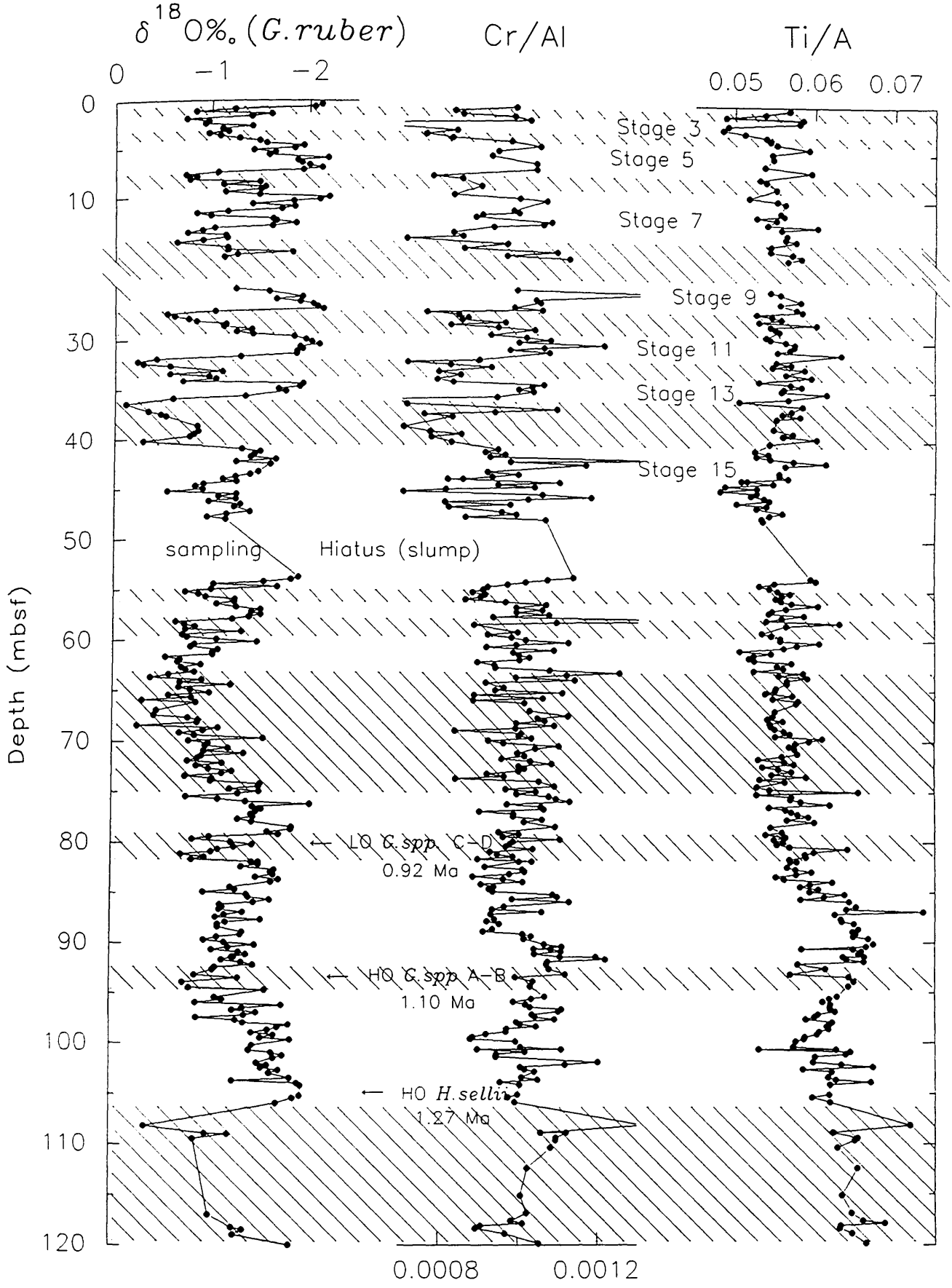

Figure 6.16. Downcore variations in the Cr/Al and Ti/Al ratios in Hole 823A periplatform muds. Also shown is the planktic oxygen isotope record from this core.

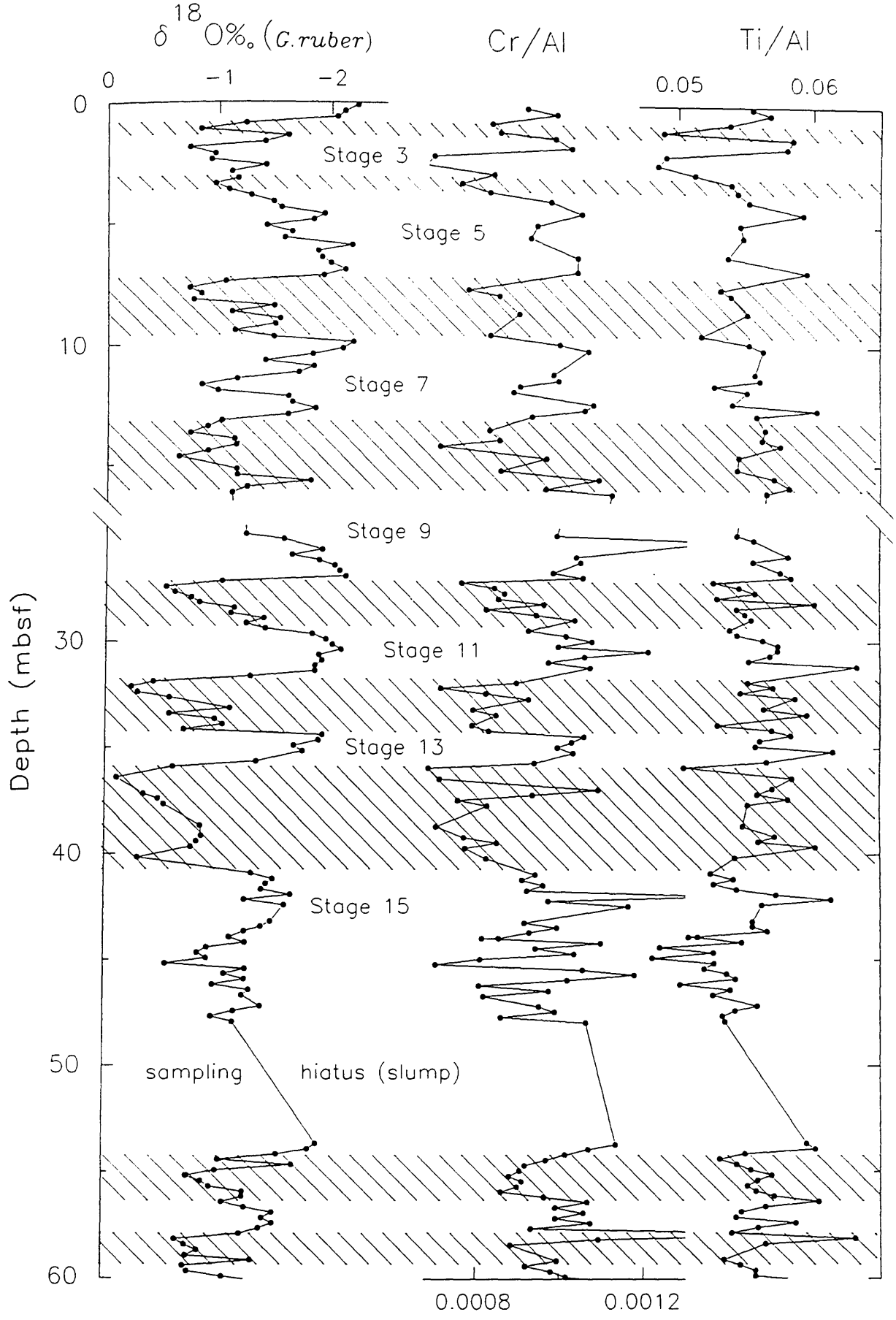

Figure 6.17. Downcore variations in the Cr/Al and Ti/Al ratios in the upper 60 m of the periplatform sequence from Hole 823A. Also shown is the planktic oxygen isotope record for this core.

In general, the late Pleistocene Cr/Al (and Ti/Al) records suggest that climatic conditions were significantly wetter on the Queensland margin during interglacial periods, than corresponding glacial periods. Enhanced river discharge during highstands of sea level, may have increased transport of terrigenous material onto the Queensland shelf, and the GBR. Increased mean annual rainfall on the northeast Queensland margin, during interglacial periods, have been reported by Kershaw (1978), based on an analysis of the pollen record. Kershaw (1978) suggested that rainfall changes in the Queensland area, over the last 125 ka have been largely controlled by global sea level and/or sea surface temperatures. However, the question remains as to how this detrital material (rich in Cr) reached the shelf edge and the Queensland Trough, particularly since the modern transport of sediment beyond the inner shelf is limited because of the dominance of along-the-shelf sediment transport in the near shore and inner-shelf regions Flood and Orme (1988). Possibly, as suggested by Davies *et al.* (1991), infrequent cyclones and extremely heavy cyclonic rainfall, particularly during the summer months and early autumn (Maxwell, 1968), may have enabled the transport of large volumes of terrigenous clastics out across the shelf and through the outer reefs. Some of this detrital material, carrying Cr rich minerals, may have reached the upper slope during periods of high sea level (Davies *et al.*, 1985).

Unlike the Ti/Al record, the Cr/Al ratio record does not show any significant shift in mean values between about 0.85 to 0.9 Ma (see Figure 6.16). Feary *et al.* (1993) argued that a fundamental change in the style of seismic sequence geometry, from mainly progradational to aggradational seismic sequence geometrys in Sites 819, 820 and 821, indicates the initiation of reef growth on the Queensland margin, at approximately 0.75 to 1.0 Ma. These authors suggested that reef development on the Queensland margin restricted sediment supply to the outer shelf and resulted in two fundamentally different types of seismic sequence geometry, and that also excluded high energy events that might otherwise have eroded inner shelf detritus and moved it seaward. However, the Cr/Al record from Hole 823A show little evidence of a significant change in depositional style during this interval (0.75-1.0 Ma), and provides no indication of a barrier to sediments discharge from the Queensland mainland.

Why one elemental ratio (Cr/Al) should show a strong relationship with sea level, and not the other (i.e., Ti/Al) is difficult to explain. Possibly the difference in the response of these elemental ratios to sea level change is related to the source of heavy minerals, or subtle changes in the degree of sorting/ grain size (see Boyle, 1983) in Hole 823A sediments. Alternatively, different dispersal mechanisms (aeolian vs. fluviatile) may

have been responsible for the pattern of heavy mineral elements seen in this core, although direct evidence of this is very scanty.

6.3.4. Origins of Aragonite.

Modern shallow-water sediments are composed of aragonite and high-magnesian calcite and subordinate amounts of low-magnesian calcite (Friedman, 1965). However, aragonite is not specific to shallow water derived carbonate. Pteropods (and other pelagic molluscs) typically secrete a shell composed of aragonite (Milliman, 1978), and are capable of producing considerable amounts of this material in both the deep-sea setting (Friedman, 1965; Chen, 1968; Berner and Honjo, 1981) and in near-platform environments (Boardman and Neumann, 1984; Droxler *et al.*, 1993). Fortunately, a measure of the influence of pelagic or planktic aragonite on the total carbonate signal within marine sediments can be gained through analysis of the strontium (Sr) content of periplatform sediments (Boardman and Neumann, 1984; Boardman *et al.*, 1986).

As mentioned earlier, strontium in marine carbonate sediments can be derived from a number of important sources, these include: molluscs; foraminifera; corals and calcareous algae (Milliman, 1974, Bathurst, 1975). The Sr content in carbonate sediments generally define two end members of concentration (Kinsman, 1969; Milliman, 1974; Bathurst, 1975). In general, calcite and molluscan aragonite contain low concentrations of strontium (<2000 ppm), whereas high concentrations of strontium (>7500 ppm) occur in aragonite from corals, calcareous green algae (e.g., *Halimeda, Penicillus*), inorganically precipitated ooids, and shallow water marine cements (Milliman, 1974).

Given the deeper water setting of Hole 823A, in comparison to Leg 133 Sites 820 to 819, it is reasonable to assume that sediments accumulating in the Queensland Trough are more under the influence of pelagic driven carbonate (and aragonite). In this section, variations in the downcore abundance of Sr and aragonite are examined in order to investigate the likely sources of aragonite in Hole 823A periplatform sediments.

Figures 6.18 and 6.19 illustrate the downcore abundance of aragonite and Sr in Hole 823A, plotted alongside the planktic oxygen isotope curve for this core. In these figures the total aragonite and Sr content in Hole 823A sediments has been normalized to 100 % carbonate (i.e., normalized value = 100/total carbonate content x total aragonite or Sr content). This enables a better comparison with carbonate sediments

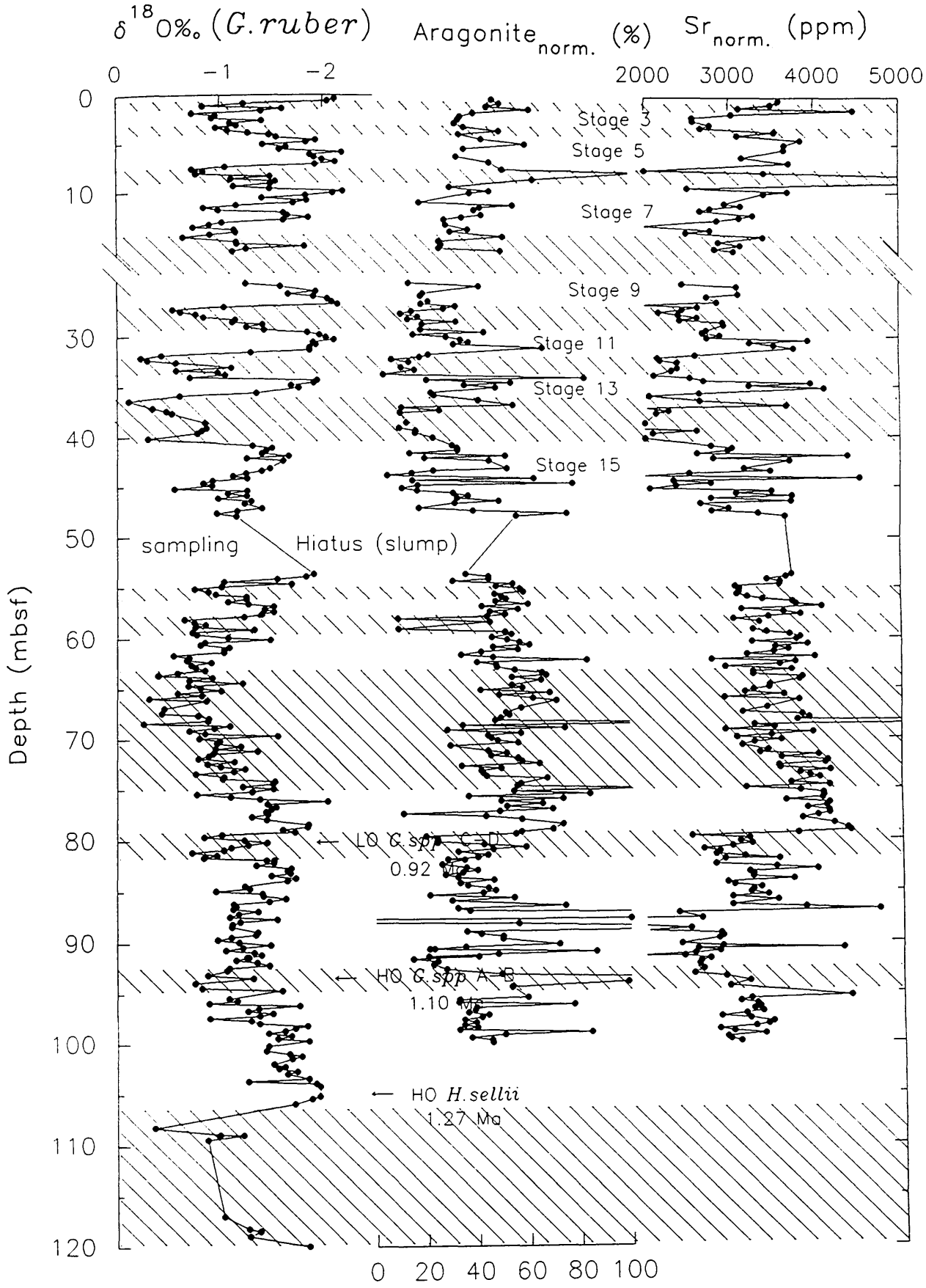

Figure 6.18. Distribution of normalized aragonite (%) and Sr (ppm) with depth in Hole 823A periplatform muds. Also shown is the planktic oxygen isotope record from this core.

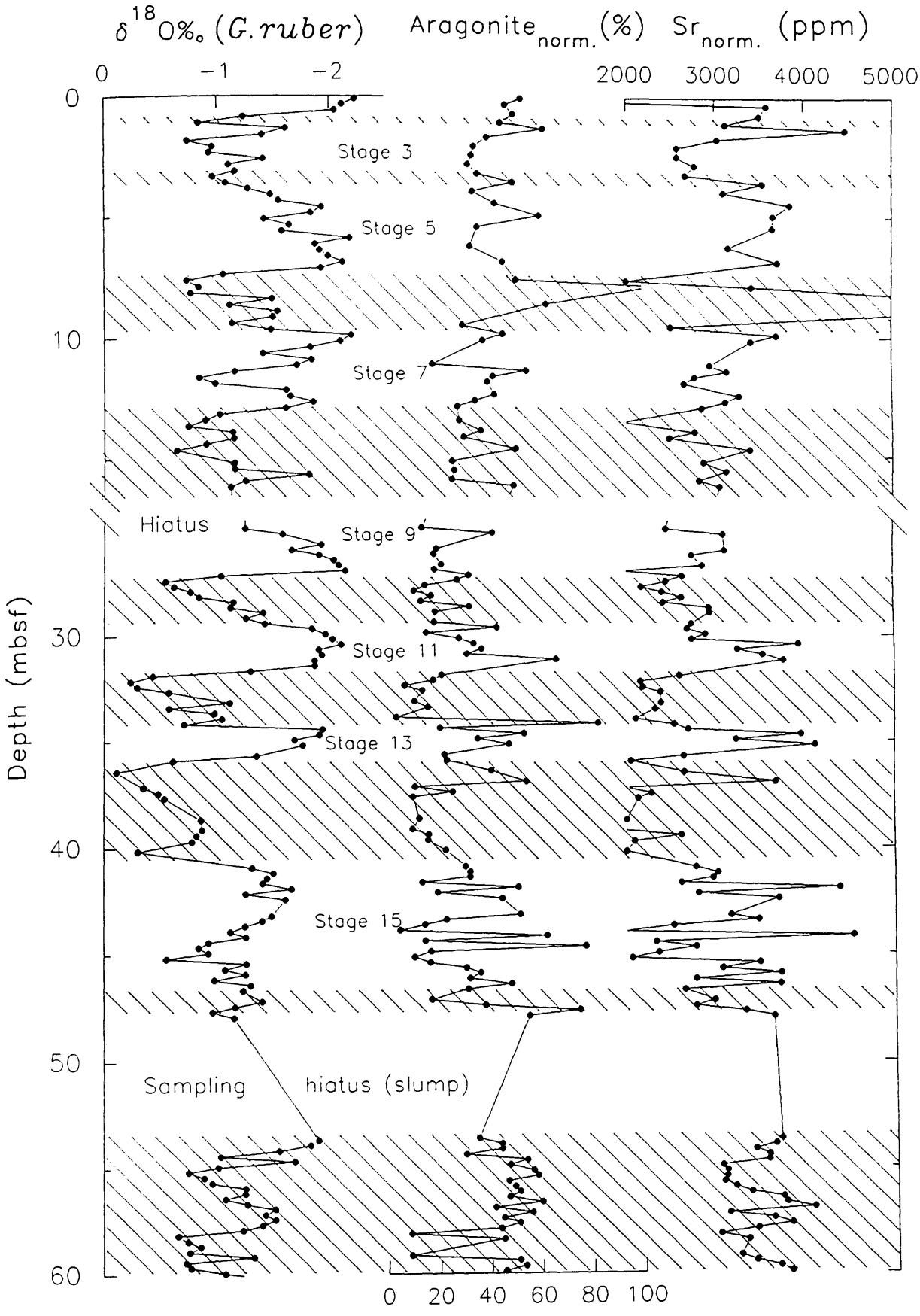

Figure 6.19. Distribution of normalized aragonite (%) and Sr (ppm), with depth, for the upper 60 m of the periplatform sequence in Hole 823A.

less under the influence of dilution by continental derived terrigenous material. Analysis of the aragonite and Sr content records in Hole 823A indicate a moderately high coefficient of correlation, r = 0.774 (where, N = 278). This suggests that variations in total Sr content in Hole 823A periplatform sediments are not unduly influenced by non-biogenic Sr.

According to Boardman and Neumann (1984) a plot of Sr concentration versus percent aragonite can be used to distinguish calcite (foraminifera, echinoids and coccoliths), low Sr aragonite (pteropods and benthic molluscs), and high Sr aragonite (Green algae, corals, ooids and cements) in periplatform sediments. Figure 6.20 shows a plot of normalized Sr ($Sr_{norm.}$) content against normalized aragonite ($aragonite_{norm.}$) content for Hole 823A periplatform sediments. Also shown in this figure is a plot of Sr against total aragonite content for Northwest Providence Channel (NWPC) periplatform sediments, Bahamas (Boardman *et al.*, 1986). In these plots a ternary field is outlined which represents the possible sources of Sr aragonite in recent marine sediments (Boardmann and Neumann, 1984). Analysis of the Hole 823A records shows that a significant proportion of the aragonite in this core is derived from a shallow water source. If low Sr aragonite (pteropods and benthic molluscs) were an important component in the Hole 823A sediments, samples would deviate significantly from a straight line connecting the calcite end member and the high Sr aragonite end member in these figures.

Examination of the scanning electron microscope (SEM) photomicrographs reveals that the only recognizable faunal and floral components, within the mud fraction in Hole 823A (and Hole 819A) periplatform sediments, are disc-shaped coccoliths and occasional immature foraminifers (see Plates 2 and 3). The remainder of the particles consist of unidentifiable equidimensional particles, plates and occasional clusters of laths or needle shaped grains (presumably of carbonate origin). In general, the carbonate needles are 4 to 20 μm in length and display poorly developed or blunt terminations. According to Macintyre and Reid (1992) blunt needles of aragonitic origin are indicative of codiacean algae (i.e., *Halimeda*). However, the concentration of needles in Hole 823A (and Hole 819A) sediments is very low (<1% by volume[2]), in comparison to many Bahamian periplatform sediments (see Lowenstam, 1955, and references therein). The general paucity of carbonate (mainly aragonite?) needles in Queensland margin Hole 823A (and upper-slope Hole 819A) periplatform sediments, however, need not be surprising given the work of Loreau (1982), who calculated that

[2]Based on the assumption that the SEM photomicrographs are representational of the bulk composition of the sample.

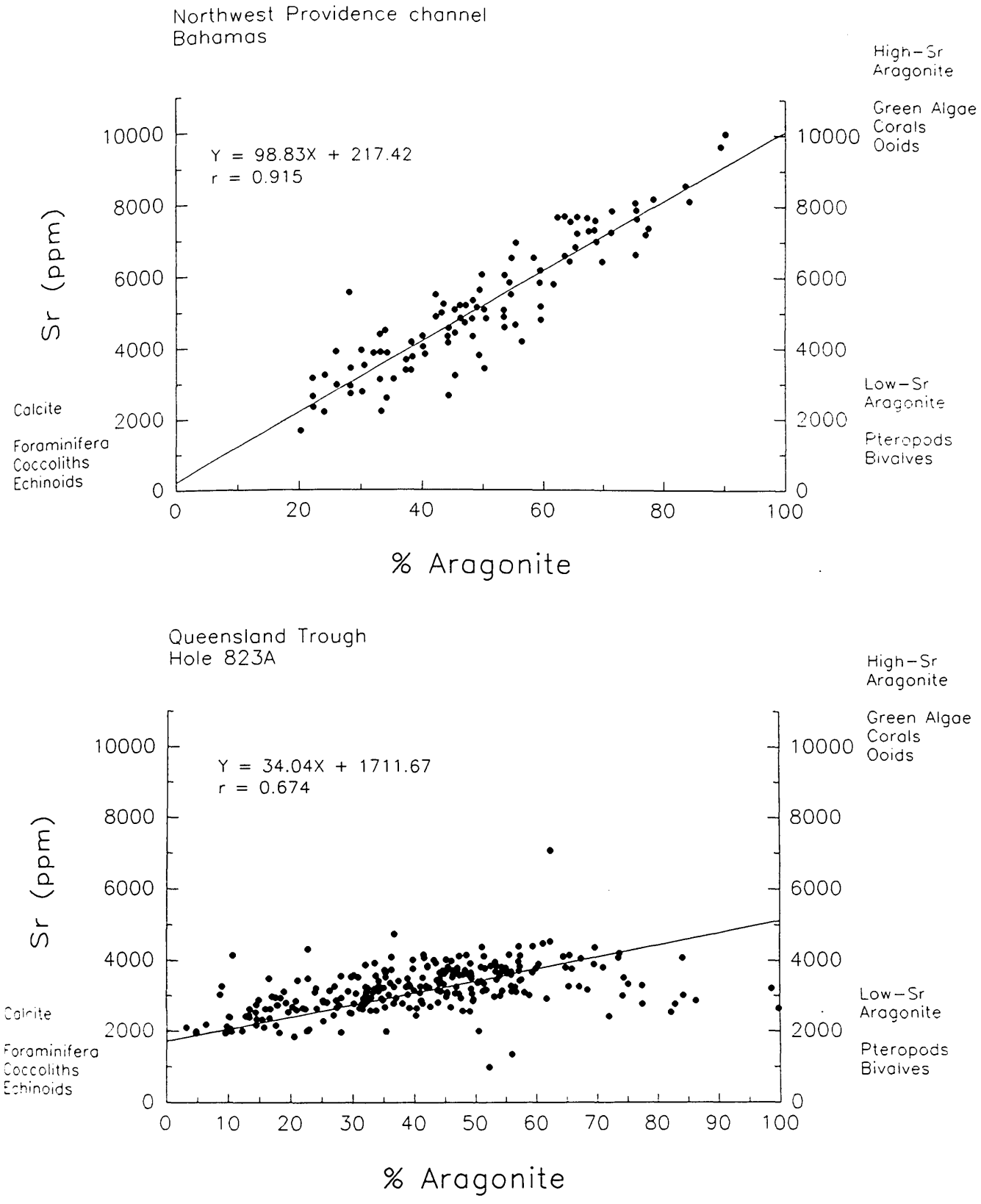

Figure 6.20. Relative proportions of sources of sediments to Hole 823A (Queensland Trough) and Northwest Providence Channel, Bahamas (after Boardman et al., 1986.

only 25-40% of the aragonite normally produced by common calcareous algae occur as laths or needles; the majority typically form clumps of very small crystals or equant nannograins. Thus, many of the 'unknown carbonate grains' seen in Hole 823A (and to a greater extent Hole 819A) periplatform sediments may well represent partly broken or dissaggregated algal material of the like described by Loreau (1982). Plate 12 (Figures A and B) show typical electron (SEM) photomicrographs of carbonate grains of possible calcareous algal origin.

These observations, combined with the Sr and Ca content (and total carbonate) data, tend to confirm the earlier work of Maxwell and Swinchatt (1970) and Tudhope and Scoffin (1988) which suggest that corals reefs generate little mud size debris (i.e., particles <63 μm), and that what little fine grained carbonate material that is produced is quickly extracted from the system via dissolution and/or biological activity (i.e., bioturbation; secretion of calcareous skeletons; etc..). Thus, it seems likely that aragonite in Hole 823A sediments is composed mainly of an admixture of calcareous algal (i.e., *Halimeda*) and molluscan debris (supplemented by minor amounts of pteropod aragonite).

6.5 Conclusions

The geochemical data presented in this chapter provide the strongest evidence of the timing of carbonate platform evolution and the influence of late Pleistocene sea level change on shallow water carbonate production and export. The variation in bank top production and export is exemplified by the ratio Sr/Ca. Using the rationale that high Sr concentrations (and high Sr/Ca ratios) indicate enhanced neritic carbonate content, the excellent correlation between the isotopic signature and Sr/Ca ratios in Hole 823A indicate that highstand shedding (Schlager, 1992: Schlager *et al.*, 1994) has dominated the pattern of carbonate deposition seen in this core. These results confirm earlier conclusions (albeit based on a slightly less convincing data set) that suggest increased bank-top production and export of shallow water carbonate during highstands of sea level in Hole 823A. These results also indicate that variations in late Pleistocene dissolution intensity (within intermediate waters on the Queensland margin), have played a minor role in modulating the pattern of carbonate deposition recorded in these sediments. Furthermore, increased shallow water carbonate production and export during highstands of sea level may have locally reduced the depth of the lysocline, on the Queensland margin, thereby facilitating metastable carbonate preservation.

Analysis of the relationship between Sr and aragonite content demonstrates the complex origins of Hole 823A periplatform sediments. These data indicate that low Sr

A

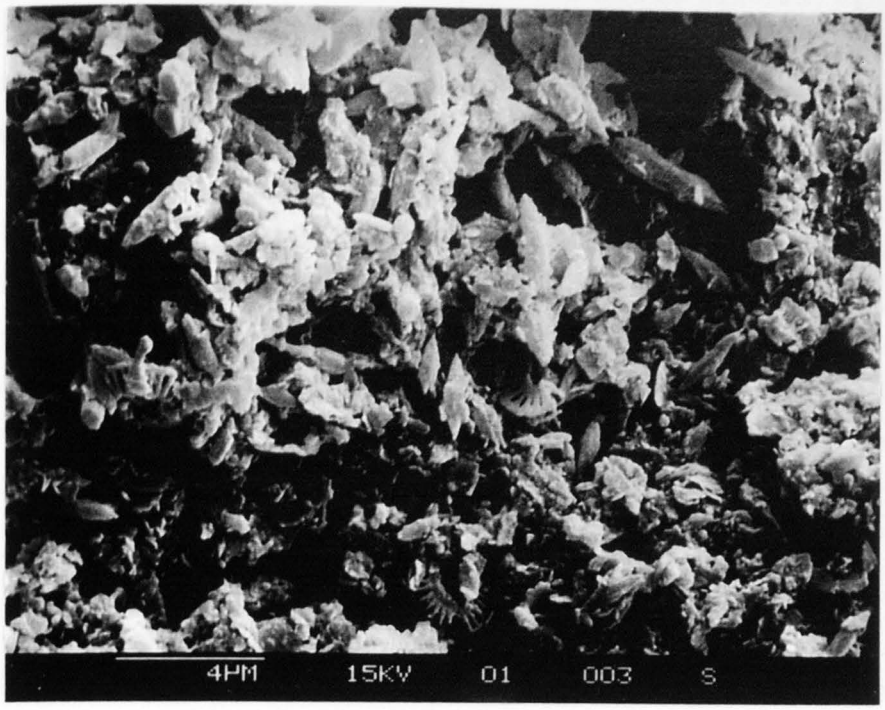

X 4750

B

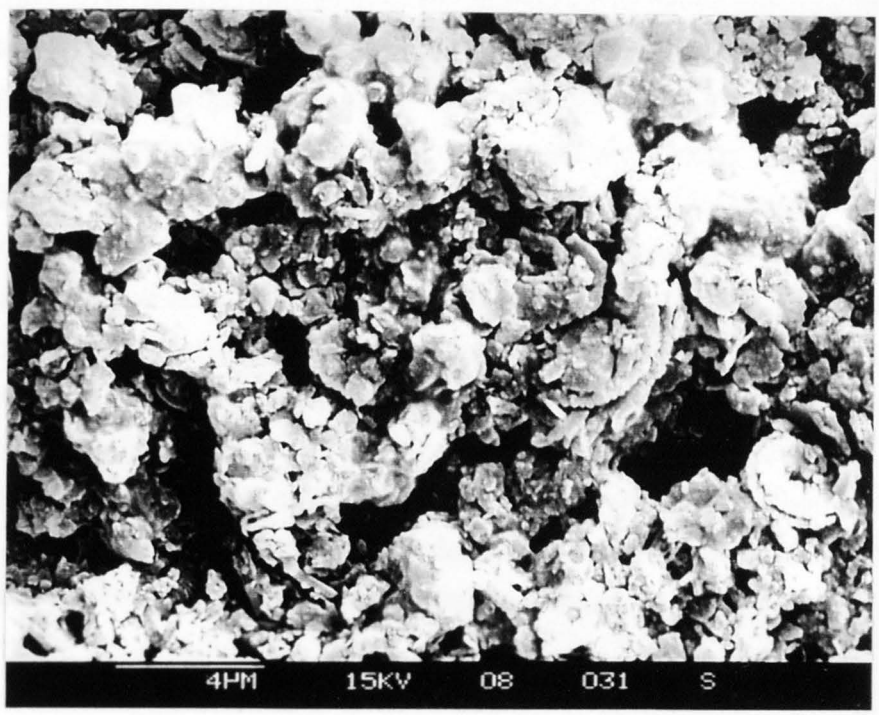

X 4750

Plate 12. Scanning electron micrographs of the mud size fraction of Hole 819A sediments (Sample 133-819A-01H02-68/70 at 2.18 mbsf) showing carbonate grains of possible calcareous algal (i.e., *Halimeda, Penicillus*) origin. (A). Note the general absence of elongate carbonate laths or needles, typical of many modern fine grained (< 63 μm) aragonite-rich sediments (i.e., Bahamas banks- Milliman et al., 1993). (B) clumps of anhedral equant grains or nanograins (Loreau, 1982; MacIntyre and Reid, 1992) of possible calcarous algal origin.

pelagic aragonite (of the type found in pteropods and benthic molluscs) has played a minor role in modulating the pattern of carbonate deposition seen in Hole 823A periplatform sediments. Preliminary SEM analysis of Hole 823A (and Hole 819A) muds suggests that the main contributor to the overall aragonite (and carbonate) signal in these cores has probably been codiacean algae (i.e., *Halimeda, Penicillus*). There is little petrological evidence to suggest that corals have been a major contributor to the overall carbonate budget in Hole 823A (or Hole 819A) periplatform sediments.

The Ba (and Ba/Al) record from Hole 823A is very disappointing in terms of providing evidence of productivity levels during the late Pleistocene. The greatly reduced Ba concentrations (and low Ba/Al ratios) below the zone of sulphate reduction, coinciding with the zone of methanogenesis, attest to the diagenetic remobilization of Ba in Hole 823A sediments. Thus, because of shallow burial diagenesis little of the original ocean fertility signal has survived in Hole 823A, and the Ba records from this core are unfortunately of little palaeoenvironmental value.

The Ti/Al and Cr/Al records (indicators of the proportion of heavy minerals in the non-carbonate fraction- Shimmield and Mowbray, 1991) demonstrate significant variation in the composition of terrigenous material being deposited in the Queensland Trough. Unlike the Ti/Al record, variations in the Cr/Al record are directly linked to sea level (as inferred from the oxygen isotope record). These records suggest that during highstands of sea level the proportion of Cr reaching the Queensland Trough and Hole 823A increases relative to glacial periods, or lowstands of sea level. These variations have been interpreted in terms of increased weathering and transport of Cr bearing material, during periods when the climate was significantly wetter. Periods of heavy (and prolonged) rainfall may have been accompanied by an increase in the intensity (and/or frequency) of cyclones on the northeast Australian margin. Significantly, the Ti/Al ratio record does not show a well defined relationship with sea level. This suggests either differences in source area or subtle differences in the hydrodynamics of Ti and Cr bearing heavy minerals.

Chapter 7 Concluding remarks and considerations

7.1 Introduction

Each of the preceding chapters has sections within it in which the main conclusions of the various investigations are individually presented. This final chapter attempts to summarize the information presented in these chapters and offers some general interpretations of these complex data collected from ODP Leg 133 Hole 819A (upper-slope of the GBR) and Site 823 (Holes 823A and 823B) (Queensland Trough).

7.2 Chronostratigraphy and the stable oxygen isotope records.

As mentioned previously in Chapter 1 (section 1.1), one of the main objectives of this thesis was to evaluate the response of the mixed carbonate-siliciclastic northeast Australian margin, including the Great Barrier Reef, to variations in Late Quaternary sea level and climate change. Crucial to this investigation has been the production of a reliable chronostratigraphy for the marine sequences recovered from Hole 819A and Site 823 (and neighbouring ODP Leg 133 Sites). This has been largely achieved using stable oxygen isotope stratigraphy, coupled with detailed biostratigraphic and magneto-stratigraphic age control. However, this has not been an easy task. Long and frustrating analytical problems arose during analysis of foraminiferal samples (particularly in the upper part of Hole 819A); duplicate and even triplicate analyses had to be run in order to resolve some of the discrepancies. Furthermore, the paucity of suitable benthos (in particular *Cibicidoides spp.*) and the pencontemporaneous redeposition of isotopically lighter foraminiferal specimens from shallower water depths (especially in Hole 823A- Watts *et al.*, 1993) has made the production of reliable benthic oxygen isotope records for Holes 819A and 823A very difficult. Problems with stage recognition and assignment have been further complicated by the presence of authigenic dolomite suggesting that diagenesis and/or dissolution may have affected the primary isotopic signal, in certain core sections (for example, between about 50-60 mbsf (0.87-0.89 Ma) and 60-74 mbsf (0.72 to 0.86 Ma) in Holes 819A and 823A, respectively) (see Figures 5.6 and 5.10).

Age models for the sequences recovered from Holes 819A and 823A have been further refined using correlation of the carbonate content stratigraphies (see section 4.4.3.). This has allowed the accurate positioning of glacial stage 4, particularly in Hole 819A. Furthermore, correlation of the carbonate records in Holes 819A and 823A with adjacent ODP Leg 133 drill sequences suggests that the isotopic stratigraphy presented by Peerdeman *et al.* (1993) for Site 820 is grossly inaccurate, particularly with respect to the identification and positioning of stages 7 to 9, corresponding to a depth interval

between 45 to 75 mbsf (see Figures 3.12 and 3.13). This interval is characterized by significant amounts of dolomite (Shipboard Scientific Party, 1991; Swart *et al.*, 1993). Peerdeman *et al.* (1993) have greatly underestimated the influence of dolomitization and shallow burial diagenesis (Dix and Mullins, 1988) on the stable oxygen isotope records from Holes 820A and 820B. Thus, the age models presented for this core, by these authors, must be regarded with extreme caution.

In Hole 823A, correlation of the downcore variations in the Sr/Ca ratio with the Hole 607A isotopic records of Ruddiman *et al* (1989) has enabled the fine-tuning of the age model[1] presented for the lower part (mid- late Pleistocene) of Hole 823A (see Figures 7.1 and 7.2). In this revised chronology the position of the prominent glacial incursions centred at 82 and 95 mbsf (corresponding to 0.875 and 1.1 Ma, respectively- based on the age model discussed in chapter 3) now become glacial stages 26 and 36, respectively. However, despite the relatively good agreement between the Sr/Ca and the Hole 607A $\delta^{18}O$ records, correlation between the planktic isotopic records from these two cores is far less convincing. Furthermore, this alternative interpretation suggests that the nannofossil datums H.O. *Gephyrocapsa spp.* C-D (80.2 mbsf/ 0.92 Ma), H.O. *Gephyrocapsa spp.* A-B (95.5 mbsf/ 1.10 Ma) and H.O. *Helicosphaera selli* (105.7 mbsf/ 1.27 Ma) (Wei and Gartner, 1993) are all misplaced. Thus, if the nannofossil datums are to be believed, then the age model discussed in chapter 3 still holds. However, if the biostratigraphy is incorrect then the age model based on Sr/Ca ratios may be a valid interpretation of the isotopic record. Clearly, there is no easy solution to stage assignment in the lower part of the record from Hole 823A.

7.3 Sea level and mixed carbonate-siliciclastic sedimentation on the northeast Australian margin since 1.1 Ma

Detailed analysis of the sedimentologic and geochemical results from the upper part of the periplatform sequences from Holes 819A and 823A (corresponding to the Brunhes Chron, 0-650 ka) indicate that highstands of sea level (and during the early regression) are distinguished by high carbonate content (or conversely low acid-insoluble material content). This relationship is particularly well developed in the high resolution Hole 819A periplatform sequence (see Figures 4.26 and 4.33). Analysis of variations in carbonate mineralogy and sediment geochemistry in Queensland margin cores (in particular the periplatform sequence from Hole 823A) indicate that highstands of sea level are distinguished by increased proportions of shallow water platform derived

[1]Amendments to the age model discussed in Chapter 3 for the lower part of the sequence from Hole 823A are given in Appendix A, Table A.9.

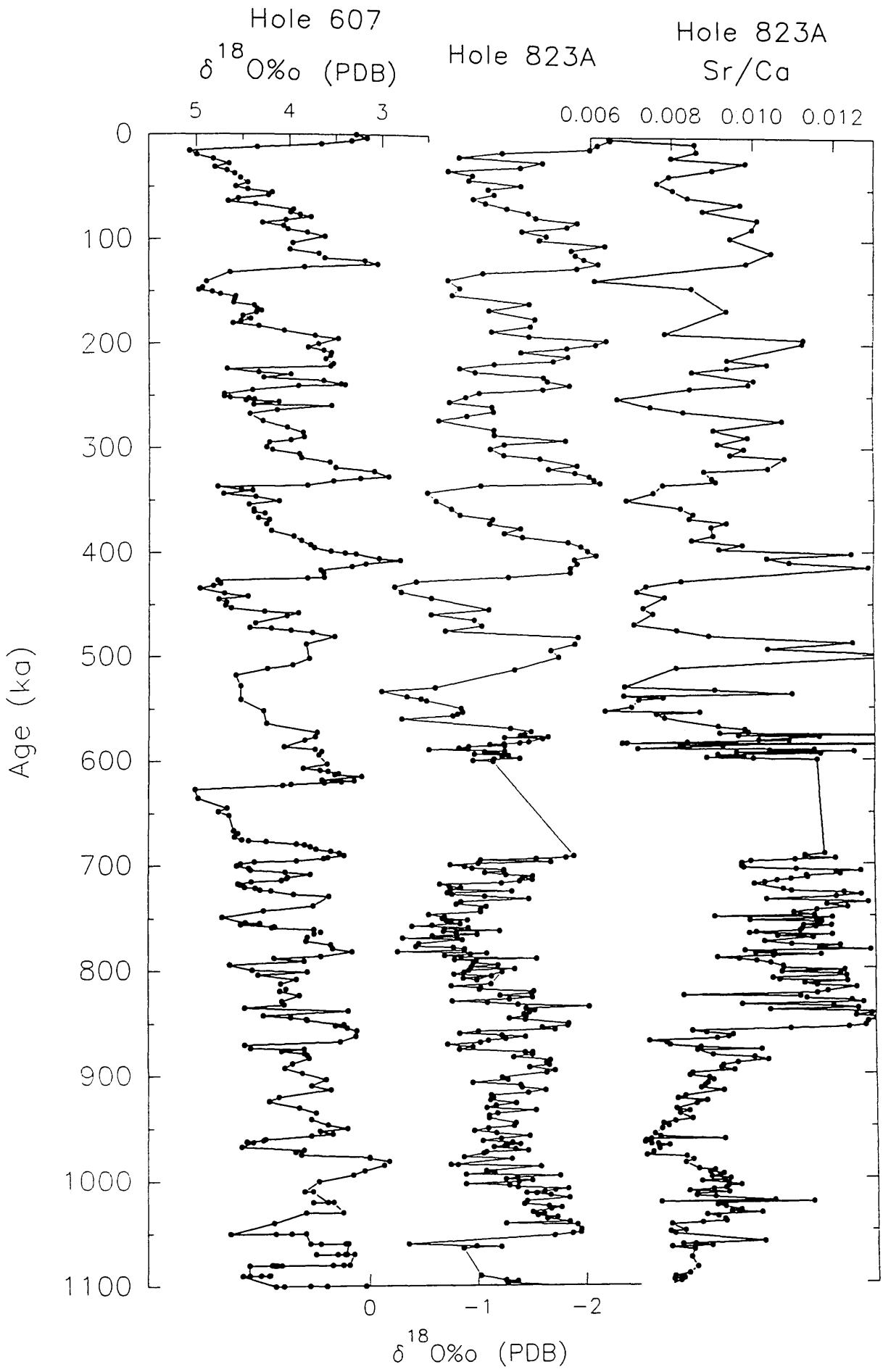

Figure 7.1. Comparison of the isotopic records from Hole 823A and Hole 607 (Ruddiman et al.,1989) with the Sr/Ca ratio record from Hole 823A.

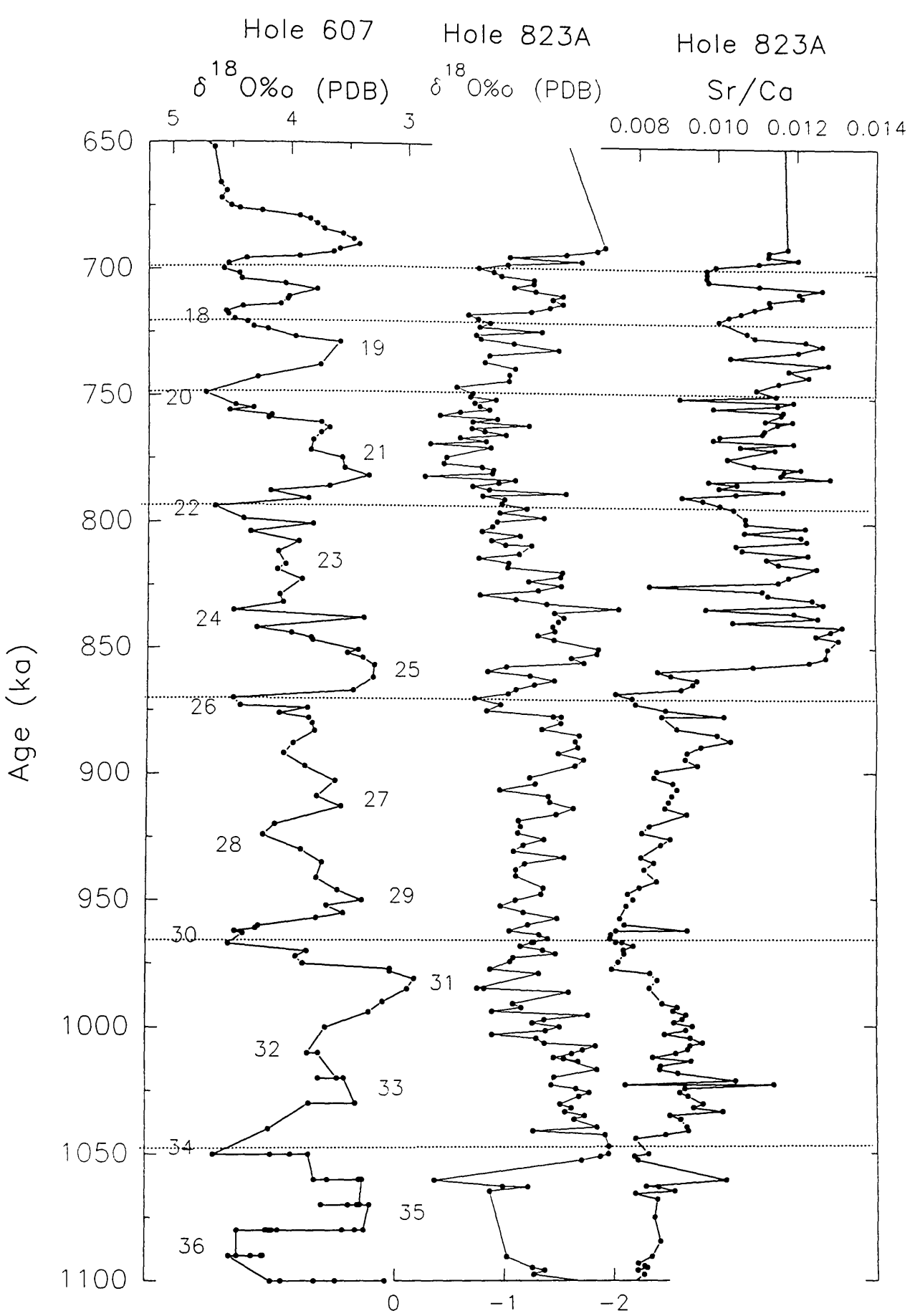

Figure 7.2. Temporal variations in the Sr/Ca record from Hole 823A, plotted alongside the isotopic records from this core and Hole 607 (Ruddiman et al., 1989). Numbers on the left hand plot represent successive oxygen isotope stages.

carbonate material (see Figure 7.3 and 7.4). This general pattern of carbonate deposition is consistent with the 'highstand' shedding scenario outlined by Schlager (1992), Droxler *et al.* (1990), and recently reviewed by Schlager *et al.* (1994).

In contrast, lowstands of sea level (and the early transgression) in Hole 819A (and Hole 823A) periplatform sediments are distinguished by increased input of continental derived terrigenous material (see Figures 7.5 and 7.6). However, unlike the sequence stratigraphic models proposed by Vail *et al.* (1977), which suggest that condensed sequences on continental slopes form during the transgression and that the highest rates of sedimentation occur during lowstands of sea level, glacial periods in Queensland shelf sediments are generally characterized by condensed sequences and/or hiatuses (see Figure 4.34). Thus, the pattern of mixed carbonate-siliciclastic sedimentation on the Queensland shelf, during the Brunhes Chron, is unlike that associated with pure siliciclastic margins.

In the lower part of the records from Holes 819A and 823A (650-1.1 Ma) the pattern of mixed carbonate-siliciclastic deposition, with respect to variations in sea level and climate change is very complex. The good correlation between the occurrence of dolomite and the lack or reduced HMC content in Hole 819A (and Hole 823A) periplatform sediments, coupled with a concomitant increase in LMC content suggest that dolomite formation occurred in response to shallow burial diagenesis and the neomorphism of HMC to LMC (see Dix and Mullins, 1988). Despite a slight diagenetic and/or dissolution overprint, the Sr/Ca record from Hole 823A clearly demonstrate that highstand shedding has been the dominant mechanism behind carbonate cyclicity in Queensland Trough sediments (see Figures 7.3 and 7.4).

Today on the Queensland continental shelf most of the energy is directed across the margin in a shoreward direction (i.e., the prevailing easterly winds tend to direct energy shoreward). This raises the question of explaining the mechanism behind highstand shedding, in which net sediment transport is in a seaward direction. How can off-bank sediment transport overcome the influence of the prevailing wind direction? Is the sediment moved offshore under the influence of tides, or as an undercurrent or undertow below the surface currents as suggested by Wolanski *et al.* (1986)? Only further detailed work on the modern sediment distribution patterns on the Queensland shelf, in particular in the region of the Arlington Reef Complex (see Figure 4.1), can provide the answers to the processes behind off-bank carbonate transport, during highstands of sea level.

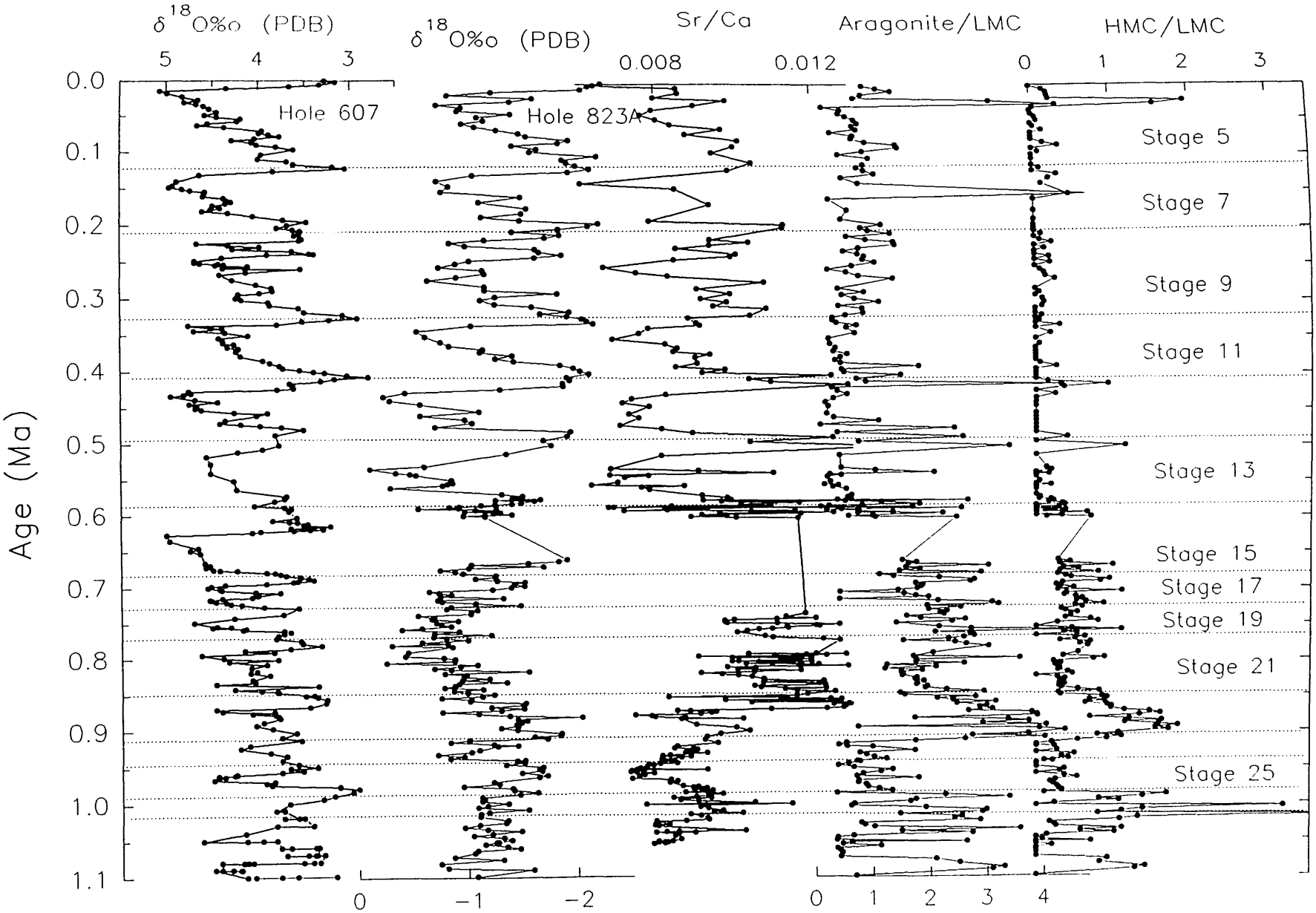

Figure 7.3. Comparison of the $\delta^{18}O$ records from Hole 607A (Ruddiman et al.,1989) and Hole 823A with the Sr/Ca , aragonite/LMC and HMC/LMC records from Hole 823A. Note that in this plot the depth to age conversion has been based on the age models discussed in chapter 3 (section 3.5.2)

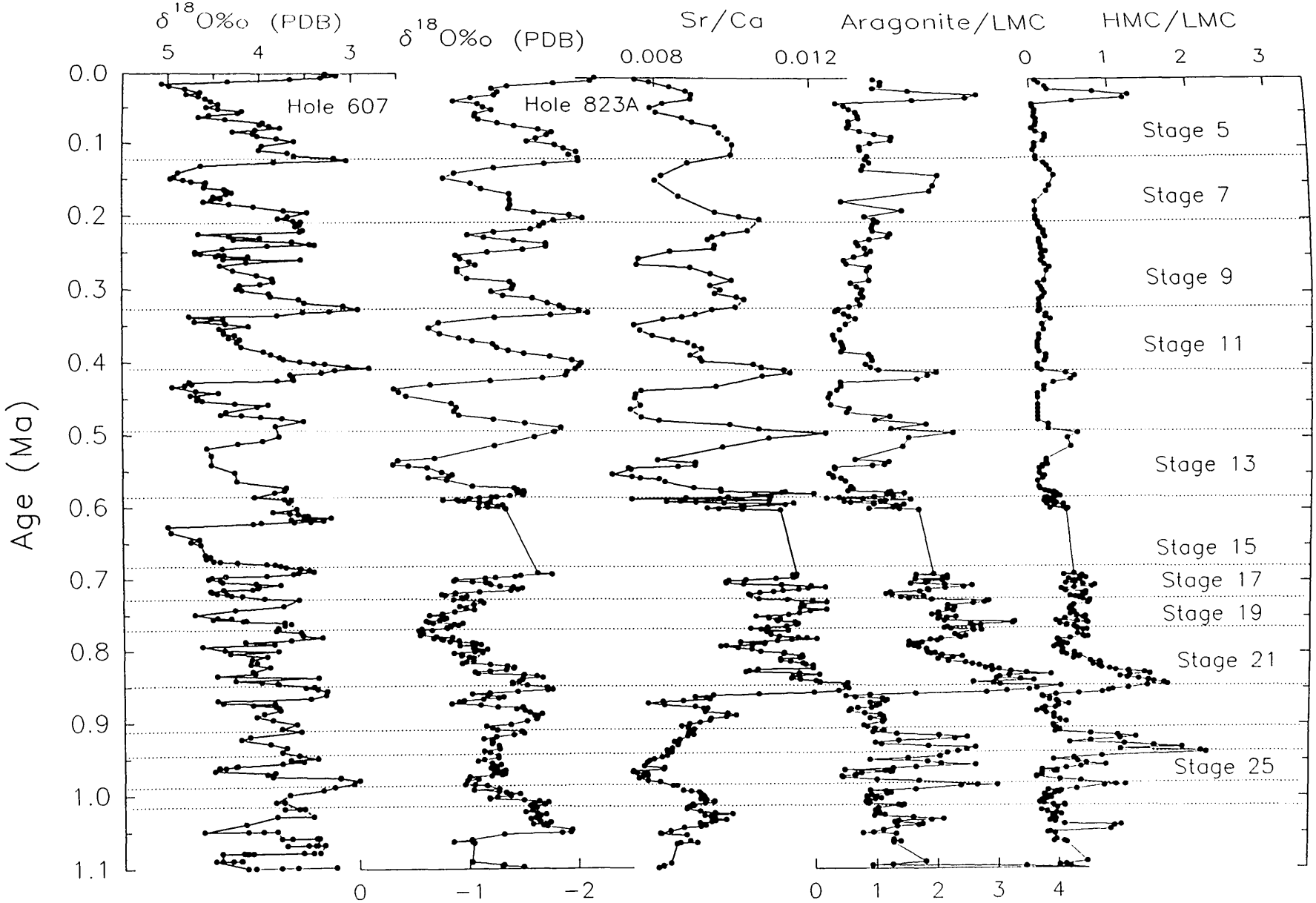

Figure 7.4. Comparison of the $\delta^{18}O$ records from Hole 607A (Ruddiman et al.,1989) and Hole 823A with the Sr/Ca, aragonite/LMC and HMC/LMC records from Hole 823A. Note that in this plot the depth/age coversion has been based on a correlation between the Sr/Ca record and the isotopic signal from Hole 607A (see text text for discussion). Note that the Sr/Ca and carbonate curves have been smoothed using a 3 point average.

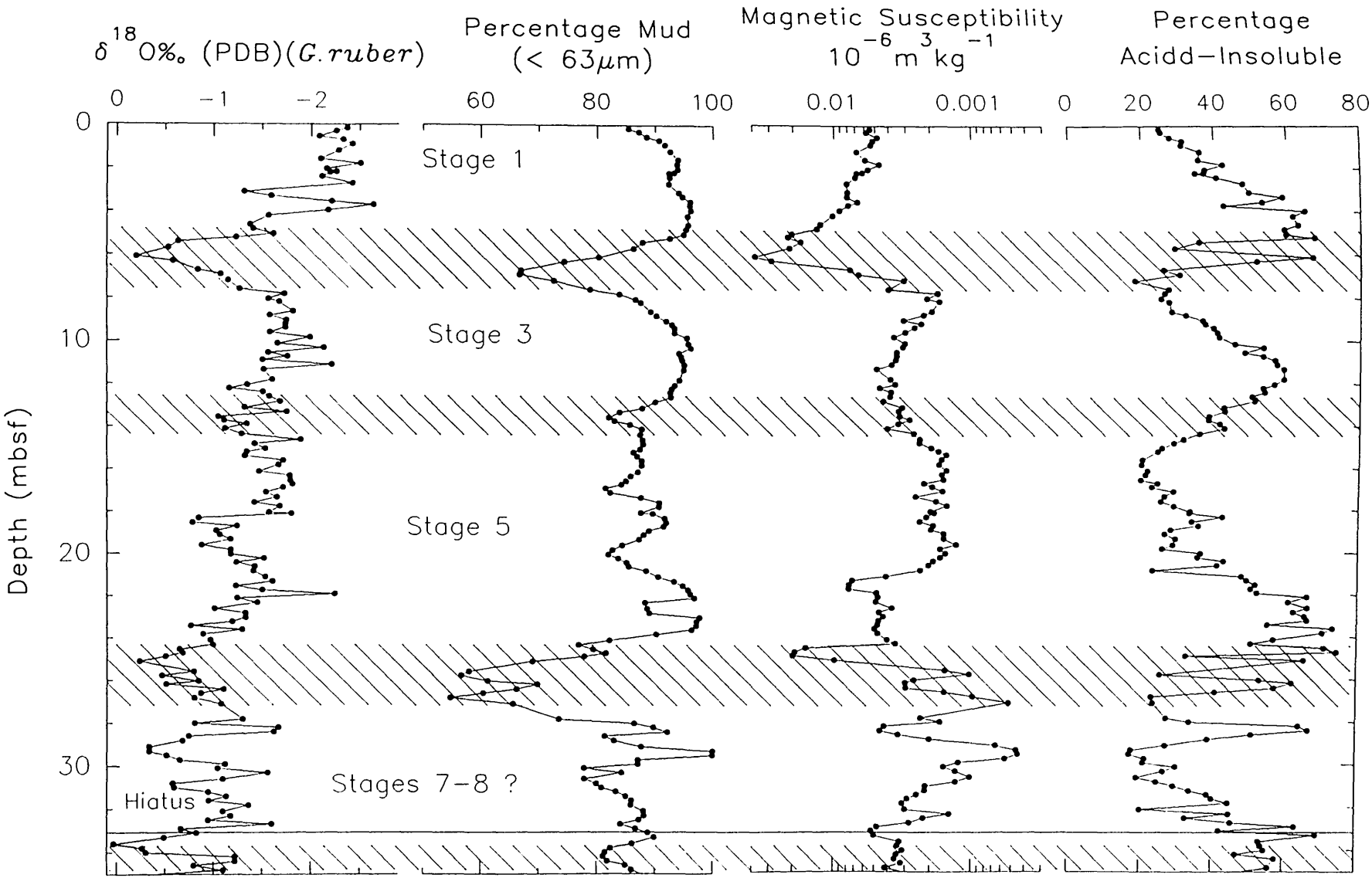

Figure 7.5 Oxygen isotope signal compared to abundance of mud, magnetic susceptibility and acid−insoluble material in Hole 819A. The numbers on the left diagram represent successive oxygen isotope stages.

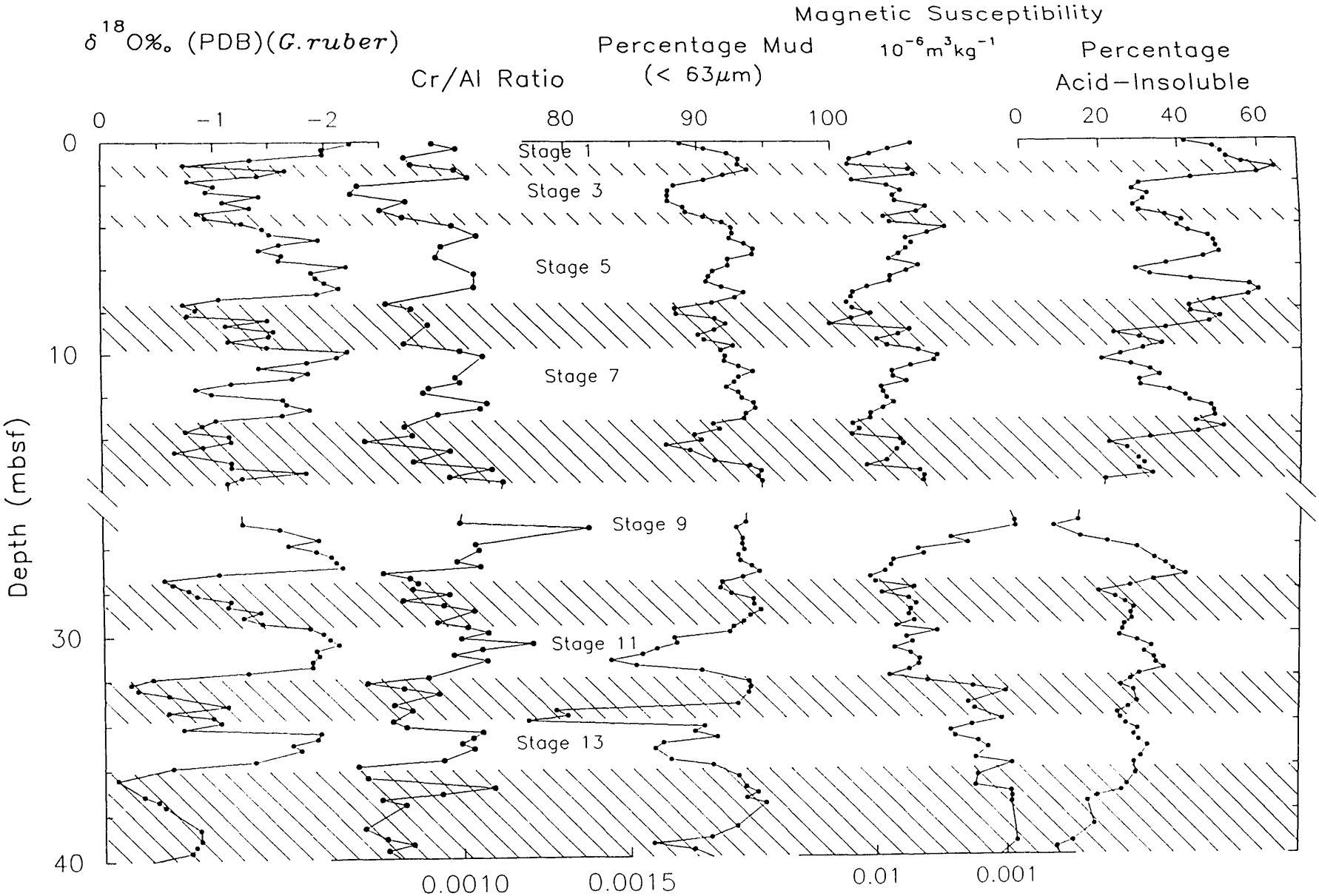

Figure 7.6 Oxygen isotope signal compared to abundance of mud, magnetic susceptibility and non–carbonate content (acid–insolubles) for sediments recovered from Hole 823A. The numbers on the left plot represent successive isotope stages. Note the presence of a haitus between 16.5–24.9 mbsf.

7.4 Long-term (Pliocene- Pleistocene) record of mixed carbonate-siliciclastic deposition on the northeast Australian margin

The record of carbonate deposition in Hole 823B (Queensland Trough basin) demonstrate that sedimentation on the northeast Australian margin was intimately linked to sea level and/or palaeotemperature during the Pliocene- Pleistocene. Detailed mineralogical (XRD) analysis of Hole 823B pelagic to hemipelagic sediments suggest that prior to about 3.4 Ma (Late Pliocene), carbonate deposition in this core was dominated by pelagic/planktonic carbonate material. However, since about 3.2 Ma, carbonate sediments in Hole 823B are characterized by a mixture of both pelagic and shallow water/neritic carbonate material. The onset of significant shallow water carbonate deposition in Hole 823B, between 3.2-3.4 Ma, coincides with a stepwise deterioration in the global climate at about this time (Jansen *et al.*, 1993), culminating with the onset of major northern hemisphere glaciation at about 2.4 Ma (Shackleton and Opdyke, 1984).

Throughout the late Pliocene to early Pleistocene the records from Hole 823B, show good correlation between aragonite (and HMC) content and the $CaCO_3$ preservation records of Farrell and Prell (1989; 1991); inasmuch, as aragonite content is generally high during periods of enhanced preservation (conversely, aragonite content is low during intervals of inferred poor carbonate preservation) (see Figures 5.45 and 5.46). This suggests that dissolution has played a more important role in determining the style of carbonate deposition seen in Hole 823B, than shallow water carbonate productivity and input. In contrast, the records from Hole 823A (and Hole 819A) show that during the late Pleistocene input has been the dominant mechanism behind carbonate cyclicity in this core (see Figure 5.40 and 5.41). It is unclear whether the switch between mainly dissolution controlled and input dominated carbonate deposition at Site 823 was abrupt or gradational. Furthermore, the exact timing of the change in depositional style between the lower part of Hole 823A and the upper portion of Hole 823B is difficult to determine. Uncertainties associated with the age models proposed for these two holes have precluded the precise dating of this feature (see Chapter 3 and section 7.2). Nonetheless, comparison of the long-term (Pliocene- Pleistocene) aragonite records from Site 823, with the preservation curves of Farrell and Prell (1991) suggest that a significant change in the relationship between these two parameters may have occurred between about 62 to 72 mbsf (corresponding to an approximate age of between 0.75 to 0.80 Ma) (see Figure 7.7). Alternatively, analysis by Kroon and Alexander (in press) suggest that the switch from mainly dissolution controlled to input dominated carbonate deposition at Site 823 may have occurred as late as 0.85 Ma (based on a correlation of the Hole 823A Sr/Ca records with the North Atlantic ODP

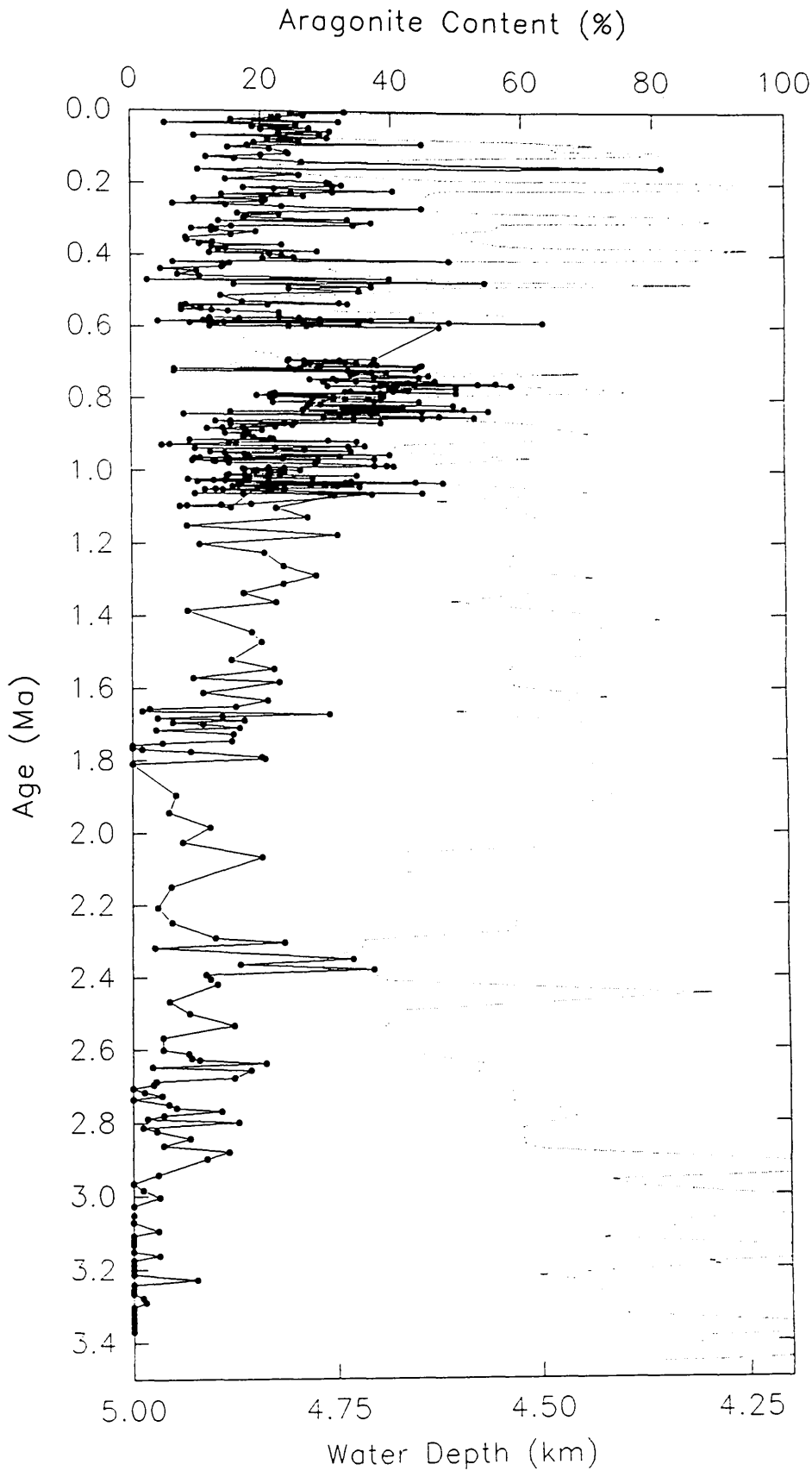

Figure 7.7. Temporal variations in the aragonite content in Site 823 (Holes 823A/B– Queensland Trough) plotted against depth and alongside the carbonate preservation record of Farrell and Prell (1991)(dotted line). Increasing $CaCO_3$ preservation is toward the left of the plot.

Hole 607 isotope stratigraphy provided by Ruddiman *et al.* (1989) (see above). However, further work is required to substantiate the exact timing of the change in dominant depositional style between these two cores.

A similar pattern of carbonate deposition to that seen in Hole 823B has been reported for periplatform sediments recovered from the flanks of the Queensland Plateau by Droxler *et al.* (1993). These authors suggest that the first appearance of aragonite in Hole 818B and 817A, at about 2.9 Ma, was related to the re-entry of parts of the Queensland Plateau into the photic zone, following a period of extensive platform drowning. The carbonate results from Hole 823B appear consistent with this interpretation, however, the precise influence of variations in palaeotemperature (see Isern *et al.*, 1993) on reef growth and development during this period remain uncertain. Droxler *et al.* (1993) propose that the Pliocene- Pleistocene carbonate records from the Queensland Plateau (Holes 817A and 818B) provide an example of lowstand shedding, unlike anything previously described for the marine record. These records, however, may have been entirely controlled by preservation. Only further work on the effects of variations in water column chemistry and palaeotemperature can provide the answers to the significance of the abrupt increase in aragonite content in Queensland margin sediments at about 0.85 Ma.

7.5 The origins and timing of the initiation of the Great Barrier Reef

There has been considerable scientific debate over the last two decades concerning the age and evolutionary development of the Great Barrier Reef (Symonds *et al.*, 1983; Davies *et al.*, 1988; Davies *et al.*, 1991; Davies and McKenzie, 1993; Feary *et al.*, 1993; Peerdeman and Davies, 1993; Montaggioni and Venec-Peyré, 1993). Early ideas based on oil company exploration and drilling in the northern and southern GBR province, suggested that the GBR may be 15 to 20 Ma old. During the early to mid-1980s, studies by the Australian Geological Survey Organization (formerly the Bureau of Mineral Resources- BMR) and the Bundesanstalt für Geowissenschaften und Rohstoffe (BGR) proposed that the reef was much younger- probably less than 3.5 Ma (Symmonds *et al.*, 1983; Davies *et al.*, 1988). More recently, Davies *et al.* (1991) suggested that a very young age for the Central GBR is supported by two lines of evidence: (1) dated seismic reflectors traceable beneath the reef and (2) the presence of reef-derived sediments only in the upper part of the section at ODP Leg 133 Hole 821A (outer-shelf/ upper-slope of the GBR). On the basis of these observations, these authors concluded that the central GBR may be between 500,000 to 900,000 yr. old (Davies *et al.*, 1991).

Studies by Peerdeman *et al.* (1993) suggest that a fundamental change in amplitude and frequency of the stable oxygen isotope signal in Hole 820A (outer-shelf/ upper-slope of the GBR), corresponding to a significant shift in seawater temperature (in the order of about 3-5 °C), coupled with a marked change in depositional style, at about 80 mbsf (~ 400 ka) may be related to the initiation of the GBR (see Figure 4.23). Peerdeman *et al.* (1993) conclude that the age of the GBR may be about 500,000 yr., or slightly younger. However, this date must be regarded with caution. Interpretation of the carbonate content record from Site 820 shows that a significant change in the frequency of the record occurs slightly earlier than the age proposed by Peerdeman *et al.* (1993), at about 0.42 Ma (corresponding to a depth of about 95 mbsf) (see Figure 4.23). Furthermore, the lack of agreement between the age models proposed for Site 820 (Peerdeman *et al.*, 1993) and stratigraphies suggested for Hole 819A and Hole 823A (this study), demonstrate that the oxygen isotope stratigraphies proposed by Peerdeman *et al.* (1993) are incorrect. Shallow burial diagenesis (Dix and Mullins, 1988), coupled with extensive dolomitization (particularly between 81.1 and 246 mbsf) in Hole 820A (Shipboard Scientific Party, 1991; Swart, 1993), is thought to have greatly altered the primary isotopic signature in this core, making accurate stage recognition and dating extremely speculative.

Feary *et al.* (1993) suggest that a fundamental change in the style of seismic sequence geometry, from mainly progradational to aggradational seismic sequence geometrys in Leg 133 Sites 819, 820 and 821 (Queensland shelf), indicates the initiation of extensive reef growth on the Queensland margin, at approximately 0.75 to 1.0 Ma. These authors suggest that significant reef development on the Queensland margin restricted sediment supply to the outer shelf and resulted in two fundamentally different types of seismic sequence geometry. However, the Cr/Al record from Hole 823A shows little evidence of a significant change in depositional style during this interval (0.75-1.0 Ma), and provides no indication of the existence of a significant barrier to sediment movement across the continental shelf during this period.

Unfortunately, the records from Hole 819A and Hole 823A provide little conclusive proof of the age of the GBR. A prominent increase in aragonite content in Hole 823A periplatform sediments at about 0.9 Ma is thought to be related to a rapid and major deepening of the calcite lysocline between 0.85 and 0.9 Ma (Farrell and Prell, 1989, 1991). A similar feature is also seen in the aragonite records from Hole 818B (Haddad *et al.*, 1993). This feature is not so well developed in the records from Hole 819A suggesting that it may represent an intermediate water phenomenon. Furthermore, an abrupt increase in aragonite content in these cores need not necessarily indicate an

increase in reefal buildup. An abrupt increase in aragonite content in periplatform sediments at this time may have been controlled by the development of extensive algal meadows (i.e., *Halimeda, Penicillus*) and banks (Davies and Marshall, 1985) on the Queensland continental shelf and on Queensland Plateau. Significantly, calcareous green algae are capable of producing significant amounts of skeletal carbonate material (Tucker and Wright, 1990), and are able to tolerate environmental conditions generally unsuitable for reef development. Thus, the prominent kick in the aragonite records at about 0.85 Ma may be related to enhanced algal production.

Despite the lack of any conclusive evidence for the timing of the GBR, in the records from Holes 819A and 823A, it seems likely that extensive reef development on the Queensland shelf was linked to a fundamental change in the frequency of isotopic variation seen in many marine sequences during the middle to late Pleistocene (Imbrie 1985; Ruddiman, 1986; 1989; Prell, 1992). The magnitude of sea level change associated with the 100 ka eccentricity cycles (i.e., in the order of ±120 m- Harris *et al.*, 1990), over the last 700 ka (late Pleistocene- Recent), may have completely flooded the continental shelf, thereby providing an extensive area suitable for the development of frame-building reefs. Furthermore, the duration of the eccentricity cycles may have allowed sufficient time for back-reef/ lagoonal basins to fill, on the continental shelf, and a state of carbonate overproduction (and hence export) to be reached. Prior to this period, the magnitude of sea level change associated with the 40 ka tilt cycles (±60-80 m- Harris *et al.*, 1990) may have been insufficient to allow the complete flooding of the Queensland shelf, and the development of extensive carbonate buildups and reefs. Furthermore, the shorter duration of the 40 ka Milankovitch cycles may have prevented a state of carbonate overproduction being reached. Thus, during the mid- late Pleistocene most of the carbonate material produced on the Queensland margin, during highstands of sea level, was easily accommodated on the shelf, and there was comparatively little off-bank transport.

7.6 Model of mixed carbonate-siliciclastic deposition on the Queensland shelf.

From the observations noted above (and from previous chapters) a model of mixed carbonate-siliciclastic deposition on the Queensland shelf during the late Pleistocene has been made, this is described in the following section. In the model presented five different phases of sea level change (corresponding to a typical glacial/ interglacial cycle) are used to explain the pattern of sedimentation, over the last two main glacial/ interglacial cycles, on the northeast Australian margin, as evidenced from Holes 819A and 823A. A graphic representation of this model is presented in Figure 7.8.

1. Highstand (and/ or Stillstand)

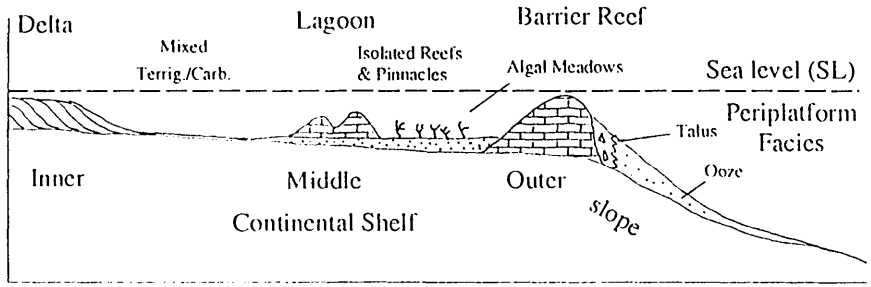

Extensive off-bank transport of shallow-water carbonate material occurs through gaps and passages between the outer reefs. Fluvial input to the upper slope is reduced. Infrequent cyclones and heavy rainfall transport fine grained terrigenous sediments (rich in heavy minerals) across the shelf and into the adjacent deep basins. Bacterial magnetite accumulates in back-reef lagoons.

2. Early Regression

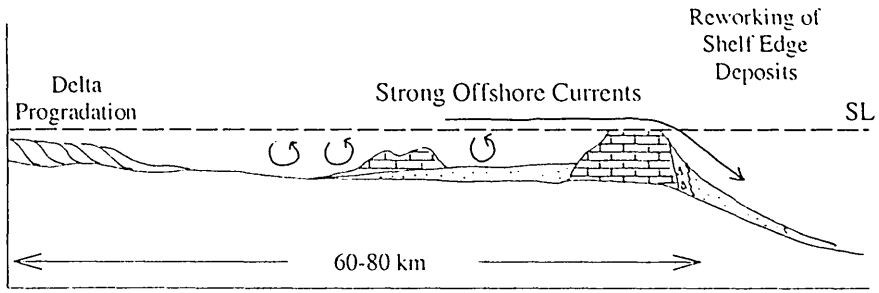

During falling sea level, currents across the continental shelf become stronger (possibly enhanced by tides) and active erosion of reefal and inter-reefal sediments occurs, leading to increased off-bank transport of carbonate clastics.

3. Lowstand (Glacial Stillstand)

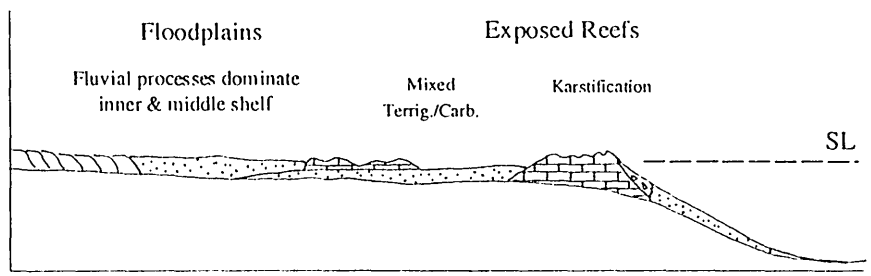

Greater influence of pelagic carbonate on sediments accumulating on the outer-shelf/ upper-slope. Exposed limestones on the shelf are incised and eroded by fluvial processes. Coarse grained siliciclastic sediments are trapped on the inner and middle shelf.

4. Early to Late Transgression

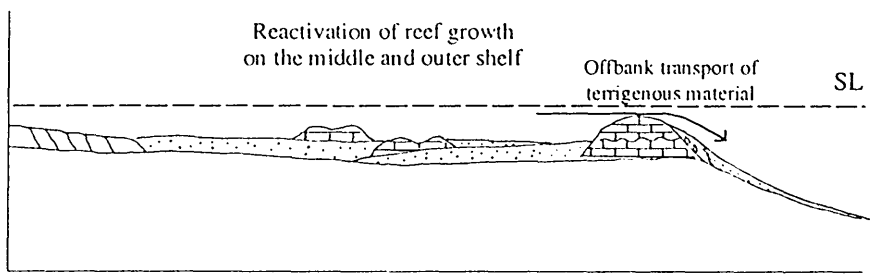

Sea level rises and encroaches onto the continental shelf. Terrigenous material, previously locked behind the outer reefs is reworked and transported off-bank. With increasing water depth limestones are submerged and shallow water carbonate production and export resumes.

Figure 7.8. Schematic diagram illustrating the influence of sea level and climate change on upper-slope/ outer-shelf sedimentation, over the last two main glacial/interglacial cycles, offshore Cairns (Queensland margin). Diagrams not drawn to scale.

- Sea level highstand (and/or stillstand).

During highstands of sea level (i.e., in the order of <120 m, Harris *et al.*, 1990), the Queensland continental shelf is completely flooded and active reef growth occurs on the margin (particularly on the outer shelf). During this period shallow water carbonate sediments are typically deposited between carbonate buildups and reefs, and in back-reef lagoons on the middle and outer shelf. However, continental shelf basins rapidly fill and excess carbonate material becomes subject to reworking and transportation across the shelf, ultimately reaching the outer-shelf/ upper-slope (although the exact mechanism behind sediment transportation remains unclear). Terrigenous material is largely restricted to the nearshore and inner shelf area, however, increased precipitation during interglacial periods, possibly associated with an increase in the frequency (and intensity) of cyclonic winds (seasonal northwest monsoon), enable the periodic transport of Cr bearing heavy minerals across the shelf toward the outer shelf, and onto the upper-slope.

- Early Regression.

As sea level begins to fall the wave base drops and active scouring of the highstand shelf sediments occurs, leading to the offbank transport of carbonate rich material. With a further decrease in sea level, carbonate sediments deposited on the outer-shelf/ upper-slope gradually become less under the influence of bank-top derived material and start to develop a more a pelagic/planktonic character. Carbonate sedimentation during this interval may have been supplemented by the reworking of previous highstand carbonate deposits ('downturn shedding') in a manner outlined by Shanmugam and Moiola (1984). This process may have been facilitated by a general lowering of wave base on the continental shelf.

- Lowstand (glacial stillstand).

During lowstands of sea level (to -120 m, Harris *et al.*, 1990), the Queensland continental shelf is exposed. Previous highstand deposits are subject to exposure and karstification. On the shelf, previous shallow water carbonate deposits are incised and eroded by fluvial processes. Terrigenous sedimentation on the continental slope during lowstands of sea level probably occurred through terrigenous point sources, such as the Barron river (although some material may have come from relic deposits on the shelf). Terrigenous debris (rich in magnetic material) is transported across the shelf, via incised rivers toward the middle and outer shelf. Some of this material reaches the upper slope (and deep sea basins), upon which it is mixed with carbonate material of a more pelagic nature. However, a significant proportion of the terrigenous material is locked behind the former highstand carbonate reefs and buildups.

- Early to late Transgression.

During the early transgression sea level rises and encroaching onto the continental shelf, flooding excavated river channels and producing an indented coastline of alternating promontories and estuaries with numerous offshore islands. Terrigenous material, previously locked up on the shelf, behind the outer or barrier reefs, becomes mobilized and is moved seaward possibly aided by strong tides. With continued sea level rise reef growth on the platform is reactivated, and carbonate sediments accumulate on the shelf. These sediments dilute out any terrigenous material reaching the middle to outer shelf, and trap previous lowstand deposits under a thin veneer of shallow water carbonate.

7.7 Suggested Future Work

Despite a detailed examination of various sedimentological and geochemical aspects of late Pleistocene sedimentation on the northeast Australian margin, several important questions still remain as to the influence of sea level and climate change on mixed carbonate-siliciclastic. For example, what combination of late Pleistocene palaeoenvironmental parameters led to the initiation of significant reef development on the Queensland shelf, and when did the GBR come into existence ?

The following could be studied in the future in order to expand on the hypotheses presented in this work and/or determine the exact cause of various geochemical/ physical sediment relationships.

1) A more detailed examination of pteropod abundances (including fragmentation records), in both Holes 819A and 823A, may provide further information about variations in Late Quaternary intermediate (and shallow) water chemistry. These data would allow a more accurate appraisal of variations in dissolution intensity, and the effects of pelagic productivity on the records from Hole 819A and Hole 823A.

2) Analysis of foraminiferal assemblages in Hole 823A sediments may provide a detailed record of variations in palaeotemperature during the Late Quaternary. These studies would help to establish whether the shift in palaeotemperature proposed by Isern *et al.* (1993), between about 0.6 and 0.8 Ma, is genuine or merely a function of the diagenetic overprinting of the Queensland margin isotopic records.

3) High resolution geochemical analysis of Queensland shelf sediments (Sites 819/ 820 and 821) may help to establish Queensland continental shelf-to-basin geochemical gradients. These may provide further evidence of climatic variations during the Late

Pleistocene, and the transport of terrigenous material across the continental margin. Furthermore, geochemical data (in particular Sr/Ca ratios) may confirm the timing of shallow water carbonate production and export relative to sea level.

4) As mentioned earlier (section 4.4.3.), ODP Leg 133 Hole 821A (the shallowest of the Queensland margin transect sites) is characterized by a well defined carbonate content stratigraphy. However, the derivation of a reliable isotopic signature for this hole has been hindered by diagenesis. As we have demonstrated carbonate content can act as an accurate proxy for sea level Therefore it is intended that a high resolution analysis of Hole 821A samples be conducted in order to examine the influence of sea level on shallow water carbonate production and export on the Queensland margin.

5) In this study, samples from Hole 823A were typically analysed every 25 cm, so there is considerable scope for improving the resolution in this core. Given the well defined nature of the isotopic record from this core (in particular stages 1 to 15, see Figure 3.2), a more detailed examination of Hole 823A sediments may provide a greater understanding of the timing of carbonate and siliciclastic deposition, relative to sea level. Furthermore, detailed isotopic and sedimentologic/ geochemical analyses of this core may serve to extend our current understanding of the complex depositional processes occurring on the northeast Australian margin during the Late Quaternary.

Finally, an international consortium[2] (Australia, UK, Japan, France, Spain, Switzerland and Germany) of marine scientists has just returned (August 1995) to the Queensland margin, and the GBR, to continue the work initiated during Ocean Drilling Program Leg 133. The intention of this group is to drill six holes through the shelf of the GBR, on a transect between Cairns and Grafton Passage (see Figures 1.3 and 2.1), enabling a unique shelf to the deep sea basin (ODP Leg 133) transect to be completed. These new boreholes were chosen in order to further evaluate the age, origin and evolution of the GBR in relation to Late Quaternary sea level and palaeoenvironmental change. Drilling is now drawing to a close and preliminary results look very encouraging (Dick Kroon, pers. comm.). The findings from Hole 819A and Site 823 (this study) will provide an invaluable framework against which the results from this latest phase of drilling can be assimilated. Combining these data will enable a greater understanding of the mechanisms behind sedimentation on mixed carbonate-siliciclastic margins, and may provide the answers to the origin and timing of the GBR.

---

[2]The international consortium is organized through a Management Committee (Dick Kroon is the U.K representative) which will run the drilling programme and arrange core curation and sampling.

REFERENCES [1]

[1] Abbreviations for names and organizations and publications follow the style given in *Chemical Abstracts Service Source Index* (published by American Chemical Society).

Adelseck, C.G. Jr. and Anderson, T.F., (1978). The late Pleistocene record of productivity fluctuations in the eastern equatorial Pacific ocean. *Geology*, 6: 388-391.

Agrawal, Y.C., McCave, I.N. and Riley, J.B., (1991). Laser diffraction size analysis. In: Syvitski, J.P.M. (Ed.). *Principles, Methods and Application of Particle Size Analysis*, Cambridge Univ. Press, 119-128.

Aharon, P. and Chappell, J., (1983). Carbon and Oxygen Isotope Probes of Reef Environment Histories. In: Barnes, D.J. (ed.). *Perspectives on coral reefs*, Australian Institute of Marine Science, Brian Clouston Publisher, Australia, 1-10.

Ahrens, L.H., (1952). The use of ionization potentials. Part 1. Ionic radii of the elements. *Geochim. Cosmochim. Acta*, 2: 155-169.

Alexander, I.T., Kroon, D. and Thompson, R., (1993). Late Quaternary paleoenvironmental change on the northeast Australian margin as evidenced in oxygen isotope stratigraphy, mineral magnetism, and sedimentology. In: McKenzie, J.A., Davies, P.J., Palmer-Julson, A., et al., *Proc. ODP, Sci. Results*, 133: College Station, TX (Ocean Drilling Program), 129-162.

Andrews, J.C., (1983). Thermal waves on the Queensland shelf. *Aust. J. Mar. Freshw. Res.*, 34: 81-96.

Andrews, J.C. and Gentien, P., (1982). Upwelling as a source of nutrients for the Great Barrier Reef ecosystems: a solution to Darwins question ? *Mar. Ecol. Prog. Ser.*, 8: 257-269.

Andrews, J.C. and Clegg, S., (1989). Coral Sea circulation and transport deduced from modal information models. *Deep-Sea Res.*, 36(6): 957-974.

Angino, E.E. and Andrews, R.S., (1968). Trace element chemistry, heavy minerals, and sediment statistics of Weddell Sea sediments. *J. Sediment. Petrol.*, 38: 634-642.

Archer, D., (1969). *X-ray Analysis of Deep-Sea Sediments*. Unpubld. Ph.D. Thesis, University of Manchester, 108 p.

Archer, D.M., Lyle, M., Rodgers, K. and Froelich, P., (1993). What controls opal preservation in Tropical deep-sea sediments ? *Paleoceanography*, 8: 7-21.

Arrhenius, G.O.S., (1952). Sediment cores from the east Pacific. *Rep. Swed. Deep Sea Exped, 1947-1948*, 5: 228 p.

Arrhenius, G.O.S., (1988). Rate of production, dissolution and accumulation of biogenic solids in the oceans. *Palaeogeogr. Palaeoclimatol. Palaeoecol.*, 67: 119-146.

Baker, P.A., Gieskes, J.M. and Elderfield, H., (1982). Diagenesis of carbonates in deep-sea sediments: evidence from Sr^{2+}/Ca^{2+} ratios and interstitial dissolved Sr^{2+} data. *J. Sediment. Petrol.*, 52: 71-82.

Barton, C.E., Lackie, M. and Peerdeman, F.M., (1993a). Environmental controls of magnetic properties of upper slope sediments near the Great Barrier Reef: results from Leg 133, Site 820. In: McKenzie, J.A., Davies, P.J., Palmer-Julson, A., et al., *Proc. ODP, Sci. Results*, 133: College Station, TX (Ocean Drilling Program), 543-562.

Barton, C.E., Omarzai, S.K., Alexander, I., Peerdeman, F. and McNeill, D., (1993). Magnetic stratigraphy and characterization of sediments from the northeast margin of Australia and their relationship to environmental change during the Quaternary. In: McKenzie, J.A., Davies, P.J., Palmer-Julson, A., et al., *Proc. ODP, Sci. Results*, 133: College Station, TX (Ocean Drilling Program), 749-754.

Bathurst, R.C.G., (1975). *Carbonate Sediments and their Diagenesis*. New York, Elsevier, 658 p.

Beget, J.E., Stone, D.B. and Hawkins, D.B., (1990). Paleoclimatic forcing of magnetic susceptibility variations in Alaskan loess during the late Quaternary. *Geology*, 18: 40-43.

Beiersdorf, H., (1989). Provenance and accumulation rates of Pliocene and Quaternary sediments from the western Coral Sea. *Geologischau Rundschau*, 78(3): 987-998.

Belperio, A.P., (1983a). Terrigenous sedimentation in the central Great Barrier Reef Lagoon; a model from the Burdekin region. *BMR Jour. Aust. Geol. and Geophys.*, 8: 179-190.

Belperio, A.P., (1983b). Late Quaternary terrigenous sedimentation in the Great Barrier Reef Lagoon. In: Baker, J.T., Carter, R.M., Sammarco, P.W. and Stark, K.P., (Eds.). *Proc. Inaugural Great Barrier Reef Conf.*, Townsville, Queensland, JCU Press, 71-76.

Belperio, A.P. and Searle, D.E., (1988). Terrigenous and carbonate sedimentation in the Great

Barrier Reef Province. In: Doyle, L.J. and Roberts, H.H. (Eds). *Carbonate-Clastic Transitions*. Elsevier, Developments in Sedimentology, (42): 143-174.

Bennett, I., (1971). *The Great Barrier Reef*. Lansdowne, Melbourne, 183 p.

Berger, W.H., (1968). Planktonic foraminifera: Selective solution and paleoclimatic interpretation. *Deep-Sea Res.*, 15: 31-43.

Berger, W.H., (1970). Planktonic Foraminifera: Selective solution and the lysocline. *Mar. Geol.*, 8: 111-138.

Berger, W.H., (1973). Deep-sea carbonates: Pleistocene dissolution cycles. *J. Foraminiferal Res.*, 3: 187-195.

Berger, W.H., (1975). Deep-sea carbonates: Dissolution profiles from foraminiferal preservation. In: Bé, A.W.H. and Berger, W.H. (Eds.). *Dissolution of Deep-Sea Carbonates*, Spec. Publ. Cushman Found. Foraminiferal Res., 13: 82-86.

Berger, W.H., (1979). Stable Isotopes in Foraminifera. In: Lipps, J.H., Berger, W.H., Buzas, M.A., Douglas, R.G., and Ross, C.A. (Eds.). *Foraminiferal Ecology and Paleocology*. Soc. Econ. Paleontol. Mineral., Short Course No.6, Houston, 154-198.

Berger, W.H., Bickert, T., Schmidt, H. and Wefer, G., (1993). Quaternary oxygen isotope record of pelagic foraminifers: Site 806, Ontong Java Plateau. In: Berger, W.H., Kroenke, L.W., Mayer, L.A., et al., *Proc. ODP, Sci. Results*, 130: College Station, TX (Ocean Drilling Program), 381-409.

Berger, W.H., Yasuda, M.K., Bickert, T., Wefer, G. and Takayama, T., (1994). Quaternary time scale for the Ontong Java Plateau: Milankovitch template for Ocean Drilling Program Site 806. *Geology*, 22: 463-467.

Berger, W.H. and Winterer, E.L., (1974). Plate stratigraphy and the fluctuating carbonate line. In: Hsu, K.J. and Jenkyns, H.C., (Eds.). *Pelagic Sediments on Land and Under the Sea*. Publ. Int. Ass. Sedimentol., 1: 11-48.

Berggren, W.A., Burckle, L.H., Cita, M.B., Cooke, H.B.S., Funnell. B.M., Gartner, S., Hays, J.D., Kennett, J.P., Opdyke, N.D., Pastouret, L., Shackleton, N.J. and Takayanagi, Y., (1980). Towards a Quaternary time scale. *Quat. Res. (N.Y.)*, 13: 277-302.

Berner, R.A., (1974). Kinetic models for the early diagenesis of nitrogen, sulphur, phosphorous, and silicon in anoxic marine sediments. In: Goldberg, E.D. (Ed.), *The Sea*, v5., Wiley, New York, 427-450.

Berner, R.A., (1980). *Early Diagenesis*: Princeton Univ. Press, Princeton, 241 p.

Berner, R.A. and Honjo, S., (1981). Pelagic sedimentation of Aragonite: Its geochemical significance. *Science*, 211: 940-942.

Betzler, C., Brachert, T.C. and Kroon, D., (1995). Role of climate in partial drowning of the Queensland Plateau carbonate platform (northeastern Australia). *Mar. Geol.*, 123: 11-32.

Biscaye, P.E., Kolla, V. and Turekian, K.K., (1976). Distribution of calcium carbonate in surface sediments of the Atlantic Ocean. *J. Geophys. Res.*, 81: 2595-2603.

Bischoff, J.L., Heath, G.R. and Leinen, M., (1979). Geochemistry of deep sea sediments from the pacific manganese nodule province: Dome sites A, B and C. In: Bischoff and Piper, (Eds.). *Marine Geology and Oceanography of the Pacific Manganese Nodule Province*. Plenum, New York, 397-473.

Bishop, J.K.B., (1988). The barite-opal organic carbon association in oceanic particulate matter. *Nature*, 332: 341-343.

Bloemendal, J., (1989). Paleoenvironmental implications of the magnetic characteristics of sediments from Deep-Sea Drilling Project Site 514, Southeast Argentine Basin. In: Ludwig, W. and Krasheninnikov, V. et al., (Eds.). *Initial Reports DSDP*, 71, Pt.2: Washington (U.S. Govt.Printing Office), 1097-1108.

Bloemendal, J. and deMenocal, P., (1989). Evidence for a change in the periodicity of tropical climate cycles at 2.4 Myr from whole-core magnetic susceptibility measurements, *Nature*, 342: 897-900.

Boardman, M.R. and Neumann, A.C., (1984). Sources of periplatform carbonates: Northwest Providence Channel, Bahamas. *J. Sediment. Petrol.*, 54(4): 1110-1123.

Boardman, M.R., Neumann, A.C., Baker, P.A., Dulin, L.A., Kenter, R.J., Hunter, G.E. and Kiefer,

K.B., (1986). Banktop responses to Quaternary fluctuations in sea level recorded in periplatform sediments. *Geology*, 14: 28-31.

Bonatti, E., Simmons, E.C., Berger, D., Hamlyn, P.R. and Lawrence, J., (1983). Ultramafic rock/ seawater interactions in the oceanic crust. Mg-silicate (sepiolite) deposit from the Indian ocean floor. *Earth Planet. Sci. Lett.*, 62: 229-238.

Bosellini, A., (1989). Dynamics of Tethyan carbonate platforms. In: Crevello, P.D., et al., (Eds.)., Controls on Carbonate Platform and Basin Development. *Soc. Econ. Paleontol. Mineral. Spec. Publ.*, 44: 3-13.

Boss, S.K. and Neumann, A.C., (1993). Impacts of hurricane Andrew on carbonate platform environments, northern Great Bahama Bank. *Geology*, 21: 897-900.

Bostrom, K., (1973). The origin and fate of metalliferous active ridge sediments. Stockholm Contrib. *Geol.*, 27: 149-243.

Bostrom, K., Jonessu, O., Moore, C., Bostrom, B., Balziel, M. and Horowitz, A., (1973). Geochemistry of barium in pelagic sediments. *Lithos*, 6: 159-174.

Bostrom, K., Jonessu, O., and Brohm, I., (1974). Plankton: its chemical composition and its significance as a source of pelagic sediments. *Chem. Geol.*, 14: 255-271.

Boyle, E.A., (1983). Chemical accumulation variations under the Peru Current during the past 130 000 years. *J. Geophys. Res.*, 88(C12): 7667-7680.

Bramlette, W.S., (1961). Pelagic sediments. In: Sears, M., (Ed.). *Oceanography*. Publ. Am. Ass. Adv. Sci., 67: 345-366.

Brandon, D.E., (1973). Waters of the Great Barrier Reef province. In: Jones, O.A., Endean, R. (Eds.)., *Biology and Geology of Coral Reefs*, Vol.1, Geology 1. Academic Press, New York, 187-232.

Broecker, W.S., (1982). Ocean chemistry during glacial time. *Geochim. Cosmochim. Acta.*, 46: 1689-1705.

Broecker, W.S. and Broecker, S., (1974). Carbonate dissolution on the western flank of the East Pacific Rise. In: Hays, W.W. (Ed.), Studies in Paleo-Oceanography. *Spec. Publ.- Soc. Econ. Paleontol. Mineral.*, 20: 44-57.

Broecker, W.S. and Takahashi, T., (1978). The relationship between lysocline depth and in-situ carbonate ion concentration. *Deep-Sea Res.*, 27: 591-613.

Broecker, W.S. and Peng, T.H., (1982). *Tracers in the sea.* Eldigio Press, Palisades, New York, 690 p.

Broecker, W.S., Spencer, W. and Craig, H., (1982). *GEOSECS Pacific Expedition, Hydrographic Data, 3.* Washington (U.S. Govt. Printing Office).

Bryne, R.H., Acker, J.G., Betzer, P.R., Feely, R.A. and Cates, M.H., (1984). Water column dissolution of aragonite in the Pacific Ocean. *Nature*, 312: 321-326.

Brummer, G.J.A. and van Eijden, A.J.M., (1992). 'Blue ocean' paleoproductivity estimates from pelagic carbonate mass accumulation rates, *Marine Micropaleontology*, 19: 99-117.

Burns, J.H. and Breding, M.A., (1956). Transformations of calcite to aragonite by grinding. *Jour. Chem. Phys.*, 25: 1281.

Burke, K. and Dewey, J.F., (1973). Plume-generated triple junctions; key indicators in applying plate tectonics to old rocks. *Jour. Geol.*, 81: 406-4433.

Cande, S.C. and Mutter, J.C. (1982). A revised identification of the oldest sea-floor anomalies between Australia and Antarctica. *Earth Planet. Sci. Lett.*, 58: 151-160.

Chan, L.H., Edmond, J.M., Stallard, R.F., Broecker, W.S., Chung, Y.C., Weiss, R.F. and Ku, T.L., (1976). Radium and barium at GEOSECS stations in the Atlantic and Pacific. *Earth Planet. Sci. Lett.*, 32: 258-267.

Chao, G.Y., (1969). *2θ ° (Cu) Table for Common Minerals.* Geological Paper 69-2, Carleton University, Ottawa, Canada. 42 p.

Chatfield, C., (1989). *The Analysis of Time Series: An Introduction.* Chapman and Hall, London. 241 p.

Chave, K.E., (1954). Aspects of the biochemistry of magnesium: 1. Calcareous marine organisms. *Jour. Geol.*, 62: 266-283.

Chave, K.E., (1962). Factors influencing the mineralogy of carbonate sediments. *Limnol.Oceanogr.*, 7: 218-223.

Chave, K.E. and Suess, E., (1970). Calcium carbonate saturation in seawater: Effects of organic matter. *Limnol. and Oceanog.*, 15: 633-637.

Chen, C., (1968). Pleistocene Pteropods in Pelagic Sediments. *Nature*, 219: 1145-1149.

Chester , R. and Aston, S.R., (1976). The geochemistry of deep sea sediments. In: Riley, J.P. and Chester, R., (Eds.). *Chemical Oceanography*, Vol.6, 281-390, Academic Press, London, 414 p.

Chilingar, G.V., Zenger, D.H., Bissell, H.J. and Wolf, K.H., (1979). Dolomites and dolomitization. In: Larsen, G. and Chilingar, G.V., (Eds.). *Diagenesis in sediments*. Elsevier, Amsterdam, 423-536.

Chow, T.J. and Goldberg, E.D., (1960). On the marine geochemistry of barium. *Geochim. Cosmochim. Acta*, 20: 192-198.

Church, J.A., (1987). East Australian current adjacent to the Great Barrier Reef. *Aust. J. Mar. Freshw. Res.*, 38: 671-683.

Church, J.A. and Boland, F.M., (1983). A permanent undercurrent adjacent to the Great Barrier Reef. *Journal of Physical Oceanography*, 13: 1746-1869.

Church, T.M., (1970). Marine Barite. Unpublished Ph.D. thesis, University of California. 325 p.

Church, T.M., (1979). Marine barite. In: Burns, R.G., (Ed.). *Marine Minerals*, Min. Soc. Am., 6:175-210.

Clark, D.N., (1980). The diagenesis of Zechstein carbonate sediments. Contrib. Sediment., 9: 167-203.

Claypool, G. and Kaplan., I.R., (1974). The origin and distribution of methane in marine sediments. In: Kaplan, I.R., (Ed.). *Natural Gases in Marine Sediments*, Plenum, New York, 99-139.

Clemens, S., Prell, W, Murray, D., Shimmield, G. and Weedon, G., (1991). Forcing mechanisms of the Indian Ocean monsoon. *Nature*, 353: 720-725.

Coleman, P.J., (1980). Plate tectonics background to biogeographic development in the Southwest Pacific over the last 100 million years. *Palaeogeogr., Palaeoclimatol., Palaeoecol.*, 31: 105-121.

Coney, P.J., Edwards, A., Hine, R., Morrison, F. and Windrim, D., (1990). The regional tectonics of the Tasman orogenic system, eastern Australia. *Jour. Structural Geol.*, 12(5/6): 519-543.

Craig, H., (1957). Isotopic standards for carbon and oxygen correction factors for mass spectrometric analysis of CO_2. *Geochim. Cosmochim. Acta*, 12: 133-149.

Craig, H. and Gordon, L.I., (1965). Deuterium and oxygen-18 variations in the ocean and marine atmosphere. In: Tongiorgi, E. (Ed.). Stable Isotopes in Oceanographic Studies and Paleotemperatures. Consiglio Nazionale delle Richerche, Laboratorio di Geologia Nucleare, Pisa, 9-130.

Cronan, D.S. and Tooms, T.S., (1969). Geochemistry of manganese nodules from the N.W. Indian ocean. *Deep-Sea Res.*, 14: 239-250.

Crowley, T.J., (1983). Calcium carbonate preservation patterns in the central North Atlantic during the last 150, 000 years. *Mar. Geol.*, 51: 1-14.

Damuth, J.E., (1977). Late Quaternary sedimentation in the western equatorial Atlantic. *Sedimentology*, 26: 825-834.

Dansgaard, W., (1964). Stable isotopes in precipitation. *Tellus*, 16: 436-468.

Dansgaard, W. and Tauber, H., (1969). Glacier oxygen-18 content and Pleistocene ocean temperatures. *Science*, 191: 1131-1137.

Davies, P.J., (1988). Evolution of the Great Barrier Reef- Reductionist Dream or Expansionist Vision ? *Proc. 6th Int. Coral Reef Symp.*, 1: 9-17.

Davies, P.J. and McKenzie, J.A., (1993). Controls on the Pliocene-Pleistocene evolution of the northeastern Australian continental margin. In: McKenzie, J.A., Davies, P.J., Palmer-Julson, A., et al., *Proc. ODP, Sci. Results*, 133: College Station, TX (Ocean Drilling Program), 755-762.

Davies, P.J, Cucuzza, J. and Marshall, J.F., (1983). Lithofacies variations on the continental shelf east of Townsville, Great Barrier Reef. In: Baker, J.T., Carter, R.M., Summarco, P.W. and Stark, K.P. (Eds.), *Proc. Inaugural GBR Conf.* (Townsville), James Cook Univ.Press, 89-93.

Davies, P.J. and Symonds, P.A., (1988). *Basin development and evolution of the continental margin of northeast Australia.* Bureau Mineral Resources, Geology and Geophysics, Yearbook., 55-60.

Davies, P.J., Symonds, P.A., Feary, D.A. and Pigram, C.J, (1987). Horizontal Plate Motion: A Key Allocyclic Factor in the Evolution of the Great Barrier Reef. *Science*, 238: 1697-1700.

Davies, P.J., Symonds, P.A., Feary, D.A. and Pigram, C.J., (1988). Facies models in exploration, the carbonate platforms of northeast Australia. *APEA J.*, 28(1): 123-143.

Davies, P.J., Symonds, P.A., Feary, D.A. and Pigram, C.J, (1989). The evolution of the carbonate platforms of northeast Australia. In: Crevello, P.D., Wilson, J.L., Sarg, J.F., Read, J.F. (Eds.), *Controls on Carbonate Platform and Basin Development.* Spec. Publ.-Soc. Econ. Paleontol. Mineral., 44: 233-258.

Davies, P.J., McKenzie, J.A., Palmer-Julson, A., et al., (1991). *Proc.ODP, Init.Repts.*, 133: College Station, TX (Ocean Drilling Program). 1-810.

Davis, J.C., (1986). Statistical Data Analysis in Geology. Wiley, New York. 225 p.

Day, R.W., Murray, C.G., and Whitaker, W.G., (1978). The eastern part of the Tasman orogenic zone. *Tectonophysics*, 48: 327-364.

Dehairs, F. Stroobants, N. and Goeyens, L., (1991). Suspended barite as a tracer of biological activity in the Southern Ocean. *Mar. Chem.*, 35: 399-410.

Dietrich, G., Kalle, K., Krauss, W. and Siedler, G., (1980). *General Oceanography: An Introduction.* New York (Wiley). 588 p.

Dix, G.R. and Mullins, H.T., (1988). A regional perspective of shallow-burial diagenesis of deep-water periplatform carbonates from the northern Bahamas. In: Austin, J., Schlager, W. et al., (Eds.)., *Proc. ODP, Sci. Results*, 101: College Station, TX,) Ocean Drilling Program), 279-302.

Donguy, J.R. and Henin, C., (1975). Evidence of the South Tropical Counter-Current in the Coral Sea. *Aust. J. Mar. Freshw. Res.*, 26: 405-409.

d'Orbigny, A.D., (1839). Foraminiferes, in R.De La Sagra, *Histoire physique, politique et naturelle de l'Ile de Cuba*, Paris, A.Bertrand, 1-224.

Doyle, L.J. and Roberts, H.H., (1988). *Carbonate-Siliciclastic Transitions: Developments in Sedimentology*. New York, Elsevier, 304 p.

Driscoll, N.W., Weissel, J.K., Karner, G.D. and Mountain, G.S., (1991). Stratigraphic response of a carbonate platform to relative sea level changes: Broken Ridge, southeast Indian Ocean. *Bull. Am. Ass. Petrol. Geol.*, 75: 808-831.

Droxler, A.W. and Schlager, W., (1985). Glacial versus interglacial sedimentation rates and turbidite frequency in the Bahamas, *Geology*, 13: 339-352.

Droxler, A.W., Schlager, W. and Whallon, C.C., (1983). Quaternary aragonite cycles and oxygen-isotope record in Bahamian carbonate ooze. *Geology*, 11: 235-239.

Droxler, A.W., Haddad, G.A., Mucciarone, D.A. and Cullen, J.L., (1990). Pliocene- Pleistocene aragonite cyclic variations in Holes 714A and 716B (The Maldives) compared with Hole 633A (The Bahamas): records of climate-induced $CaCO_3$ preservation at intermediate water depths. In: Duncan, R.A., Backman, J., Peterson, L.C., et al., *Proc. ODP, Sci. Results*, 115, College Station, TX (Ocean Drilling Program), 539-577.

Droxler, A.W., Bruce, C.H., Sager, W.W. and Watkins, D.H., (1988). Pliocene-Pleistocene variations in aragonite content and planktonic oxygen-isotope record in Bahamian periplatform ooze, Hole 633A. In: Austin, J.R., Jr. Schlager, W. et al., *Proc. ODP, Sci. Results*, 101, College Station, TX (Ocean Drilling Program), 221-244.

Droxler, A.W., Haddad, G.A., Kroon, D., Gartner, S., Wei, W. and McNeill, D., (1993). Late Pliocene (2.9 Ma) partial recovery of shallow carbonate banks on the Queensland Plateau: Signal of bank-top re-entry into the photic zone during a lowering in sea-level. In: McKenzie, J.A., Davies, P.J. and Palmer-Julson, A. (Eds.), *Proc. ODP, Sci. Results*: 133, College Station (TX), Ocean Drilling Program, 235-254.

Dunham, R., (1962). The classification of carbonate rocks according to depositional texture. In: Ham, W.E. (Ed.), *Classification of Carbonate Rocks*: Tulsa AAPG, 108-121.

Dymond, J., (1981). Geochemistry of Nazca Plate surface sediments: An evaluation of hydrothermal, biogenic, detrital, and hydrogenous sources, Nazca Plate. In: Kulm, L.D. (Ed.). *Crustal Formation and Andean Convergence*. Geol. Soc. Am. Mem., 154: 133-174.

Dymond, J., Suess, E. and Lyle, M., (1992). Barium in deep-sea sediment: A geochemical proxy for palaeoproductivity. *Paleoceanography*, 7(2): 163-181.

Eason, G., Coles, C.W. and Gettinby, G., (1980). *Mathematics for the bio-sciences*. Ellis Horwood, New York, London, 578 p.

Eberli, G.P., and Ginsburg, R.N., (1989). Cenozoic progradation of northwestern Great Bahama Bank, a record of lateral platform growth and sea level fluctuations. In: Crevello, P.D., et al., (Eds.). *Controls on Carbonate Platform and Basin Development*. Spec.Publ.- Soc. Econ. Paleontol. Mineral., 44: 339-352.

Edmond, J.M., (1974). On the dissolution of carbonate and silicate in the deep ocean. *Deep-Sea Res.*, 21: 455-480.

Edwards, A.R., (1975). Southwest Pacific Cenozoic Paleoceanography and integrated Neogene paleocirculation model. In: Andrews, J.E., Packham, G., et al. (Eds.), *Init. Repts. DSDP*: 30, Washington (US Govt. Printing Office), 667-684.

Embry, A.F. and Klovan, J.E., (1971). A late Devonian reef tract system on northeast Banks Island, Northwest Territories. *Bull. Can. Pet. Geol.*, 19: 730-781.

Emerson, S. and Bender, M., (1981). Carbon fluxes at the sediment-water interface of the deep-sea: calcium carbonate preservation. *J. Mar. Res.*, 39: 139-162.

Emiliani, C., (1954). Depth habitats of some species of pelagic foraminifera as indicated by oxygen isotope ratios. *Am. J. Sci.*, 252: 149-158.

Emiliani, C., (1955a). Pleistocene temperatures. *Jour. Geol.*, 63: 538-578.

Emiliani, C., (1955b). Mineralogical and chemical composition of the tests of certain pelagic foraminifera. *Micropalaeontology*, 1: 377-380.

Emiliani, C., (1966). Isotope paleotemperatures. *Science*, 154: 851-857.

Emiliani, C., (1972). Quaternary paleotemperatures and the duration of the high-temperature intervals. *Science*, 178: 398-401.

Emiliani, C., (1978). The cause of the ice ages. *Earth Planet Sci. Lett.*, 37: 249-354.

Emiliani, C. and Shackleton, N.J., (1974). The Brunhes epoch: Isotopic paleotemperatures and geochemistry. *Science*, 183: 511-514.

Epstein, S., Buchsbaum, R., Lowenstam, H.A., and Urey, H.C., (1951). Carbonate-water isotopic temperature scale. *Geol. Soc. Am. Bull.*, 62: 417-426.

Epstein, S., Buchsbaum, R., Lowenstam, H.A., and Urey, H.C., (1953). Revised carbonate-water isotopic temperature scale. *Geol. Soc. Am. Bull.*, 64: 1315-1326.

Ewing, M., Hawkins, L.V. and Ludwig, W.J., (1970). Crustal structure of the Coral Sea. *J. Geophys. Res.*, 75(75): 1953-1962.

Fairchild, I.J., Hendry, G., Quest, M. and Tucker, M., (1991). Chemical analysis of sedimentary rocks. In: Tucker, M. (Ed.). *Techniques in Sedimentology*, Blackwell Scientific Publications, Oxford. 274-394.

Falvey, D.A., (1972). The nature and origin of marginal plateaux and adjacent ocean basins off northern Australia. Unpublished Ph.D. Dissertation, University of new South Wales, Sydney, Australia, 239 p.

Falvey, D.A., (1974). Continental Margin Development and Plate Tectonic Theory. *Aust. Petrol. Explor. Assoc. Jnl.*, 14(1): 95-106.

Falvey, D.A. and Taylor, L.W.H., (1974). Queensland Plateau and Coral Sea Basin: Structural and Time-Stratigraphic Patterns. *Bull. Aust. Soc. Explor. Geophys.*, 5(4): 123-126.

Falvey, D.A. and Mutter, J.C., (1981). Regional plate tectonics and the evolution of Australia's passive continental margin. *.BMR Jour. Aust. Geol. and Geophys.*, 6: 1-29

Fang, J.H. and Zevin, L., (1985). Quantitative X-ray Diffractometry of Carbonate Rocks. *J. Sediment. Petrol.*, 55: 611-613.

Farrell, J.W. and Prell, W.L., (1987). Climate forcing of calcium carbonate sedimentation: a 4.0 Ma record from the central equatorial Pacific Ocean. *EOS*, Transactions American Geophysical Union, 68(16): 333.

Farrell, J.W. and Prell, W.L., (1989). Climatic change and $CaCO_3$ preservation: an 800,000 year bathymetric reconstruction from the central equatorial Pacific Ocean. *Paleoceanography*, 4: 447-466.

Farrell, J.W. and Prell, W.L., (1991). Pacific $CaCO_3$ preservation and $\delta^{18}O$ since 4 Ma: paleoceanic and paleoclimatic implications. *Paleoceanography*, 6: 485-498.

Feary, D.A. and Jarrard, R.D., (1993). Sedimentology and downhole log analysis of Site 820, central Great Barrier Reef outer shelf: the factors controlling Pleistocene progradational and aggradational seismic geometry. In: McKenzie, J.A., Davies, P.J., Palmer-Julson, A., et al., *Proc. ODP, Sci. Results*, 133: College Station, TX (Ocean Drilling Program), 315-327.

Finlay, B.J., Hetherington, N.B. and Davison, W., (1983). Active biological participation in lacustrine barium geochemistry. *Geochim. Cosmochim. Acta*, 47: 1325-1329.

Flood, P.G. and Orme, G.R., (1988). Mixed siliciclastic/carbonate sediments of the northern Great Barrier Reef Province. In: Doyle, L.J. and Roberts, H.H., (Eds.). *Carbonate-Clastic Transitions*, Elsevier, Developments in Sedimentology, 42: 175-205.

Frakes, L.A., Francis, J.E. and Syktus, J.I., (1992). *Climatic Modes of the Phanerozoic*. Cambridge University Press, 274 p.

Friedman, G.M., (1964). Early diagenesis and lithification of carbonate sediments. *J. Sediment. Petrol.*, 34: 777-813.

Friedman, G.M., (1965). Occurrence and stability relationships of aragonite, high-magnesian calcite and low-magnesian calcite under deep-sea conditions. *Geol. Soc. Am. Bull.*, 76: 1191-1196.

Frisia, S., (1994). Mechanisms of complete dolomitization in a carbonate shelf: comparison between the Norian Dolomia Principale (Italy) and the Holocene of the Abu Dhabi Sabkha. In: Purser, B., Tucker, M. and Zenger, D., (Eds.). *Dolomites*. Spec. Publs. Int. Ass. Sediment., 21: 5-74.

Gardulski, A.F., Mullins, H.T. and Oldfield, B., (1986). Carbonate mineral cycles in ramp slope sediment: Eastern Gulf of Mexico. *Palaeoceanography*, 1(4): 555-565.

Gartner, J.V., (1970). Submarine Geology of the Western Coral Sea. *Geol. Soc. Am. Bull.*, 81: 2599-2614.

Gartner, S. and Wei., W., (1993). Data report: Nannofossil biohorizons and depth-age plots for Leg 133 Sites. In: McKenzie, J.A., Davies, P.J., Palmer-Julson, A., et al., *Proc. ODP, Sci. Results*, 133: College Station, TX (Ocean Drilling Program), 773-785.

Gavish, E. and Friedman, G.M., (1973). Quantitative analysis of calcite and Mg-calcite by X-ray diffraction: effect of grinding on peak height and peak area. *Sedimentology*, 20: 437-444.

Gevirtz, J.L. and Friedman, G.M., (1966). Deep-sea carbonate sediments in the Red Sea and their implications on marine lithification. *J. Sediment. Petrol.*, 36: 143-151.

Ginsburg, R.N., Lloyd, R.M., Stockman, K.W. and McCallum, J.S., (1963). Shallow-water carbonate sediments. *In*: Hill, M.N., (Ed.). *The Seas*, Vol. 3, New York and London, John Wiley and Sons, 554-582.

Ginsburg, R.N. and James, N.P., (1974). Holocene carbonate sediments of continental shelves. In: Burk, C.A. and Drake, C.L. (Eds.), *Continental Margins*: Berlin (Springer-Verlag), 137-154.

Glasby, G.P., (1990). *Antarctic Sector of the Pacific*. Amsterdam (Elsevier). 396 p.

Glaser, K.S. and Droxler, A.W., (1991). High production and highstand shedding from deeply submerged carbonate banks, northern Nicaragua Rise. *J. Sediment. Petrol.*, 61(1): 128-142.

Glaser, K.S. and Droxler, A.W., (1993). Controls and development of late Quaternary periplatform carbonate stratigraphy in Walton Basin (Northeastern Nicaragua Rise, Caribbean Sea). *Palaeoceanography*, 8: 243-274.

Goldberg, E.D., and Arrhenius, G.O.S., (1958). Chemistry of Pacific pelagic sediments. *Geochim. Cosmochim. Acta*, 13: 153-212.

Goldhammer, R.K. and Harris, M.T., (1989). Eustatic controls on the stratigraphy and geometry of the Latemar buildup (Middle Triassic), the Dolomites of northern Italy. In: Crevello, P.D., et al., (Eds.)., *Controls on Carbonate Platform and Basin Development*. Spec.Publ.- Soc. Econ. Paleontol. Mineral., 44: 323-338.

Goldsmith, J.R., Graf, D.L. and Heard, H.C., (1961). Lattice constants of the calcium-magnesium carbonates. *Am. Min.*, 46: 453-457.

Gomberg, D.N. and Bonatti, E., (1970). High-magnesian calcite: Leaching of magnesium in the deep sea. *Science*, 168: 1451-1453.

Goodell, H.G. and Garman, R.K., (1969). Carbonate geochemistry of Superior deep testwell, Andros Island, Bahamas. *AAPG Bull.*, 53: 513-536.

Goodell, H.G. and Kunzler, R.H., (1965). Thermal inversion of aragonite to calcite (abst.). *Geol. Soc. Am. Special Paper*, No.82, p. 300.

Grammer, G.M. and Ginsburg, R.N., (1991). Morphology and development of modern carbonate foreslopes, Tongue of the Ocean, Bahamas. In: Larue, D.K. and Draper, G., (Eds.). Transactions of the 12th Caribbean Geological Conference, St. Croix, U.S. Virgin Islands. Miami Geol. Soc., 22-32.

Grammer, G.M. and Ginsburg, R.N., (1992). Highstand verses lowstand deposition on carbonate platform margins: insight from Quaternary foreslopes in the Bahamas. *Mar. Geol.*, 103: 125-136.

Grimaldi, F.S., Shapiro, L. and Schnepfe, M., (1966). Determination of carbon dioxide in limestones and dolomite by acid-base titration. *Geol. Surv. Prof. Pap. U.S.*, 550(B): B186-188.

Guoping, Wu, Yasunda, M.K. and Berger, W.H., (1991). Late Pleistocene carbonate stratigraphy on Ontong-Java Plateau in the western equatorial Pacific. *Mar. Geol.*, 99: 135-150.

Gunatilaka, H.A. and Till, R., (1971). A precise and accurate method for the quantitative determination of carbonate minerals by X-ray diffraction using a spiking technique. *Mineralog. Mag.*, 38: 481-487.

Haddad, G.A., Droxler, A.W., Kroon, D. and Muller, D.W., (1993). Quaternary $CaCO_3$ input and preservation within Antarctic Intermediate Water mineralogic and isotopic results from Holes 818B and 817A, Townsville Trough (northeast Australian margin). In: McKenzie, J.A., Davies, P.J., Palmer-Julson, A., et al., *Proc. ODP, Sci Results*, 133: College Station, TX (Ocean Drilling Program), 203-234.

Hallock, P. and Schlager, W., (1986). Nutrient excess and the demise of coral reefs and carbonate platforms. *Palaios*, 1: 389-398.

Hamon, B.V., (1970). Western Boundary currents in the South Pacific. In: Wooster, W.S. (Ed.), *Scientific Exploration of the South Pacific*: Washington (National Academy of Sciences), 50-59.

Hanshaw, B.B., Back, W. and Dicke, R.G., (1971). A geochemical hypothesis for dolomitization by groundwater. *Econ. Geol.*, 66: 710-724.

Haq, B.U., Hardenbol, J. and Vail, P.R., (1987). Chronology of fluctuating sea levels since the Triassic (250 million years ago to present). Science, 235: 1156-1167.

Hardy, R. and Tucker, M., (1988). X-ray diffraction of sediments. In: Tucker, M. (Ed.). *Techniques in Sedimentology*, Blackwell, London, 191-228.

Harris, P.T. and Davies, P.J., (1989). Submerged reefs and terraces on the shelf edge of the Great Barrier reef, Australia: morphology, occurrence and implications for reef evolution. *Sediment. Geol.*, 57: 27-297.

Harris, P.T., Davies, P.J., and Marshall, J.F., (1990). Late Quaternary sedimentation on the Great Barrier Reef continental shelf and slope east of Townsville, *Australia. Mar. Geol.*, 94: 55-77.

Hawley, J.E. and Pykowicz, R.M., (1969). Solubility of calcium carbonate in seawater at high pressure and 2°C. *Geochim. Cosmochim. Acta.*, 33: 1557-1561.

Hayes, D.E. and Ringis, J., (1973). Sea-floor spreading in the Tasman Sea. *Nature*, 243: 454-458.

Hays, J.D., Imbrie, J. and Shackleton, N.J., (1976). Variations in the Earths Orbit: Pacemaker of the Ice Ages. *Science*, 194(4270): 1121-1132.

Hays, J.D., Saito, T., Opdyke, N.D. and Burckle, L.H., (1969). Plio-Pleistocene sediments of the equatorial Pacific: their paleomagnetic, biostratigraphic and climatic records. *Geol. Soc. Am. Bull.*, 80: 1481-1514.

Heath, K.C. and Mullins, H.T., (1984). Open-ocean, off-bank transport of fine-grained carbonate sediments in northern Bahamas. In: Stow, D.A.V., and Piper, D.J.W., (Eds.). *Fine-grained sediments: Deepwater Processes and Facies*. Spec. Publ. Geol. Soc. Lond., 15: 199-208.

Hedley, C., (1925). The natural destruction of a coral reef. *Rept. Great Barrier Reef Comm.*, 1: 35-40.

Henshaw, P.C. Jr., Merrill, R.T., (1980). Magnetic and chemical changes in marine sediments. *Rev. Geophys. Space Phys.*, 18: 483-504.

Hesse, P.P., (1994). Evidence for bacterial palaeoecological origin of mineral magnetic cycles in oxic and sub-oxic Tasman Sea sediments. *Mar. Geol.*, 117: 1-17.

Hill, D. and Denmead, A.K., (1960). *The Geology of Queensland.* J. Geol. Soc. Australia, 7: 1-474.

Hirst, D.M., (1962). The geochemistry of modern sediments from the Gulf of Paria. II. The location and distribution of trace elements. *Geochim. Cosmochim. Acta*, 26: 1147-1187.

Hodell, D.A., Williams, D. and Kennett, J.P., (1985). Late Pliocene reorganization of deep vertical water mass structure in the western South Atlantic: Faunal and isotopic evidence. *Geol. Soc. Am. Bull.*, 94:495-503.

Hoefs, J., (1987). *Stable Isotope Geochemistry*. Springer-Verlag, Berlin, 241 p.

Hopley, D., (1974). The cyclone *Althea* storm surge. *Austr. Geog. Stud.*, 12: 90-106.

Hopley, D., (1982). *The Geomorphology of the Great Barrier Reef: Quaternary Development of coral Reefs*: New York (Wiley). 453 p.

Hounslow, M.W., (1990). A magnetic susceptibility stratigraphy for Pleistocene and Pliocene sediments in the vicinity of the Barbados Ridge. In: Moore, J. and Mascle, A. et al., (Eds.). *Proc. ODP, Sci. Results*, 110: College Station, TX (Ocean Drilling Program), 365-377.

Howard, W.R. and Prell, W.L., (1994). Late Quaternary $CaCO_3$ production and preservation in the Southern Ocean: Implications for oceanic and atmospheric carbon cycling, *Paleoceanography*, 9(3): 453-482.

Hutson, W.H., (1980). Bioturbation of deep-sea sediments: Oxygen isotopes and stratigraphic uncertainty. *Geology*, 8: 127-130.

Imbrie, J., (1985). A theoretical framework for the Pleistocene ice ages. *J. Geol. Soc. London*, 142: 417-432.

Imbrie, J., Hays, J.D., Martinson, D.G. et al., (1984). The orbital theory of Pleistocene climate: Support from a revised chronology of marine $\delta^{18}O$ records. In: Berger, A., Imbrie, J. Hays, J., Kukla, G. and Sultzman, B. (Eds.), *Milankovitch and Climate*, Part 1, D. Reidel, 269-305.

Irwin, H., Curtis, C.D., and Coleman, M., (1977). Isotopic evidence for source of diagenetic carbonates formed during burial of organic-rich sediments. *Nature*, 269: 209-213.

Isern, A.R., McKenzie, J.A. and Muller, D.W., (1993). Paleoceanographic changes and reef growth off the northeastern Australian margin: stable isotope data from ODP Leg 133 Sites 811 and 817 and DSDP Leg 21 Site 209. In: McKenzie, J.A., Davies, P.J., Palmer-Julson, A., et al., *Proc. ODP, Sci. Results*, 133: College Station, TX (Ocean Drilling Program), 263-280.

James, N.P. and Coquette, P.W., (1983). Diagenesis 6. Limestones- the sea floor diagenetic environment. *Geoscience Canada*, 10: 162-179.

Jansen, E., Mayer, L.A., Backman, J., Leckie, R.M. and Takayama, T., (1993). Evolution of Pliocene climate cyclicity at Hole 806B (5-2 Ma): Oxygen isotope record. In: Berger, W.H., Kroenke, L.W., Mayer, L.A., et al., *Proc. ODP, Sci. Results*, 130: College Station, TX (Ocean Drilling Program), 349-361.

Jansen, E., Bleil, U., Henrich, R., Kringstad, L. and Slettemark, B., (1988). Paleoenvironmental changes in the Norwegian Sea and the Northeast Atlantic during the last 2.8 Ma: DSDP/ ODP Sites 610, 642, 643 and 644, *Paleoceanography*, 3: 563-581.

Jansen, E. and Sjøholm, J., (1991). Reconstruction of glaciation over the past 6 million years from ice-borne deposits in the Norwegian Sea. *Nature*, 349: 600-604.

Jansen, J.H.F., Kuijpers, A. and Troelstra, S.R., (1986). A Mid-Brunhes climatic event: Long-term changes in global atmosphere and ocean circulation. *Science*, 232: 619-622.

Jarrige, F., (1968). On the eastward flow of water in the Western Pacific south of the equator. *J. Mar. Res.*, 26: 286-289.

Jell, J.S. and Flood, P.G. (1978). Guide to the geology of reefs of the Capricorn and Bunker groups, Great Barrier Reef Province, with special reference to Heron *Pap. Dep. Geol. Univ. Qd*, 8(3): 1-85.

Jenkins, G.M. and Watts, D.G., (1968). Spectral Analysis and its Applications. Holden Day, San Francisco. 320 p.

Jenkins, R. and de Vries, J.L., (1970). *Practical X-ray spectrometry*. MacMillan, London, 189 p.

Johnson, W.M. and Maxwell, J.A., (1981). *Rock and Mineral Analysis*. Wiley, New York. 420 p.

Jones, M.P., (1987). *Applied Mineralogy: A Quantitative Approach*. Graham and Trotman, Oxford, 259 p.

Karlin, R. and Levi, S., (1983). Diagenesis of magnetic minerals in recent hemipelagic sediments. *Nature*, 303: 327-330.

Kastner, M., (1984). Controls on dolomite formation. *Nature*, 311: 410-411.

Keany, J., (1978). Palaeoclimatic trends in early and middle Pliocene deep-sea sediments of the Antarctic. *Marine Micropalaeo.*, 3: 35-49.

Keigwin, L.D., (1979). Late Cenozoic stable isotope stratigraphy and paleoceanography of DSDP sites from the east equatorial and central North Pacific Ocean. *Earth Planet. Sci. Lett.*, 45: 361-382.

Kelts, K. and McKenzie, J.A., (1982). Diagenetic dolomite formation in Quaternary anoxic diatomaceous muds of Deep Sea Drilling Project Leg 64, Gulf of California. In: Curray, J.R., Moore, D.G., et al. (Eds.), *Init. Repts., DSDP*, 64(Pt.2): Washington (U.S. Govt.Printing Office), 553-569.

Kelts, K. and McKenzie, J.A., (1984). A comparison of anoxic dolomite from deep-sea sediments: Quaternary Gulf of California and Messinian Tripoli Formation of Sicily. In: Garrison, R.E., Kastner, M. and Zenger, D.H. (Eds.), *Dolomites of the Monterey Formation and Other Organic-Rich Units*: Pacific Section, Spec. Publ.-Soc. Econ. Palontol. Mineral., 119-140.

Kendal, C.C. and Skipwith, P.A., (1969). Geomorphology of a Recent shallow-water Carbonate Province: Khor Al Bazam Trucial Coast. Southwest Persian Gulf. *Geol. Soc. Am. Bull.*, 80: 865-892.

Kennett, J.P., (1982). *Marine Geology*, Prentice-Hall, Inc., London. 813 p.

Kennett, J.P., and von der Borch, C.C., (1985). Southwest Pacific Cenozoic Palaeoceanography. *In*: Kennett, J.P., and von der Borch, C.C., et al. (Eds.), *Init. Repts. DSDP*, 90, Washington, (US Govt.Printing Office), 1493-1517.

Kennett, J.P. and Hodell, D.A., (1986). Major events in Neogene oxygen isotopic records. *S. Afr. J. Sci.*, 82: 497-498.

Kent, D.V., (1982). Apparent correlation of paleomagnetic intensity and climatic records in deep-sea sediments. *Nature*, 299: 538-539.

Kershaw, A.P., (1978). Record of last interglacial-glacial cycle from northeastern Queensland. *Nature*, 272: 159-161.

Khan, A.A., (1989). *Geochemistry and Palaeoclimate change in sediments: northern Arabian Sea.* Unpublished Ph.D thesis, University of Edinburgh, 248 p.

Kier, J.S. and Pilkey, O.H., (1971). The influence of sea level changes on sediment carbonate mineralogy, Tongue of the Ocean, Bahamas. *Mar. Geol.*, 11: 189-200.

Kinsman, D.J.J., (1969). Interpretation of Sr^{2+} concentrations in carbonate minerals and rocks. *J. Sediment. Petrol.*, 39: 486-508.

Klug, H.P. and Alexander, L.E., (1974). *X-ray Diffraction Procedures for Polycrystalline and Amorphous Material.* Wiley-Interscience, New York, 966 p.

Konishi, K. and Ikehara, M., (1992). High resolution lithostratigraphy of Site 821, the most landward hole on the shelf-edge transect, Central Great Barrier Reef (ODP Leg 133, Preliminary results-unpubl. abstract).

Kroon, D., (1993). *Data Report*: Some planktonic foraminiferal datum levels during the last 10.4 Ma, Leg 133. In: McKenzie, J.A., Davies, P.J., Palmer-Julson, A., et. al., *Proc. ODP, Sci. Results*, 133: College Station, TX (Ocean Drilling Program), 787-790.

Kroon, D., Alexander, I. and Darling, K., (1993). Planktonic and benthic foraminiferal abundances and their ratios (P/B) as expressions of middle-late Quaternary changes in watermass distribution and flow intensity on the northeast Australian margin. In: McKenzie, J.A., Davies, P.J., Palmer-Julson, A., et al., *Proc. ODP Sci. Results*, 133: College Station, TX (Ocean Drilling Program), 181-188.

Lancaster, D.E., (1966). Electronic metal detectors. *Electronics World* (Dec.), 39-62.

Land, L. S., (1967). Diagenesis of skeletal carbonates. *J. Sediment. Petrol.*, 37: 914-930.

Land, L.S., (1980). The isotopic and trace element geochemistry of dolomite: The state of the art, In:

Zenger, D.H., Dunham, J.B. and Ethington, R.L., (Eds.). Concepts and models of dolomitization: Spec.Publ.- Soc.Econ.Paleontol. Mineral., 28: 87-110.

Land, L.S., (1985). The origin of massive dolomite. *J. Geol. Educ.*, 33: 112-125.

Leinen, M. and Heath, G.P., (1981). Sedimentary indicators of atmospheric activity in the Northern Hemisphere during the Cenozoiz. *Palaeogeogr., Palaeoclim., Palaeoecol.*, 36: 1-21.

Le, J. and Shackleton, N.J., (1992). Carbonate dissolution fluctuations in the western equatorial Pacific during the Late Quaternary. *Paleoceanography*, 7(1): 21-42.

Lea, D.W. and Boyle, E.A., (1989). Barium content of benthic records temporal variability in equatorial Pacific upwelling. *Nature*, 340: 373-376.

Lea, D.W., Shen, G.T. and Boyle, E.A., (1989). Coralline barium records temporal variability in equatorial Pacific upwelling. *Nature*. 340: 373-376.

Lindsay, J.F., Korsch, R.J. and Wilford, J.R., (1987). Timing and breakup of a Proterozoic supercontinent: Evidence from Australian intracratonic basins. *Geology*, 15: 1061-1064.

Lindstrom, E.R., Lukas, R., Fine, R., Firing, E., Godfrey, S., Meyers G. and Tsuchiya, M., (1987). The Western Equatorial Pacific Ocean circulation Study. *Nature*, 330: 533-537.

Lisitzin, A.P. and Petelin, V.P., (1967). Features of distribution and modification of $CaCO_3$ in bottom sediments of the Pacific Ocean. *Lithol. Miner. Resour.* Engl. Trans., 5: 565-578.

Loizeau, J.-L., Arbouille, D., Santiago, S. and Vernet, J.-P., (1994). Evaluation of a wide range of laser diffraction grain size analyser for use with sediments. *Sedimentology*, (41): 353-361.

Loreau, J.P., (1982) Sédiments aragonitiques et leur genèse: Mémoires du Muséum National d'Histoire Naturelle, Série C., Tome XLVII, 300.

Lowenstam, H.A., (1954). Factors affecting the aragonite:calcite ratios in carbonate-secreting marine organisms. *J. Geol.*, 62: 284-321.

Lowenstam, H.A., (1955). Aragonite needles secreted by algae and some sedimentary implications. *J. Sediment. Petrol.*, 25: 270-272.

Luz, B., (1973). Stratigraphic and paleoclimatic analysis of late Pleistocene tropical southeast Pacific cores. *Quat. Res.*, 3: 56-72.

Lynts, G.W., Judd, J.W., and Stehmann, C.F., (1973). Late Pleistocene history of Tongue of the Ocean, Bahamas. *Geol. Soc. Am. Bull.*, 84: 2605-2684.

Maher, B.A. and Thompson, R., (1991). Mineral magnetic record of the Chinese loess and paleosols. *Geology*, 19: 3-6.

Mankinen, E.A. and Dalrymple, G.B., (1979). Revised Geomagnetic Polarity Time Scale for the Interval 0-5 m.y. B.P. *Jour. Geophys. Res.*, 84(82): 615-626.

Marshall, J.F. and Davies, P.J., (1978). Skeletal carbonate variation on the continental shelf of eastern Australia. *BMR Jour. Aust. Geol. and Geophys.*, 3: 85-92.

Martin, J.H. and Knauer, G.A., (1973). The elemental composition of plankton. *Geochim. Cosmochim. Acta*, 37: 1639-1653.

Matthews, M.D., (1991). The effect of pretreatment on size analysis. In: Syvitski, J.P.M. (Ed.). *Principles, Methods and Application of Particle Size Analysis*, Cambridge Univ.Press), 34-42.

Maxwell, W.G.H., (1973). Sediments of the Great Barrier Reef Province. In: Jones, O.A. and Endean, R. (Eds.), *Biology and Geology of Coral Reefs*, v. 1, Geology 1, Academic Press, New York, 233-272.

Maxwell, W.G.H., (1968). *Atlas of the Great Barrier Reef*: Amsterdam (Elsevier). 258 p.

Maxwell, W.G.H. and Maiklem, W.R., (1964). Lithofacies analysis, southern part of the Great Barrier Reef. *Pap. Dep. Geol. Univ. Qd*, 5: 1-21.

Maxwell, W.G.H. and Swinchatt, J.P., (1970). Great Barrier Reef: Regional Variation in a Terrigenous-Carbonate Province. *Geol. Soc. Am. Bull.*, 81: 691-724.

McCave, I.N., Bryant, R.J., Cook, H.F. and Coughanowr, C.A., (1986). Evaluation of a laser diffraction size analyser for use with natural sediments. *J. Sediment. Petrol.*, 56: 561-564.

McCave, I.N. and Jarvis, J., (1973). Use of the Model T Coulter Counter in size analysis of the fine to coarse sand. *Sedimentology*, 20: 305-315.

McCave, I.N. and Syvitski, J.P.M., (1991). Principles and methods of geological particle size analysis. In: Syvitski, J.P.M. (Ed.). *Principles, Methods and Application of Particle Size Analysis*, Cambridge Univ.Press. 3-21.

McClune, F.W., (1987). Powder Diffraction File. Joint Committee on Powder Diffraction Standards-International Centre for Diffraction Data, U.S.A., 664 p.

McCrea, J.M., (1950). On the isotopic chemistry of carbonates and a paleotemperature scale. *Jour. Chem. Physics*. 18: 849-857.

McKenzie, J.A., Hsu, K.J. and Schneider, J.F., (1980). Movement of subsurface waters under the sabka, Abu Dhabi, U.A.E., and its relation to evaporitive dolomite genesis. In: Zenger, J.B., Dunham, J.B. and Ethington, R.L. (Eds.). Concepts and Models of Dolomitization. Spec. Publ.-Soc. Econ. Paleontol. Mineral., 28: 11-30.

McNeill, G.W., (1993). The geochemical palaeo-oceanography and mineralogy of marine sediments from the Peruvian continental margin. [Ph.D. dissert., unpubl., Univ. Edinburgh, Scotland], 411 p.

Meissner, F.C., (1972). Cyclic sedimentation in Middle Permian strata of the Permian basin, West Texas and New Mexico. In: Elam, J.C., and Chuber, S. (Eds.)., *Cyclic sedimentation in the Permian Basin*, West Texas Geological Society, Midland Texas, 203-232.

Mercer, J.H., (1987). The Antarctic ice sheet during the late Neogene. *Paleoecology of Africa*. 18: 21-32.

Middleton, G.V., (1976). Hydraulic interpretation of sand size distribution. *Jour. Geol.*, 84: 405-426.

Milliman, J.D., (1974). *Recent Sedimentary Carbonates: Marine Carbonates*, Springer-Verlag, Berlin, Heidelberg, New York, 375 p.

Milliman, J.D. and Bornhold, B.D., (1973). Peak height verses peak intensity analysis of X-ray diffraction data. *Sedimentology*, 20: 445-448.

Montaggioni, L.F. and Venec-Peyré, M.-T., (1993). Shallow-water foraminiferal taphocoenoses at Site 821: implications for the Pleistocene evolution of the central Great Barrier Reef shelf, northeast

Australia. In: McKenzie, J.A., Davies, P.J., Palmer-Julson, A., et al., *Proc. ODP, Sci. Results*, 133: College Station, TX (Ocean Drilling Program), 365-378.

Morse, J.W., (1974). Dissolution kinetics of calcium carbonate in seawater, V., Effects of natural inhibitors and the position of the lysocline, *Am.J. Sci.*, 274: 638-647.

Mountjoy, E.W. and Amthor, J.E., (1994). Has burial diagenesis come of age ? Some answers from the Wesyrtn Canada Sedimentary Basin. In: Purser, B., Tucker, M. and Zenger, D., (Eds.). *Dolomites*. Spec. Publs. Int. Ass. Sediment., 21: 203-230.

Müller, G. and Tietz, G., (1971). Dolomite replacing 'cement A' in biocalcarenites from Fuerteventura, Canary islands, Spain. In: Bricker, D.P., (Ed.). *Carbonate Cements*. Johns Hopkins University Press, Baltimore, M.D., 376 p.

Mullins, H.T., (1983). Structural controls of contemporary carbonate continental margins: Bahamas, Belize, Australia. In: Cook, H.E., Hine, A.C. and Mullins, H.T. (Eds.), *Platform margin and deep water carbonates*, Soc. Econ. Paleontol. Mineral. Short Course, No. 12, pp. 2-1 2-57.

Mullins, H.T., Gardulski, A.F. and Hine, A.C., (1986). Catastrophic collapse of the west Florida carbonate platform margin. *Geology*, 14: 167-170.

Mullins, H.T., Wise, S.W. Jr., Land, L.S., Siegel, D.I., Masters, P.M., Hinchey, E.J. and Price, K.R., (1985). Authigenic dolomite in Bahamian peri-platform slope sediments. *Geology*, 13: 292-295.

Munsell Soil Color Charts, (1971): Baltimore (Munsell Color).

Murray, J. and Renard, A.F., (1898). *Deep-Sea Deposits, Challenger reports*. Longmans, London. 525 p.

Mutter, J.C., (1977). The Queensland Plateau. *Bull. BMR Geol. and Geophys.*, 179: 1-55.

Mutter, J.C. and Karner, G.D., (1980). The continental margin off northeast Australia. In: Henderson, R.A. and Stephenson, P.J. (Eds.). *The Geology and Geophysics of Northeast Australia*; Brisbane (Geol.Soc.Australia, Queensland Div.), 47-69.

Nath, B.G., Rao, V.P. and Becker, K.P., (1989). Geochemical evidence of terrigenous influence in deep-sea sediments up to 8°S in the central Indian ocean. *Mar. Geol.*, 87: 301-313.

Neumann, A.C., (1963). Manuscript, Lehigh University, Bethlehem, Pennsylvania.

Neumann, A.C., (1965). Processes of recent carbonate sedimentation in Harrington Sound, Bermuda. *Bull. mar. Sci.*, 15: 987-1035.

Olausson, E., (1965). Evidence of climatic changes in North Atlantic deep-sea cores, with remarks on isotope paleotemperature analysis, *Prog. Oceanogr.*, 3: 221-252.

Orme, G.R., (1977). The Coral Sea Plateau: a major reef province. In: Jones, O.A. and Endean, R., (Eds.), *Biology and Geology of Coral Reefs*: Academic Press, New York , 267-306.

Orme, G.R., (1985). The sedimentological importance of *Halimeda* in the development of back reef lithofacies, northern Great Barrier Reef (Australia). *Proc. 5th. Int. Coral Reef Cong.*, 5: 31-37.

Orme, G.R. and Flood, P.G., (1977). The geological history of the Great Barrier Reef; a reappraisal of some aspects in the light of new evidence. *Proc. 3rd. Intern. Symp. Coral Reefs*, Miami, 2: 37-43.

Orme, G.R., and Salma, M.S., (1988). Form and seismic stratigraphy of *Halimeda* banks in part of the northern Great Barrier Reef Province. *Coral Reefs*, 6: 131-137.

Palfreyman, W.D., (1984). Guide to the Geology of Australia. *Bureau of Mineral Resources, Australia, Bulletin*, 181: 1-111.

Parker, F.L. and Berger, W.H., (1971). Faunal and solution patterns of foraminifera in surface sediments of the South Pacific, *Deep-Sea Res.*, 18: 73-103.

Parkin, D.W. and Shackleton, N.J., (1973). Trade wind and temperature correlation down a deep sea core off the Sahara coast. *Nature*, 245: 455-457.

Patience, A. J., (1992). Geochemical indicators of palaeoproductivity and palaeoclimate in eastern equatorial Pacific sediments. Unpub. Ph.D. thesis, University of Edinburgh, 473 p.

Patience, A. J. and Kroon, D., (1991). Oxygen Isotope Chronostratigraphy. In: Smart, P.L. and Frances, P.D. (eds.), *Quaternary Dating Methods: A Users Guide*, Quaternary Research Association, Technical Guide No.4, 199-228.

Peerdeman, F.M. and Davies, P.J., (1993). Sedimentological response of an outer-shelf, upper-slope

sequence to rapid changes in Pleistocene eustatic sea level: Hole 820A, northeastern Australian margin. In: McKenzie, J.A., Davies, P.J., Palmer-Julson, A., et al., *Proc. ODP, Sci. Results*, 133: College Station, TX (Ocean Drilling Program), 303-314.

Peerdeman, F.M., Davies, P.J. and Chivas, A.R., (1993). The stable oxygen isotope signal in shallow-water, upper-slope sediments off the Great Barrier Reef (Hole 820A). In: McKenzie, J.A., Davies, P.J., Palmer-Julson, A., et al., *Pro. ODP, Sci. Results*, 133: College Station, TX (Ocean Drilling Program), 163-174.

Perkins, R.D., Dwyer, G.S., Rosoff, D.B., Fuller, J., Baker, P.A. and Lloyd, R.M., (1994). Salina sedimentation and diagenesis: West Caicos Island, British west Indies. In: Purser, B., Tucker, M. and Zenger, D., (Eds.). *Dolomites*. Spec. Publs. Int. Ass. Sediment., 21: 37-54.

Pestiaux, P. and Berger, A., (1984). An optimal approach to the spectral characteristics of deep-sea climatic records. *In*: Berger, A, Imbrie, J., Hays, J., Kukla, G. and Sultzman, B., (Eds.), *Milankovitch and Climate*, Part 1, 417-445. D. Reidel.

Peterson, L.C. and Prell, W.L., (1985a). Carbonate preservation and rates of climatic change: an 800 kyr record from the Indian Ocean. In: Sundquist, E.T. and Broecker, W.S. (Eds.). *The Carbon cycle and Atmospheric CO_2: Natural variations Archaean to present*. Am. Geophy. Union Mono. 32, Washington D.C., 251-269.

Peterson, L.C. and Prell, W.L., (1985b). Carbonate dissolution in Recent sediments of the eastern equatorial Indian Ocean: Preservation patterns and carbonate loss above the lysocline. *Mar. Geol.*, 64: 259-290.

Pickard, G.L., Donguy, J.R., Henin, C. and Rougerie, F., (1977). A Review of the Physical Oceanography of the Great Barrier Reef and western Coral Sea. *Aust. Inst. Mar. Sci. Monogr. Ser.*, 2: 135.

Pigram, C.J. and Davies, H.L., (1987). Terranes and the accretion history of the New Guinea orogen. *BMR Jour. Aust. Geol. and Geophys.*, 10: 193-212.

Pigram, C.J., Davies, P.J., Feary, D.A. and Symonds, P.A., (1989). Tectonic controls on carbonate platform evolution in southern Papua New Guinea: Passive margin to foreland basin. *Geology*, 17: 199-202.

Pilkey, O.H., (1964). Mineralogy of the fine fraction in certain carbonate cores. *Bull. mar. Sci. Gulf Carib.*, 14: 126-139.

Piola, A.R. and Georgi, D.T., (1982). Circumpolar properties of Antarctic Intermediate Water and Subantarctic Mode water. *Deep-Sea Res.*, 29(6a): 687-711.

Pisias, N.G. and Moore, T.C., Jr., (1981). The evolution of Pleistocene climate: A time series approach. *Earth Planet. Sci. Lett.*, 52: 450-458.

Pisias, N.G. and Prell, W.L., (1985). Changes in calcium carbonate accumulation in the equatorial Pacific during the late Cenozoic: evidence from HPC Site 572. In: Sundquist, E.T. and Broecker, W.S. (Eds.). *The Carbon cycle and Atmospheric CO_2: Natural variations Archaean to present.* Am. Geophy. Union Mono. 32, Washington D.C., 443-454.

Pisias, N.G. and Rea, D.K., (1988). Late Pleistocene paleoclimatology of the central equatorial Pacific: Sea surface response to the southeast trade winds. *Paleoceanography*, 321-37.

Plumb, K.A., (1980). The Tectonic Evolution of Australia. *Earth-Science Reviews*, 14: 205-249.

Potts, P.J., (1987). *A Handbook of Silicate Rock Analysis.* Blackie, Glasgow. 622 p.

Powell, C. McA, Li, Z.X., Thrupp, G.A. and Schmidt, P.W., (1990). Australian Palaeozoic palaeomagnetism and tectonics- I. Tectonostratigraphic terrane constraints from the Tasman Fold belt. *Jour. Structural Geology*, 12(5/6): 553-565.

Prell, W.L., (1982). Oxygen and carbon isotope stratigraphy for the Quaternary of Hole 502B: evidence for two modes of isotopic variability. In: Prell, W.L., Gartner, J.V., et al., *Init. Repts. DSDP*, 68: Washington (US Govt.Printing Office), 455-464.

Prell, W.L., Imbrie, J., Martinson, D.G., Morley, J.J., Pisias, N.G., Shackleton, N.J. and Streeter, H.F., (1986). Graphic correlation of oxygen isotope stratigraphy: application to the Quaternary. *Paleoceanography*, 1: 137-162.

Prell, W.L., Niitsuma, N., et al., (1989). *Proc. ODP, Init. Repts.*, 117: College Station, TX (Ocean Drilling Program), 637 p.

Puchelt, H., (1969). Barium. In: Wedepohl, K.H., Correns, C.W., Shaw, D.M., Turekian, K.K. and Zemann, J. (Eds.). *Handbook of Geochemistry*. Springer-Verlag, Berlin Heidelberg New York, pp. 56B1-56O2.

Purdy, E.G., (1963). Recent calcium carbonate facies of the Great Bahamas Bank. *Jour. Geology*, 71: 334-355.

Pytkowicz, R.M., (1970). On the carbonate compensation depth in the Pacific Ocean. *Geochim. Cosmochi. Acta*, 34: 836-839.

Rao, C.P. and Adabi, M.H., (1992). Carbonate minerals, major and minor trace elements and oxygen and carbon isotopes and their variation with depth in deep cool, temperate carbonates, western Tasmania, Australia. *Mar. Geol.*, 103: 249-272.

Raymo, M.E., Ruddiman, W.F. and Clement, B.M., (1986). Pliocene-Pleistocene paleoceanography of the North Atlantic at Deep Sea Drilling Project Site 609. Init. Repts. DSDP. 94: 895-901.

Raymo, M.E., Ruddiman, W.F., Shackleton, N.J. and Oppo, D.W., (1990). Evolution of Atlantic-Pacific $\delta^{13}C$ gradients over the last 2.5 m.y. *Earth Planet. Sci. Lett.*, 97: 353-368.

Rea, D.K., (1990). Aspects of atmospheric circulation: the Late Pleistocene (0-950,000 yr) record of eolian deposition in the Pacific Ocean. *Palaeogeogr. Palaeoclimatol. Palaeoecol.*, 78: 217-227.

Rea, D.K. and Leinen, M., (1985). Neogene history of the calcite compensation depth and lysocline in the South Pacific Ocean. *Nature*, 316: 805-807.

Rea, D.K. and Janecek, T.R., (1982). Late Cenozoic changes in atmospheric circulation deduced from North Pacific eolian sediments. *Mar. Geol.*, 49: 149-167.

Rea, D.K. and Pisias, N.G. and Newburry, T., (1991). Late Pleistocene Paleoclimatology of the central equatorial Pacific: Flux patterns of biogenic sediments. *Paleoceanography*, 6(2): 227-244.

Reading, H.G., (1978). *Sedimentary Environments and Facies*. Blackwell Scientific Publications, Oxford. 557 p.

Reid, J.F., (1985). Carbonate platform facies models. *AAPG Bull.*, 69: 1-21.

Reineck, H.E. and Singh, I.B., (1980). *Depositional Sedimentary Environments- with reference to terrigenous clastics*. Springer-Verlag, Berlin. 439 p.

Reijmer, J.J.G., (1991). Sea level and sedimentation on the flanks of carbonate platforms [unpublished Ph.D. thesis]: Vrije Universiteit, Amsterdam, 162 p.

Reijmer, J.J.G. and Everaars, J.S.L., (1991). Carbonate platform facies reflected in carbonate basin facies (Triassic, Northern Calcereous Alps, Austria), *Facies*, 25: 253-278.

Reijmer, J.J.G., Schlager, W. and Droxler, A.W., (1988). Site 632: Pliocene-Pleistocene sedimentation cycles in a Bahamian Basin. In: Austin, J.A., Jr. Schlager, W., et al. (Eds.), *Proc. ODP., Sci. Results*, 101: College Station, TX (Ocean Drilling Program), 213-220.

Reijmer, J.J.G., Sprenger, A., Ten Kate, W.G.H.Z. and Schlager, W., (1992). Calciturbidite composition related to exposure and flooding of carbonate platforms (Triassic, Eastern Alps), *Sedimentology*, 38: 1059-1075.

Revelle, R.R., Bramlette, M., Arrhenius, G. and Goldberg, E.D., (1955). Pelagic sediments of the Pacific. *Geol. Soc. Am. Spec. Paper*, 62: 221-236.

Riggs, S.R., (1984). Palaeoceangraphic model of Neogene phosphorite deposition, U.S. Atlantic continental margin. *Science*, 223: 123-131.

Robinson, S.G., (1990). Applications for whole-core magnetic susceptibility measurements of deep-sea sediments: Leg 115 results. *In*: Duncan, R.A., Backman, J., Peterson, L.C., et al. (Eds.), *Proc .ODP, Sci. Results*, 115: College Station, TX (Ocean Drilling Program), 737-771.

Rochford, D.J., (1957). The identification and nomenclature of the surface water masses in the Tasman Sea. *Aust. J. Mar. Freshw. Res.*, 4: 369-413.

Rochford, D.J., (1959). Scientific reports of a cruise on H.M.A. Ships *Queensborough* and *Quickmatch* A. Hydrology: C.S.I.R.O. Australia Div.Fish.Oceanogr.Rept., 24: 1-24.

Rochford, D.J., (1969). Origin and circulation of water types of the 25.00 sigma-*t* surface of the south-west Pacific. *Aust. J. Mar. Freshw. Res.*, 20: 105-114.

Roof, S.R., Mullins, H.T., Gartner, S., Huang, T.C., Joyce, E., Prutzman, J. and Tjalsma, L., (1991).

Climatic forcing of cyclic carbonate sedimentation during the last 5.4 million years along the West Florida continental margin. *J. Sediment. Petrol.*, 61(7): 1070-1088.

Rösler, H.J. and Lange, H., (1972). *Geochemical Tables*. Elsevier, New York, 468 p.

Roth, P.H. and Berger, W.H., (1975). Distribution and dissolution of coccoliths in the south and central Pacific. In: Be, A.W.H. and Berger, W.H., *Spec. Publ. Cushman Found. Foraminiferal Res.*, 13: 87-113.

Rotschi, H. and Lemasson., L., (1967). Oceanography of the Coral and Tasman Seas. *Oceanogr. Mar. Biol. Ann. Rev.*, 5: 49-97.

Rucker, J.B., (1968). Carbonate mineralogy of sediments of Exuma Sound, Bahamas. *J. Sediment. Petrol.*, 38: 68-72.

Ruddiman, W.F., Cameron, D. and Clement, B.M., (1987). Sediment disturbance and correlation of offset holes drilled with the hydraulic piston corer: Leg 94. In: Ruddiman, W.F., Kidd, R.B., Thomas, E., et al., *Init. Repts. DSDP*, 94, Pt.2: Washington (U.S. Govt.Printing Office), 615-634.

Ruddiman, W.F., McInyre, A. and Raymo, M., (1986). Matuyama 41,000-year cycles: North Atlantic Ocean and northern hemisphere ice sheets. *Earth Planet. Sci. Lett.*, 80: 117-129.

Ruddiman, W.F., Raymo, M.E., Martinson, D.G., Clement, B.M. and Backman, J., (1989). Pleistocene evolution: Northern hemisphere ice sheets and North Atlantic Ocean. *Palaeoceanography*, 4: 353-412.

Runnells, D.D., (1970). Errors in X-ray analysis of carbonates due to solid-solution variation in composition of component minerals. *J. Sediment. Petrol.*, 40: 1158-1166.

Rutland, R.W.R., (1976). Orogenic evolution of Australia. *Earth-Science Reviews*, 12: 161-196.

Sandgren, P., Risberg, J. and Thompson, R., (1990). Magnetic susceptibility in sediment records of Lake Ådran, eastern Sweden: correlation among cores and interpretation. *Jour. Paleolimnology*, 3: 129-141.

Scheibner, E., (1985). Suspect terranes in the Tasman Fold Belt system, Eastern Australia. In: Howell, D.G. (Ed.). *Tectonostratigraphic Terranes in the Circum-Pacific Region*. Circum-Pacific Council Energy Miner. Resour. Earth Sci. Ser., 1: 493-514.

Scheibner, E., (1978). Tasman Fold Belt System or Orogenic System- Introduction. In: Scheibner, E. (Ed.). The Phanerozoic Structure of Australia and Variations in Tectonic Style. *Tectonophysics*, 48: 153-157.

Scheibner, E., (1987). Paleozoic tectonic development of eastern Australia in relation to the Pacific region. In: Monger, J.W.H. and Francheteau, J. (Eds.). *Circum-Pacific Orogenic Belts and Evolution of the Pacific Ocean Basin.* Am. Geophys. Un. Geodyn. Ser., 18: 133-165.

Schlager, W., (1992). Sedimentology and Sequence Stratigraphy of Reefs and Carbonate Platforms. Continuing Education Course Note Series 34, AAPG., 1-71.

Schlager, W. and James, N.P., (1978). Low-magnesium calcite limestones forming at the deep-sea floor, Tongue of the Ocean, Bahamas. *Sedimentology*, 25: 675-702.

Schlager, W., Reijmer, J.J.G. and Droxler, A., (1994). Highstand shedding of carbonate platforms. *Jour. Sed. Res.*, B64(3): 270-281.

Schmitz, B., (1987). Barium high productivity and northward wandering of the Indian continent. *Paleoceanography*, 2: 63-77.

Scholle, P.A., (1978). A color illustrated guide to carbonate rock constituents, textures, cements, and porosities. *AAPG*, Mem. 27: 1-241.

Scoffin, T.P., (1993). The geological effects of hurricanes on coral reefs and the interpretation of storm deposits. *Coral Reefs*, 12: 203-221.

Scoffin, T.P. and Tudhope, A.W., (1985). Sedimentary environments of the central region of the Great Barrier Reef of Australia. *Coral Reefs*, 4(2): 81-93.

Scott, D.L., (1993). Architecture of the Queensland Trough: implications for the structure and tectonics of the Northeastern Australian Margin. *AGSO Jour. Aust. Geol. and Geophys.*, 14: 21-34.

Sculley-Power, M., (1973a). Oceanography of the Coral Seas: the winter regime. *Roy. Aust. Naval Res.*, Lab. Tech. Note No.13/73.

Sculley-Power, M., (1973b). Coral Sea flow budgets in winter. *Aust. J. Mar. Freshw. Res.*, 24: 203-215.

Sculley-Power, M. and France, J.C., (1969). *Oceanographic cruise: Coral Sea, June 1968.* Roy. Aust. nav.res. Lab. Tech. Memo. (Ext.) 2/69.

Searle, D.E., (1983). Late Quaternary regional controls on the development of the Great Barrier Reef; geophysical evidence. *BMR Jour. Aust. Geol. and Geophys*, 8: 267-276.

Seibold, E. and Berger, W.H., (1993). *The Sea Floor: An Introduction to Marine Geology*. Springer-Verlag, Berlin, Heidelberg, 356 p.

Shackleton, N.J., Backman, J., Zimmerman, H., Kent, D.V., Hall, M.A., Roberts, D.G., Schnitker, D., Baldauf, J.G., Despraires, A., Homrighausen, R., Huddlestun, P., Keene, J.B., Kaltenback, A.J., Krumsiek, K.A.O., Morton, A.C., Murray, J.W. and Westberg-Smith, J., (1984). Oxygen isotope calibration of the onset of ice-rafting and history of glaciation in the North-Atlantic region, *Nature*, 307: 620-623.

Shackleton, N.J., Berger, A. and Peltier, W.R., (1990). An alternative astronomical calibration of the lower Pleistocene timescale based on ODP Site 677. *Trans. Roy. Soc. Edin., Earth Sci.*, 81: 251-261.

Shackleton, N.J. and Hall, M.A., (1989). Stable isotope history of the Pleistocene at ODP Site 677. In: Becker, K., Sakai, H., et al., *Proc. ODP, Sci. Results*, 111:College Station, TX (Ocean Drilling Program), 295-316.

Shackleton, N.J. and Opdyke, N.D., (1973). Oxygen isotope and palaeomagnetic stratigraphy of equatorial Pacific Core V28-238: oxygen isotope temperatures and ice volumes on a 10^5 year and 10^6 year scale. *Quat. Res. (N.Y.)*, 3: 39-55.

Shackleton, N.J. and Opdyke, N.D., (1976). Oxygen-isotope and palaeomagnetic stratigraphy of equatorial Pacific Core V28-239: late Pliocene to latest Pleistocene. In: Cline, R.M. and Hays, J.D. (Eds.), Investigations of Late Quaternary Paleoceanography and Paleoclimatology. Mem. Geol. Soc. Am., 145: 449-464.

Shankar, R., Subbarao, K.V. and Kolla, V., (1987). Geochemistry of surface sediments from the Arabian Sea. *Mar. Geol.*, 76: 253-279.

Shimmield, G.B. and Mowbray, S.R., (1991). The inorganic geochemical record of the northwest Arabian Sea: A history of productivity variation over the last 400 ka from Sites 722 and 724. In:

Prell, W.L., Niitsuma, N., et al. (Eds.). *Proc. ODP. Sci. Results*, 117: College Station, TX (Ocean Drilling Program), 409-429.

Shimmield, G.B. and Price, N.B., (1984). Recent dolomite formation in hemipelagic sediments off Baja California, Mexico. In: Garrison, R.E., Kastner, M. and Zenger, D.H. (Eds.), *Dolomites of the Monterey Formation and Other Organic-Rich Units*: Pacific Section, Spec. Publ.-Soc. Econ. Palontol. Mineral., 41: 5-18.

Shimmield, G.B. and Mowbray, S.R. and Weedon, G.P., (1990). A 350 ka history of the Indian Southwest Monsoon- evidence from deep-sea cores, northwest Arabian Sea. *Trans. R .Soc. Edinburgh*, 81: 289-299.

Shipboard Scientific Party, (1991). Site 819A. In: Davies, P.J., McKenzie, J.A., Palmer-Julson, A., et al., *Proc. ODP, Init. Repts.*, 133: College Station, TX (Ocean Drilling Program), 451-508.

Schmitz, B., (1987). The TiO_2/Al_2O_3 ratio in the Cenozoic Bengal abyssal fan sediments and its use as a palaeostream energy indicator. *Mar. Geol.*, 76: 195-206.

Shinn, E.A., (1968). Practical significance of birds eye structures in carbonate rocks. *J. Sediment. Petrol.*, 38: 215-223.

Sibley, D.F., (1980). Climatic controls of dolomitization, Seroe Domi Formation (Pliocene), Bonaire, N.A. In: Zenger, D.H., Dunham, J.B., and Ethington, R.L., (Eds.). *Concepts and models of dolomitization*. Spec. Publ.-Soc. Econ. Paleontol. Mineral., 28: 247-258.

Silver, E.A. and Smith, R.B., (1983). Comparison of terrane accretion in modern Southeast Asia and the Mesozoic North American Cordillera. *Geology*, 11: 198-202.

Singer, J.K., Anderson, J.B., Ledbetter, M.T., McCave, I.N., Jones, K.P.N. and Wright, R., (1988). An assessment of analytical techniques for the size analysis of fine-grained sediments. *J. Sediment. Pet.*, 58(3): 534-543.

Slowey, N.C., Neumann, A.C., and Baldwin, K.C., (1989). Seismic expression of Quaternary climatic cycles in the peri-platform carbonate ooze of the northern Bahamas. *Geol. Soc. Am. Bull.*, 101: 1563-1573.

Snowball, I. and Thompson, R., (1990). A mineral magnetic study of Holocene sedimentation in Lough Catherine, Northern Ireland. *Boreas*, 19: 127-146.

Spears, D.A. and Kanaris-Sotiriou, R., (1976). Titanium in some Carboniferous sediments from Great Britain. *Geochim. Cosmochim. Acta*, 40: 345-351.

Stein, R., (1986). Late Neogene evolution of paleoclimate and paleoceanic circulation in the Northern and Southern Hemisphere- A comparison, *Geologische Rundschau*, 75(1): 125-138.

Steens, T.N.F., Kroon, D., Ten Kate, W.G. and Sprenger, A., (1991). Late Pleistocene periodicities of oxygen isotope ratios, calcium carbonate contents and magnetic susceptibilities of Western Arabian Sea margin Hole 728A. In: Prell, W.L., Niitsuma, N., et al. (Eds.). *Proc. ODP. Sci. Results*, 117: College Station, TX (Ocean Drilling Program), 309-320.

Stevens, N.C., (1984). *Queensland Field Geology Guide*. Geol. Soc. Aust. (Queensland Division), Brisbane. 112 p.

Stieglitz, R.D. (1972). Scanning electron microscopy of the fine fraction of recent carbonate sediments from Bimini, Bahamas. *J. Sediment. Petrol.*, 42(1): 211-226.

Struckmeyer, H.I.M., (1990). Tectonics, climate and sea-level. In: Paine, A.G.L. (Ed.). BMR Palaeogeographic Group 1990- Australia: Evolution of a Continent. Bureau of Mineral Resources, Australia, 6-9.

Sundquist, E., (1990). Influence of deep-sea benthic processes on atmospheric CO_2. *Philos. Trans. R. Soc. Lond.*, 331: 155-165.

Summerhayes, C.P., Kroon, D., Rosell-Melé, A, Jordan, R.W., Schrader, H.-J., Hearn, R., Villanueva, J., Grimalt, J.O. and Eglington, G., in press. Variability in the Benguela current upwelling system over the last 70,000 years. *Progress in Oceanography*.

Swart, P.K. and Guzikowski, M., (1988). Interstitial-water chemistry and diagenesis of periplatform sediments from the Bahamas, ODP Leg 101. In: Austin, J.A., Jr. Schlager, W., Palmer, A.A., et al., *Proc. ODP, Sci. Results*, 101, College Station, TX (Ocean Drilling Program), 363-380.

Swart, P.K., Isern, A, Elderfield, H. and McKenzie, J.A., (1993). A summary of interstitial-water geochemistry of Leg 133. In: McKenzie, J.A., Davies, P.J., Palmer-Julson, A., et al., *Proc. ODP, Sci. Results*, 133: College Station, TX (Ocean Drilling Program), 705-722.

Swinchatt, J.P., (1968). Sedimentary facies in an area of mixed terrigenous-carbonate deposition:

Arlington Reef Complex and adjacent areas, northern Great Barrier Reef (abs.): *Bull. Am. Ass. Petrol. Geol.*, 52: 351.

Symonds, P.A., Davies, P.J. and Parisi, A., (1983). Structure and stratigraphy of the central Great Barrier Reef. *BMR Jour. Aust. Geol. and Geophys.*, 2: 284-303.

Talylor, L.W.H. and Falvey, D.A., (1977). Queensland plateau and Coral Sea Basin stratigraphy, structure and tectonics. *The APEA Journal*, 17(1): 13-29.

Takahashi, T., (1975). Carbonate chemistry of seawater and the calcite compensation depth in the oceans. In: Be, A.W.H. and Berger, W.H. (Eds.), Dissolution of deep-sea carbonates, *Spec. Publ. Cushman Found. Foraminiferal Res.*, 13: 11-26.

Tarling, D.H., (1983). *Palaeomagnetism, Principles and Applications in Geology, Geophysics and Archaeology*. New York (Chapman and Hall). 379 p.

Thiede, J., (1981). Reworked neritic fossils in upper Mesozoic and Cenozoic central Pacific deep sea sediments monitor sea-level changes. *Science*, 211: 1422-1424.

Thiede, J., Boersma, A., Schmidt, R.R. and Vincent, E., (1981). Reworked fossils in Mesozoic and Cenozoic pelagic central Pacific Ocean sediments, Deep Sea Drilling project Sites 463, 464, 465, and 466, Leg 62. In: Thiede, J., Vallier, T.J., et al. (Eds.)., *Initial Repts. DSDP.*, 62, U.S. Govt. Printing Office, Washington, D.C., 495-512.

Thierstein, H.R., Geitzenaurer, K.R., Molfino, B. and Shackleton, N.J., (1977). Global synchroneity of late Quaternary coccolith datum levels: Validation by oxygen isotopes. *Geology*, 5: 400-466.

Thompson, P.R., Be, A.W.H., Duplessy, J-C. and Shackleton, N.J., (1979). Disappearance of pink-pigmented *Globigerinoides ruber* at 120,000 yr BP in the Indian and Pacific Oceans. *Nature*, 280 (5723): 1-4.

Thompson, R., (1979). Palaeomagnetic correlation and dating. In: Berglund, B.E. (Ed.). *Palaeohydrological Changes in the temperate Zone in the Last 150 000 Years. Subproject B: Lake and Mire Environments* (vol. 2): Dep. Quat. Geol., 39-59.

Thompson, R., Battarbee, R., O'Sullivan, P. and Oldfield, F., (1975). Magnetic susceptibility of lake sediments. *Limnology and Oceanography*, 20(5): 687-698.

Thompson, R. and Oldfield, F., (1986). *Environmental magnetism*. London, George Allen and Unwin, 227 p.

Thompson, T.G. and Chow, J.J., (1956). The strontium-calcium atom ratio in carbonate secreting marine organisms. *Deep-Sea Res. Supplement*, 3: 20-39.

Thunell, R.C., (1976). Optimum indices of calcium carbonate dissolution in deep-sea sediments, *Geology*, 4: 208-227.

Thunell, R.C., (1982). Carbonate dissolution and abyssal hydrography in the Atlantic ocean. *Mar. Geol.*, 46: 165-180.

Tomczak, M. and Hao, D., (1989). Water masses in the thermocline of the Coral Sea. *Deep-Sea Res.*, 36(10): 1503-1514.

Towe, K.M., (1967). Echinoderm calcite: Single crystal or polycrystalline aggregates. *Science*, 157: 1048-1050.

Tucker, M.E., (1981). *Sedimentary Petrology: An introduction*. Blackwell Scientific Publications. 252 p.

Tucker, M.E. and Wright, V.P., (1990). *Carbonate Sedimentology*. Blackwell Scientific Publications. 482 p.

Tudhope, A.W. and Scoffin, T.P., (1988). The relative importance of benthic foraminiferans in the production of carbonate sediment on the Central Queensland Shelf. *Proc. 6th Int. Symp. Coral Reefs, Australia*, 2: 583-588.

Turekian, K.K., (1957). The significance of variations in the strontium content of deep-sea cores. *Limnol. Oceanogr.*, 2: 309-314.

Turekian, K.K., (1964). The marine geochemistry of Strontium. *Geochim. Cosmochim. Acta*, 28: 1479-1496.

Turekian, K.K. and Armstrong, R.L., (1960). Magnesium, strontium and barium concentrations and calcite-aragonite ratios of some recent mollusc shells. *Jour. Mar. Res.*, 13: 133-151.

Turekian, K.K. and Ledbetter, 1989 ?

Turekian, K.K. and Wedepohl, K.H., (1961). The distribution of the elements in some major units of the Earth's crust. *Geol. Soc. Am. Bull.*, 72: 175-192.

Urey, H.C., (1947). The thermodynamic properties of isotopic substances. *Jour. Chem. Soc.*, 562-581.

Urey, H.C., Lowenstam, H.A., Epstein, S. and McKinney, L.R., (1951). Measurement of paleotemperatures and temperatures of the Upper Cretaceous of England, Denmark, and the southeastern United States. *Geol. Soc. Am. Bull.*, 62: 399-415.

Vail, P.R., Mitchum, R.M., Todd, R.G., Widmier, J.M., Thompson, S., Sangree, J.B., Bubb, J.N. and Hatlelid, W.G., (1977). Seismic stratigraphy and global changes of sea level. In: Payton, C.E. (Ed.), *Seismic Stratigraphy -Application to Hydrocarbon Exploration*, AAPG Memoir 26: 49-212.

Van Andel, T.H., Heath, G.R. and Moore, T.C., (1975). Cenozoic history and paleoceanography of the central equatorial Pacific Ocean. *Geol. Soc. Am. Mem.*, 143.

Veevers, J.J. and McElhinny, M.W., (1976). The Separation of Australia from Other Continents. *Earth-Science Reviews*, 12: 139-159.

Volat, J.-L., Pastouret, L.P., and Vergnaud-Grazzini, C., (1980). Dissolution and carbonate fluctuations in Pleistocene deep-sea cores: A review, *Mar. Geol.*, 34: 1-28.

Von Breymann, M.T., Emeis, K.-C. and Camerlenghi, A., (1990). Geochemistry of sediments from the Peru upwelling area: Results from ODP Sites 680, 682, 685 and 688. In: Suess, E. et al., (Eds.)., *Proc. ODP., Sci. Results*, 112, 273-284.

Walter, L.M. and Morse, J.W., (1984). Magnesian calcite stabilities: A re-evaluation. *Geochim. Cosmochim. Acta*, 48: 1059-1069.

Watts, K.F., Varga, L.L. and Feary, D.A., (1993). Origins, timing and implications of Miocene to Pleistocene turbidites, debris flows, and slump deposits of the Queensland Trough, northeast Australia (Site 823). In: McKenzie, J.A., Davies, P.J., Palmer-Julson, A., et al., *Proc. ODP, Sci. Results*, 133: College Station, TX (Ocean Drilling Program), 379-446.

Wedepohl, K.H., (1960). Spurenanalytische Untersuchungen an Tiefseetonen aus Atlantik. Ein

Beitrag zur Deutung der geochemischen Sonderstellung von pelagischen Tonen. *Geochim. Cosmochim Acta*, 18: 200.

Wefer, G. and Berger, W.H., (1991). Isotope palaeontology: growth and composition of extant calcareous species. *Mar. Geol.*, 100: 207-248.

Wei, W., (1993). Calibration of upper Pliocene- lower Pleistocene nannofossil events with oxygen isotope stratigraphy. *Paleoceanography*, 8(1): 85-99.

Wei, W. and Gartner, S., (1993). Neogene calcareous nannofossils from Sites 811, 819 through 826, offshore northeastern Australia. In: McKenzie, J.A., Davies, P.J., Palmer-Julson, A., et al., *Proc. ODP, Sci. Results*, 133: College Station, TX (Ocean Drilling Program), 19-38.

Weissel, J.K. and Hayes, D.E., (1972). Magnetic anomalies in the Southeast Indian Ocean. In: Hayes, D.E. (Ed.). Antarctic Oceanography II: Australian-New Zealand Sector, *Am. Geophys. Union, Antarct. Res. Ser.*, 19: 234-249.

Weissel, J.K. and Watts, A.B., (1979). Tectonic evolution of the Coral Sea Basin. *J. Geophys. Res.*, 84: 4572-4582.

Wells, J.W., (1957). Coral Reef. In: Hedgpeth, J. (Ed.)., Treatise on marine ecology. *Geol. Soc. Am. Mem.*, 67(1): 609-631.

Wilber, R.J., Milliman, J.D. and Halley, R.B., (1990). Accumulation of bank-top sediment on the western slope of Great Bahama Bank: Rapid progradation of a carbonate megabank. *Geology*, 18: 970-974.

Williams, D.F., Lerche, I. and Full, W.E., (1988). *Isotope Chronostratigraphy: Theory and Methods*. Academic Press, Inc., (London) Ltd., 345 p.

Wilson, J.L., (1975). *Carbonate Facies in Geologic History*: Berlin (Springer-Verlag). 472 p.

Wilson, R.C.L., (1991). Sequence stratigraphy: An introduction. *Geoscientist*, 1(1): 13-23.

Winterer, E.L., (1970). Submarine valley systems around the Coral Sea Basin (Australia). *Mar. Geol.*, 8: 229-244.

Wolanski, E. and Bennett, A.F., (1983). Continental shelf waves and their influence on the

circulation around the Great Barrier Reef. *Aust. J. Mar. Freshw. Res.*, 34: 23-47.

Wolanski, E. and Jones, M., (1981). Physical properties of the Great Barrier Reef Lagoon waters near Townsville. I. Effects of Burdekin river floods. *Aust. J. Mar. Freshw. Res.*, 32: 305-319.

Wolanski, E., Jupp, D.L.B. and Pickard, G.L., (1986). Currents and Coral Reefs. *Oceanus*, 29(2): 83-89.

Wolf, K.H., Chilingar, G.V. and Beales, F.W., (1967). Elemental composition of carbonate skeletons, minerals and sediments. In: Chilingar, G.V., Bissell, H.J. and Fairbridge, R.W. (Eds.). *Developments in sedimentology 9B, Carbonate rocks: Physical and Chemical Aspects*, Elsevier, Amsterdam London New York, pp. 23-149.

Wyrtki, K., (1960). *Surface circulation in the Coral and Tasman Seas*. CSIRO Aust. Div. Fish. Oceanogr. Tech. Pap. 8.

Wyrtki, K., (1961). The flow of water into the Deep-Sea Basins of the western South Pacific Ocean. *Aust. J. Mar. Freshw. Res.*, 12: 1-16.

Wyrtki, K., (1962). The subsurface water masses in the western South Pacific Ocean. *Aust. J. Mar. Freshw. Res.*, 13: 18-47.

Wu, G., Herguera, J.C. and Berger, W.H., (1990). Differential dissolution: Modification of Late Pleistocene oxygen isotope records in the western equatorial Pacific. *Paleoceanography*, 5(4): 581-594.

Wu, G., Yasunda, M.K., and Berger, W.H., (1991). Late Pleistocene carbonate stratigraphy on Ontong-Java Plateau in the western equatorial Pacific. *Mar. Geol.*, 99: 135-150.

Yan, C.Y. and Kroenke, L.W., (1993). A plate tectonic reconstruction of the Southwest Pacific, 0-100 Ma. In: Berger, W.H., Kroenke, L.W., Mayer, L.A., et al., (Eds.). *Proc. ODP, Sci. Results*, v.130, College Station, TX (Ocean Drilling Program), 697-709.

APPENDIX - A

Stable Isotope Analysis and Operating Conditions of the VG Iosgas Precision Isotope Ratio Mass Spectrometer (PRISM).

The VG Isocarb automated carbonate preparation system is widely use in conjunction with the VG Isotech PRISM series II isotope mass spectrometer, for accurately measuring carbon and oxygen isotopes in carbonate samples. Standard PRISM analytical conditions are given in Table A.1 (see below). The Isocarb system is designed to automatically process up to 44 carbonate samples by loading the samples onto a carousel and sequentially dropping them into a reaction vessel containing 10 ml orthophosphoric acid (at 90°C and continuously mixed using a magnetic stirrer). The CO_2 evolved from the reaction between the calcium carbonate and acid, is pumped under high vacuum across a water trap (at -100°C) and collected by freezing into an external cold finger (at -196°C), located adjacent to the mass spectrometer inlet. The cold finger is then heated back to room temperature, and if the sample is large, the gas is transferred to the inlet valve of the mass spectrometer for immediate analysis. If the sample is small the gas undergoes further cryogenic transfer to the internal inlet coldfinger prior to analysis. The reference ion beam current is matched to that of the sample ion beam by use of variable-volume bellows. The mass spectrometer then measures the difference between the $^{13}C/^{12}C$ and the $^{18}O/^{16}O$ ratios of the sample and those of the reference gas, and gives the results as $\delta 1$ and $\delta 2$ values (Equation A.1).

These values are then recalculated into $\delta^{13}C$ (‰) and $\delta^{18}O$ (‰) by comparison with the average $\delta 1$ and $\delta 2$ values for the SM and MBL1 calcite standards used in the autorun and then, using Equation A.2, converted into the standard notation used in reporting foraminiferal isotopic results.

Table A.1 Standard PRISM analytical conditions

Target major ion beam	$6.00 \times E^{-09}$ A	
Maximum reference ion beam	$1.64 \times E^{-08}$ A	
Minimum reference ion beam	$2.49 \times E^{-09}$ A	
Ion Gauge base pressure	$7.60 \times E^{-10}$ Torr	
Cold finger ambient temperature	25°C	
	$\delta^{18}O$	$\delta^{13}C$
Std.dev. for SM1 standard (n = 100)	0.085 ‰	0.115 ‰

Equation A.1. Delta Calculation

$$\delta 1\ (‰) = (({}^{13}C/{}^{12}C_{smpl.} - {}^{13}C/{}^{12}C_{ref.})/{}^{13}C/{}^{12}C_{ref.}) \times 1000$$

$$\delta 1\ (‰) = (({}^{18}O/{}^{16}O_{smpl.} - {}^{18}O/{}^{16}O_{ref.})/{}^{18}O/{}^{16}O_{ref.}) \times 1000$$

where, smpl. = sample gas; ref. = reference gas

Equation A.2. $\delta^{13}C$ and $\delta^{18}O$ calculations

$$\delta^{13}C\ (PDB, ‰) = (\delta^{13}C_{sample} - \delta^{13}C_{PDB\ standard})/\delta^{13}C_{PDB\ standard} \times 1000$$

$$\delta^{18}O\ (PDB, ‰) = (\delta^{18}O_{sample} - \delta^{18}O_{\ PDB\ standard})/\delta^{18}O_{PDB\ standard} \times 1000$$

Where PDB = Pee Dee (formation) Belemnite standard (Epstein et al., 1953)

Table A.2. Duplicate stable oxygen isotope measurements of separate aliquots of *Globigerinoides ruber* and *Cibicidoides spp.* from Holes 819A and 823A.

Core section/ interval (cm)		Depth (mbsf)	$\delta^{18}O$ (‰)	$\delta^{18}O$ (‰)	$\Delta\delta^{18}O$ (‰)
Hole-819A					
Globigerinoides ruber					
3H02	10-12	19.60	-0.877	-1.067	-0.190
3H02	30-32	19.80	-1.174	-1.374	-0.200
3H02	52-54	20.02	-1.174	-1.161	0.013
3H02	70-72	20.20	-1.518	-1.940	-0.422
3H02	90-92	20.40	-1.235	-1.504	-0.269
3H02	109-111	20.59	-1.426	-1.862	-0.436
3H02	131-133	20.81	-1.410	-2.001	-0.591
3H03	10-12	21.10	-1.534	-1.846	-0.312
3H03	30-32	21.30	-1.608	-1.740	-0.132
3H03	52-54	21.52	-1.229	-1.510	-0.211
3H03	70-72	21.70	-1.502	-1.405	0.097
3H03	90-92	21.90	-2.245	-2.186	0.059
3H03	109-111	22.09	-1.246	-1.263	-0.017
3H03	131-133	22.31	-1.453	-1.411	0.042
3H04	10-12	22.60	-1.008	-1.100	-0.092
3H04	30-32	22.80	-1.330	-1.303	0.027
3H04	52-54	23.02	-1.331	-1.421	-0.090
3H04	70-72	23.20	-1.190	-1.010	0.180
3H04	90-92	23.40	-0.765	-1.120	-0.355
3H04	109-111	23.59	-1.300	-1.430	-0.130
3H04	131-133	23.81	-0.896	-1.310	-0.414
3H05	10-12	24.10	-0.967	-1.256	-0.289
3H05	30-32	24.30	-0.997	-1.211	-0.214
3H05	52-54	24.52	-0.650	-0.919	-0.269
3H05	70-72	24.70	-0.679	-0.975	-0.296
3H05	87-89	24.87	-0.506	-0.710	-0.204
3H05	109-111	25.09	-0.241	-0.561	-0.320
3H06	26-28	25.76	-0.470	-0.641	-0.171
3H06	52-54	26.02	-0.847	-0.955	-0.108
3H06	67-69	26.17	-0.511	-0.931	-0.420
3H06	109-111	26.59	-0.873	-1.220	-0.347
3H06	131-133	26.81	-0.805	-0.820	-0.015
3H07	10-12	27.10	-1.078	-1.050	0.028
12H05	10-12	109.60	-0.641	-0.677	0.036
Cibicidoides spp					
1H05	30-32	6.30	2.718	2.186	0.532
3H05	70-72	24.70	2.530	1.563	0.967
3H05	109-111	25.09	2.763	2.609	0.154
3H06	109-111	26.59	2.063	1.699	0.364

3H07	10-12	27.10	3.153	2.932	0.221
4H01	50-52	28.00	0.833	2.010	-1.177
4H01	70-72	28.20	2.114	2.207	-0.093
4H01	110-112	28.60	1.068	0.674	0.394
4H02	10-12	29.10	1.964	1.860	0.104
4H02	70-72	29.70	2.463	1.836	0.627
4H02	90-92	29.90	2.031	1.869	0.162
4H02	110-112	30.10	2.149	1.216	0.933
4H02	130-132	30.30	1.975	1.540	0.435
4H03	10-12	30.60	1.773	1.121	0.652
4H03	50-52	31.00	2.190	1.624	0.566
4H04	35-37	32.30	1.467	1.233	0.234
4H04	70-72	32.70	2.115	1.825	0.290
4H04	130-132	33.30	1.971	1.903	0.068
4H05	110-112	34.60	0.710	1.410	-0.700
5H05	10-12	43.10	0.300	1.419	-1.119

Hole-823A

Globigerinoides ruber

1H01	11-13	0.11	-2.230	-2.241	-0.011
1H01	35-37	0.35	-1.975	-2.258	-0.283
1H01	60-62	0.60	-1.985	-2.109	-0.124
1H01	85-87	0.85	-1.339	-1.132	0.207
1H01	110-112	1.10	-0.740	-0.927	-0.187
1H01	135-137	1.35	-1.651	-1.566	0.085
1H02	12-14	1.62	-1.406	-1.400	0.006
1H02	35-37	1.85	-0.778	-0.693	0.095
1H02	60-62	2.10	-1.010	-0.909	0.101
1H02	85-87	2.35	-0.938	-0.911	0.027
1H02	110-112	2.60	-1.419	-1.399	0.020
1H02	135-137	2.85	-1.092	-1.120	-0.028
1H03	13-15	3.13	-1.334	-1.115	0.219
1H03	35-37	3.35	-0.859	-1.073	-0.214
1H03	60-62	3.60	-0.931	-1.078	-0.147
1H03	85-87	3.85	-1.263	-1.298	-0.035
1H03	110-112	4.10	-1.447	-1.511	-0.064
1H03	135-137	4.35	-1.511	-1.586	-0.075
1H04	11-13	4.61	-1.945	-1.923	0.022
1H04	35-37	4.85	-1.597	-2.076	-0.479
1H04	60-62	5.10	-1.412	-1.430	-0.018
1H04	85-87	5.35	-1.619	-1.665	-0.046
1H04	110-112	5.60	-1.589	-1.574	0.015

Cibicidoides spp

2H03	88-90	9.68	3.705	3.901	-0.196
7H03	60-62	56.90	2.893	2.817	0.076

Note: Column 5 ($\Delta\delta^{18}O$) lists the difference (‰) between duplicate stable oxygen isotope measurements.

Table A.3. Planktic and benthic foraminiferal oxygen and carbon isotope ratios from ODP Leg 133 Site 819 (upper-slope of the Great Barrier Reef).

Sample Code		Depth (mbsf)	Age (Ma)	*G.ruber*		*Cibicidoides spp.*	
				$\delta^{13}C$ ‰	$\delta^{18}O$ ‰	$\delta^{13}C$ ‰	$\delta^{18}O$ ‰
1H01	16-18	0.16	0.00050	0.80	-2.37	1.66	0.37
1H01	30-32	0.30	0.00094	0.55	-2.26	1.35	1.41
1H01	54.56	0.54	0.00169	0.96	-2.08	1.07	1.15
1H01	70-72	0.70	0.00219	1.00	-2.33	1.28	0.87
1H01	90-92	0.90	0.00281	0.69	-2.42	1.13	1.06
1H01	120-122	1.20	0.00375	1.15	-2.28	1.26	1.04
1H02	10-12	1.60	0.00500	1.23	-2.09	1.70	0.69
1H02	30-32	1.80	0.00563	0.54	-2.50	1.13	1.29
1H02	54-56	2.04	0.00638	1.08	-2.15	1.37	1.36
1H02	68-70	2.18	0.00681	0.75	-2.25	1.14	1.55
1H02	70-72	2.20	0.00688	0.70	-2.19	2.11	1.13
1H02	90-92	2.40	0.00750	0.77	-2.11	1.62	0.78
1H02	120-122	2.70	0.00844	0.34	-2.42	1.08	1.31
1H03	10-12	3.10	0.00969	-0.52	-1.32	1.80	0.17
1H03	30-32	3.30	0.0103	0.87	-1.59	1.15	1.47
1H03	54-56	3.54	0.0111	0.04	-2.21	1.65	1.13
1H03	70-72	3.70	0.0116	1.85	-2.64	1.13	1.81
1H03	95-97	3.95	0.0123	0.50	-2.17	0.70	1.43
1H03	120-122	4.20	0.0134	0.53	-1.56	0.98	1.57
1H04	10-12	4.60	0.0151	0.80	-1.37	1.09	1.79
1H04	30-32	4.80	0.0159	0.65	-1.40	0.77	2.11
1H04	54-56	5.04	0.0169	0.56	-1.61	0.98	2.05
1H04	70-72	5.20	0.0176	0.54	-1.23	1.00	1.44
1H04	90-92	5.40	0.0185	0.63	-0.64	0.95	2.03
1H04	120-122	5.70	0.0197	0.60	-0.53	0.98	2.15
1H05	10-12	6.10	0.0214	0.77	-0.20	1.11	2.55
1H05	30-32	6.30	0.0223	0.76	-0.58	1.23	2.72
1H05	70-72	6.70	0.0240	0.84	-0.83	1.21	2.38
1H05	90-92	6.90	0.0246	1.07	-1.07	1.24	2.28
1H05	120-122	7.20	0.0255	0.20	-1.15	1.14	2.14
1H06	10-12	7.60	0.0267	1.00	-1.27	1.07	2.03
1H06	30-32	7.80	0.0274	1.28	-1.72	1.65	1.70
1H06	54-56	8.04	0.0281	0.82	-1.56	1.11	2.01
1H06	68-70	8.18	0.0285	1.53	-1.67	1.11	1.95
2H01	12-14	8.62	0.0298	0.54	-1.81	1.13	1.72
2H01	30-32	8.80	0.0304	0.77	-1.58	1.90	1.46
2H01	54-56	9.04	0.0311	0.57	-1.75	0.99	1.92
2H01	70-72	9.20	0.0316	0.40	-1.73	0.89	1.84
2H01	88-90	9.38	0.0322	0.66	-1.74	1.05	1.84
2H01	109-111	9.59	0.0328	0.61	-1.57	0.90	1.64
2H01	132-134	9.82	0.0335	0.68	-1.98	–	–
2H02	12-14	10.12	0.0344	0.86	-1.66	0.97	1.90
2H02	30-32	10.30	0.0350	0.31	-2.13	0.77	1.90
2H02	54-56	10.54	0.0357	0.52	-1.56	0.96	2.01
2H02	70-72	10.70	0.0362	1.10	-1.75	0.75	1.93
2H02	88-90	10.88	0.0367	0.47	-1.50	0.69	1.37
2H02	109-111	11.09	0.0374	-0.27	-2.21	0.76	1.86
2H02	132-134	11.32	0.0381	0.98	-1.51	0.90	2.10
2H03	30-32	11.80	0.0395	0.73	-1.60	1.14	1.88
2H03	54-56	12.04	0.0403	0.83	-1.35	1.10	2.02
2H03	70-72	12.20	0.0407	0.99	-1.16	0.99	2.20
2H03	88-90	12.38	0.0413	0.79	-1.51	0.91	1.88

2H03	109-111	12.59	0.0419	0.53	-1.57	1.76	2.26
2H03	132-134	12.82	0.0427	0.69	-1.68	1.12	2.27
2H04	12-14	13.12	0.0435	1.38	-1.32	1.19	1.81
2H04	30-32	13.30	0.0441	0.98	-1.75	0.71	0.67
2H04	54-56	13.54	0.0448	1.05	-1.05	1.46	2.64
2H04	70-72	13.70	0.0453	0.51	-1.11	0.78	1.04
2H04	88-90	13.88	0.0459	1.00	-1.34	0.95	2.16
2H04	109-111	14.09	0.0465	0.62	-1.11	1.03	1.94
2H04	132-134	14.32	0.0473	-0.01	-1.29	0.91	1.99
2H05	12-14	14.62	0.0481	0.84	-1.90	1.45	1.58
2H05	30-32	14.80	0.0487	0.54	-1.42	1.05	2.39
2H05	54-56	15.04	0.0494	1.00	-1.53	1.22	1.87
2H05	70-72	15.20	0.0499	1.10	-1.34	1.02	1.91
2H05	88-90	15.38	0.0504	0.71	-1.32	1.21	1.88
2H05	109-111	15.59	0.0511	0.50	-1.71	–	–
2H05	132-133	15.82	0.0518	0.34	-1.66	1.01	1.47
2H06	12-14	16.12	0.0527	1.10	-1.47	1.11	1.95
2H06	30-32	16.30	0.0532	0.43	-1.78	1.44	1.85
2H06	54-56	16.54	0.0540	0.81	-1.79	0.73	2.08
2H06	70-72	16.70	0.0544	0.82	-1.81	0.97	1.80
2H06	88-90	16.88	0.0550	0.41	-1.72	0.96	2.36
2H06	109-111	17.09	0.0556	1.12	-1.54	0.79	1.72
2H06	132-134	17.32	0.0563	0.87	-1.65	0.57	2.18
2H07	7-8	17.57	0.0571	0.82	-1.42	1.35	1.39
2H07	27-29	17.77	0.0577	0.43	-1.68	1.36	1.47
2H07	54-56	18.04	0.0585	0.40	-1.57	1.12	0.94
3H01	10-12	18.10	0.0587	0.57	-1.80	1.31	2.27
3H01	30-32	18.30	0.0598	1.34	-0.85	–	–
3H01	52-54	18.52	0.0616	0.71	-0.78	1.07	1.91
3H01	70-72	18.70	0.0630	0.29	-1.24	–	–
3H01	90-92	18.90	0.0646	0.62	-1.03	1.12	1.72
3H01	109-111	19.09	0.0661	1.15	-1.06	0.85	1.71
3H01	131-133	19.31	0.0679	0.49	-1.18	1.02	1.73
3H02	10-12	19.60	0.0702	0.51	-0.88	0.92	1.73
3H02	30-32	19.80	0.0732	0.89	-1.17	0.70	2.38
3H02	52-54	20.02	0.0780	0.81	-1.17	1.22	1.94
3H02	70-72	20.20	0.0819	0.24	-1.52	0.81	2.01
3H02	90-92	20.40	0.0863	0.56	-1.24	2.16	0.15
3H02	109-111	20.59	0.0904	1.04	-1.43	0.74	1.66
3H02	131-133	20.81	0.0952	1.07	-1.41	0.65	1.48
3H03	10-12	21.10	0.1016	0.03	-1.53	1.37	0.82
3H03	30-32	21.30	0.1059	-0.01	-1.61	0.87	1.09
3H03	52-54	21.52	0.1108	0.62	-1.23	0.65	0.91
3H03	70-72	21.70	0.1147	0.56	-1.50	0.72	1.98
3H03	90-92	21.90	0.1191	0.10	-2.25	2.30	0.20
3H03	109-111	22.09	0.1232	0.19	-1.25	–	–
3H03	131-132	22.31	0.1280	0.37	-1.45	1.34	0.16
3H04	10-12	22.60	0.1315	0.42	-1.01	0.69	1.10
3H04	30-32	22.80	0.1339	0.11	-1.33	0.43	2.03
3H04	52-54	23.02	0.1365	0.17	-1.33	0.34	0.97
3H04	70-72	23.20	0.1388	0.17	-1.19	0.74	1.19
3H04	90-92	23.40	0.1412	0.99	-0.77	1.64	2.88
3H04	109-111	23.59	0.1435	-0.30	-1.30	0.47	2.08
3H04	131-133	23.81	0.1462	0.23	-0.90	1.51	0.62
3H05	10-12	24.10	0.1597	0.16	-0.97	0.59	1.19
3H05	30-32	24.30	0.1521	0.24	-1.00	0.54	2.20
3H05	52-54	24.52	0.1548	0.14	-0.65	0.64	3.28
3H05	70-72	24.70	0.1569	0.19	-0.68	0.69	2.53
3H05	87-89	24.87	0.1590	0.42	-0.51	0.87	2.50

3H05	109-111	25.09	0.1617	0.48	-0.24	0.66	2.76
3H06	7-9	25.57	0.1675	0.24	-0.80	0.85	1.92
3H06	26-28	25.76	0.1698	0.43	-0.47	0.71	2.15
3H06	52-54	26.02	0.1729	0.66	-0.85	1.06	2.23
3H06	67-69	26.17	0.1747	0.09	-0.51	0.79	3.23
3H06	90-92	26.40	0.1775	0.64	-1.11	0.74	2.25
3H06	109-111	26.59	0.1798	1.00	-0.87	1.02	2.06
3H06	131-133	26.81	0.1822	1.10	-0.81	0.96	2.99
3H07	10-12	27.10	0.1860	0.82	-1.08	0.87	3.15
4H01	30-32	27.80	0.1945	1.11	-1.30	0.88	2.97
4H01	50-52	28.00	0.1968	0.35	-0.81	0.77	0.83
4H01	70-72	28.20	0.1993	0.49	-1.67	0.49	2.11
4H01	90-92	28.40	0.2017	0.43	-1.62	0.62	1.30
4H01	110-112	28.60	0.2042	0.46	-0.74	0.61	1.07
4H01	130-132	28.80	0.2200	0.40	-0.68	1.00	2.23
4H02	10-12	29.10	0.2240	0.24	-0.33	0.76	1.96
4H02	30-32	29.30	0.2267	0.07	-0.34	0.97	2.29
4H02	50-52	29.50	0.2293	0.72	-0.51	1.11	1.80
4H02	70-72	29.70	0.2320	0.86	-0.66	1.09	2.46
4H02	90-92	29.90	0.2347	0.72	-1.12	1.27	2.03
4H02	110-112	30.10	0.2373	0.69	-1.04	1.23	2.15
4H02	130-132	30.30	0.2400	0.59	-1.56	0.79	1.98
4H03	10-12	30.60	0.2505	0.46	-1.09	1.09	1.77
4H03	30-32	30.80	0.2575	0.53	-0.58	0.86	1.65
4H03	50-52	31.00	0.2645	0.69	-0.60	0.91	2.19
4H03	70-72	31.20	0.2715	-0.47	-0.94	0.75	1.78
4H03	90-92	31.40	0.2785	0.66	-1.13	0.89	1.93
4H03	110-112	31.60	0.2855	0.77	-0.95	0.99	1.24
4H03	130-132	31.80	0.2925	0.98	-1.36	0.89	1.85
4H04	10-12	32.10	0.3030	0.29	-1.10	0.73	2.06
4H04	30-32	32.30	0.3100	-0.46	-1.18	0.60	1.47
4H04	50-52	32.50		0.69	-0.95	0.96	2.16
4H04	70-72	32.70	0.5299	0.83	-1.60	0.76	2.12
4H04	90-92	32.90	0.5357	-0.78	-0.67	-0.87	2.39
4H04	110-112	33.10	0.5416	-0.56	-0.83	0.57	2.19
4H04	130-132	33.30	0.5474	0.55	-0.49	0.36	1.97
4H05	10-12	33.60	0.5562	-2.13	0.03	-0.46	1.61
4H05	30-32	33.80	0.5621	-0.89	-0.27	0.78	1.86
4H05	50-52	34.00	0.5662	-0.24	-0.30	0.54	1.78
4H05	70-72	34.20	0.5686	1.91	-1.22	0.47	1.95
4H05	90-92	34.20	0.5710	-0.06	-1.22	0.16	2.39
4H05	110-112	34.60	0.5735	-0.22	-0.80	-0.05	0.71
4H05	130-132	34.80	0.5759	1.62	-1.10	–	–
4H06	10-12	35.10	0.5795	-1.93	-0.04	–	–
4H06	30-32	35.30	0.5819	-0.08	-0.89	–	–
4H06	50-52	35.50	0.5845	-0.52	-0.50	0.78	1.61
4H06	70-72	35.70	0.5868	-0.37	-0.94	–	–
4H06	90-92	35.90	0.5892	0.55	-0.72	–	–
4H06	110-112	36.10	0.5916	-0.29	-0.47	–	–
4H06	130-132	36.30	0.5940	-0.03	-0.65	1.00	1.69
4H07	10-12	36.60	0.5976	-1.31	-1.00	0.86	1.64
4H07	30-32	36.80	0.6000	0.36	-1.76	–	–
4H07	50-52	37.00	0.6025	-1.00	-0.69	–	–
4H07	70-72	37.20	0.6037	-1.35	-0.41	–	–
5H01	10-12	37.10	0.6049	-1.47	-0.58	0.83	1.89
5H01	30-32	37.30	0.6061	-0.25	-0.75	–	–
5H01	50-52	37.50	0.6085	-0.54	-0.67	–	–
5H01	70-72	37.70	0.6109	-0.55	-0.59	0.86	1.62
5H01	90-92	37.90	0.6134	-0.65	-0.64	0.45	1.29

5H01	110-112	38.10	0.6158	-0.32	-0.55	–	–
5H01	130-132	38.30	0.6182	-1.35	-0.51	–	–
5H02	10-12	38.60	0.6229	-3.24	0.48	–	–
5H02	30-32	38.80	0.6267	-4.42	0.29	–	–
5H02	50-52	39.00	0.6305	-4.61	0.61	–	–
5H02	70-72	39.20	0.6343	-3.47	0.11	–	–
5H02	90-92	39.40	0.6381	-3.15	-0.17	–	–
5H02	110-112	39.60	0.6419	-4.09	-0.29	0.30	1.30
5H02	130-132	39.80	0.6457	-2.76	-0.22	–	–
5H03	10-12	40.10	0.6514	-5.47	0.97	–	–
5H03	30-32	40.30	0.6552	-3.33	-0.15	–	–
5H03	50-52	40.50	0.6590	-3.24	0.37	–	–
5H03	70-72	40.70	0.7210	-0.43	-0.84	–	–
5H03	90-92	40.90	0.7316	-0.29	-1.01	–	–
5H03	110-112	41.10	0.7349	0.03	-0.69	0.51	1.36
5H03	130-132	41.30	0.7382	0.03	-0.89	–	–
5H04	10-12	41.60	0.7432	-0.38	-1.36	0.45	1.65
5H04	30-32	41.80	0.7464	-0.38	-0.98	–	–
5H04	50-52	42.00	0.7497	0.18	-0.89	–	–
5H04	70-72	42.20	0.7530	0.26	-0.94	0.68	1.47
5H04	90-92	42.40	0.7563	-0.06	-0.61	–	–
5H04	110-112	42.60	0.7596	0.10	-0.69	–	–
5H04	130-132	42.80	0.7629	-1.03	-1.13	–	–
5H05	10-12	43.10	0.7678	0.15	-0.79	0.31	0.30
5H05	30-32	43.30	0.7711	-0.10	-1.01	–	–
5H05	50-52	43.50	0.7744	-0.32	-1.21	0.67	1.42
5H05	70-72	43.70	0.7777	-0.32	-0.92	–	–
5H05	90-92	43.90	0.7810	-0.84	-0.93	-0.64	-2.28
5H05	110-112	44.10	0.7842	-0.22	-1.16	0.51	1.36
5H05	130-132	44.30	0.7875	-0.47	-0.84	–	–
5H06	10-12	44.60	0.7932	-0.71	-0.23	–	–
5H06	30-32	44.80	0.7976	-0.73	-0.20	–	–
5H06	50-52	45.00	0.8019	-0.85	0.28	0.35	1.42
5H06	70-72	45.20	0.8062	-0.27	-0.18	–	–
5H06	90-92	45.40	0.8105	-0.43	-0.09	-0.54	1.71
5H06	110-112	45.60	0.8148	0.11	-0.39	–	–
5H06	130-132	45.80	0.8192	0.19	-0.51	-0.03	0.20
5H07	10-12	46.10	0.8256	0.08	-0.29	–	–
5H07	30-32	46.30	0.8299	-0.26	-0.14	–	–
5H07	50-52	46.50	0.8343	-0.07	-0.57	–	–
5H07	70-72	46.70	0.8364	-0.62	-0.98	0.19	1.77
6H01	10-12	46.60	0.8379	0.01	-1.02	–	–
6H01	30-32	46.80	0.8389	0.38	-1.22	0.53	1.58
6H01	50-52	47.00	0.8408	-0.20	-1.48	0.51	1.52
6H01	70-72	47.20	0.8427	0.06	-1.03	0.43	1.13
6H01	90-92	47.40	0.8446	0.30	-1.62	–	–
6H01	110-112	47.60	0.8465	-0.12	-1.73	–	–
6H01	130-132	47.80	0.8483	-0.44	-1.29	–	–
6H02	10-12	48.10	0.8512	0.64	-1.48	–	–
6H02	30-32	48.30	0.8530	0.66	-1.26	–	–
6H02	50-52	48.50	0.8549	0.40	-1.33	–	–
6H02	70-72	48.70	0.8568	0.88	-1.02	0.46	1.40
6H02	90-92	48.90	0.8587	0.15	-1.15	–	–
6H02	110-112	49.10	0.8606	0.45	-1.12	–	–
6H02	130-132	49.30	0.8625	0.13	-1.08	–	–
6H03	10-12	49.60	0.8653	-0.19	-0.92	0.59	1.91
6H03	30-32	49.80	0.8672	0.14	-1.08	0.67	1.65
6H03	50-52	50.00	0.8691	0.59	-0.17	–	–
6H03	70-72	50.20	0.8703	-0.03	-0.59	–	–

6H03	90-92	50.40	0.8709	0.61	-0.01	–	–
6H03	110-112	50.60	0.8715	0.73	-0.25	–	–
6H03	130-132	50.80	0.8720	0.33	-0.56	–	–
6H04	10-12	51.10	0.8729	0.60	-0.44	–	–
6H04	30-32	51.30	0.8735	0.54	-0.27	–	–
6H04	50-52	51.50	0.8741	0.56	-0.47	–	–
6H04	70-72	51.70	0.8747	0.79	-0.15	–	–
6H04	90-92	51.90	0.8753	0.41	-0.32	–	–
6H04	110-112	52.10	0.8758	0.28	-0.28	0.63	1.88
6H04	130-132	52.30	0.8764	0.88	-0.48	–	–
6H05	10-12	52.60	0.8773	0.92	-0.20	1.05	1.49
6H05	30-32	52.80	0.8779	0.42	-0.19	1.18	0.85
6H05	50-52	53.00	0.8785	0.91	-0.06	1.05	1.49
6H05	70-72	53.20	0.8791	0.94	-0.35	–	–
6H05	90-92	53.40	0.8796	0.58	-0.15	0.93	1.82
6H05	110-112	53.60	0.8802	0.52	-0.13	–	–
6H05	130-132	53.80	0.8808	0.61	-0.03	0.64	-0.58
6H06	10-12	54.10	0.8817	0.84	0.07	0.73	1.85
6H06	30-32	54.30	0.8823	0.28	-0.15	–	–
6H06	50-52	54.50	0.8829	0.44	-0.27	–	–
6H06	70-72	54.70	0.8834	0.81	-0.02	0.87	1.73
6H06	90-92	54.90	0.8840	0.21	0.14	0.75	1.89
6H06	110-112	55.10	0.8846	0.98	0.16	1.08	0.27
7H06	130-132	55.30	0.8852	0.36	-0.60	0.95	0.89
7H01	10-12	56.10	0.8875	0.73	-0.30	1.07	1.77
7H01	30-32	56.30	0.8881	0.47	-0.16	1.09	1.59
7H01	50-52	56.50	0.8887	1.23	-0.37	1.22	0.19
7H01	70-72	56.70	0.8893	0.84	-0.02	–	–
7H01	90-90	56.90	0.8899	1.18	-0.36	0.90	1.69
7H01	110-112	57.10	0.8904	0.86	-0.47	1.10	1.61
7H01	130-132	57.30	0.8910	0.83	-0.36	0.79	1.50
7H02	10-12	57.60	0.8919	0.56	-0.69	–	–
7H02	30-32	57.80	0.8925	0.78	-0.17	1.40	0.43
7H02	50-52	58.00	0.8931	0.59	-0.33	0.98	1.53
7H02	70-72	58.20	0.8937	0.49	-0.29	0.93	1.19
7H02	90-92	58.40	0.8942	0.85	-0.19	1.09	1.53
7H02	110-112	58.60	0.8948	0.85	-0.33	1.08	1.54
7H02	130-132	58.80	0.8954	0.84	-0.73	0.37	0.90
7H03	10-12	59.10	0.8963	0.93	-0.48	0.62	1.33
7H03	30-32	59.30	0.8969	0.62	-0.48	–	–
7H03	50-52	59.50	0.8975	–	–	0.28	1.49
7H03	70-52	59.70	0.8980	1.08	-0.62	-0.36	1.43
7H03	90-92	59.90	0.8986	0.96	-0.19	0.69	1.39
7H03	110-112	60.10	0.8992	0.94	-0.62	0.74	1.33
7H03	130-132	60.30	0.8998	0.64	-1.01	0.52	-0.39
7H04	10-12	60.60	0.9007	0.67	-0.77	–	–
7H04	30-32	60.80	0.9013	–	–	–	–
7H04	50-52	61.00	0.9018	0.92	-0.70	–	–
7H04	70-72	61.20	0.9024	–	–	–	–
7H04	90-92	61.40	0.9030	0.80	-0.64	–	–
7H04	110-112	61.60	0.9036	–	–	–	–
7H04	130-132	61.80	0.9042	1.09	-0.80	–	–
7H05	10-12	62.10	0.9051	–	–	–	–
7H05	30-32	62.30	0.9056	1.00	-0.80	–	–
7H05	50-52	62.50	0.9062	–	–	–	–
7H05	70-72	62.70	0.9068	0.77	-0.96	–	–
7H05	90-92	62.90	0.9074	–	–	–	–
7H05	110-112	63.10	0.9080	0.69	-1.21	–	–
7H06	10-12	63.60	0.9094	0.28	-1.56	–	–

7H06	30-32	63.80	0.9100	–	–	–	–
7H06	50-52	64.00	0.9106	0.68	-1.50	–	–
7H06	70-72	64.20	0.9112	0.95	-1.18	–	–
7H06	90-92	64.40	0.9118	0.86	-1.20	–	–
7H06	110-112	64.60	0.9123	1.10	-1.12	–	–
7H06	130-132	64.80	0.9129	1.05	-1.40	–	–
7H07	10-12	65.10	0.9138	0.66	-1.47	–	–
7H07	30-32	65.30	0.9144	0.88	-1.65	–	–
7H07	50-52	65.50	0.9150	1.16	-1.59	–	–
8H01	10-12	65.60	0.9153	0.99	-1.73	–	–
8H01	30-32	65.80	0.9159	0.61	-1.67	–	–
8H01	50-52	66.00	0.9164	0.38	-1.72	–	–
8H02	10-12	66.22	0.9171	0.55	-1.74	–	–
8H02	30-32	66.42	0.9177	0.52	-1.62	–	–
8H02	50-52	66.62	0.9182	0.26	-1.58	–	–
8H02	70-72	66.82	0.9188	0.31	-1.85	–	–
8H02	90-92	67.02	0.9194	0.09	-1.63	–	–
8H02	110-112	67.22	0.9200	0.48	-1.37	–	–
8H02	130-132	67.42	0.9203	0.66	-1.37	–	–
8H03	10-12	67.72	0.9207	0.69	-1.25	–	–
8H03	30-32	67.92	0.9209	0.67	-1.22	–	–
8H03	50-52	68.12	0.9212	0.44	-1.39	–	–
8H03	70-72	68.32	0.9215	0.45	-0.93	–	–
8H03	90-92	68.52	0.9217	0.37	-0.94	–	–
8H03	110-112	68.72	0.9220	0.02	-1.16	–	–
8H03	130-132	68.92	0.9223	0.59	-0.95	–	–
8H04	10-12	69.22	0.9227	0.50	-1.07	–	–
8H04	30-32	69.42	0.9229	0.96	-0.96	–	–
8H04	50-52	69.62	0.9232	0.05	-1.07	–	–
8H04	70-72	69.82	0.9235	0.42	-1.34	–	–
8H04	90-92	70.02	0.9237	0.42	-1.36	–	–
8H04	110-112	70.22	0.9240	0.61	-0.89	–	–
8H04	130-132	70.42	0.9243	0.97	-1.04	–	–
8H05	10-12	70.72	0.9247	0.35	-1.03	–	–
8H05	30-32	70.92	0.9249	0.58	-0.77	–	–
8H05	50-52	71.12	0.9252	0.38	-1.05	–	–
8H05	70-72	71.32	0.8255	0.79	-0.83	–	–
8H05	90-92	71.52	0.9257	0.37	-1.15	–	–
8H05	110-112	71.72	0.9260	1.03	-0.98	–	–
8H05	130-132	71.92	0.9263	0.64	-1.03	–	–
8H06	10-12	72.22	0.9267	0.78	-0.86	–	–
8H06	30-32	72.42	0.9269	0.84	-0.99	–	–
8H06	50-52	72.62	0.9272	0.97	-1.09	–	–
8H06	70-72	72.82	0.9275	0.81	-1.15	–	–
8H06	90-92	73.02	0.9277	0.50	-1.00	–	–
8H06	110-112	73.22	0.9280	0.70	-1.00	–	–
8H06	130-132	73.42	0.9283	–	–	–	–
8H07	10-12	73.72	0.9287	0.50	-1.02	–	–
8H07	30-32	73.92	0.9289	–	–	–	–
8H07	50-52	74.12	0.9292	–	–	–	–
8H07	70-72	74.32	0.9295	0.27	-0.90	–	–
8H07	90-92	74.52	0.9297	0.73	-1.31	–	–
8H07	110-112	74.72	0.9300	–	–	–	–
8H07	130-132	74.92	0.9308	0.83	-1.39	–	–
9H01	10-12	75.10	0.9314	–	–	–	–
9H01	30-32	75.30	0.9322	0.39	-1.41	–	–
9H02	10-12	75.45	0.9327	–	–	–	–
9H02	30-32	75.65	0.9335	0.95	-1.30	–	–
9H02	50-52	75.85	0.9342	–	–	–	–

9H02	70-72	76.05	0.9350	0.76	-1.22	–	–
9H02	90-92	76.25	0.9357	–	–	–	–
9H02	110-112	76.45	0.9365	-0.38	-1.81	–	–
9H02	130-132	76.65	0.9372	–	–	–	–
9H03	10-12	76.95	0.9384	0.57	-1.16	–	–
9H03	30-32	77.15	0.9391	–	–	–	–
9H03	50-52	77.35	0.9399	0.59	-1.56	–	–
9H03	70-72	77.55	0.9406	–	–	–	–
9H03	90-92	77.75	0.9414	0.98	-0.96	–	–
9H03	10-112	77.95	0.9421	–	–	–	–
9H03	130-132	78.15	0.9429	1.25	-1.08	–	–
9H04	10-12	78.45	0.9440	0.62	-1.33	–	–
9H04	30-32	78.65	0.9447	–	–	–	–
9H04	50-52	78.85	0.9455	1.67	-1.53	–	–
9H04	70-72	79.05	0.9462	0.83	-1.92	–	–
9H04	90-92	79.25	0.947	–	–	–	–
9H04	110-112	79.45	0.9477	0.78	-1.14	–	–
9H04	130-132	79.65	0.9485	1.10	-0.87	–	–
9H05	10-12	79.85	0.9496	–	–	–	–
9H05	30-32	80.15	0.9504	1.14	-1.61	–	–
9H05	50-52	80.35	0.9511	–	–	–	–
9H05	70-72	80.55	0.9519	0.99	-1.30	–	–
9H05	90-92	80.75	0.9526	–	–	–	–
9H05	110-112	80.95	0.9534	1.02	-1.36	–	–
9H05	130-132	81.15	0.9541	–	–	–	–
9H06	10-12	81.45	0.9552	1.10	-0.92	–	–
9H06	30-32	81.65	0.9560	–	–	–	–
9H06	50-52	81.85	0.9570	1.28	-0.73	–	–
9H06	70-72	82.05	0.9579	–	–	–	–
9H06	90-92	82.25	0.9589	1.27	-0.54	–	–
9H06	110-112	82.45	0.9598	–	–	–	–
9H06	130-132	82.65	0.9608	1.31	-0.42	–	–
9H07	10-12	82.95	0.9622	–	–	–	–
9H07	30-32	83.15	0.9632	0.88	-0.44	–	–
9H07	50-52	83.35	0.9642	–	–	–	–
9H07	70-72	83.55	0.9651	1.31	-0.51	–	–
9H07	90-92	83.75	0.9661	–	–	–	–
9H07	110-112	83.95	0.9671	1.14	-0.38	–	–
9H07	130-132	84.15	0.9680	–	–	–	–
9H08	10-12	84.45	0.9695	1.26	-0.39	–	–
9H08	30-32	84.65	0.9702	–	–	–	–
9H08	50-52	84.85	0.9704	–	–	–	–
9H08	70-72	85.05	0.9712	–	–	–	–
10H01	10-12	84.60	0.9714	0.85	-0.45	–	–
10H01	30-32	84.80	0.9721	0.87	-0.64	–	–
10H02	10-12	85.00	0.9724	–	–	–	–
10H02	30-32	85.20	0.9731	–	–	–	–
10H02	50-52	85.40	0.9740	1.14	-0.49	–	–
10H02	70-72	85.60	0.9750	–	–	–	–
10H02	90-92	85.80	0.9755	1.04	-0.63	–	–
10H02	110-112	86.00	0.9760	–	–	–	–
10H02	130-132	86.20	0.9764	0.61	-1.26	–	–
10H03	10-12	86.50	0.9772	–	–	–	–
10H03	30-32	86.70	0.9776	0.49	-1.57	–	–
10H03	50-52	86.90	0.9781	–	–	–	–
10H03	70-72	87.10	0.9786	0.57	-1.47	–	–
10H03	90-92	87.30	0.9791	–	–	–	–
10H03	110-112	87.50	0.9796	0.72	-1.46	–	–
10H03	130-132	87.70	0.9801	–	–	–	–

10H04	10-12	88.00	0.9808	0.38	-1.58	–	–
10H04	30-32	88.20	0.9813	–	–	–	–
10H04	50-52	88.40	0.9817	0.81	-1.28	–	–
10H04	70-72	88.60	0.9822	–	–	–	–
10H04	90-92	88.80	0.9827	0.77	-1.40	–	–
10H04	110-112	89.00	0.9832	–	–	–	–
10H04	130-132	89.20	0.9837	0.85	-1.54	–	–
10H05	10-12	89.50	0.9843	–	–	–	–
10H05	30-32	89.70	0.9849	0.98	-1.64	–	–
10H05	50-52	89.90	0.9853	–	–	–	–
10H05	70-72	90.10	0.9858	1.24	-1.47	–	–
10H05	90-92	90.30	0.9863	–	–	–	–
10H06	110-112	90.50	0.9868	0.72	-1.52	–	–
10H06	10-12	91.00	0.9880	–	–	–	–
10H06	30-32	91.20	0.9885	0.84	-1.49	–	–
10H06	50-52	91.40	0.9889	–	–	–	–
10H06	70-72	91.60	0.9894	0.95	-1.61	–	–
10H06	90-92	91.80	0.9899	–	–	–	–
10H06	110-112	92.00	0.9904	0.51	-1.50	–	–
10H07	130-132	92.20	0.9909	–	–	–	–
10H07	10-12	92.50	0.9916	0.67	-1.62	–	–
10H07	30-32	92.70	0.9921	–	–	–	–
10H07	50-52	92.90	0.9926	1.36	-1.58	–	–
10H07	70-72	93.10	0.9930	–	–	–	–
10H07	90-92	93.30	0.9935	1.11	-1.44	–	–
10H07	110-112	93.50	0.9940	–	–	–	–
10H07	130-132	93.70	0.9961	1.22	-1.11	–	–
10H08	10-12	94.00	0.9994	–	–	–	–
10H08	30-32	94.20	1.0015	–	–	–	–
10H08	50-52	94.40	1.0037	0.73	-1.29	–	–
10H08	70-72	94.60	1.0058	–	–	–	–
11H01	10-12	94.10	1.0004	–	–	–	–
11H02	10-12	94.42	1.0039	1.17	-1.30	–	–
11H02	30-32	94.62	1.0060	1.15	-1.40	–	–
11H02	50-52	94.82	1.0082	–	–	–	–
11H02	70-72	95.02	1.0103	1.32	-1.30	–	–
11H02	90-92	95.22	1.0125	1.41	-1.38	–	–
11H02	110-112	95.42	1.0146	–	–	–	–
11H02	130-132	95.62	1.0168	1.57	-1.50	–	–
11H03	10-12	95.92	1.0200	–	–	–	–
11H03	30-32	96.12	1.0203	0.91	-1.36	–	–
11H03	50-52	96.32	1.0205	–	–	–	–
11H03	70-72	96.52	1.0208	1.17	-1.91	–	–
11H03	90-92	96.72	1.0210	–	–	–	–
11H03	110-112	96.92	1.0213	1.35	-1.54	–	–
11H03	130-132	97.12	1.0216	–	–	–	–
11H04	10-12	97.42	1.0220	1.24	-1.41	–	–
11H04	30-32	97.62	1.0222	–	–	–	–
11H04	50-52	97.82	1.0225	1.11	-1.31	–	–
11H04	70-72	98.02	1.0227	–	–	–	–
11H04	90-92	98.22	1.0230	1.34	-1.64	–	–
11H04	110-112	98.42	1.0233	–	–	–	–
11H04	130-132	98.62	1.0235	1.60	-2.09	–	–
11H05	10-12	98.92	1.0239	–	–	–	–
11H05	30-30	99.12	1.0242	1.36	-1.74	–	–
11H05	50-52	99.32	1.0244	–	–	–	–
11H05	70-72	99.52	1.0247	1.17	-1.70	–	–
11H05	90-92	99.72	1.0249	–	–	–	–
11H05	110-112	99.92	1.0252	1.51	-1.53	–	–

11H05	130-132	100.12	1.0255	–	–	–	–
11H06	10-12	100.42	1.0259	1.17	-1.67	–	–
11H06	30-32	100.62	1.0262	–	–	–	–
11H06	50-52	100.82	1.0264	1.28	-1.87	–	–
11H06	70-72	101.02	1.0266	–	–	–	–
11H06	90-92	101.22	1.0269	1.40	-1.72	–	–
11H06	110-112	101.42	1.0272	–	–	–	–
11H06	130-132	101.62	1.0274	1.65	-1.61	–	–
11H07	10-12	101.92	1.0278	–	–	–	–
11H07	30-32	102.12	1.0281	0.92	-1.63	–	–
11H07	50-52	102.32	1.0283	1.61	-1.42	–	–
11H07	70-72	102.52	1.0286	–	–	–	–
11H07	90-92	102.72	1.0289	1.26	-1.53	–	–
11H07	110-112	102.92	1.0291	–	–	–	–
11H07	130-132	103.12	1.0294	1.41	-1.65	–	–
11H08	10-12	103.42	1.0298	1.50	-1.71	–	–
11H08	30-32	103.62	1.0301	–	–	–	–
11H08	50-52	103.82	1.0303	1.20	-1.74	–	–
11H08	70-72	104.02	1.0306	0.94	-1.27	–	–
12H01	10-12	103.60	1.0300	–	–	–	–
12H01	30-32	103.80	1.0303	1.51	-1.69	–	–
12H01	50-52	104.00	1.0305	0.77	-1.42	–	–
12H01	70-72	104.20	1.0308	–	–	–	–
12H01	90-92	104.40	1.0311	–	–	–	–
12H02	10-12	105.10	1.0320	0.26	-1.15	–	–
12H02	30-32	105.30	1.0322	–	–	–	–
12H02	50-52	105.50	1.0325	0.87	-1.36	–	–
12H02	70-72	105.70	1.0327	0.18	-1.26	–	–
12H02	90-92	105.90	1.0330	–	–	–	–
12H02	110-112	106.10	1.0332	0.25	-0.83	–	–
12H02	130-132	106.30	1.0334	–	–	–	–
12H03	10-12	106.60	1.0338	0.04	-0.47	–	–
12H03	30-32	106.80	1.0340	0.78	-1.28	–	–
12H03	50-52	107.00	1.0342	-0.67	-0.91	–	–
12H03	70-72	107.20	1.0344	-0.55	-0.58	–	–
12H03	83-85	107.33	1.0346	–	–	–	–
12H03	110-112	107.60	1.0349	-0.76	-0.63	–	–
12H04	10-12	108.10	1.0354	-1.44	-0.69	–	–
12H04	30-32	108.30	1.0356	–	–	–	–
12H04	50-52	108.50	1.0359	-0.78	-0.65	–	–
12H04	70-72	108.70	1.0361	–	–	–	–
12H04	90-92	108.90	1.0363	-1.41	-0.04	–	–
12H04	110-112	109.10	1.0365	-1.92	-0.41	–	–
12H04	130-132	109.30	1.0367	–	–	–	–
12H05	10-12	109.60	1.0371	-0.66	-0.64	–	–
12H05	30-32	109.80	1.0373	–	–	–	–
12H05	50-52	110.00	1.0375	–	–	–	–
12H05	70-72	110.20	1.0377	-0.92	-0.87	–	–
12H05	90-92	110.40	1.0379	–	–	–	–
12H05	110-112	110.60	1.0382	-1.52	-0.67	–	–
12H05	128-130	110.78	1.0384	-0.15	-0.76	–	–
13H01	10-12	111.10	1.0387	–	–	–	–
13H01	30-32	111.30	1.0389	1.09	-0.01	–	–
13H01	55-57	111.55	1.0392	–	–	–	–
13H02	10-12	111.68	1.0393	0.86	0.19	–	–
13H02	30-32	111.88	1.0396	–	–	–	–
13H02	50-52	112.08	1.0398	1.14	0.09	–	–
13H02	70-72	112.28	1.0400	–	–	–	–
13H02	88-90	112.46	1.0402	1.38	-0.14	–	–

13H02	110-112	112.68	1.0404	–	–	–	–
13H02	130-132	112.88	1.0407	1.01	0.02	–	–
13H03	10-12	113.18	1.0411	–	–	–	–
13H03	30-32	113.38	1.0412	0.98	-0.09	–	–
13H03	50-52	113.58	1.0414	–	–	–	–
13H03	70-72	113.78	1.0417	1.22	-0.05	–	–
13H03	88-90	113.96	1.0419	–	–	–	–
13H03	110-112	114.18	1.0421	1.03	-0.33	–	–
13H03	130-132	114.38	1.0423	–	–	–	–
13H04	10-12	114.68	1.0426	0.28	-0.88	–	–
13H04	30-32	114.88	1.0429	–	–	–	–
13H04	50-52	115.08	1.0431	-0.48	-0.88	–	–
13H04	70-72	115.28	1.0433	–	–	–	–
13H04	88-90	115.46	1.0435	0.31	-0.86	–	–
13H04	110-112	115.68	1.0437	–	–	–	–
13H04	130-132	115.88	1.0440	0.65	-0.55	–	–
13H05	10-12	116.18	1.0443	–	–	–	–
13H05	30-32	116.38	1.0445	0.71	-0.94	–	–
13H05	50-52	116.58	1.0447	–	–	–	–
13H05	70-72	116.78	1.0450	0.88	-0.98	–	–
13H05	88-90	116.96	1.0452	–	–	–	–
13H05	110-112	117.18	1.0454	0.92	-1.29	–	–
13H06	10-12	117.68	1.0459	–	–	–	–
13H06	30-32	117.88	1.0462	0.78	-1.54	–	–
13H06	50-52	118.08	1.0464	–	–	–	–
13H06	70-72	118.28	1.0466	0.64	-1.59	–	–
13H06	88-90	118.46	1.0468	–	–	–	–
13H06	110-112	118.68	1.0470	0.8	-1.38	–	–
13H06	130-132	118.88	1.0473	–	–	–	–
13H07	10-12	119.18	1.0476	0.56	-1.11	–	–
13H07	30-32	119.38	1.0478	–	–	–	–
13H07	50-52	119.58	1.0480	0.13	-1.28	–	–
13H07	70-72	119.78	1.0483	–	–	–	–
13H07	88-90	119.96	1.0484	0.21	-1.07	–	–
13H07	110-112	120.18	1.0487	–	–	–	–
13H07	130-132	120.38	1.0489	-0.70	-1.14	–	–
13H08	10-12	120.68	1.0492	–	–	–	–
13H08	30-32	120.88	1.0495	-0.23	-1.21	–	–
13H08	50-52	121.08	1.0497	–	–	–	–
13H08	70-72	121.28	1.0499	-0.44	-0.98	–	–
13H08	88-90	121.48	1.0501	-0.23	-1.12	–	–
13HCC	20-22	121.66	1.0503	–	–	–	–
13HCC	40-42	121.86	1.0505	–	–	–	–
14H02	71-73	122.71	1.0516	-1.08	-1.14	–	–
15X02	70-72	125.20	1.0542	1.09	-0.40	–	–
16X02	70-72	131.69	1.0613	1.34	-1.06	–	–
16X05	70-72	136.19	1.0663	0.54	-0.09	–	–
17X02	70-72	142.30	1.0730	1.05	-1.26	–	–
18X02	70-72	151.90	1.0835	1.41	0.22	–	–
18X02	70-72	161.60	1.0942	1.22	-1.05	–	–
20X02	70-72	171.30	1.1048	0.93	-0.37	–	–
20X05	70-72	175.80	1.1098	1.45	-0.67	–	–
23X02	70-72	200.40					

N.B. All isotopic values are expressed relative to PDB.

Table A.4. Planktic and benthic foraminiferal oxygen and carbon isotope ratios from ODP Leg 133 Site 823 (Queensland Trough Basin).

Sample Code		Depth (mbsf)	Age (Ma)	*G.ruber* $\delta^{13}C$ ‰	*G.ruber* $\delta^{18}O$ ‰	*Cibicidoides spp.* $\delta^{13}C$ ‰	*Cibicidoides spp.* $\delta^{18}O$ ‰
1H01	11-13	0.11	0.00196	0.46	-2.23	0.35	2.46
1H01	35-37	0.35	0.00625	0.24	-1.98	0.33	2.17
1H01	60-62	0.60	0.01072	-0.58	-1.99	0.34	2.89
1H01	85-87	0.85	0.01518	0.47	-1.34	–	–
1H01	110-112	1.10	0.01965	-0.13	-0.74	0.10	2.60
1H01	135-137	1.35	0.02411	-0.50	-1.65	–	–
1H02	12-14	1.62	0.05894	1.18	-1.41	–	–
1H02	35-37	1.85	0.03304	0.08	-0.78	–	–
1H02	60-62	2.10	0.03751	0.15	-1.01	–	–
1H02	85-87	2.35	0.04197	0.33	-0.94	–	–
1H02	110-112	2.60	0.04644	0.47	-1.42	0.07	3.73
1H02	135-137	2.85	0.05091	0.36	-1.09	–	–
1H03	13-15	3.13	0.05591	0.76	-1.33	0.23	3.49
1H03	35-37	3.35	0.05984	-0.05	-0.86	1.88	4.20
1H03	60-62	3.60	0.06430	0.40	-0.93	–	–
1H03	85-87	3.85	0.06877	0.47	-1.26	0.11	3.55
1H03	110-112	4.10	0.07316	0.48	-1.45	0.18	3.37
1H03	135-137	4.35	0.07749	1.13	-1.51	0.25	3.36
1H04	11-13	4.61	0.08198	0.32	-1.95	0.20	3.04
1H04	35-37	4.85	0.08614	0.61	-1.60	1.88	4.28
1H04	60-62	5.10	0.09046	0.74	-1.41	–	–
1H04	85-87	5.35	0.09479	0.65	-1.62	0.17	3.18
1H04	110-112	5.60	0.09911	0.88	-1.59	-0.37	3.03
2H01	9-11	5.89	0.1041	0.92	-2.19	–	–
2H01	35-37	6.15	0.1086	0.14	-1.88	-0.17	3.31
2H01	60-62	6.40	0.1130	-0.12	-1.92	0.11	3.06
2H01	85-87	6.65	0.1173	0.48	-2.00	2.25	3.71
2H01	110-112	6.90	0.1216	0.21	-2.13	–	–
2H01	135-137	7.15	0.1259	0.24	-1.93	0.37	3.26
2H02	9-11	7.39	0.1315	0.09	-1.06	–	–
2H02	35-37	7.65	0.1390	0.49	-0.73	-0.50	4.29
2H02	60-62	7.90	0.1462	-0.22	-0.84	-0.32	2.76
2H02	85-87	8.15	0.1535	0.11	-0.77	–	–
2H02	110-112	8.40	0.1607	0.41	-1.49	–	–
2H02	135-137	8.65	0.1679	0.33	-1.11	–	–
2H03	12-14	8.92	0.1757	0.32	-1.54	–	–
2H03	35-37	9.15	0.1824	-0.16	-1.50	–	–
2H03	60-62	9.40	0.1880	0.25	-1.14	–	–
2H03	88-90	9.68	0.1924	1.54	-1.48	-0.34	3.71
2H03	110-112	9.90	0.1958	0.73	-2.20	-0.01	3.07
2H03	135-137	10.15	0.1998	0.74	-2.10	0.26	2.97
2H04	9-11	10.39	0.2035	0.52	-1.84	–	–
2H04	35-37	10.65	0.2076	0.70	-1.41	0.27	2.70
2H04	60-62	10.90	0.2116	0.54	-1.85	–	–
2H04	85-87	11.15	0.2155	0.36	-1.71	–	–
2H04	110-112	11.40	0.2194	0.20	-1.16	-0.06	2.86
2H04	135-137	11.65	0.2234	0.43	-0.84	-0.18	3.50
2H05	9-11	11.89	0.2271	0.26	-0.99	–	–
2H05	35-37	12.15	0.2312	0.43	-1.62	-0.34	4.16
2H05	60-62	12.40	0.2352	0.14	-1.66	-0.42	3.31
2H05	85-87	12.65	0.2391	0.73	-1.86	–	–
2H05	110-112	12.90	0.2430	0.18	-1.62	-0.20	2.44
2H05	135-137	13.15	0.2472	0.54	-1.02	–	–

2H06	9-11	13.39	0.2515	0.44	-0.90	–	–
2H06	35-37	13.65	0.2562	0.09	-0.74	-0.10	3.89
2H06	60-62	13.90	0.2606	-0.05	-1.14	–	–
2H06	85-87	14.15	0.2651	0.14	-1.16	0.52	2.25
2H06	110-112	14.40	0.2695	-0.15	-0.90	–	–
2H06	134-136	14.64	0.2738	0.69	-0.64	-0.10	2.84
2H07	35-37	15.15	0.2829	0.78	-1.16	–	–
3H01	10-12	15.40	0.2874	1.06	-1.16	0.27	2.17
3H01	35-37	15.65	0.2918	0.50	-1.82	0.09	3.07
3H01	60-62	15.90	0.2963	0.73	-1.26	-0.07	3.13
3H01	85-87	16.15	0.3008	1.00	-1.12	–	–
4H01	10-12	24.90	0.3063	0.97	-1.25	0.18	2.61
4H01	35-37	25.15	0.3096	0.69	-1.59	–	–
4H01	85-87	25.65	0.3162	-0.11	-1.93	-0.02	2.91
4H01	110-112	25.90	0.3195	0.59	-1.66	-0.09	2.42
4H01	135-137	26.15	0.3228	0.99	-1.91	0.07	2.78
4H02	10-12	26.40	0.3261	0.60	-2.04	0.09	2.62
4H02	35-37	26.65	0.3294	0.44	-2.09	-0.93	2.79
4H02	60-62	26.90	0.3327	-0.17	-2.15	-0.17	2.37
4H02	85-87	27.15	0.3360	-0.20	-1.04	–	–
4H02	110-112	27.40	0.3434	0.43	-0.54	–	–
4H02	135-137	27.65	0.3509	0.67	-0.62	-0.27	3.92
4H03	10-12	27.90	0.3583	0.66	-0.76	–	–
4H03	35-37	28.15	0.3641	0.85	-0.84	–	–
4H03	60-62	28.40	0.3683	0.37	-1.14	-0.80	3.94
4H03	85-87	28.65	0.3725	0.71	-1.12	-0.70	3.87
4H03	110-112	28.90	0.3767	0.73	-1.41	–	–
4H03	135-137	29.15	0.3809	0.76	-1.26	-0.14	3.02
4H04	10-12	29.40	0.3851	0.77	-1.42	–	–
4H04	35-37	29.65	0.3893	0.44	-1.85	1.75	1.53
4H04	60-62	29.90	0.3936	0.82	-1.97	–	–
4H04	85-87	30.15	0.3978	1.00	-2.03	–	–
4H04	110-112	30.40	0.4020	0.05	-2.11	0.39	1.91
4H04	135-137	30.65	0.4062	0.76	-1.91	-0.02	2.73
4H05	10-12	30.90	0.4104	0.09	-1.93	-0.03	2.55
4H05	35-37	31.15	0.4146	0.32	-1.87	–	–
4H05	60-62	30.40	0.4188	-0.18	-1.87	0.02	3.05
4H05	85-87	31.65	0.4230	0.18	-1.30	-0.03	3.08
4H05	110-112	31.90	0.4282	0.00	-0.43	–	–
4H05	135-137	32.15	0.4335	0.09	-0.23	–	–
4H06	10-12	32.40	0.4387	0.54	-0.29	–	–
4H06	35-37	32.65	0.4440	0.37	-0.57	–	–
4H06	60-62	32.90	0.4492	–	–	-0.58	3.78
4H06	85-87	33.15	0.4544	-0.37	-1.11	-0.64	4.11
4H06	112-114	33.42	0.4597	0.51	-0.57	0.02	3.51
4H06	135-137	33.65	0.4649	0.46	-0.98	–	–
4H07	10-12	33.90	0.4701	0.61	-1.05	-0.18	3.77
4H07	35-37	34.15	0.4754	0.37	-0.71	–	–
5H01	10-12	34.40	0.4811	0.54	-1.94	0.29	2.36
5H01	35-37	34.65	0.4873	0.23	-1.91	0.18	2.58
5H01	60-62	34.90	0.4935	0.65	-1.69	–	–
5H01	86-88	35.16	0.5000	0.35	-1.76	–	–
5H01	135-137	35.65	0.5122	0.19	-1.35	–	–
5H02	10-12	35.90	0.5300	0.09	-0.61	0.17	3.13
5H02	60-62	36.40	0.5335	0.03	-0.11	–	–
5H02	109-111	36.89	0.5370	–	–	–	–
5H02	135-137	37.15	0.5388	0.67	-0.35	-0.52	4.00
5H03	10-12	37.40	0.5406	0.31	-0.48	-1.64	5.06
5H03	34-36	37.64	0.5423	0.59	-0.53	–	–
5H03	135-137	38.65	0.5494	0.08	-0.85	–	–
5H04	34-36	39.14	0.5529	0.51	-0.87	1.53	5.16

5H04	60-62	39.40	0.5547	0.61	-0.82	-0.63	3.89
5H04	86-88	39.66	0.5565	0.55	-0.77	–	–
5H04	135-137	40.15	0.5600	0.35	-0.30	–	–
5H05	60-62	40.90	0.5684	0.71	-1.31	-0.70	3.52
5H05	86-88	41.16	0.5713	1.00	-1.50	0.11	2.81
5H05	110-112	41.40	0.5740	0.67	-1.44	–	–
5H05	135-137	41.65	0.5750	0.86	-1.40	0.24	2.92
5H06	10-12	41.90	0.5760	1.05	-1.66	0.06	2.81
5H06	34-36	42.14	0.5770	0.54	-1.25	0.47	2.83
5H06	60-62	42.40	0.5780	0.84	-1.61	–	–
5H06	137-139	43.17	0.5811	1.02	-1.48	0.38	3.00
5H07	10-12	43.40	0.5820	0.90	-1.40	0.20	3.04
5H07	34-36	43.64	0.5830	0.92	-1.25	-0.07	3.37
5H07	60-62	43.90	0.5840	0.58	-1.12	0.13	3.68
6H01	10-12	43.90	–	–	–	–	–
6H01	35-37	44.15	0.5850	0.42	-1.26	1.06	0.37
6H01	60-62	44.40	0.5860	0.61	-0.92	–	–
6H01	85-87	44.65	0.5870	0.44	-0.83	-0.81	3.82
6H01	110-112	44.90	0.5880	0.66	-0.92	-0.47	2.71
6H01	135-137	45.15	0.5890	0.35	-0.55	–	–
6H02	10-12	45.40	0.5900	0.32	-1.26	–	–
6H02	35-37	45.65	0.5910	0.56	-1.07	-0.39	3.46
6H02	60-62	45.90	0.5920	0.35	-1.25	-0.07	3.23
6H02	85-87	46.15	0.5930	0.65	-0.97	–	–
6H02	110-112	46.40	0.5940	0.30	-1.30	1.73	4.51
6H02	135-137	46.65	0.5950	0.58	-1.23	-0.29	2.79
6H03	35-37	47.15	0.5970	0.21	-1.40	–	–
6H03	60.62	47.40	0.5980	0.50	-1.16	–	–
6H03	85-87	47.65	0.5990	0.45	-0.96	-0.25	3.60
6H03	110-112	47.90	0.6000	0.51	-1.15	–	–
7H01	35-37	53.65	0.6600	-0.14	-1.90	-0.63	2.69
7H01	60-62	53.90	0.6625	0.92	-1.83	–	–
7H01	85-87	54.15	0.6649	0.57	-1.55	–	–
7H01	110-112	54.40	0.6673	0.12	-1.03	–	–
7H01	135-137	54.65	0.6698	0.34	-1.69	–	–
7H02	10-12	54.90	0.6722	-0.34	-1.01	–	–
7H02	35-37	55.15	0.6747	-0.08	-0.75	–	–
7H02	60-62	55.40	0.6771	0.02	-0.88	–	–
7H02	85-87	55.65	0.6796	0.08	-0.95	–	–
7H02	110-112	55.90	0.6820	-0.08	-1.25	–	–
7H02	135-137	56.15	0.6845	-0.16	-1.25	-1.03	4.03
7H03	10-12	56.40	0.6869	0.10	-1.07	–	–
7H03	35-37	56.65	0.6894	0.38	-1.27	0.72	2.30
7H03	60-62	56.90	0.6918	0.35	-1.52	-1.00	2.89
7H03	85-87	57.15	0.6943	0.87	-1.42	0.20	2.38
7H03	110-112	57.40	0.6967	0.97	-1.52	-0.12	2.40
7H03	135-137	57.65	0.6992	0.61	-1.40	–	–
7H04	10-12	57.90	0.7016	0.29	-1.23	-0.82	3.24
7H04	35-37	58.15	0.7041	-0.08	-0.65	–	–
7H04	60-62	58.40	0.7065	0.48	-0.74	-1.31	3.93
7H04	85-87	58.65	0.7090	0.68	-0.85	0.78	0.95
7H04	110-112	58.90	0.7114	-0.07	-0.75	–	–
7H04	135-137	59.15	0.7139	0.53	-1.33	–	–
7H05	10-12	59.40	0.7163	0.15	-0.72	–	–
7H05	35-37	59.65	0.7188	0.52	-0.77	-0.87	3.52
7H05	60-62	59.90	0.7212	0.87	-1.07	0.21	2.52
7H05	85-87	60.15	0.7237	0.85	-1.48	0.00	1.41
7H05	110-112	60.40	0.7261	0.40	-0.85	–	–
7H05	135-137	60.65	0.7285	-0.40	-0.81	–	–
7H06	10-12	60.90	0.7310	-0.18	-1.08	-0.13	2.86
7H06	35-37	61.15	0.7334	-0.18	-1.03	-1.13	2.95

7H06	60-62	61.40	0.7359	0.28	-1.03	–	–
7H06	85-87	61.65	0.7383	0.20	-0.55	0.24	0.24
7H06	110-112	61.90	0.7408	0.29	-0.69	-0.94	3.40
7H06	135-137	62.15	0.7432	0.15	-0.67	-0.25	3.22
7H07	10-12	62.40	0.7457	0.55	-0.91	–	–
7H07	35-37	62.65	0.7481	0.38	-0.71	0.02	3.47
8H01	10-12	62.90	0.7506	0.17	-0.76	–	–
8H01	35-37	63.15	0.7530	0.21	-0.85	0.02	2.66
8H01	60-62	63.40	0.7555	0.12	-0.58	–	–
8H01	85-87	63.65	0.7579	0.64	-0.39	0.70	0.71
8H01	110-112	63.90	0.7604	0.42	-0.92	–	–
8H01	135-137	64.15	0.7628	0.12	-0.70	–	–
8H02	10-12	64.40	0.7653	0.23	-1.21	–	–
8H02	35-37	64.65	0.7677	-0.05	-0.69	–	–
8H02	60-62	64.90	0.7702	0.10	-0.80	-0.17	2.70
8H02	85-87	65.15	0.7726	0.18	-1.00	–	–
8H02	110-112	65.40	0.7751	0.11	-0.58	–	–
8H02	135-137	65.65	0.7775	-0.01	-0.82	–	–
8H03	10-12	65.90	0.7800	-0.17	-0.31	–	–
8H03	35-37	66.15	0.7824	0.22	-0.86	–	–
8H03	110-112	66.90	0.7898	0.07	-0.46	-0.11	2.72
8H04	10-12	67.40	0.7947	0.14	-0.43	–	–
8H04	35-37	67.65	0.7971	0.49	-0.78	-0.80	0.94
8H04	60-62	67.90	0.7995	0.03	-0.88	–	–
8H04	85-87	68.15	0.8020	0.09	-0.88	–	–
8H04	110-112	68.40	0.8044	0.29	-0.26	-1.33	3.03
8H04	135-137	68.65	0.8069	0.12	-1.09	0.10	1.58
8H05	10-12	68.90	0.8093	0.03	-0.93	-0.01	2.53
8H05	35-37	69.15	0.8118	0.12	-0.70	–	–
8H05	60-62	69.40	0.8142	0.44	-0.85	1.15	0.314
8H05	85-87	69.65	0.8167	-0.12	-1.55	-0.99	2.59
8H05	110-112	69.90	0.8191	0.20	-0.79	–	–
8H05	135-137	70.15	0.8216	0.32	-1.00	–	–
8H06	10-12	70.40	0.8240	0.29	-0.96	–	–
8H06	35-37	70.65	0.8265	0.20	-1.20	-0.29	2.42
8H06	60-62	70.90	0.8289	0.04	-0.94	–	–
8H06	85-87	71.15	0.8314	0.07	-1.35	–	–
8H06	110-112	71.40	0.8338	0.57	-0.92	-0.40	2.58
8H06	135-137	71.65	0.8363	0.09	-0.88	0.34	1.10
8H07	10-12	71.90	0.8387	0.09	-0.78	–	–
8H07	35-37	72.15	0.8412	0.20	-1.13	–	–
9H01	9-11	72.39	0.8436	0.77	-0.87	–	–
9H01	35-37	72.65	0.8461	0.28	-1.00	-0.13	2.66
9H01	60-62	72.90	0.8485	0.14	-1.23	0.19	2.58
9H01	85-87	73.15	0.8510	0.42	-1.13	–	–
9H01	110-112	73.40	0.8534	0.32	-0.76	–	–
9H01	135-137	73.65	0.8559	0.69	-1.03	–	–
9H02	9-11	73.89	0.8582	0.73	-1.02	–	–
9H02	35-37	74.15	0.8608	1.20	-1.52	–	–
9H02	60-62	74.40	0.8632	1.18	-1.51	–	–
9H02	85-87	74.65	0.8656	0.45	-1.21	-0.06	3.09
9H02	110-112	74.90	0.8681	0.56	-1.51	–	–
9H02	135-137	75.15	0.8706	0.92	-1.30	–	–
9H03	9-11	75.39	0.8730	0.72	-0.77	–	–
9H03	35-37	75.65	0.8754	0.28	-1.09	–	–
9H03	60-62	75.90	0.8779	0.92	-1.38	0.78	2.07
9H03	85-87	76.15	0.8803	0.33	-2.04	-0.09	2.25
9H03	110-112	76.40	0.8828	0.80	-1.45	–	–
9H03	135-137	76.65	0.8852	0.49	-1.54	–	–
9H04	9-11	76.89	0.8876	0.19	-1.48	-0.62	3.24
9H04	35-37	77.15	0.8901	-0.09	-1.43	–	–

9H04	60-62	77.40	0.8926	-0.01	-1.45	–	–
9H04	85-87	77.65	0.8950	0.54	-1.30	–	–
9H04	110-112	77.90	0.8975	0.15	-1.45	–	–
9H05	9-11	78.39	0.8023	1.02	-1.85	–	–
9H05	35-37	78.65	0.9048	0.97	-1.84	0.73	1.15
9H05	60-62	78.90	0.9073	0.48	-1.60	0.63	1.36
9H05	85-87	79.15	0.9097	0.52	-1.72	0.57	1.06
9H05	110-112	79.40	0.9122	0.94	-1.01	0.35	0.89
9H05	135-137	79.65	0.9146	0.75	-0.84	-0.36	3.54
9H06	9-11	79.89	0.9171	0.77	-1.23	–	–
9H06	35-37	80.15	0.9195	0.46	-1.45	–	–
9H06	60-62	80.40	0.9224	0.45	-1.26	–	–
9H06	85-87	80.65	0.9253	0.45	-1.10	–	–
9H06	110-112	80.90	0.9283	0.33	-1.03	-0.32	3.27
9H06	135-137	81.15	0.9312	0.22	-0.72	-0.60	3.64
9H07	9-11	81.39	0.9341	0.43	-0.96	-0.73	3.87
9H07	35-37	81.65	0.9371	0.27	-0.83	-1.01	3.86
9H07	60-62	81.90	0.9399	0.74	-1.51	–	–
10H01	9-11	81.89	0.9400	0.70	-1.44	-0.91	3.73
10H01	35-37	82.15	0.9429	0.82	-1.51	–	–
10H01	60-62	82.40	0.9459	0.96	-1.34	–	–
10H01	85-87	82.65	0.9488	0.78	-1.68	–	–
10H01	110-112	82.90	0.9518	0.72	-1.64	–	–
10H01	135-137	83.15	0.9547	0.43	-1.67	–	–
10H02	9-11	83.39	0.9575	0.84	-1.49	–	–
10H02	35-37	83.65	0.9606	0.73	-1.72	–	–
10H02	60-62	83.90	0.9635	0.52	-1.64	–	–
10H02	85-87	84.15	0.9665	–	–	–	–
10H02	110-112	84.40	0.9694	0.51	-1.23	–	–
10H02	135-137	84.65	0.9724	0.93	-1.28	–	–
10H03	9-11	84.89	0.9753	0.63	-0.95	–	–
10H03	35-37	85.15	0.9782	0.87	-1.40	–	–
10H03	60-62	85.40	0.9811	0.73	-1.41	–	–
10H03	85-87	85.65	0.9841	0.45	-1.63	–	–
10H03	110-112	85.90	0.9871	1.02	-1.47	–	–
10H03	135-137	86.15	0.9900	0.90	-1.12	–	–
10H04	9-11	86.39	0.9928	0.77	-1.15	–	–
10H04	35-37	86.65	0.9959	0.72	-1.12	–	–
10H04	60-62	86.90	0.9988	0.68	-1.36	–	–
10H04	85-87	87.15	1.0018	0.31	-1.17	–	–
10H04	110-112	87.40	1.0047	0.96	-1.08	–	–
10H04	135-137	87.65	1.0076	0.72	-1.54	–	–
10H05	9-11	87.89	1.0106	1.30	-1.19	–	–
10H05	35-37	88.15	1.0135	0.91	-1.11	–	–
10H05	60-62	88.40	1.0165	0.66	-1.11	–	–
10H05	85-87	88.65	1.0194	–	–	–	–
10H05	110-112	88.90	1.0224	0.40	-1.36	–	–
10H05	135-137	89.15	1.0253	0.11	-1.34	–	–
10H06	9-11	89.39	1.0282	1.01	-1.10	–	–
10H06	35-37	89.65	1.0312	1.19	-0.96	–	–
10H06	60-62	89.90	1.0341	0.91	-1.17	–	–
10H06	85-87	90.15	1.0371	0.55	-1.48	–	–
10H06	110-112	90.40	1.0400	0.58	-1.21	–	–
10H06	135-137	90.65	1.0429	0.31	-1.05	–	–
10H07	9-11	90.89	1.0459	0.62	-1.32	–	–
10H07	35-37	91.15	1.0488	0.31	-1.39	–	–
10H07	60-62	91.40	1.0518	0.15	-1.27	–	–
11H01	10-12	91.40	1.0518	0.63	-1.25	–	–
11H01	35-37	91.65	1.0547	0.52	-1.15	–	–
11H01	60-62	92.90	1.0576	1.19	-1.35	–	–
11H01	85-87	92.15	1.0606	0.49	-1.47	–	–

11H01	110-112	92.40	1.0635	0.63	-1.08	–	–
11H01	135-137	92.65	1.0665	0.34	-1.05	–	–
11H02	35-37	93.15	1.0724	0.22	-0.87	–	–
11H02	64-66	93.44	1.0758	0.59	-1.31	–	–
11H02	110-112	93.90	1.0812	0.51	-0.75	–	–
11H03	10-12	94.40	1.0871	0.89	-0.81	–	–
11H03	35-37	95.65	1.0900	1.26	-1.59	–	–
11H03	110-112	95.40	1.0988	0.22	-1.08	–	–
11H03	135-137	95.65	1.1025	0.99	-1.15	–	–
11H04	10-12	95.90	1.1067	0.61	-0.89	–	–
11H04	35-37	96.15	1.1110	1.00	-1.76	–	–
11H04	64-66	96.44	1.1157	0.72	-1.37	–	–
11H04	85-87	96.65	1.1192	-0.08	-1.26	–	–
11H04	110-112	96.90	1.1233	0.71	-1.50	–	–
11H04	135-137	97.15	1.1275	0.58	-1.38	–	–
11H05	10-12	97.40	1.1317	-0.03	-0.89	–	–
11H05	35-37	97.65	1.1358	0.02	-1.29	–	–
11H05	64-66	97.94	1.1407	0.09	-1.37	–	–
11H05	85-87	98.15	1.1440	0.66	-1.83	–	–
11H05	110-112	98.40	1.1830	-0.18	-1.72	–	–
11H05	135-137	98.65	1.1525	0.25	-1.62	–	–
11H06	10-12	98.90	1.1567	0.13	-1.45	–	–
11H06	35-37	99.15	1.1608	0.84	-1.68	–	–
11H06	64-66	99.44	1.1657	0.57	-1.54	–	–
11H06	85-87	99.65	1.1692	-0.17	-1.85	–	–
11H06	110-112	99.90	1.1733	–	–	–	–
11H06	135-137	100.15	1.1775	-1.80	-1.46	–	–
11H07	10-12	100.40	1.1817	–	–	–	–
11H07	35-37	100.65	1.1858	-1.12	-1.43	–	–
12H01	10-12	100.90	1.1900	0.78	-1.66	–	–
12H01	36-38	101.16	1.1943	0.52	-1.77	–	–
12H01	61-63	101.41	1.1985	0.53	-1.68	–	–
12H01	111-113	101.91	1.2068	0.44	-1.51	–	–
12H01	136-138	102.16	1.2110	0.68	-1.61	–	–
12H02	10-12	102.40	1.215	0.59	-1.55	–	–
12H02	36-38	102.66	1.2193	0.29	-1.73	–	–
12H02	61-63	102.91	1.2235	0.60	-1.64	–	–
12H02	111-113	103.41	1.2318	-0.28	-1.85	–	–
12H02	136-138	103.66	1.2360	0.33	-1.26	–	–
12H03	10-12	103.90	1.2400	0.93	-1.92	–	–
12H03	36-38	104.16	1.2440	0.45	-1.95	–	–
12H03	136-138	105.16	1.2610	0.77	-1.95	–	–
12H04	10-12	105.40	1.2650	0.01	-1.88	–	–
12H04	36-38	105.66	1.2730	0.42	-1.71	–	–
12H05	136-138	108.16	1.3110	0.54	-0.36	–	–
12H06	36-38	108.66	1.3230	0.38	-0.98	–	–
12H06	61-63	108.91	1.3235	0.34	-1.21	–	–
12H06	111-113	109.41	1.3318	0.38	-0.87	–	–
12H06	136-138	109.66	1.3360	–	–	–	–
13H01	10-12	110.40	1.3480	–	–	–	–
13H02	60-62	112.40	1.3817	–	–	–	–
13H04	35-37	115.15	1.4275	–	–	–	–
13H05	60-62	116.90	1.4567	0.76	-1.02	–	–
13H05	135-137	117.65	1.4691	–	–	–	–
13H06	10-12	117.90	1.4733	–	–	–	–
13H06	35-37	118.15	1.4775	0.66	-1.26	–	–
13H06	60-62	118.40	1.4817	0.60	-1.37	–	–
13H06	110-112	118.90	1.4900	1.12	-1.27	–	–
13H07	60-62	119.90	1.5067	2.01	-1.84	–	–

N.B. All isotopic values are expressed relative to PDB

Table A.5 Magnetic susceptibility measurements for Hole 819A samples

Sample code		Depth (mbsf)	Age (Ma)	Magnetic Susceptibility ($\mu m^3 kg^{-1}$)	Sample code		Depth (mbsf)	Age (Ma)	Magnetic Susceptibility ($\mu m^3 kg^{-1}$)
1H01	16-18	0.16	0.00050	0.0055	2H04	12-14	13.12	0.0435	0.0032
1H01	30-32	0.30	0.00094	0.0058	2H04	30-32	13.30	0.0441	0.0034
1H01	54.56	0.54	0.00169	0.0048	2H04	54-56	13.54	0.0448	0.0034
1H01	70-72	0.70	0.00219	0.0052	2H04	70-72	13.70	0.0453	0.0029
1H01	90-92	0.90	0.00281	0.0054	2H04	88-90	13.88	0.0459	0.0035
1H01	120-122	1.20	0.00375	0.0068	2H04	109-111	14.09	0.0465	0.0042
1H02	10-12	1.60	0.00500	0.0059	2H04	132-134	14.32	0.0473	0.0027
1H02	30-32	1.80	0.00563	0.0047	2H05	12-14	14.62	0.0481	0.0024
1H02	54-56	2.04	0.00638	0.0057	2H05	30-32	14.80	0.0487	0.0024
1H02	68-70	2.18	0.00681	0.0063	2H05	54-56	15.04	0.0494	0.0020
1H02	70-72	2.20	0.00688	0.0069	2H05	70-72	15.20	0.0499	0.0018
1H02	90-92	2.40	0.00750	0.0070	2H05	88-90	15.38	0.0504	0.0015
1H02	120-122	2.70	0.00844	0.0081	2H05	109-111	15.59	0.0511	0.0017
1H03	10-12	3.10	0.00969	0.0080	2H05	132-133	15.82	0.0518	0.0018
1H03	30-32	3.30	0.0103	0.0081	2H06	12-14	16.12	0.0527	0.0015
1H03	54-56	3.54	0.0111	0.0068	2H06	30-32	16.30	0.0532	0.0017
1H03	70-72	3.70	0.0116	0.0080	2H06	54-56	16.54	0.0540	0.0016
1H03	95-97	3.95	0.0123	0.0092	2H06	70-72	16.70	0.0544	0.0023
1H03	120-122	4.20	0.0134	0.0104	2H06	88-90	16.88	0.0550	0.0020
1H04	10-12	4.60	0.0151	0.0127	2H06	109-111	17.09	0.0556	0.0016
1H04	30-32	4.80	0.0159	0.0135	2H06	132-134	17.32	0.0563	0.0026
1H04	54-56	5.04	0.0169	0.0208	2H07	7-8	17.57	0.0571	0.0018
1H04	70-72	5.20	0.0176	0.0222	2H07	27-29	17.77	0.0577	0.0015
1H04	90-92	5.40	0.0185	0.0178	2H07	54-56	18.04	0.0585	0.0020
1H04	120-122	5.70	0.0197	0.0213	3H01	10-12	18.10	0.0587	0.0019
1H05	10-12	6.10	0.0214	0.0385	3H01	30-32	18.30	0.0598	0.0022
1H05	30-32	6.30	0.0223	0.0293	3H01	52-54	18.52	0.0616	0.0024
1H05	70-72	6.70	0.0240	0.0780	3H01	70-72	18.70	0.0630	0.0019
1H05	90-92	6.90	0.0246	0.0068	3H01	90-92	18.90	0.0646	0.0020
1H05	120-122	7.20	0.0255	0.0031	3H01	109-111	19.09	0.0661	0.0016
1H06	10-12	7.60	0.0267	0.0041	3H01	131-133	19.31	0.0679	0.0016
1H06	30-32	7.80	0.0274	0.0018	3H02	10-12	19.60	0.0702	0.0013
1H06	54-56	8.04	0.0281	0.0022	3H02	30-32	19.80	0.0732	0.0017
1H06	68-70	8.18	0.0285	0.0018	3H02	52-54	20.02	0.0780	0.0016
2H01	12-14	8.62	0.0298	0.0020	3H02	70-72	20.20	0.0819	0.0017
2H01	30-32	8.80	0.0304	0.0023	3H02	90-92	20.40	0.0863	0.0019
2H01	54-56	9.04	0.0311	0.0032	3H02	109-111	20.59	0.0904	0.0021
2H01	70-72	9.20	0.0316	0.0024	3H02	131-133	20.81	0.0952	0.0024
2H01	88-90	9.38	0.0322	0.0027	3H03	10-12	21.10	0.1016	0.0042
2H01	109-111	9.59	0.0328	0.0031	3H03	30-32	21.30	0.1059	0.0074
2H01	132-134	9.82	0.0335	0.0038	3H03	52-54	21.52	0.1108	0.0078
2H02	12-14	10.12	0.0344	0.0031	3H03	70-72	21.70	0.1147	0.0078
2H02	30-32	10.30	0.0350	0.0033	3H03	90-92	21.90	0.1191	0.0049
2H02	54-56	10.54	0.0357	0.0036	3H03	109-111	22.09	0.1232	0.0048
2H02	70-72	10.70	0.0362	0.0036	3H03	131-132	22.31	0.1280	0.0050
2H02	88-90	10.88	0.0367	0.0036	3H04	10-12	22.60	0.1315	0.0038
2H02	109-111	11.09	0.0374	0.0039	3H04	30-32	22.80	0.1339	0.0047
2H02	132-134	11.32	0.0381	0.0050	3H04	52-54	23.02	0.1365	0.0044
2H03	30-32	11.80	0.0395	0.0040	3H04	70-72	23.20	0.1388	0.0047
2H03	54-56	12.04	0.0403	0.0036	3H04	90-92	23.40	0.1412	0.0048
2H03	70-72	12.20	0.0407	0.0047	3H04	109-111	23.59	0.1435	0.0051
2H03	88-90	12.38	0.0413	0.0039	3H04	131-133	23.81	0.1462	0.0048
2H03	109-111	12.59	0.0419	0.0040	3H05	10-12	24.10	0.1597	0.0041
2H03	132-134	12.82	0.0427	0.0045	3H05	30-32	24.30	0.1521	0.0036

3H05	52-54	24.52	0.1548	0.0161
3H05	70-72	24.70	0.1569	0.0193
3H05	87-89	24.87	0.1590	0.0199
3H05	109-111	25.09	0.1617	0.0098
3H06	7-9	25.57	0.1675	0.0016
3H06	26-28	25.76	0.1698	0.0010
3H06	52-54	26.02	0.1729	0.0026
3H06	67-69	26.17	0.1747	0.0030
3H06	90-92	26.40	0.1775	0.0030
3H06	109-111	26.59	0.1798	0.0016
3H06	131-133	26.81	0.1822	0.0010
3H07	10-12	27.10	0.1860	0.0005
4H01	30-32	27.80	0.1945	0.0023
4H01	50-52	28.00	0.1968	0.0017
4H01	70-72	28.20	0.1993	0.0043
4H01	90-92	28.40	0.2017	0.0046
4H01	110-112	28.60	0.2042	0.0034
4H01	130-132	28.80	0.2200	0.0020
4H02	10-12	29.10	0.2240	0.0007
4H02	30-32	29.30	0.2267	0.0005
4H02	50-52	29.50	0.2293	0.0005
4H02	70-72	29.70	0.2320	0.0006
4H02	90-92	29.90	0.2347	0.0012
4H02	110-112	30.10	0.2373	0.0016
4H02	130-132	30.30	0.2400	0.0013
4H03	10-12	30.60	0.2505	0.0010
4H03	30-32	30.80	0.2575	0.0013
4H03	50-52	31.00	0.2645	0.0021
4H03	70-72	31.20	0.2715	0.0022
4H03	90-92	31.40	0.2785	0.0025
4H03	110-112	31.60	0.2855	0.0029
4H03	130-132	31.80	0.2925	0.0032
4H04	10-12	32.10	0.3030	0.0030
4H04	30-32	32.30	0.3100	0.0014
4H04	50-52	32.50		0.0022
4H04	70-72	32.70	0.5299	0.0028
4H04	90-92	32.90	0.5357	0.0048
4H04	110-112	33.10	0.5416	0.0053
4H04	130-132	33.30	0.5474	0.0050
4H05	10-12	33.60	0.5562	0.0033
4H05	30-32	33.80	0.5621	0.0034
4H05	50-52	34.00	0.5662	0.0031
4H05	70-72	34.20	0.5686	0.0034
4H05	90-92	34.20	0.5710	0.0036
4H05	110-112	34.60	0.5735	0.0032
4H05	130-132	34.80	0.5759	0.0042
4H06	10-12	35.10	0.5795	0.0028
4H06	30-32	35.30	0.5819	0.0031
4H06	50-52	35.50	0.5845	0.0033
4H06	70-72	35.70	0.5868	0.0029
4H06	90-92	35.90	0.5892	0.0031
4H06	110-112	36.10	0.5916	0.0031
4H06	130-132	36.30	0.5940	0.0032
4H07	10-12	36.60	0.5976	0.0031
4H07	30-32	36.80	0.6000	0.0030
4H07	50-52	37.00	0.6025	0.0026
4H07	70-72	37.20	0.6037	0.0023
5H01	10-12	37.10	0.6049	0.0033
5H01	30-32	37.30	0.6061	0.0026
5H01	50-52	37.50	0.6085	0.0026
5H01	70-72	37.70	0.6109	0.0025
5H01	90-92	37.90	0.6134	0.0024
5H01	110-112	38.10	0.6158	0.0025
5H01	130-132	38.30	0.6182	0.0022
5H02	10-12	38.60	0.6229	0.0024
5H02	30-32	38.80	0.6267	0.0024
5H02	50-52	39.00	0.6305	0.0025
5H02	70-72	39.20	0.6343	0.0025
5H02	90-92	39.40	0.6381	0.0020
5H02	110-112	39.60	0.6419	0.0022
5H02	130-132	39.80	0.6457	0.0023
5H03	10-12	40.10	0.6514	0.0021
5H03	30-32	40.30	0.6552	0.0021
5H03	50-52	40.50	0.6590	0.0025
5H03	70-72	40.70	0.7210	0.0028
5H03	90-92	40.90	0.7316	0.0026
5H03	110-112	41.10	0.7349	0.0027
5H03	130-132	41.30	0.7382	0.028
5H04	10-12	41.60	0.7432	0.0033
5H04	30-32	41.80	0.7464	0.0031
5H04	50-52	42.00	0.7497	0.0029
5H04	70-72	42.20	0.7530	0.0027
5H04	90-92	42.40	0.7563	0.0029
5H04	110-112	42.60	0.7596	0.0026
5H04	130-132	42.80	0.7629	0.0027
5H05	10-12	43.10	0.7678	0.0031
5H05	30-32	43.30	0.7711	0.0027
5H05	50-52	43.50	0.7744	0.0026
5H05	70-72	43.70	0.7777	0.0033
5H05	90-92	43.90	0.7810	0.0024
5H05	110-112	44.10	0.7842	0.0026
5H05	130-132	44.30	0.7875	0.0023
5H06	10-12	44.60	0.7921	0.0026
5H06	30-32	44.80	0.7950	0.0024
5H06	50-52	45.00	0.7978	0.0022
5H06	70-72	45.20	0.8006	0.0027
5H06	90-92	45.40	0.8035	0.0025
5H06	110-112	45.60	0.8063	0.0030
5H06	130-132	45.80	0.8091	0.0030
5H07	10-12	46.10	0.8134	0.0035
5H07	30-32	46.30	0.8162	0.0034
5H07	50-52	46.50	0.8190	0.0026
5H07	70-72	46.70	0.8219	0.0026
6H01	10-12	46.60	0.8204	0.0035
6H01	30-32	46.80	0.8233	0.0036
6H01	50-52	47.00	0.8261	0.0035
6H01	70-72	47.20	0.8289	0.0036
6H01	90-92	47.40	0.8318	0.0040
6H01	110-112	47.60	0.8346	0.0040
6H01	130-132	47.80	0.8374	0.0039
6H02	10-12	48.10	0.8417	0.0041
6H02	30-32	48.30	0.8445	0.0040
6H02	50-52	48.50	0.8473	0.0034
6H02	70-72	48.70	0.8502	0.0037
6H02	90-92	48.90	0.8530	0.0037
6H02	110-112	49.10	0.8558	0.0035
6H02	130-132	49.30	0.8587	0.0034
6H03	10-12	49.60	0.8629	0.0033

6H03	30-32	49.80	0.8658	0.0030
6H03	50-52	50.00	0.8686	0.0025
6H03	70-72	50.20	0.8703	0.0021
6H03	90-92	50.40	0.8709	0.0019
6H03	110-112	50.60	0.8715	0.0022
6H03	130-132	50.80	0.8720	0.0020
6H04	10-12	51.10	0.8729	0.0017
6H04	30-32	51.30	0.8735	0.0020
6H04	50-52	51.50	0.8741	0.0025
6H04	70-72	51.70	0.8747	0.0019
6H04	90-92	51.90	0.8753	0.0020
6H04	110-112	52.10	0.8758	0.0020
6H04	130-132	52.30	0.8764	0.0017
6H05	10-12	52.60	0.8773	0.0016
6H05	30-32	52.80	0.8779	0.0014
6H05	50-52	53.00	0.8785	0.0017
6H05	70-72	53.20	0.8791	0.0016
6H05	90-92	53.40	0.8796	0.0012
6H05	110-112	53.60	0.8802	0.0014
6H05	130-132	53.80	0.8808	0.0013
6H06	10-12	54.10	0.8817	0.0013
6H06	30-32	54.30	0.8823	0.0015
6H06	50-52	54.50	0.8829	0.0014
6H06	70-72	54.70	0.8834	0.0014
6H06	90-92	54.90	0.8840	0.0013
6H06	110-112	55.10	0.8846	0.0014
7H06	130-132	55.30	0.8852	0.0022
7H01	10-12	56.10	0.8875	0.0016
7H01	30-32	56.30	0.8881	0.0016
7H01	50-52	56.50	0.8887	0.0014
7H01	70-72	56.70	0.8893	0.0014
7H01	90-90	56.90	0.8899	0.0015
7H01	110-112	57.10	0.8904	0.0018
7H01	130-132	57.30	0.8910	0.0017
7H02	10-12	57.60	0.8919	0.0016
7H02	30-32	57.80	0.8925	0.0016
7H02	50-52	58.00	0.8931	0.0017
7H02	70-72	58.20	0.8937	0.0017
7H02	90-92	58.40	0.8942	0.0017
7H02	110-112	58.60	0.8948	0.0016
7H02	130-132	58.80	0.8954	0.0016
7H03	10-12	59.10	0.8963	0.0020
7H03	30-32	59.30	0.8969	0.0018
7H03	50-52	59.50	0.8975	0.0018
7H03	70-52	59.70	0.8980	0.0018
7H03	90-92	59.90	0.8986	0.0017
7H03	110-112	60.10	0.8992	0.0021
7H03	130-132	60.30	0.8998	0.0018
7H04	10-12	60.60	0.9007	0.0021
7H04	30-32	60.80	0.9013	0.0026
7H04	50-52	61.00	0.9018	0.0019
7H04	70-72	61.20	0.9024	0.0020
7H04	90-92	61.40	0.9030	0.0025
7H04	110-112	61.60	0.9036	0.0024
7H04	130-132	61.80	0.9042	0.0027
7H05	10-12	62.10	0.9051	0.0027
7H05	30-32	62.30	0.9056	0.0026
7H05	50-52	62.50	0.9062	0.0025
7H05	70-72	62.70	0.9068	0.0031
7H05	90-92	62.90	0.9074	0.0029
7H05	110-112	63.10	0.9080	0.0028
7H06	10-12	63.60	0.9094	0.0030
7H06	30-32	63.80	0.9100	0.0032
7H06	50-52	64.00	0.9106	0.0027
7H06	70-72	64.20	0.9112	0.0029
7H06	90-92	64.40	0.9118	0.0033
7H06	110-112	64.60	0.9123	0.0035
7H06	130-132	64.80	0.9129	0.0034
7H07	10-12	65.10	0.9138	0.0037
7H07	30-32	65.30	0.9144	0.0039
7H07	50-52	65.50	0.9150	0.0036
8H01	10-12	65.60	0.9153	0.0027
8H01	30-32	65.80	0.9159	0.0027
8H01	50-52	66.00	0.9164	0.0034
8H02	10-12	66.22	0.9171	0.0036
8H02	30-32	66.42	0.9177	0.0037
8H02	50-52	66.62	0.9182	0.0041
8H02	70-72	66.82	0.9188	0.0055
8H02	90-92	67.02	0.9194	0.0060
8H02	110-112	67.22	0.9200	0.0064
8H02	130-132	67.42	0.9203	0.0062
8H03	10-12	67.72	0.9207	0.0064
8H03	30-32	67.92	0.9209	0.0056
8H03	50-52	68.12	0.9212	0.0050
8H03	70-72	68.32	0.9215	0.0042
8H03	90-92	68.52	0.9217	0.0037
8H03	110-112	68.72	0.9220	0.0036
8H03	130-132	68.92	0.9223	0.0043
8H04	10-12	69.22	0.9227	0.0042
8H04	30-32	69.42	0.9229	0.0035
8H04	50-52	69.62	0.9232	0.0038
8H04	70-72	69.82	0.9235	0.0042
8H04	90-92	70.02	0.9237	0.0034
8H04	110-112	70.22	0.9240	0.0041
8H04	130-132	70.42	0.9243	0.0047
8H05	10-12	70.72	0.9247	0.0041
8H05	30-32	70.92	0.9249	0.0052
8H05	50-52	71.12	0.9252	0.0051
8H05	70-72	71.32	0.8255	0.0049
8H05	90-92	71.52	0.9257	0.0050
8H05	110-112	71.72	0.9260	0.0055
8H05	130-132	71.92	0.9263	0.0055
8H06	10-12	72.22	0.9267	0.0052
8H06	30-32	72.42	0.9269	0.0052
8H06	50-52	72.62	0.9272	0.0040
8H06	70-72	72.82	0.9275	0.0043
8H06	90-92	73.02	0.9277	0.0044
8H06	110-112	73.22	0.9280	0.0042
8H06	130-132	73.42	0.9283	0.0044
8H07	10-12	73.72	0.9287	0.0040
8H07	30-32	73.92	0.9289	0.0043
8H07	50-52	74.12	0.9292	0.0042
8H07	70-72	74.32	0.9295	0.0047
8H07	90-92	74.52	0.9297	0.0046
8H07	110-112	74.72	0.9300	0.0046
8H07	130-132	74.92	0.9308	0.0053
9H01	10-12	75.10	0.9314	0.0048
9H01	30-32	75.30	0.9322	0.0056

9H02	10-12	75.45	0.9327	0.0059
9H02	30-32	75.65	0.9335	0.0067
9H02	50-52	75.85	0.9342	0.0056
9H02	70-72	76.05	0.9350	0.0063
9H02	90-92	76.25	0.9357	0.0071
9H02	110-112	76.45	0.9365	0.0058
9H02	130-132	76.65	0.9372	0.0060
9H03	10-12	76.95	0.9384	0.0058
9H03	30-32	77.15	0.9391	0.0059
9H03	50-52	77.35	0.9399	0.0056
9H03	70-72	77.55	0.9406	0.0051
9H03	90-92	77.75	0.9414	0.0049
9H03	10-112	77.95	0.9421	0.0051
9H03	130-132	78.15	0.9429	0.0045
9H04	10-12	78.45	0.9440	0.0046
9H04	30-32	78.65	0.9447	0.0047
9H04	50-52	78.85	0.9455	0.0046
9H04	70-72	79.05	0.9462	0.0051
9H04	90-92	79.25	0.947	0.0045
9H04	110-112	79.45	0.9477	0.0049
9H04	130-132	79.65	0.9485	0.0048
9H05	10-12	79.85	0.9496	0.0026
9H05	30-32	80.15	0.9504	0.0026
9H05	50-52	80.35	0.9511	0.0021
9H05	70-72	80.55	0.9519	0.0023
9H05	90-92	80.75	0.9526	0.0025
9H05	110-112	80.95	0.9534	0.0022
9H05	130-132	81.15	0.9541	0.0026
9H06	10-12	81.45	0.9552	0.0024
9H06	30-32	81.65	0.9560	0.0020
9H06	50-52	81.85	0.9570	0.0023
9H06	70-72	82.05	0.9579	0.0023
9H06	90-92	82.25	0.9589	0.0027
9H06	110-112	82.45	0.9598	0.0027
9H06	130-132	82.65	0.9608	0.0026
9H07	10-12	82.95	0.9622	0.0028
9H07	30-32	83.15	0.9632	0.0027
9H07	50-52	83.35	0.9642	0.0023
9H07	70-72	83.55	0.9651	0.0027
9H07	90-92	83.75	0.9661	0.0026
9H07	110-112	83.95	0.9671	0.0022
9H07	130-132	84.15	0.9680	0.0020
9H08	10-12	84.45	0.9695	0.0024
9H08	30-32	84.65	0.9702	0.0024
9H08	50-52	84.85	0.9704	0.0028
9H08	70-72	85.05	0.9712	0.0025
10H01	10-12	84.60	0.9714	0.0021
10H01	30-32	84.80	0.9721	0.0029
10H02	10-12	85.00	0.9724	0.0030
10H02	30-32	85.20	0.9731	0.0029
10H02	50-52	85.40	0.9740	0.0028
10H02	70-72	85.60	0.9750	0.0026
10H02	90-92	85.80	0.9755	0.0026
10H02	110-112	86.00	0.9760	0.0027
10H02	130-132	86.20	0.9764	0.0030
10H03	10-12	86.50	0.9772	0.0032
10H03	30-32	86.70	0.9776	0.0032
10H03	50-52	86.90	0.9781	0.0030
10H03	70-72	87.10	0.9786	0.0034
10H03	90-92	87.30	0.9791	0.0033
10H03	110-112	87.50	0.9796	0.0031
10H03	130-132	87.70	0.9801	0.0033
10H04	10-12	88.00	0.9808	0.0037
10H04	30-32	88.20	0.9813	0.0039
10H04	50-52	88.40	0.9817	0.0041
10H04	70-72	88.60	0.9822	0.0044
10H04	90-92	88.80	0.9827	0.0046
10H04	110-112	89.00	0.9832	0.0050
10H04	130-132	89.20	0.9837	0.0055
10H05	10-12	89.50	0.9843	0.0045
10H05	30-32	89.70	0.9849	0.0056
10H05	50-52	89.90	0.9853	0.0000
10H05	70-72	90.10	0.9858	0.0059
10H05	90-92	90.30	0.9863	0.0051
10H06	110-112	90.50	0.9868	0.0053
10H06	10-12	91.00	0.9880	0.0049
10H06	30-32	91.20	0.9885	0.0042
10H06	50-52	91.40	0.9889	0.0043
10H06	70-72	91.60	0.9894	0.0045
10H06	90-92	91.80	0.9899	0.0033
10H06	110-112	92.00	0.9904	0.046
10H07	130-132	92.20	0.9909	0.0046
10H07	10-12	92.50	0.9916	0.0045
10H07	30-32	92.70	0.9921	0.0044
10H07	50-52	92.90	0.9926	0.0048
10H07	70-72	93.10	0.9930	0.0042
10H07	90-92	93.30	0.9935	0.0044
10H07	110-112	93.50	0.9940	0.0048
10H07	130-132	93.70	0.9961	0.0048
10H08	10-12	94.00	0.9994	0.0047
10H08	30-32	94.20	1.0015	0.0045
10H08	50-52	94.40	1.0037	0.0048
10H08	70-72	94.60	1.0058	0.0044
11H01	10-12	94.10	1.0004	0.0049
11H02	10-12	94.42	1.0039	0.0051
11H02	30-32	94.62	1.0060	0.0041
11H02	50-52	94.82	1.0082	0.0041
11H02	70-72	95.02	1.0103	0.0043
11H02	90-92	95.22	1.0125	0.0041
11H02	110-112	95.42	1.0146	0.0036
11H02	130-132	95.62	1.0168	0.0037
11H03	10-12	95.92	1.0200	0.0038
11H03	30-32	96.12	1.0203	0.0037
11H03	50-52	96.32	1.0205	0.0037
11H03	70-72	96.52	1.0208	0.0035
11H03	90-92	96.72	1.0210	0.0034
11H03	110-112	96.92	1.0213	0.0037
11H03	130-132	97.12	1.0216	0.0036
11H04	10-12	97.42	1.0220	0.0042
11H04	30-32	97.62	1.0222	0.0036
11H04	50-52	97.82	1.0225	0.0035
11H04	70-72	98.02	1.0227	0.0037
11H04	90-92	98.22	1.0230	0.0034
11H04	110-112	98.42	1.0233	0.0030
11H04	130-132	98.62	1.0235	0.0030
11H05	10-12	98.92	1.0239	0.0028
11H05	30-30	99.12	1.0242	0.0034
11H05	50-52	99.32	1.0244	0.0029

11H05	70-72	99.52	1.0247	0.0029
11H05	90-92	99.72	1.0249	0.0033
11H05	110-112	99.92	1.0252	0.0027
11H05	130-132	100.12	1.0255	0.0023
11H06	10-12	100.42	1.0259	0.0027
11H06	30-32	100.62	1.0262	0.0032
11H06	50-52	100.82	1.0264	0.0028
11H06	70-72	101.02	1.0266	0.0025
11H06	90-92	101.22	1.0269	0.0028
11H06	110-112	101.42	1.0272	0.0028
11H06	130-132	101.62	1.0274	0.0026
11H07	10-12	101.92	1.0278	0.0026
11H07	30-32	102.12	1.0281	0.0026
11H07	50-52	102.32	1.0283	0.0025
11H07	70-72	102.52	1.0286	0.0023
11H07	90-92	102.72	1.0289	0.0027
11H07	110-112	102.92	1.0291	0.0025
11H07	130-132	103.12	1.0294	0.0024
11H08	10-12	103.42	1.0298	0.0022
11H08	30-32	103.62	1.0301	0.0025
11H08	50-52	103.82	1.0303	0.0025
11H08	70-72	104.02	1.0306	0.0022
12H01	10-12	103.60	1.0300	0.0024
12H01	30-32	103.80	1.0303	0.0030
12H01	50-52	104.00	1.0305	0.0031
12H01	70-72	104.20	1.0308	0.0029
12H01	90-92	104.40	1.0311	0.0000
12H02	10-12	105.10	1.0320	0.0035
12H02	30-32	105.30	1.0322	0.0029
12H02	50-52	105.50	1.0325	0.0029
12H02	70-72	105.70	1.0327	0.0024
12H02	90-92	105.90	1.0330	0.0024
12H02	110-112	106.10	1.0332	0.0021
12H02	130-132	106.30	1.0334	0.0018
12H03	10-12	106.60	1.0338	0.0022
12H03	30-32	106.80	1.0340	0.0024
12H03	50-52	107.00	1.0342	0.0019
12H03	70-72	107.20	1.0344	0.0013
12H03	83-85	107.33	1.0346	0.0017
12H03	110-112	107.60	1.0349	0.0022
12H04	10-12	108.10	1.0354	0.0019
12H04	30-32	108.30	1.0356	0.0022
12H04	50-52	108.50	1.0359	0.0020
12H04	70-72	108.70	1.0361	0.0022
12H04	90-92	108.90	1.0363	0.0019
12H04	110-112	109.10	1.0365	0.0020
12H04	130-132	109.30	1.0367	0.0021
12H05	10-12	109.60	1.0371	0.0018
12H05	30-32	109.80	1.0373	0.0015
12H05	50-52	110.00	1.0375	0.0021
12H05	70-72	110.20	1.0377	0.0019
12H05	90-92	110.40	1.0379	0.0017
12H05	110-112	110.60	1.0382	0.0025
12H05	128-130	110.78	1.0384	0.0034
13H01	10-12	111.10	1.0387	0.0014
13H01	30-32	111.30	1.0389	0.0014
13H01	55-57	111.55	1.0392	0.0017
13H02	10-12	111.68	1.0393	0.0015
13H02	30-32	111.88	1.0396	0.0013
13H02	50-52	112.08	1.0398	0.0013
13H02	70-72	112.28	1.0400	0.0013
13H02	88-90	112.46	1.0402	0.0013
13H02	110-112	112.68	1.0404	0.0019
13H02	130-132	112.88	1.0407	0.0017
13H03	10-12	113.18	1.0411	0.0019
13H03	30-32	113.38	1.0412	0.0022
13H03	50-52	113.58	1.0414	0.0021
13H03	70-72	113.78	1.0417	0.0019
13H03	88-90	113.96	1.0419	0.0024
13H03	110-112	114.18	1.0421	0.0022
13H03	130-132	114.38	1.0423	0.0023
13H04	10-12	114.68	1.0426	0.0027
13H04	30-32	114.88	1.0429	0.0023
13H04	50-52	115.08	1.0431	0.0026
13H04	70-72	115.28	1.0433	0.0025
13H04	88-90	115.46	1.0435	0.0031
13H04	110-112	115.68	1.0437	0.0031
13H04	130-132	115.88	1.0440	0.0035
13H05	10-12	116.18	1.0443	0.0030
13H05	30-32	116.38	1.0445	0.0036
13H05	50-52	116.58	1.0447	0.0033
13H05	70-72	116.78	1.0450	0.0033
13H05	88-90	116.96	1.0452	0.0038
13H05	110-112	117.18	1.0454	0.0035
13H06	10-12	117.68	1.0459	0.0041
13H06	30-32	117.88	1.0462	0.0045
13H06	50-52	118.08	1.0464	0.0043
13H06	70-72	118.28	1.0466	0.0035
13H06	88-90	118.46	1.0468	0.0033
13H06	110-112	118.68	1.0470	0.0029
13H06	130-132	118.88	1.0473	0.0023
13H07	10-12	119.18	1.0476	0.0028
13H07	30-32	119.38	1.0478	0.0034
13H07	50-52	119.58	1.0480	0.0032
13H07	70-72	119.78	1.0483	0.0029
13H07	88-90	119.96	1.0484	0.0028
13H07	110-112	120.18	1.0487	0.0034

Table A.6 Magnetic susceptibility measurements for Hole 823A samples

Sample code	Depth (mbsf)	Age (Ma)	Magnetic Susceptibility ($\mu m^3 kg^{-1}$)
1H01 11-13	0.11	0.00196	0.0050
1H01 35-37	0.35	0.00625	0.0075
1H01 60-62	0.60	0.01072	0.0104
1H01 85-87	0.85	0.01518	0.0149
1H01 110-112	1.10	0.01965	0.0155
1H01 135-137	1.35	0.02411	0.0053
1H02 12-14	1.62	0.05894	0.0049
1H02 35-37	1.85	0.03304	0.0143
1H02 60-62	2.10	0.03751	0.0078
1H02 85-87	2.35	0.04197	0.0062
1H02 110-112	2.60	0.04644	0.0071
1H02 135-137	2.85	0.05091	0.0069
1H03 13-15	3.13	0.05591	0.0041
1H03 35-37	3.35	0.05984	0.0047
1H03 60-62	3.60	0.06430	0.0084
1H03 85-87	3.85	0.06877	0.0076
1H03 110-112	4.10	0.07316	0.0029
1H03 135-137	4.35	0.07749	0.0040
1H04 11-134	4.61	0.08198	0.0058
1H04 35-37	4.85	0.08614	0.0053
1H04 60-62	5.10	0.09046	0.0058
1H04 85-87	5.35	009479	0.0066
1H04 110-112	5.60	0.09911	0.0078
2H01 9-11	5.89	0.1041	0.0047
2H01 35-37	6.15	0.1086	0.0058
2H01 60-62	6.40	0.1130	0.0077
2H01 85-87	6.65	0.1173	0.0078
2H01 110-112	6.90	0.1216	0.0115
2H01 135-137	7.15	0.1259	0.0148
2H02 9-11	7.39	0.1315	0.0453
2H02 35-37	7.65	0.1390	0.0165
2H02 60-62	7.90	0.1462	0.0150
2H02 85-87	8.15	0.1535	0.0109
2H02 110-112	8.40	0.1607	0.0152
2H02 135-137	8.65	0.1679	0.0225
2H03 12-14	8.92	0.1757	0.0055
2H03 35-37	9.15	0.1824	0.0068
2H03 60-62	9.40	0.1880	0.0098
2H03 88-90	9.68	0.1924	0.0082
2H03 110-112	9.90	0.1958	0.0047
2H03 135-137	10.15	0.1998	0.0034
2H04 9-11	10.39	0.2035	0.0036
2H04 35-37	10.65	0.2076	0.0055
2H04 60-62	10.90	0.2116	0.0076
2H04 85-87	11.15	0.2155	0.0075
2H04 110-112	11.40	0.2194	0.0059
2H04 135-137	11.65	0.2234	0.0092
2H05 9-11	11.89	0.2271	0.0089
2H05 35-37	12.15	0.2312	0.0083
2H05 60-62	12.40	0.2352	0.0074
2H05 85-87	12.65	0.2391	0.0089
2H05 110-112	12.90	0.2430	0.0110
2H05 135-137	13.15	0.2472	0.0111
2H06 9-11	13.39	0.2515	0.0150
2H06 60-62	13.90	0.2606	0.0153
2H06 85-87	14.15	0.2651	0.0066
2H06 110-112	14.40	0.2695	0.0063
2H06 134-136	14.64	0.2738	0.0070
2H07 35-37	15.15	0.2839	0.0083
3H01 10-12	15.40	0.2874	0.0117
3H01 35-37	15.65	0.2918	0.0047
3H01 60-62	15.90	0.2963	0.0043
3H01 85-87	16.15	0.3008	0.0044
4H01 10-12	24.90	0.3063	0.0009
4H01 35-37	25.15	0.3096	0.0009
4H01 85-87	25.65	0.3162	0.0027
4H01 110-112	25.90	0.3195	0.0020
4H01 135-137	26.15	0.3228	0.0048
4H02 10-12	26.40	0.3261	0.0044
4H02 35-37	26.65	0.3294	0.0075
4H02 60-62	26.90	0.3327	0.0078
4H02 85-87	27.15	0.3360	0.0087
4H02 110-112	27.40	0.3434	0.0112
4H02 135-137	27.65	0.3509	0.0102
4H03 10-12	27.90	0.3583	0.0052
4H03 35-37	28.15	0.3641	0.0091
4H03 60-62	28.40	0.3683	0.0057
4H03 85-87	28.65	0.3725	0.0050
4H03 110-112	28.90	0.3967	0.0055
4H03 135-137	29.15	0.3809	0.0057
4H04 10-12	29.40	0.3851	0.0052
4H04 35-37	29.65	0.3893	0.0071
4H04 60-62	29.90	0.3936	0.0035
4H04 85-87	30.15	0.3978	0.0060
4H04 110-112	30.40	0.4020	0.0054
4H04 135-137	30.65	0.4062	0.0073
4H05 10-12	30.90	0.4104	0.0055
4H05 35-37	31.15	0.4146	0.0047
4H05 60-62	30.40	0.4188	0.0048
4H05 85-87	31.65	0.4230	0.0057
4H05 110-112	31.90	0.4282	0.0080
4H05 135-137	32.15	0.4335	0.0041
4H06 10-12	32.40	0.4387	0.0019
4H06 35-37	32.65	0.4440	0.0011
4H06 60-62	32.90	0.4492	-
4H06 85-87	33.15	0.4544	0.0020
4H06 112-114	33.42	0.4597	0.0018
4H06 135-137	33.65	0.4649	0.0000
4H07 10-12	33.90	0.4701	0.0011
4H07 35-37	34.15	0.4754	0.0019
5H01 10-12	34.40	0.4811	0.0028
5H01 35-37	34.65	0.4873	0.0026
5H01 60-62	34.90	0.4935	0.0017
5H01 86-88	35.16	0.5000	0.0014
5H01 135-137	35.65	0.5122	0.0018
5H02 10-12	35.90	0.5300	0.0009

5H02	60-62	36.40	0.5335	0.0017
5H02	109-111	36.89	0.5370	0.0018
5H02	135-137	37.15	0.5388	0.0009
5H03	10-12	37.40	0.5406	0.0009
5H03	34-36	37.64	0.5423	0.0009
5H03	135-137	38.65	0.5494	0.0000
5H04	34-36	39.14	0.5529	0.0000
5H04	60-62	39.40	0.5547	0.0008
5H04	86-88	39.66	0.5565	0.0000
5H04	135-137	40.15	0.5600	0.0000
5H05	60-62	40.90	0.5684	0.0017
5H05	86-88	41.16	0.5713	0.0025
5H05	110-112	41.40	0.5740	0.0015
5H05	135-137	41.65	0.5750	0.0000
5H06	10-12	41.90	0.5760	0.0008
5H06	34-36	42.14	0.5770	0.0008
5H06	60-62	42.40	0.5780	0.0032
5H06	137-139	43.17	0.5811	0.0019
5H07	10-12	43.40	0.5820	0.0024
5H07	34-36	43.64	0.5830	0.0018
5H07	60-62	43.90	0.5840	0.0009
6H01	10-12	43.90	-	0.0017
6H01	35-37	44.15	0.5850	0.0016
6H01	60-62	44.40	0.5860	0.0009
6H01	85-87	44.65	0.5870	0.0009
6H01	110-112	44.90	0.5880	0.0010
6H01	135-137	45.15	0.5890	0.0009
6H02	10-12	45.40	0.5900	0.0018
6H02	35-37	45.65	0.5910	0.0008
6H02	60-62	45.90	0.5920	0.0017
6H02	85-87	46.15	0.5930	0.0017
6H02	110-112	16.40	0.5940	0.0016
6H02	135-137	46.65	0.5950	0.0017
6H03	35-37	47.15	0.5970	0.0025
6H03	60-62	47.40	0.5980	0.0034
6H03	85-87	47.65	0.5990	0.0022
6H03	110-112	47.90	0.6000	0.0024
7H01	35-37	53.65	0.6600	0.0018
7H01	60-62	53.90	0.6625	0.0026
7H01	85-87	54.15	0.6649	0.0018
7H01	110-112	54.40	0.6673	0.0009
7H01	135-137	54.65	0.6698	0.0034
7H02	10-12	54.90	0.6722	0.0017
7H02	35-37	55.15	0.6747	0.0024
7H02	60-62	55.40	0.6771	0.0017
7H02	85-87	55.65	0.6796	0.0026
7H02	110-112	55.90	0.6820	0.0025
7H02	135-137	56.15	0.6845	0.0017
7H03	10-12	56.40	0.6869	0.0009
7H03	35-37	56.65	0.6894	0.0018
7H03	60-62	56.90	0.6918	0.0018
7H03	85-87	57.15	0.6943	0.0018
7H03	110-112	57.40	0.6967	0.0025
7H03	135-137	57.65	0.6992	0.0035
7H04	10-12	57.90	0.7016	0.0028
7H04	35-37	58.15	0.7041	0.0019
7H04	60-62	58.40	0.7065	0.0033
7H04	85-87	58.65	0.7090	0.0009
7H04	110-112	58.90	0.7114	0.0018
7H04	135-137	59.15	0.7139	0.0019
7H05	10-12	59.40	0.7163	0.0018
7H05	35-37	59.65	0.7188	0.0024
7H05	60-62	59.90	0.7212	0.0021
7H05	85-87	60.15	0.7237	0.0027
7H05	110-112	60.40	0.7261	0.0033
7H05	135-137	60.65	0.7285	0.0017
7H06	10-12	60.90	0.7310	0.0018
7H06	35-37	61.15	0.7334	0.0018
7H06	60-62	61.40	0.7359	0.0028
7H06	85-87	61.65	0.7383	0.0009
7H06	110-112	61.90	0.7408	0.0009
7H06	135-137	62.15	0.7432	0.0033
7H07	10-12	62.40	0.7457	0.0018
7H07	35-37	62.65	0.7481	0.0027
8H01	10-12	62.90	0.7506	0.0018
8H01	35-37	63.15	0.7530	0.0017
8H01	60-62	63.40	0.7555	0.0017
8H01	85-87	63.65	0.7579	0.0000
8H01	110-112	63.90	0.7604	0.0008
8H01	135-137	64.15	0.7628	0.0021
8H02	10-12	64.40	0.7653	0.0009
8H02	35-37	64.65	0.7677	0.0025
8H02	60-62	64.90	0.7702	0.0024
8H02	85-87	65.15	0.7726	0.0009
8H02	110-112	65.40	0.7751	0.0028
8H02	135-137	65.65	0.7775	0.0008
8H03	10-12	65.90	0.7800	0.0017
8H03	35-37	66.15	0.7824	0.0016
8H03	110-112	66.90	0.7898	0.0016
8H04	10-12	67.40	0.7947	0.0008
8H04	35-37	67.65	0.7971	0.0009
8H04	60-62	67.90	0.7995	0.0016
8H04	85-87	68.15	0.8020	0.0016
8H04	110-112	68.40	0.8044	0.0008
8H04	135-137	68.65	0.8069	0.0025
8H05	10-12	68.90	0.8093	0.0036
8H05	35-37	69.15	0.8118	0.0017
8H05	60-62	69.40	0.8142	0.0016
8H05	85-87	69.65	0.8167	0.0042
8H05	110-112	69.90	0.8191	0.0040
8H05	135-137	70.15	0.8216	0.0033
8H06	10-12	70.40	0.8240	0.0016
8H06	35-37	70.65	0.8265	0.0017
8H06	60-62	70.90	0.8289	0.0017
8H06	85-87	71.15	0.8314	0.0017
8H06	110-112	71.40	0.8338	0.0017
8H06	135-137	71.65	0.8363	0.0008
8H07	10-12	71.90	0.8387	0.0009
8H07	35-37	72.15	0.8412	0.0018
9H01	09-11	72.39	0.8436	0.0008
9H01	35-37	72.65	0.8462	0.0019
9H01	60-62	72.90	0.8485	0.0016
9H01	85-87	73.15	0.8510	0.0008
9H01	110-112	73.40	0.8534	0.0016
9H01	135-137	73.65	0.8559	0.0009
9H02	09-11	73.89	0.8582	0.0009
9H02	35-37	74.15	0.8608	0.0015
9H02	60-62	74.40	0.8632	0.0017
9H02	85-87	74.65	0.8656	0.0018
9H02	110-112	74.90	0.8681	0.0018
9H02	135-137	75.15	0.8706	0.0018
9H03	09-11	75.39	0.8730	0.0016

9H03	35-37	75.65	0.8754	0.0008
9H03	60-62	75.90	0.8779	0.0009
9H03	85-87	76.15	0.8803	0.0052
9H03	110-112	76.40	0.8828	0.0017
9H03	135-137	76.65	0.8852	0.0008
9H04	09-11	76.89	0.8876	0.0020
9H04	35-37	77.15	0.8901	0.0000
9H04	60-62	77.40	0.8926	0.0000
9H04	85-87	77.65	0.8950	0.0000
9H04	110-112	77.90	0.8975	0.0008
9H05	09-11	78.39	0.8023	0.0010
9H05	35-37	78.65	0.9048	0.0016
9H05	60-62	78.90	0.9073	0.0017
9H05	85-87	79.15	0.9097	0.0018
9H05	110-112	79.40	0.9122	0.0017
9H05	135-137	79.65	0.9146	0.0018
9H06	09-11	79.89	0.9171	0.0026
9H06	35-37	80.15	0.9195	0.0017
9H06	60-62	80.40	0.9224	0.0018
9H06	85-87	81.65	0.9253	0.0017
9H06	110-112	80.90	0.9283	0.0036
9H06	135-137	81.15	0.9312	0.0060
9H07	09-11	81.39	0.9341	0.0050
9H07	35-37	81.65	0.9371	0.0052
9H07	60-62	81.90	0.9399	0.0038
10H01	09-11	81.89	0.9400	0.0043
10H01	35-37	82.15	0.9429	0.0055
10H01	60-62	82.40	0.9459	0.0036
10H01	85-87	82.65	0.9488	0.0033
10H01	110-112	82.90	0.9518	0.0041
10H01	135-137	83.15	0.9547	0.0040
10H02	09-11	83.39	0.9575	0.0037
10H02	35-37	83.65	0.9606	0.0034
10H02	60-62	83.90	0.9635	0.0059
10H02	85-87	84.15	0.9665	0.0052
10H02	110-112	84.40	0.9694	0.0088
10H02	135-137	84.65	0.9724	0.0062
10H03	09-11	84.89	0.9753	0.0055
10H03	35-37	85.15	0.9782	0.0032
10H03	60-62	85.40	0.9811	0.0042
10H03	85-87	85.65	0.9841	0.0026
10H03	110-112	85.90	0.9871	0.0028
10H03	135-137	86.15	0.9900	0.0040
10H04	09-11	86.39	0.9928	0.0148
10H04	35-37	86.65	0.9959	0.0067
10H04	60-62	86.90	0.9988	0.0187
10H04	85-87	87.15	1.0018	0.0280
10H04	110-112	87.40	1.0047	0.0115
10H04	135-137	87.65	1.0076	0.0158
10H05	09-11	87.89	1.0106	00137
10H05	35-37	88.15	1.0235	0.0228
10H05	60-62	88.40	1.0165	0.0019
10H05	85-87	88.65	1.0194	0.0042
10H05	110-112	88.90	1.0224	0.0050
10H05	135-137	89.15	1.0253	0.0045
10H06	09-11	89.39	1.0282	0.0045
10H06	35-37	89.65	1.0312	0.0036
10H06	60-62	89.90	1.0341	0.0011
10H06	85-87	90.15	1.0371	0.0035
10H06	110-112	90.40	1.0400	0.0027
10H06	135-137	90.65	1.0429	0.0042
10H07	09-11	90.89	1.0459	0.0037
10H07	35-37	91.15	1.0488	0.0034
10H07	60-62	91.40	1.0518	0.0027
11H01	10-12	91.40	1.0518	0.0017
11H01	35-37	91.65	1.0547	0.0019
11H01	60-62	92.90	1.0576	0.0027
11H01	85-87	92.15	1.0606	0.0025
11H01	110-112	92.40	1.0635	0.0041
11H01	135-137	92.65	1.0665	0.0027
11H02	35-37	93.15	1.0724	0.0035
11H02	64-66	93.44	1.0758	0.0041
11H02	110-112	93.90	1.0812	0.0046
11H03	10-12	94.40	1.0871	0.0043
11H03	35-37	95.65	1.0900	0.0010
11H03	110-112	95.40	1.0988	0.0027
11H03	135-137	95.65	1.1025	0.0032
11H04	10-12	95.90	1.1067	0.0035
11H04	35-37	96.15	1.1110	0.0050
11H04	85-87	96.65	1.1192	0.0037
11H04	110-112	96.90	1.1233	0.0026
11H04	135-137	97.15	1.1275	0.0035
11H05	10-12	97.40	1.1317	0.0031
11H05	35-37	97.65	1.1358	0.0020
11H05	64-66	97.94	1.1407	0.0020
11H05	85-87	98.15	1.1440	0.0034
11H05	110-112	98.40	1.1830	0.0035
11H05	135-137	98.65	1.1525	0.0039
11H06	10-12	98.90	1.1567	0.0035
11H06	35-37	99.15	1.1608	0.0034
11H06	64-66	99.44	1.1657	0.0036
11H06	85-87	99.65	1.1692	0.0018
11H06	110-112	99.90	1.1733	0.0018
11H06	135-137	100.15	1.1775	0.0020
11H07	10-12	100.40	1.1817	0.0027
11H07	35-37	100.65	1.1858	0.0037
12H01	10-12	100.90	1.1900	0.0044
12H01	36-38	101.16	1.1943	0.0051
12H01	61-63	101.41	1.1985	0.0037
12H01	111-113	101.91	1.2068	0.0019
12H01	136-138	102.16	1.2110	0.0038
12H02	10-12	102.40	1.2150	0.0036
12H02	36-38	102.66	1.2193	0.0027
12H02	61-63	102.90	1.2235	0.0035
12H02	111-113	103.41	1.2318	0.0037
12H02	136-138	103.66	1.2360	0.0026
12H03	10-12	103.90	1.2400	0.0036
12H03	36-38	104.16	1.2440	0.0037
12H03	136-138	105.16	1.2610	0.0036
12H04	10-12	105.40	1.2650	0.0038
12H04	36-38	105.66	1.2730	0.0042
12H05	136-138	108.16	1.3110	0.0016
12H06	36-38	108.66	1.3230	0.0019
12H06	61-63	108.91	1.3235	0.0035
12H06	111-113	109.41	1.3318	0.0020
12H06	136-138	109.66	1.3360	0.0028
13H01	10-12	110.40	1.3480	0.0048
13H02	60-62	112.40	1.3817	0.0045
13H04	35-37	115.15	1.4275	0.0053
13H05	60-62	116.90	1.4567	0.0148
13H05	135-137	117.65	1.4691	0.0126
13H06	10-12	117.90	1.4733	0.0247

13H06	35-37	118.15	1.4775	0.0463
13H06	60-62	118.40	1.4817	0.0183
13H06	110-112	118.90	1.4900	0.0210
13H07	60-62	119.90	1.5067	0.0056

Table A.7. Amendments to Hole 819A age model, based on correlation of carbonate stratigraphies across the Queensland margin.

Sample code		Depth (mbsf)	Age (Ma)	Sample code		Depth (mbsf)	Age (Ma)
1H05	70-72	6.70	0.0240	2H05	54-56	15.04	0.0672
1H05	90-92	6.90	0.0251	2H05	70-72	15.20	0.0678
1H05	120-122	7.20	0.0268	2H05	88-90	15.38	0.0685
1H06	10-12	7.60	0.0290	2H05	109-111	15.59	0.0694
1H06	30-32	7.80	0.0301	2H05	132-133	15.82	0.0703
1H06	54-56	8.04	0.0314	2H06	12-14	16.12	0.0721
1H06	68-70	8.18	0.0322	2H06	30-32	16.30	0.0737
2H01	12-14	8.62	0.0347	2H06	54-56	16.54	0.0759
2H01	30-32	8.80	0.0357	2H06	70-72	16.70	0.0773
2H01	54-56	9.04	0.0370	2H06	88-90	16.88	0.0789
2H01	70-72	9.20	0.0379	2H06	109-111	17.09	0.0808
2H01	88-90	9.38	0.0389	2H06	132-134	17.32	0.0829
2H01	109-111	9.59	0.0401	2H07	7-8	17.57	0.0852
2H01	132-134	9.82	0.0413	2H07	27-29	17.77	0.0870
2H02	12-14	10.12	0.0430	2H07	54-56	18.04	0.0894
2H02	30-32	10.30	0.0440	3H01	10-12	18.10	0.0900
2H02	54-56	10.54	0.0453	3H01	30-32	18.30	0.0918
2H02	70-72	10.70	0.0462	3H01	52-54	18.52	0.0938
2H02	88-90	10.88	0.0472	3H01	70-72	18.70	0.0954
2H02	109-111	11.09	0.0484	3H01	90-92	18.90	0.0972
2H02	132-134	11.32	0.0497	3H01	109-111	19.09	0.0989
2H03	30-32	11.80	0.0523	3H01	131-133	19.31	0.1009
2H03	54-56	12.04	0.0537	3H02	10-12	19.60	0.1035
2H03	70-72	12.20	0.0546	3H02	30-32	19.80	0.1053
2H03	88-90	12.38	0.0556	3H02	52-54	20.02	0.1073
2H03	109-111	12.59	0.0567	3H02	70-72	20.20	0.1089
2H03	132-134	12.82	0.0580	3H02	90-92	20.40	0.1107
2H04	12-14	13.12	0.0595	3H02	109-111	20.59	0.1125
2H04	30-32	13.30	0.0602	3H02	131-133	20.81	0.1145
2H04	54-56	13.54	0.0612	3H03	10-12	21.10	0.1171
2H04	70-72	13.70	0.0618	3H03	30-32	21.30	0.1189
2H04	88-90	13.88	0.0625	3H03	52-54	21.52	0.1209
2H04	109-111	14.09	0.0634	3H03	70-72	21.70	0.1225
2H04	132-134	14.32	0.0643	3H03	90-92	21.90	0.1243
2H05	12-14	14.62	0.0655	3H03	109-111	22.09	0.1260
2H05	30-32	14.80	0.0662	3H03	131-132	22.31	0.1280

Note: Stages 3/ 4 and 4/ 5 boundaries are now located at 13 and 16 mbsf, respectively.

Table A.8. Depth to age conversion for Hole 823B sediments, based on a combination of calcareous nannofossil and foraminiferal datums (column A), and foraminiferal datums (column B) (see main text)

Sample code	Depth (mbsf)	A	B	Sample code	Depth (mbsf)	A	B
12H01 50-52	103.80	1.261	1.020	19X05 50-52	177.30	1.694	1.694
12H02 50-52	105.30	1.272	1.023	19X06 50-52	178.80	1.700	1.700
12H03 50-52	106.80	1.275	1.026	20X01 50-52	181.00	1.709	1.709
12H04 50-52	108.30	1.282	1.029	20X02 50-52	182.50	1.714	1.714
12H05 50-52	109.80	1.289	1.032	20X04 50-52	185.50	1.726	1.726
12H06 50-52	111.30	1.296	1.035	21X01 50-52	190.70	1.746	1.746
12H07 50-52	112.80	1.303	1.038	21X02 50-52	192.20	1.752	1.752
13X01 50-52	113.30	1.305	1.039	21X03 50-52	193.70	1.758	1.758
13H02 50-52	114.80	1.312	1.042	21X04 50-52	195.20	1.764	1.764
13X03 50-52	116.30	1.319	1.045	21X05 50-52	196.70	1.770	1.770
13X04 50-52	117.80	1.326	1.048	21X06 50-52	198.20	1.776	1.776
13X05 50-52	119.30	1.333	1.052	22X02 49-51	201.79	1.789	1.789
13X06 50-52	120.80	1.341	1.068	22X03 49-51	203.25	1.795	1.795
14X01 50-52	122.90	1.350	1.102	22X04 49-51	204.75	1.808	1.804
14X02 50-52	124.40	1.357	1.127	22X06 62-64	207.92	1.895	1.845
14X03 50-52	125.90	1.364	1.152	23X01 55-57	209.65	1.943	1.867
14X04 50-52	127.40	1.371	1.177	23X02 55-57	211.15	1.984	1.886
14X05 50-52	128.90	1.378	1.202	23X03 55-57	212.65	2.025	1.905
14X06 50-52	130.40	1.385	1.226	23X04 55-57	214.15	2.066	1.924
15X01 48-50	132.58	1.395	1.262	23X06 55-57	217.15	2.149	1.963
15X02 48-50	134.08	1.402	1.287	24X01 55-57	219.25	2.206	1.990
15X03 48-50	135.58	1.409	1.312	24X02 55-57	220.75	2.248	2.001
15X04 48-50	137.08	1.416	1.337	24X03 55-57	222.28	2.290	2.029
15X05 48-50	138.58	1.423	1.362	24X04 55-57	223.75	2.304	2.048
15X06 48-50	140.08	1.430	1.386	24X05 55-57	225.25	2.318	2.067
16X02 50-52	143.70	1.447	1.446	25X01 58-60	228.58	2.349	2.110
16X03 50-52	145.20	1.454	1.471	25X02 58-60	230.08	2.363	2.129
16X05 50-52	148.20	1.468	1.521	25X03 58-60	231.58	2.377	2.148
16X06 50-52	149.70	1.474	1.545	25X04 58-60	233.08	2.391	2.167
16X07 50-52	151.20	1.496	1.570	25X05 58-60	234.58	2.405	2.187
17X01 50-52	151.90	1.533	1.582	25X06 58-60	236.08	2.419	2.206
17X04 50-52	156.40	1.613	1.613	26X01 56-80	238.26	2.466	2.234
18X01 50-52	161.60	1.633	1.633	26X02 56-80	239.76	2.499	2.253
18X04 50-52	166.10	1.651	1.651	26X03 56-80	241.26	2.532	2.272
18X05 50-52	167.60	1.656	1.656	26X04 56-80	242.76	2.566	2.291
18X06 50-52	169.10	1.662	1.662	26X05 56-80	244.26	2.599	2.311
19X01 50-52	171.30	1.671	1.671	26X06 56-80	245.80	2.610	2.330
19X02 50-52	172.80	1.677	1.677	27X01 50-52	247.80	2.623	2.356
19X03 50-52	174.30	1.682	1.682	27X02 50-52	248.52	2.628	2.365
19X04 50-52	175.80	1.688	1.688	27X03 50-52	250.02	2.637	2.385

27X04 50-52	251.52	2.647	2.404
27X05 50-52	253.02	2.657	2.423
27X07 50-52	256.02	2.677	2.462
28X01 51-52	257.51	2.686	2.481
28X02 51-52	259.01	2.696	2.500
28X03 51-52	260.51	2.706	2.519
28X04 51-52	262.01	2.716	2.538
28X05 51-52	263.51	2.726	2.558
28X06 45-47	264.95	2.735	2.576
29X01 50-52	267.20	2.750	2.605
29X02 50-52	268.70	2.760	2.624
29X03 50-52	270.20	2.769	2.643
29X04 55-57	271.75	2.779	2.663
29X05 57-59	273.27	2.789	2.683
29X06 57-59	274.77	2.800	2.702
30X01 65-67	276.95	2.813	2.730
30X02 65-67	278.45	2.823	2.749
30X04 72-74	281.52	2.843	2.790
30X06 61-63	284.41	2.862	2.826
31X02 62-64	287.18	2.880	2.861
31X04 56-58	290.12	2.900	2.899
31X06 66-68	293.22	2.942	2.942
31X07 82-84	294.88	2.965	2.965
32X01 70-72	296.30	2.984	2.984
32X02 70-72	297.80	3.003	3.002
32X04 70-72	300.80	3.028	3.016
32X06 70-72	303.80	3.052	3.030
33X01 70-72	306.00	3.071	3.040
33X03 70-72	309.00	3.095	3.054
33X04 67-69	310.47	3.107	3.061
33X05 67-69	311.97	3.120	3.058
33X06 67-69	313.45	3.132	3.075
34X01 70-72	315.60	3.150	3.085
34X02 70-72	317.10	3.162	3.092
34X03 70-72	318.60	3.174	3.100
34X04 70-72	320.10	3.187	3.106
34X05 70-72	321.60	3.200	3.113
34X06 70-72	323.10	3.212	3.120
35X01 50-52	325.10	3.228	3.130
35X02 50-52	326.60	3.240	3.137
35X03 50-52	328.10	3.253	3.144
35X04 50-52	329.60	3.265	3.151
35X05 50-52	331.10	3.278	3.158
35X06 50-52	332.60	3.290	3.165
35X07 50-52	334.10	3.302	3.172
36X01 50-52	334.70	3.307	3.175
36X02 50-52	336.20	3.320	3.182
36X03 53-55	337.73	3.332	3.189
36X04 50-52	339.20	3.344	3.196
36X05 50-52	340.70	3.357	3.203
36X06 51-53	342.21	3.369	3.210

Table A.9. Amendments to the age model proposed for Hole 823A based on a comparison between Sr/Ca ratios and the Hole 607 oxygen isotope stratigraphy (Ruddiman et al., 1989).

Sample Code		Depth (mbsf)	Age (Ma)	Sample Code		Depth (mbsf)	Age (Ma)
6H03	110-112	47.90	0.600	8H02	135-137	65.65	0.768
7H01	35-37	53.65	0.690	8H03	10-12	65.90	0.769
7H01	60-62	53.90	0.692	8H03	35-37	66.15	0.771
7H01	85-87	54.15	0.693	8H03	110-112	66.90	0.775
7H01	110-112	54.40	0.695	8H04	10-12	67.40	0.777
7H01	135-137	54.65	0.696	8H04	35-37	67.65	0.778
7H02	10-12	54.90	0.698	8H04	60-62	67.90	0.779
7H02	35-37	55.15	0.699	8H04	85-87	68.15	0.781
7H02	60-62	55.40	0.701	8H04	110-112	68.40	0.782
7H02	85-87	55.65	0.702	8H04	135-137	68.65	0.783
7H02	110-112	55.90	0.704	8H05	10-12	68.90	0.785
7H02	135-137	56.15	0.705	8H05	35-37	69.15	0.786
7H03	10-12	56.40	0.707	8H05	60-62	69.40	0.787
7H03	35-37	56.65	0.708	8H05	85-87	69.65	0.789
7H03	60-62	56.90	0.709	8H05	110-112	69.90	0.790
7H03	85-87	57.15	0.711	8H05	135-137	70.15	0.791
7H03	110-112	57.40	0.713	8H06	10-12	70.40	0.793
7H03	135-137	57.65	0.715	8H06	35-37	70.65	0.795
7H04	10-12	57.90	0.716	8H06	60-62	70.90	0.796
7H04	35-37	58.15	0.718	8H06	85-87	71.15	0.798
7H04	60-62	58.40	0.719	8H06	110-112	71.40	0.800
7H04	85-87	58.65	0.721	8H06	135-137	71.65	0.802
7H04	110-112	58.90	0.722	8H07	10-12	71.90	0.804
7H04	135-137	59.15	0.724	8H07	35-37	72.15	0.805
7H05	10-12	59.40	0.726	9H01	9-11	72.39	0.807
7H05	35-37	59.65	0.727	9H01	35-37	72.65	0.809
7H05	60-62	59.90	0.729	9H01	60-62	72.90	0.811
7H05	85-87	60.15	0.732	9H01	85-87	73.15	0.813
7H05	110-112	60.40	0.734	9H01	110-112	73.40	0.814
7H05	135-137	60.65	0.737	9H01	135-137	73.65	0.816
7H06	10-12	60.90	0.739	9H02	9-11	73.89	0.817
7H06	35-37	61.15	0.742	9H02	35-37	74.15	0.820
7H06	60-62	61.40	0.744	9H02	60-62	74.40	0.822
7H06	85-87	61.65	0.747	9H02	85-87	74.65	0.823
7H06	110-112	61.90	0.749	9H02	110-112	74.90	0.825
7H06	135-137	62.15	0.750	9H02	135-137	75.15	0.827
7H07	10-12	62.40	0.752	9H03	9-11	75.39	0.829
7H07	35-37	62.65	0.753	9H03	35-37	75.65	0.831
8H01	10-12	62.90	0.754	9H03	60-62	75.90	0.832
8H01	35-37	63.15	0.755	9H03	85-87	76.15	0.834
8H01	60-62	63.40	0.757	9H03	110-112	76.40	0.836
8H01	85-87	63.65	0.759	9H03	135-137	76.65	0.838
8H01	110-112	63.90	0.760	9H04	9-11	76.89	0.839
8H01	135-137	64.15	0.761	9H04	35-37	77.15	0.841
8H02	10-12	64.40	0.762	9H04	60-62	77.40	0.843
8H02	35-37	64.65	0.763	9H04	85-87	77.65	0.845
8H02	60-62	64.90	0.764	9H04	110-112	77.90	0.847
8H02	85-87	65.15	0.766	9H05	9-11	78.39	0.850
8H02	110-112	65.40	0.767	9H05	35-37	78.65	0.852

9H05	60-62	78.90	0.854
9H05	85-87	79.15	0.856
9H05	110-112	79.40	0.857
9H05	135-137	79.65	0.859
9H06	9-11	79.89	0.861
9H06	35-37	80.15	0.863
9H06	60-62	80.40	0.865
9H06	85-87	80.65	0.866
9H06	110-112	80.90	0.868
9H06	135-137	81.15	0.870
9H07	9-11	81.39	0.872
9H07	35-37	81.65	0.875
9H07	60-62	81.90	0.877
10H01	9-11	81.89	0.877
10H01	35-37	82.15	0.879
10H01	60-62	82.40	0.882
10H01	85-87	82.65	0.885
10H01	110-112	82.90	0.887
10H01	135-137	83.15	0.889
10H02	9-11	83.39	0.892
10H02	35-37	83.65	0.894
10H02	60-62	83.90	0.897
10H02	85-87	84.15	0.899
10H02	110-112	84.40	0.902
10H02	135-137	84.65	0.904
10H03	9-11	84.89	0.906
10H03	35-37	85.15	0.909
10H03	60-62	85.40	0.911
10H03	85-87	85.65	0.914
10H03	110-112	85.90	0.916
10H03	135-137	86.15	0.919
10H04	9-11	86.39	0.921
10H04	35-37	86.65	0.923
10H04	60-62	86.90	0.926
10H04	85-87	87.15	0.928
10H04	110-112	87.40	0.931
10H04	135-137	87.65	0.933
10H05	9-11	87.89	0.935
10H05	35-37	88.15	0.938
10H05	60-62	88.40	0.941
10H05	85-87	88.65	0.943
10H05	110-112	88.90	0.945
10H05	135-137	89.15	0.948
10H06	9-11	89.39	0.950
10H06	35-37	89.65	0.952
10H06	60-62	89.90	0.955
10H06	85-87	90.15	0.957
10H06	110-112	90.40	0.960
10H06	135-137	90.65	0.962
10H07	9-11	90.89	0.964
10H07	35-37	91.15	0.965
10H07	60-62	91.40	0.967
11H01	10-12	91.40	0.967
11H01	35-37	91.65	0.968
11H01	60-62	92.90	0.969
11H01	85-87	92.15	0.971
11H01	110-112	92.40	0.973
11H01	135-137	92.65	0.974
11H02	35-37	93.15	0.977
11H02	64-66	93.44	0.979
11H02	110-112	93.90	0.982
11H03	10-12	94.40	0.985
11H03	35-37	94.65	0.987
11H03	110-112	95.40	0.991
11H03	135-137	95.65	0.992
11H04	10-12	95.90	0.994
11H04	35-37	96.15	0.995
11H04	64-66	96.44	0.997
11H04	85-87	96.65	0.998
11H04	110-112	96.90	0.999
11H04	135-137	97.15	1.001
11H05	10-12	97.40	1.003
11H05	35-37	97.65	1.005
11H05	64-66	97.94	1.006
11H05	85-87	98.15	1.008
11H05	110-112	98.40	1.009
11H05	135-137	98.65	1.011
11H06	10-12	98.90	1.012
11H06	35-37	99.15	1.014
11H06	64-66	99.44	1.015
11H06	85-87	99.65	1.017
11H06	110-112	99.90	1.018
11H06	135-137	100.15	1.020
11H07	10-12	100.40	1.021
11H07	35-37	100.65	1.023
12H01	10-12	100.90	1.024
12H01	36-38	101.16	1.026
12H01	61-63	101.41	1.027
12H01	111-113	101.91	1.030
12H01	136-138	102.16	1.032
12H02	10-12	102.40	1.033
12H02	36-38	102.66	1.035
12H02	61-63	102.91	1.036
12H02	111-113	103.41	1.040
12H02	136-138	103.66	1.041
12H03	10-12	103.90	1.042
12H03	36-38	104.16	1.044
12H03	136-138	105.16	1.050
12H04	10-12	105.40	1.051
12H04	36-38	105.66	1.053
12H05	136-138	108.16	1.060
12H06	36-38	108.66	1.063
12H06	61-63	108.91	1.063
12H06	111-113	109.41	1.065
12H06	136-138	109.66	1.066
13H01	10-12	110.40	1.068
13H02	60-62	112.40	1.075
13H04	35-37	115.15	1.085
13H05	60-62	116.90	1.091
13H05	135-137	117.65	1.093
13H06	10-12	117.90	1.094
13H06	35-37	118.15	1.095
13H06	60-62	118.40	1.096
13H06	110-112	118.90	1.098
13H07	60-62	119.90	1.101

APPENDIX - B

Additional notes on the acid-base titration method of carbonate content determination

Solutions

0.5N HCL
0.35N NaOH
Bromophenol blue indicator

Standardization

Either $CaCO_3$ or Na_2CO_3 can be used as primary standards to standardise the HCL; the former was used as calculations are easier and the titration is performed in the same way as a sample titration (where most of the carbonate is present as $CaCO_3$). Any titration errors should then cancel out and be negligible.

Ideally the $CaCO_3$ should be oven-dried at 110°C before weighing. Excess 0.5 N HCL is added and after reaction 0.35 N NaOH used to titrate to a bromophenol blue endpoint.

Symbols are used below to show the calculation and actual values (for a working example) obtained are shown in brackets.

Let W = weight (wt) of $CaCO_3$ taken for standardisation which should be approximately 0.5 g (0.47552 g.)

Let V = volume (vol.) of 0.5N HCL added to $CaCO_3$ (25 ml.)

Let V_1= vol. of 0.35N NaOH required to neutralise the solution after the carbonate has reacted (8.72 ml.)

It is now necessary to titrate the NaOH directly against the HCL using the bromophenol blue as indicator

Let V_2 = vol. of HCL used (25 ml.), Let V_3 = vol. of NaOH used (37.52 ml.)

Then 1 ml. of NaOH is equivalent to V_2/V_3 ml. of HCL, and the HCL equivalent to the NaOH used to titrate excess HCL after reaction with $CaCO_3$ is:

$V_1 \times V_2/V_3$ ml. (8.72 x 25/37.52 = 5.81)

Therefore the volume of HCL consumed by the $CaCO_3$ is:

$V - (V_1 \times V_2/V_3)$, (25 - 5.81 = 19.19)

Therefore 1ml. of HCL is equal to,

$W/ V - (V1 \times V_2/V_3)$ g $CaCO_3$ (0.02478) Call this value Wg

Sample titration.
Let W_2 be the weight in g of sample. This was attacked with 25 ml. of the HCL solution and the excess acid titrated with the NaOH to the bromophenol blue endpoint.

Let V_4 be the volume of NaOH used (6.27). This is equivalent to $V_4 \times V_2/V_3$ ml. of HCL (4.18)

Therefore the volume of HCL consumed by $CaCO_3$ within the sample is:

$$25 - (V_4 \times V_2/V_3) = V \quad (20.82)$$

$$\% \ CaCO_3 \text{ in sample} = V \times Wg/W_2 \times 100$$

$$(21.82 \times 0.02478/ 0.50092 \times 100 = 109.6 \ \%$$

Note: this result is high because some of the carbonate is present as $MgCO_3$

In the final calculation of percentage carbonate content, in Hole 819A and Hole 823A samples, mean values of 0.02478 (N = 26) and 37.52 (N =12) were taken for Wg and V_3, respectively.

Table B.1. Particle size distribution for samples collected from Hole 819A.

(Note: column B data calculated using the Sieving method -see Chapter 4, data in column A and mean particle size are generated using the Coulter LS-100 particle size analyser).

Depth (mbsf)	A % Fine Fraction (< 63 μm)	B % Fine Fraction (< 63 μm)	Mean Particle Size (μm)	Depth (mbsf)	A % Fine Fraction (< 63 μm)	B % Fine Fraction (< 63 μm)	Mean Particle Size (μm)
0.16	81.82	86.39	37.78	12.20	98.11	92.68	25.46
0.30	81.56	84.35	48.99	12.38	86.28	93.52	38.53
0.54	81.79	90.69	47.07	12.59	86.11	91.36	37.17
0.70	85.49	90.51	40.47	12.82	89.02	92.89	33.11
0.90	83.27	90.58	42.13	13.12	77.06	85.46	54.00
1.20	88.12	93.71	36.47	13.30	68.35	84.62	80.88
1.60	80.08	93.32	39.50	13.54	61.16	81.29	102.30
1.80	95.74	94.71	25.71	13.70	66.29	80.00	81.05
2.04	88.43	93.11	35.69	13.88	70.21	87.48	73.55
2.18	91.97	93.51	32.45	14.09	78.13	89.11	51.53
2.20	88.68	93.04	33.86	14.34	71.95	86.17	68.46
2.40	87.16	90.49	38.21	14.62	76.94	86.75	60.38
2.70	88.70	93.78	35.89	14.80	84.71	90.38	44.20
3.10	83.42	92.50	40.03	15.04	74.22	86.55	59.43
3.30	87.18	95.73	35.10	15.20	68.12	85.19	102.30
3.54	96.88	95.58	22.77	15.38	78.15	86.84	57.24
3.70	91.06	96.45	29.69	15.59	84.05	88.40	44.48
3.95	96.03	95.59	22.61	15.82	79.10	87.68	52.09
4.20	94.15	95.96	24.89	16.12	81.69	86.84	57.77
4.60	92.57	93.43	38.34	16.30	82.13	86.39	45.47
5.40	79.73	88.78	50.32	16.54	73.77	84.05	59.80
5.70	71.65	81.01	69.26	16.70	73.91	84.29	64.04
6.10	84.07	88.69	32.73	16.88	76.69	84.06	58.91
6.30	63.97	70.89	88.96	17.09	61.17	75.80	123.90
6.70	53.59	63.26	113.10	17.32	77.75	86.71	58.04
6.90	59.26	66.31	96.85	17.57	72.22	100.00	70.03
7.20	58.10	70.10	97.77	17.77	79.67	85.41	52.97
7.60	65.56	80.85	82.09	18.04	76.09	86.45	56.48
7.80	64.94	85.00	77.52	18.10	81.23	90.58	46.83
8.04	78.84	85.15	52.00	18.30	88.41	91.50	35.54
8.18	80.80	89.12	47.82	18.52	86.98	92.81	34.53
8.62	79.47	87.64	53.63	18.70	87.48	91.22	35.95
8.80	84.70	90.62	43.25	18.90	82.19	90.13	40.78
9.04	84.19	92.06	42.81	19.09	75.21	85.33	64.10
9.20	85.39	92.59	41.05	19.31	78.83	88.66	54.22
9.38	90.12	93.55	35.71	19.60	74.02	87.78	65.87
9.59	87.39	93.54	31.94	19.80	57.47	76.61	129.30
9.82	89.42	92.55	32.08	20.02	72.58	83.43	77.20
10.12	86.23	100.00	38.64	20.20	82.35	85.88	51.03
10.30	89.70	94.21	28.38	20.40	75.49	81.63	57.03
10.54	90.66	93.91	32.37	20.59	80.98	87.81	50.24
10.70	87.23	93.96	35.97	20.81	80.23	86.99	46.16
10.88	84.19	95.18	39.20	21.10	85.14	90.81	40.48
11.09	90.06	94.34	32.59	21.30	91.12	93.86	28.50
11.32	90.70	95.13	32.95	21.52	92.33	95.32	28.35
11.80	82.68	94.98	41.39	21.70	90.21	95.21	31.61
12.04	90.57	92.16	30.30	21.90	92.84	96.59	27.09

22.09	92.75	96.69	27.95	35.30	88.21	89.56	31.39
22.31	99.70	97.15	17.26	35.50	82.79	87.72	38.46
22.60	48.20	71.23	107.10	35.70	84.57	89.82	35.40
22.80	92.95	97.53	26.44	35.90	82.96	89.27	37.51
23.02	97.59	98.27	18.94	36.10	84.51	86.94	36.18
23.20	96.15	97.27	21.73	36.30	83.63	87.33	37.16
23.40	89.74	96.05	32.51	36.60	86.39	86.77	29.87
23.59	98.22	98.26	19.34	36.80	68.00	85.49	56.15
23.81	83.78	94.93	42.00	37.00	78.55	84.50	42.44
24.10	76.87	77.49	57.93	37.20	78.74	82.27	41.88
24.30	70.61	74.13	85.47	37.10	85.43	86.05	36.86
24.52	62.95	78.92	128.80	37.30	84.53	84.46	36.95
24.70	84.73	85.13	45.76	37.50	82.23	86.12	39.31
24.87	74.84	80.55	67.81	37.70	75.77	85.54	41.91
25.09	73.72	67.81	80.88	37.90	76.91	86.24	44.30
25.57	60.55	58.76	112.60	38.10	79.86	84.33	41.61
25.76	50.10	47.59	150.50	38.30	83.34	87.63	37.25
26.02	59.81	63.61	120.00	38.60	81.31	75.48	48.70
26.17	71.06	72.52	78.98	38.80	83.95	81.62	36.19
26.40	73.59	73.30	79.62	39.00	83.67	81.05	41.69
26.59	55.44	52.87	148.50	39.20	87.78	88.13	31.10
26.81	57.07	55.30	135.90	39.40	87.26	76.84	39.86
27.10	52.98	56.34	147.40	40.10	89.48	75.36	30.63
27.80	79.44	85.37	59.01	40.30	86.32	85.26	35.15
28.00	82.97	78.82	49.75	40.50	87.50	89.52	32.00
28.20	99.98	95.46	16.57	40.70	82.37	90.23	38.57
28.40	100.00	95.25	15.97	40.90	85.24	87.23	36.89
28.60	77.50	85.93	71.87	41.10	82.56	84.89	40.84
28.80	68.32	63.06	99.97	41.60	82.93	87.88	38.81
29.10	63.62	100.00	121.30	41.80	79.22	83.98	41.58
29.30	58.29	100.00	127.90	42.00	79.91	85.89	40.12
29.50	56.15	100.00	126.10	42.20	82.82	81.43	37.98
29.70	55.41	100.00	114.40	42.40	81.60	84.41	40.57
29.90	59.75	61.48	130.90	42.60	78.13	83.76	42.99
30.10	68.55	100.00	104.90	42.80	79.00	81.69	43.15
30.30	73.59	72.20	70.35	43.10	72.80	79.39	48.80
30.60	79.98	80.86	57.69	43.30	76.22	79.63	45.00
30.80	79.11	80.50	61.56	43.50	68.28	77.68	55.28
31.00	79.36	78.69	69.10	43.70	76.96	81.17	42.82
31.20	81.55	83.38	62.43	43.90	71.51	74.48	51.59
31.40	89.91	87.94	30.74	44.10	75.09	80.03	46.89
31.60	83.76	83.68	47.56	44.30	77.88	81.39	43.30
31.80	79.80	86.35	52.78	44.60	76.36	79.82	45.20
32.10	83.15	87.82	45.73	44.80	78.99	84.17	42.78
32.30	88.94	90.15	38.62	45.00	81.29	85.63	38.81
32.50	84.33	86.83	38.27	45.20	84.94	85.41	34.12
32.70	85.40	85.06	38.24	45.40	81.74	85.75	39.03
32.90	81.22	80.65	37.77	45.60	84.04	88.38	35.91
33.10	93.38	94.49	24.07	45.80	79.44	87.47	40.98
33.30	88.44	91.40	30.22	46.10	80.48	89.19	40.07
33.60	78.33	83.88	42.81	46.30	83.67	87.49	37.63
33.80	78.93	83.12	46.00	46.50	78.62	80.02	43.13
34.00	77.05	80.25	53.32	46.60	81.16	81.87	41.13
34.20	71.91	81.14	51.37	46.70	84.75	87.51	36.65
34.40	73.34	82.15	49.01	46.80	86.50	91.22	36.30
34.60	75.02	82.14	49.12	47.00	87.96	91.05	31.49
34.80	90.14	90.53	24.94	47.20	81.48	88.87	39.51
35.10	82.71	85.37	37.33	47.40	81.47	89.43	39.84

47.60	87.51	89.35	31.72	61.00	84.22	91.03	37.73
47.80	89.09	91.57	29.35	61.20	86.89	89.95	30.68
48.10	91.2	92.57	27.65	61.40	84.68	92.17	36.79
48.30	88.14	92.09	32.60	61.60	88.82	91.36	29.66
48.50	77.26	87.76	43.86	61.80	88.84	92.90	28.63
48.70	87.09	90.79	31.78	62.10	87.79	88.07	30.69
48.90	85.63	91.80	34.18	62.30	87.32	92.86	31.18
49.10	90.00	91.67	27.44	62.50	78.11	88.50	45.09
49.30	90.96	92.38	28.63	62.70	90.88	94.97	29.77
49.60	86.31	92.53	33.28	62.90	85.07	91.89	37.33
49.80	84.18	91.00	36.45	63.10	89.03	91.17	28.92
50.00	84.46	89.87	34.67	63.60	88.38	91.30	28.83
50.20	82.06	89.04	38.13	63.80	90.70	93.29	30.29
50.40	85.86	88.85	35.40	64.00	82.87	89.66	34.47
50.60	83.75	87.17	36.27	64.20	87.29	93.08	30.83
50.80	83.37	87.93	36.58	64.40	90.23	92.79	29.89
51.10	85.61	88.93	34.55	64.60	91.74	94.00	26.83
51.30	85.02	88.48	35.44	64.80	87.76	93.94	33.34
51.50	85.48	90.72	35.60	65.10	89.16	90.68	33.55
51.70	85.93	88.46	33.66	65.30	86.19	90.47	34.56
51.90	86.10	89.11	33.48	65.50	83.94	86.82	37.89
52.10	87.04	88.20	33.15	65.60	74.93	87.00	43.87
52.30	79.92	85.67	41.15	65.70	69.34	77.26	61.12
52.60	81.26	87.91	34.55	65.80	64.80	77.34	58.53
52.80	84.63	87.36	37.24	66.00	79.06	84.90	38.06
53.40	80.2	87.08	40.24	66.22	67.64	83.28	51.73
53.60	84.78	87.28	36.50	66.42	72.47	81.78	47.53
53.80	81.57	85.74	39.72	66.62	77.30	87.21	40.62
54.10	84.97	87.96	36.72	66.82	84.89	86.06	37.71
54.30	82.90	86.40	39.76	67.02	81.17	88.90	36.85
54.50	82.74	86.31	39.50	67.22	83.46	87.44	33.31
54.70	85.86	87.35	35.96	67.42	79.89	87.82	36.78
54.90	82.93	84.51	38.55	67.72	73.86	89.12	42.96
55.10	82.91	85.86	38.91	67.92	65.91	80.87	52.05
55.30	81.60	87.73	39.39	68.12	77.53	86.84	40.30
56.10	86.95	85.05	33.81	68.32	73.23	85.77	44.13
56.30	84.18	86.68	36.72	68.52	74.50	83.31	43.17
56.50	76.71	82.00	45.27	68.72	70.60	83.70	53.48
56.70	78.11	86.15	38.71	68.92	75.60	85.40	47.05
56.90	83.04	92.08	35.26	69.22	70.25	87.88	47.16
57.10	81.23	88.50	35.39	69.42	67.58	79.77	56.68
57.30	82.84	90.35	35.20	69.62	68.49	77.39	48.39
57.60	80.49	89.24	39.05	69.82	72.23	85.59	51.43
57.80	88.66	91.00	29.75	70.02	55.61	75.50	63.20
58.00	80.79	89.10	36.46	70.22	68.48	83.17	55.13
58.20	81.04	89.76	37.24	70.42	81.21	88.57	36.41
58.40	86.24	88.92	32.10	70.72	84.67	86.51	33.04
58.60	80.11	88.42	37.80	70.92	66.44	85.89	49.92
58.80	76.85	81.70	40.80	71.12	78.95	88.69	43.29
59.10	86.77	90.53	31.20	71.32	82.63	91.27	38.39
59.30	81.44	85.69	36.70	71.52	85.07	92.00	32.51
59.50	84.15	88.49	33.06	71.72	84.65	91.84	32.14
59.70	84.99	87.23	35.62	71.92	88.93	91.43	29.99
59.90	85.89	87.77	33.69	72.22	81.84	91.90	39.21
60.10	83.45	89.28	34.45	72.42	82.32	92.86	38.73
60.30	88.42	88.96	30.09	72.62	83.65	87.73	36.85
60.60	85.34	90.80	35.75	72.82	86.85	90.93	33.04
60.80	86.13	92.16	32.78	73.02	76.80	91.90	45.02

73.22	77.76	86.60	33.37	86.00	72.70	82.08	43.28
73.72	90.00	89.33	26.19	86.20	88.46	91.85	29.12
73.92	85.77	91.33	29.79	86.50	90.33	91.42	27.77
74.12	88.66	91.35	27.60	86.70	75.45	87.29	41.05
74.92	84.25	93.28	30.75	86.90	86.85	89.82	31.08
75.10	79.63	87.16	36.60	87.10	76.95	87.59	40.22
75.30	87.68	92.21	27.38	87.30	75.85	88.73	40.97
75.45	94.59	94.72	22.29	87.50	86.41	90.35	30.87
75.65	90.29	94.25	24.87	87.70	81.84	90.26	35.80
75.85	92.03	92.87	24.51	88.00	83.58	90.29	34.40
76.05	92.55	94.04	23.47	88.20	86.11	91.98	32.00
76.25	87.31	90.14	27.54	88.40	86.36	91.67	32.61
76.45	90.48	93.02	25.25	88.60	89.65	93.72	28.83
76.65	89.92	92.00	25.12	88.80	90.67	90.56	29.88
76.95	89.53	92.86	26.52	89.00	91.45	92.30	28.49
77.15	89.56	93.16	25.86	89.20	85.25	95.21	29.78
77.35	81.25	91.66	34.06	89.50	66.29	90.42	50.74
77.55	87.73	92.78	27.72	89.70	92.80	95.28	26.55
77.75	86.59	90.62	30.60	89.90	86.24	92.96	32.81
77.95	85.38	91.34	29.76	90.10	92.98	95.99	26.06
78.15	85.26	90.43	30.72	90.30	91.06	93.50	27.38
78.45	88.91	90.94	27.10	90.50	89.76	95.01	28.89
78.65	75.37	90.00	41.24	91.00	87.06	92.91	31.26
78.85	85.48	91.04	31.21	91.20	83.43	90.37	34.61
79.05	82.91	92.94	33.24	91.40	82.68	94.14	35.17
79.25	77.28	89.14	38.04	91.60	87.21	92.16	28.72
79.45	85.95	91.70	28.92	91.80	69.95	79.77	47.72
79.65	90.71	94.55	25.80	92.00	84.12	90.57	32.76
79.95	82.43	88.44	33.60	92.20	89.16	93.03	27.09
80.15	80.58	89.75	38.39	92.50	86.6	92.57	31.63
80.35	86.13	88.32	30.42	92.70	88.62	93.48	27.14
80.55	82.52	89.28	34.05	92.90	91.12	94.94	26.17
80.75	82.50	87.45	34.68	93.10	88.07	91.49	28.23
80.95	82.73	88.81	34.96	93.30	88.71	90.57	27.74
81.15	89.32	89.02	27.17	93.50	85.83	93.21	30.43
81.45	88.31	90.59	27.72	93.70	87.69	92.74	29.01
81.65	85.79	90.36	31.97	94.00	86.45	93.39	28.92
81.85	89.81	90.45	27.14	94.10	91.28	93.14	24.97
82.05	89.42	89.30	26.91	94.20	81.18	93.58	34.13
82.25	91.06	91.79	25.84	94.40	84.70	87.41	31.18
82.45	90.94	91.72	25.31	94.42	87.62	93.60	28.00
82.65	80.10	90.54	38.09	94.60	89.95	91.18	25.28
82.95	85.92	90.42	31.81	94.62	79.65	89.18	36.16
83.15	86.52	92.37	31.30	94.82	79.99	92.63	36.22
83.35	88.06	86.13	28.19	95.02	88.95	93.86	25.85
83.55	92.64	90.06	27.27	95.22	85.41	91.87	29.91
83.75	90.27	92.03	26.45	95.42	85.94	90.22	29.55
83.95	85.05	89.62	32.11	95.62	83.85	91.23	31.55
84.15	81.81	89.79	35.66	95.92	87.08	92.31	28.15
84.45	85.71	89.29	30.90	96.12	88.83	92.35	27.04
84.60	79.45	86.22	39.34	96.32	84.17	91.89	31.05
84.65	82.12	89.41	35.46	96.52	80.74	88.01	35.62
84.80	90.23	92.09	25.86	96.72	85.83	90.62	30.36
84.85	91.37	91.37	24.75	96.92	84.16	90.15	29.12
85.00	91.61	93.36	25.69	97.42	90.37	91.89	25.13
85.05	88.72	90.86	30.73	97.62	85.65	91.10	29.89
85.60	89.26	91.81	26.92	97.82	85.45	90.35	30.50
85.80	84.14	88.25	32.56	98.02	87.89	92.03	27.50

98.22	84.70	90.31	30.89
98.42	85.92	90.62	30.57
98.62	84.50	88.43	33.60
98.92	87.90	90.83	29.37
99.12	91.90	93.11	24.20
99.32	89.18	87.32	26.90
99.52	83.75	89.20	32.67
99.72	90.70	92.78	25.20
99.92	87.44	89.57	29.15
100.12	86.16	89.10	30.32
100.42	85.25	86.12	31.24
100.62	87.57	87.96	30.04
100.82	89.55	89.20	27.27
101.02	85.17	89.34	31.60
101.22	86.19	89.59	30.51
101.42	86.31	87.03	30.40
101.62	85.78	87.78	31.75
101.92	89.74	91.17	28.21
102.12	88.13	85.29	29.16
102.32	84.45	88.31	32.78
102.52	88.65	90.71	28.28
102.72	82.36	87.31	34.29
102.92	81.96	88.32	35.26
103.12	82.44	89.06	34.98
103.42	82.02	85.91	39.14
103.62	86.07	89.24	31.92
104.02	82.06	85.71	35.16
104.00	77.73	86.31	39.45
104.20	81.44	85.60	35.67
105.10	74.95	84.72	42.38
105.30	74.39	84.83	43.61
105.50	76.78	84.51	40.25
105.70	79.94	82.25	37.23
105.90	72.28	80.16	45.01
106.10	68.91	73.12	47.56
106.30	72.49	78.72	44.44
106.60	73.98	82.13	42.50
106.80	77.28	82.55	40.04
107.00	75.90	80.21	41.14
107.20	64.17	73.47	53.87
107.33	66.18	69.36	54.06
107.60	73.97	76.67	43.39
108.10	77.40	81.77	41.59
108.30	66.67	34.88	56.72
108.50	82.49	79.50	33.07
108.70	84.11	58.78	31.28
108.90	79.36	80.37	36.43
109.10	76.55	73.32	44.33
109.30	79.19	82.58	36.73
109.60	75.63	84.15	40.62
109.80	77.82	82.04	38.63
110.00	83.30	19.33	32.97
110.20	75.89	79.01	41.11
110.40	78.15	79.84	37.94
110.60	73.05	80.52	45.87
110.78	71.50	81.40	46.64
111.10	85.99	86.66	30.70
111.30	87.29	89.58	30.45
111.55	91.42	85.57	27.40
111.68	89.28	89.88	29.39
111.88	87.67	88.04	30.54
112.08	88.32	76.54	29.99
112.28	93.75	89.83	24.11
112.46	85.16	90.34	32.44
112.68	90.97	91.92	27.03
112.88	91.22	85.81	25.92
113.13	88.64	83.91	8.74
113.38	91.46	89.10	26.90
113.58	90.50	88.82	26.07
113.78	88.18	86.68	29.63
113.96	87.92	89.30	29.38
114.18	90.40	86.14	27.37
114.38	85.31	88.22	32.27
114.68	82.39	87.45	35.45
114.88	88.45	88.55	29.26
115.08	87.40	86.69	30.59
115.28	79.45	83.08	41.47
115.46	90.96	91.62	26.08
115.68	91.68	90.49	26.11
115.88	88.58	89.40	30.69
116.18	89.82	90.03	27.13
116.38	92.33	88.77	24.56
116.58	89.60	88.63	27.57
116.78	80.97	89.96	39.38
116.96	87.56	89.22	29.76
117.18	83.40	90.65	35.70
117.68	83.83	88.49	35.70
117.88	84.89	87.23	32.63
118.08	79.84	85.66	37.90
118.28	74.39	81.87	43.14
118.46	73.59	83.02	44.97
118.68	72.61	78.39	44.71
118.88	77.64	77.37	40.64
119.18	69.50	76.16	48.27
119.38	67.25	78.53	49.00
119.58	72.05	76.49	46.39
119.78	74.34	78.93	43.58
119.96	70.31	80.02	46.06
120.18	73.73	80.76	43.16

Table B.2. Particle size distribution for samples collected from Hole 823A

Depth (mbsf)	% Fine Fraction (< 63 μm)	Depth (mbsf)	% Fine Fraction (< 63 μm)	Depth (mbsf)	% Fine Fraction (< 63 μm)
0.11	86.60	14.64	84.80	39.66	85.50
0.35	90.90	15.15	93.80	40.15	94.70
0.60	94.10	15.40	94.60	40.90	93.90
0.85	91.80	15.65	92.80	41.16	94.40
1.10	93.40	15.90	96.40	41.40	96.80
1.35	94.00	16.15	94.00	41.65	91.60
1.62	93.90	24.90	93.60	41.90	91.50
1.85	88.00	25.15	92.70	42.14	91.00
2.10	89.60	25.65	91.80	42.40	98.60
2.35	87.10	25.90	95.00	43.17	90.40
2.60	86.70	26.15	92.60	43.40	91.20
2.85	89.40	26.40	92.30	43.64	88.90
3.13	87.20	26.65	93.60	43.90	88.70
3.35	90.10	26.90	93.10	43.90	88.70
3.60	89.90	27.15	94.80	44.15	81.50
3.85	91.20	27.40	95.40	44.40	87.50
4.10	94.20	27.65	89.30	44.65	92.20
4.35	92.00	27.90	90.20	44.90	85.50
4.61	91.40	28.15	95.00	45.15	87.60
4.85	93.60	28.40	91.80	45.40	95.30
5.10	95.30	28.65	95.10	45.65	91.50
5.35	93.40	28.90	95.20	45.90	96.60
5.60	93.30	29.15	93.30	46.15	93.10
5.89	89.80	29.40	92.70	46.40	86.50
6.15	93.40	29.65	93.70	46.65	91.70
6.40	89.90	29.90	91.00	47.15	94.30
6.65	88.80	30.15	91.80	47.40	94.20
6.90	92.90	30.40	81.30	47.65	94.20
7.15	93.40	30.65	91.60	47.90	98.80
7.39	93.80	30.90	87.40	53.65	96.00
7.65	90.90	31.15	78.10	53.90	95.70
7.90	88.20	31.40	84.50	54.15	95.10
8.15	85.50	31.65	93.00	54.40	89.90
8.40	91.20	32.15	92.80	54.65	95.20
8.65	96.80	32.40	95.00	54.90	88.70
8.92	87.90	32.65	93.40	55.15	89.40
9.90	95.10	33.15	92.30	55.40	88.20
10.15	90.40	33.40	92.60	55.65	91.00
10.39	90.30	33.65	52.80	55.90	87.20
10.65	94.90	33.90	94.80	56.15	82.80
10.90	93.50	34.15	83.90	56.40	83.50
11.15	93.50	34.40	92.10	56.65	89.90
11.40	91.80	34.6	92.60	56.90	95.40
11.65	92.50	34.90	89.00	57.15	92.90
11.89	91.70	35.16	80.00	57.40	95.00
12.15	94.40	35.65	90.70	58.15	91.90
12.40	93.30	35.90	92.50	58.65	63.00
12.65	94.40	36.40	89.50	58.90	75.90
12.90	94.80	36.89	96.50	59.15	91.90
13.15	91.20	37.15	94.20	59.40	89.10
13.39	94.00	37.40	92.10	59.65	88.60
13.65	87.80	37.64	94.00	60.40	92.00
13.90	92.70	38.65	98.50	60.65	90.30
14.15	88.40	39.14	85.60	60.90	91.80
14.40	89.30	39.40	88.30	61.15	91.40

61.40	92.60	77.65	77.70	94.65	20.40
61.65	91.70	77.90	76.10	95.40	93.00
61.90	93.90	78.39	95.00	95.65	88.30
62.15	93.00	78.65	92.40	95.90	89.90
62.40	90.90	78.90	91.60	96.15	94.80
62.65	89.00	79.15	87.50	96.44	91.00
62.90	94.50	79.40	88.90	96.65	91.60
63.15	91.60	79.65	92.70	96.90	92.20
63.40	90.50	79.90	92.50	97.15	90.00
63.65	86.10	80.15	87.70	97.40	91.30
63.90	92.70	80.40	91.60	97.65	89.60
64.15	29.70	80.65	84.80	97.94	85.50
64.40	91.90	80.90	91.10	98.15	94.50
64.65	88.90	81.15	93.20	98.40	93.30
64.90	91.00	81.40	89.20	98.65	94.00
65.15	94.50	81.65	83.50	98.90	91.40
65.40	92.00	81.89	90.60	99.15	74.60
65.65	86.30	82.65	84.50	99.44	87.40
65.90	88.90	82.90	88.20	99.65	88.30
66.15	85.30	83.15	83.90	99.90	86.30
66.90	86.90	83.39	83.90	100.15	90.90
67.40	84.40	83.90	88.90	100.40	93.00
67.90	82.20	84.15	88.40	100.65	95.40
68.15	92.00	84.40	85.20	100.90	93.20
68.40	90.80	84.65	91.30	101.16	97.20
68.65	92.20	84.90	85.60	101.41	91.80
68.90	91.80	85.15	69.60	101.91	89.90
69.15	94.50	85.39	96.00	102.16	92.10
69.40	94.30	85.65	90.30	102.40	93.80
69.65	96.10	85.90	83.30	102.66	90.20
69.90	92.00	86.15	90.50	102.91	88.40
70.15	93.80	86.39	89.90	103.41	86.00
70.40	94.10	86.65	77.50	103.66	82.20
70.65	92.90	86.90	97.00	103.90	85.80
70.90	91.80	87.40	77.30	104.16	87.80
71.15	93.10	87.65	83.70	105.16	89.60
71.40	92.00	87.90	75.50	105.88	84.00
71.65	91.10	88.15	89.60	108.16	72.90
71.90	93.20	88.40	47.10	108.88	87.00
72.15	91.80	88.65	73.40	108.91	95.10
72.40	89.00	88.90	89.40	109.41	86.20
72.90	92.90	89.15	86.50	109.66	84.70
73.15	89.60	89.40	89.80	110.40	98.20
73.40	87.10	89.65	89.80	112.40	90.50
73.65	84.10	90.15	88.20	115.15	80.80
73.89	78.80	90.40	75.50	116.90	97.60
74.15	95.50	90.65	87.50	117.65	80.20
74.40	94.40	90.90	89.60	117.90	99.50
74.65	94.80	91.15	88.90	118.15	86.80
74.90	94.00	91.40	80.30	118.40	95.60
75.15	93.00	91.40	85.80	118.90	98.30
75.40	93.40	91.65	89.20	119.90	92.30
75.6	81.20	91.90	84.60		
75.90	76.80	92.15	90.60		
76.15	96.70	92.40	92.00		
76.40	89.80	92.65	93.70		
76.65	83.60	93.15	90.30		
76.89	84.70	93.44	87.90		
77.15	77.20	93.90	87.30		
77.40	77.00	94.40	91.20		

Table B.3. Grain size distribution data and characteristics for Hole 819A sediments generated using the Coulter LS-100 particle size analyser

Depth (mbsf)	% Clay (<3.91μm)	% Silt (3.91-63μm)	% VF.Sand (63-125μm)	% F.Sand (125-250μm)	% M.Sand (250-500μm)	% C.Sand (>500μm)	Mean (μm)	Median (μm)	Mode (μm)
0.16	8.49	72.13	14.71	3.47	0.00	1.20	37.78	29.06	39.48
0.30	8.82	72.62	10.31	5.00	2.97	0.31	48.99	24.22	27.26
0.54	13.58	68.01	11.21	4.49	2.44	0.27	47.07	27.84	27.26
0.70	13.53	70.96	10.44	2.01	2.05	1.01	40.47	25.18	27.26
0.90	13.54	69.73	12.30	2.68	1.23	0.52	42.13	28.70	27.26
1.20	15.77	72.24	9.25	1.13	1.50	0.11	36.47	24.57	27.26
1.60	5.98	74.00	16.14	3.68	0.00	0.20	39.50	29.52	39.48
1.80	16.17	79.57	4.26	0.00	0.00	0.00	25.71	21.56	27.26
2.04	15.25	73.01	9.35	1.00	1.22	0.17	35.69	24.88	27.26
2.18	16.52	75.31	5.89	0.91	1.23	0.14	32.45	22.89	27.26
2.20	15.08	73.51	9.72	0.95	0.65	0.09	33.86	24.44	27.26
2.40	14.80	72.21	10.33	1.17	1.34	0.15	38.21	26.17	27.26
2.70	15.44	73.14	9.76	1.15	0.39	0.12	35.89	26.87	57.24
3.10	14.71	68.61	13.75	2.38	0.45	0.10	40.03	29.39	57.24
3.30	15.60	71.51	11.19	1.29	0.34	0.07	35.10	25.91	57.24
3.54	20.29	76.59	3.12	0.00	0.00	0.00	22.77	16.43	27.26
3.70	20.27	70.48	6.74	1.79	0.41	0.31	29.69	18.22	27.26
3.95	21.85	74.06	3.51	0.16	0.30	0.12	22.61	13.95	27.26
4.20	20.23	73.92	5.85	0.00	0.00	0.00	24.89	17.59	27.26
4.60	21.57	70.91	6.78	0.23	0.42	0.09	25.78	14.61	27.26
4.80	22.06	70.02	7.05	0.40	0.36	0.11	25.88	13.97	27.26
5.04	24.00	68.78	4.41	2.28	0.36	0.17	26.57	13.49	27.26
5.20	20.20	64.20	8.20	4.51	1.78	1.10	38.34	16.54	25.10
5.40	14.22	64.21	12.28	5.51	2.48	1.30	50.32	29.31	48.54
5.70	11.76	57.80	15.72	6.55	6.08	2.09	69.26	37.28	57.24
6.10	9.03	75.04	13.99	1.94	0.00	0.00	32.73	21.30	39.48
6.30	7.41	53.46	18.52	8.92	8.59	3.10	88.96	48.84	62.16
6.70	7.71	43.88	21.52	11.07	11.56	4.30	113.10	64.30	62.16
6.90	7.79	50.47	20.42	9.02	9.69	2.61	96.85	56.34	62.16
7.20	7.31	50.39	21.35	10.77	8.74	1.40	97.77	57.94	62.16
7.60	10.13	53.12	17.25	9.09	8.10	2.31	82.09	46.48	62.16
7.80	8.18	56.06	18.51	9.84	5.70	1.70	77.52	49.40	62.16
8.04	13.04	65.70	14.58	3.67	2.91	0.10	52.00	31.46	57.24
8.18	13.65	67.02	12.44	4.61	2.15	0.13	47.82	28.61	57.24
8.62	13.36	65.01	12.81	4.26	3.46	1.10	53.63	31.39	57.24
8.80	14.02	70.61	10.49	2.90	1.91	0.07	43.25	28.47	52.72
9.04	12.28	71.80	10.63	4.22	0.96	0.11	42.81	29.48	52.72
9.20	14.49	70.90	10.80	1.96	1.85	0.00	41.05	26.79	27.26
9.38	15.84	74.28	5.44	3.36	1.08	0.00	35.71	23.50	27.26
9.59	6.34	81.05	10.74	1.87	0.00	0.00	31.94	23.36	39.48
9.82	13.75	75.67	8.30	1.72	0.56	0.00	32.08	20.14	27.26
10.12	15.64	70.59	9.74	2.67	1.36	0.00	38.64	24.55	27.26
10.30	7.87	81.83	9.61	0.69	0.00	0.00	28.38	20.16	31.97
10.54	16.85	73.81	7.16	1.23	0.95	0.00	32.37	21.61	27.26
10.70	16.42	70.81	8.78	3.20	0.77	0.00	35.97	22.87	27.26
10.88	15.38	68.81	11.03	4.18	0.60	0.00	39.20	24.64	27.26
11.09	16.23	73.74	8.21	0.91	0.82	0.09	32.59	22.46	27.26
11.32	16.30	74.33	7.20	0.94	1.16	0.07	32.95	22.10	27.26
11.80	15.75	64.83	11.62	4.38	1.32	2.10	41.39	23.87	27.26
12.04	16.89	72.70	8.64	0.55	0.24	0.90	30.30	21.90	27.26
12.20	16.00	82.11	1.89	0.00	0.00	0.00	25.46	21.79	52.72
12.38	16.78	68.60	9.62	2.30	1.77	0.93	38.53	22.94	27.26

12.59	16.00	70.11	10.99	1.81	1.09	0.00	37.17	24.12	27.26
12.82	16.84	72.18	9.84	0.47	0.69	0.00	33.11	23.76	27.26
13.12	14.47	61.59	12.47	7.36	2.90	1.21	54.00	29.50	57.24
13.30	12.61	52.74	14.14	8.57	8.93	3.01	80.88	36.01	57.24
13.54	11.31	46.35	13.56	10.24	13.52	5.02	102.3	47.71	57.24
13.70	13.31	50.87	13.46	12.07	6.18	4.11	81.05	43.81	57.24
13.88	15.41	53.50	13.04	9.12	7.33	1.80	73.55	33.20	57.24
14.09	16.61	60.64	12.51	6.17	3.19	0.88	51.53	26.60	57.24
14.34	14.13	55.32	14.18	6.44	6.93	3.00	68.46	33.79	57.24
14.62	14.51	60.13	12.07	5.83	5.16	2.30	60.38	29.15	57.24
14.80	6.80	76.91	9.78	3.41	2.10	1.00	44.20	26.56	27.26
15.04	13.14	60.38	14.22	7.85	3.71	0.70	59.43	32.35	57.24
15.20	12.20	52.62	10.03	7.56	13.28	4.21	102.30	35.67	57.24
15.38	12.90	64.25	12.84	4.76	4.23	1.02	57.24	31.48	57.24
15.59	13.00	71.05	10.01	3.34	2.60	0.00	44.48	26.04	27.26
15.82	12.19	66.13	12.01	6.03	2.86	0.77	52.09	27.89	27.26
16.12	5.74	73.95	10.44	3.54	4.33	2.00	57.77	30.74	29.60
16.30	11.01	71.12	12.82	3.51	1.52	0.02	45.47	30.83	57.24
16.54	9.30	63.37	16.19	6.65	3.39	1.10	59.80	34.78	57.24
16.70	10.06	62.86	13.95	7.73	4.41	0.99	64.04	34.41	29.60
16.88	10.49	64.20	12.44	6.65	4.19	2.03	58.91	29.47	27.26
17.09	8.23	51.93	13.01	8.40	16.42	4.01	123.90	47.03	57.24
17.32	12.66	65.01	10.40	6.23	4.62	1.80	58.04	26.67	27.26
17.57	10.86	61.36	13.12	8.08	5.76	0.82	70.03	31.59	57.24
17.77	12.77	65.70	12.39	4.32	3.62	1.20	52.97	28.76	27.26
18.04	12.98	63.11	13.69	6.99	3.23	0.00	56.48	30.53	27.26
18.10	14.93	66.30	11.97	4.78	2.02	0.00	46.83	27.90	27.26
18.30	17.63	69.78	7.77	2.18	1.64	1.00	35.54	20.89	27.26
18.52	17.48	69.50	9.70	2.40	0.92	0.00	34.53	20.50	27.26
18.70	16.81	70.67	9.00	2.16	1.36	0.00	35.95	22.30	27.26
18.90	17.20	64.99	11.86	5.14	0.81	0.00	40.78	23.10	27.26
19.09	12.43	62.80	13.43	5.89	5.49	0.98	64.10	32.74	27.26
19.31	13.59	64.14	11.42	6.08	3.67	1.10	54.22	27.47	27.26
19.60	11.27	60.75	13.23	6.68	5.77	2.30	65.87	31.58	27.26
19.80	9.32	46.15	13.35	10.25	16.92	4.01	129.30	52.05	57.24
20.02	11.15	60.43	12.06	6.16	8.49	1.71	77.20	34.92	29.60
20.20	6.59	75.76	10.76	4.02	2.87	0.00	51.03	27.09	27.26
20.40	11.04	64.45	13.68	7.60	3.21	0.00	57.03	29.64	27.26
20.59	13.45	67.53	11.37	4.77	2.88	0.00	50.24	28.26	27.26
20.81	13.76	66.47	12.57	5.63	1.57	0.00	46.16	27.27	27.26
21.10	16.73	68.41	8.93	4.28	1.65	0.00	40.48	23.42	27.26
21.30	20.71	70.41	5.58	2.42	0.88	0.00	28.50	12.60	25.10
21.52	12.09	80.24	5.01	2.03	0.63	0.00	28.35	15.63	25.10
21.70	18.76	71.45	6.25	2.81	0.53	0.00	31.61	20.45	27.26
21.90	20.97	71.87	4.96	2.01	0.19	0.00	27.09	17.37	27.26
22.09	21.65	71.10	4.47	1.93	0.85	0.00	27.95	15.40	25.10
22.31	25.85	73.85	0.27	0.01	0.02	0.00	17.26	11.64	25.10
22.60	7.63	38.57	26.60	16.91	8.26	2.03	107.10	71.10	73.31
22.80	24.17	68.78	4.41	2.28	0.36	0.00	26.44	13.96	25.10
23.02	28.74	68.85	0.90	1.24	0.27	0.00	18.94	9.948	25.01
23.20	28.70	67.45	1.05	2.32	0.48	0.00	21.73	10.08	25.10
23.40	21.14	68.60	6.33	3.53	0.50	0.00	32.51	19.47	27.26
23.59	28.44	69.78	0.31	1.00	0.47	0.00	19.34	10.23	25.10
23.81	18.08	65.70	9.97	4.79	1.46	0.00	42.00	25.21	48.54
24.10	18.03	57.44	10.20	7.61	5.12	1.60	57.93	25.40	27.26
24.30	14.37	53.14	9.90	8.24	11.27	3.10	85.47	28.37	27.26
24.52	13.92	48.03	9.00	8.23	18.63	4.11	128.80	36.37	57.24
24.70	9.10	75.61	7.50	2.85	4.05	0.08	45.76	18.11	25.10
24.87	12.33	60.41	12.27	5.07	7.12	2.80	67.81	28.19	57.24

25.09	9.88	61.84	10.72	5.14	10.40	3.02	80.88	26.70	57.24
25.57	4.30	54.25	17.00	7.16	14.49	2.80	112.60	50.86	57.24
25.76	5.17	41.93	15.55	11.54	22.78	3.03	150.50	68.19	62.16
26.02	9.39	48.31	15.56	8.37	16.26	2.11	120.00	51.12	62.16
26.17	11.03	60.03	14.11	5.46	9.37	0.00	78.98	34.64	57.24
26.40	7.88	64.71	11.03	5.61	8.97	1.80	79.62	29.49	57.24
26.59	5.01	49.43	11.02	9.77	21.67	3.10	148.5	53.75	41.40
26.81	6.95	50.12	11.91	9.81	19.11	2.11	135.9	52.43	57.24
27.10	7.48	44.51	13.76	10.83	22.43	0.99	147.4	61.54	57.24
27.80	7.59	71.15	11.80	4.40	4.36	0.70	59.01	30.56	29.60
28.00	7.07	75.90	10.44	3.16	3.43	0.00	49.75	27.42	29.60
28.20	28.68	71.30	0.02	0.00	0.00	0.00	16.57	10.68	25.10
28.40	28.62	71.38	0.00	0.00	0.00	0.00	15.97	10.11	25.10
28.60	19.59	56.92	7.53	5.16	9.81	0.99	71.87	20.58	27.26
28.80	5.05	61.27	12.03	5.78	12.67	3.20	99.97	38.67	57.24
29.10	5.09	58.53	11.75	6.95	17.57	0.11	121.30	44.31	57.24
29.30	5.60	51.69	13.71	9.02	17.98	2.00	127.90	53.11	57.24
29.50	7.78	48.37	17.26	9.07	16.21	1.31	126.10	57.76	62.16
29.70	6.88	46.53	24.07	6.28	13.44	2.80	114.40	60.74	62.16
29.90	8.28	51.37	12.65	6.59	18.01	3.10	130.90	48.06	57.24
30.10	11.53	55.22	9.81	6.47	15.17	1.90	104.90	28.23	25.10
30.30	16.22	57.33	11.42	5.30	9.29	0.44	70.35	29.66	57.24
30.60	6.81	73.17	12.48	2.39	5.15	0.00	57.69	29.50	27.26
30.80	13.17	65.44	9.23	4.81	6.80	0.55	61.56	22.99	25.10
31.00	7.06	71.00	9.12	3.02	8.10	1.70	69.10	27.91	27.26
31.20	12.34	67.21	6.37	4.02	7.96	2.10	62.43	20.17	25.10
31.40	13.01	76.90	8.81	0.46	0.82	0.00	30.74	18.88	27.26
31.60	17.76	65.01	8.17	3.28	4.79	0.99	47.56	20.76	27.26
31.80	15.33	63.47	12.29	3.55	4.06	1.10	52.78	28.21	57.24
32.10	9.24	73.91	11.28	2.74	2.83	0.00	45.73	24.44	27.26
32.30	12.71	76.23	6.80	2.16	2.10	0.00	38.62	22.83	27.26
32.50	6.38	77.95	13.62	1.88	0.17	0.00	38.27	28.36	29.60
32.70	9.53	75.87	10.86	2.53	1.21	0.00	38.24	22.75	27.26
32.90	15.39	65.83	17.23	0.99	0.56	0.00	37.77	24.81	62.16
33.10	15.47	77.91	6.62	0.00	0.00	0.00	24.07	14.80	25.10
33.30	21.20	67.24	9.20	1.75	0.71	0.00	30.22	13.93	25.10
33.60	9.79	68.54	16.89	4.57	0.21	0.00	42.81	26.75	57.24
33.80	9.39	69.54	14.80	4.92	1.35	0.00	46.00	25.67	57.24
34.00	6.34	70.71	16.41	4.38	2.19	0.00	53.32	30.70	57.24
34.20	10.53	61.38	21.42	6.15	0.52	0.00	51.37	36.55	62.16
34.40	9.91	63.43	21.54	4.82	0.30	0.00	49.01	36.19	62.16
34.60	10.93	64.09	19.11	5.01	0.86	0.00	49.12	34.49	57.24
34.80	11.28	78.86	9.82	0.04	0.00	0.00	24.94	14.81	12.36
35.10	14.25	68.46	14.26	2.99	0.04	0.00	37.33	24.25	57.24
35.30	13.01	75.20	10.39	1.29	0.11	0.00	31.39	20.51	57.24
35.50	13.29	69.50	13.70	3.37	0.14	0.00	38.46	25.47	57.24
35.70	16.71	67.86	12.50	2.90	0.03	0.00	35.40	22.82	57.24
35.90	16.94	66.02	14.06	2.83	0.15	0.00	37.51	25.48	57.24
36.10	13.82	70.69	12.95	2.29	0.25	0.00	36.18	24.13	57.24
36.30	15.38	68.25	13.73	2.44	0.20	0.00	37.16	25.77	57.24
36.60	9.26	77.13	13.31	0.30	0.00	0.00	29.87	20.13	39.48
36.80	9.67	58.33	24.47	7.40	0.13	0.00	56.15	46.80	62.16
37.00	14.45	64.10	17.14	4.27	0.04	0.00	42.44	29.17	57.24
37.20	13.85	64.89	17.19	3.99	0.08	0.00	41.88	28.20	57.24
37.10	9.82	75.61	12.68	1.89	0.00	0.00	36.86	28.33	48.54
37.30	10.10	74.43	12.86	2.60	0.01	0.00	36.95	25.93	27.26
37.50	10.48	71.75	14.12	3.59	0.06	0.00	39.31	26.25	27.26
37.70	4.57	71.20	22.28	1.95	0.00	0.00	41.91	34.43	54.19
37.90	15.07	61.84	18.22	4.84	0.05	0.00	44.30	30.85	57.24

38.10	14.66	65.20	15.58	4.47	0.09	0.00	41.61	27.99	57.24
38.30	12.27	71.07	13.37	3.18	0.11	0.00	37.25	23.96	27.26
38.60	11.45	69.86	10.85	4.42	3.42	0.00	48.70	21.61	14.10
38.80	13.93	70.02	12.50	3.40	0.15	0.00	36.19	21.19	57.24
39.00	1.47	72.20	10.48	4.02	1.83	0.00	41.69	21.44	11.95
39.20	15.78	72.00	9.92	2.18	0.12	0.00	31.10	17.50	25.10
39.40	7.75	79.51	10.18	2.54	0.02	0.00	33.91	22.38	27.26
39.60	7.10	69.41	17.63	5.01	0.85	0.00	47.30	29.95	57.24
39.80	11.21	72.48	11.22	3.68	1.41	0.00	39.86	20.06	11.95
40.10	6.89	82.59	9.03	1.13	0.36	0.00	30.63	18.14	14.10
40.30	7.15	79.17	10.07	3.28	0.33	0.00	35.15	19.65	14.10
40.50	15.61	71.89	10.50	1.82	0.18	0.00	32.00	19.77	27.26
40.70	15.54	66.83	14.39	3.13	0.11	0.00	38.57	26.55	57.24
40.90	7.79	77.45	12.81	1.95	0.00	0.00	36.89	27.36	29.60
41.10	9.03	73.53	14.57	2.81	0.06	0.00	38.68	26.57	27.26
41.30	8.67	72.12	15.95	3.26	0.02	0.00	40.84	28.56	57.24
41.60	8.85	74.08	14.29	2.77	0.01	0.00	38.81	27.51	27.26
41.80	11.36	67.86	16.74	4.01	0.03	0.00	41.58	27.38	57.24
42.00	14.78	65.13	15.57	4.34	0.18	0.00	40.12	23.62	57.24
42.20	10.43	72.39	13.43	3.68	0.05	0.00	37.98	24.10	27.26
42.40	8.56	73.04	14.69	3.70	0.01	0.00	40.57	28.07	29.60
42.60	11.29	66.84	16.80	5.01	0.06	0.00	42.99	27.21	57.24
42.80	7.36	71.64	16.87	4.13	0.00	0.00	43.15	29.92	27.26
43.10	11.90	60.90	21.99	5.18	0.03	0.00	48.80	36.75	62.16
43.30	10.11	66.11	18.95	4.79	0.04	0.00	45.00	30.32	62.16
43.50	10.52	57.76	24.68	6.81	0.23	0.00	55.28	44.53	62.16
43.70	12.68	64.28	20.54	2.50	0.00	0.00	42.82	32.71	62.16
43.90	5.96	65.55	22.04	6.38	0.07	0.00	51.59	37.04	62.16
44.10	8.25	66.84	19.62	5.24	0.05	0.00	46.89	31.98	57.24
44.30	9.66	68.22	18.93	3.19	0.00	0.00	43.30	31.83	57.24
44.60	7.66	68.70	20.31	3.33	0.00	0.00	45.20	34.02	57.24
44.80	9.66	69.33	17.00	3.98	0.03	0.00	42.78	29.59	57.24
45.00	11.51	69.78	15.98	2.73	0.00	0.00	38.81	26.58	57.24
45.20	14.89	70.05	12.92	2.14	0.00	0.00	34.12	22.19	27.26
45.40	9.60	72.14	16.29	1.97	0.00	0.00	39.03	28.67	57.24
45.60	10.48	73.56	13.97	1.99	0.00	0.00	35.91	24.66	27.26
45.80	15.35	64.09	17.25	3.28	0.03	0.00	40.98	28.78	57.24
46.10	15.58	64.90	16.62	2.90	0.00	0.00	40.07	29.08	57.24
46.30	9.06	74.61	13.40	2.92	0.01	0.00	37.63	25.72	27.26
46.50	8.73	69.89	16.95	4.42	0.01	0.00	43.13	29.13	57.24
46.70	7.48	73.68	16.13	2.71	0.00	0.00	41.13	30.47	57.24
46.60	8.78	75.97	13.04	2.21	0.00	0.00	36.65	26.15	27.26
46.80	6.86	79.64	11.83	1.67	0.00	0.00	36.30	27.88	29.60
47.00	11.07	76.89	10.62	1.28	0.14	0.00	31.49	20.55	25.10
47.20	16.18	65.00	15.35	3.01	0.16	0.00	39.51	27.84	57.24
47.40	16.58	64.89	15.02	3.24	0.27	0.00	39.84	27.42	57.24
47.60	10.72	76.79	11.20	1.29	0.00	0.00	31.72	21.10	27.26
47.80	16.15	72.94	10.90	0.01	0.00	0.00	29.35	21.08	57.24
48.10	11.42	79.78	8.22	0.57	0.01	0.00	27.65	18.17	25.10
48.30	9.20	78.94	10.93	0.93	0.00	0.00	32.60	24.18	27.26
48.50	14.15	63.11	18.81	3.92	0.01	0.00	43.86	32.01	57.24
48.70	11.48	75.61	11.62	1.29	0.00	0.00	31.78	20.88	25.10
48.90	17.36	68.27	12.80	1.32	0.25	0.00	34.18	23.93	57.24
49.10	7.73	82.27	9.87	0.13	0.00	0.00	27.44	19.07	39.48
49.30	9.70	81.26	8.62	0.42	0.00	0.00	28.63	20.38	25.10
49.60	18.90	67.41	12.32	1.05	0.32	0.00	33.28	23.17	57.24
49.80	18.86	65.32	13.18	2.20	0.44	0.00	36.45	24.79	57.24
50.00	21.89	62.57	13.84	1.29	0.41	0.00	34.67	23.87	57.24
50.20	20.26	61.80	15.38	2.02	0.54	0.00	38.13	26.58	57.24

50.40	11.64	74.22	12.45	1.53	0.16	0.00	35.40	25.83	57.24
50.60	16.36	67.39	13.26	2.71	0.28	0.00	36.27	23.17	57.24
50.80	16.84	66.53	13.27	3.00	0.36	0.00	36.58	22.12	57.24
51.10	12.84	72.77	12.04	2.34	0.01	0.00	34.55	23.37	27.26
51.30	13.00	72.02	12.75	2.13	0.10	0.00	35.44	24.50	27.26
51.50	16.67	68.81	11.69	2.75	0.08	0.00	35.60	25.10	52.72
51.70	16.25	69.68	13.22	0.85	0.00	0.00	33.66	25.66	57.24
51.90	14.00	72.10	12.77	1.11	0.02	0.00	33.48	24.29	27.26
52.10	13.05	73.99	11.95	0.99	0.02	0.00	33.15	24.84	27.26
52.30	13.12	66.80	16.43	3.34	0.31	0.00	41.15	27.51	57.24
52.60	14.57	66.69	18.57	0.17	0.00	0.00	34.55	29.23	39.48
52.80	9.12	71.55	16.38	2.87	0.08	0.00	42.01	31.48	57.24
53.00	10.29	74.42	13.49	1.76	0.04	0.00	37.26	28.22	57.24
53.20	10.67	73.96	12.98	2.32	0.07	0.00	37.24	27.04	29.60
53.40	16.86	63.34	17.70	1.98	0.12	0.00	40.24	30.89	57.24
53.60	15.70	69.08	12.78	2.00	0.44	0.00	36.50	25.61	27.26
53.80	13.73	67.84	15.03	3.02	0.38	0.00	39.72	26.55	57.24
54.10	15.25	69.72	12.07	2.43	0.53	0.00	36.72	24.56	27.26
54.30	9.76	73.14	14.75	2.04	0.31	0.00	39.76	29.41	57.24
54.50	11.58	71.16	14.13	2.87	0.26	0.00	39.50	27.93	57.24
54.70	11.82	74.04	12.11	1.82	0.21	0.00	35.96	26.17	29.60
54.90	14.23	68.70	14.06	2.57	0.44	0.00	38.55	26.24	57.24
55.10	13.30	69.61	13.93	2.86	0.30	0.00	38.91	27.01	57.24
55.30	17.02	64.58	14.96	3.31	0.13	0.00	39.39	27.60	57.24
56.10	18.28	68.67	11.32	1.36	0.37	0.00	33.81	24.30	52.72
56.30	13.83	70.35	13.68	2.08	0.06	0.00	36.72	26.60	57.24
56.50	11.58	65.13	18.69	4.42	0.18	0.00	45.27	31.70	62.16
56.70	9.77	68.34	19.69	2.19	0.00	0.00	38.71	30.40	43.88
56.90	12.07	70.97	14.45	2.51	0.00	0.00	35.26	27.22	39.48
57.10	12.76	68.47	17.88	0.89	0.00	0.00	35.39	28.85	43.88
57.30	8.76	74.08	16.10	1.06	0.00	0.00	35.20	28.41	39.48
57.60	5.29	75.20	17.77	1.74	0.00	0.00	39.05	32.95	43.88
57.80	9.60	79.06	11.34	0.00	0.00	0.00	29.75	23.98	39.48
58.00	10.09	70.70	18.59	0.62	0.00	0.00	36.46	30.82	43.88
58.20	8.02	73.02	16.92	2.04	0.00	0.00	37.24	29.61	39.48
58.40	12.46	73.78	13.76	0.00	0.00	0.00	32.19	28.83	43.88
58.60	11.04	69.07	18.12	1.77	0.00	0.00	37.48	30.93	43.88
58.80	10.85	66.00	21.53	1.62	0.00	0.00	40.18	34.46	43.88
59.10	10.02	76.75	12.82	0.41	0.00	0.00	31.20	24.29	39.48
59.30	6.42	75.02	17.81	0.75	0.00	0.00	36.70	30.45	43.88
59.50	12.61	71.54	15.69	0.16	0.00	0.00	33.06	27.62	39.48
59.70	15.58	69.41	14.74	0.27	0.00	0.00	35.62	29.39	57.24
59.90	6.93	78.96	12.52	1.59	0.00	0.00	33.69	26.36	39.48
60.10	8.91	74.54	16.34	0.21	0.00	0.00	34.45	29.08	39.48
60.30	7.83	80.59	11.58	0.00	0.00	0.00	30.09	24.13	39.48
60.60	16.43	68.91	12.38	2.23	0.05	0.00	35.75	26.09	57.24
60.80	5.95	80.18	13.69	0.18	0.00	0.00	32.78	26.73	39.48
61.00	12.85	71.37	12.82	2.75	0.21	0.00	37.73	26.44	57.24
61.20	11.15	75.74	12.99	0.12	0.00	0.00	30.68	24.15	39.48
61.40	13.94	70.74	13.02	2.30	0.00	0.00	36.79	27.21	57.24
61.60	13.04	75.78	11.18	0.00	0.00	0.00	29.66	25.04	39.48
61.80	13.26	75.58	11.16	0.00	0.00	0.00	28.63	22.13	39.48
62.10	7.61	80.18	12.04	0.17	0.00	0.00	30.69	24.05	39.48
62.30	14.76	72.56	12.61	0.07	0.00	0.00	31.18	27.05	39.48
62.50	13.85	64.26	17.46	4.28	0.15	0.00	45.09	33.85	57.24
62.70	16.39	74.49	8.09	0.98	0.05	0.00	29.77	22.32	27.26
62.90	15.85	69.22	12.40	2.43	0.10	0.00	37.33	28.23	52.72
63.10	8.72	80.31	10.97	0.00	0.00	0.00	28.92	22.12	39.48
63.60	9.12	79.26	11.52	0.10	0.00	0.00	28.83	20.56	39.48

63.80	9.06	81.64	9.29	0.01	0.00	0.00	30.29	23.99	27.26
64.00	9.10	73.77	16.75	0.38	0.00	0.00	34.47	28.51	43.88
64.20	10.15	77.14	12.52	0.19	0.00	0.00	30.83	24.57	39.48
64.40	18.27	71.96	9.77	0.00	0.00	0.00	29.89	24.97	52.72
64.60	13.83	77.91	8.26	0.00	0.00	0.00	26.83	21.09	39.48
64.80	15.94	71.82	9.34	2.59	0.31	0.00	33.34	21.55	27.26
65.10	18.44	70.72	8.43	1.78	0.63	0.00	33.55	23.88	48.54
65.30	18.35	67.84	12.08	0.98	0.77	0.00	34.56	23.48	57.24
65.50	16.72	67.22	11.62	3.80	0.64	0.00	37.89	22.51	57.24
65.70	12.64	62.29	18.05	7.02	0.00	0.00	43.87	31.49	43.88
65.60	9.71	59.63	20.96	6.93	2.77	0.00	61.12	38.63	62.16
65.80	6.44	58.36	22.96	11.19	1.05	0.00	58.53	41.76	66.94
66.00	10.01	69.05	17.94	3.00	0.00	0.00	38.06	28.33	43.88
66.22	8.10	59.54	25.17	7.19	0.00	0.00	51.73	43.14	54.19
66.42	10.00	62.47	20.25	7.28	0.00	0.00	47.53	36.99	43.88
66.62	10.50	66.80	19.74	2.96	0.00	0.00	40.62	33.11	43.88
66.82	9.15	75.74	12.24	2.35	0.52	0.00	37.71	25.61	27.26
67.02	12.04	69.13	16.69	2.14	0.00	0.00	36.85	29.84	39.48
67.22	8.14	75.32	15.15	1.39	0.00	0.00	33.31	22.98	39.48
67.42	13.11	66.78	18.14	1.97	0.00	0.00	36.78	28.59	39.48
67.72	10.78	63.08	20.68	5.46	0.00	0.00	42.96	31.24	66.94
67.92	8.35	57.56	26.16	7.90	0.00	0.00	52.05	42.49	66.94
68.12	9.15	68.38	20.19	2.28	0.00	0.00	40.30	33.41	43.88
68.32	8.80	64.43	23.78	2.99	0.00	0.00	44.13	37.77	54.19
68.52	8.16	66.34	21.70	3.80	0.00	0.00	43.17	34.98	54.19
68.72	9.78	60.82	23.24	6.06	0.10	0.00	53.48	43.50	62.16
68.92	11.25	64.35	20.70	3.63	0.07	0.00	47.05	37.84	57.24
69.22	8.29	61.96	25.46	4.29	0.00	0.00	47.16	39.77	54.19
69.42	9.10	58.48	25.56	6.81	0.05	0.00	56.68	48.01	62.16
69.62	8.47	60.02	27.18	4.33	0.00	0.00	48.39	41.67	66.94
69.82	10.61	61.62	21.95	5.70	0.12	0.00	51.43	40.77	57.24
70.02	4.31	51.30	32.88	11.51	0.00	0.00	63.20	55.79	82.67
70.22	8.50	59.98	25.59	5.93	0.00	0.00	55.13	47.64	62.16
70.42	10.72	70.49	18.05	0.74	0.00	0.00	36.41	30.75	43.88
70.72	6.74	77.93	14.37	0.93	0.00	0.00	33.04	24.27	39.48
70.92	8.11	58.33	29.36	4.20	0.00	0.00	49.92	43.81	66.94
71.12	13.86	65.09	16.97	4.06	0.02	0.00	43.29	31.64	57.24
71.32	15.85	66.78	14.74	2.63	0.00	0.00	38.39	28.08	57.24
71.52	12.84	72.23,	14.71	0.22	0.00	0.00	32.51	26.59	39.48
71.72	14.31	70.34	14.78	0.57	0.00	0.00	32.14	24.61	39.48
71.92	19.15	69.78	11.01	0.06	0.00	0.00	29.99	23.05	27.26
72.22	16.60	65.24	15.27	2.84	0.05	0.00	39.21	28.42	57.24
72.42	15.91	66.41	14.88	2.80	0.00	0.00	38.73	28.33	57.24
72.62	16.44	67.21	13.55	2.79	0.01	0.00	36.85	25.64	57.24
72.82	17.13	69.72	11.66	1.49	0.00	0.00	33.04	24.06	57.24
73.02	14.05	62.75	19.28	3.90	0.02	0.00	45.02	34.57	57.24
73.22	16.24	61.52	17.56	4.61	0.04	0.00	43.44	30.34	57.24
73.42	19.03	67.30	11.64	2.03	0.00	0.00	33.37	23.27	57.24
73.72	12.92	77.08	9.95	0.05	0.00	0.00	26.19	17.38	39.48
73.92	11.91	73.86	13.42	0.81	0.00	0.00	29.79	18.53	39.48
74.12	19.33	67.57	12.94	0.16	0.00	0.00	27.78	17.58	39.48
74.32	13.61	69.69	16.43	0.27	0.00	0.00	32.12	23.29	43.88
74.52	11.48	66.91	21.27	0.34	0.00	0.00	36.39	28.99	66.94
74.72	10.28	78.38	11.34	0.00	0.00	0.00	27.60	18.52	39.48
74.92	12.10	72.15	15.22	0.53	0.00	0.00	30.75	19.36	39.48
75.10	7.49	72.14	18.31	2.06	0.00	0.00	36.60	25.40	39.48
75.30	13.86	73.82	12.22	0.10	0.00	0.00	27.38	16.77	39.48
75.45	11.62	82.97	5.41	0.00	0.00	0.00	22.29	14.72	12.36
75.65	12.29	78.00	9.60	0.11	0.00	0.00	24.87	14.96	12.36

75.85	14.77	77.26	7.97	0.00	0.00	0.00	24.51	16.32	39.48
76.05	13.71	78.84	7.45	0.00	0.00	0.00	23.47	15.13	39.48
76.25	14.92	72.39	12.38	0.31	0.00	0.00	27.54	16.57	39.48
76.45	12.89	77.59	9.52	0.00	0.00	0.00	25.25	16.00	39.48
76.65	15.98	73.94	10.04	0.04	0.00	0.00	25.12	15.13	39.48
76.95	11.20	78.31	10.45	0.02	0.00	0.00	26.52	17.25	39.48
77.15	12.29	77.27	10.35	0.09	0.00	0.00	25.86	15.89	39.48
77.35	14.87	66.38	18.05	0.70	0.00	0.00	34.06	25.53	39.48
77.55	13.61	74.12	12.08	0.19	0.00	0.00	27.72	17.34	39.48
77.75	8.51	78.08	13.22	0.19	0.00	0.00	30.60	22.39	39.48
77.95	12.35	73.03	14.41	0.21	0.00	0.00	29.76	19.10	39.48
78.15	9.04	76.22	14.52	0.22	0.00	0.00	30.72	20.99	39.48
78.45	12.06	76.85	11.09	0.00	0.00	0.00	27.10	17.99	39.48
78.65	10.96	64.41	21.41	3.22	0.00	0.00	41.24	32.55	54.19
78.85	12.86	72.62	14.46	0.06	0.00	0.00	31.21	24.39	39.48
79.05	13.15	69.76	16.37	0.72	0.00	0.00	33.24	24.87	39.48
79.25	12.48	64.80	20.93	1.79	0.00	0.00	38.04	29.11	54.19
79.45	12.43	73.52	13.09	0.96	0.00	0.00	28.92	16.32	39.48
79.65	16.95	73.76	9.29	0.00	0.00	0.00	25.80	17.93	39.48
79.95	10.31	72.12	15.85	1.72	0.00	0.00	33.60	22.35	39.48
80.15	6.44	74.14	16.85	2.57	0.00	0.00	38.39	30.14	39.48
80.35	10.06	76.07	13.76	0.11	0.00	0.00	30.42	22.13	39.48
80.55	11.19	71.33	16.90	0.58	0.00	0.00	34.05	26.69	39.48
80.75	8.62	73.88	16.18	1.32	0.00	0.00	34.68	25.94	39.48
80.95	7.65	75.08	16.34	0.93	0.00	0.00	34.96	27.41	39.48
81.15	12.50	76.82	10.35	0.33	0.00	0.00	27.17	17.85	39.48
81.45	14.54	73.77	11.55	0.14	0.00	0.00	27.72	18.67	39.48
81.65	9.58	76.21	13.34	0.87	0.00	0.00	31.97	24.02	39.48
81.85	14.07	75.74	10.15	0.04	0.00	0.00	27.14	19.47	39.48
82.05	14.73	74.69	10.55	0.03	0.00	0.00	26.91	18.61	39.48
82.25	14.20	76.86	8.94	0.00	0.00	0.00	25.84	18.17	39.48
82.45	15.32	75.62	9.06	0.00	0.00	0.00	25.31	16.81	39.48
82.65	7.72	72.38	18.85	1.05	0.00	0.00	38.09	32.16	43.88
83.95	9.42	76.50	13.90	0.18	0.00	0.00	31.81	25.24	39.48
83.15	10.67	75.85	12.96	0.52	0.00	0.00	31.30	24.20	39.48
83.35	16.04	72.02	10.96	0.98	0.00	0.00	28.19	18.07	39.48
83.55	13.15	79.49	7.38	0.00	0.00	0.00	27.27	22.95	39.48
83.75	13.69	76.58	9.73	0.00	0.00	0.00	26.45	18.46	39.48
83.95	10.53	74.52	13.88	1.07	0.00	0.00	32.11	23.22	39.48
84.15	9.07	72.74	16.80	1.39	0.00	0.00	35.66	27.77	39.48
84.45	13.96	71.75	13.79	0.50	0.00	0.00	30.90	23.01	39.48
84.60	6.32	73.13	18.07	2.48	0.00	0.00	39.34	31.97	43.88
84.65	13.05	69.07	13.72	4.16	0.00	0.00	35.46	22.67	39.48
84.80	14.35	75.88	9.76	0.01	0.00	0.00	25.86	16.85	39.48
84.85	14.92	76.45	8.52	0.11	0.00	0.00	24.75	15.66	39.48
85.00	11.30	80.31	8.39	0.00	0.00	0.00	25.69	18.10	39.48
85.05	10.10	78.62	11.18	0.10	0.00	0.00	29.56	23.17	39.48
85.20	14.95	72.56	12.10	0.39	0.00	0.00	28.97	20.18	39.48
85.40	12.82	72.95	13.82	0.44	0.00	0.00	30.73	22.48	39.48
85.60	14.64	74.62	10.65	0.09	0.00	0.00	26.92	18.18	39.48
85.80	15.16	68.98	15.55	0.31	0.00	0.00	32.56	26.45	39.48
86.00	8.02	64.68	24.05	3.25	0.00	0.00	3.28	34.65	66.94
86.20	15.16	73.30	11.49	0.05	0.00	0.00	29.12	23.18	39.48
86.50	15.58	74.75	9.67	0.00	0.00	0.00	27.77	22.47	39.48
86.70	7.79	67.66	23.20	1.35	0.00	0.00	41.05	35.09	54.19
86.90	11.65	75.20	13.15	0.00	0.00	0.00	31.08	25.73	39.48
87.10	8.19	68.76	20.36	2.69	0.00	0.00	40.22	31.96	43.88
87.30	8.62	67.23	23.15	1.00	0.00	0.00	40.97	36.33	54.19
87.50	9.32	74.26	16.33	0.09	0.00	0.00	34.40	29.89	43.88

88.20	11.43	74.68	13.87	0.02	0.00	0.00	32.00	27.16	39.48
88.40	10.57	75.79	13.64	0.00	0.00	0.00	32.61	29.28	43.88
88.60	12.91	76.74	10.35	0.00	0.00	0.00	28.83	23.79	39.48
88.80	10.91	79.76	9.33	0.00	0.00	0.00	29.88	26.77	48.77
89.00	11.10	80.35	8.55	0.00	0.00	0.00	28.49	24.34	43.88
89.20	21.78	63.47	14.55	0.20	0.00	0.00	29.78	21.67	39.48
89.50	4.85	61.44	30.60	2.81	0.00	0.00	50.74	47.19	66.94
89.70	12.79	80.01	7.20	0.00	0.00	0.00	26.55	21.50	39.48
89.90	10.62	75.62	13.76	0.00	0.00	0.00	32.81	29.47	43.88
90.10	13.16	79.82	7.02	0.00	0.00	0.00	26.06	20.47	39.48
90.30	13.45	7.61	8.94	0.00	0.00	0.00	27.38	21.70	39.48
90.50	11.95	77.81	10.23	0.00	0.00	0.00	28.89	23.67	39.48
91.00	11.61	75.45	12.60	0.34	0.00	0.00	31.26	25.26	39.48
91.20	10.93	72.50	15.99	0.58	0.00	0.00	34.61	28.91	39.48
91.40	11.15	71.53	16.23	1.09	0.00	0.00	35.17	28.57	39.48
91.60	11.47	75.74	12.79	0.00	0.00	0.00	28.72	19.84	39.48
91.80	11.07	78.09	10.72	0.12	0.00	0.00	27.09	17.60	39.48
92.50	10.40	76.20	13.40	0.00	0.00	0.00	31.63	26.42	39.48
92.70	12.21	76.41	11.25	0.13	0.00	0.00	27.14	16.80	39.48
92.90	13.90	77.22	8.88	0.00	0.00	0.00	26.17	18.84	39.48
93.10	13.59	74.48	11.83	0.10	0.00	0.00	28.23	19.53	39.48
93.30	8.99	79.72	10.82	0.47	0.00	0.00	27.74	17.65	39.48
93.50	14.89	70.94	13.09	1.08	0.00	0.00	30.43	20.40	39.48
93.70	15.45	72.24	11.97	0.34	0.00	0.00	29.01	20.85	39.48
94.00	11.31	75.14	12.31	1.24	0.00	0.00	28.92	16.26	39.48
94.20	15.27	76.01	8.72	0.00	0.00	0.00	24.97	16.04	39.48
94.40	15.61	65.57	17.40	1.42	0.00	0.00	34.13	24.18	39.48
94.60	10.14	74.56	13.30	2.00	0.00	0.00	31.18	18.17	39.48
94.10	16.16	71.46	12.04	0.34	0.00	0.00	28.00	18.08	39.48
94.42	14.14	75.81	9.97	0.08	0.00	0.00	25.28	14.90	39.48
94.62	12.34	67.31	19.07	1.28	0.00	0.00	36.16	27.96	43.88
94.82	12.77	67.22	18.75	1.26	0.00	0.00	36.22	28.63	39.48
95.02	14.32	74.63	10.97	0.08	0.00	0.00	25.85	14.61	39.48
95.22	14.86	70.55	14.37	0.22	0.00	0.00	29.91	20.17	39.48
95.42	11.91	74.03	13.20	0.86	0.00	0.00	29.55	17.64	39.48
95.62	12.19	74.89	12.48	0.44	0.00	0.00	28.15	16.47	39.48
96.12	9.98	78.85	10.96	0.21	0.00	0.00	27.04	16.69	39.48
96.32	11.86	72.31	14.39	1.44	0.00	0.00	31.05	18.00	39.48
96.52	9.78	70.96	16.66	2.60	0.00	0.00	35.62	24.12	39.48
96.72	9.05	76.78	13.58	0.59	0.00	0.00	30.36	19.74	39.48
96.92	12.67	71.49	15.12	0.72	0.00	0.00	31.50	21.31	39.48
97.12	12.14	73.89	13.36	0.61	0.00	0.00	29.12	17.32	39.48
97.42	10.76	79.61	9.49	0.14	0.00	0.00	25.13	14.84	10.01
97.62	13.54	72.11	13.87	0.48	0.00	0.00	29.89	19.43	39.48
97.82	13.46	71.99	14.32	0.23	0.00	0.00	30.50	21.79	39.48
98.02	11.94	75.95	11.49	0.62	0.00	0.00	27.50	15.95	39.48
98.22	12.73	71.97	14.17	1.13	0.00	0.00	30.89	19.26	39.48
98.42	12.39	73.53	13.95	0.13	0.00	0.00	30.57	22.87	39.48
98.62	7.32	77.18	13.53	1.97	0.00	0.00	33.60	24.04	39.48
98.92	8.52	79.38	11.59	0.51	0.00	0.00	29.37	20.40	39.48
99.12	12.45	79.45	8.08	0.02	0.00	0.00	24.20	15.06	39.48
99.32	10.97	78.21	10.65	0.17	0.00	0.00	26.90	17.11	39.48
99.52	12.74	71.01	15.58	0.67	0.00	0.00	32.67	24.53	39.48
99.72	13.33	77.37	9.23	0.07	0.00	0.00	25.20	15.83	39.48
99.92	10.88	76.56	12.43	0.13	0.00	0.00	29.15	20.59	39.48
100.12	9.63	76.53	13.25	0.59	0.00	0.00	30.32	20.58	39.48
100.42	12.43	72.82	14.57	0.18	0.00	0.00	31.24	23.64	39.48
100.62	11.55	76.02	12.39	0.04	0.00	0.00	30.04	23.70	39.48
100.82	10.28	79.27	10.03	0.42	0.00	0.00	27.27	18.22	31.97

101.02	9.54	75.63	13.09	1.74	0.00	0.00	31.60	20.54	39.48
101.22	10.40	75.79	13.19	0.62	0.00	0.00	30.51	21.25	39.48
101.42	11.87	74.44	12.67	1.02	0.00	0.00	30.40	20.79	39.48
101.62	11.78	74.00	14.16	0.06	0.00	0.00	31.75	25.98	39.48
101.92	15.52	74.22	10.26	0.00	0.00	0.00	28.21	23.00	39.48
102.12	9.88	78.25	11.04	0.83	0.00	0.00	29.16	20.01	39.48
102.32	12.91	71.54	14.48	1.07	0.00	0.00	32.78	25.05	39.48
102.52	11.35	77.30	10.68	0.67	0.00	0.00	28.28	19.09	39.48
102.72	10.72	71.64	16.84	0.80	0.00	0.00	34.29	26.43	39.48
102.92	11.78	70.18	16.12	1.92	0.00	0.00	35.26	26.60	39.48
103.12	13.62	68.82	16.10	1.46	0.00	0.00	34.98	27.90	39.48
103.42	12.31	69.71	16.60	1.38	0.00	0.00	35.32	28.07	39.48
103.60	7.12	71.75	17.55	3.58	0.00	0.00	39.14	28.56	39.48
103.62	12.81	73.26	13.81	0.12	0.00	0.00	30.44	22.81	39.48
103.80	10.91	66.00	20.94	2.15	0.00	0.00	39.63	32.17	54.19
103.82	14.56	70.22	15.12	0.10	0.00	0.00	31.92	25.90	39.48
104.02	11.36	70.70	17.60	0.34	0.00	0.00	35.16	29.60	39.48
104.00	10.26	67.47	21.24	1.03	0.00	0.00	39.45	34.17	54.19
104.20	11.65	69.79	18.35	0.21	0.00	0.00	35.67	30.88	43.88
105.10	9.17	65.78	22.46	2.59	0.00	0.00	42.38	35.81	54.19
105.30	7.69	66.70	22.98	2.63	0.00	0.00	43.61	37.27	54.19
105.50	8.51	68.27	22.29	0.97	0.00	0.00	40.25	34.75	54.19
105.70	8.30	71.64	19.20	0.86	0.00	0.00	37.23	30.55	48.77
105.90	8.03	64.25	24.74	2.98	0.00	0.00	45.01	38.52	54.19
106.10	9.38	59.53	27.24	3.85	0.00	0.00	47.56	41.10	66.94
106.30	9.35	63.14	22.77	4.74	0.00	0.00	44.44	34.36	66.94
106.60	9.58	64.4	22.87	3.15	0.00	0.00	42.50	34.01	54.19
106.80	8.27	69.01	20.08	2.64	0.00	0.00	40.04	31.31	39.48
107.00	9.58	66.32	22.25	1.85	0.00	0.00	41.10	34.55	54.19
107.20	7.03	57.14	26.61	9.22	0.00	0.00	53.87	42.65	74.39
107.33	3.79	62.39	25.10	8.72	0.00	0.00	54.06	42.84	54.19
107.60	7.15	66.82	21.73	4.63	0.00	0.00	43.39	33.05	54.19
108.10	4.83	72.57	20.52	2.08	0.00	0.00	41.59	35.12	43.88
108.30	7.70	58.97	19.93	13.07	0.33	0.00	56.72	38.41	54.19
108.50	13.69	68.80	16.75	0.96	0.00	0.00	33.07	23.50	43.88
108.70	13.91	70.20	14.35	1.54	0.00	0.00	31.28	19.04	39.48
108.90	12.00	67.36	19.33	1.31	0.00	0.00	36.43	28.55	54.19
109.10	7.98	68.57	15.97	7.13	0.35	0.00	44.33	28.44	39.48
109.30	8.92	70.27	19.00	1.81	0.00	0.00	36.73	26.75	43.88
109.60	9.63	66.00	22.25	2.12	0.00	0.00	40.62	32.69	54.19
109.80	9.09	68.73	20.35	1.83	0.00	0.00	38.63	29.95	39.48
110.00	9.86	73.44	16.36	0.34	0.00	0.00	32.97	24.78	39.48
110.20	8.90	66.99	20.53	3.58	0.00	0.00	41.11	31.16	39.48
110.40	10.66	67.49	20.71	1.14	0.00	0.00	37.94	30.40	39.48
110.60	5.83	67.22	20.86	6.09	0.00	0.00	45.87	34.04	39.48
110.78	6.97	64.53	22.65	5.85	0.00	0.00	46.64	35.97	54.19
111.10	12.84	73.15	12.95	1.06	0.00	0.00	30.70	20.78	39.48
111.30	11.21	76.08	12.28	0.43	0.00	0.00	30.45	23.10	39.48
111.55	11.68	79.74	8.58	0.00	0.00	0.00	27.40	21.83	39.48
111.68	11.88	77.40	10.72	0.00	0.00	0.00	29.39	24.40	39.48
111.88	12.80	74.87	11.88	0.45	0.00	0.00	30.54	24.44	39.48
112.08	12.77	75.55	11.64	0.04	0.00	0.00	29.99	24.76	39.48
112.28	16.89	76.86	6.25	0.00	0.00	0.00	24.11	17.67	39.48
112.46	11.75	73.41	14.45	0.39	0.00	0.00	32.44	26.09	39.48
112.68	14.37	76.60	8.89	0.04	0.00	0.00	27.03	20.74	39.48
112.88	14.36	76.86	8.78	0.00	0.00	0.00	25.92	18.46	39.48
113.13	15.00	73.64	11.06	0.30	0.00	0.00	28.74	21.70	39.48
113.38	14.28	77.18	8.54	0.00	0.00	0.00	26.90	21.29	39.48
113.58	18.49	72.01	9.50	0.00	0.00	0.00	26.07	18.46	39.48

113.78	12.29	75.89	11.68	0.14	0.00	0.00	29.63	23.14	39.48
113.96	12.96	74.96	11.77	0.31	0.00	0.00	29.38	21.92	39.48
114.18	14.75	75.65	9.60	0.00	0.00	0.00	27.37	21.16	39.48
114.38	11.14	74.17	13.68	1.01	0.00	0.00	32.27	24.35	39.48
114.68	12.30	70.09	14.87	2.76	0.00	0.00	35.45	26.29	39.48
114.88	11.02	77.43	11.55	0.00	0.00	0.00	29.26	22.58	39.48
115.08	10.26	77.14	11.98	0.62	0.00	0.00	30.59	23.03	39.48
115.28	6.57	72.88	14.97	5.50	0.01	0.00	41.47	29.61	43.88
115.46	12.69	78.27	9.04	0.00	0.00	0.00	26.08	17.00	39.48
115.68	11.75	79.93	8.32	0.00	0.00	0.00	26.11	18.91	39.48
115.88	7.67	80.91	11.36	0.06	0.00	0.00	30.69	25.31	39.48
116.18	13.78	76.04	9.95	0.23	0.00	0.00	27.13	18.78	39.48
116.38	17.42	74.91	7.67	0.00	0.00	0.00	24.56	17.02	39.48
116.58	11.60	78.00	10.27	0.13	0.00	0.00	27.57	19.56	39.48
116.78	5.88	75.09	15.66	3.37	0.00	0.00	39.38	31.14	39.48
116.96	11.96	75.60	11.28	1.16	0.00	0.00	29.76	20.46	39.48
117.18	4.71	78.69	15.31	1.29	0.00	0.00	35.70	28.27	39.48
117.68	12.12	71.71	14.81	1.36	0.00	0.00	35.70	28.27	39.48
117.88	13.32	71.57	13.69	1.42	0.00	0.00	32.63	24.64	39.48
118.08	10.23	69.61	18.11	2.05	0.00	0.00	37.90	30.75	43.88
118.28	8.18	66.21	22.36	3.25	0.00	0.00	43.14	35.90	54.19
118.46	7.53	66.06	22.53	3.88	0.00	0.00	44.97	37.81	54.19
118.68	7.69	64.92	24.24	3.15	0.00	0.00	44.71	38.05	54.19
118.88	4.93	72.71	18.66	3.70	0.00	0.00	40.64	30.02	39.48
119.18	4.38	65.12	25.19	5.31	0.00	0.00	48.27	39.09	66.94
119.38	5.49	61.76	28.56	4.19	0.00	0.00	49.00	42.37	66.94
119.58	3.19	68.86	24.70	3.25	0.00	0.00	46.39	39.01	54.19
119.78	3.59	70.75	23.60	2.06	0.00	0.00	43.58	36.46	54.19
119.96	4.43	65.88	26.94	2.75	0.00	0.00	46.06	39.14	66.94
120.18	7.58	66.15	22.90	3.37	0.00	0.00	43.16	35.10	54.19

Grain size: VF = very fine, F = fine, M = medium, C = coarse

Table B.4. Percentage carbonate content in coarse (> 63μm) fraction and bulk Hole 819A samples, as determined using the acid-base titration method outlined by Grimaldi et al. (1966).

Depth (mbsf)	% $CaCO_3$ Coarse fraction	% $CaCO_3$ Bulk samples	Depth (mbsf)	% $CaCO_3$ Coarse fraction	% $CaCO_3$ Bulk samples	Depth (mbsf)	% $CaCO_3$ Coarse fraction	% $CaCO_3$ Bulk samples
0.16	88.85	74.90	12.20	85.90	46.68	22.80	73.16	37.66
0.30	88.40	74.41	12.38	83.97	46.27	23.02	65.87	34.52
0.54	86.69	72.05	12.59	78.20	49.84	23.20	69.63	33.86
0.70	89.39	68.73	12.82	85.36	49.04	23.40	49.95	44.94
0.90	88.06	68.89	13.12	90.94	57.50	23.59	78.88	26.66
1.20	89.43	63.88	13.30	75.06	57.13	23.81	66.62	29.48
1.60	88.71	64.31	13.54	92.12	61.57	24.10	77.83	43.21
1.80	90.56	57.68	13.70	93.00	61.78	24.30	71.83	49.54
2.04	93.80	62.63	13.88	93.05	58.62	24.52	64.55	28.97
2.18	97.56	62.85	14.09	93.60	57.35	24.70	49.19	25.42
2.20	88.63	65.30	14.34	93.24	64.12	24.87	62.14	67.58
2.40	79.74	59.42	14.62	91.93	68.45	25.09	79.68	34.52
2.70	78.12	52.22	14.80	93.49	71.28	25.57	88.21	-
3.10	75.84	50.51	15.04	95.13	74.40	25.76	83.43	74.57
3.30	75.49	41.37	15.20	95.34	75.58	26.02	72.39	46.98
3.54	87.40	47.04	15.38	95.71	-	26.17	66.50	37.91
3.70	89.99	57.57	15.59	95.44	79.89	26.40	69.59	42.74
3.95	64.56	35.29	15.82	93.87	80.16	26.59	82.40	59.14
4.20	64.00	38.52	16.12	92.52	78.42	26.81	85.29	76.82
4.60	88.14	37.14	16.30	89.12	79.06	27.10	84.59	76.49
4.80	83.93	40.97	16.54	91.21	80.26	27.80	85.20	72.82
5.04	88.23	40.47	16.70	90.35	75.68	28.00	84.34	66.22
5.20	87.15	32.57	16.88	91.04	77.26	28.20	65.90	35.84
5.40	85.79	64.58	17.09	91.24	71.37	28.40	62.23	33.17
5.70	69.97	71.09	17.32	90.72	73.74	28.60	64.70	49.05
6.10	57.93	32.93	17.57	92.23	74.80	28.80	75.38	61.20
6.30	72.40	48.52	17.77	88.09	71.27	29.10	84.43	72.89
6.70	85.83	74.24	18.04	91.57	66.70	29.30	89.00	82.43
6.90	87.39	69.74	18.10	86.17	67.03	29.50	86.50	82.81
7.20	87.90	82.04	18.30	87.90	57.83	29.70	85.63	78.58
7.60	90.66	72.77	18.52	86.39	66.23	29.90	84.59	79.02
7.80	89.26	73.99	18.70	91.20	64.50	30.10	85.98	69.89
8.04	89.43	74.93	18.90	90.53	72.12	30.30	87.30	73.43
8.18	85.64	72.85	19.09	89.25	73.61	30.60	82.10	80.89
8.62	88.47	71.91	19.31	91.53	70.63	30.80	89.09	75.32
8.80	89.32	68.08	19.60	88.57	71.34	31.00	88.02	70.51
9.04	85.05	63.50	19.80	88.93	74.36	31.20	90.38	66.07
9.20	92.71	62.77	20.02	83.53	63.75	31.40	88.82	61.21
9.38	87.52	60.40	20.20	68.02	64.64	31.60	88.81	59.90
9.59	84.28	59.42	20.40	83.41	57.33	31.80	90.50	55.31
9.82	84.04	58.85	20.59	82.34	58.99	32.10	93.33	79.87
10.12	85.09	54.52	20.81	90.98	76.85	32.30	91.85	55.03
10.30	80.59	46.55	21.10	73.91	52.26	32.50	89.17	67.27
10.54	83.13	51.85	21.30	77.96	50.83	32.70	82.94	54.60
10.70	82.76	46.67	21.52	74.87	48.40	32.90	57.58	36.71
10.88	82.33	43.42	21.70	85.64	49.70	33.10	54.72	57.75
11.09	76.32	42.87	21.90	91.89	47.90	33.30	54.05	30.69
11.32	76.90	40.97	22.09	74.78	33.80	33.60	58.80	46.75
11.80	96.38	40.89	22.31	74.50	39.04	33.80	61.13	46.19
12.04	80.01	43.66	22.60	51.03	33.73	34.00	59.36	45.12

34.20	62.35	53.15	46.70	71.73	51.65	59.50	70.61	61.33
34.40	61.10	42.15	46.60	72.79	48.16	59.70	69.50	59.81
34.80	68.50	44.03	46.80	77.70	45.66	59.90	75.42	61.25
35.10	69.40	54.74	47.00	74.31	44.06	60.10	70.70	59.40
35.30	63.56	49.11	47.20	69.67	40.46	60.30	71.21	59.03
35.50	66.29	47.30	47.40	70.44	41.44	60.60	70.71	62.48
35.70	73.88	49.54	47.60	73.83	41.43	60.80	67.36	52.71
35.90	74.96	49.97	47.80	74.29	42.08	61.00	72.15	61.39
36.10	73.05	56.61	48.10	78.46	45.05	61.20	75.16	62.19
36.30	74.96	62.04	48.30	75.92	43.37	61.40	75.48	60.47
36.60	71.59	53.94	48.50	74.55	52.33	61.60	71.60	60.09
36.80	69.83	51.31	48.70	75.84	43.14	61.80	74.90	61.59
37.00	69.69	51.61	48.90	76.53	44.78	62.10	66.99	59.94
37.20	75.56	50.74	49.10	76.35	46.01	62.30	73.17	58.98
37.10	72.05	57.64	49.30	75.55	45.13	62.50	72.74	58.42
37.30	71.38	53.94	49.60	75.77	57.05	62.70	73.28	54.55
37.50	73.95	55.65	49.80	75.61	47.44	62.90	71.67	57.07
37.70	74.12	52.18	50.00	75.25	60.11	63.10	70.94	59.00
37.90	78.69	55.79	50.20	74.84	63.33	63.60	69.83	55.09
38.10	74.15	56.55	50.40	75.83	62.52	63.80	71.79	50.19
38.30	79.42	59.29	50.60	74.46	57.60	64.00	69.53	54.66
38.60	71.20	65.41	50.80	73.93	65.72	64.20	68.15	56.97
38.80	71.31	59.60	51.10	77.94	64.31	64.40	72.37	48.80
39.00	70.22	56.61	51.30	75.57	64.47	64.60	72.14	52.77
39.20	70.18	52.07	51.50	74.66	63.02	64.80	70.64	50.27
39.40	70.91	58.49	51.70	73.97	64.93	65.10	71.58	49.87
39.60	72.85	57.45	51.90	74.54	64.66	65.30	74.44	48.06
39.80	74.38	63.91	52.10	75.68	64.43	65.50	69.58	46.41
40.10	68.96	56.69	52.30	71.57	64.51	65.70	71.69	49.14
40.30	67.23	55.70	52.60	73.86	64.78	65.60	75.74	67.42
40.50	66.91	51.78	52.80	73.02	65.90	65.80	75.08	60.79
40.70	66.33	47.84	53.00	74.65	67.75	66.00	70.97	56.94
40.90	66.97	47.41	53.20	73.05	65.59	66.22	69.57	57.35
41.10	59.19	46.56	53.40	69.31	68.84	66.42	65.60	54.90
41.30	69.90	51.31	53.60	68.35	68.02	66.62	67.53	50.73
41.60	70.88	50.81	53.80	67.05	69.76	66.82	65.22	43.47
41.80	71.56	53.79	54.10	67.09	71.25	67.02	62.63	42.33
42.00	71.01	47.58	54.30	64.90	70.72	67.22	55.45	40.92
42.20	70.59	51.85	54.50	71.29	70.66	67.42	58.86	34.14
42.40	74.68	50.22	54.70	70.76	71.83	67.72	59.90	33.23
42.60	74.58	50.68	54.90	72.15	70.53	67.92	63.58	42.10
42.80	73.83	50.00	55.10	70.21	70.49	68.12	71.01	46.07
43.10	71.75	52.87	55.30	73.16	62.19	68.32	68.80	47.14
43.30	74.31	51.33	56.10	72.91	71.38	68.52	68.70	56.34
43.50	75.86	52.42	56.30	71.05	87.31	68.72	68.51	51.84
43.70	75.49	51.06	56.50	70.17	51.46	68.92	70.28	49.71
43.90	78.97	57.05	56.70	68.92	66.17	69.22	71.34	52.74
44.10	73.43	49.94	56.90	75.07	67.58	69.42	69.10	52.29
44.30	77.15	59.13	57.10	62.66	63.95	69.62	69.41	52.69
44.60	73.72	57.66	57.30	72.31	67.37	69.82	66.63	44.37
44.80	77.61	58.25	57.60	73.11	63.02	70.02	71.82	60.52
45.00	78.06	47.20	57.80	74.64	66.52	70.22	69.25	48.19
45.20	74.13	56.85	58.00	72.03	65.40	70.42	71.76	49.28
45.40	77.92	54.69	58.20	70.48	63.73	70.72	68.49	49.25
45.60	74.92	48.38	58.40	72.87	64.45	70.92	69.07	48.44
45.80	75.71	48.18	58.60	73.03	62.91	71.12	66.77	45.84
46.10	60.73	41.48	58.80	68.93	63.67	71.32	68.76	48.59
46.30	73.43	49.44	59.10	73.83	60.68	71.52	72.09	48.73
46.50	72.38	50.51	59.30	66.69	59.87	71.72	70.82	48.68

71.92	79.83	42.73	84.45	68.45	59.00	95.92	85.16	53.95
72.22	71.44	42.44	84.60	68.84	64.65	96.12	85.87	54.92
72.42	68.41	48.07	84.65	68.24	60.52	96.32	83.32	53.08
72.62	71.87	41.96	84.80	72.84	65.31	96.52	84.18	56.62
72.82	70.22	51.73	84.85	70.02	-	96.72	84.35	55.47
73.02	65.88	47.48	85.00	69.16	61.46	96.92	82.28	55.80
73.22	63.70	47.00	85.05	68.98	64.66	97.12	80.91	53.80
73.42	65.08	51.38	85.20	69.58	58.42	97.42	81.02	52.55
73.72	72.87	51.98	85.40	67.99	63.07	97.62	85.91	53.80
73.92	68.98	48.96	85.60	64.60	60.78	97.82	78.64	52.98
74.12	67.74	48.49	85.80	64.40	60.84	98.02	82.23	50.20
74.32	71.69	47.14	86.00	60.27	59.08	98.22	81.99	58.93
74.52	70.36	50.19	86.20	67.81	58.90	98.42	79.65	60.81
74.72	69.73	49.74	86.50	66.95	55.93	98.62	81.44	57.68
74.92	73.44	49.85	86.70	64.34	56.96	98.92	81.37	59.56
75.10	72.97	50.76	86.90	66.18	57.80	99.12	82.39	56.85
75.30	71.11	38.79	87.10	63.70	51.89	99.32	81.56	61.74
75.45	66.90	42.92	87.30	63.92	51.09	99.52	80.29	60.82
75.65	75.50	42.96	87.50	67.63	50.31	99.72	80.10	57.06
75.85	69.01	44.12	87.70	64.11	49.33	99.92	85.02	63.46
76.05	71.56	38.93	88.00	83.44	48.56	100.12	82.28	62.35
76.25	72.11	41.90	88.20	67.45	49.23	100.42	77.06	63.96
76.45	73.32	40.55	88.40	65.36	48.47	100.62	76.54	66.95
76.65	63.48	42.56	88.60	62.77	45.13	100.82	79.70	65.19
76.95	70.74	42.90	88.80	65.51	45.03	101.02	76.78	62.56
77.15	72.41	43.32	89.00	60.43	38.57	101.22	80.21	68.41
77.35	75.23	43.46	89.20	58.05	32.33	101.42	79.32	65.39
77.55	74.74	42.70	89.50	65.92	41.46	101.62	80.85	66.69
77.75	71.05	44.48	89.70	56.11	30.98	101.92	81.70	67.10
77.95	75.48	44.78	89.90	62.25	36.20	102.12	69.70	64.01
78.15	71.81	45.00	90.10	57.23	33.09	102.32	76.79	64.21
78.45	63.19	43.74	90.30	60.68	38.00	102.52	77.90	64.33
78.65	70.49	44.35	90.50	67.66	37.97	102.72	72.00	61.20
78.85	67.94	44.60	91.00	69.60	44.69	102.92	79.48	62.66
79.05	73.43	34.89	91.20	73.38	49.33	103.12	78.95	63.97
79.25	66.08	36.77	91.40	76.99	44.36	103.42	78.42	65.47
79.45	59.52	36.15	91.60	82.00	49.79	103.60	75.54	64.88
79.65	61.92	34.78	91.80	83.98	61.77	103.62	76.54	62.56
79.95	77.61	62.19	92.00	74.55	53.58	103.80	74.36	66.85
80.15	74.78	61.89	92.20	77.45	46.30	103.82	82.02	64.52
80.35	76.13	57.66	92.50	79.91	47.18	104.00	69.15	52.57
80.55	75.67	62.96	92.70	83.16	47.47	104.02	74.68	51.19
80.75	72.26	63.49	92.90	72.41	41.65	104.20	68.27	50.41
80.95	73.47	61.37	93.10	74.49	45.55	104.40	-	-
81.15	74.35	61.35	93.30	77.41	49.45	105.10	73.54	51.02
81.45	77.19	63.32	93.50	78.24	48.75	105.30	76.30	58.85
81.65	76.28	64.10	93.70	79.19	46.49	105.50	76.80	56.07
81.85	74.92	63.76	94.00	84.51	48.34	105.70	72.29	57.57
82.05	75.82	64.19	94.10	78.16	45.74	105.90	76.66	60.67
82.25	75.71	62.40	94.20	81.66	48.14	106.10	79.23	61.69
82.45	-	62.43	94.40	78.39	54.78	106.30	81.04	67.27
82.65	74.96	65.65	94.42	84.27	43.09	106.60	82.65	66.50
82.95	71.32	68.04	94.60	63.27	44.49	106.80	78.20	65.04
83.15	74.04	67.80	94.62	83.34	51.43	107.00	79.53	65.28
83..35	71.24	63.20	94.82	86.45	47.63	107.20	79.68	65.45
83.55	71.78	60.16	95.02	84.74	48.08	107.33	82.41	73.30
83.75	73.81	63.30	95.22	85.28	47.52	107.60	77.01	65.23
83.95	73.64	64.97	95.42	82.58	54.94	108.10	78.96	64.89
84.15	69.62	66.67	95.62	80.50	53.70	108.30	78.97	72.55

108.50	77.10	65.29	112.46	79.60	70.33	116.38	63.26	55.84
108.70	77.60	69.94	112.68	-	-	116.58	64.90	57.06
108.90	74.75	64.59	112.88	78.32	58.96	116.78	70.38	53.54
109.10	78.34	68.75	113.18	76.02	69.28	116.96	64.59	49.89
109.30	76.98	66.50	113.38	77.05	70.42	117.18	67.75	51.30
109.60	81.49	62.40	113.58	78.57	66.24	117.68	73.33	41.68
109.80	77.95	63.45	113.78	76.93	66.88	117.88	60.60	38.54
110.00	82.81	65.24	113.96	48.62	64.28	118.08	62.90	41.39
110.40	76.53	64.39	114.18	74.94	66.72	118.28	66.48	35.80
110.60	77.15	64.54	114.38	77.61	70.85	118.46	69.60	46.31
110.78	81.31	66.14	114.68	72.24	61.01	118.68	72.85	50.54
111.10	81.27	72.69	114.88	72.67	64.03	118.88	71.33	50.96
111.30	77.72	70.29	115.08	67.86	62.90	119.18	46.87	52.01
111.55	75.93	70.48	115.28	72.50	71.25	119.38	73.73	57.03
111.68	79.49	71.60	115.46	67.77	58.98	119.58	70.32	53.80
111.88	80.03	72.53	115.68	72.94	55.07	119.78	73.99	55.04
112.08	77.32	68.90	115.88	70.89	58.00	119.96	81.84	53.80
112.28	80.83	69.57	116.18	61.24	54.77	120.18	72.10	50.39

Table B.5. Carbonate content values for Hole 823A muds (< 63 μm), as determined using the acid-base titration method outlined by Grimaldi et al. (1966).

Depth (mbsf)	% $CaCO_3$	Depth (mbsf)	% $CaCO_3$	Depth (mbsf)	% $CaCO_3$	Depth (mbsf)	% $CaCO_3$
0.11	62.92	13.15	61.24	34.65	69.46	55.90	53.96
0.35	53.41	13.39	58.71	34.90	69.26	56.15	72.25
0.60	36.99	13.65	50.25	35.16	74.18	56.40	80.50
0.85	57.60	13.90	39.88	35.65	62.64	56.65	74.67
1.10	49.13	14.15	78.10	35.90	74.69	56.90	69.96
1.35	25.39	14.40	86.68	36.40	79.27	57.15	79.25
1.62	33.16	14.64	70.72	36.89	61.44	57.40	63.86
1.85	62.46	15.15	64.92	37.15	81.14	57.65	47.69
2.10	75.26	15.40	77.83	37.40	83.45	57.90	59.25
2.35	72.50	15.65	66.56	37.64	79.46	58.15	75.61
2.60	68.13	15.9	68.84	38.65	88.63	58.40	56.12
2.85	63.53	16.15	67.34	39.14	-	58.65	79.63
3.13	76.10	24.90	101.87	39.4	78.21	58.90	69.34
3.35	75.73	25.15	90.30	39.66	95.29	59.15	73.36
3.60	59.25	25.65	85.39	40.15	100.87	59.40	72.70
3.85	62.60	25.90	81.78	40.90	75.50	59.65	73.76
4.61	48.70	26.15	69.67	41.16	70.98	59.90	76.19
4.85	48.56	26.40	-	41.40	80.56	60.15	66.37
5.10	58.88	26.65	63.18	41.65	90.61	60.40	59.82
5.35	47.08	26.90	68.37	41.90	84.75	60.65	75.78
5.60	46.15	27.15	61.11	42.14	86.73	60.90	81.03
5.89	70.58	27.40	57.62	42.40	65.24	61.15	79.34
6.15	75.19	27.65	58.95	43.17	71.44	61.4	75.25
6.40	69.43	27.90	85.57	43.40	70.70	61.65	82.10
6.65	60.25	28.15	75.19	43.64	77.60	61.90	68.55
6.90	44.36	28.40	82.47	43.90	85.78	62.15	56.40
7.15	24.79	28.65	73.22	44.15	78.64	62.40	74.23
7.39	53.05	28.90	67.57	44.40	85.82	62.65	73.27
7.65	52.11	29.15	76.23	44.65	81.65	62.90	81.21
7.90	51.15	29.40	75.24	44.90	86.54	63.15	78.12
8.15	71.59	29.65	67.16	45.15	87.95	63.40	86.02
8.40	51.28	29.90	81.51	45.40	79.91	63.65	79.59
8.65	28.62	30.15	76.77	45.65	87.12	63.90	73.57
8.92	79.90	30.40	69.28	45.90	80.16	64.15	67.44
9.15	84.12	30.65	68.52	46.15	86.89	64.4	85.65
9.40	68.13	30.90	65.82	46.4	72.66	64.65	71.65
9.68	60.55	31.15	74.37	46.65	86.86	64.90	70.14
9.90	67.05	31.40	61.30	47.15	71.13	65.15	73.87
10.15	82.13	31.65	64.30	47.40	63.64	65.40	59.64
10.39	77.96	31.90	68.48	47.65	63.02	65.65	77.30
10.65	81.19	32.15	79.73	47.90	67.85	65.90	81.05
10.90	60.07	32.40	71.04	53.65	68.95	66.15	66.81
11.15	63.38	32.65	76.04	53.90	60.24	66.90	69.45
11.40	74.17	32.90	-	54.15	72.34	67.40	83.37
11.65	75.21	33.15	70.06	54.40	79.50	67.65	76.90
11.89	62.98	33.42	68.36	54.65	55.29	67.90	68.68
12.15	51.98	33.65	82.67	54.90	69.49	68.15	70.03
12.40	63.49	33.90	78.26	55.15	58.10	68.40	36.22
12.65	59.43	34.15	66.17	55.40	59.69	68.65	64.61
12.90	35.76	34.40	77.94	55.65	58.88	68.90	51.48

69.15	77.42	76.89	47.34	84.65	42.45	92.15	57.61
69.40	68.20	77.15	76.22	84.89	45.56	92.40	56.66
69.65	48.40	77.40	75.20	85.15	51.86	92.65	54.33
69.90	42.47	77.65	74.17	85.40	42.27	93.15	57.51
70.15	46.09	77.90	82.72	85.65	55.93	93.44	36.56
70.40	69.66	78.39	71.63	85.90	50.09	93.90	37.92
70.65	72.93	78.65	69.33	86.15	18.02	94.40	39.64
70.90	71.28	78.90	64.21	86.39	21.66	94.65	-
71.15	62.97	79.15	59.89	86.65	18.25	95.40	60.57
71.40	71.13	79.40	62.23	86.90	12.73	95.65	52.76
71.65	72.80	79.65	77.69	87.15	18.61	95.90	54.03
71.90	68.62	79.89	53.36	87.40	19.59	96.15	33.42
72.15	65.25	80.15	63.52	87.65	22.10	96.44	49.28
72.39	68.76	80.40	59.27	87.89	44.15	96.65	48.43
72.65	64.59	80.65	65.05	88.15	44.14	96.90	52.78
72.90	63.11	80.90	51.17	88.40	20.65	97.15	52.00
73.15	66.21	81.15	47.21	88.65	21.68	97.40	57.10
73.40	65.19	81.39	56.30	88.90	34.31	97.65	61.83
73.65	66.85	81.65	55.25	89.15	34.85	97.94	54.14
73.89	73.63	81.89	60.89	89.39	35.02	98.15	43.53
74.15	66.60	81.90	63.62	89.65	-	98.40	-
74.40	73.27	82.15	66.09	89.90	37.47	98.65	45.04
74.65	58.46	82.40	67.40	90.15	44.49	98.90	41.10
74.90	36.46	82.65	56.68	90.40	42.69	99.15	45.34
75.15	60.68	82.90	44.48	90.65	46.26	99.44	48.49
75.39	60.82	83.15	53.08	90.89	43.32	99.65	49.79
75.65	72.57	83.39	52.92	91.15	48.55	99.90	61.28
75.90	74.72	83.65	56.03	91.40	71.24		
76.15	30.91	83.90	32.88	91.40	-		
76.40	68.35	84.15	52.75	91.65	64.48		
76.65	73.69	84.40	47.70	91.90	51.96		

APPENDIX - C

Table C.1. Summary of the Philips PW 1011/1050 automatic powder diffractometer operating conditions used in analysis of Site 819 and Site 823 samples.

Tube type	Cu
Generator Settings	40kV, 50mA
Take off angle	6.00°
Cu Alpha 1,2 wavelengths	1.54060, 1.554439 Å
Intensity ratio	0.50000
Tube focus	Long fine
Step size (degree), sample time (sec.), total time	0.04, 1.0, 0:14:35
Monochromator used	Yes
Detector type	Proportional
PHD window	35-70%
Divergence slit	Automatic (specimen length: 10.0mm)
Receiving slit	0.2 mm
Scatter slit	None
Analysis program	22
Peak angle range	5-40 2θ°
Spinner	On
High angular limit	140°

Table C.2. Dominant X-ray diffraction peaks of selected minerals in order of decreasing intensities (I/I_{Max}), crystallographic (Miller) indices (*hkl*), and 2θ angles for Cu radiation.

Aragonite [5-453]								
I/I_{Max}	100	65	52	46	38	32	32	30
hkl	111	221	021	012	112	200	041	130
$2\theta_{Cu}$	26.23	45.85	27.23	*33.16	37.89	36.18	48.36	38.42
Low $MgCO_3$ Calcite [5-586]								
I/I_{Max}	100	18	18	17	17	14	12	8
hkl	104	113	202	108	116	110	102	212
$2\theta_{Cu}$	*29.40	39.40	43.16	47.47	48.51	35.97	23.02	57.38
Dolomite [11-078]								
I/I_{Max}	100	30	30	20	15	15	10	10
hkl	104	113	009	018	202	030	110	119
$2\theta_{Cu}$	*30.97	41.14	51.18	50.56	44.94	67.35	37.36	65.14
Quartz, Low [5-490]								
I/I_{Max}	100	34	17	15	12	12	11	9
hkl	101	100	112	211	110	102	203	200
$2\theta_{Cu}$	*26.64	20.83	50.17	59.98	36.52	36.2	68.14	42.44

The figures bounded by parentheses refer to the Powder Diffraction File Index presented by McClune (1987). 2θ degree values marked with an asterisk denotes those intensities used in calculating peak heights.

Table C.3. XRD peak heights for selected minerals in Hole 819A bulk sediments.

Sample Code		Depth (mbsf)	Quartz	Low Mg Calcite	High Mg Calcite	Dolomite	Aragonite	Chlorite /Kaolinite
01H01	16-18	0.16	286	534	650	0	185	0
01H01	30-32	0.30	317	894	876	25	324	0
01H01	54-56	0.54	484	762	708	0	296	0
01H01	70-72	0.70	380	751	697	0	234	10
01H01	90-92	0.90	408	697	620	53	253	10
01H01	120-122	1.20	488	702	571	0	222	10
01H02	10-12	1.60	635	773	660	0	276	0
01H02	30-32	1.80	590	671	1927	0	246	12
01H02	54-56	2.04	24	713	566	0	237	10
01H02	68-70	2.18	454	571	590	0	199	18
01H02	70-72	2.20	630	692	790	0	234	18
01H02	90-92	2.40	630	595	655	0	234	10
01H02	120-122	2.70	392	900	493	0	279	0
01H03	10-12	3.10	882	404	548	0	174	0
01H03	30-32	3.30	1362	502	590	0	182	14
01H03	54-56	3.54	1005	480	538	0	137	0
01H03	70-72	3.70	1340	581	566	0	202	18
01H03	95-97	3.95	1806	100	404	0	112	27
01H03	120-122	4.20	1253	493	635	0	188	31
01H04	10-12	4.60	1232	353	365	0	123	19
01H04	30-32	4.80	1761	292	416	0	117	32
01H04	54-56	5.04	784	346	400	0	125	12
01H04	70-72	5.20	1246	520	460	0	213	32
01H04	90-92	5.40	600	480	724	0	204	10
01H04	120-122	5.70	992	697	818	0	276	14
01H05	10-12	6.10	1884	552	471	0	154	32
01H05	30-32	6.30	205	986	600	0	193	25
01H05	70-72	6.70	357	999	625	0	299	0
01H05	90-92	6.90	1050	882	986	0	292	29
01H05	120-122	7.20	635	967	829	0	296	0
01H06	10-12	7.60	534	918	818	0	324	10
01H06	30-32	7.80	437	824	829	31	269	0
01H06	54-56	8.04	520	986	847	0	376	0
01H06	68-70	8.18	424	801	708	0	310	0
02H01	12-14	8.62	396	973	745	0	279	0
02H01	30-32	8.80	961	864	934	0	346	10
02H01	54-56	9.04	692	566	697	0	213	10
02H01	70-72	9.20	876	756	818	0	303	10
02H01	88-90	9.38	671	493	548	0	172	0
02H01	109-111	9.59	961	697	1421	0	177	11
02H01	132-134	9.82	745	557	548	0	169	10
02H02	12-14	10.12	1050	835	734	0	259	18
02H02	30-32	10.30	949	566	543	0	177	15
02H02	54-56	10.54	1149	692	718	0	279	23
02H02	70-72	10.70	818	502	471	0	159	10
02H02	88-90	10.88	1005	605	562	0	190	28
02H02	109-111	11.09	906	428	449	0	137	20
02H02	132-134	11.32	1296	543	610	0	182	19
02H03	30-32	11.80	740	548	369	0	125	14
02H03	54-56	12.04	1414	534	506	0	174	29
02H03	70-72	12.20	762	404	576	0	132	14

02H03	88-90	12.38	1204	586	620	0	216	23
02H03	109-111	12.59	767	454	557	0	161	23
02H03	132-134	12.82	1043	640	702	0	250	27
02H04	12-14	13.12	361	520	369	0	139	10
02H04	30-32	13.30	557	778	538	0	222	16
02H04	54-56	13.54	497	676	552	0	188	10
02H04	70-72	13.70	562	876	600	0	286	20
02H04	88-90	13.88	458	681	515	0	182	10
02H04	109-111	14.09	671	829	676	0	266	20
02H04	132-134	14.34	400	841	718	0	246	10
02H05	12-14	14.62	610	876	829	0	303	14
02H05	30-32	14.80	384	697	645	0	228	10
02H05	54-56	15.04	339	918	973	0	317	0
02H05	70-72	15.20	320	767	702	0	303	0
02H05	88-90	15.38	462	1178	1056	0	445	0
02H05	109-111	15.59	266	853	767	0	339	0
02H05	132-134	15.82	454	1056	955	0	404	0
02H06	12-14	16.12	296	767	864	0	313	0
02H06	30-32	16.30	576	773	1030	0	365	0
02H06	54-56	16.54	346	756	835	0	313	0
02H06	70-72	16.70	576	841	924	0	376	0
02H06	88-90	16.88	412	660	620	0	276	0
02H06	109-111	17.09	576	930	1056	0	353	0
02H06	132-134	17.32	615	762	807	0	306	14
02H07	07-08	17.57	310	595	734	0	289	0
02H07	27-29	17.77	420	888	906	0	372	0
02H07	54-56	18.04	335	681	751	0	276	0
03H01	10-12	18.10	595	807	745	0	317	12
03H01	30-32	18.30	416	590	557	0	228	10
03H01	52-54	18.52	762	784	756	0	320	18
03H01	70-72	18.70	313	524	524	0	185	10
03H01	90-92	18.90	384	767	660	0	339	0
03H01	109-111	19.09	303	620	548	0	237	0
03H01	131-133	19.31	615	894	829	0	369	11
03H02	10-12	19.60	339	708	697	45	317	10
03H02	30-32	19.80	412	949	1253	92	392	0
03H02	52-54	20.02	534	773	724	42	346	0
03H02	70-72	20.20	650	936	807	117	392	0
03H02	90-92	20.40	557	676	708	76	269	0
03H02	109-111	20.59	882	807	795	41	380	0
03H02	131-133	20.81	762	576	615	30	207	0
03H03	10-12	21.10	1218	713	734	0	386	18
03H03	30-32	21.30	906	408	600	0	169	0
03H03	52-54	21.52	1544	562	734	0	246	18
03H03	70-72	21.70	961	462	676	0	177	22
03H03	90-92	21.90	1391	488	666	0	188	23
03H03	109-111	22.09	906	396	488	0	117	10
03H03	131-133	22.31	1260	424	548	0	128	18
03H04	10-12	22.60	2070	216	462	0	110	10
03H04	30-32	22.80	1399	346	557	0	128	27
03H04	52-54	23.02	824	276	416	0	62	12
03H04	70-72	23.20	1030	353	493	0	112	31
03H04	90-92	23.40	906	262	392	0	59	24
03H04	109-111	23.59	1459	207	488	0	72	37
03H04	131-133	23.81	1030	250	365	0	88	24
03H05	10-12	24.10	1030	467	515	0	196	29
03H05	30-32	24.30	801	528	506	0	213	14
03H05	52-54	24.52	1962	795	320	29	250	38

03H05	70-72	24.70	1806	620	199	0	137	38
03H05	87-89	24.87	1971	824	433	0	123	40
03H06	26-28	25.76	462	1475	610	90	557	0
03H06	52-54	26.02	1082	1037	372	0	231	10
03H06	67-69	26.17	1600	876	400	0	177	37
03H06	90-92	26.40	1560	888	353	0	204	22
03H06	109-111	26.59	1384	1490	1289	0	250	30
03H06	131-133	26.81	497	949	511	0	335	0
03H07	10-12	27.10	506	1102	620	53	424	0
04H01	30-32	27.80	384	666	562	0	204	0
04H01	50-52	28.00	581	713	829	0	335	0
04H01	70-72	28.20	1211	342	369	0	125	24
04H01	90-92	28.40	930	289	324	0	154	41
04H01	110-112	28.60	824	493	595	0	156	21
04H01	130-132	28.80	835	894	605	0	204	0
04H02	10-12	29.10	655	870	548	0	256	10
04H02	30-32	29.30	480	1011	605	34	272	0
04H02	50-52	29.50	339	1037	807	0	303	0
04H02	70-72	29.70	380	676	600	0	282	0
04H02	90-92	29.90	286	961	471	56	202	10
04H02	110-112	30.10	543	1218	630	234	317	12
04H02	130-132	30.30	462	986	557	0	276	10
04H03	10-12	30.60	388	1102	762	0	384	0
04H03	30-32	30.80	428	888	524	0	292	0
04H03	50-52	31.00	506	1005	562	0	404	0
04H03	70-72	31.20	388	756	420	0	210	0
04H03	90-92	31.40	620	740	520	0	237	0
04H03	110-112	31.60	400	590	380	48	149	10
04H03	130-132	31.80	1005	829	605	0	276	10
04H04	10-12	32.10	506	718	408	38	196	20
04H04	30-32	32.30	511	1362	864	0	433	0
04H04	50-52	32.50	428	676	660	0	210	10
04H04	70-72	32.70	1082	655	600	0	240	14
04H04	90-92	32.90	1197	365	437	88	137	36
04H04	110-112	33.10	2228	335	342	0	108	64
04H04	130-132	33.30	1156	210	222	0	88	41
04H05	10-12	33.60	1211	484	493	388	174	0
04H05	30-32	33.80	807	449	484	142	130	26
04H05	50-52	34.00	1246	497	773	142	172	10
04H05	70-72	34.20	745	365	441	46	135	10
04H05	90-92	34.40	1656	520	745	71	222	10
04H05	110-112	34.60	1170	650	408	199	204	10
04H05	130-132	34.80	1282	424	515	146	204	38
04H06	10-12	35.10	835	548	502	416	174	18
04H06	30-32	35.30	1260	493	566	231	202	25
04H06	50-52	35.50	1018	526	566	225	169	34
04H06	70-72	35.70	1866	620	515	279	243	16
04H06	90-92	35.90	1239	524	520	231	159	22
04H06	110-112	36.10	1011	524	548	182	207	18
04H06	130-132	36.30	1156	449	562	110	166	18
04H07	10-12	36.60	1149	538	676	119	219	20
04H07	30-32	36.80	992	462	543	117	199	21
04H07	50-52	37.00	1362	620	835	317	296	0
04H07	70-72	37.20	610	441	445	502	202	19
05H01	10-12	37.10	2172	655	576	388	299	0
05H01	50-52	37.50	1632	630	681	94	303	21
05H01	70-72	37.70	999	412	557	58	196	14
05H01	90-92	37.90	1325	681	630	156	282	16

05H01	110-112	38.10	864	471	595	202	231	16
05H01	130-132	38.30	1089	790	562	396	253	16
05H02	10-12	38.60	1354	357	234	655	137	0
05H02	30-32	38.80	1005	590	388	1122	286	0
05H02	50-52	39.00	835	454	276	1318	216	26
05H02	70-72	39.20	1648	671	276	420	328	24
05H02	90-92	39.40	906	475	193	888	246	15
05H02	110-112	39.60	1043	557	166	1043	282	29
05H02	130-132	39.80	864	369	117	1452	231	10
05H03	10-12	40.10	1089	557	168	1673	272	23
05H03	30-32	40.30	930	433	202	1246	231	10
05H03	50-52	40.50	1122	586	350	847	289	14
05H03	70-72	40.70	882	404	380	64	169	18
05H03	90-92	40.90	1332	620	557	0	339	20
05H03	110-112	41.10	795	595	571	44	199	13
05H03	130-132	41.30	1467	778	918	83	303	0
05H04	10-12	41.60	801	666	581	102	199	10
05H04	30-32	41.80	1082	858	835	204	296	26
05H04	50-52	42.00	586	475	515	92	177	21
05H04	70-72	42.20	818	581	835	69	262	18
05H04	90-92	42.40	590	676	502	0	166	10
05H04	110-112	42.60	1218	773	790	74	262	30
05H04	130-132	42.80	784	548	645	0	193	38
05H05	10-12	43.10	1225	734	801	0	286	21
05H05	30-32	43.30	784	552	548	0	164	38
05H05	50-52	43.50	1267	751	778	0	250	86
05H05	70-72	43.70	818	818	605	79	207	21
05H05	90-92	43.90	1910	718	681	55	272	10
05H05	130-132	44.30	605	1076	557	142	204	0
05H06	10-12	44.60	488	992	502	85	190	14
05H06	30-32	44.80	870	1190	524	144	266	0
05H06	50-52	45.00	1362	762	396	100	216	0
05H06	70-72	45.20	900	1149	566	88	286	0
05H06	90-92	45.40	635	973	511	102	193	10
05H06	110-112	45.60	734	740	605	0	207	0
05H06	130-132	45.80	650	671	497	52	172	12
05H07	10-12	46.10	1096	870	692	0	266	0
05H07	30-32	46.30	955	734	590	0	188	15
05H07	50-52	46.50	1063	906	790	0	256	32
05H07	70-72	46.70	1303	697	506	76	204	14
06H01	10-12	46.60	1362	773	538	0	199	31
06H01	30-32	46.80	1197	835	581	0	216	10
06H01	50-52	47.00	1267	729	600	0	216	35
06H01	70-72	47.20	1011	697	515	92	202	10
06H01	90-92	47.40	1183	600	692	0	231	31
06H01	110-112	47.60	1421	543	462	0	169	0
06H01	130-132	47.80	1421	745	973	0	262	25
06H02	10-12	48.10	1116	538	506	0	154	23
06H02	30-32	48.30	912	635	697	0	222	27
06H02	50-52	48.50	853	493	480	0	177	0
06H02	70-72	48.70	930	702	906	0	216	22
06H02	90-92	48.90	702	543	454	0	161	0
06H02	110-112	49.10	818	571	480	0	199	0
06H02	130-132	49.30	773	497	557	41	159	16
06H03	10-12	49.60	876	635	497	0	182	27
06H03	30-32	49.80	713	660	515	61	202	10
06H03	50-52	50.00	600	1043	350	169	204	0
06H03	70-72	50.20	807	1296	368	262	279	0

06H03	90-92	50.40	571	1122	643	196	240	0
06H03	110-112	50.60	900	1163	296	193	289	0
06H03	130-132	50.80	576	1043	279	207	272	0
06H04	10-12	51.10	640	1122	392	303	276	0
06H04	30-32	51.30	552	1197	277	256	296	0
06H04	50-52	51.50	888	1136	1096	269	342	10
06H04	70-72	51.70	697	1050	443	228	279	0
06H04	90-92	51.90	961	1163	408	193	310	0
06H04	110-112	52.10	515	1037	571	188	262	12
06H04	130-132	52.30	586	1069	577	196	320	0
06H05	30-32	52.80	600	1406	597	237	346	0
06H05	50-52	53.00	441	949	383	159	234	0
06H05	70-72	53.20	655	1232	0	210	328	0
06H05	90-92	53.40	449	955	283	177	272	10
06H05	110-112	53.60	645	1142	0	207	269	0
06H05	130-132	53.80	515	1142	177	219	269	0
06H06	10-12	54.10	548	1640	847	428	350	0
06H06	30-32	54.30	520	1142	350	0	289	0
06H06	50-52	54.50	697	1459	0	471	350	0
06H06	70-72	54.70	388	745	83	253	156	0
06H06	90-92	54.90	576	1414	0	475	328	10
06H06	110-112	55.10	548	1362	0	449	246	0
06H06	130-132	55.30	692	1183	511	202	313	0
07H01	10-12	56.10	557	1576	123	266	310	0
07H01	30-32	56.30	1246	1176	0	276	335	0
07H01	50-52	56.50	497	1050	185	396	276	0
07H01	70-72	56.70	581	1436	190	313	328	0
07H01	90-92	56.90	462	1482	217	282	324	0
07H01	110-112	57.10	980	1521	209	303	384	10
07H01	130-132	57.30	515	1211	110	262	282	10
07H02	10-12	57.60	454	1063	0	250	313	0
07H02	30-32	57.80	924	1529	0	400	313	0
07H02	50-52	58.00	729	1289	510	276	317	10
07H02	70-72	58.20	493	1024	0	306	259	0
07H02	90-92	58.40	992	1142	304	250	320	0
07H02	110-112	58.60	543	1253	170	213	299	0
07H02	130-132	58.80	1376	980	380	180	52	0
07H03	10-12	59.10	484	1109	417	146	282	0
07H03	30-30	59.30	961	1225	671	182	384	0
07H03	50-52	59.50	724	1030	383	132	243	0
07H03	70-72	59.70	888	1267	548	121	380	10
07H03	90-92	59.90	576	906	369	98	231	0
07H03	110-112	60.10	745	1043	548	86	328	0
07H03	130-132	60.30	778	967	484	94	272	0
07H04	10-12	60.60	778	1239	475	92	328	10
07H04	30-32	60.80	818	697	350	85	240	0
07H04	50-52	61.00	829	1030	449	72	292	0
07H04	70-72	61.20	692	841	400	53	231	0
07H04	90-92	61.40	610	967	471	67	253	12
07H04	110-112	61.60	615	967	433	69	250	0
07H04	130-132	61.80	708	967	538	58	292	20
07H05	10-12	62.10	538	924	384	53	219	0
07H05	30-32	62.30	870	986	557	0	276	10
07H05	50-52	62.50	660	876	365	56	219	10
07H05	70-72	62.70	790	853	534	0	335	13
07H05	90-92	62.90	635	773	586	40	213	10
07H05	110-112	63.10	1109	858	543	96	317	11
07H06	10-12	63.60	1030	864	625	0	320	18

07H06	30-32	63.80	900	684	484	0	210	12
07H06	50-52	64.00	1901	801	462	56	246	14
07H06	90-92	64.40	1082	900	467	79	303	12
07H06	110-112	64.60	864	615	350	46	225	12
07H06	130-132	64.80	1204	778	433	0	231	17
07H07	10-12	65.10	790	645	372	38	177	18
07H07	30-32	65.30	1063	870	912	0	253	18
07H07	50-52	65.50	912	666	458	0	204	20
07H07	70-72	65.70	1537	1005	605	0	303	0
08H01	10-12	65.60	645	818	467	0	299	10
08H01	30-32	65.80	1089	906	729	0	313	10
08H01	50-52	66.00	566	756	480	0	210	0
08H02	10-12	66.22	1459	767	660	0	310	10
08H02	30-32	66.42	1444	767	586	0	259	11
08H02	50-52	66.62	1706	590	571	0	213	23
08H02	70-72	66.82	1163	557	511	0	199	0
08H02	90-92	67.02	2088	630	590	102	199	32
08H02	130-132	67.42	1747	660	676	0	246	10
08H03	10-12	67.72	1467	404	441	64	161	18
08H03	30-32	67.92	1176	724	870	0	213	21
08H03	50-52	68.12	1303	428	449	125	125	11
08H03	70-72	68.32	1163	708	795	0	231	11
08H03	90-92	68.52	1142	566	581	0	180	0
08H03	110-112	68.72	882	552	734	0	172	21
08H03	130-132	68.92	829	562	666	0	169	10
08H04	10-12	69.22	1310	676	655	55	216	14
08H04	30-32	69.42	645	625	615	0	159	0
08H04	50-52	69.62	1289	650	942	37	222	11
08H04	70-72	69.82	1149	666	702	0	266	14
08H04	110-112	70.22	900	924	538	0	182	16
08H04	130-132	70.42	1260	645	713	0	222	22
08H05	10-12	70.72	942	520	566	0	159	14
08H05	30-32	70.92	1176	645	729	0	246	10
08H05	50-52	71.12	1102	566	595	0	177	0
08H05	70-72	71.32	942	595	1303	0	177	22
08H05	90-92	71.52	1789	610	692	0	190	17
08H05	110-112	71.72	801	497	595	0	142	10
08H06	30-32	72.42	812	681	650	77	172	0
08H06	50-52	72.62	882	534	2172	0	190	13
08H06	70-72	72.82	1296	605	625	0	193	15
08H06	90-90	73.02	888	538	625	0	159	14
08H06	110-112	73.22	864	576	973	0	207	10
08H07	10-12	73.72	666	511	581	35	149	18
08H07	30-32	73.92	1232	697	824	0	225	22
08H07	50-52	74.12	973	562	605	0	164	14
08H07	70-72	74.32	1163	666	1475	71	219	26
08H07	90-92	74.52	912	449	552	0	169	14
08H07	110-112	74.72	1197	566	708	0	177	20
08H07	130-132	74.92	762	605	562	0	13	18
09H01	10-12	75.10	1142	600	666	0	246	23
09H01	30-32	75.30	1282	449	396	0	169	35
09H02	10-12	75.45	1089	529	515	0	159	31
09H02	30-32	75.65	1050	529	562	0	132	29
09H02	50-52	75.85	1096	767	645	0	188	38
09H02	70-72	76.05	778	428	400	0	100	26
09H02	90-92	76.25	1399	595	552	0	166	29
09H02	110-112	76.45	740	445	353	0	110	24
09H02	130-132	76.65	1260	320	256	0	149	17

09H03	10-12	76.95	924	630	488	0	146	27
09H03	30-32	77.15	1260	576	546	24	169	36
09H03	50-52	77.35	882	566	484	0	161	29
09H03	70-72	77.55	1183	586	686	0	193	34
09H03	90-92	77.75	1063	660	497	0	169	32
09H03	110-112	77.95	1421	713	635	98	222	27
09H03	130-132	78.15	818	557	497	34	193	16
09H04	10-12	78.45	1156	681	586	35	204	26
09H04	30-32	78.65	1063	620	511	0	185	30
09H04	50-52	78.85	1063	702	515	0	169	18
09H04	70-72	79.05	912	420	350	31	130	17
09H04	90-92	79.25	1384	571	475	0	172	37
09H04	110-112	79.45	1190	520	420	0	149	32
09H04	130-132	79.65	1082	571	357	0	169	29
09H05	10-12	79.95	961	936	562	0	210	0
09H05	30-32	80.15	515	773	488	0	222	0
09H05	50-52	80.35	404	801	493	36	199	10
09H05	70-72	80.55	681	1116	708	36	335	10
09H05	90-92	80.75	702	829	488	40	234	0
09H05	110-112	80.95	676	1260	566	108	335	11
09H05	130-132	81.15	488	1183	420	81	282	0
09H06	10-12	81.45	812	1274	420	100	313	0
09H06	30-32	81.65	428	1116	290	96	234	0
09H06	50-52	81.85	1076	1384	237	30	292	0
09H06	70-72	82.05	605	1362	350	69	256	0
09H06	90-92	82.25	756	1260	273	58	256	0
09H06	110-112	82.45	471	1260	223	55	240	10
09H06	130-132	82.65	392	1347	330	108	313	0
09H07	10-12	82.95	543	1467	163	71	250	0
09H07	30-32	83.15	595	1697	171	96	317	0
09H07	70-72	83.55	1391	1608	62	98	292	0
09H07	90-92	83.75	697	1399	0	102	246	0
09H07	110-112	83.95	795	1498	138	119	296	0
09H07	130-132	84.15	543	1459	0	159	237	11
09H08	10-12	84.45	1096	1211	100	196	276	0
10H01	10-12	84.60	1096	1429	0	282	303	0
09H08	30-32	84.65	992	1325	147	151	253	0
10H01	30-32	84.80	751	1109	83	154	219	0
09H08	50-52	84.85	841	1369	0	137	262	0
10H02	10-12	85.00	1183	1218	397	117	269	0
9H08	70-72	85.05	506	1269	382	172	243	0
10H02	30-32	85.20	724	1163	163	151	231	0
10H02	50-52	85.40	912	1218	458	61	279	0
10H02	70-72	85.60	640	773	286	67	177	0
10H02	90-92	85.80	1129	1011	524	96	266	0
10H02	110-112	86.00	924	767	506	61	210	0
10H02	130-132	86.20	1096	1063	671	69	269	10
10H03	10-12	86.50	751	702	586	68	228	0
10H03	30-32	86.70	1076	1089	829	45	306	0
10H03	50-52	86.90	1096	778	718	0	225	0
10H03	70-72	87.10	1260	767	1163	62	292	0
10H03	90-92	87.30	1421	692	745	0	225	22
10H03	110-112	87.50	1050	590	595	0	182	19
10H03	130-132	87.70	1274	595	566	0	172	12
10H04	10-12	88.00	1467	724	702	0	234	0
10H04	30-32	88.20	936	529	605	0	174	17
10H04	50-52	88.40	1832	640	801	0	256	10
10H04	70-72	88.60	1122	571	524	0	177	19

10H04	90-92	88.80	1910	524	655	49	225	10
10H04	110-112	89.00	1998	506	538	64	142	30
10H04	130-132	89.20	1681	515	620	0	182	10
10H05	10-12	89.50	1384	480	600	77	169	17
10H05	30-32	89.70	1747	433	454	0	154	29
10H05	50-52	89.90	1260	400	384	0	108	14
10H05	70-72	90.10	2098	467	502	0	154	37
10H05	90-92	90.30	1384	502	488	0	156	24
10H05	110-112	90.50	1354	471	571	0	188	31
10H06	10-12	91.00	1183	625	676	0	204	27
10H06	30-32	91.20	841	590	666	0	193	28
10H06	50-52	91.40	1109	630	734	0	289	15
10H06	70-72	91.60	801	480	615	0	169	27
10H06	90-92	91.80	762	801	967	0	299	10
10H06	110-112	92.00	620	449	488	0	149	10
10H06	130-132	92.20	1505	605	778	0	250	24
10H07	10-12	92.50	829	506	511	0	177	10
10H07	30-32	92.70	992	562	660	0	188	10
10H07	50-52	92.90	692	408	480	0	169	14
10H07	70-72	93.10	980	645	610	0	210	20
10H07	90-92	93.30	708	484	511	0	196	21
10H07	110-112	93.50	1030	697	681	0	243	29
10H07	130-132	93.70	702	557	454	0	161	24
10H08	10-12	94.00	1183	734	697	0	228	22
11H01	10-12	94.10	1239	829	548	0	199	30
10H08	30-32	94.20	756	557	548	38	166	13
10H08	50-52	94.40	1037	724	686	0	210	20
11H02	10-12	94.42	1030	524	488	0	174	27
10H08	70-72	94.60	812	620	1024	0	166	19
11H02	30-32	94.62	835	676	718	0	262	21
11H02	50-52	94.82	671	506	534	0	185	18
11H02	70-72	95.02	841	740	595	0	202	23
11H02	90-92	95.22	475	369	346	0	117	12
11H02	110-112	95.42	762	740	660	45	213	14
11H02	130-132	95.62	581	660	515	0	188	12
11H03	10-12	95.92	1136	969	1056	41	296	27
11H03	30-32	96.12	506	660	511	0	159	22
11H03	50-52	96.32	681	942	762	0	243	26
11H03	70-72	96.52	640	734	506	0	202	14
11H03	90-92	96.72	807	980	745	0	292	18
11H03	110-112	96.92	734	767	650	0	253	12
11H03	130-132	97.12	767	906	697	0	276	18
11H04	10-12	97.42	718	605	576	0	174	18
11H04	30-32	97.62	853	949	708	49	313	31
11H04	50-52	97.82	566	666	502	0	164	12
11H04	70-72	98.02	900	888	718	0	243	12
11H04	90-92	98.22	515	676	543	0	216	0
11H04	110-112	98.42	824	1116	740	0	313	14
11H04	130-132	98.62	543	847	605	0	225	19
11H05	10-12	98.92	745	967	708	0	306	0
11H05	30-32	99.12	388	640	502	0	199	0
11H05	50-52	99.32	576	841	640	0	296	10
11H05	70-72	99.52	437	692	471	0	182	0
11H05	90-92	99.72	576	818	538	110	234	0
11H05	110-112	99.92	493	734	600	0	228	10
11H05	130-132	100.12	1005	961	729	128	299	15
11H06	10-12	100.42	475	795	595	0	253	10
11H06	30-32	100.62	497	936	790	0	310	0

11H06	50-52	100.82	310	581	660	0	190	0
11H06	70-72	101.02	548	1037	718	0	296	0
11H06	90-92	101.22	388	740	515	0	202	0
11H06	110-112	101.42	630	1024	949	0	342	0
11H06	130-132	101.62	511	930	740	0	266	0
11H07	10-12	101.92	697	1156	812	0	289	0
11H07	30-32	102.12	502	906	543	0	204	10
11H07	50-52	102.32	640	1102	729	0	279	15
11H07	70-72	102.52	713	835	640	0	276	10
11H07	90-92	102.72	713	876	724	102	262	10
11H07	110-112	102.92	529	807	676	0	256	0
11H07	130-132	103.12	506	847	713	0	317	0
11H08	10-12	103.42	702	1176	708	0	272	0
12H01	10-12	103.60	529	697	666	0	282	0
11H08	30-32	103.62	702	660	835	0	335	0
12H01	30-32	103.80	692	1018	515	0	182	0
11H08	50-52	103.82	666.	818	650	0	250	0
12H01	50-52	104.00	1116	635	543	0	219	11
11H08	70-72	104.02	692	1018	818	0	352	0
12H01	70-72	104.20	1781	888	640	0	282	10
12H02	10-12	105.10	751	576	506	0	182	0
12H02	30-32	105.30	1011	906	924	0	306	0
12H02	50-52	105.50	548	610	818	0	204	10
12H02	70-72	105.70	1037	1109	778	0	272	0
12H02	90-92	105.90	1063	1043	745	204	276	10
12H02	110-112	106.10	767	1030	600	0	276	0
12H02	130-132	106.30	566	1069	529	0	320	0
12H03	10-12	106.60	493	961	408	71	279	0
12H03	30-32	106.80	458	1246	552	0	306	0
12H03	50-52	107.00	734	942	430	52	272	0
12H03	70-72	107.20	605	1232	408	108	353	0
12H03	83-85	107.33	543	1163	574	600	350	0
12H03	110-112	107.60	497	1037	483	193	266	0
12H04	10-12	108.10	484	676	388	177	237	0
12H04	30-32	108.30	645	876	347	1283	313	0
12H04	50-52	108.50	534	718	424	801	231	0
12H04	90-92	108.90	713	906	557	0	306	0
12H04	110-112	109.10	992	924	421	818	310	0
12H04	130-132	109.30	724	841	357	424	250	0
12H05	10-12	109.60	762	1069	474	190	420	0
12H05	30-32	109.80	729	894	490	188	269	0
12H05	50-52	110.00	942	853	339	967	306	0
12H05	70-72	110.20	571	870	328	159	269	0
12H05	90-92	110.40	812	949	1665	324	317	0
12H05	110-112	110.60	396	841	310	71	225	0
12H05	128-130	110.78	610	1030	231	114	282	12
13H01	10-12	111.10	445	1498	0	346	256	0
13H01	30-32	111.30	562	1989	231	0	225	0
13H01	55-57	111.55	801	1568	0	125	231	0
13H02	10-12	111.68	534	2016	0	161	303	0
13H02	30-32	111.88	534	1706	0	102	225	12
13H02	50-52	112.08	433	1989	0	98	262	0
13H02	70-72	112.28	416	1467	0	71	225	0
13H02	88-90	112.46	650	2480	0	85	328	0
13H02	110-112	112.68	380	1584	0	53	193	0
13H02	130-132	112.88	625	2134	0	83	324	0
13H03	10-12	113.18	428	1624	0	69	246	0
13H03	30-32	113.38	692	2153	0	76	303	0

13H03	50-52	113.58	1129	1232	0	41	190	0
13H03	70-72	113.78	1082	2034	0	88	310	0
13H03	88-90	113.96	506	1318	0	53	225	0
13H03	110-112	114.18	640	1954	0	139	331	0
13H03	130-132	114.38	762	1608	0	86	266	12
13H04	10-12	114.68	1406	1714	0	151	357	0
13H04	30-32	114.88	557	1211	0	228	243	12
13H04	50-52	115.08	1267	1399	0	467	350	0
13H04	70-72	115.28	876	289	864	795	253	10
13H04	88-90	115.46	1043	1239	0	502	328	0
13H04	110-112	115.68	605	1018	0	384	222	0
13H04	130-132	115.88	1260	1369	131	276	331	0
13H05	10-12	116.18	686	876	723	123	216	10
13H05	30-32	116.38	1056	942	239	102	250	14
13H05	50-52	116.58	1109	999	0	45	204	0
13H05	70-72	116.78	986	1005	388	106	259	0
13H05	88-90	116.96	992	686	353	0	185	10
13H05	110-112	117.18	1798	625	467	76	213	10
13H06	10-12	117.68	1332	713	645	50	266	16
13H06	30-32	117.88	961	433	388	0	151	14
13H06	50-52	118.08	1789	590	534	0	210	0
13H06	70-72	118.28	858	441	369	44	151	32
13H06	88-90	118.46	1600	729	576	0	228	0
13H06	110-112	118.68	1109	590	576	0	172	0
13H06	130-132	118.88	1239	718	666	0	243	0
13H07	10-12	119.18	1267	718	586	0	210	0
13H07	30-32	119.38	1490	773	740	0	250	18
13H07	50-52	119.58	762	676	625	0	231	0
13H07	70-72	119.78	2134	812	617	0	262	13
13H07	88-90	119.96	625	488	548	0	137	0
13H07	110-112	120.18	1714	912	751	0	228	0

Peak heights (counts above background) can be converted into semi-quantitative mineral abundances using the calibration graphs presented in the back of Appendix B (Figures I to V).

Table C.4. XRD peak heights for selected minerals in Hole 823A bulk sediments.

Sample Code	Depth (mbsf)	Quartz	Low Mg Calcite	High Mg Calcite	Dolomite	Aragonite	Chlorite /Kaolinite
01H01 11-13	0.11	310	2500	0	0	225	0
01H01 35-37	0.35	445	1482	177	0	169	0
01H01 60-62	0.60	666	1303	205	0	182	10
01H01 85-87	0.85	433	1772	297	0	156	0
01H01 110-112	1.10	586	1998	369	0	149	18
01H01 135-137	1.35	1082	339	493	0	106	25
01H02 12-14	1.62	1552	511	595	0	219	42
01H02 35-37	1.85	400	2007	57	21	36	0
01H02 60-62	2.10	225	3516	0	0	174	0
01H02 85-87	2.35	146	2704	30	0	128	0
01H02 110-112	2.60	416	3170	131	0	188	13
01H02 135-137	2.85	437	1849	103	0	137	0
01H03 13-15	3.13	213	2621	0	0	210	10
01H03 35-37	3.35	146	2228	57	0	156	10
01H03 60-62	3.60	520	2581	270	0	199	12
01H03 85-87	3.85	250	2162	0	0	67	10
01H03 110-112	4.10	392	2884	0	0	207	14
01H03 135-137	4.35	320	2116	0	0	144	0
01H04 11-13	4.61	249	1927	205	0	177	0
01H04 35-37	4.85	365	894	223	0	130	0
01H04 60-62	5.10	502	2061	0	0	306	0
01H04 85-87	5.35	369	1421	77	0	123	0
01H04 110-112	5.60	576	2314	0	0	102	21
02H01 09-11	5.89	174	1498	0	0	146	0
02H01 60-62	6.40	353	1866	0	0	164	10
02H01 85-87	6.65	303	2162	143	0	166	0
02H01 110-112	6.90	882	1544	0	0	137	0
02H01 135-135	7.15	543	740	170	0	79	16
02H02 09-11	7.39	576	2237	334	0	109	18
02H02 35-37	7.65	610	2304	187	0	180	25
02H02 85-87	8.15	1325	1163	388	0	557	0
02H02 110-112	8.40	458	2830	0	0	71	0
02H03 12-14	8.92	246	3069	0	0	177	0
02H03 60-62	9.40	424	2172	0	0	100	10
02H03 110-112	9.90	331	1772	0	0	207	0
02H03 135-137	10.15	342	2601	0	0	210	0
02H04 09-11	10.39	353	2372	0	0	222	10
02H04 35-37	10.65	286	1608	103	0	213	0
02H04 60-62	10.90	404	2134	0	0	119	15
02H04 85-87	11.15	353	1689	90	0	151	10
02H04 110-112	11.40	412	2007	334	0	276	0
02H04 135-137	11.65	361	1521	0	0	213	0
02H05 09-11	11.89	488	2209	205	0	169	22
02H05 35-37	12.15	44	1927	0	0	96	23
02H05 60-62	12.40	486	2430	0	0	182	10
02H05 85-87	12.65	615	1624	223	0	139	0
02H05 110-112	12.90	475	801	0	0	67	40
02H05 135-137	13.15	400	1362	97	0	142	10
02H06 09-11	13.39	778	2153	0	0	139	40
02H06 35-37	13.65	671	2107	97	36	44	26
02H06 60-62	13.90	973	1858	159	0	100	19
02H06 85-87	14.15	269	2098	210	0	159	15
02H06 110-112	14.40	253	2258	420	0	306	14
02H07 35-37	15.15	595	2830	0	0	112	0

03H01	10-12	15.40	228	1840	70	0	156	0
03H01	35-37	15.65	400	2621	0	0	121	0
03H01	60-62	15.90	357	1722	123	0	119	16
03H01	85-87	16.15	529	2052	169	0	228	23
04H01	10-12	24.90	128	2294	150	0	92	0
04H01	35-37	25.15	361	3102	0	0	253	0
04H01	85-87	25.65	331	2809	0	0	234	0
04H01	110-112	25.90	219	2025	123	0	106	0
04H01	135-137	26.15	380	2959	0	0	85	0
04H02	10-12	26.40	256	2190	83	0	64	0
04H02	35-37	26.65	458	2490	0	0	90	14
04H02	60-62	26.90	635	1190	277	0	85	15
04H02	85-87	27.15	511	2480	0	0	132	12
04H02	110-112	27.40	484	1552	216	0	106	0
04H02	135-137	27.65	681	2591	0	0	58	14
04H03	10-12	27.90	121	2381	83	0	59	0
04H03	35-37	28.15	346	2510	0	0	86	0
04H03	60-62	28.40	231	2362	0	0	72	0
04H03	85-87	28.65	433	2905	0	0	159	0
04H03	110-112	28.90	256	1989	0	0	85	0
04H03	135-137	29.15	289	2970	0	0	100	14
04H04	10-12	29.40	317	2144	90	0	92	0
04H04	35-37	29.65	416	1089	215	0	196	0
04H04	60-62	29.90	137	1875	0	0	83	0
04H04	85-87	30.15	350	3014	0	0	146	0
04H04	110-112	30.40	590	1076	0	0	159	0
04H04	135-137	30.65	515	2440	0	0	172	0
04H05	10-12	30.90	488	1600	183	0	139	12
04H05	35-37	31.15	640	784	534	0	335	0
04H05	60-62	31.40	433	1592	424	0	44	0
04H05	85-87	31.65	303	2841	0	0	104	0
04H05	110-112	31.90	416	1815	330	0	98	10
04H05	135-137	32.15	590	3170	0	0	96	10
04H06	10-12	32.40	234	1901	0	0	31	0
04H06	35-37	32.65	253	3249	0	0	69	0
04H06	85-87	33.15	286	2632	0	0	49	12
04H06	112-114	33.42	445	2372	0	0	72	14
04H06	135-137	33.65	392	2490	0	67	272	0
04H07	10-12	33.90	204	2144	0	0	17	0
04H07	35-37	34.15	576	1544	0	0	372	0
05H01	10-12	34.40	279	2938	0	0	108	10
05H01	35-37	34.65	310	992	296	0	253	0
05H01	60-62	34.90	424	2256	0	0	166	14
05H01	86-88	35.16	484	713	600	0	240	0
05H01	135-137	35.65	369	2314	0	0	94	0
05H02	10-12	35.90	292	2663	260	0	117	15
05H02	60-62	36.40	412	2125	303	0	219	0
05H02	109-111	36.89	635	1109	0	0	228	10
05H02	135-137	37.15	256	2460	297	0	58	0
05H03	10-12	37.40	317	3329	0	0	144	0
05H03	34-36	37.64	190	2694	0	0	53	0
05H03	135-137	38.65	77	3014	102	0	74	0
05H04	34-36	39.14	169	3636	0	0	53	0
05H04	60-62	39.40	234	2190	310	0	85	0
05H04	86-88	39.66	282	3564	0	0	102	0
05H04	135-137	40.15	193	2959	0	45	156	0
05H05	60-62	40.90	234	2540	0	58	156	10
05H05	86-88	41.16	441	2852	104	56	156	15
05H05	110-112	41.40	292	2884	77	36	177	0

05H05	135-137	41.65	137	2237	317	0	83	0
05H06	10-12	41.90	202	1122	169	0	296	0
05H06	34-36	42.14	137	2256	370	0	114	0
05H06	60-62	42.40	339	1756	204	0	199	12
05H06	137-139	43.17	480	1406	353	0	253	0
05H07	10-12	43.40	190	1369	370	0	110	0
05H07	34-36	43.64	282	3387	0	45	76	0
05H07	60-62	43.90	137	3600	0	22	28	0
06H01	10-12	43.90	77	2209	450	0	45	13
06H01	35-37	44.15	445	1998	0	72	335	0
06H01	60-62	44.40	630	2144	470	0	85	0
06H01	85-87	44.65	424	1714	0	64	433	0
06H01	110-112	44.90	123	2247	403	0	98	0
06H01	135-137	45.15	219	3469	0	0	62	0
06H02	10-12	45.40	135	1225	343	0	90	0
06H02	35-37	45.65	117	2470	0	34	182	0
06H02	60-62	45.90	292	1490	370	0	199	0
06H02	85-87	46.15	182	2632	0	42	190	0
06H02	110-112	46.40	388	1089	523	96	240	0
06H03	35-37	47.15	361	1892	0	40	185	10
06H03	60-62	47.40	253	1490	363	0	83	0
06H03	85-87	47.65	272	1624	159	0	166	0
06H03	110-112	47.90	299	1325	683	0	324	0
07H01	35-37	53.65	471	1706	353	0	256	0
07H01	60-62	53.90	534	949	303	0	166	0
07H01	85-87	54.15	339	1136	253	0	182	10
07H01	110-112	54.40	671	729	529	0	219	0
07H01	135-137	54.65	610	1056	272	53	164	23
07H02	10-12	54.90	571	1129	454	0	204	30
07H02	35-37	55.15	992	1560	353	0	225	0
07H02	60-62	55.40	635	824	484	0	237	0
07H02	85-87	55.65	1109	1714	342	0	188	0
07H02	110-112	55.90	801	1354	376	0	182	22
07H02	135-137	56.15	328	1183	392	94	253	0
07H03	10-12	56.40	342	942	650	36	259	0
07H03	35-37	56.65	353	1142	692	0	306	0
07H03	60-62	56.90	296	1149	289	0	199	0
07H03	85-87	57.15	296	1632	303	0	303	0
07H03	110-112	57.40	445	1069	253	0	196	0
07H03	135-137	57.65	778	942	339	0	166	0
07H04	10-12	57.90	445	1239	253	0	177	10
07H04	35-37	58.15	342	1102	894	88	45	0
07H04	60-62	58.40	676	1122	320	0	172	18
07H04	85-87	58.65	467	1722	458	0	299	0
07H04	110-112	58.90	313	1163	437	0	228	0
07H04	135-137	59.15	388	1122	493	164	45	0
07H05	10-12	59.40	339	1190	458	0	253	0
07H05	35-37	59.65	795	876	412	0	269	0
07H05	60-62	59.90	306	745	475	0	237	0
07H05	85-87	60.15	449	1211	449	100	234	0
07H05	110-112	60.40	353	918	400	106	231	0
07H05	135-137	60.65	272	1600	384	59	313	0
07H06	10-12	60.90	313	1122	313	146	256	0
07H06	35-37	61.15	231	1406	552	237	303	0
07H06	60-62	61.40	237	955	317	117	213	0
07H06	85-87	61.65	847	1197	396	0	188	21
07H06	110-112	61.90	292	1183	328	104	216	0
07H06	135-137	62.15	625	1232	640	49	320	0
07H07	10-12	62.40	292	853	502	66	202	0

07H07	35-37	62.65	292	1697	343	193	237	0
08H01	35-37	63.15	369	1362	0	139	292	0
08H01	60-62	63.40	289	1421	480	292	384	0
08H01	85-87	63.65	296	756	610	72	365	0
08H01	110-112	63.90	306	1296	339	139	269	0
08H01	135-137	64.15	1096	1116	433	41	299	0
08H02	10-12	64.40	324	1452	0	313	400	0
08H02	35-37	64.65	497	1018	467	59	262	0
08H02	60-62	64.90	566	1197	445	79	276	0
08H02	85-87	65.15	234	1369	310	146	207	0
08H02	110-112	65.40	392	1156	595	94	279	0
08H02	135-137	65.65	320	980	404	38	256	0
08H03	10-12	65.90	497	1136	557	534	342	0
08H03	110-112	66.90	697	1332	534	159	272	0
08H04	10-12	67.40	571	1722	445	190	292	0
08H04	35-37	67.65	282	778	506	190	276	0
08H04	60-62	67.90	471	1325	724	110	231	10
08H04	85-87	68.15	462	1296	210	137	225	15
08H04	110-112	68.40	159	1325	310	296	342	0
08H04	135-137	68.65	317	1225	217	64	151	10
08H05	10-12	68.90	600	1253	261	38	262	0
08H05	35-37	69.15	246	1246	283	146	149	10
08H05	60-62	69.40	331	1436	297	142	266	10
08H05	85-87	69.65	784	986	299	0	146	0
08H05	110-112	69.90	773	870	299	0	132	0
08H05	135-137	70.15	365	1011	0	85	151	0
08H06	10-12	70.40	396	1513	306	250	266	0
08H06	35-37	70.65	204	847	230	94	146	0
08H06	60-62	70.90	234	1136	278	98	213	0
08H06	85-87	71.15	376	1076	237	100	190	11
08H06	110-112	71.40	361	1429	380	59	250	0
08H06	135-137	71.65	243	1163	250	37	225	0
08H07	10-12	71.90	369	1376	331	128	262	0
08H07	35-37	72.15	384	1129	445	52	256	10
09H01	09-11	72.39	376	1037	620	0	303	0
09H01	35-37	72.65	396	1018	213	41	149	10
09H01	60-62	72.90	502	1384	320	64	213	0
09H01	85-87	73.15	475	676	424	45	188	0
09H01	110-112	73.40	552	894	600	48	188	0
09H01	135-137	73.65	320	835	424	0	199	0
09H02	09-11	73.89	650	1082	702	0	339	0
09H02	35-37	74.15	250	756	353	0	185	0
09H02	60-62	74.40	342	961	645	0	286	0
09H02	85-87	74.65	497	778	557	35	222	0
09H02	110-112	74.90	534	906	645	0	279	10
09H02	135-137	75.15	475	847	713	0	225	14
09H03	09-11	75.40	342	930	1005	0	350	0
09H03	35-37	75.65	216	467	552	0	180	0
09H03	60-62	75.90	620	973	961	0	376	0
09H03	85-87	76.15	1156	605	310	0	104	4
09H03	110-112	76.40	441	912	812	0	306	0
09H03	135-137	76.65	346	697	835	0	259	0
09H04	09-11	76.89	835	773	655	0	225	0
09H04	35-37	77.15	269	630	734	0	253	0
09H04	60-62	77.40	548	751	1018	0	55	0
09H04	85-87	77.65	289	562	640	44	219	0
09H04	110-112	77.90	324	745	942	0	324	0
09H05	09-11	78.39	80	973	762	0	361	16
09H05	35-37	78.65	282	740	433	0	202	0

09H05	60-62	78.90	445	767	625	0	306	10
09H05	85-87	79.15	392	900	605	0	234	0
09H05	110-112	79.40	520	1354	534	0	234	0
09H05	135-137	79.65	237	1980	290	0	104	0
09H06	09-11	79.89	441	2285	0	0	88	0
09H06	35-37	80.15	335	1954	0	0	104	0
09H06	60-62	80.40	384	1756	306	0	172	11
09H06	85-87	80.65	660	1521	296	42	262	12
09H06	110-112	80.90	534	2134	0	0	161	0
09H06	135-137	81.15	529	1197	433	0	104	20
09H07	09-11	81.40	571	1673	404	0	169	11
09H07	35-37	81.65	286	1232	376	0	151	10
09H07	60-62	81.89	237	1632	123	0	117	0
10H01	09-11	81.90	416	1998	310	0	151	0
10H01	35-37	82.15	213	1739	0	0	96	0
10H01	60-62	82.40	328	2107	0	0	79	0
10H01	85-87	82.65	480	1815	0	0	119	18
10H01	110-112	82.90	635	1030	276	0	137	12
10H01	135-137	83.15	488	1076	243	0	121	10
10H02	09-11	83.39	515	1505	0	0	123	21
10H02	35-37	83.65	360	1399	373	0	98	10
10H02	60-62	83.90	1050	686	269	0	123	27
10H02	85-87	84.15	784	1399	257	0	104	0
10H02	110-112	84.40	1056	1624	215	0	119	23
10H02	135-137	84.65	751	1347	217	0	117	21
10H03	09-11	84.90	924	1414	276	0	128	10
10H03	35-37	85.15	543	1340	289	0	146	14
10H03	60-62	85.39	697	1122	276	0	149	22
10H03	85-87	85.65	199	1697	130	0	61	0
10H03	110-112	85.90	595	918	1142	0	207	0
10H03	135-137	86.15	246	702	713	0	237	0
10H04	09-11	86.39	1183	586	350	0	102	28
10H04	35-37	86.65	504	671	529	0	110	0
10H04	60-62	86.90	980	605	104	0	40	24
10H04	85-87	87.15	955	524	0	0	32	49
10H04	110-112	87.40	262	1289	3047	0	246	0
10H04	135-137	87.65	724	767	778	0	228	10
10H05	09-11	87.89	306	520	424	0	151	0
10H05	35-37	88.15	992	458	269	0	67	38
10H05	60-62	88.40	369	718	2391	0	182	0
10H05	85-87	88.65	801	702	681	0	169	10
10H05	110-112	88.90	590	807	640	0	231	0
10H05	135-137	89.15	676	1063	137	0	83	10
10H06	09-11	89.40	718	1163	196	0	98	12
10H06	35-37	89.65	853	1170	219	37	119	22
10H06	60-62	89.90	346	762	625	0	272	0
10H06	85-87	90.15	484	824	350	0	123	0
10H06	110-112	90.40	188	801	600	0	219	0
10H06	135-137	90.65	520	1568	163	0	102	0
10H07	09-11	90.89	595	1892	0	0	72	0
10H07	35-37	91.15	615	1849	117	0	66	18
10H07	60-62	91.40	279	973	506	0	256	0
11H01	10-12	91.40	299	2520	0	0	159	0
11H01	35-37	91.65	310	2172	0	0	100	0
11H01	60-62	91.90	718	1747	261	137	196	0
11H01	85-87	92.15	313	1756	0	76	64	15
11H01	110-112	92.40	357	2034	0	62	86	10
11H01	135-137	92.65	416	1936	0	67	88	0
11H02	35-37	93.15	462	2372	0	81	102	0

11H02	64-66	93.44	807	924	625	104	193	0
11H02	110-112	93.90	999	1076	645	0	269	24
11H03	10-12	94.40	681	778	807	0	256	0
11H03	35-37	94.65	151	894	841	0	276	0
11H03	110-112	95.40	497	2070	0	41	144	0
11H03	135-137	95.65	566	1459	325	44	161	18
11H04	10-12	95.90	437	1384	183	0	117	10
11H04	35-37	96.15	1197	801	286	0	119	31
11H04	64-66	96.44	681	1325	230	0	177	12
11H04	110-112	96.90	697	1731	103	21	128	11
11H04	135-137	97.15	784	1176	224	0	130	19
11H05	10-12	97.40	671	1391	219	299	156	14
11H05	35-37	97.65	493	1681	150	0	161	0
11H05	64-66	97.94	751	1781	130	56	146	10
11H05	85-87	98.15	1011	1731	0	52	144	0
11H05	110-112	98.40	847	1289	117	0	102	14
11H05	135-137	98.65	762	1176	0	49	119	12
11H06	10-12	98.90	790	1303	177	31	100	21
11H06	35-37	99.15	600	1050	369	0	237	0
11H06	64-66	99.44	708	1340	467	56	156	14
11H06	85-87	99.65	543	1399	159	0	123	19
11H06	110-112	99.90	467	1544	243	0	154	0
11H06	135-137	100.15	380	2237	0	0	190	0
11H07	10-12	100.40	256	1109	0	0	117	0
11H07	35-37	100.65	581	1340	0	0	59	10
12H01	10-12	100.90	692	767	246	0	123	27
12H01	36-36	101.16	858	1109	303	0	98	14
12H01	61-63	101.41	600	1354	163	0	117	22
12H01	111-113	101.91	475	2088	177	0	231	0
12H01	136-138	102.16	876	1069	282	0	299	19
12H02	10-12	102.40	1296	967	217	0	225	0
12H02	36-38	102.66	353	2088	0	32	112	10
12H02	61-63	102.91	876	1714	283	83	202	26
12H02	111-113	103.41	1063	882	331	64	188	15
12H02	136-138	103.66	524	1116	310	202	213	0
12H03	10-12	103.90	745	1069	1918	0	106	21
12H03	36-38	104.16	400	1414	283	41	151	0
12H03	136-138	105.16	671	1325	203	0	161	14
12H04	10-12	105.40	734	1681	83	0	88	25
12H04	36-38	105.88	640	1384	190	0	77	0
12H05	136-138	108.16	756	1082	383	243	306	0
12H06	36-38	108.88	745	1592	150	0	66	35
12H06	61-63	108.91	480	1318	97	67	117	10
12H06	111-113	109.41	428	1024	660	121	253	0
12H06	136-138	109.66	595	1731	283	35	77	0
13H01	10-12	110.40	847	751	346	0	137	10
13H02	60-62	112.40	511	864	458	0	156	0
13H04	35-37	115.15	506	784	412	0	128	10
13H05	69-62	116.90	835	784	299	0	125	25
13H05	135-137	117.65	924	697	408	0	151	20
13H06	10-12	117.90	1232	380	207	0	67	37
13H06	35-37	118.15	835	713	246	0	94	27
13H06	60-62	118.40	406	841	0	0	58	55
13H06	110-112	118.90	1030	650	230	0	50	30
13H07	60-62	119.90	671	117	77	0	104	14

Peak heights (counts) can be converted into semi-quantitative mineral abundances using the calibration curves listed at the back of Appendix C.

Table C.5. XRD peak heights (counts) for selected minerals in Hole 823B samples

Sample Code	Depth (mbsf)	Quartz	Low Mg Calcite	High Mg Calcite	Dolomite	Aragonite	Chlorite/ Kaolinite
12H01 50-52	103.80	529	1452	114	0	144	0
12H02 50-52	105.30	437	2034	68	182	121	40
12H03 50-52	106.80	595	1681	55	0	86	72
12H04 50-52	108.30	400	2581	68	0	69	0
12H05 50-52	109.80	219	1037	955	119	328	53
12H06 50-52	111.30	949	1369	784	0	204	44
12H07 50-52	112.80	511	1901	68	0	112	56
13X01 50-52	113.30	610	708	795	0	240	92
13X02 50-52	114.80	506	762	1176	0	216	0
13X03 50-52	116.30	449	870	615	0	240	0
13X04 50-52	117.80	666	1656	278	53	144	53
13X05 50-52	119.30	445	1429	292	0	96	0
13X06 50-52	120.80	595	1798	412	0	213	66
14X01 50-52	122.90	529	1927	134	0	151	53
14X02 50-52	124.40	396	1347	441	0	185	49
14X03 50-52	125.90	864	1246	68	0	58	132
14X04 50-52	127.40	506	686	695	0	216	0
14X05 50-52	128.90	548	488	213	0	71	0
14X06 50-52	130.40	1156	1005	234	0	139	69
15X01 48-50	132.58	660	1436	416	0	159	62
15X02 48-50	134.08	882	1183	365	0	193	64
15X03 48-50	135.58	882	1340	286	0	159	98
15X04 48-50	137.08	620	2372	28	0	117	61
15X05 48-5-	138.58	773	1037	237	0	151	79
15X06 48-50	140.08	762	1399	134	50	58	74
16X02 50-52	143.70	692	2116	88	0	125	59
16X03 50-52	145.20	484	1376	292	0	135	64
16X05 50-52	148.20	882	1089	234	0	104	104
16X06 50-52	149.70	992	1490	147	0	149	79
16X07 50-52	151.20	475	1576	68	0	64	55
17X01 50-52	151.90	471	1576	147	0	154	41
17X04 50-52	156.40	357	2107	161	0	74	37
18X01 50-52	161.60	734	1640	320	0	142	58
18X04 50-52	166.10	729	1910	292	0	108	46
18X05 50-52	167.60	234	2209	0	0	18	36
18X06 50-52	169.10	818	1421	0	0	10	110
19X01 50-52	171.30	692	1303	595	0	207	67
19X02 50-52	172.80	615	1954	0	0	94	61
19X03 50-52	174.30	1011	1239	0	0	26	88
19X04 50-52	175.80	702	1731	202	0	117	66
19X05 50-52	177.30	708	2162	0	0	42	0
19X06 50-52	178.80	454	2560	0	0	74	72
20X01 50-52	181.00	437	2016	278	0	112	74
20X02 50-52	182.50	497	1063	0	0	25	67
20X04 50-52	185.50	900	1892	213	0	106	49
21X01 50-52	190.70	219	1918	147	0	104	0
21X02 50-52	192.20	515	2043	0	0	31	56
21X03 50-52	193.70	380	1875	0	0	0	0
21X04 50-52	195.20	666	2043	0	52	0	74
21X05 50-52	196.70	428	2247	0	69	10	169
21X06 50-52	198.20	595	2079	0	357	61	37

22X01 49-51	200.29	713	1689	260	0	135	48
22X02 49-51	201.79	906	1136	353	0	169	135
22X04 45-47	204.75	234	2916	0	35	0	25
22X06 62-64	207.92	497	1858	0	25	45	42
23X01 55-57	209.65	605	1624	0	35	38	58
23X02 55-57	211.15	346	2134	0	110	81	0
23X03 55-57	212.65	445	2052	0	50	52	45
23X04 55-57	214.15	484	1936	0	71	135	71
23X06 55-57	217.15	416	1789	0	45	40	44
24X01 55-57	219.25	660	1722	0	55	26	42
24X02 55-57	220.75	630	1600	0	81	41	45
24X03 58-60	222.28	708	1798	0	85	86	69
24X04 55-57	223.75	1170	1225	0	0	159	108
24X05 55-57	225.25	515	2905	0	0	23	740
25X01 58-60	228.58	906	1616	0	0	231	88
25X02 58-60	230.08	581	2275	0	0	112	56
25X03 58-60	231.58	1384	1122	534	0	253	144
25X04 58-60	233.08	506	2401	0	0	76	48
25X05 58-60	234.58	824	955	751	0	81	72
25X06 58-60	236.08	1568	1253	253	0	88	94
26X01 56-58	238.26	445	2391	0	0	38	36
26X02 56-58	239.76	534	2209	0	0	59	53
26X03 56-58	241.26	524	2266	161	0	106	42
26X04 56-58	242.76	515	2352	0	0	31	52
26X05 56-58	244.26	253	2601	187	0	31	0
26X06 60-62	245.80	437	2725	0	0	58	38
27X01 50-52	247.80	538	2025	0	0	61	58
27X02 50-52	248.52	702	1513	0	0	69	32
27X03 50-52	250.02	590	1673	220	0	139	64
27X04 50-52	251.52	384	2381	0	0	20	49
27X05 50-52	253.02	1011	1945	161	0	123	38
27X07 50-52	256.02	538	2540	134	0	106	42
28X01 51-52	257.51	369	2611	0	0	24	58
28X02 51-52	259.01	392	2460	0	114	21	85
28X03 51-52	260.51	497	2560	0	0	0	69
28X04 51-52	262.01	416	2314	0	0	12	49
28X05 51-52	263.51	256	2401	0	0	30	41
28X06 51-52	264.95	228	2352	0	0	0	0
29X01 50-52	267.20	420	2777	0	0	37	49
29X02 50-52	268.70	484	2323	0	0	45	67
29X03 50-52	270.20	506	2362	75	0	92	61
29X04 55-57	271.75	289	2352	0	0	32	28
29X05 55-57	273.27	630	2304	0	0	15	86
29X06 57-59	274.77	493	2440	0	0	110	42
30X01 65-67	276.95	306	2314	0	0	10	34
30X02 65-67	278.45	253	2788	0	0	24	0
30X04 72-74	281.52	488	2079	0	0	59	55
30X06 61-63	284.41	388	2125	0	0	31	45
31X02 62-64	287.18	702	2520	0	0	100	61
31X04 56-58	290.12	562	1764	0	0	77	46
31X06 66-68	293.22	342	2352	0	0	26	37
31X07 82-84	294.88	193	2550	0	0	0	0
32X01 70-72	296.30	207	2621	0	0	10	0
32X02 70-72	297.80	282	2025	0	0	27	0
32X04 70-72	300.80	493	1747	0	0	0	34
32X06 70-72	303.80	404	2381	0	0	0	0
33X01 70-72	306.00	125	2809	0	71	0	102
33X03 70-72	309.00	841	1102	0	0	26	20

33X04 67-69	310.47	243	2663	0	0	0	0
33X05 67-69	311.97	117	2323	0	18	0	0
33X06 65-67	313.45	81	1918	0	0	0	0
34X01 70-72	315.60	132	2247	0	14	0	0
34X02 70-72	317.10	361	2530	0	0	27	28
34X03 70-72	318.60	433	2162	0	0	0	29
34X04 70-72	320.10	292	2591	0	0	0	0
34X05 70-72	321.60	225	2959	0	0	0	32
34X06 70-72	323.10	339	2570	0	0	0	64
35X01 50-52	325.10	524	1806	0	0	66	0
35X02 50-52	326.60	135	2746	0	58	0	38
35X03 50-52	328.10	339	2391	0	0	0	0
35X04 50-52	329.60	196	2304	0	28	0	161
35X05 50-52	331.10	246	2079	0	0	10	30
35X06 50-52	332.60	320	2581	0	0	13	67
35X07 50-52	334.10	524	1892	0	0	0	20
36X01 50-52	334.70	213	1681	0	0	0	44
36X02 50-52	336.20	219	2237	0	0	0	0
36X03 53-55	337.73	282	2591	0	139	0	0
36X04 50-52	339.20	1076	2767	0	0	0	0
36X05 50-52	340.70	234	2830	0	0	0	0
36X06 51-53	342.21	137	3147	0	0	0	0
37X01 50-52	344.40	515	2228	0	41	0	0
37X02 50-52	345.90	259	2430	0	0	0	0
37X03 50-52	347.40	645	1832	0	0	35	123
37X04 50-52	348.90	79	1429	0	0	0	79
37X05 50-52	350.40	172	2884	0	0	0	23
37X06 50-52	351.90	292	3147	0	0	0	37

XRD Peak heights (counts above background) can be converted into semi-quantitative mineral abundances using the calibration curves presented in the back of Appendix C (Figures I to V).

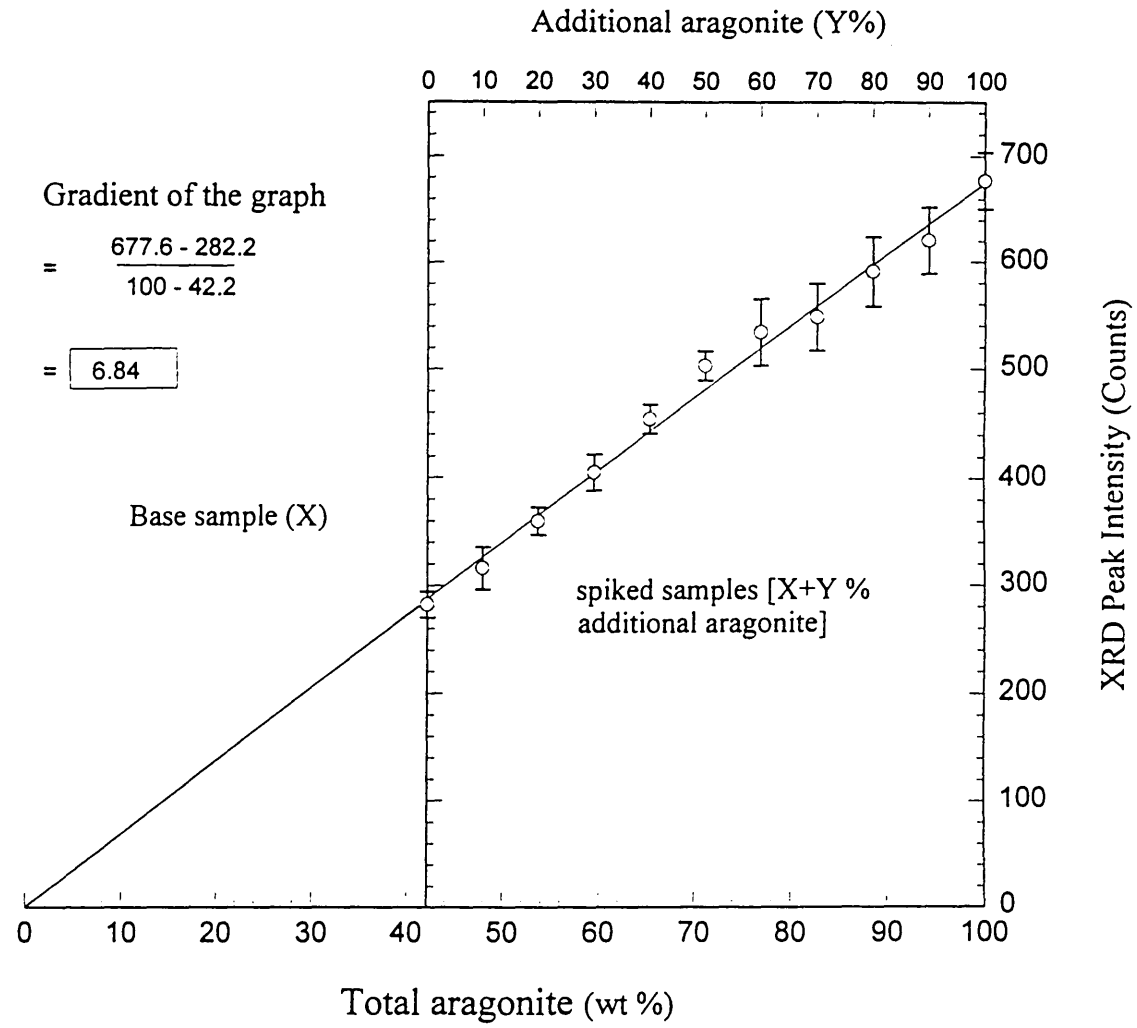

Additional aragonite (wt.%)

Peak height (counts)											
	293	331	358	392	459	489	537	543	566	626	628
	268	320	363	410	435	486	551	508	590	646	678
	281	331	365	402	483	511	545	557	584	596	658
	281	304	337	435	448	500	569	554	560	562	671
	268	300	354	412	459	503	500	575	565	614	681
	306	262	358	417	433	494	569	520	554	639	694
	300	320	354	412	462	483	497	563	578	581	642
	278	320	356	385	451	500	511	599	621	605	671
	275	311	354	395	462	508	503	551	554	633	700
	283	283	373	415	469	525	506	514	602	665	652
	289	293	365	415	459	478	478	508	604	576	655
	268	322	335	381	438	497	543	593	580	655	717
	264	340	382	407	443	528	514	525	621	593	670
	283	322	358	392	475	508	503	511	608	602	684
	278	317	358	415	454	514	548	593	524	665	652
	277	326	377	422	459	525	587	528	595	614	681
	275	337	347	363	441	500	560	578	655	617	678
	277	333	385	407	446	511	578	590	646	681	731
	296	308	356	397	464	501	557	551	621	615	688
	304	337	358	425	443	511	545	518	602	633	721
Mean	282.2	315.9	359.7	405.0	454.2	503.7	535.1	549.0	591.5	620.9	677.6
SD	12.2	19.8	12.8	16.88	13.4	13.8	31.2	31.4	32.7	37.8	26.5

Figure C.1. XRD calibration data and graph for aragonite. Aragonite peak heights (counts) measured at 33.16 2θ degrees, for samples collected at Sites 819 and 823 were converted into absolute values (weight %) by dividing the XRD counts by the gradient of the calibration graph (i.e., 6.84). Error bars indicate standard deviation (SD) of the mean for additional proportions of aragonite.

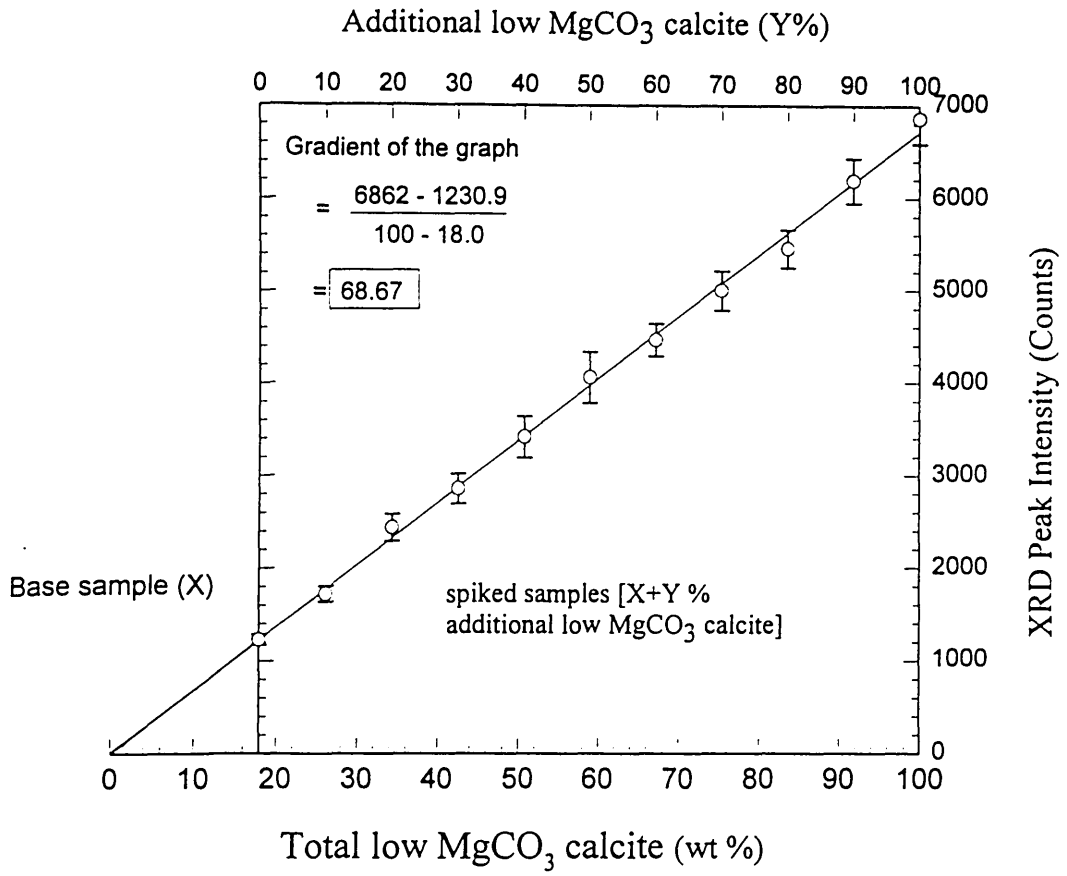

Additional low $MgCO_3$ calcite (wt.%)

Peak height (counts)

	1300	1730	2222	3037	3169	3709	4481	4934	5263	6281	6879
	1278	1669	2400	2743	3724	4432	4532	5137	5678	6364	7141
	1238	1710	2414	2976	2848	4090	4452	4978	5300	6284	6435
	1264	1659	2525	3044	3427	4271	4507	4961	5810	6314	6890
	1230	1593	2582	3017	3574	3732	4259	4873	5102	6413	6862
	1200	1788	2222	2691	3304	3801	4471	5040	5591	6079	6903
	1203	1783	2187	2633	3150	3847	4692	5155	5418	6294	7130
	1114	1762	2317	2841	3544	3980	4300	5327	5254	6205	6726
	1273	1825	2361	3134	3536	4306	4498	5281	5715	5963	7120
	1156	1679	2433	2928	3529	3839	4590	4978	5409	6102	6860
	1238	1720	2495	2769	3204	3785	4473	4726	5301	6523	6870
	1238	1694	2426	2736	3492	3980	4667	4675	5445	6493	6354
	1238	1730	2451	2815	3717	4186	4565	5455	5308	6164	6382
	1359	1590	2451	2601	3211	3940	4194	5111	5608	5819	7183
	1247	1938	2544	2749	3204	4390	4162	5058	5678	6534	6932
	1256	1809	2698	2981	3574	3679	4709	4735	5381	5744	7268
	1182	1767	2457	2627	3589	4035	4590	5093	5464	6403	6914
	1243	1767	2359	2996	3551	4114	4138	4692	5227	6011	7109
	1131	1730	2582	2963	3463	4574	4587	4859	5327	6103	6473
	1230	1612	2730	2901	3515	4457	4333	4877	5791	5763	6808
Mean	1230.9	1727.8	2442.8	2859.1	3416.3	4057.4	4460.0	4997.3	5453.5	6192.8	6862.0
SD	56.6	83.9	145.5	159.3	222.9	274.8	173.9	213.4	204.8	242.9	271.4

Figure C.2. XRD calibration data and graph for low $MgCO_3$ calcite. Low $MgCO_3$ calcite peak heights (counts) measured at 29.40 2θ degrees, for samples collected at Sites 819 and 823, were converted into absolute values (wt %) by dividing the by dividing the XRD counts by the gradient of the calibration graph (i.e., 68.67). Error bars indicate standard deviation of the mean for additional amounts of low $MgCO_3$ calcite.

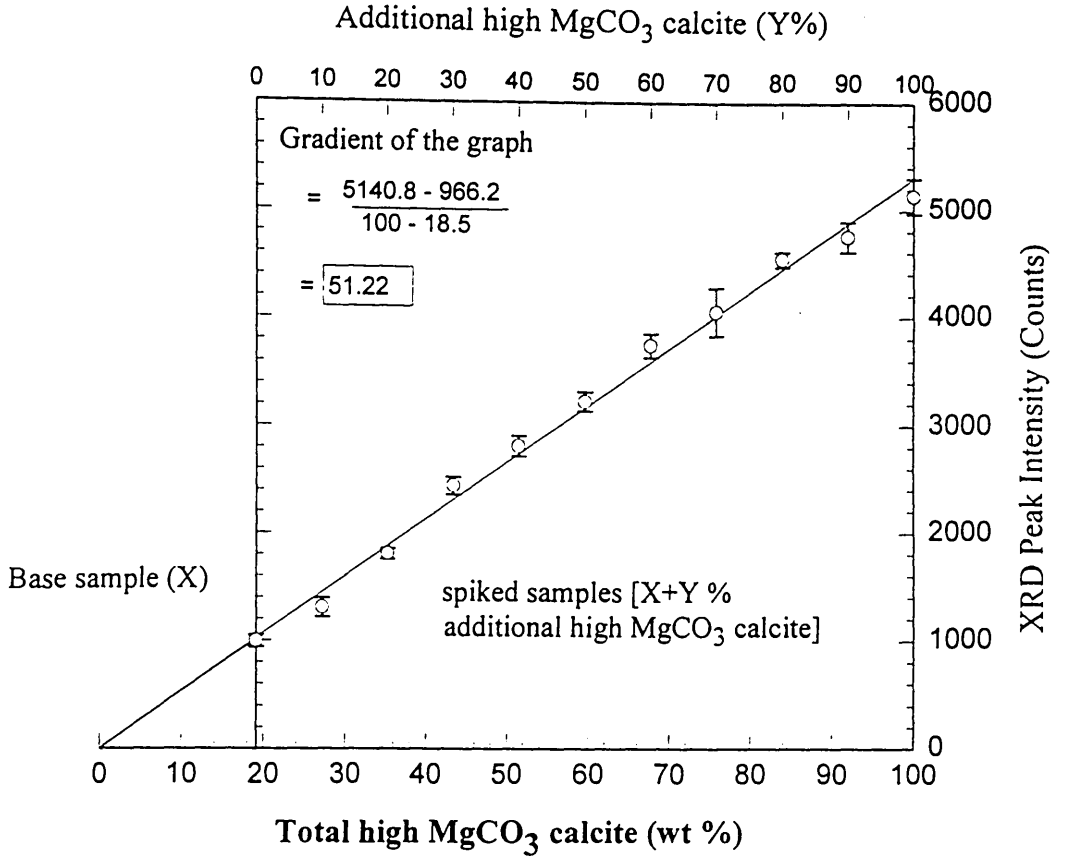

Additional high $MgCO_3$ calcite (wt.%)

Peak height (counts)	0	10	20	30	40	50	60	70	80	90	100
	999	1252	1789	2450	2704	3238	3856	4264	4597	4775	4706
	1006	1332	1892	2541	2788	3125	3807	4109	4516	4900	5170
	1011	1391	1866	2500	2746	3341	3795	3894	4543	5013	5184
	980	1316	1747	2314	2894	3170	3700	3931	4422	4556	5055
	1018	1429	1884	2440	2862	3181	3856	4020	4502	4844	5271
	1050	1296	1789	2411	2820	3204	3446	4212	4422	4516	5242
	1011	1347	1731	2391	2788	3272	3672	4083	4692	4928	5170
	967	1459	1800	2450	2684	3295	3721	4277	4556	4692	4950
	960	1340	1731	2495	2852	3069	3733	4122	4436	4900	5001
	967	1170	1815	2440	2970	3249	3648	4109	4570	4751	5015
	1018	1300	1789	2372	2777	3422	3832	4369	4560	4956	5112
	1082	1310	1892	2450	2852	3192	3807	4160	4543	4775	5300
	1122	1318	1798	2421	2673	3058	3660	3711	4626	4802	5402
	964	1282	1781	2391	2761	3203	3969	4212	4462	4583	4958
	894	1176	1756	2381	2820	3238	3684	4343	4543	4638	5358
	1030	1211	1832	2323	2970	3216	3733	4096	4597	4740	5084
	864	1303	1781	2652	2823	3329	3672	3794	4529	4706	5227
	1002	1475	1815	2570	2663	3226	3844	4173	4597	4775	5141
	982	1136	1858	2401	2981	3192	3709	3624	4597	4583	5141
	996	1331	1790	2352	2798	3318	3788	3660	4568	4665	5329
Mean	966.2	1308.7	1806.8	2437.3	2811.3	3226.9	3746.6	4058.2	4543.9	4754.9	5140.8
SD	56.8	90.5	50.1	83.3	94.7	88.7	109.7	221.5	69.8	140.4	165.4

Figure C.3. XRD calibration data and graph for high $MgCO_3$ calcite. High $MgCO_3$ calcite peak heights (counts) measured between 29.4 and 30.4 2θ degrees, for samples collected at Sites 819 and 823, were converted into absolute values (weight %) by dividing the XRD peak counts by the gradient of the graph (i.e., 51.22). Error bars indicate the standard deviation of the mean for additional amounts of high $MgCO_3$.

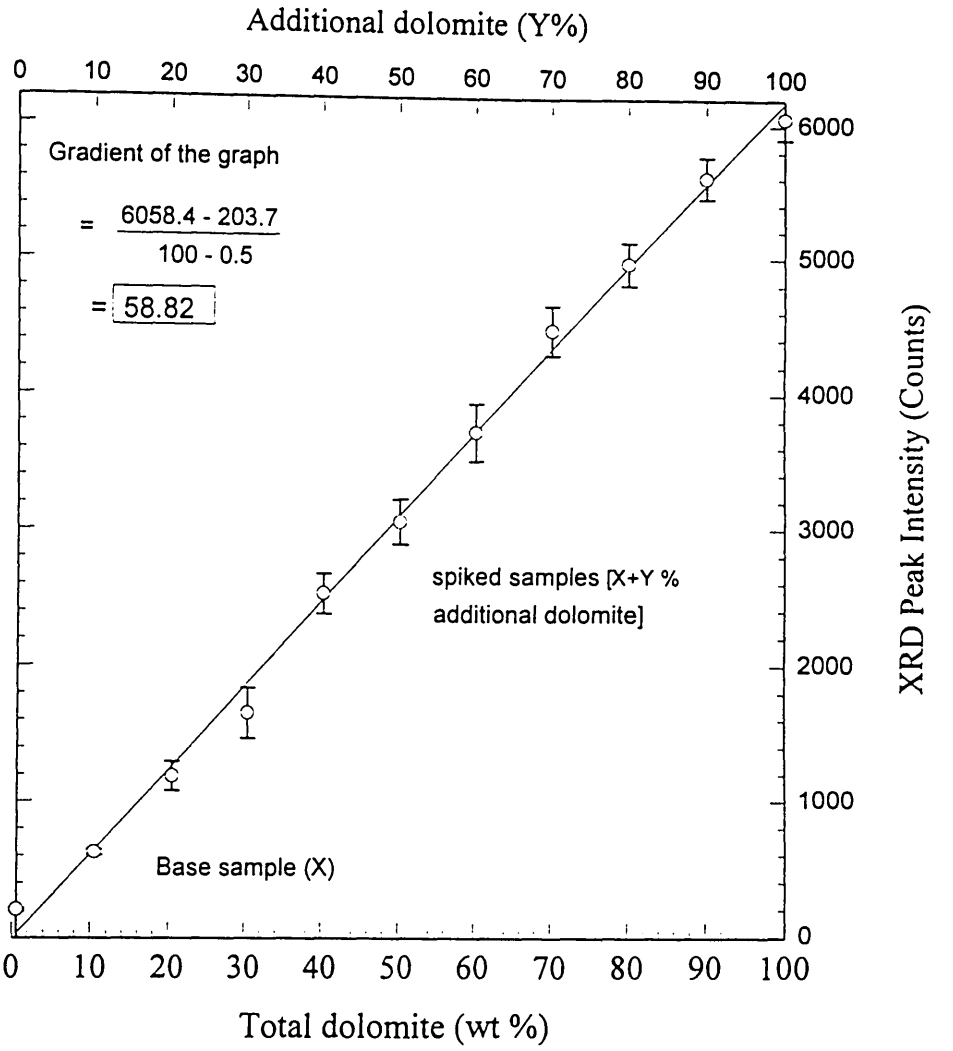

Additional dolomite (wt.%)

Peak height (counts)											
	214	602	1359	1429	2420	2841	3605	4570	5003	5592	6078
	203	602	997	1628	2769	3007	3434	4351	4709	5413	5875
	186	611	1256	1472	2582	3127	3383	4490	5001	5866	5953
	207	671	1200	1944	2659	2901	3893	4146	5081	5433	5998
	195	627	1287	1873	2482	2955	3758	4284	5151	5500	6005
	221	649	1215	1498	2264	2895	3656	4401	4804	5712	5900
	200	624	1114	1539	2438	3166	4019	4521	4790	5489	6278
	207	627	1160	1664	2501	3275	3785	4507	5116	5621	6225
	211	615	1057	1582	2476	3072	3971	4795	4898	5681	5983
	193	626	1220	1868	2678	3325	3641	4633	5136	5813	6289
Mean	203.7	625.4	1186.5	1649.7	2526.9	3056.4	3714.5	4469.8	4968.9	5612.0	6058.4
SD	10.5	21.2	108.2	184.1	147.4	165.5	212.6	184.1	159.6	156.2	153.3

Figure C.4. XRD calibration data and graph for dolomite. Dolomite peak heights (counts) measured at 30.97 2θ degrees, for samples collected at Sites 819 and 823, were converted into absolute values (weight %) by dividing the XRD peak counts by the gradient of the calibration graph (i.e., 58.82). Error bars indicate the standard deviation (SD) of the mean for additional proportions of dolomite.

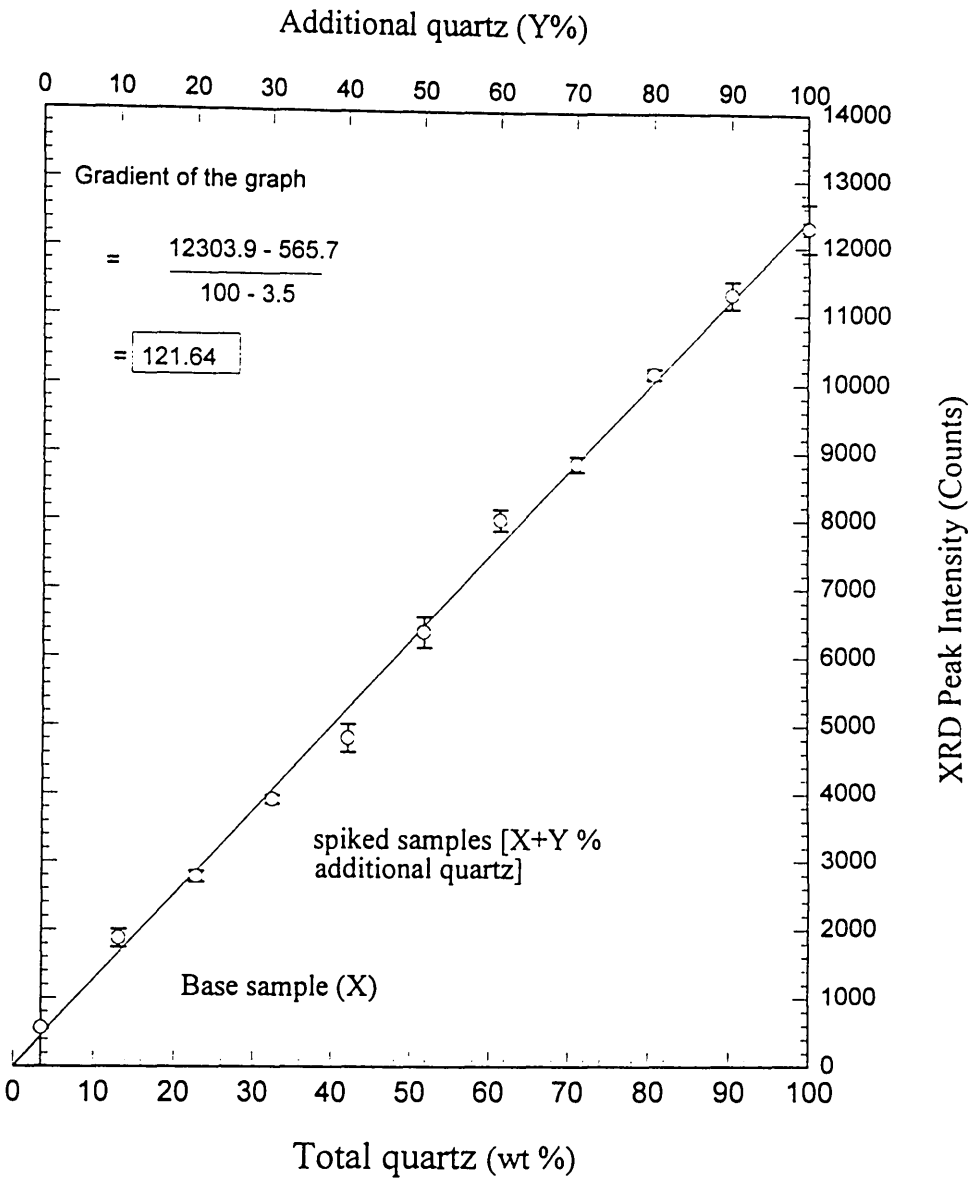

Additional quartz (wt.%)

Peak height (counts)											
	559	1961	2875	3900	4709	5991	7852	9061	10064	11634	11859
	548	1881	2723	4035	4890	6186	7910	8830	10165	11149	12072
	600	1949	2698	3924	4675	6201	7955	8902	10106	11300	12604
	555	1782	2789	3917	5200	6655	8187	8803	10283	11453	12985
	568	1691	2751	3956	4590	6513	7941	8681	10201	11039	12015
	572	1691	2804	3870	4624	6635	8198	8932	10192	11030	12058
	563	1908	2855	3944	5100	6276	7743	8715	10118	11517	12200
	558	1908	2678	3948	4899	6373	8008	8762	10036	11342	12794
	572	2113	2730	3832	4773	6217	8008	8866	10223	11204	12245
	562	1909	2929	3816	4692	6594	8221	8798	10196	11419	12207
Mean	565.7	1879.2	2783.2	3914.2	4814.9	6364.1	8002.3	8835.0	10158.4	11308.7	12303.9
SD	14.2	128.7	82.4	64.1	204.7	226.1	158.0	111.5	76.3	202.8	367.2

Figure C.5. XRD calibration data and graph for quartz. Quartz peak heights (counts) measured at 26.64 2θ degrees, for samples collected at Sites 819 and 823, were converted into absolute values (weight %) by dividing the XRD peak counts by the gradient of the calibration graph (i.e., 121.64). Error bars indicate the standard deviation (SD) of the mean for additional amounts of quartz.

APPENDIX - D

Table D.1. A selection of the standards used in XRF calibration.

STANDARDS
Ba-1 (I-III), Ba-2 (I-III), Ba-3 (I-III), Ba-4 (I-III), Ba-5 (I-III), Ba-6 (I-III)
BRIMO-1 (I-III), BRIMO-2 (I-III), BRIMO-3 (I-III), BRIMO-4 (I-III), BRIMO-5 (I-III), BRIMO-6 (I-III), BRIMO-7 (I-III).
MAG-1, BCR-1, AGV-1, GA, BR, GH, SY2, SY3, JB-1, PCC1, SGR-1, GSP-1.

Ba- and BRIMO- standards are a synthetic dilution series made up from the following SPECPURE compounds: $Ba(IO_3)_2$, $KBrO_3$, $(NH_4)Mo_7O_{24}.4H_2O$ and $BaCO_3$. Each was prepared using CaCO3 (I), Salisbury Crag Dolomite (II), and Shap Granite (III) matrices which represented a range of possible sediments compositions and mass absorption effects. Calibration lines are periodically revised and some standards are added and some removed, depending on what range of concentrations is required for each element.

Table D.2. Analytical conditions for XRF. Fl = Flow; Sc = Scintilation; FS = Flow + Scintilation

Element	Line	Tube	kV	mA	Crystal	Peak °2θ	+ Offset °2θ	- Offset °2θ	Counter/ Detector	Pulse Height Lower	Pulse Height Upper	Collimator	Sample Prep.	Count Time
Al	kα	Rh	40	60	PE	144.955	0.00	0.00	Fl	28	76	Coarse	P.D	50
Ba	Lα	Rh	50	50	Ge220	87.970	1.60	2.70	Fl	32	70	Fine	P.D	100
Br	kα	Rh	80	30	Lif200	29.940	0.00	0.60	FS	27	75	Fine	P.D	20
Ca	kα	Rh	50	50	Lif200	113.145	0.00	4.00	Fl	30	75	Fine	P.D	20
Ce	Lα	Rh	50	50	Lif200	71.625	2.50	1.00	Fl	32	70	Fine	P.D	100
Cr	kα	Rh	50	50	Lif200	69.375	1.62	0.88	Fl	32	70	Fine	P.D	40
Cu	kα	Rh	50	50	Lif200	45.040	1.70	0.70	Fl	40	70	Fine	P.D	40
Fe	kα	Rh	50	50	Lif200	57.530	0.00	2.50	Fl	18	68	Fine	P.D	10
I	kα	Rh	80	30	Lif200	12.375	0.50	0.50	Sc	25	75	Fine	P.D	20
K	kα	Rh	80	30	Lif200	136.720	0.00	5.00	Fl	32	75	Fine	P.D	20
La	Lα	Rh	50	50	Lif200	82.950	1.20	1.20	Fl	32	70	Fine	P.D	100
Mg	kα	Rh	40	60	PX1	22.605	3.10	0.00	Fl	25	80	Coarse	P.D	50
Mn	kα	Rh	50	50	Lif200	63.000	2.50	0.00	Fl	14	72	Fine	P.D	10
Mo	kα	Rh	80	30	Lif200	20.300	0.44	0.44	Sc	28	70	Fine	P.D	100
Na	kα	Rh	40	60	PX1	27.275	2.30	2.30	Fl	25	75	Coarse	P.D	50
Ni	kα	Rh	50	50	Lif200	48.685	1.30	0.00	Fl	40	70	Fine	P.D	40
Nb	kα	Rh	80	30	Lif200	21.360	0.40	0.40	FS	20	75	Fine	P.D	40
Nd	Lα	Rh	50	50	Lif200	72.160	2.30	0.00	Fl	32	70	Fine	P.D	100
P	kα	Rh	40	60	Ge111	140.915	3.00	0.00	Fl	34	75	Coarse	P.D	50
Pb	kα	Rh	80	30	Lif200	28.245	0.30	0.30	FS	20	75	Fine	P.D	100
Rb	kα	Rh	80	30	Lif200	26.585	0.54	0.70	FS	20	75	Fine	P.D	40
Sc	kα	Rh	50	50	Lif200	97.750	0.00	2.00	Fl	30	70	Fine	P.D	40
Si	kα	Rh	40	60	PE	109.070	4.00	0.00	Fl	30	75	Coarse	P.D	50
Sr	kα	Rh	80	30	Lif200	21.110	0.76	0.76	FS	20	75	Fine	P.D	40
Ti	kα	Rh	50	50	Lif200	86.185	3.50	0.00	Fl	28	72	Fine	P.D	20
Th	Lα	Rh	80	30	Lif200	27.465	0.00	0.30	FS	20	75	Fine	P.D	100
U	Lα	Rh	80	30	Lif200	26.130	0.00	0.36	FS	20	75	Fine	P.D	100
V	kα	Rh	50	50	Lif200	123.260	3.65	1.30	Fl	32	70	Fine	P.D	40
Y	kα	Rh	80	30	Lif200	23.760	0.60	0.60	FS	20	75	Fine	P.D	40
Zn	kα	Rh	50	50	Lif200	41.795	0.66	0.66	FS	22	75	Fine	P.D	40
Zr	kα	Rh	80	30	Lif200	22.500	0.66	0.76	FS	20	75	Fine	P.D	40

Table D3. XRF analytical precision for selected Hole 823A major and minor elements

Sample:

01H01 35-37			02H02 135-137			01H03 60-62		
Element	Mean[1] (N = 6)	1σ	Element	Mean[1] (N = 6)	1σ	Element	Mean[1] (N = 6)	1σ
Al	3.01	0.02	Al	6.88	0.30	Al	2.85	0.009
Ca	23.38	0.07	Ca	9.27	0.75	Ca	22.84	0.05
Sr	1969.80	15.59	Sr	651.78	13.81	Sr	2133.68	12.41
Ba	149.18	7.18	Ba	290.60	25.57	Ba	331.55	9.91
Ti	0.19	0.003	Ti	0.41	0.04	Ti	0.18	0.0062
Cr	35.47	1.04	Cr	68.15	6.63	Cr	27.76	1.0689

Sample:

04H01 35-37			13H05 60-62			13H06 60-62		
Element	Mean[1] (N = 6)	1σ	Element	Mean[1] (N = 6)	1σ	Element	Mean[1] (N = 6)	1σ
Al	1.16	0.01	Al	6.08	0.03	Al	7.58	0.04
Ca	27.47	0.10	Ca	11.16	0.07	Ca	7.92	0.04
Sr	2882.92	12.88	Sr	948.75	10.95	Sr	631.35	8.93
Ba	206.13	13.11	Ba	228.10	6.29	Ba	253.03	9.59
Ti	0.07	0.002	Ti	0.48	0.006	Ti	0.55	0.004
Cr	17.60	1.34	Cr	80.08	1.29	Cr	82.72	1.42

[1]Major element mean concentrations and accuracy in wt.%, Sr, Ba, and Cr in ppm. XRF analytical accuracy is given as standard deviations (1σ) about the mean.

Table D.4. Major element concentrations in Hole 823A periplatform muds.

Depth (mbsf)	Si %	Al %	Fe %	Mg %	Ca %	Na %	K %	Mn %	Ti %	P %	Total %
0.11	18.05	8.10	2.72	0.78	9.66	0.56	1.41	0.03	0.45	0.05	78.26
0.35	5.96	3.38	0.92	0.54	22.37	0.40	0.61	0.03	0.19	0.06	55.16
0.75	7.38	4.23	1.17	0.80	20.06	0.50	0.65	0.03	0.23	0.06	57.85
1.10	7.65	4.41	1.19	0.81	19.22	0.50	0.76	0.03	0.22	0.06	57.75
1.35	17.54	7.58	2.01	1.39	11.55	0.73	1.26	0.05	0.44	0.04	78.26
1.74	12.62	5.68	1.60	1.21	16.10	0.70	0.93	0.04	0.33	0.05	68.65
2.10	1.09	1.83	0.53	0.42	24.42	0.32	0.27	0.05	0.09	0.06	42.96
2.48	2.48	2.35	0.71	0.40	23.70	0.40	0.38	0.05	0.11	0.06	46.55
2.85	5.15	3.28	0.95	0.53	21.94	0.45	0.54	0.04	0.17	0.05	52.64
3.24	1.13	1.78	0.48	0.49	24.14	0.35	0.29	0.06	0.10	0.06	42.62
3.60	5.43	3.20	0.87	0.65	21.64	0.44	0.54	0.04	0.17	0.05	52.69
3.98	6.02	3.47	0.96	0.55	21.23	0.47	0.61	0.04	0.19	0.06	54.09
4.48	6.65	3.44	0.95	0.68	21.16	0.47	0.57	0.04	0.20	0.06	55.43
4.98	8.97	4.50	1.22	0.86	19.64	0.59	0.77	0.04	0.25	0.05	61.69
5.48	10.36	4.81	1.48	0.84	18.00	0.64	0.83	0.04	0.26	0.05	63.64
6.28	6.86	3.68	1.03	0.74	21.83	0.44	0.57	0.04	0.20	0.06	57.54
6.90	12.15	5.23	1.80	0.82	16.70	0.43	0.90	0.05	0.31	0.05	67.05
7.65	10.75	5.53	1.52	0.55	17.16	0.46	0.88	0.05	0.29	0.06	64.17
7.90	6.85	3.89	1.08	0.75	20.59	0.47	0.63	0.05	0.21	0.06	56.46
8.65	4.47	2.83	0.84	0.45	21.62	0.36	0.46	0.04	0.16	0.05	49.26
9.54	7.19	4.05	1.09	0.57	20.61	0.46	0.67	0.05	0.21	0.05	57.27
9.90	7.15	3.58	1.12	0.69	22.02	0.49	0.62	0.03	0.20	0.04	58.42
10.15	2.31	2.02	0.57	0.42	24.97	0.36	0.30	0.04	0.11	0.05	46.89
11.15	8.30	3.98	1.26	0.71	19.96	0.56	0.72	0.04	0.22	0.05	59.37
11.40	5.06	2.99	0.87	0.80	22.47	0.42	0.53	0.05	0.17	0.05	52.85
11.65	4.30	2.84	0.80	0.81	22.31	0.47	0.52	0.05	0.15	0.06	50.65
11.89	8.48	4.46	1.25	0.69	19.68	0.47	0.74	0.05	0.25	0.06	60.21
12.40	8.16	4.10	1.17	0.63	20.76	0.47	0.66	0.04	0.22	0.05	59.91
12.65	9.48	4.47	1.25	0.85	18.76	1.55	0.80	0.04	0.27	0.05	62.88
12.90	16.51	7.30	2.02	0.90	12.09	0.72	1.31	0.04	0.41	0.04	75.49
13.48	11.06	5.41	1.50	0.57	16.50	0.53	0.90	0.04	0.31	0.05	63.79
13.90	13.63	5.96	1.70	0.65	14.81	0.48	1.14	0.03	0.34	0.04	68.79
14.15	2.92	2.39	0.67	0.43	23.45	0.37	0.42	0.05	0.14	0.05	47.23
14.64	5.84	3.30	0.85	0.92	22.39	0.47	0.53	0.03	0.18	0.04	55.21
15.15	7.57	3.96	1.07	0.49	20.65	0.48	0.70	0.03	0.22	0.04	57.81
15.53	4.95	2.94	0.83	0.48	22.91	0.42	0.51	0.02	0.17	0.05	52.46
15.90	6.42	3.50	0.92	0.58	21.31	0.45	0.62	0.02	0.20	0.04	55.03
16.15	7.91	4.02	1.03	0.75	21.00	0.47	0.69	0.02	0.23	0.04	59.47
24.90	-0.41	1.10	0.32	0.23	26.35	0.30	0.17	0.03	0.06	0.04	40.00
25.15	0.22	1.29	0.37	0.33	25.84	0.28	0.20	0.03	0.07	0.04	41.30
25.90	2.94	2.27	0.60	0.42	24.47	0.33	0.34	0.04	0.13	0.05	48.09
26.15	6.17	3.45	0.95	0.51	21.62	0.47	0.59	0.03	0.19	0.05	54.76
26.65	7.98	4.05	1.09	0.55	20.01	0.87	0.71	0.04	0.23	0.05	58.69
26.90	14.07	6.36	1.69	0.95	14.61	0.58	1.15	0.03	0.37	0.04	70.88
27.15	6.53	3.75	0.97	0.59	20.60	0.64	0.66	0.05	0.20	0.05	55.18
27.40	9.00	4.61	1.24	0.59	18.64	0.50	0.80	0.04	0.25	0.05	60.04
27.65	9.26	4.62	1.26	0.46	18.52	0.50	0.86	0.04	0.26	0.04	60.34
27.90	1.24	1.81	0.49	0.35	24.93	0.29	0.31	0.05	0.10	0.05	43.71

28.15	4.45	2.69	0.84	0.45	23.11	4.98	0.52	0.05	0.16	0.05	57.37
28.40	2.98	2.31	0.64	0.31	23.60	0.33	0.41	0.05	0.13	0.04	47.03
28.65	5.03	3.05	0.82	0.46	22.87	0.40	0.51	0.03	0.17	0.04	52.71
28.90	5.65	3.24	0.91	0.46	22.07	0.44	0.58	0.03	0.18	0.04	53.66
29.40	5.13	3.00	0.84	0.46	22.71	0.45	0.54	0.02	0.16	0.04	52.74
29.65	6.77	3.74	1.10	0.61	21.22	0.36	0.67	0.04	0.20	0.05	56.53
29.90	2.77	2.23	0.62	0.42	24.15	0.47	0.36	0.05	0.13	0.05	47.44
30.15	4.44	2.82	0.81	0.49	22.89	0.42	0.51	0.04	0.16	0.07	51.12
30.40	6.25	3.23	0.97	0.77	21.86	0.52	0.52	0.02	0.19	0.04	55.31
30.65	6.65	3.58	0.95	0.57	21.48	0.49	0.62	0.04	0.20	0.05	56.05
30.90	7.81	3.90	0.91	0.81	21.31	0.36	0.68	0.04	0.22	0.04	59.11
31.15	5.29	2.65	0.63	0.87	21.73	0.47	0.46	0.02	0.17	0.04	51.20
31.90	5.33	3.04	0.99	0.62	21.59	0.36	0.58	0.03	0.17	0.04	52.23
32.15	3.29	2.52	0.67	0.41	23.32	0.29	0.45	0.05	0.14	0.05	47.95
32.40	5.30	3.18	0.89	0.42	21.69	0.39	0.60	0.04	0.17	0.04	52.08
32.65	3.38	2.55	0.71	0.34	23.17	0.32	0.44	0.04	0.15	0.05	48.00
33.15	4.11	2.87	0.76	0.30	22.93	0.28	0.50	0.04	0.16	0.04	49.91
33.42	6.70	3.72	0.87	0.45	21.01	0.33	0.61	0.04	0.22	0.04	55.14
33.90	3.47	2.60	0.64	0.28	23.30	0.33	0.45	0.05	0.14	0.04	48.20
34.15	6.69	3.68	1.00	0.44	20.63	0.43	0.61	0.03	0.21	0.04	54.94
34.40	4.04	2.67	0.73	0.49	23.55	0.40	0.45	0.03	0.16	0.05	50.60
34.65	6.65	3.31	0.93	0.90	22.04	0.48	0.56	0.02	0.19	0.04	56.68
34.90	6.55	3.54	0.90	0.52	21.57	0.50	0.61	0.03	0.20	0.05	55.68
35.15	4.88	2.14	0.54	1.15	21.78	0.53	0.42	0.02	0.13	0.03	49.66
35.65	8.21	4.33	1.13	0.59	20.38	0.33	0.80	0.04	0.25	0.05	59.78
35.90	4.46	3.08	0.76	0.51	22.39	0.37	0.56	0.04	0.16	0.05	50.85
36.40	3.20	2.36	0.58	0.65	23.17	0.33	0.42	0.03	0.14	0.04	47.41
36.89	8.08	4.20	0.87	1.13	20.59	0.45	0.70	0.02	0.24	0.04	59.80
37.15	3.19	2.46	0.65	0.39	23.69	0.30	0.43	0.03	0.14	0.05	48.02
37.40	1.77	1.85	0.57	0.40	24.46	0.28	0.35	0.03	0.11	0.04	44.60
37.64	3.17	2.49	0.61	0.36	23.61	0.93	0.44	0.03	0.14	0.04	48.64
38.65	0.33	1.42	0.35	0.59	25.35	0.27	0.25	0.03	0.08	0.04	41.55
39.14	1.25	1.78	0.39	0.24	24.90	0.25	0.31	0.04	0.10	0.04	43.15
39.40	4.20	2.67	0.66	0.48	23.52	0.33	0.48	0.02	0.15	0.04	50.63
39.66	-0.76	0.99	0.25	0.35	26.20	0.22	0.17	0.03	0.06	0.04	38.76
40.15	0.10	1.32	0.35	0.60	25.85	0.25	0.22	0.04	0.07	0.05	41.56
40.90	5.22	3.19	0.84	0.69	22.92	0.37	0.54	0.03	0.17	0.04	53.86
41.16	6.53	3.65	0.88	0.66	21.92	0.47	0.62	0.03	0.20	0.04	56.43
41.40	3.51	2.50	0.61	0.55	24.24	0.33	0.42	0.02	0.13	0.04	49.72
41.65	0.83	1.54	0.38	0.37	25.80	0.24	0.24	0.02	0.08	0.04	43.15
41.90	2.31	1.98	0.46	0.73	25.30	0.42	0.30	0.02	0.11	0.04	47.57
42.14	1.52	1.76	0.41	0.45	25.23	0.36	0.29	0.02	0.11	0.04	44.66
42.40	7.90	4.15	1.01	1.00	20.78	0.60	0.80	0.02	0.23	0.05	60.02
43.17	5.83	3.34	0.85	0.54	22.34	0.47	0.61	0.02	0.19	0.04	54.66
43.40	5.75	3.34	0.78	0.55	22.59	0.45	0.61	0.02	0.19	0.05	54.68
43.64	3.81	2.75	0.67	0.47	23.41	0.37	0.53	0.02	0.16	0.05	49.93
43.90	1.67	2.00	0.50	0.33	24.74	0.27	0.36	0.02	0.10	0.05	44.77
43.90	1.70	1.97	0.51	0.37	24.47	0.30	0.32	0.03	0.10	0.05	44.51
44.15	3.88	2.40	0.68	0.71	23.66	0.47	0.44	0.02	0.13	0.04	50.16
44.40	1.72	1.96	0.45	0.51	24.40	0.33	0.37	0.04	0.10	0.04	44.58
44.65	2.63	2.27	0.53	0.51	24.47	0.44	0.39	0.03	0.12	0.05	47.57
44.90	1.54	1.86	0.52	0.50	24.73	0.30	0.32	0.04	0.09	0.05	44.52
45.15	1.25	1.82	0.42	0.42	25.27	0.30	0.30	0.04	0.10	0.05	44.18
45.40	3.36	2.53	0.63	0.58	24.21	0.42	0.42	0.02	0.13	0.04	49.62

45.65	0.85	1.56	0.38	0.47	25.74	0.29	0.24	0.03	0.08	0.05	43.41
45.90	3.60	2.42	0.55	0.70	23.94	0.47	0.42	0.02	0.13	0.05	49.68
46.15	1.72	1.91	0.44	0.52	25.15	0.31	0.30	0.04	0.10	0.05	45.45
46.40	5.00	2.88	0.69	0.98	23.15	0.49	0.47	0.02	0.16	0.05	53.36
46.65	1.67	1.93	0.47	0.51	25.18	0.35	0.30	0.03	0.10	0.04	45.49
47.15	6.25	3.32	1.04	0.85	21.70	0.45	0.66	0.03	0.19	0.05	55.64
47.40	8.54	4.41	1.11	0.73	19.96	1.48	0.76	0.02	0.24	0.05	61.72
47.65	8.11	4.26	1.13	0.81	20.97	0.45	0.68	0.02	0.23	0.04	60.57
47.90	7.29	3.91	0.98	0.69	21.34	0.51	0.69	0.02	0.21	0.05	58.18
53.65	6.72	3.42	0.78	0.93	21.77	0.51	0.61	0.03	0.20	0.06	56.53
53.90	9.61	4.48	1.03	0.99	19.48	0.61	0.81	0.04	0.27	0.05	62.64
54.15	6.68	3.59	0.81	0.83	21.96	0.56	0.59	0.02	0.20	0.05	56.95
54.40	3.55	2.48	0.53	1.06	23.65	0.36	0.42	0.02	0.13	0.06	49.66
54.65	11.37	5.39	1.33	1.06	17.90	0.63	1.01	0.03	0.29	0.05	67.03
54.90	6.13	3.56	0.76	0.95	21.34	0.47	0.58	0.02	0.20	0.05	54.79
55.15	9.12	4.62	1.05	0.86	18.58	0.54	0.77	0.02	0.26	0.05	60.26
55.40	8.84	4.60	0.94	0.92	19.04	0.53	0.75	0.03	0.26	0.05	60.10
55.65	9.39	4.66	1.05	0.92	18.61	1.68	0.79	0.02	0.26	0.05	62.62
55.90	11.28	5.36	1.16	0.90	17.67	0.48	0.88	0.03	0.30	0.04	65.47
56.15	6.24	3.35	0.71	1.05	22.07	0.47	0.55	0.02	0.19	0.05	55.64
56.40	2.97	2.08	0.46	1.23	23.75	0.42	0.33	0.02	0.13	0.05	47.90
56.65	4.92	2.96	0.63	1.21	23.36	0.54	0.48	0.02	0.17	0.05	53.96
56.90	4.25	2.73	0.59	0.89	23.47	0.47	0.44	0.02	0.15	0.05	51.45
57.15	6.68	3.63	0.79	0.89	21.94	0.54	0.61	0.02	0.20	0.05	57.01
57.40	8.61	4.08	0.93	0.97	20.40	0.68	0.73	0.02	0.24	0.05	60.73
57.65	12.99	5.88	1.47	1.02	16.66	0.42	1.08	0.03	0.33	0.04	69.78
57.90	10.09	4.98	1.22	1.03	19.29	0.35	0.89	0.02	0.27	0.05	64.55
58.15	4.89	2.75	0.69	1.10	22.27	4.01	0.52	0.02	0.17	0.06	56.70
58.40	11.50	5.19	1.18	1.07	18.64	0.38	0.90	0.03	0.29	0.05	67.14
59.15	5.82	3.36	0.81	0.99	22.26	0.52	0.56	0.02	0.18	0.05	55.22
59.40	6.15	3.39	0.72	1.17	22.72	0.38	0.53	0.02	0.19	0.05	56.52
59.65	5.67	3.11	0.61	1.28	22.26	0.52	0.53	0.02	0.17	0.05	54.40
59.90	5.64	3.22	0.67	1.37	22.95	0.35	0.52	0.02	0.18	0.05	55.57
60.15	8.52	3.95	0.89	1.27	20.76	0.50	0.66	0.02	0.24	0.05	60.89
60.40	10.44	4.76	1.09	1.28	18.81	0.41	0.81	0.02	0.28	0.05	64.39
60.65	4.32	2.66	0.53	1.45	23.06	0.47	0.46	0.02	0.15	0.05	51.70
60.90	3.84	2.59	0.53	1.44	24.19	0.50	0.42	0.02	0.13	0.05	52.08
61.15	3.67	2.52	0.53	1.21	23.69	0.60	0.46	0.02	0.14	0.06	50.69
61.40	5.01	2.96	0.65	1.42	22.84	0.47	0.50	0.02	0.16	0.05	53.73
61.65	3.58	2.54	0.54	1.77	23.86	0.45	0.41	0.02	0.13	0.05	51.45
61.90	4.73	2.85	0.61	1.32	23.77	0.47	0.46	0.02	0.15	0.04	53.88
62.15	12.14	5.44	1.20	1.04	17.28	0.51	0.95	0.03	0.31	0.04	67.34
62.40	4.87	2.92	0.58	1.30	23.37	0.47	0.47	0.02	0.16	0.04	53.70
62.65	5.81	3.20	0.65	1.30	22.73	0.50	0.51	0.02	0.18	0.04	55.59
62.90	3.61	2.51	0.55	1.41	24.08	0.28	0.40	0.02	0.13	0.05	50.94
63.15	2.48	2.04	0.47	1.42	24.83	0.36	0.32	0.02	0.12	0.05	48.52
63.40	2.10	1.94	0.42	2.00	24.12	0.40	0.30	0.02	0.11	0.05	47.37
63.65	3.94	2.43	0.53	1.62	23.15	0.39	0.40	0.02	0.14	0.05	50.63
63.90	3.65	2.43	0.54	1.46	23.71	0.41	0.40	0.02	0.14	0.05	50.60
64.15	6.59	3.49	0.73	1.25	22.26	0.38	0.56	0.02	0.20	0.04	57.21
64.65	7.24	3.68	0.76	1.25	22.12	0.42	0.61	0.02	0.20	0.04	58.95
64.90	7.45	3.80	0.84	1.29	21.72	0.42	0.63	0.02	0.21	0.05	59.34
65.15	3.69	2.55	0.55	1.32	23.96	0.31	0.41	0.02	0.14	0.05	50.94
65.40	9.96	4.81	1.08	1.04	19.04	0.44	0.85	0.02	0.28	0.05	63.40

65.65	5.12	2.94	0.65	1.30	23.46	0.37	0.46	0.02	0.16	0.04	54.42
65.90	4.04	2.48	0.52	2.39	22.39	0.32	0.42	0.02	0.14	0.05	51.08
66.15	5.63	3.11	0.69	1.42	22.12	0.39	0.53	0.02	0.18	0.05	54.38
66.90	5.20	2.93	0.66	1.54	23.16	0.34	0.48	0.02	0.16	0.05	54.55
67.40	2.94	2.18	0.49	1.41	23.93	0.34	0.35	0.02	0.12	0.05	48.53
67.65	2.89	2.21	0.48	1.85	24.34	0.34	0.32	0.02	0.12	0.04	49.72
67.90	5.13	2.98	0.68	1.42	23.02	0.33	0.48	0.02	0.17	0.05	54.15
68.15	5.64	3.18	0.70	1.26	22.81	0.48	0.54	0.02	0.17	0.05	55.38
68.40	0.79	1.42	0.31	1.82	24.47	0.36	0.22	0.02	0.08	0.04	43.34
68.65	6.47	3.47	0.86	1.16	21.64	0.42	0.57	0.03	0.19	0.06	56.28
68.90	12.44	5.53	1.27	1.05	17.22	0.54	0.95	0.02	0.31	0.05	68.30
69.15	4.71	2.84	0.65	1.44	22.60	0.38	0.46	0.02	0.16	0.05	52.43
69.40	5.49	3.14	0.68	1.37	23.20	0.41	0.51	0.02	0.17	0.05	55.53
69.65	13.66	5.79	1.27	1.23	16.07	0.62	1.02	0.03	0.35	0.05	70.37
69.90	15.60	6.55	1.54	1.16	14.31	0.56	1.19	0.02	0.39	0.04	74.14
70.15	12.30	5.49	1.27	1.13	17.18	0.39	0.95	0.02	0.32	0.05	67.79
70.40	5.00	2.94	0.69	1.44	22.68	0.42	0.49	0.02	0.17	0.06	53.51
70.65	6.47	3.43	0.80	1.33	21.94	0.33	0.56	0.02	0.20	0.05	56.61
71.15	8.52	4.03	0.96	1.20	20.16	0.45	0.72	0.02	0.23	0.05	60.23
71.40	6.60	3.52	0.82	1.00	22.14	0.30	0.61	0.02	0.20	0.05	56.88
71.65	3.99	2.59	0.55	1.25	23.96	0.39	0.42	0.02	0.14	0.05	51.68
71.90	5.20	2.97	0.66	1.39	23.02	0.33	0.48	0.02	0.17	0.06	54.24
72.15	6.66	3.54	0.81	1.36	22.25	0.36	0.62	0.02	0.20	0.05	57.86
72.39	5.11	3.01	0.66	1.33	22.99	0.45	0.48	0.02	0.16	0.05	54.06
72.65	6.82	3.55	0.77	1.29	21.99	0.44	0.59	0.02	0.20	0.06	57.73
72.90	7.40	3.76	0.87	1.34	21.27	0.42	0.61	0.02	0.22	0.06	58.74
73.15	5.58	3.06	0.60	1.28	22.42	0.42	0.52	0.02	0.17	0.05	54.18
73.40	6.15	3.24	0.62	1.31	22.11	0.37	0.55	0.02	0.19	0.05	55.44
73.65	7.10	3.70	0.74	1.25	22.72	0.38	0.61	0.02	0.20	0.05	59.44
73.89	3.35	2.23	0.52	1.35	23.77	0.52	0.37	0.02	0.13	0.05	49.52
74.40	6.72	3.61	0.78	1.35	22.97	0.42	0.55	0.02	0.19	0.04	59.01
74.65	8.84	4.39	0.95	1.36	21.02	0.52	0.71	0.02	0.24	0.05	63.10
74.90	16.74	6.85	1.83	1.19	13.99	0.57	1.16	0.03	0.45	0.05	77.52
75.15	9.33	4.64	1.05	1.36	20.76	0.60	0.72	0.02	0.25	0.04	64.61
75.39	8.58	4.29	0.95	1.39	21.98	0.42	0.68	0.02	0.25	0.04	63.57
75.65	4.00	2.51	0.56	1.47	23.90	0.43	0.37	0.02	0.14	0.04	51.82
75.90	3.08	2.15	0.47	1.54	23.97	0.49	0.32	0.02	0.13	0.04	49.20
76.15	18.55	7.44	1.74	1.25	11.59	0.72	1.30	0.04	0.46	0.04	79.43
76.40	5.28	3.07	0.65	1.44	23.70	0.43	0.46	0.02	0.17	0.05	55.66
76.65	3.70	2.43	0.53	1.54	24.15	0.42	0.36	0.02	0.14	0.04	51.38
76.89	13.02	5.96	1.20	1.19	17.72	0.50	0.95	0.02	0.34	0.04	71.10
77.15	1.99	1.65	0.38	1.59	24.00	0.54	0.26	0.02	0.10	0.04	45.74
77.40	2.46	1.92	0.42	1.50	24.20	0.44	0.27	0.02	0.11	0.04	47.41
77.65	3.37	2.32	0.53	1.70	23.80	0.45	0.35	0.02	0.13	0.04	50.26
77.90	2.46	1.89	0.41	1.47	24.23	0.44	0.27	0.02	0.11	0.04	47.33
78.39	4.88	2.85	0.63	1.35	23.50	0.52	0.42	0.02	0.16	0.05	53.96
78.90	7.67	3.84	0.89	1.38	21.95	0.42	0.61	0.02	0.22	0.05	60.45
79.15	8.23	4.21	1.07	1.36	21.34	0.53	0.68	0.02	0.23	0.05	62.16
79.40	7.19	3.70	0.91	1.05	21.60	0.47	0.63	0.02	0.21	0.05	58.30
79.65	4.01	2.72	0.82	0.75	23.23	0.42	0.49	0.05	0.15	0.06	50.91
79.89	10.05	4.79	1.32	0.67	19.41	0.40	0.88	0.03	0.27	0.05	64.00
80.15	8.47	4.21	1.14	0.65	20.78	0.40	0.81	0.04	0.23	0.06	60.88
80.40	7.95	3.99	1.07	0.84	20.49	0.50	0.80	0.03	0.23	0.06	59.21
80.65	5.41	2.89	0.80	0.83	21.54	2.10	0.59	0.04	0.19	0.06	54.39

80.90	9.81	4.69	1.18	0.77	18.41	0.56	0.92	0.05	0.28	0.05	62.07
81.15	12.20	5.49	1.34	1.15	17.23	0.63	1.03	0.03	0.32	0.04	68.26
81.39	9.16	4.46	1.15	0.91	19.97	0.56	0.85	0.04	0.26	0.05	62.47
81.65	9.55	4.73	1.12	0.99	20.05	0.55	0.85	0.04	0.27	0.05	63.95
81.89	7.87	4.03	1.10	0.66	21.29	0.45	0.75	0.03	0.23	0.05	59.86
81.90	6.86	3.77	0.95	0.69	21.61	0.49	0.69	0.04	0.22	0.05	57.35
82.40	7.27	3.69	1.14	0.53	21.08	0.45	0.71	0.05	0.21	0.07	57.51
82.65	8.99	4.25	1.11	0.68	19.94	0.61	0.81	0.04	0.25	0.06	61.19
82.90	12.41	5.41	1.39	0.99	17.21	0.73	1.13	0.03	0.32	0.05	68.68
83.15	11.51	5.28	1.33	0.88	17.73	0.62	1.04	0.03	0.31	0.05	66.64
83.39	10.36	5.09	1.32	0.76	18.63	0.42	0.94	0.04	0.28	0.06	64.42
83.65	8.70	4.25	1.14	0.79	19.79	0.54	0.83	0.04	0.24	0.06	60.52
83.90	16.58	6.73	1.77	1.10	12.85	0.93	1.40	0.03	0.42	0.04	75.78
84.15	10.12	4.63	1.20	0.83	18.35	0.59	0.90	0.03	0.28	0.05	62.66
84.40	11.70	5.33	1.33	0.78	17.17	0.66	0.97	0.03	0.31	0.05	66.14
84.65	13.95	5.93	1.36	0.88	15.98	0.58	1.06	0.03	0.36	0.04	70.75
84.89	12.81	5.54	1.33	0.89	16.48	0.70	1.04	0.02	0.33	0.04	68.28
85.15	10.71	4.69	1.21	0.93	18.87	0.50	0.86	0.03	0.30	0.05	64.83
85.40	13.39	5.57	1.45	1.00	16.48	0.59	1.08	0.04	0.34	0.06	70.01
85.65	8.79	4.31	1.15	0.70	19.33	1.46	0.80	0.04	0.25	0.05	61.24
85.90	10.69	4.74	1.19	1.07	19.17	0.65	0.81	0.03	0.31	0.05	65.65
86.39	22.61	8.73	2.21	1.10	7.84	0.98	1.54	0.04	0.57	0.05	86.95
86.65	21.68	8.51	2.12	1.09	8.68	0.85	1.46	0.04	0.55	0.05	85.19
86.90	19.30	6.76	2.15	0.83	6.81	13.87	1.40	0.03	0.50	0.05	91.20
87.15	24.23	9.28	2.55	1.03	5.15	1.30	1.69	0.03	0.58	0.05	88.99
87.65	22.55	8.89	2.26	1.10	7.23	1.00	1.56	0.04	0.56	0.05	86.41
87.89	22.12	8.68	2.29	1.11	8.40	0.92	1.49	0.03	0.55	0.05	86.63
88.15	22.99	8.84	2.35	1.15	7.26	0.98	1.57	0.04	0.58	0.05	87.61
88.65	23.96	9.32	2.36	1.16	6.43	0.78	1.59	0.04	0.61	0.05	89.30
88.90	21.91	8.59	2.18	1.05	8.45	0.69	1.50	0.03	0.56	0.04	85.41
89.15	16.79	6.80	1.78	0.90	12.90	0.63	1.24	0.04	0.44	0.05	75.58
89.39	16.51	6.65	1.76	0.89	12.85	0.81	1.22	0.04	0.43	0.05	74.77
89.65	16.74	6.73	1.77	0.90	13.38	0.59	1.21	0.04	0.45	0.05	75.91
90.15	15.85	6.40	1.70	0.92	14.18	0.62	1.17	0.04	0.43	0.05	74.31
90.40	13.06	5.31	1.49	0.84	16.05	0.76	0.98	0.04	0.35	0.05	68.16
90.65	7.01	3.68	0.91	0.77	21.49	1.16	0.66	0.03	0.22	0.04	58.22
90.65	13.07	5.54	1.46	0.80	16.13	0.62	1.00	0.05	0.36	0.05	68.45
90.89	12.23	5.27	1.41	0.73	16.89	0.46	0.95	0.04	0.35	0.06	66.67
91.15	12.23	5.30	1.40	0.70	17.07	0.48	0.96	0.04	0.35	0.06	66.96
91.40	11.51	4.97	1.36	0.75	17.63	0.49	0.90	0.04	0.33	0.06	65.47
91.40	4.29	2.64	0.72	0.54	22.87	0.40	0.48	0.05	0.17	0.07	50.29
91.65	5.62	3.09	0.81	0.59	22.39	0.43	0.56	0.04	0.20	0.06	53.77
91.90	10.40	4.53	1.17	0.89	17.92	0.70	0.80	0.03	0.30	0.05	62.54
92.15	8.25	4.02	1.06	0.71	19.69	0.59	0.73	0.04	0.23	0.06	58.64
92.65	9.69	4.39	1.19	0.86	19.25	0.45	0.81	0.03	0.27	0.06	62.27
93.15	8.28	3.98	1.09	0.77	19.99	0.50	0.72	0.04	0.23	0.07	59.06
93.44	16.99	6.99	1.71	1.09	12.87	0.86	1.22	0.03	0.45	0.05	76.77
93.90	16.13	6.64	1.69	1.14	14.32	0.60	1.16	0.03	0.43	0.05	75.91
94.40	16.30	6.71	1.63	1.19	14.20	0.70	1.15	0.03	0.43	0.05	76.29
95.40	8.73	4.10	1.09	0.71	20.17	0.39	0.76	0.04	0.26	0.05	60.32
95.65	10.98	4.93	1.23	0.97	18.85	0.41	0.86	0.03	0.31	0.05	65.82
95.90	10.95	5.00	1.24	0.92	18.77	0.46	0.88	0.03	0.31	0.05	65.82
96.15	17.58	7.14	1.71	1.19	11.90	0.91	1.25	0.03	0.44	0.05	77.22
96.44	11.56	5.12	1.31	0.92	17.93	0.48	0.90	0.03	0.32	0.05	66.42

96.65	11.82	5.21	1.31	1.13	17.64	0.50	0.93	0.03	0.32	0.05	67.14
96.90	10.02	4.49	1.12	0.78	18.86	0.64	0.82	0.04	0.28	0.05	62.63
97.15	11.63	5.14	1.29	0.98	17.82	0.58	0.91	0.03	0.31	0.05	66.65
97.40	8.74	4.18	1.13	2.12	18.84	0.43	0.76	0.05	0.25	0.05	61.14
97.65	7.62	3.85	0.91	0.84	21.25	0.51	0.69	0.03	0.23	0.05	58.82
97.94	8.97	4.13	1.05	0.78	19.50	0.59	0.71	0.03	0.26	0.06	60.19
98.15	13.40	5.70	1.41	0.87	15.96	0.75	1.06	0.03	0.35	0.05	69.45
98.40	14.18	5.83	1.45	0.95	15.61	0.76	1.14	0.03	0.36	0.05	71.19
98.65	15.13	6.30	1.55	1.03	14.30	0.87	1.23	0.03	0.39	0.05	72.92
98.90	14.64	6.22	1.59	1.02	14.76	0.72	1.21	0.03	0.38	0.04	72.19
99.15	12.79	5.35	1.76	1.13	16.38	0.65	0.94	0.02	0.32	0.04	68.91
99.44	11.87	5.28	1.29	0.96	16.61	2.02	0.98	0.03	0.31	0.04	67.68
99.65	11.96	5.39	1.33	0.92	17.30	0.82	0.96	0.03	0.32	0.04	67.45
99.90	8.23	4.14	0.99	0.90	21.02	0.41	0.70	0.03	0.24	0.04	60.48
100.40	6.74	3.65	0.85	0.69	18.96	0.52	0.58	0.03	0.21	0.04	52.81
100.65	13.96	5.73	1.57	0.80	14.16	3.98	1.08	0.03	0.36	0.04	72.79
100.65	9.57	4.72	1.05	1.39	21.22	0.47	0.73	0.02	0.25	0.04	65.84
100.90	16.49	6.59	1.79	1.06	12.62	3.75	1.19	0.03	0.43	0.04	78.50
101.16	18.75	7.49	2.05	1.03	11.12	0.78	1.34	0.03	0.48	0.04	79.78
101.41	14.84	6.27	1.66	0.93	14.56	0.91	1.15	0.03	0.38	0.04	72.66
101.91	6.40	3.40	0.87	0.71	22.08	0.54	0.60	0.03	0.20	0.06	56.11
102.16	11.27	5.01	1.35	0.80	18.44	0.50	0.90	0.03	0.32	0.04	66.22
102.40	13.24	5.25	1.32	0.82	16.55	0.60	0.95	0.02	0.35	0.04	68.42
102.66	9.31	4.39	1.16	0.74	19.78	0.50	0.80	0.03	0.26	0.05	61.94
102.91	10.96	4.91	1.25	0.99	18.40	0.42	0.88	0.03	0.31	0.05	65.21
103.41	14.16	5.91	1.49	1.20	15.43	0.72	1.03	0.03	0.37	0.04	71.37
103.66	7.59	3.63	0.97	1.60	20.37	0.53	0.69	0.03	0.23	0.05	58.50
103.90	15.82	6.16	1.53	0.90	13.67	0.60	1.10	0.03	0.41	0.05	72.54
104.16	15.14	6.37	1.79	0.83	14.25	0.47	1.15	0.03	0.40	0.04	72.60
105.16	14.45	6.19	1.57	0.89	15.29	0.56	1.11	0.03	0.38	0.04	71.89
105.40	15.00	6.40	1.70	0.78	13.67	0.95	1.19	0.03	0.38	0.04	71.97
105.88	16.42	6.76	1.67	0.89	13.16	0.62	1.23	0.03	0.42	0.04	74.70
108.16	4.96	2.58	0.66	1.87	21.80	0.69	0.43	0.02	0.19	0.04	52.47
108.88	8.55	4.12	0.99	1.08	20.34	0.52	0.71	0.02	0.26	0.05	60.69
108.91	11.27	5.00	1.21	1.16	17.77	0.91	0.90	0.02	0.31	0.04	66.03
109.41	11.04	4.85	1.17	1.17	18.37	0.68	0.86	0.02	0.32	0.04	65.68
109.66	11.83	5.15	1.28	0.90	17.33	0.68	0.95	0.03	0.34	0.04	66.45
110.40	16.12	6.57	1.62	1.23	14.10	0.68	1.25	0.03	0.41	0.05	75.59
112.40	14.15	5.77	1.46	1.03	14.98	1.49	1.14	0.04	0.38	0.05	71.30
115.15	12.10	5.28	1.34	0.98	17.10	0.71	0.94	0.04	0.34	0.06	67.25
116.90	18.89	7.59	1.97	1.13	10.99	1.06	1.37	0.04	0.49	0.05	80.51
117.65	20.68	8.07	2.20	1.16	9.39	0.85	1.39	0.04	0.53	0.05	83.40
117.90	23.91	8.80	2.73	1.26	6.05	0.89	1.60	0.04	0.61	0.05	88.79
118.15	21.43	8.32	2.09	0.99	8.46	1.11	1.47	0.03	0.53	0.05	84.09
118.40	22.37	8.72	2.20	0.95	7.59	1.11	1.54	0.03	0.55	0.05	85.92
118.90	23.15	8.71	2.27	0.98	7.36	0.99	1.59	0.03	0.56	0.04	87.35
119.90	17.51	6.94	1.76	0.88	12.62	0.85	1.30	0.04	0.46	0.05	77.32

Table D.5. Minor element concentrations in Hole 823A periplatform muds.

Depth (mbsf)	Ba (ppm)	V (ppm)	La (ppm)	Ce (ppm)	Nd (ppm)	Cr (ppm)	Ni (ppm)	Cu (ppm)	Zn (ppm)	Pb (ppm)	Th (ppm)	U (ppm)	Rb (ppm)	Sr (ppm)	Y (ppm)	Zr (ppm)	Nb (ppm)	Mo (ppm)	I (ppm)	Br (ppm)	Sc (ppm)
0.11	327.7	91.00	34.80	60.70	28.70	74.20	38.50	52.00	76.10	20.00	12.20	3.20	101.50	623.7	25.80	111.60	11.80	0.60	26.10	20.60	12.60
0.35	165.9	38.20	7.90	22.40	10.80	33.30	14.60	26.60	52.80	7.30	6.30	1.00	39.40	1918.1	12.80	43.40	4.20	0.30	8.00	10.70	10.80
0.75	321.5	39.50	13.20	27.20	13.50	35.20	23.90	66.50	58.50	18.50	5.90	-2.40	55.20	1728.4	18.90	65.20	5.00	0.60	29.80	28.80	9.40
1.10	328.6	42.40	15.80	23.10	15.80	37.60	21.50	46.30	56.80	11.80	7.50	3.40	56.20	1535.6	20.80	63.90	6.80	0.50	34.60	44.10	8.50
1.35	166.2	75.70	16.40	43.00	22.50	74.50	38.20	28.00	59.40	14.60	9.50	2.60	83.20	1135.7	18.90	121.70	9.10	1.00	18.20	35.80	12.60
1.74	263.4	63.80	19.00	35.00	18.00	58.00	33.50	37.80	60.10	10.10	6.80	1.40	64.80	1452.0	20.00	87.10	7.70	0.40	14.50	32.30	12.20
2.10	376.0	16.70	7.40	11.40	14.10	12.70	12.00	24.70	41.50	6.90	4.60	0.80	19.90	1939.1	20.70	25.30	2.20	0.10	4.90	16.50	11.90
2.48	411.9	29.40	14.90	9.70	10.40	15.80	18.00	36.80	42.00	8.20	2.60	1.30	28.00	1813.7	19.00	31.20	3.90	-0.10	12.30	29.80	6.10
2.85	364.4	36.20	8.90	22.50	15.80	27.40	22.50	35.60	48.00	8.10	6.10	-0.10	40.80	1764.9	17.90	48.40	5.00	0.20	19.10	19.10	4.60
3.24	359.7	19.90	8.50	14.80	8.60	13.50	13.70	32.10	38.40	5.70	2.10	2.40	19.60	2029.1	16.80	15.60	1.20	0.30	11.70	32.20	8.90
3.60	323.0	36.00	8.10	20.40	12.80	26.40	21.30	34.10	45.20	7.40	5.50	1.60	36.20	2098.2	21.70	59.60	4.50	0.50	15.60	28.30	9.10
3.98	389.7	43.80	10.30	28.50	16.60	33.80	26.10	41.50	56.80	7.90	4.90	2.40	41.00	1865.0	19.60	48.60	4.40	0.80	9.60	32.70	8.60
4.48	268.0	37.30	9.50	21.40	12.40	36.00	24.40	32.70	53.10	6.30	5.80	0.20	40.60	2142.0	14.60	54.30	4.10	0.50	24.50	24.10	9.20
4.98	268.1	49.60	15.20	24.60	16.00	42.30	26.00	39.30	63.50	8.50	4.40	3.20	51.90	1965.0	16.60	56.20	5.70	0.30	16.70	38.10	8.10
5.48	342.1	51.70	11.40	27.70	14.70	44.50	27.80	41.20	63.60	9.80	6.80	4.20	55.00	1702.7	17.30	64.70	5.70	0.50	18.10	34.50	15.30
6.28	360.8	41.80	13.90	16.70	13.70	38.20	29.70	62.50	56.40	8.60	3.50	1.60	38.90	2284.5	16.60	43.10	4.80	0.30	14.40	17.60	7.80
6.90	335.0	66.40	12.60	31.10	12.70	54.30	30.80	49.10	62.30	9.50	7.70	2.50	62.00	1646.7	19.20	82.50	6.30	0.40	7.10	12.40	12.50
7.65	432.8	61.90	21.90	43.60	19.10	42.90	31.60	48.10	60.40	13.10	7.90	0.90	66.60	1044.8	22.80	85.00	8.60	0.30	8.60	15.90	14.60
7.90	367.1	40.20	16.00	22.50	13.20	33.10	21.40	50.50	51.70	9.80	5.00	0.80	45.90	1750.5	20.70	71.70	6.00	0.30	21.00	16.40	5.80
8.65	227.3	28.70	2.00	11.40	7.60	25.40	17.10	22.10	49.20	7.90	4.70	2.20	32.20	2024.1	11.10	38.10	4.30	0.40	0.30	14.10	11.60
9.54	412.9	44.50	10.90	20.70	15.80	33.60	22.20	44.30	56.30	8.70	5.60	0.90	47.40	1615.7	20.50	55.90	5.70	0.80	12.20	35.90	10.40
9.90	319.5	44.20	13.20	20.50	13.90	35.60	24.80	32.00	52.40	7.30	5.20	3.20	39.50	2478.5	16.50	43.40	5.30	0.40	12.00	15.00	7.10
10.15	276.8	20.10	7.40	10.00	10.50	21.50	16.80	29.60	41.60	5.10	2.00	0.70	18.10	2804.7	13.80	16.90	1.90	0.40	7.60	14.20	12.70
11.15	258.5	40.30	7.80	33.00	13.00	39.00	19.80	36.40	55.50	6.30	5.00	1.10	47.00	1872.5	15.00	56.60	5.30	-0.20	8.80	22.70	12.00
11.40	220.3	31.00	1.80	7.00	11.90	29.70	16.30	25.40	42.50	8.10	4.80	1.70	35.10	2329.1	13.90	37.10	4.20	0.50	7.20	19.00	11.70
11.65	247.8	33.20	5.30	26.00	13.40	25.60	15.20	34.40	41.40	9.40	4.10	2.80	31.90	2090.3	17.60	36.10	4.80	0.20	16.10	47.70	9.30
11.89	362.3	53.30	14.60	22.10	13.90	39.40	26.20	58.90	54.90	13.20	6.00	2.80	49.00	1675.3	17.60	54.30	6.00	0.50	6.00	18.70	7.70

12.40	305.1	42.30	13.30	26.10	15.10	44.10	24.70	36.40	56.20	5.90	5.00	2.10	42.90	2083.9	14.20	56.30	5.10	0.40	15.50	18.70	13.50
12.65	252.4	46.80	17.60	30.10	15.30	47.20	23.80	40.30	53.50	7.20	5.90	0.40	50.10	1858.2	14.40	69.80	6.10	0.30	12.60	65.20	8.10
12.90	263.6	81.10	22.90	44.10	19.90	67.80	33.50	46.00	69.50	13.00	7.90	0.00	87.30	1023.5	19.80	103.10	9.20	0.80	15.50	30.20	13.40
13.48	342.4	54.00	18.30	34.90	24.10	44.80	30.30	47.90	63.50	15.80	10.20	1.80	69.40	1099.4	22.40	91.10	8.30	0.70	22.00	23.40	11.60
13.90	344.6	64.60	13.80	48.80	24.40	50.80	26.10	43.80	66.60	13.80	9.10	1.40	79.40	1108.6	21.10	102.10	9.70	0.40	10.80	14.80	11.40
14.15	271.0	22.30	12.80	16.60	9.50	17.00	19.00	46.00	45.70	3.00	2.60	2.70	27.90	1947.3	15.10	39.10	3.80	0.40	18.50	21.70	6.90
14.64	221.2	36.70	12.30	22.80	13.00	31.80	18.20	35.40	44.30	8.90	5.20	4.20	34.20	2406.6	16.30	52.30	4.70	0.80	6.40	13.60	8.60
15.15	314.1	43.50	11.40	24.80	18.20	33.90	19.70	31.20	50.70	9.70	4.60	1.90	47.20	1867.1	19.40	55.70	5.10	0.30	10.50	21.80	9.50
15.53	220.9	33.60	7.00	17.40	9.70	32.00	18.90	28.00	47.60	5.40	4.00	0.90	33.60	2265.0	12.10	35.50	2.90	0.10	18.10	23.00	11.00
15.90	216.2	34.00	17.90	27.20	12.00	33.70	19.80	28.80	50.30	8.40	5.50	1.20	42.70	1948.4	13.50	49.30	4.10	0.50	14.60	21.70	10.90
16.15	220.5	45.90	12.90	28.30	12.50	45.10	22.50	24.20	52.50	7.60	6.20	2.50	45.60	2056.8	14.60	55.10	5.60	0.50	23.30	19.70	6.20
24.90	216.4	14.90	-0.50	8.50	11.10	10.90	10.30	19.00	33.10	6.10	2.60	0.00	8.30	2490.3	8.30	2.30	0.70	-0.20	9.60	15.80	7.50
25.15	205.7	13.70	-2.80	12.70	8.70	17.80	10.70	15.80	36.20	1.40	1.90	2.90	11.40	2791.7	8.10	5.30	1.30	-0.10	19.90	12.70	9.20
25.90	241.6	30.30	6.70	13.50	10.60	23.50	16.10	22.00	42.50	4.80	2.30	1.10	22.10	2542.1	12.10	22.70	2.20	0.20	10.80	12.10	9.70
26.15	295.7	34.70	10.70	20.00	11.50	36.10	18.80	24.90	50.50	7.00	4.70	1.90	37.60	1905.3	13.30	42.70	4.10	0.30	9.70	31.30	9.90
26.65	286.0	39.80	6.50	23.90	14.10	39.80	19.10	30.90	56.30	9.90	5.70	2.60	46.40	1803.7	14.50	57.50	5.90	0.60	1.20	25.60	8.80
26.90	234.9	75.10	17.00	42.30	22.10	67.00	40.20	39.80	73.20	12.40	8.30	2.70	77.70	1330.1	17.80	97.90	8.20	1.00	23.50	24.80	9.70
27.15	254.3	37.80	11.30	28.10	14.10	28.60	17.30	28.30	52.50	11.30	8.50	-0.80	47.30	1605.2	16.60	56.90	5.30	0.30	12.60	20.30	8.60
27.40	255.3	47.60	11.70	33.00	14.80	38.80	29.50	39.10	55.80	13.70	6.60	2.00	59.10	1409.2	19.90	76.20	8.20	0.10	9.40	20.00	7.70
27.65	400.0	49.00	17.20	25.90	14.90	40.00	24.10	31.10	53.50	13.80	8.20	1.10	60.80	1275.7	21.70	69.20	7.00	0.30	8.80	22.10	10.40
27.90	260.7	22.00	0.60	13.80	7.30	15.40	13.30	19.70	32.40	6.70	3.00	1.60	19.60	2051.0	14.10	19.10	2.70	0.40	4.10	14.80	12.40
28.15	283.0	28.90	13.50	20.30	15.30	25.80	17.40	31.40	43.60	6.10	4.50	0.40	33.70	1971.8	19.10	37.40	5.50	0.40	12.70	18.70	9.50
28.40	255.4	24.20	10.00	13.00	11.30	19.00	14.50	17.00	40.20	5.60	3.10	0.50	28.00	1991.7	15.60	31.60	3.80	0.30	6.40	19.10	6.80
28.65	247.9	31.60	14.60	19.30	14.20	28.70	18.90	20.90	47.00	8.50	2.80	1.90	34.20	2142.8	15.10	39.80	4.30	0.10	13.50	12.10	10.50
28.90	244.1	37.70	18.60	23.10	14.20	33.50	22.30	31.40	49.90	6.90	3.70	1.10	37.90	1983.1	15.10	41.70	4.90	0.20	10.00	21.70	11.20
29.40	281.1	32.20	8.10	13.70	11.90	27.70	17.00	28.50	46.10	4.80	5.70	2.60	34.10	2051.7	13.30	34.90	3.80	-0.40	18.70	28.70	11.50
29.65	254.6	34.10	11.70	12.90	9.80	37.90	23.00	32.30	52.80	7.10	4.60	0.40	45.70	1803.0	14.10	43.90	5.10	0.20	7.40	10.20	10.20
29.90	208.1	24.00	4.10	22.50	12.70	24.00	16.00	23.30	40.00	5.20	3.10	3.80	23.70	2353.6	11.40	23.40	3.50	0.30	2.60	15.30	9.40
30.15	213.0	28.20	3.40	11.10	9.90	28.00	17.30	20.60	44.00	4.60	4.60	1.10	32.50	2098.3	12.90	33.00	4.20	0.10	14.10	28.00	8.70
30.40	222.8	29.50	9.20	22.20	13.30	39.10	47.30	23.30	46.70	7.30	5.00	0.50	32.70	2720.1	11.70	56.90	4.40	1.20	14.10	24.70	5.90
30.65	252.4	34.20	16.20	20.20	16.30	37.90	16.40	29.80	48.50	7.60	4.10	1.00	40.40	2223.9	13.30	47.00	4.30	0.50	10.00	27.90	10.20
30.90	216.7	36.10	5.00	25.90	12.60	37.90	18.60	37.50	47.90	8.20	4.60	3.00	43.40	2323.1	13.40	59.80	4.70	0.40	5.70	6.20	8.30

31.15	174.0	23.40	5.40	21.70	10.70	28.40	17.00	16.70	37.10	6.90	5.50	1.40	30.00	2796.9	9.80	73.40	3.40	0.80	9.50	16.20	4.40
31.90	200.6	32.10	15.10	22.70	11.30	27.20	16.40	19.90	43.20	7.30	5.10	0.90	40.20	1778.3	15.50	53.40	5.00	0.40	6.30	8.50	7.90
32.15	238.0	27.90	10.60	17.00	10.60	18.00	14.30	16.60	43.40	8.40	3.30	0.70	30.20	1717.4	14.90	37.30	4.10	0.30	12.60	7.00	9.50
32.40	284.2	40.10	10.60	22.10	17.40	26.10	17.00	22.40	44.70	8.30	5.20	0.40	40.10	1548.5	19.10	47.70	4.10	0.20	16.80	18.90	7.10
32.65	265.7	26.50	3.90	15.50	14.10	23.60	18.50	31.30	41.20	6.30	4.00	0.10	28.90	1813.4	15.00	37.00	4.00	0.10	5.50	10.40	6.40
33.15	267.8	31.00	4.50	22.20	13.80	22.70	13.80	18.30	42.20	6.60	5.70	1.20	37.00	1673.9	14.60	40.70	3.90	-0.20	7.70	9.70	6.20
33.42	233.7	46.20	13.60	30.50	16.40	31.50	20.80	34.60	50.30	8.50	5.10	1.10	44.80	1585.7	17.90	61.50	6.30	0.30	7.80	7.00	8.00
33.90	236.3	24.60	9.00	15.00	11.40	20.50	14.90	17.60	41.70	8.50	3.30	2.80	32.80	1648.1	15.30	36.70	4.80	0.10	7.00	12.90	12.30
34.15	217.2	42.90	6.20	35.50	14.20	30.50	31.70	31.40	48.90	8.80	4.60	2.40	43.40	1678.5	17.00	70.30	5.60	0.80	-3.10	12.70	12.80
34.40	251.5	30.20	1.80	22.40	11.60	28.20	19.00	32.90	51.40	5.00	3.60	1.20	29.60	2100.6	13.40	30.70	3.20	0.40	11.10	12.40	8.60
34.65	210.9	33.00	7.00	13.00	9.40	34.00	16.80	18.20	41.60	5.70	2.10	5.00	34.80	2749.2	11.80	45.70	4.40	0.20	13.10	9.50	1.30
34.90	263.5	34.30	8.80	26.40	12.40	35.20	16.40	25.60	46.80	5.60	3.40	4.10	39.10	2237.2	12.40	46.40	5.00	0.50	12.90	18.60	6.50
35.15	144.2	22.20	1.10	17.20	6.60	22.10	10.30	14.60	31.80	5.20	4.60	0.20	26.80	3051.7	9.10	59.70	2.90	0.10	11.80	11.40	7.60
35.65	256.4	45.00	9.30	23.80	15.30	40.70	17.80	21.40	52.30	9.90	7.20	4.30	53.70	1656.0	14.80	61.60	6.20	0.10	2.90	7.90	7.40
35.90	260.0	29.20	7.80	16.40	7.40	21.10	14.00	19.60	45.70	8.20	5.20	1.00	41.30	1531.2	14.30	40.00	5.00	0.40	2.60	20.50	10.20
36.40	208.5	24.60	6.40	15.90	10.50	16.80	11.70	10.90	36.80	5.20	3.20	1.80	28.00	2100.8	13.70	47.20	4.50	0.20	18.10	7.40	7.70
36.89	170.1	46.10	3.60	28.10	14.50	45.80	17.40	15.40	43.80	10.30	5.80	0.90	47.20	2257.3	13.30	74.30	7.00	0.30	17.20	15.90	8.30
37.15	258.9	29.10	11.20	12.40	11.70	23.00	13.40	12.20	42.20	7.50	5.20	0.40	28.00	1614.4	15.40	38.50	4.30	0.10	5.30	8.40	12.00
37.40	218.1	23.30	8.10	7.90	7.90	14.00	11.00	8.20	33.20	4.70	3.20	1.00	22.80	1905.0	10.70	25.20	3.00	0.00	-4.20	14.70	5.50
37.64	237.6	25.00	4.10	15.30	9.30	20.60	12.70	20.80	38.60	7.40	5.70	3.80	31.90	1696.4	13.20	38.20	4.30	0.40	-4.70	19.80	6.10
38.65	148.8	19.80	1.80	14.00	8.00	10.00	9.10	2.40	30.80	5.90	1.70	1.80	15.70	1778.1	10.10	15.70	2.00	0.00	4.40	14.20	9.80
39.14	253.9	22.00	8.90	12.90	8.90	13.70	16.90	17.10	39.50	7.70	4.00	2.90	22.60	1580.9	10.80	24.50	3.30	0.10	6.10	14.00	10.20
39.40	229.3	32.50	9.60	20.00	15.40	22.70	13.90	22.40	41.20	6.50	3.80	0.60	32.00	2046.2	15.20	34.10	4.60	0.70	2.90	5.50	8.50
39.66	208.4	13.70	2.30	2.00	6.00	7.70	7.80	7.90	28.00	2.70	1.80	3.10	9.60	1996.4	10.00	9.60	1.60	0.40	7.90	6.90	6.10
40.15	187.7	18.30	8.80	9.30	8.10	10.90	9.60	9.40	28.60	4.90	2.60	2.60	12.40	2021.5	11.40	12.70	1.80	0.10	-3.70	3.80	8.90
40.90	306.4	31.80	4.10	14.10	11.90	30.10	16.60	15.80	48.20	5.10	5.40	1.10	34.90	2098.1	13.90	34.60	2.60	0.20	1.70	11.20	9.60
41.16	265.3	40.50	9.10	18.00	7.50	33.20	19.90	27.30	51.20	6.70	4.50	2.00	40.70	2147.5	14.50	43.10	5.10	0.40	13.30	15.50	7.60
41.40	209.5	24.20	5.10	15.70	11.00	24.00	12.90	15.70	39.00	4.70	2.20	-0.40	24.40	2395.2	11.70	28.30	2.30	0.40	10.50	10.00	14.40
41.65	283.9	15.00	1.60	15.10	8.70	14.20	10.00	16.30	38.00	4.30	2.30	0.10	13.80	2369.6	11.20	15.90	1.50	0.10	9.30	6.10	9.50
41.90	163.5	23.80	-3.40	16.70	6.70	27.80	13.20	11.50	33.10	3.10	1.40	1.70	16.70	3714.2	7.30	16.00	1.10	0.10	16.50	16.90	8.50
42.14	401.2	18.80	-3.20	13.10	9.30	17.10	10.30	12.70	32.70	2.50	2.60	0.30	17.30	2431.7	10.30	15.40	1.90	0.90	10.00	20.10	4.80
42.40	217.9	42.80	5.60	26.40	8.30	48.30	18.50	22.00	54.90	3.90	5.30	1.40	48.20	2415.0	12.40	46.90	6.00	0.30	16.40	36.30	6.30

43.17	378.0	48.80	13.90	15.50	11.00	30.60	23.90	33.80	52.70	5.60	5.60	-1.30	37.00	2265.6	12.60	37.30	3.80	0.90	11.90	23.20	10.10
43.40	312.3	31.40	9.60	22.10	14.70	33.20	20.40	26.90	46.40	5.20	5.00	2.60	37.80	2459.0	13.30	38.90	3.60	0.50	3.60	13.70	8.20
43.64	360.0	32.60	16.40	15.40	10.80	25.50	16.70	37.80	47.70	7.10	4.50	0.30	35.80	1960.9	14.40	35.10	4.20	0.20	7.60	10.20	10.20
43.90	302.1	20.60	14.00	10.90	3.90	17.10	17.30	34.50	40.80	4.80	4.10	-1.10	23.30	1706.1	12.20	23.40	3.10	0.20	-6.40	7.90	9.90
43.90	374.6	18.60	7.60	-7.20	3.30	16.10	35.20	9.20	32.10	3.60	4.50	1.80	24.10	1657.5	11.90	22.70	4.20	0.30	-1.70	16.00	8.10
44.15	180.4	24.60	0.50	24.80	10.90	26.40	21.30	26.40	40.00	5.30	4.90	0.90	26.30	3562.5	10.70	32.60	3.00	0.40	11.20	11.60	6.80
44.40	142.6	16.10	9.40	12.80	8.00	18.50	12.10	14.50	36.60	5.50	4.40	-0.60	23.80	2003.7	10.40	19.80	3.10	0.70	15.00	23.80	5.70
44.65	136.7	29.60	5.90	18.30	13.50	23.50	14.40	34.00	38.70	2.20	4.50	1.10	24.00	2267.1	13.60	22.90	2.70	-0.30	8.80	20.10	13.10
44.90	138.4	21.00	5.50	12.90	10.90	15.10	12.50	19.00	37.50	5.00	3.60	2.80	20.40	2044.1	12.00	18.20	2.90	0.20	7.30	11.60	7.20
45.15	117.3	22.90	4.90	3.40	7.50	12.80	12.90	23.10	35.50	4.90	4.10	3.10	19.00	1810.3	14.00	18.90	3.70	-0.20	6.80	16.40	10.50
45.40	143.0	21.30	6.70	23.80	13.60	26.70	16.00	24.50	42.00	2.90	2.90	3.00	25.40	2786.6	14.10	21.40	2.80	0.30	6.70	14.80	11.00
45.65	137.2	14.60	0.80	4.70	7.40	18.40	10.40	17.00	36.20	1.70	1.60	0.90	13.00	2678.9	12.00	9.30	1.60	0.20	-3.90	5.80	7.40
45.90	161.7	21.00	5.40	11.20	9.00	24.70	15.00	12.40	39.50	3.60	2.50	1.60	24.20	2989.4	11.60	22.30	2.60	0.30	13.00	17.30	11.60
46.15	128.8	22.70	0.60	10.50	8.40	15.40	13.20	19.40	36.30	4.90	4.10	-0.20	17.60	2412.7	12.60	16.20	2.00	0.00	3.00	11.20	8.90
46.40	140.2	27.90	3.60	10.80	7.30	28.10	13.40	17.80	40.40	6.00	3.20	1.90	29.60	2699.7	11.80	37.10	2.70	0.30	18.20	12.40	9.50
46.65	138.0	18.00	2.90	16.30	8.10	15.80	10.60	10.60	36.30	4.50	3.80	3.60	19.40	2301.3	9.10	16.30	2.20	0.00	-0.80	12.10	7.80
47.15	165.9	38.70	7.10	20.00	14.90	31.60	16.30	20.50	49.30	7.20	2.20	1.60	41.30	2121.3	14.40	39.30	4.50	0.20	-3.50	21.00	7.60
47.40	187.4	46.70	13.20	22.30	14.30	43.60	23.30	45.40	59.20	8.90	5.80	3.80	52.90	1769.0	15.40	55.20	5.80	0.00	1.70	25.60	12.50
47.65	183.0	41.10	12.70	20.90	11.90	36.70	21.10	25.30	53.40	5.10	5.00	0.00	44.10	2099.4	16.40	48.80	5.00	0.60	7.40	12.70	12.30
47.90	199.8	38.20	1.60	19.50	12.50	41.60	27.10	25.40	48.70	6.50	3.10	-0.20	42.70	2471.6	13.10	43.50	5.10	0.40	18.90	29.30	3.60
53.65	166.2	34.90	3.90	19.00	11.90	38.80	14.20	14.00	44.60	5.50	3.90	1.40	37.00	2562.3	12.80	47.30	4.10	0.20	13.70	20.70	10.00
53.90	171.4	45.40	5.00	26.10	14.60	47.90	18.90	21.00	50.90	6.90	5.10	1.30	49.60	2198.3	13.60	65.60	5.90	0.30	4.90	20.30	10.20
54.15	159.1	39.00	9.40	16.70	11.30	36.40	16.60	17.40	46.40	4.80	3.90	2.60	36.00	2476.7	12.80	40.10	3.90	0.20	12.80	21.20	11.80
54.40	143.4	21.60	4.10	13.90	11.50	24.00	10.70	10.00	35.00	4.50	4.70	1.50	27.20	2845.8	11.40	32.50	3.50	0.10	13.00	9.70	7.50
54.65	206.1	54.50	14.70	40.90	16.50	49.50	23.30	25.20	58.20	10.20	7.50	4.50	64.20	1976.2	14.50	72.20	6.90	0.40	9.80	22.10	6.30
54.90	156.3	35.30	7.50	13.30	7.00	32.30	16.00	16.70	44.70	5.90	5.00	0.60	38.30	2124.9	13.70	62.30	6.30	0.20	10.80	19.80	6.30
55.15	198.9	45.60	11.40	26.50	16.60	40.70	18.70	23.00	50.60	10.00	6.40	1.00	54.30	1806.6	17.50	90.50	7.00	0.40	11.20	20.00	9.50
55.40	188.4	40.70	15.70	35.10	17.70	41.90	19.30	18.80	47.70	7.10	6.50	2.90	51.90	1851.5	17.90	90.00	6.50	0.70	12.60	21.80	11.10
55.65	178.8	47.80	13.70	32.30	18.20	42.00	18.90	24.50	52.20	9.10	7.00	0.10	55.30	1810.6	17.00	84.00	7.70	0.70	20.30	27.00	10.00
55.90	205.6	51.30	16.70	36.20	17.90	46.20	21.70	23.10	53.30	10.00	7.90	5.70	62.20	1727.1	18.30	104.30	7.80	0.80	17.20	12.60	8.50
56.15	171.0	36.30	10.20	22.60	13.10	32.30	15.10	17.60	40.70	4.60	5.60	1.00	35.30	2440.1	13.60	59.00	4.20	0.40	5.60	10.20	10.00
56.40	135.9	22.10	4.20	19.60	11.30	22.20	10.90	7.70	33.00	3.40	3.20	4.90	18.90	3001.2	10.80	43.50	2.30	0.30	10.00	8.30	9.00

56.65	160.0	31.10	63.40	20.10	10.90	29.40	13.20	16.10	38.60	4.80	6.30	2.80	28.60	2814.2	10.90	36.10	3.30	-0.10	13.50	18.10	7.30
56.90	150.6	30.80	3.70	15.70	9.20	28.90	13.60	11.40	40.00	3.10	3.70	1.40	26.90	2849.1	10.30	26.60	3.20	0.50	10.10	20.60	7.60
57.15	146.8	38.30	4.70	25.00	12.00	36.00	17.50	19.20	46.50	4.80	1.80	3.10	36.50	2479.7	14.30	41.20	4.20	0.50	11.60	25.00	6.30
57.40	170.2	42.20	11.00	30.10	14.90	43.80	16.60	17.20	46.00	6.60	6.70	3.20	44.50	2311.5	15.30	60.00	5.00	0.10	4.40	23.60	11.20
57.65	212.9	65.10	16.80	42.20	21.20	54.90	25.90	34.40	65.40	11.00	7.70	2.60	71.40	1821.4	16.90	80.40	7.40	0.90	15.40	10.70	12.20
57.90	178.9	54.40	19.70	37.10	14.90	82.40	29.80	27.20	58.30	8.80	6.40	2.10	57.50	2041.1	15.30	65.70	7.60	1.40	10.30	7.30	11.00
58.15	129.8	31.70	1.60	19.60	13.70	30.10	14.60	17.90	42.70	7.30	4.60	-0.40	33.40	2292.5	12.90	50.20	3.60	-0.10	4.90	14.00	8.80
58.40	195.6	57.50	13.20	30.80	18.10	45.90	21.20	27.10	54.30	9.60	6.20	1.50	57.50	1871.7	16.20	83.50	6.80	0.50	14.60	4.80	7.00
59.15	153.9	34.00	4.90	22.50	15.70	33.40	16.30	16.70	42.30	5.60	5.50	-6.90	32.10	2390.6	16.10	44.00	3.40	0.60	7.90	18.40	9.30
59.40	161.4	37.90	5.10	23.80	8.50	31.20	14.80	17.10	41.00	6.50	5.20	2.30	32.40	2484.9	13.20	47.40	4.20	-0.10	15.60	6.80	10.50
59.65	155.5	25.90	6.10	24.20	13.10	30.50	13.60	7.80	37.10	5.20	4.20	2.10	34.10	2722.2	11.20	52.20	3.90	0.50	16.40	18.60	6.60
59.90	154.3	32.90	4.10	15.40	9.40	32.70	14.70	17.80	44.70	5.70	4.20	1.60	32.90	2905.2	10.80	40.40	4.80	0.90	15.00	9.70	11.10
60.15	165.3	42.10	11.30	22.40	9.10	44.40	17.90	11.10	41.20	3.90	4.60	1.90	41.70	2501.4	13.80	59.00	4.80	0.40	12.10	12.00	11.10
60.40	196.1	45.10	7.80	39.80	17.00	47.20	19.20	26.50	54.60	8.30	7.00	1.30	52.90	1943.0	16.30	77.80	8.00	0.70	13.80	6.80	10.30
60.65	153.8	19.70	12.60	21.80	13.00	24.40	11.70	6.50	35.40	3.40	2.80	33.50	43.40	2955.3	7.00	40.00	3.20	0.10	5.50	16.30	9.30
60.90	133.9	28.50	6.60	19.90	13.50	28.20	12.40	8.40	35.90	-0.70	2.50	2.10	23.70	2854.7	8.90	20.60	2.40	0.00	7.00	15.80	9.30
61.15	140.0	25.50	4.60	21.60	8.80	24.80	10.80	11.10	38.10	4.10	3.20	0.80	29.40	2917.3	10.00	27.80	2.60	-0.10	4.20	27.80	4.30
61.40	159.1	34.90	8.60	19.80	12.00	29.60	13.60	11.30	38.70	3.70	3.80	1.90	30.90	2639.2	10.10	33.80	3.70	0.40	11.90	11.50	9.70
61.65	153.2	25.50	5.60	12.70	7.40	26.00	11.70	8.20	36.50	3.00	3.00	2.30	23.60	2621.7	8.50	24.30	4.10	-0.10	8.30	12.50	6.60
61.90	137.9	28.70	7.40	8.80	12.70	28.50	14.50	12.00	38.20	8.60	3.20	2.00	26.10	2731.5	8.60	29.20	3.50	0.10	10.60	9.10	13.90
62.15	191.3	53.00	22.30	30.10	17.80	48.60	23.60	22.20	55.50	8.00	7.40	2.40	60.80	1563.6	15.50	86.50	7.20	0.80	11.30	23.40	9.40
62.40	148.7	28.50	8.20	10.90	10.00	27.30	13.20	10.80	38.60	5.20	6 20	2.10	27.90	2788.7	10.90	40.00	3.80	0.30	17.40	11.30	9.50
62.65	149.3	29.30	4.10	18.50	8.40	30.00	13.00	13.90	35.90	5.90	5.80	2.30	31.70	2620.0	12.10	47.00	4.00	0.30	15.80	12.60	10.00
62.90	136.5	26.10	6.20	12.60	6.00	27.00	13.10	6.90	41.90	3.60	4.30	4.80	25.60	2386.5	10.60	24.80	3.40	0.00	0.40	4.80	13.00
63.15	128.7	28.30	-0.60	8.80	9.40	25.60	12.50	7.10	34.50	2.30	1.40	0.80	18.20	2897.8	8.20	16.60	2.00	-0.20	14.10	7.00	12.30
63.40	141.9	14.60	2.40	14.80	7.90	21.70	10.10	4.40	21.00	2.90	3.90	-1.00	17.50	2804.8	7.30	20.90	2.10	-0.10	20.20	21.80	7.50
63.65	131.3	22.20	6.10	14.50	9.00	24.10	13.90	9.80	35.60	4.00	4.10	2.20	23.50	2597.4	10.50	33.80	2.50	0.30	5.90	8.80	8.70
63.90	133.4	23.10	-1.30	19.40	7.90	27.70	14.10	7.20	36.50	4.40	4.70	3.50	24.70	2824.3	9.30	28.10	2.70	0.30	5.40	10.00	8.20
64.15	155.8	36.20	8.30	16.30	14.60	31.90	15.70	9.90	43.10	6.20	6.30	-1.30	33.00	2565.7	13.60	49.00	4.30	0.60	14.50	7.40	10.00
64.65	173.3	36.50	-3.20	26.70	16.90	35.40	13.70	13.30	41.60	6.00	5.60	1.70	36.80	2474.9	12.40	53.90	4.60	0.10	39.80	8.30	9.10
64.90	176.5	35.60	9.40	24.70	15.30	35.70	17.00	14.60	44.00	6.20	6.10	4.80	39.50	2420.3	11.70	53.90	5.30	0.60	7.10	6.30	8.60
65.15	137.6	29.00	0.80	12.40	8.40	28.30	13.80	8.60	38.00	3.10	1.80	1.50	24.80	2413.3	9.80	27.00	2.80	0.30	7.80	6.40	8.80

65.40	182.5	47.00	13.40	34.70	13.70	42.60	20.30	22.60	52.00	10.20	7.00	-0.50	55.90	1886.5	16.40	74.60	7.60	0.40	14.80	10.20	8.30
65.65	132.6	29.40	8.90	17.70	9.90	31.20	13.30	10.80	38.70	6.60	4.50	3.20	28.20	2799.0	10.50	39.50	3.20	0.70	15.80	5.60	6.60
65.90	154.6	22.60	1.50	11.80	9.10	21.90	9.00	4.20	31.50	4.70	4.30	2.10	26.00	2370.7	8.90	39.10	3.70	0.10	6.00	3.60	7.30
66.15	146.1	31.30	8.50	10.00	9.60	31.50	13.70	10.80	40.30	6.10	5.20	1.00	33.80	2535.9	11.20	54.00	4.20	0.20	16.20	7.30	4.80
66.90	159.2	25.60	11.10	12.90	9.40	30.10	15.10	11.50	38.70	3.70	5.00	1.20	29.80	2378.0	10.60	44.10	3.70	0.40	11.40	6.70	7.40
67.40	148.3	21.00	4.10	10.20	13.00	24.50	12.10	5.40	35.00	3.90	4.50	0.60	21.60	2616.2	8.40	27.80	3.00	0.20	11.00	8.20	8.10
67.65	122.9	20.80	1.60	9.40	6.00	23.10	9.80	4.60	31.90	10.10	4.80	-1.80	16.50	2949.6	8.70	27.70	3.10	2.00	11.50	5.30	7.80
67.90	147.1	28.70	3.10	26.40	12.50	31.80	14.80	10.20	37.30	5.20	4.50	1.70	30.70	2688.6	11.10	43.80	0.40	15.30	10.40	4.20	9.50
68.15	166.5	32.40	6.40	26.40	16.20	31.60	14.70	13.80	37.90	7.30	24.20	0.80	31.50	2648.7	17.40	40.80	4.00	0.70	6.30	12.40	6.60
68.40	134.7	14.90	2.00	11.30	10.30	15.50	11.00	2.30	30.80	0.00	1.60	1.70	12.00	3149.3	7.60	12.10	2.00	0.30	10.10	13.00	9.00
68.65	160.6	32.40	6.60	17.00	6.10	34.40	18.00	15.90	45.20	2.70	3.90	1.10	37.40	2118.8	11.70	53.80	4.50	0.50	3.80	12.20	10.30
68.90	198.1	52.70	15.90	39.70	20.00	46.30	22.80	23.00	56.90	9.10	8.00	0.60	62.20	1809.0	17.00	94.80	8.50	0.40	5.80	13.80	10.60
69.15	148.8	32.50	9.30	17.00	10.50	28.50	14.80	8.40	40.30	5.20	3.90	1.70	30.10	2271.5	10.40	38.60	3.00	-0.10	-0.60	10.40	9.90
69.40	149.5	32.30	2.30	17.60	9.60	31.40	15.70	13.30	41.30	3.80	3.60	2.00	30.90	2703.8	10.40	36.90	3.60	0.10	9.50	13.50	7.80
69.65	191.8	59.40	13.80	40.10	17.60	59.70	23.80	18.50	57.10	9.10	7.00	3.30	64.50	1683.5	16.90	98.10	7.50	0.20	12.00	16.90	8.60
69.90	221.5	66.70	19.40	49.90	22.00	60.40	26.70	25.80	65.70	11.80	8.70	1.90	74.50	1304.0	21.50	116.90	10.00	0.20	13.50	12.90	7.60
70.15	215.5	52.80	15.10	39.20	17.10	52.80	22.40	26.60	56.80	7.80	6.50	1.00	60.60	1656.4	16.80	97.10	8.00	0.50	8.30	8.40	13.60
70.40	152.2	33.60	1.50	11.10	8.20	32.40	14.40	12.70	43.20	3.50	4.40	1.70	30.80	2283.0	10.90	39.10	4.50	0.30	1.90	11.30	8.80
70.65	175.1	34.80	2.90	22.60	14.70	35.70	16.30	13.10	44.80	7.60	4.10	0.50	37.00	2285.0	11.30	52.00	5.20	-0.10	3.00	5.70	9.20
71.15	187.3	39.90	10.30	24.70	13.00	40.10	17.70	17.70	48.50	7.30	6.70	2.80	45.90	2161.2	14.00	68.70	5.40	0.10	-2.20	12.30	11.00
71.40	151.8	36.00	9.30	19.30	12.50	35.70	18.00	17.40	44.40	5.00	4.20	-1.10	39.00	2376.0	13.50	55.60	5.30	0.40	13.30	9.00	7.60
71.65	156.9	27.70	1.90	14.80	7.70	24.80	13.10	8.10	36.00	3.40	4.10	3.10	25.70	2931.1	11.20	31.80	2.80	0.10	11.60	9.90	10.20
71.90	140.3	27.40	6.40	17.70	10.40	30.60	14.10	13.50	44.40	3.70	4.10	0.10	28.30	2463.3	10.30	37.80	3.60	0.50	10.40	10.20	11.60
72.15	185.6	36.60	10.30	27.70	10.30	38.30	17.30	16.30	45.80	5.70	3.90	2.60	39.10	2697.4	10.80	50.30	4.20	0.10	8.10	12.50	6.90
72.39	179.1	26.60	2.30	23.40	10.50	30.10	13.10	8.90	38.10	5.90	3.00	3.60	29.80	2821.1	10.90	43.10	3.60	0.20	14.30	13.50	7.10
72.65	169.2	30.80	13.50	25.20	11.40	36.00	15.70	13.80	44.60	4.10	5.80	2.30	37.70	2303.2	11.60	46.40	3.60	0.20	10.60	13.00	11.00
72.90	175.1	35.70	2.10	31.90	18.80	37.60	18.20	15.30	45.00	5.60	4.30	1.80	39.30	2261.5	12.10	58.10	5.30	0.80	5.40	13.00	9.80
73.15	165.1	25.70	8.10	20.00	10.00	28.10	11.10	8.00	36.80	6.00	4.30	3.80	34.80	2758.9	11.40	54.00	4.10	0.30	3.50	10.40	13.50
73.40	179.5	29.40	3.20	26.00	10.40	31.20	13.80	8.90	42.00	5.90	6.20	2.50	35.40	2488.0	11.80	62.10	4.80	0.50	12.80	8.60	7.90
73.65	173.8	38.70	1.40	26.30	13.10	31.10	14.50	14.00	43.00	4.80	5.40	0.50	37.30	2625.9	11.70	56.90	5.60	0.60	14.60	8.60	9.10
73.89	157.8	20.70	8.30	18.40	11.50	23.40	11.40	4.70	31.80	4.10	4.90	0.00	21.70	2978.5	8.90	39.20	2.50	0.30	16.70	15.70	8.80
74.40	170.0	34.70	9.10	17.40	9.50	39.40	17.90	13.20	40.60	6.90	4.50	2.00	32.80	2715.5	11.40	41.10	3.70	0.50	19.80	14.00	7.00

74.65	185.2	42.80	6.00	30.50	13.70	42.40	19.30	15.70	46.10	8.40	6.30	3.30	44.90	2429.9	12.60	59.80	6.20	0.30	20.30	16.70	9.80
74.90	247.5	82.20	24.50	35.00	17.40	71.50	28.30	30.50	64.10	9.80	8.10	1.50	62.10	1159.5	18.70	118.80	8.90	0.60	12.50	13.30	11.90
75.15	192.0	51.70	6.30	28.30	14.70	46.10	20.60	18.10	49.80	5.30	4.60	2.40	44.60	2313.7	13.10	55.30	6.40	0.30	16.80	21.20	12.40
75.39	184.0	44.70	10.80	18.10	8.00	46.10	18.20	12.80	45.30	5.30	5.60	3.00	42.70	2482.4	11.20	58.00	4.40	0.40	9.80	14.80	5.90
75.65	166.3	24.30	5.10	19.60	11.50	27.50	12.50	7.90	32.50	4.90	4.30	3.60	22.90	2965.5	8.80	41.80	2.80	-0.20	11.60	11.40	7.80
75.90	159.7	20.30	-0.70	20.10	13.90	24.30	10.90	5.00	29.40	3.80	3.70	0.00	19.00	3041.5	9.30	40.00	2.40	0.40	3.40	13.30	9.90
76.15	238.2	91.80	19.50	50.70	24.60	72.20	28.10	22.10	63.50	13.80	8.50	4.30	80.80	1126.3	20.00	126.10	10.80	2.40	10.50	15.60	9.30
76.40	174.2	29.00	1.10	24.00	10.60	32.50	13.60	10.80	34.90	3.60	4.70	4.00	28.50	2835.0	10.60	39.40	3.10	0.80	10.20	13.80	4.10
76.65	183.0	25.30	4.20	21.00	9.30	25.90	11.60	5.00	32.10	3.10	4.50	1.30	20.70	3033.2	9.00	38.70	4.00	0.00	6.50	10.30	8.10
76.89	241.1	57.80	15.70	34.40	15.70	53.70	21.30	26.50	52.10	9.90	8.90	2.30	63.10	1843.8	17.40	104.80	8.40	0.30	7.00	11.70	7.70
77.15	167.6	17.80	6.60	16.20	10.40	16.30	8.90	0.60	25.60	1.30	3.20	1.50	14.30	3160.1	7.40	40.10	2.20	0.50	9.10	10.20	5.60
77.40	166.7	17.60	6.70	7.80	8.70	18.90	8.40	3.30	28.40	4.00	2.70	2.80	16.60	3119.1	9.40	41.60	2.10	0.50	11.50	10.10	6.70
77.65	179.9	23.90	12.50	18.60	10.10	24.60	12.70	6.70	31.50	4.40	4.00	1.10	20.70	2976.2	9.70	39.00	3.40	0.50	15.80	12.00	7.00
77.90	170.6	19.10	6.20	13.60	5.70	19.20	10.00	3.50	28.50	2.00	3.10	0.50	16.40	3169.1	9.00	38.40	3.00	-0.10	9.60	11.10	8.50
78.39	164.9	27.80	-2.70	16.40	10.60	31.10	13.60	9.60	35.90	5.20	3.70	0.70	25.40	3008.8	10.20	32.10	3.50	0.50	11.50	18.30	9.10
78.90	214.9	38.40	1.30	19.90	13.40	36.50	16.20	13.90	41.10	6.00	4.90	2.10	38.10	2798.9	12.10	56.00	4.30	0.40	15.20	11.50	2.70
79.15	198.6	41.40	20.10	26.70	12.70	42.10	15.50	12.40	43.50	4.90	6.50	1.10	43.30	2632.4	11.30	61.00	5.50	0.50	14.70	17.00	9.00
79.40	196.0	36.70	7.60	28.20	13.50	35.60	18.40	15.30	44.20	4.40	5.20	3.60	40.00	2356.6	13.20	59.70	4.70	0.50	12.10	13.30	9.10
79.65	157.1	34.90	3.70	14.90	13.10	30.00	15.00	18.80	43.40	4.10	4.40	0.20	30.40	1975.8	15.40	36.50	3.80	0.90	8.80	12.60	7.60
79.89	192.3	52.80	9.40	30.50	17.50	47.20	24.00	30.20	61.70	8.80	5.00	2.20	55.50	1715.5	17.80	63.60	6.00	0.70	-1.90	5.50	11.00
80.15	182.5	40.50	10.50	31.50	13.70	41.10	22.20	25.50	56.60	6.40	5.80	4.60	52.00	1972.7	14.50	57.40	5.30	0.70	10.20	6.90	11.90
80.40	168.4	42.70	14.00	25.60	14.70	38.60	18.70	26.40	52.00	9.70	5.80	0.40	49.00	1922.9	13.50	56.80	5.00	0.50	7.70	13.30	8.30
80.65	164.9	36.30	9.90	21.20	13.20	30.00	15.40	21.60	46.20	8.20	4.70	1.20	36.00	1960.9	14.30	57.30	4.30	-0.20	0.90	17.60	9.80
80.90	192.5	47.80	15.00	28.70	22.50	43.50	19.80	21.30	54.50	9.40	7.80	1.50	58.00	1370.4	18.70	75.50	7.00	0.70	10.40	16.20	9.00
81.15	210.5	53.60	16.70	35.50	18.90	51.90	22.40	28.90	60.60	9.90	7.60	2.40	63.40	1353.5	19.40	84.60	8.40	-0.10	17.80	16.30	13.80
81.39	184.3	52.30	19.60	30.70	18.10	44.00	16.70	32.20	50.60	6.30	5.40	4.40	50.30	1587.0	19.20	66.10	6.30	0.70	10.30	13.90	8.90
81.65	199.0	49.00	17.20	27.20	15.70	42.40	20.80	22.60	52.30	5.40	4.30	3.70	50.00	1745.8	17.70	69.10	6.40	0.40	9.60	11.90	8.70
81.89	182.3	43.10	10.70	29.00	15.20	41.70	21.00	30.70	61.60	8.60	4.70	3.40	45.70	2167.5	15.90	54.20	4.90	0.40	4.90	12.50	6.60
81.90	194.0	42.40	11.80	17.10	12.60	37.80	20.70	33.10	53.60	7.60	5.80	3.50	42.20	1861.5	16.50	50.00	5.10	0.10	7.70	16.30	9.60
82.40	192.7	38.60	10.60	18.10	10.40	33.80	16.80	16.80	49.80	6.40	6.50	0.20	45.90	1896.4	15.80	50.80	4.00	0.10	6.30	13.10	6.40
82.65	180.9	41.50	8.10	21.70	13.60	42.90	18.80	21.80	59.10	7.50	5.60	1.00	49.20	1997.1	15.70	71.20	5.60	0.50	8.90	16.10	8.10
82.90	215.0	47.10	19.80	43.10	16.90	55.00	24.80	20.70	59.10	8.30	8.40	2.10	65.90	1780.8	17.20	91.10	7.60	0.60	1.80	19.40	12.70

83.15	216.1	47.80	16.80	36.00	19.10	51.60	24.50	29.70	59.60	7.60	6.10	-0.50	63.50	1703.7	16.90	81.30	8.20	0.20	8.30	17.80	10.90
83.39	206.6	51.00	13.70	28.30	17.50	45.00	36.80	30.10	62.60	8.90	6.80	0.40	59.60	1724.4	17.30	69.90	6.20	0.30	12.20	7.50	12.70
83.65	179.1	38.50	11.50	31.70	15.40	40.90	18.60	24.30	54.20	8.20	5.70	2.10	51.40	1820.9	13.90	63.60	5.80	0.40	13.90	15.50	6.40
83.90	249.3	69.90	21.20	52.60	26.50	68.10	25.60	24.50	63.50	10.50	8.50	2.00	83.70	1224.2	20.00	117.00	9.70	0.60	0.40	23.70	9.80
84.15	193.1	40.40	13.30	36.80	11.70	41.90	18.30	25.60	52.50	10.60	7.80	3.10	56.40	1559.0	17.60	85.80	6.00	0.40	1.00	14.40	10.30
84.40	223.5	54.00	16.70	39.50	17.20	50.00	21.20	31.60	59.20	9.90	7.60	0.90	60.20	1446.6	18.40	93.10	7.70	0.10	15.80	18.40	9.20
84.65	239.2	61.00	21.20	37.00	19.10	54.90	22.80	27.20	65.10	8.70	7.00	2.20	64.20	1421.6	18.20	118.00	8.00	0.20	15.20	13.20	13.30
84.89	216.2	58.30	15.10	31.30	17.40	51.80	23.30	21.60	59.00	10.40	8.40	1.90	63.50	1484.1	16.60	98.80	8.30	0.30	21.90	20.40	10.40
85.15	218.5	56.60	19.80	37.80	13.80	51.00	25.40	27.30	61.00	7.50	6.00	-0.20	48.70	1674.2	16.90	94.60	6.50	0.70	7.80	12.30	8.70
85.40	227.6	52.10	13.90	36.50	17.50	61.20	24.80	25.50	55.90	8.40	7.90	4.40	62.30	1449.1	16.40	89.80	7.00	0.70	6.10	14.70	11.30
85.65	191.0	45.90	15.50	26.90	14.40	42.40	20.00	22.90	55.60	7.20	5.00	2.10	48.90	1682.7	15.30	68.30	6.30	0.60	5.20	35.10	8.80
85.90	217.4	53.00	15.60	32.90	17.20	53.50	22.10	21.10	49.60	6.30	6.20	0.50	44.80	1773.9	15.70	80.70	6.40	0.10	7.60	19.60	10.20
86.39	281.1	107.20	24.10	57.30	27.50	84.10	37.80	32.40	74.30	13.50	9.10	2.90	79.40	651.7	21.40	151.50	11.60	0.70	16.00	22.90	16.00
86.65	297.1	102.70	22.70	51.90	25.50	79.50	30.90	30.40	69.70	12.30	9.50	1.70	77.30	705.4	22.40	148.70	11.10	0.60	14.90	21.70	13.90
86.90	251.1	100.50	18.10	55.40	30.10	71.60	31.60	34.70	74.00	13.20	8.80	1.40	83.10	602.2	23.50	141.30	11.60	0.70	11.30	48.40	13.50
87.15	292.9	117.60	28.30	63.50	27.90	86.40	33.90	38.80	80.70	16.60	9.80	2.50	91.00	443.0	22.50	154.60	12.40	0.70	17.30	31.80	18.00
87.65	287.5	107.70	25.90	45.50	25.60	83.50	34.30	36.40	74.20	15.30	9.90	4.40	82.80	585.4	23.00	149.10	11.10	0.30	18.90	24.00	16.30
87.89	273.8	100.70	21.80	54.80	23.90	79.90	41.00	33.30	87.70	12.80	9.20	3.70	78.10	706.8	22.00	150.20	11.10	0.90	0.10	22.40	15.70
88.15	297.7	106.80	27.10	55.30	24.50	84.20	35.20	35.40	74.80	12.40	10.00	2.20	82.30	593.9	22.80	150.80	11.60	0.70	12.00	20.80	16.70
88.65	305.5	111.30	21.80	50.40	22.50	87.20	35.80	34.30	76.40	14.00	9.30	3.60	86.20	545.9	22.20	164.40	11.90	0.80	10.70	15.80	13.70
88.90	295.4	101.20	65.00	51.80	23.60	78.40	33.80	34.80	77.10	12.50	10.50	3.60	80.60	681.3	21.90	149.60	11.60	0.50	9.90	15.60	13.00
89.15	249.6	83.30	18.90	38.80	21.70	68.80	29.80	31.50	69.00	10.00	6.80	2.40	68.60	1001.7	19.30	120.40	9.50	0.40	15.80	13.40	10.70
89.39	251.0	78.00	15.50	38.60	16.30	68.60	28.40	28.10	68.90	9.20	8.10	1.70	67.50	1014.2	19.10	117.50	9.70	0.50	18.40	24.20	9.20
89.65	252.2	86.40	16.70	47.70	24.00	68.30	28.90	30.80	70.60	10.60	7.70	3.30	67.00	1034.2	19.30	116.60	9.10	0.60	6.20	14.60	11.90
90.15	243.3	70.20	19.30	32.60	22.60	68.20	29.10	28.60	68.10	10.60	7.10	3.70	64.90	1071.9	18.60	117.40	9.20	0.70	7.30	16.20	9.70
90.40	223.2	68.10	14.40	33.70	17.30	59.00	28.40	27.30	61.90	7.20	6.10	2.30	55.20	1232.3	16.70	108.10	8.20	0.70	10.40	24.20	7.60
90.65	183.8	43.00	8.20	21.60	9.30	38.30	18.30	24.00	53.80	7.00	5.80	2.20	39.70	1992.3	14.90	55.10	5.60	0.30	6.80	21.90	11.10
90.65	220.4	64.60	14.00	36.60	15.00	60.00	25.40	29.20	67.30	7.70	7.80	1.10	57.00	1204.7	18.30	100.30	7.60	0.40	13.00	17.80	10.10
90.89	229.0	67.80	13.80	28.30	18.50	58.40	26.60	31.50	67.30	10.20	6.00	0.50	55.10	1238.9	17.20	93.80	7.60	0.10	-2.10	12.00	9.60
91.15	212.5	60.90	12.00	31.30	13.80	55.20	27.60	29.10	67.80	7.30	6.50	3.60	56.00	1247.5	16.80	91.60	7.60	0.70	14.20	13.30	12.30
91.40	194.3	58.30	13.60	24.30	15.30	55.00	26.80	32.50	64.50	5.60	6.60	0.90	52.20	1315.6	16.80	88.70	7.00	0.20	17.20	14.10	9.70
91.40	315.5	32.30	9.20	16.90	9.90	31.50	15.50	19.30	144.00	7.60	3.30	2.10	28.90	1742.8	12.60	45.70	4.20	0.60	9.20	13.10	11.10

91.65	155.1	35.90	2.00	20.00	9.90	37.60	15.50	17.60	47.70	4.20	3.80	1.20	33.80	1769.7	12.70	50.10	4.90	-0.20	12.10	14.70	11.10
91.90	205.3	44.90	17.40	33.60	16.10	48.60	20.10	20.40	52.00	7.70	7.40	1.70	47.90	1370.9	15.20	91.80	7.30	0.70	13.90	22.90	8.70
92.15	186.1	39.00	11.30	23.30	17.20	43.10	16.60	25.70	55.90	7.30	4.50	2.70	44.50	1509.7	14.20	64.40	5.10	0.10	1.90	21.00	9.60
92.65	202.4	41.40	13.80	31.60	12.80	47.30	16.20	23.00	54.90	4.20	5.00	0.00	48.50	1448.3	15.80	72.60	5.20	0.20	5.00	10.50	10.00
93.15	173.7	38.30	8.40	27.90	13.30	44.50	18.10	20.40	53.50	6.00	5.30	0.50	44.10	1471.1	14.70	66.10	5.40	0.10	7.60	15.70	7.90
93.44	240.4	87.90	18.10	35.20	16.80	69.40	28.20	29.80	67.60	11.10	7.40	1.50	66.10	1072.4	18.80	119.30	10.00	0.90	14.00	26.50	13.30
93.90	247.2	77.80	21.90	43.60	20.90	68.90	26.80	28.10	61.20	10.80	8.40	1.30	63.30	1216.7	18.70	115.50	9.40	0.50	-2.10	12.70	13.00
94.40	251.7	82.10	15.80	37.80	18.50	69.20	25.40	25.70	57.70	9.30	8.90	2.40	62.30	1180.2	18.20	116.30	9.70	0.70	13.60	17.70	11.60
95.40	200.1	52.20	16.80	23.20	13.10	43.70	20.50	24.60	54.80	5.50	4.90	1.70	44.80	1741.2	15.30	71.80	5.30	0.10	7.20	10.80	10.10
95.65	215.2	54.50	14.40	35.40	14.50	51.00	23.00	24.80	56.70	7.50	5.30	1.40	50.80	1700.5	16.10	85.90	6.60	0.90	5.80	8.80	9.00
95.90	222.4	53.80	13.00	42.90	19.00	49.40	22.50	23.60	57.60	8.60	7.90	1.60	52.70	1671.9	17.00	81.60	6.20	0.30	15.10	12.60	10.60
96.15	256.1	72.40	19.70	42.80	20.10	72.80	29.80	22.40	64.90	11.80	8.30	3.50	75.10	1099.4	18.50	126.90	10.40	0.80	6.50	30.60	8.60
96.44	225.5	55.50	13.60	30.40	18.30	52.80	24.60	21.50	59.30	6.50	6.90	3.70	55.60	1638.5	16.70	90.60	7.20	0.90	8.20	14.30	12.60
96.65	225.4	55.50	12.50	33.00	14.80	57.90	25.60	22.20	59.00	8.50	7.40	2.30	55.30	1575.9	16.70	89.70	7.10	0.10	9.30	12.00	12.50
96.90	204.1	48.10	8.20	32.90	15.30	49.50	19.60	23.00	59.10	8.50	5.60	3.80	49.50	1772.2	15.00	82.00	6.60	0.70	9.50	21.60	9.30
97.15	209.2	55.40	15.40	29.20	18.00	53.30	27.70	19.70	57.70	8.00	5.80	0.90	53.40	1646.4	17.60	88.40	7.30	0.50	12.20	17.20	14.40
97.40	226.2	47.20	17.60	31.50	15.50	43.60	21.40	17.00	50.80	7.70	5.30	1.70	44.20	1639.1	15.00	72.90	5.60	0.30	12.30	10.20	13.20
97.65	183.3	39.60	9.50	19.80	11.30	42.10	24.70	20.70	50.30	5.40	4.30	1.00	39.30	1986.2	15.50	60.40	4.40	0.90	9.10	17.60	12.30
97.94	196.9	44.80	9.30	19.80	13.00	41.20	24.00	20.10	51.60	6.70	5.80	2.10	45.30	1882.7	14.30	79.90	6.00	0.20	16.20	15.70	11.50
98.15	222.8	60.30	31.90	34.00	19.70	57.30	24.00	21.90	59.80	9.90	6.40	3.70	64.00	1490.1	18.50	101.30	8.00	0.30	6.90	21.40	15.30
98.40	215.4	61.90	29.40	43.10	21.80	61.00	24.50	27.90	63.90	10.00	7.70	1.40	66.90	1447.9	17.90	102.60	8.40	0.40	11.00	21.40	14.90
98.65	257.4	67.10	15.90	36.50	15.70	61.20	24.70	27.80	64.80	10.70	9.00	2.60	72.70	1283.8	18.20	107.30	9.40	0.10	7.50	22.30	12.00
98.90	252.4	63.50	20.40	42.80	22.70	60.30	24.30	27.50	63.50	10.30	8.00	1.10	70.70	1239.2	18.50	102.40	8.90	0.30	10.40	21.10	10.10
99.15	226.6	54.00	11.50	34.60	17.70	49.20	33.70	21.60	55.50	8.60	6.00	2.90	55.10	1533.1	15.80	101.40	7.20	1.00	11.40	18.30	8.50
99.44	223.3	56.10	13.70	23.50	14.10	46.80	23.40	32.60	57.60	10.50	7.70	3.80	57.60	1427.4	16.90	83.10	7.30	0.80	13.40	40.40	9.60
99.65	217.1	58.70	14.70	30.90	17.80	47.50	22.50	27.10	59.90	8.30	6.90	1.90	56.50	1483.3	16.70	91.90	7.60	0.50	3.00	24.50	8.90
99.90	186.5	44.10	9.20	19.40	12.60	41.20	19.50	23.20	52.50	7.00	7.10	1.50	42.80	1897.0	15.50	60.10	4.90	0.40	12.40	10.10	8.50
100.40	163.5	40.90	2.00	22.80	8.00	36.70	18.50	15.60	49.50	6.60	5.80	2.20	38.10	1987.7	15.60	64.10	5.20	0.70	13.20	16.00	9.00
100.65	214.8	70.40	20.60	38.30	18.00	63.50	29.30	31.40	69.30	9.80	6.40	1.40	65.50	1091.3	18.90	96.80	8.20	0.50	10.80	43.10	13.40
100.65	191.0	47.30	9.90	26.50	12.50	42.40	21.60	19.60	48.00	5.60	4.60	1.90	44.50	2426.8	12.60	54.60	4.90	0.40	16.00	16.60	9.00
100.90	236.7	70.50	20.60	34.80	15.80	67.10	29.20	36.60	68.90	10.70	7.30	3.40	70.20	1161.3	18.50	114.10	10.40	0.60	11.10	34.50	11.90
101.16	253.9	73.90	21.20	50.80	21.40	70.90	33.40	33.10	70.60	12.40	8.40	5.00	80.00	1009.7	22.10	127.50	10.50	0.60	1.50	19.80	15.00

101.41	221.9	69.00	19.50	34.40	19.90	59.20	28.70	29.00	66.50	6.60	7.30	2.70	67.50	1351.1	19.10	97.90	8.40	0.90	10.80	30.70	10.40
101.91	159.5	39.00	9.90	16.00	14.40	40.80	18.10	21.50	49.70	6.00	4.00	3.00	35.40	2133.5	14.40	59.60	4.50	0.00	4.90	18.60	7.40
102.16	205.2	58.10	13.50	36.90	17.30	56.00	33.70	27.30	62.10	7.20	6.90	1.90	52.00	1737.4	17.20	85.10	6.40	0.80	10.90	10.80	9.20
102.40	221.4	54.10	11.70	37.10	14.20	52.80	30.10	19.50	55.50	7.60	6.10	-0.70	53.30	1681.0	15.50	110.80	6.50	0.40	12.90	13.10	11.10
102.66	190.4	41.40	13.00	27.00	16.90	44.60	22.20	23.70	55.20	7.30	5.60	1.40	49.50	1745.1	14.60	67.30	5.50	0.70	2.70	13.10	7.70
102.91	207.0	52.80	14.30	30.80	16.80	51.10	23.20	25.30	60.90	6.60	6.10	1.90	52.10	1673.6	15.90	89.50	6.50	0.30	11.70	9.20	11.00
103.41	207.5	67.30	14.70	29.80	17.60	59.70	23.00	23.30	58.90	8.00	6.10	2.10	58.90	1427.3	16.90	114.30	8.00	0.00	11.30	16.40	10.40
103.66	185.7	39.20	11.10	27.10	16.50	38.10	12.90	14.70	45.00	7.60	4.10	3.10	39.60	1892.0	13.40	69.10	5.60	0.60	16.10	14.00	10.00
103.90	235.2	61.50	12.80	30.60	17.80	58.90	34.60	26.80	61.40	7.00	7.60	2.90	64.50	1191.5	18.30	138.20	8.70	0.80	20.20	14.80	10.80
104.16	233.7	66.70	14.80	38.70	18.60	64.00	29.50	32.80	71.50	11.00	7.80	2.10	70.80	1134.3	19.60	105.90	8.60	0.20	8.40	12.40	11.70
105.16	233.2	70.40	23.30	40.60	19.80	61.90	27.80	31.00	67.30	9.40	7.70	1.50	65.80	1266.9	17.70	101.60	8.90	0.40	12.00	12.90	11.60
105.40	210.3	70.20	21.80	40.50	18.90	62.50	28.00	31.50	69.80	10.80	9.20	4.10	72.70	1083.2	19.70	111.50	9.30	0.40	14.30	37.80	14.20
105.88	231.8	65.60	22.20	36.50	22.00	67.10	30.50	28.70	68.90	10.20	7.80	1.40	73.20	1055.6	18.90	118.80	10.10	1.00	7.90	13.80	10.20
108.16	173.5	26.70	7.30	22.40	11.10	34.00	15.40	3.40	35.40	5.00	5.30	2.50	22.80	2232.0	10.70	71.50	3.70	1.00	9.80	20.40	6.40
108.88	190.2	50.60	9.90	21.30	12.00	43.60	19.40	18.60	51.70	6.00	3.80	1.20	40.30	1672.9	14.30	76.00	6.00	0.20	2.00	15.50	9.70
108.91	208.4	53.30	23.80	31.50	12.60	56.10	21.10	21.80	56.40	7.60	5.60	3.80	50.20	1517.6	16.00	79.60	7.00	0.00	13.20	33.80	10.20
109.41	191.7	57.70	12.10	30.20	19.40	53.20	22.20	23.20	53.20	7.50	4.80	2.10	47.50	1643.8	16.10	86.80	6.60	-0.10	14.30	21.30	10.20
109.66	209.9	61.40	15.90	27.70	14.30	56.50	26.40	26.80	61.90	8.10	6.00	2.30	54.10	1378.7	18.40	93.80	7.80	0.40	9.00	22.00	13.00
110.40	248.8	65.20	16.80	42.00	17.50	71.10	24.50	22.00	62.00	10.90	7.40	1.20	69.10	1200.8	17.90	108.50	8.60	0.50	6.90	20.50	13.20
112.40	209.8	66.30	15.60	30.40	16.10	59.10	24.60	22.80	59.80	7.90	6.60	0.90	62.90	1264.0	17.90	106.40	7.60	0.70	12.80	41.20	12.20
115.15	205.3	63.10	16.70	36.20	21.60	53.20	24.80	22.50	62.80	6.40	5.60	2.80	51.20	1468.6	17.00	96.60	7.70	0.30	3.00	20.60	11.00
116.90	245.6	92.80	16.00	41.90	20.30	77.70	28.20	28.70	70.10	9.00	7.40	1.40	74.00	921.1	19.90	126.50	9.60	0.90	15.60	27.70	15.10
117.65	279.8	96.70	19.80	50.60	23.50	79.30	36.30	33.90	71.90	10.90	7.50	0.40	73.50	752.9	22.90	142.50	10.40	0.30	17.70	18.70	12.80
117.90	300.8	115.60	22.80	54.40	27.10	89.00	37.30	36.20	76.00	14.80	9.00	3.50	86.50	495.4	21.90	154.00	12.80	0.60	3.20	17.00	14.50
118.15	278.0	104.50	29.30	48.90	20.80	75.50	30.10	36.60	73.60	13.40	7.90	0.60	78.80	698.2	22.20	137.70	11.50	0.30	15.00	30.50	15.60
118.40	271.0	106.50	27.30	51.60	27.10	78.00	32.60	38.80	76.40	15.60	10.50	2.90	81.70	607.9	22.70	143.70	11.70	0.60	18.10	25.70	16.00
118.90	275.7	105.50	25.10	55.60	30.00	84.40	32.60	34.50	77.40	12.30	9.50	1.90	85.90	600.7	22.00	147.70	11.20	0.60	7.90	20.00	16.70
119.90	260.8	81.30	16.40	34.40	17.00	73.10	30.80	32.40	69.40	10.50	6.10	1.10	70.40	996.4	19.50	118.50	9.40	0.50	11.10	22.00	11.70

APPENDIX - E

McKenzie, J.A., Davies, P.J., Palmer-Julson, A., et al., 1993
Proceedings of the Ocean Drilling Program, Scientific Results, Vol. 133

11. LATE QUATERNARY PALEOENVIRONMENTAL CHANGE ON THE NORTHEAST AUSTRALIAN MARGIN AS EVIDENCED IN OXYGEN ISOTOPE STRATIGRAPHY, MINERAL MAGNETISM, AND SEDIMENTOLOGY[1]

Ian Alexander,[2] Dick Kroon,[2] and Roy Thompson[2]

ABSTRACT

To investigate late Quaternary paleoclimatic and paleoceanographic change in the sedimentary record, preserved on the Australian Continental Margin during the late Quaternary, core material was collected from Ocean Drilling Program, Leg 133, Site 819. An expanded sequence of late Quaternary, rhythmically bedded, predominantly hemipelagic sediments were recovered from Hole 819A. The foraminiferal $\delta^{18}O$ record preserved at Hole 819A suggests that the late Quaternary section is incomplete. Both benthic and planktonic $\delta^{18}O$ stratigraphies can be traced tentatively downcore to stage 9 at about 32.5 mbsf, where a major hiatus occurs. At this level, a slump detachment surface has been identified (Shipboard Scientific Party, 1991). This slump has removed marine oxygen isotope stages 10 to 13. Below 32.5 mbsf, continuous correlation can be achieved in the planktonic $\delta^{18}O$ curve, with existing deep-sea foraminiferal oxygen isotope stratigraphies from stage 14 through stage 28.

The major hiatus at 32.5 mbsf marks the position of a significant change in the character of the sedimentation at Site 819. Sediments below 32.5 mbsf, relative to those above 32.5 mbsf, are characterized by less variation in mean particle size; lower percentages of carbonate content in the coarse fraction (>63 µm); a stronger relationship between the percentage of fine fraction and magnetic mineral concentration, and lower foraminiferal abundances. Above the hiatus, large fluctuations in mean particle size occurred, which have been interpreted to be the result of high foraminiferal abundances. Early highstands show high terrigenous influx in the fine fraction above the hiatus. This is the opposite of the general idea of high terrigenous influx during lowstands of sea level on siliciclastic dominated continental margins. We are far from understanding the origin of this material and further investigation will be required (see also Glenn et al., this volume).

All our records, except the planktonic foraminiferal oxygen isotope record, indicate that the major hiatus marks the position of a significant change in the environment at Site 819. The planktonic foraminiferal $\delta^{18}O$ record suggests that environmental change occurred prior to the formation of the hiatus (i.e., near the Brunhes/Matuyama [B/M] boundary). The interval between the B/M boundary and the hiatus represents a transitional period between two different patterns of ocean circulation.

Throughout most of the lower part of the sequence, Site 819 was at a shallow-water depth and local oceanographic conditions were dominated by sluggish Subtropical Central Water (SCW) flow. However, near the B/M boundary, ocean circulation patterns intensified, reflecting a worldwide change in paleoenvironment. Enhanced ocean circulation patterns were possibly aided by tectonic subsidence. During this period Site 819 became progressively more under the influence of Antarctic Intermediate Water (AAIW), than SCW.

In the upper part of the sequence at Hole 819A, we see a continuation of the pattern of oceanographic reorganization suggested during stages 21 through 14. Intensification of the subsurface oceanographic circulation was also accompanied by the progressive wedging southward of surface waters associated with the East Australian Current (EAC).

The change in the nature of the records in the lower and upper parts of the sequence at Site 819 are thought to reflect perturbations by the orbital eccentricity cycle.

INTRODUCTION

The region offshore of the Australian continental margin is an extremely complex product of rifting, seafloor spreading, and margin accretion (Shipboard Scientific Party, 1991). During the evolution of the continental margin patterns of sediment production, transport and deposition have changed in response to fluctuations in both climatic and ocean circulation. The modern day physiographical setting on the continental margin, east of Cairns, is dominated by the presence of extensive carbonate bioherms (Davies et al., 1989; Harris et al., 1990). However, prior to the development of carbonate builds patterns of sediment production, transport and deposition, were most likely different and more open to the influence of ocean circulation pattern and sea level change.

To investigate the potential paleoclimatic and paleoceanographic change on the Australian Continental Margin, core material was collected from Ocean Drilling Program (ODP) Leg 133 Site 819 (NE-3). Site 819 forms part of an eastward-extending transect from the outer shelf and slope of the continental margin (Sites 819 through 822) into the Queensland Trough (Site 823) and onto the Queensland Plateau (Sites 811/825 and 824) (Shipboard Scientific Party, 1991). This transect was designed to investigate the evolution of a basin and its adjacent platforms, with emphasis on developing sedimentary sequences.

Site Description

Site 819 (NE-3), drilled during Leg 133, is located in 565.2 m of water in Grafton Passage on the upper slope off the Great Barrier Reef (GBR) east of Cairns (Fig. 1). Sediments were recovered from Site 819 using an advanced hydraulic piston corer (APC) between 0–123 meters below seafloor (mbsf) and by the use of an extended piston core barrel (XCB) to 123–400 mbsf. Above 123 mbsf, 133.5 m of sediment was recovered (gas expansion of cored sediments gave 108.6% recovery) at Site 819. Below 123 mbsf, 277 m of sediment was cored, with a 205.5-m (74.3%) recovery.

Site 819 yielded an expanded Pleistocene section (spanning <1.48 Ma) of rhythmically bedded, hemipelagic, carbonate and siliciclastic sand and mud. Five major sedimentary units were identified by the Shipboard Scientific Party (1991), of which only the upper two fall within the scope of this study. Sedimentary Unit I, representing Cores 133-819A-1H through to -4H-3 (0–32.5 mbsf), were found to consist

[1] McKenzie, J.A., Davies, P.J., Palmer-Julson, A., et al., 1993. *Proc. ODP, Sci. Results*, 133: College Station, TX (Ocean Drilling Program).

[2] Department of Geology and Geophysics, University of Edinburgh, West Mains Road, Edinburgh EH9 3JW, Scotland.

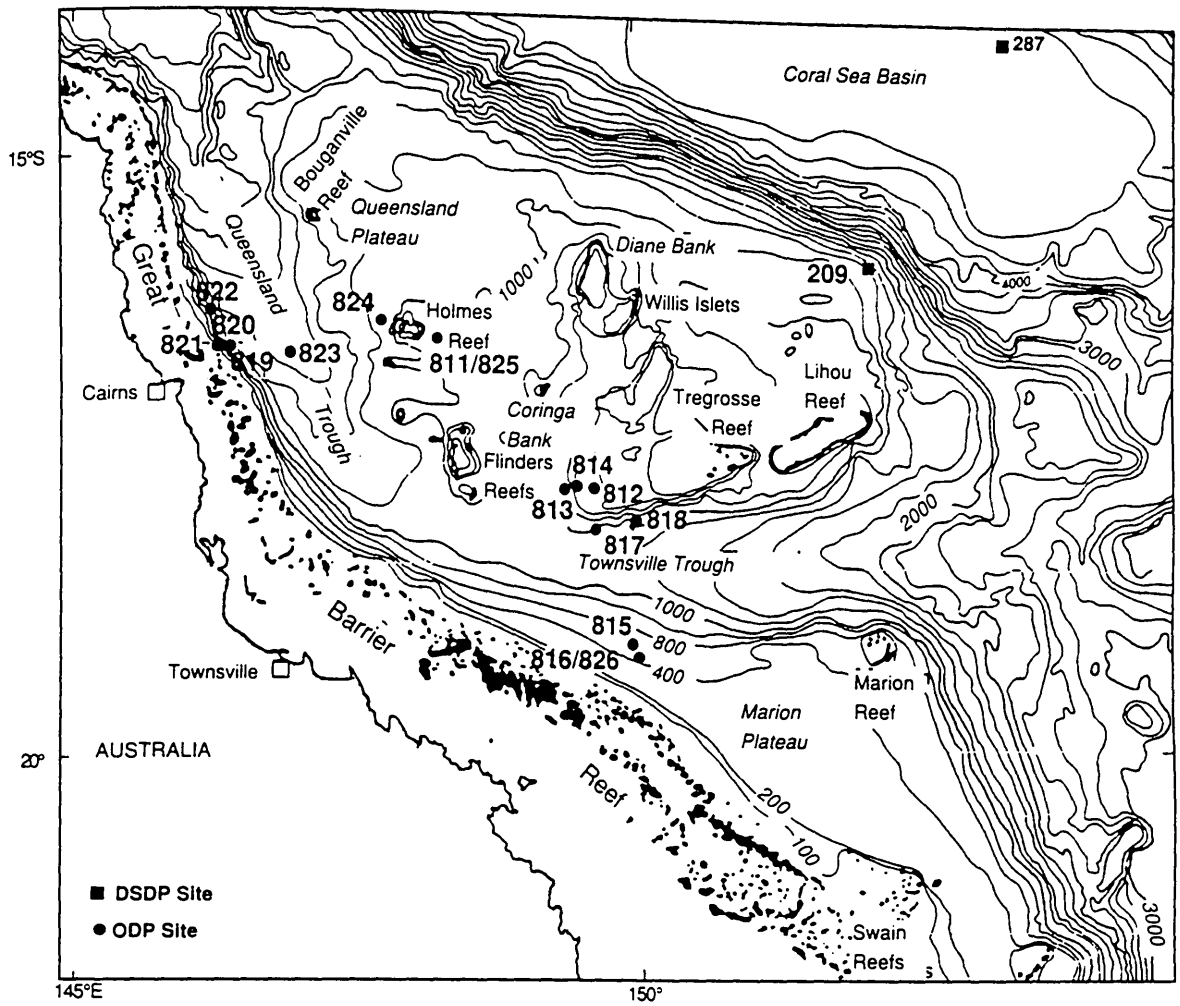

Figure 1. Map of northeastern Australian margin showing Leg 133 drill sites. Bathymetry in meters.

of rhythmically bedded sediment couplets about 9.6 m long; the upper half-couplet consisting of light greenish-gray clayey nannofossil ooze with assorted shallow-water bioclasts and the lower half-couplet made up of dark greenish gray clayey nannofossil ooze with numerous silt intercalations. Unit II, Cores 133-819A-4H-3 through to -11H-2 (32.5–97 mbsf), made up five rhythmic couplets approximately 13 m thick. The lower half-couplets, in Unit II, were characterized by the presence of abundant intercalations of silt; these graded upward into the dolomitized clayey nannofossil oozes of the upper half-couplet. A stratigraphic hiatus separates sedimentary Unit I from Unit II and was visually characterized by steeply inclined bedding and a rapid change in contents of calcium carbonate (Shipboard Scientific Party, 1991).

The general depositional setting for all five sedimentary units has been interpreted as being that of an upper-slope environment, perhaps distally tapping fluviodeltaic terrigenous sources (Shipboard Scientific Party, 1991). Benthic foraminiferal assemblages indicate an upper bathyal paleodepth (200–600 m) for Hole 819A. Tentative interpretation of the sedimentary couplets suggests that the basal clay-rich half-couplets of each cycle may relate to periods of sea level lowstand and enhanced terrigenous influx, while coarser upper portions are related to periods of sea level highstand with enhanced neritic carbonate production and detrital shedding onto the slope (Shipboard Scientific Party, 1991).

ANALYTICAL TECHNIQUES

Shipboard samples were collected routinely at 20 cm intervals down the core to a depth of 400 mbsf. Samples from the uppermost 120 mbsf at Hole 819A form the basis of this study. Post-cruise (laboratory-based) measurements on discrete samples included magnetic susceptibility and laboratory-induced remanences, particle size characteristics, planktonic and benthic foraminiferal oxygen isotope analysis, and carbonate content determination. With the exception of benthic foraminiferal oxygen isotope analysis, all parameters were successfully completed downcore to 120 mbsf.

Magnetic Mineralogy

Five different types of laboratory-induced magnetization were employed to ascertain the likely composition and grain size of the assemblage of magnetic minerals in the Hole 819A sediments. Since single magnetic parameters, such as susceptibility (X), anhysteretic,

Table 1 (continued).

Depth (mbsf)	χ ($\mu m^3 kg^{-1}$)	ARM (mAm^3kg^{-1})	IRM (40mT) (mAm^3kg^{-1})	IRM (100mT) (mAm^3kg^{-1})	SIRM (mAm^3kg^{-1})	ARM/χ (K Am^{-1})	SIRM/χ (K Am^{-1})	S ratio
108.1	0.0019	0.11	0.44	0.72	0.82	0.60	4.35	0.87
108.3	0.0022	0.07	0.27	0.45	0.58	0.34	2.63	0.77
108.5	0.0020	0.03	0.32	0.53	0.67	0.45	3.33	0.73
108.7	0.0022	0.08	0.24	0.49	0.62	0.38	2.73	0.73
108.9	0.0019	0.03	0.34	0.57	0.70	0.48	3.63	0.81
103.1	0.0020	0.03	0.31	0.54	0.64	0.46	3.22	0.85
103.3	0.0021	0.08	0.31	0.50	0.64	0.38	3.02	0.78
103.6	0.0018	0.11	0.48	0.71	0.91	0.63	4.95	0.73
103.8	0.0015	0.10	0.37	0.64	0.82	0.65	5.35	0.78
110	0.0021	0.09	0.27	0.52	0.66	0.43	3.03	0.73
110.2	0.0019	0.03	0.36	0.63	0.80	0.50	4.24	0.80
110.4	0.0017	0.03	0.36	0.63	0.78	0.50	4.53	0.81
110.6	0.0025	0.10	0.36	0.65	0.81	0.39	3.24	0.81
110.78	0.0034	0.03	0.35	0.63	0.74	0.26	2.20	0.85
111.1	0.0014	0.03	0.26	0.44	0.47	0.65	3.37	0.93
111.3	0.0014	0.08	0.25	0.42	0.54	0.58	3.88	0.73
111.55	0.0017	0.03	0.22	0.48	0.62	0.55	3.70	0.77
111.68	0.0015	0.03	0.26	0.44	0.56	0.61	3.67	0.73
111.88	0.0013	0.09	0.28	0.44	0.55	0.66	4.15	0.81
112.08	0.0013	0.03	0.26	0.44	0.56	0.65	4.14	0.78
112.28	0.0013	0.03	0.29	0.52	0.56	0.69	4.24	0.92
112.46	0.0013	0.10	0.26	0.55	0.67	0.75	5.19	0.82
112.68	0.0019	0.03	0.30	0.53	0.65	0.49	3.47	0.81
112.88	0.0017	0.10	0.29	0.55	0.61	0.57	3.55	0.90
113.13	0.0019	0.10	0.31	0.61	0.72	0.52	3.75	0.85
113.38	0.0022	0.11	0.37	0.65	0.77	0.50	3.48	0.84
113.58	0.0021	0.10	0.33	0.58	0.76	0.48	3.57	0.77
113.78	0.0019	0.10	0.39	0.65	0.78	0.52	4.03	0.83
113.96	0.0024	0.10	0.35	0.67	0.78	0.41	3.22	0.87
114.18	0.0022	0.11	0.38	0.67	0.82	0.51	3.74	0.81
114.38	0.0023	0.11	0.36	0.80	0.73	0.46	3.15	1.03
114.68	0.0027	0.13	0.41	0.77	0.98	0.47	3.66	0.78
114.88	0.0023	0.12	0.42	0.85	1.04	0.54	4.59	0.82
115.08	0.0026	0.14	0.42	0.81	0.98	0.52	3.77	0.84
115.28	0.0025	0.12	0.44	0.77	0.94	0.49	3.78	0.83
115.46	0.0031	0.13	0.47	0.84	0.98	0.42	3.20	0.85
115.68	0.0031	0.13	0.51	0.94	1.08	0.42	3.44	0.87
115.88	0.0035	0.13	0.46	0.84	1.08	0.37	3.08	0.79
116.18	0.0030	0.12	0.51	0.36	1.03	0.41	3.59	0.88
116.38	0.0036	0.15	0.55	0.95	1.17	0.41	3.21	0.81
116.58	0.0033	0.16	0.61	1.06	1.31	0.48	3.97	0.81
116.78	0.0033	0.12	0.59	1.12	1.37	0.37	4.19	0.82
116.96	0.0038	0.13	0.74	1.32	1.48	0.34	3.88	0.89
117.18	0.0035	0.13	0.67	1.31	1.61	0.39	4.65	0.81
117.68	0.0041	0.19	0.77	1.41	1.66	0.46	4.07	0.85
117.88	0.0045	0.15	0.76	1.42	1.62	0.33	3.58	0.88
118.08	0.0043	0.14	0.73	1.46	1.70	0.33	3.98	0.86
118.28	0.0035	0.18	0.68	1.48	1.68	0.53	4.81	0.88
118.46	0.0033	0.15	0.84	1.55	1.81	0.45	5.46	0.86
118.68	0.0029	0.17	0.70	1.38	1.70	0.57	5.84	0.81
118.88	0.0023	0.15	0.69	1.30	1.60	0.65	6.93	0.81
119.18	0.0028	0.13	0.65	1.29	1.51	0.46	5.46	0.85
119.38	0.0034	0.17	0.66	1.24	1.55	0.50	4.53	0.80
119.58	0.0032	0.15	0.66	1.30	1.53	0.49	4.86	0.85
119.78	0.0029	0.11	0.65	1.20	1.46	0.40	5.07	0.82
119.96	0.0028	0.12	0.69	1.34	1.62	0.45	5.88	0.83
120.18	0.0034	0.11	0.67	1.21	1.45	0.32	4.31	0.84

Gartner, this volume) were used to constrain isotopic stage assignment. The lowest occurrence (LO) of *Emiliania huxleyi* was located at 29.4 mbsf and indicates the position of stages 9 through 8, while the highest occurrence (HO) of *Pseudoemiliania lacunosa* at 32.4 mbsf indicates the position of stage 12. The foraminiferal datum event, the HO of the pink-pigmented foraminifer *Globigerinoides ruber*, was used to fix the position of the stage 6/5e oxygen isotope boundary (Thompson et al., 1979) at about 18 mbsf.

The Brunhes/Matuyama boundary has been identified at 41 mbsf, and the top of the Jaramillo Subchron was recorded between 115 and 120 mbsf (Barton et al., this volume); both were used to define the approximate position of the stage 19/20 boundary and stage 28, respectively.

According to the biostratigraphy the foraminiferal $\delta^{18}O$ stratigraphy at Hole 819A appears to be incomplete. A major hiatus is present at 32.5 mbsf, as indicated by the condensed nature of the nannofossil stratigraphy (i.e., the HO of *P. lacunosa*, 0.465 Ma) is almost at the same depth as the location of *E. huxleyi* (0.275 Ma). Also, the upper part of the isotopic record is punctuated with several minor hiatuses. In our interpretation, part of glacial stage 6 and possibly stage 5 is absent. Clearly, no easy solution is available for the problem of isotopic stage assignment above 32.5 mbsf at Hole 819A.

Table 1 (continued).

Depth (mbsf)	χ ($\mu m^3 kg^{-1}$)	ARM (mAm^3kg^{-1})	IRM (40mT) (mAm^3kg^{-1})	IRM (100mT) (mAm^3kg^{-1})	SIRM (mAm^3kg^{-1})	ARM/χ ($K\ Am^{-1}$)	SIRM/χ ($K\ Am^{-1}$)	S ratio
90.5	0.0053	0.15	0.90	1.41	1.68	0.29	3.18	0.84
91	0.0049	0.13	0.71	1.13	1.37	0.27	2.79	0.82
91.2	0.0042	0.13	0.66	1.04	1.26	0.31	3.00	0.83
91.4	0.0043	0.12	0.65	1.06	1.29	0.28	3.02	0.83
91.6	0.0045	0.10	0.59	0.92	1.14	0.22	2.56	0.81
91.8	0.0033	0.09	1.03	0.80	0.99	0.27	3.02	0.81
92	0.0046	0.12	0.58	0.94	1.16	0.27	2.53	0.80
92.2	0.0046	0.10	0.60	0.96	1.17	0.22	2.57	0.82
92.5	0.0045	0.13	0.62	0.99	1.19	0.28	2.67	0.83
92.7	0.0044	0.15	0.69	1.09	1.32	0.33	2.98	0.83
92.9	0.0048	0.12	0.62	0.97	1.15	0.24	2.41	0.84
93.1	0.0042	0.12	0.62	0.97	1.18	0.28	2.78	0.82
93.3	0.0044	0.12	0.63	0.98	1.21	0.28	2.77	0.81
93.5	0.0048	0.14	0.61	0.95	1.16	0.28	2.38	0.82
93.7	0.0048	0.11	0.64	0.98	1.17	0.22	2.46	0.84
94	0.0047	0.10	0.60	0.91	1.15	0.21	2.47	0.79
94.2	0.0045	0.11	0.64	1.01	1.22	0.25	2.70	0.83
94.4	0.0048	0.12	0.61	0.96	1.18	0.25	2.45	0.81
94.6	0.0044	0.12	0.55	0.90	1.16	0.27	2.63	0.77
94.1	0.0049	0.09	0.60	1.01	1.17	0.18	2.38	0.86
94.42	0.0051	0.13	0.61	0.76	1.24	0.26	2.42	0.61
94.62	0.0041	0.11	0.50	0.78	0.96	0.27	2.36	0.81
94.82	0.0041	0.13	0.54	0.84	1.05	0.32	2.57	0.80
95.02	0.0043	0.11	0.47	0.78	0.98	0.26	2.27	0.80
95.22	0.0041	0.12	0.54	0.90	1.11	0.30	2.70	0.81
95.42	0.0036	0.11	0.47	0.79	0.93	0.30	2.60	0.85
95.62	0.0037	0.07	0.46	0.78	0.93	0.19	2.51	0.83
95.92	0.0038	0.11	0.46	0.77	0.94	0.29	2.47	0.82
96.12	0.0037	0.06	0.44	0.79	0.91	0.16	2.50	0.86
96.32	0.0037	0.11	0.45	0.74	0.86	0.29	2.31	0.87
96.52	0.0035	0.11	0.43	0.71	0.81	0.31	2.35	0.88
96.72	0.0034	0.13	0.50	0.81	1.00	0.38	2.98	0.81
96.92	0.0037	0.06	0.44	0.73	0.92	0.16	2.48	0.79
97.12	0.0036	0.12	0.50	0.81	1.02	0.33	2.81	0.79
97.42	0.0042	0.12	0.47	0.80	1.00	0.29	2.37	0.81
97.62	0.0036	0.10	0.44	0.72	0.87	0.29	2.41	0.83
97.82	0.0035	0.11	0.43	0.71	0.87	0.32	2.49	0.82
98.02	0.0037	0.08	0.46	0.77	0.97	0.21	2.64	0.79
98.22	0.0034	0.08	0.43	0.74	0.92	0.22	2.70	0.80
98.42	0.0030	0.06	0.41	0.69	0.88	0.21	2.89	0.79
98.62	0.0030	0.12	0.43	0.73	0.92	0.40	3.07	0.79
98.92	0.0028	0.06	0.36	0.73	0.91	0.23	3.27	0.80
99.12	0.0034	0.07	0.45	0.75	0.89	0.20	2.66	0.84
99.32	0.0029	0.12	0.44	0.71	0.89	0.41	3.13	0.80
99.52	0.0029	0.06	0.39	0.68	0.87	0.21	2.99	0.79
99.72	0.0033	0.10	0.34	0.71	0.87	0.32	2.67	0.82
99.92	0.0027	0.11	0.39	0.71	0.84	0.39	3.08	0.84
100.12	0.0023	0.07	0.42	0.76	0.93	0.29	3.99	0.81
100.42	0.0027	0.06	0.40	0.67	0.85	0.23	3.14	0.78
100.62	0.0032	0.10	0.38	0.67	0.83	0.31	2.62	0.81
100.82	0.0028	0.12	0.42	0.72	0.87	0.42	3.14	0.82
101.02	0.0025	0.09	0.38	0.63	0.81	0.38	3.29	0.78
101.22	0.0028	0.10	0.40	0.68	0.89	0.36	3.13	0.77
101.42	0.0028	0.09	0.38	0.67	0.84	0.34	3.03	0.80
101.62	0.0026	0.11	0.37	0.65	0.75	0.41	2.90	0.86
101.92	0.0026	0.10	0.42	0.70	0.87	0.39	3.31	0.80
102.12	0.0026	0.11	0.42	0.76	0.94	0.40	3.58	0.81
102.32	0.0025	0.05	0.39	0.65	0.83	0.21	3.36	0.79
102.52	0.0023	0.11	0.42	0.70	0.92	0.47	3.97	0.76
102.72	0.0027	0.08	0.37	0.80	0.98	0.28	3.62	0.81
102.92	0.0025	0.07	0.43	0.75	0.94	0.28	3.76	0.80
103.12	0.0024	0.10	0.37	0.67	0.83	0.40	3.47	0.80
103.42	0.0022	0.08	0.34	0.74	0.89	0.37	3.98	0.84
103.62	0.0025	0.12	0.45	0.77	0.95	0.48	3.73	0.81
103.82	0.0025	0.10	0.45	0.80	0.96	0.42	3.86	0.83
104.02	0.0022	0.07	0.43	0.75	0.93	0.30	4.26	0.81
103.6	0.0024	0.12	0.41	0.76	0.92	0.48	3.76	0.83
103.8	0.0030	0.15	0.58	0.99	1.27	0.51	4.20	0.79
104	0.0031	0.16	0.58	1.05	1.28	0.51	4.15	0.82
104.2	0.0029	0.10	0.57	1.03	1.25	0.35	4.34	0.83
104.4	0.0000							
105.1	0.0035	0.17	0.69	1.16	1.47	0.49	4.25	0.79
105.3	0.0029	0.13	0.54	0.95	1.20	0.45	4.21	0.79
105.5	0.0029	0.13	0.55	0.99	1.19	0.47	4.16	0.83
105.7	0.0024	0.12	0.52	0.92	1.17	0.50	4.90	0.79
105.9	0.0024	0.13	0.45	0.89	1.08	0.52	4.42	0.82
106.1	0.0021	0.10	0.43	0.79	0.98	0.47	4.72	0.81
106.3	0.0018	0.08	0.33	0.60	0.81	0.44	4.50	0.74
106.6	0.0022	0.08	0.33	0.57	0.74	0.36	3.34	0.77
106.8	0.0024	0.09	0.31	0.63	0.81	0.39	3.36	0.78
107	0.0019	0.08	0.29	0.58	0.72	0.43	3.73	0.80
107.2	0.0013	0.03	0.32	0.59	0.74	0.64	5.58	0.80
107.33	0.0017	0.07	0.26	0.49	0.59	0.44	3.44	0.84
107.6	0.0022	0.10	0.38	0.66	0.77	0.43	3.47	0.86

and isothermal remanent magnetization (ARM and IRM, respectively) are largely dependent on the concentration of magnetic minerals present in a sample, several "interparametric" ratios (e.g., S ratio [Bloemendal, 1983], ARM/*X*, and ARM/SIRM) were determined to investigate changes in magnetic mineralogy (Kent, 1982; Robinson, 1986).

Specific Magnetic Susceptibility (X)

Susceptibility is a measure of the ease with which a sample can be magnetized. It is primarily dependent on the concentration of magnetic minerals present in a sample, such as magnetite and maghemite (Thompson, 1979), although it is also related to other parameters, such as magnetic grain size and shape.

Susceptibility measurements were taken on 10 cm^3 sample core plugs using a Bartington Instruments susceptibility meter. Calibration was achieved using a paramagnetic salt ($FeSO_4 \cdot 7H_2O$) standard. Noise levels were below 0.1 $10^{-6}m^3kg^{-1}$. Mass specific susceptibility measurements were obtained for samples by dividing the total susceptibility by the sample weight and expressed in units of 10^{-6} m^3kg^{-1} (Table 1).

Anhysteretic Remanent Magnetization (ARM)

Anhysteretic remanence is a laboratory-induced magnetization acquired when a sample is subjected to a declining alternating field in the presence of a direct magnetic field. The magnitude of the remanence depends on the strength of the direct magnetic field, the amplitude of the alternating magnetic field, and the susceptibility of the sample (Tarling, 1983).

ARM growth was performed using a modified Molyneux, variac-type demagnetizer. Sample magnetic moments produced by the ARM growth were measured using a slow-spin Molspin fluxgate magnetometer. Results have been expressed as the square root of the sum of squares of the instrument readings (two orthogonal magnetic moments) divided by sample weight (Table 1) and are in $10^{-3}Am^2kg^{-1}$ units. Calibration of the magnetometer was achieved using a strip of magnetic tape of known magnetic moment.

Isothermal Remanent Magnetization (IRM)

Isothermal remanence is a remanent magnetization acquired by the application of steady magnetic fields at a constant temperature, for a few seconds (Tarling, 1983). By increasing the magnetic field strength, eventually a point will be reached beyond which the remanent magnetization of the sample cannot be increased. The resulting magnetization is conventionally referred to as the saturation isothermal remanent magnetization (SIRM), although it is recognized that hematite and goethite minerals will not be strictly saturated even in high laboratory fields (Tarling, 1983).

A high-powered electromagnet was used to generate the magnetic fields for producing IRMs. Field strengths of 40, 100, and 1000 Mt were used in our IRM acquisition work. Sample IRMs, were measured using the Molspin fluxgate magnetometer, in the same manner as outlined above for ARMs. The data obtained were divided by individual sample weights to give mass specific results, expressed in 10^{-3} A^2kg^{-1} (Table 1). Ratios of IRM acquired by samples in different magnetic fields, such as the S-ratio (Bloemendal, 1983), are mainly influenced by changes in the mineralogical composition of a sediments magnetic assemblage, especially the proportion of ferrimagnetic (magnetite-type) to imperfect antiferromagnetic (hematite-type) particles.

Particle Size Characteristics

Discrete sediment samples (taken from shipboard cores) were oven-dried at 60°C, for 24 hr, weighed, and a 0.5 g subsample taken from each. Samples were then wet-sieved through a No. 250 mesh (63 µm) stainless steel sieve. Both sediment fractions fine (<63 µm) and coarse (>63 µm) were retained, oven-dried at 60°C, and later weighed to five decimal places. Fine fraction and coarse fraction dry weights were then expressed as percentages of the original dry sample weight.

Subsamples were analyzed for particle size variations using a Coulter LS-100 particle size analyzer. This instrument uses the principle of Fraunhofer diffraction of laser light in which light falling on suspended sediment particles is deflected (diffracted) by an amount that depends on the size of the particle (Agrawal et al., 1991). Subsamples were allowed to soak overnight in water, facilitating deflocculation. After a visual check for good dispersion, the samples were wet-sieved through a mesh 32 (500 µm) stainless steel sieve, and the suspension retained. Sample volume was then made up, with water, to approximately 150 mL. During the sieving procedure, scatted shell fragments greater than the upper running limit of the Coulter LS-100 particle size analyzer (i.e., 800 µm) were found in some of the samples (these samples were not included in the calculation of mean particle size). Samples were further disaggregated with ultrasound for 3 min before being run through the instrument.

Oxygen Isotope Analysis

The coarse sediment sample fraction was dry-sieved through mesh No. 45 (355 µm) and mesh No. 60 (250 µm) stainless steel sieves. Tests of the foraminifer species *Globigerinoides ruber* (planktonic) and *Cibicidoides* spp. (benthic) were hand-picked under a binocular microscope from the 250- to 355-µm sediment fraction (Table 2). Care was taken to select only complete and undamaged foraminiferal tests. After selection, tests were soaked in methyl alcohol (analytical reagent) for several minutes and later cleaned in an ultrasonic bath to remove adherent contaminants. Following ultrasonic cleaning, excess methyl alcohol was drawn off with tissue paper and any residual alcohol allowed to evaporate. Foraminiferal sample weights were typically <0.1 mg and composed of between five to eight planktonic specimens and between two to four benthic specimens.

Following cleaning, foraminiferal tests were reacted in orthophosphoric acid (specific gravity, 1.9) at 90°C, and the resulting CO_2 gas analyzed using a VG Isogas Prism mass spectrometer. Foraminiferal samples were analyzed using a standard marble reference (SM1), and values thus obtained were converted to a PDB standard (Craig, 1957). Precision for oxygen isotope analysis was 0.085% (standard deviation for 100 analyses of a standard carbonate (SM1) conducted over several months) using SM1 sample weights of between 0.05 and 0.1 mg. Standard deviations for duplicate samples gave typical ranges from 0.015 to 0.275 for planktonic oxygen isotope ratios and 0.093 to 0.250 for benthic oxygen isotope ratios.

Carbonate Content Determination

Percentages of carbonate contents were found using dried, 0.5-g subsamples of the washed coarse fraction and on archive (unprocessed) sediment samples. We used the acid-base titration method to determine carbonate content, as described by Grimaldi et al. (1966).

RESULTS

Oxygen Isotope Stratigraphy

An attempt was made to correlate the foraminiferal oxygen isotope stratigraphy of Hole 819A with the stacked record of Raymo et al. (1990). However, isotopic stage recognition and assignment has proved difficult, given the incomplete nature of the isotopic record at Hole 819A. Therefore, our presented isotopic stage assignment (Figs. 2 and 3, Table 3) is only tentative and requires further corroboration, possibly from the isotopic stratigraphies of Holes 821 and 820 (Barton et al.; Peerdeman et al., both this volume) and/or other "Pacific type" isotope stratigraphies. Both biostratigraphic datum and magnetostratigraphic data have been used to validate our tentative foraminiferal oxygen isotope stratigraphy. Mainly nannofossil data (Wei and

Table 1. Magnetic susceptibility and laboratory-imparted magnetization at Hole 819A.

Depth (mbsf)	χ ($\mu m^3 kg^{-1}$)	ARM ($mAm^3 kg^{-1}$)	IRM (40mT) ($mAm^3 kg^{-1}$)	IRM (100mT) ($mAm^3 kg^{-1}$)	SIRM ($mAm^3 kg^{-1}$)	ARM/χ (K Am^{-1})	SIRM/χ (K Am^{-1})	S ratio
0.16	0.0055	3.85	5.26	8.78	10.05	7.03	18.36	0.87
0.3	0.0058	4.32	5.22	8.99	9.58	7.48	16.58	0.94
0.54	0.0048	4.48	5.40	9.38	10.27	9.24	21.19	0.91
0.7	0.0052	4.25	5.66	9.61	10.35	8.16	19.87	0.93
0.9	0.0054	4 .30	5 .53	9.49	10.75	7.94	19.84	0.88
1.2	0.0068	4.45	6.01	10.21	11.13	6.54	16.35	0.92
1.6	0.0059	4.32	5.35	8.87	10.07	7.27	16.93	0.88
1.8	0.0047	3.38	4.56	7.33	8.31	7.22	17.73	0.88
2.04	0.0057	4.62	6.43	10.80	12.31	8.11	21.58	0.88
2.18	0.0063	5.33	6.69	11.29	12.12	8.50	19.31	0.93
2.2	0.0069	5.49	6.48	10.84	12.18	7.98	17.71	0.89
2.4	0.0070	5.94	7.06	12.25	13.28	8.43	18.84	0.92
2.7	0.0081	6.17	7.59	13.46	14.72	7.59	18.12	0.91
3.1	0.0080	5.24	6.79	11.99	13.61	6.53	16.95	0.88
3.3	0.0081	5.49	7.57	13.20	15.03	6.75	18.48	0.88
3.54	0.0068	5.75	7.41	12.68	14.10	8.41	20.64	0.90
3.7	0.0080	6.06	7.69	12.85	13.04	7.59	16.33	0.99
3.95	0.0092	5.92	8.21	12.99	15.04	6.40	16.27	0.86
4.2	0.0104	5.24	7.74	12.46	13.78	5.06	13.30	0.90
4.6	0.0127	6.25	9.47	14.72	16.24	4.91	12.77	0.91
4.8	0.0135	5.88	9.43	13.99	15.29	4.35	11.31	0.92
5.04	0.0208	6.72	13.52	17.39	19.06	3.24	9.18	0.91
5.2	0.0222	6.98	13.55	17.81	19.63	3.15	8.85	0.91
5.4	0.0178	6.52	12.60	17.05	17.93	3.66	10.07	0.95
5.7	0.0213	5.33	13.74	18.09	19.76	2.50	9.26	0.92
6.1	0.0385	3.77	23.88	35.13	40.75	0.98	10.60	0.86
6.3	0.0293	2.95	20.64	27.35	29.92	1.01	10.21	0.91
6.7	0.0078	1.81	5.07	7.60	8.69	2.33	11.21	0.87
6.9	0.0068	2.38	5.33	8.38	9.24	3.51	13.59	0.91
7.2	0.0031	2.05	2.81	5.10	5.56	6.51	17.67	0.92
7.6	0.0041	2.71	3.63	5.71	6.14	6.64	15.05	0.93
7.8	0.0018	0.08	0.38	0.64	0.97	0.42	5.38	0.66
8.04	0.0022	0.10	0.52	0.86	1.21	0.48	5.61	0.71
8.18	0.0018	0.07	0.39	0.67	1.02	0.42	5.80	0.66
8.62	0.0020	0.12	0.53	0.86	1.22	0.61	6.16	0.70
8.8	0.0023	0.08	0.46	0.79	1.10	0.37	4.85	0.71
9.04	0.0032	0.09	0.55	0.92	1.24	0.27	3.88	0.74
9.2	0.0024	0.09	0.54	0.88	1.25	0.37	5.28	0.70
9.38	0.0027	0.09	0.57	0.94	1.34	0.34	5.06	0.70
9.59	0.0031	0.09	0.54	0.89	1.25	0.30	4.04	0.71
9.82	0.0038	0.09	0.52	0.84	1.17	0.25	3.10	0.72
10.12	0.0031	0.09	0.58	0.95	1.35	0.29	4.33	0.70
10.3	0.0033	0.11	0.58	0.96	1.42	0.33	4.35	0.68
10.54	0.0036	0.11	0.73	1.08	1.56	0.31	4.37	0.69
10.7	0.0036	0.11	0.65	1.09	1.67	0.30	4.69	0.65
10.88	0.0036	0.11	0.68	1.13	1.74	0.31	4.79	0.65
11.09	0.0039	0.12	0.74	1.25	1.95	0.31	5.03	0.64
11.32	0.0050	0.12	0.74	1.22	1.83	0.24	3.66	0.67
11.8	0.0040	0.11	0.63	1.02	1.35	0.28	3.41	0.75
12.04	0.0036	0.11	0.64	1.06	1.49	0.31	4.08	0.71
12.2	0.0047	0.10	0.58	0.97	1.30	0.21	2.76	0.74
12.38	0.0039	0.10	0.57	0.89	1.18	0.27	3.00	0.76
12.59	0.0040	0.10	0.52	0.83	1.09	0.25	2.72	0.76
12.82	0.0045	0.10	0.64	0.85	1.08	0.22	2.42	0.79
13.12	0.0032	0.08	0.41	0.69	0.96	0.25	2.98	0.72
13.3	0.0034	0.08	0.37	0.60	0.82	0.22	2.38	0.73
13.54	0.0034	0.06	0.32	0.49	0.63	0.19	1.85	0.78
13.7	0.0029	0.06	0.32	0.49	0.68	0.22	2.37	0.72
13.88	0.0035	0.07	0.38	0.57	0.72	0.21	2.07	0.79
14.09	0.0042	0.08	0.36	0.53	0.68	0.18	1.63	0.79
14.34	0.0027	0.06	0.30	0.46	0.58	0.22	2.18	0.78
14.62	0.0024	0.05	0.32	0.47	0.60	0.22	2.49	0.77
14.8	0.0024	0.05	0.27	0.44	0.57	0.21	2.33	0.77
15.04	0.0020	0.05	0.24	0.37	0.46	0.23	2.32	0.81
15.2	0.0018	0.05	0.21	0.33	0.43	0.28	2.45	0.77
15.38	0.0015	0.05	0.23	0.36	0.49	0.34	3.15	0.74
15.59	0.0017	0.05	0.23	0.37	0.49	0.31	2.94	0.75
15.82	0.0018	0.05	0.24	0.39	0.50	0.31	2.86	0.78
16.12	0.0015	0.06	0.28	0.45	0.54	0.41	3.50	0.83
16.3	0.0017	0.06	0.25	0.41	0.56	0.34	3.35	0.74
16.54	0.0016	0.06	0.28	0.47	0.59	0.37	3.68	0.78
16.7	0.0023	0.06	0.29	0.46	0.58	0.25	2.56	0.80
16.88	0.0020	0.06	0.32	0.49	0.65	0.32	3.32	0.76
17.09	0.0016	0.05	0.26	0.41	0.53	0.33	3.20	0.78
17.32	0.0026	0.08	0.32	0.51	0.65	0.30	2.52	0.78
17.57	0.0018	0.07	0.28	0.42	0.49	0.37	2.66	0.86
17.77	0.0015	0.06	0.25	0.37	0.50	0.37	3.26	0.74
18.04	0.0020	0.06	0.25	0.38	0.50	0.27	2.49	0.75
18.1	0.0019	0.06	0.27	0.21	0.56	0.33	2.97	0.37
18.3	0.0022	0.06	0.30	0.40	0.62	0.28	2.86	0.65
18.52	0.0024	0.07	0.33	0.52	0.65	0.29	2.70	0.79
18.7	0.0019	0.06	0.27	0.43	0.55	0.32	2.86	0.78
18.9	0.0020	0.06	0.27	0.43	0.57	0.31	2.88	0.75
19.09	0.0016	0.06	0.23	0.38	0.52	0.35	3.23	0.72

Table 1 (continued).

Depth (mbsf)	χ ($\mu m^3 kg^{-1}$)	ARM (mAm^3kg^{-1})	IRM (40mT) (mAm^3kg^{-1})	IRM (100mT) (mAm^3kg^{-1})	SIRM (mAm^3kg^{-1})	ARM/χ ($K Am^{-1}$)	SIRM/χ ($K Am^{-1}$)	S ratio
37.7	0.0025	0.11	0.48	0.80	1.00	0.44	3.98	0.80
37.9	0.0024	0.10	0.43	0.71	0.88	0.43	3.67	0.81
38.1	0.0025	0.11	0.45	0.77	0.96	0.44	3.88	0.80
38.3	0.0022	0.09	0.39	0.69	0.86	0.41	3.86	0.80
38.6	0.0024	0.09	0.37	0.65	0.81	0.36	3.40	0.80
38.8	0.0024	0.08	0.35	0.62	0.81	0.35	3.37	0.77
39	0.0025	0.08	0.33	0.56	0.70	0.33	2.76	0.80
39.2	0.0025	0.09	0.38	0.65	0.83	0.36	3.27	0.79
39.4	0.0020	0.09	0.36	0.61	0.77	0.42	3.78	0.80
39.6	0.0022	0.09	0.46	0.77	0.97	0.42	4.41	0.79
39.8	0.0023	0.08	0.36	0.63	0.76	0.37	3.37	0.82
40.1	0.0021	0.07	0.34	0.60	0.77	0.33	3.78	0.78
40.3	0.0021	0.06	0.30	0.54	0.63	0.27	2.99	0.86
40.5	0.0025	0.09	0.37	0.64	0.81	0.36	3.18	0.79
40.7	0.0028	0.09	0.41	0.75	0.92	0.33	3.25	0.81
40.9	0.0026	0.14	0.53	0.94	1.15	0.53	4.40	0.82
41.1	0.0027	0.17	0.55	1.00	1.19	0.64	4.34	0.84
41.3	0.0028	0.16	0.54	1.21	1.51	0.55	5.31	0.80
41.6	0.0033	0.15	0.53	0.84	1.03	0.45	3.17	0.82
41.8	0.0031	0.17	0.54	1.00	1.25	0.53	4.03	0.80
42	0.0029	0.17	0.67	1.66	2.12	0.60	7.23	0.78
42.2	0.0027	0.17	0.64	1.20	1.46	0.64	5.51	0.82
42.4	0.0029	0.16	0.59	1.02	1.19	0.54	4.14	0.86
42.6	0.0026	0.17	0.61	1.00	1.20	0.64	4.57	0.83
42.8	0.0027	0.21	0.61	0.95	1.11	0.76	4.11	0.85
43.1	0.0031	0.20	0.68	1.03	1.22	0.64	3.92	0.84
43.3	0.0027	0.21	0.71	1.14	1.29	0.81	4.86	0.89
43.5	0.0026	0.22	0.68	1.03	1.18	0.86	4.58	0.87
43.7	0.0033	0.23	0.72	1.13	1.34	0.71	4.13	0.84
43.9	0.0024	0.19	0.64	0.97	1.14	0.78	4.72	0.85
44.1	0.0026	0.18	0.57	0.88	1.03	0.67	3.89	0.86
44.3	0.0023	0.15	0.48	0.74	0.90	0.64	3.95	0.82
44.6	0.0026	0.13	0.46	0.74	0.92	0.50	3.54	0.80
44.8	0.0024	0.13	0.43	0.66	0.81	0.56	3.38	0.81
45	0.0022	0.11	0.44	0.69	0.86	0.49	3.90	0.80
45.2	0.0027	0.13	0.44	0.71	0.88	0.49	3.23	0.81
45.4	0.0025	0.13	0.46	0.70	0.87	0.53	3.46	0.80
45.6	0.0030	0.19	0.57	0.87	1.06	0.61	3.51	0.82
45.8	0.0030	0.16	0.56	0.86	1.04	0.54	3.48	0.83
46.1	0.0035	0.21	0.62	1.03	1.26	0.58	3.55	0.82
46.3	0.0034	0.21	0.62	1.03	1.19	0.61	3.49	0.86
46.5	0.0026	0.23	0.67	1.03	1.17	0.89	4.49	0.88
46.7	0.0026	0.19	0.64	0.96	1.11	0.76	4.32	0.86
46.6	0.0035	0.29	0.87	1.31	1.53	0.82	4.38	0.86
46.8	0.0036	0.30	0.91	1.37	1.59	0.84	4.45	0.86
47	0.0035	0.31	1.03	1.51	1.71	0.88	4.95	0.88
47.2	0.0036	0.33	1.03	1.53	1.78	0.92	4.91	0.86
47.4	0.0040	0.32	0.98	1.54	1.60	0.82	4.04	0.96
47.6	0.0040	0.33	0.97	1.54	1.72	0.83	4.31	0.89
47.8	0.0039	0.29	0.86	1.40	1.64	0.74	4.24	0.86
48.1	0.0041	0.28	0.85	1.41	1.63	0.69	3.99	0.87
48.3	0.0040	0.26	0.76	1.19	1.36	0.65	3.44	0.87
48.5	0.0034	0.27	0.78	1.15	1.34	0.79	3.99	0.85
48.7	0.0037	0.21	0.64	0.96	1.15	0.55	3.07	0.84
48.9	0.0037	0.21	0.70	1.02	1.20	0.55	3.20	0.85
49.1	0.0035	0.18	0.58	0.86	1.00	0.52	2.83	0.87
49.3	0.0034	0.14	0.45	0.72	0.86	0.42	2.54	0.84
49.6	0.0033	0.09	0.35	0.58	0.75	0.29	2.29	0.78
49.8	0.0030	0.10	0.32	0.58	0.73	0.33	2.43	0.79
50	0.0025	0.09	0.31	0.53	0.67	0.34	2.65	0.79
50.2	0.0021	0.08	0.32	0.49	0.55	0.39	2.67	0.90
50.4	0.0019	0.09	0.27	0.49	0.65	0.47	3.44	0.75
50.6	0.0022	0.07	0.26	0.48	0.62	0.32	2.85	0.77
50.8	0.0020	0.07	0.27	0.49	0.63	0.38	3.20	0.77
51.1	0.0017	0.07	0.24	0.42	0.56	0.41	3.22	0.74
51.3	0.0020	0.07	0.25	0.44	0.57	0.35	2.87	0.78
51.5	0.0025	0.07	0.26	0.47	0.62	0.26	2.42	0.76
51.7	0.0019	0.06	0.25	0.45	0.59	0.33	3.01	0.76
51.9	0.0020	0.06	0.26	0.45	0.54	0.33	2.73	0.84
52.1	0.0020	0.07	0.24	0.47	0.57	0.37	2.86	0.82
52.3	0.0017	0.07	0.25	0.45	0.59	0.42	3.60	0.76
52.6	0.0016	0.07	0.25	0.45	0.57	0.46	3.63	0.79
52.8	0.0014	0.06	0.23	0.42	0.62	0.43	4.47	0.68
53	0.0017	0.09	0.29	0.51	0.67	0.54	4.01	0.75
53.2	0.0016	0.08	0.23	0.47	0.53	0.48	3.37	0.88
53.4	0.0012	0.06	0.23	0.41	0.50	0.48	4.08	0.83
53.6	0.0014	0.06	0.23	0.41	0.53	0.43	3.73	0-77
53.8	0.0013	0.06	0.21	0.39	0.48	0.44	3.59	0.82
54.1	0.0013	0.05	0.20	0.38	0.52	0.36	3.98	0.73
54.3	0.0015	0.08	0.28	0.51	0.71	0.51	4.67	0.72
54.5	0.0014	0.07	0.25	0.43	0.56	0.55	4.12	0.77
54.7	0.0014	0.07	0.23	0.42	0.55	0.50	3.97	0.76
54.9	0.0013	0.06	0.19	0.36	0.50	0.48	3.81	0.72
55.1	0.0014	0.08	0.24	0.45	0.60	0.57	4.39	0.75

Table 1 (continued).

Depth (mbsf)	χ ($\mu m^3 kg^{-1}$)	ARM ($mAm^3 kg^{-1}$)	IRM (40mT) ($mAm^3 kg^{-1}$)	IRM (100mT) ($mAm^3 kg^{-1}$)	SIRM ($mAm^3 kg^{-1}$)	ARM/χ ($K Am^{-1}$)	SIRM/χ ($K Am^{-1}$)	S ratio
55.3	0.0022	0.07	0.25	0.47	0.55	0.31	2.49	0.84
56.1	0.0016	0.07	0.22	0.40	0.52	0.44	3.32	0.78
56.3	0.0016	0.07	0.26	0.47	0.61	0.43	3.80	0.78
56.5	0.0014	0.07	0.29	0.52	0.67	0.47	4.69	0.76
56.7	0.0014	0.09	0.30	0.56	0.68	0.64	4.77	0.82
56.9	0.0015	0.08	0.28	0.49	0.58	0.54	3.96	0.85
57.1	0.0018	0.07	0.32	0.58	0.76	0.42	4.24	0.77
57.3	0.0017	0.08	0.28	0.49	0.62	0.46	3.55	0.79
57.6	0.0016	0.08	0.35	0.60	0.79	0.51	4.78	0.77
57.9	0.0016	0.09	0.28	0.51	0.65	0.57	4.17	0.78
58	0.0017	0.08	0.26	0.51	0.62	0.48	3.73	0.82
58.2	0.0017	0.08	0.30	0.56	0.73	0.49	4.29	0.78
58.4	0.0017	0.09	0.33	0.59	0.78	0.51	4.52	0.75
58.6	0.0016	0.08	0.36	0.65	0.83	0.51	5.09	0.78
58.8	0.0016	0.09	0.35	0.63	0.82	0.55	5.20	0.77
59.1	0.0020	0.09	0.36	0.64	0.82	0.46	4.16	0.78
59.3	0.0018	0.09	0.37	0.65	0.81	0.51	4.48	0.80
59.5	0.0018	0.10	0.35	0.62	0.82	0.52	4.47	0.76
59.7	0.0018	0.09	0.35	0.60	0.75	0.47	4.15	0.79
59.9	0.0017	0.09	0.35	0.62	0.80	0.51	4.68	0.77
60.1	0.0021	0.09	0.34	0.61	0.74	0.42	3.57	0.82
60.3	0.0018	0.09	0.34	0.60	0.78	0.50	4.45	0.76
60.6	0.0021	0.09	0.38	0.67	0.80	0.41	3.80	0.84
60.8	0.0026	0.11	0.42	0.74	0.93	0.42	3.61	0.80
61	0.0019	0.08	0.34	0.60	0.74	0.40	3.93	0.81
61.2	0.0020	0.10	0.33	0.59	0.77	0.49	3.78	0.77
61.4	0.0025	0.08	0.33	0.56	0.73	0.33	2.88	0.77
61.6	0.0024	0.11	0.39	0.71	0.95	0.43	3.87	0.75
61.8	0.0027	0.09	0.34	0.59	0.70	0.34	2.58	0.84
62.1	0.0027	0.10	0.40	0.71	0.86	0.37	3.23	0.82
62.3	0.0026	0.09	0.38	0.65	0.83	0.35	3.15	0.78
62.5	0.0025	0.09	0.38	0.65	0.79	0.34	3.09	0.83
62.7	0.0031	0.10	0.42	0.71	0.90	0.33	2.94	0.79
62.9	0.0029	0.10	0.41	0.68	0.84	0.34	2.92	0.82
63.1	0.0028	0.10	0.43	0.72	0.87	0.36	3.10	0.83
63.6	0.0030	0.09	0.43	0.71	0.91	0.31	3.01	0.77
63.8	0.0032	0.10	0.45	0.75	0.92	0.32	2.91	0.82
64	0.0027	0.10	0.43	0.71	0.95	0.38	3.49	0.75
64.2	0.0029	0.10	0.44	0.75	0.94	0.33	3.20	0.80
64.4	0.0033	0.10	0.46	0.79	0.93	0.31	2.84	0.85
64.6	0.0035	0.11	0.51	0.80	1.01	0.30	2.88	0.79
64.8	0.0034	0.08	0.47	0.79	0.98	0.24	2.88	0.80
65.1	0.0037	0.09	0.58	0.93	1.12	0.25	3.05	0.83
65.3	0.0039	0.11	0.62	1.02	1.23	0.29	3.20	0.83
65.5	0.0036	0.10	0.58	0.96	1.19	0.29	3.32	0.80
65.7	0.0038	0.14	0.71	1.20	1.48	0.36	3.88	0.81
65.6	0.0027	0.15	0.66	1.09	1.39	0.55	5.21	0.79
65.6	0.0027	0.15	0.66	1.09	1.39	0.55	5.21	0.79
65.8	0.0027	0.15	0.71	1.19	1.44	0.57	5.40	0.83
66	0.0034	0.17	0.77	1.30	1.59	0.51	4.70	0.82
66.22	0.0036	0.24	1.05	1.81	2.18	0.67	5.99	0.83
66.42	0.0037	0.25	1.08	1.91	2.42	0.67	6.48	0.79
66.62	0.0041	0.40	1.50	2.73	3.35	0.99	8.19	0.81
66.82	0.0055	0.55	3.42	6.97	9.18	0.99	16.69	0.76
67.02	0.0060	0.46	1.72	3.49	4.88	0.77	8.15	0.72
67.22	0.0064	0.45	1.73	3.24	4.52	0.71	7.12	0.72
67.42	0.0062	0.33	1.47	2.72	3.90	0.54	6.34	0.70
67.72	0.0064	0.26	1.33	2.32	3.47	0.40	5.42	0.67
67.92	0.0056	0.26	1.29	2.21	3.27	0.47	5.88	0.68
68.12	0.0050	0.20	1.17	2.03	3.07	0.41	6.15	0.66
68.32	0.0042	0.16	1.04	1.80	2.69	0.37	6.39	0.67
68.52	0.0037	0.14	0.94	1.61	2.31	0.37	6.25	0.70
68.72	0.0036	0.12	1.01	1.73	2.63	0.34	7.40	0.66
68.92	0.0043	0.14	1.05	1.75	2.67	0.33	6.26	0.66
69.22	0.0042	0.13	0.97	1.67	2.62	0.32	6.31	0.63
69.42	0.0035	0.13	0.93	1.57	2.46	0.38	7.09	0.64
69.62	0.0038	0.16	1.00	1.70	2.65	0.41	6.96	0.64
69.82	0.0042	0.16	0.92	1.64	2.54	0.38	6.06	0.65
70.02	0.0034	0.15	0.88	1.52	2.32	0.44	6.77	0.66
70.22	0.0041	0.16	1.17	1.92	2.86	0.38	7.02	0.67
70.42	0.0047	0.16	1.22	2.07	2.98	0.35	6.32	0.70
70.72	0.0041	0.15	0.88	1.52	2.43	0.36	5.91	0.62
70.92	0.0052	0.17	1.38	2.20	3.23	0.34	6.23	0.68
71.12	0.0051	0.16	1.42	2.27	3.18	0.32	6.28	0.71
71.32	0.0049	0.17	1.34	2.18	3.23	0.34	6.52	0.68
71.52	0.0050	0.16	1.28	2.12	2.96	0.32	5.87	0.72
71.72	0.0055	0.18	1.46	2.34	3.43	0.33	6.24	0.68
71.92	0.0055	0.19	1.49	2.36	3.30	0.34	5.96	0.72
72.22	0.0052	0.18	1.39	2.21	3.14	0.34	6.05	0.70
72.42	0.0055	0.16	1.19	1.92	2.88	0.28	5.20	0.67
72.62	0.0040	0.15	0.85	1.45	2.26	0.38	5.71	0.64
72.82	0.0043	0.15	0.81	1.39	2.00	0.34	4.65	0.69
73.02	0.0044	0.16	0.86	1.43	2.01	0.37	4.59	0.71
73.22	0.0042	0.14	0.78	1.33	1.77	0.33	4.21	0.76

Table 1 (continued).

Depth (mbsf)	χ ($\mu m^3 kg^{-1}$)	ARM (mAm^2kg^{-1})	IRM (40mT) (mAm^2kg^{-1})	IRM (100mT) (mAm^2kg^{-1})	SIRM (mAm^2kg^{-1})	ARM/χ (K Am^{-1})	SIRM/χ (K Am^{-1})	S ratio
73.42	0.0044	0.14	0.84	1.40	1.80	0.31	4.12	0.77
73.72	0.0040	0.16	0.81	1.38	1.81	0.40	4.51	0.77
73.92	0.0043	0.18	0.89	1.50	1.91	0.43	4.49	0.79
74.12	0.0042	0.19	0.83	1.40	1.80	0.46	4.34	0.78
74.32	0.0047	0.20	0.91	1.58	1.90	0.42	4.07	0.83
74.52	0.0046	0.25	1.01	1.78	2.23	0.55	4.90	0.80
74.72	0.0046	0.27	1.08	1.88	2.37	0.58	5.14	0.80
74.92	0.0053	0.55	0.98	1.66	2.01	1.04	3.82	0.83
75.1	0.0048	0.40	1.40	2.60	3.26	0.84	6.86	0.80
75.3	0.0056	0.31	1.30	2.37	2.82	0.56	5.08	0.84
75.45	0.0059	0.31	1.43	2.74	3.56	0.52	6.06	0.77
75.65	0.0067	0.29	1.38	2.41	3.46	0.43	5.18	0.70
75.85	0.0056	0.30	1.50	2.47	3.56	0.54	6.38	0.69
76.05	0.0063	0.34	1.64	2.81	4.13	0.54	6.51	0.68
76.25	0.0071	0.79	2.00	6.37	8.08	1.11	11.39	0.79
76.45	0.0058	0.42	2.40	7.14	8.89	0.74	15.47	0.80
76.65	0.0060	0.34	1.53	2.56	3.66	0.57	6.08	0.70
76.95	0.0058	0.35	1.52	2.59	3.64	0.60	6.25	0.71
77.15	0.0059	0.34	1.44	2.48	3.57	0.58	6.07	0.69
77.35	0.0056	0.36	1.48	2.51	3.73	0.65	6.68	0.67
77.55	0.0051	0.28	1.16	2.01	2.81	0.55	5.54	0.71
77.75	0.0049	0.30	1.31	2.14	2.92	0.62	5.94	0.73
77.95	0.0051	0.28	1.21	2.11	2.82	0.55	5.57	0.75
78.15	0.0045	0.19	0.90	1.49	1.95	0.42	4.38	0.77
78.45	0.0046	0.19	0.98	1.68	2.16	0.42	4.71	0.78
78.65	0.0047	0.20	0.96	1.58	2.08	0.43	4.42	0.76
78.85	0.0046	0.18	0.95	1.69	2.17	0.38	4.73	0.78
79.05	0.0051	0.19	0.93	1.59	2.08	0.38	4.08	0.76
79.25	0.0045	0.15	0.84	1.41	1.80	0.33	3.99	0.78
79.45	0.0049	0.15	0.79	1.29	1.65	0.31	3.39	0.78
79.65	0.0048	0.15	0.75	1.24	1.61	0.31	3.38	0.77
79.95	0.0026	0.08	0.40	0.56	0.81	0.30	3.06	0.69
80.15	0.0026	0.11	0.44	0.70	0.84	0.43	3.24	0.84
80.35	0.0021	0.09	0.42	0.67	0.80	0.42	3.78	0.84
80.55	0.0023	0.10	0.46	0.76	0.92	0.42	3.95	0.83
80.75	0.0025	0.09	0.46	0.73	0.90	0.38	3.68	0.81
80.95	0.0022	0.10	0.46	0.69	0.88	0.46	4.04	0.78
81.15	0.0026	0.10	0.42	0.64	0.80	0.39	3.13	0.80
81.45	0.0024	0.10	0.42	0.67	0.81	0.42	3.32	0.83
81.65	0.0020	0.09	0.40	0.69	0.87	0.43	4.30	0.79
81.85	0.0023	0.10	0.42	0.69	0.84	0.44	3.65	0.82
82.05	0.0023	0.10	0.44	0.69	0.89	0.44	3.90	0.78
82.25	0.0027	0.10	0.47	0.72	0.88	0.38	3.21	0.83
82.45	0.0027	0.10	0.46	0.73	0.89	0.37	3.35	0.82
82.65	0.0026	0.10	0.44	0.69	0.86	0.36	3.23	0.81
83.95	0.0028	0.10	0.46	0.82	0.88	0.37	3.18	0.93
83.15	0.0027	0.08	0.44	0.68	0.89	0.32	3.36	0.76
83.35	0.0023	0.08	0.43	0.67	0.84	0.33	3.57	0.810
83.55	0.0027	0.09	0.48	0.84	0.99	0.34	3.68	0.84
83.75	0.0026	0.11	0.50	0.79	0.97	0.42	3.67	0.81
83.95	0.0022	0.10	0.46	0.77	1.00	0.48	4.63	0.77
84.15	0.0020	0.10	0.43	0.69	0.83	0.50	4.12	0.83
84.45	0.0024	0.10	0.43	0.74	0.86	0.42	3.59	0.86
84.65	0.0024	0.09	0.43	0.75	0.96	0.39	4.04	0.78
84.85	0.0028	0.11	0.46	0.75	0.89	0.39	3.19	0.84
85.05	0.0025	0.10	0.45	0.72	0.86	0.39	3.44	0.84
84.6	0.0021	0.10	0.45	0.77	0.94	0.46	4.54	0.82
84.8	0.0029	0.09	0.56	0.92	1.12	0.30	3.85	0.82
85	0.0030	0.10	0.74	1.14	1.32	0.34	4.41	0.86
85.2	0.0029	0.11	0.60	0.97	1.21	0.37	4.24	0.80
85.4	0.0028	0.11	0.58	1.08	1.24	0.41	4.45	0.87
85.6	0.0026	0.12	0.62	1.00	1.22	0.44	4.67	0.82
85.8	0.0026	0.12	0.57	0.96	1.18	0.46	4.54	0.81
86	0.0027	0.13	0.59	1.01	1.22	0.47	4.48	0.82
86.2	0.0030	0.12	0.58	0.94	1.14	0.40	3.81	0.82
86.5	0.0032	0.12	0.55	0.88	1.11	0.37	3.52	0.79
86.7	0.0032	0.15	0.74	1.19	1.40	0.48	4.43	0.84
86.9	0.0030	0.13	0.74	1.22	1.48	0.42	4.87	0.82
87.1	0.0034	0.12	0.71	1.16	1.42	0.36	4.17	0.82
87.3	0.0033	0.14	0.73	1.28	1.48	0.42	4.50	0.87
87.5	0.0031	0.14	0.71	1.15	1.41	0.44	4.47	0.82
87.7	0.0033	0.13	0.72	1.15	1.42	0.39	4.31	0.81
88	0.0037	0.15	0.84	1.39	1.64	0.41	4.38	0.85
88.2	0.0039	0.15	0.77	1.23	1.48	0.39	3.77	0.83
88.4	0.0041	0.16	0.62	1.36	1.69	0.40	4.15	0.81
88.6	0.0044	0.13	0.75	1.24	1.53	0.30	3.50	0.81
88.8	0.0046	0.17	0.93	1.50	1.84	0.37	3.96	0.82
89	0.0050	0.14	0.86	1.41	1.76	0.29	3.55	0.80
89.2	0.0055	0.17	0.97	1.54	1.90	0.30	3.48	0.81
89.5	0.0045	0.17	1.00	1.67	2.03	0.38	4.48	0.82
89.7	0.0056	0.16	0.97	1.57	1.90	0.28	3.38	0.83
89.9	0.0000	0.19	1.03	1.63	2.02			0.81
90.1	0.0059	0.17	0.92	1.48	1.73	0.28	2.91	0.85
90.3	0.0051	0.15	0.73	1.19	1.47	0.29	2.87	0.81

Table 1 (continued).

Depth (mbsf)	X ($\mu m^3 kg^{-1}$)	ARM ($mAm^3 kg^{-1}$)	IRM (40mT) ($mAm^3 kg^{-1}$)	IRM (100mT) ($mAm^3 kg^{-1}$)	SIRM ($mAm^3 kg^{-1}$)	ARM/X ($K\ Am^{-1}$)	SIRM/X ($K\ Am^{-1}$)	S ratio
90.5	0.0053	0.15	0.90	1.41	1.68	0.29	3.18	0.84
91	0.0049	0.13	0.71	1.13	1.37	0.27	2.79	0.82
91.2	0.0042	0.13	0.66	1.04	1.26	0.31	3.00	0.83
91.4	0.0043	0.12	0.65	1.06	1.29	0.28	3.02	0.83
91.6	0.0045	0.10	0.59	0.92	1.14	0.22	2.56	0.81
91.8	0.0033	0.09	1.03	0.80	0.99	0.27	3.02	0.81
92	0.0046	0.12	0.58	0.94	1.16	0.27	2.53	0.80
92.2	0.0046	0.10	0.60	0.96	1.17	0.22	2.57	0.82
92.5	0.0045	0.13	0.62	0.99	1.19	0.28	2.67	0.83
92.7	0.0044	0.15	0.69	1.09	1.32	0.33	2.98	0.83
92.9	0.0048	0.12	0.62	0.97	1.15	0.24	2.41	0.84
93.1	0.0042	0.12	0.62	0.97	1.18	0.28	2.78	0.82
93.3	0.0044	0.12	0.63	0.98	1.21	0.28	2.77	0.81
93.5	0.0048	0.14	0.61	0.95	1.16	0.28	2.38	0.82
93.7	0.0048	0.11	0.64	0.98	1.17	0.22	2.46	0.84
94	0.0047	0.10	0.60	0.91	1.15	0.21	2.47	0.79
94.2	0.0045	0.11	0.64	1.01	1.22	0.25	2.70	0.83
94.4	0.0048	0.12	0.61	0.96	1.18	0.25	2.45	0.81
94.6	0.0044	0.12	0.55	0.90	1.16	0.27	2.63	0.77
94.1	0.0049	0.09	0.60	1.01	1.17	0.18	2.38	0.86
94.42	0.0051	0.13	0.61	0.76	1.24	0.26	2.42	0.61
94.62	0.0041	0.11	0.50	0.78	0.96	0.27	2.36	0.81
94.82	0.0041	0.13	0.54	0.84	1.05	0.32	2.57	0.80
95.02	0.0043	0.11	0.47	0.78	0.98	0.26	2.27	0.80
95.22	0.0041	0.12	0.54	0.90	1.11	0.30	2.70	0.81
95.42	0.0036	0.11	0.47	0.79	0.93	0.30	2.60	0.85
95.62	0.0037	0.07	0.46	0.78	0.93	0.19	2.51	0.83
95.92	0.0038	0.11	0.46	0.77	0.94	0.29	2.47	0.82
96.12	0.0037	0.06	0.44	0.79	0.91	0.16	2.50	0.86
96.32	0.0037	0.11	0.45	0.74	0.86	0.29	2.31	0.87
96.52	0.0035	0.11	0.43	0.71	0.81	0.31	2.35	0.88
96.72	0.0034	0.13	0.50	0.81	1.00	0.38	2.98	0.81
96.92	0.0037	0.06	0.44	0.73	0.92	0.16	2.48	0.79
97.12	0.0036	0.12	0.50	0.81	1.02	0.33	2.81	0.79
97.42	0.0042	0.12	0.47	0.80	1.00	0.29	2.37	0.81
97.62	0.0036	0.10	0.44	0.72	0.87	0.29	2.41	0.83
97.82	0.0035	0.11	0.43	0.71	0.87	0.32	2.49	0.82
98.02	0.0037	0.08	0.46	0.77	0.97	0.21	2.64	0.79
98.22	0.0034	0.08	0.43	0.74	0.92	0.22	2.70	0.80
98.42	0.0030	0.06	0.41	0.69	0.88	0.21	2.89	0.79
98.62	0.0030	0.12	0.43	0.73	0.92	0.40	3.07	0.79
98.92	0.0028	0.06	0.36	0.73	0.91	0.23	3.27	0.80
99.12	0.0034	0.07	0.45	0.75	0.89	0.20	2.66	0.84
99.32	0.0029	0.12	0.44	0.71	0.89	0.41	3.13	0.80
99.52	0.0029	0.06	0.39	0.68	0.87	0.21	2.99	0.79
99.72	0.0033	0.10	0.34	0.71	0.87	0.32	2.67	0.82
99.92	0.0027	0.11	0.39	0.71	0.84	0.39	3.08	0.84
100.12	0.0023	0.07	0.42	0.76	0.93	0.29	3.99	0.81
100.42	0.0027	0.06	0.40	0.67	0.85	0.23	3.14	0.78
100.62	0.0032	0.10	0.38	0.67	0.83	0.31	2.62	0.81
100.82	0.0028	0.12	0.42	0.72	0.87	0.42	3.14	0.82
101.02	0.0025	0.09	0.38	0.63	0.81	0.38	3.29	0.78
101.22	0.0028	0.10	0.40	0.68	0.89	0.36	3.13	0.77
101.42	0.0028	0.09	0.38	0.67	0.84	0.34	3.03	0.80
101.62	0.0026	0.11	0.37	0.65	0.75	0.41	2.90	0.86
101.92	0.0026	0.10	0.42	0.70	0.87	0.39	3.31	0.80
102.12	0.0026	0.11	0.42	0.76	0.94	0.40	3.58	0.81
102.32	0.0025	0.05	0.39	0.65	0.83	0.21	3.36	0.79
102.52	0.0023	0.11	0.42	0.70	0.92	0.47	3.97	0.76
102.72	0.0027	0.08	0.37	0.80	0.98	0.28	3.62	0.81
102.92	0.0025	0.07	0.43	0.75	0.94	0.28	3.76	0.80
103.12	0.0024	0.10	0.37	0.67	0.83	0.40	3.47	0.80
103.42	0.0022	0.08	0.34	0.74	0.89	0.37	3.98	0.84
103.62	0.0025	0.12	0.45	0.77	0.95	0.48	3.73	0.81
103.82	0.0025	0.10	0.45	0.80	0.96	0.42	3.86	0.83
104.02	0.0022	0.07	0.43	0.75	0.93	0.30	4.26	0.81
103.6	0.0024	0.12	0.41	0.76	0.92	0.48	3.76	0.83
103.8	0.0030	0.15	0.58	0.99	1.27	0.51	4.20	0.79
104	0.0031	0.16	0.58	1.05	1.28	0.51	4.15	0.82
104.2	0.0029	0.10	0.57	1.03	1.25	0.35	4.34	0.83
104.4	0.0000							
105.1	0.0035	0.17	0.69	1.16	1.47	0.49	4.25	0.79
105.3	0.0029	0.13	0.54	0.95	1.20	0.45	4.21	0.79
105.5	0.0029	0.13	0.55	0.99	1.19	0.47	4.16	0.83
105.7	0.0024	0.12	0.52	0.92	1.17	0.50	4.90	0.79
105.9	0.0024	0.13	0.45	0.89	1.08	0.52	4.42	0.82
106.1	0.0021	0.10	0.43	0.79	0.98	0.47	4.72	0.81
106.3	0.0018	0.08	0.33	0.60	0.81	0.44	4.50	0.74
106.6	0.0022	0.08	0.33	0.57	0.74	0.36	3.34	0.77
106.8	0.0024	0.09	0.31	0.63	0.81	0.39	3.36	0.78
107	0.0019	0.08	0.29	0.58	0.72	0.43	3.73	0.80
107.2	0.0013	0.03	0.32	0.59	0.74	0.64	5.58	0.80
107.33	0.0017	0.07	0.26	0.49	0.59	0.44	3.44	0.84
107.6	0.0022	0.10	0.38	0.66	0.77	0.43	3.47	0.86

Table 1 (continued).

Depth (mbsf)	χ ($\mu m^3 kg^{-1}$)	ARM ($mAm^2 kg^{-1}$)	IRM (40mT) ($mAm^2 kg^{-1}$)	IRM (100mT) ($mAm^2 kg^{-1}$)	SIRM ($mAm^2 kg^{-1}$)	ARM/χ (K Am^{-1})	SIRM/χ (K Am^{-1})	S ratio
108.1	0.0019	0.11	0.44	0.72	0.82	0.60	4.35	0.87
108.3	0.0022	0.07	0.27	0.45	0.58	0.34	2.63	0.77
108.5	0.0020	0.03	0.32	0.53	0.67	0.45	3.33	0.73
108.7	0.0022	0.08	0.24	0.49	0.62	0.38	2.73	0.73
108.9	0.0019	0.03	0.34	0.57	0.70	0.48	3.63	0.81
103.1	0.0020	0.03	0.31	0.54	0.64	0.46	3.22	0.85
103.3	0.0021	0.08	0.31	0.50	0.64	0.38	3.02	0.78
103.6	0.0018	0.11	0.48	0.71	0.91	0.63	4.95	0.73
103.8	0.0015	0.10	0.37	0.64	0.82	0.65	5.35	0.78
110	0.0021	0.09	0.27	0.52	0.66	0.43	3.03	0.73
110.2	0.0019	0.03	0.36	0.63	0.80	0.50	4.24	0.80
110.4	0.0017	0.03	0.36	0.63	0.78	0.50	4.53	0.81
110.6	0.0025	0.10	0.36	0.65	0.81	0.39	3.24	0.81
110.78	0.0034	0.03	0.35	0.63	0.74	0.26	2.20	0.85
111.1	0.0014	0.03	0.26	0.44	0.47	0.65	3.37	0.93
111.3	0.0014	0.08	0.25	0.42	0.54	0.58	3.88	0.73
111.55	0.0017	0.03	0.22	0.48	0.62	0.55	3.70	0.77
111.68	0.0015	0.03	0.26	0.44	0.56	0.61	3.67	0.73
111.88	0.0013	0.09	0.28	0.44	0.55	0.66	4.15	0.81
112.08	0.0013	0.03	0.26	0.44	0.56	0.65	4.14	0.78
112.28	0.0013	0.03	0.29	0.52	0.56	0.69	4.24	0.92
112.46	0.0013	0.10	0.26	0.55	0.67	0.75	5.19	0.82
112.68	0.0019	0.03	0.30	0.53	0.65	0.49	3.47	0.81
112.88	0.0017	0.10	0.29	0.55	0.61	0.57	3.55	0.90
113.13	0.0019	0.10	0.31	0.61	0.72	0.52	3.75	0.85
113.38	0.0022	0.11	0.37	0.65	0.77	0.50	3.48	0.84
113.58	0.0021	0.10	0.33	0.58	0.76	0.48	3.57	0.77
113.78	0.0019	0.10	0.39	0.65	0.78	0.52	4.03	0.83
113.96	0.0024	0.10	0.35	0.67	0.78	0.41	3.22	0.87
114.18	0.0022	0.11	0.38	0.67	0.82	0.51	3.74	0.81
114.38	0.0023	0.11	0.36	0.80	0.73	0.46	3.15	1.03
114.68	0.0027	0.13	0.41	0.77	0.98	0.47	3.66	0.78
114.88	0.0023	0.12	0.42	0.85	1.04	0.54	4.59	0.82
115.08	0.0026	0.14	0.42	0.81	0.98	0.52	3.77	0.84
115.28	0.0025	0.12	0.44	0.77	0.94	0.49	3.78	0.83
115.46	0.0031	0.13	0.47	0.84	0.98	0.42	3.20	0.85
115.68	0.0031	0.13	0.51	0.94	1.08	0.42	3.44	0.87
115.88	0.0035	0.13	0.46	0.84	1.08	0.37	3.08	0.79
116.18	0.0030	0.12	0.51	0.36	1.03	0.41	3.59	0.88
116.38	0.0036	0.15	0.55	0.95	1.17	0.41	3.21	0.81
116.58	0.0033	0.16	0.61	1.06	1.31	0.48	3.97	0.81
116.78	0.0033	0.12	0.59	1.12	1.37	0.37	4.19	0.82
116.96	0.0038	0.13	0.74	1.32	1.48	0.34	3.88	0.89
117.18	0.0035	0.13	0.67	1.31	1.61	0.39	4.65	0.81
117.68	0.0041	0.19	0.77	1.41	1.66	0.46	4.07	0.85
117.88	0.0045	0.15	0.76	1.42	1.62	0.33	3.58	0.88
118.08	0.0043	0.14	0.73	1.46	1.70	0.33	3.98	0.86
118.28	0.0035	0.18	0.68	1.48	1.68	0.53	4.81	0.88
118.46	0.0033	0.15	0.84	1.55	1.81	0.45	5.46	0.86
118.68	0.0029	0.17	0.70	1.38	1.70	0.57	5.84	0.81
118.88	0.0023	0.15	0.69	1.30	1.60	0.65	6.93	0.81
119.18	0.0028	0.13	0.65	1.29	1.51	0.46	5.46	0.85
119.38	0.0034	0.17	0.66	1.24	1.55	0.50	4.53	0.80
119.58	0.0032	0.15	0.66	1.30	1.53	0.49	4.86	0.85
119.78	0.0029	0.11	0.65	1.20	1.46	0.40	5.07	0.82
119.96	0.0028	0.12	0.69	1.34	1.62	0.45	5.88	0.83
120.18	0.0034	0.11	0.67	1.21	1.45	0.32	4.31	0.84

Gartner, this volume) were used to constrain isotopic stage assignment. The lowest occurrence (LO) of *Emiliania huxleyi* was located at 29.4 mbsf and indicates the position of stages 9 through 8, while the highest occurrence (HO) of *Pseudoemiliania lacunosa* at 32.4 mbsf indicates the position of stage 12. The foraminiferal datum event, the HO of the pink-pigmented foraminifer *Globigerinoides ruber*, was used to fix the position of the stage 6/5e oxygen isotope boundary (Thompson et al., 1979) at about 18 mbsf.

The Brunhes/Matuyama boundary has been identified at 41 mbsf, and the top of the Jaramillo Subchron was recorded between 115 and 120 mbsf (Barton et al., this volume); both were used to define the approximate position of the stage 19/20 boundary and stage 28, respectively.

According to the biostratigraphy the foraminiferal $\delta^{18}O$ stratigraphy at Hole 819A appears to be incomplete. A major hiatus is present at 32.5 mbsf, as indicated by the condensed nature of the nannofossil stratigraphy (i.e., the HO of *P. lacunosa*, 0.465 Ma) is almost at the same depth as the location of *E. huxleyi* (0.275 Ma). Also, the upper part of the isotopic record is punctuated with several minor hiatuses. In our interpretation, part of glacial stage 6 and possibly stage 5 is absent. Clearly, no easy solution is available for the problem of isotopic stage assignment above 32.5 mbsf at Hole 819A.

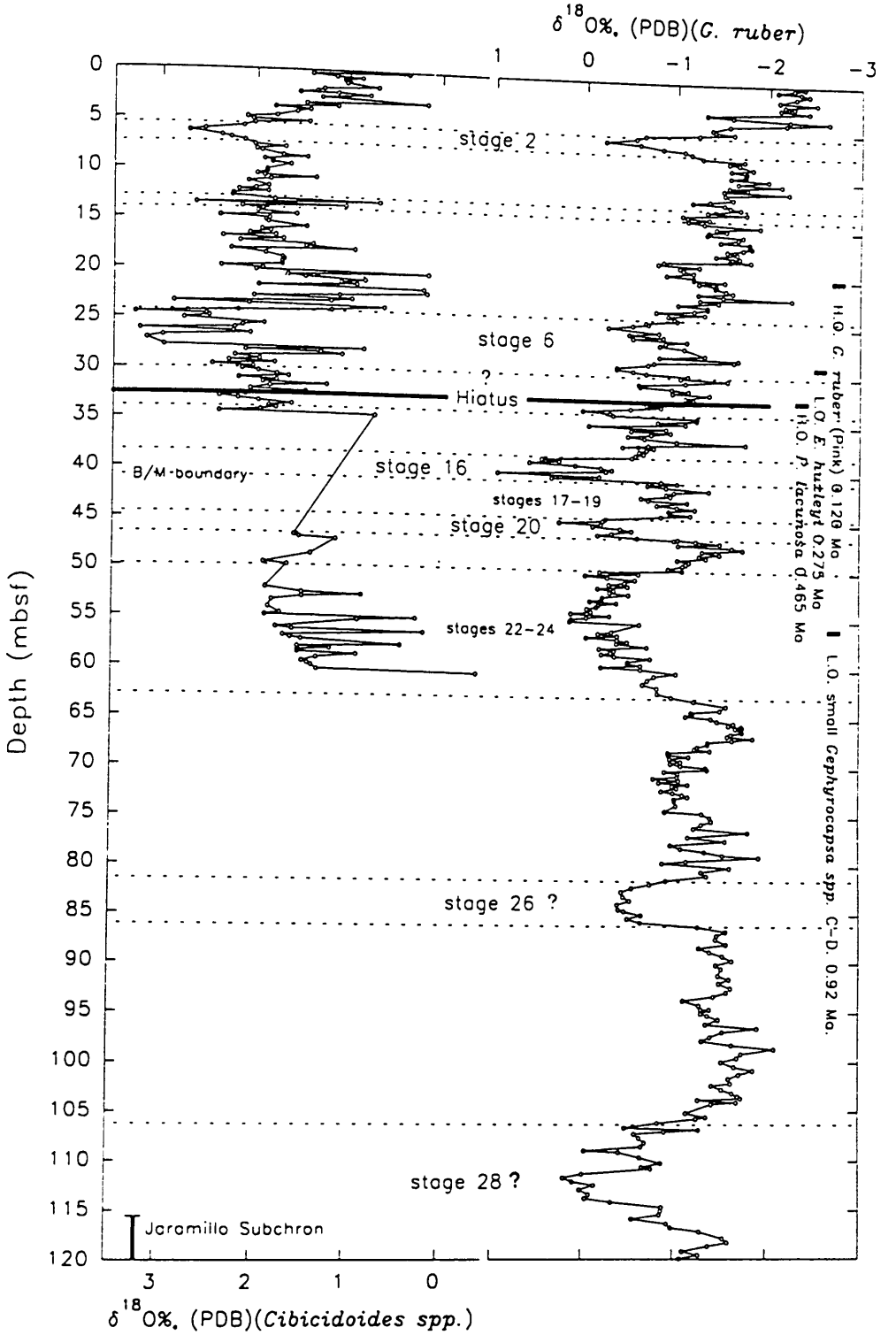

Figure 2. Planktonic (*G. ruber*) and benthic (*Cibicidoides* spp.) foraminiferal oxygen isotope records plotted vs. depth at Hole 819A. The solid horizontal line at 32.5 mbsf marks the position of a major stratigraphical hiatus.

Table 2. Planktonic and benthic foraminiferal oxygen isotope ratios.

Sample	Depth (mbsf)	*G. ruber* $\delta^{18}O$‰ (PDB)	*Cibicidoides* spp. $\delta^{18}O$‰ (PDB)
1H-1, 16–18	0.16	−2.407	0.332
1H-1, 30–32	0.3	-2.295	1.368
1H-1, 54–56	0.54	−2.117	1.106
1H-1, 70–72	0.7	−2.366	0.827
1H-1, 90–92	0.9	−2.46	1.018
1H-1, 120–122	1.2	−2.315	0.995
1H-2, 10–12	1.6	−2.133	0.652
1H-2, 30–32	1.8	−2.544	1.247
1H-2, 54–56	2.04	−2.194	1.319
1H-2, 68–70	2.18	−2.293	1.506
1H-2, 70–72	2.2	−2.232	1.091
1H-2, 90–92	2.4	−2.47	0.743
1H-2, 120–122	2.7	−2.458	1.266
1H-3, 10–12	3.1	−1.355	0.13
1H-3, 30–32	3.3	−1.633	1.434
1H-3, 54–56	3.54	−2.247	1.091
1H-3, 70–72	3.7	−2.676	1.769
1H-3, 95–97	3.95	−2.21	1.392
1H-3, 120–122	4.2	−1.601	1.534
1H-4, 10–12	4.6	−1.412	1.752
1H-4, 30–32	4.8	−1.442	2.073
1H-4, 54–56	5.04	−1.649	2.011
1H-4, 70–72	5.2	−1.269	1.403
1H-4, 90–92	5.4	−0.675	1.988
1H-4, 120–122	5.7	−0.573	2.107
1H-5, 10–12	6.1	−0.24	2.514
1H-5, 30–32	6.3	−0.621	2.678
1H-5, 70–72	6.7	−0.872	2.337
1H-5, 90–92	6.9	−1.109	2.242
1H-5, 120–122	7.2	−1.186	2.095
1H-6, 10–12	7.6	−1.306	1.991
1H-6, 30–32	7.8	−1.761	1.658
1H-6, 54–56	8.04	−1.599	1.968
1H-6, 68–70	8.18	−1.708	1.914
2H-1, 12–14	8.62	−1.853	1.683
2H-1, 30–32	8.8	−1.617	1.421
2H-1, 54–56	9.04	−1.787	1.883
2H-1, 70–72	9.2	−1.772	1.797
2H-1, 88–90	9.38	−1.776	1.8
2H-1, 109–111	9.59	−1.613	1.597
2H-1, 132–134	9.82	−2.022	
2H-2, 12–14	10.12	−1.695	1.86
2H-2, 30–32	10.3	−2.165	1.855
2H-2, 54–56	10.54	−1.599	1.965
2H-2, 70–72	10.7	−1.793	1.885
2H-2, 88–90	10.88	−1.539	1.327
2H-2, 109–111	11.09	−2.245	1.819
2H-2, 132–134	11.32	−1.55	2.057
2H-3, 30–32	11.8	−1.639	1.84
2H-3, 54–56	12.04	−1.386	1.978
2H-3, 70–72	12.2	−1.198	2.157
2H-3, 88–90	12.38	−1.545	1.842
2H-3, 109–111	12.59	−1.61	2.216
2H-3, 132–134	12.82	−1.722	2.225
2H-4, 12–14	13.12	−1.362	1.771
2H-4, 30–32	13.3	−1.792	0.634
2H-4, 54–56	13.54	−1.089	2.602
2H-4, 70–72	13.7	−1.145	0.996
2H-4, 88–90	13.88	−1.381	2.12
2H-4, 109–111	14.09	−1.154	1.901
2H-4, 132–134	14.34	−1.328	1.953
2H-5, 12–14	14.62	−1.936	1.537
2H-5, 30–32	14.8	−1.461	2.351
2H-5, 54–56	15.04	−1.571	1.827
2H-5, 70–72	15.2	−1.38	1.868
2H-5, 88–90	15.38	−1.36	1.841
2H-5, 109–111	15.59	−1.754	
2H-5, 132–134	15.82	−1.704	1.425
2H-6, 12–14	16.12	−1.511	1.908
2H-6, 30–32	16.3	−1.824	1.811
2H-6, 54–56	16.54	−1.826	2.035
2H-6, 70–72	16.7	−1.847	1.759
2H-6, 88–90	16.88	−1.755	2.321
2H-6, 109–111	17.09	−1.579	1.675
2H-6, 132–134	17.32	−1.69	2.142
2H-7, 7–8	17.57	−1.458	1.354
2H-7, 27–29	17.77	−1.719	1.431
2H-7, 54–56	18.04	−1.611	0.897
3H-1, 10–12	18.1	−1.839	2.233
3H-1, 30–32	18.3	−0.886	
3H-1, 52–54	18.52	−0.824	1.868
3H-1, 70–72	18.7	−1.278	
3H-1, 90–92	18.9	−1.065	1.683
3H-1, 109–111	19.09	−1.101	1.666
3H-1, 131–132	19.31	-1.216	1.689
3H-2, 10–12	19.6	−0.917	1.688
3H-2, 30–32	19.8	−1.214	2.339
3H-2, 52–54	20.02	−1.214	1.897
3H-2, 70–72	20.2	−1.558	1.97
3H-2, 90–92	20.4	−1.275	0.108
3H-2, 109–111	20.59	−1.466	1.624
3H-2, 130–132	20.81	−1.45	1.435
3H-3, 10–12	21.1	−1.574	0.784
3H-3, 30–32	21.3	−1.648	1.856
3H-3, 52–54	21.52	−1.269	0.87
3H-3, 70–72	21.7	−1.542	1.94
3H-3, 90–92	21.9	−2.285	0.16
3H-3, 109–111	22.09	−1.286	
3H-3, 131–132	22.31	−1.493	0.121
3H-4, 10–12	22.6	−1.048	1.062
3H-4, 30–32	22.8	−1.37	1.988
3H-4, 52–54	23.02	−1.371	0.927
3H-4, 70–72	23.2	−1.23	1.154
3H-4, 90–92	23.4	−0.805	2.835
3H-4, 109–111	23.59	−1.34	2.042
3H-4, 131–133	23.81	−0.936	0.576
3H-5, 10–12	24.1	−1.009	3.158
3H-5, 30–32	24.3	−1.037	2.156
3H-5, 52–54	24.52	−0.69	3.238
3H-5, 70–72	24.7	−0.719	2.49
3H-5, 87–89	24.87	−0.546	2.461
3H-5, 109–111	25.09	−0.281	2.723
3H-6, 7–9	25.57	−0.837	1.878
3H-6, 26–28	25.76	−0.51	2.109
3H-6, 52–54	26.02	-0.887	
3H-6, 67–69	26.17	−0.551	3.188
3H-6, 90–92	26.4	−1.147	2.206
3H-6, 109–111	26.59	−0.913	2.023
3H-6, 131–133	26.81	−0.845	2.948
3H-7, 10–12	27.1	−1.118	3.113
4H-1, 30–32	27.8	−1.343	2.934
4H-1, 50–52	28	−0.848	0.793
4H-1, 70–72	28.2	−1.71	2.074
4H-1, 90–92	28.4	−1.663	1.261
4H-1, 110–112	28.6	−0.783	1.028
4H-1, 130–132	28.8	−0.721	2.185
4H-2, 10–12	29.1	−0.373	1.924
4H-2, 30–32	29.3	−0.376	2.248
4H-2, 50–52	29.5	−0.554	1.76
4H-2, 70–72	29.7	−0.697	2.423
4H-2, 90–92	29.9	−1.16	1.991
4H-2, 110–112	30.1	−1.082	2.109
4H-2, 130–132	30.3	−1.599	1.935
4H-3, 10–12	30.6	−1.134	1.733
4H-3, 30–32	30.8	−0.62	1.607
4H-3, 50–52	31	−0.638	2.147
4H-3, 70–72	31.2	−0.984	1.738
4H-3, 90–92	31.4	−1.17	1.888
4H-3, 110–112	31.6	−0.991	1.196
4H-3, 130–132	31.8	−1.4	1.807
4H-4, 10–12	32.1	−1.135	2.02
4H-4, 30–32	32.3	−1.222	1.427
4H-4, 50–52	32.5	−0.987	2.122
4H-4, 70–72	32.7	−1.642	2.075
4H-4, 90–92	32.9	−0.707	2.346
4H-4, 110–112	33.1	−0.865	2.149
4H-4, 130–132	33.3	−0.531	1.931
4H-5, 10–12	33.6	−0.008	1.574
4H-5, 30–32	33.8	−0.308	1.821
4H-5, 50–52	34	−0.342	1.74
4H-5, 70–72	34.2	−1.264	1.911
4H-5, 90–92	34.4	−1.263	2.345
4H-5, 110–112	34.6	−0.835	0.67
4H-5, 130–132	34.8	−1.139	
4H-6, 10–12	35.1	−0.076	
4H-6, 30–32	35.3	−0.925	
4H-6, 50–52	35.5	−0.541	
4H-6, 70–72	35.7	−0.977	
4H-6, 90–92	35.9	−0.76	
4H-6, 110–112	36.1	−0.506	
4H-6, 130–132	36.3	−0.686	
4H-7, 10–12	36.6	−1.041	
4H-7, 30–32	36.8	−1.795	
4H-7, 50–52	37	−0.728	
4H-7, 70–72	37.2	−0.448	
5H-1, 10–12	37.1	−0.62	
5H-1, 30–32	37.3	−0.79	
5H-1, 50–52	37.5	−0.713	
5H-1, 70–72	37.7	−0.629	
5H-1, 90–92	37.9	−0.679	
5H-1, 110–112	38.1	-0.59	
5H-1, 130–132	38.3	−0.553	
5H-2, 10–12	38.6	0.441	
5H-2, 30–32	38.8	0.245	
5H-2, 50–52	39	0.573	
5H-2, 70–72	39.2	0.071	
5H-2, 90–92	39.4	-0.213	
5H-2, 110–112	39.6	-0.333	
5H-2, 130–132	39.8	-0.264	
5H-3, 10–12	40.1	0.927	
5H-3, 30–32	40.3	−0.193	
5H-3, 50–52	40.5	0.329	
5H-3, 70–72	40.7	−0.876	
5H-3, 90–92	40.9	−1.052	
5H-3, 110–112	41.1	−0.725	
5H-3, 130–132	41.3	−0.93	
5H-4, 10–12	41.6	−1.398	
5H-4, 30–32	41.8	−1.016	
5H-4, 50–52	42	−0.932	
5H-4, 70–72	42.2	−0.979	
5H-4, 90–92	42.4	−0.653	
5H-4, 110–112	42.6	−0.731	
5H-4, 130–132	42.8	−1.165	
5H-5, 10–12	43.1	−0.829	
5H-5, 30–32	43.3	−1.052	
5H-5, 50–52	43.5	−1.247	
5H-5, 70–72	43.7	−0.959	
5H-5, 90–92	43.9	−0.971	
5H-5, 110–112	44.1	−1.197	
5H-5, 130–132	44.3	−0.876	
5H-6, 10–12	44.6	−0.267	
5H-6, 30–32	44.8	−0.235	
5H-6, 50–52	45	0.244	
5H-6, 70–72	45.2	−0.217	
5H-6, 90–92	45.4	−0.126	
5H-6, 110–112	45.6	−0.426	
5H-6, 130–132	45.8	−0.55	
5H-7, 10–12	46.1	−0.334	
5H-7, 30–32	46.3	−0.18	
5H-7, 50–52	46.5	−0.614	
5H-7, 70–72	46.7	−1.024	
6H-1, 10–12	46.6	−1.062	
6H-1, 30–32	46.8	−1.262	1.579
6H-1, 50–52	47	−1.524	1.524
6H-1, 70–72	47.2	−1.068	1.127
6H-1, 90–92	47.4	−1.66	
6H-1, 110–112	47.6	−1.774	
6H-1, 130–132	47.8	−1.334	
6H-2, 10–12	48.1	−1.52	
6H-2, 30–32	48.3	-1.299	
6H-2, 50–52	48.5	−1.373	
6H-2, 70–72	48.7	−1.059	1.398
6H-2, 90–92	48.9	−1.191	
6H-2, 110–112	49.1	−1.156	
6H-2, 130–132	49.3	−1.117	
6H-3, 10–12	49.6	−0.959	1.907
6H-3, 30–32	49.8	−1.115	1.652
6H-3, 50–52	50	−0.206	
6H-3, 70–72	50.2	−0.63	
6H-3, 90–92	50.4	−0.048	
6H-3, 110–112	50.6	−0.291	
6H-3, 130–132	50.8	−0.595	
6H-4, 10–12	51.1	−0.479	
6H-4, 30–32	51.3	−0.307	
6H-4, 50–52	51.5	-0.514	
6H-4, 70–72	51.7	−0.185	
6H-4, 90–92	51.9	−0.362	
6H-4, 110–112	52.1	−0.317	1.883
6H-4, 130–132	52.3	−0.523	
6H-5, 10–12	52.6	−0.235	1.49
6H-5, 30–32	52.8	−0.232	0.849
6H-5, 50–52	53	−0.1	1.49
6H-5, 70–72	53.2	−0.39	
6H-5, 90–92	53.4	−0.192	1.816
6H-5, 110–112	53.6	−0.174	
6H-5, 130–132	53.8	−0.067	
6H-6, 10–12	54.1	−0.114	1.852
6H-6, 30–32	54.3	0.108	
6H-6, 50–52	54.5	−0.314	
6H-6, 70–72	54.7	−0.062	1.725
6H-6, 90–92	54.9	0.102	1.885
6H-6, 110–112	55.1	0.123	0.269

Table 2 (continued).

Sample	Depth (mbsf)	*G. ruber* $\delta^{18}O$‰ (PDB)	*Cibicidoides* spp. $\delta^{18}O$‰ (PDB)
6H-6, 130–132	55.3	–0.644	0.886
7H-1, 10–12	56.1	–0.341	1.768
7H-1, 30–32	56.3	–0.196	1.591
7H-1, 50–52	56.5	–0.406	0.188
7H-1, 70–72	56.7	–0.063	
7H-1, 90–92	56.9	–0.403	1.69
7H-1, 110–112	57.1	–0.511	1.614
7H-1, 130–132	57.3	–0.395	1.495
7H-2, 10–12	57.6	–0.727	
7H-2, 30–32	57.8	–0.207	0.433
7H-2, 50–52	58	–0.369	1.531
7H-2, 70–72	58.2	–0.334	1.185
7H-2, 90–92	58.4	–0.233	1.534
7H-2, 110–112	58.6	–0.374	1.535
7H-2, 130–132	58.8	–0.765	0.897
7H-3, 10–12	59.1	–0.516	1.333
7H-3, 30–32	59.3	–0.519	
7H-3, 50–52	59.5	1.487	
7H-3, 70–72	59.7	–0.663	1.43
7H-3, 90–92	59.9	–0.228	1.387
7H-3, 110–112	60.1	–0.659	1.328
7H-3, 130–132	60.3	–1.01	-0.394
7H-4, 10–12	60.6	-0.768	
7H-4, 30–32	60.8		
7H-4, 50–52	61	–0.696	
7H-4, 70–72	61.2		
7H-4, 90–92	61.4	–0.64	
7H-4, 110–112	61.6		
7H-4, 130–132	61.8	–0.801	
7H-5, 10–12	62.1		
7H-5, 30–32	62.3	–0.804	
7H-5, 50–52	62.5		
7H-5, 70–72	62.7	–0.962	
7H-5, 90–92	62.9		
7H-5, 110–112	63.1	–1.208	
7H-6, 10–12	63.6	–1.561	
7H-6, 30–32	63.8		
7H-6, 50–52	64	–1.495	
7H-6, 70–72	64.2	–1.179	
7H-6, 90–92	64.4	–1.197	
7H-6, 110–112	64.6	–1.122	
7H-6, 130–132	64.8	–1.397	
7H-7, 10–12	65.1	–1.467	
7H-7, 30–32	65.3	–1.647	
7H-7, 50–52	65.5	–1.592	
7H-7, 70–72	65.7	–1.737	
8H-1, 10–12	65.6	–1.728	
8H-1, 30–32	65.8	–1.667	
8H-1, 50–52	66	–1.723	
8H-2, 10–12	66.22	–1.739	
8H-2, 30–32	66.42	–1.615	
8H-2, 50–52	66.62	–1.58	
8H-2, 70–72	66.82	–1.851	
8H-2, 90–92	67.02	–1.628	
8H-2, 110–112	67.22	–1.366	
8H-2, 130–132	67.42	–1.366	
8H-3, 10–12	67.72	–1.249	
8H-3, 30–32	67.92	–1.222	
8H-3, 50–52	68.12	–1.391	
8H-3, 70–72	68.32	–0.928	
8H-3, 90–92	68.52	–0.936	
8H-3, 110–112	68.72	–1.157	
8H-3, 130–132	68.92	–0.947	
8H-4, 10–12	69.22	–1.071	
8H-4, 30–32	69.42	–0.958	
8H-4, 50–52	69.62	-1.07	
8H-4, 70–72	69.82	-1.342	
8H-4, 90–92	70.02	–1.362	
8H-4, 110–112	70.22	–0.891	
8H-4, 130–132	70.42	–1.043	
8H-5, 10–12	70.72	–1.034	
8H-5, 30–32	70.92	–0.768	
8H-5, 50–52	71.12	–1.048	
8H-5, 70–72	71.32	–0.83	
8H-5, 90–92	71.52	–1.149	
8H-5, 110–112	71.72	–0.978	
8H-5, 130–132	71.92	–1.03	
8H-6, 10–12	72.22	–0.858	
8H-6, 30–32	72.42	–0.986	
8H-6, 50–52	72.62	–1.09	
8H-6, 70–72	72.82	–1.149	
8H-6, 90–92	73.02	–1	
8H-6, 110–112	73.22	–1.004	
8H-6, 130–132	73.42		
8H-7, 10–12	73.72	–1.021	
8H-7, 30–32	73.92		
8H-7, 50–52	74.12		
8H-7, 70–72	74.32	–0.897	
8H-7, 90–92	74.52	–1.307	
8H-7, 110–112	74.72		
8H-7, 130–132	74.92	–1.393	
9H-1, 10–12	75.1		
9H-1, 30–32	75.3	–1.412	
9H-2, 10–12	75.45		
9H-2, 30–32	75.65	–1.301	
9H-2, 50–52	75.85		
9H-2, 70–72	76.05	–1.217	
9H-2, 90–92	76.25		
9H-2, 110–112	76.45	–1.806	
9H-2, 130–132	76.65		
9H-3, 10–12	76.95	–1.156	
9H-3, 30–32	77.15		
9H-3, 50–52	77.35	–1.56	
9H-3, 70–72	77.55		
9H-3, 90–92	77.75	–0.962	
9H-3, 110–112	77.95		
9H-3, 130–132	78.15	–1.075	
9H-4, 10–12	78.45	–1.333	
9H-4, 30–32	78.65		
9H-4, 50–52	78.85	–1.533	
9H-4, 70–72	79.05	–1.921	
9H-4, 90–92	79.25		
9H-4, 110–112	79.45	–1.136	
9H-4, 130–132	79.65	–0.872	
9H-5, 10–12	79.95		
9H-5, 30–32	80.15	–1.608	
9H-5, 50–52	80.35		
9H-5, 70–72	80.55	–1.302	
9H-5, 90–92	80.75		
9H-5, 110–112	80.95	–1.362	
9H-5, 130–132	81.15		
9H-6, 10–12	81.45	–0.916	
9H-6, 30–32	81.65		
9H-6, 50–52	81.85	–0.734	
9H-6, 70–72	82.05		
9H-6, 90–92	82.25	–0.535	
9H-6, 110–112	82.45		
9H-6, 130–132	82.65	–0.423	
9H-7, 10–12	83.95		
9H-7, 30–32	83.15	–0.444	
9H-7, 50–52	83.35		
9H-7, 70–72	83.55	–0.514	
9H-7, 90–92	83.75		
9H-7, 110–112	83.95	–0.381	
9H-7, 130–132	84.15		
9H-8, 10–12	84.45	–0.391	
9H-8, 30–32	84.65		
9H-8, 50–52	84.85	–1.365	
9H-8, 70–72	85.05		
10H-1, 10–12	84.6	–0.453	
10H-1, 30–32	84.8		
10H-2, 10–12	85	–0.642	
10H-2, 30–32	85.2		
10H-2, 50–52	85.4	–0.49	
10H-2, 70–72	85.6		
10H-2, 90–92	85.8	–0.634	
10H-2, 110–112	86		
10H-2, 130–132	86.2	–1.262	
10H-3, 10–12	86.5		
10H-3, 30–32	86.7	-1.57	
10H-3, 50–52	86.9		
10H-3, 70–72	87.1	–1.474	
10H-3, 90–92	87.3		
10H-3, 110–112	87.5	–1.461	
10H-3, 130–132	87.7		
10H-4, 10–12	88	–1.575	
10H-4, 30–32	88.2		
10H-4, 50–52	88.4	–1.282	
10H-4, 70–72	88.6	88.8	
10H-4, 90–92			-1.398
10H-4, 110–112	89		
10H-4, 130–132	89.2	–1.538	
10H-5, 10–12	89.5		
10H-5, 30–32	89.7	–1.638	
10H-5, 50–52	89.9		
10H-5, 70–72	90.1	–1.465	
10H-5, 90–92	90.3		
10H-5, 110–112	90.5	–1.523	
10H-6, 10–12	91		
10H-6, 30–32	91.2	-1.492	
10H-6, 50–52	91.4		
10H-6, 70–72	91.6	-1.609	
10H-6, 90–92	91.8		
10H-6, 110–112	92	-1.5	
10H-6, 130–132	92.2		
10H-7, 10–12	92.5	-1.622	
10H-7, 30–32	92.7		
10H-7, 50–52	92.9	-1.578	
10H-7, 70–72	93.1		
10H-7, 90–92	93.3	-1.439	
10H-7, 110–112	93.5		
10H-7, 130–132	93.7	-1.107	
10H-8, 10–12	94		
10H-8, 30–32	94.2	-1.286	
10H-8, 50–52	94.4		
10H-8, 70–72	94.6	-1.304	
11H-1, 10–12	94.1		
11H-2, 10–12	94.42		
11H-2, 30–32	94.62	-1.398	
11H-2, 50–52	94.82		
11H-2, 70–72	95.02	-1.303	
11H-2, 90–92	95.22	-1.375	
11H-2, 110–112	95.42		
11H-2, 130–132	95.62	-1.495	
11H-3, 10–12	95.92		
11H-3, 30–32	96.12	-1.357	
11H-3, 50–52	96.32		
11H-3, 70–72	96.52	-1.91	
11H-3, 90–92	96.72		
11H-3, 110–112	96.92	-1.536	
11H-3, 130–132	97.12		
11H-4, 10–12	97.42	-1.407	
11H-4, 30–32	97.62		
11H-4, 50–52	97.82	-1.314	
11H-4, 70–72	98.02		
11H-4, 90–92	98.22	-1.639	
11H-4, 110–112	98.42		
11H-4, 130–132	98.62	-2.091	
11H-5, 10–12	98.92		
11H-5, 30–32	99.12	-1.744	
11H-5, 50–52	99.32		
11H-5, 70–72	99.52	-1.695	
11H-5, 90–92	99.72		
11H-5, 110–112	99.92	-1.527	
11H-5, 130–132	100.12		
11H-6, 10–12	100.42	-1.666	
11H-6, 30–32	100.62		
11H-6, 50–52	100.82	-1.866	
11H-6, 70–72	101.02		
11H-6, 90–92	101.22	-1.715	
11H-6, 110–112	101.42		
11H-6, 130–132	101.62	-1.607	
11H-7, 10–12	101.92		
11H-7, 30–32	102.12	-1.629	
11H-7, 50–52	102.32	-1.424	
11H-7, 70–72	102.52		
11H-7, 90–92	102.72	-1.53	
11H-7, 110–112	102.92		
11H-7, 130–132	103.12	-1.647	
11H-8, 10–12	103.42	-1.708	
11H-8, 30–32	103.62	-1.736	
11H-8, 50–52	103.82		
11H-8, 70–72	104.02	-1.69	
12H-1, 10–12	103.6		
12H-1, 30–32	103.8	-1.274	
12H-1, 50–52	104		
12H-1, 70–72	104.2	-1.421	
12H-1, 90–92	104.4		
12H-2, 10–12	105.1	-1.147	
12H-2, 30–32	105.3		
12H-2, 50–52	105.5	-1.364	
12H-2, 70–72	105.7	-1.259	
12H-2, 90–92	105.9		
12H-2, 110–112	106.1	-0.834	
12H-2, 130–132	106.3		
12H-3, 10–12	106.6	-0.472	
12H-3, 30–32	106.8	-1.283	
12H-3, 50–52	107	-0.913	
12H-3, 70–72	107.2	-0.578	
12H-3, 83–85	107.33		
12H-3, 110–112	107-6	-0.634	
12H-4, 10–12	108.1	-0.691	

Table 2 (continued).

Sample	Depth (mbsf)	*G. ruber* $\delta^{18}O$‰ (PDB)	*Cibicidoides* spp. $\delta^{18}O$‰ (PDB)
12H-4, 30-32	108.3		
12H-4, 50-52	108.5	-0.654	
12H-4, 70-72	108.7		
12H-4, 90-92	108.9	-0.036	
12H-4, 110-112	109.1	-0.409	
12H-4, 130-132	109.3	-0.767	
12H-5, 10-12	109.6		
12H-5, 30-32	109.8		
12H-5, 50-52	110		
12H-5, 70-72	110.2	-0.874	
12H-5, 90-92	110.4		
12H-5, 110-112	110.6	-0.665	
12H-5, 128-130	110.78	-0.762	
13H-1, 10-12	111.1		
13H-1, 30-32	111.3	-0.013	
13H-1, 55-57	111.55		
13H-2, 10-12	111.68	0.193	
13H-2, 30-32	111.88		
13H-2, 50-52	112.08	0.093	
13H-2, 70-72	112.28		
13H-2, 88-90	112.46	-0.144	
13H-2, 110-112	112.68		
13H-2, 130-132	112.88	0.015	
13H-3, 10-12	113.13		
13H-3, 30-32	113.38	-0.085	
13H-3, 50-52	113.58		
13H-3, 70-72	113.78	-0.045	
13H-3, 88-90	113.96		
13H-3, 110-112	114.18	-0.328	
13H-3, 130-132	114.38		
13H-4, 10-12	114.68	-0.882	
13H-4, 30-32	114.88		
13H-4, 50-52	115.08	-0.875	
13H-4, 70-72	115.28		
13H-4, 88-90	115.46	-0.856	
13H-4, 110-112	115.68		
13H-4, 130-132	115.88	-0.552	
13H-5, 10-12	116.18		
13H-5, 30-32	116.38	-0.935	
13H-5, 50-52	116.58		
13H-5, 70-72	116.78	-0.981	
13H-5, 88-90	116.96		
13H-5, 110-112	117.18	-1.291	
13H-6, 10-12	117.68		
13H-6, 30-32	117.88	-1.543	
13H-6, 50-52	118.08		
13H-6, 70-72	118.28	-1.594	
13H-6, 88-90	118.46		
13H-6, 110-112	118.68	-1.384	
13H-6, 130-132	118.88		
13H-7, 10-12	119.18	-1.107	
13H-7, 30-32	119.38		
13H-7, 50-52	119.58	-1.28	
13H-7, 70-72	119.78		
13H-7, 88-90	119.96	-1.073	
13H-7, 110-112	120.18		
13H-7, 130-132	120.38	-1.138	

Below 32.5 mbsf, the isotopic record is thought to be more complete. Isotopic stages 14 through 21, at about 47 mbsf, can be recognized in the record at hole 819A, except for the absence of a clear stage 18. Below about 50 mbsf continuous correlation with the isotopic record of Raymo et al. (1990) becomes more difficult. For example, some uncertainty exists as to whether the slight enrichment event between 68 and 74 mbsf is in point of fact stage 24, and not part of stage 25. Oxygen isotope stage 28 has been placed at about 114 mbsf, which is supported by the tentative location of the Jaramillo subchron (0.97–0.91 Ma) between 115–120 mbsf (Barton et al., this volume). This implies that the recorded nannofossil datum level of HO of small *Gephyrocapsa* spp. C-D at 56 mbsf (Wei and Gartner, this volume) is unreliable and possibly indicates either reworking or sample contamination.

In general, the benthic foraminiferal oxygen isotope record, relative to the planktonic oxygen isotope record, displays a greater intrastage amplitudinal variation in isotopic value. This greater amplitudinal variation, in isotopic value, is particularly evident within isotope stages 4, 7, and 8. Benthic oxygen isotope values are typically about 2.5 to 3.5 ‰ heavier than corresponding planktonic oxygen isotope values. The oxygen isotope difference between benthic and planktonic foraminifers ($\Delta\delta^{18}O_{B\text{-}P}$) are shown in Figure 4. Comparison of the $\Delta\delta^{18}O_{B\text{-}P}$ record in the upper and lower parts of the sequence at Hole 819A indicates that during stages 22 through 24 the mean isotopic difference is about 1.5‰ . This compares with about 3.0‰ during stage 9 and 3.5‰ during the Holocene.

The planktonic foraminiferal oxygen isotope record displays a trend of depletion in mean $\delta^{18}O$ value, from 32.5 mbsf through the Holocene, of about 1.5‰. This upward decreasing trend is not so clear in the benthic foraminiferal curve and is not present below about 42 mbsf in the planktonic curve. Below 42 mbsf, the planktonic foraminiferal curve displays a trend, similar to that displayed by the benthic foraminiferal $\delta^{18}O$ record, of depletion in mean $\delta^{18}O$ value, with depth.

Mineral Magnetic Properties

Figures 5 and 6 summarize the variations of mineral magnetic properties and planktonic foraminiferal oxygen isotope ratio with depth in Hole 819A. Magnetic susceptibility and saturation isothermal magnetization (Fig. 5) predominantly reflect the concentration of magnetite in the sediments. The highest concentrations are found in the top 7 m and at four horizons at 21.7, 24.6, 67.2, and 76.2 mbsf. Other sediment horizons have dramatically reduced magnetite concentrations, thus necessitating the use of logarithmic X and SIRM scales to display the magnetic variations.

Below the marked change in magnetic concentration at 7 mbsf and excluding the peaks at 21.7 and 24.6 mbsf, specific magnetic susceptibility and saturation IRM display a general trend of decreasing value with depth to about 32.5 mbsf, roughly following the foraminiferal $\delta^{18}O$ trend (Fig. 5). In general, below 32.5 mbsf, high magnetite content occurs during the interglacial periods and low concentrations during the glacial periods (e.g., stages 22 to 24 and stages 26 and 28). By contrast, above 32.5 mbsf the relationship between specific magnetic susceptibility and SIRM is more capricious, with no clear relationship between magnetic concentration and foraminiferal $\delta^{18}O$ values and with the peaks in magnetic mineral content occurring in both the glacial and interglacial periods.

The mineral magnetic ratios of S-ratio ($IRM_{100\ mT}/IRM_{1000\ mT}$) and ARM/$X$ were plotted down the core to 120 mbsf for Hole 819A in Figure 6 (Table 1). Both ratios display a marked change in value at about 7.5 mbsf, the same depth at which the magnetic concentrations were found to change (Figs. 5 and 7). Both the S-ratio and ARM/X ratio are again high at depths of 21.7 and 24.6 mbsf, where the magnetic concentrations also are high. Below 7.5 mbsf, both ratios show a slight overall trend of increasing mean value with depth.

Below 32.5 mbsf, peaks in magnetic mineral concentration tend to be associated with relatively low percentage carbonate content (see Fig. 8). This inverse relationship is particularly evident in the percentage of carbonate content archive (bulk) sample plot alongside magnetic susceptibility (see Fig. 8). However, subtle variations in this overall antithetical relationship occur, for example, at about 5 and 32 mbsf. Curves for percentages of carbonate and susceptibility exhibit a positive correlation.

Particle Size Characteristics

The relative proportions of fine fraction (<63 μm) and mean particle size (μm) with depth at Hole 819A are illustrated in Figure 9

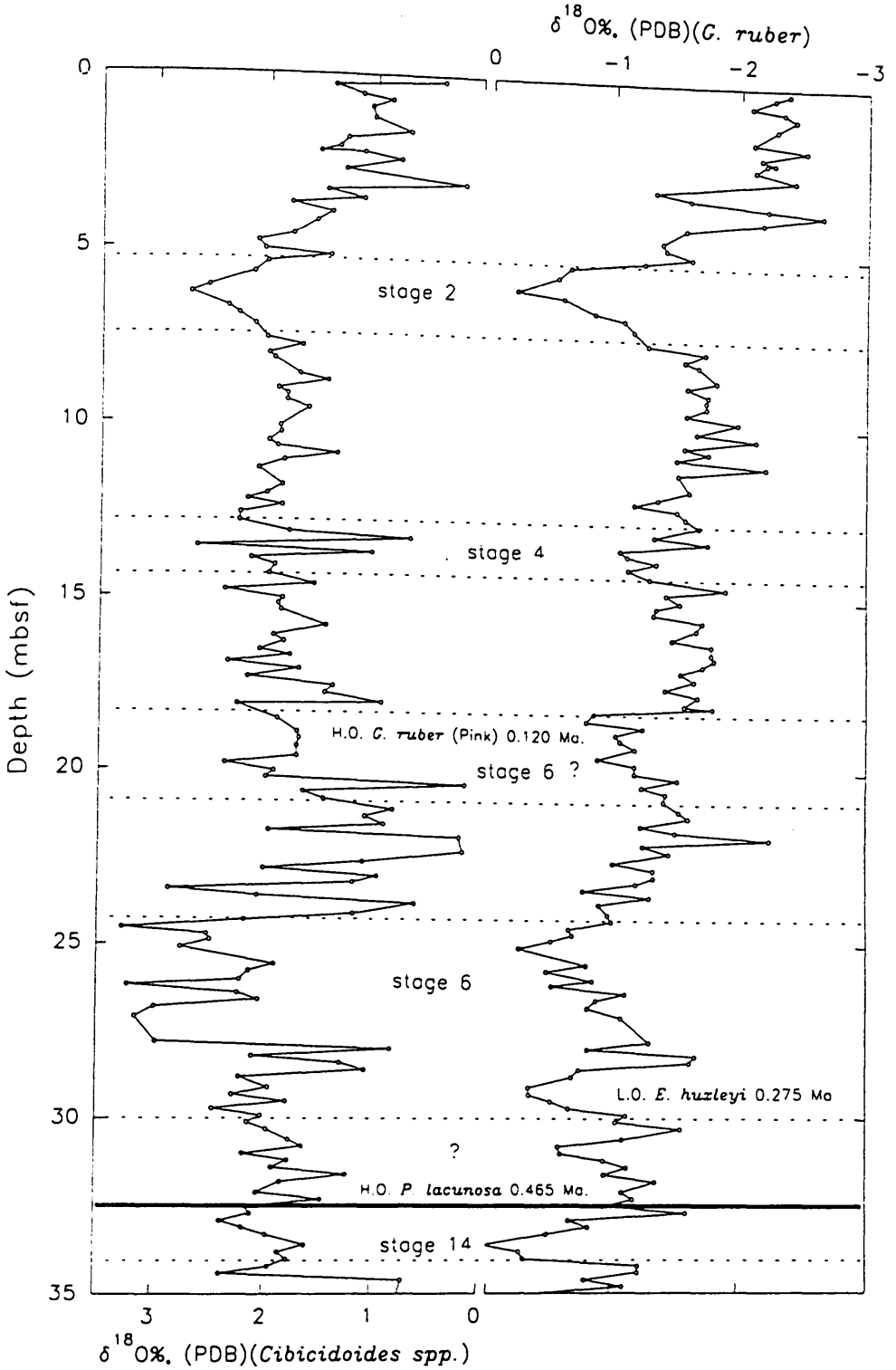

Figure 3. Planktonic (*G. ruber*) and benthic (*Cibicidoides* spp.) foraminiferal oxygen isotope records at Hole 819A plotted downcore to 35 mbsf. The solid horizontal line at 32.5 mbsf marks the position of a major stratigraphical hiatus.

Table 3. Particle size distribution for samples collected at Hole 819A.

Sample depth (mbsf)	A % fine fraction (<63 µm)	B % fine fraction (<63 µm)	Mean particle size (µm)
0.16	81.8	86.4	37.8
0.3	81.6	84.4	49.0
0.54	81.8	90.7	47.1
0.7	85.5	90.5	40.5
0.9	83.3	90.6	42.1
1.2	88.1	93.7	36.5
1.6	80.1	93.3	39.5
1.8	95.7	94.7	25.7
2.04	88.4	93.1	35.7
2.18	92.0	93.5	32.5
2.2	88.7	93.0	33.9
2.4	87.2	90.5	38.2
2.7	88.7	93.8	35.9
3.1	83.4	92.5	40.0
3.3	87.2	95.7	35.1
3.54	96.9	95.6	22.8
3.7	91.1	96.5	29.7
3.95	96.0	95.6	22.6
4.2	94.2	96.0	24.9
4.6	92.6	95.0	25.8
4.8	92.2	95.8	25.9
5.04	93.0	95.0	26.6
5.2	85.5	93.4	38.3
5.4	79.7	88.8	50.3
5.7	71.7	81.0	69.3
6.1	84.1	88.7	32.7
6.3	64.0	70.9	89.0
6.7	53.6	63.3	113.1
6.9	59.3	66.3	96.9
7.2	58.1	70.1	97.8
7.6	65.6	80.9	82.1
7.8	64.9	85.0	77.5
8.04	78.8	85.2	52.0
8.18	80.8	89.1	47.8
8.62	79.5	87.6	53.6
8.8	84.7	90.6	43.3
9.04	84.2	92.1	42.8
9.2	85.4	92.6	41.1
9.38	90.1	93.6	35.7
9.59	87.4	93.5	31.9
9.82	89.4	92.6	32.1
10.12	86.2		38.6
10.3	89.7	94.2	28.4
10.54	90.7	93.9	32.4
10.7	87.2	94.0	36.0
10.88	84.2	95.2	39.2
11.09	90.1	94.3	32.6
11.32	90.7	95.1	33.0
11.8	82.7	95.0	41.4
12.04	90.6	92.2	30.3
12.2	98.1	92.7	25.5
12.38	86.3	93.5	38.5
12.59	86.1	91.4	37.2
12.82	89.0	92.9	33.1
13.12	77.1	85.5	54.0
13.3	68.4	84.6	80.9
13.54	61.2	81.3	102.3
13.7	66.3	80.0	81.1
13.88	70.2	87.5	73.6
14.09	78.1	89.1	51.5
14.34	72.0	86.2	68.5
14.62	76.9	86.8	60.4
14.8	84.7	90.4	44.2
15.04	74.2	86.6	59.4
15.2	68.1	85.2	102.3
15.38	78.2	86.8	57.2
15.59	84.1	88.4	44.5
15.82	79.1	87.7	52.1
16.12	81.7	86.8	57.8
16.3	82.1	86.4	45.5
16.54	73.8	84.1	59.8
16.7	73.9	84.3	64.0
16.88	76.7	84.1	58.9
17.09	61.2	75.8	123.9
17.32	77.8	86.7	58.0
17.57	72.2	100.0	70.0
17.77	79.7	85.4	53.0
18.04	76.1	86.5	56.5
18.1	81.2	90.6	46.8
18.3	88.4	91.5	35.5
18.52	87.0	92.8	34.5
18.7	87.5	91.2	36.0
18.9	82.2	90.1	40.8
19.09	75.2	85.3	64.1
19.31	78.8	88.7	54.2
19.6	74.0	87.8	65.9
19.8	57.5	76.6	129.3
20.02	72.6	83.4	77.2
20.2	82.4	85.9	51.0
20.4	75.5	81.6	57.0
20.59	81.0	87.8	50.2
20.81	80.2	87.0	46.2
21.1	85.1	90.8	40.5
21.3	91.1	93.9	28.5
21.52	92.3	95.3	28.4
21.7	90.2	95.2	31.6
21.9	92.8	96.6	27.1
22.09	92.8	96.7	28.0
22.31	99.7	97.2	17.3
22.6	48.2	71.2	107.1
22.8	93.0	97.5	26.4
23.02	97.6	98.3	18.9
23.2	96.2	97.3	21.7
23.4	89.7	96.1	32.5
23.59	98.2	98.3	19.3
23.81	83.8	94.9	42.0
24.1	76.9	77.5	57.9
24.3	70.6	74.1	85.5
24.52	63.0	78.9	128.8
24.7	84.7	85.1	45.8
24.87	74.8	80.6	67.8
25.09	73.7	67.8	80.9
25.57	60.6	58.8	112.6
25.76	50.1	47.6	150.5
26.02	59.8	63.6	120.0
26.17	71.1	72.5	79.0
26.4	73.6	73.3	79.6
26.59	55.4	52.9	148.5
26.81	57.1	55.3	135.9
27.1	53.0	56.3	147.4
27.8	79.4	85.4	59.0
28	83.0	78.8	49.8
28.2	100.0	95.5	16.6
28.4	100.0	95.3	16.0
28.6	77.5	85.9	71.9
28.8	68.3	63.1	100.0
29.1	63.6		121.3
29.3	58.3		127.9
29.5	56.2		126.1
29.7	55.4		114.4
29.9	59.8	61.5	130.9
30.1	68.6		104.9
30.3	73.6	72.2	70.4
30.6	80.0	80.9	57.7
30.8	79.1	80.5	61.6
31	79.4	78.7	69.1
31.2	81.6	83.4	62.4
31.4	89.9	87.9	30.7
31.6	83.8	83.7	47.6
31.8	79.8	86.4	52.8
32.1	83.2	87.8	45.7
32.3	88.9	90.2	38.6
32.5	84.3	86.8	38.3
32.7	85.4	85.1	38.2
32.9	81.2	80.7	37.8
33.1	93.4	94.5	24.1
33.3	88.4	91.4	30.2
33.6	78.3	83.9	42.8
33.8	78.9	83.1	46.0
34	77.1	80.3	53.3
34.2	71.9	81.1	51.4
34.4	73.3	82.2	49.0
34.6	75.0	82.1	49.1
34.8	90.1	90.5	24.9
35.1	82.7	85.4	37.3
35.3	88.2	89.6	31.4
35.5	82.8	87.7	38.5
35.7	84.6	89.8	35.4
35.9	83.0	89.3	37.5
36.1	84.5	86.9	36.2
36.3	83.6	87.3	37.2
36.6	86.4	86.8	29.9
36.8	68.0	85.5	56.2
37	78.6	84.5	42.4
37.2	78.7	82.3	41.9
37.1	85.4	86.1	36.9
37.3	84.5	84.5	37.0
37.5	82.2	86.1	39.3
37.7	75.8	85.5	41.9
37.9	76.9	86.2	44.3
38.1	79.9	84.3	41.6
38.3	83.3	87.6	37.3
38.6	81.3	75.5	48.7
38.8	84.0	81.6	36.2
39	83.7	81.1	41.7
39.2	87.8	88.1	31.1
39.4	87.3	90.6	33.9
39.6	76.5	80.5	47.3
39.8	93.7	76.8	39.9
40.1	89.5	75.4	30.6
40.3	86.3	85.3	35.2
40.5	87.5	89.5	32.0
40.7	82.4	90.2	38.6
40.9	85.2	87.2	36.9
41.1	82.6	85.2	38.7
41.3	80.8	84.9	40.8
41.6	82.9	87.9	38.8
41.8	79.2	84.0	41.6
42	79.9	85.9	40.1
42.2	82.8	81.4	38.0
42.4	81.6	84.4	40.6
42.6	78.1	83.8	43.0
42.8	79.0	81.7	43.2
43.1	72.8	79.4	48.8
43.3	76.2	79.6	45.0
43.5	68.3	77.7	55.3
43.7	77.0	81.2	42.8
43.9	71.5	74.5	51.6
44.1	75.1	80.0	46.9
44.3	77.9	81.4	43.3
44.6	76.4	79.8	45.2
44.8	79.0	84.2	42.8
45	81.3	85.6	38.8
45.2	84.9	85.4	34.1
45.4	81.7	85.8	39.0
45.6	84.0	88.4	35.9
45.8	79.4	87.5	41.0
46.1	80.5	89.2	40.1
46.3	83.7	87.5	37.6
46.5	78.6	80.0	43.1
46.7	81.2	81.9	41.1
46.6	84.8	87.5	36.7
46.8	86.5	91.2	36.3
47	88.0	91.1	31.5
47.2	81.5	88.9	39.5
47.4	81.5	89.4	39.8
47.6	87.5	89.4	31.7
47.8	89.1	91.6	29.4
48.1	91.2	92.6	27.7
48.3	88.1	92.1	32.6
48.5	77.3	87.8	43.9
48.7	87.1	90.8	31.8
48.9	85.6	91.8	34.2
49.1	90.0	91.7	27.4
49.3	91.0	92.4	28.6
49.6	86.3	92.5	33.3
49.8	84.2	91.0	36.5
50	84.5	89.9	34.7
50.2	82.1	89.0	38.1
50.4	85.9	88.9	35.4
50.6	83.8	87.2	36.3
50.8	83.4	87.9	36.6
51.1	85.6	88.9	34.6
51.3	85.0	88.5	35.4
51.5	85.5	90.7	35.6
51.7	85.9	88.5	33.7
51.9	86.1	89.1	33.5
52.1	87.0	88.2	33.2
52.3	79.9	85.7	41.2
52.6	81.3	87.9	34.6
52.8	80.7	86.5	42.0
53	84.7	87.3	37.3
53.2	84.6	87.4	37.2
53.4	80.2	87.1	40.2
53.6	84.8	87.3	36.5
53.8	81.6	85.7	39.7
54.1	85.0	88.0	36.7

Table 3 (continued).

Sample depth (mbsf)	A % fine fraction (<63 µm)	B % fine fraction (<63 µm)	Mean particle size (µm)
54.3	82.9	86.4	39.8
54.5	82.7	86.3	39.5
54.7	85.9	87.4	36.0
54.9	82.9	84.5	38.6
55.1	82.9	85.9	38.9
55.3	81.6	87.7	39.4
56.1	87.0	85.1	33.8
56.3	84.2	86.7	36.7
56.5	76.7	82.0	45.3
56.7	78.1	86.2	38.7
56.9	83.0	92.1	35.3
57.1	81.2	88.5	35.4
57.3	82.8	90.4	35.2
57.6	80.5	89.2	39.1
57.8	88.7	91.0	29.8
58	80.8	89.1	36.5
58.2	81.0	89.8	37.2
58.4	86.2	88.9	32.2
58.6	80.1	88.4	37.5
58.8	76.9	81.7	40.2
59.1	86.8	90.5	31.2
59.3	81.4	85.7	36.7
59.5	84.2	88.5	33.1
59.7	85.0	87.2	35.6
59.9	85.9	87.8	33.7
60.1	83.5	89.3	34.5
60.3	88.4	89.0	30.1
60.6	85.3	90.8	35.8
60.8	86.1	92.2	32.8
61	84.2	91.0	37.7
61.2	86.9	90.0	30.7
61.4	84.7	92.2	36.8
61.6	88.8	91.4	29.7
61.8	88.8	92.9	28.6
62.1	87.8	88.1	30.7
62.3	87.3	92.9	31.2
62.5	78.1	88.5	45.1
62.7	90.9	95.0	29.8
62.9	85.1	91.9	37.3
63.1	89.0	91.2	28.9
63.6	88.4	91.3	28.8
63.8	90.7	93.3	30.3
64	82.9	89.7	34.5
64.2	87.3	93.1	30.8
64.4	90.2	92.8	29.9
64.6	91.7	94.0	26.8
64.8	87.8	93.9	33.3
65.1	89.2	90.7	33.6
65.3	86.2	90.5	34.6
65.5	83.9	86.8	37.9
65.7	74.9	87.0	43.9
65.6	69.3	77.3	61.1
65.8	64.8	77.3	58.5
66	79.1	84.9	38.1
66.22	67.6	83.3	51.7
66.42	72.5	81.8	47.5
66.62	77.3	87.2	40.6
66.82	84.9	86.1	37.7
67.02	81.2	88.9	36.9
67.22	83.5	87.4	33.3
67.42	79.9	87.8	36.8
67.72	73.9	89.1	43.0
67.92	65.9	80.9	52.1
68.12	77.5	86.8	40.3
68.92	75.6	85.4	47.1
69.22	70.3	87.9	47.2
69 42	67.6	79 8	56.7
69 62	68.5	77.4	48.4
69 82	72.2	85.6	51.4
70.02	55.6	75.5	63.2
70.22	68.5	83.2	55.1
70 42	81.2	88.6	36.4
70.72	84.7	86.5	33.0
70.92	66.4	85.9	49.9
71.12	79.0	88 7	43.3
71.32	82.6	91.3	38.4
71.52	85.1	92.0	32.5
71 72	84.7	91.8	32.1
71.92	88.9	91.4	30.0
72.22	81.8	91.9	39.2
72.42	82.3	92.9	38.7
72.62	83.7	87.7	36.9
72.82	86.9	90.9	33.0
73.02	76.8	91.9	45.0
73.22	77.8	86.6	43.4
73.42	86.3	89.5	33.4
73.72	90.0	89.3	26.2
73.92	85.8	91.3	29.8
74.12	86.9	92.1	27.8
74.32	83.3	90.8	32.1
74.52	78.4	90.0	36.4
74.72	88.7	91.4	27.6
74.92	84.3	93.3	30.8
75.1	79.6	87.2	36.6
75.3	87.7	92.2	27.4
75.45	94.6	94.7	22.3
75.65	90.3	94.3	24.9
75.85	92.0	92.9	24.5
76.05	92.6	94.0	23.5
76.25	87.3	90.1	27.5
76.45	90.5	93.0	25.3
76.65	89.9	92.1	25.1
76.95	89.5	92.9	26.5
77.15	89.6	93.2	25.9
77.35	81.3	91.7	34.1
78.15	85.3	90.4	30.7
78.45	88.9	90.9	27.1
78.65	75.4	90.0	41.2
78.85	85.5	91.0	31.2
79.05	82.9	92.9	33.2
79.25	77.3	89.1	38.0
79.45	86.0	91.7	28.9
79.65	90.7	94.6	25.8
79.95	82.4	88.4	33.6
80.15	80.6	89.8	38.4
80.35	86.1	88.3	30.4
80.55	82.5	89.3	34.1
80.75	82.5	87.5	34.7
80.95	82.7	88.8	35.0
81.15	89.3	89.0	27.2
81.45	88.3	90.6	27.7
81.65	85.8	90.4	32.0
81.85	89.8	90.5	27.1
82.05	89.4	89.3	26.9
82.25	91.1	91.8	25.8
82.45	90.9	91.7	25.3
82.65	80.1	90.5	38.1
83.95	85.9	90.4	31.8
83.15	86.5	92.4	31.3
83.35	88.1	86.1	28.2
83.55	92.6	90.1	27.3
83.75	90.3	92.0	26.5
83.95	85.1	89.6	32.1
84.15	81.8	89.8	35.7
84.45	85.7	89.3	30.9
84.65	82.1	89.4	35.5
84.85	91.4	91.4	24.8
85.05	88.7	90.3	29.6
84.6	79.5	86.2	39.3
84.8	90.2	92.1	25.9
85	91.6	93.4	25.7
85.2	87.5	92.1	29.0
85.4	85.8	90.9	30.7
85.6	89.3	91.8	26.9
85.8	84.1	88.3	32.6
86	72.7	82.1	43.3
86.2	88.5	91.9	29.1
86.5	90.3	42.4	27.8
86.7	75.5	87.3	41.1
86.9	86.9	89.8	31.1
87.1	77.0	87.6	40.2
87.3	75.9	88.7	41.0
87.5	86.4	90.4	30.9
87.7	81.8	90.3	35.8
88	83.6	90.3	34.4
88.2	86.1	92.0	32.0
88.4	86.4	91.7	32.6
88.6	89.7	93.7	28.8
88.8	90.7	90.6	29.9
89	91.5	92.3	28.5
89.2	85.3	95.2	29.8
89.5	66.3	90.4	50.7
89.7	92.8	95.3	26.6
89.9	86.2	93.0	32.8
90.1	93.0	96.0	26.1
90.3	91.1	93.5	27.4
90.5	89.8	95.0	28.9
91	87.1	92.9	31.3
91.2	83.4	90.4	34.6
91.4	82.7	94.1	35.2
91.6	87.2	92.2	28.7
91.8	70.0	79.8	47.7
92	84.1	90.6	32.8
92.2	89.2	93.0	27.1
92.5	86.6	92.6	31.6
92.7	88.6	93.5	27.1
92.9	91.1	94.9	26.2
93.1	88.1	91.5	28.2
93.3	88.7	90.6	27.7
93.5	85.8	93.2	30.4
93.7	87.7	92.7	29.0
94	86.5	93.4	28.9
94.2	91.3	93.1	25.0
94.4	81.2	93.6	34.1
94.6	84.7	87.4	31.2
94.1	87.6	93.6	28.0
94.42	90.0	91.2	25.3
94.62	79.7	89.2	36.2
94.82	80.0	92.6	36.2
95.02	89.0	93.9	25.9
95.22	85.4	91.9	29.9
95.42	85.9	90.2	29.6
95.62	83.9	91.2	31.6
95.92	87.1	92.3	28.2
96.12	88.8	92.4	27.0
96.32	84.2	91.9	31.1
96.52	80.7	88.0	35.6
96.72	85.8	90.6	30.4
96.92	84.2	90.2	31.5
97.12	86.0	91.8	29.1
97.42	90.4	91.9	25.1
97.62	85.7	91.2	29.9
97.82	85.5	90.4	30.5
98.02	87.9	92.0	27.5
98.22	84.7	90.3	30.9
98.42	85.9	90.6	30.6
98.62	84.5	88.4	33.6
98.92	87.9	90.8	29.4
99.12	91.9	93.1	24.2
99.32	89.2	87.3	26.9
99.52	83.8	89.2	32.7
99.72	90.7	92.8	25.2
99.92	87.4	89.6	29.2
100.12	86.2	89.1	30.3
100.42	85.3	86.1	31.2
100.62	87.6	88.0	30.0
100.82	89.6	89.2	27.3
101.02	85.2	89.3	31.6
101.22	86.2	89.6	30.5
101.42	86.3	87.0	30.4
101.62	85.8	87.8	31.8
101.92	89.7	91.2	28.2
102.12	88.1	85.3	29.2
102.32	84.5	88.3	32.8
102.52	88.7	90.7	28.3
102.72	82.4	87.3	34.3
102.92	82.0	88.3	35.3
103.12	82.4	89.1	35.0
103.42	82.0	86.1	35.3
103.62	86.1	88.3	30.4
103.82	84.8	89.2	31.9
104.02	82.1	85.7	35.2
103.6	78.9	85.9	39.1
103.8	76.9	86.6	39.6
104	77.7	86.3	39.5
104.2	81.4	85.6	35.7
104.4			
105.1	75.0	84.7	42.4
105.3	74.4	84.8	43.6
105.5	76.8	84.5	40.3
105.7	79.9	82.3	37.2
105.9	72.3	80.2	45.0
106.1	68.9	73.1	47.6
106.3	72.5	78.7	44.4
106.6	74.0	82.1	42.5
106.8	77.3	82.6	40.0
107	75.9	80.2	41.1
107.2	64.2	73.5	53.9
107.33	66.2	69.4	54.1

Table 3 (continued).

Sample depth (mbsf)	A % fine fraction (<63 µm)	B % fine fraction (<63 µm)	Mean particle size (µm)
107.6	74.0	76.7	43.4
108.1	77.4	81.8	41.6
108.3	66.7	34.9	56.7
108.5	82.5	79.5	33.1
108.7	84.1	58.8	31.3
108.9	79.4	80.4	36.4
109.1	76.6	73.3	44.3
109.3	79.2	82.6	36.7
109.6	75.6	84.2	40.6
109.8	77.8	82.0	38.6
110	83.3	19.3	33.0
110.2	75.9	79.0	41.1
110.4	78.2	79.8	37.9
110.6	73.1	80.5	45.9
110.78	71.5	81.4	46.6
111.1	86.0	86.7	30.7
111.3	87.3	89.6	30.5
111.55	91.4	85.6	27.4
111.68	89.3	89.9	29.4
111.88	87.7	88.0	30.5
112.08	88.3	76.5	30.0
112.28	93.8	89.8	24.1
112.46	85.2	90.3	32.4
112.68	91.0	91.9	27.0
112.88	91.2	85.8	25.9
113.13	88.6	83.9	28.7
113.38	91.5	89.1	26.9
113.58	90.5	88.8	26.1
113.78	88.2	86.7	29.6
113.96	87.9	89.3	29.4
114.18	90.4	86.1	27.4
114.38	85.3	88.2	32.3
114.68	82.4	87.5	35.5
114.88	88.5	88.6	29.3
115.08	87.4	86.7	30.6
115.28	79.5	83.1	41.5
115.46	91.0	91.6	26.1
115.68	91.7	90.5	26.1
115.88	88.6	89.4	30.7
116.18	89.8	90.0	27.1
116.38	92.3	88.8	24.6
116.58	89.6	88.6	27.6
116.78	81.0	90.0	39.4
116.96	87.6	89.2	29.8
117.18	83.4	90.7	35.7
117.68	83.8	88.5	35.7
117.88	84.9	87.2	32.6
118.08	79.8	85.7	37.9
118.28	74.4	81.9	43.1
118.46	73.6	83.0	45.0
118.68	72.6	78.4	44.7
118.88	77.6	77.4	40.6
119.18	69.5	76.2	48.3
119.38	67.3	78.5	49.0
119.58	72.1	76.5	46.4
119.78	74.3	78.9	43.6
119.96	70.3	80.0	46.1
120.18	73.7	80.8	43.2

Column B data generated using sieving method (see analytical techniques), data in columns A and mean particle size generated using Coulter particle size analyzer.

(Table 3). Particle size characteristics obtained from the sieving method (see analytical techniques) show a general decrease in mean percentage of fine fraction down the core to about 32.5 mbsf. The amplitude of fluctuations of the percentage of fine fraction is significantly higher above rather than below 32.5 mbsf for both sieving and Coulter methods of particle size analysis.

The mean particle size curve for Hole 819A (generated by the Coulter LS-100 particle size analyzer) shows that little variation in mean grain size occurs below 32.5 mbsf, but considerable variation occurs above 32.5 mbsf.

The relationships between particle grain size distribution and planktonic foraminiferal oxygen isotope ratios are particularly complicated and are illustrated in Figures 9 and 10. Below 32.5 mbsf, no clear relationship exists between these two parameters. However, above 32.5 mbsf, the relationship between particle size and planktonic

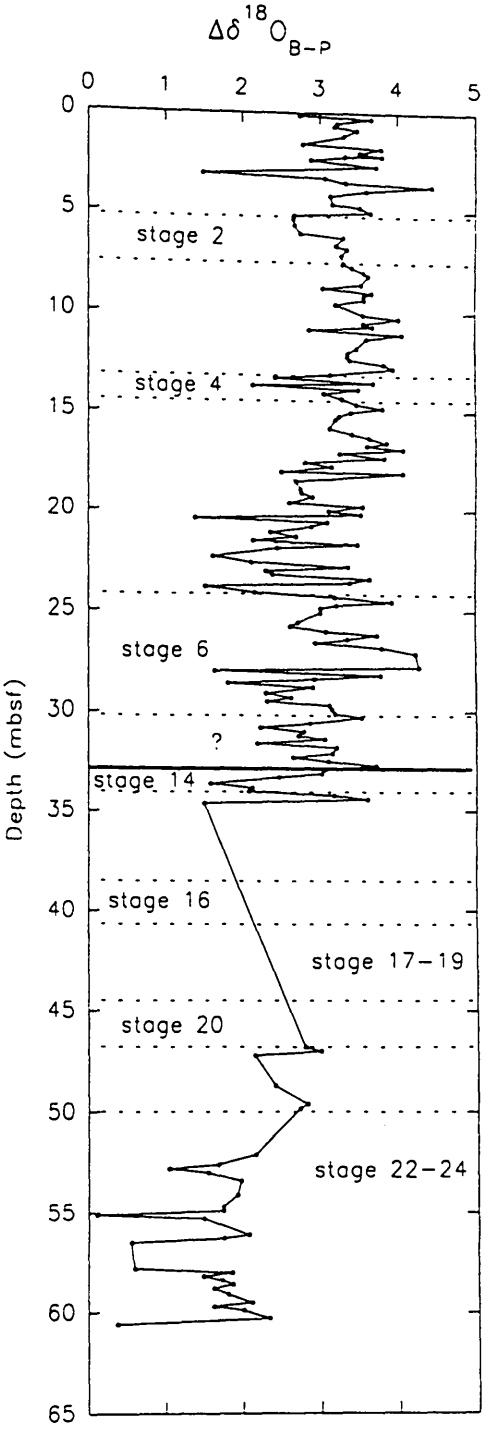

Figure 4. The difference between the planktonic and benthic foraminiferal oxygen isotope records ($\Delta\delta^{18}O_{B-P}$) plotted vs. depth at Hole 819A. Note the difference in the mean $\Delta\delta^{18}O_{B-P}$ values above and below the Brunhes/Matuyama boundary at 41 mbsf.

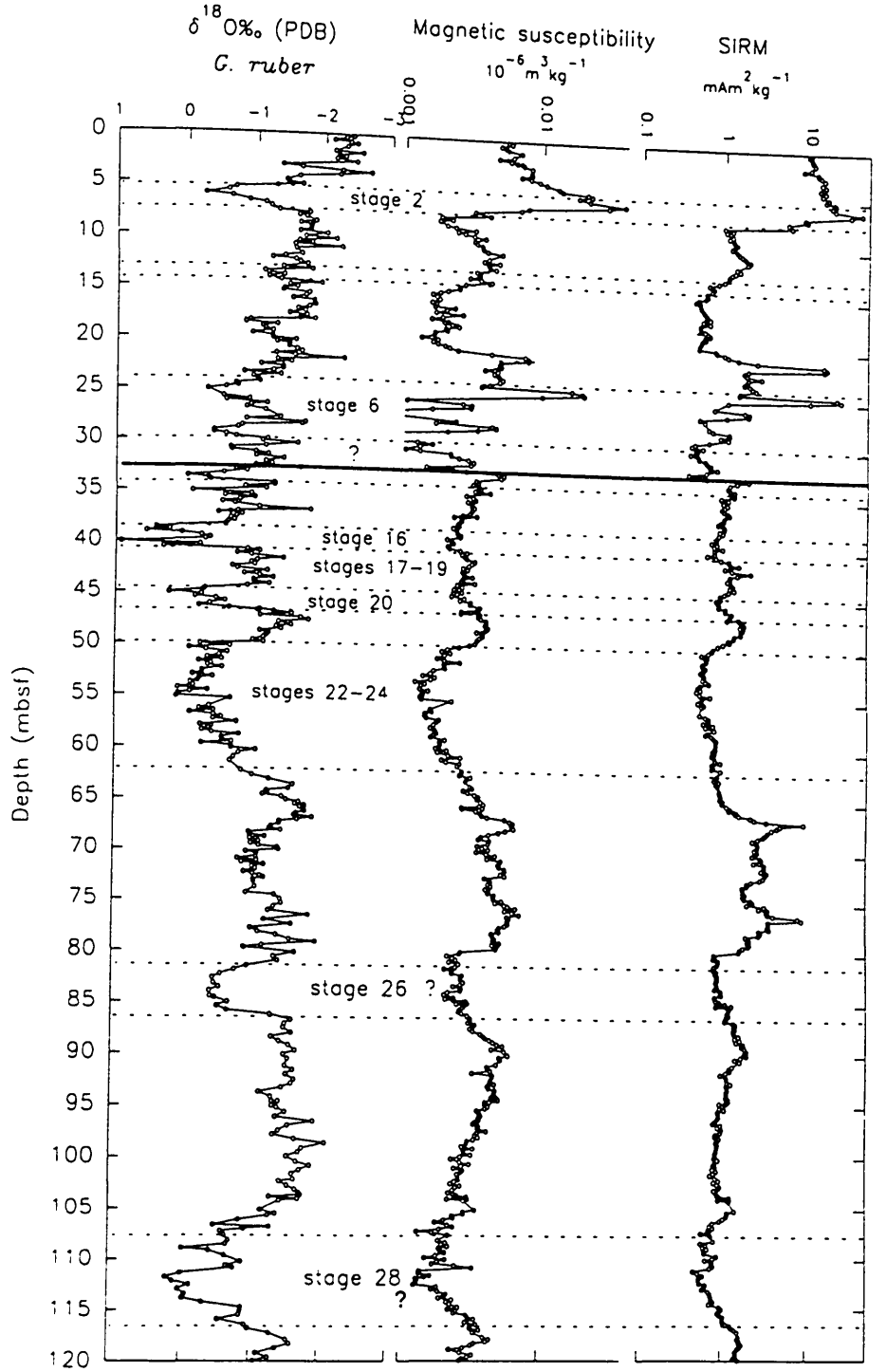

Figure 5. Magnetic mineral measurements (*X* and SIRM) and planktonic foraminiferal oxygen isotope record at Hole 819A plotted vs. depth. Note the magnetic relic dissolution layers at 21.7, 24.6, 67.2, and 76.2 mbsf and the antithetic relationships among *X*, SIRM, and the oxygen isotope record below the hiatus (solid horizontal line) at 32.5 mbsf. Both *X* and SIRM values were plotted on a common logarithmic scale.

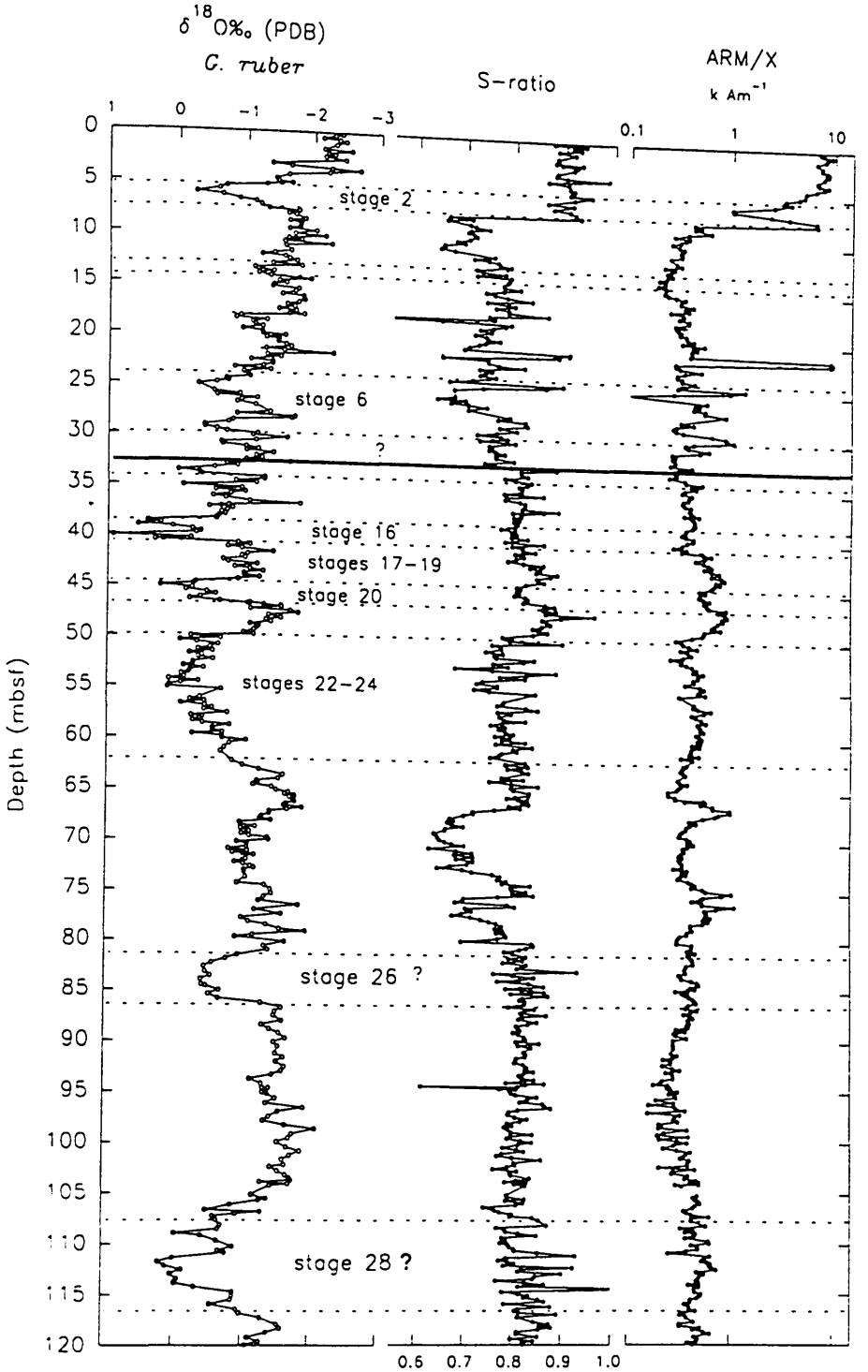

Figure 6. Magnetic mineral ratios (S and ARM/*X*) and planktonic foraminiferal oxygen isotope record at Hole 819A plotted vs. depth. The solid horizontal line at 32.5 mbsf marks the position of a major stratigraphical hiatus. ARM/*X* ratios have been plotted on a common logarithmic scale.

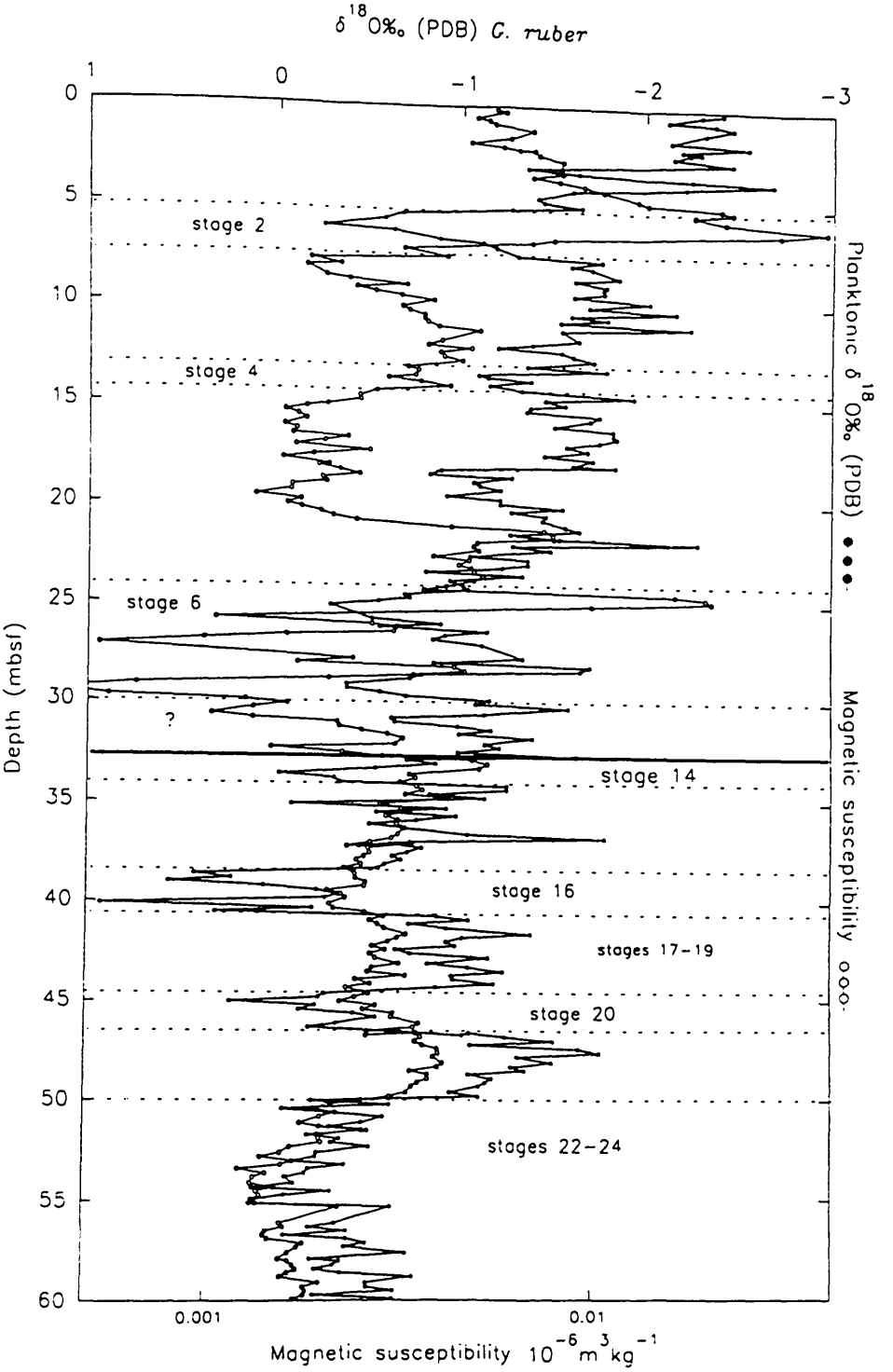

Figure 7. Specific magnetic susceptibility (open circles) and planktonic foraminiferal oxygen isotope record (closed circles) plotted vs. depth at Hole 819A. Note the complex relationship between the records above and below the hiatus (solid horizontal line) at 32.5 mbsf. Magnetic susceptibility values have been plotted on a common logarithmic scale.

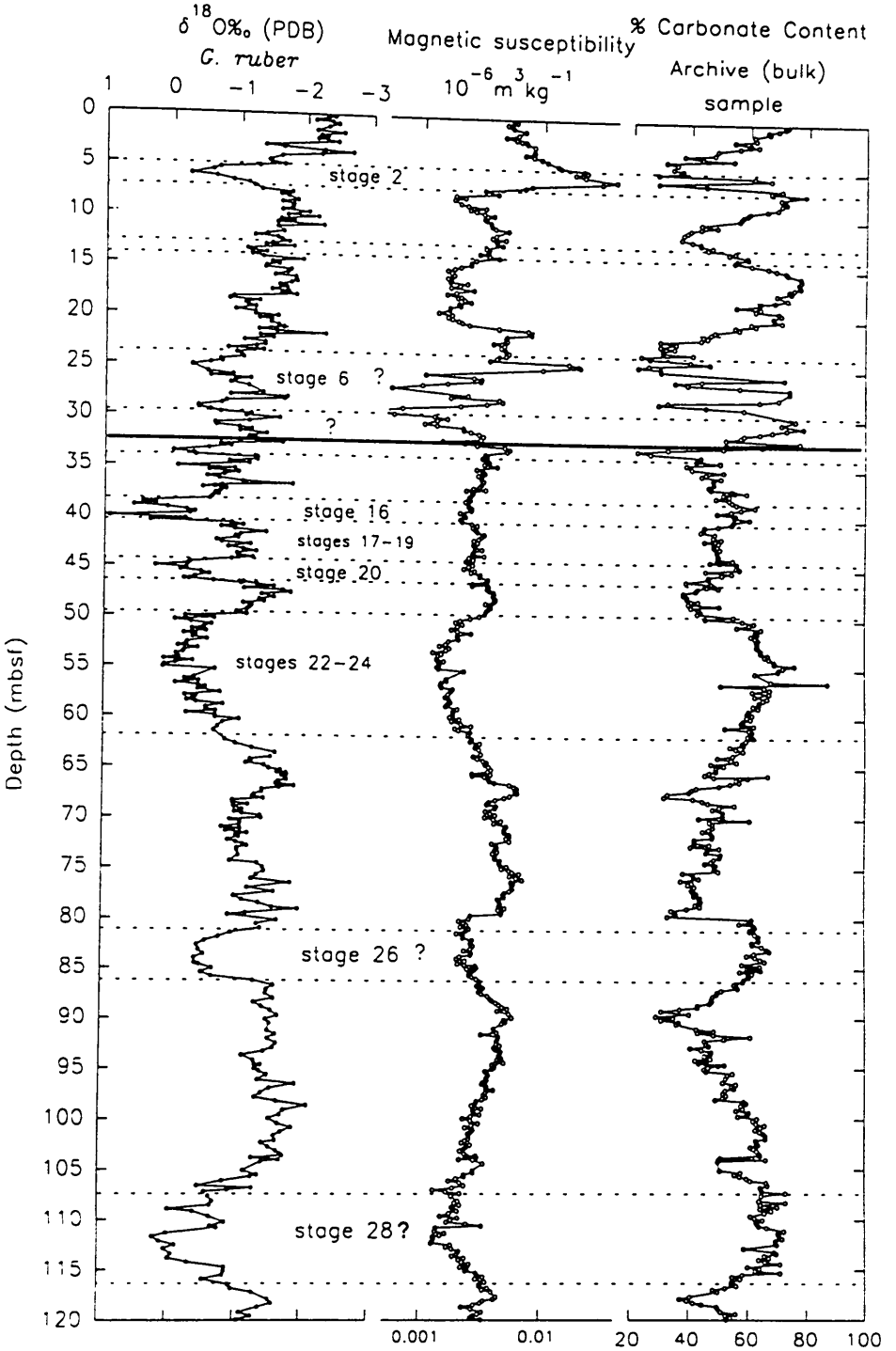

Figure 8. Planktonic foraminiferal oxygen isotope record, magnetic susceptibility, and percentage of carbonate (archive sample) plotted vs. depth. Magnetic susceptibility values have been plotted on a common logarithmic scale.

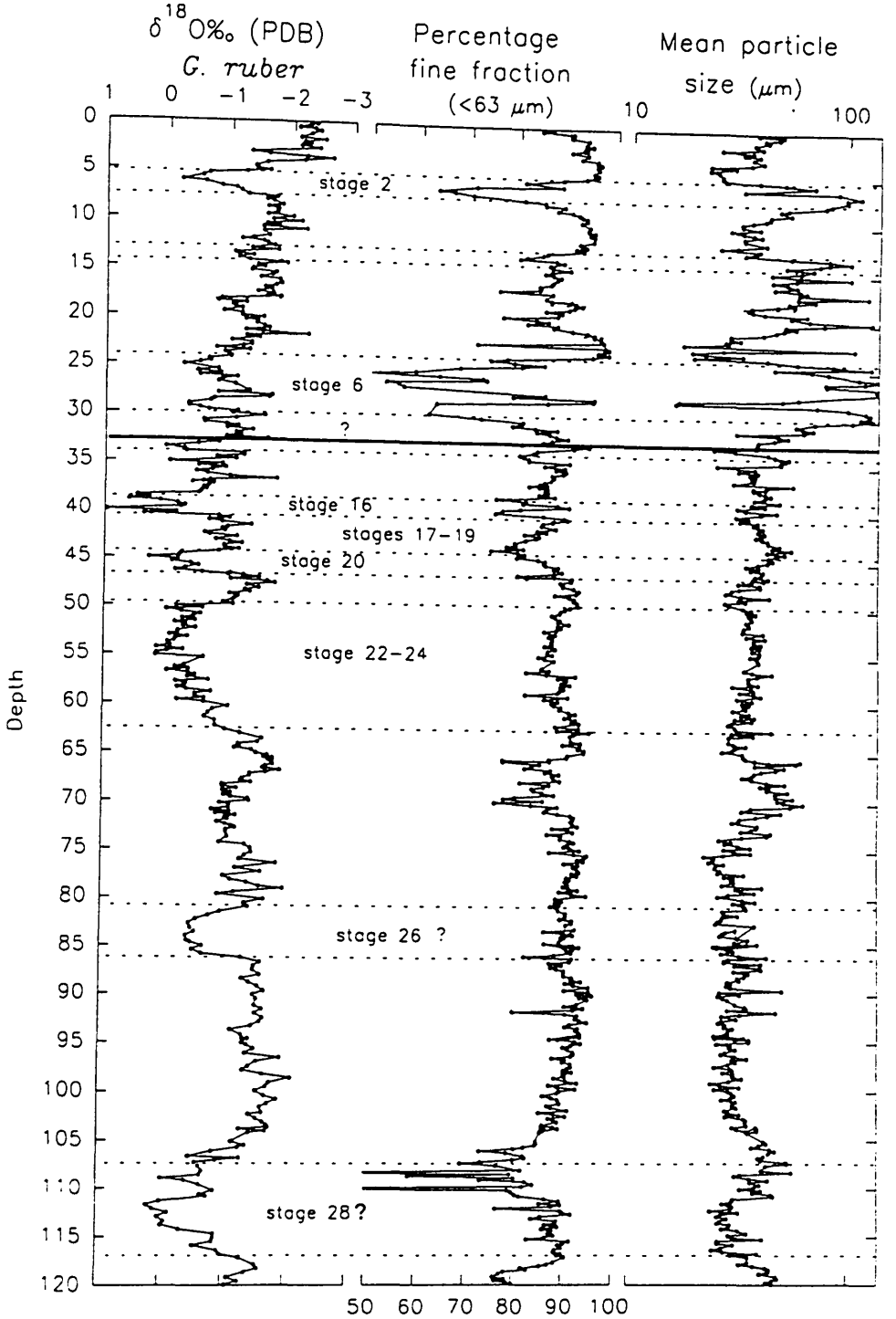

Figure 9. Composite plot showing the percentage of fine fraction (values derived from the wet-sieving method, see analytical techniques) plotted vs. planktonic foraminiferal oxygen isotope record. Note the significant offset of curves at approximately 6 and 25 mbsf. The adjoining plot displays mean particle size values, generated by the Coulter LS-100 counter and shows diminished mean particle size fluctuations below about 32.5 mbsf.

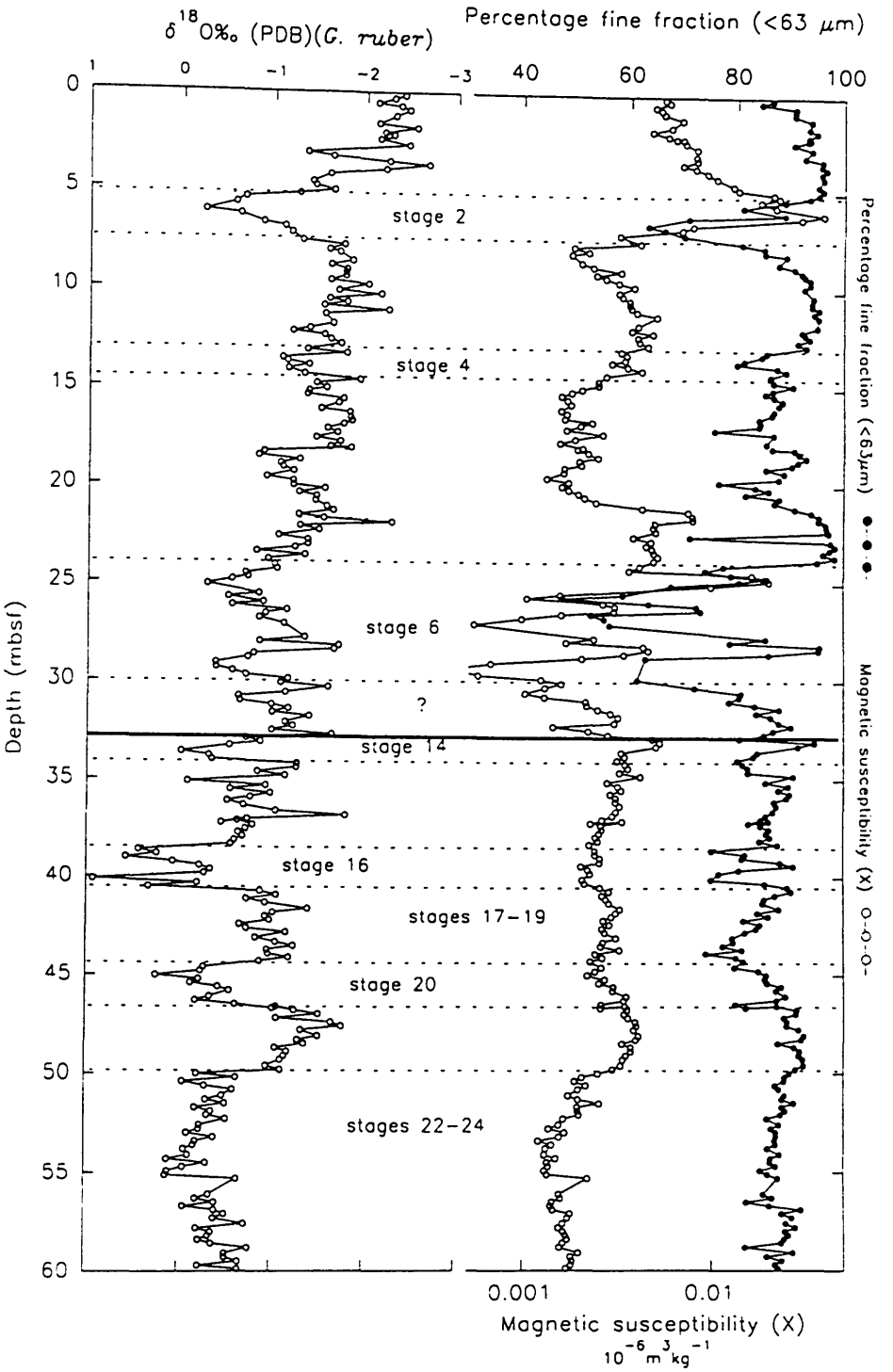

Figure 10. Planktonic foraminiferal oxygen isotope record, percentage of fine fraction (< 63 μm: closed circles) and magnetic susceptibility (open circles) plotted vs. depth. Magnetic susceptibility values have been plotted on a common logarithmic scale.

foraminiferal oxygen isotope values is more clearly developed. Above 32.5 mbsf, glacial periods were mainly dominated by low percentages of the fine fraction content, while high percentages of the fine fraction content dominate the interglacial periods. Although broadly similar, both particle grain size and planktonic foraminiferal oxygen isotope curves above 32.5 mbsf may be significantly out of phase in places; for example, during stages 2 and 6, the peak in percentages of the fine fraction clearly occurred before the glacial maxima.

Carbonate Content Determination

The percentage carbonate content for samples collected at Hole 819A ranged from 21% to 87% (see Fig. 11 and Table 4). The percentages of carbonate content within both the coarse fraction and the archive (bulk) sample, at Hole 819A, display less variation below 32.5 mbsf than above 32.5 mbsf. Compared with the archive samples, the coarse fraction samples displayed significantly higher values (by as much as 45%) of carbonate content. Below 32.5 mbsf, glacial horizons of the sequence (relative to interglacial horizons) are characterized by a higher percentage of carbonate content. Above 32.5 mbsf, relationships between planktonic foraminiferal oxygen isotope values and the percentage of carbonate content are more complex. For example, high percentage of carbonate peaks occur in both stages 5 and 8. Although the curve for the coarse fraction is broadly similar to the archive sample curve, it does display subtle differences, particularly in the peak positions at 5 mbsf and between 10 to 15 mbsf.

The comparison of the percentage of fine fraction with the percentage of carbonate content (Fig. 12), particularly in the upper part of the sequence at Hole 819A, shows that when the fine fraction content is high, the percentage of carbonate content generally is low. Thus, the fine fraction is primarily controlled by detrital influx of a terrigenous origin, resulting in a low carbonate content. A high percentage of fine fraction content generally occurs during early interglacial stages.

DISCUSSION

The mineral magnetic, particle size, and percentage of carbonate content records all show a major change at 32.5 mbsf, which marks the position of a major stratigraphic hiatus. A tentative interpretation of our isotopic data suggests that the hiatus at Hole 819A represents missing marine isotopic stages 10 to 13 (a stratigraphic time gap of about 200 k.y.), or possibly a longer period of time, depending on isotopic stage assignment. The seemingly abrupt change in the nature of sedimentation thus is an artifact of the major hiatus at 32.5 mbsf. It is most likely that a gradual or transitional change occurred in the records, between the lower and upper portions of the sequence at Hole 819A.

Mineral Magnetism

Mineral magnetic characteristics in many marine sediment sequences, for example, on bathymetric highs of the King's Trough area in the North Atlantic (Oldfield and Robinson, 1985; Robinson, 1986) or the Owen Ridge in the Indian Ocean (Bloemendal, 1989) have been found to reflect paleoclimatic changes closely. In these regions, the mineral magnetic variations involve both mineralogical fluctuations and changes in concentration. Mineral magnetic variations often repeat extremely well between neighboring core segments and between drill holes (Bloemendal et al., 1988; Hounslow, 1990). As such, they form the basis of a precise form of lithostratigraphic core correlation. Despite the value of magnetic signatures in core matching and paleoclimatic studies, the cause of magnetic signatures remains poorly understood.

The concentration of magnetic minerals in marine sediments is diluted by any carbonate (or biogenic silica) component (Kent, 1982). Reductive dissolution of iron oxides in the organic-rich upper layers also can profoundly reduce the magnetic content and also change the magnetic grain size (Karlin and Levi, 1983). Diagenesis and authigenic changes also can produce additional post-depositional magnetic minerals (Henshaw and Merrill, 1980).

For Hole 819A, we propose that the main processes controlling the overall magnetic signature have, in order of importance, been as follows:

1. Dissolution of terrigenous magnetic particles by reductive diagenesis.
2. Dilution by high concentrations of carbonate minerals, and
3. Heavy mineral concentration variations associated with sedimentological particle size changes.

The overriding importance of dissolution at Hole 819A can be seen in the 10-fold decline of magnetic concentration (as measured by, *X*, ARM, or IRM) at a depth of about 7 mbsf (see Figs. 5 and 6). Occasionally, such dissolution processes at Hole 819A have been interrupted, and magnetic mineral relics have been preserved in the sediment sequence. We interpret the magnetic concentration peaks at depths of 21.7, 24.6, 67.2, and 76.2 mbsf as horizons that have escaped dissolution. As described by Karlin and Levi (1983), dissolution changes the grain size of the magnetic minerals as well as the concentration. Such grain size changes clearly are seen in the downcore log of the S and ARM/*X* ratios (see Fig. 6). Above 6 mbsf, S ratios of 0.9 or more were found. These ratios are characteristic of large (>10 μm), easily magnetized magnetic grains. Following dissolution below 7 mbsf, S ratios were reduced to about 0.7. These lower ratios are typical of stable, single-domain grains having diameters of less than 0.1 μm that are more difficult to magnetize (e.g., Thompson, 1986; Dankers, 1978). A likely source of these small magnetite crystals that have survived reductive diagenesis, are inclusions in "dusty" feldspar or other silicate grains (Morgan and Smith, 1981).

A change can be seen in the magnetic characteristics at about 32.5 mbsf. Below this depth, magnetic concentration is inversely related to the $\delta^{18}O$ ratio. Again, the overall low concentrations are attributable to reductive diagenesis, but the variations that remain in this part of the sequence have been caused by dilution by carbonates (Kent, 1982). This inverse relationship between magnetic concentration and carbonate concentration also holds above the magnetic relic dissolution layers at depths of about 21 to 18 mbsf (see Figs. 5, 6, and 10). Dilution by carbonates, however, is not the only process affecting the magnetic properties in these horizons, because the S ratio also is changing in parallel with the $\delta^{18}O$ profile. Low S ratios of about 0.75 (corresponding to smaller magnetic grain size) are found in the glacial stages, while S ratios of about 0.9 are found in the interglacial stages. In these deposits, a relationship also has been observed between the particle size distribution (% fine fraction) and magnetic concentration (see Figs. 10 and 13). Higher magnetic concentrations are associated with finer-grained sediments. These variations may be explained by changing heavy-mineral fractions that are associated with transportation or by variable dissolution related to changes in the original organic carbon content and productivity.

Present-day Oceanic Circulation

As we are concerned with the late Quaternary paleoenvironmental history of the continental margin, the question arises of what environmental factors caused the change in the records. The records represent a major shift in the dominant sedimentological regime between the lower and upper parts of the sequence at Hole 819A. Was it a change in the paleoclimate that caused different influxes of sediment, or was it a reorganization of the paleoceanographic circulation, or a combination of these factors? In an attempt to answer these questions, the modern oceanographic setting of Site 819 may provide some clues.

Today's ocean circulation patterns for the western Coral Sea are illustrated in Figure 14 (Pickard et al., 1977; Church, 1987). Surface-water circulation patterns in the western Coral Sea are largely dominated by the westward-flowing South Equatorial Current (SEC; see

Table 4. Percentage carbonate content determination for samples collected at Hole 819A.

Sample, interval (cm)	Depth (mbsf)	% Carbonate content Coarse fraction	% Carbonate content Archive (bulk)
1H-1, 16–18	0.16	86.4	72.4
1H-1, 30–32	0.30	86.9	71.6
1H-1, 54–56	0.54	84.7	69.3
1H-1, 70–72	0.70	86.7	65.6
1H-1, 90–92	0.90	86.3	66.2
1H-1, 120–122	1.20	85.9	61.0
1H-2, 10–12	1.60	86.2	61.5
1H-2, 30–32	1.80	87.8	54.4
1H-2, 54–56	2.04	92.1	59.7
1H-2, 68–70	2.18	94.9	59.4
1H-2, 70–72	2.20	86.2	62.5
1H-2, 90–92	2.40	77.4	56.1
1H-2, 120–122	2.70	75.6	48.6
1H-3, 10–12	3.10	71.1	47.5
1H-3, 30–32	3.30	69.9	37.3
1H-3, 54–56	3.54	82.2	43.6
1H-3, 70–72	3.70	84.4	54.1
1H-3, 95–97	3.95	61.1	31.1
1H-3, 120–122	4.20	60.9	34.9
1H-4, 10–12	4.60	84.2	33.3
1H-4, 30–32	4.80	80.3	36.7
1H-4, 54–56	5.04	84.1	36.0
1H-4, 70–72	5.20	84.2	28.4
1H-4, 90–92	5.40	83.0	61.2
1H-4, 120–122	5.70	67.6	66.8
1H-5, 10–12	6.10	54.5	28.5
1H-5, 30–32	6.30	68.8	44.8
1H-5, 70–72	6.70	83.1	70.6
1H-5, 90–92	6.90	84.8	66.9
1H-5, 120–122	7.20	86.3	78.6
1H-6, 10–12	7.60	88.1	70.2
1H-6, 30–32	7.80	87.0	71.5
1H-6, 54–56	8.04	87.0	72.0
1H-6, 68–70	8.18	83.7	70.5
2H-1, 12–14	8.62	86.3	69.0
2H-1, 30–32	8.80	86.5	65.6
2H-1, 54–56	9.04	82.4	59.6
2H-1, 70–72	9.20	88.8	58.9
2H-1, 88–90	9.38	84.4	57.4
2H-1, 109–111	9.59	82.4	56.6
2H-1, 132–134	9.82	81.6	56.0
2H-2, 12–14	10.12		
2H-2, 30–32	10.03	77.3	43.2
2H-2, 54–56	10.54	81.0	48.5
2H-2, 70–72	10.70	80.6	43.1
2H-2, 88–90	10.88	78.6	39.5
2H-2, 109–111	11.09	73.3	38.5
2H-2, 132–134	11.32	74.4	37.1
2H-3, 30–32	11.80	93.7	36.4
2H-3, 54–56	12.04	77.3	40.0
2H-3, 70–72	12.20	82.3	43.0
2H-3, 88–90	12.38	81.6	43.0
2H-3, 109–111	12.59	75.0	47.0
2H-3, 132–134	12.82	81.8	45.4
2H-4, 12–14	13.12	88.6	54.7
2H-4, 30–32	13.30	71.9	52.5
2H-4, 54–56	13.54	89.5	58.8
2H-4, 70–72	13.70	91.4	59.1
2H-4, 88–90	13.88	89.8	55.2
2H-4, 109–111	14.09	91.5	54.5
2H-4, 132–134	14.34	90.5	60.3
2H-5, 12–14	14.62	89.0	65.9
2H-5, 30–32	14.80	91.7	68.7
2H-5, 54–56	15.04	92.5	72.0
2H-5, 70–72	15.20	93.3	72.6
2H-5, 88–90	15.38		
2H-5, 109–111	15.59	92.9	77.0
2H-5, 132–134	15.82	91.8	77.3
2H-6, 12–14	16.12	89.2	76.4
2H-6, 30–32	16.30	87.5	76.8
2H-6, 54–56	16.54	89.3	77.0
2H-6, 70–72	16.70	88.4	75.0
2H-6, 88–90	16.88	88.0	73.1
2H-6, 109–111	17.09	88.3	73.9
2H-6, 132–134	17.32	88.1	69.0
2H-7, 7–8	17.57		
2H-7, 27–29	17.77	89.3	72.5
2H-7, 54–56	18.04	86.5	68.3
3H-1, 10–12	18.10	88.7	63.4
3H-1, 30–32	18.30	83.3	63.1
3H-1, 52–54	18.52	84.8	55.2
3H-1, 70–72	18.70	84.6	63.5
3H-1, 90–92	18.90	89.1	61.8
3H-1, 109–111	19.09	87.3	69.7
3H-1, 131–132	19.31	86.6	70.5
3H-2, 10–12	19.60	89.9	67.8
3H-2, 30–32	19.80	87.0	68.3
3H-2, 52–54	20.02	87.4	70.9
3H-2, 70–72	20.20	81.8	60.3
3H-2, 90–92	20.40	78.5	61.9
3H-2, 109–111	20.59	80.9	54.8
3H-2, 130–132	20.81	79.6	56.2
3H-3, 10–12	21.10	71.0	48.0
3H-3, 30–32	21.30	74.4	46.7
3H-3, 52–54	21.52	72.2	44.1
3H-3, 70–72	21.70	82.5	45.5
3H-3, 90–92	21.90	88.9	43.3
3H-3, 109–111	22.09	71.6	29.3
3H-3, 131–132	22.31	70.5	34.9
3H-4, 10–12	22.60	46.8	29.3
3H-4, 30–32	22.80	67.9	34.2
3H-4, 52–54	23.02	57.9	30.2
3H-4, 70–72	23.20	64.8	30.2
3H-4, 90–92	23.40	46.3	40.7
3H-4, 109–111	23.59	70.4	22.7
3H-4, 131–133	23.81	62.7	25.6
3H-5, 10–12	24.10	74.9	39.8
3H-5, 30–32	24.30	69.8	46.5
3H-5, 52–54	24.52	61.4	25.3
3H-5, 70–72	24.70	46.3	21.7
3H-5, 87–89	24.87	58.6	29.5
3H-5, 109–111	25.09	76.6	29.6
3H-6, 7–9	25.57		
3H-6, 26–28	25.76	81.5	71.7
3H-6, 52–54	26.02	69.8	43.7
3H-6, 67–69	26.17	63.9	34.5
3H-6, 90–92	26.40	66.7	38.8
3H-6, 109–111	26.59	80.2	56.5
3H-6, 131–133	26.81	83.5	73.7
3H-7, 10–12	27.10	82.9	73.6
4H-1, 30–32	27.80	83.5	69.9
4H-1, 50–52	28.0	81.0	63.4
4H-1, 70–72	28.20	62.5	32.0
4H-1, 90–92	28.40	59.1	29.0
4H-1, 110–112	28.60	75.4	45.1
4H-1, 130–132	28.80	73.0	57.9
4H-2, 10–12	29.10		
4H-2, 30–32	29.30		
4H-2, 50–52	29.50		
4H-2, 70–72	29.70		
4H-2, 90–92	29.90	82.5	75.5
4H-2, 110–112	30.10	85.7	67.7
4H-2, 130–132	30.30	85.3	70.8
4H-3, 10–12	30.60	86.5	78.4
4H-3, 30–32	30.80	86.1	72.6
4H-3, 50–52	31.0	85.7	67.7
4H-3, 70–72	31.20	88.3	63.4
4H-3, 90–92	31.40	86.5	58.2
4H-3, 110–112	31.60	86.0	57.0
4H-3, 130–132	31.80	87.5	51.9
4H-4, 10–12	32.10	90.7	77.3
4H-4, 30–32	32.30	89.1	52.0
4H-4, 50–52	32.50	87.2	64.2
4H-4, 70–72	32.70	80.2	51.1
4H-4, 90–92	32.90	54.1	32.2
4H-4, 110–112	33.10	51.4	21.7
4H-4, 130–132	33.30	50.6	26.3
4H-5, 10–12	33.60	55.3	43.5
4H-5, 30–32	33.80	57.8	42.6
4H-5, 50–52	34.0	55.6	41.9
4H-5, 70–72	34.20	59.3	50.0
4H-5, 90–92	34.40	57.6	38.6
4H-5, 110–112	34.60		
4H-5, 130–132	34.80	65.3	40.5
4H-6, 10–12	35.10	66.2	51.2
4H-6, 30–32	35.30	59.9	45.2
4H-6, 50–52	35.50	63.4	43.8
4H-6, 70–72	35.70	68.6	50.3
4H-6, 90–92	35.90	67.9	47.5
4H-6, 110–112	36.10	66.5	47.6
4H-6, 130–132	36.30	72.2	47.8
4H-7, 10–12	36.60	71.4	46.1
4H-7, 30–32	36.80	71.9	46.8
4H-7, 50–52	37.0	70.5	53.9
4H-7, 70–72	37.20	72.3	58.9
5H-1, 10–12	37.10	69.8	55.0
5H-1, 30–32	37.30	68.8	51.0
5H-1, 50–52	37.50	71.5	53.1
5H-1, 70–72	37.70	71.6	48.6
5H-1, 90–92	37.90	75.2	53.0

Table 4 (continued).

Sample, interval (cm)	Depth (mbsf)	% Carbonate content Coarse fraction	% Carbonate content Archive (bulk)
5H-1, 110–112	38.10	72.2	54.0
5H-1, 130–132	38.30	76.0	55.5
5H-2, 10–12	38.60	68.5	61.9
5H-2, 30–32	38.80	69.5	57.2
5H-2, 50–52	39.0	68.5	53.8
5H-2, 70–72	39.20	67.4	49.0
5H-2, 90–92	39.40	68.9	55.2
5H-2, 110–112	39.60	69.1	54.8
5H-2, 130–132	39.80	71.3	60.0
5H-3, 10–12	40.10	67.3	54.4
5H-3, 30–32	40.30	63.3	53.9
5H-3, 50–52	40.50	63.4	49.5
5H-3, 70–72	40.70	63.5	44.6
5H-3, 90–92	40.90	64.6	44.5
5H-3, 110–112	41.10	56.3	43.5
5H-3, 130–132	41.30	67.7	48.3
5H-4, 10–12	41.60	67.3	47.7
5H-4, 30–32	41.80	68.7	50.5
5H-4, 50–52	42.0	67.0	44.8
5H-4, 70–72	42.20	68.3	49.5
5H-4, 90–92	42.40	71.5	47.9
5H-4, 110–112	42.60	72.0	48.0
5H-4, 130–132	42.80	71.8	50.0
5H-5, 10–12	43.10	68.9	48.9
5H-5, 30–32	43.30	71.6	49.1
5H-5, 50–52	43.50	72.5	49.6
5H-5, 70–72	43.70	72.1	49.2
5H-5, 90–92	43.90	76.2	54.4
5H-5, 110–112	44.10	69.8	46.6
5H-5, 130–132	44.30	75.5	55.8
5H-6, 10–12	44.60	71.3	55.5
5H-6, 30–32	44.80	75.3	56.7
5H-6, 50–52	45.0	74.8	45.3
5H-6, 70–72	45.20	72.7	54.1
5H-6, 90–92	45.40	74.3	50.7
5H-6, 110–112	45.60	72.2	46.1
5H-6, 130–132	45.80	73.3	46.2
5H-7, 10–12	46.10	57.5	38.6
5H-7, 30–32	46.30	72.2	47.3
5H-7, 50–52	46.50	69.7	48.1
5H-7, 70–72	46.70	70.0	49.5
6H-1, 10–12	46.60	70.5	45.7
6H-1, 30–32	46.80	75.5	42.5
6H-1, 50–52	47.0	71.4	41.9
6H-1, 70–72	47.20	66.1	37.7
6H-1, 90–92	47.40	67.2	37.8
6H-1, 110–112	47.60	70.2	39.0
6H-1, 130–132	47.80	70.7	38.9
6H-2, 10–12	48.10	75.2	42.7
6H-2, 30–32	48.30	73.5	39.4
6H-2, 50–52	48.50	70.3	49.9
6H-2, 70–72	48.70	73.3	40.3
6H-2, 90–92	48.90	72.8	42.9
6H-2, 110–112	49.10	72.7	43.6
6H-2, 130–132	49.30	72.8	42.5
6H-3, 10–12	49.60	73.4	54.8
6H-3, 30–32	49.80	72.6	45.2
6H-3, 50–52	50.0	71.5	57.8
6H-3, 70–72	50.20	72.8	61.7
6H-3, 90–92	50.40	72.6	60.2
6H-3, 110–112	50.60	71.3	56.0
6H-3, 130–132	50.80	71.5	64.2
6H-4, 10–12	51.10	74.3	62.1
6H-4, 30–32	51.30	72.4	62.9
6H-4, 50–52	51.50	71.6	60.7
6H-4, 70–72	51.70	71.5	62.1
6H-4, 90–92	51.90	72.5	63.2
6H-4, 110–112	52.10	73.2	62.6
6H-4, 130–132	52.30	69.7	62.9
6H-5, 10–12	52.600	71.4	62.6
6H-5, 30–32	52.80	71.1	63.5
6H-5, 50–52	53.0	72.4	64.2
6H-5, 70–72	53.20	71.6	64.1
6H-5, 90–92	53.40	67.4	66.5
6H-5, 110–112	53.60	65.6	65.5
6H-5, 130–132	53.80	63.1	67.0
6H-6, 10–12	54.10	64.9	68.7
6H-6, 30–32	54.30	60.9	68.7
6H-6, 50–52	54.50	70.9	75.6
6H-6, 70–72	54.70	70.1	71.7
6H-6, 90–92	54.90	72.2	70.1
6H-6, 110–112	55.10	70.0	70.0
6H-6, 130–132	55.30	73.1	62.2
7H-1, 10–12	56.10	73.0	67.7
7H-1, 30–32	56.30	70.9	86.9
7H-1, 50–52	56.50	69.6	50.6
7H-1, 70–72,	56.70	68.5	65.4
7H-1, 90–92	56.90	74.4	67.2
7H-1, 110–112	57.10	62.3	61.3
7H-1, 130–132	57.30	71.4	67.1
7H-2, 10–12	57.60	73.0	62.2
7H-2, 30–32	57.80	74.2	66.4
7H-2, 50–52	58.0	70.0	65.1
7H-2, 70–72	58.20	70.1	63.5
7H-2, 90–92	58.40	72.0	63.6
7H-2, 110–112	58.60	72.3	61.6
7H-2, 130–132	58.80	68.7	63.3
7H-3, 10–12	59.10	73.2	60.0
7H-3, 30–32	59.30	65.8	59.6
7H-3, 50–52	59.50	70.5	61.3
7H-3, 70–72	59.70	69.0	59.4
7H-3, 90–92	59.90	75.2	60.7
7H-3, 110–112	60.10	70.3	58.1
7H-3, 130–132	60.30	70.8	57.6
7H-4, 10–12	60.60	70.4	61.9
7H-4, 30–32	60.80	66.3	52.0
7H-4, 50–52	61.0	72.3	60.3
7H-4, 70–72	61.20	75.1	61.3
7H-4, 90–92	61.40	74.8	60.8
7H-4, 110–112	61.60	71.1	59.8
7H-4, 130–132	61.80	74.1	61.7
7H-5, 10–12	62.10	66.8	59.2
7H-5, 30–32	62.30	72.8	58.0
7H-5, 50–52	62.50	72.7	58.4
7H-5, 70–72	62.70	72.4	53.8
7H-5, 90–92	62.90	71.0	55.8
7H-5, 110–112	63.10	70.2	58.2
7H-6, 10–12	63.60	69.3	54.7
7H-6, 30–32	63.80	71.1	49.6
7H-6, 50–52	64.0	68.6	54.2
7H-6, 70–72	64.20	67.3	56.0
7H-6, 90–92	64.40	71.7	47.4
7H-6, 110–112	64.60	71.2	51.8
7H-6, 130–132	64.80	69.8	48.9
7H-7, 10–12	65.10	71.0	49.1
7H-7, 30–32	65.30	73.7	46.8
7H-7, 50–52	65.50	69.4	45.4
7H-7, 70–72	65.70	71.5	48.5
8H-1, 10–12	65.60	75.9	66.7
8H-1, 30–32	65.80	74.8	59.8
8H-1, 50–52	66.0	71.0	55.9
8H-2, 10–12	66.22	69.1	57.0
8H-2, 30–32	66.42	65.3	54.0
8H-2, 50–52	66.62	66.6	50.1
8H-2, 70–72	66.82	64.8	42.5
8H-2, 90–92	67.02	61.9	40.9
8H-2, 110–112	67.22	54.9	40.0
8H-2, 130–132	67.42	58.1	32.6
8H-3, 10–12	67.72	59.5	31.5
8H-3, 30–32	67.92	63.0	41.4
8H-3, 50–52	68.12	70.4	44.5
8H-3, 70–72	68.32	68.7	46.3
8H-3, 90–92	68.52	68.4	55.4
8H-3, 110–112	68.72	68.2	50.2
8H-3, 130–132	68.92	70.2	48.0
8H-4, 10–12	69.22	71.4	51.5
8H-4, 30–32	69.42	68.9	51.3
8H-4, 50–52	69.62	69.0	51.4
8H-4, 70–72	69.82	65.9	43.4
8H-4, 90–92	70.02	72.0	60.4
8H-4, 110–112	70.22	69.0	47.0
8H-4, 130–132	70.42	71.1	48.0
8H-5, 10–12	70.72	67.7	48.1
8H-5, 30–32	70.92	69.0	46.7
8H-5, 50–52	71.12	66.7	44.7
8H-5, 70–72	71.32	68.0	47.5
8H-5, 90–92	71.52	71.6	48.0
8H-5, 110–112	71.72	70.7	47.8
8H-5, 130–132	71.92	79.1	41.9
8H-6, 10–12	72.22	70.6	41.9
8H-6, 30–32	72.42	68.4	47.0
8H-6, 50–52	72.62	71.8	40.6
8H-6, 70–72	72.82	69.5	50.3
8H-6, 90–92	73.02	65.3	46.2
8H-6, 110–112	73.22	63.2	45.9
8H-6, 130–132	73.42	64.9	50.7
8H-7, 10–12	73.72	72.4	50.4
8H-7, 30–32	73.92	68.2	48.4
8H-7, 50–52	74.12	67.0	47.6
8H-7, 70–72	74.32	70.9	45.5

Table 4 (continued).

Sample, interval (cm)	Depth (mbsf)	% Carbonate content Coarse fraction	% Carbonate content Archive (bulk)
8H-7, 90–92	74.52	70.1	49.2
8H-7, 110–112	74.72	69.0	48.6
8H-7, 130–132	74.92	73.1	48.5
9H-1, 10–12	75.10	72.5	50.0
9H-1, 30–32	75.30	70.3	38.0
9H-2, 10–12	75.45	66.1	41.5
9H-2, 30–32	75.65	75.1	41.8
9H-2, 50–52	75.85	68.5	43.4
9H-2, 70–72	76.05	70.9	37.3
9H-2, 90–92	76.25	71.3	41.2
9H-2, 110–112	76.45	72.6	39.8
9H-2, 130–132	76.65	62.8	42.0
9H-3, 30–32	77.15	71.7	41.6
9H-3, 50–52	77.35	74.6	42.7
9H-3, 70–72	77.55	74.6	41.9
9H-3, 90–92	77.75	70.3	43.9
9H-3, 110–112	77.95	75.0	43.7
9H-3, 130–132	78.15	71.6	44.2
9H-4, 10–12	78.45	62.7	42.3
9H-4, 30–32	78.65	69.7	43.9
9H-4, 50–52	78.85	67.7	39.4
9H-4, 70–72	79.05	72.5	34.0
9H-4, 90–92	79.25	65.6	35.6
9H-4, 110–112	79.45	58.6	35.6
9H-4, 130–132	79.65	61.0	32.8
9H-5, 10–12	79.95	77.1	61.3
9H-5, 30–32	80.15	74.2	60.7
9H-5, 50–52	80.35	76.2	57.2
9H-5, 70–72	80.55	75.4	62.0
9H-5, 90–92	80.75	71.6	62.4
9H-5, 110–112	80.95	73.1	60.8
9H-5, 130–132	81.15	73.9	60.7
9H-6, 10–12	81.45	76.9	62.5
9H-6, 30–32	81.65	75.9	63.8
9H-6, 50–52	81.85	74.6	63.5
9H-6, 70–72	82.05	75.5	63.7
9H-6, 90–92	82.25	75.4	61.5
9H-6, 110–112	82.45	61.6	
9H-6, 130–132	82.65	74.6	64.7
9H-7, 10–12	82.95	70.8	66.5
9H-7, 30–32	83.15	73.8	67.4
9H-7, 50–52	83.35	70.9	62.1
9H-7, 70–72	83.55	71.4	60.0
9H-7, 90–92	83.75	73.4	62.7
9H-7, 110–112	83.95	73.3	64.3
9H-7, 130–132	84.15	69.0	65.8
9H-8, 10–12	84.45	69.1	58.1
9H-8, 30–32	84.65	68.6	
9H-8, 50–52	84.85	67.6	59.8
9H-8, 70–72	85.05	72.4	64.6
10H-1, 10–12	84.60	69.7	
10H-1, 30–32	84.80	68.7	60.7
10H-2, 10–12	85.0	68.4	64.1
10H-2, 30–32	85.20	69.0	57.3
10H-2, 50–52	85.40	67.4	61.6
10H-2, 70–72	85.6	63.8	60.2
10H-2, 90–92	85.8	63.7	60.5
10H-2, 110–112	86.0	59.6	58.7
10H-2, 130–132	86.20	67.1	58.4
10H-3, 10–12	86.50	66.2	55.4
10H-3, 30–32	86.70	63.9	56.3
10H-3, 50–52	86.90	65.6	56.6
10H-3, 70–72	87.10	62.9	51.1
10H-3, 90–92	87.30	63.2	49.7
10H-3, 110–112	87.50	67.0	49.6
10H-3, 130–132	87.70	63.6	48.3
10H-4, 10–12	88.0	66.6	47.8
10H-4, 30–32	88.20	66.7	48.0
10H-4, 50–52	88.40	64.7	47.2
10H-4, 70–72	88.60	62.0	43.2
10H-4, 90–92	88.80	65.0	43.1
10H-4, 110–112	89.0	59.7	37.1
10H-4, 130–132	89.20	57.1	30.8
10H-5, 10–12	89.50	65.2	40.3
10H-5, 30–32	89.70	55.2	29.0
10H-5, 50–52	89.90	61.5	35.0
10H-5, 70–72	90.10	56.2	30.8
10H-5, 90–92	90.30	59.8	36.9
10H-5, 110–112	90.50	67.0	35.9
10H-6, 10–12	91.0	69.1	42.8
10H-6, 30–32	91.20	73.3	48.6
10H-6, 50–52	91.40	76.7	43.2
10H-6, 70–72	91.60	81.9	48.6
10H-6, 90–92	91.80	84.1	60.8
10H-6, 110–112	92.0	74.1	52.1
10H-6, 130–132	92.20	77.3	45.6
10H-7, 10–12	92.50	79.6	46.2
10H-7, 30–32	92.70	83.1	47.0
10H-7, 50–52	92.90	71.9	40.7
10H-7, 70–72	93.10	74.1	44.6
10H-7, 90–92	93.30	77.1	47.8
10H-7, 110–112	93.50	78.0	47.6
10H-7, 130–132	93.70	79.0	45.5
10H-8, 10–12	94.0	84.4	47.5
10H-8, 30–32	94.20	83.8	42.3
10H-8, 50–52	94.40	78.0	44.0
10H-8, 70–72	94.60	81.4	46.1
11H-1, 10–12	94.10	63.0	43.7
11H-2, 10–12	94.42	78.3	52.1
11H-2, 30–32	94.62	83.3	50.1
11H-2, 50–52	94.82	86.5	46.8
11H-2, 70–72	95.02	84.7	45.4
11H-2, 90–92	95.22	85.1	46.1
11H-2, 110–112	95.42	82.2	55.0
11H-2, 130–132	95.62	80.3	53.3
11H-3, 10–12	95.92	85.0	52.7
11H-3, 30–32	96.12	85.6	54.3
11H-3, 50–52	96.32	83.2	51.6
11H-3, 70–72	96.52	84.2	56.1
11H-3, 90–92	96.72	84.3	54.7
11H-3, 110–112	96.92	82.2	55.4
11H-3, 130–132	97.12	80.8	52.6
11H-4, 10–12	97.42	80.9	51.7
11H-4, 30–32	97.62	85.6	52.7
11H-4, 50–52	97.82	78.1	51.6
11H-4, 70–72	98.02	82.0	49.2
11H-4, 90–92	98.22	81.8	58.7
11H-4, 110–112	98.42	79.4	59.5
11H-4, 130–132	98.62	81.4	57.7
11H-5, 10–12	98.92	81.2	58.5
11H-5, 30–32	99.12	82.2	56.1
11H-5, 50–52	99.32	81.3	60.4
11H-5, 70–72	99.52	80.0	60.0
11H-5, 90–92	99.72	79.9	56.9
11H-5, 110–112	99.92	84.8	63.1
11H-5, 130–132	100.12	82.0	61.9
11H-6, 10–12	100.42	76.8	62.9
11H-6, 30–32	100.62	76.2	65.8
11H-6, 50–52	100.82	79.8	64.4
11H-6, 70–72	101.02	76.5	62.6
11H-6, 90–92	101.22	79.9	64.2
11H-6, 110–112	101.42	79.0	65.3
11H-6, 130–132	101.62	80.7	66.0
11H-7, 10–12	101.92	81.5	66.0
11H-7, 30–32	102.12	69.4	62.7
11H-7, 50–52	102.32	76.6	63.1
11H-7, 70–72	102.52	77.4	63.6
11H-7, 90–92	102.72	71.4	61.0
11H-7, 110–112	102.92	79.2	62.1
11H-7, 130–132	103.12	78.8	63.3
11H-8, 10–12	103.42	77.9	64.0
11H-8, 30–32	103.62	78.1	64.3
11H-8, 50–52	103.82	75.5	64.4
11H-8, 70–72	104.02	68.5	50.8
12H-1, 10–12	103.60	76.1	61.6
12H-1, 30–32	103.08	74.1	50.3
12H-1, 50–52	104.0	73.9	66.3
12H-1, 70–72	104.20	67.6	50.0
12H-1, 90–92	104.40		
12H-2, 10–12	105.10	73.1	50.7
12H-2, 30–32	105.30	76.2	57.7
12H-2, 50–52	105.50	76.8	55.7
12H-2, 70–72	105.70	71.8	57.4
12H-2, 90–92	105.90	76.5	59.7
12H-2, 110–112	106.10	75.3	61.0
12H-2, 130–132	106.30	81.0	66.4
12H-3, 10–12	106.60	82.3	66.7
12H-3, 30–32	106.80	78.1	64.4
12H-3, 50–52	107.0	79.2	64.7
12H-3, 70–72	107.20	79.5	64.9
12H-3, 83–85	107.33	82.2	73.0
12H-3, 110–112	107.60	76.5	64.7
12H-4, 10–12	108.10	78.7	64.0
12H-4, 30–32	108.30	78.9	72.9
12H-4, 50–52	108.50	77.0	64.6
12H-4, 70–72	108.70	77.7	70.2
12H-4, 90–92	108.90	74.3	64.4
12H-4, 110–112	109.10	78.3	68.1
12H-4, 130–132	109.30	76.8	65.8
12H-5, 10–12	109.60	81.3	61.0

Table 4 (continued).

Sample, interval (cm)	Depth (mbsf)	% Carbonate content Coarse fraction	% Carbonate content Archive (bulk)
12H-5, 30–32	109.80	77.7	62.3
12H-5, 50–52	110.0	82.3	65.0
12H-5, 70–72	110.20	76.7	63.0
12H-5, 90–92	110.40	76.4	63.2
12H-5, 110–112	110.60	77.1	63.8
12H-5, 128–130	110.78	81.2	66.5
13H-1, 10–12	111.10	81.0	72.3
13H-1, 30–32	111.30	77.5	70.2
13H-1, 55–57	111.55	75.7	70.6
13H-2, 10–12	111.68	79.2	70.7
13H-2, 30–32	111.88	80.0	71.7
13H-2, 50–52	112.08	77.4	69.3
13H-2, 70–72	112.28	80.7	69.4
13H-2, 88–90	112.46	79.3	69.8
13H-2, 110–112	112.68		
13H-2, 130–132	112.88	78.3	58.6
13H-3, 10–12	113.13	75.6	69.0
13H-3, 30–32	113.38	77.0	69.6
13H-3, 50–52	113.58	78.3	65.6
13H-3, 70–72	113.78	76.6	67.2
13H-3, 88–90	113.96	76.1	63.8
13H-3, 110–112	114.18	74.6	65.9
13H-3, 130–132	114.38	77.4	71.0
13H-4, 10–12	114.68	71.7	60.0
13H-4, 30–32	114.88	72.3	64.0
13H-4, 50–52	115.08	67.6	62.6
13H-4, 70–72	115.28	72.1	71.1
13H-4, 88–90	115.46	67.1	58.3
13H-4, 110–112	115.68	72.4	54.7
13H-4, 130–132	115.88	70.3	57.5
13H-5, 10–12	116.18	60.4	54.6
13H-5, 30–32	116.38	62.4	54.4
13H-5, 50–52	116.58	64.3	56.3
13H-5, 70–72	116.78	69.7	52.4
13H-5, 88–90	116.96	64.0	48.2
13H-5, 110–112	117.18	67.1	50.0
13H-6, 10–12	117.68	73.0	40.7
13H-6, 30–32	117.88	60.0	37.1
13H-6, 50–52	118.08	62.1	39.6
13H-6, 70–72	118.28	66.0	41.7
13H-6, 88–90	118.46	69.0	44.5
13H-6, 110–112	118.68	72.4	49.6
13H-6, 130–132	118.88	70.9	50.0
13H-7, 10–12	119.18	73.0	51.0
13H-7, 30–32	119.38	73.3	56.0
13H-7, 50–52	119.58	69.9	52.4
13H-7, 70–72	119.78	73.6	54.2
13H-7, 88–90	119.96	81.5	52.8
13H-7, 110–112	120.18	71.7	49.8
13H-7, 130–132	120.38	73.3	48.9

Fig. 14). Upon entering the western Coral Sea, the SEC either diverges or is turned southward, depending on the austral season (Pickard et al., 1977). The southward-flowing component of the SEC becomes the East Australian Current (EAC) at about 20°S (Orme, 1973). Intensification of the northwest monsoon, during the austral summer, may account for the increased southerly currents near the Australian continental margin (Isern et al., this volume). Pickard et al. (1977) suggested that because of the build-up and sinking of watermasses associated with the SEC along today's Australian continental margin, currently, little significant upwelling is occurring.

Typical vertical profiles of temperature (T), salinity (S), density (σ) and dissolved oxygen (O_2) for the western Coral Sea are illustrated in Figure 15 (Pickard et al., 1977). Although Figure 15 shows a set of typical physiochemical profiles from the western Coral Sea in 1200 m of water, we postulate that this model can be applied directly to the shallower upper slope setting at Hole 819A without significant modification. The important point to note is that the present-day position of Site 819 (water depth of 565.2 m) is just below the main thermocline, the zone of rapid physiochemical oceanographic change (see Fig. 15).

In terms of watermasses, Site 819 today is situated between the cores of Subtropical Central Water (SCW; water depth of 50–250 m) and Antarctic Intermediate Water (AAIW; water depth of 650–1150 m), see Pickard et al. (1977) and Wyrtki (1962). Temperature ranges for these watermasses at the time are between 18°–25°C and 4.2°–6°C for SCW and AAIW, respectively (Wyrtki, 1962). Given the proximity of Site 819 to the core of AAIW, it is reasonable to assume that sediments today are more likely to be influenced by AAIW during deposition than SCW. However, any changes in relative sea level in the past might have been accompanied by a change in the prevailing watermass.

Paleodepth and Paleoceanography

The dramatic upward decrease in sedimentation rates at Hole 819A and the overall increase in nannofossil percentages (Shipboard Scientific Party, 1991) below the hiatus (during sedimentological Units 5 through 2) suggest that the lower part of the section was at a shallower depth than the upper portion. Planktonic/benthic (P/B) foraminiferal ratio data (see Kroon et al., this volume), which are available for the upper 45 m of the sedimentary sequence at Hole 819A, also suggest shallower water depths during isotopic stages 15 to 28. Possibly, tectonic subsidence across the continental margin caused deepening at Site 819. Subsidence may not have been restricted to the continental margin, but also may have involved the adjoining Marion and Queensland plateaus. Subsidence across these ocean-circulation modulating bathymetric highs would enhance local AAIW circulation patterns and would enable these waters to encroach farther up the continental margin. With increasing water depth, a restructuring of the water column occurred, involving the intensification of both AAIW and SCW flow on the continental margin during the upper part of the sequence at Hole 819A. In addition, the regional spatial watermass distribution might have changed over time in a response to worldwide reorganization of watermasses (see below).

Assuming that Site 819 was at a shallower depth below the hiatus, the dominant watermass affecting sedimentation at Site 819 was most likely the SCW. This part of the record at Site 819 is dominated by predominantly fine-grained sediments (Fig. 9). High concentrations of fine-grained sediments indicate the absence of erosive currents and imply that SCW circulation was reasonably sluggish. The presence of SCW in this part of the record is also suggested by the low $\Delta\delta^{18}O_{B-P}$ values, during stages 22 to 24 (Fig. 4), which imply little temperature difference between surface and bottom waters. Thus, cool AAIWs were unable to affect sedimentation at Site 819 during this period, as they had most likely been displaced farther down the slope by shallower water depths. However, at about stage 21 (i.e., close to the Brunhes/Matuyama boundary), the $\Delta\delta^{18}O_{B-P}$ shows a marked increase in value. Higher $\Delta\delta^{18}O_{B-P}$ values during stages 21 to 14 suggest the decoupling of surface and bottom water temperatures. Enhanced temperature stratification may have occurred in response to a change in the distribution of the watermasses, associated with the resurgence of cold AAIW flow at Hole 819A.

Throughout the upper part of the sequence at Hole 819A, we see a further continuation of the pattern of ocean-circulation intensification and reorganization, suggested during stages 21 to 14. The upcore trend of increasing $\Delta\delta^{18}O_{B-P}$ values, during the upper part of the sequence at Hole 819A, suggests the progressive decoupling of surface and bottom water temperatures. Furthermore, the planktonic foraminiferal oxygen isotopic record indicates (assuming that salinity changes are negligible) a gradual increase in mean surface-water temperatures above the hiatus. This trend might reflect depletion of ^{16}O, associated with the progressive wedging southward of warm EAC surface waters. Increased southerly currents may reflect a long-term trend in the intensification of the northwest monsoon, in a similar manner to that outlined by Isern et al. (this volume).

The upper part of the sequence is also characterized by high P/B ratios (Kroon et al., this volume), which possibly indicates higher productivity in the surface waters. This might reflect the increased influence of AAIW flow across the continental margin, although on a glacial/interglacial basis, no significant relationship can be seen. The presence of upwelling is difficult to substantiate using our foraminiferal isotopic data. Warm, well-stratified surface waters may have prevented AAIWs from reaching the ocean surface and only occasionally was the thermocline sufficiently eroded to allow these waters to "outcrop." However, the zone of mixing between the surface and

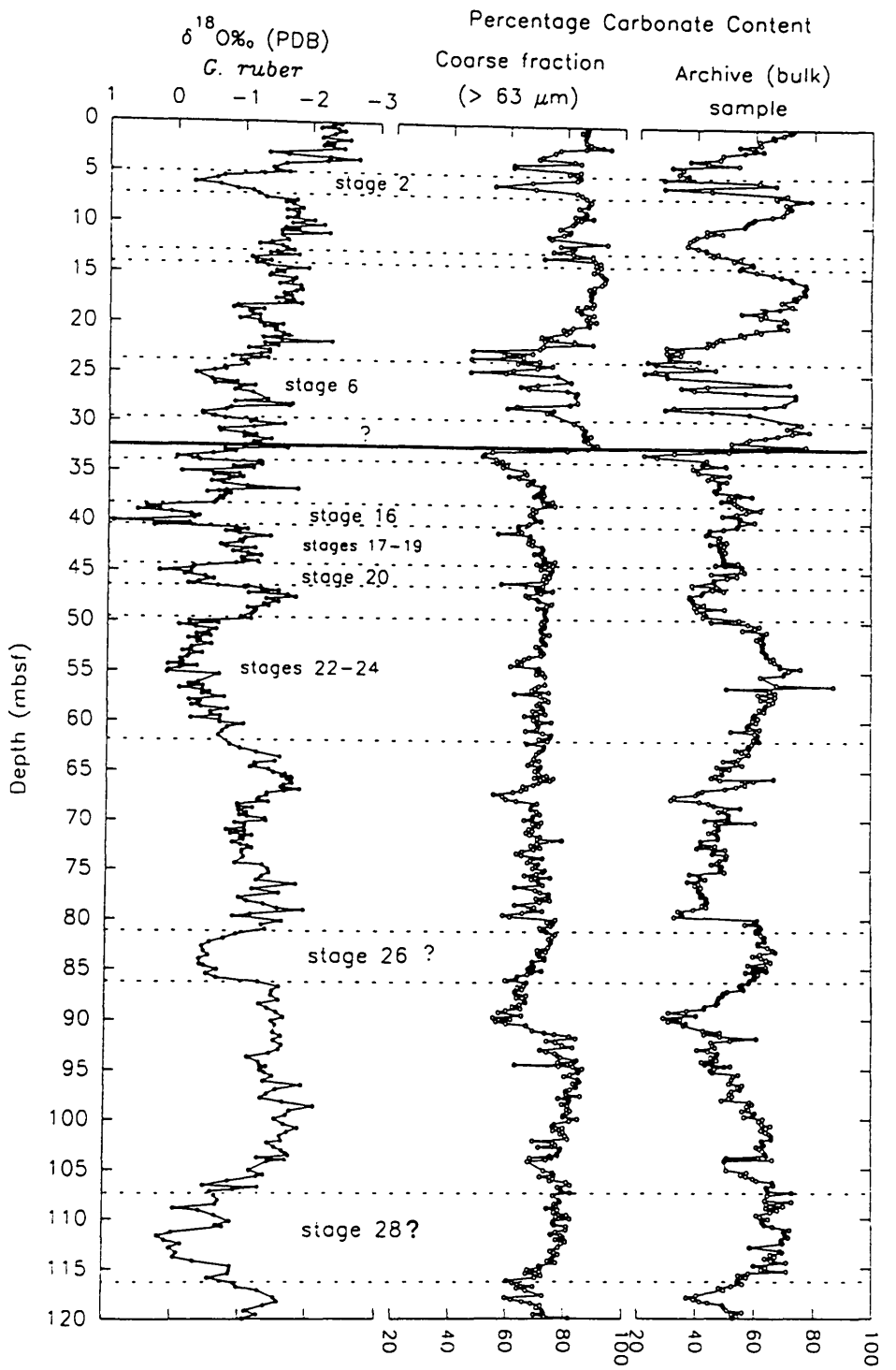

Figure 11. Percentage of carbonate content for coarse fraction (>63 μm) and archive (bulk) samples and planktonic foraminiferal oxygen isotope record plotted vs. depth.

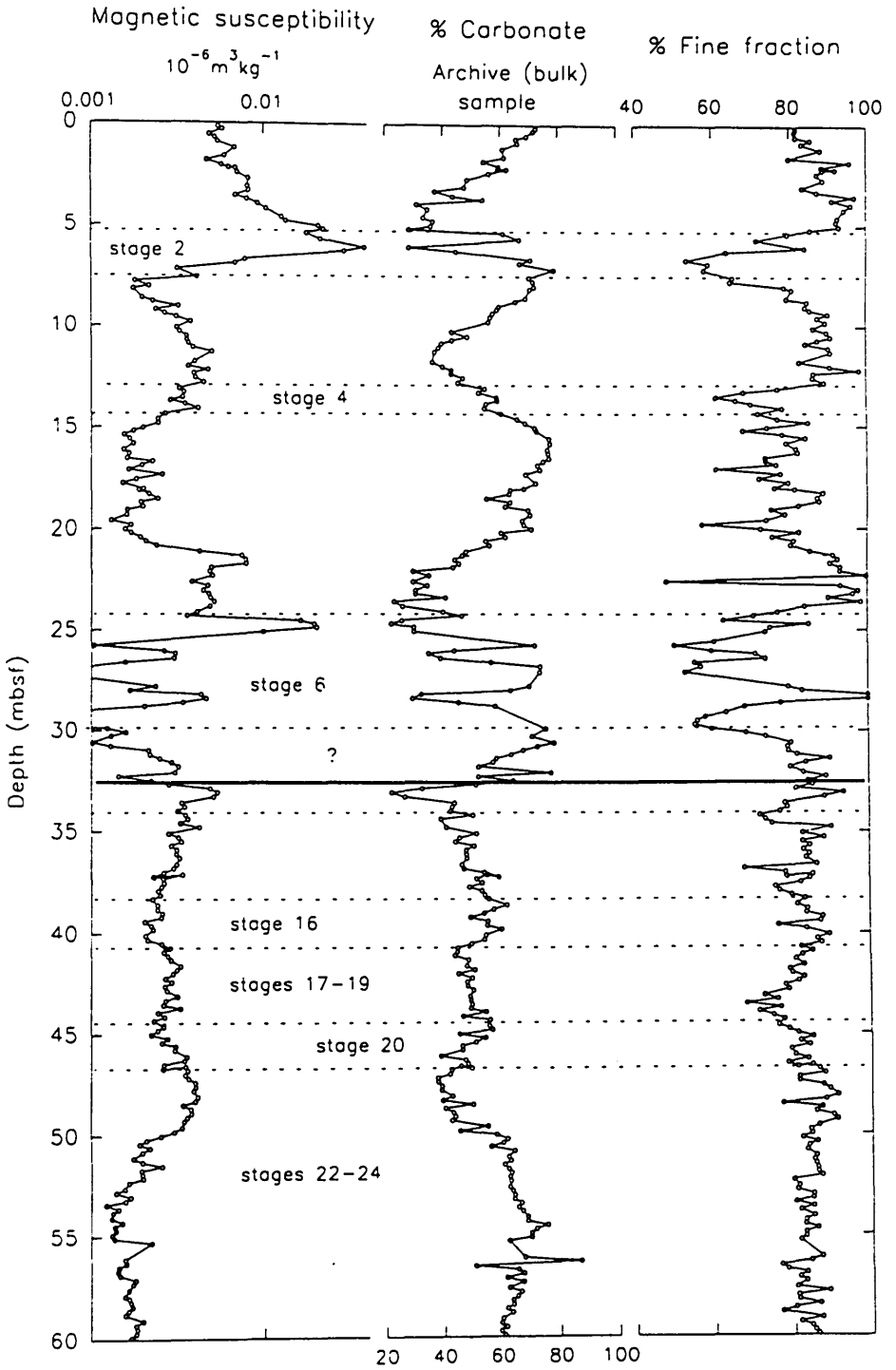

Figure 12. Magnetic susceptibility values, percentage of carbonate (archive sample) and percentage of fine fraction plotted vs. depth. Magnetic susceptibility has been plotted on a common logarithmic scale.

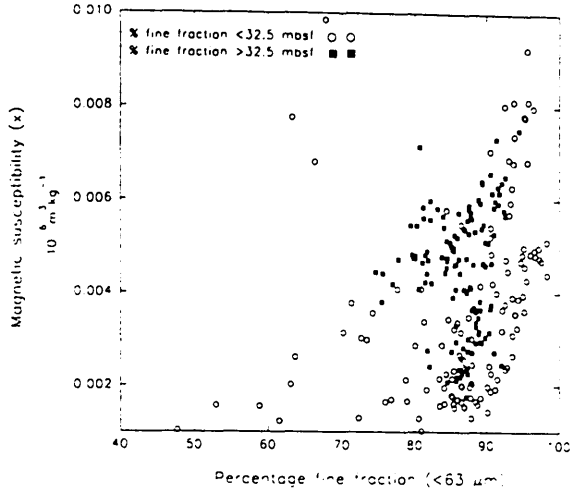

Figure 13. Scatter graph of magnetic susceptibility (X) plotted vs. percentage of fine fraction (<63 μm) above (open circles) and below (filled squares) 32.5 mbsf. The plot shows that no relationship occurred between the two variables below 35 mbsf and a strong positive relationship above 35 mbsf (Matthews, 1981). Magnetic susceptibility is plotted on a common logarithmic scale.

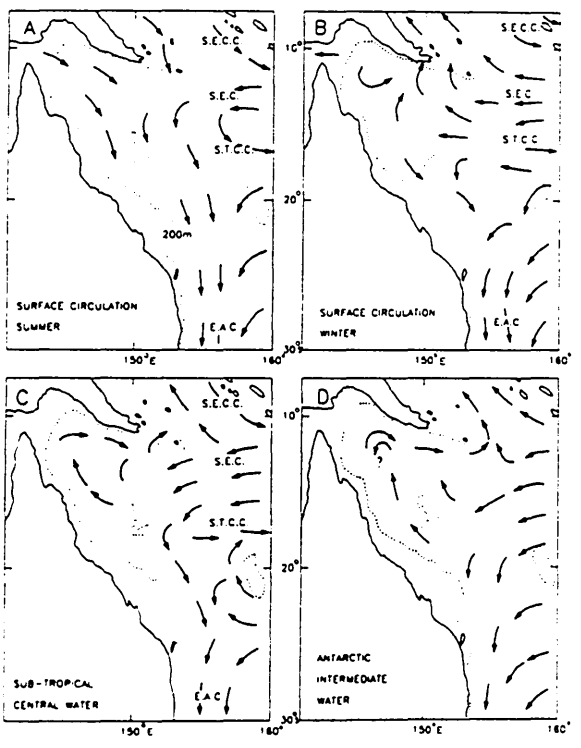

Figure 14. Surface and subsurface circulation patterns in austral summer and winter in the western Coral Sea (modified after Pickard et al., 1977). The South Equatorial Counter Current (SECC), the South Equatorial Current (SEC), the South Tropical Counter Current (STCC), and the East Australian Current (EAC) are illustrated in blocks A through D.

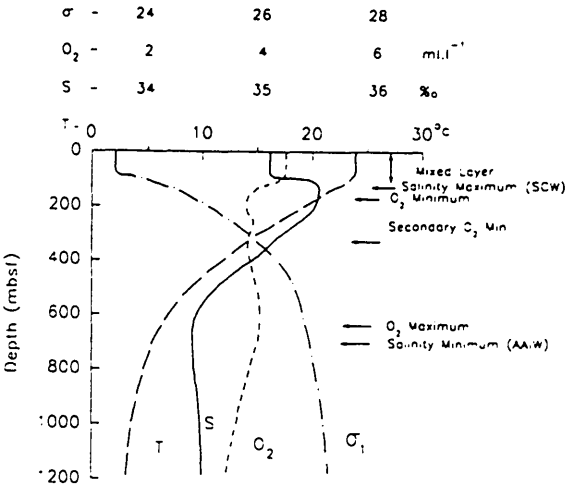

Figure 15. Typical vertical profiles of temperature (T), salinity (S), density (σ) and dissolved oxygen (O_2) in 1200 m of water for the western Coral Sea (redrawn after Pickard et al., 1977). Note the changes in the structure of the thermocline/mixed layer in a water depth of between 200 and 550 m.

subsurface watermasses may have become sufficiently shallow to facilitate nutrient transfer, thereby enabling the surface waters to support high abundances of planktonic foraminifers. Unfortunately, biogenic silica as a possible indicator of enhanced nutrient supply associated with upwelling (Codispoti, 1983) was not investigated in this study, and as such, our present data set is inconclusive. Further stable isotope and micropaleontological research will be required to substantiate the occurrence of periods of enhanced upwelling on the continental margin during the late Pleistocene at Hole 819A.

Most of our records suggest that a major change in the environment occurred across the major stratigraphic hiatus at Hole 819A. However, the foraminiferal record indicates that the change possibly occurred prior to the formation of the hiatus. Although some inconsistency can be seen among our records as to the exact timing of change, our data imply a significant reorganization of the climate and oceanography at or near the Brunhes/Matuyama boundary at Hole 819A.

The middle to late Pleistocene has been variously interpreted as a period of significant environmental change. Studies by Keany and Kennett (1972) indicated that mean temperatures were generally cooler during the Matuyama Chron than those during the Brunhes Chron. These results conflict with previous determinations of paleotemperature on the basis of radiolarian assemblages, which suggest mean warmer conditions throughout the Matuyama Chron (Hays, 1968; Bandy et al., 1971). Further, Keany and Kennett (1972) imply that climatic fluctuations during the Matuyama Chron were of lower magnitude than those in the Brunhes Chron. Although we did not see any convincing evidence of the temperature differences suggested by Keany and Kennett (1972), our records do suggest an intensification of glacial/interglacial climatic change above the hiatus. Kuijpers (1989) has interpreted the middle Pleistocene, between about 0.7 and 0.4 Ma (early Brunhes), as a period of reduced AAIW flow at depths of its present depth stratum. However, Nelson et al. (1988) interpreted sedimentological data collected from the Challenger Plateau, South Tasman Sea, as indicating an increase in mean AAIW velocities after 0.5 Ma (i.e. close to the timing of the major stratigraphic hiatus at Hole 819A). This suggests an absence of synchroneity in the timing of major oceanographic change throughout the world oceans. Jansen et al. (1986) reported a transition toward higher sea-surface temperatures (SSTs) and more "interglacial" conditions in the equatorial

regions during the mid-Brunhes period (between 0.4 and 0.3 Ma.) and attributed the longterm climatic change in the Southern Ocean circulation to a worldwide reorganization of paleoclimate and paleoceanography, possibly linked to perturbation by the orbital eccentricity cycle. Thus, the records obtained from Hole 819A indicate the occurrence of environmental change during the mid- to late Pleistocene. Our records, when combined with those from other Leg 133 holes, offer insight into the response of the Australian continental margin to fluctuations in paleoclimate and paleoceanography.

ACKNOWLEDGMENTS

We thank Tony Fallick and Terry Donnelly of the Scottish Universities Research Reactor Centre at East Kilbride for their assistance and endless patience with the "Prism." Ann Mennim and Kate Darling for their help with choosing foraminifers, and Mike Saunders and Tim Brand for their guidance during carbonate analysis. I.T. Alexander and D. Kroon gratefully acknowledge financial support from NERC (Grant No.GST/02/524).

REFERENCES*

Agrawal, Y.C., McCave, I.N., and Riley, J.B., 1991. Laser diffraction size analysis. *In* Syvitski, J.P.M. (Ed.), *Principles, Methods, and Application of Particle Size Analysis:* (Cambridge Univ. Press), 368.

Bandy, O.L., Casey, R.E., and Wright, R.C., 1971. Late Neogene planktonic zonation, magnetic reversals and radiometric dates, Antarctic to tropics. *Antarct. Res. Ser.*, 15:1–26.

Bloemendal, J., 1983. Paleoenvironmental implications of the magnetic characteristics of sediments from Deep Sea Drilling Project Site 514, southeast Argentine Basin. *In* Ludwig, W.J., Krasheninnikov, V.A., et al., *Init. Repts. DSDP*, 71 (Pt. 2): Washington (U.S. Govt. Printing Office), 1097–1108.

———, 1989. Evidence for a change in the periodicity of tropical climate cycles at 2.4 Myr from whole-core magnetic susceptibility measurements. *Nature*, 342:897–900.

Bloemendal, J., Tauxe, L., Valet, J.-P., and Shipboard Scientific Party, 1988. High-resolution, whole-core magnetic susceptibility logs from Leg 108. *In* Ruddiman, W., Sarnthein, M., Baldauf, J., et al., *Proc. ODP, Init. Repts.*, 108: College Station, TX (Ocean Drilling Program), 1005–1014.

Church, J.A., 1987. East Australian current adjacent to the Great Barrier Reef. *Aust. J. Mar. Freshwater Res.*, 38:671–683.

Codispoti, L.A., 1983. On nutrient variability and sediments in upwelling regions. *In* Suess, E., and Thiede, J. (Eds.), *Coastal Upwelling: Its Sediment Record:* New York (Plenum), 125–145.

Craig, H., 1957. Isotopic standards for carbon and oxygen correction factors for mass spectrometric analysis of CO_2. *Geochim. Cosmochim. Acta*, 12:133–149.

Dankers, P.H.M., 1978. Magnetic properties of dispersed natural iron-oxides of known grain-size [Ph.D. thesis]. Univ. of Utrecht.

Davies, P.J., Symonds, P.A., Feary, D.A., and Pigram, C.J., 1989. The evolution of the carbonate platforms of northeast Australia. *In* Crevello, P.D., Wilson, J.L., Sarg, J.F., Read, J.F. (Eds.), *Controls on Carbonate Platform and Basin Development.* Spec. Publ.—Soc. Econ. Paleontol. Mineral., 44:233–258.

Grimaldi, F.S., Shapiro, L., and Schnepfe, M., 1966. Determination of carbon dioxide in limestones and dolomite by acid-base titration. *Geol. Surv. Prof. Pap. U.S.*, 550-B:B186–188.

Harris, P.T., Davies, P.J., and Marshall, J.F., 1990. Late Quaternary sedimentation on the Great Barrier Reef continental shelf and slope east of Townsville, Australia. *Mar. Geol.*, 94:55–77.

Hays, J.D., 1968. Climatic record of late Cenozoic Antarctic Ocean sediments related to the record of world climate. *In* van Zinreren Bakker, E.M. (Ed.), *Paleoecology of Africa and Antarctica:* Cape Town (Balkema), 5:139–163.

Henshaw, P.C., Jr., and Merrill, R.T., 1980. Magnetic and chemical changes in marine sediments. *Rev. Geophys. Space Phys.*, 18:483–504.

Hounslow, M.W., 1990. A magnetic susceptibility stratigraphy for Pleistocene and Pliocene sediments in the vicinity of the Barbados Ridge. *In* Moore, J.C., Mascle, A., et al., *Proc. ODP, Sci. Results*, 110: College Station, TX (Ocean Drilling Program), 365–377.

Jansen, J.H.F., Kuijpers, A., and Troelstra, S.R., 1986. A mid-Brunhes climatic event: long-term changes in global atmospheric and ocean circulation. *Science*, 232:619–622.

Karlin, R., and Levi, S., 1983. Diagenesis of magnetic minerals in recent hemipelagic sediments. *Nature*, 303:327–330.

Keany, J., and Kennett, J.P., 1972. Pliocene-early Pleistocene palaeoclimatic history recorded in Antarctic-Subantarctic deep-sea cores. *Deep-Sea Res. Part A*, 19:529–548.

Kent, D.V., 1982. Apparent correlation of paleomagnetic intensity and climatic records in deep-sea sediments. *Nature*, 299:538–539.

Kuijpers, A., 1986. Southern Ocean circulation and global climate in the Middle Pleistocene (early Brunhes). *Palaeogeogr., Palaeoclimatol., Palaeoecol.*, 76:000–000.

Matthews, J.A., 1981. *Quantitative and Statistical Approaches to Geography: A Practical Manual:* Oxford (Pergamon Press), 138–154.

Morgan, G.E., and Smith, P.P.K., 1981. Transmission electron microscope and rock magnetic investigations of remanance carriers in a Precambrian metadolerite. *Earth Planet. Sci. Lett.*, 53:226–240.

Nelson, C.S., Hendy, C.H., and Dudley, W.C., 1986. Quaternary isotope stratigraphy of Hole 593, Challenger Plateau, South Tasman Sea: preliminary observations based on foraminifers and calcareous nannofossils. *In* Kennett, J.P., von der Borch, C.C. et al., *Init. Repts. DSDP*, 90 (Pt. 2): Washington (U.S. Govt. Printing Office), 1413–1424.

Oldfield, F., and Robinson, S.G., 1985. Geomagnetism and palaeoclimate. *In* Tooley, M.J., and Sheail, G.M. (Eds.), *The Climatic Scene:* London (Allen and Unwin), 186–205.

Orme, G.R., 1973. The Coral Sea Plateau: a major reef province. *In* Jones, O.A., and Endean, R. (Eds.), *Biology and Geology of Coral Reefs:* New York (Academic Press), 267–306.

Pickard, G.L., Donguy, J.R., Henin, C., and Rougerie, F., 1977. *A Review of the Physical Oceanography of the Great Barrier Reef and western Coral Sea.* Aust. Inst. Mar. Sci. Monogr. Ser., 2.

Raymo, M.E., Ruddiman, W.F., Shackleton, N.J., and Oppo, D.W., 1990. Evolution of global ice volume and Atlantic-Pacific $\delta^{13}C$ gradients over the last 2.5 m.y. *Earth Planet. Sci. Lett.*, 97:353–368.

Robinson, S.G., 1986. The late Pleistocene paleoclimatic record of North Atlantic deep-sea sediments revealed by mineral-magnetic measurements. *Phys. Earth Planet. Inter.*, 42:22–47.

Shipboard Scientific Party, 1991 Site 819. *In* Davies, P.J., McKenzie, J.A., Palmer-Julson, A., et al., *Proc. ODP, Init. Repts.*, 133: College Station, TX (Ocean Drilling Program).

Tarling, D.H., 1983. *Palaeomagnetism, Principles and Applications in Geology, Geophysics and Archaeology:* New York (Chapman and Hall).

Thompson, P.R., Allan, W.H.B., Duplessy, J.-C., and Shackleton, N.J., 1979. Disappearance of pink-pigmented *Globigerinoides ruber* at 120,000 yr BP in the Indian and Pacific oceans. *Nature*, 280:554–558.

Thompson, R., 1979. Palaeomagnetic correlation and dating. *In* Berglund, B.E. (Ed.), *Palaeohydrological Changes in the Temperate Zone in the Last 150,000 Years, Subproject B: Lake and Mire Environments* (Vol. 2): Dep. Quat. Geol., 39–59.

———, 1986. Modelling magnetization data using SIMPLEX: *Phys. Earth. Planet. Int.*, 42:113–127.

Wyrtki, K., 1962. The subsurface water masses in the western South Pacific Ocean. *Aust. J. Mar. Freshwater Res.*, 13:18–47.

* Abbreviations for names of organizations and publication titles in ODP reference lists follow the style given in *Chemical Abstracts Service Source Index* (published by American Chemical Society).

Date of initial receipt: 30 April 1992
Date of acceptance: 12 February 1993
Ms 133SR-224